

Harish Sharma
Mukesh Kumar Gupta
G. S. Tomar
Wang Lipo *Editors*

Communication and Intelligent Systems

Proceedings of ICCIS 2020

Lecture Notes in Networks and Systems

Volume 204

Series Editor

Janusz Kacprzyk, Systems Research Institute, Polish Academy of Sciences,
Warsaw, Poland

Advisory Editors

Fernando Gomide, Department of Computer Engineering and Automation—DCA,
School of Electrical and Computer Engineering—FEEC, University of Campinas—
UNICAMP, São Paulo, Brazil

Okyay Kaynak, Department of Electrical and Electronic Engineering,
Bogazici University, Istanbul, Turkey

Derong Liu, Department of Electrical and Computer Engineering, University
of Illinois at Chicago, Chicago, USA; Institute of Automation, Chinese Academy
of Sciences, Beijing, China

Witold Pedrycz, Department of Electrical and Computer Engineering,
University of Alberta, Alberta, Canada; Systems Research Institute,
Polish Academy of Sciences, Warsaw, Poland

Marios M. Polycarpou, Department of Electrical and Computer Engineering,
KIOS Research Center for Intelligent Systems and Networks, University of Cyprus,
Nicosia, Cyprus

Imre J. Rudas, Óbuda University, Budapest, Hungary

Jun Wang, Department of Computer Science, City University of Hong Kong,
Kowloon, Hong Kong

The series “Lecture Notes in Networks and Systems” publishes the latest developments in Networks and Systems—quickly, informally and with high quality. Original research reported in proceedings and post-proceedings represents the core of LNNS.

Volumes published in LNNS embrace all aspects and subfields of, as well as new challenges in, Networks and Systems.

The series contains proceedings and edited volumes in systems and networks, spanning the areas of Cyber-Physical Systems, Autonomous Systems, Sensor Networks, Control Systems, Energy Systems, Automotive Systems, Biological Systems, Vehicular Networking and Connected Vehicles, Aerospace Systems, Automation, Manufacturing, Smart Grids, Nonlinear Systems, Power Systems, Robotics, Social Systems, Economic Systems and other. Of particular value to both the contributors and the readership are the short publication timeframe and the world-wide distribution and exposure which enable both a wide and rapid dissemination of research output.

The series covers the theory, applications, and perspectives on the state of the art and future developments relevant to systems and networks, decision making, control, complex processes and related areas, as embedded in the fields of interdisciplinary and applied sciences, engineering, computer science, physics, economics, social, and life sciences, as well as the paradigms and methodologies behind them.

Indexed by SCOPUS, INSPEC, WTI Frankfurt eG, zbMATH, SCImago.

All books published in the series are submitted for consideration in Web of Science.

More information about this series at <http://www.springer.com/series/15179>

Harish Sharma · Mukesh Kumar Gupta ·
G. S. Tomar · Wang Lipo
Editors

Communication and Intelligent Systems

Proceedings of ICCIS 2020



Springer

Editors

Harish Sharma
Department of Computer Science
and Engineering
Rajasthan Technical University
Kota, Rajasthan, India

G. S. Tomar
Birla Institute of Applied Sciences
Nainital, Uttarakhand, India

Mukesh Kumar Gupta
Department of Computer Science
and Engineering
Swami Keshvanand Institute of Technology
Jaipur, India

Wang Lipo
School of Electrical and Electronic
Engineering
Nanyang Technological University
Singapore, Singapore

ISSN 2367-3370

ISSN 2367-3389 (electronic)

Lecture Notes in Networks and Systems

ISBN 978-981-16-1088-2

ISBN 978-981-16-1089-9 (eBook)

<https://doi.org/10.1007/978-981-16-1089-9>

© The Editor(s) (if applicable) and The Author(s), under exclusive license to Springer Nature Singapore Pte Ltd. 2021

This work is subject to copyright. All rights are solely and exclusively licensed by the Publisher, whether the whole or part of the material is concerned, specifically the rights of translation, reprinting, reuse of illustrations, recitation, broadcasting, reproduction on microfilms or in any other physical way, and transmission or information storage and retrieval, electronic adaptation, computer software, or by similar or dissimilar methodology now known or hereafter developed.

The use of general descriptive names, registered names, trademarks, service marks, etc. in this publication does not imply, even in the absence of a specific statement, that such names are exempt from the relevant protective laws and regulations and therefore free for general use.

The publisher, the authors and the editors are safe to assume that the advice and information in this book are believed to be true and accurate at the date of publication. Neither the publisher nor the authors or the editors give a warranty, expressed or implied, with respect to the material contained herein or for any errors or omissions that may have been made. The publisher remains neutral with regard to jurisdictional claims in published maps and institutional affiliations.

This Springer imprint is published by the registered company Springer Nature Singapore Pte Ltd.
The registered company address is: 152 Beach Road, #21-01/04 Gateway East, Singapore 189721,
Singapore

Preface

This volume contains the papers presented at the 2nd International Conference on Communication and Intelligent Systems (ICCIS 2020) jointly organized in virtual format by Global Institute of Technology, Jaipur, and Rajasthan Technical University Kota in association with Birla Institute of Applied Sciences, Uttarakhand, and Soft Computing Research Society during December 26–27, 2020. The International Conference on Communication and Intelligent Systems (ICCIS 2020) invited ideas, developments, applications, experiences, and evaluations in intelligent system, intelligent data analytics and computing, informatics and applications, and communication from academicians, research scholars, and scientists. The conference deliberation included topics specified within its scope. The conference offered a platform for bringing forward extensive research and literature across the arena of communication and intelligent systems. It provided an overview of the upcoming technologies. ICCIS 2020 provided a platform for leading experts to share their perceptions, provide supervision, and address participant's interrogations and concerns. ICCIS 2020 received 376 research submissions from 38 different countries, viz. Algeria, Australia, Bangladesh, Benin, Bulgaria, Chile, China, Colombia, Ecuador, Egypt, Ethiopia, France, Germany, Honduras, Iceland, India, Indonesia, Iraq, Ireland, Japan, Jordan, Lithuania, Malaysia, Mexico, Morocco, New Zealand, Nigeria, Portugal, Russia, Saudi Arabia, Senegal, South Africa, South Korea, Spain, Ukraine, United Arab Emirates, USA, and Vietnam. The papers included topics about various advanced technologies such as artificial intelligence, machine learning, and the like. After a rigorous peer review by program committee members and 90 external reviewers, 80 papers were approved.

ICCIS 2020 is a flagship event of Soft Computing Research Society, India. The conference was inaugurated by Prof. R. A. Gupta, Honorable Vice-Chancellor, Rajasthan Technical University Kota, and other eminent dignitaries, including Sh. Naman Kandoi, CEO, GIT, and Prof. Dhirendra Mathur, RTU (ATU) TEQIP-III Coordinator. The conference witnessed keynote addresses from eminent speakers, namely Kusum Deep, Indian Institute of Technology Roorkee, India; Xin-She Yang, Middlesex University, The Burroughs, Hendon, London; Wang

Lipo, Nanyang Technological University, Singapore; Joong Hoon Kim, Korea University, South Korea; Ajit K. Verma, Western Norway University of Applied Sciences, Norway; and Amir H. Gandomi, University of Technology Sydney, Australia. The organizers wish to thank Dr. Aninda Bose, Senior Editor, Springer Nature, and Mr. Radhakrishnan Madhavamani, Springer Nature, New Delhi, India, for their support and guidance.

Kota, India

Jaipur, India

Nainital, India

Singapore

Harish Sharma

Mukesh Kumar Gupta

G. S. Tomar

Wang Lipo

Contents

Neural Network Imitation Model of Realization of the Business Analysis Process	1
Katerina Kolesnikova, Olga Mezentseva, and Olena Savielieva	
Thermal Modeling of the GaN HEMT Device Using Decision Tree Machine Learning Technique	13
Niketa Sharma, Yogendra Gupta, Ashish Sharma, and Harish Sharma	
Low-Cost FPGA-Based On-board Computer	21
Dirk van Wyk and Vipin Balyan	
A Survey on Solution of Imbalanced Data Classification Problem Using SMOTE and Extreme Learning Machine	31
Ankur Goyal, Likhita Rathore, and Sandeep Kumar	
Thermal Imaging-Assisted Infection Classification (BoF) for Brinjal Crop	45
Shubhangi Verma, O. P. Singh, Sachin Kumar, and Sumita Mishra	
Preterm Delivery Prediction Using Gradient Boosting Algorithms	59
Monarch Saha, Soumen Nayak, Nirjharini Mohanty, Vishal Baral, and Imlee Rout	
Analysis Urban Traffic Vehicle Routing Based on Dijkstra Algorithm Optimization	69
Truong-Giang Ngo, Thi-Kien Dao, Jothiswaran Thandapani, Trong-The Nguyen, Duc-Tinh Pham, and Van-Dinh Vu	
A Comprehensive Overview of Quality Enhancement Approach-Based Biometric Fusion System Using Artificial Intelligence Techniques	81
Gaurav Jindal and Gaganpreet Kaur	

Rainfall Prediction Using Deep Neural Network	99
Chitra Desai	
A Comparative Analysis of Supervised Word Sense Disambiguation in Information Retrieval	111
Chandrakala Arya, Manoj Diwakar, and Shobha Arya	
Real-Time Deep Learning Face Mask Detection Model During COVID-19	121
Amit Juyal and Aditya Joshi	
Prediction of California Bearing Ratio of Subgrade Soils Using Artificial Neural Network Principles	133
T. V. Nagaraju, R. Gobinath, Paul Awoyer, and Mohd Abbas H. Abdy Sayyed	
Real-Time Bangladeshi Currency Recognition Using Faster R-CNN Approach for Visually Impaired People	147
Md. Tobibul Islam, Mohiuddin Ahmad, and Akash Shingha Bappy	
Bearing Fault Detection Using Comparative Analysis of Random Forest, ANN, and Autoencoder Methods	157
Pooja Kamat, Pallavi Marni, Lester Cardoz, Arshan Irani, Anuj Gajula, Akash Saha, Satish Kumar, and Rekha Sugandhi	
Selection of a Mesh Network Routing Protocol for Underground Mines	173
Prenern Reddy and Theo G. Swart	
An Energy-Efficient Communication Scheme for Multi-robot Coordination Deployed for Search and Rescue Operations	187
M. Rajesh and S. R. Nagaraja	
Butterfly Optimization Algorithm-Based Optimal Sizing and Integration of Photovoltaic System in Multi-lateral Distribution Network for Interoperability	201
Thandava Krishna Sai Pandraju and Varaprasad Janamala	
Document Classification in Robotic Process Automation Using Artificial Intelligence—A Preliminary Literature Review	211
Jorge Ribeiro, Rui Lima, and Sara Paiva	
Artificial Intelligence Optimization Strategies for Invoice Management: A Preliminary Study	223
Rui Lima, Sara Paiva, and Jorge Ribeiro	
A Comparative Study Between Data-Based Approaches Under Earlier Failure Detection	235
Hadjidj Nadjiha, Benbrahim Meriem, Berghout Tarek, and Mouss Leila Hayet	

Contents	ix
Survey Analysis for Medical Image Compression Techniques	241
Baidaa A. Al-Salamee and Dhiah Al-Shammary	
Performance Evaluation of SEIG Under Unbalanced Load Operations Using Genetic Algorithm	265
Yatender Chaturvedi, Varun Gupta, Arunesh Chandra, and Ankit Goel	
Suppliers Selection Using Fuzzy AHP and Fuzzy TOPSIS Method—A Case Study of a Bearing Manufacturing Company	275
Ramesh Karwal, Pradeep Kumar, Manish Bhandari, and M. L. Mittal	
A New Approach to Classify the Boolean Functions Based on Heuristic Technique	289
Rajni Goyal and Harshit Grewal	
Influence of Object-Oriented Software Design Measures on Reliability: Fuzzy Inference System Perspective	297
Syed Wajahat Abbas Rizvi	
Test Case Prioritization Based on Requirement	309
Amrita and Prateek Gupta	
Mining and Predicting No-Show Medical Appointments: Using Hybrid Sampling Technique	315
Albtool Alaiddah, Eman Alamoudi, Dauaa Shalabi, Malak AlQahtani, Hajar Alnamshan, and Nirase Fathima Abubacker	
Adaptive Strategy for Environment Exploration in Search and Rescue Missions by Autonomous Robot	335
Rokas Semenas and Romualdas Bausys	
Investigating the Effect of Lockdown During COVID-19 on Land Surface Temperature Using Machine Learning Technique by Google Earth Engine: Analysis of Rajasthan, India	355
Amita Jangid and Mukesh Kumar Gupta	
Emotion Distribution Profile for Movies Recommender Systems	365
Mala Saraswat and Shampa Chakraverty	
Prediction of Modulus of Subgrade Reaction Using Machine Language Framework	375
K. S. Grover, Jitendra Khatti, and Amit Kumar Jangid	
Enyo: A Multistage Partition and Transposition Based Cipher	395
Apratim Shukla, Mayank K. Tolani, Dipan Polley, Abhishek Thazhethe Kalathil, and N. Subhashini	
Exploring Cognitive Process in Extended Data Mining	409
Zexi Xing and Zhengxin Chen	

Sentiment Analysis from Bangla Text Review Using Feedback Recurrent Neural Network Model	423
Pratim Saha and Naznin Sultana	
Improved Vehicle Detection and Tracking Using YOLO and CSRT	435
I. C. Amitha and N. K. Narayanan	
A Comparative Analysis of Japan and India COVID-19 News Using Topic Modeling Approach	447
Piyush Ghasiya and Koji Okamura	
Double-Sided Split Ring Resonator-Based Probe Feed Patch Antenna with Enhanced Bandwidth for 5G and Ku Band Applications	461
E. Kusuma Kumari, M. Vinod Kumar, Purnima K. Sharma, and S. Murugan	
A Soft Computing Technique to Optimize Energy Consumption in Wireless Sensor Networks	475
Anupma Sangwan, Rishi Pal Singh, Garima Popli, and Anju Sangwan	
Witty City—Smart City on an Intelligent Conway Grid	489
Prakash Hegade and Girish P. Mallya	
Reinforcement Learning-Based Clustering Algorithm for Cognitive Wireless Sensor Networks	503
Anu Maria Joykutty and B. Baranidharan	
An Exploratory Analysis and Prediction of Factors Influencing the Debugging Behavior of Computer Science Students	513
Sherna Mohan and E. R. Vimina	
Automated Short Video Caption Generation Using Video Features and Audio Content	533
Shubhra Choudhary, Yogesh Kumar Ahuja, Nishkarsh Makhija, Srihitha Tangudu, and B. Rajitha	
A Method of Polytexture Modeling in 3D Anatomy Simulators	545
Alexandr Kolsanov, Sergey Chaplygin, Aikush Nazaryan, and Anton Ivaschenko	
An Impact of Different Uncertainties and Attacks on the Performance Metrics and Stability of Industrial Control System	557
Brijraj Singh Solanki, Renu Kumawat, and Seshadhri Srinivasan	
Parallel Matrix Sort Using MPI and CUDA	575
Priyanka Ojha, Pratibha Singh, Gopalakrishna N. Kini, B. Ashwath Rao, and Shwetha Rai	

Experiences Involving Student Assistants in Interdisciplinary R&D Projects Using the Example of Aerospace Computing and Bioeconomics: The “HONEYCLOUD” Project	585
Alexander Hilgarth, Diego Gormaz-Lobos, Claudia Galarce-Miranda, and Sergio Montenegro	
Multidimensional Ensemble LSTM for Wind Speed Prediction	595
Ashapurna Marndi and G. K. Patra	
A Novel Diagnosis System for Parkinson’s Disease Using K-means Clustering and Decision Tree	607
L. Sherly Puspha Annabel, S. Sreenidhi, and N. Vishali	
An Investigation of Ground Barriers and Teachers’ Attitude Towards Technology-Enabled Education in Schools	617
Gopal Datt and Naveen Tewari	
An Improved Ant Colony Optimization with Correlation and Gini Importance for Feature Selection	629
Tanvi Joshi, Ashwin Lahorkar, Gaurav Tikhe, Hrushikesh Bhosale, Aamod Sane, and Jayaraman K. Valadi	
Automated Sleep Staging Using Convolution Neural Network Based on Single-Channel EEG Signal	643
Santosh Kumar Satapathy, S. Sharathkumar, and D. Loganathan	
Spark-Based FP-Growth Algorithm for Generating Association Rules from Big Data	659
D. K. Chandrashekhar, K. C. Srikantaiah, and K. R. Venugopal	
A Univariate Data Analysis Approach for Rainfall Forecasting	669
V. P. Tharun, Prakash Ramya, and S. Renuga Devi	
Improved Adaboost Algorithm with Regression Imputation for Prediction of Chronic Type 2 Diabetes Mellitus	691
M. Dhilsath Fathima and S. Justin Samuel	
Kardex: Platformer	709
Santiago Jones, Susana Flores, Claudia Torrero, Lamia Hamdan, Everardo Torrero, and Silvana Flores	
Automatic Generation Control of Multi-area Multi-source Deregulated Power System Using Moth Flame Optimization Algorithm	717
B. V. S. Acharyulu, Tulasichandra Sekhar Gorripotu, Ahmad Taher Azar, Banaja Mohanty, Ramana Pilla, Sandeep Kumar, Fernando E. Serrano, and Nashwa Ahmad Kamal	
Spam Review Detection Using K-Means Artificial Bee Colony	731
Prateek Saini, Sakshi Shringi, Nirmala Sharma, and Harish Sharma	

Mutual Learning-Based Spider Monkey Optimization for Constraint Optimization	745
Meghna Singh, Nirmala Sharma, and Harish Sharma	
Budget-Oriented Reliable WDO Algorithm for Workflow Scheduling in Cloud Systems	759
Poonam Singh, Maitreyee Dutta, and Naveen Aggarwal	
Classification of Fundus Images Based on Non-binary Patterns for the Automated Screening of Retinal Lesions	773
Mekhana Suresh, Sreelekshmi Indira, and Sivakumar Ramachandran	
A Modulo ($2^n - 2^{n-2} - 1$) Adder Design	789
Ahmad Hiasat	
Entity-Based Knowledge Graph Information Retrieval for Biomedical Articles	803
Vikash Kumar Prasad, Shashvat Bharti, and Nishanth Koganti	
Human Activity Recognition Using Deep Learning-Based Approach	813
Maruf Rahman and Tanuja Das	
Time Fractionalized Lattice Boltzmann Model-Based Image Denoising	831
P. Upadhyay and K. N. Rai	
Distributed and Anonymous E-Voting Using Blockchain and Ring Signatures	839
Nishay Madhani, Vikrant Gajria, and Pratik Kanani	
Neuronal Unit of Thoughts (NUTs); A Probabilistic Formalism for Higher-Order Cognition	855
Nordin Zakaria	
Real-Time Multi-obstacle Detection and Tracking Using a Vision Sensor for Autonomous Vehicle	873
Sobers Francis, Sreenatha G. Anavatti, Matthew Garratt, and Hussein A. Abbass	
Healthcare Security: Usage of Generative Models for Malware Adversarial Attacks and Defense	885
Shymala Gowri Selvaganapathy and Sudha Sadasivam	
Human Identification System Based on Latent Fingerprint	899
Shashi Shreya and Kakali Chatterjee	
Data Quality Requirements Methodology for an Adapted PHM Implementation	911
N. Omri, Z. Al Masry, N. Mairot, S. Giampiccolo, and N. Zerhouni	

Contents	xiii
Scaling Depression Level Through Facial Image Processing and Social Media Analysis	921
Akshar Bhayani, Pratiksha Meshram, Bhishman Desai, Ayushi Garg, and Shivam Jha	
Classification of Social Media Users Based on Temporal Behaviors and Interests	935
Murad Hossen, Tamanna Afrose, Atashi Mani Ghosh, and Md. Musfique Anwar	
Stability and Dynamic Power Analysis of Novel 9T SRAM Cell for IoT Applications	945
Ashish Sachdeva and V. K. Tomar	
Leveraging Deep Learning Techniques on Remotely Sensing Agriculture Data	955
Ajaysinh Vikramsinh Kathiya, Jai Prakash Verma, and Sanjay Garg	
Unsupervised Classification of Zero-Mean Data Based on L1-Norm Principal Component Analysis	967
José Luis Camargo, Rubén Martín-Clemente, Susana Hornillo-Mellado, and Vicente Zarzoso	
Social Network Analysis Based on Combining Probabilistic Models with Graph Deep Learning	975
Xuan Truong Dinh and Hai Van Pham	
Data Confidentiality and Integrity in Cloud Storage Environment	987
Essohanam Djeki, Carlyna Bondiombouy, and Jules Degila	
Social Media Analytics: Current Trends and Future Prospects	1005
Sonam Srivastava, Mahesh Kumar Singh, and Yogendra Narain Singh	
A Study on Application of Interplanetary File System	1017
Ankur Biswas, Riya Sil, and Abhishek Roy	
A Hybrid LWT and DCT-Based Lossless Watermarking Scheme for Color Images	1027
Roop Singh, Alaknanda Ashok, and Mukesh Saraswat	
Author Index	1037

Editors and Contributors

About the Editors

Harish Sharma is Associate Professor at Rajasthan Technical University, Kota, in the Department of Computer Science and Engineering. He has worked at Vardhaman Mahaveer Open University Kota and Government Engineering College Jhalawar. He received his B.Tech. and M.Tech. degrees in Computer Engineering from Government Engineering College, Kota, and Rajasthan Technical University, Kota, in 2003 and 2009, respectively. He obtained his Ph.D. from ABV—Indian Institute of Information Technology and Management, Gwalior, India. He is Secretary and one of the Founder Members of Soft Computing Research Society of India. He is Lifetime Member of Cryptology Research Society of India, ISI, Kolkata. He is Associate Editor of *International Journal of Swarm Intelligence* (IJSI) published by Inderscience. He has also edited special issues of the many reputed journals like *Memetic Computing*, *Journal of Experimental and Theoretical Artificial Intelligence* and *Evolutionary Intelligence*. His primary area of interest is nature-inspired optimization techniques. He has contributed to more than 65 papers published in various international journals and conferences.

Dr. Mukesh Kumar Gupta is currently working as Professor in the Department of Computer Science and Engineering at the Swami Keshvanand Institute of Technology, Jaipur, where he has joined as a lecturer in 2002. He has more than 18-year experience in research and teaching. Prior to this college, he had worked with CEERI Pilani and many other organizations. He received the B.E. degree in Computer Science and Engineering from Government Engineering College, Kota, in 1999, and the M.Tech. from IIT Bombay and Ph.D. from MNIT Jaipur, in 2008 and 2016, respectively. His current research interests include security of web applications using machine learning techniques and modeling of web applications. Dr. Gupta is Member of Standing Executive Board (SEB) in Software Technology Parks (STPI) of India, Jaipur, Member of the Board of Governors, Swami Keshvanand Institute of Technology, Management and Gramothan, Jaipur, and Member of IEEE and IEEE Computer Society. He is Life Member of the Indian

Society for Technical Education (ISTE). Dr. Gupta has received many grants from different agencies for conducting FDP, workshops and other programs. He has felicitated at the 5th Principal and Teachers Awards-2016 ceremony at Birla Auditorium on 3rd September 2016. He is Chief Coordinator of TEQIP-III RTU-ATU Project in SKIT, Jaipur, since February 2018, and has organized various activities in this project. He has received a letter of appreciation for proactively participating on the Editorial Board of *SKIT Research Journal of Engineering, Science, Humanities and Management*, recognized as SILVER partner faculty under Inspire-The Campus Connect Faculty Partnership Model by Infosys Limited, received a certificate of recognition from Infosys for outstanding contribution to Campus Connect Program and recognized as a one of the Torch Bearer Persons in the SKIT Times annual Issue.

Prof. G. S. Tomar is Director of Rajkiya (Govt.) Engineering College, Sonbhadra, Uttar Pradesh, India. He received his UG, PG and Ph.D. degrees in Electronics Engineering from Institution of Engineers Calcutta, MNREC Allahabad and RGPV Bhopal, respectively. He completed Postdoc from the University of Kent, UK, in Computer Engineering. He worked with MITS and IIITM Gwalior, University of Kent, UK, and University of West Indies, Trinidad and Tobago. He also served as Director in 3 private colleges along with additional charge of Director of Machine Intelligence Research Labs, Gwalior, India. He served in Indian Air Force for 17 Years. His research interests are digital systems, air interface and advanced communication networks. He has many sponsored research projects to his credit. He has been a guest faculty at Thapar University Patiala, Hannam University Korea and many other universities of international repute. He received International Plato Award for academic excellence in 2009 from IBC Cambridge UK. He has published more than 220 research papers and 07 patents. He is Chief Editor of 5 international journals and has written 11 books and 10 book chapters. He organized many IEEE conferences and delivered keynote lectures at many IEEE conferences in various countries.

Dr. Wang Lipo received the Bachelor's degree from National University of Defense Technology (China) and Ph.D. from Louisiana State University (USA). He is presently on the faculty of the School of Electrical and Electronic Engineering, Nanyang Technological University, Singapore. His research interest is artificial intelligence with applications to image/video processing, biomedical engineering and data mining. He has 330+ publications, a U.S. patent in neural networks and a patent in systems. He has co-authored 2 monographs and (co-)edited 15 books. He has 8000+ Google Scholar citations, with H-index 43. He was Keynote Speaker for 36 international conferences. He is/was Associate Editor/Editorial Board Member of 30 international journals, including 4 IEEE Transactions, and Guest Editor for 10 journal special issues. He was Member of the Board of Governors of the International Neural Network Society, IEEE Computational Intelligence Society (CIS) and the IEEE Biometrics Council. He served as CIS Vice President for Technical Activities and Chair of Emergent Technologies Technical Committee, as

well as Chair of Education Committee of the IEEE Engineering in Medicine and Biology Society (EMBS). He was President of the Asia-Pacific Neural Network Assembly (APNNA) and received the APNNA Excellent Service Award. He was Founding Chair of both the EMBS Singapore Chapter and CIS Singapore Chapter. He serves/served as Chair/Committee Member of over 200 international conferences.

Contributors

Hussein A. Abbass School of Engineering and IT, University of New South Wales, Canberra, Australia

Mohd Abbas H. Abdy Sayyed Department of Civil Engineering, SR University, Warangal, India

Nirase Fathima Abubacker School of Computing, Dublin City University, Dublin, Ireland

B. V. S. Acharyulu Department of Electrical and Electronics Engineering, Lendi Institute of Technology and Management, Srikakulam, Andhra Pradesh, India

Tamanna Afroze Computer Science and Engineering Department, Jahangirnagar University, Savar, Bangladesh

Naveen Aggarwal UIET, Panjab University, Chandigarh, India

Mohiuddin Ahmad Department of Electrical and Electronic Engineering, Khulna University of Engineering & Technology, Khulna, Bangladesh

Yogesh Kumar Ahuja Department of Computer Science and Engineering, Motilal Nehru National Institute of Technology Allahabad, Uttar Pradesh, Prayagraj, India

Z. Al Masry FEMTO-ST Institute, Univ. Bourgogne Franche-Comté, CNRS, ENSMM, Besançon Cedex, France

Albtool Alaidah School of Computing, Dublin City University, Dublin, Ireland

Eman Alamoudi School of Computing, Dublin City University, Dublin, Ireland; Taif University, Taif, Saudi Arabia

Hajar Alnamshan School of Computing, Dublin City University, Dublin, Ireland

Malak AlQahtani School of Computing, Dublin City University, Dublin, Ireland

Baidaa A. Al-Salamee College of Computer Science and Information Technology, University of Al-Qadisiyah, Diwaniyah, Iraq

Dhiah Al-Shammary College of Computer Science and Information Technology, University of Al-Qadisiyah, Diwaniyah, Iraq

I. C. Amitha Department of Information Technology, Kannur University, Kannur, Kerala, India

Amrita Banasthali Vidyapith, Vanasthali, Rajasthan, India

Sreenatha G. Anavatti School of Engineering and IT, University of New South Wales, Canberra, Australia

Md. Musfiq Anwar Computer Science and Engineering Department, Jahangirnagar University, Savar, Bangladesh

Chandrakala Arya Graphic Era Hill University, Dehradun, Uttarakhand, India

Shobha Arya Gurukul Kangri Vishwavidyalaya, Haridwar, Uttarakhand, India

Alaknanda Ashok Dean College of Technology, G.B. Pant University of Agriculture and Technology, Pantnagar, Uttarakhand, India

Paul Awoyeria Department of Civil Engineering, Covenant University, Ota, Nigeria

Ahmad Taher Azar College of Computer and Information Sciences, Prince Sultan University, Riyadh, Saudi Arabia;

Faculty of Computers and Artificial Intelligence, Benha University, Benha, Egypt

Vipin Balyan Cape Peninsula University of Technology, Cape Town, South Africa

Akash Shingha Bappy Department of Electronics and Communication Engineering, Khulna University of Engineering & Technology, Khulna, Bangladesh

Vishal Baral Department of Computer Science and Information Technology, ITER, S'O'A Deemed to be University, Bhubaneswar, India

B. Baranidharan SRM Institute of Science and Technology, Tamil Nadu, India

Romualdas Bausys Department of Graphical Systems, Vilnius Gediminas Technical University, Vilnius, Lithuania

Manish Bhandari Department of Mechanical Engineering, MBM Engineering College, J.N.V University, Jodhpur, India

Shashvat Bharti GEP Worldwide Inc., Hyderabad, India

Akshar Bhayani Information Technology—Bachelor of Technology, SVKM's NMIMS MPSTME, Shirpur, India

Hrushikesh Bhosale Flame University, Pune, India

Ankur Biswas Department of Computer Science and Engineering, Adamas University, Kolkata, India

Carlyna Bondiombouy Centre d'Excellence Africain—Science Mathématiques et Applications, Porto-Novo, Benin

José Luis Camargo Signal Processing and Communications Department, University of Seville, Seville, Spain

Lester Cardoz Department of Computer Science and Information Technology, Symbiosis Institute of Technology, Pune, Maharashtra, India

Shampa Chakraverty Netaji Subhas University of Technology, Delhi, India

Arunesh Chandra KIET Group of Institutions, Ghaziabad, Uttar Pradesh, India

D. K. Chandrashekhar Department of CSE, SJB Institute of Technology, Bengaluru, Karnataka, India

Sergey Chaplygin Samara State Medical University, 89 Chapayevskaya st., Samara, Russia

Kakali Chatterjee Computer Science and Engineering, National Institute of Technology Patna, Patna, Bihar, India

Yatender Chaturvedi KIET Group of Institutions, Ghaziabad, Uttar Pradesh, India

Zhengxin Chen College of IS&T, University of Nebraska, Omaha, NE, USA

Shubhra Choudhary Department of Computer Science and Engineering, Motilal Nehru National Institute of Technology Allahabad, Uttar Pradesh, Prayagraj, India

Thi-Kien Dao Fujian Provincial Key Laboratory of Big Data Mining and Applications, Fujian University of Technology, Fuzhou, China

Tanuja Das Department of Information Technology, GUIST, Guwahati, Assam, India

Gopal Datt School of Vocational Studies, Uttarakhand Open University, Haldwani, India

Jules Degila Institut de Mathématiques et de Sciences Physiques, Porto-Novo, Benin

Bhishman Desai Information Technology—Bachelor of Technology, SVKM's NMIMS MPSTME, Shirpur, India

Chitra Desai National Defence Academy, Pune, India

M. Dhilsath Fathima Sathyabama Institute of Science and Technology, Chennai, India

Xuan Truong Dinh Hanoi University of Science and Technology, Hanoi, Vietnam; CMC Institute of Science and Technology, Hanoi, Vietnam

Manoj Diwakar Graphic Era Deemed To Be University, Dehradun, Uttarakhand, India

Essohanam Djeki Institut de Mathématiques et de Sciences Physiques, Porto-Novo, Benin

Maitreyee Dutta NITTTR, Chandigarh, India

Silvana Flores Tecnológico Nacional de México/Instituto Tecnológico de La Laguna, Torreón, Coah, México

Susana Flores Tecnológico Nacional de México/Instituto Tecnológico de La Laguna, Torreón, Coah, México

Sobers Francis School of Engineering and IT, University of New South Wales, Canberra, Australia

Vikrant Gajria Dwarkadas J. Sanghvi College of Engineering, Mumbai, Maharashtra, India

Anuj Gajula Department of Computer Science and Information Technology, Symbiosis Institute of Technology, Pune, Maharashtra, India

Claudia Galarce-Miranda Faculty of Engineering, International Center of Engineering Education, Universidad de Talca, Talca, Chile

Ayushi Garg Information Technology—Bachelor of Technology, SVKM's NMIMS MPSTME, Shirpur, India

Sanjay Garg Institute of Technology, Nirma University, Ahmedabad, India

Matthew Garratt School of Engineering and IT, University of New South Wales, Canberra, Australia

Piyush Ghasiya Kyushu University, Fukuoka, Japan

Atashi Mani Ghosh Computer Science and Engineering Department, Jahangirnagar University, Savar, Bangladesh

S. Giampiccolo SCODER 1 rue de la Forêt Z.A. l'Orée du Bois, Pirey, France

R. Gobinath Department of Civil Engineering, SR Engineering College, Warangal, India

Ankit Goel KIET Group of Institutions, Ghaziabad, Uttar Pradesh, India

Diego Gormaz-Lobos Faculty of Engineering, International Center of Engineering Education, Universidad de Talca, Talca, Chile

Tulasichandra Sekhar Gorripotu Department of Electrical and Electronics Engineering, Sri Sivani College of Engineering, Srikakulam, Andhra Pradesh, India

Ankur Goyal KL (Deemed to be University), Hyderabad, India

Rajni Goyal Amity University, Noida, UP, India

Harshit Grewal Amity University, Noida, UP, India

K. S. Grover Rajasthan Technical University, Kota, Rajasthan, India

Mukesh Kumar Gupta Department of CSE, Swami Keshvanand Institute of Technology Management & Gramothan, Jaipur, Rajasthan, India

Prateek Gupta UPES, Dehradun, India

Varun Gupta KIET Group of Institutions, Ghaziabad, Uttar Pradesh, India

Yogendra Gupta Swami Keshvanand Institute of Technology Management & Gramothan, Jaipur, India

Lamia Hamdan Tecnológico Nacional de México/Instituto Tecnológico de La Laguna, Torreón, Coah, México

Mouss Leila Hayet Laboratory of Automation and Manufacturing Engineering, University of Batna2, Batna, Algeria

Prakash Hegade KLE Technological University, Vidyanagar, Hubli, Karnataka, India

Ahmad Hiasat Princess Sumaya University for Technology, Amman, Jordan

Alexander Hilgarth Faculty of Mathematics and Computer Science, Julius Maximilians Universität Würzburg, Würzburg, Germany

Susana Hornillo-Mellado Signal Processing and Communications Department, University of Seville, Seville, Spain

Murad Hossen Computer Science and Engineering Department, Jahangirnagar University, Savar, Bangladesh

Sreelekshmi Indira Department of Electronics and Communication Engineering, College of Engineering Trivandrum, Thiruvananthapuram, Kerala, India

Arshan Irani Department of Computer Science and Information Technology, Symbiosis Institute of Technology, Pune, Maharashtra, India

Md. Tobibul Islam Department of Biomedical Engineering, Khulna University of Engineering & Technology, Khulna, Bangladesh

Anton Ivaschenko Samara State Technical University, Samara, Russia

Varaprasad Janamala Department of Electrical and Electronics Engineering, School of Engineering and Technology, Christ (Deemed to be University), Bangalore, Karnataka, India

Amit Kumar Jangid Rajasthan Technical University, Kota, Rajasthan, India

Amita Jangid Department of CSE, Swami Keshvanand Institute of Technology Management & Gramothan, Jaipur, Rajasthan, India

Shivam Jha Information Technology—Bachelor of Technology, SVKM's NMIMS MPSTME, Shirpur, India

Gaurav Jindal Department of Computer Science and Engineering, Sri Guru Granth Sahib World University, Fatehgarh Sahib, Punjab, India

Santiago Jones Tecnológico Nacional de México/Instituto Tecnológico de La Laguna, Torreón, Coah, México

Aditya Joshi Graphic Era Deemed to be University, Dehradun, India

Tanvi Joshi Centre for Modeling and Simulation, SPPU, Pune, India

Anu Maria Joykutty Rajagiri School of Engineering and Technology, Kerala, India

S. Justin Samuel Department of Computer Science and Engineering, PSN Engineering College, Tirunelveli, India

Amit Juyal Graphic Era Hill University, Dehradun, India

Abhishek Thazheth Kalathil Vellore Institute of Technology, Chennai, Tamil Nadu, India

Nashwa Ahmad Kamal Faculty of Engineering, Cairo University, Giza, Egypt

Pooja Kamat Department of Computer Science and Information Technology, Symbiosis Institute of Technology, Pune, Maharashtra, India

Pratik Kanani Dwarkadas J. Sanghvi College of Engineering, Mumbai, Maharashtra, India

Ramesh Karwal Water Resources Department, Jaipur, Rajasthan, India

Ajaysinh Vikramsinh Kathiya Institute of Technology, Nirma University, Ahmedabad, India

Gaganpreet Kaur Department of Computer Science and Engineering, Sri Guru Granth Sahib World University, Fatehgarh Sahib, Punjab, India

Jitendra Khatti Rajasthan Technical University, Kota, Rajasthan, India

Gopalakrishna N. Kini Department of Computer Science and Engineering, Manipal Institute of Higher Education, Manipal, Karnataka, India

Nishanth Koganti GEP Worldwide Inc., Hyderabad, India

Katerina Kolesnikova Department of Management Technology, Taras Shevchenko National University, Kyiv, Ukraine

Alexandr Kolsanov Samara State Medical University, Samara, Russia

Pradeep Kumar Department of Mechanical Engineering, MBM Engineering College, J.N.V University, Jodhpur, India

Sachin Kumar Amity University, Lucknow, India

Sandeep Kumar CHRIST (Deemed to be University), Bangalore, Karnataka, India

Satish Kumar Department of Mechanical Engineering, Symbiosis Institute of Technology, Pune, Maharashtra, India

M. Vinod Kumar ECE Department, Sri Vasavi Engineering College, Tadepalligudem, Andhra Pradesh, India

E. Kusuma Kumari ECE Department, Sri Vasavi Engineering College, Tadepalligudem, Andhra Pradesh, India

Renu Kumawat Manipal University Jaipur, Jaipur, India

Ashwin Lahorkar Centre for Modeling and Simulation, SPPU, Pune, India

Rui Lima Instituto Politécnico de Viana do Castelo, Viana do Castelo, Portugal

D. Loganathan Department of CSE, Pondicherry Engineering College, Puducherry, India

Nishay Madhani Dwarkadas J. Sanghvi College of Engineering, Mumbai, Maharashtra, India

N. Mairot SCODER 1 rue de la Forêt Z.A. l'Orée du Bois, Pirey, France

Nishkarsh Makhija Department of Computer Science and Engineering, Motilal Nehru National Institute of Technology Allahabad, Uttar Pradesh, Prayagraj, India

Girish P. Mallya KLE Technological University, Vidyanagar, Hubli, Karnataka, India

Ashapurna Marndi Academy of Scientific and Innovative Research, Ghaziabad, Uttar Pradesh, India;

Council of Scientific and Industrial Research, Fourth Paradigm Institute, Bengaluru, Karnataka, India

Pallavi Marni Department of Computer Science and Information Technology, Symbiosis Institute of Technology, Pune, Maharashtra, India

Rubén Martín-Clemente Signal Processing and Communications Department, University of Seville, Seville, Spain

Benbrahim Meriem Laboratory of Automation and Manufacturing Engineering, University of Batna2, Batna, Algeria

Pratiksha Meshram Department of Information Technology, SVKM's NMIMS MPSTME, Shirpur, India

Olga Mezentseva Department of Management Technology, Taras Shevchenko National University, Kyiv, Ukraine

Sumita Mishra Amity University, Lucknow, India

M. L. Mittal Department of Mechanical Engineering, MNIT, Jaipur, India

Sherna Mohan Department of Computer Science and IT, Amrita School of Arts and Sciences, Amrita Vishwa Vidyapeetham, Kochi, India

Banaja Mohanty Department of Electrical Engineering, Veer Surendra Sai University of Technology, Burla, Odisha, India

Nirjharini Mohanty Department of Computer Science and Information Technology, ITER, S‘O’A Deemed to be University, Bhubaneswar, India

Sergio Montenegro Faculty of Mathematics and Computer Science, Julius Maximilians Universität Würzburg, Würzburg, Germany

S. Murugan ECE Department, Sri Vasavi Engineering College, Tadepalligudem, Andhra Pradesh, India

Hadjidj Nadjiha Laboratory of Automation and Manufacturing Engineering, University of Batna2, Batna, Algeria

S. R. Nagaraja Department of Mechanical Engineering, Amrita School of Engineering, Amrita Vishwa Vidyapeetham, Bengaluru, India

T. V. Nagaraju Department of Civil Engineering, S.R.K.R. Engineering College, Bhimavaram, India

N. K. Narayanan Indian Institute of Information Technology Kottayam, Kottayam, Kerala, India

Soumen Nayak Department of Computer Science and Engineering, ITER, S‘O’A Deemed to be University, Bhubaneswar, India

Aikush Nazaryan Samara State Medical University, Samara, Russia

Truong-Giang Ngo Faculty of Computer Science and Engineering, Thuyloi University, Hanoi, Vietnam

Trong-The Nguyen Fujian Provincial Key Laboratory of Big Data Mining and Applications, Fujian University of Technology, Fuzhou, China;
Haiphong University of Management and Technology, Haiphong, Vietnam

Priyanka Ojha Department of Computer Science and Engineering, Manipal Institute of Higher Education, Manipal, Karnataka, India

Koji Okamura Kyushu University, Fukuoka, Japan

N. Omri FEMTO-ST Institute, Univ. Bourgogne Franche-Comté, CNRS, ENSMM, Besançon Cedex, France;
SCODER 1 rue de la Forêt Z.A. l’Orée du Bois, Pirey, France

Sara Paiva Instituto Politécnico de Viana do Castelo, Viana do Castelo, Portugal

Thandava Krishna Sai Pandraju Department of Electrical and Electronics Engineering, Dhanekula Institute of Engineering & Technology, Vijayawada, Andhra Pradesh, India

G. K. Patra Academy of Scientific and Innovative Research, Ghaziabad, Uttar Pradesh, India;

Council of Scientific and Industrial Research, Fourth Paradigm Institute, Bengaluru, Karnataka, India

Duc-Tinh Pham Center of Information Technology, Hanoi University of Industry, Hanoi, Vietnam;

Graduate University of Science and Technology, Vietnam Academy of Science and Technology, Hanoi, Vietnam

Ramana Pilla Department of Electrical and Electronics Engineering, GMR Institute of Technology, Rajam, Srikakulam, Andhra Pradesh, India

Dipan Polley Vellore Institute of Technology, Chennai, Tamil Nadu, India

Garima Popli Department of Computer Science and Engineering, Guru Jambheshwar University of Science and Technology, Hisar, Haryana, India

Vikash Kumar Prasad GEP Worldwide Inc., Hyderabad, India

Maruf Rahman Department of Information Technology, GUIST, Guwahati, Assam, India

K. N. Rai Department of Mathematical Sciences IIT (B.H.U.), DST-CIMS Banaras Hindu University, Varanasi, Uttar Pradesh, India

Shwetha Rai Department of Computer Science and Engineering, Manipal Institute of Higher Education, Manipal, Karnataka, India

M. Rajesh Department of Computer Science and Engineering, Amrita School of Engineering, Amrita Vishwa Vidyapeetham, Bengaluru, India

B. Rajitha Department of Computer Science and Engineering, Motilal Nehru National Institute of Technology Allahabad, Uttar Pradesh, Prayagraj, India

Sivakumar Ramachandran Department of Electronics and Communication Engineering, College of Engineering Trivandrum, Thiruvananthapuram, Kerala, India

Prakash Ramya British Telecom, Bengaluru, India

B. Ashwath Rao Department of Computer Science and Engineering, Manipal Institute of Higher Education, Manipal, Karnataka, India

Likhita Rathore Yagyavalkya Institute of Technology, Jaipur, India

Preneern Reddy Department of Electrical and Electronic Engineering Science, Center for Telecommunications, University of Johannesburg, Johannesburg, South Africa

S. Renuga Devi Vellore Institute of Technology University, Vellore, India

Jorge Ribeiro Instituto Politécnico de Viana do Castelo, Viana do Castelo, Portugal

Syed Wajahat Abbas Rizvi Department of Computer Science and Engineering, Amity University, Uttar Pradesh, Lucknow, India

Imlee Rout Department of Computer Science and Information Technology, ITER, S'O'A Deemed to be University, Bhubaneswar, India

Abhishek Roy Department of Computer Science and Engineering, Adamas University, Kolkata, India

Ashish Sachdeva GLA University, Mathura, India

Sudha Sadasivam Department of Computer Science and Engineering, PSG college of Technology, Coimbatore, India

Akash Saha Department of Computer Science and Information Technology, Symbiosis Institute of Technology, Pune, Maharashtra, India

Monarch Saha Department of Computer Science and Information Technology, ITER, S'O'A Deemed to be University, Bhubaneswar, India

Pratim Saha Daffodil International University, Dhaka, Bangladesh

Prateek Saini Rajasthan Technical University, Kota, India

Aamod Sane Flame University, Pune, India

Anupma Sangwan Department of Computer Science and Engineering, Guru Jambheshwar University of Science and Technology, Hisar, Haryana, India

Anju Sangwan Department of Computer Science and Engineering, Guru Jambheshwar University of Science and Technology, Hisar, Haryana, India

Mala Saraswat ABES Engineering College, Ghaziabad, U.P., India

Mukesh Saraswat Jaypee Institute of Information Technology, Noida, India

Santosh Kumar Satapathy Department of CSE, Pondicherry Engineering College, Puducherry, India

Olena Savielieva South Ukrainian National Pedagogical University Named After K. D. Ushynsky, Odessa, Ukraine

Shymala Gowri Selvaganapathy Department of Information Technology, PSG college of Technology, Coimbatore, India

Rokas Semenas Department of Graphical Systems, Vilnius Gediminas Technical University, Vilnius, Lithuania

Fernando E. Serrano Universidad Tecnologica Centroamericana (UNITEC), Tegucigalpa, Honduras

Dauaa Shalabi School of Computing, Dublin City University, Dublin, Ireland

S. Sharathkumar Department of CSE, Pondicherry Engineering College, Puducherry, India

Ashish Sharma Indian Institute of Information Technology, Kota, India

Harish Sharma Rajasthan Technical University, Kota, Rajasthan, India

Niketa Sharma Swami Keshvanand Institute of Technology Management & Gramothan, Jaipur, India

Nirmala Sharma Rajasthan Technical University, Kota, Rajasthan, India

Purnima K. Sharma ECE Department, Sri Vasavi Engineering College, Tadepalligudem, Andhra Pradesh, India

L. Sherly Puspha Annabel Department of Information Technology, St. Joseph's College of Engineering, Chennai, India

Shashi Shreya Computer Science and Engineering, National Institute of Technology Patna, Patna, Bihar, India

Sakshi Shringi Rajasthan Technical University, Kota, India

Apratim Shukla Vellore Institute of Technology, Chennai, Tamil Nadu, India

Riya Sil Department of Computer Science and Engineering, Adamas University, Kolkata, India

Mahesh Kumar Singh Institute of Engineering and Technology, Dr. APJ Abdul Kalam Technical University, Lucknow, Uttar Pradesh, India

Meghna Singh Rajasthan Technical University, Kota, Rajasthan, India

O. P. Singh Amity University, Lucknow, India

Poonam Singh NITTTR, Chandigarh, India

Pratibha Singh Department of Computer Science and Engineering, Manipal Institute of Higher Education, Manipal, Karnataka, India

Rishi Pal Singh Department of Computer Science and Engineering, Guru Jambheshwar University of Science and Technology, Hisar, Haryana, India

Roop Singh Department of Electronics and Communication Engineering, Uttarakhand Technical University, Dehradun, Uttarakhand, India

Yogendra Narain Singh Institute of Engineering and Technology, Dr. APJ Abdul Kalam Technical University, Lucknow, Uttar Pradesh, India

Brijraj Singh Solanki Poornima College of Engineering, Jaipur, India; Manipal University Jaipur, Jaipur, India

S. Sreenidhi Department of Information Technology, St. Joseph's College of Engineering, Chennai, India

K. C. Srikantaiah Department of CSE, SJB Institute of Technology, Bengaluru, Karnataka, India

Seshadri Srinivasan Kalasalingam Academy of Research and Education, Krishnankoil, Tamil Nadu, India

Sonam Srivastava Institute of Engineering and Technology, Dr. APJ Abdul Kalam Technical University, Lucknow, Uttar Pradesh, India

N. Subhashini Vellore Institute of Technology, Chennai, Tamil Nadu, India

Rekha Sugandhi Department of Information Technology, MIT School of Engineering, Pune, India

Naznin Sultana Daffodil International University, Dhaka, Bangladesh

Mekhana Suresh Department of Electronics and Communication Engineering, College of Engineering Trivandrum, Thiruvananthapuram, Kerala, India

Theo G. Swart Department of Electrical and Electronic Engineering Science, Center for Telecommunications, University of Johannesburg, Johannesburg, South Africa

Srihitha Tangudu Department of Computer Science and Engineering, Motilal Nehru National Institute of Technology Allahabad, Uttar Pradesh, Prayagraj, India

Berghout Tarek Laboratory of Automation and Manufacturing Engineering, University of Batna2, Batna, Algeria

Naveen Tewari School of Computing, Graphic Era Hill University, Bhimtal, India

Jothiswaran Thandapani Fujian Provincial Key Laboratory of Big Data Mining and Applications, Fujian University of Technology, Fuzhou, China; Anna University, Chennai, India

V. P. Tharun Wipro Ltd., Bengaluru, India

Gaurav Tikhe Centre for Modeling and Simulation, SPPU, Pune, India

Mayank K. Tolani Vellore Institute of Technology, Chennai, Tamil Nadu, India

V. K. Tomar GLA University, Mathura, India

Claudia Torrero Tecnológico Nacional de México/Instituto Tecnológico de La Laguna, Torreón, Coah, México

Everardo Torrero MAQTEC, Gómez Palacio, Dgo, México

P. Upadhyay DST-CIMS Banaras Hindu University, Varanasi, Uttar Pradesh, India

Dirk van Wyk Cape Peninsula University of Technology, Cape Town, South Africa

Jayaraman K. Valadi Flame University, Pune, India

Hai Van Pham Hanoi University of Science and Technology, Hanoi, Vietnam

K. R. Venugopal Bangalore University, Bengaluru, Karnataka, India

Jai Prakash Verma Institute of Technology, Nirma University, Ahmedabad, India

Shubhangi Verma Amity University, Lucknow, India

E. R. Vimina Department of Computer Science and IT, Amrita School of Arts and Sciences, Amrita Vishwa Vidyapeetham, Kochi, India

N. Vishali Department of Information Technology, St. Joseph's College of Engineering, Chennai, India

Van-Dinh Vu Faculty of Information Technology, Electric Power University, Hanoi, Vietnam

Zexi Xing College of IS&T, University of Nebraska, Omaha, NE, USA

Nordin Zakaria High-Performance Cloud Computing Center, Universiti Teknologi PETRONAS, Seri Iskandar, Malaysia

Vicente Zarzoso I3S Laboratory, CNRS, Université Côte d'Azur, Sophia Antipolis Cedex, France

N. Zerhouni FEMTO-ST Institute, Univ. Bourgogne Franche-Comté, CNRS, ENSMM, Besançon Cedex, France

Neural Network Imitation Model of Realization of the Business Analysis Process



Katerina Kolesnikova , Olga Mezentseva , and Olena Savielieva

Abstract The article reflects the results of research related to the reorganization of the business analysis processes of an IT enterprise by building a neural network simulation model. For comparison, an analysis of the business process “as is” was carried out using standard software tools on the basis of expert assumptions, and notations were made in BPMN. Ways to optimize the process are proposed. Then, based on the same initial data, a simulation model is proposed for generating virtual indicators based on various kinds of business process load scenarios and initial independent conditions. Using neural network modeling based on simulation data, a “as it should be” model is proposed. A possible economic effect was obtained from each optimization project from the received 25 scenarios. The article offers a mathematical description of the model and method for modeling these interactions from the perspective of game theory. This allows you to build appropriate formal models.

Keywords Simulation · Business processes · Reinforced neural networks · Process reorganization

1 Introduction

Simulation of a business process is used to reduce uncertainty in decision making. It also optimally solves the complexity of the process, its variability and the resulting efficiency. Since when planning any business process in a company, management almost always encounters a lack of experience in the proposed actions and the lack of information about similar decisions in other companies, and it has no concrete reason to predict the results and consequences.

K. Kolesnikova · O. Mezentseva ()

Department of Management Technology, Taras Shevchenko National University, Bohdan Gavrilishin Str., 24, Kyiv 01601, Ukraine

O. Savielieva

South Ukrainian National Pedagogical University Named After K. D. Ushynsky,
Staroportofrankivska Str. 2/4, Odessa 65029, Ukraine

To address such issues, business analysis primarily raises the question of collecting baseline information and the current state of affairs. One of such methods is the notation and analysis of the processes “as is”. Based on the shortcomings and obvious losses of the constructed notation, an experienced analyst analyzes the “how it should be” analysis. In the future, this analysis is implemented in the company’s activities and over time turns into “as is”. For complex processes, this manual optimization becomes partial and only by repeating many implementations (iterations) has a real economic effect. The use of popular programs and services based on simulation modeling, in turn, does not solve the problem of multiple iterations of optimized processes, which is often more expensive for a business than the effect obtained from implementation.

We propose to solve such a problem by using simulation models of many and various variants of the “as is” processes as a virtual environment for training a neural network to obtain the final optimal “as it should be” solution among many possible options. Thus, we avoid the repeated and possibly costly implementation of optimized processes, since a simulation model predicts for us, and the best option is built using the implementation of a neural network [1].

Artificial intelligence technologies using simulation data have shown their high efficiency in the field of computer and board games. According to [2], games are a simpler and more limited simulation environment than a real business in market instability. Therefore, in this area today, there is a great potential. And the potential branch of research itself is in demand and necessary in the field of making cost-effective decisions.

2 Analysis of Recent Research and Publications

The issues of using simulation to effectively control production processes were considered in [3–5]. The work [3] provides a description of the forms and types of simulation modeling, selected for use by large industrial organizations and projects. Here, methods for optimizing production are proposed, but automation of calculations and optimization of such processes is not given.

In [5], the basic mathematical principles of effective simulation were proposed, sufficient for medium and large-scale enterprises, while far from all processes the task of constructing scenarios of possible options was posed. In [6, 7], models of reinforced neural networks and neural networks without a teacher are considered for predicting the design activities of IT companies, but without using a virtual simulation environment.

In [8, 9], the basic algorithms and principles for constructing neural networks with reinforcement and combining various methodologies were proposed. In [10], the problems of constructing effective simulation models are considered, which can significantly affect the implementation of a neural network; however, what methods can be used to take into account the entire spectrum of necessary data are not indicated. This approach can be used in the future for the development of scenario

building of scenarios of possible business processes; however, the efficiency assessment by the business owner on the results of such processes is practically not carried out.

3 Setting the Objective

Formulating objectives. The purpose of this research is the justification and development of a neural network simulation model of optimization for business analysis processes in an IT company. Evaluation of such interaction will be evaluated with simulation and construction of a neural network with reinforcement [2]. The results of the evaluation will be used to draw up an action program to improve the development process and plan the organization of the IT company with maximum efficiency. This will provide an opportunity to improve the quality of business processes management of such projects and companies and will also increase their commercial effectiveness over time.

To achieve these goals, the following tasks were identified:

- identify the stages of modeling, which form the basis for obtaining a wide range of possible options for building business processes, their sequence and duration;
- build a conceptual simulation model for creating a virtual environment for training a neural network with reinforcement;
- conduct a formal description of the elements and build a mathematical model of the neural network of the interaction process of key stakeholders and explore the resulting model;
- conduct modeling and research the results obtained, analyze them and determine the main conclusions.

A novelty in the solution to optimize business processes for IT companies is the use of a neural network trained on simulated data. This allows the neural network to determine the order and properties of processes with the most accurate understanding of the specifics of a company or project.

4 The Case Study

For the most visual analysis of the process, we considered a simulation model of the real process “Review and approval of support applications” of a large IT company. For comparative analysis, we use classic simulation tools (ELMA, Business Studio, ARIS).

Applications for withdrawal to processing are submitted subject to preliminary study of the possibility of withdrawing certain services and products for support, i.e., considering the following:

- working hours of departments;
- the current sequence of business processes;
- previously approved applications;
- combining the implementation of different types of work units.

As a result, we want to get a coordinated, approved application included in the shift task.

The analysis of the current model consists in determining the directions of optimization of the business process by calculating the average duration (one process instance) and the total monthly costs for the implementation of the business process “Consideration and approval of support requests”. BPMN diagram of the “as is” process (Fig. 1).

The process involves the following: the client—the initiator submitting the application; personnel in charge of working with clients; team-lead project; personnel with whom the development is located.

The time cost of the above resources has been determined. The functional cost scheme is also used, and the general optimization of processes is taken into account. The diagram shows excessive parallelism, dead-end processes, and excessive complexity.

The first operations of the process “Review and approval of applications for support” are not permanent. Less than 64% of all applications are implemented within 5 min. In 27% of cases, there is a need to collect data for the application. For the analysis, a discrete distribution was chosen in view of the fact that there is no business process accounting for this section. Conditional data are collected from the words of specialists of the client department.

In Fig. 1, the process diagram is fully reflected, and the probability of moving along the arrows after the gateways (places of choice) is also shown. So, the transition

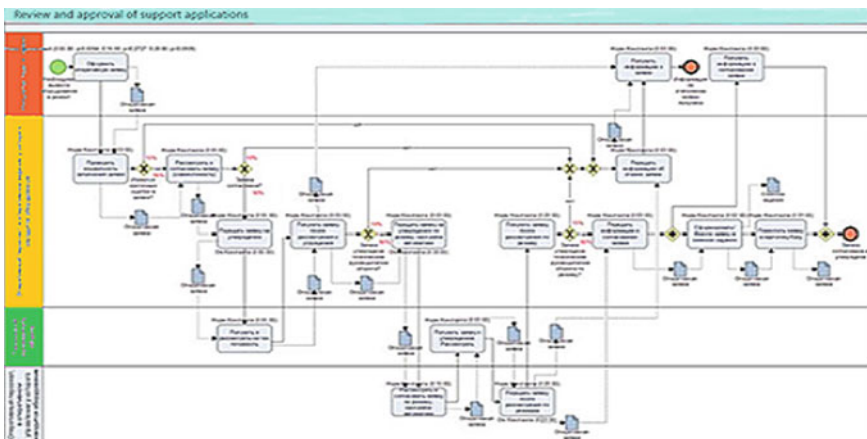


Fig. 1 “as is” model of the business process “Review and approval of applications for support”

along the arrow “yes” after the selection/gateway “Are there critical errors in the application?” will be carried out with a probability of 78%, etc.

The results of the simulation business process of this application through the program “Business Studio” were carried out for the period 2018–2019. Based on the simulation results, the following data were obtained.

The analysis of the report on the results of the simulation generated by the program shows that the most expensive operation within a single process instance is the operation “Submit a support request”. The simulation was carried out for the case of a full load of the process, subject to 10% of applications with critical errors (they need to be returned for replenishment). The last step is necessary to optimize the process [11].

Simulation of the “as is” process for the business process “Review and approval of support requests” for the case with 10% incorrect applications in the program gave the following results:

- increased average execution time for one process instance—30 h;
- too high total monthly cost of the process. Since there is a 100% load of the business process, when simulating, a queue arises for processing incoming applications. At high loads, the length of this queue reaches 10 h.

As a result of the analysis of the “as is” model, a complete list of improvements for the “as it should be” scenario was created as follows:

- reduce the time required to generate applications by 65% of cases;
- eliminate auxiliary operations “Send” and “Receive”;
- automate a number of operations, such as “Generate/Submit an Application”.

Based on these optimization suggestions, the following “as it should be” process flow diagram was formed using Business Studio tools (Fig. 2).

Based on the simulation results of an optimized process, the following data were obtained:

- The average execution time for one instance of the business process is now 1 h 37 min.
- The cost of the business process for the month decreased by 7%.

5 Research Method

Simulation provides a realistic and diverse virtual environment for training and testing students of different types of intelligent systems [12]. Simulation for training a neural network for optimizing business processes has several advantages as follows:

- The base created by simulation is wider and more diverse than the accumulated historical data, which limit the experience only to the scenarios that have happened.

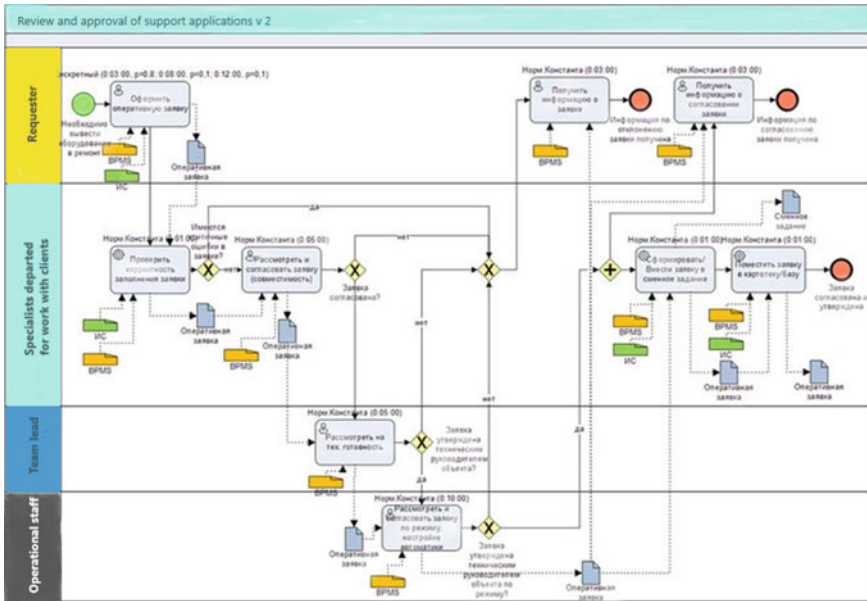


Fig. 2 Scheme of the optimized process “to be” of “Review and approval of applications for support”

- Unimported data often need to be obtained during experiments, and they are expensive and create unreasonable risks for the business process.
- The process of achieving the optimal chain of processes “as it should be” is often too long, a process for effective solutions compared to the development of a neural simulation model.

Since the model is faced with the task of building the best (from the so-called economic effect) chains of business processes almost independently, the analyst cannot mark the data that the simulation model creates as bad or good. Also, we do not set the task for the model to find the relationship between the data obtained. Therefore, modeling in terms of network learning should be used with the reinforcement learning (RL) method [13]. A feature of this method is that the result will be a certain chain of business processes, i.e., management strategy, which is carried out by choosing an action by the agent, and a chain of these actions based on the observation of the virtual environment. However, simulation modeling is used not only for such a method. Also, simulation modeling is used to obtain any number of synthetic, labeled data, providing any desired set of options and levels of detail for the development of events for training with a teacher [14].

In our case, we consider the business process as a continuously changing system, dependent on some independent variable (time). To formalize such systems, network dynamics models are used. Their mathematical basis is a system of differential equations. Describing the general structural diagram, we have a vector of functions $f(x, u)$

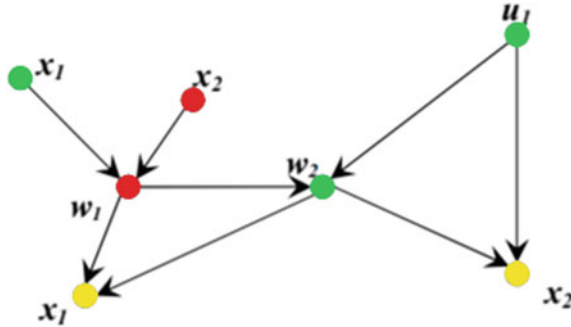


Fig. 3 Graph of functional dependencies of variables of a differential model [15]

and use a graph where the model variables correspond to the vertices and the model arcs show the functional relationships between the variables (Fig. 3).

The model considers executable business processes as a network of threads. Each component of this network corresponds to a single set of homogeneous ingredients (e.g., business processes of one group of performers), the dynamics of which are taken into account in the model.

$$X(t + r) = x(t) + r * V(t), \quad (1)$$

where

t is the model (system) time;

r —change (increment) of time—step of modeling (integration);

$x(t), x(t + r)$ —level value at time instants;

$V(t)$ is the speed of the level dynamics, i.e., its change per unit time.

To train the neural network, a simulation model [8] was used using the DL4J library for deep machine learning [16]. This library works in the Java programming language. To compare the calculations, we took the functional cost indicators of business processes in IT companies for past periods in order to simulate them for the future (Figs. 4 and 5).

After the preparation of simulation data, a neural network with reinforcement starts processing it. Briefly describe the principles of its work. The main purpose of the enhanced learning algorithm is to maximize rewards, taking into account future actions and their rewards [17].

$$J(\theta) = E \left[\sum_{t=0}^{T-1} r_{t+1} \right] \quad (2)$$

Function $J()$ waits for the next time step t to update the value estimates. At time $t + 1$, they immediately form the TD target, using the observed reward r_{t+1} and

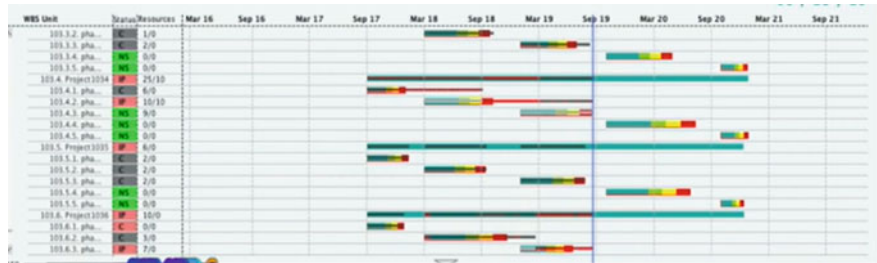


Fig. 4 Simulation indicators “Review and approval of applications for support”

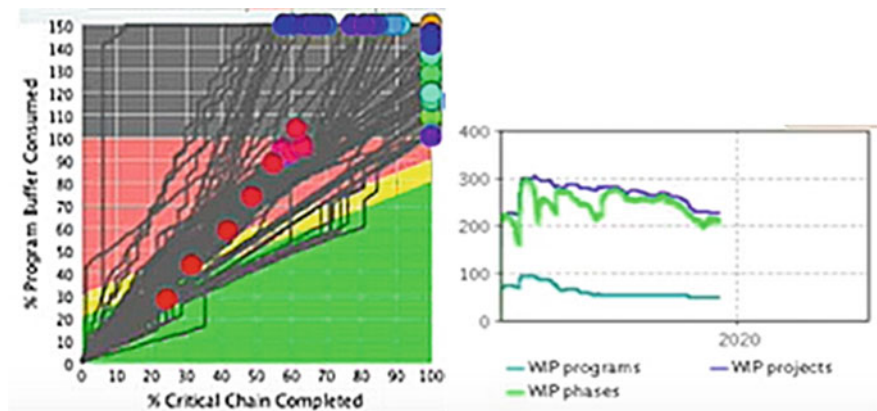


Fig. 5 Results of the simulation of the business process “Review and approval of applications for support” in the DL4J package

the current estimate of $J(r_t + 1)$. The final expression for the gradient is

$$\nabla_{\theta} J(\theta) = \sum_{t=0}^{T-1} \nabla_{\theta} \log \pi_{\theta}(a_t | s_t) G_t \nabla_{\theta} J(\theta) = \sum_{t=0}^{T-1} \nabla_{\theta} \log \pi_{\theta}(a_t | s_t) G_t \quad (3)$$

$$\sum_{t'}^T = t + 1 \gamma^{t'-t-1} r_{t'} \quad (4)$$

where

$J()$ is a function that tells us the maximum expected future reward that the agent will receive in each state:

γ is a discount factor:

γ is a discount factor,
 $\pi(s)$ is a behavior function:

$\pi(a | s)$ —return of probability of distribution by actions:

A is the set of all possible moves that an agent can make.

So now we can bring both actor (softmax) and critique (logit) closer together using a single neural network. But further study suggested a slight improvement in expression, and instead of using G , the advantage function is defined as follows:

$$A(s_t, a_t) = Q_w(s_t, a_t) - V_v(s_t) \quad (5)$$

The reward function A for performing an action has the following conditions [18]:

- (1) $A = 1000$ if the action moves the chain to the target (short) function;
- (2) $A = 1$ if the result of the completed action proceeds to the next action;
- (3) $A_n = -1$ in all other cases. A_1 is a low reward for actions that potentially increase the likelihood of reaching a target position. Suppose that A_i is small enough that repeated movement of the business process between executors (the sum of awards A_i) could not exceed the reward from reaching the target position (A_p) and lead to a false interpretation of the function [5].

The Valohai platform was used as an infrastructure for conducting training experiments and model evaluation [11]. When setting up a neural network, 0.0001–0.1 for learning speed and integer values of 16–256 for layer size will be considered (Fig. 6).

The main task of managing the process of “Consideration and approval of support applications” was broken down into complex sub-tasks (moving processes to a specific executor). After that, a neural network training was performed for each sub-task [5]. DDQN was chosen as the trained algorithm, as it allows to obtain more accurate results in the final set of actions. In this task, there are only 28 possible actions for any business process chain configuration. The accuracy of training is 88.8%, and the accuracy of testing is only 74.3%.

As a result of the application of the neural network to the virtual simulation data, more than 25 possible “as it should be” scenarios were obtained, which were also carried out over a period of time—during the year. Table 1 shows the four most significant neural network variants proposed, taking into account their economic effect within a year after reproducible changes.

```

val configuration = new OptimizationConfiguration.Builder()
    .candidateGenerator(candidateGenerator)
    .dataProvider(dataProvider)
    .modelSaver(modelSaver)
    .scoreFunction(scoreFunction)
    .terminationConditions(terminationConditions)
    .build()

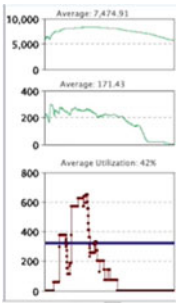
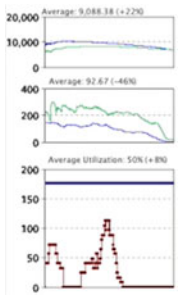
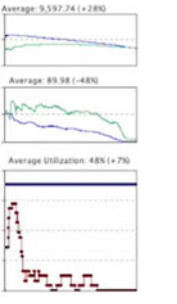
val runner = new LocalOptimizationRunner(configuration, new MultiLayerNetworkTaskCreator())

//Start the hyperparameter optimization
runner.execute()

```

Fig. 6 Creating an optimization configuration

Table 1 Most significant variants proposed

	Scenario 1	Scenario 2 (results 365 days after)	Scenario 3 (results 365 days after)	Scenario 4 (results 365 days after)
% program finished on time	2%	9% (+7%)	6% (+4%)	8% (+6%)
% processes within planned time	19%	78% (+59%)	3% (-16%)	3% (-16%)
% phases on time	33%	100% (+67%)	19% (-13%)	5% (-28%)
Costs,	384.76	321.47 (-63.28)	31.78 (-352.98)	16.22 (-368.54)
Net profit, %	-44%	23% (+67%)	-1393% (-1349%)	-1242% (-1198%)
Dynamics of indicators and accuracy of the obtained data	 <p>Average: 7,474.91 Average: 171.43 Average Utilization: 42%</p>  <p>Average: 9,088.38 (+220) Average: 92.67 (-460) Average Utilization: 50% (+80)</p>  <p>Average: 9,597.74 (+280) Average: 89.98 (-480) Average Utilization: 48% (+70)</p>  <p>Average: 9,989.74 (+340) Average: 100.83 (-410) Average Utilization: 54% (+130)</p>			

At the beginning of the neural network training with reinforcement, the agent offers randomly selected actions, many of which are not feasible (e.g., moving the process to a position occupied by another process), but as a result of repeated repetitive learning cycles under the influence of the reward function (5) forms an effective chain of action for achievement of the goal. As a result, the ensemble of trained neural network agents successfully moves business processes among themselves, increasing efficiency in time and cost [19].

6 Conclusions

The using of neural network simulation models has shown a significant increase in the overall variability of the business process horizon compared to manual planning. We have obtained a wide range (more than 25) of possible sequences of processes and operations, their duration and parallelization at a sufficiently low, however, accuracy. Each individual model is not always successful and optimal, which depends on the simulation indicators and corresponds to the real situation in the business.

As a result of the model implementation, five optimal scenarios and sets of simulation data were obtained. The best case scenario (Table 1, Scenario 2) resulted in an increase in net profit and a decrease in overall costs. In comparison with manual optimization, economic indicators have been obtained to compare them between different scenarios [20].

In further studies [21], it should be borne in mind that neural network simulation is complicated by the fact that in larger tasks of business analysis, both the state space and the action space may be too large, which consequently slows down the convergence of the learning process of the neural network, since it requires a larger size of the processes of the algorithm continuing education.

References

1. Molnar C, Interpretable machine learning. In: A guide for making black box models explainable. Available at: <https://christophm.github.io/interpretable-ml-book/>. Last accessed 1 April 2020
2. Gogunskii V, Kolesnikov O, Kolesnikova K, Lukianov D (2016) “Lifelong learning” is a new paradigm of personnel training in enterprises. Eastern-Eur J Enterp Technol 4(2(82)):4–10. <https://doi.org/10.15587/1729-4061.2016.74905>
3. Aguado JV, Borzacchiello D, Chinesta F, Upadhyay R, Binetruy CA (2017) Simulation App based on reduced order modeling for manufacturing optimization of composite outlet guide vanes. Adv Model Simul Eng Sci 4(1):110–112
4. Li T, Guilbaud D, Potapov S, Marigo JJ (2016) Numerical investigation of dynamic brittle fracture via gradient damage models. Adv Model Simul Eng Sci 3(1):215–221
5. Morozov V, Kalnichenko O, Mezentseva O (2020) The method of interaction modeling on basis of deep learning the neural networks in complex IT-projects. Int J Comput 19(1):88–96
6. Neural Networks and Deep Learning. Homepage, <https://neuralnetworksanddeeplearning.com/>. Last accessed 1 April 2020

7. Sutton A, Barto G (2018) Reinforcement learning: an introduction. Adaptive computation and machine learning, 2nd edn. A Bradford Book, UK, 552 p. <https://balka-book.com/search/filter=1;235331/>
8. Simonini T, An introduction to reinforcement learning. <https://www.freecodecamp.org/news/an-introduction-to-reinforcement-learning-4339519de419/>
9. Géron A (2019) Hands-on machine learning with Scikit-Learn, Keras, and TensorFlow. Concepts, tools, and techniques to build intelligent systems. O'Reilly Media Inc., UK
10. Lantsev E, Dorrer M (2013) Obtaining an agent simulation model from a discrete-event description of a business process. Scientific and Technical Statements of SPbSPU 3(174)
11. Liu D, Li H, Wang D (2017) Feature selection and feature learning for high-dimensional batch reinforcement learning: a survey. Int J Autom Comput 12:229–242
12. Durst PJ, Anderson DT, Bethel CL (2017) A historical review of the development of verification and validation theories for simulation models. Int J Model Simul Sci Comput 8(2)
13. Wu J (2017) The key technology research for integrated simulation of multi-disciplinary complex product system. Int J Model Simul Sci Comput 8(2)
14. Hastie T, Tibshirani R, Friedman J (2014) The elements of statistical learning. Springer, 739 p
15. Lukianov D, Bespanskaya-Paulenka K, Gogunskii V, Kolesnikov O, Moskaliuk A, Dmitrenko K (2017) Development of the markov model of a project as a system of role communications in a team. Eastern-Eur J Enterp Technol 3(87):21–28. <https://doi.org/10.15587/1729-4061.2017.103231>
16. Free Simulation Software for Education. AnyLogic Personal Learning Edition. Homepage, <https://www.anylogic.ru/s/download-free-simulation-software-for-education/>, last accessed 1 April 2020
17. Parast K, Dowdy D, Kelton D (2013) Agent-based simulation of a tuberculosis epidemic. In: Proceedings of the 2013 winter simulation conference (2013)
18. Goodfellow I, Bengio Y, Courville A (2017) Deep learning. Adaptive computation and machine learning, 652 p
19. Michie D, Spiegelhalter DJ, Taylor CC (1994) Machine learning, neural and statistical classification, 298 p. Available at: <https://www1.maths.leeds.ac.uk/~charles/statlog/whole.pdf>. Last accessed 1 April 2020
20. Trask A (2019) Grokking deep learning. Print Inc., USA, 310 p
21. Litvin Y (2017) Development of a simulation and analytical complex modeling the operation of gas and gas condensate fields. In: IMMOD-2017, St. Petersburg

Thermal Modeling of the GaN HEMT Device Using Decision Tree Machine Learning Technique



Niketa Sharma, Yogendra Gupta, Ashish Sharma, and Harish Sharma

Abstract In this paper, we have proposed electrothermal modeling of GaN-based HEMT devices. A data-driven approach has been implemented for a temperature range varying from 300 to 600 K, based on one of the core methods of machine learning techniques based on decision tree (DT). The performance of the proposed models was validated through the simulated test examples. The attained outcomes depicted that the developed models predict the HEMT device characteristics accurately depending on the determined mean-squared error (MSE) between the actual and anticipated characteristics. The paper also indicates that the decision tree technique could be specifically beneficial when data are nonlinear and multidimensional, with the different process parameters exhibited profoundly complex interactions.

Keywords AlGaN/GaN HEMT · Decision tree · Device modeling · Machine learning

1 Introduction

The gallium nitride-based HEMTs are considered as one of the most promising devices to realize the “high-power,” “high-frequency,” and “high-temperature” applications due to their inherent material properties such as wide band gap, high saturation velocity, and high thermal stability [1–4]. Technology enhancement in material science and devices in the last decade has led to the advancement in the performance of GaN-based HEMTs. Larger breakdown, electric field, and good thermal conductivity make it an interesting device for the high-temperature applications [5]. In comparison with other III–V semiconductor materials, GaN material devices can

N. Sharma (✉) · Y. Gupta

Swami Keshvanand Institute of Technology Management & Gramothan, Jaipur 302021, India
e-mail: drniketa@skit.ac.in

A. Sharma

Indian Institute of Information Technology, Kota 302021, India

H. Sharma

Rajasthan Technical University, Kota 324010, India

operate at a much higher temperature (750°C), without degradation in performance. The ability of GaN-based devices to operate at high temperature makes it useful for extreme environmental conditions [6]. An assortment of chemical, gas, and biosensor gave HEMT technology which has been operated at lifted temperatures [7–9]. The durability and high-temperature operation are significant prerequisites for gas sensors. The Si-based gas sensor has a point of confinement to be operated underneath 250°C , prohibiting them from being utilized as “hydrocarbon detectors.” Therefore, semiconductor devices based on AlGaN/GaN heterostructure have great potential for sensor applications in harsh environments.

It is always needed to accurately predict the device electrical characteristics by simulation before fabrication. It reduces the development cost and time required for long and tedious growth and processing steps. That helped in the interpretation of the fundamental device physics. Many series of simulations have been executed on various methods of GaN-based HEMTs such as “transport and mobility properties,” [10, 11] “self-heating effects,” [12, 13] and “carrier lifetime”. The combined investigations on simulation study of these devices for high temperatures are greatly required.

The circuit simulations always play a key role while testing circuits and to predict device performance. The fabrication cost of integrated circuits is very high. That is why modeling and simulation of characteristics of semiconductor devices become vital prior to fabrication [14]. Several models were reported for GaN HEMT devices [15–18]. These models are empirical and followed the induction process for development. In which, the user needs to give an initial estimate of the empirical parameters and apply some presumption that might be erroneous [19]. Additionally, these models were ordinarily generated for low-temperature values, e.g., RF applications [20, 21].

The best method to model the extracted device data is machine learning (ML). Through this method, the user can identify the parameters that can be with the desired data with the least interference. Machine learning technique finds more efficiently and accurately as compared to traditional modeling techniques and additionally can direct to a model that is not just useful for interpolation but also for extrapolation [22]. The work related to short-range temperature modeling using an ML technique was reported in [23]. Nonetheless, reported work focused on neural network modeling for a shorter temperature range ($25\text{--}80^{\circ}\text{C}$). This range is extremely constrained for GaN devices which could be operated at considerably higher temperatures [24]. The GaN HEMT device modeling techniques using a machine learning algorithm are hardly observed in the reported research with respect to high temperatures. There are very few reports available in the literature on the modeling for GaN HEMT devices based on AI in relation to high temperatures. Kumar et al. used machine learning approaches for soil prediction [25] and disease identification [26].

Machine learning has become one of the most promising modeling techniques nowadays, for device modeling [27]. In [27], an intelligent algorithm for device modeling based on a decision tree is used to predicting the lithographic process parameters semiconductor manufacturing. The exceptional model performance obtained shows the remarkable ability of this modeling technique. Shekhawat

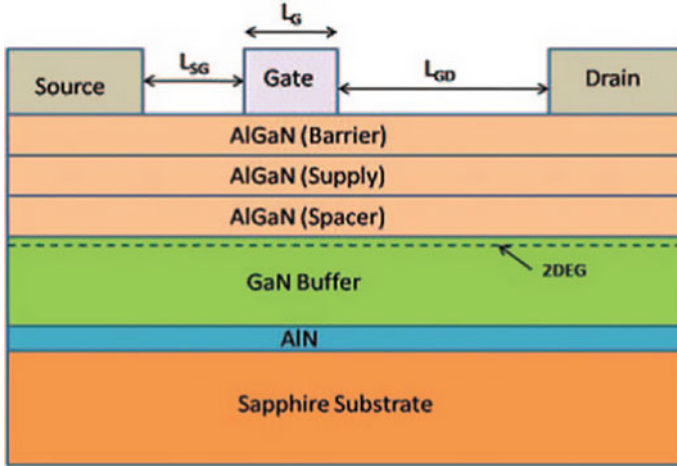


Fig. 1 Layered representation of simulated device

et al. [28] proposed data transformation approach to improve machine learning approaches.

This paper reports on the nonlinear data modeling for the output characteristics of the GaN-based HEMT device over large temperature ranges using the machine learning regression technique specifically: the decision tree (DT).

2 Experimental Setup

A single gate finger device of 100 μm unit gate width was used for simulation as shown in Fig. 1. The epitaxial structure comprised of a 25 nm $\text{Al}_{0.25}\text{Ga}_{0.75}\text{N}$ layer, 2.7 μm GaN buffer, and an AlN layer with sapphire as a substrate. The gate length (L_G), source-to-gate length (L_{SG}), and gate-to-drain length (L_{GD}) of the device are 1 μm , 1 μm , and 2 μm , respectively.

The data extracted from the device simulations [29] using TCAD tool were utilized to train the machine learning algorithm for development of the GaN HEMT device model.

3 Device Modeling Using Machine Learning

The machine learning algorithm used to model the device characteristics is the decision tree algorithm. It is an extensively used algorithm for “inductive inference” by which it approximates the target function [30]. Here, every single node signifies a

test on a variable. All branches denote test outcome, and the cost of the class variables is located at the leaves of the tree [31]. This algorithm uses training examples to build a classification model, which express the connection between “classes” and “attributes.” Once it has learned, the regression model can order new, obscure cases. The benefit of the decision tree models is that they are vigorous to noisy data and effective in learning disjunctive expressions [32].

In this paper, an exceptionally efficient and extensively utilized classification-based algorithm named C4.5 [33–35] is employed. The C4.5 uses top-down, greedy approaches for the construction of a decision tree. This approach starts with inspecting in which characteristic (input variable) ought to be tried at the root of the tree. All the instance feature is assessed via a statistical assay to decide performance level for classification of the training examples. The best attribute is chosen and employed as a test at the root node of the tree. Afterward, a relative of the root hub is formerly made for every viable estimate of this characteristic (discrete or continuous), and the training models are arranged to the fitting relative nodes. The whole cycle is then continued utilizing the training models related to every relative node to choose the best ascribed to test by then in the tree. The developed DT could be employed to group the specific data element. It could be done with beginning the root and progressing across the leaf node demonstrating a class come across. All the nodes indicate a test that is executed on a specific parameter. These tests could be executed with the chosen data element besides branches for every viable outcome of the test. A decision was taken while reaching a terminal node.

By every non-leafy decision node, the characteristic is determined by the node being examined. This progress prompts the root of the subtree relating to the test’s result. After putting the attributes by superior information gain nearest to the root, the algorithm prefers choosing shorter trees over longer ones.

The algorithm can likewise retrace to re-examine prior decisions by utilizing a pruning strategy called rule post-pruning [34, 35]. The “rule post-pruning” technique is used to conquer the overfitting issue, which regularly emerges in learning errands.

4 Results

A dataset is used to train the machine learning models with the different gate-to-source voltage (V_{gs}) and temperature oscillating from 300 to 600 K. The temperature values higher than 300 K are used to test the model’s capability to extrapolate outside the input range.

The “hyperparameters optimization” of the decision tree function gives three different optimized parameters: the `MinParentSize` = 1, the `MaxNumSplits` = 2000, and the `NumVariablesToSample` = 3. The output curves related to the GaN HEMT device in a temperature range varying from 300 and 600 K are presented in Fig. 2. The applied voltage between gate and the source is 2 V. The data extracted from the decision tree model are compared with simulated outcomes, and a mean-squared error between these two was calculated as 5.32×10^{-8} . The temperature dependence of

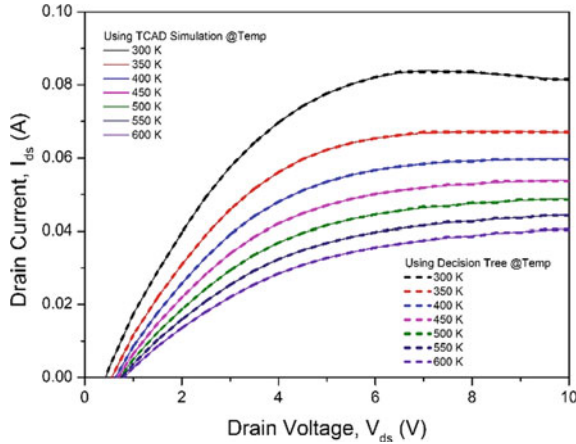


Fig. 2 Comparison of drain current at different temperatures (300–600 K) at $V_{\text{gs}} = +2$ V

the maximum current and transconductance of different devices was further studied. The transconductance (g_m) versus gate–source voltage (V_{ds}) for drain bias $V_{\text{ds}} = +10$ V of the simulated AlGaN/GaN HEMT is shown in Fig. 3.

We observed a reduction in I_{ds} ($\approx 52\%$) with an increase in temperature from 300 to 600 K. The gate bias was ramped from -6 to 2 V for each of the drain biases. The peak current density was reached of $V_{\text{gs}} = +2$ V, $V_{\text{ds}} = +10$ V @ 300 K with a current density of 0.84 A/mm.

The high current density could be attributed to the extremely high charge that was accumulated in the channel because of the polarization effects and high saturation peak velocity of electrons in GaN.

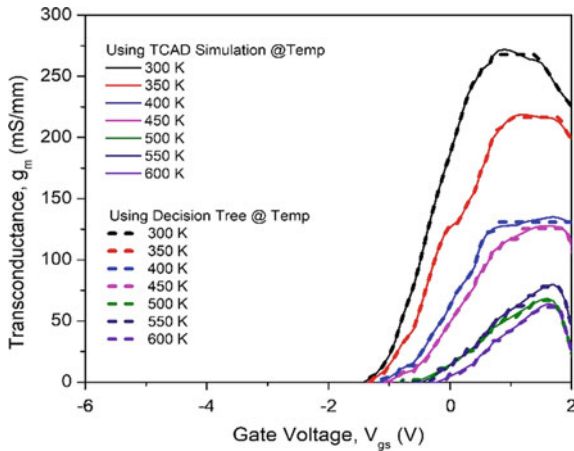


Fig. 3 Comparison of transconductance at different Temp (300–600 K) at $V_{\text{ds}} = +5$ V

The output drain current becomes degrading with the temperature hike from 300 to 600 K, to comprehend the explanation for, we have tested for different parameters, for example, electron concentration and mobility.

Figure 4 describes the behavior of electric concentration versus depth (μm) at different temperatures. Peak electron concentration along the channel was about $1.3 \times 10^{19}/\text{cm}^3$ @ 300 K corresponded to the highest $I_{ds} = 0.84 \text{ A/mm}$ when the device was turned on.

Such an effect could be explained, looking at the differences between the electron mobility values at different temperatures as displayed in Fig. 5. The electron mobility

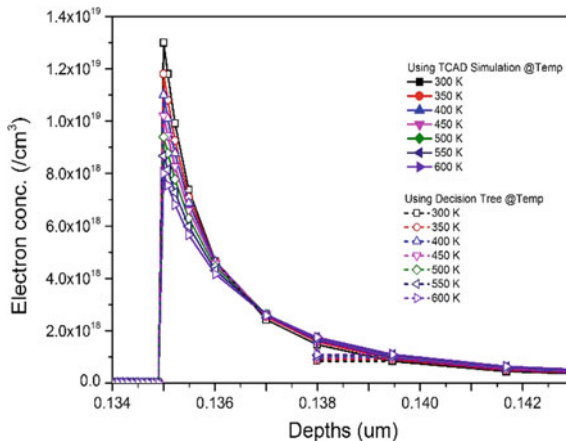


Fig. 4 Comparison of electron concentration at different temperatures

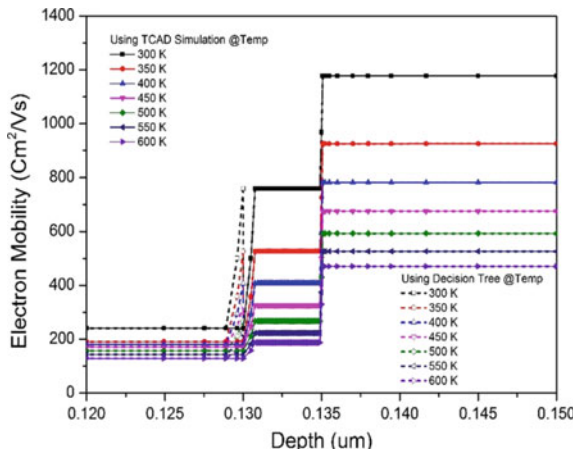


Fig. 5 Comparison of electron mobility at different temperatures

in the channel was $1181 \text{ cm}^2/\text{Vs}$ @ 300 K. When the temperature was increased, electron mobility degrades along channel due to phonon and impurity scattering.

The predicted I_{ds} values at 300–600 K are close to the actual simulations. These approximations show the mean-squared error of 2.17×10^{-6} . The predicted characteristics utilizing the decision tree algorithm almost overlap alongside the simulation's ones.

5 Conclusion

We have done the measurements of I-V characteristics for GaN-based HEMT devices for temperature range from 300 to 600 K. The proposed data modeling method for the I-V characteristics is the decision tree machine learning algorithm. The inputs to this model are V_{gs} , V_{ds} , and temperature. The predicted I_{ds} values at 300–600 K are close to the actual simulations. These approximations show the mean-squared error of 2.17×10^{-6} . The predicted characteristics utilizing the decision tree algorithm almost overlap alongside the simulation's ones. In our next future work, we have planned to increase the temperature range by training the model over higher temperature range, beyond 600 K to improve the model performance.

Acknowledgements Authors acknowledge the fund provided by TEQIP III-RTU (ATU) CRS project scheme under the sanction no. “TEQUIP-III/RTU (ATU)/CRS/2019-20/19”.

References

1. Ambecher O, Foutz B, Smart J, Shealy JR, Weimann NG, Chu K, Murph M, Sierakowski AJ, Schaff WJ, Eastman LF, Dimitrov R, Mitchell A, Stutzmann M (2000) Two dimensional electron gases induced by spontaneous and piezoelectric polarization in undoped and doped AlGaN/GaN heterostructures. *J Appl Phys* 87:334–344
2. Osvald J (2007) Polarization effects and energy band diagram in AlGaN/GaN heterostructure. *Appl Phys A Mater Sci Process* 87:679
3. Gelmont B, Kim KS, Shur M (1993) Monte Carlo simulation of electron transport in gallium nitride. *J Appl Phys* 74:1818–1821
4. Pearton SJ, Zolper JC, Shul RJ, Ren F (1999) GaN: processing, defects, and devices. *J Appl Phys* 86:1–78
5. Levinshtein M, Rumyantsev S, Shur M (2001) Properties of advanced semiconductor materials. Wiley, New York
6. Vitanov S, Palankovski V, Maroldt S, Quay R (2010) High-temperature modeling of AlGaN/GaN HEMTs. *Solid-State Electron* 54:1105–1112
7. Luther BP, Wolter SD, Mohney SE (1999) High temperature Pt Schottky diode gas sensors on n-type GaN. *Sens Actuators B* 56:164–168
8. Rýger I, Vanko G, Kunzo P, Lalinský T, Vallo M, Plecenik A, Satrapinský L, Plecenik T (2012) AlGaN/GaN HEMT based hydrogen sensors with gate absorption layers formed by high temperature oxidation. *Procedia Eng* 47:518–521

9. Lalinsky T, Ryger I, Vanko G, Tomaska M, Kostic I, Hascik S, Valloa M (2010) AlGaN/GaN based SAW-HEMT structures for chemical gas sensors. *Procedia Eng* 5:152–155
10. Albrecht JD, Wang RP, Ruden PP (1998) Electron transport characteristics of GaN for high temperature device modelling. *J Appl Phys* 83:4777–4781
11. Corderier Y, Hugues M, Lorenzini P, Semond F, Natali F, Massies J (2005) Electron mobility and transfer characteristics in AlGaN/GaN HEMTs. *Physica Status Solidi (C)* 2:2720–2723
12. Turin VO, Balandin AA (2006) Electrothermal simulation of the self-heating effects in GaN-based field-effect transistors. *J Appl Phys* 100:054501–054508
13. Islam SK, Huq HF (2007) Improved temperature model of AlGaN/GaN HEMT and device characteristics at variant temperature. *Int J Electron* 94:1099–1108
14. Galup-Montoro C (2007) MOSFET modeling for circuit analysis and design. World Scientific
15. Deng W, Huang J, Ma X, Liou JJ (2015) An explicit surface potential calculation and compact current model for AlGaN/GaN HEMTs. *IEEE Electron Device Lett* 36(2):108–110
16. Oishi T, Otsuka H, Yamanaka K, Inoue A, Hirano Y, Angelov I (2010) Semi-physical nonlinear model for HEMTs with simple equations. In: Integrated nonlinear microwave and millimeter-wave circuits (INMMIC). IEEE, pp 20–23
17. Sang L, Schutt-Aine J (2012) An improved nonlinear current model for GaN HEMT high power amplifier with large gate periphery. *J Electromagn Waves Appl* 26(2–3):284–293
18. Linsheng L (2011) An improved nonlinear model of HEMTs with independent transconductance tail-off fitting. *J Semicond* 32(2):024004–024006
19. Gunn SR (1998) Support vector machines for classification and regression. *ISIS Tech Rep* 14:85–86
20. Huque M, Eliza S, Rahman T, Huq H, Islam S (2009) Temperature dependent analytical model for current–voltage characteristics of AlGaN/GaN power HEMT. *Solid-State Electron* 53(3):341–348
21. Chang Y, Tong K, Surya C (2005) Numerical simulation of current–voltage characteristics of AlGaN/GaN HEMTs at high temperatures. *Semicond Sci Technol* 20(2):188–192
22. Breiman L (2001) Statistical modeling: the two cultures. *Statist Sci* 16(3):199–231
23. Marinković Z et al (2015) Neural approach for temperature-dependent modeling of GaN HEMTs. *Int J Numer Model Electron Networks Devices Fields* 28(4):359–370
24. Neudeck PG, Okojie RS, Chen L-Y (2002) High temperature electronics-a role for wide bandgap semiconductors. *Proc IEEE* 90(6):1065–1076
25. Kumar S, Sharma B, Sharma VK, Poonia RC (2018) Automated soil prediction using bag-of-features and chaotic spider monkey optimization algorithm. *Evol Intell*, 1–12. <https://doi.org/10.1007/s12065-018-0186-9>
26. Kumar S, Sharma B, Sharma VK, Sharma H, Bansal JC (2018) Plant leaf disease identification using exponential spider monkey optimization. *Sustain Comput Inf Syst* 28. <https://doi.org/10.1016/j.suscom.2018.10.004>
27. Braha D, Shmilovici A (2003) On the use of decision tree induction for discovery of interactions in a photolithographic process. *IEEE Trans Semicond Manuf* 16(4):644–652
28. Shekhawat SS, Sharma H, Kumar S, Nayyar A, Qureshi B, bSSA: Binary Salp Swarm Algorithm with hybrid data transformation for feature selection. *IEEE Access*. <https://doi.org/10.1109/ACCESS.2021.3049547>
29. Sharma N, Periasamy C, Chaturvedi N (2016) Investigation of high temperature effects on the performance of AlGaN/GaN High electron mobility transistors. *J Nanoelectron Optoelectron* 11(6):694–701
30. Quinlan JR (1986) Induction of decision trees. *Mach Learn* 1(1):81–106
31. Witten IH, Frank E, Hall MA, Pal CJ (2016) Data mining: practical machine learning tools and techniques. Morgan Kaufmann
32. Mitchell TM (1997) Machine learning. McGraw Hill, Burr Ridge, IL, pp 45, 37
33. Braha D (ed) (2001) Data mining for design and manufacturing: methods and applications. Kluwer Academic, Boston, MA
34. Mitchell TM (1997) Machine learning. McGraw-Hill, New York
35. Quinlan JR (1986) Induction of decision trees. *Mach Learn* 1:81–106

Low-Cost FPGA-Based On-board Computer



Dirk van Wyk  and Vipin Balyan 

Abstract This paper discusses the feasibility for the use of commercially available reconfigurable field-programmable gate arrays as the main system processor for small satellite systems and subsystems. FPGAs are in high demand as the space industry and applications are rapidly increasing and evolving. The use of FPGAs within the design of spacecraft systems reduces the design cost, as well as the turnaround time. It is anticipated that the single-board computer can be used as a configurable on-board computer with high flexibility allowing in-orbit reconfiguration (Thai in Applications for FPGAs on nanosatellites, 2014 [1]). Modern FPGAs are designed with embedded processing systems integrated inside the core allowing monotonous performance task to execute more easily with flexibility. One single printed circuit board with the computing power will handle all the challenging requirements for performance and functionality of the payload data handling.

Keywords On-board computer · FPGA · Small satellite · LEO

1 Introduction

The small satellite industry has grown rapidly over the past few years with designs for a variety of applications and missions. The satellite system structure can be considered as the core structure and a varying one. The payload of the satellite will be the variable component specific to the mission at hand. The development of small satellites can be of great advantage for low earth orbit (LEO) space applications at a lower cost and less development time. The typical small satellite structure consists of several subsystems, namely the OBC as the main component of the satellite for control and data handling (CDH) [2]. Additional structures include the communication system used amid the ground station and with the OBC, making it probable to retrieve remote control as well as sending commands to the satellite. The satellite will have a power control unit (PCU) for all the power demands and the application-specific payload firmware with the actual hardware.

D. van Wyk · V. Balyan ()
Cape Peninsula University of Technology, Cape Town, South Africa

Most on-board computers that have been used in the space environment are based on the microcontroller architecture, although these MCUs provide robust and predictable performance outcomes in the harsh space environment. Factors that will affect electronics in space include single event radiation effects and charged particles, which need to be considered when choosing the main components of the SBC [3].

The overwhelming demand for performance and functionality of new on-board computers creates more complex challenges. The FPGA technology allows for comprehensive functionality of the OBC on a single PCB, with highly integrated and configurable system-on-chip approach. The whole concept is to have a fully reconfigurable system within the OBC in orbit due to the high flexibility of the FPGA technology. The digital FPGAs are used as the main processor for the OBC to compute rigorous tasks and commands that can be done in parallel [4].

The COTS FPGA platform designed in this paper is used as a reconfigurable computing processor in small satellite systems for low-cost development and high-speed computing. This paper mainly introduces the OBC board development using the Xilinx Spartan-3E device and the architecture for this platform and simulations are done for the processes to read and write into memory, as well as the communication interface through UART. The use of commercially off-the-shelf (COTS) components is to build small satellites, CubeSats, at lower costs with endless mission possibilities. The standard CubeSat is $100\text{ mm} \times 100\text{ mm} \times 100\text{ mm}$ in structure known as a 1U satellite. These satellites can be stacked for greater flexibility of applications with structures as 2U or 3U. Nanosatellites or picosatellites are extremely small in physical size and consist of lightweight structures [5].

The internal electronic hardware is based on the PC/104 form specifications. The OBC's printed circuit board will have a PC/104 format with all the peripheral support and functionality. The OBC includes the memory subsystem while being the centre of all communication through the serial bus interface.

The remaining of the work in this article is arranged as follows, where Sect. 2 gives an overview and refers to related work done. The OBC interface layout is given in Sect. 3. The memory access and UART communication interface are explained in Sect. 3. In Sect. 4, the simulation results are demonstrated and explained. Finally, the article is concluded in Sect. 5.

2 Related Work

The FPGA-based on-board computer for a small satellite acts as the primary source for all the monitoring of various subsystems and commands to payload systems. The architecture embraces a system-wide I2C and UART bus from which numerous sensors and payloads are interfaced. A universal asynchronous receiver/transmitter, UART, interface is used between the on-board processor and payload systems which will transfer all the required data for housekeeping, payload data and further required information [6]. Figure 1 illustrates the board's layout and interfacing.

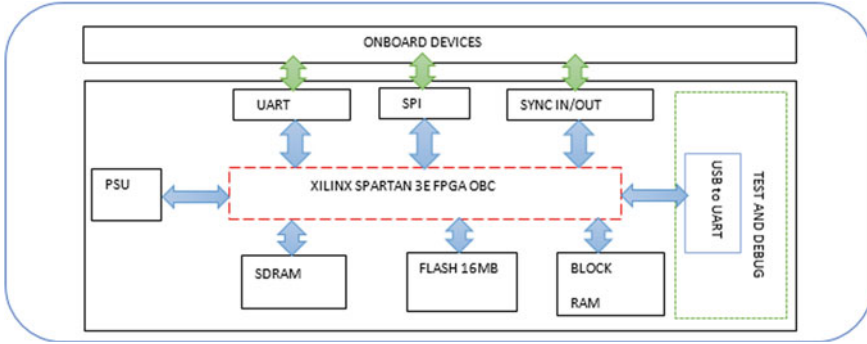


Fig. 1 Proposed OBC interface layout

Previous implementation has been done where the satellite functions on different modes of operation and can be modelled as a finite state machine, where the modes are the states of the FSM and the state transitions are the changes in the operation modes that depend on certain health conditions and parameters as measured by the various on-board sensors.

Satellites have many applications in the new space age, with earth observation (EO) being one of the most popular missions and primary applications. EO satellites use smart image sensors to monitor and capture data from the earth's surface, with infrared for in-depth data collection. This data may then be utilized to monitor urban development, vegetation growth, natural disaster, etc. The use of satellite imaging technology is constantly evolving and improving, the capture information provides more informations due to the improvement in resolution of the images captured. It is all achieved through the use of a wide range of spectral band cameras [7]. Earth observation has been performed since the mid 1900s by the US meteorological satellite. The purpose of earth observation is to measure the earth's characteristic to better understand weather patterns, natural disasters, water behaviour and pollutions [8].

3 Proposed Work

Detailing the hardware components is used to design the FPGA-based OBC platform. The design and development are aimed at providing support for most of the standard devices used on board a small satellite such as various payload systems and mission-specific applications. This board is designed to be used as a development board as there are no specified requirements for the board during the research and project period; therefore, it is customizable and can be integrated into commercial small satellite components to control and read/send data. The board is designed on the PC/104 form factor for small satellites. The proposed testing and verification of the

platform are done by testing the memory and communication interfaces through HIL simulations.

For the hardware development, a commercial FPGA is used as the processing system (PS), namely the Xilinx Spartan-3E with an on-board flash memory component from Atmel with a rich set of peripheral connectivity interfaces. It was found that in comparison with general-purpose processors (GPPs), the FPGAs are definitely more versatile and configurable when compared to application-specific integrated circuits (ASICs) [6]. The software development and simulations are done using the VHDL programming language for the test bench of the external flash memory and the communication interface. The type of storage is dependent on the application at hand. It is during storage that errors are most likely to arise. Errors usually occur when radiated particles penetrate the memory cells contained within the RAM. These types of errors are defined as bit flips in the memory [9].

4 Results and Simulations

Focus is on the hardware being utilized for the main processor of the OBC as well as the design structure. The simulations and verification of the memory system and communication of the FPGA are discussed with simulated results.

First In First Out (FIFO) helps in data transfer and cross clock domains. FIFOs are used within FPGAs mostly throughout and ASIC designs as basic building blocks [10]. FIFOs have various purposes which include crossing clock domains, storing data and buffering data prior to sending it to the RAM modules. The on-board memory is from Atmel, model AT45DB161E, Fig. 2. This module allows for simple in-system programmability and re-programmability which does not necessitate high

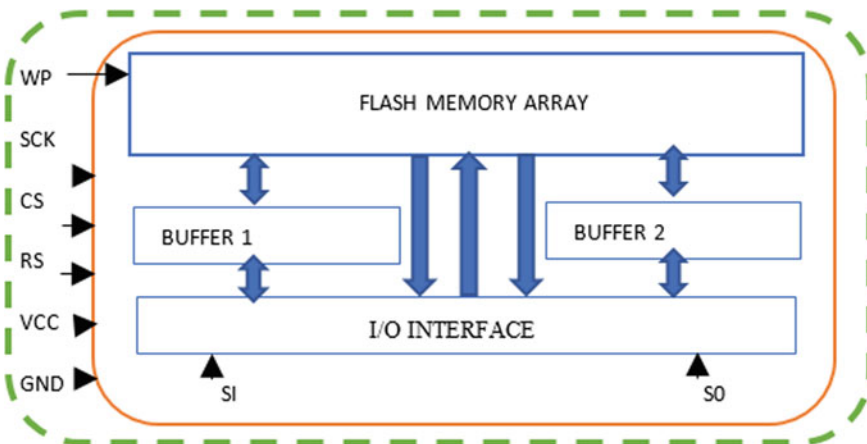


Fig. 2 16 MB flash memory block diagram

input voltages, where the flash memory operates off a single 2.5 V power source for the erase, write and read commands. This flash memory is ideal for the use within various applications to store data, images and program code. Rapid serial interface through the three-wire interface is done using the serial input (SI), serial output (SO) and the serial clock (SCK) pins [11].

The FPGA OBC needs to be programmable and configurable to suite an end user's requirements. Therefore, it has been designed to be able to connect to the Xilinx XC3S250E FPGA through the on-board JTAG connection or via the micro-USB port. The FT2232D is used in for the USB interface which incorporates the functionality of two second-generation BM chips into a single device. The stand-alone downstream USB port is converted to two IO channels which can be individually configured as a UART interface or as a FIFO interface. This makes it more convenient to programme the FPGA through an on-board USB port. For additional support, the FPGA may be programmed through the JTAG configuration as an alternative. To programme the FPGA using the JTAG, a USB blaster module is required. The Xilinx Spartan-3E family FPGAs and the Platform Flash PROMs all make use of a four-wire JTAG port compliant with the international IEEE 1149.1/1532 standard. They divide the JTAG TCK, USB_TCK, clock input and the select input function through TMS mode. These components can connect in any order with the TDO output on the JTAG string of one device transmitting the TDI/USB_TDI input from the other device in the sequence. The TDO output from the last device in the JTAG string leads the JTAG connector. This programming interface on the FPGA is powered through the VCC_AUX supply. Subsequently, the PROM's VCC supply must additionally be 2.5 V [12]. For the HIL simulation, a local computer with Xilinx IDE is used. The FPGA board is programmed through the use of a USB blaster via the JTAG pins. Figure 3 illustrates the basic flow of the hardware-in-the-loop simulation set-up. The UART mode of communication transfers data in blocks of 8 bits, also known as frames, which are user-configurable in terms of contents. The USART can function in either synchronous or asynchronous modes, which are application dependent [13].

The Write Enable (WR_EN) is used to write data into the FIFO with the Write Data (WR_DATA) holding the data that is sent to the FIFO. The FIFO model has a clock and reset trigger points. The clock is used for every action to execution upon trigger of the clock on the rising (high) edge or falling (low) edge of the clock frequency based on your application. As the name states, reset is the signal used to reset the FIFO memory when a high signal is transmitted.

From the read side, there is the Read_Enable (RD_EN) which allows the reading of the current data from the FIFO memory. To read data, the RD_EN input must receive a high input during one clock cycle and the data that is stored first will be read first from the Read_Data (RD_DATA) pin. When reading data constantly or at a high rate, the RD_EN pin's state may be set high for a longer period than one clock cycle.

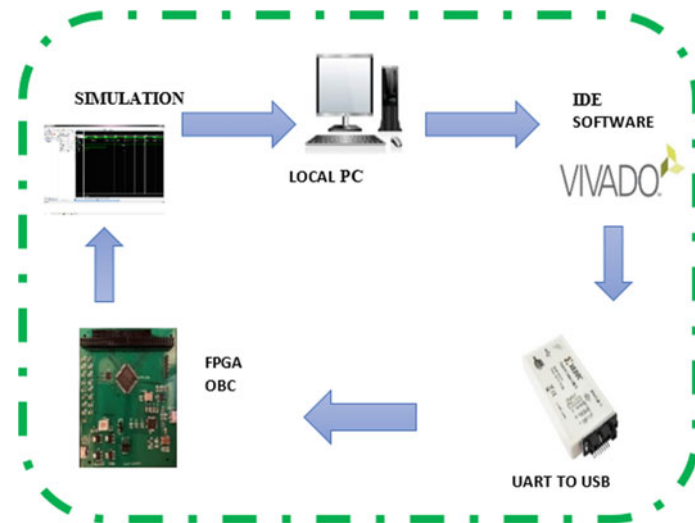


Fig. 3 HIL set-up sequence flow diagram

The write and read functions are implemented on the designed FPGA Spartan-3E board. This verifies the memory operation of the OBC with 16 MB flash memory on board. A basic write sequence is done in VHDL using the Xilinx IDE platform to configure the OBC. Figure 4 shows the read and write sequence on the flash memory through a FIFO model from the simulated VHDL code in the flow diagram illustrated in Fig. 5. The is done through every clock pulse, and the write of data is enabled.

Figure 4 shows the outcomes of the write/read operation for a full cycle where the FIFO buffer is full. In simultaneous read and write FIFOs, there is no dependency between the write and read operations of the data. Instantaneous reading and writing are possible in an overlapping manner or continuously. In other words, the two systems with different frequencies can be connected to the FIFO buffer. When designing a platform, you do not need to concern regarding harmonizing these two

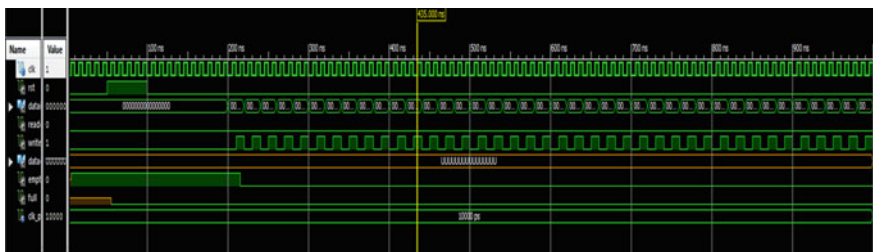


Fig. 4 Full FIFO cycle simulated on FPGA OBC

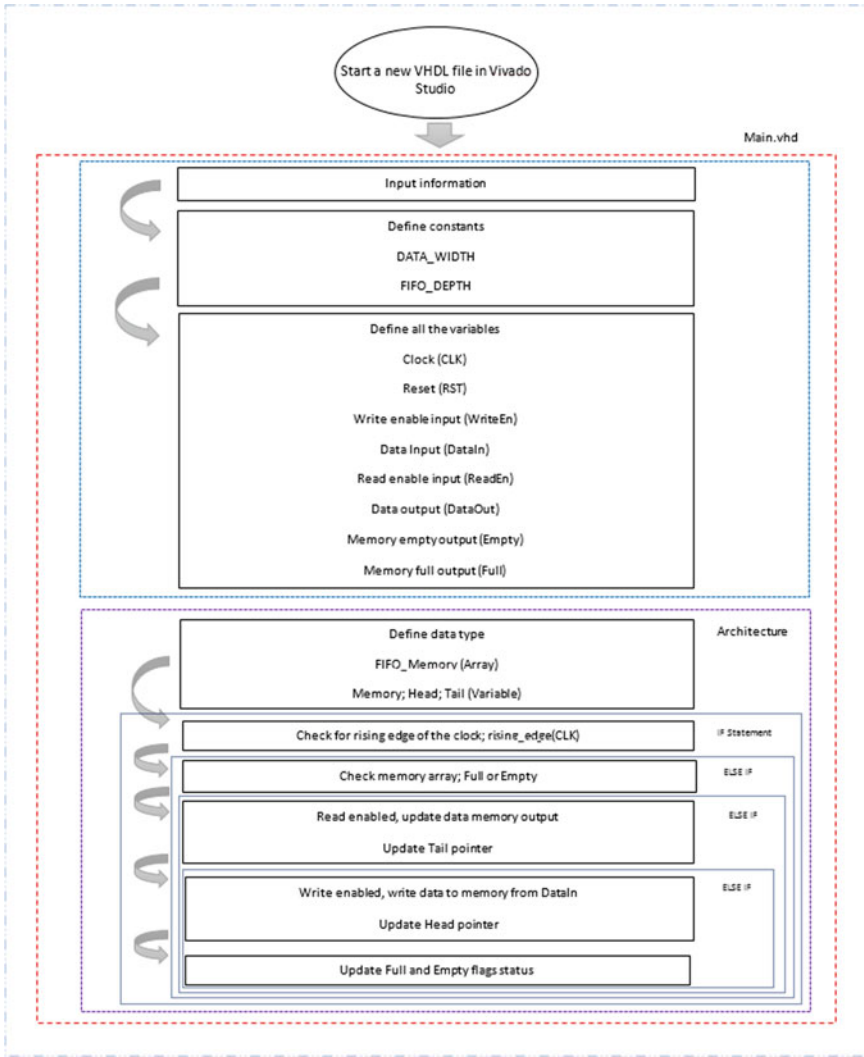


Fig. 5 VHDL memory test flow sequence

systems as this is taken into consideration by the FIFO. Parallel read and write operations of the FIFOs depend on the command signals for reading and writing which are based in two groups, synchronous and asynchronous FIFO banks.

For this simulation, the synchronous standard FIFO was used. The DATA_IN signal is the input to the FIFO with the DATA_OUTPUT as the output. WR_EN is the signal used to write data into the FIFO memory when the CLK is triggered on the positive edge. RN_EN is used for reading data from the FIFO buffer and is able to be reset through RS as high. The FIFO buffer will indicate when it is full with the

FULL signal at high and the same for the EMPTY signal when the buffer is empty, the signal will be high.

There are numerous ways to optimize VHDL code. Some of the main topics when it comes to optimization are efficient adder implementation, state machines, signal selection, storage structure, placement and routing [14]. In this paper, the Vivado package is used to code, analyse, compile and optimize the VHDL code.

For this simulation, the synchronous standard FIFO was used. The DATA_IN signal is the input to the FIFO with the DATA_OUTPUT as the output. WR_EN is the signal used to write data into the FIFO memory when the CLK is triggered on the positive edge. RD_EN is used for reading data from the FIFO buffer and is able to be reset through RS as high. The FIFO buffer will indicate when it is full with the FULL signal at high and the same for the EMPTY signal when the buffer is empty, the signal will be high. Figure 6 illustrates the basic FIFO write and read procedure.

The UART transmission is of a serial-type communication. Nonconcurrent transmission suggests that both the receiver and the transmitter have singular local clock signals which are established before the proceeding of the communication instead of simultaneous, where the communication transmission is synchronized on both ends through a common clock (Fig. 7).

Fig. 6 FIFO memory read/write sequence

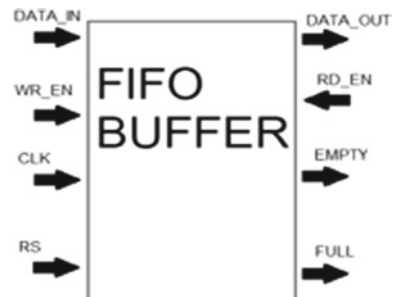


Fig. 7 JTAG in-circuit schematic

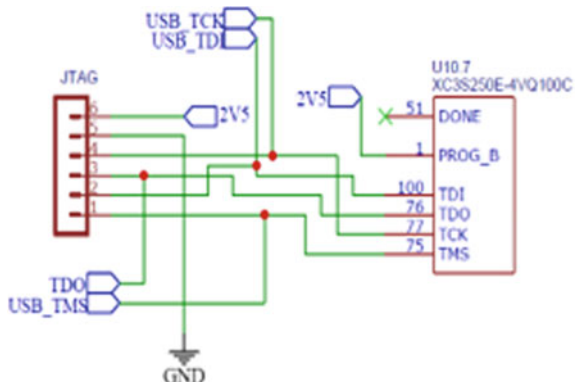




Fig. 8 UART simulation from VHDL test bench file

The UART communication for the FPGA-based on-board computer is also tested through the HIL simulation using a small VHDL script file to test the transfer of data between the OBC and the IDE platform. Figure 8 shows the UART communication between the FPGA-based OBC designed platform with successful WRITE and READ commands of 8 bits.

5 Conclusion

The first step presented for this research was to establish the various parameters governing an on-board computer for small satellites within low earth orbit and the space environment. Emphasis was put on the main components that are proposed for the OBC by using commercially available electronic components. The FPGA device had to be of commercial grade for the operating temperature and durability that will most likely survive in the space environment, as well as the current systems and electronic components being used in the small satellite industry that are of space grade and/or radiation-hardened components. Research was done on various FPGA manufacturers and current commercial OBC platforms available for satellite systems. A comparison is done on the most feasible and readily available FPGA packages as to which one will be used for the design implementation and verification of the OBC.

The final FPGA that was used is one from Xilinx Spartan-3E family manufactured in 2018 which has been available by Xilinx for several years now. The Spartan chip has 250 K system gates with a distributed RAM 38 K and 68 differential I/O pairs. This processor was designed to operate in temperature ranges of -40°C to $+100^{\circ}\text{C}$ which is suitable for low earth orbit missions and applications, at low voltage. The FPGA can be programmed through the USB interface and the JTAG header pins. Programming can be stored on the on-board external 16 MB flash memory. Generic programming is done using Verilog or VHDL to configure payloads or subsystems to control and/or read data from. The designed OBC has an on-board power supply unit to power the various electronic components from the FPGA to the flash memory.

This FPGA OBC was tested under a semi-controlled environment and not simulated under conditions similar to that of the space environment. The reliability will

only be confirmed upon vacuum testing and vibration testing under heat. The electronic components are susceptible to radiation damage or SEE from the cosmic rays, as the electronic component used is COTS components. In future, work will be compared with results from hardware.

References

1. Thai T (2014) Applications for FPGAs on nanosatellites
2. Hanafi A, Latachi I (2017) FPGA-based secondary on-board computer system for low-earth-orbit nano-satellite, pp 1–6
3. Uryu AN (2013) A combined data and power management infrastructure
4. Varnavas K, Sims WH, Casas J (2015) The use of field programmable gate arrays (FPGA) in small satellite communication systems, pp 86–89 (2015). https://www.thinkmind.org/download.php?articleid=spacomm_2015_4_30_20063
5. Sandy A (2015) DIY Comms and control for amateur Space. Maker Media, Inc
6. Prasad A, Jain Y, Joshi N, Gupta N, Singhania V, Sreedharan Y (2020) Interfacing architecture between telemetry and on-board computer for a nanosatellite, pp 1–6
7. Hillier C, Balyan V (2019) Error detection and correction on-board nanosatellites using hamming codes. *J Electr Comput Eng*
8. Lokman AH (2017) A Review of antennas for picosatellite applications. *Int J Antennas Propag*
9. Hillier C, Balyan V (2019) Effect of space radiation on LEO nanosatellites. *J Eng Appl Sci*
10. Kuwahara T (2010) FPGA-based reconfigurable on-board computing systems for space applications
11. Extra D (2012) Atmel AT45DB161E pin configurations and pinouts, pp 1–70
12. UG332 (2015) Spartan-3 generation configuration. Xilinx User Guid 332
13. Lumbwe LT (2013) Development of an onboard computer (OBC) for a CubeSat, pp 1–178
14. Gschwind M, Salapura V, Optimizing VHDL code for FPGA targets 1 Introduction, pp 1–13

A Survey on Solution of Imbalanced Data Classification Problem Using SMOTE and Extreme Learning Machine



Ankur Goyal, Likhita Rathore, and Sandeep Kumar

Abstract Imbalanced data are a common classification problem. Since it occurs in most real fields, this trend is increasingly important. It is of particular concern for highly imbalanced datasets (when the class ratio is high). Different techniques have been developed to deal with supervised learning sets. SMOTE is a well-known method for over-sampling that discusses imbalances at the level of the data. In the area, unequal data are widely distributed, and ensemble learning algorithms are a more efficient classifier in classifying imbalances. SMOTE synthetically contrasts two closely connected vectors. The learning algorithm itself, however, is not designed for imbalanced results. The simple ensemble idea, as well as the SMOTE algorithm, works with imbalanced data. There are detailed studies about imbalanced data problems and resolving this problem through several approaches. There are various approaches to overcome this problem, but we mainly focused on SMOTE and extreme learning machine algorithms.

Keywords Machine learning · Synthetic minority over-sampling technique (SMOTE) · Imbalanced data (ID) · Imbalanced data classification · Extreme learning machine (ELM) · Machine learning (ML)

1 Introduction

Imbalanced data apply when a single interest class is superfluous (discussed to as a minority or a positive class), resulting in uneven distribution of the sample by another interesting class (referred to as a majority class or a negative class). Imbalanced data are a traditional credit rating problem where positive evaluations are considerably greater than bad results. It leads to a phenomenon in which the study's outcomes are

A. Goyal
KL (Deemed to be University), Hyderabad 500075, India

L. Rathore
Yagyavalkya Institute of Technology, Jaipur, India

S. Kumar (✉)
CHRIST (Deemed to be University), Bangalore, Karnataka 560074, India

biased by a statistical prejudice toward the ruling party, while substantial financial damages are incurred by a wrong sample analysis, as a perfect illustration. Form II credit rating errors tend to riskier for loan consumers than Form I errors because they often create savings gains. Data mining techniques for commercial and management decision-making have been broadly applied while class mismatch problems remain a task for classification models. These models aim to improve overall accuracy (optimal global solutions) while knowledge distribution. [1].

ID classification issues have arisen from the advancement of ML from science fiction to technology. Differing datasets that are very prevalent in academic science, accounting, development, and industry are responsible for the problems found in data mismatch classification. Some of the well-known problems include spam filters, fraud detection of credit cards, medical anomaly detection, and software defect prediction. The significance of tackling this challenge has become particularly relevant as the researchers have discovered that the accessible data collection in these areas is not balanced [2].

Several methods are available for the over-sampling dataset used in the standard grading problem (a classification algorithm is used to classify an image, provided a labeled image training set). The most popular approach is known as SMOTE: an over-sampling technique for the synthetic minority. For example, specific training data that have samples and functionalities in the data feature region would be included in this technique. Note that these features are ongoing for simplicity. Consider a bird's dataset for clarification, for example. The space we want to excess for the minority class could be size, span, and weight (all continuous). Take a sample from the dataset, and then consider its nearest thing (in functional space) k-neighbors. Take vector amid k-neighbors and the current data point to establish a synthetic data point. Multiply a vector by an arbitrary number x between 0 and 1. Fill in everything in the existing data point to build the latest synthetic knowledge point [3].

ELM is a system applied as a single hidden layer feed-forward neural network (FNN) that selects random and calculates output weights, with a single layer of inputs, an occult layer of occult nodes, and a single output layer. It varies a bit from traditional algorithms for backpropagation. This procedure sets the number of occult neurons, and weights are distributed arbitrarily amid input and hidden layers (HLs) of a biased measure, so utilizing the Moore–Penrose process, the output layer is measured pseudo-inverse. This algorithm offers excellent speed and incredible precision for processing. Compared with conventional neural network approaches, ELM is more persuasive when it comes to solving challenges [4].

2 Imbalanced Data

Imbalanced data or datasets have been found to have particular relations between them essential for real-world applications. We obtain highly imbalanced datasets when using ML techniques and algorithms in real scenarios. From now on, we saw the appearance in the aftermath of ROC curves. There are several situations in which ML

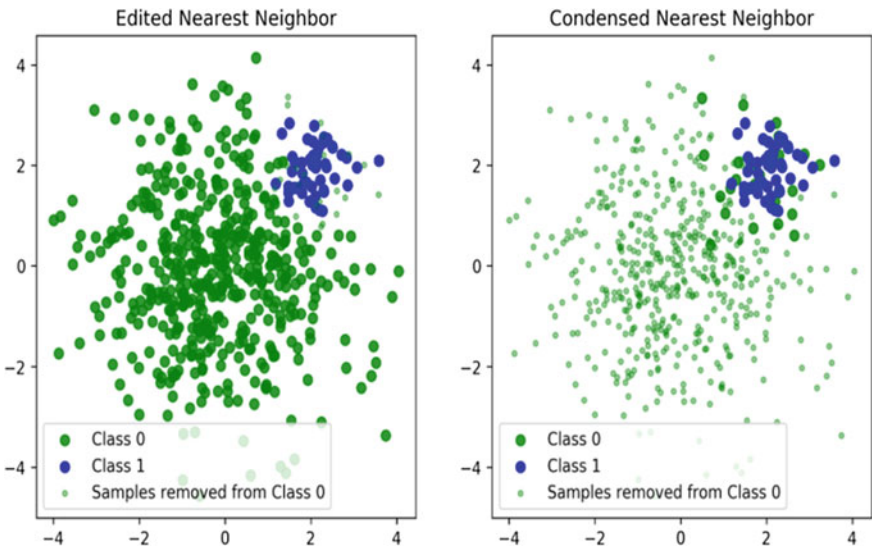


Fig. 1 Imbalance data

is used to collect datasets. Many of the primary applications are language recognition and description, output analysis, etc. The imbalances in our dataset may reflect an unsuitable class of error distribution. To computer scientists and software learners worldwide, this issue has drawn interest [5] (Fig. 1).

Imbalanced data classification is a concern, with a relatively wide variation of a dataset's proportional class size. At least one class is seen with few samples (known as a minority class), and the remainder goes to another class (known as a majority class). By theory, the output of a classifier in the ID set is partial to other classes (main class).

2.1 Approaches to Overcome Class Imbalance

There are various approaches by which we can solve the class imbalance problem. For this, we should be aware of supervised classification. The objective of classification is to estimate explicit labels where input and output are known. Many approaches are developed to overcome the challenges faced in imbalanced data.

Data-level approaches: The data-level approach or external technology involving preprocessing to re-equalize the class distribution is classified into two methods: sampling and data sampling. The sampling procedure may be conducted with or without the dataset substitution if a dataset is balanced by deleting the sample class instances. If we add similar minority class instances to balance the class ratio, an

over-sampling is done. With or without replacement, we can resample. We should look in depth at each solution below.

Resampling: Resampling is known as the process of recreating the sample data from the original datasets. It can be achieved through either non-statistical predictions or statistics. We take random samples from the real dataset of non-statistical calculations to expect the results to be broken into an equal division with the actual data.

Under-sampling: Under-sampling is a method in which the bulk of tests is automatically picked and the remainder is rejected. We presume that every random sampling approximately represents the data division.

Over-sampling: Using the process of sampling, we obtain fair distribution by eliminating samples from majority groups. In our over-sampling, we replicate the samples in minorities to ensure equal and balanced distribution. SMOTE is another prevalent over-sampling technique. SMOTE also measures and produces a different survey interval for the minority group below the maximum decision. The judgment cap would be influenced to step away from the main groups to eradicate the problem.

Algorithm-Level Approach: In general, an approach at the algorithm level can be classified as specific algorithms that take the distribution of imbalances from groups in the datasets directly. We comprise classifying, cost-sensitive learning, and ensemble approach focused on identification.

Improved algorithm: This is a procedure for classification developed by researchers to classify datasets to handle class imbalance. It has been updated to match the need for the unbalanced class distribution to understand explicitly. That algorithms recognize the class distribution before extracting essential knowledge to create a model focused on the target.

- One-class learning
- Cost-sensitive learning.

Ensemble Method: Ensemble learning for class imbalance problem is another choice. Many classifiers are educated on training data and are evaluated to make the final judgment on classification. Methods of assembly can be described as general boosting. This method is used to reduce the estimation gap by producing different samples of the actual results' training [12].

Hybrid Approach: New classification algorithm technology for handling imbalanced datasets has been developed in recent years. In comparison with one-class instruction, this method is cost-sensitive but ensemble. More than one machine learning algorithm is applied to boost the classification's accuracy, mostly by hybridization and others, to produce better performance. With the goal of the issue in samples, choosing the feature base, optimizing the cost matrix, and polishing the learning algorithms, the homologous recombination is created. The hybridizer classifiers were used to boost the consistency of classification for class mismatch issues.

2.2 *Advantages and Disadvantages of the Approaches*

Advantages: Classification performance is made better by using the data generation and boosting methods. The use of various classifiers in the ensemble method preserves the regularity with the training data, which is a significant factor in ensuring correctness. It improves the execution time of the model and solves memory problematic by decreasing no. of samples when the training dataset is more. There is no loss of information in over-sampling. To adjust the division of sample data boosting is used to handle uneven division in datasets by assigning weight to examples.

Disadvantages: There is a loss of information in the under-sampling technique. Over-sampling is feasible as it generates the same replica of minority class samples as samples from minority production tests. Another issue with an over-sampling method is that the amount of samples is rising; the model becomes more complex, expanding the models' running time. One-class algorithm is restricted only to specific learning algorithms. Cost-sensitive learning, we do not know the real cost in many applications, even if the dataset is balanced. It also has an issue of overfitting during training. It is the same as the over-sampling technique, and there is no difference in the performance of both methods [6].

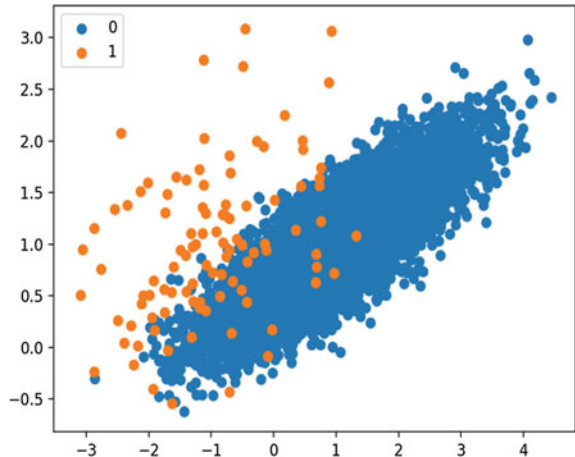
3 Synthetic Minority Over-sampling Technique

The so-called synthetic minority over-sampling technique or SMOTE is a widespread tool for generating new data. It is based on sampling minority class data by modestly making segment data points connecting one of its nearest K-nearest data points to a randomly selected data point. It is an elementary method and has become widely shared in use. The only problem of SMOTE was that it was not founded on a sound theory in mathematics. The purpose of this research is to fix this flaw and to study the SMOTE protocol thoroughly (Fig. 2).

While SMOTE is not intended to imitate = underlying distribution, distribution is essential for establishing classification limits. We also explain SMOTE's impact on classification results, as classification efficacy is the primary goal when utilizing SMOTE, in addition to our proposed distributional analysis. In reality, our priorities are the same.

- Improve the mathematical model of SMOTE and calculate to what degree it emulates, similar to the underlying distribution (check its moments). The presented theory is universal and is valid for any distribution.
- Put on terms of identity statistical analysis to 2 distributions: Gaussian or multi-variate Gaussian distribution to achieve simpler, closed-form for medium or covariant sequence distribution over-sampled.
- Include a thorough laboratory analysis of SMOTE, analyzing factors influencing its accuracy (imitating distribution). For instance, we find both statistically and

Fig. 2 SMOTE for imbalance classification



empirically, the number of initial minority trends decreases as scale grows, and as no. of neighbors applied to analyze SMOTE grows, the accuracy deteriorates.

- Analyze utility of SMOTE for other classifiers, both logically and empirically, by examining the impact of specific variables on their efficacy.
- Give a detailed analytical study of SMOTE, including three common SMOTE extensions (borderline SMOTE1, borderline SMOTE2, or ADASYN) to analyze the distribution or classification efficiency of these over-sampling methods [7].

4 Extreme Learning Machine (ELM)

In many fields of research and technology, it has drawn extensive attention. With hidden neuron weights dynamically set, ELM efficiently eliminates the limitations of conventional SLFN learning algorithms. ELM incorporates ML problems like regression, sorting, clustering, and compression in the approach. The benefits of ELM in this method include high productivity (rapid testing with high accuracy), excellent overall results, a painless procedure, and uniform approximation ability. ELM has also been extended to ship identification, picture quality measurement, and human behavior recognition [8] (Fig. 3).

4.1 Variants of ELM

This portion introduces and describes a few common ELM variants.

Incremental ELM (I-ELM): I-ELM is to create an incremental input network. In the hidden layer, I-ELM inserted random nodes. It was added one at a time. That froze the performance weights of currently hidden nodes (HNs) when a new HN

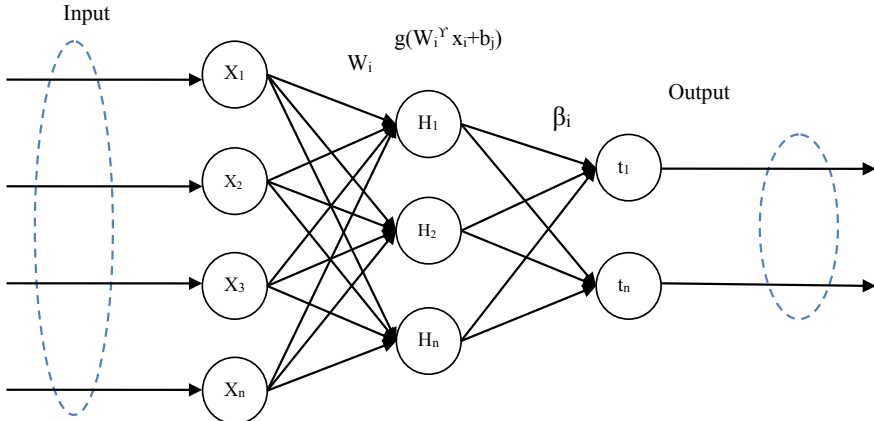


Fig. 3 Extreme learning machine

was inserted. In addition to the continuous (and differentiable) enabling functions of the SLFN, I-ELM is useful for SLFNs with partly continuous (such as threshold) activation functions. Huang et al. introduced I-ELM convex (CI-ELM) and improved I-ELM (EI-ELM) given this I-ELM sense.

Pruning ELM: If very few/many hidden nodes are deployed, the underfitting/overfitting of a P-ELM algorithm built for an ELM network design will lead to problems. P-ELM starts with many HNs before less relevant or irrelevant HNs are eliminated by taking into account their significance for class labels in learning.

Error-Minimized ELM: This system can automatically increase group-by-group hidden nodes and know the amount of HNs in generalized SLFNs. During network development, performance weights are changed slowly, and thus the device complexity is significantly reduced. For secret nodes of sigmoid form, the simulation results indicate that this technique will dramatically reduce the computation difficulty of ELM and help build an efficient application of ELM.

Online Sequential ELM: Both preparation details will be accessible for training purposes by utilizing traditional ELM. However, training data can be accessed one by one or one element per line in actual applications. It proposed an algorithm called the online ELM (OS-ELM) for sequential learning. This algorithm can be used in a unified environment with both RBF and additive nodes.

Ordinary ELM: ELM algorithm is used for common problems in regression, three ordinal algorithms based on ELM have been implemented, and one framework is based on encoding.

Fully Complex ELM: The ELM algorithm was generalized from the real domain to the abstract domain. C-ELM's secret layer preferences and input weights were randomly chosen based on the ongoing likelihood of spread like ELM. The performance weights were then measured analytically rather than iterating [9].

5 Machine Learning

ML is an IT field where computers can learn from data and are not explicitly programmed. The study ML subfield requires marked information to learn. Data are identified by human experts and methods that should be mimicked for behavior. The algorithm attempts to establish relationships between input (data) and output (labels) throughout the training process. After training on unlisted data, the system can be used. The methods used in this paper are those used for supervised learning algorithms. With the Internet increasing, online reviews have become increasingly relevant information sources. Sellers also seek to mislead buyers by posting false comments, realizing that customer reviews depend on their products' popularity. Sellers themselves may post reviews or pay for them by other individuals [7].

5.1 ML Techniques

Artificial Neural Network: That combines computational computing power with human brain logic. Neurons are used to determine the location or boundaries between neurons to measure each neuron's contribution to the last layer and result. It relies on pattern recognition.

Decision Tree: Classification or estimation is a method of computation. The internal node tree displaying a check on a particular feature shows each branch's outcome, and a class label will be used for each leaf node (terminal node). It divided a dataset, by either a breadth-first greedy approach or a depth-first greedy method, and stopped when a different class was assigned for each variable.

Fuzzy Logic: Fuzzy logic is used where the reality's values are not discrete; that is, they are continuous. It is logical with a multivalued. There are several rules which classify transactions as a genuine or fraudulent transaction.

Support Vector Machine: SVM is a supervised learning algorithm partitioned into distinct classes in one hyperplane by a dataset. The hyperplane is to be discovered by SVM. There may be many hyperplanes available, but we are dedicated to an optimal hyperplane. Nearest hyperplane points are considered multiclass support vectors, and these support vectors are used to infer new data point classes (Fig. 4).

Bayesian Network (BN): The probability hypothesis of Bayes theorem is used and is thus a probabilistic method used to correctly predict various events. It consists of nodes and rims. They calculate the fraud or legal crime with predefined minimum and average risks. Therefore, we find that perhaps the probability of a valid transaction for an incoming transaction is less than a given minimum value, which is more than a specified maximum value for a fraud transaction.

K-Nearest Neighbor (KNN): One of the most common technologies is the statistical classification or regression problems. The usefulness varies according to three factors: estimating distances, distance law, and K value. Range metrics suggest the closest neighbors are to be found at every data point.

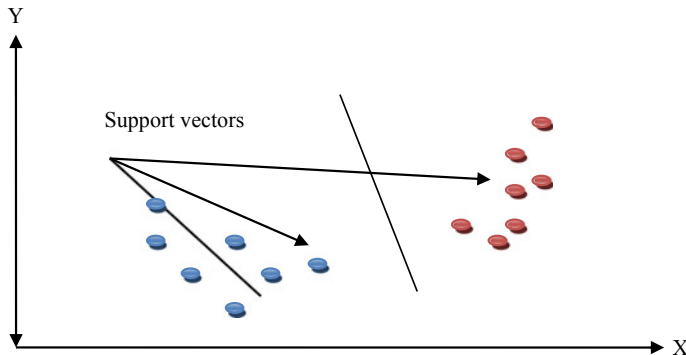


Fig. 4 Support vector machine

K-Means: It can be used to shape a category of K-means. It is a vector quantization method produced initially by signal processing and used for information mining cluster processing. We may use one nearest neighbor categorization in K-means cluster centers to efficiently incorporate new knowledge into established categories.

Genetic Algorithm: GA is an approach of locally searching to partially solve a problem and partially refine search parameters. GA is an evolutionary algorithm class that uses crossover and inheritance-based methods or evolutionary biology selection. GA is conducted primarily as a computer simulation so that the abstract population of candidate solutions grows to strengthen solutions to the O problem [10].

6 Convolutional Neural Network (CNN)

CNN is close to feeding neural networks with learning weights and biases in neurons. It has been used for signal processing and image recognition in the field of vision with OpenCV. Modular neural networks provide an independent set of different networks that contribute to the output. The neural network has a collection of unique inputs to the build-up and executes subtasks of other networks. When carrying out functions, these networks do not communicate or warn each other. A modular neural network's benefit was that significant computational function reduces complexity into smaller parts [11] (Fig. 5).

7 Related Work

Rustogi and Prasad proposed a hybrid method in the paper, followed by extreme learning machine, to classify binary variable data using SMOTE. This method and rapid learning rate are effective in forecasting the desired class. This system has

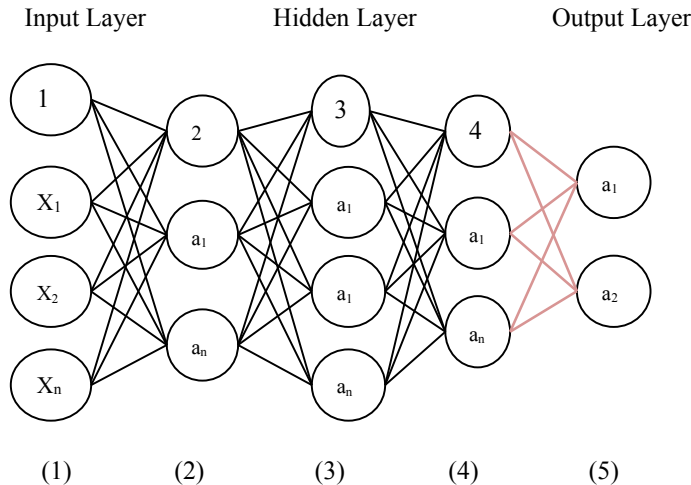


Fig. 5 Convolutional neural network

been checked for five regular imbalanced datasets, and a higher F, G, and ROC score has been achieved for the entire dataset. The continuous growth of S and T has contributed to outstanding data quality and usability in every region. Throughout the decision-making process, it is essential to grasp and evaluate these details critically. While the prevalent computer engineering and mining methods have achieved great success, there is still rapid detection of imbalanced data in academia and industry. Data up-sampling or down-sampling can solve a potential solution to the problem of skewness in data. Several approaches eradicate bias first and then define, but such strategies suffer from challenges such as abortive accuracy or slower learning rates [2].

Yuan and Zhao discussed that data mining requires common imbalanced data, so EL algorithms are a more efficient classification for detecting imbalanced data. The learning algorithm itself, however, is not designed for imbalanced results. Therefore, a system of data processing is suggested, which is imbalanced and focused on the SE-gcForest stage of ensemble instruction. This approach incorporates the concept of data-level processing after the gcForest algorithm's multi-grain scanning method. The SMOTE and easy ensemble algorithms manage imbalanced results. Experiments demonstrate that this approach is more effective if the data balancing ratio is lower and higher [12].

Gameng et al. described that the discrepancy would decrease classification algorithms' capacity to identify cases of interest that misclassify valid samples as negative or false valid. It is one of the existing super-sampling techniques. One of its many variants is the adaptive synthetic (ADASYN) SMOTE. ADASYN incorporates K-nearest neighbor (KNN). Manhattan distance in the KNN calculations is applied in this study. The performance of this updated ADASYN calculation in the overall quality, precision, retrieval, and F1 calculation was calculated in six unbalanced datasets using

logistic regression as a classification algorithm. The updated ADASYN was over 66.67% of the overall value metric count over SMOTE and the initial ADASYN. It leads to the accuracy and recalls the number of 4 of 6, the accuracy of 3 of 6, and the F1 of 5 of 6. Therefore, proof should prove that the updated ADASYN may give a successful remedy for ID sets [13].

Khadijah et al. proposed that when the data collection has a multiclass purpose, and the number of observations is not distributed correctly (called the distribution of imbalances), it is getting more challenging. This work's specific methods are researched to tackle imbalances in the data flow: SMOTE (data-based) and ELM (algorithmic). The proposed approach's efficiency was evaluated using two imbalanced public mul and cycle microarray datasets, Global Cancer Map (GCM) and leukemia subtype datasets. Experimental results show that GCM dataset implementation of SMOTE and weighted ELM does not substantially affect classification performance. Unlike leukemia subtypes, the improvement of classification efficiency by SMOTE and weighted ELM implementations follows previous investigations. Overall, the results show the weighted ELM to enhance the minority class's precision a bit better than SMOTE [14].

Mohasseb et al. explained that throughout ML or data mining, the detection of ID became a big concern. In this article, the authors proposed to use a hierarchical SMOTE algorithm to address different kinds of questions on the inequality of gender. The grammar pattern is applied for each question, and it is classified using algorithms for machine learning. The experimental findings suggest that various questions are correct, and class imbalances are established [15].

Sanguanmak and Hanskunatai discussed that many real-life systems face class inequality. The performance of the prediction is affected by this problem. The resampling method is now a popular method for dealing with class imbalances such as over-sampling, under-sampling, and hybrid sampling. Therefore, this paper offers a new approach for the hybrid resampling of class inequality, known as DBSM. The DBSM idea is to use the DBSCAN under-sampling algorithm as well as the DBSCAN over-sampling methodology. An initial dataset and various other comparison techniques, including SMOTE, Tomek L connections, SMOTE + Tomek, and DBSCAN, contrast with the DBSM algorithm's experimental performance. The results show that DBSM can improve classification predictive efficiency. It also provides the highest AUC, F-measurement, and precision on average [16].

Matsuda and Murase proposed that ID detection is one of the classifications' most common topics. Inappropriate handling contributes to weaker guidance and fewer effective marking. They used complex NN (CVNN) to classify IDs in this analysis with a single sheet. In addition to overcoming the ID issue, we use the well-known over-sample, something called the CVNN SMOTE. SMOTE is the method for over-proving minority class results. Authors use five imbalanced datasets from the UCI collection relative to real-valued NN (RV NN) to determine the effectiveness of CVNN with SMOTE for unbalanced data classification issues. It results in better sensitivity and accuracy of CVNN using SMOTE than the other part with most of the datasets tested [17].

Fang et al. described that classification had been a hotspot problem in DM in the ID collection. The main principle for the traditional classification algorithms is that the distribution of classes is balanced, and therefore it is not possible to produce an ideal effect for the algorithms used in the imbalanced classification set. To guide people through selecting samples of a minority class and generating new samples of minority classes, we propose a supportive over-sampling method based on a disability classification. Because of the assisted stage, the detection of minority class boundary samples is now feasible, and a range of new samples can be generated between the boundary samples or their neighboring countries. Experimental findings indicate that the approach has a decisive benefit in the control of imbalanced data [18] (Table 1).

8 Conclusion

Data sets are usually imbalanced in real-world applications. It becomes a hotspot issue to properly characterize the imbalance information. Synthetic minority over-sampling technique is the full name of SMOTE and is a synthetic over-sampling process. It is a more robust scheme based on the algorithm of random samples.

Table 1 Comparison of related work

Author	Paper title	Problem	Method	Advantages
Rastogi and Prasad [2]	Swift Imbalance Data Classification using SMOTE and Extreme Learning Machine	Huge computer transparency and usability Rapid imbalanced data classification	ELM leads SMOTE	Remove skewness and then perform classification
Yuan and Zhao [12]	An Improved Ensemble Learning for ID Classification	Something is not optimized itself for unequaled data	SE-gcForest	More efficient at high and low data unequaled ratio
Zhu and Qin [19]	An Improved Weighted KNN Algorithm for ID Classification	To determine the appropriate value of k	Training method	Better performance in class-imbalanced data
Chen et al. [20]	GAN-based ID Classification Semi-supervised	The classification performance drops sharply	Increased generative adversarial network (GAN) algorithm	Good applicability for the classification of structured data
WeiShimizu et al. [21]	Safe Mini-Batch Instruction with NN Image Classification	The difference in the amount of test application-level samples	A balanced mini-batch training method	Higher classification ability

(continued)

Table 1 (continued)

Author	Paper title	Problem	Method	Advantages
Li et al. [22]	An Improved AdaBoost for ID Focused on KNN	Problem of identification Minority class accuracy	AdaBoost changed slightly dependent on KNN (K-AdaBoost) weighted	Avoid weight distortion
Matsuda and Murase [17]	CNN with SMOTE for ID Classification of Single-Layered	Reduction of the classification's precision and flexibility	Single-layered complex-valued neural network (CVNN)	Better sensitivity and accuracy
Fang et al. [18]	An Improved Help Degree SMOTE ID Classification System	Classification cannot produce an optimal result with imbalanced datasets	Over the help degree sampling system	Handling the imbalance set of data

ELM is a novel way of classifying the pattern and of approaching the function. It is primarily an outstanding feed-forward neural network and has a single layer of hidden knots where weights are uniformly distributed between inputs and hidden nodes and are constant during exercise and prediction. This study is useful for providing information about various ELM algorithms and SMOTE as a solution to ID problems.

References

1. Shen F, Zhao X, Li Z, Li K, Meng Z (2019) A novel ensemble classification model based on neural networks and a classifier optimization technique for imbalanced credit risk evaluation. *Phys A Statist Mech Its Appl* 526:1–17. <https://doi.org/10.1016/j.physa.2019.121073>
2. Rustogi R, Prasad A (2019) Swift imbalance data classification using SMOTE and extreme learning machine. In: Second international conference on computational intelligence in data science (ICCIDIS), vol 978, pp 1–8
3. Shelke MS (2017) A review on imbalanced data handling using undersampling and oversampling technique. *Int J Recent Trends Eng Res (IJRTER)* 03(04):1–7
4. Gupta C, Gill NS (2020) ML techniques and extreme learning machine for early breast cancer prediction. *Int J Innov Technol Explor Eng (IJITEE)* 9(4). ISSN: 2278-3075
5. Birla S, Kohli K, Dutta A (2016) Machine learning on imbalanced data in credit risk. In: 2016 IEEE 7th annual information technology, electronics and mobile communication conference (IEMCON), vol 978, pp 1–6. <https://doi.org/10.1109/iemcon.2016.7746326>
6. Ochani M, Sawarkar SD, Narwane S (2019) A novel approach to handle class imbalance: a survey. *Int J Eng Dev Res (IJEDR)* 7(2): 1–9. ISSN: 2321-9939
7. Elreedy D, Atiya AF (2019) A Comprehensive analysis of synthetic minority oversampling technique (SMOTE) for handling class imbalance. *Inf Sci* 502:32–63. <https://doi.org/10.1016/j.ins.2019.07.070>
8. Deng B, Zhang X, Gong W, Shang D (2019) An overview of extreme learning machine. In: 2019 4th international conference on control, robotics and cybernetics (CRC), vol. 978, pp. 1–7. <https://doi.org/10.1016/j.ins.2019.07.070>

9. Abbas M, Albadra A, Tiuna S (2017) Extreme learning machine: a review. *Int J Appl Eng Res* 12(14):4610–4623. ISSN 0973-4562
10. Kajaree D (2007) A survey on machine learning: concept, algos and applications. *Int J Innov Res Comput Commun Eng* 5(2):1–12. (An ISO 3297: Certified Organization), Website: www.ijircce.com
11. <https://analyticsindiamag.com/6-Types-Of-Artificial-Neural-Networks-Currently-Being-Used-In-Todays-Technology/>
12. Yuan Z, Zhao P (2019) An improved ensemble learning for imbalanced data classification. In: 2019 IEEE 8th joint international information technology and artificial intelligence conference (ITAIC), vol 978, pp 1–4. <https://doi.org/10.1109/itaic.2019.8785887>
13. Gameng HA, Gerardo BB, Medina RP (2019) Modified adaptive synthetic SMOTE to improve classification performance in imbalanced datasets. In: IEEE 6th international conference on engineering technologies and applied sciences (ICETAS), Kuala Lumpur, Malaysia, vol 978, pp 1–5. <https://doi.org/10.1109/ICETAS48360.2019.9117287>
14. Khadijah SNE, Kusumaningrum R (2018) The study of synthetic minority over-sampling technique (SMOTE) and weighted extreme learning machine for handling imbalance problem on multiclass microarray classification. In: International conference on informatics and computational sciences (ICICoS), Semarang, Indonesia, pp 1–6. <https://doi.org/10.1109/ICICOS.2018.8621657>
15. Mohasseb M, Cocea M, Liu H (2018) improving imbalanced question classification using structured smote based approach. In: International conference on machine learning and cybernetics (ICMLC), Chengdu, pp 593–597. <https://doi.org/10.1109/ICMLC.2018.8527028>
16. Sangwanmak Y, Hanskunatai A (2016) DBSM: the combination of DBSCAN and SMOTE for imbalanced data classification. In: international joint conference on computer science and software engineering (JCSSE), KhonKaen, pp 1–5. <https://doi.org/10.1109/JCSSE.2016.7748928>
17. Matsuda K, Murase K (2016) Single-layered complex-valued neural network with SMOTE for imbalanced data classification. In: 2016 joint 8th international conference on soft computing and intelligent systems (SCIS) and 17th international symposium on advanced intelligent systems (ISIS). <https://doi.org/10.1109/scis-isis.2016.0079>
18. Li K, Zhang W, Lu Q, Fang X (2014) An improved SMOTE, imbalanced data classification method, based on support degree. In: 2014 international conference on identification, information, and knowledge in the internet of things. <https://doi.org/10.1109/iiki.2014.14>
19. Liu S, Zhu P, Qin S (2018) An improved weighted KNN algorithm for imbalanced data classification. In: 2018 IEEE 4th international conference on computer and communications (ICCC). <https://doi.org/10.1109/compcomm.2018.8780580>
20. Zhou T, Liu W, Zhou C, Chen L (2018) GAN-based semi-supervised for imbalanced data classification. In: 2018 4th international conference on information management (ICIM). <https://doi.org/10.1109/infoman.2018.8392662>
21. Shimizu R, Asako K, Ojima H, Morinaga S, Hamada M, Kuroda T (2018) Balanced mini-batch training for imbalanced image data classification with neural network. In: 2018 first international conference on artificial intelligence for industries (AI4I). <https://doi.org/10.1109/ai4i.2018.8665709>
22. Li K, Xie P, Zhai J, Liu W (2017) An improved Adaboost algorithm for imbalanced data based on weighted KNN. In: 2017 IEEE 2nd international conference on big data analysis (ICBDA). <https://doi.org/10.1109/icbda.2017.8078849>

Thermal Imaging-Assisted Infection Classification (BoF) for Brinjal Crop



Shubhangi Verma, O. P. Singh, Sachin Kumar, and Sumita Mishra

Abstract In the development of economy, agriculture has always played an important role for different nations; since it is considered to be the main source of income, food, and employment to rural populations in the country, owing to diversified geographical locations, environmental conditions, and pest attacks, it is of prime importance to devise technological-assisted methods to monitor and provide early remedial actions for the damage and infections to the crop. Algorithm proposed focuses on health monitoring of brinjal crop using digital thermal imaging. Paper aims to identify the plant disease by analyzing thermal images of brinjal leaves. Infrared images are rich in important hidden details that are not visible due to their low contrast and blurring. Experiment was conducted on two sets of images, first set comprising of healthy and infected thermal images and second comprising of normal RGB capture of healthy and infected images; 30 to 35 images per crop per set were acquired, total dataset analyzed had 1160 images, and the process of identification was implemented via bag of features (BoF), under the umbrella; feature extraction was carried out by SIFT operator, and classification was performed using classification MLSTSVM. Simulation was implemented using MATLAB 2018b. Results showed that duration of the process was less for RGB images by a margin of approximately 6 secs, but the accuracy efficiency achieved was more for thermal images by margin of 3%, having 87% in all. From the results, it can be concluded that however duration required for the identification was more for thermal images but still percentage accuracy is more for thermal images; thus, thermal image-assisted algorithm can be employed for crops in remote scenarios where accuracy plays a vital role.

Keywords Brinjal plant · Thermal images · RGB · BoF · Accuracy

S. Verma · O. P. Singh · S. Kumar (✉) · S. Mishra
Amity University, Lucknow campus, Lucknow, India
e-mail: skumar3@lko.amity.edu

O. P. Singh
e-mail: opsingh@amity.edu

S. Mishra
e-mail: smishra3@lko.amity.edu

1 Introduction

In the development of economy, agriculture has always played an important role of different countries since it is the main source of income, food, and employment to rural populations in the country. USA, China, and India are some top countries in food exporters which produce more food together than European Union put together. Brazil is in the fourth place which is more toward the production of sugarcane, soybeans, and beef. India stands second largest food producer in terms of intake of total calorie, and if total value of agriculture production is measured, India falls in fourth position followed by China, USA, and Brazil. Agriculture in India contributes to 19.5% of the GDP [1–6].

In order to increase the agriculture's contribution toward GDP, it is essential for us to take necessary actions toward the development in agriculture sector by helping rural communities in understanding the India's situation of leading crop production. As India tops in producing some vegetables like potato, tomato, sugarcane, and many more, monitoring health of these crops is an important factor in order to increase its productivity and its contribution in India's economy as well. Here, we are specifically focusing on brinjal plants since it is poor man's vegetable and popular with low-income consumers and small-scale farmers which are grown mostly in all states of our country, and India is a second largest producer after China. In the year 2017–2018, West Bengal tops the list in production of brinjal and produced its total share of 23.69%, whereas Haryana is in 10th position and its share is 2.50% as shown in Fig. 1 [4–6].

Monitoring the health of the crops is an important step toward the growth in productivity. There are certain factors which should be kept in mind while monitoring

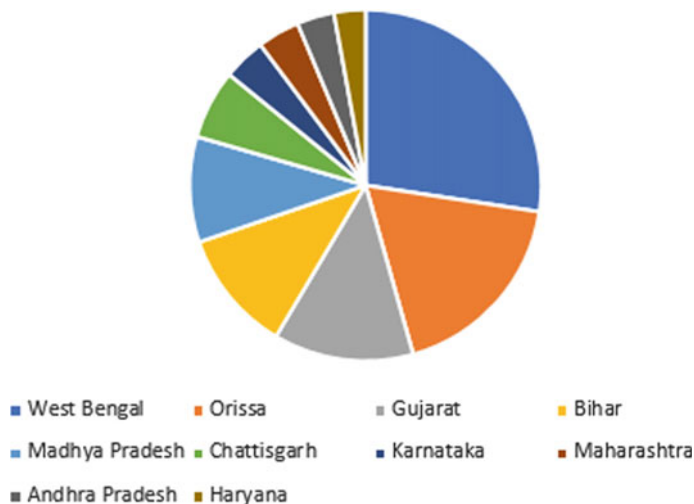


Fig. 1 Top 10 leading brinjal producers of India [4–6]

crop's growth like light, water, temperature, nutrients, diseases, and many more. Early detection of whatever issues associated with any one of the above factors can help us to monitor the growth in an efficient way and without wasting our resources in later stage. In this paper, we are specifically focusing on identification of diseases in brinjal plants [5, 7–9].

The paper is arranged as follows: Sect. 2 presents the motivation for conducting the study, Sect. 3 presents the material and methods employed for implementing the algorithm adopted for classification of thermal and RGB images for disease identification in brinjal plant, Sect. 4 discusses in brief the results obtained from the implementation conducted, and finally conclusion is presented in Sect. 5.

2 Motivation

Over the years, diversified techniques have evolved for early identification and cure of infection in crops. D.M. Bulanon et al. presented the paper on the thermal temporal variation in citrus fruit as a technique for enhancing fruit identification; in this work, canopy was examined after every twenty-four-hour period employing a thermal infrared camera and samples were segregated successfully in the dataset employing image processing algorithms at the instant of highest temperature variation; the results obtained gave improved results as compared to existing algorithms. Model presented a combination of thermal and RGB datasets with learning algorithms to remotely identify plants infected with disease. Shan-e-Ahmed Raza et al. obtained a group of features from the sample data employing global and local mathematical processing and displayed that combining normal and thermal identification methods provided depth information and improved the accuracy and precision of disease identification in infected plants [8–11].

IR sensor applications include detecting drought phenotype samples for studies from rice fields and grape farms, samples have issues of sensitivity, such as plant temperature variations of 15 °C happening between portions of shaded area and complete sunlight. Hamlyn G. Jones et al. employed the techniques in data analytics; displaying about variation, may be identified despite visible variations in soil water content using normalization methods [11]. Carmen M. Ortiz-Bustos et al. studied BGF emission by benign sunflower plant leaves and employed a combination of thermal and BGF imaging techniques for the identification of the diseases. Lower BGF was identified in parasitized samples via leaf expansion, and low pigment concentration was identified at final time [12].

Zulkifli Bin Husin et al. presented a technique for early identification of chili infection via leaf feature monitoring. Image dataset was acquired and processed to identify the infection level of the sample. Method ensures that pesticides or insecticides are applied only if the samples are infected. The system proposed is extremely cost-effective and inexpensive [13]. With farming process, processing of image is employed to identify the infectious diseases on samples. Ashwani Kumar et al. employed ANN for the purpose. Grapes and apples were the samples used for

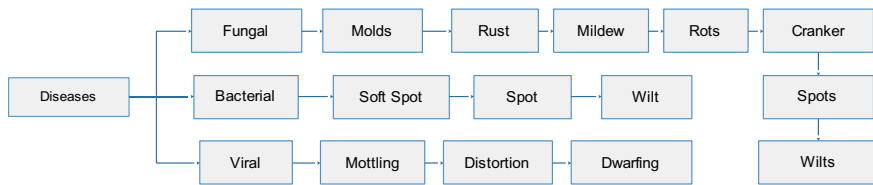
the algorithm. The technique proposed employed two datasets, first one for training of infected samples and the second one for testing of queried sample images. Work presents algorithms for the spread of infection and counting of fruits. MATLAB 2018b was employed for the implementation [14]. Automated disease identification is achieved employing multiple AI algorithms. The model proposed has three blocks, i.e., color segmentation from sample dataset, disease segmentation from segregated samples, and classification of infection. Segmentation via colors of leaf is a preprocessing block, this segments out unnecessary information that is not required for identification, and this helps in segmenting grape leaf regions in the dataset. P. Kumsawat et al. presented the model which displays the output segmented sample, which is subjected to filtering process and permits the system to study disease through color features. Model proposed can successfully categorize the dataset into three classes, rust infection, scab infection, and benign samples [15]. S. Bani-Ahmad et al. presented a soft solution for automated identification of plant diseases. Model developed comprises four main components. First is the process of segmentation; after this phase, two steps are there; first, identify region of interest, i.e., green colored, and in second regions are masked depending upon threshold value defined, employing Otsu's technique; second step involves subdivision into clusters with RGB values defining region of interest for elimination. Algorithm developed efficiently detects and classifies the infected region [16].

Disease identification comprises steps such as acquiring image dataset, preprocessing, segregating, feature extraction, and benign or infected classification. A.B. Patil et al. presented techniques for detection of infections in plants employing health of leaves and feature extraction from these leaves for disease identification [17]. The automated platform for rice infection based on the feature extraction of different rice plants is presented by Jaya Sil et al. Dataset of images is obtained from live images acquired from camera, rice crop was taken for the work, and images acquired are processed to be fed to NN for classification of infected regions [18]. Kumar et al. classified soil into different categories [19] and also developed a method for disease identification in plants [20].

Owing to potential dependency and importance crops play in world's economy, it is important to monitor and save crops timely for healthy production. Therefore, there is a potential requirement of pioneering and out of box results in the area, supported by relevant research results. Work proposed is an effort to increase productivity through early and precise disease detection with thermal images and thus plant for early remedial action, and the process is executed by analyzing thermal images.

3 Material and Methods

In crops, diseases can be classified as biotic and abiotic diseases. Biotic diseases originate from living organisms. They can be caused by fungi, bacteria, and viruses. Abiotic disease originates from non-living substances like hail, spring frosts, weather

**Fig. 2** Categorical division of diseases

conditions, burning of chemicals, etc. Figure 2 depicts categorical division of diseases.

Before extracting the features of diseases, it is important for us to know about the diseases caused in brinjal plant. Table 1 shows the different diseases' name along with its symptoms and images of the respective disease in plant [4–6, 17–20].

Table 1 Diseases in brinjal plant

S. No.	Disease	Symptoms	Images
1	Bacterial wilt	Leaf surface wilting, yellowing of foliage	
2	Cercospora leaf spot	Leaf spots by chlorotic lesions and irregular in shape	
3	Alternaria leaf spot	Cracks appear in leaf with concentric rings	
4	Damping off	Collapse of seed lines and spread through fungus present in soil	
5	Tobacco mosaic virus	Leaves are deformed and develop blisters in the advance case	
6	Collar rot	Caused by the accumulation of water around stem	

3.1 Experimental Setup

Experimental setup is a combination of hardware and software modules, both functioning in together for brinjal plant disease detection, and modules are as follows.

3.1.1 Hardware

The images are captured by FLIR one camera, which can be interfaced with the smartphone. The smartphone which we have used in this work is Motorola G6. The reason to choose this phone is that it has C-type USB slot so that this camera can be easily interfaced. Other smartphones with same feature can also be selected for this proposed model. This camera helps us to take the thermal images, and we have option to choose the palette of our choice. In the proposed work, we have chosen rainbow HC palette as it helps us to see the minute temperature difference.

3.1.2 Software

Thermal images acquired are cleaned to reach optimum-level acceptable quality for further processing, and the process is known as preprocessing of images and is done using MATLAB software. This software allows us to implement various filter algorithms, creation of user interfaces, segmentation techniques, and data analysis procedures. In preprocessing of images, techniques like image enhancement and noise filters are used to clean image, features linked with affected portions are extracted via segmentation techniques to process for disease identification, in data analysis standard parameters are correlated with segmented portions to conclude about infection in affected regions, and the processes mentioned are incorporated on a single platform through user interface built in MATLAB.

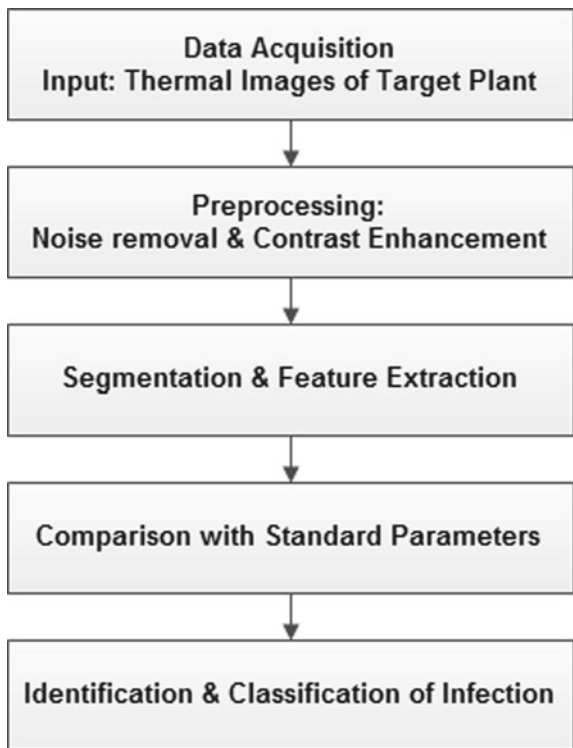
3.2 Proposed Methodology

For the detection of diseases, the following set procedure has been taken; the first step is thermal image acquisition, the second step is preprocessing, the third step is segmentation, and the fourth and last step is disease identification. Figure 3 shows the detailed flowchart of the procedure taken in this work.

3.2.1 Image Acquisition

The sample image was collected from a crop nursery, located at A block, Indira Nagar, Lucknow, images were acquired from 30 brinjal plants, images were captured in two

Fig. 3 Methodology proposed



sets, first set comprising healthy and infected thermal images and second comprising normal RGB capture of healthy and infected images, and 40 to 45 images per crop per set were acquired, total dataset analyzed had 2160 images; Fig. 4 depicts thermal samples collected.

3.2.2 Thermal Image Preprocessing

Images acquired were subjected to preprocessing steps that involved cleaning and contrast enhancement of acquired thermal image of brinjal leaves, in cleaning images are first processed for noise removal and image degradation, this is achieved by the adaptive median filter and wiener filter, after noise removal dataset is further processed to improve image contrast, and dualistic sub-image histogram equalization is employed for the process as depicted in Fig. 5. The processed dataset comprising two sets each having healthy and infected categories is then fed for classification to BoF.

Fig. 4 Sample of thermal dataset acquired

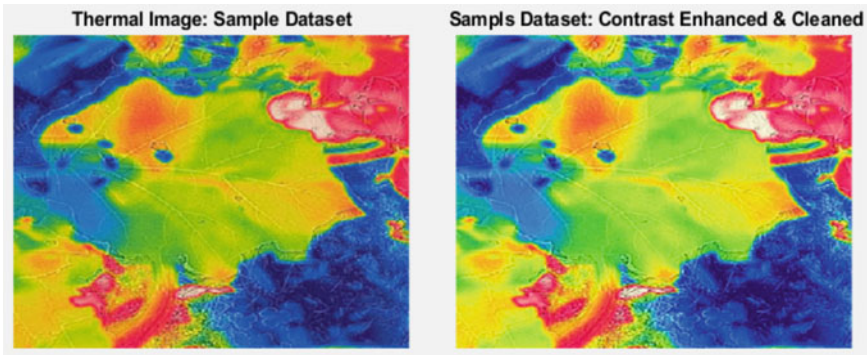
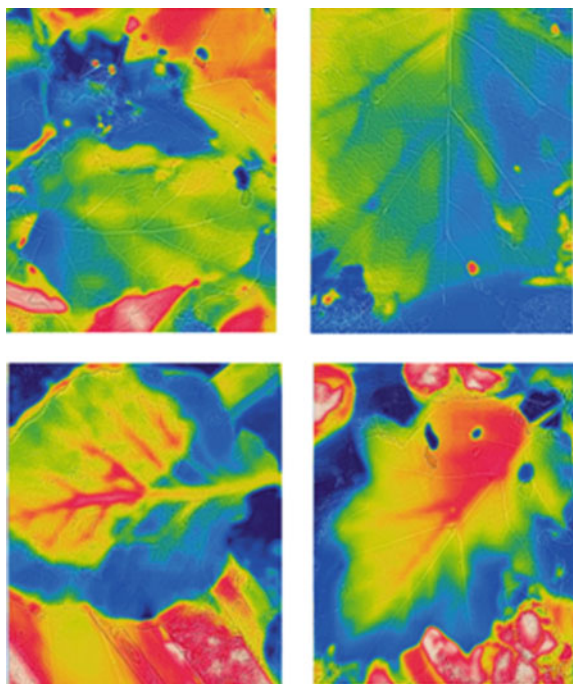


Fig. 5 Preprocessed image

3.3 Classification: BoF

Bag of feature has been employed for disease classification of the brinjal plant; two datasets one for thermal images and other for RGB images of healthy and infected leaves are passed to the training model, one set at a time to train the network. Once trained, the classifier is capable of efficiently classifying infected crops. BoF

primarily involves five steps, feature extraction, codebook creation, encoding feature, feature pooling, and learning and classification phase.

The primary objective is to identify features which is achieved by the quantization of local descriptors of images in the dataset according to visual vocabulary. The vocabulary is formulated by clustering a large volume of local descriptors employing the K-means algorithm. The algorithm processes the training data as input and clusters of similar datasets as output. The individual cluster would be described by one visual feature. Images will now be depicted as a BoF. Features are extracted in two phases; in first, patches are sampled employing their interest points [17] or densely with a regular grid. In second, the extraction of features and descriptors is obtained. The dataset with thermal capture of healthy and infected samples is first fed, and implementation process can be summarized as follows:

1. Acquiring Data: The sample image was collected from a crop nursery, located at A block, Indira Nagar, Lucknow, images were acquired from 25 brinjal plants, images were captured in two sets, first set comprising healthy and infected thermal images and second comprising normal RGB capture of healthy and infected images, 30 to 35 images per crop per set were acquired, total dataset analyzed had 1160 images, and dataset obtained was cleaned and labeled as healthy and infected. The process was first performed on thermal dataset.
2. Feature Identification and Segregation: Objective is to segregate a representative group of images with the most significant information in the data. After identifying the critical features in each dataset, computation of vector takes place which describes the features. The tasks of object recognition and image categorization are completed using SIFT descriptor. SIFT descriptor consists of feature extraction and detection both. Figure 6 depicts creation of BoF for thermal healthy and infected images and extraction of features.
3. Formulation of Codebook and Quantization: In encoding phase, the local descriptor is obtained in a new form by utilizing visual vocabulary.
 - (a) Codebook formulation: K-means clustering—Construction of visual vocabulary: A vector quantization technique is utilized. In this, N descriptors are partitioned into K clusters; here, each descriptor is associated with a cluster with closest mean. Trial-and-error iterations lead to $K = 500$ that gave optimum result, as K need not be sufficiently large and not too small too for a feature set of magnitude 1,587,788. K-means clustering of healthy and infected thermal images is depicted in Fig. 7.
 - (b) Encoding: BoF methodology for encoding converts the local descriptor into a more adapted form through codebook [1, 12]. Soft assignment algorithm has been utilized in this case; it keeps more information about the original image features.
4. Classification Phase: During categorization of image, the primary objective is to automatically annotate images with predefined groups. Image labels are predicted as soon as descriptors are extracted using a set of classifiers. BoF

Creating Bag-Of-Features.

- * Image category 1: Thermal Images-Healthy Leaf
- * Image category 2: Thermal Images-Infected Leaf
- * Selecting feature point locations using the Grid method.
- * Extracting SURF features from the selected feature point locations.
- ** The GridStep is [8 8] and the BlockWidth is [32 64 96 128].

- * Extracting features from 292 images in image set 1...done. Extracted 7992368 features.
- * Extracting features from 233 images in image set 2...done. Extracted 8778432 features.

- * Keeping 80 percent of the strongest features from each category.

Fig. 6 Feature extraction of healthy and infected thermal images

- * Using K-Means clustering to create a 500 word visual vocabulary.
- * Number of features : 1587788
- * Number of clusters (K) : 500

- * Initializing cluster centers...100.00%.
- * Clustering...completed 60/100 iterations (~39.87 seconds/iteration)...converged in 60 iterations.

- * Finished creating Bag-Of-Features

Fig. 7 K-means clustering of healthy and infected thermal images

employed SVM classifier from machine learning toolbox for classification. For the task, we have two categories of labeled dataset as healthy and infected.

Several “one-versus-all” classifications are performed for discriminating the multi-class problem. One-versus-all MLSTSVM—In this methodology, training of each class is done with rest of the other classes. Assume the scenario of K class, and OVA MLSTSVM classifier solves K-linear equations and generates K non-parallel hyperplanes, one hyperplane for each class.

Hyperplanes for the classification of images are obtained such that data points of each class lie in the close affinity of its respective hyperplane and maintain a clear separation. *i*th hyperplane is obtained as given in Eq. 1:

$$f_i = (w_i x) + b_i = 0 \quad (1)$$

where $w_i \in R_n$ refers to the normal vector to the hyperplane and $b_i \in R$ refers to the bias term. The objective function of i th linear OVA MLSTSVM classifier is expressed as given in Eq. 2:

$$\begin{aligned} \min(w_i, b_i, \xi_i) & \frac{1}{2} \|X_i w_i + e_{i1} b_i\| + \frac{c_i}{2} \xi_i^T \xi_i \\ \text{s.t. } & (Y_i w_i + e_{i2} b_i) + \xi_i = e_{i2} \end{aligned} \quad (2)$$

where c_i denotes penalty parameter, $e_{i1} \in R_{l_i}$ and $e_{i2} \in R_{l-l_i}$ are two vectors of one's, and ξ_i is the slack variable. OVAMLSTSVM classifier decision function that classifies samples as healthy or infected is given in Eq. 3:

$$d(x) = \arg \min_{i=1 \dots K} \frac{|w_i x + b_i|}{\|w_i\|} \quad (3)$$

5. **Performance of Model:** The algorithm trained the image category classifier for 2 categories—healthy and infected, following which encoding was done for each category and finished training the category classifier. Confusion matrix and accuracy achieved for the images with BoF are depicted in Fig. 8.

The procedure for classification was repeated for RGB dataset of healthy and infected images; Fig. 9 depicts the confusion matrix and accuracy achieved for RGB images.

4 Result and Discussion

The experiment for the methodology proposed was conducted to estimate efficiency of disease identification through thermal images as compared to RGB images; for the experiment, dataset was collected from a crop nursery located in Lucknow, images were acquired from 25 brinjal plants, images were captured in two sets, first set comprising healthy and infected thermal images and second comprising normal RGB capture of healthy and infected images, 30 to 35 images per crop per set were acquired, total dataset analyzed had 1160 images, and the process of identification was implemented via BoF, under the umbrella; feature extraction was carried out by SIFT operator, and classification was performed using classification MLSTSVM; results obtained are displayed in Table 2; strongest features were retained for the K-means clustering before classification. Classification took 60 iterations for thermal images whereas 51 iterations for RGB images; duration of the process was less for RGB images by a margin of approximately 6 secs, but the accuracy efficiency achieved was more for thermal images by margin of 3%, having 87% in all. From the results,

Evaluating image category classifier for 2 categories.

- * Category 1: Thermal Images-Healthy Leaf
- * Category 2: Thermal Images-Infected Leaf
- * Evaluating 292 images from category 1...done.
- * Evaluating 233 images from category 2...done.
- * Finished evaluating all the test sets.
- * The confusion matrix for this test set is:

KNOWN	PREDICTED	
	Thermal Images-Healthy Leaf	Thermal Images-Infected Leaf
Thermal Images-Healthy Leaf	0.92	0.08
Thermal Images-Infected Leaf	0.18	0.82

- * Average Accuracy is 0.87.

Fig. 8 Confusion matrix and accuracy achieved for thermal images with BoF

it can be concluded that however duration required for the identification was more for thermal images but still percentage accuracy is more for thermal images. The algorithm proposed can be very useful for more accurate disease identification of crops with a little compromise on duration elapsed for identification.

5 Conclusion

Damages caused due to erratic environmental conditions, diseases, and pest attacks cause substantial losses in the yield and quality of vegetables produced worldwide. Food and Agriculture Organization (FAO) report says that more than half world's population depends on agriculture for their survival. Paper proposes an algorithm to identify infected leaves and thus plant for early remedial action, the process is executed by analyzing thermal and RGB images of Brinjal leaves, and BoF has been employed for classification procedure. Simulation was implemented using MATLAB 2018b. Classification took 60 iterations for thermal images whereas 51 iterations for RGB images; duration of the process was less for RGB images by a margin of approximately 6 secs, but the accuracy efficiency achieved was more for thermal images by margin of 3%, having 87% in all. From the results, it can

Evaluating image category classifier for 2 categories.

- * Category 1: Healthy Leaves
- * Category 2: Infected Leaves
- * Evaluating 236 images from category 1...done.
- * Evaluating 291 images from category 2...done.
- * Finished evaluating all the test sets.
- * The confusion matrix for this test set is:

		PREDICTED	
KNOWN		Healthy Leaves	Infected Leaves
Healthy Leaves		0.81	0.19
Infected Leaves		0.13	0.87

* Average Accuracy is 0.84.

Fig. 9 Confusion matrix and accuracy achieved for RGB images with BoF

Table 2 Obtained parameters values for thermal and RGB images

Type of image/algorithm parameters	Healthy leaf features extracted	Infected leaf features extracted	Strongest features employed for K-means	Iterations	Duration (s)	Accuracy (%)
Thermal	7,992,368	8,778,432	1,587,788	60	39.87	87
RGB	9,180,288	9,297,064	1,475,302	51	33.22	54

be concluded that however duration required for the identification was more for thermal images but still percentage accuracy is more; thus, thermal image-assisted algorithm can be employed for crops in remote scenarios where accuracy plays a vital role. The proposed model can also be used for other crop plants as well with minor modifications in methodology.

References

1. Alston JM, Pardey PG (2014) Agriculture in the global economy. *J Econ Perspect* 28(1):121–146
2. Wen D, Ren A, Ji T et al (2020) Segmentation of thermal infrared images of cucumber leaves using K-means clustering for estimating leaf wetness duration. *Int J Agric Biol Eng* 13(3):161–167
3. Zeng X, Miao Y, Ubaid S, Gao X et al (2020) Detection and classification of bruises of pears based on thermal images. *Postharvest Biol Technol* 161. <https://doi.org/10.1016/j.postharvbio.2019.111090>
4. www.apeda.in/agriexchange/
5. www.kisansuvidha.com;brinjal-diseases/
6. www.indiastat.com/agriculture-data/2/stats.aspx
7. Lydia MS, Aulia I, Jaya I et al (2019) Preliminary study for identifying rice plant disease based on thermal images. *J Phys Conf Ser* 1566; 4th international conference on computing and applied informatics 2019 (ICCAI 2019), 26–27 November 2019, Medan, Indonesia
8. Haris KM, Kumar S, Mishra S, Pragya (2018) Precision crop monitoring for sugarcane and corn. *Int J Latest Trends Eng Technol* 9(3):289–293. e-ISSN: 2278-621X
9. Kumar S, Mishra S, Khanna P, Pragya (2017) Precision sugarcane monitoring using SVM classifier. *Procedia Comput Sci* 122:881–887. Information Technology and Quantitative Management (ITQM 2017), Elsevier
10. Raza S-e-A, Prince G et al (2015) Automatic detection of diseased tomato plants using thermal and stereo visible light images. *PLoS Journal*
11. Jones HG, Serraj R, Loveys BR et al (2009) Thermal infrared imaging of crop canopies for the remote diagnosis and quantification of plant responses to water stress in the field. *Funct Plant Biol* J
12. Ortiz-Bustos CM et al (2017) Use of blue-green fluorescence and thermal imaging in the early detection of sunflower infection by the root parasitic Orobanche cumana Wallr. *Advances in oil crops research. Front Plant Sci*
13. Bin Husin Z, Bin Abdul Aziz AH et al (2012) Feasibility study on plant Chili disease detection using image processing techniques. In: 2012 third international Conference on Intelligent Systems Modelling and Simulation
14. Jhuria M, Kumar A, Borse R (2013) Image processing for smart farming: detection of disease and fruit grading. In: Proceedings of the 2013 IEEE second international conference on image information processing (ICIIP-2013)
15. Meunkaewjinda A, Kumsawat P, Attakitmongkol K et al (2008) Grape leaf disease detection from color imagery using hybrid intelligent system. In: Proceedings of ECTI-CON 2008
16. Al-Hiary H et al (2011) Fast and accurate detection and classification of plant diseases. *Int J Comp Appl* (0975 – 8887) 17(1)
17. Khirade SD, Patil AB (2015) Plant disease detection using image processing. In: IEEE conference
18. Phadikar S, Sil J (2008) Rice disease identification using pattern recognition. In: Proceedings of 11th international conference on computer and information technology (ICCIT 2008), 25–27 Dec 2008, Khulna, Bangladesh
19. Kumar S, Sharma B, Sharma VK, Poonia RC (2018) Automated soil prediction using bag-of-features and chaotic spider monkey optimization algorithm. *Evol Intell*, 1–12. <https://doi.org/10.1007/s12065-018-0186-9>.
20. Kumar S, Sharma B, Sharma VK, Sharma H, Bansal JC (2018) Plant leaf disease identification using exponential spider monkey optimization. *Sustain Comput Inf Syst* 28. <https://doi.org/10.1016/j.suscom.2018.10.004>

Preterm Delivery Prediction Using Gradient Boosting Algorithms



Monarch Saha, Soumen Nayak, Nirjharini Mohanty, Vishal Baral,
and Imlee Rout

Abstract Even with the scientific and medical advancements in today's world, the number of preterm births keeps increasing. The preterm babies continue to face the consequences of their early birth, lifelong. If predicted accurately, these agony experiences with financial exhaustion can be dodged, with proper care and attention. The preterm delivery means when babies are born before the thirty-seventh week of pregnancy, arise of infants, who has a greater risk of death than those born at full term. This work will intimate the mother about the preterm delivery, so that they can take proper precaution and both mother and child will be healthy during the birth time. The classification method in machine learning has enabled us to attain the desired goal in most of the spheres of biomedicine. The need for accuracy calls out for the best possible classification method for a prediction that can help both the mothers and their babies. This paper's central idea is figuring out if the birth is going to be premature or not by implementing gradient boosting classifiers of machine learning and conducting a comparative study between two such classification algorithms, namely XGB classifier and LGBM classifier, to select the most precise algorithm for prediction. The paper additionally highlights the factors on which the final deduction is made.

Keywords Machine learning · Gradient boosting · Preterm deliveries · Classification algorithms

M. Saha · N. Mohanty · V. Baral · I. Rout

Department of Computer Science and Information Technology, ITER, S.O'A Deemed to be University, Bhubaneswar, India

S. Nayak (✉)

Department of Computer Science and Engineering, ITER, S.O'A Deemed to be University, Bhubaneswar, India

e-mail: soumennayak@soa.ac.in

1 Introduction

Preterm or premature birth occurs in only 11 births out of a hundred but somehow has managed to be the leading cause of deaths in infants. While the average gestation period in a human lasts for around 40 weeks, the children born before 37 weeks are considered premature babies [1, 2]. The early delivery of a child can be due to the untimely rupture of the membranes, premature labor, or induced labor ahead of time for the advantage of both mother and the child [1]. Even factors like the environment and the circumstances in which the mother is living, health conditions and proper care, and inherited genes can affect the duration of a woman's gestation period eventually concluding if the baby will be healthy and delivery will be with complexities or not [3].

The paper on preterm birth by García-Blanco et al. [17] explores the threat of preterm labor in women. And they have also worked on the effect of stress bookmarks on preterm birth. The women who were pregnant for 24 to 31 gestational weeks are threatened for preterm labor.

As the consequences are dire, in preterm deliveries, the need for extensive care is necessary. Some of the inconveniences and risks during the delivery can be not receiving adequate or complete prenatal care absence, among other factors [2]. The call for a suitable method of prediction is urgent. The infant mortality can be reduced with the help of beforehand understanding of the pregnancy. We intend to do just that by using classification algorithms and focusing on the comparative study between two of the classifiers.

When it comes to the medical industry, the prognosis of various diseases or disorders is notably favorable. It gives healthcare professionals a head start to provide patients with the best possible treatment, services, and adequate maintenance preparation. The application of machine learning on proper medical datasets can help humankind achieve those, as mentioned earlier. By feeding the algorithms a set of data, the classifiers will learn and predict the necessary details regarding the patient like recovery and progress among other constituents [4]. When it concerns both regression and classification, the gradient boosting of regression trees provides us with competitor, remarkably robust, understandable methods, and is eminently suitable for mining somewhat unclear data [5].

This paper revolves around the central idea of finding out the particular classifier among eXtreme gradient boosting (XGB) classifier and light gradient boosting machine (LGBM) classifier that performs better in the prognosis of premature birth in a set of various cases. Most of the time, the application of boosting to a classification algorithm enhances the same performance. The procedure followed to attain this is by sequentially employing any one of the classifiers to numerous reweighted variants of the training data and selecting a weighted majority vote of the classifiers' array consequently generated [6].

2 Related Work

As evident in the previous section, it is highly needed for the pregnancies to be held under systematic review. The desperate demand for proper prediction and care was stated by Ahumada-Barrios et al. [2] in their paper while calling out the medical facilities being unable to handle a proper premature delivery. The authors concluded that the risk factors for premature births are absence or inadequacy of care before birth, a history of the patient dealing with premature delivery, etc. And that, there can always be further research. The study focused on the risks that could be faced by the pregnancy to be avoided along with the essential need to prevent premature deliveries by taking a step forward to enhance prenatal care, early detection, etc.

A lot of research and predictions have been conducted on any medical dataset. The implementation of machine learning helps by predicting the value or giving the desired outputs based on the dataset's analysis. One of the many deployments is the study conducted by Li and Zhang [7]. The main focus was to develop a model to predict the orthopedic auxiliary and provide better treatment. It focuses on the treatment and caring of the musculoskeletal system. The use of an XGB classifier to create an orthopedic additional classification prediction model was studied upon.

The research paper on gastric cancer risk by Taninage et al. [8] used machine learning classifiers. The study is centering the cause to improve patients' prediction accuracy at higher or lower risk of raising gastric cancer. The model of the paper was generated by XGBoost classification. The authors worked on an 80–20 split and finally concluded that the XGBoost model gave a higher accuracy than logistic regression.

The XGB model was used by Dong et al. [9] to predict the concrete of electrical resistivity derived from the demonstration of the database. The XGB algorithm generates the prediction model in which all the factors are given to get the desired outcome on the electrical resistivity. The experiment was done on data with 16 different attributes for experimentation purposes. The factor or the statistics used to evaluate the model was RMSE, MAE, and R2. The result of the training and testing data on the XGB model demonstrated by the regression fitting line's high coefficient value is 0.991 and 0.943, respectively.

In the Sentimental Analysis of Drugs research paper by Bemila et al. [10], there was an analysis of data on the price, user experiences, proper dosage, and side effects of the drugs and many prediction models are derived like the LSTM model and LGBM classifier, whose input was the dataset with certain health conditions in any case and gave an accuracy of 83%.

Acknowledging the involvement of machine learning in the cases of preterm deliveries, we can shed light on the research conducted by Fergus et al. [11] by applying machine learning to the results and data of electrohysterography to predict the premature birth of an infant. The paper gave an AUC value of 55% on the clinical dataset.

Article by Linda et al. [12] discussed the risk of preterm (premature) birth while revealing that almost 8–12% of deliveries can be premature in the USA. After

applying machine learning algorithm and data analysis on various datasets, a prediction model was built to determine preterm delivery with an accuracy of 53–88%. Dyne et al. [13] used machine learning and statistical analysis to build a prototype expert system with an accuracy of 53–88%. The experiment was carried on with the help of a dataset with 9,419 prenatal records. Researchers applied machine learning in field medical field for prediction of disease like COVID-19 [14–16].

3 Backgrounds

Data mining is one of the most crucial and necessary aspects of biomedical data analysis. Data mining is the process of extracting useful and significant information from large volumes of raw data using various statistical and analytical techniques. Data mining can be applied to any dataset to extract data from enormous medical datasets that can be used to train and test the machine to predict future cases according to specified parameters with the maximum accuracy. This paper revolves around the idea of using two classification algorithms on a premature delivery dataset and then compares those algorithms to find out which of those two classifiers can predict if someone is going to deliver a preterm baby accurately.

In this work, we are comparing between two gradient boosting machine-based classification algorithms called XGB and LGBM classifiers.

XGB Classifier: XGB classifier also stands for the eXtreme gradient boosting machine classifier. It is mainly an implementation of standard gradient boosting machines. XGB classifier is a library that offers various features and has the prime focus on classification of model, execution speed, and performance of the model. XGB classifier mainly focuses on speed of execution and hence becomes fast, i.e., more quickly than other gradient boosting classifiers as shown in Fig. 1.

LGBM Classifier: The light gradient boosting machine classifier is another type of a gradient boosting algorithm, where it is based on the gradient-based one-side sampling (GOSS) technique to find a value to split the dataset and also speeds up the training process. It has a higher accuracy among any other gradient boosting algorithm; also, it breaks the tree down by node/leaf (Fig. 2) while still not being heavy on the resources it is implemented on.

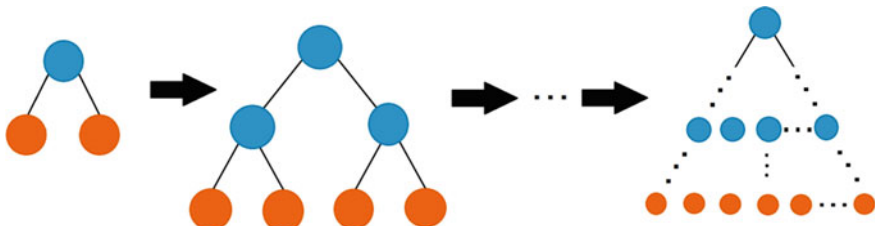


Fig. 1 Level-wise split in eXtreme gradient boosting

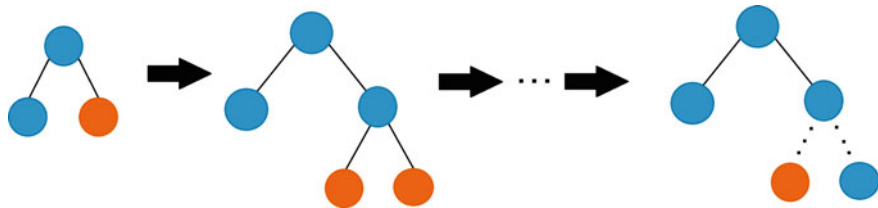


Fig. 2 Leaf-wise split in light gradient boosting machine

4 Result and Discussion

In this paper, we use the premature delivery dataset (from Kaggle) in order to get the machine trained and tested and be ready for predicting preterm delivery with the highest precision possible. The premature delivery dataset contains a huge set of data classified into 14 columns carrying 391 rows of data. The variables predictive are expressed as follows:

1. GEST: Gestational age (in weeks)
2. DILATE: Cervical dilation (in cm)
3. EFFACE: Effacement of the collar (in %)
4. CONSID: Consistency of the neck (1 = soft, 2 = medium, 3 = firm)
5. CONTR: The presence (=1) or not (=2) of contraction
6. MEMBRAN: Membranes ruptured (=1) or not (=2) or uncertain (=3)
7. AGE: The patient's age
8. STRAT: Period of pregnancy
9. GRAVID: Number of previous pregnancies inclusive of the current one
10. PARIT: Parity (number of previous term pregnancies)
11. DIAB: Presence (=1) or not (=2) of a diabetes problem or missing value (=9)
12. BEBAGE: Gestational age (in days) of the baby at birth
13. TRANSF: Transfer (=1) or not (=2) to a hospital for specialized care
14. GEMEL: Single (=1) or multiple (=2) pregnancies.

In the premature delivery dataset, the target class or the variable to be predicted is:

PREMATURE: Premature delivery (positive or negative).

Positive: The patient is susceptible to have a premature delivery.

Negative: The patient is not susceptible to have a premature delivery.

In this work, the dataset is used to train and test the model to classify whether the patient has a chance of premature delivery or not. The training data is used to train the data by making it acquainted with the columns and values. The testing data is used to test the model for accuracy, i.e., check how accurately the model predicts if the patient has a chance of premature delivery against the actual result that is in the table. For doing that, we split the data in the dataset into two parts which is also known as the train-test split. In this experiment, the dataset is split into 80% of training data

Table 1 Average precision, precision, and recall of the classifiers

Classification algorithm	Avg. precision	Precision	Recall
LGBM classifier	0.538	0.534	0.648
XGB classifier	0.501	0.506	0.61

and 20% of testing data. Scaling law has proved that the 80/20 spilt gives a better accuracy value and also improves the precision, recall, and f1-score.

The classification techniques that we use in this paper to compare between are XGB classifier and LGBM classifier, both of which are types of gradient boosting machine classifiers. In this experiment, we came to find that both the classification techniques showcase different levels of accuracy and various other performances examining parameters.

Firstly, the factor that affects the model in prediction is average precision, precision, and recall. Table 1 represents the values corresponding to the classifiers.

Average Precision: Average precision is calculated by calculating the area covered under both the curve of precision and curve of recall. The value of the area covered always ranges between 0 and 1. It is denoted as

$$AP = \int_0^1 p(r)dr \quad (1)$$

Precision: Precision is used to calculate the accuracy of the model with respect to prediction. It is the ratio of the true positives (TPs) with respect to the total cases of positives which is the sum of true positives (TPs) and false positives (FPs).

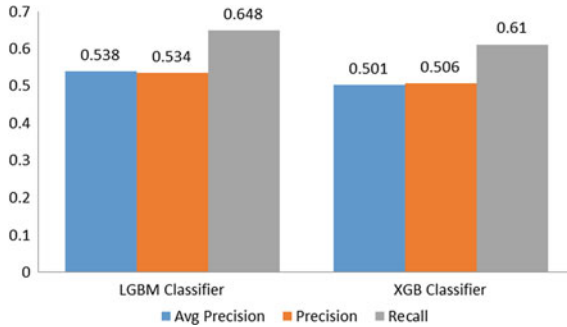
$$\text{Precision} = \frac{\text{TP}}{\text{TP} + \text{FP}} \quad (2)$$

Recall: Recall calculates the true positives (TPs) which was accurately predicted by the classification model.

$$\text{Recall} = \frac{\text{TP}}{\text{TP} + \text{FN}} \quad (3)$$

After observing Graph 1, the value of precision for LGBM classifier is 0.534 and value of XGB classifier is 0.506, whereas the average precision of LGBM classifier is slightly greater than XGB classifier. So, for better clarity, the next measuring factor is accuracy for both the classifiers in Table 2.

Accuracy: Accuracy is the criteria that define the fitness of the classification algorithm. It describes the ratio of the number of correct predictions with respect to the total number of cases.



Graph 1 The bar and line graph comparing the attributes of LGBM and XGB classifiers

Table 2 Accuracy of LGBM and XGB classifiers

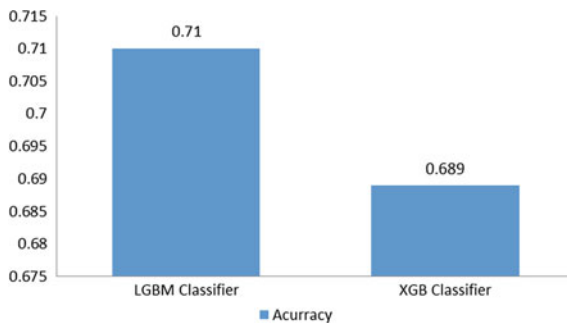
Classification algorithm	Accuracy
LGBM classifier	0.71
XGB classifier	0.689

$$\text{Accuracy} = \frac{\text{Number of correct predictions}}{\text{Total number of predictions}} \quad (4)$$

From Graph 2, we can clearly see that the accuracy value of LGBM classifier is 0.71 which is 71%, whereas the accuracy value of XGB classifier is 0.689 which is 68.9%. The other factors like F1 score, Log Loss, Normalized Gini Coefficient, ROC AUC, and the model's build time are represented in Table 3.

F1-Score: It is a better measuring factor to seek a balance between the recall and precision and use the uneven class distribution. It is represented by:

$$F1 = 2 \times \frac{\text{Precision} \times \text{Recall}}{\text{Precision} + \text{Recall}} \quad (5)$$



Graph 2 Bar and line graph comparing the accuracy of the two algorithms

Table 3 Additional attributes of the algorithms

Classification algorithm	F1	Log loss	Normalized Gini coefficient	ROC AUC	Build time (in sec)
LGBM classifier	0.584	0.669	0.4	0.766	1
XGB classifier	0.551	0.606	0.363	0.745	1

Log Loss: This loss function is used in extension of logistic regression and also in logistic regression. It is defined as the negative value of log-likelihood of a logistic model. It is said that lesser the log loss is equivalent to the higher the accuracy score of the classification.

Normalized Gini Coefficient: It is used to find how far away we are with our sorted actual values from random state measured in number of swaps:

$$\text{NGini} = \frac{\text{Srandom} - \text{Ssorted}}{\text{Srandom}} \% \quad (6)$$

where Srandom is the random state and Ssorted is the sorted actual values.

ROC AUC: It is used to measure the different threshold settings of classification problem. ROC is representing the probability curve, and AUC is used to define the degree or measure of separability. By analogy, the model with better result will have higher AUC value.

From Graph 3 depicted, we can observe that the LGBM classifier is able to predict if a patient is susceptible to premature delivery with higher accuracy and precision as compared to the XGB classifier.

The comparison is made with the García-Blanco et al. [17] who have used predicting of preterm birth in women, and they have used parametric survival model which was based on α -amylase, cortical, age, parity, and multiple pregnancy factors.

After observing Table 4 for the prediction of the preterm delivery, García-Blanco et al. [17] model's AUC value and the proposed work (the LGBM Classifier and

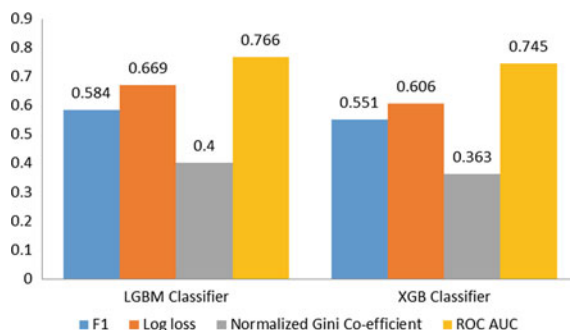
**Graph 3** Graphical representation of the factors in Table 3

Table 4 Comparative study using AUC value

Classification algorithm	AUC	AUC percentage (%)
Previous work [17]	0.63	63
Proposed work	0.766	76.6

XGB Classifier) AUC values are 0.63, 0.766, and 0.745, respectively. The previous work's AUC value is comparatively less than the proposed classifier obtained values.

There are various other factors that contribute to the performance of a classification model. For the two classifiers used in this paper, those factors are:

Considering all the observations above, it can be concluded that among the two classification techniques, namely LGBM classifier and XGB classifier that were used as a medium of comparison to find the classification technique with more accurate prediction, the LGBM classifier is able to predict if a patient is susceptible to premature delivery with higher accuracy of 0.71 (71%) and higher precision of 0.534 (53.4%) than the XGB classifier which has the accuracy of 0.689 (68.9%) and precision of 0.506 (50.6%).

5 Conclusions

The comparative study was done between the two classification algorithms, particularly, the eXtreme gradient boosting (XGB) classifier and LightGBM classifier on the premature data with a split of 80–20 for training–testing dataset, respectively. The objective was to find a better prediction model among the two to predict an infant's premature birth. As shown in Table 2, the accuracy value of the LGBM classifier is 71%, whereas the accuracy value of the XGB classifier is 68.9%. Therefore, LGBM is better at predicting classifiers over the XGB classifier. The average precision value of LGBM is 0.538, which is greater than the XGB classifier average precision value of 0.501. The comparison study shows the better AUC value we got from the proposed work. In the future, there will be more techniques to predict with better accuracy on the targeted dataset. Furthermore, different models and algorithms can be combined to get more accurate predictions.

References

1. Goldenberg RL, Rouse RJ (1998) Prevention of premature birth. *N Engl J Med* 339(5):313–320
2. Ahumada-Barrios ME, Alvarado GF (2016) Risk Factors for premature birth in a hospital. *Revista latino-americana de enfermagem*, vol 24
3. Muglia LJ, Katz M (2010) The enigma of spontaneous preterm birth. *N Engl J Med* 362(6):529–535
4. Rajkomar A, Dean J, Kohane I (2019) Machine learning in medicine. *N Engl J Med* 380(26):2588–2588
5. Friedman JH (2001) Greedy function approximation: a gradient boosting machine. *Ann Statist*, 1189–1232
6. Friedman J, Hastie T, Tibshirani R (2000) Additive logistic regression: a statistical view of boosting (With discussion and a rejoinder by the authors). *Ann Statist* 28(2):337–407
7. Li S, Zhang X (2020) Research on orthopedic auxiliary classification and prediction model based on XGBoost algorithm. *Neur Comput Appl* 32:1971–1979
8. Taninaga J, Nishiyama Y, Fujibayashi K (2019) Prediction of future gastric cancer risk using a machine learning algorithm and comprehensive medical check-up data: a case-control study. *Sci Rep* 9
9. Dong W, Huang Y, Lehane B, Ma G (2020) XGBoost algorithm-based prediction of concrete electrical resistivity for structural health monitoring. *Autom Constr* 114:103–155
10. Bemila T, Kadam I, Sidana A, Zemse S (2020) An approach to sentimental analysis of drug reviews using RNN-BiLSTM model. In: Proceedings of the 3rd international conference on advances in science & technology (ICAST)
11. Fergus P, Cheung P, Hussain A, Al-Jumeily D, Dobbins C, Iram S (2013) Prediction of preterm deliveries from EHG signals using machine learning. *PLoS ONE* 8(10):e77154
12. Woolery LK, Grzymala-Busse J (1994) Machine learning for an expert system to predict preterm birth risk. *J Am Med Inf Assoc* 1(6):439–446
13. Van Dyne MM, Woolery L, Gryzmala-Busse J, Tsatsoulis C (1994) Using machine learning and expert systems to predict preterm delivery in pregnant women. In: Proceedings of the tenth conference on artificial intelligence for applications, pp 344–350, San Antonio, TX, USA
14. Singh V, Poonia RC, Kumar S, Dass P, Agarwal P, Bhatnagar V, Raja L (2020) Prediction of COVID-19 corona virus pandemic based on time series data using Support Vector Machine. *J Discrete Math Sci Cryptogr*, 1–15
15. Bhatnagar V, Poonia RC, Nagar P, Kumar S, Singh V, Raja L, Dass P (2020) Descriptive analysis of COVID-19 patients in the context of India. *J Interdiscip Math*, 1–16
16. Kumari R, Kumar S, Poonia RC, Singh V, Raja L, Bhatnagar V, Agarwal P (2020) Analysis and predictions of spread, recovery, and death caused by COVID-19 in India. *Big Data Min Anal*. <https://doi.org/10.26599/BDMA.2020.9020013>
17. García-Blanco A, Diago V, De La Cruz VS, Hervás D, Cháfer-Pericás C, Vento M (2017) Can stress biomarkers predict preterm birth in women with threatened preterm labor? *Psychoneuroendocrinology* 83:19–24

Analysis Urban Traffic Vehicle Routing Based on Dijkstra Algorithm Optimization



Truong-Giang Ngo, Thi-Kien Dao, Jothiswaran Thandapani, Trong-The Nguyen, Duc-Tinh Pham, and Van-Dinh Vu

Abstract The transportation cost, running vehicle time, duration, and distance cost, the route network of revealed urban vehicles, are considered to need to be analyzed meaningfully and reasonably planned. This paper suggests an analysis of urban traffic vehicle routing based on the Dijkstra algorithm optimization that is as a solution to the road selection and optimization under various constraints jointly built in the central metropolitan area. The leading metropolitan area road network's various constraints are to consider the road condition factors and the risk resistance in road planning. The analysis and realization are verified with the geocoding, network topology, and network analysis. The results show that the integration of network analysis technology and the Dijkstra algorithm realizes the urban vehicle route's optimization decision. Still, the improved Dijkstra algorithm reduces the number of node visiting and time complexity. Under the driving time and distance constraints, the speed limit, road hierarchy, and road condition are the line selection's restrictive factors. The graphical description could provide technical support and reference for the driver's driving strip and traffic management department for decision making.

Keywords Urban traffic · Dijkstra algorithm · Constraint conditions · Path analysis

T.-G. Ngo

Faculty of Computer Science and Engineering, Thuyloi University, Hanoi, Vietnam

T.-K. Dao · J. Thandapani · T.-T. Nguyen (✉)

Fujian Provincial Key Laboratory of Big Data Mining and Applications, Fujian University of Technology, Fuzhou, China

J. Thandapani

Anna University, Chennai, India

T.-T. Nguyen

Haiphong University of Management and Technology, Haiphong, Vietnam

D.-T. Pham

Center of Information Technology, Hanoi University of Industry, Hanoi, Vietnam

Graduate University of Science and Technology, Vietnam Academy of Science and Technology, Hanoi, Vietnam

V.-D. Vu

Faculty of Information Technology, Electric Power University, Hanoi, Vietnam

1 Introduction

Path observation is one of the research materials of an overview of urban traffic networks [1] and a part of the spatial analysis method's spatial analysis method [2]. It is commonly used in urban road maintenance, network coordination [3], traffic planning, and others [4]. The center of route analysis is the shortest path and the safest path, and the path optimization is to use the concept of tactical research planning to maximize the organizational efficiency and usage and road network, vehicle routing, delivery of goods, etc. [5]

In the case of confidence, there have been several studies on the shortest path analysis algorithm, e.g., Bellman algorithm [6], Dijkstra algorithm [7], and Dreyfus algorithm [8] have been the traditional algorithms. Nonetheless, under complexity, the shortest path problem can be loosely separated into four parts. This paper looks at the most straightforward path of random road length change, the shortest route with different cost functions, the shortest path with random road length change under the condition of time independence, and the shortest path of interval length.

Nevertheless, in the actual driving of urban vehicles, the above shortest path studies do not consider unknown considerations of the other road route conditions, e.g., rush hours, limited speed, or road situation [9]. Therefore, this study does more work focused on optimization allocation based on the Dijkstra algorithm. First, the urban road network is transformed into a driven graph, including nodes and connections, using the geographic information network mapping technology. The municipal road is transformed into a directed graph. Second, we consider several factors, e.g., the type of route, node stay time, speed limit, the direction of driving of vehicles, and other factors. A starting point to the endpoint is measured and evaluated with the time and cost to optimize global results. It means that the time or expense from the starting point to the parameter is calculated according to the time cost and distance.

Besides the expense restriction considerations and the calculated optimum paths, the shortest route scenarios under unconstrained conditions [10], hazard road condition, and speed limit mode are also considered for testing on the spot.

2 Related Work

2.1 Dijkstra Algorithm

Dijkstra algorithm is a standard algorithm for finding the shortest path in graph theory proposed by Dijkstra, a Dutch computer scientist, in 1959 [11]. The algorithm can find the shortest path from a point in a graph to any other vertex. Dijkstra algorithm divides network nodes into three parts: unlabeled in the network graph, all nodes are initialized as unlabeled nodes. In the process of searching, the nodes that are connected in any path and travel nodes are temporarily marked nodes. In each cycle, the shortest path length from the origin point is searched from the temporarily marked

nodes as the permanently marked nodes until the nodes are found. As shown in Fig. 1, assuming that the origin point of the node network is node 0 and the target point is node 4, the shortest path distance between node 0 and node 4 is calculated (the length between nodes is assumed).

Suppose each node has a pair of labels (w_i, p_j) , w_i is the length of the shortest path from the origin point to the target point, w_j is the shortest path length from the origin point s to any node j (the shortest path from the vertex to itself is the zero path (the path without arc), and its length is equal to zero), and p_j is the length from the origin point s to the node j . The shortest path from the origin point I to the target node j is solved. The basic process is as follows:

- (1) Initialization. The origin point is set to
 - (i) If the shortest path length $w_s = 0$, p_s is null;
 - (ii) The path length of all other nodes is $w_i = \infty$, $p_i = s$;
 - (iii) Mark the origin point S . mark all marked nodes $k = s$, and set other nodes as unmarked.
- (2) Verify the distance from all marked nodes K to their directly connected unlabeled nodes J , and set

$$w_j = \min\{w_j, w_k + d_{kj}\} \quad (1)$$

where w_j is the shortest path length of unlabeled node j , w_k is the shortest path length of labeled node k , and d_{kj} is the direct connection distance from node k to node j .

- (3) Select the next point. From all unlabeled nodes w_j , select the smallest labeled node i , that is, $w_i = \min w_j$ (all unlabeled nodes j), and node i is selected as the point in the shortest path and set as the marked point

Fig. 1 Meshed network of the route

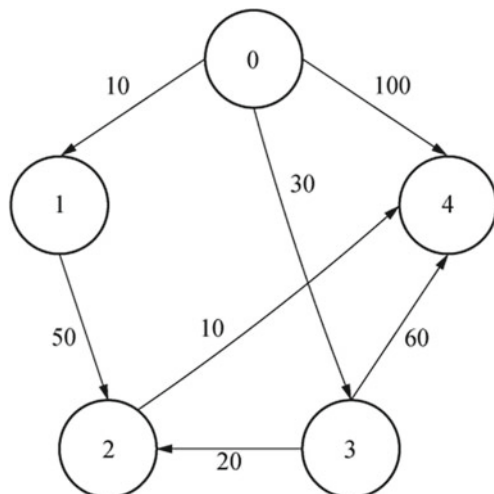


Table 1 List of an example of the shortest path of node 0 to node 4 processing

Cycle	Node set s	Number of marked nodes K	Distance d between node 0 and 1 D{0}	Distance d between node 0 and 1 D{1}	Distance d between node 0 and 2 D{2}	Distance d between node 0 and 3 D{3}	Distance d between node 0 and 4 D{4}
Initialization	{0}	–	0	10	∞	30	100
1	{0,1}	1	0	10	60	30	100
2	{0,1,3}	3	0	10	50	30	90
3	{0,1,3,2}	2	0	10	50	30	60
4	{0,1,3,2,4}	4	0	10	50	30	60

- (4) Find the previous point of node I . find the point j' directly connected to node i from the marked node. As the previous point, set $i = j'$
- (5) If all nodes have been marked, the algorithm will find the shortest path; otherwise, mark $k = i$ and go to step (2). Table 1 shows a list of an example of the shortest path of node 0 to node 4 processing.

2.2 Algorithm Optimization

The optimization is implemented based on the Dijkstra algorithm as follows: firstly, the temporary set NB_s of the starting point, the neighbor nodes k with the smallest distance is selected as the transition point, and at the same time, it is assigned to the identification set S . The union of the temporary set of all nodes in the identification set s and the difference set of the identification set ($\cup NB_s S, i \in S$), a node W_k with the minimum path distance value is selected as the next transition point and is assigned to the identification set S . Repeat the above process until all nodes are identified $|s| = n$, and the algorithm ends. Let NB_i be the temporary set of nodes i , S be the identification set, w_i be the shortest path length from source point s to node j , P_i be the previous node of j point in the shortest path from s to j , and D_{ij} is the distance from node i to node j .

- (1) Initialize identity collection $S = \{s\}$, $w_i = d_{si} \quad i \in NB_s$ otherwise $w_i = \infty \quad i \in NB_s; P_i = s$.
- (2) If the distance between k temporary set node and origin point is the smallest $d_{sk} = \min d_{si}$, then $S = S \cup \{k\}, j \in NB_s$
- (3) Modify the w_i value in k temporary set node $NB_k = S, w_i = \min\{w_i + d_{ki}\}$; if w_i value changes, then $P_j = k, j \in NB_s - S$
- (4) Select the minimum value of w_i in the marked temporary node, set a and classify it into s , $w_k = \min w_i, S = S \cup \{k\}$ if $|s| = n$, the node has been identified, and then the algorithm is terminated; otherwise, go to step (3).

For the network graph with n nodes, the Dijkstra algorithm needs a total of $n - 1$ iterations to solve the shortest path, and a new node is added to the temporary node set in each iteration. Because the number of nodes not in the temporary node set is $n - i$ in the i th iteration, then $n - i$ is needed in the i th iteration. The number of nodes processed is

$$\sum_{i=1}^{n-1} (n - i) = \frac{n(n - 1)}{2} \quad (2)$$

When the number of network nodes in Eq. (2) is n , the time complexity of the path solution is $O(n^2)$, which is the time complexity of the shortest path from the origin point to the other nodes in the network graph. With the increase of the total number of nodes n , the calculation efficiency and storage efficiency decrease.

The time complexity $O(n^2)$ depends on the number of elements in the temporary set NB_s of the transition point k , and then the space complexity of the optimization algorithm is $O(n \times P)$, where p is the space occupied by the node object under the adjacency matrix storage structure $N \times N$, which is a constant. According to the number of points and road sections, the average out degree e of nodes can be obtained, i.e.,

$$e = \frac{m}{n} \quad (3)$$

where m is the number of road sections.

Generally, in the geographic information system network diagram, $e \in [1, 4]$, because step (3) and step (4) are search and V_i ($i = 1, 2, 3, \dots, n$). The time complexity of step 4 is $O(m)$, i.e., $O(n \times e)$.

3 Model Construction

We assume the road network of a center city by generating randomly to facilitate the experiment. The vector elements of options are imported into the local geographic database, e.g., the expressway, national road, provincial road, and county road. The topological grade is specified as vector elements of the participating road network. The tolerance limit value, such as the speed limit and traffic restriction and turning model, is set up, and the road arc segment node is established. The cost and constraint variables are set according to the connection rule between the road network node and arc segment. The cost variable is path cost expense, and the attribute field of the constraint variable is a Boolean value, namely a single line or double line, respectively.

$$\begin{cases} R_w = (N, R, L_R) \\ R = \{(x, y) | x, y \in N, \text{ and } L(x, y)\} \\ L_R = \{l_{xy} | (x, y) \in R\} \end{cases} \quad (4)$$

where R_w represents the road network; N represents the node set; R represents the set of road sections, whose elements are ordered pair (x, y) , and indicates that there is a directed path from node x to node y ; L_R represents the weighted length of the section, and its elements $L(x, y)$ denote the weighted length of the directed section (x, y) ; l_{xy} is the length of any section from node x to node y .

The weighted length L_R of a road segment refers to the optimal path which is solved by integrating various dynamic and static attribute constraints according to the multi-objective function and planning requirements, rather than the actual distance or length of the path. Therefore, the optimal path not only refers to the shortest distance in the general geospatial sense. It can also be extended to time, cost, and line capacity.

Some constraints are also considered when nodes or sections in the network cannot operate due to some emergencies, such as traffic accidents, or the original optical path needs to be modified. For example, the road is under maintenance, the distance of the optimal path changes, and maintenance status. If there is a traffic accident at the intersection, it is temporarily not passable; that is, the nodes in the network cannot run, thus, prolonging vehicles' travel time.

The comprehensive road resistance C of any path is calculated by the weighted summation method

$$C = \sum_{i=1}^n C_i = \sum_{i=1}^n (D_{i1}a_1 + D_{i2}a_2 + \dots + D_{ij}a_j) \quad (5)$$

where C_i is the comprehensive road resistance of section i , D_{ij} is the score of the road resistance factor, and a_j is the weight of j road resistance factor. A parameter is used to adjust the weight according to the situation of environmental conditions.

$$a_j^t = \mu \times a_j^{t-1} \quad (6)$$

where μ is an adjusting variable based on the scenario of environmental conditions.

The upper limit measure is used to calculate the D_{ij} a score of any road section, and the calculation formula is

$$D_{ij} = d_{ij} / d_{j,\max} \quad (7)$$

where D_{ij} is the score of j road resistance factor of section i ; d_{ij} is the actual value of road resistance factor; $d_{j,\max}$ is the maximum actual value of J road resistance factor.

Algorithm 1. The adjusted optimal path based on the Dijkstra algorithm

Input: A bi-directed graph with weights $D_{ij} = (N_{ij}; C_{ij})$, the set of all nodes N , and the set of weighted edges of connected nodes C . The source and target node n_s and n_t , respectively.

Output: Shortest path and the length from the source node n_s to the target node n_t

1: Initialization

Visited nodes $Ne = ns.d(ns) = 0$, where $d(nti)$ is the minimum cost of the shortest path from n_s to n_{ti} . $Nu = N - Ne$, where N_u is the set of nodes to n_s with the undetermined shortest path. $d(nti) = \min(C(ns; nti))$, if nti is a successor to n_s , or else, $d(n_{ti}) = 1$, where $C(i; j)$ is the cost between node i and node j as Eq. (5)

2: Repeat the following steps until there are no nodes in the set N_u

2.1 Put the node in N_u that has the minimum cost to the old n_s as the new source n_s . Move the new source node n_s to N_e ; adjust the weight according to the situation of environmental conditions as Eq. (6)

2.2 Set $d(n_{ti}) = d(n_s) + \min(C(ns; n_{ti}))$

3: Find the shortest path from the source node n_s to the target node n_t

4: Return $d(nt), N_e$

The initial work of the Dijkstra algorithm is only dealing with the shortest path between two points. Mathematically, these points must be represented by nodes in the graph network. Bellman Ford implemented the possibility of fixing

4 Results and Discussion

In order to test the performance of the proposed scheme, some lines assuming roads are generated randomly in a specified metro urban area based on the grid and sample points under constraints of the condition roads and obstacles. Table 2 lists the comparison of theoretical and actual driving time of the optimized route. It is seen that the travel time of the optimized route, the real travel time is longer, and the difference between the minimum and maximum travel time is 1.2 min and 2.9 min, respectively. In the obstacle mode, the driving time of line 4 is 1.0 min longer than that of line 3. The driving time of line 4 is 1.0 min longer than that of line 3. In the speed limit mode, the actual driving time of urban vehicles inline 5 is limited by road congestion, traffic capacity, and traffic information, which is 1.2 min longer than the real driving time on line 6 is 2.3 min longer than the theoretical driving time of line 6. In the case of a 30 s delay at the intersection node, the actual driving distance is more reasonable, and the real driving time is longer. Therefore, the node delay, road conditions, and speed limit are the main factors affecting the urban vehicle route selection. The number of nodes in the optimal path plays a leading role in the driving time and distance.

Figure 2a displays the setting for generating points in the road network. Figure 2b shows the generated obstacle maps and the roads' points as road network grade and speed limit mode, randomly prioritizing provincial roads, national highways, and urban trunk roads and then choosing urban secondary trunk roads and township roads. Figure 2c displays the proposed method's optimal paths close to the actual travel time and distance cost. Drivers would be advised as a priority to these kinds of

Table 2 Obtained results of the optimization of the Dijkstra algorithm for actual driving time and vehicle routing

Serial number	Line selection conditions	Distance (m)	Theoretical driving time (min)	Actual driving time (min)	Travel time difference (min)	Number of nodes
Line 1	The shortest distance in unlimited road class and speed mode	4377.8	10.7	11.9	1.2	19
Line 2	Minimum time in unlimited road class and speed mode	4385.2	9.7	11.5	1.8	17
Line 3	Shortest distance in obstacle mode	4610.3	10.7	12.1	1.4	20
Line 4	Shortest time in obstacle mode	4630.6	10.2	13.1	2.9	18
Line 5	The shortest distance under speed limit mode	4455.2	10.9	13.2	2.3	17
Line 6	The shortest time under speed limit mode	4739.3	10.5	12.0	1.5	21
Line 7	The delay time of 30 s at the node is the shortest	4463.3	15.9	18.4	2.5	17

conditions as assuming that the speed limit of trunk roads is 30 km/h, and of crowded streets is 35 km/h. In the speed limit mode, the shortest path needs to drive 4455.3 m, and the travel time cost is 13.2 min.

Figure 2d shows the shortest distance between Hoabinh park and the Linhnam-Hoang Mai, Hanoi, as an example of the most straightforward under the condition of daily road status and vehicle speed in the middle afternoon. Assuming that Hoa Bin the park, Hanoi is the initial source point and the Linhnam–Hoangmai, Hanoi as the target node, the optimal distance, and time path between Hoa Bin park and

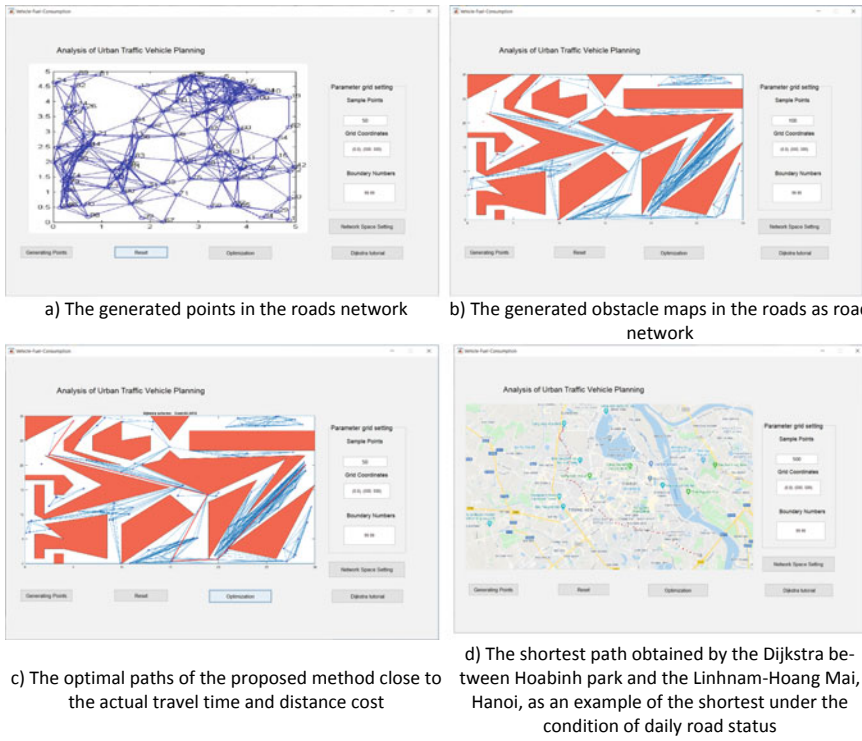


Fig. 2 Proposed scheme's optical paths based on the Dijkstra for analysis of urban traffic vehicle routing in terms of the travel time and distance cost

the Linhnam–Hoangmai can be calculated at any intersection. The route length is 19,377.8 m, and the time cost is 25.7 min, while the route distance under time constraint mode is 19,374.9 m, and the minimum driving time is 24.7 min. In actual driving, route selection is affected by drivers' preference for the shortest time and shortest distance. Figure 3 shows a comparison of the suggested approach's outcomes regarding the average optimization error rate with the A* algorithm and dynamic programming schemes to analyze urban traffic vehicle paths. It can be seen that the suggested approach based on Dijkstra algorithm optimization produces the lowest average converge error rate in comparison with other methods.

Table 3 illustrates the comparison of the proposed scheme's results with the A-star algorithm and dynamic programming methods. It is seen that the proposed approach produces the results efficiently for the analysis of urban traffic vehicle routing planning.

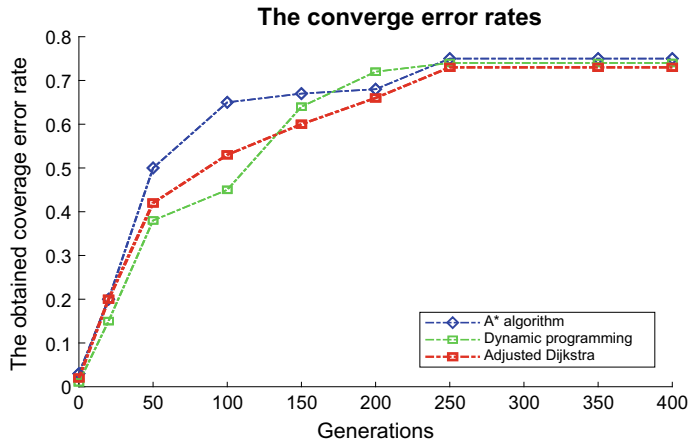


Fig. 3 Comparison of the suggested approach's outcomes regarding the average optimization error rate with the A^* algorithm and dynamic programming schemes to analyze urban traffic vehicle paths

Table 3 Comparison of the results of the proposed scheme with the A^* -star algorithm and dynamic programming methods

Approach	The obtained best cost	The averaged the optimal cost	The executed time
A^* algorithm [12]	19,378	20,263	2670
Dynamic programming algorithm [13]	19,375	20,623	2580
Proposed scheme	19,368	20,233	2376

5 Conclusion

This study proposed an analysis of urban traffic vehicle routing based on the Dijkstra algorithm optimization for suggesting road selection and optimization under various constraints jointly built in the central metropolitan area. The optimal path cost depends on the number of path nodes, link constraints, and speed limit conditions. In this planned scheme of the road network, the specified for both origin point and the target point, the Dijkstra's obtained optimal path was implemented under distance and time cost constraints. The analysis and realization are verified with the geocoding, network topology, and network analysis tools. The results show that the integration of network analysis technology and the Dijkstra algorithm realizes the urban vehicle route's optimization decision. Also, the Dijkstra algorithm reduced the number of node visiting and time complexity. Under the driving time and distance

constraints, the speed limit, road hierarchy, and road conditions are the line selection's restrictive factors. The graphical description could provide technical support and reference for the driver's driving strip and traffic management department for decision making.

References

1. Dao T, Nguyen T, Pan J, Qiao Y, Lai Q (2020) Identification failure data for cluster heads aggregation in WSN based on improving classification of SVM. IEEE Access 8:61070–61084. <https://doi.org/10.1109/ACCESS.2020.2983219>
2. dan Stucky J (1998) On applying viewshed analysis for determining least-cost paths on digital elevation models. Int J Geogr Inf Sci 12:891–905
3. Dao T, Yu J, Nguyen T, Ngo T (2020) A hybrid improved MVO and FNN for identifying collected data failure in cluster heads in WSN. IEEE Access 8:124311–124322. <https://doi.org/10.1109/ACCESS.2020.3005247>
4. Bang S, Heo J, Han S, Sohn H-G (2010) Infiltration route analysis using thermal observation devices (TOD) and optimization techniques in a GIS environment. Sensors 10:342–360
5. Magzhan K, Jani HM (2013) A review and evaluations of shortest path algorithms. Int J Sci Technol Res 2:99–104
6. Awerbuch B, Bar-Noy A, Gopal M (1994) Approximate distributed bellman-ford algorithms. IEEE Trans Commun 42:2515–2517
7. Jianya YYG (1999) An efficient implementation of shortest path algorithm based on dijkstra algorithm. J Wuhan Tech Univ Surv Mapp 3
8. Fuchs B, Kern W, Wang X (2007) Speeding up the Dreyfus-Wagner algorithm for minimum Steiner trees. Math Methods Oper Res 66:117–125
9. Nguyen T-T, Qiao Y, Pan J-S, Chu S-C, Chang K-C, Xue X, Dao T-K (2020) A hybridized parallel bats algorithm for combinatorial problem of traveling salesman. J Intell Fuzzy Syst 38:5811–5820. <https://doi.org/10.3233/jifs-179668>
10. Nguyen T-T, Dao T-K, Kao H-Y, Horng M-F, Shieh C-S (2017) Hybrid particle swarm optimization with artificial bee colony optimization for topology control scheme in wireless sensor networks. J Internet Technol 18. <https://doi.org/10.6138/JIT.2017.18.4.20150119>
11. Dijkstra EW (1959) A note on two problems in connexion with graphs (PDF). Numerische Mathematik 1:269–271. <https://doi.org/10.1007/BF01386390>. S2CID 123284777
12. Duchoň F, Babinec A, Kajan M, Beňo P, Florek M, Fico T, Jurišica L (2014) Path planning with modified a star algorithm for a mobile robot. Procedia Eng 96:59–69
13. Psarafitis HN, Tsitsiklis JN (1993) Dynamic shortest paths in acyclic networks with Markovian arc costs. Oper Res 41:91–101

A Comprehensive Overview of Quality Enhancement Approach-Based Biometric Fusion System Using Artificial Intelligence Techniques



Gaurav Jindal and Gaganpreet Kaur

Abstract Biometric authentication has been reported to be one of the most emerging research fields and its attainments are inseparable from the aid of a heterogeneity of single-modal and multi-modal biometric traits (e.g., fingerprint, hand geometry, iris, face, ear, gait, and so on). Normally, biometric traits are used as authentication information for the security system. Sometimes, the characteristics of biometric traits are difficult to acquire in an appropriate means, and it is essential to practice numerous pre-processing and post-processing algorithms to improve the feature of traits on the security system. In this case, this review paper presents a comprehensive overview of the biometric fusion system (BFS) with some pre-processing and post-processing approaches using the concept of artificial intelligence/machine learning techniques. In this regard, the following subject matters are discussed: 1. Biometric traits quality improvement techniques in the BFS. 2. Feature extraction and optimization approaches. 3. Analysis of classifiers to improve biometric fusion accuracy. 4. Existing challenges of BFS. Besides, a review of existing work based on their accuracy of classification is also discussed. The main aim of this survey is to make available a complete overview of BFS with the role of a different biometric trait in biometrics fusion.

Keywords Biometric authentication system · Biometric modalities · Biometric traits · Image quality improvement techniques · Feature extraction approaches · Optimization approaches · Classifiers · Artificial intelligence/machine learning techniques

G. Jindal () · G. Kaur

Department of Computer Science and Engineering, Sri Guru Granth Sahib World University, Fatehgarh Sahib, Punjab, India

1 Introduction

Biometric fusion system (BFS) refers to the automated process of recognizing and validating a user based on their behavior as well as physical traits for instance finger-print, hand geometry, iris, face, ear, signature, gait, voice, etc. The human biological characteristics are inherent characteristics and the chances of changes are less. These types of biological features frequently have high differences of character, which are considered by constancy, assortment, and openness. Biometrics authentication system (BAS) is a well-known advancement that practices human behavior as well as physiological features for mechanical identification (recognition/verification). In this decade, the mainstream biometrics technologies include physiological biometric traits such as the face, iris, ear, lip, and gait. The BAS with different behavioral as well as physiological biometric traits is shown in Fig. 1.

With the progress of science and innovation with the evolution of the times, in view of the neighborliness and comfort of biometrics innovation, this innovation has been broadly utilized in the banking, transportation, internet business, judicial, security, and diverse fields. The different types of physiological as well as behavioral biometric traits are shown in Fig. 2.

With the ever-increasing advancement of computer technology, single-modal BAS is unable to meet the security requirements of users in most cases, so multi-modal BAS has also become a novel research hotspot. The advantage of the multi-modal BAS is that it can fully utilize the information provided by each biometric to complement the defects of the single-modal BAS, thereby improving the rate of recognition and robustness of the BAS with the concept of feature fusion. For BFS to be effectual in real-time applications, researchers need to prevail over certain associated challenges:

- ***Distorted and noisy scanned input data:*** In BFS, physiological biometric data composed in real-time applications are distorted and noisy due to boisterous

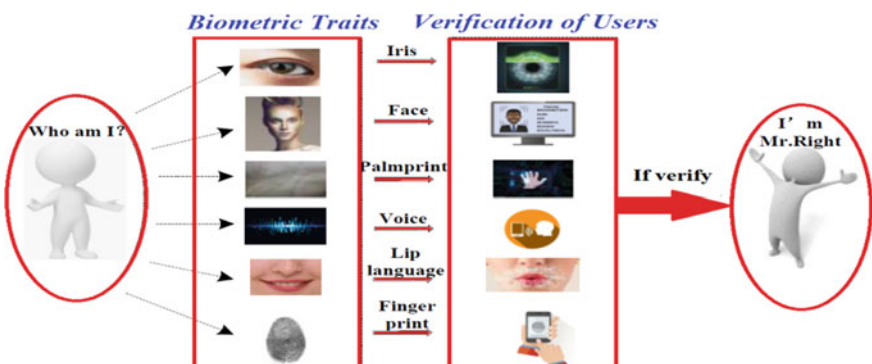


Fig. 1 BAS with different biometric traits

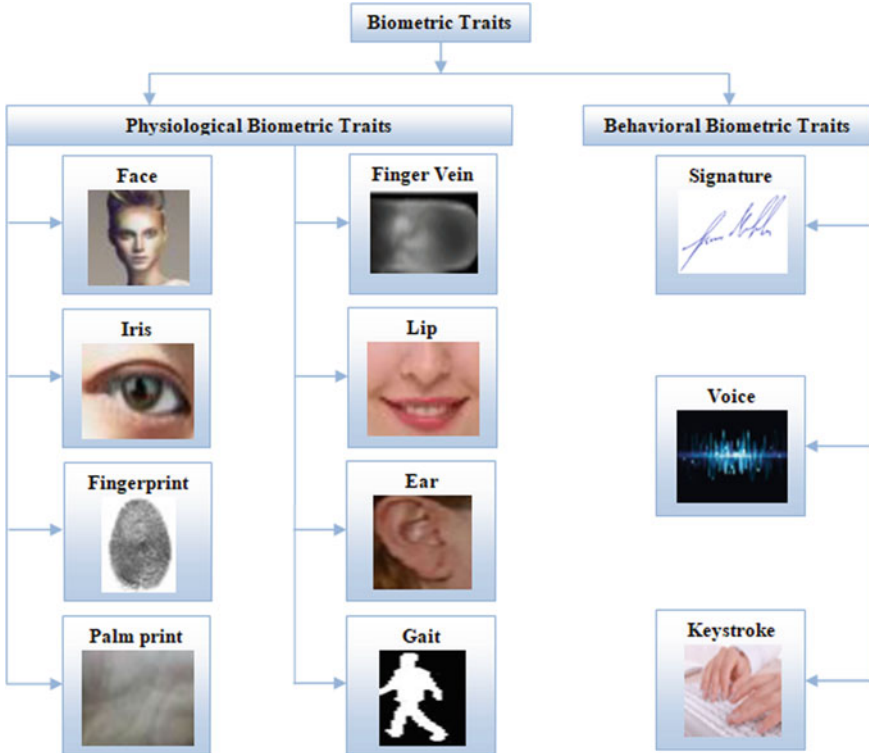


Fig. 2 Types of biometric traits

biometric sensors. The quality of input as a scanned image to be clear when biometric data are captured covertly due to completely unimpeded conditions.

- **Selection of irregular region of interest (ROI):** The selection of proper ROI of scanned input data is the biggest task in any BFS which depends on the pre-processing phases like segmentation, morphological operations, etc.
- **Biometric feature extraction:** Extracting the appropriate biometric features from distorted and noisy input data needs lots of substantial pre-processing techniques, and if extracted features are not unique as per user, then the chances of misclassification are more.
- **Permanence:** Since biological features are based on human factors, they may be unreliable. Physical biometrics vary with time, while biometric behaviors are further discriminated against by socio-ecological factors.
- **Large identities:** BFS includes recognizing possibly a great many people in whom recognizing variables might be unobtrusive. This entails profoundly intricate models to distinguish people at such a scale.
- **Uniqueness:** It is not clear whether a particular biometric model could identify a person differently. In particular, many biometric behavioral features do not apply to human identification and are only used for verification purposes.

- **Attacks on biometric systems:** Biometric systems are often attacked at various levels. Such an attack must be identified as part of the recognition process.

With the current success of machine learning methods, we expect them to be of assistance in addressing the many challenges mentioned above in BFS. Artificial intelligence or machine learning methods learn features from biometric data and, when they are discriminated against, can learn subtle features that can differentiate between a large number of individual users. In addition, if there are satisfactory numbers of feature samples for various biometric features are available, then artificial intelligence or machine learning techniques can train the system to separate such discriminative features based on the users.

Under such scenarios, generative artificial intelligence or machine learning methods might be utilized to synthesize such differences and proved better results. Because of its ability to read biometric data, artificial intelligence or machine learning can also help to differentiate biometric data from a noisy environment. Given these opportunities, we present a comprehensive study to investigate how biometric detection methods have taken advantage of the intrinsic worth of artificial intelligence or machine learning techniques and aspects where artificial intelligence or machine learning can help improve the efficiency of BFS.

This paper presents a survey of the existing trends in BFS with different artificial intelligence or machine learning approaches. Specifically, in Sect. 2, we introduce a literacy study (background survey) of existing work with their advantages and disadvantages. Section 3 of this survey represents a comparative analysis of biometric traits' quality enhancement. The current results-based research is available in Sect. 4 and concludes through discussions on current challenges and future outcomes in Sect. 5.

2 Background Survey

In this segment, we introduce a study of work that is already based on biometric integration with dissimilar techniques. UQi Zhang et al. [1] presented a deep fusion feature network (using the convolution neural network (CNN)) that uses complementary information presented in the iris and periocular regions to improve mobile screening performance. Conventional iris detection systems cannot detect high levels of fragmentation using these low-resolution images and improve the user-identifiable functionality of a cell phone, creating an integrated network of learning features that utilize complementary information proposed in the iris and periocular areas. In this study, the authors are not trying to avoid the problems of distortion of images. Proen  a et al. [2] presented a model of periocular recognition without iris and sclera with the concept of deep learning frameworks. As a young adult, they describe a series of analysis based on CNN. Talreja et al. [3] proposed a secure biometric system that uses deep neural networks and encrypted error correction codes. The authors introduced a feature-level mixing in the biometric framework to produce a secure biometric

template from multiple biometric for each user. They show that phase performance can be improved in many ways while maintaining good safety and durability. Xu and Lu [4] proposed a model using a flexible set method to set the default settings for all test samples and do not require manual setup. Detailed experiments indicate that the method used exceeds previous contemporary art approaches and they need to improve their results through an in-depth prepared learning approach. Liu et al. [5] introduced a safe and effective framework for producing safe, effectual, and removable biometric templates. The advanced framework uses networks of deep trust and random biometric data predictions using secure keys from user authentication passwords. A great bright spot for the introduced system is that it can store the most significant data of biometric data, even the password used. They did not focus on complex design and experimentation with other recognition algorithms capable of image protection. Muthu Kumar and Kavipriya [6] proposed a biometric system model based on the extraction of the Gabor element with the SVM classifier of Finger-Knuckle-Print (FKP). The authors focused on using FKP recognition through the process of integrating the Gabor and SVM features. Security with FKP and other biometric features should be greatly improved. Srivastava and Srivastava [7] presented a multidisciplinary framework using palm, and fingerprint, a combination of face. The SVM separator produces better results in the approval framework and the ids and accuracy and errors are worse. Leghari et al. [8] proposed a biometric validation development model using a combined learning method as dividers. Researchers systematically explored a variety of biometric recognition classification techniques. The three types of biometric data used include fingerprints, online signature, and offline signature. Class algorithms include nearest neighbors algorithm (k-NN), support vector machine (SVM), and multilayer perceptron (MLP) neural network and ensemble learning algorithms included by extra tree classifier (ETC) and random forest classifier (RFC). They did not use large datasets and did not use an in-depth study of various types of biometric data.

Raja [9] proposed a kernel-based manager support program (ESVM-KM) to improve the recognition of multiple chemical reactions using facials, fingerprints, and iris images. Rane [10] proposed a multidisciplinary biometric recognition system using face and palm print as biometric methods. The author's main goal is to increase the robustness of recognition systems. Both uni-methods and multiple methods are combined using various biometric fusion techniques. Garg et al. [11] proposed a multi-modal biometric system based on the decision-making process. The authors want to present a model with k-NN and a neural classifier that participated in the decision-making process. This research work uses 100 samples of iris and fingerprint from a CASIA database compiled by 50 familiar individuals where each person entered two samples and extracted a feature, counting the texture factors used for the continuation of the identification process. After that, the consolidation of the decision level was done using k-NN and neural classifiers. Many datasets can be used because, in the case of user identification, the data used are insufficient. Gayathri Rajagopal and RamamoorthyPalaniswamy [12] proposed a biometric system with multiple human recognition features using two components, namely, palm print, and iris. The resolution of this study was to evaluate multi-modal integration to attain

better performance. The main objectives of the authors are to increase the accuracy of the detection using fusion-level fusion and to obtain good accuracy but not safety precautions. Cheniti et al. [13] proposed that multi-modal biometric systems, which include data from a wide range of biometric sources, have been revealed to advance the performance of character recognition by overcoming the weaknesses and specific environmental restrictions of illegal systems. An innovative outline for consolidating school standards based on symmetrical statistics (S-sums) has been introduced, and the authors are developing a benchmark of information available on a public bench. Sharma et al. [14] proposed an integrated point-level integration scheme that is a combination of the standard GEV distribution process and fm-based DS_mT application. They did not use any encryption algorithm to protect their system. Vishi and Josang [15] introduced a multi-biometric fusion for multi-biometric fusion based on subjective logic, and their results demonstrate that in most phases, subjective logic fusion accomplishes better than classical fusion approaches but they did not test with different modalities for instance the face, finger vein, fingerprint, voice, and iris and with a variety of databases.

The Solution of Existing Challenges in BAS and BFS: From the survey, artificial intelligence or machine learning has outperformed previous state-of-the-art methods in various domains. The following factors which help to solve the current challenges and issues of BAS or BFS:

Biometric Quality Improvement: It is the basic and necessary step to solve the current BFS challenges. If the quality of the biometric image is better, then the chances of higher accuracy are more. A brief description of different biometric quality improvement methods is described in Sect. 3.

Biometric Feature Learning: Artificial intelligence or machine learning methods learn features from biometric data that help to perform other related tasks. A variety of integrated features are analyzed in this paper to the trained system compared to some specific named features. Several feature extraction techniques are available to train the system using feature metrics instead of a particular named feature set. The uniqueness of the named feature is less as compare to the unnamed feature extraction approaches like PCA, SIFT, SURF, etc.

Feature Selection/Optimization: These methods help to learn BFS by selecting a useful feature set of particular biometric data. There are several feature selection/optimization algorithms are available but the selection of an appropriate approach helps to achieve better performance of biometric recognition.

The fusion of Features: The fusion of biometric features is a necessary process to train the system with maximum accuracy. There are several types of methods that are available to fusion the extracted feature which are the following:

- *Sensor-level fusion*
- *Feature-level fusion*
- *Score-level fusion*
- *Rank-level fusion*
- *Decision-level fusion.*

Training with Large-Scale Biometric Datasets: Artificial intelligence or machine learning is the better option for the training of the system but a large-scale biometric dataset helps to achieve a better classification accuracy of the system.

3 Biometric Quality Enhancement

Biometric quality improvement strategies are used to obtain better biometric quality, where ‘quality improvement’ is occasionally defined as neutral and sometimes individual that means making the process of debugging and classification easier by modifying the colors, contrast, or intensities of biometric data. There are a lot of biometric quality improvement techniques are available.

Intensity-based Biometric Quality Improvement (IBQI): Intensity quality-based development is a way to adjust the strength of the biometric image strength values in a series of novels and create a biometric image with better durability. Prior to the improvement of data quality, it is essential to set limits on the maximum and minimum pixel value for which the biometric image will be made. Prior to this, we know that at 8-bit gray-level any images, lower and upper limits, can range from 0 to 255. We look at the lower and upper limits by LR and HR, respectively with the iris sample shown in Fig. 3. Then check the biometric image to find the lowest and highest pixel value currently existing in the biometric image that needs enrichment. These pixel values are called LN and HN. Thereafter, each pixel (P) of the biometric image is developed by means of the following equation:

$$P_{\text{Enh}} = (P_{\text{Bimg}} - L_N) \left(\frac{H_R - L_R}{H_N - L_N} \right) + L \quad (1)$$

where P_{Enh} is the enhanced biometric image and P_{Bimg} the original biometric image. To illustrate, the third image below shows a low biometric image (iris) with its histogram and enhances its biometric image and its histogram using the IBQI method.

The IBQI method enhances the biometric image strength by transferring each grayscale value to a new pixel series using a collector scatter function from the path of the hardness histogram. Figure 3 represents the IBQI process representing the biometric iris image and the enhanced image after the development process. In this figure, (a) represents the first biometric iris image, (b) signifies an advanced biometric iris image using IBQI, (c) is the histogram of the first biometric iris image, and (d) is the histogram of iris biometric iris image. To improve the image of the biometric iris, below is the IBQI algorithm used.

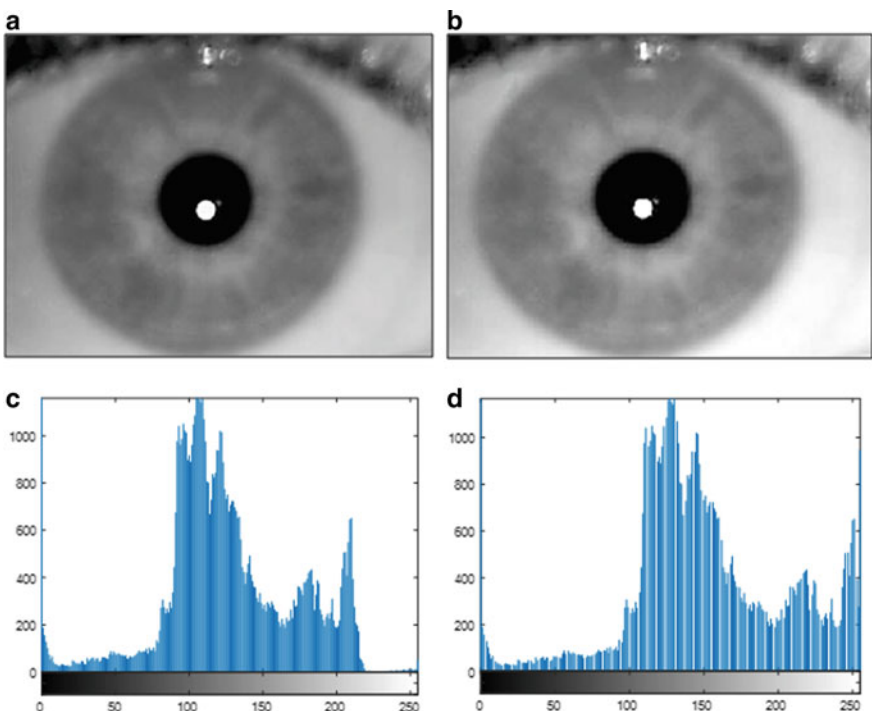


Fig. 3 **a** Biometric image, **b** enhanced biometric image, **c** histogram of biometric image, and **d** histogram of biometric enhanced image

Algorithm 1: IBQI

Input: $B_{img} \leftarrow$ Biometric Image

Output: $E_{Bimg} \leftarrow$ Enhanced Biometric Image

1. Calculate the dimension (D) of B_{img}

2. If $D == 3$

3. $B_{img_R} =$ Red component of B_{img}

4. $B_{img_G} =$ Green component of B_{img}

5. $B_{img_B} =$ Blue component of B_{img}

6. Using equation (1)

7. Enhanced $R_{img} = P_E(B_{img_R})$

8. Enhanced $G_{img} = P_E(B_{img_G})$

9. Enhanced $B_{img} = P_E(B_{img_B})$

10. Enhanced Image = cat (3, Enhanced R_{img} , Enhanced G_{img} , Enhanced B_{img})

11. Else

12. Enhanced Image = $P_E(B_{img})$

13. End

14. **Return:** Enhanced Image as a Enhanced Biometric Image

15. End

Histogram Equalization-based Biometric Quality Improvement (HEBQI):

Biometric quality improvement using the histogram equalization approach is a procedure of image intensities adjustment to advance the contrast of a biometric image. It is not indispensable that the contrast of the image will always be a rise in quality improvement using the histogram equalization approach. There may be various cases where quality improvement using the histogram equalization approach to generate an inferior quality image. In that situation, the contrast of a biometric image is reduced.

Consider B_{img} be a given biometric iris image represented as an R by C matrix of integer pixel intensities ranging from 0 to Int, where Int is the number of feasible intensity values of the image. Let N_H denote the normalized histogram of B_{img} with a number of feasible bins intensity. The formula to calculate the normalized histogram of B_{img} is given in Eq. 2.

$$N_H = \frac{\text{No. of pixels with } n \text{ intensity}}{\text{Total Pixels}} \quad (2)$$

$$n = 0, 1, 2, \dots, \text{Int} - 1$$

The histogram equalized biometric image B_{imgH_E} is well defined by

$$B_{imgH_E}(i, j) = R((\text{Int} - 1) \sum_{n=0}^{B_{img}(i, j)} H_{Enh}) \quad (3)$$

where $R()$ is the function that is used to rounds down the pixel value to the nearest integer. Let us start biometric quality improvement using a histogram equalization approach by taking an instance of a biometric image below as a simple image.

Figure 4 represents the process of biometric quality improvement using a histogram equalization approach, representing the first biometric image and the enhanced biometric image after development. In this figure, (a) represents the first biometric image, (b) signifies the advanced biometric image using the HEBQI process, (c) the histogram of the first biometric image, and (d) is a biometric image enhancement histogram. To make a biometric image, use the HEBQI algorithm mentioned below.

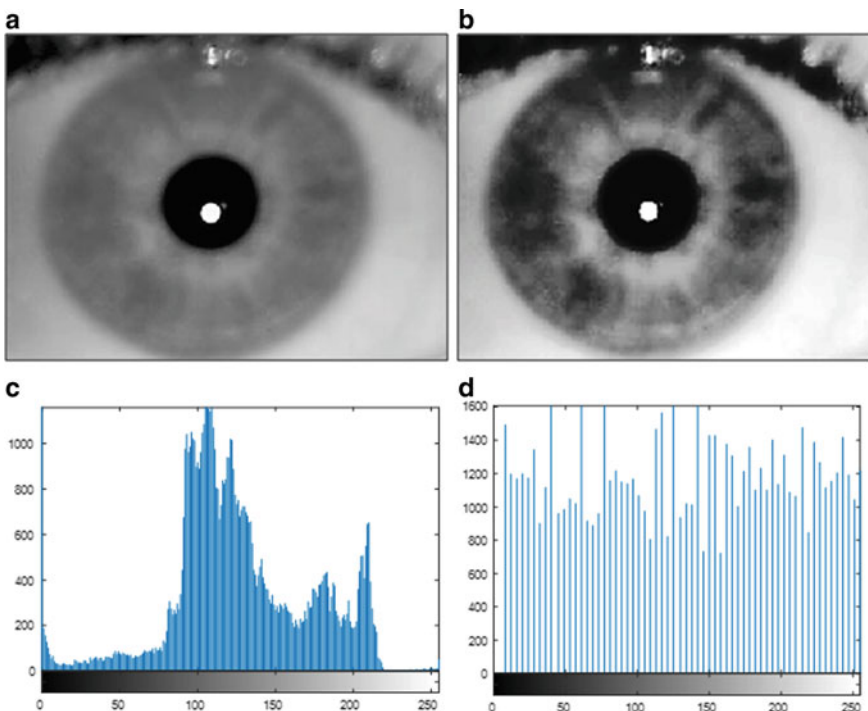


Fig. 4 **a** Biometric image, **b** enhanced biometric image, **c** histogram of biometric image, and **d** histogram of biometric enhanced image

Algorithm 2: HEBQI

```

Input: Bimg  $\leftarrow$  Biometric Image
Output: EBimg  $\leftarrow$  Enhanced Biometric Image
1. Calculate the dimension (D) of Bimg
2. If D==3
3.Bimg_R=Red component of Bimg
4.Bimg_G=Green component of Bimg
5.Bimg_B=Blue component of Bimg
6. Using equation (3)
7. Enhanced Rimg= $H_{Enh}$  (Bimg _R)
8. EnhancedGimg = $H_{Enh}$ (Bimg _G)
9. EnhancedBimg = $H_{Enh}$ (Bimg _B)
10. Enhanced Image=cat (3, Enhanced Rimg, EnhancedGimg, EnhancedBimg)
11. Else
12. Enhanced Image= $H_{Enh}$  (Bimg)
13. End
14. Return: Enhanced Image as an Enhanced Biometric Image
15. End
```

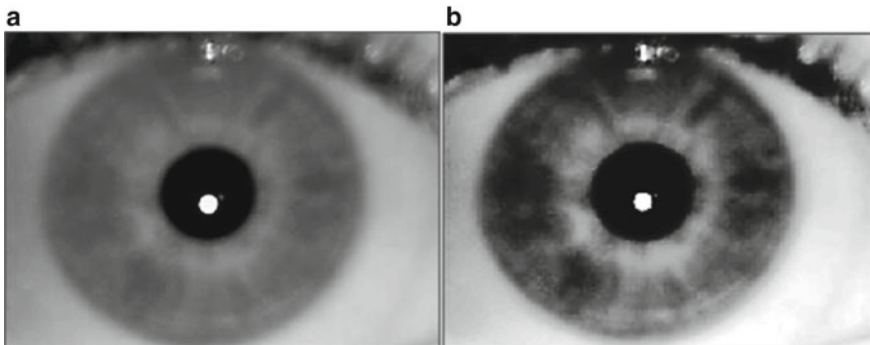


Fig. 5 **a** Before global HEBQI and **b** after HEBQI

Contrast Limited Adaptive Histogram Equalization-based Biometric Quality Improvement (CLAHEBQI): It is the improvisation of HEBQI. In the HEBQI method, we have just considered, it looks at the global difference of biometric image in Eq. (3). In most cases, it is not good for improving the quality of the biometric image. For instance, the below image demonstrates an input biometric iris image and its consequence after global HEBQI.

It is correct that the background contrast of biometric iris image (Fig. 5) has improved after HEBQI but compares the iris part of the eye in both (Fig. 5 a, b) biometric images. We founded that much information is lost due to the problem of overhead. This is because the histogram of the iris image is not limited to a specific region as we have seen in previous cases. The difference does not have to always be an increase in the HEBQI approach. There may be some cases where the HEBQI process may be of poor quality. If so, the biometric image difference is decreasing so we need to use the comparison limit to advance the quality of the biometric image, and this method is known as CLAHEBQI. The CLAHEBQI method is described below:

Phase 1: Firstly provide a biometric image for further process of image quality improvement.

Phase 2: Acquire altogether the input pixel values used in the image quality improvement process such as number of regions in row and column, the total number of drums used in comparison clip limit, histogram conversion function distribution, parameter.

Phase 3: After that, apply to pre-process on the biometric image to split an image into sub-regions.

Phase 4: Process applied over the plane of a biometric image (proper sub-region).

Phase 5: At last, construct gray-level mapping and clipped histogram for the pre-processed part of the image. Unsuitable sub-region, numbers of pixels are divided alike in each gray level so a typical number of pixels for gray level is defined using the given Eq. 4:

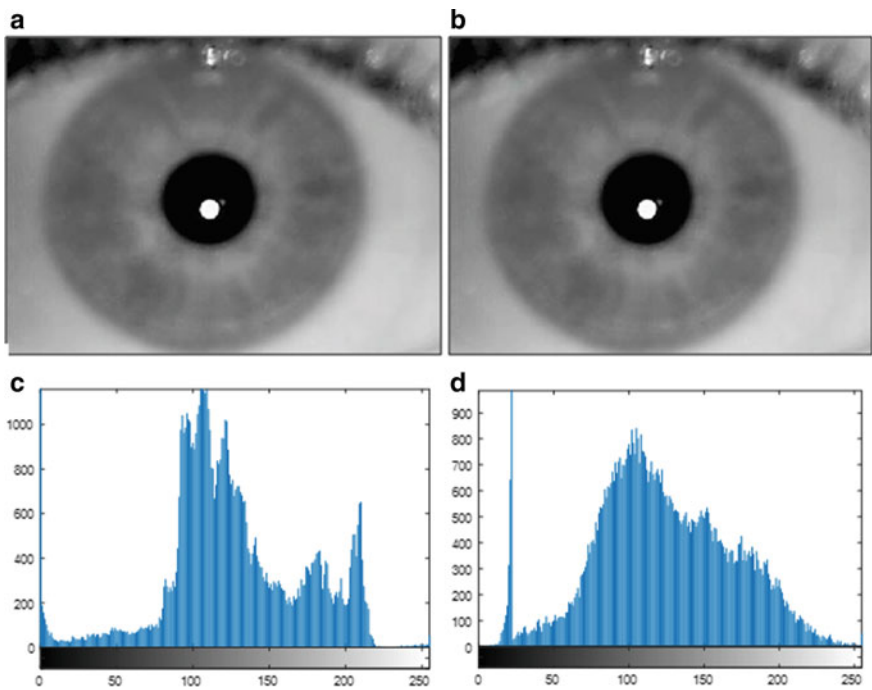


Fig. 6 **a** Biometric image, **b** enhanced biometric image, **c** histogram of biometric image, and **d** histogram of biometric enhanced image

$$Pix_{\text{average}} = \frac{Pix_{(CR-Xp)} \times Pix_{(CR-Yp)}}{Pix_{\text{Gray}}} \quad (4)$$

where Pix_{average} is an average number of pixels presents in the biometric image, Pix_{Gray} is the number of gray levels in the appropriate sub-region, Pix_{CR-Xp} is the number of pixels with the x -axis of suitable sub-region, and Pix_{CR-Yp} is the number of pixels with the y -axis of the apposite sub-region. After that, compute the genuine clip limit of a biometric image using the given formula:

$$Pix_{CL} = Pix_{Clip} - Pix_{\text{average}} \quad (5)$$

where Pix_{CL} is the pixel clip limit that is used to set the contrast limitation of a biometric image.

Phase 6: Apply the HEBQI technique with Eq. (3) with a clip limit to advance the quality of the original biometric image.

To exemplify, below-mentioned figure displays the CLAHEBQI process by its histogram and compares it with the original biometric image.

Figure 6 signifies the procedure of the CLAHEBQI method which characterizes the original biometric iris image and enhanced iris image after the quality improvement. In CLAHEBQI technique, quality improvement function is applied over all neighborhood pixels of a biometric image and then the transformation function is derived with limitation. This is differing from the HEBQI method because of its contrast limiting method. In Fig. 6, (a) signifies the first biometric image, (b) signifies the enhanced biometric image using the CLAHEBQI process, (c) is the histogram of the original biometric image, and (d) is the histogram of the enhanced image. The quality of biometric images improved using the CLAHEBQI algorithm.

In this survey, we present a comparative analysis of biometric fusion and the impact of image quality improvement techniques on BFS using different image quality improvement algorithms such as IBQI, HEBQI, and CLAHEBQI.

4 Analysis of Existing Work

From the survey and above observation, we concluded the accurateness in terms of genuine acceptance rate (GAR) for different biometric modalities and techniques is described in the below table.

Figure 7 characterizes the relative analysis of existing work based on the accuracy of classification in terms of GAR. From the figure, we observe that the accuracy attains by using the concept of artificial intelligence/machine learning is better than another author because they present a module by using the concept of CNN using different feature extraction techniques.

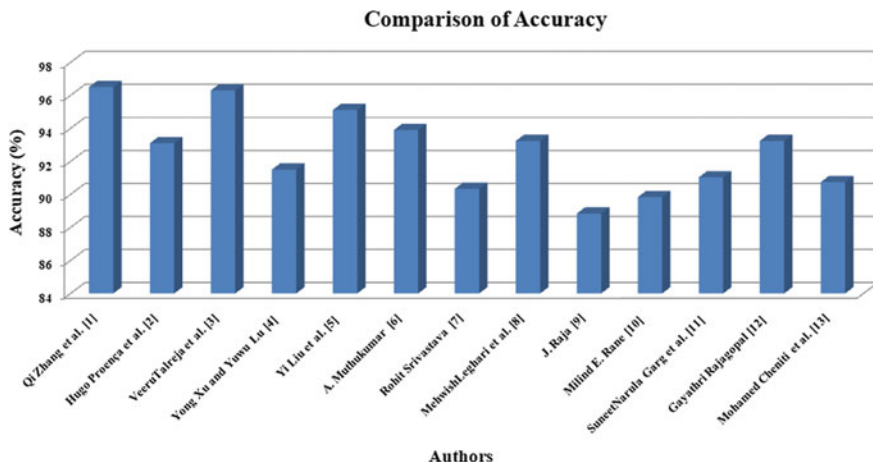


Fig. 7 Comparison of accuracy of proposed work with existing works

5 Conclusion and Future Work

In this paper, a comprehensive overview of the quality enhancement approach-based biometric fusion system via artificial intelligence or machine learning techniques is presented with an analysis of biometric image quality enhancement approaches. It provides a comprehensive view of the various applications and potential challenges of the biometric system which is a tough task in the science and technology field from a security point of view. From the survey, as it provides a large number of different techniques and algorithms, artificial intelligence or machine learning techniques offer numerous advantages over other methods for the biometric pattern recognition system. In this approach, the requirements of capable techniques satisfy a growing need for security and shrewder applications in this world. Also, it could be appreciated that all the given artificial intelligence algorithms congregate the crucial features proposed in Sect. 2 for biometric survey dealing and attained high classification accuracy demonstrates they are appropriate for real-time applications for BAS or BFS. So this survey finds out a better solution to an existing problem in BFS by integrating the concept of artificial intelligence or machine learning techniques with feature extraction and feature optimization approaches with feature fusion in the future trends. In the future, artificial intelligence or machine learning techniques that are utilized as a classifier to train BFS based on hybridization of feature descriptor with soft computing-based feature optimization algorithm could be a better option.

Table 1 Brief summary of traditional BAS

No	Bas with advantages		Adopted approaches disadvantages	
1	System	Finger print-based BAS	Approach	1. Minutiae feature-based methods 2. Image pixel-based approaches
	Advantages	1. Highly mature technique 2. Trouble-free to use and it is a non-intrusive technology 3. Classification accuracy is high 4. Long-term constancy and capability to store and enroll multiple fingerprints 5. A low-cost system with respect to others BAS	Disadvantages	1. Failure to enroll some users 2. Affected by human skin circumstance 3. Used sensor need to clean up again and again 4. Association with forensic applications
2	System	Face-based BAS	Approach	1. Image pixel-based methods i. A model with Eigenfaces ii. A model with Fischer's faces 2. Image feature-based methods i. A model with geometric feature ii. A model with features metric iii. Morphological models
	Advantages	1. Non-intrusive model 2. Designing cost is low 3. Capability to function covertly 4. Potential for isolation abuse	Disadvantages	1. Mat be affected by appearance surroundings 2. High false acceptance rates 3. Twins attacks are applicable

(continued)

Table 1 (continued)

No	Bas with advantages		Adopted approaches disadvantages	
3	System	Iris-based BAS	Approach	<ol style="list-style-type: none"> 1. A model with complex-valued 2D Gabor wavelets 2. Gaussian filters for feature extraction from iris 3. A model with zero-crossing wavelet transform as a feature 4. Hough circular transform with filters
	Advantages	<ol style="list-style-type: none"> 1. Potential for high recognition accuracy 2. Confrontation to impostors 3. Long-period constancy 	Disadvantages	<ol style="list-style-type: none"> 1. Intrusive and normalization of data is difficult 2. High designing cost 3. Time-consuming
4	System	Hand geometry-based BAS	Approach	<ol style="list-style-type: none"> 1. A feature-based model such as finger length, width, thickness curvatures and relative location of features
	Advantages	<ol style="list-style-type: none"> 1. Affection rate of the environment is minimum 2. Mature BAS technology 3. The relatively more stable and secure technique of BAS 	Disadvantages	<ol style="list-style-type: none"> 1. Low accuracy 2. High cost 3. Relatively large readers 4. Difficult to use for some users
5	System	Finger vein based BAS	Approach	<ol style="list-style-type: none"> 1. Feature-based model
	Advantages	<ol style="list-style-type: none"> 1. Resistance to forgery 2. Commonly secured and accepted 3. Non-intrusive 4. No need to record 	Disadvantages	<ol style="list-style-type: none"> 1. Pattern inconsistencies 2. Difficult to utilize 3. Required large matching templates 4. Problem with small data

Table 2 Artificial intelligence or machine learning approaches in biometrics

Algorithms	Biometric applications	Analysis
Deep learning	Iris recognition [1] Iris and sclera recognition [2] Face and iris fusion [3] Palm and face [4] Finger vein recognition [5]	Deep learning techniques (CNN, ANN, etc.) are used as a classifier to train and classify the user using their different biometric traits. Using the concept of deep learning techniques, the achieved accuracy is lies between 90 to 96% in different scenarios
SVM	The fusion of Finger-Knuckle-Print [6] The fusion of face, fingerprint, and palm print [7] The fusion of fingerprint, online and offline signature [8] The fusion of face, iris, and fingerprint [9]	SVM (binary classification) is used to train the model based on the different types of features like principal component analysis (PCA), Gabor filter, stroked-based feature, etc. The accuracy of the system is calculated in terms of Genuine acceptance rate and it is near to 90% but needs improvement in the feature selection process
Decision tree, k-NN, random forest, etc.	The fusion of face and palm print [10] The fusion of iris and face [11] The fusion of iris and palm print [12] Face and fingerprint-based fusion model [13]	With the decision tree, k-NN, random forest, etc. as a classifier, they have a limitation of training data and these types of classifiers are applicable for a few amounts of data

Table 3 Analysis of GAR in multi-modal biometric system

Authors	Accuracy (%)
Zhang et al. [1]	96.5
Proen��a et al. [2]	93.1
Talreja et al. [3]	96.3
Xu and Lu [4]	91.5
Liu et al. [5]	95.11
Muthukumar and Kavipriya [6]	93.9
Srivastava and Srivastava [7]	90.34
Leghari et al. [8]	93.24
Raja [9]	88.84
Rane [10]	89.83
Garg et al. [11]	91.03
Rajagopal [12]	93.24
Cheniti et al. [13]	90.74

References

1. Zhang Qi, Li H, Sun Z, Tan T (2018) Deep feature fusion for iris and periocular biometrics on mobile devices. *IEEE Trans Inf Forensics Secur* 13(11):2897–2912
2. Proen  a H, Neves JC (2018) Reminiscence of ‘mastermind’: Iris/periocular biometrics by “In-Sets” CNN iterative analysis. In: *IEEE transactions on information forensics and security*
3. Talreja V, Soleimani S, Valenti MC, Nasrabadi NM (2019) Learning to authenticate with deep multibiometric hashing and neural network decoding. *arXiv preprint arXiv: 1902.04149*
4. Xu Y, Yuwu Lu (2015) Adaptive weighted fusion: a novel fusion approach for image classification. *Neurocomputing* 168:566–574
5. Liu Y, Ling J, Liu Z, Shen J, Gao C (2018) Finger vein secure biometric template generation based on deep learning. *Soft Comput* 22(7):2257–2265 (2018)
6. Muthukumar A, Kavipriya A (2019) A biometric system based on Gabor feature extraction with SVM classifier for Finger-Knuckle-Print. *Pattern Recogn Lett* 125:150–156
7. Srivastava R, Srivastava P (2019) A framework design for human authentication based on biometric fusion mechanism. Available at SSRN 3391051
8. Leghari M, Memon S, Sahito F, Chandio AA, Leghari M (2018) Biometric verification enhancement with ensemble learning classifiers. In: *2018 5th international multi-topic ICT conference (IMTIC)*. IEEE, pp 1–6
9. Raja J, Gunasekaran K, Pitchai R (2018) Prognostic evaluation of multimodal biometric traits recognition based human face, fingerprint and iris images using ensembled SVM classifier. *Cluster Comput* 1–14
10. Rane ME, Pande AJ (2018) Multi-modal biometric recognition of face and palm-print using matching score level fusion. In: *2018 fourth international conference on computing communication control and automation (ICCUBEA)*. IEEE, pp 1–6
11. Garg SN, Vig R, Gupta S (2016) Multimodal biometric system based on decision level fusion. In: *2016 international conference on signal processing, communication, power and embedded system (SCOPES)*. IEEE, pp 753–758
12. Rajagopal G, Palaniswamy R (2015) Performance evaluation of multimodal multi-feature authentication system using KNN classification. *Sci World J* 2015
13. Cheniti M, Boukezzoula N-E, Akhtar Z (2017) Symmetric sum-based biometric score fusion. *IET Biometr* 7(5):391–395
14. Sharma R, Das S, Joshi P (2018) Score-level fusion using generalized extreme value distribution and DSmT, for multi-biometric systems. *IET Biometr* 7(5):474–481
15. Vishi K, J  sang A (2017) A new approach for multi-biometric fusion based on subjective logic. In: *Proceedings of the 1st international conference on internet of things and machine learning*. ACM, p 68
16. Abdullah-Al-Wadud M, Kabir MH, Dewan MAA, Chae O (2007) Dynamic histogram equalization for image contrast enhancement. *IEEE Trans Cons Electron* 53(2)
17. Yadav G, Maheshwari S, Agarwal A (2014) Contrast limited adaptive histogram equalization based enhancement for real time video system. In: *Advances in computing, communications and informatics (ICACCI, 2014 International Conference on)*. IEEE, pp 2392–2397
18. Gillespie AR (1992) Enhancement of multispectral thermal infrared images: Decorrelation contrast stretching. *Remote Sens Environ* 42(2):147–155
19. Mustapha A, Hussain A, Samad SA (2011) A new approach for noise reduction in spine radiograph images using a non-linear contrast adjustment scheme based adaptive factor. *Sci Res Essays* 6(20):4246–4258
20. Restaino R, Vivone G, Dalla Mura M, Chanussot J (2016) Fusion of multispectral and panchromatic images based on morphological operators. *IEEE Trans Image Process* 25(6):2882–2895
21. Sarhan S, Alhassan S, Elmougy S (2017) Multimodal biometric systems: a comparative study. *Arab J Sci Eng* 42(2):443–457

Rainfall Prediction Using Deep Neural Network



Chitra Desai

Abstract A model when stated in simple terms is a mathematical equation, which is true when it implies to any model in machine learning including deep neural network. Every model will generate output for a given input, but important is to get output of desired accuracy. Machine learning models are trained on training data, and their best fit is judged on testing data. Before fitting the training data to the model to predict on unknown (test) data, pre-processing of data is essential to ensure model accuracy to acceptable level. This paper presents steps involved in pre-processing raw labelled dataset (Seattle weather) with 25,551 records (from year 1948 to 2017) to make it suitable for input to a deep neural network model. The data is split into 80% of training data and 20% of testing data. Scaling is performed on the data before it is passed to the deep neural network model. Deep neural network model that is multilayer perceptron model using sequential model API with dense layer is built and compiled using Adam optimizer resulting accuracy of 97.33% in predicting rainfall on a particular day.

Keywords Data pre-processing · Deep neural network · Adam optimizer · Sequential model

1 Introduction

Artificial neural network (ANN) models have been used for rainfall prediction [1, 2] and found suitable for handling complex large dataset, particularly of nonlinear nature. There are several methods [3] apart from artificial neural networks which have been used for forecasting rainfall; however, ANN has proved to be useful in identifying complex nonlinear relationship between input–output variables. As the number of hidden layers are increased for better performance [4], the concept of deep learning comes in, which are useful for rainfall prediction. The deep neural network models have mathematics behind them, the understanding of which enables one for the selection of architecture for fine tuning of deep learning models, setting of values

C. Desai (✉)
National Defence Academy, Pune, India

for hyperparameters and applying appropriate optimization. However, the success of a model for prediction or classification is directly impacted by the data used for training the model. The real-world data in its raw form may not be suitable to train the model, which signifies the importance of data pre-processing.

Pre-processing of data refers to improving the quality of data, which involves data cleaning, data reduction, data transformation and data encoding. In data cleaning, the missing values, duplicate values and outliers are dealt with. Data reduction refers to number of features being reduced, particularly adopted to reduce the effect of curse of dimensionality. Data transformation is applied to scale the data either using normalization or standardization. Data encoding ensures the categorical features in text format are encoded to numbers.

This paper presents steps involved in pre-processing raw labelled dataset (Seattle weather) with 25,551 records, to make it suitable for input to a deep neural network model. Insight into the data is further gained to identify the architecture suitable for chosen problem. Deep learning model, that is multilayer perceptron model using sequential model API with dense layer, is built and compiled using Adam optimizer for desired accuracy.

2 Methodology

Data obtained in raw form is suitably pre-processed to ensure all feature variables and target variable fit the DNN model. Using quantitative approach, the relationship between variables is identified. On pre-processing, the number of input neurons is identified. After pre-processing, data is divided into train–test data and scaling is applied. The DNN-sequential approach is adopted, and dense layers are added. At hidden layers, the activation function is chosen. As the problem belongs to the class of binary classification, sigmoid function is applied at the output layer. The epoch size is identified by observing the model loss and model accuracy curve. The test accuracy is further computed using the prediction capability of the model trained.

3 Data and Data Pre-processing

3.1 Data Set

The present study is made on Seattle, US weather dataset [5]. The dataset contains records of daily rainfall patterns from Jan 1st, 1948 to Dec 12th, 2017. The dataset consists of five columns, and the description of these columns is as follows as shown in Table 1.

There are total number of records which are 25,551. The memory usage is approximately 998 KB. Here DATE, PRCP, TMAX and TMIN are features (X),

Table 1 Data description for Seattle weather dataset

Column name	Data description
DATE	The date of the observation
PRCP	The amount of precipitation, in inches
TMAX	The maximum temperature for that day, in degrees Fahrenheit
TMIN	The minimum temperature for that day, in degrees Fahrenheit
RAIN	TRUE if rain was observed on that day, FALSE if it was not. [target]

Table 2 First five records of Seattle weather dataset

Date	PRCP	TMAX	TMIN	RAIN
1948-01-01	0.47	51	42	True
1948-01-02	0.59	45	36	True
1948-01-03	0.42	45	35	True
1948-01-04	0.31	45	34	True

Table 3 Statistical description of Seattle weather dataset

	PRCP	TMAX	TMIN
Count	25,548.000000	25,551.000000	25,551.000000
Mean	0.106222	59.544206	44.514226
Std.	0.239031	12.772984	8.892836
Min.	0.000000	4.000000	0.000000
25%	0.000000	50.000000	38.000000
50%	0.000000	58.000000	45.000000
75%	0.100000	69.000000	52.000000
Max.	5.020000	103.000000	71.000000

and RAIN is our target variable Y . RAIN is categorical in nature which has two possible output—True (RAIN) or False (Not RAIN). Thus, the problem belongs to the class—binary classification. Features—PRCP, TMAX and TMIN—are numerical continuous values, and DATE is in format YYYY-MM-DD. Sample five records are displayed below from the dataset as shown in Tables 2 and 3 which shows the statistical description of the dataset:

3.2 Data Pre-processing

Deep neural network (DNN) models like any other machine learning model requires pre-processing of data, before the data is passed to input neuron. One of the important

step is to identify the missing values and if found treat them appropriately. Missing values can be dropped and can be substituted by either mean, median or any other relevant value like 0 or 1. It is also necessary to check for duplicate data to make our model more impactful. Often, the raw dataset may contain columns which are less important and can be ignored or avoided as input to the model which are identified during pre-processing. Also, certain new columns may be required to be generated from the existing one for extracting more feature value for the model. Deep learning model takes input to the input layer neurons in the form of real values, essentially it is to be ensured that text to number encoding is done prior to that.

It is observed that the dataset consists of three null values in PRCP and RAIN columns as shown in Table 4. Before we send our data to the model, it is required that the null values to be treated with appropriate action. In this case compared to the huge number of records dropping, the three records with null values in PRCP and RAIN are recommended, and accordingly, they are removed from the dataset leaving 25,548 records for further processing. Next, the dataset is checked for duplicate values and it is observed that there are no duplicate records in the dataset.

The DATE field is broken into ‘YEAR’, ‘MON’, ‘DAY’. The value true is replaced by 1 and False by 0 in the field ‘RAIN’, that is the text (Boolean) data is converted to numeric. Thus, feature X will consist of ‘PRCP’, ‘TMAX’, ‘TMIN’, ‘YEAR’, ‘MON’, ‘DAY’ and ‘RAIN’ as target column Y . So now the data appears as shown in Table 5.

Table 4 NaN values in dataset

Date	PRCP	TMAX	TMIN
1998-06-02	NaN	72	52
1998-06-03	NaN	66	51
2005-09-05	NaN	70	52

Table 5 Sample data after splitting DATE column

PRCP	TMAX	TMIN	RAIN	YEAR	MON	DAY
0.47	51	42	1	1948	1	1
0.59	45	36	1	1948	1	2
0.42	45	35	1	1948	1	3
0.31	45	34	1	1948	1	4
0.17	45	32	1	1948	1	5

3.3 Data Insight

The dataset contains data from the year 1948 to 2017, and the month-wise distribution of data from the 1948 to 2017 is shown in Table 6.

The rainfall experience in a particular month for the period 1948 to 2017 is shown in Table 7. It is observed that lowest rainfall is observed in the month of July every year, and highest rainfall is observed in the month of December every year.

The histogram for the column rainfall is shown in Fig. 1. The number of records with no rainfall is 14,648, and number of records with rainfall is 10,900.

To get the scatter plot of precipitation with the temperature, additional column AVGTEMP is created from TMAX and TMIN. The obtained scatter plot is shown in Fig. 2. On referring to Table 3, it is observed that the maximum value of PRCP is 5.02, which as shown in Fig. 2 is an outlier. Except for few cases where the average temperature is in between 48 and 60°F, we observe PRCP value above 2.0.

The precipitation is the water released from clouds in the form of rainfall [6]. Refer to Table 8 [7] below and observe Fig. 3, it is seen that October to April every year, moderate rainfall is experienced and from May to September light rainfall is experienced in Seattle.

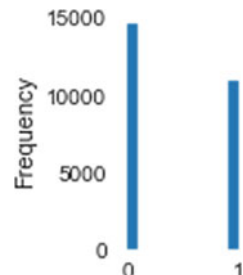
Table 6 Month-wise total records since 1948–2017

Month	1	2	3	4	5	6	7	8	9	10	11	12
Number of records	2170	1978	2170	2100	2170	2098	2170	2170	2099	2170	2100	2153

Table 7 Month-wise rainfall records since 1948–2017

Month	1	2	3	4	5	6	7	8	9	10	11	12
Number of records	1298	1103	1212	998	771	632	343	413	609	950	1264	1307

Fig. 1 Histogram for column RAIN



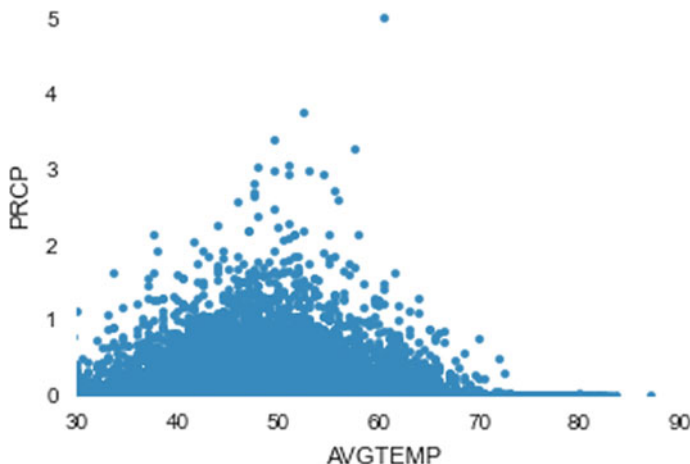


Fig. 2 Scatter plot

Table 8 Precipitation intensity

	Intensity in./h (cm/hour)	Median diameter (mm)	Velocity of fall ft/s (m/s)	Drops per second per square foot (m ²)
Fog	0.005 (0.013)	0.01	0.01 (0.003)	6,264,000 (67,425,000)
Mist	0.002 (0.005)	0.1	0.7 (0.21)	2510 (27,000)
Drizzle	0.01 (0.025)	0.96	13.5 (4.1)	14 (151)
Light rain	0.04 (0.10)	1.24	15.7 (4.8)	26 (280)
Moderate rain	0.15 (0.38)	1.60	18.7 (5.7)	46 (495)
Heavy rain	0.60 (1.52)	2.05	22.0 (6.7)	46 (495)
Excessive rain	1.60 (4.06)	2.40	24.0 (7.3)	76 (818)
Cloudburst	4.00 (10.2)	2.85	25.9 (7.9)	113 (1220)

Source Refer [6, 7]

3.4 Train–Test Split

To estimate the performance of machine learning algorithms, the data is split into training and testing data. Usually, the data is split into train–validate–test data. The train data is used to train the model; using validation data, the model is validated and tested using test data. In the present experiment, the data is split into only train and test data. The ratio chosen here is 80:20, that is 80% of training data and 20% of testing data.

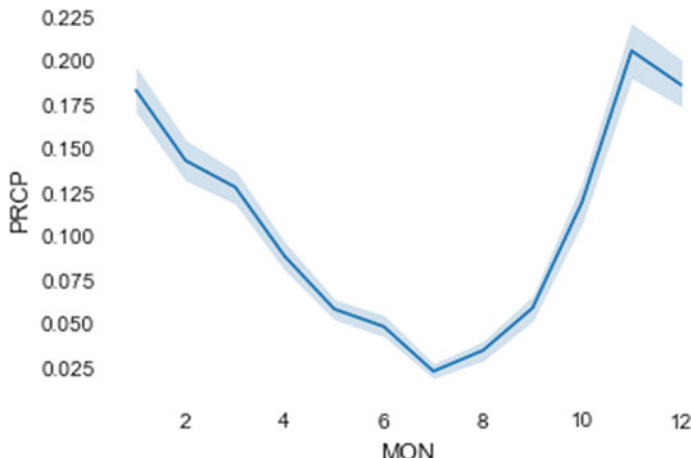


Fig. 3 Precipitation trend

3.5 Feature Scaling

Machine learning algorithms like linear regression, logistic regression and neural network that use gradient descent as an optimization technique require data to be scaled [8]. On observing the values across different columns in the Seattle weather dataset, we find there is varying range of values. By applying scaling, all values are brought on same scale before giving it to our deep neural network model. Scaling can be done using either normalization or standardization. In normalization, values are scaled in the range from 0 to 1, while in standardization values are centred around the mean. As we see outliers with respect to PRCP and AVGTEMP in the data, standardization on train and test data is applied.

4 Deep Neural Network Model

Neural network models in simple terms described as mathematical function which maps the input to generate the desired output. It comprises of input layer, output layer, arbitrary number of hidden layers, a set of weights, and bias between each layer and a choice of activation function and loss function.

On completion of transformation of the data, DNN-sequential model is applied here on the pre-processed data as it allows layer by layer model building, which forms network of dense layer. As there are six input features (except ‘RAIN’ which is target variable) as shown in Table 5, the first dense input layer is set with six features. Activation function rectified linear activation function ‘ReLU’ is used at hidden layers. Another dense layer with four neurons is added with ‘ReLU’ activation. As the problem belongs to the class of binary classification, ‘sigmoid’ function is used

Table 9 Model summary

Layer (type)	Output shape	Param #
dense_1 (Dense)	(None, 6)	42
dense_2 (Dense)	(None, 4)	28
dense_3 (Dense)	(None, 1)	5
Total Params: 75		
Trainable params: 75		
Non-trainable params: 0		

at the output layer, which will generate output either 1 or 0, for rainfall or no rainfall, respectively. Thus, the model has 6 input, two hidden layers with 6 and 4 neurons and output layer with one output. The model is implemented using keras.io [9]. The model summary is shown in Table 9.

To train deep neural network models, adaptive optimization algorithms are used. The examples include Adam [10], Adagrad [11], RMSprop [12]. Adaptive here refers that it computes individual learning rate for different parameters. The model is compiled using Adam optimizer which is seen as a combination of RMSprop and stochastic gradient descent [13] with momentum with few distinctions. The nature of problem being binary classification and as the target variables are {0,1}, the loss function is computed using cross-entropy [14]. The model is fitted to training data using 10 epochs and batch size of 64. One epoch is the complete pass through the training data. Epoch is a hyperparameter, and there is no thumb rule for that. Batch size is the number of sample processed in the single mini-batch.

5 Result and Conclusion

In this section, the results generated at various stages are discussed.

5.1 Weights and Bias

The model weights for first layer dense_1, with the output shape (None, 6) generates 42 parameters, that is 36 weights and 6 bias, similarly 24 weights and 4 bias for dense_2 and 4 weights and 1 bias for dense_3, total 75 parameters. The values generated across each weight and bias is as shown in Table 10.

Table 10 Weight and bias at hidden layers

Layer (type)	Weights	Bias
dense_1 (Dense)	[1.141973, 1.97442, -1.734192, 1.275294, -2.042584, -2.0059183], [-0.29253215, 0.12715897, 0.83936656, -0.2561121, 0.21438691, -0.00820558], [0.3164518, -0.1136589, -0.19223101, 0.4917892, -0.0732223, -0.07245291], [-0.12871715, 0.03039517, -0.18574753, -0.15315911, -0.12539569, 0.00333604], [-0.14801866, 0.07896663, 0.93043214, 0.5128609, -0.35926303, 0.29292443], [0.16915724, 0.00389614, -0.38254952, -0.28463966, 0.22222997, 0.00662909]	[1.0052627, 1.0992466, 0.28027502, 0.6150749, 0.31144813, -0.14159845]
dense_2 (Dense)	[-0.51795757, -0.85841197, -0.616253, 1.39788], [-0.87039506, -1.31375, -0.62691236, 2.1033716], [0.5722295, 0.95757383, -0.6314308, 0.10791895], [-0.78557706, -0.5372498, 0.2611877, 0.39101806], [-0.44372734, 1.4242774, 0.0454119, -0.62419903], [-0.6753952, 0.69929206, -0.34458962, -0.95543414]	[-0.19212776, 0.28099677, 0.08030465, 0.6100016]
dense_3 (Dense)	[0.5681466], [-1.3521026], [-0.12679887], [2.3315494]	[-0.08006777]

5.2 Training and Validation: Loss and Accuracy

After the model is complied, the training data is fit using 10 epoch and 64 batch size. As the number of epochs increases, more information is learned. Both training and validation accuracy increase as the number of epochs increases. The resultant training and validation loss and accuracy in each epoch are shown in Table 11. The model took 2.48 s to train.

Figure 4 shows at each increasing epoch the model loss and decreases and the model accuracy increases. From 8th epoch onwards, the curve starts flattening, and by 10th epoch, it becomes stagnant. Here, the batch size is 64. Thus, further training is stopped and model used for testing data.

Table 11 Training and validation loss and accuracy

Epoch	Training loss	Training accuracy	Validation loss	Validation accuracy
1	0.5548	0.7310	0.4685	0.7852
2	0.4041	0.8349	0.3324	0.8774
3	0.2866	0.8939	0.2363	0.9132
4	0.2210	0.9145	0.1939	0.9271
5	0.1839	0.9308	0.1654	0.9376
6	0.1547	0.9442	0.1415	0.9503
7	0.1326	0.9527	0.1224	0.9557
8	0.1143	0.9582	0.1067	0.9606
9	0.0990	0.9642	0.0938	0.9655
10	0.0859	0.9670	0.0819	0.9667

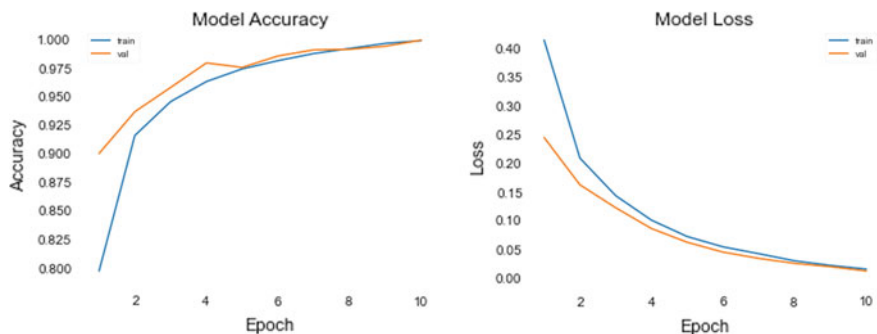


Fig. 4 Model accuracy and model loss

Table 12 Test loss and test accuracy

Test loss	0.07455659657716751
Test accuracy	0.9733855128288269

5.3 *Test Loss and Test Accuracy*

The model is applied on testing data, and the resultant test loss and test accuracy is shown in Table 12.

5.4 *Comparative Analysis*

The target variable in the present problem statement is binary, that is 1 for it will rain and 0 for will not rain. Thus, it is a classification problem and several machine learning classification algorithms can be fitted to this dataset on appropriate pre-processing. Logistic regression model [15] is one such model which best fits for binary classification. The training data is fitted to logistic regression model, and it is observed that test accuracy obtained is 0.9330724070450098.

6 Conclusion

The paper presents the steps involved in pre-processing the raw data before passing it to a deep neural network model. The architecture of the deep neural network model is influenced by the feature vectors that go as input and the target variable which is the expected output. The activation function and optimizer used impacts the loss function. Here, the Seattle weather data is used for rainfall prediction which is available for a period from 1948 to 2017. The prediction of rainfall on a particular day which belongs to the class of binary classification is trained using deep neural network model. The sequential model with dense layer, ReLU activation function at hidden layer, sigmoid function at output layer, Adam optimizer, 10 epochs with batch size 64 is implemented on the dataset to achieve the test accuracy of 97.33%. The training data when was fitted to logistic regression model also, and it gave accuracy of 93.30%. Thus, it is recommended to use DNN model, as in logistic regression the classification is linear, whereas the DNN model will be useful for more complex and nonlinear data.

References

1. Nayak DR, Mahapatra A, Mishra P (2013) A survey on rainfall prediction using artificial neural network. *Int J Comput Appl*
2. Lee S, Cho S, Wong PM (1998) Rainfall prediction using artificial neural networks. *J Geogr Inf Decis Anal* 2(2):233–242
3. Lee J, Kim C-G, Lee JE, Kim NW, Kim H (2018) Application of artificial neural networks to rainfall forecasting in the Geum River Basin, Korea. *Water* 10:1448. <https://doi.org/10.3390/w10101448>
4. Aswin S, Srikanth G, Vinayakumar R (2018) Deep learning models for the prediction of rainfall. In: Conference: 2018 international conference on communication and signal processing (ICCPSP). <https://doi.org/10.1109/ICCPSP.2018.8523829>
5. <https://www.kaggle.com/rtatman/did-it-rain-in-seattle-19482017>
6. Rain: A Water Resource. USGS General Interest Publication. https://www.usgs.gov/special-topic/water-science-school/science/precipitation-and-water-cycle?qt-science_center_objects=0#qt-science_center_objects. Last accessed 12/10/2020
7. Lull HW (1959) Soil compaction on forest and range lands. U.S. Dept. of Agriculture, Forestry Service, Misc. Publication No. 768
8. Bhandari A (2020) Feature scaling for machine learning: understanding the difference between normalization versus standardization, <https://www.analyticsvidhya.com/blog/2020/04/feature-scaling-machine-learning-normalization-standardization/>
9. Keras Homepage. <https://keras.io/>. Last accessed 14/10/2020
10. Kingma DP, Ba JL (2014) Adam: a method for stochastic optimization. [arXiv:1412.6980v9](https://arxiv.org/abs/1412.6980v9)
11. Duchi J, Hazan E, Singer Y (2011) Adaptive subgradient methods for online learning and stochastic optimization. *J Mach Learn Res* 12:2121–2159
12. Tieleman T, Hinton G (2012) Lecture 6.5-rmsprop: divide the gradient by a running average of its recent magnitude. COURSERA: neural networks for machine learning 4(2):26–31
13. Ashia C, Wilson RR, Stern M, Srebro N, Recht B (2017) The marginal value of adaptive gradient methods in machine learning. [arXiv:1705.08292v2](https://arxiv.org/abs/1705.08292v2)
14. Mannor S, Peleg D, Reuven R (2005) The cross entropy method for classification, ICML. In: '05: proceedings of the 22nd international conference on machine learning, pp 561–568. <https://doi.org/10.1145/1102351.1102422>
15. Jakaitiene A (2019) Nonlinear regression models. In: Encyclopedia of bioinformatics and computational biology

A Comparative Analysis of Supervised Word Sense Disambiguation in Information Retrieval



Chandrakala Arya, Manoj Diwakar, and Shobha Arya

Abstract As the amount of information increases every day, there is a need of information retrieval for finding useful information from large amount of information. This paper presents and evaluates supervised word sense disambiguation (WSD) algorithms in information retrieval (IR). Word ambiguity problem is a key issue in the information retrieval systems. Supervised WSD is considered as the effective method than other methods in information retrieval. The effective usage of supervised WSD in IR is the main objectives of this research paper. The paper defines the role of supervised WSD in IR and discusses the best-known supervised algorithms in detail. We use Weikato environment for knowledge analysis (WEKA) tool to assess four supervised WSD algorithms Naïve Bayes, support vector machine (SMO), decision tree (J48), and KNN (IBK) through a series of experiments, and the result concludes that the algorithms performance is based on the features of the datasets.

Keywords Word sense disambiguation · Information retrieval · WEKA · Supervised word sense disambiguation

1 Introduction

The performance of IR system is measured by the usefulness of the system to the typical user, and the use of WSD in IR systems significantly affects its performance. It is one of the fundamental problems in numerous NLP applications such as machine translation [1, 2] and IR, etc. In natural language, ambiguous words have multiple meanings, each meaning is called a “sense” of the word, and the process of classifying precise meaning of a word in a given context is known as WSD. Overall IR systems performance can improve by identifying correct meanings of words provided by

C. Arya (✉)
Graphic Era Hill University, Dehradun, Uttarakhand, India

M. Diwakar
Graphic Era Deemed To Be University, Dehradun, Uttarakhand, India

S. Arya
Gurukul Kangri Vishwavidyalaya, Haridwar, Uttarakhand, India

WSD system; therefore, lack of disambiguation power is one of the reasons of poor IR performance. In IR systems, WSD is used to resolve ambiguity in queries, relevance ranking, and classification of documents. WSD combines with IR in such a way that it improves the performance of an IR system.

The performance evaluation parameters of IR systems are the retrieval precision and recall; these are the assessment measures of retrieval results. The correct use of WSD in IR shows improvements in precision and recall, retrieval precision can hurt by the ambiguities in query words, and therefore, correct classification of the sense of the ambiguous word in both queries and documents can improve the retrieval precision. In retrieval recall, the words in query may have tightly related meaning with other words which are not present in the query, while by using these relations between words can lead to improved retrieval recall. Previous researches in the field of WSD in IR show conflicting results. Firstly Weiss [3] in 1973 discussed the work of disambiguation and IR. Weiss used a disambiguator in which he constructed set of rules manually to disambiguate five words. The disambiguator used by Weiss shows 90% accuracy wherever the improvement in IR performance was reported 1%. Later, Krovetz and Croft in 1992 [4] and Voorhees in 1993 [5] also show no improvement in IR using word senses. Some other experiments performed by Schite and Pedersen in 1995 [6], Gonzalo et al. in 1998 [7], Sanderson in 2000 [8], and Donia Tatar in 2004 [9] also used the word senses in IR systems for the performance improvement. Kumar et al. [10, 11] employed machine learning approaches for classification and achieved significant improvement in accuracy.

WSD approaches can be classified into four categories: Supervised approach, unsupervised approach, semi-supervised approach, and knowledge-based approach. This paper mainly focuses on the supervised WSD approach in the context of classification in IR. In IR, we often want to learn many related classes over same data where users have related interest and categories have relationships. Supervised method generally tends to reduce WSD to a classification problem that depends on the occurrence of words in trained systems. IR performance can be improved by the correct classification of the documents.

The remaining paper is ordered as follows: Sect. 2 discusses the several approaches of WSD. Section 3 describes the detail of supervised approach and its various algorithms in detail. Comparative analysis of supervised algorithms is discussed in Sect. 4. Discussion is presented in Sect. 5, and finally, Sect. 6 covers the conclusion of the paper.

2 WSD Approaches

WSD approaches are classified as:

Supervised approach: Supervised approach is based on annotated corpora, and strongly supervised is defined as a system which employs sense labeled training data.

Unsupervised approach: Unsupervised approach is completely relying on external information and does not use sense-tagged data (training data).

Semi-supervised approach: Semi-supervised system has both sense-tagged and untagged data to learn a classifier using different proportions.

Knowledge-Based Approach: Those methods depend on glossaries, dictionaries, and other lexical knowledge bases without using any corpus are named knowledge-based approach.

In this paper, we discuss supervised WSD approach to improve the performance of IR. Supervised WSD approach is considered as the best approach among the others. Other WSD methods show some limitations which affects the IR performance. The main drawback of knowledge-based approach is that it requires knowledge source for providing the word senses, but sense inventories and rule database are not always available; therefore, supervised approach shows better performance than knowledge-based approach. Unsupervised approach determines unidentified but valuable objects classes [12]. It is useful when sense-tagged corpora are not available. In spite of this, unsupervised methods are difficult to implement, because tagged corpora is unavailable for comparing results. Figure 1 shows the classification of WSD approaches.

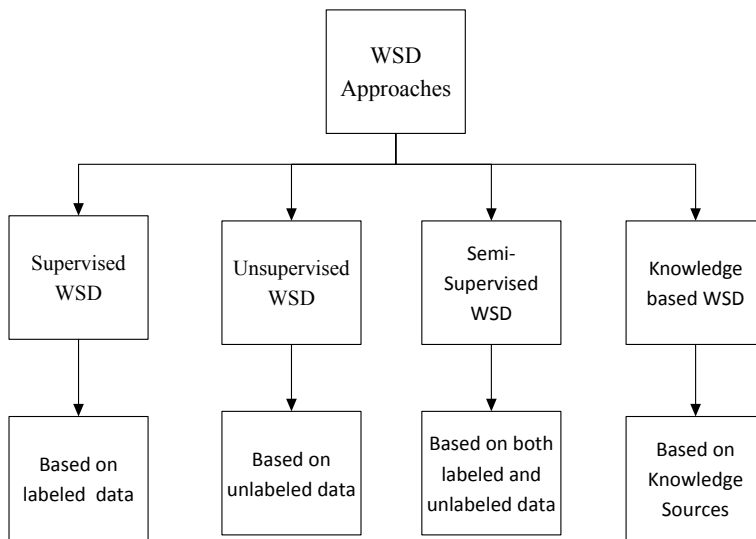


Fig. 1 WSD approaches

3 Supervised WSD for IR

In current scenario, the supervised approaches have been recognized as the most commonly used approach for disambiguation. Supervised WSD approach requires a set of labeled documents and maps the documents with predefined class labels. Earlier research shows that supervised WSD approach increases IR performance and is better than other WSD approaches.

Kotsiantis [13] in 2007 describe the best-known supervised algorithms and show that classification accuracy is increased without decreasing comprehensibility of feature selection procedure. Zhong and Ng [14] in 2012 show improvements in IR by using supervised WSD methods.

The main task of IR is to find that whether a particular sense is connected with a particular instance of word or likely that whether the document is relevant to a query. Appropriate classification of documents can improve IR performance. It is established that a good WSD program can improve IR performance by 2% [9]. In classification, a set of input documents or datasets are divided into one or more classes. It is used to classify given set of words to the correct domain and presented with a training set which consists a set of input context labeled with their appropriate sense. Some important methods of supervised approach are as follows.

3.1 Naïve Bayes Algorithm

Naïve Bayes algorithm is based on the probabilistic approach of Bayes' theorem [15]. A naïve Bayes classifier is assuming that features are statistically independent and computes the conditional probability of each independent sense S_i of a word w where f_j are features of the given context. Classification is based on the selection of most appropriate sense S from the context. According to the concept of independent features, the algorithm can be stated as:

$$\begin{aligned} S &= \arg \max P(S_i | f_1, \dots, f_m) \\ &= \arg \max P(f_1, \dots, f_m | S_i) P(S_i) / P(f_1, \dots, f_m) \end{aligned} \quad (1)$$

where $P(S_i)$ and $P(S_i/f_i)$ are calculated in the training process.

3.2 Support Vector Machine (SVM) Algorithm

SVM is a binary classifier; i.e., it solves classification problem of binary classes [16]. It depends upon the vector space. SVM separated two classes by the decision boundary. A maximum decisions margin shows the good classification results. The training set is divided into two ways by the SVM; the first one is linear separation,

and the second is kernel function, which is used to take data as input and convert it into essential form such as linear, nonlinear, polynomial, etc. Shekhawat et al. [17] proposed a new approach for data transformation that leads to efficient classification. There is no way to select a best kernel for a specific problem; therefore, it is better to try all possible kernels and choose the best one according to the particular task.

3.3 Decision Tree Algorithm

Decision tree is defined by a hierarchy of rule in the form of a tree. Internal nodes of a tree are formed by the rules, and the root node is defined by the highest internal node. Each rule (internal node) is used to test the value of some property of data. For the construction of decision tree, training data is used. The list of rules is checked first whenever a new sample is classified, and the first matched rule is applied. Features are ranked according to their information content. Decision tree is used to predict label y for test input x .

There are numerous specific decision tree's versions are available like C 4.5, ID3, 48, and CART, etc.

In this paper, we used J48 algorithm. The concept of information entropy is used by the J48 to build a decision trees from a labeled training dataset. While building a tree, J48 ignores the missing values.

3.4 K-Nearest Neighbor (KNN) Algorithm

This algorithm performed classification, by comparing a given test set with training set which are comparable to it. It contains three primary components: a set of labeled approach, a closeness or resemblance metrical for the purpose of measuring the objects distance, the k value, and the nearest neighbor's count. Class label of the object can be measured by the nearest neighbor's class labels.

Likeness of the test objects $z = (x'', y'')$ and training objects $x = (x, y)$ is obtained from the equation:

$$\text{Dist}(z, x) = \sqrt{(x'' - x)^2 + (y'' - y)^2} \quad (2)$$

In this paper, we used IBK for comparison. It is a K-nearest neighbor algorithm that uses the same distance metric. It used the distance function as a parameter for the searching. The predictions about the neighbor can be measured by the test instances distances, and for converting the distance into weight, there are two different formulas (Witten and Frank) [18, 19].

4 Comparison of Algorithms

Supervised WSD methods are relevant in numerous domains. Classification is an important part of information retrieval; in classification, it classifies an object into multiple classes. This paper shown a comparative analysis of SVM based (SMO algorithm), Naïve Bayes, KNN based (IBK algorithm), and decision based (J48 algorithm). For classification, we used WEKA tool. There are numeric and nominal types of dataset attributes. We used four datasets, namely lymph dataset, breast cancer dataset, gesture phase segmentation, and Iris dataset containing instances and attributes as 149 and 19, 286 and 9, 1747 and 20, and 150 and 5, respectively, primarily from UCI repository [20]. Percentage split method, where dataset is randomly separated into two distinct datasets, known as training set and test set used for the dataset evaluation. Once the experiments are carried out on the selected dataset, it is split into training with 66% objects from the original dataset and remaining for the testing dataset, and comparison is conducted on the overall results.

Experiments are applied on the four datasets. Main features of these datasets are enumerated in Table 1.

Table 2 shows the comparison of accuracies of the four classifiers for four different datasets.

From Table 1, the overall best accuracy is obtained as 96% for iris dataset. For the datasets, gesture phase segmentation and breast cancer IBK show high accuracy of 95 and 72%. For the dataset lymph, Naïve Bayes shows the lowest accuracy of 91% and then the other three classifiers. Table shows that the accuracy of classifiers varies according to the characteristics of datasets.

Table 1 Datasets characteristics

Datasets	Total No. of instances	Number of attributes
Iris	150	5
Gesture phase segmentation	1747	20
Lymph	149	19
Breast cancer	268	9

Table 2 Comparison of accuracies of all datasets

Algorithms	Gesture phase segmentation (%)	Breast cancer (%)	Lymph (%)	Iris (%)
Naïve Bayes	74	71	91	94
SVM (SMO)	79	70	93	96
KNN (IBK)	95	72	93	96
Decision tree (J48)	93	68	93	96

In an information retrieval system, documents are known as instances, and the task is to return a set of relevant documents given a search term and categorize documents as relevant and not relevant. The performance of the classifier is evaluated on the basis of some parameters such as true positive (TP), false positive (FP), precision, recall, *F*-measure, and Mathew correlation coefficient (MCC). These parameters were calculated using the predictive classification table known as confusion matrix. Confusion matrix shows the accuracy of the solution to a classification problem.

Precision: Precision measures the fraction of retrieved instances that are relevant.

$$\text{Precision} = \text{TP}/(\text{FP} + \text{TP}) \quad (3)$$

Recall: Recall is measured by the fraction of true positive and the total number of elements that truly go to the positive class.

$$\text{Recall} = \text{TP}/(\text{FN} + \text{TP}) \quad (4)$$

F-measure: *F*-measure is used to measure the accuracy of test. It computes the score with the help of both precision and recall.

$$F\text{-measure} = (2 * \text{precision} * \text{recall})/(\text{precision} + \text{recall}) \quad (5)$$

MCC: MCC is used to measure the binary classification quality.

$$\begin{aligned} \text{MCC} = & (\text{TP} * \text{TN} - \text{FP} * \text{FN}) \\ & /(\sqrt{(\text{TP} + \text{FP})(\text{TP} + \text{FN})(\text{TN} + \text{FP})(\text{TN} + \text{FN})}) \end{aligned} \quad (6)$$

The comparison of performance of different classifiers with different datasets is measured on the basis of these parameters. Firstly, compare four classifiers with lymph dataset, weighted average parameters of four classifiers are shown in Table 3.

Table 3 shows that parameters values of Naïve Bayes are lower than other algorithms for lymph dataset. SMO, KNN (IBK), and DT (J48) show best precision and recall value as 0.945 and 0.941, respectively, and also, higher F-measure and MCC values as 0.941 and 0.901, respectively.

Weighted average comparison of four classifiers for breast cancer dataset is listed in Table 4.

Table 3 Comparison of parameters of lymph dataset

Algorithms	Precision	Recall	<i>F</i> -Measure	MCC
Naïve Bayes	0.937	0.921	0.921	0.898
SVM (SMO)	0.945	0.941	0.941	0.901
KNN (IBK)	0.945	0.941	0.941	0.901
Decision tree (J48)	0.945	0.941	0.941	0.901

Table 4 Comparison of parameters of breast cancer dataset

Algorithms	Precision	Recall	<i>F</i> -Measure	MCC
Naïve Bayes	0.701	0.711	0.703	0.331
SVM (SMO)	0.699	0.701	0.691	0.302
KNN (IBK)	0.714	0.722	0.690	0.326
Decision tree (J48)	0.657	0.680	0.650	0.217

From Table 4, parameters values of KNN (IBK) show the highest value among others for breast cancer dataset. IBK shows overall best precision and recall value as 0.714 and 0.722, respectively, but higher *F*-measure J48 shows lowest parameters value.

Weighted average of four classifiers for gesture phase segmentation dataset is listed in Table 5.

According to Table 5, parameters value of KNN (IBK) algorithm is higher than the algorithms DT (J48), SMO, and Naïve Bayes, respectively. Lowest precision shows by the SMO while lowest recall by Naïve Bayes algorithm.

Weighted average comparison of four classifiers for iris dataset is listed in Table 6.

In Table 6, parameters value of three classifiers, namely SMO, KNN (IBK), and DT (J48) are exactly same. Only Naïve Bayes shows lower parameter value.

Table 5 Comparison of parameters of gesture phase segmentation dataset

Algorithms	Precision	Recall	<i>F</i> -Measure	MCC
Naïve Bayes	0.756	0.741	0.736	0.653
SVM (SMO)	0.741	0.793	0.739	0.672
KNN (IBK)	0.959	0.958	0.958	0.942
Decision tree (J48)	0.939	0.939	0.938	0.917

Table 6 Comparison of parameters of weighted average of iris dataset

Algorithms	Precision	Recall	<i>F</i> -Measure	MCC
Naïve Bayes	0.756	0.741	0.736	0.653
SVM (SMO)	0.741	0.793	0.739	0.672
KNN (IBK)	0.959	0.958	0.958	0.942
Decision tree (J48)	0.939	0.939	0.938	0.917

5 Discussion

Supervised WSD approach shows significant effect in IR. The automatic extraction of information from supervised learning algorithms is the best explored approach to mine the information. Accurate mining of information improves IR performance. We have attempted to describe the algorithms of supervised WSD approach and give a comparison. We compare four algorithms Naïve Bayes, SMO, decision tree (J48), and KNN (IBK) on four different datasets.

SVM can be a useful tool for analysis of data which are not regularly distributed or have an unknown distribution. Naïve Bayes classifier is easy to implement and obtain good results in most of the cases. The fast classification time by decision tree is due to the absence of calculation in its classification process. The weaknesses of KNN are slow runtime performance and large memory requirement.

Similarly, based on the findings of our experimental results, IBK and SMO perform better than other algorithms but no one performs best for all the datasets. It can be seen that the same classifier is not the best one for all datasets and always outperforms the other classifiers. For each dataset, the best predictive classifier is defined.

6 Conclusion

The relationship of WSD and IR is one of the most challenging problems on the Internet. The main aim of the paper is to discuss about the role of supervised WSD approach in IR and describe the best-known supervised algorithms in detail and provided comparison of these algorithms with four different datasets. There are four classifiers used in the experiment, namely Naïve Bayes, SMO, J48, and IBK. According to the experimental results, IBK and SMO algorithms show the best performances; however, none of the algorithms outperforms the other algorithms, so we can say that the classifiers performance can be affected by the characteristics of datasets; any difference in characteristic of dataset can change the performance of classifier.

References

1. Sanderson M (1994) Word sense disambiguation and information retrieval. In: SIGIR'94. Springer, London, pp 142–151
2. Stokoe C, Oakes MP, Tait J (2003) Word sense disambiguation in information retrieval revisited. In: Proceedings of the 26th annual international ACM SIGIR conference on research and development in information retrieval, pp 159–166
3. Weiss SF (1973) Learning to disambiguate. Inf Stor Retr 9(1):33–41
4. Krovetz R, Croft WB (1992) Lexical ambiguity and information retrieval. ACM Trans Inf Syst (TOIS) 10(2):115–141

5. Voorhees EM (1993) Using WordNet to disambiguate word senses for text retrieval. In: Proceedings of the 16th annual international ACM SIGIR conference on research and development in information retrieval, pp 171–180
6. Schütze H, Pedersen JO (1995) Information retrieval based on word senses
7. Gonzalo J, Verdejo F, Chugur I, Cigarran J (1998) Indexing with WordNet synsets can improve text retrieval. arXiv preprint cmp-lg/9808002
8. Sanderson M (2000) Retrieving with good sense. Inf Retrieval 2(1):49–69
9. Tatar D (2005) Word sense disambiguation by machine learning approach: a short survey. Fund Inform 64(1–4):433–442
10. Kumar S, Sharma B, Sharma VK, Poonia RC (2018) Automated soil prediction using bag-of-features and chaotic spider monkey optimization algorithm. Evol Intel 1–12. <https://doi.org/10.1007/s12065-018-0186-9>
11. Kumar S, Sharma B, Sharma VK, Sharma H, Bansal JC (2018) Plant leaf disease identification using exponential spider monkey optimization. Sustain Comput Inf Syst 28. <https://doi.org/10.1016/j.suscom.2018.10.004>
12. Jain AK, Murty MN, Flynn PJ (1999) Data clustering: a review. ACM Comput Surv (CSUR) 31(3):264–323
13. Kotsiantis SB, Zaharakis I, Pintelas P (2007) Supervised machine learning: a review of classification techniques. Emerg Artif Intel Appl Comput Eng 160(1):3–24
14. Zhong Z, Ng HT (2012) Word sense disambiguation improves information retrieval. In: Proceedings of the 50th annual meeting of the association for computational linguistics, vol 1: long papers, pp 273–282
15. Huang J, Lu J, Ling CX (2003) Comparing naive Bayes, decision trees, and SVM with AUC and accuracy. In: Third IEEE international conference on data mining. IEEE, pp 553–556
16. Burges CJ (1998) A tutorial on support vector machines for pattern recognition. Data Min Knowl Disc 2(2):121–167
17. Shekhawat SS, Sharma H, Kumar S, Nayyar A, Qureshi B bSSA: binary salp swarm algorithm with hybrid data transformation for feature selection. IEEE Access. <https://doi.org/10.1109/ACCESS.2021.3049547>
18. Deepajothi S, Selvarajan S (2012) A comparative study of classification techniques on adult data set. Int J Eng Res Technol 1(8):1–8
19. Shazmeen SF, Baig MMA, Pawar MR (2013) Performance evaluation of different data mining classification algorithm and predictive analysis. J Comput Eng 10(6):01–06
20. <https://archive.ics.uci.edu/ml/>. Accessed on 10 Oct 2020

Real-Time Deep Learning Face Mask Detection Model During COVID-19



Amit Juyal and Aditya Joshi

Abstract COVID-19 pandemic has affected the whole world not only physically but also financially. Thousands of people have died due to this COVID-19 (Coronavirus) epidemic, and still the whole world is struggling to prevent this epidemic. Initially, the government had only an option to stop this epidemic and that was to declare complete lockdown. But during this time phase of lockdown, many people became unemployed. To stop this scenario and for the sake of employment and other financial economy, our government has decided to unlock various sectors. This unlock phase has increased the risk of outbreak of COVID-19 so to avoid risk and to stop spreading of this pandemic disease, the government has issued some important guidelines to be followed mandatorily by each individual during this unlock process. The face mask is one of the compulsory guidelines issued by the government. Wearing a face mask may reduce the chances of spreading corona virus. Many people roaming in public places without wearing a face mask. To monitor such kind of people at a time is not easy manually. So in this paper, we are proposing deep learning-based model that can automatically detect person wearing a mask or not. In this method, a model convolutional neural network (CNN) was trained over thousands of images to detect whether a person wearing a mask or not. Proposed model achieved 93.36 validation accuracy and 98.71 training accuracy. This model can be helpful to stop spreading of coronavirus in such organizations where human interaction is necessary for smooth functioning like hospitals, colleges, gyms, supermarkets.

Keywords CNN · Face mask · Deep learning · Keras

A. Juyal (✉)
Graphic Era Hill University, Dehradun, India

A. Joshi
Graphic Era Deemed to be University, Dehradun, India

1 Introduction

During this crucial phase of COVID-19 pandemic, to stop spreading of the virus some important guidelines were issued by government, out of these, wearing a face mask in public is one of the most important guidelines. Wearing a face mask, frequent hand wash and social distancing by maintaining one meter distance from others are the ways to be safe from corona. Most of the countries have decided to punish those who are not wearing a mask in public. But it is impossible to invigilate everyone in public for a face mask. Thus to overcome this problem, we have proposed a deep learning (CNN)-based model that can detect a person wearing a mask or not. For this work, we have created our own image dataset containing thousand of images. In the image dataset, we have created two categories, namely “with face mask” and “without face mask.” We have created five hundred images for both of the above-mentioned categories. Then our model was trained on the bases of image dataset and validated. For real-time video stream, we have used webcam to record person appearing in front of the camera. We have used keras library to build our model. Frame was extracted from the captured video containing person face. Using Haar cascade library, we have extracted region of interest which is face in our present study. Then we loaded our model that we have trained earlier. By using this model, we have predicted if a person is wearing a mask or not.

2 Literature Survey

Deep learning technique has emerged as a promising method to solve out various real-world problems. CNN model nowadays is widely used as a computational technique in different areas. This model has been used to solve problems of various fields like image recognition, recognition of action, face recognition, an estimation of human pose documentation analysis, scene labeling, speech recognition, and text classification for natural language processing [1]. CNN method has described as the best model in field of face recognition. Many researchers used CNN-based approach for face recognition [2]. This model was simplified by layering the convolutional and sampling layers together for face recognition [3]. It is also used in biomedical imaging. Medical image classification is applied for computer-aided diagnosis by the use of CNN model [4]. It has also been fused with some other technique to produce a new improvise fusion model like color two-dimensional principal component analysis (2DPCA)-convolutional neural network (C2D-CNN) for facial feature robust face recognition [5]. Singh et al. [6] analyzed time series data for COVID-19 using SVM. Bhatnagar et al. [7] also data do COVID-19. CNN model showed very good performance for face recognition [7, 8]. When it combined with SVM, it showed high recognition rate and less training time in face recognition [9]. Prediction for spread rate and recovery also performed by researchers [10] using machine learning.

Recently CNN model was used as an improvised technique named as Mask R-CNN for face recognition, which include face detection and segmentation simultaneously [11].

3 Methodology

The COVID-19 pandemic has affected all of humanity today, physically as well as financially. Presently, government has suggested everyone to wear mask and has made it mandatory in public places. To restrict spreading of corona virus, wearing a mask in public/crowd is very important.

3.1 Algorithm

Step 1: Person appears at the entrance

Step 2: CCTV will capture the video

Step 3: Extract frame containing person image from video

Step 4: Feed image into CNN model

Step 5: Input image will be classified from step 4 in two classes “With Face Mask” or “Without Face Mask”

Step 6: If image classified as Without Face Mask, then entry of a person will be prohibited else person allowed to enter

Step 7: End.

The overall working of our proposed model has showed in Fig. 1. Person appears at the entrance may wear a mask or not. CCTV camera will capture the video of the person who is coming to the entrance. The video is made up of a sequence of frames. The video captured in step 2 will be processed to obtain an image from a frame. Captured image in step 3 will be feed into the CNN-based model to detect whether a person wearing a mask or not. If the person is identified without wearing a face mask, he or she will be refused to enter.

In this paper, CNN model was trained with thousand of images with good accuracy. CNN is a feed forward type of neural network. Mainly CNN has three layers, convolutional, rectified linear unit (ReLU), pooling and fully connected layer. Each layer in CNN is made up of neurons. For image classification, CNN is considered better than fully connected network. In a fully connected network, each neurons of one layer is connected to all the neurons of next layer which eventually lead to overfitting. While in CNN, a neuron in the layer will only be connected to small regions of the layer before it. Figure 2 shows the working of CNN model.

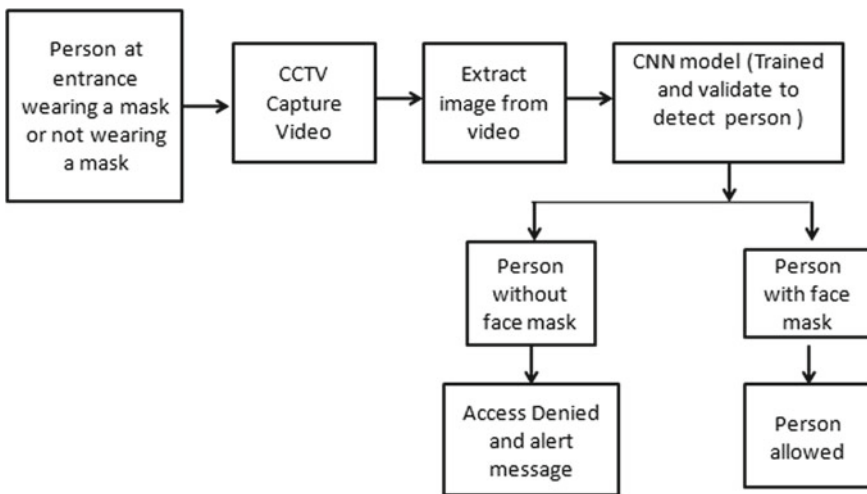


Fig. 1 Working of entire proposed model

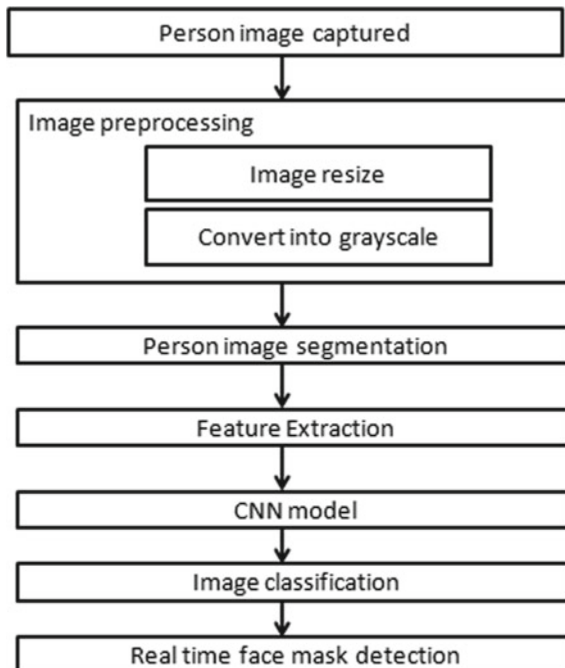


Fig. 2 Layered architecture of proposed model



Fig. 3 Images of a same person from different angles with mask and without mask

3.2 Dataset

In this paper, we have created a labeled image dataset of thousand images. Dataset consists of mainly two classes, having five hundred images in each class. Dataset contains different types of human face images. Dataset images shown in Fig. 3 belong to same person from different angles.

The proposed model used two sets of images, with face mask and without face mask. Table 1 shows the distribution of human faces dataset in training and testing phases. Total thousand images were created.

The dataset distributed into 70:30 ratios. 70% of image dataset is used for training purpose, and 30% of image dataset is used for validation purpose. The dataset contains both JPG files and .png files. Dataset contains different size of colored images. It requires lots of computing resources to process color images. Because each pixel contains RGB channel information so to overcome this problem, first images are converted into grayscale as shown in Figs. 4 and 5. The images were resized according to proposed model requirement.

Table 1 Distribution of images for training and validation

Classes	Number of images for training	Number of images for testing	Total images
Without face mask	350	150	500
With face mask	350	150	500

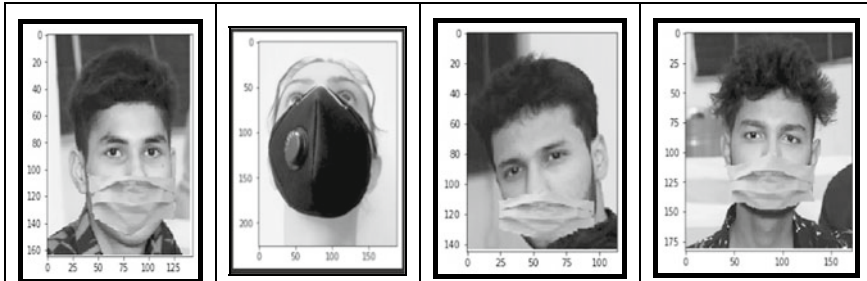


Fig. 4 Images are converted into gray scale

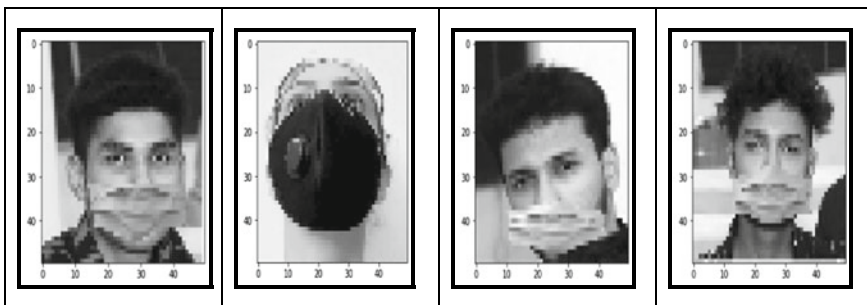


Fig. 5 Resized images in to equal size

4 Implementation

In this work, we have built deep learning CNN model using Keras that uses TensorFlow as a back end engine. Every Keras model is either built using sequential class, which represents linear CNN layers that allow creating model layer by layer or functional model class. For prediction, two classes were categorized on the bases of with mask or without. Sequential model was invoked to initiate the neural network. After initiating sequential model, a first layer was added. In the first layer, convolutional (Conv2D), ReLU, and Max Pooling layers were added as shown in Fig. 6.

The convolutional layer which is represented as Conv2D which has three parameters. The first parameter is feature or filter detector, second parameter is kernel size, and the third parameter is input image shape. First parameter is feature or filter detector which is a set of learnable weights which learnt from backpropagation algorithm. In the present work, there are 64 features or filter detectors. CNN works differently to identify images. To train a CNN model, first of all small pieces of image are provided to the CNN, and these small region of image is called features or filters. The second parameter is kernel size and it should be an odd number; here we have taken kernel size 3×3 . The third parameter is input image_shape that represents input shape of one image, numeric value 1 represents that image is in grayscale.

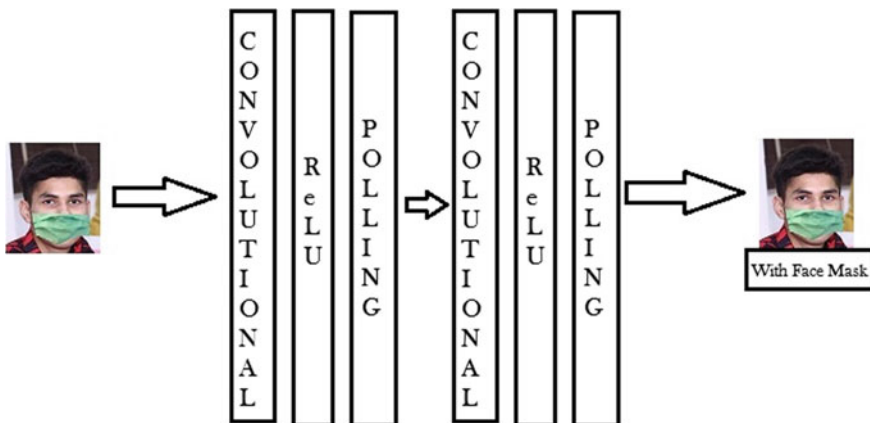


Fig. 6 Hidden layers in CNN model

The next layer is rectified linear unit (ReLU). In the ReLU layer, all the negative values will be replaced with some other value. ReLU is an activation function which replaces every negative value with zero in the filtered image. ReLU function only activates the node, if the input is below zero, then the output will be zero. If the input rises above certain threshold, it has a linear relationship with dependent variables.

$$\text{if } x = -\text{ve} \text{ then } f(x) = 0$$

$$\text{if } x = +\text{ve} \text{ then } f(x) = x$$

ReLU activation function only activates a node if the input is above certain quantity, if the input is zero, output is also zero (Fig. 7).

Therefore, activation is done using ReLU. The next layer is MaxPooling layer. In this layer, the image stack will be shrunked into a smaller size. Maxpooling layers

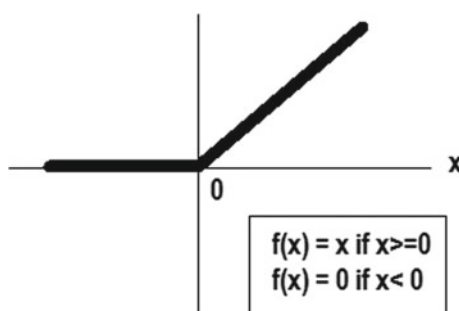


Fig. 7 Representation of ReLU function. If x value is negative then $f(x)$ value remains as 0 otherwise $f(x)$ value will be same as x value

operate on each feature map independently. Similarly in second layer, convolutional (Conv2D), ReLU, and MaxPooling were added. In the second layer, the filter size is 128 which was just double from previous layer. Next, fully connected layer was created using flatten. Flatten is used to convert the data into one-dimensional array for inputting to next layer. The overall neural network architecture is representing in Fig. 8. This overall summary was generated by invoking `model.summary()` method.

Figure 9 depicts accuracy achieved while training and validation. Number of epochs is defined as 22. Training accuracy achieved 98.71% and validation accuracy achieved 93.36%. These training and validation accuracies are directly proportional to number of epochs that means with the increase in number of epochs, the accuracy will increase. But due to small dataset, proposed model achieved good accuracy.

Figure 10 depicts the line graph progress with each epochs for training and validation loss. It is clear from the plot of loss that the model is little over fitted. The gap between training and validation is no minimal, and for a good model, the gap between training and validation should be less. The curve for training loss started approx. 0.38 and end with approx. 0.28. Similarly, validation loss started approx. 0.48 and end with approx. 0.04. It is clearly shown in Fig. 10 that there is a gap between

```
In [13]: print(model.summary());
Model: "sequential_2"

Layer (type)          Output Shape       Param #
=====
conv2d_4 (Conv2D)     (None, 48, 48, 64)    640
activation_6 (Activation) (None, 48, 48, 64)    0
max_pooling2d_4 (MaxPooling2D) (None, 24, 24, 64) 0
conv2d_5 (Conv2D)     (None, 22, 22, 128)   73856
activation_7 (Activation) (None, 22, 22, 128) 0
max_pooling2d_5 (MaxPooling2D) (None, 11, 11, 128) 0
flatten_2 (Flatten)   (None, 15488)        0
dense_4 (Dense)       (None, 64)           991296
dense_5 (Dense)       (None, 1)            65
activation_8 (Activation) (None, 1)           0
=====
Total params: 1,065,857
Trainable params: 1,065,857
Non-trainable params: 0
```

Fig. 8 Showing the overall CNN layers summary

```

Console 1/A
accuracy: 0.9900 - val_loss: 0.2244 - val_accuracy: 0.9302
Epoch 16/20
22/22 [=====] - 26s 1s/step - loss: 0.0305 -
accuracy: 0.9900 - val_loss: 0.2437 - val_accuracy: 0.9402
Epoch 17/20
22/22 [=====] - 26s 1s/step - loss: 0.0281 -
accuracy: 0.9886 - val_loss: 0.2215 - val_accuracy: 0.9435
Epoch 18/20
22/22 [=====] - 26s 1s/step - loss: 0.0226 -
accuracy: 0.9929 - val_loss: 0.2326 - val_accuracy: 0.9402
Epoch 19/20
22/22 [=====] - 26s 1s/step - loss: 0.0248 -
accuracy: 0.9929 - val_loss: 0.2316 - val_accuracy: 0.9535
Epoch 20/20
22/22 [=====] - 27s 1s/step - loss: 0.0285 -
accuracy: 0.9871 - val_loss: 0.2551 - val_accuracy: 0.9336

```

Fig. 9 Training accuracy is 98.71%, and validation accuracy is 93.36%

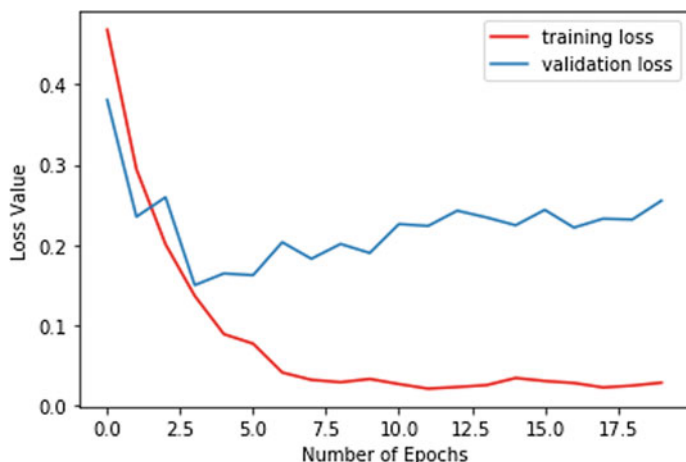


Fig. 10 Plot of training and validation loss

training and validation loss. From epoch 0–27, there is minimum gap between training and validation but as epochs increases the gap also increases between training and validation.

Figure 11 illustrates the plot of training and validation accuracy. It is clearly shown that for training dataset our model achieves 98.71% accuracy, and for validation, our model achieves 93.36% accuracy. The trained model could detect whether a person wearing a mask or not.

For the real-time face mask detection webcam was used. Then the deep learning model “h5” file was loaded which was trained on image dataset earlier. Open CV Haarcascade classifier was used to detect the face in the video frame. Using this

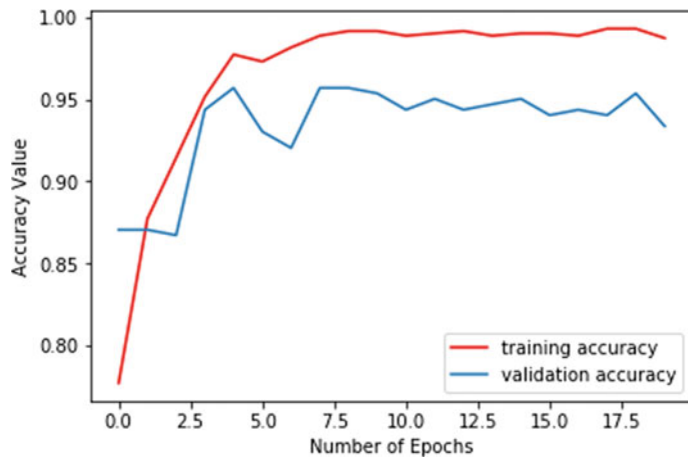


Fig. 11 Plot of training accuracy and validation accuracy

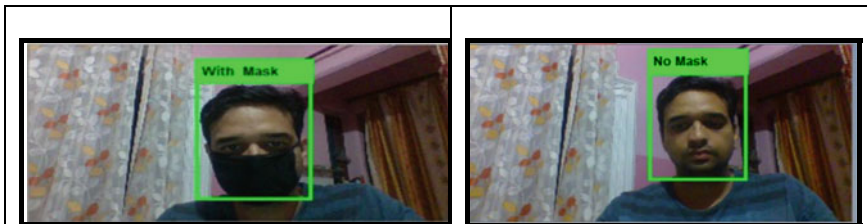


Fig. 12 Detecting face mask or without face mask

classifier, region of interest (ROI) was found in the video frame, and in the present study, ROI is human face.

The result of the present model in real time is shown in Fig. 12. The model detected a person appeared in front of webcam and showed whether a person wearing a mask or not.

5 Conclusion

During COVID-19 pandemic, people have to apply minor but very important change in their lifestyle to control spreading of Corona virus. Wearing a face mask is one of the essential habits to prevent spreading of this virus. In this paper, a deep learning model CNN was proposed that can detect whether a person wearing a face mask or not using webcam. For this study, a three-layer CNN model was used. A dataset of thousand images was created and categorized in two classes: “with face mask” class and “without face mask” with 500 images in each class. The proposed model was

trained on testing image dataset and achieved 98.71% training accuracy and 93.36% validation accuracy.

References

1. Bhandare A, Bhide M, Gokhale P, Chandavarkar R (2016) Applications of convolutional neural networks. *Int J Comput Sci Inf Technol* 7(5):2206–2215
2. Hui HCWYH, Yanjiao X (2008) Recognition of partial-face expression affected by the facial arrangements. *J Shandong Normal Univ (Nat Sci)* 2
3. Wang J, Li Z (2018) Research on face recognition based on CNN. In: Proceedings of the IOP conference, pp 170–177
4. Shin HC, Roth HR, Gao M, Lu L, Xu Z, Nogues I, Summers RM (2016) Deep convolutional neural networks for computer-aided detection: CNN architectures, dataset characteristics and transfer learning. *IEEE Trans Med Imag* 35(5):1285–1298
5. Li J, Qiu T, Wen C, Xie K, Wen FQ (2018) Robust face recognition using the deep C2D-CNN model based on decision-level fusion. *Sensors* 18(7):2080
6. Singh V, Poonia RC, Kumar S, Dass P, Agarwal P, Bhatnagar V, Raja L (2020) Prediction of COVID-19 corona virus pandemic based on time series data using support vector machine. *J Discrete Math Sci Cryptogr* 23(8):1583–1597
7. Lu J, Wang G, Zhou J (2017) Simultaneous feature and dictionary learning for image set based face recognition. *IEEE Trans Image Process* 26(8):4042–4054
8. Hu G, Peng X, Yang Y, Hospedales TM, Verbeek J (2017) Frankenstein: learning deep face representations using small data. *IEEE Trans Image Process* 27(1):293–303
9. Guo S, Chen S, Li Y (2016) Face recognition based on convolutional neural network and support vector machine. In: 2016 IEEE international conference on information and automation (ICIA). IEEE, pp 1787–1792
10. Kumari R, Kumar S, Poonia RC, Singh V, Raja L, Bhatnagar V, Agarwal P Analysis and predictions of spread, recovery, and death caused by COVID-19 in India. In Big data mining and analytics. IEEE. <https://doi.org/10.26599/BDMA.2020.9020013>
11. Lin K, Zhao H, Lv J, Li C, Liu X, Chen R, Zhao R (2020) Face detection and segmentation based on improved mask R-CNN. In: Discrete dynamics in nature and society
12. Bhatnagar V, Poonia RC, Nagar P, Kumar S, Singh V, Raja L, Dass P (2020) Descriptive analysis of COVID-19 patients in the context of India. *J Interdisc Math* 1–16. <https://doi.org/10.1080/09720502.2020.1761635>

Prediction of California Bearing Ratio of Subgrade Soils Using Artificial Neural Network Principles



T. V. Nagaraju, R. Gobinath, Paul Awoyer, and Mohd Abbas H. Abdy Sayyed

Abstract In soil mechanics, prediction of soil properties is necessary due to the large-scale construction activities and time-consuming testing. California Bearing Ratio (CBR) is one of the soil parameters used as strength and stiffness indicator for subgrade soil. However, for investigating soil subgrade in the field, there is a need of more soil samples to be tested; it may be time-consuming and cumbersome task. Moreover, certain issues like lack of funding, unavailability of skilled labour and poor laboratory infrastructure to handle large number of samples put thrust on development of models to predict strength with reference to certain amount of data. Nowadays, the potentiality of prediction models has been gaining importance in every discipline. Numerous tools and techniques were evolved focusing on model development; which will be able to perform iteration-based techniques. In this study, CBR values of subgrade along a proposed road are collected. Nearly, 480 samples were collected in which 15 samples were used for comparison (control value). The results revealed that the artificial neural networks (ANN) prediction models were significant promising tool for predicting CBR of subgrade soil by using index properties as input parameters.

Keywords California Bearing Ratio (CBR) · Artificial neural networks (ANN) · Backpropagation · Pavements

T. V. Nagaraju (✉)

Department of Civil Engineering, S.R.K.R. Engineering College, Bhimavaram, India

R. Gobinath

Department of Civil Engineering, SR Engineering College, Warangal, India

P. Awoyer

Department of Civil Engineering, Covenant University, Ota, Nigeria

M. A. H. Abdy Sayyed

Department of Civil Engineering, SR University, Warangal, India

1 Introduction

Recent years, rapid increase in urbanization leads to increase in the potential of new pavements to each and every nook for sustainable development. Moreover, the main parameter that affects the pavement design and construction is subgrade soil. The properties of soils are varied with place to place and layer to layer from surface. In India, most of the regions covered with the expansive soil, and it possesses variation in swell-shrink behaviour in the field [1, 2]. Further, the distresses caused by the subsoil exposed with moisture content effects the pavements, embankments, and houses. Many researchers are come up with promising findings to counteract the swelling and shrinkage behaviour of expansive clays such as mechanical alteration, chemical alteration and hydraulic modifications [3–6].

Engineering construction of modern highways and transportation modes requires high strength subgrades due to the intensity of loading pattern which is highly demanding. The subgrades that are provided should have sufficient strength, durability, bearing capacity settlement and swelling characteristics [7–9]. Hence, for assessing and investigating the strength and stiffness of the subgrades for new pavements, suitable testing and quality control are needed. Many experimental procedures were available to test the strength of subsoil in which CBR is widely regarded as preferable test which is used frequently throughout the world [10, 11]. It is recommended test for pavement analysis in terms of strength and stiffness. In California Bearing Ratio (CBR) test, the soil strength (penetration resistance) is compared with the penetration resistance of standard crushed rock.

CBR is the ratio between penetration resistance offered by soil to a piston which is travelling at a velocity of 1.27 mm/min and the resistance offered by standard crushed rock for the same penetration depth. CBR of soil subgrades was influenced by various parameters in the field such as moisture content, compaction characteristics, type of soil and method of construction. The presence of excess moisture content not only reduces the maximum density of the soil but also leads to transferring structure of flocculated expansive grains into the dispersed structures [12]. Moreover, subgrade CBR was influenced or altered by chemical alteration of soils using fly ash, rice husk ash, lime and cement. Most of the existing chemical additives such as lime and cement as a stabilizer are not enough sound in the field for higher performance. So, geosynthetics are polymeric materials gaining potential usage in the field of highways, and they can serve as a separator, filter and reinforcement member [13, 14].

On the other hand, few studies show that there will be changes in the experimental values which are caused due to the geographical area all over the world [15]. Despite the reason that it is widely used test, engineers often face issues in obtaining CBR values for longer length of a section due to funding and other related issues, but these values are required for design purpose. Also, concerned with laboratory testing of CBR, it is found that many times the data obtained become inaccurate due to the no control over the soil sampling especially in case of undisturbed sample. CBR can be obtained by other methods, tools and techniques too; researchers had studied CBR by using conic penetrometer experiment, by correlating the soil index with calculated

CBR values and also by using statistical analysis and ANN [16, 17]. Hence, there occurs a need for prediction models utilization in obtaining CBR values which can be validated against real-time data [16, 18]. Research works were undertaken for developing prediction models, since CBR of soil will be affected by index properties in a variety of ways. Most of the models tried to correlate between CBR and the grain size distribution of soils as well as plastic characteristics. Agarwal and Ghanekar [19] made an attempt to correlate CBR with plasticity index (PI), but they failed to obtain convergent correlation. They found that there exists correlation between compaction characteristics and plasticity characteristics instead and they suggested a correlation of sufficient accuracy that can be employed for preliminary identification of material. Even though models are designed to be accurate, reliable and effective, not all models that are available are providing satisfactory results. Stephens [20] reported the models using the single and multi-variable forms for estimating the CBR values based on the soil classification. He found that the estimation models were not convergent. Recent advances arrived in the field of artificial intelligence (AI), techniques such as ANN, support vector machine, natural language processing and algorithms which are gaining potentiality in soil parameters prediction. Moreover, there are not so many research works related to application of soft computing approaches for successful estimation of CBR. Some attempts were made to develop models to predict CBR but most of the models are related to statistical correlations which produce unsatisfactory results. Some attempts of such prediction model development were found in the literature. Many researchers have been attempted for developing prediction models, but reliable models were not developed. Most of the reports, prediction models on CBR of soils, were based on the traditional single and multi-variable regression analysis. Besides, many studies only considered two or three variables to estimate CBR value. For example, compaction characteristics alone do not have significant influence on subgrade CBR value. In similar fashion, plasticity characteristics or soil classification alone do not have profound significance over prediction models [18]. Prediction of CBR of fine-grained soils using artificial intelligence methods was emerging [18, 21]. Recent decade seen splurge in the research works dedicated to the usage of artificial neural networks (ANNs) concerned with the application of geotechnical engineering and allied disciplines; this is used particularly for prediction of critical parameters in soil mechanics [22–24].

For overcoming these problems, implementation of soft computing methods is used, many researchers have studied the behaviour of the soil and they done the experiments on soft computing methods such as artificial neuron networks (ANN), adaptive neuro-fuzzy interface systems (ANFIS) and support vector machine (SVM), and also traditional mathematical regression analysis is in vogue. Patel and Desai [25] reported the convergent correlations between CBR values and soil properties. His research also found that the compaction characteristics and index properties have significant effect on CBR values of soils. Taskiran [18] suggested that AI approaches such as ANN and gene expression programming (GEP) results show best estimation of CBR values.

Trivedi et al. [26] reported that the subgrade soils altered with fly ash can be assessed or predicted using genetic algorithm. Katte et al. [27] reported the estimation models of CBR value using multiple linear regression analysis based on the input variables as OMC and MDD. Especially in construction materials, not only soils but there are also more uncertainties in the concrete composition, which influences strength properties [28]. So, using AI tools gives validate results for predicting the concrete behaviour [29]. This paper presents the prediction of California Bearing Ratio (CBR) of subgrade soil using artificial neural networks (ANN). The predicted model equations have been developed, use five input parameters namely particle sizes (gravel, sand and fines) contents, liquid limit (LL), plastic limit (PL), optimum moisture content (OMC) and maximum dry density (MDD). The paper also focuses on the potentiality of ANN models for predicting soil properties.

2 Materials

Obtaining California Bearing Ratio (soaked or unsoaked) in tandem with other soil characteristics requires considerable effort, resources and time to make a preliminary assessment for the soil suitability for a particular project. In this scenario, implementing prediction models will be suitable considering the reason that they are easy to perform, take less time and also cost-effective comparing the cost required to obtain index and engineering properties of soils. In this research, an attempt is made to use ANN to predict the CBR values of soil with various input parameters.

Considering the neural network usage of relatively less influential parameters in tandem with strong parameters will be definitely beneficial and not like generic statistical procedures which will end up in unpredictable and not so favourable results. Mostly, very weak parameters that are related to the output parameters alone need to be avoided for ANN [30]. Studies suggest that usage of less influential parameters will lead to better prediction of CBR values in case of clays and silts [30]. Their results found that ANN models have significant ability to predict CBR values with very less input variables than the multiple regression analysis.

The soil samples were collected from the road network of S-Yanam to CheeraYanam, Andhra Pradesh, India, at a depth of 0.5 m for every 250 m longitudinal interval of proposal road stretch. Moreover, for any road or pavement design, only soil parameters can decide the road thickness. The strength and stiffness of the road can be assessed by the CBR value, which further affects by the index properties of soils.

2.1 Particle Sizes

In general, soils consist of fine-grained (silts and clays) and coarse-grained particles (gravels and sand). Fine-grained particles are dominant in surface forces and coarse-grained particles are higher in gravity forces, which further affect the compaction characteristics such as OMC and MDD. Moreover, based on the local availability of sources and conditions, the composition of sand may vary certainly. But, silica in the form of quartz is the most general constituent of sand followed by calcium carbonate.

Fines are the smaller-sized particles. These finer particles are used for binding the soil materials. Fines are the first particles move on the surface of the earth when erosion takes place. Finer particles are smaller than 0.0075 mm such as silt and clay.

2.2 Plasticity Characteristics

The amount of water required to transfer soil from plastic state to liquid state is known as liquid limit. It also defined as a soil sample cut into two parts in a cup by a groove of standard dimension of 1 cm deep should join by $\frac{1}{2}$ inches fewer than 25 blows of using the mechanical liquid limit device. Plastic limit is the stage of the soil at which the soils start crumbling when it is rolled into 3 mm diameter threads under the palm of the hand.

2.3 Compaction Characteristics

Compaction characteristics such as optimum moisture content and maximum dry density influence the stiffness of the subgrade soil. The maximum dry density can be achieved by the proper gradation of soil and the compaction effort, which results in the reduction of air voids and strength improvement.

2.4 California Bearing Ratio (CBR)

California Bearing Ratio is a parameter for evaluating the mechanical strength characteristics of ground beneath pavement construction. The standard test is done by penetrating the plunger of fixed area and measure the pressure generated. Measuring load-bearing capacity is the crucial part while constructing roads. CBR can be used for evaluating the strength and the stiffness of both low and heavy-volume roads.

3 Artificial Neuron Network

ANN is brought into usage in 1958 which is the outcome of a fundamental research carried out to develop them such as Hopfields work in 1982 and McClelland and Rumelhart in 1986 considered to be the most important studies. Artificial neuron network model is a computational model which is based on the structure and functions of biological neural networks [18]. They are most reliable of learning complexity in the data and also capture convergent relationships with the given data sets [33, 34].

ANN methods are mostly adopted when direct mathematical formulae do not exist and obtaining the results may take more time for accurate results. Modern research works done in the last two decades had shown that artificial neural networks (ANN) have powerful pattern classification and pattern recognition capabilities too. Since they are biological system inspired, it will learn generally from experience and more iteration produce better results. Standard algorithm used mostly in ANNs includes backpropagation algorithms that will be employed to find the optimal choices for training a model, and the network will comprise of three layers: input, hidden and output layers [35, 36]. Compared with generic statistical methods, the effectiveness and flexibility of ANNs are more, and they are nonlinear in nature. One of the major applications they are used is in forecasting [37]. ANN models were the best tools for both researchers and engineering in the field owing to several features which are efficient and effective. Even though forecasting is a domain of linear statistics, ANNs that are nonlinear perform well [38]. They are capable of performing nonlinear modelling without any knowledge about the input and output variable relationship. But ANNs can often generalize since they are learning from the data that is presented to them; if the data contains noisy information, they can see the unseen part of a population. Also, they are universal functional approximators; they can approximate any continuous function focusing on obtaining desired accuracy.

The results obtained from the models developed using the ANN and MR were compared with the field results or experimental results. By comparison, ANN models were very efficient and effective based on the performance indices than the MR. In spite of the reason that ANN has many advantages such as easiness in applying, robustness, the main disadvantage being it is a black-box model in which no explicit relationship between input and output variables can be obtained, and hence, the results are difficult to interpret sometimes [39].

The typical structure of a feed-forward artificial neural network is shown in Fig. 1. The train program allows the user to determine the number of iterations [17]. The complexity of any problem depends on the hidden layer neurons, the connection between the neurons to their adjacent layer and the weights [23, 40–42]. Once if the system is trained, the trained file is called into the main program. In this process, there are seven input layers, ten hidden layers and one output layer.

ANN forecasting model of single hidden layer was constructed with the training and learning functions. The output of ANN model was calculated as:

$$Y = f_2(W_2 f_1(W_1 X + b_1) + b_2)$$

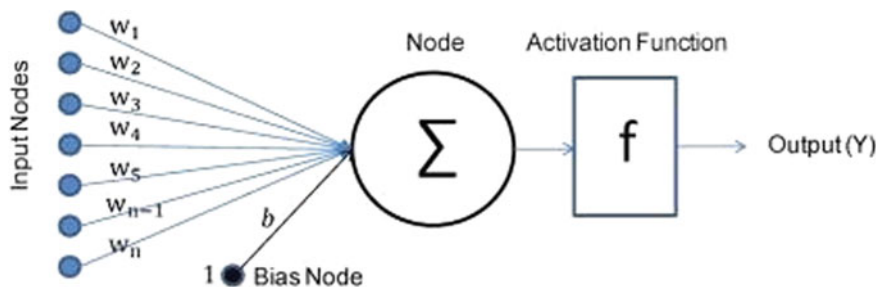


Fig. 1 Schematic representation of an artificial neuron

where y is the output. X is the input vector; f_1 and f_2 are transfer functions of the hidden and output layer, respectively; b_1 and b_2 are biases of the hidden and output layer, respectively; w_1 and w_2 are weights of the input and hidden layer, respectively.

4 Results and Discussion

In this study, for prediction of CBR value, a data set of 90 soil samples was preferred. All the 90 samples were tested for various geotechnical properties, in which 68 sample data was used for training and the remaining 22 sample data utilized for testing the ANN model. Prediction models were generated using the ANN tool from MATLAB software. Hidden layers and input layers are one and five, respectively, and preferred hyperbolic tangent sigmoid for activating layers of input, output and hidden.

Artificial neural network technique has been applied to develop a better predictive model to find California Bearing Ratio (CBR) of soil samples. Several soil samples consisting gravel, fines and sand in varying proportions were prepared to find the CBR values. The statistics such as minimum, maximum, average and standard deviation of the soil samples are listed in Table 1.

The experimental data was used for training the network, and it was divided as 70% for training, 15% for testing and 15% for validation. Various data learning techniques are available in artificial neural networks; within that, Levenberg Marquardt

Table 1 Statistics of soil data used for training the network

	Gravel (%)	Sand (%)	Fines (%)	Liquid limit	Plastic limit	OMC (%)	MDD (g/cc)	CBR (%)
Min	0	4	1	0	0	1.92	1	0.5
Max	86	99	96	60	26	24.5	6.8	35
Average	18.293	47.298	34.191	28.214	17.731	11.761	1.928	10.986
Standard deviation	17.61	16.583	19.288	9.359	5.822	2.838	0.278	7.997

algorithm was chosen based on previous studies which portraits its high accuracy of predicting targets. The input parameters considered for this study are gravel, sand and fines, LL, PL, OMC and MDD; and the output layer is having one node, California Bearing Ratio (CBR). Several iterations were conducted by retraining as well as by changing the number of hidden layers to get the best-fitting model. The final architecture selected for this network is 7–101, and it was taken by considering least mean squared error (MSE). The developed model will be considered best for prediction only if the R^2 value is more and MSE is less.

Figure 2 represents regression plot for the trained model. The linear plots clearly indicate the valid prediction plots as well as deviating plots. The regression value was found to be 0.90943 for training data, 0.92681 for validation data and 0.94597 for testing data. Overall R^2 value for the network was 0.91906 which is very close to unity

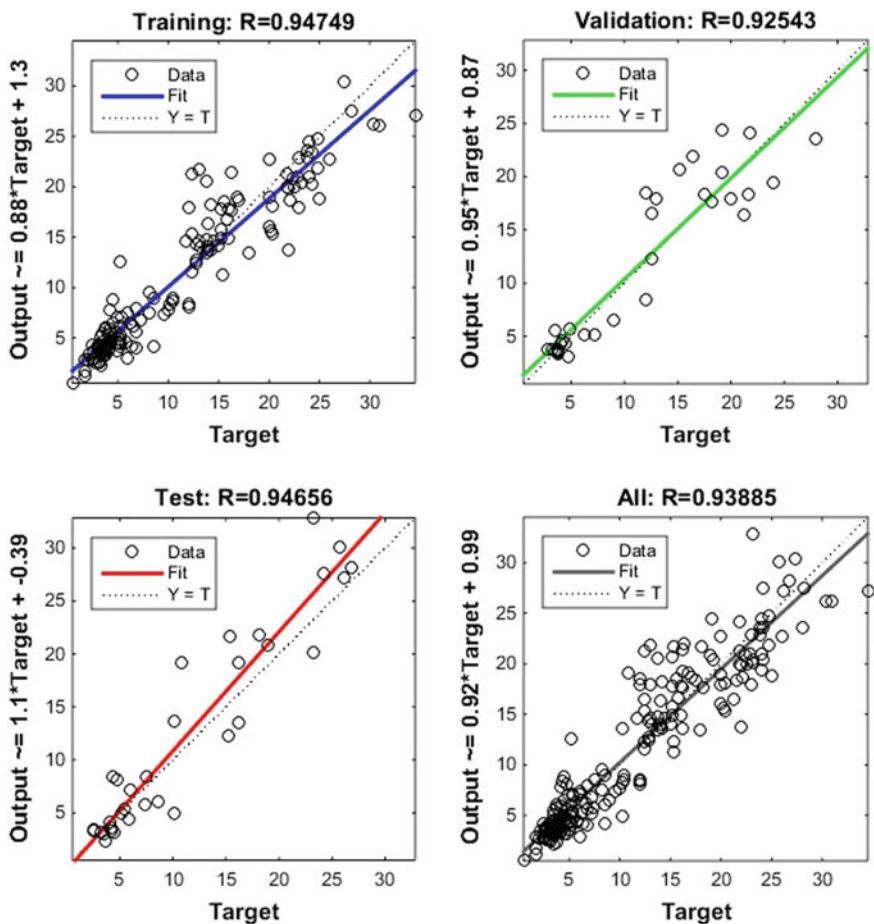


Fig. 2 Data correlations: actual and predicted values

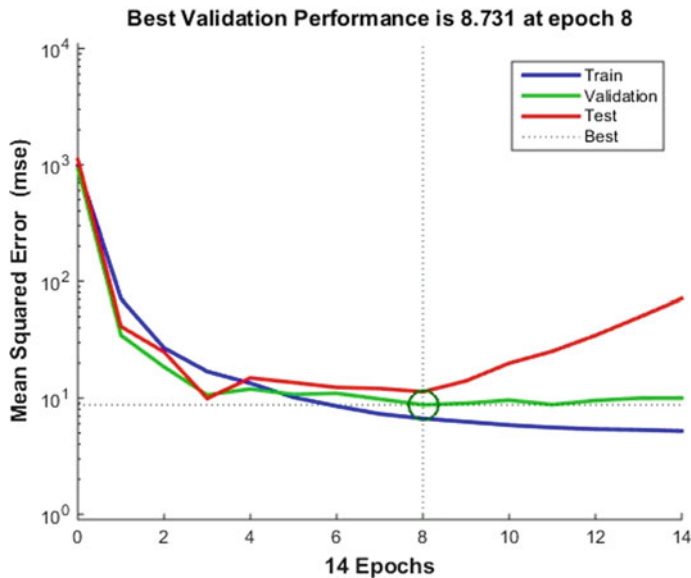


Fig. 3 Performance plot for finding CBR

indicating high accuracy. R^2 values obtained in the four cases were quite different; it implies that input data aforementioned was sensitive to choose for prediction. Best performance was observed as 9.0352 at epoch 10 and it was shown in Fig. 3. Also, the error histogram and gradient plots were shown in Figs. 4 and 5, respectively.

After training the network with 480 soil experimental data sets, 15 samples were used for testing the generated model's accuracy. The experimental data used for this is shown in Table 2. The predictions from generated neural network model are precisely matching with the actual results obtained in the laboratory. The comparison between actual and predicted CBR is shown in Fig. 6. By comparing predicted and experimental results of soil data, it is clearly evident that the best performance was occurred. Even though predicted CBR values have variation with the experimental laboratory results, it does not make any sense, because the maximum error percentage is 15%. In general, CBR values were soul parameters for pavement or road construction. This study is evident that index properties of soils such as gravel, sand and fines, LL, PL, OMC and MDD influence the subgrade CBR value. CBR prediction models using ANN can be ideal for estimating CBR values in the field.

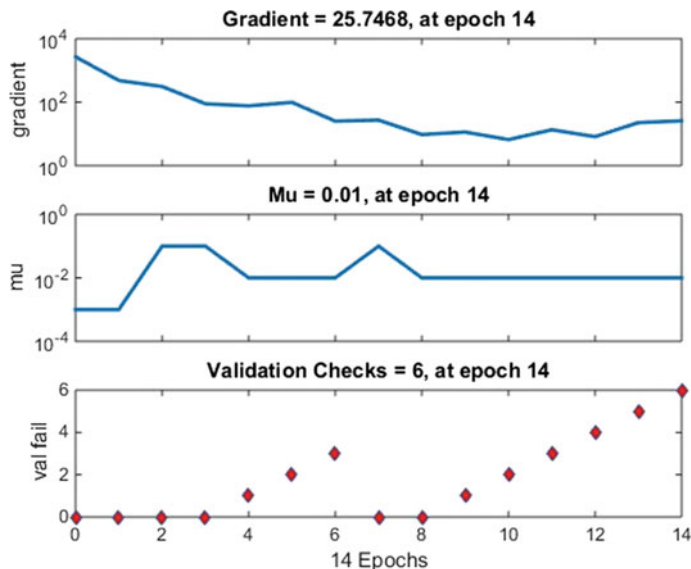


Fig. 4 Gradient plot for Soil CBR

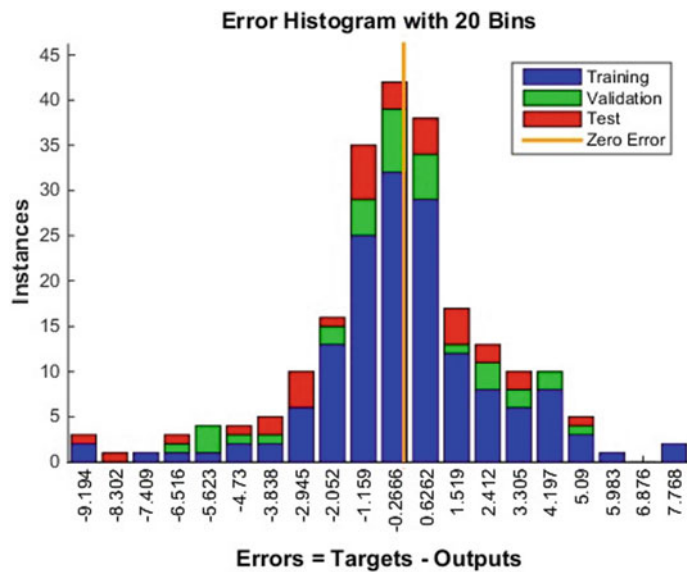
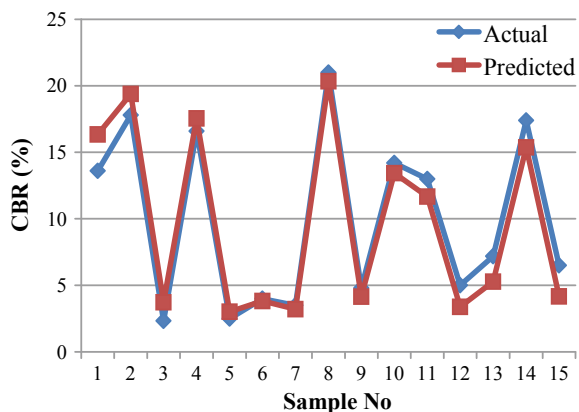


Fig. 5 Error histogram of soil samples

Table 2 Data used for testing the ANN model

S. No	Gravel (%)	Sand (%)	Fines (%)	Liquid limit	Plastic limit	OMC (%)	MDD (g/cc)	Actual CBR (%)	Predicted CBR (%)
1	20	44	36	37	20	15.2	1.9	8	8.462
2	7	60	33	26	19	11	1.98	4	6.14
3	14	53	33	36	21	15	1.86	5.3	5.363
4	25	44	31	27	19	10.5	2.04	14	13.68
5	7	35	58	42	23	18	1.76	3.6	3.299
6	25	50	25	25	18	11.2	1.93	12.8	12.72
7	0	55	45	26	19	11.8	1.81	4.5	4.328
8	19	61	20	27	18	10	2.01	15	14.09
9	20	52	28	23	18	8.3	1.95	5	6.497
10	24	45	31	25	18.5	9	1.96	6	8.016

Fig. 6 Comparison between actual and predicted CBR



5 Conclusions

The research mainly focuses on developing prediction models for finding the California Bearing Ratio (CBR) of soil samples by using experimental data. The following conclusions were drawn from the study:

1. The study illustrates the properties of soils such as grain size, plasticity characteristics and compaction characteristics have significant influence on the CBR of subgrade soils.
2. The selected model for the study consists of three input layers, six hidden layers and one output layer.
3. The overall regression value was found to be 0.91906. The high regression value for training, testing and validation represents more accuracy of the network. Best performance of the model is experienced at epoch 10. The high R^2 defines that the inputs and outputs of the model are having strong correlation. Apart from training data, 15 samples were used for prediction of CBR with generated model, and interestingly, they were very close to experimental results.
4. Soft computing techniques were potential and promising tools for the prediction of geotechnical parameters and helpful for practising engineers in the field.

References

1. Chen FH (2012) Foundations on expansive soils, vol 12. Elsevier
2. Nagaraju TV, Satyanarayana PVV (2019) Geotechnical aspects of various constructions along the canal embankment using rice husk ash as stabilizer. In: Ground improvement techniques and geosynthetics. Springer, Singapore, pp 143–150
3. Moseley MP Kirsch K (2004) Ground improvement. CRC Press

4. Yarbaşı N, Kalkan E, Akbulut S (2007) Modification of the geotechnical properties, as influenced by freeze-thaw, of granular soils with waste additives. *Cold Reg Sci Technol* 48(1):44–54
5. Gobinath R, Ganapathy GP, Akinwumi II (2020a) Stabilisation of natural slopes using natural plant root as reinforcing agent, *Materials Today: Proceedings* Available online 18 September (2020a) <https://doi.org/10.1016/j.matpr.2020.08.227>
6. Gobinath R, Raja, G, Prasath E, Shyamala G (2020b) Amelec viloria & noel varela.: studies on strength characteristics of black cotton soil by using novel SiO₂ combination as a stabilizing agent, *materials today: proceedings*, vol 27, Part 1, pp 657–663
7. Heydinger AG (2003) Evaluation of seasonal effects on subgrade soils. *Transp Res Rec* 1821(1):47–55
8. Jones D, Jones D (2010) Guidelines for the stabilization of subgrade soils in California. University of California Pavement Research Center
9. Gobinath R, Akinwumi I, Ganapathy GP, Mithuna R (2020c) Compaction and shear strength enhancement of weak soil by copper slag addition. *Materials Today: Proceedings*
10. Magnan JP, Ndiaye M (2015) Determination and assessment of deformation moduli of compacted lateritic gravels, using soaked CBR tests. *Transp Geotechnics* 5:50–58
11. Rehman ZU, Khalid U, Farooq K, Mujtaba H (2017) Prediction of CBR value from index properties of different soils. *Technical journal university of engineering and technology Taxila, Pakistan* 22
12. Phanikumar BR, Nagaraju TV (2018) Engineering behaviour of expansive clays blended with cement and GGBS. *Proc Inst Civil Eng Ground Improv* 171(3):167–173
13. Koerner RM (1991) Geosynthetics in geotechnical engineering. In: *Foundation Engineering Handbook*. Springer, Boston, MA, pp 796–813
14. Brandl H (2011) Geosynthetics applications for the mitigation of natural disasters and for environmental protection. *Geosynthetics Int* 18(6):340–390; Chen FH (2012) Foundations on expansive soils; vol 12. Elsevier (2011)
15. Linveh M (1989) Validation of correlations between a number of penetration tests and in situ California bearing ratio test. *Transp Res Rec* 1219:56–67
16. Kin MW (2006) California bearing ratio correlation with soil index properties. Faculty of Civil Engineering, University Technology Malaysia, Master degree Project
17. Günaydin O (2009) Estimation of soil compaction parameters by using statistical analyses and artificial neural networks. *Environ Geol* 57(1):203
18. Taskiran T (2010) Prediction of California bearing ratio (CBR) of fine grained soils by AI methods. *Adv Eng Softw* 41(6):886–892
19. Agarwal KB, Ghanekar KD (1970) Prediction of CBR from plasticity characteristics of soil. In Proceeding of 2nd south-east Asian conference on soil engineering, Singapore, pp 571–576
20. Stephens DJ (1990) The prediction of the California bearing ratio. *Civ Eng Siviele Ingenieurwese* 1990(v32i12):523–528
21. Nagaraju TV, Prasad CD, Raju MJ (2020) Prediction of California Bearing Ratio using particle swarm optimization. In: *Soft computing for problem solving*. Springer, Singapore, pp 795–803
22. Das SK, Basudhar PK (2008) Prediction of residual friction angle of clays using artificial neural network. *Eng Geol* 100(3–4):142–145
23. Gunaydin O, Gokoglu A, Fener M (2010) Prediction of artificial soil's unconfined compression strength test using statistical analyses and artificial neural networks. *Adv Eng Softw* 41(9):1115–1123
24. Abdalla JA, Attom MF, Hawileh R (2015) Prediction of minimum factor of safety against slope failure in clayey soils using artificial neural network. *Environ Earth Sci* 73(9):5463–5477
25. Patel RS, Desai MD (2010) CBR predicted by index properties for alluvial soils of South Gujarat. In *Proceedings of the Indian geotechnical conference*, Mumbai, pp 79–82
26. Trivedi JS, Nair S, Iyyunni C (2013) Optimum utilization of fly ash for stabilization of sub-grade soil using genetic algorithm. *Procedia Eng* 51:250–258
27. Katte VY, Mfoyet SM, Manefouet B, Wouatong ASL, Bezeng LA (2019) Correlation of California bearing ratio (CBR) value with soil properties of road subgrade soil. *Geotech Geolog Eng* 37(1):217–234

28. Kumar S, Murthi P, Awoyera P, Gobinath R, Sathiskumar (2020) Impact resistance and strength development of fly ash based self-compacting concrete. *Silicon*. <https://doi.org/10.1007/s12633-020-00842-2>
29. Udaya Banu T, Rajamane NP, Awoyera PO, Gobinath R (2020) Strength characterisation of self cured concrete using AI tools, materials today: proceedings available online (11 November 2020) In Press. <https://doi.org/10.1016/j.matpr.2020.10.101>
30. Venkatasubramanian C, Dhinakaran G (2011) ANN model for predicting CBR from index properties of soils. *Int J Civ Struct Eng* 2(2):614620
31. Hopfield JJ (1982) Neural networks and physical systems with emergent collective computational abilities. *Proc Nat Acad Sci* 79(8):2554–2558
32. Parallel distributed processing (1986) McClelland, J. L., Rumelhart, D. E., & PDP Research Group. *Explor Microstruct Cognit* 2:216–271
33. Ripley BD (1993) Statistical aspects of neural networks. *Networks Chaos—Statist Probab Aspects* 50:40–123(1993).
34. Cheng B, Titterington DM (1994) Neural networks: a review from a statistical perspective. *Statist Sci* 2–30
35. Erzin Y, Turkoz D (2016) Use of neural networks for the prediction of the CBR value of some Aegean sands. *Neural Comput Appl* 27(5):1415–1426
36. Widrow B, Rumelhart DE, Lehr MA (1994) Neural networks: applications in industry, business and science. *Commun ACM* 37(3):93–106
37. Sharda R (1994) Neural networks for the MS/OR analyst: an application bibliography. *Interfaces* 24(2):116–130
38. Hu MJC (1964) Application of the adaline system to weather forecasting Doctoral dissertation Department of Electrical Engineering, Stanford University
39. Tayfur G, Erdem TK, Kirca Ö (2014) Strength prediction of high-strength concrete by fuzzy logic and artificial neural networks. *J Mater Civ Eng* 26(11):04014079
40. Zhang G, Patuwo BE, Hu MY (1998) Forecasting with artificial neural networks
41. Betaubun P (2018) Engineering of clay soil stabilization with cement and fiber on cbr value for road materials in merauke district. *Int J Civ Eng Technol (IJCIET)* 9(8):562–567
42. Reddy RA, Sivakrishna A, Gobinath R, Babu DR (2020) A novel method to predict pozzolanic nature of concrete with sintered clay using soft computing techniques. *IOP Conf Ser Mater Sci Eng* 872(1):012159 (IOP Publishing)

Real-Time Bangladeshi Currency Recognition Using Faster R-CNN Approach for Visually Impaired People



Md. Tobibul Islam, Mohiuddin Ahmad, and Akash Shingha Bappy

Abstract In this research work, we represent a new method for recognition of Bangladeshi money using Raspberry Pi 4 and the faster R-CNN approach. Here we represent a microprocessor-based smart blind glass where one of the important features is Bangladeshi money recognition. Money is a very important element for all the people in the world including blind people. They cannot recognize the banknotes without the help of others. Sometimes they cheat by wrong people in various money issues. So, they suffer a lot in their day-to-day life. Through this paper, we introduce a smart blind glass that can recognize money and provide audio information to the blind man's ears. In this recognition, we introduced a new method faster R-CNN approach which is widely used for object and face recognition. By using a faster R-CNN model in money dataset training, we found about average 97.8% real-time accuracy. Our recognition accuracy was high compared with other state-of-the-art research work.

Keywords Currency recognition · Faster R-CNN · Raspberry Pi · Money · Region of interest (RoI)

1 Introduction

In the present world, around 253 million people live-in vision impairment of which 36 million are completely blind [1] and the rest of them are partially blinding. So a huge number of people, all over the world as well as in our country depend on

Md. T. Islam (✉)

Department of Biomedical Engineering, Khulna University of Engineering & Technology, Khulna 9200, Bangladesh

M. Ahmad

Department of Electrical and Electronic Engineering, Khulna University of Engineering & Technology, Khulna 9200, Bangladesh

A. S. Bappy

Department of Electronics and Communication Engineering, Khulna University of Engineering & Technology, Khulna 9200, Bangladesh

other people. They cannot do anything without the help of other people. About 253 million, people all over the world are blind, so there are also another 250 million people needed to help them. So about 506 million people are unproductive for the world economy. Through this research work, we are working to give the blind man independent life, so that they can live without the help of anyone. We are working to develop a smart blind glass which can provide all the necessary formations. It can recognize any type of objects, holes in front of the blind man using a machine learning TensorFlow approach [2]. It also provides all types of safety information like any type of hole in front of the blindman's ears and provides location and safety information to the blindman's family members. Money is an important issue for any human being, and we try to solve the money recognition problem for the blind man.

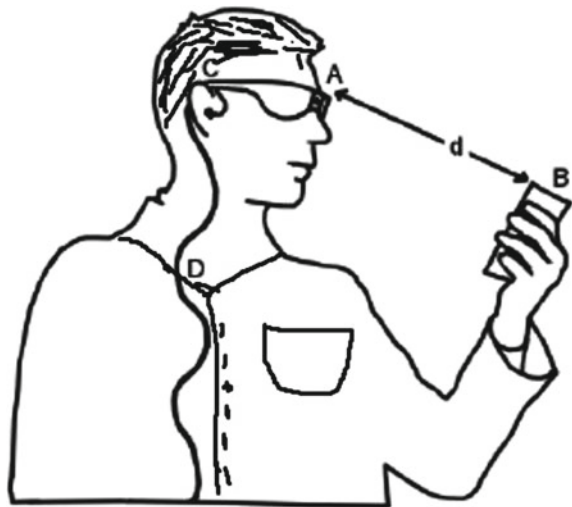
In this paper, we solve money recognition problems for the blind man using a faster R-CNN approach. In the very beginning, a deep CNN-based approach was widely used for computer vision. Nowadays, all types of objects can easily recognize using, Keras, TensorFlow, and region-based convolution neural network. In R-CNN, the performance was too slow in the recognition process. Then fast R-CNN [3] approach was spread in the recognition process, and its recognition process was acceptable. Nowadays, third-generation faster R-CNN is widely used in computer vision as well as in the machine learning approach. In this procedure, we fund faster recognition and high accuracy. Many research work used optical character recognition (OCR) [4] and oriented fast and rotated brief (ORB) algorithm for money recognition. In OCR, optical characteristics of money are the main features for the recognition process. This process is widely used for fake banknote detection. In ORB technology, the orientation [5] of the money can be invariant so that it is easy for the recognition processor to recognize the money easily. In our proposed method, we can easily recognize Bangladeshi money in real time with high accuracy. Our smart glass module can easily recognize the money and provides associated audio information.

Figure 1 represents the money recognition procedure of our proposed system. In our proposed system, we use a Raspberry Pi 4 (microprocessor like minicomputer), a Raspberry Pi camera module, a headphone. From the picture, we can understand that when the blind man takes money in their hand the camera module captures the video frame and microprocessor process the image and recognize the amount. Then it produces specific audio information and sends it to the blindman's ears. From the figure, we also see that a blind man knowing about a currency. Here the distance d between the currency and the glass frame will be about 60 cm or less for proper focusing.

2 Related Works

Some methods have been proposed for currency recognition worldwide. In the paper [6], the researcher proposed a method that is based on OBR (Oriented FAST and rotated BRIEF) algorithm. Actually, with this procedure, currency can recognize in

Fig. 1 Sketch representation of the blind man recognizes money using smart glass



very fast. In this method, the rotation of the notes is not dependent on its recognition accuracy. In the paper [7], another currency recognition system based on speeded up robust features (SURF) where the recognition rate was very high. Various shapes, sizes, and other conditions are also easily identified using this technique. Firstly, the regulatory features of all images are mined by using SURF. Then all these factors are examined with a precomputed SURF factor for each currency image. Then the value of matches is compared with a threshold. In this way, it can categorize the currency. In [8], the authors proposed a device for the blind man which can detect banknotes and provide audio notification for the blind man. They build it for the recognition of Australian currency by using the light property. First of all, light is passed through the paper currency and automated sensors automatically identified a series of values. Those values are then comprised of ideal stored value and recognize the specific currency.

3 System Design

Figure 2 represents the basic block diagram, and Fig. 3 represents the 3D printed hardware support of our proposed system. It contains Raspberry Pi 4, a Pi camera, power supply, headphones. The Pi camera grabs video frame, then it is processed in the Raspberry Pi 4 and produces audio instruction for associated recognized money. The Raspberry Pi sends audio instructions to the headphone as well as the ears of the blind man.

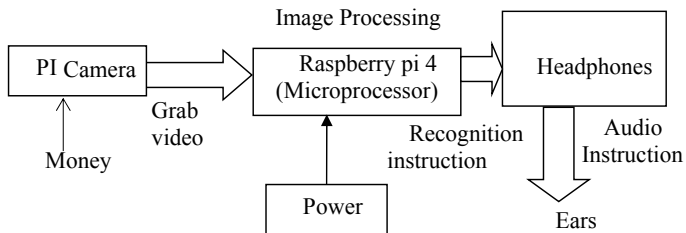


Fig. 2 System architecture of our proposed glass

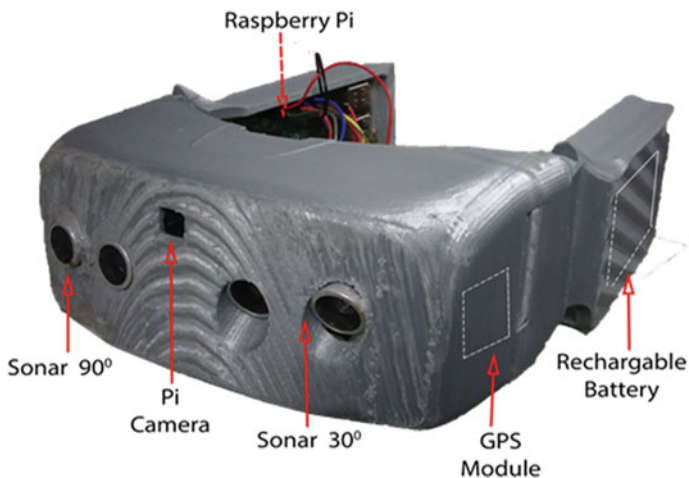


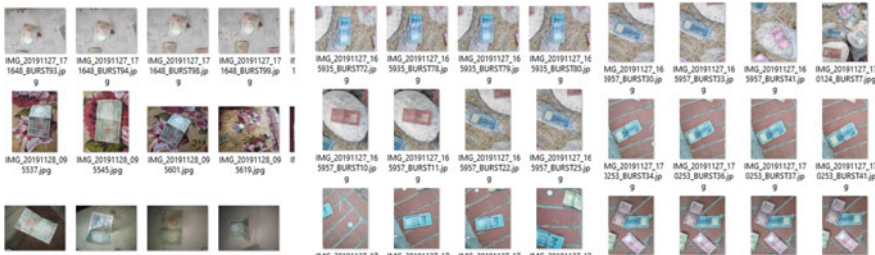
Fig. 3 Hardware architecture of our proposed system

4 Dataset Developing and Training

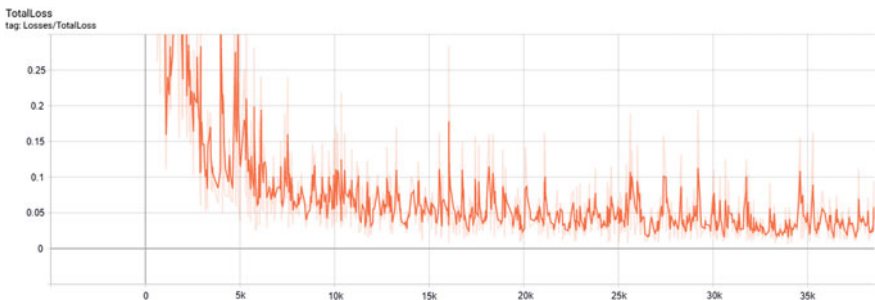
In this proposed research work, we used a set of Bangladeshi banknotes that are created by us. We only used the banknotes as 1000, 500, 100, 50, 20, 10, 5, 2, and 1 taka notes for our datasets. About 4507 images are captured for these datasets. These images are captured by us which is in different locations in indoor and outdoor environments like on the table, chair, street, bench, hand, laptop, bed, mouse, in hand, etc. It also collected in different positions like full, half, one-third, a sliced part, folding, and different light illumination too. We capture both sides of the notes properly. For better training images, it equals the amount of both sides' images. We put 3571 images in the train section and 936 images for the test section which is about one-fourth of training images. Table 1 represents all the train and test images numbers in associated categories, and Fig. 4 represents the snapshots of images in different locations. After collecting the images, we performed level mapping all the images with the corresponding currency amount very carefully. Then we performed training the image by using the faster R-CNN inception V2 coco-2018 model. We

Table 1 Categorization and distribution of data

Category	Train	Test	Image format
One thousand taka	403	115	jpg
Five hundred taka	400	102	jpg
One hundred taka	380	105	jpg
Fifty taka	385	100	jpg
Twenty taka	385	110	jpg
Ten taka	430	100	jpg
Five taka	390	96	jpg
Two taka	398	108	jpg
One taka	400	100	jpg
Total	3571	936	

**Fig. 4** Snapshots of the training images in different places and different shapes

found our training loss very small. Figure 5 represents our classifier total training loss where we showed that after 35 thousand, iterations the loss is less than 0.05 where preferable is about 0.05. It means our classifier training accuracy was very high enough.

**Fig. 5** Training loss of our proposed classifier

5 Currency Recognition via Faster R-CNN

Faster R-CNN is a little different from R-CNN and CNN because it has two parts. This first part is fully connected convolution layers, and the second part is fast R-CNN detectors [9]. This is the newest technology mainly for object detection, but we performed the technology for currency recognition. In this method, it trains the VGG16 training network very fast nine times faster and 213 times faster in the test time than the R-CNN. Figure 6 represents our proposed currency recognition system by using the fast R-CNN model. It processes the whole money image with numerous convolution layers and max-pooling layers for the feature mapping. After that, it identifies each money image region of interest (RoI) pooling layers feature vector value. Then for each feature, vector value fed into a fully connected layer.

Faster R-CNN has two familial output stages. The first stage describes probability distribution for every region of interest as $P = (P^0 + P^1 + \dots + P^n)$ in $n + 1$ categories. Probability P finds out from the softmax by using $n + 1$ output fully connected layers. Then second familial stage describes bounding box recreation as $T_n = T_n x, T_n y, T_n w, T_n h$ for each n money classes [10]. For the training of every RoI with a ground truth class o and box regression m . Now the task loss L will be:

$$L(p; o; t_o; m) = L_{\text{cls}}(p; o) + \gamma[0 \geq 1]L_{\text{loc}}(t_o; m) \quad (1)$$

where $L_{\text{cls}}(p; o) = -\log p_o$ is a log loss for class o and task loss is L_{loc} , then $m = (mx; my; mw; mh)$, and predicted tuple $t^o = (t^o x; t^o y; t^o w; t^o h)$. For the classification of the bank currency inversion indicator value $[o \geq 1]$ set to value 1 and 0 for other conditions. The loss function L_{loc} for the bounding box regression, we can write:

$$L_{\text{loc}}(t^o, m) = \sum_{i \in \{x, y, w, h\}} \text{smooth}_{L_1}(t_i^o - m_i), \quad (2)$$

where

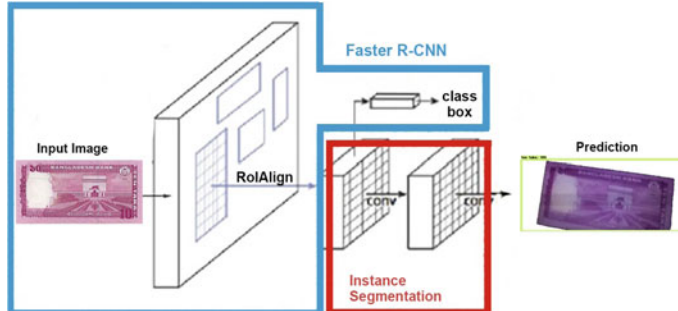


Fig. 6 Our proposed faster R-CNN architecture for currency recognition

$$\text{smooth}_{L_1}(x) = \begin{cases} 0.5x^2 & \text{if } x < 1 \\ |x| - 0.5 & \text{otherwise} \end{cases}; \quad (3)$$

In the outlines where we found L_1 loss which is less sensitive than L_2 loss which mainly used in SPPnet and R-CNN. Two task loss is balanced by hyperparameter γ . We use it $\gamma = 1$ for all experiments for normalizing the ground truth regression.

6 Results and Discussions

In this research work at first, we capture images by using a Raspberry Pi camera module, then it sends to the main processing unit of the Raspberry Pi module. In the Raspberry Pi module, we already train a Faster R-CCN model using 4507 images where 3571 images were in the training section and 936 images were in the test section. We placed the frozen interference graph in the Pi model. Now it is ready to predict Bangladeshi currency in real time. It automatically recognizes the taka and provides associated audio information like “one thousand taka note at your hand.”

In the previous Fig. 7, this paper represents the real-time recognition process after completing the softer section for this research work. We perform our accuracy test in different light illumination, but we found the accuracy very high. We perform an accuracy test with associated audio information on all the Bangladeshi currency notes and found high accuracy compared with other researches. Table 1 represents the real-time performance identification of our proposed system where we use each note 50 times in the recognition process. Then we observed the associated audio instruction, and it was strong enough to help the blind man to know which note is on their hand. In this research, we use pre-trained faster R-CNN models for our currency recognition which used previously for object recognition and we found high accuracy comparing to other works. Table 2 is given below which compares our work with other research works (Table 3).

7 Conclusions

In this research, we used a new currency recognition system by using the faster R-CNN approach. It is an important feature of our smart glass system. We completed the software and hardware part and insert the software into the hardware successfully. Now our module can easily recognize the Bangladeshi bank notes and provides associated audio instruction to the blind person ears. We identify the real-time recognition accuracy in different conditions like different illuminations, in different shapes, and our system accuracy was good enough to use it. We are still working on it for adding more features like blind man safety issues, voice recognizes system for making the module more convenient for a blind individual.

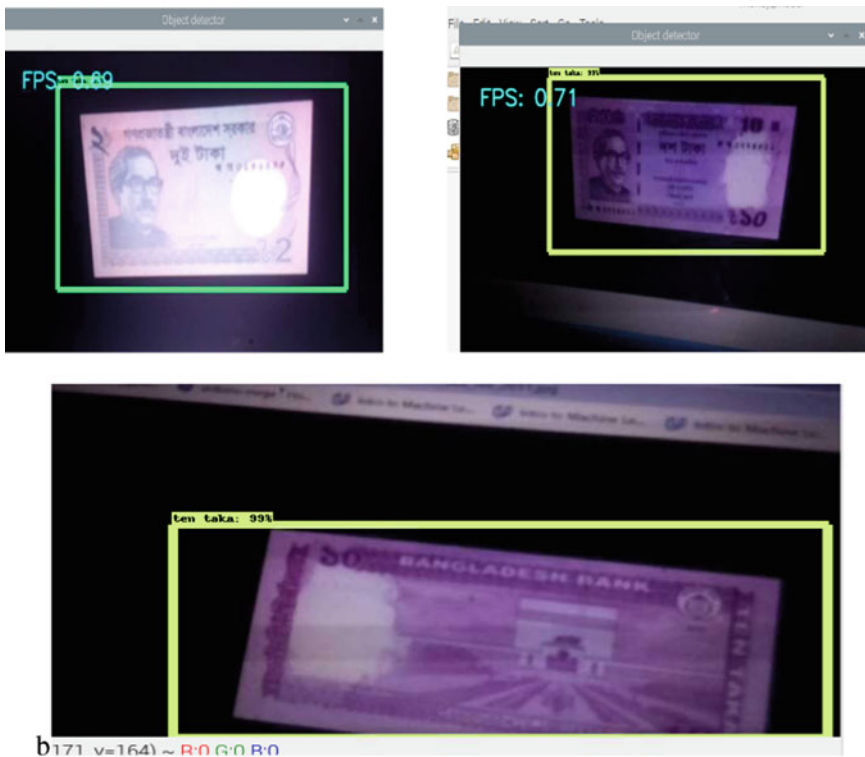


Fig. 7 Represents the real-time recognition process with percentage accuracy

Table 2 Accuracy identification of our currency recognition system

SL#	Note name	Currency recognition	Accuracy (%)	Audio output
01	One taka	49	98	“One taka note in your hand”
02	Two taka	50	100	“Two taka note in your hand”
03	Five taka	48	96	“Five taka note in your hand”
04	Ten taka	49	98	“Ten taka note in your hand”
05	Twenty taka	49	98	“Twenty taka note in your hand”
06	Fifty taka	47	94	“Fifty taka note in your hand”

(continued)

Table 2 (continued)

SL#	Note name	Currency recognition	Accuracy (%)	Audio output
07	One hundred taka	49	98	“One hundred taka note in your hand”
08	Five hundred taka	49	98	“Five hundred note in your hand”
09	One thousand taka	50	100	“One thousand taka note in your hand”

Table 3 Compare with our currency recognition process with some state-of-the-art other researches

References	Research work is done
[6]	Egyptian currency recognition system using FAST ORB algorithm where recognition accuracy is about 96%
[4]	Indian currency recognition with the android platform by using the SIFT algorithm
[5]	Indian currency recognition for visually disabled people using image processing where accuracy is 90%
[7]	Fake banknote recognition by using the SURF algorithm where recognition accuracy 100%
Our proposed system	Real-time Bangladeshi currency recognition is using faster R-CNN approach and provides audio information to the blind man ears where recognition accuracy is 97.8%

Acknowledgements We are working to develop smart blind glass, and it is supported by the access to information (A2I) project (Idea bank ID: 12504) under the supervision of the prime minister office. It is a series work, and this paper represents an important feature of the Bangladeshi currency recognition for the blind individual.

References

1. Blindness and vision impairment prevention. https://www.who.int/blindness/world_sight_day/2017/en/
2. Islam T, Ahmad M, Bappy AS (2018) Microprocessor-based smart blind glass system for visually impaired people. In: Proceedings of IJCCI, chap 13. Springer Nature Singapore, Dhaka, Bangladesh
3. Girshick RB (2015) Fast R-CNN. In: ICCV, pp 1440–1448
4. Saraf S, Sindhikar V, Sonawane A, Thakare S (2017) Currency recognition system for visually impaired. IJARIE-ISSN(O) 3(2):2395–4396
5. Bhagat SP, Patil SB (2016) Indian currency recognition for visually disabled people using image processing. Int J Adv Res Comput Commun Eng 5(6)
6. Yousry A, Taha M, Selim M (2018) Currency recognition system for blind people using ORB algorithm. Int Arab J Inf Technol 5:34–40
7. Hasanuzzaman FM, Yang X, Tian YL (2012) Robust and effective component-based banknote recognition for the blind. IEEE Trans 42(6)

8. Calonder M, Lepetit V, Strecha C, Fua P (2010) BRIEF: binary robust independent elementary features. In: Daniilidis K, Maragos P, Paragios N (eds) Computer vision—ECCV 2010. Lecture notes in computer science, vol 6314. Springer, Berlin, Heidelberg
9. Girshick R (2015) Fast R-CNN. In: IEEE International conference on computer vision (ICCV)
10. Girshick R, Donahue J, Darrell T, Malik J (2014) Rich feature hierarchies for accurate object detection and semantic segmentation. In: CVPR

Bearing Fault Detection Using Comparative Analysis of Random Forest, ANN, and Autoencoder Methods



Pooja Kamat, Pallavi Marni, Lester Cardoz, Arshan Irani, Anuj Gajula, Akash Saha, Satish Kumar, and Rekha Sugandhi

Abstract The manufacturing industry is currently witnessing a huge revolution in terms of the Industry 4.0 paradigm, which aims to automate most of the manufacturing processes from condition monitoring of the machinery to optimizing production efficiency with automated robots and digital twins. One such valuable contribution of the Industry 4.0 paradigm is the concept of predictive maintenance (PdM), which aims to explore the contributions of artificial intelligence to get meaningful insights into the health of the machinery to enable timely maintenance. As majority of these machineries consist of bearings, bearing fault detection using artificial intelligence has been a popular choice for researchers. This paper provides a systematic literature survey of the existing research works in bearing fault detection. Further in this paper, we have done comparative analysis of bearing fault detection using the techniques of random forest classification, artificial neural network, and autoencoder on the benchmarked dataset provided by CWRU. The deep learning model of autoencoders provides the highest accuracy of 91% over the algorithms of artificial neural network and random forest.

Keywords Fault detection · Machine learning · Industry 4.0 · Artificial neural networks · Random forest · Autoencoder · Bearing fault diagnosis

P. Kamat (✉) · P. Marni · L. Cardoz · A. Irani · A. Gajula · A. Saha

Department of Computer Science and Information Technology, Symbiosis Institute of Technology, Pune, Maharashtra, India

e-mail: pooja.kamat@sitpune.edu.in

S. Kumar

Department of Mechanical Engineering, Symbiosis Institute of Technology, Pune, Maharashtra, India

R. Sugandhi

Department of Information Technology, MIT School of Engineering, Pune, India

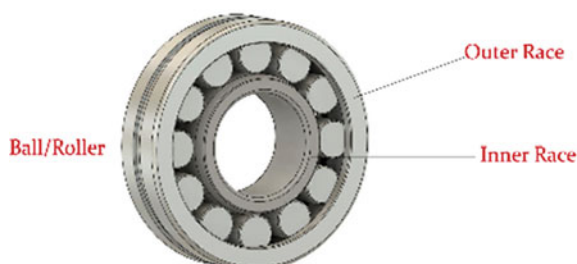
1 Introduction

Under the umbrella of Industry 4.0, predictive maintenance (PdM) is a technique of analyzing the production data to detect faults before they happen. Factory managers up until now had to regularly repair machine parts and carry out scheduled maintenance in order to prevent downtime. Most predictive maintenance activities are ineffective, driving productivity losses and leading to consumption of unnecessary resources. Therefore, predictive maintenance using machine learning has quickly emerged as highly useful in Industry 4.0 for manufacturers and asset managers. Manufacturers maximize uptime and lower the service costs by using deep learning algorithms and machine learning. This helps in improving production throughput, observing asset health, and gaining real-time alerts to future operational risks. It can be observed that machines operating on electricity are widely used for various purposes of electronic application and for certain industrial purposes which rely on electricity. Faults present in electric machines are divided into different categories including stator winding insulation breakdown, bearing faults, drive inverter failures, and air gap eccentricity. Surveys show that the most common form of fault is the bearing fault, which accounts for 30–40% of all machine failures. Therefore, we have focused our research on bearing fault diagnosis.

The causes for faults in bearings are inappropriate use of bearings due to overload, faulty installation or improper processing, improper lubricant, lubrication method for sealing device, inappropriate speed and operating temperature, and contamination by foreign matter during installation.

Figure 1 shows the typical structure of a roller-element bearing. Zhang et al. describe the four forms of misalignment most likely to cause failures in the bearings [1]. The first one is the out-of-line misalignment, the second one is shaft deflection, the third one is crooked or tilted outer race, and the fourth one is crooked or tilted inner race. This paper focuses on how AI algorithms can empower manufacturing industry in making predictive analytics of the bearing health. The remaining paper is structured as follows: Sect. 2 shows work similar to our research, Sect. 3 describes the algorithms of random forest, artificial neural networks, and autoencoders in detail, Sect. 4 presents the proposed methodology and dataset description used in the study, and Sect. 5 provides results and comparative analysis.

Fig. 1 Structure of rolling-element bearing



2 Related Work

In 2018, Heo and Lee [2] used datasets published online to solve the problem of fault detection. They used neural networks to do this and found the accuracy of the network by changing the count of hidden layers (0, 1, 2, 3, 4). They also analyzed the effects on accuracy by changing the number of neurons (1, 2, 3, 12) in the last hidden layer. They also performed analysis using data augmentation where the input data is augmented by combining consecutive samples. A classification accuracy of 97.26% was achieved in this study. It also proved that accuracy of fault detection can be further increased by data augmentation.

Zhang et al. [1] performed a study using different deep learning algorithms on Case Western Reserve University (CWRU) dataset. Results showed sparse autoencoder (SAE) and stacked denoising autoencoder (SDAE) have the highest average accuracy of 99.83%. They also provided detailed recommendations and suggestions regarding how to choose the right category of deep learning algorithm for different application scenarios.

Ademujimi et al. [3] published a paper reviewing all papers published from 2007 to 2017 on present techniques of fault diagnosis in manufacturing, which are based on different machine learning algorithms. They provided summaries for four important techniques (Bayesian network, hidden Markov model, artificial neural network, support vector machine). They concluded that both BN and HMM techniques are beneficial for modeling. However, BN requires less computational power than HMM. The paper also shows that ANN gave faultless results, but the model being a black-box algorithm, it was very tedious to visualize what is happening within the model. Compared to ANN, SVM generates a high-fault classification rate at less computation time.

Li et al. [4] wrote a paper on imbibing deep statistical feature learning from vibration recordings of rotating machinery. They validated the potency of the model by using it to diagnose the health of a gearbox and bearing system. The model that was proposed by them was Gaussian–Bernoulli deep Boltzmann machine (GDBM) which is based on Gaussian–Bernoulli restricted Boltzmann machines (GRBMs). Classifying fault patterns using deep statistical feature learning provide much better results compared to other models (unsupervised GRBM, the SVM, combination of SVM and GRBM).

Munirathnam et al. [5] proposed ML procedures to produce a precise predictive model that predicts equipment failures during the wafer fabrication process in semiconductor industries. This particular paper aims to construct a decision model which helps to detect any equipment faults as quickly as possible to sustain high process yields in manufacturing. They propose a method of predictive maintenance which includes the following steps: data preparation phase, data cleansing phase, feature scaling, feature reduction, and feature selection. The right features are selected from implementing three techniques: subject matter expert (SME) knowledge, correlation analysis (CA), principal component analysis (PCA). These features obtained from the dataset are used for various machine learning models such as k-nearest neighbor

method (KNN), decision tree, artificial neural network (ANN), and support vector machine (SVM), naïve Bayes (NB), logistic regression (LR).

Amruthnath and Gupta [6] in this paper have taken simple vibration data collected from an exhaust fan and used various unsupervised learning algorithms such as fuzzy C-means clustering, hierarchical clustering, PCA T2 statistic, K-Means and model-based clustering to examine its precision and execution. Finally, a technique has been proposed to standardize different algorithms and select the ultimate model. They provided a summary for all the models. Results showed that T2 statistics provide more accurate results than the GMM method. However, clustering methodology is better comparatively in detecting different levels of faults while the T2 statistics would face problems in detecting after certain levels. In conclusion, T2 is an excellent tool if the application must only detect faults. For performing fault detection under different levels, clustering algorithms should be used.

Ferreira and Warzecha [7] examined a synchronous machine. The methodology implemented here can be used for condition-monitoring-based maintenance. In stator and rotor winding, mainly currents and voltages, and rotational speed and electromechanical torque, they observed. Next, the signals were cleaned and preprocessed and about 5038 features were deliberated and made into a dataset. As there are a huge number of features that were present in the data collected from the machine linear discriminant analysis algorithm were implemented to remove the features needed for this model. A total of 37 sensors were used to collect data from the machine. All the signals are defined as variables, in numerical form, and are stored collectively as columns in a table. Every row in the table is a sample which represents a machine condition. Lastly, these datasets are made ready for preprocessing, where the data is transformed into features. It was noted that the time it took to systemize a new observation was close to the real time. In the case of this paper, the time taken to process/systemize a new observation was 0.23 s. The amount of time to classify, store, preprocess, and collect was less than 4 s. Finally, in this paper the authors suggested to better the technique by incorporating other domains of features and to advance features extraction and classification free from the workload of the machine.

Seera et al. [8] here, faults in ball bearings were classified with the help of vibration signals using FMM (Fuzzy Min–Max)–RF (Random Forest) as the hybrid model. The two methods of feature extraction, namely power spectrum (PS) and sample entropy (SampEn), were primarily used. Here, Welch's method was used to execute and estimate the power spectrum of the signal, and for every vibration signal, three sample entropy features were taken. Two experiments were carried out, namely benchmark and real world. Benchmark experiment consisted of a test setup which had a dynamometer, torque encoder, and three-phase motor. Data for the real-world experiment was obtained by using a small test rig. The FMM-RF hybrid model was used. For comparison, other models such as FMM, CART, RF, FMM-CART were also used. The experiments were divided into three, where PS, SampEn, and PS + SampEn features were considered. Decision tree is made use of to find out the feature which is most important from FMM-RF. It was concluded that the performances shown by both the experiments with the FMM-RF model were precise. The best outcomes of real world and benchmark datasets were at 99.8% and 99.9%, respectively.

Korba and Arbaoui [9], the major aim of this paper was the categorization of the bearing's defects with the help of vibratory analysis using SVM with EMD. Kernel function and maximum margin are the two ideas on which SVM algorithm is based. The testing rig consisted of an induction machine, dynamometer, and torque transducer. The main steps in the methodology were feature selection, feature extraction, and classification. EMD generates IMFs of vibratory signals. Three classifiers were used for the process of classification for comparison, namely SVM, ANN, and NFN. Relevant IMFs were compared with the original signal to find the correlation factor. Classification time and classification rate were used as metrics for the comparison of performances of the classifiers. After the tests and the comparative study between the classifiers, it was concluded that the SVM had slightly better results than the other classifiers.

Patel and Giri [10] published a paper which was on fault detection and diagnosis, proposing the election and categorization of mechanical defects of induction motors utilizing random forest classification. This paper in question examines the developing algorithm of random forest (RF) classification. The proposed algorithm could be used for multi-class fault diagnostics in induction motor. The paper discusses the effect of random forest taxonomies on misdiagnosis. The results were obtained in comparison with current artificial intelligence techniques and neural networks. The examination of the results demonstrated that the proposed method showed better performance and higher accuracy when compared to other technologies.

Seryasat et al. [11] managed a study on the intelligent misalignment of ball bearing. This study introduces ANNs into a roll bearing fault detection system by removing features in the time zone from the vibration signals. Synthetic neural networks (ANNs) and support vector machines (SMVs) are the proposed models used in this study.

Yang and Fu [12] wrote a paper based on the concepts of rolling-element bearing fault automatic data clustering, whose datasets are related to wavelets and deep neural networks. For automatic clustering of rolling-element fault data, a method based on wavelet and deep neural networks has been proposed. This method without human knowledge can achieve intelligent signal classification. Datasets are roughly classified by distance-based clustering method. The proposed methodology was tested with data bearing case data from Case Western Reserve University.

Lei et al. [13] wrote a paper based on the concepts of rolling bearings in relation to rotary machine systems. The incorrect dataset is calculated using the various items described in the paper.

Rolling bearings with defects from both aspects of mechanism study and diagnostic analysis have been extensively and deeply investigated. Mechanism studies mainly involve the theoretical examination of rolling bearings with surface defects from the perspective of the design of mechanical models and the theory of mechanical dynamics. This paper introduces Siemen's method for researching the dimensionality and purity of vibrational signals. Currently, the theory of symplectic geometry is mainly studied in nonlinear differential systems.

Zhang et al. [14] wrote a paper on intelligent status monitoring and misdiagnosis by analyzing sensor data. The paper proposed a deep neural networks model.

The feature choosing process and the temporary compatibility with advanced time series data without erroneous confirmation were considered. The proposed prototype machines can automatically learn the features that will help in the diagnosis. This paper shows that the classification accuracy can reach 100%. The paper proposes that prognosticators have a significant advantage over the proposed method compared to traditional error diagnostic methods. Classifying a faulty model using DNN yields better results than other models, including continuous wavelet transition with SVM, and isolation with ANN. Wavelet transitions include statistically isolated embedding with SVM.

Khorram and Khalooei [15] wrote a paper on intelligent error diagnosis and prognosis. The model they proposed is the traditional long-term-short-memory recurrent neural network (CRNN), which detects bearing defects on benchmarked datasets. The overall classification accuracy was seen as 97.13%-IMS and 99.77%-CWRU bearing datasets. The paper demonstrates the experiments for selecting each element of the proposed network and the network structure which is used to achieve high accuracy.

3 Algorithms

There are several algorithms used today for fault detection, i.e., predicting accuracy, precision, finding anomalies, etc., in ball bearing such as support vector machine, stochastic gradient descent, regularized extreme learning machine, principal component analysis, deep neural networks, and convolutional neural network. In this study, we have used random forest classification, artificial neural networks, and autoencoders. Recently, researchers deployed machine learning algorithm for automated prediction [16], classification [17], and data transformation [18].

3.1 Random Forest Classification

Random forest classification is a model which consists of many decision trees. It follows a divide-and-conquer approach where the dataset is split randomly, and the decision trees are generated on it. Attribute selection indicators (information gain, gain ratio, etc.) are used to generate these individual decision trees.

When performing a random forest presentation based on taxonomic data, you need to find out the formula you use to determine, if you use the Gini index, often decide how the nodes on the branch of the tree.

$$\text{Gini} = 1 - \sum_{i=1}^c (p_i)^2 \quad (1)$$

This formula uses squares and probabilities to determine the guinea of each branch at a node, which determines which branches are most likely to occur. Here, p denotes the relative frequency and C denotes the number of classes. You can also use entropy to find out how nodes branch out in a decision tree.

$$\text{Entropy} = \sum_{i=1}^c -p_i * \log_2(p_i) \quad (2)$$

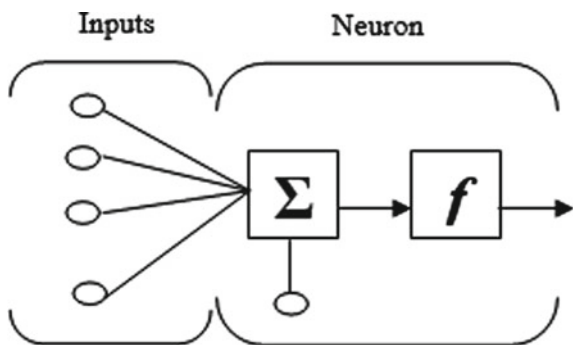
Entropy uses the probability of a specific outcome so that the node can determine how to branch. Unlike the Gini index, it is more mathematical due to the logarithmic function used in computation.

3.2 Artificial Neural Network

Artificial neural networks behave like a biological system which is composed of neurons. It consists of many nodes that work together and process information. Meaningful results are also generated from it. As mentioned before, it is composed of collectively three layers: input layer, hidden layer, and output layer. The input layer accepts inputs which the programmer can provide in different formats. The hidden layer is situated between the input and the output layer. The calculations to find patterns and features hidden in the data are performed here. Finally, the output layer is the layer which provides the output after the inputs have undergone computations in the hidden layer.

As shown in Fig. 2, except those in the input layer, each node provides a range of the same value that is associated with their input value p_i and the equivalent weight value y . Then by adding this weight value (total), the net input value of the neuron becomes n , for which b , the bias term. Relative to the actual amount, a bias is added. The net input value is then processed to the transfer function f , which manufactures the neuron output.

Fig. 2 A neuron



$$a = f\left(\sum_{i=1}^F w_i \cdot p_i + b\right) \quad (3)$$

The transfer function f is usually a nonlinear function that converts weighted inputs into output. The sigmoid/logistic function is a transfer function that limits the nodes output amid 0 and 1.

3.3 Autoencoder

Autoencoder is a dimensionality compression algorithm. Autoencoders have three main properties: They are data-specific, the compression is lossy, and it is an unsupervised learning technique. The three parts of an autoencoder network are the encoder, the code, and the decoder. The encoder and the decoder are essentially artificial neural networks, whereas code is an individual layer of an ANN whose dimensionality is provided by us. The hyperparameters needed to train an autoencoder are code size (number of nodes present in the middle layer), number of layers, number of nodes per layer, and loss function (mean squared error or binary cross-entropy).

Autoencoders consists of encoder interpreted as transitions Φ and the decoder as ψ , such that:

$$\Phi = X \rightarrow F \quad (4)$$

$$\psi = F \rightarrow X \quad (5)$$

$$\Phi, \psi = \arg \arg \min ||X - (\psi \circ \Phi)X||^2 \quad (6)$$

In a single hidden layer, the encoding stage of the model takes the input $x \in \mathbb{R}^d = X$ and maps it to $h \in \mathbb{R}^p = F$

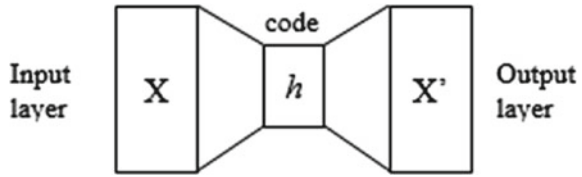
$$h = \sigma Wx + b \quad (7)$$

Here, equation h is cited as latent variables or latent representation or code and σ is known as an element-wise activation function. W is a weight matrix, and b is a bias vector, both are usually initialized randomly. W and b through backpropagation, are then updated iteratively during training. Then the decoder maps h to the reconstruction x' of the same shape as x :

$$x' = \sigma'(W'h + b') \quad (8)$$

Now σ' , W' and b' of the decoder may not be related to the equivalent σ' , W' and b' of the encoder. Autoencoders are further optimized and trained to minimize

Fig. 3 Autoencoder architecture



reconstruction errors mainly referred to as the “loss” as L , where x is usually average of the input training set.

$$L(x, x') = \|x - x'\|^2 = \|x - \sigma'(W'(\sigma(Wx+b)) + b')\|^2 \quad (9)$$

A typical structure of the autoencoder is shown in Fig. 3.

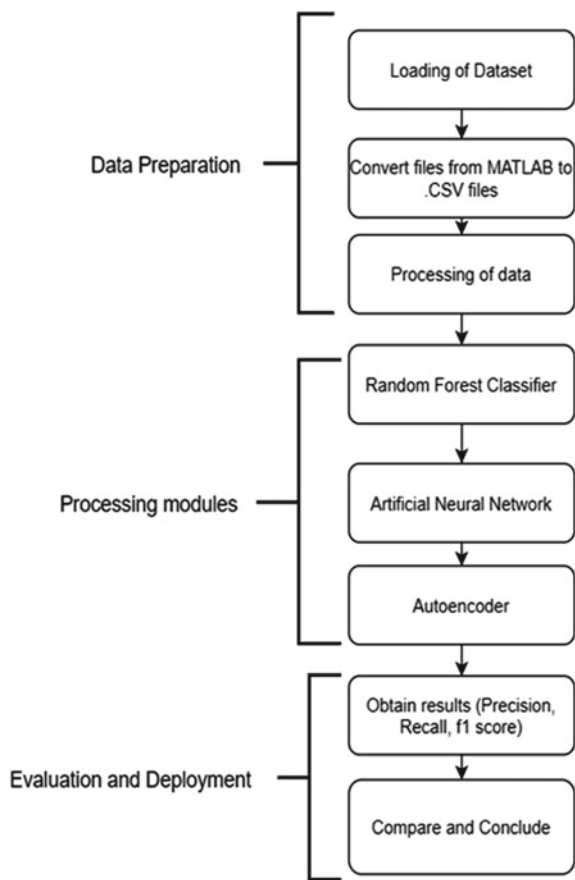
4 Proposed Methodology

4.1 Dataset Description

The dataset is collected from Case Western Reserve University Bearing Data Center (Case Western Reserve University 2017). Data files obtained in MATLAB format are converted to comma separated values (.csv). Each data files were exported to CSV spreadsheet file on MATLAB, using the writetable function available on MATLAB. Datasets used in the study are normal baseline and 12k drive end bearing fault data [Inner Race (0.007”), Outer Race (0.007”), Inner Race (0.021”), Outer Race (0.021”)]. The 12k drive end bearing fault data is anomalous. All the datasets are taken at approx. motor speed of 1750 rpm. Each dataset of the 12k drive end bearing fault is merged with normal baseline for 0.007” fault diameter and simultaneously for 0.021” fault diameter. We have chosen 121,155 data-points for each state of health.

4.2 Methodology

Figure 4 presents the system architecture used in this study. In order to obtain the results regarding accuracy, precision, and anomalies, three models are used, i.e., random forest classification, artificial neural networks, and autoencoder. After collecting and preparing the data, feature extraction was performed, i.e., removing the unnecessary features and data from the dataset and keeping only the ones which will be used by the models. Next, all the features are standardized in addition to that only the independent features are standardized. The datasets are then modeled using

Fig. 4 System architecture

various algorithms. In order to do this, the datasets are evaluated, and parameters tuned accordingly to give better results.

5 Results and Discussion

The precision, recall, f_1 -score, and anomalies using random forest classification and artificial neural networks are shown. Accuracy represents the number of correctly predicted observations over the total number of predicted observations.

$$\text{Accuracy} = \frac{\text{TP} + \text{TN}}{\text{TP} + \text{TN} + \text{FP} + \text{FN}} \quad (10)$$

Precision is the ratio of positive observations that are correctly predicted to the total number of positive observations.

$$\text{Precision} = \frac{\text{TP}}{\text{TP} + \text{FP}} \quad (11)$$

Recall is the ratio of positive observations correctly forecast to all observations in real class.

$$\text{Recall} = \frac{\text{TP}}{\text{TP} + \text{FN}} \quad (12)$$

The weighted average for accuracy and recall is the *F1 Score*.

$$\text{F1 Score} = 2 \cdot \frac{\text{precision} \cdot \text{recall}}{\text{precision} + \text{recall}} \quad (13)$$

where TP = true positive, TN = true negative, FP = false positive, FN = false negative. Similar results were obtained by Lei et al. [13] when studying the fault detection of ball bearing using symplectic entropy method. The loss mean absolute error and the anomalies calculated using autoencoders. The comparison between the different models is also shown. The results are presented in the following sections.

5.1 Random Forest Classification

As shown in Table 1, comparison of results using random forest classification with normal baseline and 12k drive end bearing fault data is shown. Two models with different fault diameters were used, consisting of 0.007" fault diameter and 0.021"

Table 1 Random forest classification results

	Normal (%)	Inner race (%)	Normal (%)	Outer race (%)
<i>Random forest classification (0.007" fault diameter)</i>				
Precision	82	89	81	88
Recall	90	81	89	78
<i>F1-score</i>	86	85	85	83
Anomalies	7045		7823	
<i>Random forest classification (0.021" fault diameter)</i>				
Precision	81	87	73	78
Recall	88	79	80	70
<i>F1-score</i>	84	83	76	74
Anomalies	7905		12,093	

Table 2 Artificial neural network results

	Normal (%)	Inner race (%)	Normal (%)	Outer race (%)
<i>Artificial neural networks (0.007" fault diameter)</i>				
Precision	74	88	75	90
Recall	91	69	92	69
F1-score	82	77	83	78
Anomalies	9844		9410	
<i>Artificial neural networks (0.021" fault diameter)</i>				
Precision	76	88	67	87
Recall	90	72	92	55
F1-score	83	79	78	67
Anomalies	9206		12,918	

fault diameter. Results were computed using 10n-estimators and entropy criterion. The precision, recall, *f*1-score, and faults defined by anomalies using random forest classification is shown in Table 1.

5.2 Artificial Neural Network

The results are differentiated with the help of artificial neural networks with 12k drive end bearing and normal baseline and the same is shown in Table 2. The precision, recall, *f*1-score, and faults defined by anomalies using artificial neural networks are also shown. Fault diameters of two different models which are 0.007" and 0.021" are being used. The final end product is calculated by using Adam optimizer and binary cross-entropy loss.

5.3 Autoencoder

Table 3 shows the loss mean absolute error and the anomalies of the different datasets present in the 12k drive end bearing fault which were calculated using autoencoders.

Table 3 Autoencoder results

	Loss (mean absolute error)	Anomalies
Inner race (0.007")	0.01747204981317849	643
Outer race (0.007")	0.013837332365064396	952
Inner race (0.021")	0.011308336521063111	698
Outer race (0.021")	0.011221625310020175	812

The highest number of anomalies were noted in outer race (0.007''). Alternatively, the inner race (0.007) had the lowest number of anomalies. Figure 5 shows the interpretation of the models on a graph using autoencoders. The anomaly marked shows that the loss mean absolute error exceeds the threshold. A parameter referred to as the threshold governs the decision to transform an expected likelihood or ranking into a class mark. Threshold is calculated using another graph interpreting the loss distribution. The anomalies are marked as red dots on the graph, and the threshold is marked by the orange line.

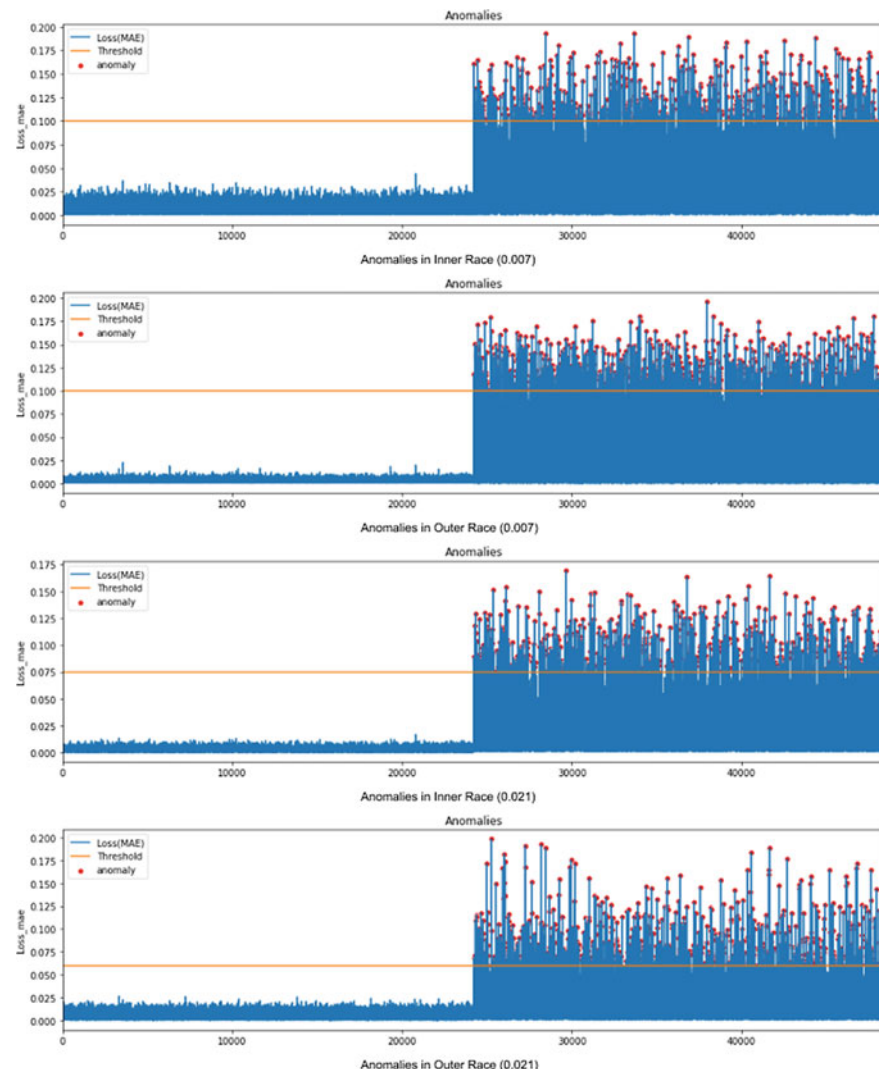


Fig. 5 Anomalies in autoencoder models

Table 4 Comparison of the models based on accuracy

	Accuracy		
	RF (%)	ANN (%)	Autoencoders (%)
Inner race (0.007")	85	80	91
Outer race (0.007")	84	81	96
Inner race (0.021")	84	81	97
Outer race (0.021")	75	73	99

5.4 Comparing the Various Models

The accuracy acquired across all the three models are shown in Table 4. While the results of autoencoders acquired the highest accuracy rate, on the other hand, artificial neural networks had the least accuracy rate. The results show that the model created using autoencoders is the best fit for this study.

6 Conclusion

In this study, we researched and explored the different algorithms that are used in machine learning and deep learning to predict anomalies in the bearing machinery. The three algorithms used in the study were random forest classification and artificial neural network and autoencoder algorithm to CWRU dataset. Our results showed better accuracy for autoencoders in comparison with random forest classification and artificial neural networks. Also, the feature preprocessing techniques required in autoencoders were less in comparison with random forest and ANN. The authors propose to extend their work by applying other variants of autoencoder and other deep learning models to derive further bearing performance parameter values for predictive maintenance.

Acknowledgements The dataset was downloaded from the Case Western Reserve University Bearing Data Centre website at <https://csegroups.case.edu/bearingdatacenter/pages/welcome-case-western-reserveuniversity-bearing-data-center-website>.

References

1. Zhang S, Zhang S, Wang B, Habetler T (2019) Deep learning algorithms for bearing fault diagnostics—a comprehensive review. [arXiv:1901.08247](https://arxiv.org/abs/1901.08247)
2. Heo S, Lee JH (2018) Fault detection and classification using artificial neural networks. IFAC (International Federation of Automatic Control) PapersOnLine 51:470–475
3. Ademujimi T, Brundage M, Prabhu V (2017) A review of current machine learning techniques used in manufacturing diagnosis, pp 407–415. https://doi.org/10.1007/978-3-319-66923-6_48

4. Li C, Sánchez R, Zurita G, Cerrada M, Cabrera D (2016) Fault diagnosis for rotating machinery using vibration measurement deep statistical feature learning. *Sensors* 2016(16):895. <https://doi.org/10.3390/s16060895>
5. Munirathnam S, Ramadoss B (2016) Predictive models for equipment fault detection in the semiconductor manufacturing process. *IACSIT Int J Eng Technol* 8:273–285. <https://doi.org/10.7763/IJET.2016.V8.898>
6. Amruthnath N, Gupta T (2018) A research on unsupervised machine learning algorithms for early fault detection in predictive maintenance. In: 5th Conference on industrial engineering and applications. <https://doi.org/10.13140/RG.2.2.28822.24648>
7. Ferreira JG, Warzecha A (2017) An application of machine learning approach to fault detection of a synchronous machine. In: 2017 International symposium on electrical machines (SME). <https://doi.org/10.1109/ISEM.2017.799354>
8. Seera M, Wong M, Nandi A (2017) Classification of ball bearing faults using a hybrid intelligent model. *Appl Soft Comput* 57:427–435
9. Korba KA, Arbaoui F (2018) SVM Multi-classification of induction machine's bearings defects using vibratory analysis based on empirical mode decomposition. *Int J Appl Eng Res* 13(9):6579–6586. ISSN 0973-4562
10. Patel R, Giri V (2016) Feature selection and classification of mechanical fault of an induction motor using random forest classifier. *Perspect Sci* 8:334–337
11. Seryasat OR, Haddadnia J, Arabnia Y, Zeinali M, Aboozalizadeh Z, Taherkhani A, Tabrizy S, Maleki F (2012) Intelligent fault detection of ball-bearings using artificial neural networks and support-vector machine. *Life Sci J* 9(4):4186–4189. ISSN: 1097-8135. <https://www.lifesciencesite.com>
12. Yang Y, Fu P (2018) Rolling-element bearing fault data automatic clustering based on wavelet and deep neural network. *Shock Vib* 2018:1–11
13. Lei M, Meng G, Dong G (2017) Fault detection for vibration signals on rolling bearings based on the symplectic entropy method. *Entropy* 19(11):607
14. Zhang R, Peng Z, Wu L, Yao B, Guan Y (2017) Fault diagnosis from raw sensor data using deep neural networks considering temporal coherence. *Sensors* 17(3):549
15. Khorram A, Khalooei M (2019) Intelligent bearing fault diagnosis with convolutional long-short-term-memory recurrent neural network
16. Kumar S, Sharma B, Sharma VK, Poonia RC (2018) Automated soil prediction using bag-of-features and chaotic spider monkey optimization algorithm. *Evol Intell* 1–12. <https://doi.org/10.1007/s12065-018-0186-9>
17. Kumar S, Sharma B, Sharma VK, Sharma H, Bansal JC (2018) Plant leaf disease identification using exponential spider monkey optimization. *Sustain Comput Inf Syst* 28. <https://doi.org/10.1016/j.suscom.2018.10.004>
18. Shekhawat SS, Sharma H, Kumar S, Nayyar A, Qureshi B (2021) bSSA: binary Salp Swarm algorithm with hybrid data transformation for feature selection. *IEEE Access*. <https://doi.org/10.1109/ACCESS.2021.3049547>

Selection of a Mesh Network Routing Protocol for Underground Mines



Prenern Reddy and Theo G. Swart

Abstract Research into determining the optimum routing protocol for underground mines was conducted in a mock stope at the University of Johannesburg comparing B.A.T.M.A.N., Babel and OLSR by transferring different types of network traffic. It was found that the B.A.T.M.A.N. routing protocol offered the best performance due to its layer 2 implementation; however, OLSR, a layer 3 routing protocol, was also found to be an acceptable routing protocol. This may have been due to OLSR's ability to skip nodes when routing data. It was also found that the optimal internode spacing was 60 m as this allows for a reported -3 dB RSSI enabling a good balance between transfer speed and coverage distance.

Keywords Wireless mesh networks · Routing protocol · Mining · Telecommunications

1 Introduction

The use of IoT sensors to collect data is increasing drastically as the Fourth Industrial Revolution progresses, and thus, there are multiple cases where these IoT sensors may be used in underground mines to improve day-to-day operations as well as safety amongst other things. However, it is necessary for these sensors and devices to have access to some form of network in order to transfer collected data for processing, and this is where wireless mesh networks (WMNs) have an advantage as they allow for easy to set up and maintain wireless access points that allow sensors to be installed wirelessly as well as be mobile. Thus, to bring such IoT devices into underground mines, it is apt to study the capabilities of the network required and determine what is needed to make these networks run optimally with the hardware available so as

P. Reddy (✉) · T. G. Swart

Department of Electrical and Electronic Engineering Science, Center for Telecommunications, University of Johannesburg, Johannesburg, South Africa

T. G. Swart

e-mail: tgswart@uj.ac.za

to attain the best performance given the large amounts of data that is required to be transmitted when considering a mining environment.

In this study, three different types of routing protocols were compared, namely B.A.T.M.A.N., Babel and OLSR using different types of network traffic, transmission control protocol (TCP) and user datagram protocol (UDP), to determine which routing protocol provided not only the best network transfer speed and the lowest latency but also the largest internode spacing so as to reduce the number of nodes required, thus potentially reducing the overall cost of implementation.

It was found that the B.A.T.M.A.N. routing protocol performed the best when transferring TCP data and that Babel slightly outperformed the other routing protocols when transferring UDP data and that B.A.T.M.A.N. had the lowest latency on an uncongested network, thus indicating that B.A.T.M.A.N. routing protocol is the most suited to being used in a mining environment.

2 Literature Review

The literature review will discuss similar work done, the main points with regards to wireless mesh network routing protocols as well as the three routing protocols used for testing.

2.1 *Current Networking Methods Used in Mines*

ABB Tropos Mesh Network ABB offers a mesh networking solution that utilizes ABBs Tropos wireless mesh networking system consisting of Tropos mobile and outdoor mesh routers and a Tropos wireless control system. The system utilizes mobile nodes capable of withstanding high dust and vibration which ensures reliable connectivity when placed in vehicles. The high-capacity Tropos Mesh Network system has proven that it is able to facilitate mining operations reliably in extreme environments and allows nodes to be relocated and associated easily should they be moved around the mine site.

The ABB Tropos mesh network system was tested in one of the largest iron ore mines which spans over 25 ha in Australia, the open pit mine operates 24/7 and has between 1500 and 2000 workers on site per day with the ore lying 20–70 m below the surface [1].

General Electric's Industrial Communication Solutions for the Mining Industry General electric's networking and communication solutions for the mining industry offer world leading end-to-end wireless industrial communications. Multiple systems such as wellheads, utility substations and SCADA applications can be monitored. The industrial grade wireless modems and routers are required to operate in harsh

environments during testing, such as operating in temperature ranges from -40 to $+70$ °C and environments with high continuous vibration, and as a result, the devices have hazardous location approvals, such as class 1, division 2 which state that the system can operate in hazardous environments and is blast proof [2].

The system comprises wireless radios which can operate in both the licensed and unlicensed narrowband as well as industrial 2G, 3G and 4G LTE routers and gateways. These networks can be used to carry a variety of traffic including serial and ethernet traffic as well as analogue and digital I/O signals connected directly to field devices and sensors [3].

Nokia Intelligent Communications for Mining The Nokia provides high performance networks for mining companies which allow the use of digital technologies enabling ease of adaptation to address safety and environmental concerns as well as adapt to fluctuating demand and control and operational costs.

To support machine-to-machine communications in today's wireless network, the traffic needs to either travel to a hub location via a layer two protocol tunnel or an IPsec tunnel (if encryption is required) first or hop on a mesh of tunnels, which requires substantial efforts to manage, before arriving at the destination router. The complexities and inefficiencies incurred by the tunnels impede the adoption and performance of mine automation, and thus, the Nokia system does not rely exclusively on mesh networks.

Two global standards-based networking technologies are used, long-term evolution and IP/multi-protocol label switching (a technique to improve network speeds as well as shape traffic flows across large networks [4]), together with an agile network services platform from the basis for the Nokia system [5].

Cambium Networks utilize a point-to-point backhaul based on a licensed microwave radio band, and this backhaul then connects to access points or nodes. The Wi-Fi access points are part of the cnPilot series and are available in either an outdoor or indoor version depending on the intended location of the access point. Both versions offer reliable and secure 802.11ac Wi-Fi capable of 1 Gbps and industry standard connectivity for a multitude of devices. The access points are typically utilized in mining camp configurations where 100 or more access points support thousands of workers [6].

2.2 *Similar Work on Selecting WMN Routing Protocols for Underground Mines*

A Routing Protocol for Multisink Wireless Sensor Networks (WSNs) in Underground Coal mine Tunnels [7] The network observed was designed to be implemented in haulage coal mine tunnels which have a long strip shape whose length is much greater than width. As a result, multiple sinks or mesh nodes are needed to

form a chain, and these nodes are required to negotiate their communication radius and transmission power to ensure full coverage of the mine tunnel. Unequal clustering in individual regions was established in relation to the actual coverage of each sink to optimize the network topology and reduce the clustering interference, energy consumption and prolong the network lifetime with the goal being to ensure optimum connectivity.

The power control and energy balance monitoring system (PCEB-MS) protocol (similar to TORA routing protocol) used in the coal mine tunnel places a sink at non-specific locations along a link with the only restriction being that the intervals are less than the radius of communication of each sink.

Each sink location is determined by UWB technology, and power control message or PCM is then broadcasted within its radius of communication the nodes can also communicate with each other using a buried cable. If it is assumed that two sinks are able to communicate with one another in the initialization stages, each sink can then receive regional monitoring data from a sensor node, thus ensuring a PCM exchange.

The PCEB-MS algorithm attempts to address the problems which occur when using wireless technology in coal mines which have a long strip shape. The sensor network in this study achieved a solution to the traditional problems which exist in underground coal mine tunnels and shows that relative to power control, network connectivity was improved, and latency was decreased, thus achieving a balance based on the clustering of the network.

An Underground Mobile Wireless Sensor Network (UWSN) Routing Protocol for Coal Mine Environment using Mobile Node-Based Routing (MNBR) [8] The USWN observed in this study consisted of three kinds of nodes: a beacon node which was responsible for monitoring the environment and deployed only at one end of a tunnel due to the narrow underground tunnel, a mobile node, which was uniquely numbered and was attached to mobile equipment. The mobile nodes unique number acts as an identification for tracing and locating mobile equipment underground and finally a base station which was connected to an unlimited power supply and could thus communicate over a very large distance was used. The base station was capable of storage and computing, the base station was also used as the exit of the UWSN and responsible for the exchange of the collected data and control commands.

The MNBR protocol can save the energy consumption of nodes greatly and is more suitable for UWSN whose nodes' energy is imbalance. The MNBR protocol can elect the appropriate relay node to build up the routing path through neighbor information table, which can adapt to the fast-changed topology caused by the movement of the mobile node.

An Experimental Comparison of Routing Protocols in Multi-hop Ad Hoc Networks [9] In this study, the performance of B.A.T.M.A.N., Babel and OLSR was compared. Since it has been shown that traditional routing protocols are inadequate when used on wireless ad hoc networks, resulting in the need for ad hoc specific routing protocols, and this study tested the three main classes of routing

protocols, link state, distance vector and hybrid approaches to routing protocols. The importance of OSI layers is also taken into consideration, and it is concluded that the routing protocol's overhead has the greatest impact on performance in small multi-hop ad hoc networks and that the results show that Babel outperforms both OLSR and B.A.T.M.A.N. routing protocols, as well as concluding that the OSI layer of the routing protocol has little to no impact on performance.

2.3 Wireless Mesh Network Routing Protocols

Wireless mesh network routing protocols can be arranged into the following types of protocols:

- Reactive protocols: This type of protocol can construct a route at whatever point there is a request. If a node is required to send data to another node and if there is no route accessible, at that point, the route required will be built up by the reactive protocol in order to make communication possible. These are normally distance vector-based protocols.
- Proactive protocols: In proactive routing, every node of a network maintains one table at the least, and this table is used to speak to the overall network, i.e., each node has at least one routing table that it uses to direct data. These are normally link state-based routing protocols.
- Hybrid routing protocols combine both reactive and proactive protocols as the name implies. Hybrid type protocols attempt to locate the optimal destination and can also generate a report should there be any changes to the WMN. Hybrid protocols are generally, a combination of link state and distance vector routing protocols.

There are two main classes of routing protocol that are derived from the above types, distance vector which normally implements reactive techniques and link state which normally implements proactive techniques [10], and this can be used to classify the routing protocol used as there are a great number of protocols available which achieve the same result either through distance vectoring or monitoring the link state using different algorithms. These algorithms then implement a proactive, reactive or hybrid response to route data depending on the routing protocol used, and Table 1 provides the differences between distance vector and link state-based protocols.

The following discussion will cover the three main routing protocols used during testing, namely B.A.T.M.A.N., a hybrid proactive and reactive-based protocol, Babel, a reactive distance vector-based protocol and finally optimized link state routing (OLSR), a proactive link state-based protocol.

Better Approach to Mobile Ad Hoc Networking (B.A.T.M.A.N.) B.A.T.M.A.N. operates by requiring each node to store and maintain information about only the next best hop toward other nodes in the network, and this results in a reduction of unnecessary knowledge regarding the global topology, thus reducing overheads [11].

Table 1 Differences between distance vector and link state routing [10]

Distance vector	Link state
Sends entire routing table	Sends only link state information
Slow to converge	Fast to converge
Updates are sent using broadcast technique	Updates are sent using multicast technique
Does not have the network topology	Has the network topology
Simple to configure	Difficult to configure
Susceptible to routing loops	Less susceptible to routing loops

B.A.T.M.A.N. does not attempt to determine the full routing path but rather only determines which link-local neighbor is the optimal gateway to each originator, keeps track of new originators and informs neighboring nodes about originators existence, and B.A.T.M.A.N. also ensures that routes only consist of bidirectional links.

Babel routing protocol, a loop-avoiding layer 3 distance vector routing protocol, is robust and efficient. Babel is suitable for unstable networks as it limits the frequency and duration of routing pathologies such as routing loops. After a mobility event is detected, Babel is able to remain loop free and will converge to a configuration which preserves the loop-freedom of the network. This may not be optimal as this operation may not require a packet exchange resulting in Babel converging to an optimal configuration in a time scale of minutes and is achieved by utilizing sequenced routes a technique used in destination-sequenced distance vector routing [12].

Optimized link state routing protocol is a proactive layer 3 routing protocol for mobile ad hoc networks, and the stability of the link state algorithm is inherent in OLSR and can have routes immediately available as it is a proactive protocol and is the optimization of the link state protocol.

OLSR minimizes overheads by controlling flooding of control traffic through the use of selected nodes, called multi-point relays, to send control messages to the network. This technique enables a reduction in the number of transmissions required to send a message to the whole network. OLSR also only needs a partial link state flooded in order to determine the shortest routes, and the minimum link state information that OLSR requires is that nodes, selected as multi-point relays, must declare the links to their respective multi-point relay selectors [13].

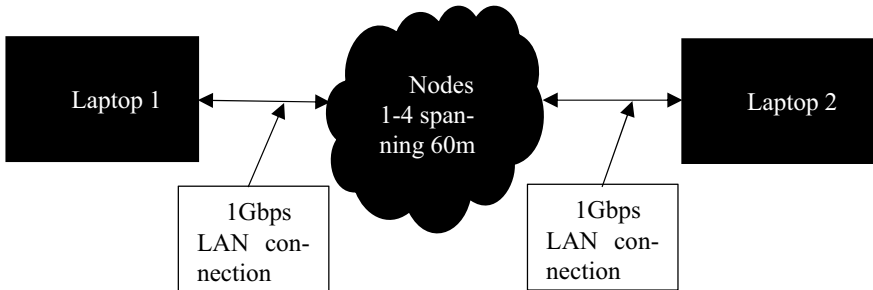


Fig. 1 Overview of the network setup in the mock stope

3 Setup and Procedure

3.1 Setup

Four wireless mesh network nodes were used to collect data, these nodes were flashed with OpenWRT firmware as this enabled the routing protocols to be switched, the three routing protocols, B.A.T.M.A.N, Babel and OLSR, were then configured on the seven mesh nodes, and preliminary testing conducted to ensure that the mesh network was still operational and that the routing protocols could be switched after configuring the firmware.

The network setup consisted of the four mesh nodes powered by four 12 V batteries and two laptops connected to the first and last nodes via 1 Gbps LAN similar to the setup found in J. Shibalabala and T. G. Swart, “Performance analysis of wireless mesh networks for underground mines”, International Conference on Artificial Intelligence, Big Data, Computing and Data Communication Systems, Durban, South Africa, August 6–7, 2020.) [14] as the current study builds upon these findings. The physical topology of the network was linear with the two laptops at each end of the linear mesh. The network traffic that was used for testing consisted of file transfer using a 18 MB file, video streaming from one laptop to another using TCP streaming of a 1080p video, and finally, VoIP calls were made over the network using UDP. Figure 1 shows an overview of the network setup.

3.2 Procedure

Due to the pandemic faced in 2020, it was not possible to conduct testing of the wireless mesh network in an actual stope, and thus, testing had to be conducted in a mock stope in the basement of University of Johannesburg’s Doornfontein campus. As such, the length of the stope was severely limited to only 60 m, and testing had to be reduced to having fixed internode spacing of 20 m between nodes giving a

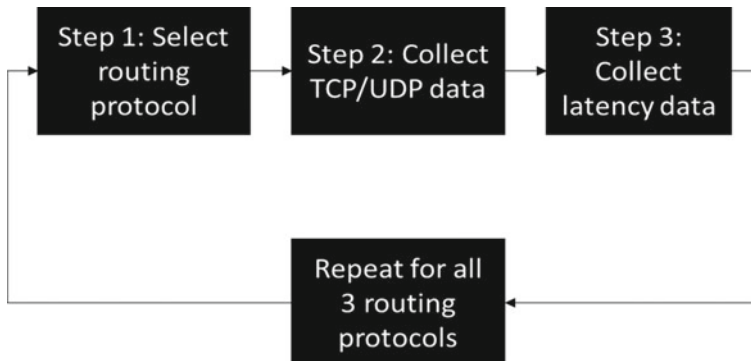


Fig. 2 Flow diagram indicating the procedure used to collect data

maximum coverage length of 60 m which was the entire length of the mock stope and only four of the seven nodes are being used.

To collect data, a routing protocol was selected, the 18 MB file was transferred from the second laptop to the first, the transfer speeds recorded using Wireshark, the same was done for VoIP and video streaming traffic; finally, the uncongested network latency data was collected once this was completed for a single routing protocol, the next protocol was selected, the testing restarted, and this process can be seen in Fig. 2.

3.3 *Equipment and Software*

The main equipment used for testing in the mock stope was four open mesh OM2P wireless mesh nodes and two laptops equipped with 1Gbps LAN interfaces, and the software that was used was the aforementioned OpenWRT, Wireshark, Team Viewer and PC VoIP Extreme 2.0. A discussion follows with regards to the equipment and software used.

Open mesh OM2P wireless mesh nodes were used to create the WMN from the first laptop to the second laptop where the second laptop was specified as the end point. The OM2P wireless mesh network nodes use B.A.T.M.A.N as the standard routing protocol with the supplied firmware, and thus, to change the routing protocol, it was required to flash the devices firmware with an open source version. The OM2P hardware supports 2.4 GHz with a transmit power of 23 dBm or 200 mW and a range of 23–45 m indoors and an outdoor range of 122–152 m [15].

OpenWRT, an open source Linux-based router firmware, was used to replace the firmware on the mesh nodes as well as on the router as the CloudTrax firmware supplied only utilizes the B.A.T.M.A.N routing protocol and cannot be changed. OpenWRT supports B.A.T.M.A.N, OSLR and Babel routing protocols as such these

are the protocols that were tested on the mesh network, which was sufficient as this allowed for testing of a hybrid, link state and a distance vector protocol [16].

Team Viewer, an application that allows remote control of a computer over a network, was used to control the second laptop remotely to answer VoIP calls.

PC VoIP extreme was used for VoIP calls as this eliminates the need for VoIP phones which require external power to the base, and this also makes the network easier to set up as only the two laptops are required to be connected continuously.

3.4 Requirements

The system must

- Transfer data at or above 5 Mbps for file transfer, 2.5 Mbps for video streaming via the transmission control protocol and 120 kbps for VoIP communication via user datagram protocol, and all tests should occur with less than 100 ms latency across the entire network.
- Be able to operate underground.
- Be able to transmit data at the required bandwidth with at least 60 m between nodes so that the system may operate at the largest distance with the least number of nodes.
- Be able to operate in the presence of electrical noise that may be emitted by machinery operating in the vicinity.
- Be easy to maintain and replace nodes should a node get damaged.

4 Results

Figure 3 shows the network in the mock mine stope, and the following results were obtained from the tests conducted in the mock stope.

From Fig. 4, it can be seen that Babel, a layer 3 distance vector-based routing protocol, performed the worst under test conditions during TCP video streaming, and B.A.T.M.A.N. performed the best; however, OLSR, an OSI layer 3-based routing protocol, achieved performance that was surprisingly close to B.A.T.M.A.N., a layer 2-based routing protocol. This may be due to the link state nature of OLSR as well as the short internode spacing, as this routing protocol is capable of skipping nodes should there be congestion whereas B.A.T.M.A.N is a hybrid protocol which monitors both link state and distance.

The next test conducted was transferring a file across the mesh network, and the result seen in Fig. 5 shows that B.A.T.M.A.N again outperforms Babel and OLSR by almost 2 Mbps and OLSR transferring the file slightly faster than Babel with a 0.4 Mbps difference.

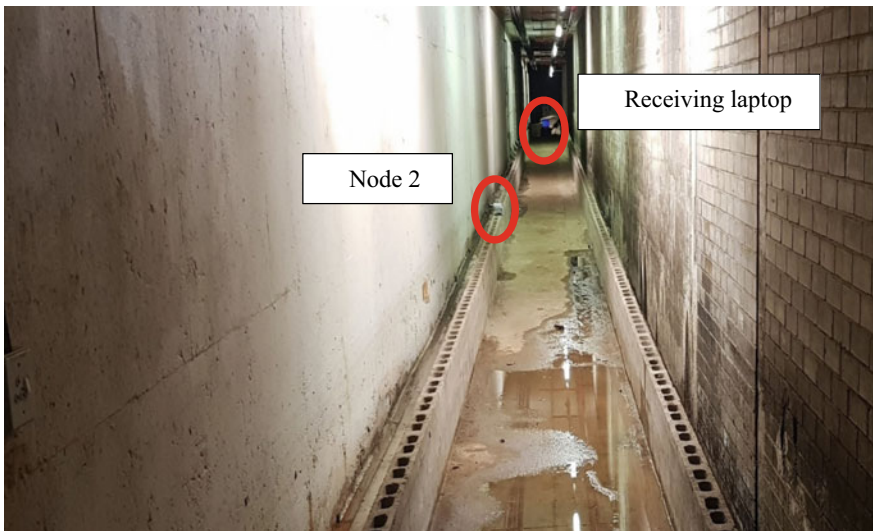


Fig. 3 Network setup in mock stope

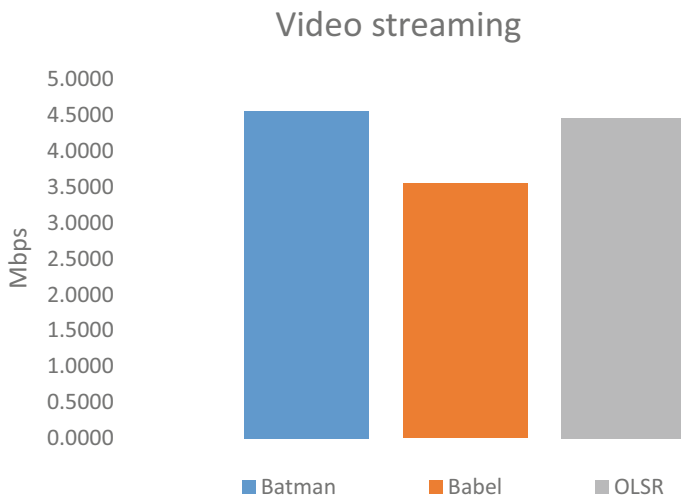


Fig. 4 Results of the video streaming tests using TCP, as can be seen B.A.T.M.A.N and OLSR performed similarly with B.A.T.M.A.N streaming at 4.55 Mbps and OLSR at 4.45 Mbps

Following the file transfer test, a VoIP call was initiated between the end point laptops for approximately one minute and network data recorded. This test provided perhaps the most surprising result as seen in Fig. 6. OLSR outperformed both B.A.T.M.A.N. and Babel while streaming VoIP data using UDP, which may again be due to the internode spacing. This implies that OLSR may be better to use when

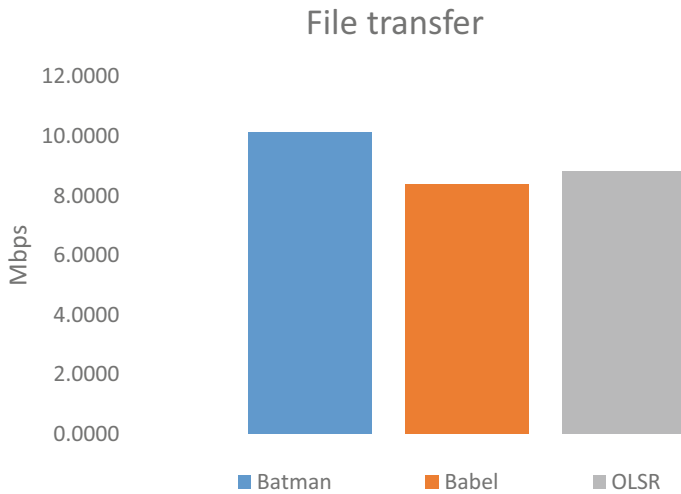


Fig. 5 Results of the file transfer test where B.A.T.M.A.N. far outperformed Babel and OLSR

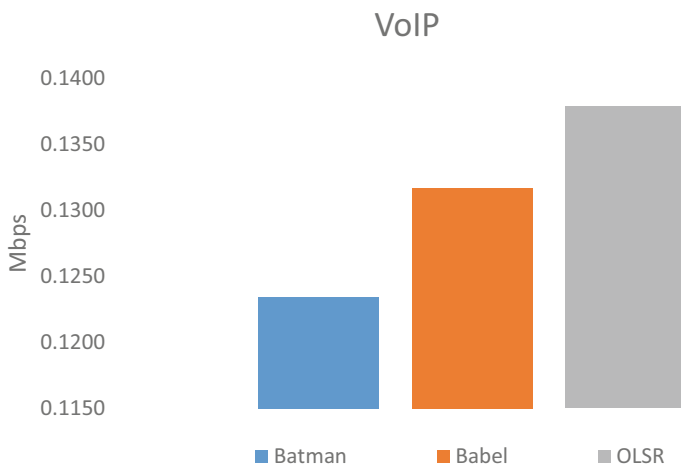


Fig. 6 Results obtained from VoIP testing using UDP showing OLSR outperforming B.A.T.M.A.N. and Babel routing protocols

transferring data from IoT sensors for instance. However, B.A.T.M.A.N., the poorest performing routing protocol, had a data rate above 120 Kbps equivalent to the bitrate of FM radio, and thus, the call quality is still acceptable using B.A.T.M.A.N.

The final test that was conducted was the uncongested latency test where the delay between the two end point laptops was measured, and in this case, lower values are better. As expected, B.A.T.M.A.N. performed the best due to its layer

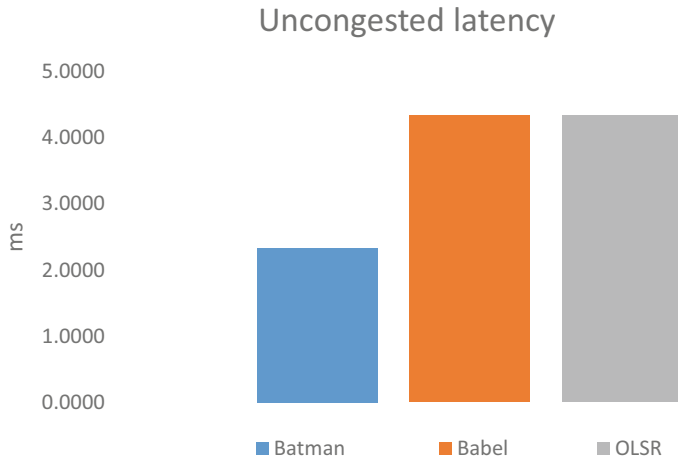


Fig. 7 Results obtained from the uncongested latency test showing B.A.T.M.A.N. with the lowest latency and both Babel and OLSR with a latency of 4 ms

2-based construction, and this resulted in a latency of almost half that of Babel and OLSR, the layer 3-based protocols as seen in Fig. 7.

5 Discussion

From the results above, it can be deduced that B.A.T.M.A.N. is suitable for most applications in underground mines; however, OLSR is an alternative that may be considered as it has shown adequate performance. However, further testing should be conducted to ensure that OLSR performance is acceptable when the internode spacing is changed. The current recommendation for the optimum routing protocol for wireless mesh networks in mines is to use the B.A.T.M.A.N. routing protocol with an internode spacing of 60 m. Both OLSR and Babel outperformed B.A.T.M.A.N. as shown in Fig. 6, and this indicates that B.A.T.M.A.N. is not as well suited to dealing with UDP traffic as its layer 3-based competitors and thus shows that the main network traffic should be considered when selecting a routing protocol.

Observing Figs. 4, 5 and 6 again, OLSR outperforms Babel across all tests, and this result was unexpected as it was postulated that the link state-based routing protocol would be the worst performing protocol because if the nodes were to be lined up sequentially, knowing the link state would be unnecessary since the data only needs to be transmitted to the next required node, thus a distance vector protocol should have outperformed a link state protocol as the distance vector would have known to transmit to its nearest neighbor. Perhaps the results would change should there be an increase in internode spacing as the results obtained between Babel and OLSR could be explained since the distance vector protocol may only be transmitting to

its nearest neighbor whereas the link state protocol may be skipping nodes and transmitting directly to the receiving node given the overall distance of 60 m.

The uncongested latency from Fig. 7 was clearly lower by 2 ms when utilizing B.A.T.M.A.N. This performance may lead to faster real-time communications but does not impact the network too heavily when using Babel and OLSR overall, and given that B.A.T.M.A.N. operates on layer 2, this result is expected.

6 Conclusion

Overall, the research can be seen as somewhat successful as all the requirements that could be met given the circumstances were met and the network was able to transfer the required data at the required data rates and latency. The network could be implemented in a mine stope and used to transmit some less critical data, this could then be used as a long-term study into the performance of the WMN and to gauge if the mesh network can handle the actual data rate that may be required by equipment and communications devices as the tests conducted only handled one data type at a time.

Regarding the physical testing of the WMN, it would be advisable to conduct the testing in a longer stope to determine a concrete distance and data rate that each routing protocol can achieve, which will result in an accurate depiction of which routing protocol to select when attempting to develop a WMN for use in underground mines. However, the current data shows that the B.A.T.M.A.N. routing protocol with internode spacing of 50–60 m is best suited for this task and notably OLSR can also be used despite being a layer 3-based protocol that considers the link state. The viability of OLSR, however, needs to be tested further as the results obtained could indicate that the OLSR routing protocol was in fact skipping nodes given the short distance of the stope used for testing.

A similar case can be made for Babel; however, given that it is a distance vector-based protocol, the results should be similar when testing with larger distances, as the routing protocol will be searching for all of its available neighbors (this increases overheads and has been eliminated in B.A.T.M.A.N. in favor of only keeping records of the next available nodes at each node) and selecting the ones with the highest signal strength/data rate which is what took place with the current testing conducted. Thus, given the sequential nature of a WMN set up in a stope, it is not necessary to keep a record of all neighboring nodes, rather only the closest ones to improve performance.

In conclusion, it can be seen that valuable insights into implementing mesh networking in underground mines were gained, this is one of the first steps of many to improve mining operations using current technology, thus bringing underground mines up to date with the Fourth Industrial Revolution.

Acknowledgements A special thanks goes to Schauenburg Systems for sponsoring this research.

References

1. Mining iron ore in Australia. Search.abb.com (2015) [Online]. Available: <https://search.abb.com/library/Download.aspx?DocumentID=1KHA%20-%20001%20379%20-%20REN%20-%201002-%2011-2015&LanguageCode=en&DocumentPartId=&Action=Launch>. Accessed: 06 Mar 2020
2. 1910.399—Definitions applicable to this subpart. Occupational Safety and Health Administration. Osha.gov (2020) [Online]. Available: <https://www.osha.gov/laws-regulations/standardnumber/1910/1910.399>. Accessed: 06 Mar 2020
3. Industrial wireless: GE grid solutions. Geagridsolutions.com [Online]. Available: <https://www.geagridsolutions.com/Communications/wireless.htm>. Accessed: 07 Mar 2020
4. Rouse M (2020) What is multiprotocol label switching (MPLS)? SearchNetworking [Online]. Available: <https://searchnetworking.techtarget.com/definition/Multiprotocol-Label-Switching-MPLS>. Accessed: 07 Mar 2020
5. Nokia: Nokia converged mining automation networks white paper. OneStore [Online]. Available: <https://onestore.nokia.com/asset/202095>. Accessed: 07 Mar 2020
6. Wireless digital connectivity for mining operations. Cdn.cambiumnetworks.com (2017) [Online]. Available: https://cdn.cambiumnetworks.com/wp-content/uploads/2017/10/SP_WirelessMiningOperations_09122017.pdf. Accessed: 09 Mar 2020
7. Xia X, Chen Z, Liu H, Wang H, Zeng F (2016) A routing protocol for multisink wireless sensor networks in underground coalmine tunnels. Sensors 16(12):2032
8. Qiao G, Jianchao Z (2011) An underground mobile wireless sensor network routing protocol for coal mine environment. J Comput Inf Syst 7(7):2488, 2493
9. Murray D, Dixon M, Koziniec T (2010) An experimental comparison of routing protocols in multi hop ad hoc networks. In: Australasian telecommunication networks and applications conference, pp 159–164
10. Ahmad W, Qazi A (2018) Comparison of routing protocols in wireless mesh network on the basis of performance. Int J Netw Commun 8(2):29–33
11. Venkat M, Kasiviswanath N (2011) Routing protocols for wireless mesh networks. Int J Sci Eng Res 2(8):1–3
12. Chroboczek J (2020) RFC 6126—The babel routing protocol. Tools.ietf.org (2011) [Online]. Available: <https://tools.ietf.org/html/rfc6126>. Accessed: 04 Mar 2020
13. Destination-sequenced distance vector routing (DSDV). <https://mti.binus.ac.id> (2020) [Online]. Available: <https://mti.binus.ac.id/2014/08/15/destination-sequenced-distance-vector-routing-dsdv/>. Accessed: 04 Mar 2020
14. Shibalabala J, Swart TG (2020) Performance analysis of wireless mesh networks for underground mines. In: International conference on artificial intelligence, big data, computing and data communication systems, Durban, South Africa, 6–7 Aug 2020
15. Openmesh.com [Online]. Available: <https://www.openmesh.com/resource-downloads/OM-Series-Datasheet.pdf>. Accessed: 19 Mar 2020
16. OpenWrt Project: welcome to the OpenWrt Project. Openwrt.org [Online]. Available: <https://openwrt.org/>. Accessed: 22 Sept 2020

An Energy-Efficient Communication Scheme for Multi-robot Coordination Deployed for Search and Rescue Operations



M. Rajesh and S. R. Nagaraja

Abstract Robots are assisting humans in various fields of life such as in industry, health care, defense, and entertainment. Rescue robotics is an evolving division of robotics where robots are used to replace humans from hazardous situations to carry out rescue operations. Examples of human fire fighters are getting replaced by team of robots to carry out search and rescue operation. The major challenge in the use of multi-robot systems is the battery life of the robots. Efficient use of the battery power is the essential task of robots. In a multi-robot system, coordination among robots will be effective if there is proper communication scheme is available among the robots. In this paper, an energy-efficient communication scheme is proposed which will avoid unnecessary messages being communicated among robots and limit the message exchanges between interested parties only. Heterogeneous robots will classify themselves into groups of robots with similar functionalities, and they will publish the details of services (data) which they can offer. Robots which need those details will subscribe these groups, and communication will be limited to subscribed robots. This will reduce the number of messages exchanged in the system and thus by reducing the use of energy for communication. Simulation of the proposed system provides strong support for the claim that the proposed system is much more effective than existing strategies in terms of energy efficiency. The proposed system is able to reduce the energy consumption of the entire network by around 24% compared to the traditional schemes.

Keywords Multi-robot system · Energy efficiency · Publish–subscribe · Heterogeneous robots · Robot coordination

M. Rajesh (✉)

Department of Computer Science and Engineering, Amrita School of Engineering, Amrita Vishwa Vidyapeetham, Bengaluru, India
e-mail: m_rajesh@blr.amrita.edu

S. R. Nagaraja

Department of Mechanical Engineering, Amrita School of Engineering, Amrita Vishwa Vidyapeetham, Bengaluru, India
e-mail: sr_nagaraja@blr.amrita.edu

1 Introduction

Robotics is the branch of studies which focus on designing and developing robots to assist humans in performing hazardous and complex tasks. Initially, robots were designed to help humans in industry to complete jobs such as assembly of vehicles and painting. Later robots are built to assist humans in every aspects of life like space missions, health care, search, and rescue missions. Robots are nowadays designed to entertain people, elderly people monitoring, etc. Initially, the design aspect of developing a robotic solution is to build a single robot which can complete the required services. But nowadays, multi-robot systems are developed for providing a solution. This will reduce the amount of time spend to complete the task as well as it will enhance the performance. But the major challenge in multi-robot systems is coordination and communication among robots.

Multi-robot systems are used in complex tasks where individual robots are not capable of completing the entire task alone, but with proper coordination and communication among the team of robots, the complex task is completed [1]. This feature also allows the developers to build a multi-robot system made of heterogeneous robots with different capabilities so that complicated tasks can be completed.

The heterogeneous behavior of robots among the team introduces more challenges as coordination and communication become more complicated as general messages will not be effective as robots are not having homogenous behavior as well as the robots will not have to perform jobs of similar nature [2]. When the jobs need to be performed are different from each other, instructions to perform the jobs also should be specific [3]. Also, the type of data collected by the robots will be different and a specific end user may not be interested in all the data together, rather the user will be interested in specific types of data. These requirements lead to the development of various communication schemes which focuses on utilizing the heterogeneous nature of robots. Energy efficiency is another aspect which is considered while developing communication protocols.

Generally, a communication scheme uses broadcasting mechanism to pass data to the members of the team. The broadcasting mechanism consumes large amount of energy as lots of messages are shared irrespective of the fact that not all members will be interested in the messages being passed. If we consider a team of robots with heterogeneous capabilities, instead of general messages, messages specific to each sub groups will be a better option in terms of energy usage. This is the base of the proposed system where a team of robots are considered with sub groups of different capabilities and end users with different interest. This will enable the communication model to be developed in such a way that team of robots are divided into different sub-groups with different data collection schemes and end users with different interest on the data being collected by the robots. Team of robots publish about the type of data being collected and users subscribe based on their interest on the data.

The proposed system is simulated using network simulator (NS2), and the results are analyzed by comparing with other existing communication schemes. The results indicate that the proposed system performs better in terms of energy usage compared

to the existing communication schemes. The remaining part of the paper is organized as follows: Related works section describes the various communication schemes existing and summarizing about the research gaps in the existing schemes. Proposed system section describes the entire architecture of the system, and implementation section describes the simulation setup. Results section compares the results with existing systems, and conclusion part briefly summarizes the advantageous of the proposed system.

2 Related Works

Zia [4] discusses the advantages of data-centric approach over address-centric approach and lists out the various data-centric protocols developed for wireless sensor networks. The disadvantages of data-centric approaches are also described such as challenges in naming the communication entities, inability of query-driven approach to cater continuous monitoring application. The major challenge is the naming issues. In data-centric WSNs, naming plays a crucial role as address is not being used. But the naming will be application-dependent, and this will not allow generalization.

Data-centric networks generally use on-demand approach for collecting data. This is implemented using query-driven approach where the node which is need of the data generates a query to the network to which the data is send back as response. This approach is perfect for an application which requires the data based on the occurrence of some event which happens not continuously. But if the application demands continuous monitoring of the environment, then data collection needs to happen quite often and a query-driven approach will not be able to cater the continuous data collection requirements [5].

Different approaches are suggested by researchers to implement data-centric WSNs which will avoid the challenges faced in the earlier implementations of data-centric networks. Content-based networks or content-driven routing is an approach suggested by many researchers to overcome the common challenges a data-centric network faces. The content-based networking scheme has further studied more in detail and an approach named publish—subscribe model is designed [6]. The very basic idea of publish—subscribe approach is that, in a wireless sensor network, multiple sensors will be interfaced which introduces different categories of data being collected [7]. Also, various sensor nodes or sinks which are trying to gather information from the network will have different priorities or selection parameters for the data they collect. This leads to an idea of categorizing nodes in to data collection agents of specific types of data and data gathering agents which focuses on specific types of data [8].

It describes the challenges involved in a typical address-centric wireless sensor network and suggests a data-centric approach. To implement such a data-centric approach, a publish—subscribe system has been suggested [9]. The authors also describe multiple types of publish—subscribe systems based on the use. Out of the

various types, topic-based publish–subscribe model is observed to be better in terms of performance.

Based on the application, publishers and subscribers can be identified and the model can be used to avoid general broadcasting approach which is commonly seen most of the wireless sensor networks [10, 11]. The reduction in messages attributes to the reduction in energy consumption and increases in lifetime of the network.

The proposed system is an extension to the publish–subscribe model, and it is applied to a specific multi-robot system which is designed to carry out search and exploration of an unknown area. This is an alternative to the approaches and efforts of reducing the protocol overheads suggested by various communication protocols [12–14].

3 Proposed System

The context in which the proposed system is going to be used is a collection of autonomous robots which are heterogeneous in their capabilities assigned to perform a search and explore task. The term capabilities refer to the various functionalities associate with each robot, and these functionalities are directly related the type of sensors and actuators interfaced with the robots. The main reason behind having a team of heterogeneous robots is that the cost will be less if a team of robots formed from robots with different capabilities.

To address the various needs which can come across during the search and explore operation, generally robots are equipped with all the different capabilities together. This will make the robot complex and of high cost. Also in any scenario, not all robots are utilized their complete capabilities. Instead of having robots which are equipped with complete functionalities, a heterogeneous team of robots is deployed where each robot is equipped with the subset of capabilities and they work together to achieve the goal assigned.

To have coordination among the robots, a proper communication scheme is essential. The publish/Subscribe scheme is coming handy in such a situation where the members of the communication network are heterogeneous in nature. Also the fact that the data which is being shared in the network is also heterogeneous. The entire system consists of robots with different sensing capabilities. These robots collect different types of data. The robots in the system which looks for data also will be having specific requirement about the type of data it is looking for. Such a situation is the ideal one for implementing publish/subscribe model communication as the model consists of publishers who provides data and subscribers are those who would like to receive the data.

The proposed system consists of three parts: publisher robots, subscriber robots, and coordinator Robot. Figure 1 explains the various elements of the proposed system. The publisher robots are those who are equipped with specific sensors which collects data from the environment. These publishers notify other robots in the network that, and it can provide certain type of data. Subscriber robots are those

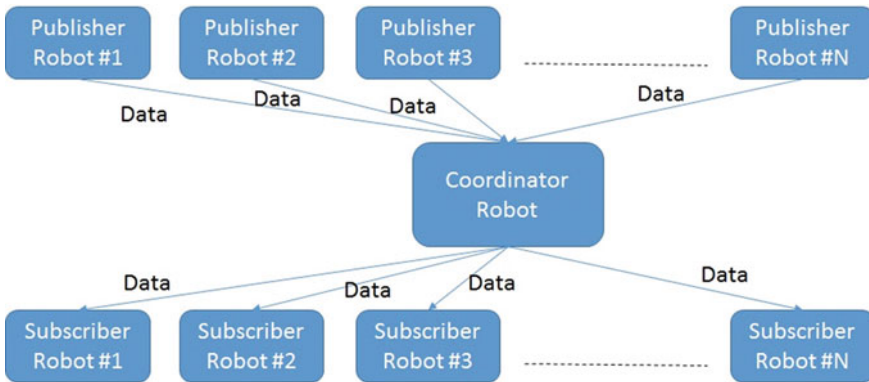


Fig. 1 Architecture of the proposed system

who generally the robots which need specific data from other fellow robots to make a decision such as when to collect data, what action to be performed, what data need to be communicated to the users. The role of coordinator robot is to maintain the details about publisher robots, type of data publisher can provide, subscription requests, etc. The coordinator also categorizes subscription requests for the same data and create subscription lists for easier maintenance.

The context in which the proposed system is implemented is one in which, a team of heterogeneous robots are deployed to carry out exploration of an unknown area. The output of this process can be used for rescue operations which may be carried out by another set of robots or humans. The major constraints in the problem are the size of the area need to be covered and the absence of any prior knowledge about the area to be explored. Also similar to any other exploration strategies, time and energy are two additional parameters which need to be optimized. Compared to the traditional broadcasting or multicasting communication strategies which are normally used for communication among a team of robots, the concept of publish/subscribe model will certainly reduce the energy consumption as the number of messages generated and transmitted over the communication network will be less compared to traditional schemes.

The large size of the area which is to be explored can be addressed by the distributed nature of the proposed system in which the team of autonomous robots carry out exploration locally, and the outputs are merged together for the goal. The availability of an efficient communication scheme will handle the challenges posed by the absence of prior knowledge about the area to be explored.

3.1 Publisher Robots

The publisher robots are equipped with specific set of sensors to collect data. Rather than having robots equipped with all the various types of sensors, in the proposed model, robots are equipped with only few sensors to reduce the complexity of individual robots. The sequence of actions performed by publisher robots is as follows:

- Initially robots are deployed, and the communication network is formed.
- Robots with sensors attached are identified as publishers.
- Publishers announce its presence, and the type of data it can provide to the network.
- The sensors attached starts collecting data periodically or event-driven based.
- Based on the subscription request, publisher communicates the data to those robots who have subscribed.

3.2 Subscriber Robots

The subscriber robots are the ones which require certain data for either decision making or for collecting the data as the node is a data aggregator. Since the system consists with limited sensors attached on each individual robot, instead of collecting data itself, robots will subscribe the data which it requires from others. The sequence of actions performed by subscriber robots is as follows:

- Initially robots are deployed, and the communication network is formed.
- The subscriber robots send its set of data requirements to coordinator robot.
- The coordinator identifies the corresponding publisher nodes and informs the publishers about subscriptions.
- Once the subscribed data is arrived from publisher nodes, it is either used for decision making or data collection as part of data aggregation step is performed.

3.3 Coordinator Robot

The coordinator robots are the ones which coordinates the subscribers and publishers. Coordinator robots manage the list of publisher robots and the category of data which is published by each publisher robots. Coordinator robots also manage the subscription lists requested by each subscriber robots. The sequence of actions performed by subscriber robots is as follows:

- Coordinator robots get publisher lists from publisher robots which consists of publisher robot address, category of data it publishes.
- Subscriber robots also send its subscription lists to coordinator robots.
- When a subscription request is received, the publish list is checked and corresponding publisher robot is informed about the subscription request.

4 Implementation

To implement the proposed system of publish–subscribe concept-based communication scheme among multi-robot system, Network Simulator 2 (NS2) is chosen as it is the most effective network simulator for implementing communication protocols. The collection of built-in libraries for deploying various network protocols provided along with NS2 along with the flexibility of developing user-based customized communication protocols and deployment techniques have made the NS2 one of most successful network simulators. The support of OTcl libraries and C++ libraries has made NS2 rich and efficient.

The three categories of robots are simulated by adding corresponding methods in the NS2 library. The robots are implemented as nodes in the network, and these nodes are deployed using random deployment strategy available in NS2. Once deployed, these nodes will identify its neighbors and form ad-hoc network. Once the network is formed, nodes are categorized in to three groups as publisher robots, subscriber robots, and coordinator robot. These nodes communicate among each other using the most commonly wireless ad-hoc routing protocol ad-hoc on-demand vector (AODV) routing protocol. NS2 has AODV routing protocol code available in the library which is modified by appending functionalities specific to publisher, subscriber, and coordinator robots.

Functions named `publisher_initialize()`, `publisher_dataGenerate()`, `publisher_send()` are developed for publisher node which is used to initialize generate the publisher data and send the publisher data, respectively. Functions named `subscriber_initialize()`, `subscriber_generateRequest()`, `subscriber_recv()` for subscriber node which is used to initialize, generate the request for data and receive data, respectively. Same way functions named `coordinator_initialize()`, `coordinator_generatePublisherList()`, `coordinator_generateSubscriberList()` for coordinator node to initialize, generate the list of publisher nodes with its corresponding type of data, and generate the list of subscribers with its corresponding data requests, respectively (Figs. 2, 3, 4, 5, 6, 7, 8, 9 and 10).

These functions are invoked after deployment of the nodes and formation of the ad-hoc network. The sequence of these function calls is shown in Fig. 11.

```
void PUBLISHER::publisher_initialize()
{
    PUB_initVal *iv;
    iv = initial_setup(rand().deploy);
    if(iv == -1)
        ERROR(INIT_ERR);
}
```

Fig. 2 Code snippet for `publisher_initialize()`

```

void PUBLISHER::publisher_dataGenerate(Packet *p)
{
    struct hdr_PUB_reply *rp = HDR_PUB_REPLY(p);
    PUB_tt_entry tt;
    nb = nb_lookup(rp->rp_dst);
    p->msg = HDR_PUB_REQUEST("Publisher Data")
    if(nb == 0)
        nb_insert(rp->rp_dst)
    Packet::free(p);
    Node *sender_node = Node::get_node_by_address(rp->rp_dst);
    Node * receiver_node = Node::get_node_by_address(index);
    sender_node->addNeighbour(receiver_node);
    receiver_node->addNeighbour(sender_node);

    tt->value = PUB_Neighbour::get_value(rp->rp_tval);
}

```

Fig. 3 Code snippet for publisher_dataGenerate()

```

void PUBLISHER::publisher_send(Packet *p)
{
    struct hdr_PUB_request *rq = HDR_PUB_REQUEST(p);
    PUB_Neighbour *nb;

    nb = nb_lookup(rq->rq_dst);
    p->msg = HDR_PUB_REQUEST("Publisher Data")
    if(nb == 0)
        ERROR(NO_DST);
    send_echo(nb, rq, p);
}

```

Fig. 4 Code snippet for publisher_send()

```

void SUBSCRIBER::subscriber_initialize()
{
    SUB_initVal *iv;
    iv = initial_setup(rand().deploy);
    if(iv == -1)
        ERROR(INIT_ERR);
}

```

Fig. 5 Code snippet for subscriber_initialize()

```

void SUBSCRIBER::subscriber_generateRequest(Packet *p)
{
    struct hdr_SUB_reply *rp = HDR_SUB_RESP(p);
    SUB_tt_entry tt;
    nb = nb_lookup(rp->rp_dst);
    p->msg = HDR_SUB_REQUEST("Subscriber Data")
    if(nb == 0)
        nb_insert(rp->rp_dst)
    Packet::free(p);
    Node *sender_node = Node::get_node_by_address(rp->rp_dst);
    Node * receiver_node = Node::get_node_by_address(index);
    sender_node->addNeighbour(receiver_node);
    receiver_node->addNeighbour(sender_node);

    tt->value = SUB_Neighbour::get_value(rp->rp_tval);
}

```

Fig. 6 Code snippet for subscriber_generateRequest()

```

void SUBSCRIBER::subscriber_recv(Packet *p)
{
    struct hdr_SUB_request *rq = HDR_SUB_REQUEST(p);
    PUB_Neighbour *nb;

    nb = nb_lookup(rq->rq_dst);
    p->msg = HDR_SUB_REQUEST("Subscriber Data")
    if(nb == 0)
        ERROR(NO_DST);
    recv_echo(nb, rq, p);
}

```

Fig. 7 Code snippet for subscriber_recv()

```

void COORDINATOR::coordinator_initialize()
{
    CORD_initVal *iv;
    iv = initial_setup(rand().deploy);
    if(iv == -1)
        ERROR(INIT_ERR);
}

```

Fig. 8 Code snippet for coordinator_initialize()

```

Node * CORD_rt_entry CORD::coordinator_generatePublisherList()
{
    CORD_tt_entry *tt, *tt1;
    for(tt = ttable.head(); tt!= ttable.end; tt = tt->tt_link.next)
    {
        for(tt1 = ttable.head(); tt1 != ttable.end; tt1 = tt1->tt_link.next)
        {
            if(tt->pubvalue < tt1->pubvalue)
            {
                tt->swap_entry(tt_pubvalue, tt1->pubvalue);
            }
            tt1 = tt1->tt_link.next;
        }
        tt = tt->tt_link.next;
    }
    return (*CORD_rt_entry) ttable.head;
}

```

Fig. 9 Code snippet for coordinator_generatePublisherList()

```

Node * CORD_rt_entry CORD::coordinator_generateSubscriberList()
{
    CORD_tt_entry *tt, *tt1;
    for(tt = ttable.head(); tt!= ttable.end; tt = tt->tt_link.next)
    {
        for(tt1 = ttable.head(); tt1 != ttable.end; tt1 = tt1->tt_link.next)
        {
            if(tt->subvalue < tt1->subvalue)
            {
                tt->swap_entry(tt_subvalue, tt1->subvalue);
            }
            tt1 = tt1->tt_link.next;
        }
        tt = tt->tt_link.next;
    }
    return (*CORD_rt_entry) ttable.head;
}

```

Fig. 10 Code snippet for coordinator_generateSubscriberList()

5 Results and Discussion

The proposed system is simulated using NS2. NS2 provides features to extract network parameters to analyze the performance of the proposed communication scheme and compare against traditional existing communication schemes. In case of the proposed system, the major advantage suggested is the optimal use of energy by

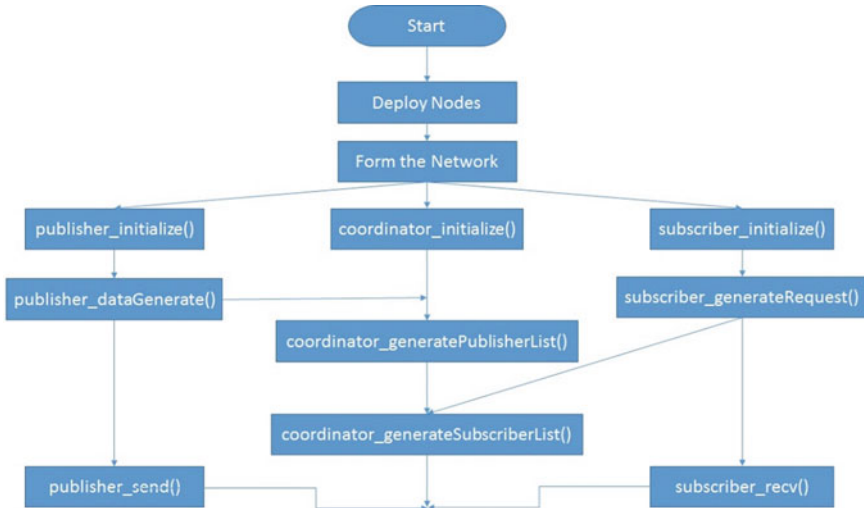


Fig. 11 Function call sequence

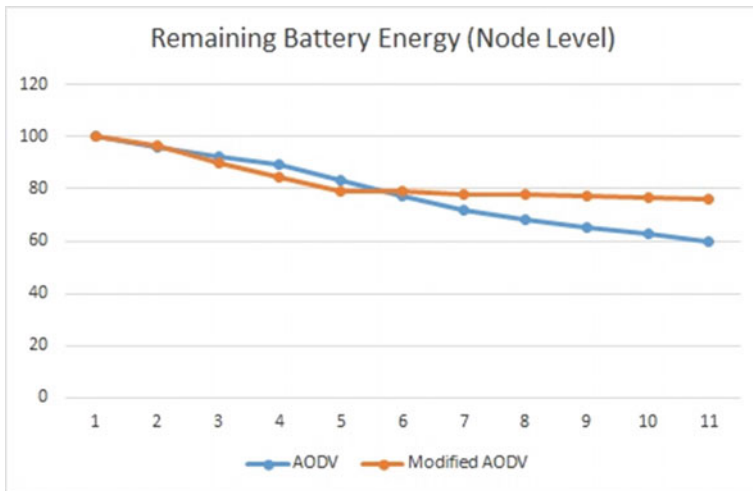


Fig. 12 Comparison of node-level energy consumption

avoiding the commonly used broadcasting. To prove this claim, energy consumption of each node is evaluated. Also energy consumption of the entire network which directly decides the lifetime of the WSN is also evaluated and compared against the traditional schemes.

The results of individual node-level energy consumption and network-level energy consumptions are plotted. Figures 12 and 13 illustrate the comparison of individual node-level and network-level energy consumption of proposed and existing schemes.

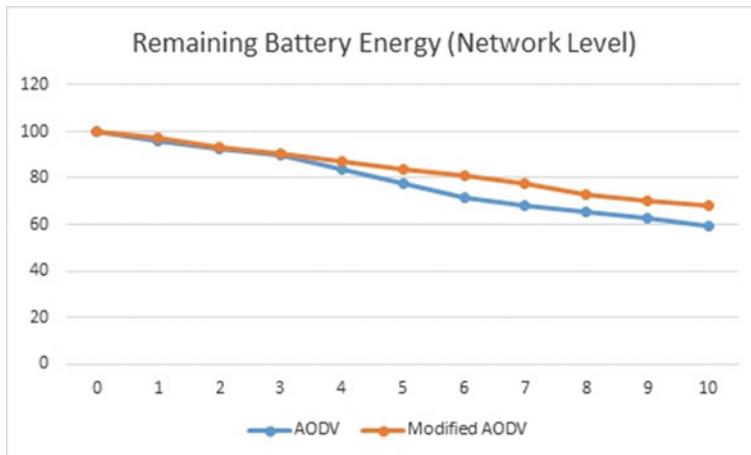


Fig. 13 Comparison of network-level energy consumption

In the network-level energy consumption comparison, the average remaining energy of the traditional scheme is around 78 while the proposed system is around 84. This indicates that the energy consumption of the existing and proposed schemes is 22 and 16, respectively. This proves that around 24% energy consumption is reduced by the proposed scheme compared to the traditional scheme of communication. The above diagrams indicate that the proposed scheme of multi-robot communication based on publish–subscribe scheme performs better than traditional communication schemes in terms of energy consumption. So it is proven that the proposed system improves the lifetime of the WSN.

6 Conclusion

In a multi-robot system deployed for carrying out tasks, communication and coordination are the most important aspects. An efficient communication scheme is vital in sharing control and coordination information among the team of robots to carry out the tasks effectively. The challenge in the context is the energy usage of robots for communication. The traditional communication schemes generally depend on broadcasting options for exchanging the information among team of robots. But the broadcasting scheme generates a lot of packets, and this will obviously consume more energy. So an energy-efficient communication scheme is proposed which uses the publish–subscribe scheme. The nodes which are ready to share the data are termed as publishers, and the nodes which require the data are termed as subscribers. With the help of coordinator node, the publishers and subscribers share the data. The total number of messages are very less compared to a traditional broadcasting-based communication and obviously the energy consumption is also less. The simulation

of the proposed system provides results which prove the energy efficiency claim to be true.

References

1. Rajesh M, Jose GR, Sudarshan TSB (2014) Multi robot exploration and mapping using frontier cell concept. In: 11th IEEE International conference Indicon 2014
2. Banfi J, Quattrini Li A, Rekleitis I et al (2018) Strategies for coordinated multirobot exploration with recurrent connectivity constraints. *Auton Robot* 42:875–894
3. Rajesh M, George A, Sudarshan TSB (2015) Energy efficient deployment of wireless sensor network by multiple mobile robots. In: International conference on computing and network communications (CoCoNet'15)
4. Zia Q (2015) A survey of data-centric protocols for wireless sensor networks. *J Comput Sci Syst* 8:127–131
5. Sreevidya B, Rajesh M (2017) Enhanced energy optimized cluster based on demand routing protocol for wireless sensor networks. In: International conference on advances in computing, communications & informatics (ICACCI'17)
6. Tekin Y, Sahingoz OK (2016) A publish/subscribe messaging system for wireless sensor networks. In: Sixth international conference on digital information and communication technology and its applications (DICTAP), Konya, pp 171–176
7. Hunkeler U, Truong HL, Stanford-Clark A (2008) MQTT-S—a publish/subscribe protocol for wireless sensor networks. In: 3rd International conference on communication systems software and middleware and workshops (COMSWARE'08), India, pp 791–798
8. Davis EG, Augé AC (2018) Publish/Subscribe protocol in wireless sensor networks: improved reliability and timeliness. *KSI Trans Internet Inf Syst* 12(4):1527–1552
9. Gerkey BP, Matari MJ (2000) MURDOCH: publish/subscribe task allocation for heterogeneous agents. In: Proceedings of autonomous agents, Spain, pp 203–204
10. Gerkey BP, Matari MJ (2002) Pusher-watcher: an approach to fault-tolerant tightly-coupled robot coordination. In: IEEE International conference on robotics and automation (ICRA 2002), pp 464–469
11. Gerkey BP, Matari MJ (2002) Sold!: auction methods for multirobot coordination. *IEEE Trans Robot Autom* 18(5):758–768
12. Sreevidya B, Rajesh M (2018) Design and performance evaluation of an efficient multiple access protocol for virtual cellular networks. In: International conference on computer networks and communication technologies (ICCNCT)
13. Ramesh MV, Divya PL, Kulkarni RV, Manoj R (2012) A swarm intelligence based distributed localization technique for wireless sensor network. In: International conference on advances in computing, communications and informatics, pp 367–373
14. Meera MS, Rao S (2017) Comparative analysis of IoT protocols for a marine IoT system. In: International conference on advances in computing, communications and informatics (ICACCI), Bangalore

Butterfly Optimization Algorithm-Based Optimal Sizing and Integration of Photovoltaic System in Multi-lateral Distribution Network for Interoperability



Thandava Krishna Sai Pandraju and Varaprasad Janamala

Abstract In this paper, a new and simple nature-inspired meta-heuristic search algorithm, namely butterfly optimization algorithm (BOA), is proposed for solving the optimal location and sizing of solar photovoltaic (SPV) system. An objective function for distribution loss minimization is formulated and minimized via optimally allocating the SPV system on the main feeder. At the first stage, the computational efficiency of BOA is compared with various other similar works and highlights its superiority in terms of global solution. In the second stage, the interoperability requirement of SPV system while determining the location and size of SPV system among multiple laterals in a distribution system is solved without compromises in radiality constraint. Various case studies on standard IEEE 33-bus system have shown the effectiveness of proposed concept of interline-photovoltaic (I-PV) system in improving the distribution system performance in terms of reduced losses and improved voltage profile via redistributing the feeder power flows effectively.

Keywords Butterfly optimization algorithm · Interline-photovoltaic system · Interoperability · Loss minimization · Radial distribution system · Radiality constraint

1 Introduction

Optimization of distribution system performance is always an important criterion in power system operation and control. Network reconfiguration, installation of capacitor banks (CBs) and integration of distribution generation (DGs) are some of the

T. K. S. Pandraju

Department of Electrical and Electronics Engineering, Dhanekula Institute of Engineering & Technology, Vijayawada, Andhra Pradesh 521139, India
e-mail: thandava.pandraju@res.christuniversity.in

V. Janamala

Department of Electrical and Electronics Engineering, School of Engineering and Technology, Christ (Deemed to be University), Bangalore, Karnataka 560074, India
e-mail: varaprasad.janamala@christuniversity.in

remedial ways for some extent to improve the radial distribution system (RDS) performance without curtailing the load. The problem of optimal allocation of DGs in RDSs is one of important planning aspects for minimizing the distribution losses, improving the voltage profile, improving the power factor and consequently reducing the burden on transformer or system capacity release stability enhancement and minimization of total cost, etc. Based on the meteorological conditions, some locations are suitable to install a specific type of RE units at a large-scale capacity. But high penetrations levels of RE at a single location can cause degraded feeder performance considerably. In order to avoid this problem, the interline-photovoltaic (I-PV) concept is highly adaptable to inject the total yielded PV power at multiple points in to the network. As introduced in 2011, Khadkikar and Kirtley [1], the I-PV system consists of a common PV source for the different voltage source converters (VSC), which is used to inject PV output power into the AC grid via shunt coupling transformers (T_{sh}). In this work, the configuration of basic I-PV system is modified for easy adoption in the conventional load flow studies.

Since in real time the faults can take place at any section of the distribution system, it is required to isolate the faulty section immediately and continue the service for healthy sections, which can improve reliability of the utility. In this connection, the planning of DGs considering interoperability among multiple feeders is essential and has not been considered in the reviewed works. For the first time, strengthening the distribution network via simultaneous allocation of the solar PV system and interoperability features is handled in this paper. While solving the DG allocation problem in the distribution system, maintaining radial configuration is also important for avoiding misconduct of protection systems. Hence, a novel methodology is proposed for solving the simultaneous allocation of solar photovoltaic-type DG and integration of new branches between multiple feeders considering radiality constraint.

2 Literature Review

The problem of optimal allocation of DGs in RDSs has paid high attention, and still it is a complex problem needs to focus w.r.t. intermittency of RESs. A comprehensive literature survey on DG allocation problem by various heuristic search algorithms (HSAs) can be seen in 2016, Muthukumar and Jayalalitha [2]. In 2018, Dinakara Prasad Reddy et al. [3], power loss index (PLI) and whale optimization algorithm (WOA) are presented for optimal location and sizing of different types of DGs considering loss minimization as main objective. In 2018, Dinakara Prasad Reddy et al. [4], index vector (IV) method is used to find potential candidate locations for DGs at initial stage and later ant lion optimization (ALO) is proposed for determining optimal location and size of different type of DGs for minimizing real power losses. In 2018, Suresh and Belwin [5], loss sensitivity factors have been proposed for limiting search space of locations and later dragonfly algorithm (DA) is applied for determining the optimal location and sizes of DG considering objective of loss

minimization. In 2017, Dinakara Prasad Reddy et al. [6], IV method and WOA are used for loss minimization via different type of DG technologies integration at best location with optimal sizes. In 2017, Hassan et al. [7], augmented Lagrangian genetic algorithm (ALGA) is proposed for finding location and sizes of different type of DGs for loss minimization. In 2016, Sudabattula and Kowsalya [8], bat algorithm (BA) is proposed for location and sizing of SPV DGs towards real power loss reduction. In 2020, Suresh and Edward [9], a hybrid algorithm GOA-CS is proposed using grasshopper optimization and algorithm (GOA) and cuckoo search (CS) for optimal allocation of DG problem. In comparison, the results of GOA-CS are better than lightning search algorithm (LSA) and sarp swarm optimization (SSO) algorithm in terms of reduced loss and improved profile. In 2017, Dixit et al. [10], Gbest-guided artificial bee colony (GABC) algorithm is proposed for deducing the optimal locations of DGs from IV-based initial search space of locations and sizes towards loss reduction in the distribution system. In 2018, Prakash and Lakshminarayana [11], WOA is proposed for loss minimization, voltage profile improvement, voltage stability enhancement and total cost minimization via optimal allocation of DGs.

From all these works, potential benefits can be obtained via optimal allocation of DGs in RDS. Considering the complexity of the optimization problem with continuous and discrete variables, the problem is solved effectively using different heuristic approaches [2]. On the other side, there is no single specific algorithm which can solve all types of optimization problems as proved in the no-free-launch theorem defined in 1997, Wolpert and Macready [12]. Hence, the researchers are still aspiring to introduce new heuristic algorithms and also improvements to the existing algorithms for solving different kinds of optimization problems. The optimization problem considering loss is solved using a novel nature-inspired meta-heuristic, namely butterfly optimization algorithm (BOA) in 2019, Arora and Singh [13]. In comparison with the most popular and existing other meta-heuristic algorithms such as ABC, CS, DE, FA, GA, MBO and PSO, BOA proposed based on unique food foraging behaviour of butterflies and stands ideally for solving complex and nonlinear optimization problems.

3 Problem Formulation

Loss minimization in the operation of RDS is an important operational requirement for improving the utilization of DGs power. The real power loss of all branches in a distribution system is given by,

$$\min f(P_{\text{loss}}) = \sum_{mn} r_{(mn)} \left(\frac{P_{(n)}^2 + Q_{(n)}^2}{|V_{(n)}|^2} \right) \quad (1)$$

The following voltage, current, DGs power and radiality constraints are considered in solving the proposed objective function.

$$|V_i|_{\min} \leq |V_i| \leq |V_i|_{\max} \quad i = 1, 2, \dots, nb \quad (2)$$

$$|I_i| \leq |I_i|_{\max} \quad i = 1, 2, \dots, nl \quad (3)$$

$$P_{dg(T)} \leq P_{load(T)} \quad (4)$$

$$n_{br} = n_b - 1 \quad (5)$$

where P_{loss} is the total real power loss in the feeder distribution, mn , nb and nl are the branch index, number of buses and number of branches, respectively; $P_{(n)}$, $Q_{(n)}$, $P_{dg(T)}$, $P_{load(T)}$ and $|V_{(n)}|$ are the real, reactive power loads, DG real power, total real power demand and voltage magnitude of n th bus, respectively.

4 Overview of Butterfly Optimization Algorithm

In this section, the modelling of food foraging behaviour of butterflies is explained. Also, the proposed methodology to determine optimal location and size of a photovoltaic (PV) system along with its optimal interline-photovoltaic (I-PV) system is presented.

4.1 Modelling of Food Foraging Behaviour of Butterflies

Butterfly optimization algorithm (BOA) is a new nature-inspired optimization algorithm developed using unique features of butterflies for their food search in 2019, Arora and Singh [13]. The accurate sense of butterflies for locating the source of fragrance is the main motivation for BOA and is idealized as follows: (i) each butterfly emits some fragrance by which other butterflies can sense and attracts each other, (ii) the random movement nature of a butterfly depends on the magnitude of fragrance emitted by other butterflies and (iii) for a sensed fragrance, the reaction of a butterfly depends on and affected by the environmental conditions of landscape or search space.

The perceived magnitude of the fragrance of butterflies (f) depends on stimulus intensity, i.e. fitness function (I) and related mathematically,

$$f = cI^a \quad (6)$$

where c and a are the sensory modality of butterflies, i.e. fragrance and power of exponent dependent on modality for accounting the nature of varying degree of fragrance absorption, respectively.

The search process of BOA is modelled in three phases as briefed here. In the initialization phase, artificial butterflies equal to the number of designed variables in the optimization problem. At this stage, it is required to define sensor modality c , power exponent a , switch probability p , maximum number iterations k_{\max} , dimension of search space d and number of butterflies n . The lower and upper boundaries of design variables relate the search space or landscape region for foraging food and initial fitness values using Eq. (6), which relates their magnitude of fragrance.

After completion of the initialization phase, the iteration phase takes place up to the maximum number of iteration defined for stopping criterion in the optimization problem. In each iteration, the position of butterflies' changes within the search space and their fitness values is evaluated simultaneously. At this stage, the fragrance sensing behaviour of butterflies is modelled for global search phase ($r_i < p$) or local search phase ($r_i > p$), given by Eqs. (7) and (8), respectively.

$$x_{i(k+1)} = x_{i(k)} + (r_i^2 - g^* - x_{i(k)}) \times f_i \quad (7)$$

$$x_{i(k+1)} = x_{i(k)} + (r_i^2 \times x_{j(k)} - x_{i(k)}) \times f_i \quad (8)$$

where $x_{i(k)}$ and $x_{j(k)}$ are the solution vectors in iteration k relate to butterflies x_i and x_j , respectively; g^* is the current global best among all solutions; r_i is a random number generated in $[0, 1]$ and f_i is the fragrance of butterfly i .

The switching phenomena global search (i.e. attracting towards high fragrance emitting food or butterfly for mating, results for towards global optima) and local search (i.e. trapping towards local minima) depends on switch probability relates the environmental conditions in search space or landscape like rain and wind. Updating power exponent and switch probability in each iteration can result in adoptive BOA, which is still in research stage Arora and Singh [13].

At the third stage, BOA results for the best solution vector and corresponding global fitness obtained within the maximum iterations and stops. By relating the mating characteristics and food searching behaviour of butterflies considering environmental conditions using simple mathematical relations, BOA stands for simple and easy to adopt for global optimization problems.

4.2 Proposed Methodology for Optimal I-PV Configuration

The following steps are followed to determine optimal I-PV configuration by optimizing the different variables within their search space as defined here.

- St 1. Read test system data and perform load flow for determining total power loss using Eq. (1), minimum voltage magnitude and corresponding bus. Save the result as a base case.
- St 2. Define BOA control variables and dimension of search space (i.e. population size is equal to the number of search variables, i.e. one for PV location on

- main feeder, one for PV size and number of branches to open while forming I-PV configuration) and maximum number iterations, k_{\max} .
- St 3. Generate the initial random population vector or pollinators consisting of the vector of locations and sizes of DG.
 - St 4. Using all the control variables generated at step 3, determine intensity (I), i.e. total loss using Eq. (1).
 - St 5. Define sensor modality c , power exponent a and switch probability p .
 - St 6. Set iteration count $k = 1$. Repeat step 4 for all butterflies and find the current best fitness value or fragrance using Eq. (6) over the initial population.
 - St 7. Generate a random number r between [0, 1]. Update each butterfly movement towards best butterfly using Eq. (7), if $r < p$, else using Eq. (8).
 - St 8. Update power exponent a and set iteration count $k = k + 1$.
 - St 9. Repeat St (6) to St (8) until $k = k_{\max}$. At each iteration, compare the new fragrance with the global fitness so far. If current fitness (fragrance) is better than global fitness, then replace global fitness by current fitness and current pollinators as a global solution vector.
 - St 10. Display the global fitness and global solution vector and stop.

5 Results and Discussion

The proposed methodology is applied on IEEE 33-bus test systems. In this system, it is assumed that the buses 1–18 as main feeder and buses 19–22, buses 23–25 and buses 26–33 as lateral feeders.

Case 1: Uncompensation and base case From the data given in [14], the system is serving totally a load of ($3715 \text{ kW} + j 2300 \text{ kVAr}$) and suffering with total distribution losses of ($210.9983 \text{ kW} + j 143.0329 \text{ kVAr}$), respectively. Also, the system has a poor voltage profile (i.e. $<0.95 \text{ p.u.}$) at some locations and the lowest voltage magnitude 0.9038 p.u is registered at 18th bus.

Case 2: Single PV allocation considering loss minimization Initially, BOA is applied to determine the optimal location and sizing of a single PV system considering only loss minimization as objective function, since the system has already satisfied radiality constraint. The search space for location and size is considered as [2, 33] and [0, 3715], respectively. The optimized solution by BOA is as follows: The best location: 6th bus; best PV size: 2590 kW; global optima: 111.0299 kW. Under these conditions, the feeder voltage profile is improved considerably but not yet satisfied by the lower voltage magnitude constraint (i.e. $\leq 0.95 \text{ p.u.}$) due to 0.9424 p.u at 18th bus.

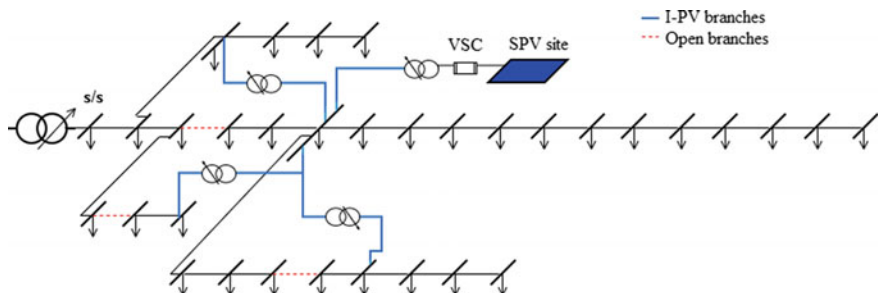
Also, the competitiveness of BOA with other HSAs, the literature works is compared and given in Table 1. It is observed that BOA is superior than WOA [3] and ALO [4], DA [5], WOA [6], BA [8], GOA-CS [9], SSA [9], LSA [9], GABC [10], WIPSO and SADE [14], and well in agreement with the results of WOA [11], HGWO [15] and EA-OPF [16].

Table 1 Comparison of BOA results with the literature works

Reference	PV location	PV size (kW)	P_{loss} (kW)
WOA [3] and ALO [4]	30	1542.67	125.161
DA [5]	16	1000	136.7533
WOA [6]	15	1061	133.503
BA [8]	15	816.30	137.20
GOA-CS [9]	24	926.99	139.5915
SSA [9]	16	853.8882	143.0741
LSA [9]	13	757.097	148.6011
GABC [10]	30	1543	125.15
WIPSO and SADE [14]	30	1600	125.267
WOA [11]	6	2589.6	111.03
HGWO [15]	6	2589.6	111.03
EA-OPF [16]	6	2589.6	111.03
Proposed BOA	6	2589.6	111.0299

Case 3: Optimal I-PV configuration with three laterals In this case, BOA needs to identify simultaneously for best PV location and sizes on main feeder as well as for forming I-PV configuration with three laterals, it needs to identify three integrating points among 15 and 3 branches for opening among 22. The optimized results of BOA are as follows: PV location: 6th bus; PV size: 3356 kW; I-PV integration points on lateral 1 is 19th bus, lateral 2 is 25th bus and lateral 3 is 30th bus; and branch numbers to open: 3 (3–4), 23 (23–24) and 28 (28–29). The overall I-PV configuration with three laterals without radial structure is given in Fig. 1. Under these conditions, the losses ($51.7086 \text{ kW} + j 54.8051 \text{ kVAr}$) and minimum voltage at 18th bus are 0.9469 p.u.

The convergence characteristics of BOA for Case 2 and Case 3 are given in Fig. 2, and the voltage profiles for all cases are given in Fig. 3, respectively. From

**Fig. 1** Optimal I-PV configuration with three laterals in IEEE 33-bus system

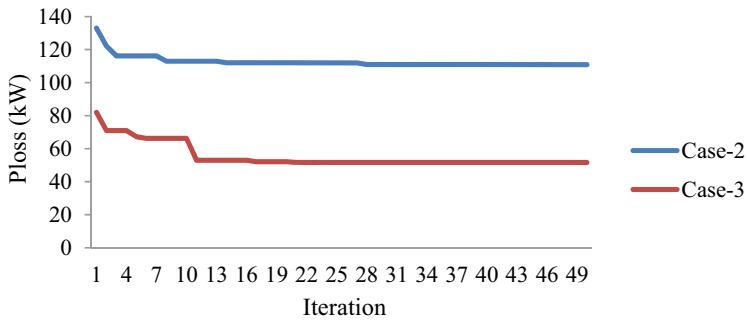


Fig. 2 Convergence characteristics of BOA for Case 2 and Case 3

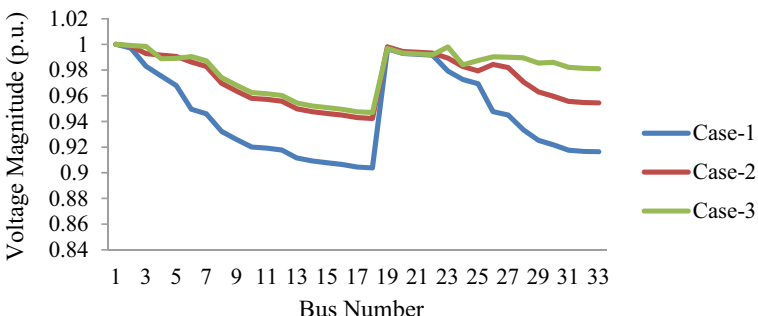


Fig. 3 Voltage profile for three cases

the voltage profile shown in Fig. 3, it can be seen that the optimal I-PV configuration has improved the performance of the distribution system significantly.

6 Conclusion

In order to meet the requirements of interconnected networks, the power exports and imports need interoperability features from generation sources. In this paper, optimal allocation, sizing and power sharing from a solar photovoltaic system (SPV) among multi-laterals (I-PV) is proposed without compromising operational constraints of the radial distribution system (RDS). Loss minimization as an objective function, a new and efficient optimization algorithm, namely butterfly optimization algorithm (BOA), is proposed for evaluating the global solution. From the comparison study, it has shown that the proposed BOA has outperformed than various other algorithms in terms of global optima. The simulations are performed on IEEE 33-bus system. The base case real power loss of 210.99 kW is reduced to 111.03 kW (which is equal to 47.37% reduction) with optimal PV allocation and is further reduced to

51.7086 kW (which is equal to 77.87% reduction) with optimal I-PV configuration. These results have shown the ability of the I-PV system concept in improving the RDS performance in terms of reduced losses and improved voltage profile and need for real-time adoption.

References

1. Khadkikar V, Kirtley JL (2011) Interline photovoltaic (I-PV) power system—a novel concept of power flow control and management. In: 2011 IEEE Power and energy society general meeting, Detroit, MI, USA. IEEE, pp 1–6
2. Muthukumar K, Jayalalitha S (2016) Optimal placement and sizing of distributed generators and shunt capacitors for power loss minimization in radial distribution networks using hybrid heuristic search optimization technique. *Int J Electr Power Energy Syst* 78:299–319
3. Dinakara Prasad Reddy P, Veera Reddy VC, Gowri Manohar T (2018) Optimal renewable resources placement in distribution networks by combined power loss index and whale optimization algorithms. *J Electr Syst Inf Technol* 5:175–191
4. Dinakara Prasad Reddy P, Veera Reddy VC, Gowri Manohar T (2018) Ant lion optimization algorithm for optimal sizing of renewable energy resources for loss reduction in distribution systems. *J Electr Syst Inf Technol* 5:663–680
5. Suresh MCV, Belwin EJ (2018) Optimal DG placement for benefit maximization in distribution networks by using Dragonfly algorithm. *Renew Wind Water Solar* 5(4):1–8
6. Dinakara Prasad Reddy P, Veera Reddy VC, Gowri Manohar T (2017) Whale optimization algorithm for optimal sizing of renewable resources for loss reduction in distribution systems. *Renew Wind Water Solar* 4(3):1–13
7. Hassan AA, Fahmy FH, Nafeh AE-SA, Abuelmagd MA (2015) Genetic single objective optimisation for sizing and allocation of renewable DG systems. *Int J Sustain Energy* 1–18
8. Sudabattula SK, Kowsalya M (2016) Optimal allocation of solar based distributed generators in distribution system using bat algorithm. *Perspect Sci* 8:270–272
9. Suresh MCV, Edward JB (2020) A hybrid algorithm based optimal placement of DG units for loss reduction in the distribution system. *Appl Soft Comput J* 91:106191
10. Dixit M, Kundu P, Jariwala HR (2017) Incorporation of distributed generation and shunt capacitor in radial distribution system for techno-economic benefits. *Eng Sci Technol Int J* 20:482–493
11. Prakash DB, Lakshminarayana C (2018) Multiple DG placements in radial distribution system for multi objectives using whale optimization algorithm. *Alex Eng J* 57:2797–2806
12. Wolpert DH, Macready WG (1997) No free lunch theorems for optimization. *IEEE Trans Evolut Comput* 1(1):67–82
13. Arora S, Singh S (2019) Butterfly optimization algorithm: a novel approach for global optimization. *Soft Comput* 23(3):715–734
14. Rajeswaran S, Nagappan K (2016) Optimum simultaneous allocation of renewable energy DG and capacitor banks in radial distribution network. *Circ Syst* 7:3556–3564
15. Sanjay R, Jayabarathi T, Raghunathan T, Ramesh V, Mithulanthan N (2017) Optimal allocation of distributed generation using hybrid grey wolf optimizer. *IEEE Access* 5:14807–14818
16. Mahmoud K, Yorino N, Ahmed A (2016) Optimal distributed generation allocation in distribution systems for loss minimization. *IEEE Trans Power Syst* 31(2):60–969

Document Classification in Robotic Process Automation Using Artificial Intelligence—A Preliminary Literature Review



Jorge Ribeiro, Rui Lima, and Sara Paiva

Abstract In recent decades, combined with technological evolution, numerous operational activities of companies are supported by information systems. Despite its advantages, countless routine tasks of the organizations are done manually. In recent years, robotic process automation (RPA) has emerged allowing to create automatic processes to deal with routine tasks. One typical feature of these systems is reading documents via optical character recognition (OCR) that are associated with the classification of documents. This paper aims to present a general study on the document classification process using OCR in RPA processes combined with the application of artificial intelligence. It was intended to carry out a survey of the state of the art of tools and approaches for the classification of documents using AI. Conclusions show that despite the challenges associated with the classification and categorization of documents, the applicability of AI techniques shows good results of accuracy to allow a better efficiency in the automation of RPA processes.

Keywords Artificial intelligence · Document classification · Robotic process automation

1 Introduction

Information systems are nowadays crucial in any company and we assist to the massive use of enterprise resource planning (ERP), customer relationship management or supply chain management. It is very common for companies to receive invoices in paper or digital format and have a collaborator to manually transform this data to a digital structure that can be inserted in an ERP. This work is quite time consuming, given the volume of communication transactions through digital means, hence the need to find a way to automate this process. Robotic process automation (RPA) processes are characterized by a set of processes automation processes at the computer level that map the routine and repetitive tasks triggered by the employees of

J. Ribeiro · R. Lima · S. Paiva (✉)

Instituto Politécnico de Viana do Castelo, Viana do Castelo, Portugal

e-mail: sara.paiva@estg.ipvc.pt

the organizations, in order to increase the performance and efficiency of employees and a greater speed and transparency in organizations' business processes. Artificial intelligence (AI) is also nowadays a key concept in these scenarios where its techniques and algorithms can be combined with RPA processes to achieve a better and smart document classification, enhancing achieved results. The main contribution of this paper is to provide a comprehension review on the document classification process using OCR in RPA processes as well as the use of techniques and algorithms of AI throughout the process.

Following research papers in the field of document classification, text classification in documents and algorithms to optimize the process of classification, recently, several opinions and implementation articles have been presented as guidelines for the implementation of the document classification process, such [1–3]. The need to contemplate a prior analysis of the information associated with "data preparation for document classification" and "machine learning options for document processing" [3], namely a strategy for detecting type of documents and detecting language, of the documents is highlighted. In this context, the general process of document classification using artificial intelligence (implemented as RPA processes) can be described as a set of steps as:

1. Document upload and optical character recognition (OCR) technology: upload documents and apply OCR methods to extract information from the documents.
2. Identification/recognition of the document type: according to the context of the documents (e.g., accounting, supply chain, etc.), apply artificial intelligence algorithms to identify or recognize the type of the document (e.g., using a trained algorithm collection);
3. Language detection: identification of the country language expressed in the document.
4. Data extraction per extraction field: extraction of data from the document (e.g., document date, entity, address, etc.);
5. Selection of an extraction strategy (e.g., trained deep learning, trained neural networks, trained natural language processing (NLP) libraries or configuration of extraction patterns).

In Sect. 3, it is described with more detail the document classification process as well as the use of AI and RPA techniques/approaches/algorithms.

In this study, research papers were studied from scientific digital libraries such as Scopus, Elsevier, Web of Science and Google Scholar, between the last five years where the main search terms used have been "document classification," "artificial intelligence," "machine learning" and "robotic process automation." Additionally, in order to complement the work, some documentation and institutional information of software tools were studied, and tools were tested.

This document is structured as follows. Section 2 presents the general concept of RPA. Section 3 presents the problematic of classifying documents as a base activity in an RPA process, describing the analysis in the conversion of files with various formats to text and the conversion of PDF files to a structured format. Sections 4

and 5 present the discussion and conclusions of the study carried out and, finally, the bibliographic references that supported this work.

2 Robotic Process Automation

RPA is the automation of service tasks that reproduce the work that humans do [4]. The automation is done with the help of software robots or AI workers that are able to accurately perform repetitive tasks. The task instructions are set by the developer using some form of screen recording and defining variables. These tasks include actions like logging into applications, copying and pasting data, opening emails, filling forms, among others [5]. For business processes, RPA is the extrapolation of a human worker's repetitive tasks by a robot. This aims to replace people by automation in an outside-in manner. Unlike traditional methods, RPA is not part of the information infrastructure but rather sits on top of it, implying a low level of intrusiveness [6] possibly reducing costs. Some reports present a 30–50% decrease in operational costs of transactional activities within shared services with the use of RPA technologies complemented with AI techniques or algorithms [7]. In the last decades, several studies on RPA were presented at the academic level [8–12], as well as several companies started the implementation of optimization processes, as was the case of SAP, Oracle or Microsoft Dynamics. With the success of the applicability of more intelligent automation processes [7], RPA tools, in most cases, provide a more intelligent interaction with the user interface. Thus, RPA does not need users with programming skills to configure the software robots [5] and can also work with virtually any existing desktop software [6], offering a comparable low entry point for new clients. The use of RPA can also bring some limitations that might be overlooked at first [5]: (1) robot reprogramming might be required if structural changes occur to the interface; (2) software might not be able to use RPA as a technique due to lack of compatibility; and (3) human interaction is still needed to attend for the automation when triggering a robot or addressing the resulting content. RPA is more appropriate in situations with the following traits [6]: (1) well-defined processes where precise instructions can be given; (2) high volume of similar tasks (mundane and recurring actions are usually good candidates); and (3) mature tasks with predictable outcomes and well-known costs. In this context, one of the basic processes of the RPA tools is the document classification challenging using OCR tools [10–12]. In another way, the AI can be defined as a concept divided into major fields of application. Some of those fields were natural language processing, automatic programming, robotics, computer vision, automatic theorem proving, intelligent data retrieval, etc.

3 Document Classification Process

Typically, in a document classification process via optical character recognition (OCR), the user uploads one or more PDFs to the document list. The user starts loading PDF documents and then the inference system dematerializes the documents in a structure of digital data compatible with an ERP. In order to carry out this process, it becomes necessary to ensure a set of prerequisites, such as converting files with various formats to text, converting PDF files to a structured format and preprocessing the inference process for the document classification. Afterward, when the document has been previously treated, the inference system dematerializes the added PDFs and generates a document structure. Then the inference system uses an OCR system to read the document data and extract with the highest quality possible.

3.1 Conversion of Files with Various Formats to Text and Conversion of PDF Files to a Structured Format

In order to facilitate the work of analyzing the data structure, it is necessary to convert the content of the files to plain text. Table 1 shows a comparison of tools for converting files to and from different formats, and the aspects compared are as follows: type of files treated (source and destination files), whether or not the layout, price and license type. Table 1 presents five software tools using open-source license, in particular the LibreOffice (www.libreoffice.org), PDFMiner (www.pypi.org/project/pdfminer), Tesseract (github.com/tesseract-ocr/tesseract) and the PdfToText (www.pdftotext.com) using command line and web platform. Applicable to different document types, the LibreOffice and PDF to Text are more widespread. However, it does not keep the original layout in comparison with the pdftotext and Tesseract.

Table 1 Comparison of tools for converting files to and from different formats

	LibreOffice	PdfToText (command line)	pdf2txt (PDFMiner)	Tesseract	pdftotext (web)
Source file type	Various formats	PDF	PDF	Various image formats	PDF
Destination file type	Various formats	Simple text	Simple text	Simple text	Simple text, DOC and DOCX
Keeps the layout?	No	Yes	No	Yes	No
Price	Free	Free	Free	Free	Free
License	MLP-2	GPL-2/GPL-3	MIT	Apache 2	Proprietary

Table 2 Comparison of tools to extract data from tables stored in PDF files

	Tabula	PDFTables	PDFix
Fields identification	No	No	No
Reading order and table detection	Manual or automatic	Automatic	Automatic
Fields hierarchy?	No	No	Automatic
Extraction to a structured format?	Yes	Yes	Yes
Scalability (API)	No	Yes	Yes
Source files	PDF	PDF	PDF
Graphical interface	Yes	Yes	No
Price	Free	0.02\$ to 0.04\$ per page	Negotiable

Analyzing the online and business literature, it is concluded that there are some tools to extract data from tables stored in PDF files. Table 2 makes an analysis and comparison between them.

Three tools have been analyzed the Tabula (www.github.com/tabulapdf/tabula), PDFTables (www.pdftables.com) and PDFix (www.pdfix.net/) where the first tool is free, and all extracts the structure of a PDF file.

3.2 Alternative Approach to Converting PDFs to a Structured Format

The solutions presented in the previous sections are not completely satisfactory despite the conversion of the files to CSV or JSON. Several problems arise with the approach of these tools: (1) content marking: the values present in the tables often do not have the name that defines them. It becomes necessary way to mark the fields; (2) reading order: while for a human being it is second nature to identify the reading order of tables, for a machine, it is a process that sometimes becomes confusing. It becomes necessary to define the reading order; (3) relationship between content: the simple fact that the content is in the same row or column can mean that these values belong to the same field or just a coincidence to be ignored. The content must be segmented in order to define the correct relationship between the values of a table and (4) content hierarchy: if, for example, a PDF shows a total amount paid as well as the itemized amounts for each item, the dimension with the total amount is a hierarchical grade above the values for each item. The total value must show a “one to many” relationship with the values of each article. All of these problems have to be solved by a human in an abstract enough way to be applied to several files with the same format. An alternative solution can be found in a module, called PositionParser, created as part of another work carried out in 2018 [13], which reveals a more suitable solution. Similar to what is done in natural language processing, the

data is “tokenized,” but in this case, the position of each token in the original text is preserved. The process can be described as follows: (1) tokenize the data, segmenting the original text into small parts. Each part has the value of the token, the position of the token in the overall structure of the text and a label to identify the field to which the token belongs (if any); (2) label the tokens by checking or changing the values of the fields; (3) define the tables and reading order, decomposing and choosing the group of tokens in smaller and ordered segments; (4) visualize the tokenized data, reconstructing the tokens again to get an idea of how the document is being labeled and segmented; (5) define the hierarchy of the fields, taking into account that there may be some more generalist fields than others and (6) extract the labeled values to a CSV or JSON file, keeping the implicit relationships between the data.

3.3 Preprocessing of the Inference Process for Classifying Documents

In this context and considering that the PDF files correspond to document files that can use various formats and layout structures in the documents, the generation of data from the PDF file to text format is peaceful. However, for N structures of PDF file layouts, we can have N data structures in CSV format. For this reason, there is no standard CSV file structure format for importing directly into a table structure. In this context and following some implementation guidelines, it is recommended to characterize a typical configuration file for different types of PDF document layout formats so that maintaining a structure of tables (e.g., to store sales documents, human resources, shopping, etc.), it may be possible to import CSV files in various formats. Recently, several opinions and implementation articles have been presented as guidelines for carrying out the classification process, such as references [1–3, 14] with regard to the “data preparation for document classification” and the “machine learning options for document processing,” namely a strategy for detecting the type of documents and detecting the language of the documents. An example of the processing flow includes an input data stage, followed by a data preprocessing stage, keyword extraction and transformation and finally through classification and scoring stage. In turn, the process of implementing the AI algorithms in classification processes is well described which is presented in [2] and [15] and characterized the process in [16] as illustrated in Table 3.

3.4 Execution of the Inference Process in the Classification of Documents

Various tools associated with the implementation of RPA processes are made available on the market, at the proprietary level (UiPath [17], Kofax [18], Automation

Table 3 Document classification with artificial intelligence (AI): manual process to train and create the AI document classifier algorithm [16]

-
1. Human Step: Train a classifier on N document types using samples. Samples of each document class are imported into the system and a training process is started
 2. Machine Step: During training, the classifier will take each group of samples used for a document class and examine them for similar characteristics or features. These features can be text-based or visual features. Algorithms are then created to identify incoming documents as being part of one class or another
 3. Human Step: Next, the classifier will be tested by inputting a stream of documents and generating class assignment results
 4. Human Step: Analyze the output and compare against the “answer key” (technically called Ground Truth Data) which is the actual class assignment for each document
 5. Human Step: Note errors where a document belonging to “class a” actually belongs to “class b.”
 6. Human Step: Analyze the examples of errors against the samples used to train the document class. Do they contain new features that need to be trained? Do the documents have a lot of similarities that require adding new samples to each class for training?
 7. Human Step: Add new samples and retrain the classifier
 8. Human Step: Analyze results against what the results should be (using ground truth). Does the performance improve for those “tuned” document classes? Is there degradation to other document classes that requires adjustment by adding samples?
 9. Human Step: Repeat until performance is improved
-

Anywhere [19], WinAutomation [20], IBM-RPA [21]) and open-source tools (TagUI [22], AssistEdge [23], Automagica [24] and some other initiatives [25, 26]), being that mainly the proprietors provide implementations and extensibilities of AI techniques and algorithms. In this context, combined with the RPA process with the application of machine learning/artificial intelligence techniques/algorithms, it is considered important to characterize some indications so that the system proceeds to automate more efficiently. The CuneSoft company (www.cunesoft.com) in their module “distiller” presents a clear process of document classification using AI that has six main steps: (1) document upload and optional OCR; (2) document type detection; (3) language detection; (4) data extraction per extraction field; (5) selection extraction strategy; and (6) calculate and filter by confidence value.

3.5 Artificial Intelligence Application

The classification of documents (or text in documents) using AI algorithms has been investigated in recent years [1, 2, 14, 27–32]. The work of Talib et al. [14] shows the link between text classification [14, 29] and the various areas of applicability of AI (web mining, natural language processing, information extraction, etc.), as well as the challenges to proceed with this type of classification [1, 28–30, 33, 34]. Using supervised learning in the machine learning concept, the system can learn through

the rectification / correction by the manager (or user) of the incorrect classifications made by the inference system, as well as updating this knowledge base with new indications, which they may not be specific for an item for a field to be checked in the data structure, but also for an item to correspond to several fields in the data structure, allowing for some autonomy of decision of routing/categorization/classification to the inference system. To implement this type of intelligent approaches, code made available by proprietary or open-source technologies can be used for processes of classification, categorization, recognition and text analysis:

- Image and Character Recognition: Recognition of elements on a screen within a visual interface [35] of a user's work. Mix of machine learning approaches (supervised, unsupervised and by reinforcement), fuzzy matching text, multianchoring systems [36], artificial neural networks [37–40], mining text [14, 29, 41] and natural language processing [42, 43].
- Classification: Classification of documents through the application of natural language processing techniques on the text; use artificial neural networks [37–39, 44] to classify the reading of key elements (“keywords”) on web pages.

Associated with the objectives of classification and recognition, the various tools described in this study, mainly the proprietary ones, trigger processes of optimization, information extraction, potentiating recommendation and forecasting processes, such as exploring the multiclass of attributes in text of documents, using Microsoft Azure Decision Tree and multiclass neural network as an example.

4 Discussion

As the RPA process can be applied to various types of domains within an ERP and the scope of the AI objectives and taking into account the context of applicability of this project, it is recommended in a classification and documents process: (i) Circumscribe the type of analysis format of PDF documents associated with an ERP, due to the type of data structure extracted from different document formats, and the recommendations described in the section “preprocessing of the inference process” should be analyzed. (ii) The contextualization of the applicability of AI objectives (classification, categorization and text analysis), for example, in PDFs through the use and exploration of tools/programming languages already with implementations of AI algorithms, as in.NET or using the languages of R or Python programming. For the convenience to integrate an ERP implemented in.NET technologies, it is recommended to implement the algorithms for classifying documents made available by Microsoft, namely: artificial neural networks: Microsoft document classification using artificial neural networks [30, 38, 44], decision trees [31, 33, 44], support vector machine models [44]. (iii) Based on the schematic of the illustrative procedural flows (example of the Knime.com and Cunesoft.com platforms) and following the fundamentals of the classification of documents and texts, create support structures by creating a knowledge database to proceed with the referral of processes, in the

sense of the inference system proceed to the training for the automation processes of learning robots, through supervised automatic learning. In this way, a user will register the association of fields extracted from documents and tables where the data will be inserted so that the processes are routed efficiently and the system is autonomous. (iv) Associate a database or knowledge base (ex: “table” associated with the context with a “dictionary” of fields for and routing/classification so that the inference system can learn and add new item associations, and this process must be monitored by a user to validate that valid and consistent rules are being created by the inference system.

5 Conclusions

Tools oriented toward robotic process automation have been increasingly adding functionalities to improve the routine operations of organizations, optimizing work processes and consequently the profitability of the work of the employees of the organizations. One of the most important processes in this type of system is that of receiving documents in digital format, either via email, files or via optical character recognition technology, which is associated with the classification and categorization of documents. Being a challenge with several peculiarities, these RPA processes have been complemented with the success of the applicability of artificial intelligence techniques and algorithms. In this context, this work aimed to conduct a recent research on tools and approaches to the applicability of AI in more intelligent automatic processes. For this, several proprietary and open-source tools were analyzed, as well as academic and business approaches as a way of reviewing the literature carried out in recent years. In terms of the objectives of artificial intelligence, the applicability of classification and recognition (of images and text) is verified, enhancing the triggering of optimization processes, information extraction, enhancing recommendation and forecasting processes. In turn, it is concluded that despite the challenges associated with the classification and categorization of documents, the applicability of techniques and algorithms associated with artificial intelligence has been showing good accuracy results to allow a better efficiency in the automation of RPA processes. It appears that for processes of recognition, classification, information extraction and categorization of documents, the applicability of artificial neural networks, support vector machines, decision trees, combined with natural language processing techniques, is successfully applied in RPA tools, particularly in the task of reading digital documents.

Customizing certain tasks with RPA tools is still difficult which represents an open field for further work and research. The introduction of artificial intelligence into RPA processes can improve the scalability when automating common repetitive tasks like invoice management, data migration or expense management. Allowing for the end user to also train their own artificial intelligence models could provide a benefit to the healthcare, banking or marketing fields, among others, which represent some of the future work we intend to carry out.

References

1. Under the hood of AI document classification. <https://www.bizdata.com.au/blogpost.php?p=under-the-hood-of-ai-document-classification>. Last accessed 2020/09/11
2. Automatic machine learning document classification—an introduction. <https://provalisresearch.com/blog/automatic-machine-learning-document-classification/>. Last accessed 2020/09/11
3. Problem-solving with ML: automatic document classification. AI & Machine Learning. <https://cloud.google.com/blog/products/gcp/problem-solving-with-ml-automatic-document-classification>. Last accessed 2020/09/11
4. Aalst W, Bichler M, Heinzl A (2018) Robotic process automation. Bus Inf Syst Eng 60
5. Asquith A, Horsman G (2019) Let the robots do it!—taking a look at robotic process automation and its potential application in digital forensics. Forensic Sci Int Rep 1:100007
6. Enriquez JG, Jiménez-Ramírez A, Domínguez-Mayo FJ, García-García JA (2020) Robotic process automation: a scientific and industrial systematic mapping study. IEEE Access 8:39113–39129
7. Williams D, Allen I (2017) Using artificial intelligence to optimize the value of robotic process automation
8. Anagnoste S (2017) Robotic automation process—the next major revolution in terms of back office operations improvement. In: Proceedings of the international conference on business excellence 11
9. William W, William L (2019) Improving corporate secretary productivity using robotic process automation. In: International conference on technologies and applications of artificial intelligence, pp 1–5
10. Syed R, Suriadi S, Adams M, Bandara W el al (2020) Robotic process automation: contemporary themes and challenges. Comput Ind 115
11. Kaya C, Turkyilmaz M, Birol B (2019) Impact of RPA technologies on accounting systems. J Acc Financ 82:235–249
12. Enriquez JG, Jimenez-Ramirez A, Dominguez-Mayo FJ, Garcia-Garcia JA (2020) Robotic process automation: a scientific and industrial systematic mapping study. IEEE Access 8:39113–39129
13. Lima R (2018) Extração e análise multidimensional de dados de atletismo a partir de dados não estruturados (Master's thesis), Mestrado em Engenharia de Software, Instituto Politécnico de Viana do Castelo
14. Talib R, Hanif MK, Ayesha S, Fatima F (2016) Text mining: techniques, applications and issues. Int J Adv Comput Sci Appl 7(11):414–418
15. Text analysis, classification and categorization. <https://monkeylearn.com/text-analysis/>. Last accessed 2020/09/11
16. AI Document Classification Process. <https://www.parascript.com/blog/leveraging-ai-in-document-classification/>. Last accessed 2020/09/11
17. Artificial intelligence RPA capabilities. <https://www.uipath.com/product/ai-rpa-capabilities>. Last accessed 2020/09/11
18. Kofax intelligent automation platform. <https://www.kofax.com/Products/intelligent-automation-platform>. Last accessed 2020/09/11
19. IQBot—Intelligent document processing. <https://www.automationanywhere.com/products/iq-bot>. Last accessed 2020/09/11
20. About Softomotive. <https://www.winutomation.com/about-softomotive/>. Last accessed 2020/09/11
21. IBM RPA. <https://www.ibm.com/products/robotic-process-automation>. Last accessed 2020/09/11
22. TagUI—AI Singapore platform—National Institute. <https://makerspace.aisingapore.org/do-ai/tagui/>. Last accessed 2020/09/11
23. RPA. <https://www.edgeverve.com/assistededge/robotic-process-automation/>. Last accessed 2020/09/11

24. Automagica GitHub repository. <https://github.com/automagica/automagica>. Last accessed 2020/09/11
25. Robocorp hub. <https://hub.robohub.org/new-to-robohub-suite/get-started/quickstart-guide/>. Last accessed 2020/09/11
26. TaskT RPA .NET platform. <https://github.com/saucereez/taskt/wiki/Automation-Commands>. Last accessed 2020/09/11
27. Bilski A (2011) A review of artificial intelligence algorithms in document classification. *Int J Electron Telecommun* 57:263–270
28. Chakravarthy T, Arivoli P (2015) Document classification using machine learning algorithms—a review. *Int J Sci Eng Res (IJSER)* 2347–3878
29. Thangaraj M, Sivakami M (2018) Text classification techniques: a literature review
30. Tripathi K, Vyas R, Gupta A (2019) Document classification using artificial neural networks. Research Gate Publication
31. Noormanshah W, Nohuddin P, Zainol Z (2018) Document categorization using decision tree: preliminary study. *Int J Eng Technol* 7:437–440
32. Thangaraj M, Sivakami M (2018) Text classification techniques: a literature review. *Interdiscip J Inf Knowl Manag* 13:117–135
33. Sivakumar R, Manikandan R (2018) Machine learning algorithms for text-documents classification: a review. *Int J Acad Res Dev.* ISSN: 2455-4197
34. Anderlucci L, Guastadisegni L, Viroli C (2019) Classifying textual data: shallow, deep and ensemble methods
35. UIPath—Element recognition in user visual interface. <https://www.uipath.com/product/platform/ai-computer-vision-for-rpa>. Last accessed 2020/09/11
36. Fritsch J, Kleinehagenbrock M et al (2003) Multi-modal anchoring for human–robot interaction. *Robot Auton Syst* 43(2–3):133–147
37. Kofax—Cognitive document automation. <https://www.kofax.com/Blog/Categories/Cognitive-Document-Automation>. Last accessed 2020/09/11
38. Google Tensorflow. <https://www.tensorflow.org/>. Last accessed 2020/09/11
39. Automation anywhere—Artificial neural networks. https://www.automationanywhere.com/images/Datasheet_IQ_Bot.pdf. Last accessed 2020/09/11
40. AssistEdge—Use of artificial neural networks to analyze business process variations. <https://www.edgeverve.com/assistededge/assistededge-discover/>. Last accessed 2020/09/11
41. Natural Processing Language usage. <https://makerspace.aisingapore.org/do-ai/hotdocs-nlp>. Last accessed 2020/09/11
42. Microsoft Text Analytics API [Online]. <https://docs.microsoft.com/en-us/azure/cognitive-services/text-analytics/>. Last accessed 2020/09/11
43. Google Natural Language API. <https://cloud.google.com/natural-language/docs/languages>. Last accessed 2020/09/11
44. Microsoft Azure machine learning algorithm cheat sheet. <https://docs.microsoft.com/pt-pt/azure/machine-learning/algorithms-cheat-sheet>. 2020/09/11

Artificial Intelligence Optimization Strategies for Invoice Management: A Preliminary Study



Rui Lima, Sara Paiva, and Jorge Ribeiro

Abstract It is very common for companies to receive invoices (and other semi-structured documents) in paper and PDF files and someone has to manually enter that data into a digital structure like a database or comma-separated values (CSV) file. This type of work is very time-consuming (making it expensive) and exhaustive (making it prone to errors). Data entry activities also force high-paying specialized workers to do repetitive tasks or to outsource that work, making it hard to manage the data workflow. There is a need to automate this type of process. In this context, the following paper presents a preliminary study and review of technologies, tools and recent research strategies for invoice management mainly in the scope of robotic process automation tools.

Keywords Artificial intelligence · Computer vision · Machine learning · Natural language processing · Optical character recognition · Robotic process automation

1 Introduction

The digitalization of paper documents is one of the most commercially important interests worldwide. After a document is scanned, various operations involving artificial intelligence (AI) need to be performed. The first step involves the application of optical character recognition (OCR) methods to generate textual information and computer vision (CV) for automatic document layout extraction and analyzing text segments represented as bounding boxes [1]. Natural language processing (NLP) can be used in the encoding process of the text into numeric values, while maintaining context (e.g., semantic, spatial) [2]. After the text is encoded, it can be used to train machine learning (ML) models like artificial neural networks (NNs) or support vector machines (SVMs).

R. Lima · S. Paiva (✉) · J. Ribeiro
Instituto Politécnico de Viana do Castelo, Viana do Castelo, Portugal
e-mail: sara.paiva@estg.ipvc.pt

Currently, most companies have some system to deal with receipts and other documents with semi-structured text. Many times, the system resorts to the data being entered manually into a database. This type of manual labor is prone to errors and is time-consuming, making it expensive. For this reason, and for some years now, we assist to a set of commercial tools, usually referred to as robotic process automation (RPA) tools that can automate tasks (like the management of scanned documents) at a user level, by using some AI methods referred above. RPA tools and other processes can be used to transform this manual labor into an automatic one. It is possible to extract the text from an image of the physical documents using an OCR approach, while ML could be used to infer the knowledge and find out what information to extract [3].

When extracting data from semi-structured documents, even if the data conversion to text keeps the structure of the original content, it is still virtually impossible to accurately recover the correspondence between the values and the data meaning. Resorting to programmable automation becomes a requirement [4].

For this study, research articles were downloaded from scientific digital libraries (e.g., mainly through the www.b-on.pt platform) such as Scopus, Elsevier, Web of Science and Google Scholar, between the year 2017 and December 2020. The search terms used have been “document classification,” “artificial intelligence,” “machine learning,” “optimization,” “robotic process automation” and both or a mixture of these keywords. To complement the research, documentation and institutional information of robotic process automation software tools were studied and tested.

The main contributions of this paper are: (1) a summary of the main techniques that are used in the scope of AI, invoice management and processing in robotic process automation tools; (2) an overview of several RPA tools and their comparison; and also (3) a reference to recent optimization strategy for invoice management. To that purpose, the paper follows the following structure: In Sect. 2, an overview of common AI techniques that are used for invoice management is presented. Section 3 presents tools and methods used to automate and improve invoice handling. In Sect. 4, we present an analysis and conclusions are presented in Sect. 5.

2 AI Techniques

This section presents a brief description of the technologies associated with AI that are usually used in the process of automatic processing of invoices.

2.1 Computer Vision

CV relies on image features like describing points, edges, objects or color to generate information from the image perception. To describe an image, visual features must be detected and represented. Most of the times the image description takes the form

of vectors [5]. The modern approaches for context-based image retrieval and classification are to gradually generalize information from an image using methods based on ML, like convolutional NN. NN models can be trained to classify elements of an image by reducing the quantity of visual feature data present to describe the entire image (at the highest possible level) [5]. CV solutions are increasingly being applied into production processes to ensure their correct operation. These methods are vital in various fields like engineering, science and business [5]. Image comparison algorithms can simplify large amounts of data to make images easier to compare but developing CV capable of simulating human visual perception is a complicated process. Image recognition is a simple process for humans but when an algorithm tries to mimic the process, it does not take into account imagination or human knowledge. In some cases, this makes the image description not satisfactory for human users [5].

2.2 *Optical Character Recognition*

OCR is the technique for converting handwritten, physical text into machine-encoded text. It is one of the most popular fields in pattern recognition because of its vast application potential. It is used as a way to automate data entry from printed documents (e.g., passport documents, receipts, invoices) into data records. The benefits of OCR are that text can then be electronically edited, searched, occupy less memory and be used in machine processes like ML and NLP [6]. An OCR system is capable of liberating the information on paper. After the information is retrieved, it is possible to extract material of interest and process it [7]. The major concern of OCR is the accuracy of the character recognition. There is always a degree of imprecision present in real-life documents. To tackle this problem, the models are trained with fuzzy and rough sets to simulate indeterminate uncertainty. Studies, evaluated through different performance metrics, show that soft computing models of OCR systems perform better than traditional models [6]. Although soft OCR methods perform better, the conversion is not always flawless. OCR models make errors and, if too many mistakes happen, the electronic version of the document might not be properly extracted. When a document has too many errors, the application of an OCR model might not be useful, but OCR technology advanced to the point where it can process a large variety of documents with accuracies of 99% or more in cleanly printed pages [7].

2.3 *Natural Language Processing*

It is the attempt to extract the meaning representation from free text. To do this, it makes use of multiple knowledge representations like lexicon of words or grammar rules. A specific technique of NLP is text mining. Text mining is the discovery and

extraction of nontrivial knowledge from unstructured text; this encompasses information retrieval and text classification/clustering [8]. Text classification is an important part of the information workflow [9]. Text classification and information retrieval are also used in invoice management. NLP benefited notably from the resurgence of artificial NN, namely deep NN. Artificial NN is a type of ML algorithm currently popular due to their high performance with less need for engineered features. There are two main types of deep NN: recurrent NN (that performs well on document-level sentiment classification) and convolutional NN (that performs well on language modeling tasks) [10].

2.4 Machine Learning

ML and statistical techniques are techniques that are not yet fully incorporated with NLP. Some of the prevailing techniques for addressing NLP tasks are SVM, Naïve Bayes and deep NN for supervised learning and clustering for unsupervised learning [11]. Unlike rule-based approached, ML solutions automatically generate rules from training data. ML algorithms are usually capable of learning with historical data. The historical data needs to be synthesized into features before being used as parameters for these algorithms. These features can later be used to make predictions or classify data. Without ML approaches, NLP tasks have to be done manually using rule-based approaches [11].

The encoding of text into values is currently done using word embeddings (e.g., word2vec, glove), but in the case of semi-structured texts (e.g., invoice documents), the named entity recognition (NER) performance is limited. This happens because it is difficult to produce meaningful word embedding vectors when the input is a page image. Although there are recent improvements in ML algorithms, the extraction of information from unstructured or semi-structured document images is still a challenge that needs human supervision [12]. Gradually, the vanguard of research made in NLP is being based on ML models. In such models, a real value is attached to each input feature, generating stochastic, probabilistic decisions. The benefit of this approach is the capability of representing a relation quality in different dimensions. The use of ML is not only limited to the NLP field [11].

3 Invoice Improvement Strategies

There are many tools and methods available to analyze information from documents with semi-structured information, including invoices. These tools usually resort to multiple AI fields (e.g., CV and NLP [13]) to classify documents or extract their information. In this section, we present an overview of the currently used tools and methods being researched. We make a comparison between commonly used RPA

tools in section A and present new optimization methods being developed for invoices and other semi-structured texts in section B.

3.1 Robotic Process Automation Tools

Due to the repetitious transactional nature of invoice processing, RPA tools are perfect solutions that bring immediate value to the core business process [13, 14]. We provide a comparison between six of the most used platforms: UiPath, Kofax, Automation Anywhere, TagUI, AssistEdge and Automagica. Most of the RPA tools apply AI techniques to automate manual processes done by human workers, reducing the burden of recurring tasks [13, 15]. These techniques can be grouped into four categories: CV, OCR, NLP and ML. A comparison of the AI methods used by each RPA solution is made in Table 1.

UiPath is capable of image [16] and text [17] recognition from the computer screen. It can recognize elements from the user interface using ML approaches and learn, through visualization, human interactions (e.g., drag and drop files). It can extract text and classify documents through the process that use keywords, regex or pre-trained machine learning models. UiPath started in 2005 as an outsourcing company and later developed an industry standard platform for training software robots. Their source code is now being used by a large number of companies ranging from call centers to healthcare and financial institutions [15].

Kofax is a proprietary software that uses artificial NN to recognize document types. It allows the use of sentiment analysis combined with NLP algorithms [18] for document classification. This tool uses artificial NN to classify and read keyword elements from webpages [19]. Kofax is capable of cognitive document automation that goes beyond the normal OCR functionality [20]. Kofax automatically extracts and classifies data from paper and digital sources with reduced human intervention and error. As the demand for single platform software with mobile applications increased, Kofax introduced document workflow, imaging, intelligent capture and business process management [13].

Automation Anywhere uses artificial NN, CV and OCR to recognize types of documents, images or fields of text [21]. It combines NLP, fuzzy logic and ML to

Table 1 Comparison of AI methods used by RPA tools

	CV	OCR	NLP	ML	License Type
UiPath	Yes	Yes	No	Yes	Proprietary
Kofax	Yes	Yes	Yes	Yes	Proprietary
Automation Anywhere	Yes	Yes	Limited	Yes	Proprietary
TagUI	No	Yes	No	No	Open-Source
Automagica	Yes	Yes	Limited	Yes	Proprietary Open-Source

automatically classify, extract and validate information. Automation Anywhere has a script-based design. This allows for higher accuracy in the bot development but might decrease the number of potential users [15]. The company provides RPA technology to leading healthcare, financial, manufacturing and insurance firms for over a decade. [13].

TagUI can recognize text via OCR using techniques commonly not associated with IA [22]. The automation is done using a natural language-like syntax with support of over 20 languages. Although this tool does not have native support for ML, it can be integrated with Python or R for AI or ML [23].

Automagica is capable of recognizing image and text from documents using CV and OCR techniques. It is built on open-source technologies like Python language and the ML platform TensorFlow [24]. TensorFlow is commonly used for image and text classification.

Some of the most common ML algorithms used by RPA tools, for document classification, are artificial NN and SVM, among others (e.g., k-nearest neighbor and Naïve Bayes [25]). Artificial NN is applied with great success in document analysis, document recognition, image preprocessing and OCR. Tasks like preprocessing, layout analysis, character segmentation and word recognition also show promising results. They are extensively used in almost all document image analysis and recognition tasks. Studies show that 65% of papers deal with OCR tasks and 15% with word recognition, involving artificial NN [26]. A NN is an algorithm inspired by the functioning of animal brains when processing information. This algorithm is made of a large number of nodes (also called neurons) that are associated with a transfer function. Nodes usually operate in parallel and are highly interconnected (with one another) between each layer [25], through edges. Each edge is associated with a numeric value known as weight [27]. NN has an input and an output, where the data used as input must be numeric. The network model needs to be trained before it can be applied, with new values, to make predictions [27, 28]. Algorithms based on the artificial NN made a huge success in many types of classification activities, and the emergence of new theories seems promising. Nevertheless, one of their drawbacks is that they lack transparency and act like a “black box.” During the classification, a target model can find common features and then be able to group values into different categories [29].

There are three types of methods for classification (also known as the regression issue); the first one is based on statistical methods (e.g., SVM), the second is rule-based methods (e.g., decision trees) and the third is based on connection methods (e.g., artificial NN) [29]. SVM (an algorithm introduced in 1992 by Vladimir Vapnik and Alexey Chervonenkis at AT&T Bell Laboratories [30]) is also another method commonly used in RPA, namely OCR. SVM is at the borderline between artificial NN and other statistical algorithms [26]. This algorithm is primarily used for classification such as image classification and categorization of large bodies of text. It is particularly useful in complex data with a high number of dimensions and for small training samples. SVM uses a supervised learning approach where it classifies new data based on preexisting labeled training data. Since this type of model works well with

a small dataset, it offers a cost-effective method for classifying large volumes of documents in big organizations [31].

Studies have shown that SVM surpassed other ML methods in text categorization and is vastly accepted in the academic and industrial fields. As an example, Health Discovery Corporation uses it in medical image analysis and Reuters uses it for text classification [31]. SVM is accurate, scalable, predictable and (unlike artificial NN) is auditable, ideal for automatic text classification made by corporations [31].

3.2 Recently Researched Optimization Strategies

In order to use the invoice text with a ML algorithm, it first needs to be converted into a vector representation. To optimize the recognition of named entities or the classification process of documents, the text needs to be encoded into numerical vectors. There are three major NLP methods that encode text: one-hot, term frequency-inverse document frequency (TF-IDF) and word embeddings. One-hot encoding is the simplest method to implement, but frequency information and context of words are lost in the process. TF-IDF takes into account the frequency information [32]. Word embeddings try to maintain the context of words by producing a co-occurrence matrix where every row corresponds to a word and every column corresponds to the context of a word (e.g., in the same paragraph). The cell values correspond to the number of appearances of a word in the context of another word [33]. A small example of a co-occurrence matrix can be seen in Fig. 1.

Although word embeddings are able to encode continuous text, they are not ideal for semi-structured layouts. This happens because the spatial information is lost during the conversion. Until recently, there was not an efficient way of encoding semi-structured text while maintaining spatial information. In June 2019, Xiaohui Zhao et al. proposed a new language representation model called Convolutional Universal Text Information Extractor (CUTIE). This model can maintain information of both

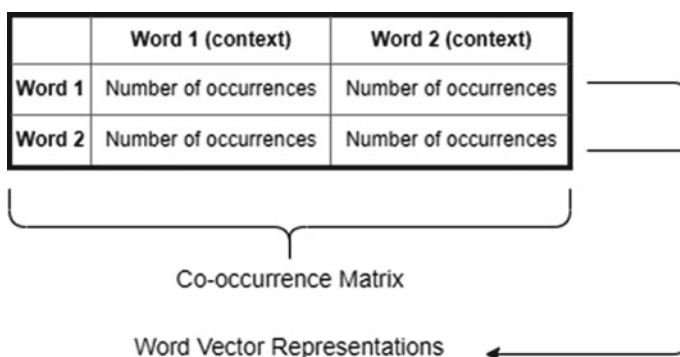


Fig. 1 Example of a co-occurrence matrix

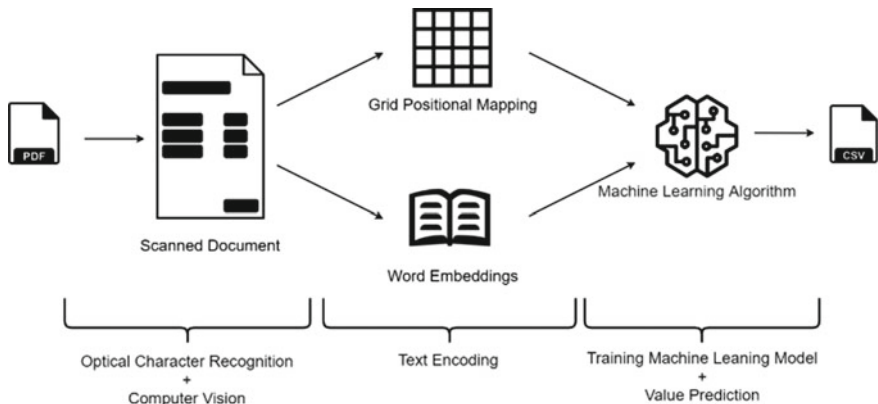


Fig. 2 Workflow for NER of semi-structured documents

the semantic meaning and spatial distribution of the text. This is done by applying convolutional NN on gridded text where words are embedded as features (Fig. 2) [2]. The embedding of each word is placed in the respective location in the grid. The layout is maintained because cells without words have no embeddings. The matrix is then ready to be processed by a convolutional NN.

Drobac and Lindén present a solution for printed documents with multiple languages and fonts. Those types of documents have a high error rate when applying the usual tools like Tesseract or Ocrpy. The solution involves finding an optimal deep NN using training data, performing the OCR by applying the pre-trained model to the images, and performing a post-correction to the resulting text. There are multiple approaches to OCR post-processing but all of them have at least two steps. The first step is the generation of correction candidates. The second step is the decision to accept or reject the corrections. Using this approach, they claim an increase in accuracy from 8 and 13% to 1.7 and 2.7% of character error rate [34].

Clausner et al. presented an effective approach to train an OCR model using the Aletheia document analysis tool. This tool can be integrated with different OCR engines, but Tesseract is available by default and Tesseract 3 is the only one that allows model training [35].

Li et al. present a CV solution for text detection on natural scenes. Natural scene text detection is difficult to perform due to the randomness of the background and the multiple existing languages and fonts. In this solution, a deep convolutional NN is used but the training samples rely on pixels instead of default character boxes. The model can be broken into three parts: convolutional module, aggregated feature module and prediction layer [36].

For scanned documents, the character distance and direction often change based on the content. This is a challenge for character detection and combining those characters into words and text lines. Zhao et al. present a four-channel directional text score map so that the direction of the character is acquired. This process helps

the recognition process by introducing a GAN framework into the OCR task of the document [37].

4 Analysis

It is fairly easy to digitalize paper documents into images and recognize words and their location on the document using CV and OCR methods. But to fully convert semi-structured text into a structured format like CSV, or a database, some problems arise:

1. Content tagging: The values presented in tables sometimes do not have a name to define their values. It becomes a necessary way to do the NER of the fields.
2. Reading order: For a human being, it is second nature to identify the reading order in semi-structured text, but for a machine, it sometimes is a confusing process. The reading order is something that might have to be taken into account.
3. Relation between content: The fact of the content being on the same line or column might mean those values belong to the same field or just a coincidence to be ignored. The content needs to define the correct relation between the values from a text structure.
4. Content hierarchy: As an example, if an invoice presents the total value as well as the discriminated values for each article, the total value dimension is one hierarchical level above the values for each separated article. The total value should present a “one-to-many” relation with the values from each article.

These problems need to be resolved in a sufficiently comprehensive way to be applied to multiple files with the same format.

Although RPA tools tackle these problems, they usually resort to the absolute location of a value in a previously tagged document to fetch new values. This means that if the position of values changes slightly, the values might not be found or incorrect values might be extracted instead. Some RPA tools use pre-trained ML models but cannot be retrained for the user's specific group of documents. Since last year (2019), there is a solution to keep the spatial distribution information, when encoding words, presented by Xiaohui Zhao et al. with the CUTIE model. In theory, the application of ML algorithms would be the perfect solution for documents with slightly inconsistent formats, but the words in the text need to first be encoded into numerical values without losing their positional values. For that purpose, new language representation processes (like CUTIE) are currently being developed.

5 Conclusion

In this paper, we describe the use of robotic process automation (RPA) tools and other methods as solutions for invoice management, following recent research/works/tools

from the web (e.g., software companies) and articles from scientific digital libraries such as Scopus, Elsevier, Web of Science and Google Scholar (e.g., mainly through the www.b-on.pt platform).

RPA tools can improve the workflow of invoice handling, usually without the need for the user to have knowledge about programming. Although practical tools, RPAs are somewhat limited with the use of ML for semi-structured documents. In this sense, a proper encoding method for semi-structured texts opens the door for the use of ML algorithms that previously were not able to be used accurately. For this to happen, the language representation needs to keep both the semantic understanding as well as the spatial distribution context. With proper encoding, and some pre-tagged documents, it is possible to train ML algorithms like artificial NN or SVM. The trained model can be used to infer information like: (i) the hierarchical level of the information; (ii) the content's NER tag value; and (iii) the element's group number.

We conclude that, in the context of AI optimization strategies for invoice management, RPA tools are useful for practical implementations without the need for the end users to have specialized AI knowledge. We also conclude that, with the development of recent word embedding techniques, the use of ML algorithms became more accurate in the automation of mining semi-structured texts like invoice documents.

An RPA tool, like UiPath, is recommended for generalized automated invoice analysis in semi-structured text, but there are scenarios where someone will need to train their own model. On those cases, a programmable solution, using grid positional mapping and word embeddings, is advised.

References

1. Gupta G, Niranjan S, Shrivastava A, Sinha RMK (2006) Document layout analysis and classification and its application in OCR. In: 2006 10th IEEE international enterprise distributed object computing conference workshops (EDOCW'06). IEEE, pp 58–58
2. Zhao X, Niu E, Wu Z, Wang X (2019) Cutie: learning to understand documents with convolutional universal text information extractor. arXiv preprint [arXiv:1903.12363](https://arxiv.org/abs/1903.12363)
3. Odd J, Theologou E (2018) Utilize OCR text to extract receipt data and classify receipts with common machine learning algorithms
4. McCallum QE (2012) Bad data handbook: cleaning up the data so you can get back to work. O'Reilly Media, Inc.
5. Scherer R, Scherer D (2020) Computer vision methods for fast image classification and retrieval. Springer International Publishing
6. Chaudhuri A, Mandaviya K, Badelia P, Ghosh SK (2017) Optical character recognition systems. In: Optical character recognition systems for different languages with soft computing. Springer, Cham, pp 9–41
7. Nagy G, Nartker TA, Rice SV (1999) Optical character recognition: an illustrated guide to the frontier. In: Document recognition and retrieval VII, vol 3967. International Society for Optics and Photonics, pp 58–69
8. Kao A, Poteet SR (eds) (2007) Natural language processing and text mining. Springer Science & Business Media
9. Bilski A (2011) A review of artificial intelligence algorithms in document classification. Int J Electron Telecommun

10. Yin W, Kann K, Yu M, Schütze H (2011) Comparative study of cnn and rnn for natural language processing. arXiv preprint [arXiv:1702.01923](https://arxiv.org/abs/1702.01923)
11. Khan W, Daud A, Nasir JA, Amjad T (2016) A survey on the state-of-the-art machine learning models in the context of NLP. Kuwait J of Sci 43(4)
12. Carbonell M, Fornés A, Villegas M, Lladós J (2019) TreyNet: a neural model for text localization, transcription and named entity recognition in full pages. arXiv preprint [arXiv:1912.10016](https://arxiv.org/abs/1912.10016)
13. Madakam S, Holmukhe RM, Jaiswal DK (2019) The future digital work force: robotic process automation (RPA). JISTEM-J Inf Syst Technol Manag 16
14. Kaya CT, Turkyilmaz M, Birol B (2019) Impact of RPA technologies on accounting systems. J Account Financ (82)
15. Issac R, Muni R, Desai K (2018) Delineated analysis of robotic process automation tools. In: 2018 second international conference on advances in electronics, computers and communications (ICAEEC). IEEE, pp 1–5
16. About the UIAutomation Activities Pack, <https://docs.uipath.com/activities/docs/about-the-ui-automation-activities-pack>. Last accessed 2020/09/11
17. About the IntelligentOCR Activities Pack, <https://docs.uipath.com/activities/docs/about-the-intelligent-ocr-activities-pack>. Last accessed 2020/09/11
18. Scaling, Expanding and excelling in automation is how organizations. <https://www.kofax.com/Products/intelligent-automation-platform>. Last accessed 2020/09/11.
19. Kofax Robotic Process Automation. https://www.kofax.com/-/media/files/solution-overview/en/so_kofax-robotic-process-automation_en.pdf. Last accessed 2020/09/11
20. Beyond RPA and Cognitive Document Automation: Intelligent Automation at Scale. <https://www.kofax.com/blog/beyond-rpa-and-cognitive-document-automation-intelligent-automation-at-scale>. Last accessed 2020/09/11
21. Automation Anywhere IQ Bot Datasheet. https://www.automationanywhere.com/images/Datasheet_IQ_Bot.pdf. Last accessed 2020/09/11
22. Kelaberetiv/TagUI. <https://github.com/kelaberetiv/TagUI>. Last accessed 2020/09/11
23. TagUI. <https://makerspace.aisingapore.org/do-ai/tagui/>. Last accessed 2020/09/11
24. Open Source Smart Robotic Process Automation, <https://automagica.com/>. Last accessed 2020/09/11
25. Kothari VM, Rana ZD, Naik C (2015) Document classification using neural networks based on words. Int J Adv Res Comput Sci 6(2)
26. Marinai S, Gori M, Soda G (2005) Artificial neural networks for document analysis and recognition. IEEE Trans Pattern Anal Mach Intell 27(1):23–35
27. Tripathi K, Vyas RG, Gupta AK (2019) Document classification using artificial neural network. Asian J Comput Sci Technol 8(2):55–58
28. de Mello RF, Senger LJ, Yang LT (2005) Automatic text classification using an artificial neural network. In: High performance computational science and engineering. Springer, Boston, MA, pp 215–238
29. Gu XF, Liu L, Li JP, Huang YY, Lin J (2008) Data classification based on artificial neural networks. In: 2008 International conference on apperceiving computing and intelligence analysis. IEEE, pp 223–226
30. Mayor S, Pant B (2012) Document classification using support vector machine. Int J Eng Sci Technol 4(4)
31. Mertsalov K, McCreary M (2009) Document classification with support vector machines. ACM Comput Surv CSUR 42:1–47
32. Vector Representations of Text for Machine Learning. <https://medium.com/@athif.shaffy/one-hot-encoding-of-text-b69124bef0a7>. Last accessed 2020/09/11
33. Søgaard A, Vučić I, Ruder S, Faruqui M (2019) Cross-lingual word embeddings. Synth Lect Hum Lang Technol 12(2):1–132
34. Drobac S, Lindén K (2020) Optical character recognition with neural networks and post-correction with finite state methods. Int J Doc Anal Recogn (IJDAR) 23(4):279–295

35. Clausner C, Antonacopoulos A, Pletschacher S (2020) Efficient and effective OCR engine training. *Int J Doc Anal Recogn (IJDAR)* 23(1):73–88
36. Li X, Liu J, Zhang S, Zhang G, Zheng Y (2020) Single shot multi-oriented text detection based on local and non-local features. *Int J Doc Anal Recogn (IJDAR)* 23(4):241–252
37. Zhao J, Wang Y, Xiao B, Shi C, Jia F, Wang C (2020) DetectGAN: GAN-based text detector for camera-captured document images. *Int J Doc Anal Recogn (IJDAR)* 23(4):267–277

A Comparative Study Between Data-Based Approaches Under Earlier Failure Detection



Hadjidj Nadjiha, Benbrahim Meriem, Berghout Tarek,
and Mouss Leila Hayet

Abstract A comparative study between a set of chosen machine learning tools for direct remaining useful life prediction is presented in this work. The main objective of this study is to select the appropriate prediction tool for health estimation of aircraft engines for future uses. The training algorithms are evaluated using “time-varying” data retrieved from Commercial Modular Aero-Propulsion System Simulation (C-MAPSS) developed by NASA. The training and testing processes of each algorithm are carried out under the same circumstances using the similar initial condition and evaluation sets. The results prove that among the studied training tools, Support vector machine (SVM) achieved the best results.

Keywords Machine learning · SVM · Remaining useful life · C-MAPSS

1 Introduction

Recently, and since health state estimation of equipments or subsystems plays an important role in conditional-based maintenance (CBM) operations, remaining useful life (RUL) prediction became a very crucial task for prognostic health management (PHM) [1]. Thanks to advancement sensors technologies, the availability of rich dynamic data makes the application of machine learning tools for this mission very reliable [2].

H. Nadjiha (✉) · B. Meriem · B. Tarek · M. L. Hayet

Laboratory of Automation and Manufacturing Engineering, University of Batna2, 01 Rue Chahid Bokhlouf, 05000 Batna, Algeria
e-mail: n.hadjidj@univ-batna2.dz

B. Meriem
e-mail: m.benbrahim@univ-batna2.dz

B. Tarek
e-mail: t.berghout@univ-batna2.dz

M. L. Hayet
e-mail: h.mouss@univ-batna2.dz

Many “data-driven” approaches were introduced in the literature for solving or enhancing RUL prediction models. Several architectures and schemes for data pre-processing, training and post-processing were developed in order to obtain the optimal solution for this case. According to the literature, SVM and artificial neural networks (ANN) with different architectures were the most used training tools before deep learning emerged [1, 3]. The problem that we are facing in this case is finding the optimal training tools among these developed ones.

Therefore, the objective of this study is to replicate RUL prediction experiments using the common training tools attempting to find the most adaptable solution.

The rest of this paper is organized as follows: a brief description of the studied system and its data set is introduced in Sect. 2. Section 3 elaborates experiences and results discussion. This work is concluded in Sect. 4.

2 Data Set and System Description

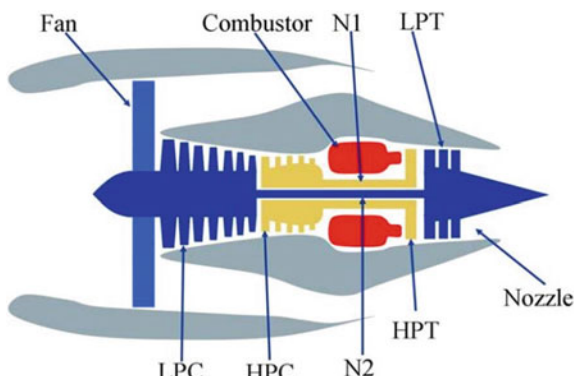
The studied system in this research is a two spool, double flow turbofan engine with 90.000 lb thrust class that is illustrated in the diagram of Fig. 1. This propulsion power is produced when the high-pressure (HPT) and low-pressure (LPT) turbines are driven by a tremendous force of pressure produced in the combustion chamber.

The heated air by the burners is previously accumulated from the fan and compressed in different stages using low-pressure (LPC) and high-pressure compressors (HPC). More detailed explanation of the engine can be found in C-MAPSS user guide in [4].

Data that is used to estimate the health state of the engine during operating cycles is retrieved from a simulated engine model [6]. The data set contains 26 measurements (engine number, operating conditions, sensors measurements, RUL labels) of 100 different life cycles of the engine in different operating condition and failure modes.

In each life cycle, the sensors measurements are changed gradually to describe certain kind of deterioration attitude of the engine. In the beginning of each life cycle,

Fig. 1 Diagram of the studied type of engines [5]



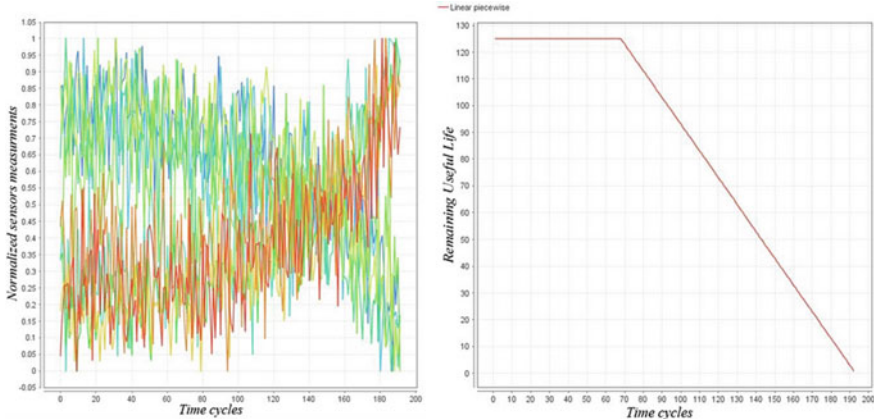


Fig. 2 Example of aircraft engine sensors measurements variation and its RUL function

the engine is normally working under the initial conditions, and at certain number of flights, it starts gradually losing its performances towards a predefined failure mode.

An example of the behaviour of sensors measurements and RUL function of one life cycle of the engine is illustrated in Fig. 2. The RUL degradation law is proposed in [1] as a linear piecewise continuous function with threshold equal to 125 time cycles.

C-MAPSS data set is divided into four different subsets according to different operating conditions and failure modes with the notations: FD001, FD002, FD003 and FD004. Each subset is divided into training and testing sets.

3 Experimental Results and Discussion

The experimental results are carried out using the first subset FD001 from C-MAPSS dataset, which means that only one fault mode (HPC degradation) and one single operating condition (sea level) are considered.

Before any application, the input training and testing data were prepared by using min–max normalization as illustrated previously in Fig. 1. The targets were defined using a linear piecewise continuous function, and the prepared FD001 can be found online in “FD001.mat” file [7].

The comparative study is achieved using well-known basic learning algorithms without any hybridization or additive parameters such as regularization parameters, weighting or irregular feature mapping paradigms. The used algorithms are as follows: a simple linear regression algorithm (LR), polynomial regression algorithm (PR), Gaussian process (GP), support vector machines (SVM), sigmoid neural network (SNN) and a deep neural network (DNN) with H₂O type.

Table 1 Performance evaluation

Algorithms	SVM	LR	PR	GP	DNN	SNN
<i>Training</i>						
RMSE	13.938	13.020	12.952	10.472	11.748	9.347
MAE	11.460	10.594	10.398	8.132	9.303	6.581
<i>Testing</i>						
RMSE	55.632	61.252	64.093	69.324	71.220	73.549
MAE	52.982	58.190	59.595	66.685	65.817	70.499

Results of the comparison are given in Table 1 using two essential metrics for evaluation as follows: the root mean-squared error (RMSE) and mean absolute error (MAE).

The results show that the SNN has the best training attitude (trained well) and the worst testing accuracy in the same time. That means that it has no resistance towards over-fitting and empirical risks.

SVM has an acceptable average accuracy of training (not the best and not the worst), but it proves its resistance towards ill-posed problems by achieving the best testing accuracy in both used metrics.

The order of the algorithms in Table 1 is addressed by using the testing accuracy starting from the best average. The results also prove that the simple training tools LR, PR and SVM work better than other neural networks and Gaussian process which might need a lot of computational cost due to their algorithmic complexity.

An example of curve fitting of the RUL degradation function using all the trained approximation models with the previously mentioned algorithms for one life cycle of the engine from FD001 subset is illustrated in Fig. 3.

4 Conclusion

In this work, in order to determine the optimal algorithm for future uses in RUL prediction of aircraft engines, a comparative study between several approaches is aborted. The comparison experiences were carried out under “time-varying” data retrieved from C-MAPPSS software.

Only a single subset from the data set is studied in this paper. The subset FD001 describes one single failure mode related to the health deterioration of the high-pressure compressor under sea level operating conditions.

In this benchmark, the results prove that SVM and basic linear and polynomial regression algorithms work better than recent training tools such as DNN, SNN and GP.

The subject of the future works will focus on optimizing or studying SVM variants to enhance and construct a more competitive data-driven approach to the others in the literature.

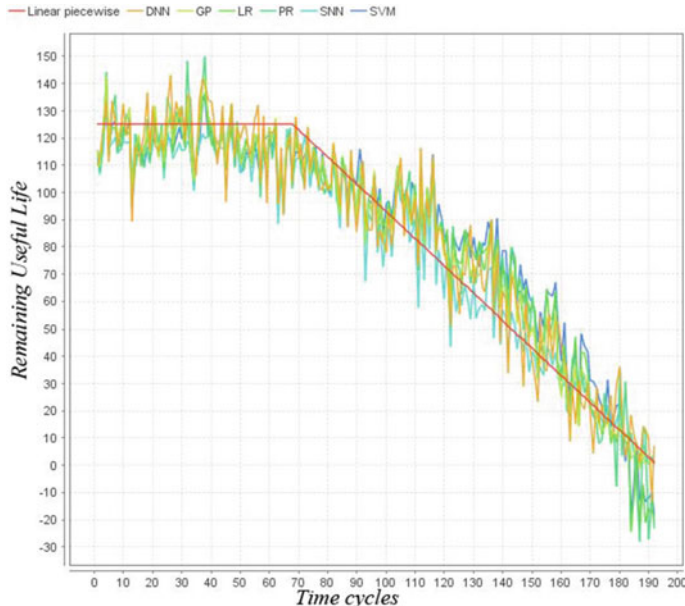


Fig. 3 RUL curve fitting with different algorithms

References

1. Navathe SB, Wu W, Shekhar S, Du X, Sean Wang X, Xiong H (2016) Database systems for advanced applications: 21st international conference, DASFAA 2016 Dallas, TX, USA, April 16–19, 2016 Proceedings, Part I, Lect. Notes Comput. Sci. (including Subser. Lect. Notes Artif. Intell. Lect. Notes Bioinformatics), vol 9642, pp 214–228
2. Zhao Z, Liang B, Wang X, Lu W (2017) Remaining useful life prediction of aircraft engine based on degradation pattern learning. Reliab Eng Syst Saf 164(457):74–83
3. Ordóñez C, Sánchez Lasheras F, Roca-Pardiñas J, de C. Juez FJ, A hybrid ARIMA–SVM model for the study of the remaining useful life of aircraft engines. J Comput Appl Math 346:184–191 (2019)
4. Parker K, Melcher K (2004) The modular aero-propulsion system simulation (MAPSS) users' guide
5. Saxena A, Goebel K, Simon D, Eklund N (2008) Damage propagation modeling
6. Saxena A, Ieee M, Goebel K, Simon D, Eklund N (2008) Damage propagation modeling for aircraft engine prognostics. Response
7. BERGHOUT Tarek, Mouss LH, Kadri O (2019) RUL prediction (C-MAPSS dataset), [Online]. Available: <https://www.mathworks.com/matlabcentral/fileexchange/73629-rul-prediction-c-mapss-dataset>

Survey Analysis for Medical Image Compression Techniques



Baidaa A. Al-Salamee and Dhiah Al-Shammary

Abstract This paper presents a survey for medical image compression for both lossy and lossless approaches. This survey discusses twenty-five publications with several applied lossy and lossless compression techniques. All approaches are distributed into seven groups based on the applied technique. Fractals, wavelet, region of interest (ROI) and non-region of interest (Non-ROI), and other approaches represent four lossy compression groups. Adaptive block size, least square, and other approaches represent three lossless medical image compression techniques. Technically, medical image communication requires large space to be represented and sent over the network creating a number of challenges in terms of interaction, processing, storage, and transmission operations. Therefore, significant compression ratio (CR) and peak signal-to-noise ratio (PSNR) are always targeted in image communication. Both CR and PSNR are considered in this survey as the main metrics to investigate and evaluate models performance. As a result of this survey analysis, ROI and Non-ROI has shown the best average CR with 91, and wavelet has shown the best average PSNR with 80.

Keywords Medical · Image · Compression · CT image · MRI

1 Introduction

Medically, the demand for remote imaging systems is increasing rapidly [1]. Several medical services are provided by remote imaging communication such as remote diagnose and monitoring [2]. Evidently, the number of remote patients utilizing of telecommunications and for clinical services is growing up potentially [3]. CT and

B. A. Al-Salamee · D. Al-Shammary (✉)

College of Computer Science and Information Technology, University of Al-Qadisiyah,

Diwaniyah, Iraq

e-mail: d.alshammary@qu.edu.iq

B. A. Al-Salamee

e-mail: baidaa.alsalamee@qu.edu.iq

MRI images are widely used over remote medical imaging applications in addition to few more types [4].

1.1 Motivation

Telemedicine applications are relied on various forms to represent data such as videos and images transmitted over the network systems and applications [5]. Technically, medical forms usually require large amounts of data to construct highly quality elements in order to avoid wrong or inaccurate diagnosis [6]. Consequently, there are some potential challenges facing telemedicine applications such as:

- **Storage Problem:** The tremendous data for thousands patients would be stored and probably for a long time. Therefore, devices with high storage capacity are essential.
- **Network Low Bandwidth:** Low bandwidth is technically caused by high number and large size of medical images sent/received over the network. High bandwidth is usually required for medical imaging applications in order to satisfy the significant quality obligated by medical requirements.

1.2 Existing Solutions

This paper presents a survey for potential medical image compression techniques. Both lossy and lossless approaches for medical images are included and analyzed. Twenty-five compression approaches are described and distributed into seven groups based on applied method. These groups represent four groups for lossy medical image approaches: fractals, wavelet, ROI and Non-ROI, and other lossy approaches. Moreover, three groups represent lossless medical image approaches: adaptive block size, least square, and other lossless approaches. Wide range of approaches has been developed for medical image compression with successful performance. Technically, all included approaches have targeted high image quality and efficient compression ratio. However, some lossless models have been applied in such an interesting architecture with the ability to control image quality (PSNR) over the remote image communication system in order to adjust network bandwidth utilization, although they are designed to reconstruct identical images with infinity PSNR.

1.3 Evaluation and Analysis

The main strategy used to investigate the efficiency of the presented models relies on compression ratio (CR) and peak signal-to-noise ratio (PSNR). Therefore, CR and PSNR are extracted from all included publications and listed in corresponding

tables in regard to the designed analysis groups. In principle, compression approaches are compared with each other inside their groups. Furthermore, summarized results such as average CR and average PSNR are calculated for each approach group and compared with other groups in order to investigate models persistent performance. Technically, ROI and Non-ROI-based compression approaches have outperformed other lossy medical image compression in terms of average CR up to 91. On the other hand, wavelet-based lossy approaches have outperformed other lossy approaches in terms of image quality with average PSNR up to 80. In regards to lossless approaches, least square-based approaches have achieved the highest CR (8) while both least square and adaptive block-based approaches have achieved the highest PSNR (60). Evidently, ROI and Non-ROI has shown the best CR and wavelet has shown the best PSNR.

1.4 Paper Organization

The rest of this paper is organized as follows: Sect. 2 describes lossy compression for medical images include four subsections illustrating main approaches groups: fractals, wavelet, ROI and Non-ROI, and other approaches. Lossless compression for medical images is illustrated in Sect. 3 including three subsections allocated to main approaches groups: adaptive block size, least square, and other approaches. Analysis and evaluation are presented in Sect. 4. Finally, conclusions are presented in Sect. 5.

2 Lossy Compression for Medical Images

Lossy compression approaches have represented a potential solution in medical network services and especially for medical images like CT and MRI. Technically, lossy compression for medical images faces a significant challenge of preserving high quality and keeping sensitive information available without damage. This section has addressed the main proposed solutions based on different methodologies such as fractals and wavelet transform and more.

2.1 Fractal-Based Compression Technique

Fractal similarity measurement has been a potential direction of many compression solutions for images [7]. Fractal-based image compression has shown significant efficiency evident by high compression ratio and PSNR [8]. Furthermore, several fractal-based models have been developed specifically for CT and MRI medical images [9]. Maha Lakshmi [4] has addressed the MRI high volume problem trying

to find the best models to reduce its size. The research has focused on fractals image compression significant processing time as a main obstacle against developers using fractals. This research has proposed fractal image compression as a potential model to reduce MRI size. Moreover, a new model has been developed using neural network as an efficient strategy to solve the time-consuming problem for fractals. The fractals range blocks index is dedicated to be the input for trained system. In order to evaluate their proposed solution, compression ratio and processing time are computed and compared with other techniques. Several original images reconstructed brain MRI samples are used to investigate the capabilities of their models. The best obtained results are around 36 PSNR with average of 10 compression ratio. Although the neural network algorithm has shown great improvement for the proposed FIC processing time (more than 400 s), it is still considered to be time consuming, especially with low size MRI samples (about 193 KB). Furthermore, the not persistent PSNR values (drop from 36–25) for the IFIC (fractals with neural network) do not confirm IFIC as the right approach to reduce processing time for fractals.

Another study achieved by Suresh Kumar et al. [5] that has addressed the problem of MRI images compression and how to develop fractals compression to achieve better quality with higher performance. Presented a novel model that attempt to estimate affine parameters of fractals with the aim to minimize the complexity of computation for MRI compressed images. The paper has proposed near-lossless image compression using fractal texture identification (NLICPFTI) which have used pattern dictionary to utilize repeated fractal patterns after the detection for maximum fractal patterns from an image. Furthermore, oriented Gaussian filter has been proposed as an edge detection for fractal patterns identification. Five metrics: PSNR, EPSNR, FSIM, SSIM, and CR are used to investigate the proposed model performance. Moreover, NLICPFTI has been compared with three other models: an improved image compression algorithm using wavelet and fractional cosine transform (AIICA), high level synthesis for retiming stochastic VLSI signal processing architectures (HLSRSVS), and VLSI implementation of a cost-efficient near-lossless CFA image compressor for wireless capsule endoscopy (VICENLCFAIC). The obtained PSNR for the proposed model starts from 39.98 to 42.88 which is considered to be high quality while the other models have achieved PSNR from 29.11 to 35.86. For EPSNR, NLICPFTI has resulted in a high EPSNR start from 31.17 to 34.02 while other models are 18.48–26.93. Furthermore, the proposed model has achieved CR about 2.36–2.41 which are higher than other models (1.20–1.56). Ten datasets are used for experiments and evaluation. Each dataset contains five MRI images. This paper has resulted in CR of 2.4 and PSNR of 42.88 as best values in comparison with other models. Although the proposed model has shown higher results in comparison with three other models, the obtained CR is considered to be very low for a lossy compression model. The proposed architecture for parallel fractals and affine parameters is not clarified in detail and not clear how the complexity has been reduced. Moreover, the processing time is missing from this paper, and therefore it is hard to recognize its performance.

With the aim to reduce image size with quality preservation, Magar et al. [6] have addressed the problem of large amounts of the medical image size that requires large storage and bandwidth to be sent/received over the networks. This paper has produced

a hybrid compression technique using the oscillation concept and quasi-fractal-based on the concepts of region of interest (ROI) and non-region of interest (Non-ROI). Technically, ROI—represent a vital part of a medical image—has been compressed using lossless compression (oscillation concept). On the other hand, Non-ROI has been compressed using lossy compression (quasi-fractal). The hybrid model has been implemented using morphological filter and adaptive thresholding. PSNR and CR were the main metrics used for evaluation. Furthermore, the proposed model results have been compared with other models instance: hybrid coding using biomedical-set partitioning in hierarchical trees (BTC-SPIHT), fractal, and discrete wavelet transform (DWT). CR has reached about (24) for the proposed model while other models have reached about (5, 3, and 1) for BTC-SPIHT, fractal, and DWT, respectively. Likewise, the resultant PSNR for the proposed model has reached about 33, while other models have reached about (33, 31, and 29) for BTC-SPIHT, fractal, and DWT, respectively. Several medical images have been used to test the performance of the proposed model. The best obtained results of this paper were: PSNR about 33 and CR about 24. PSNR and CR metrics have reached high scores. However, the evaluation was missing the time metric—encoding and decoding time—that made it unclear for the model efficiency.

2.2 *Wavelet Transform-Based Compression Technique*

Transform-based image compression (encoding) is one of the most effective models like wavelet methods [5]. The encoder function transforms the data to remove redundancy, then the transform coefficients are quantized and lastly entropy encoding is applied on the quantization output. Uma Vetri Selvi et al. [7] have discussed the problem of large amount of medical image size causing many limitations for both fast transfer and efficient storage. They have attempted to achieve suitable size reduction and maintain high quality. This article has proposed wavelet-based contourlet transform (WBCT) and binary array technique (BAT) in order to construct a rapid 2-D lossy compression technique. Both computed tomography (CT) and magnetic resonance imaging (MRI) have been applied. First, a high frequency subband has obtained from a wavelet transform. Then, it has further decomposed using directional filter bank in order to obtain more directional subbands in WBCT. Consequently, coefficients have included more direction though the relationship of subbands has been changed in WBCT. A repositioning algorithm has been applied to handle differences of relationships. Then, the quantization process has been applied on the repositioned coefficient. Finally, further compression has been implemented on the quantized coefficients by (BAT) as the high frequent value is coded only once. The main metrics have been applied to evaluate the performance of the proposed model are: PSNR, CR, and time processing. Moreover, there is a comparison between the proposed method and two other models called wavelet + SPIHT (wavelet-based set partitioning in hierarchical trees) and wavelet + SPECK (wavelet-based set partitioning embedded block). Empirically, the proposed method has resulted in CR about (4.9–6.3) while

other models resultant CR are about (6.08–6.66) and (5.8–6.9) for wavelet + SPIHT and wavelet + SPECK, respectively. On the other hand, the proposed method has achieved PSNR about (81–101) while (87–99) for wavelet + SPIHT and (87–98) for wavelet + SPECK. Finally, the proposed method has outperformed other models in terms of processing time as it mainly consumes about 5 s for both encoding and decoding while other models have consumed about (20–100 s). Twenty-one sets of real-time MRI 16-bit images and forty-five sets of real-time CT 16-bit have been applied in this article for analysis and evaluation. Best obtained results are: PSNR about 101, CR about 6.3, and processing about 5 s. The researchers have achieved excellent results in this paper, especially in terms of time processing in comparison with other models. However, CR is considered to be low according to lossy compression methods.

In order to reduce image size with an attempt for keeping high quality, Paul Nii Tackie Ammah et al. [8] have addressed the problem of large data required to construct accurate medical images in order to avoid wrong diagnosis. Therefore, several problems are rising in terms of storage capacity and transmission rate. This paper has proposed a compression model named: wavelet transform-vector quantization. The hybrid technique has largely reduced speckle and salt and pepper noises of ultrasound imagery. Otherwise, the process has preserved the edge with a little effect. Then, DWT has been applied to filter images. Moreover, coefficients have been generated using efficient means of threshold approach. Finally, obtained results have been vector quantized and encoded using Huffman technique. DWD-VQ model was evaluated and tested using two metrics: PSNR and CR. Additionally, the results of the proposed model have been compared with other models instance: region of interest (ROI)-based medical image compression for telemedicine application and wavelet-based medical image compression for telemedicine application. Empirically, the resultant PSNR for the proposed model was (43–60) while other models about 53 and 37 for ROI and wavelet, respectively. Meanwhile, obtained CR was (90–91) for the proposed model, whereas other models have shown 89 and 87 for ROI and wavelet, respectively. In order to evaluate the proposed model performance, different types of medical images have been used. The best achieved results are: PSNR about 60 and CR about 91. Despite significantly efficient results have been achieved using DWT-VQ, execution time was not computed. Therefore, the performance accurate metrics are considered to be insufficient.

2.3 Lossy Approaches Based on ROI and Non-ROI

Several researches have been achieved in target of developing both lossy and lossless approaches by utilizing region of interest (ROI) and Non-ROI with promising efficiency. In order to keep the vital information from being lost in medical images that represent a valuable data for diagnosing diseases, several techniques divide the image to two parts region of interest (ROI) and non-region of interest (Non-ROI) [4]. Consequently, ROI would be compressed with lossless technique while Non-ROI would

be compressed by lossy method. Sabbavarapu et al. [9] have discussed the large medical image sizes such as MR and CT as they have attempted to minimize their size and decrease the redundancies in order to resolve storage issues and bandwidth problems. Based on region of interest (ROI) and Non-ROI concepts, this paper has presented a hybrid compression (i.e., the combination of lossy and lossless compression) by using recurrent neural network RNN and discrete wavelet transform (DWT). Region growing and Otsu thresholding have been proposed to identify and separate the ROI and Non-ROI regions of the image. ROI should contain vital information, and therefore DWT (lossless compression) has been applied to completely maintain vital information. On the other hand, Non-ROI has considered image background information (not vital), and therefore RNN (lossy compression) has been applied. PSNR and CR results have been computed and compared with three other models, namely fractional-order Darwinian PSO (FODPSO), quasi-fractal and oscillation method (QFOM), and Burrows–Wheeler transform (BWT-MTF). Average PSNR obtained by the proposed model is about 35. In comparison, other models have achieved PSNR 22, 33, and 34 for FODPSO, QFOM, and BWT-MTF, respectively. Likewise, resultant CR is about 23 while other models have achieved 2, 24, and 4 for FODPSO, QFOM, and BWT-MTF, respectively. Experimentally, fifteen different MR and CT medical images have been used to analyze and validate the model's performance. These samples have been taken from MedPix database. The best obtained results are 35 for PSNR and 23 for CR. Although the proposed model has achieved high PSNR and CR results, encoding time was missing from this paper and leaves the reader with unclear picture for performance analysis. Furthermore, this model has been designed for images that may be contain important and not important information, and the evaluation had not considered general samples in order to provide a clear behavior analysis on this kind of images.

Eben Sophia et al. [10] have aimed to develop a technique to produce good quality at lower bit rate by discussed how to optimize and develop the contextual compression technique that plays an important role of medical image compression with preserving their diagnostics information. This article has proposed a hybrid method using wavelet and contourlet transform for contextual compression and particle swarm optimization (PSO). PSO was applied to mask transformed coefficients before prediction in order to obtain optimized threshold value. Contextual region has been detected as a portion containing region of interest (ROI) and the remaining image as non-region of interest (Non-ROI). ROI part has been coded as lossless or with less loss while Non-ROI part has been coded with more loss. LGD (Gaussian distribution) has been used to identify ROI and Non-ROI. ROI has been compressed near-lossless using wavelet transform. On the other hand, lossy compression has been applied on Non-ROI using wavelet and contourlet transform then arithmetic coding technique to encode the compressed data. In order to check the performance of the proposed model, two metrics have been used: PSNR and CR. Furthermore, PSNR results have been compared with other models named, EBCOT-ROI, maxshift, and implicit. Experimentally, the resultant CR for the proposed model started from 16 to 144. On the other hand, PSNR has been achieved for the proposed model (30–40) while other models have achieved (24–38), (27–38), (24–35) for EBCOT-ROI, maxshift,

and implicit, respectively. The samples have been used for experimentation and evaluation obtained from multimedia digital archiving system, <https://overcode.yak.net/15?size15> O&size and <https://www.osirix-viewer.com/datasets/> databases. The best shown results are: PSNR about 40 and CR about 144. High results of PSNR and CR have been achieved in this paper. However, the execution time—represent an important metric for an efficient compression model—was missing. Furthermore, the size of testing images was relatively small (512×512), especially for medical images that usually have large amount of data. Technically, PSO has relatively caused an increase in both encoding time and bit rate.

Another compression method by Manimekalai et al. [11] that have been proposed for magnetic resonance imaging (MRI) based on the concepts region of interest (ROI) and non-region of interest (Non-ROI) after addressed the problem of large amount of medical images size which representing an obstacle for networks bandwidth and storage. They have aimed to minimize images size with high quality for diagnostics and analysis objectives. Initially, the pre-process step has been manipulated them by means of median filter. It is also involved detection and separation ROI and Non-ROI using deep fully convolution networks with Jaccard distance. Next, the ROI edge has been taken out which was encrypted with freeman chain coding. Furthermore, ROI part has been compressed by hybrid Lempel-ZIV-Welch and clipped histogram equalization (CHF). Technically, particle swarm optimization (PSO) technique has been used in order to choose an ideal threshold value in CHE for enhanced the brightness. Finally, Non-ROI has been compressed using enhanced zero tree wavelet (EZW). Moreover, firefly algorithm has been used in EZW technique involved to choose a preliminary threshold. PSNR and CR have been used as main metrics in order to validate the efficiency of the proposed model (hybrid LZW and CHE). Moreover, the proposed method has been compared with other models called: LZW, fully convolutional networks (FCN) with Jaccard distance in terms of evaluation metrics. Hybrid LZW and CHE model has resulted in CR about (85–94) while other models about (80–87) and (83–90) for FCN and LZW, respectively. On the other hand, PSNR has reached about (41–56) by the proposed model while other models have obtained less values (38–52) and (40–54) for FCN and LZW, respectively. Many MRI images have been used as evaluation samples for the analysis process. CR about 94 and PSNR about 56 have been achieved as best result. Despite the excellent results have been achieved in this article, the performance metrics were insufficient since their evaluation was lacking of the processing time measurements. Furthermore, a number and size of evaluation samples were missing from this paper which made the model behavior not guaranteed.

With the estimation of the brain tumor location, Kumarganesh et al. [12] have proposed a brain tissue compression method to solve the problem of the large amount of the brain images (tissue) size contained a tumor that require high storage and more transmission time. They have aimed to reduce the size without quality degradation. The model has detected and segmented the tissue and the tumor based on mathematical morphological operations. Then, lossless compression technique has been applied on the brain tissue with tumor and lossy compression technique on the brain tissue without tumor. In order to validate the proposed model performance, two

metrics have been used: PSNR and CR. Empirically, PSNR has reached about 31. Moreover, the proposed model has resulted in CR about 37. Twenty normal images and ten abnormal images have been used for analysis and evaluation purposes. The best achieved results are: PSNR about 31 and CR about 37. The proposed system has reached significant results. However, the lacking for computing the execution time made the model efficiency not clear. Moreover, some comparison results between the proposed model and other models were not shown.

By the visual saliency representing an emulation of the human visual system, Paramveer Kaur Sran et al. [13] have proposed a compression algorithm based on the concept of region of interest (ROI) and non-region of interest (Non-ROI). They have discussed the problem of medical images that construct of large amount of data that caused many obstacles in healthcare systems, especially in terms of storage areas and transmission speed. The researchers have attempted to reduce the size of images without impact the quality. The proposed technique has been performed in two phases. Firstly, the detection and extraction of ROI were applied using an automatic saliency-based fuzzy C-means clustering algorithm (SAL-FCM). Secondly, ROI set partitioning in hierarchical trees (ROI-SPIHT) algorithm was applied to encode both ROI and Non-ROI at high and low bit rate, respectively. Furthermore, wavelet using a lifting scheme has been executed to minimize the computational complexity for the proposed method. ROI-SPIHT model has been evaluated using two main metrics: PSNR and CR. Furthermore, the results of the proposed system have been compared with other models called: JPEG, JPEG2000, and SPIHT. Experimentally, PSNR has reached about (29–39) while other models have obtained about (23–30), (24–31), and (33–42) for JPEG, JPEG2000, and SPIHT, respectively. Meanwhile, ROI-SPIHT has resulted in CR about (25–160). The BRATS database from <https://www.smir.ch/BRATS/Start2015>. has been used for testing and analyzing the proposed model. The size of database images was 256×256 . The best obtained results are: PSNR about 39 and CR about 160. The results of ROI-SPIHT model were practically excellent. However, the execution time was not computed. Therefore, the performance elements are insufficient. Moreover, the SPIHT model has outperformed the proposed model in terms of PSNR. Additionally, the size of MRI images used for evaluation was small according to the usual large sizes of medical image. Finally, CR comparison between the model and other models was missing made the efficiency of the model is unguaranteed.

2.4 Other Lossy Approaches

There are several other irreversible lossy approaches used by many researchers to get a minimum image size with high compression ratio. Parikh et al. [14] have addressed the problem of the large amount of medical image sizes that represent an obstacle for storing and retrieval operation over the network. Generally, this has significant effects on costs and accessibility for cloud-based healthcare services. They have attempted to minimize image size with preserving quality. They have proposed high

efficiency video coding (HEVC) as a new format for medical images. Technically, HEVC has provided better compression efficiency in comparison with JPEG2000 (is commonly used format for medical images alongside with DICOM digital imaging and communication in medicine). Three metrics (PSNR, CR, and encoding time) have been used in order to validate HEVC efficiency. Moreover, the proposed model results have been compared with JPEG2000 (J2K) results. PSNR and CR for the model are about (from 45 to 62 and from 8 to 50), respectively. On the other hand, J2K results are from 48 to 65 for PSNR and from 8 to 40 for CR. Finally, HEVC has potentially outperformed J2K in terms of time as it consumes about (50–55%) in comparison with J2K. Different MRI, CT, and CR images have been used as samples for evaluation and experimentation. The best results were: PSNR and CR about 62 and 50, respectively. Furthermore, HEVC consumes about 55% of J2K. Despite the superiority is evident to the model in terms of encoding time and CR, there is an increase rate in compressed file size in some cases when complexity is reduced. Moreover, the medical image samples have relatively little resolution that did not assure the same system behavior for high definition medical images.

To produce a method capable of reducing sizes and preserving high quality, Ranjeet Kumar et al. [15] have addressed the problem of big data size of images that consume large amounts of storage space and transmission time. This paper has proposed matrix completion technique for image compression and quality retrieval. This approach was based on low-rank matrix using a unique truncation and thresholding value. The decomposition (SVD) to get a low rank of image data that has been approximated in compressed form. Visual quality of the compressed image has been retrieved using singular value thresholding algorithm. Three essential metrics (PSNR, CR, and encoding time) have been used to test the performance of the proposed model. The proposed model has resulted in [5, (9–26), 0.03 s.] for CR, PSNR, and encoding time, respectively. Six different types of images have been used for evaluation and testing purposes. Five images with size of 512×512 and only one image has size of 1024×1024 . CR about 5, PSNR about 26, and encoding time about 0.03 s. have been achieved as best results. PSNR results for the proposed model are considered to be very low as they obtain PSNR of 9 in some samples. On the other hand, a CR of 5 is not a potential achievement for a lossy model. Moreover, several values for PSNR, CR, and encoding time have been missed for other models when compared to the proposed model. Finally, the usage of only six samples to evaluate the performance considered to be insufficient.

Anitha et al. [16] have attempted to curtail images size with maintain their quality through their addressed the problem of a large data in digital medical images that is caused several problems in visualization, interaction, transmission, and storage. This article has proposed a compression method based on improved ripplet transform. The traditional ripplet transform has progressed by lossless predicted and decomposed lossy singular value for the coefficients of the transform. Lossless prediction has benefited the correlation between image pixels with facilitated the transform operation. Furthermore, singular value decomposition technique has carried out to get the vital information of the high frequency coefficients. Therefore, fast and efficient computationally randomization has been obtained. Finally, the components of

low and high frequency have been encoded by entropy method. The analyzing and testing performance of RT-prediction-RSVD (proposed model) has been performed using PSNR and execution time metrics. Moreover, results of the proposed method have been compared with other models such as ripplet and JPEG2000. Technically, RT-prediction-RSVD model has resulted in PSNR about (28–37) while other models have obtained about (26–33) and (27–35) for ripplet and JPEG2000, respectively. On the other hand, (3–12 s) of execution time has been consumed by the proposed model while ripplet model has consumed about (3–14 s) MRI and CT images downloaded from Osirix online database have been used for evaluation purposes. Their sizes start from 256×256 to 512×512 . The best achieved results are: PSNR about 37 and processing time about 3 s. Although the effective results have been obtained using this improved technique, CR was entirely missing. Therefore, the efficiency analysis was insufficient. Furthermore, the size of testing samples was very little according to usual large size of medical images.

Neural networks have several applications in the field of telecommunication and computer science in addition to simulating the learning approach of human brains [10]. With the widespread multimedia applications and their products where information processing and communication is the main problem, neural networks play an essential role in this special area [11]. Recent publications have clarified a substantial increase in neural networks for medical image compression and decompression [12]. K. J. et al. [17] have discussed the problem of potential losing vital information when using lossy JPEG compression approach with medical images. They have attempted to improve the decompression of lossy JPEG model by achieving high quality. The researchers have proposed a novel cross-domain cascade of U-Net named: the W-Net. The degradation of the image using traditional lossy JPEG compression has usually occurred because of the lossy precision in discrete cosine transform (DCT) domain resulting from 8×8 image blocks quantization. The proposed method using operated DCT domain network has shown significant ability to recover the discarded DCT coefficients benefited from neighbor blocks information. Then, these information and image domains have been used to resolve any artifacts at the image pixel level. PSNR has been computed as a main metric for evaluating the proposed method (DIW-Net). Furthermore, there is a comparison between the proposed model and other model instances: JPEG and DI-AUTOMAP. Experimentally, PSNR of (30–37) have been obtained for DIW-Net while other models have obtained (29–36) and (28–35) for DI-AUTOMAP and JPEG, respectively. Many MRI images from the Calgary-Campinas-359 (CC-359) dataset have been used as testing samples. PSNR about 37 has been achieved as best result. Despite the obvious improvement in PSNR results for the proposed model, the percentage change in results compared to traditional JPEG decompression technically was very simple. Furthermore, the decoding time was missing from this article. Therefore, the performance of the model is unguaranteed.

3 Lossless Compression for Medical Images

Lossless compression approaches for medical images are an obligatory direction in many medical applications because of the sensitivity of their medical information. Medically, some medical cases cannot be diagnosed as a result of the lost information occurred by lossy compression. Therefore, lossless approaches represent a potential motivation for researchers and developers in order to satisfy medical applications requirements. This section has addressed main potential lossless approaches for medical images such as adaptive block size and least square methods in addition to several other models.

3.1 Adaptive Block Size-Based Compression Technique

Many approaches for image compression are based on adaptive block size method in order to achieve higher efficiency [15]. Sharma et al. [18] have discussed the problem of tremendous data required for representing medical images. Technically, storage, interaction, and transmission operations on these images would be very expensive. The researchers have tried to reduce images size with the attempt to keep high quality. This article has suggested near-lossless compression algorithm. The proposed algorithm has used predictor based on modality and resolution independent threshold, optimal level quantization, and encoding of adaptive block size. In order to remove the redundancy inter-pixel, resolution independent gradient edge detector (RIGED) has been applied. Furthermore, BAAT block adaptive arithmetic encoding has been implemented after quantization to take off coding redundancy. PSNR has been measured as an essential metric for evaluating the proposed model performance. Moreover, there is a comparison between the proposed model and other models named: differential pulse code modulation (DPCM) and set partitioning in hierachal trees (SPIHT). Technically, the proposed model has resulted in a PSNR about 60 while other models have obtained about 45 for both DPCM and SPIHT. Many CT and MRI images—sizes between 256×256 and 512×512 —have been used for experimentation and evaluation. The images have been acquired from CIPR and MRI images from the Computer Vision Group at the University of Granada. PSNR about 60 has been obtained as best result. Although the excellent quality results have been achieved by the proposed model, CR and execution time were missing from this article. Furthermore, the size of the samples was very little. Therefore, the efficiency of the proposed model is considered to be ambiguous.

Song et al. [19] have had an effort to minimize images size without impact the quality through discussed the challenge of large amount of medical sequence images size representing a bottleneck for storage, processing, and communication requirements. The research paper has proposed a novel near-lossless compression algorithm. The proposed method has used spatial prediction based on adaptive block size for blocks prediction in the spatial domain directly. Furthermore, lossless Hadamard

transform has been applied before quantization to refine the reconstructed image quality. In order to check the proposed model efficiency, PSNR has been computed as a main metric. Furthermore, the obtained results of the proposed method have been compared with other models named: differential pulse code modulation (DPCM), set partitioning in hierachal trees (SPIHT). Empirically, the proposed model has resulted in a PSNR about 59 while other models have achieved about 45 for all other models. Nine datasets that contained different types of images have been used for testing and analyzing objectives. The images were captured from Mallinckrodt Institute of Radiology Image Processing Laboratory, at CIPR <https://www.cipr.rpi.edu/resource/sequences/sequence01.html>, and MRI images from the Computer Vision Group at the University of Granada. About 59 PSNR has been obtained as best result. The proposed model has achieved significant PSNR result. However, the efficiency and performance metrics were insufficient since their lacking for CR and processing time.

3.2 Least Square-Based Compression Technique

Least square method is a statistical procedure to find the best fit for a set of data points by reducing the sum of the offsets or residuals of points from the plotted curve [6]. Song et al. [20] have addressed the problem of large medical images size that playing an essential role for high-speed transmission and efficient storage between healthcare organizations. They have aimed to minimize the sizes vs high quality. This article has proposed a lossless compression algorithm. Firstly, adaptive irregular segmentation of images has been performed based on hybrid technique constructed of geometry-adaptive partitioning with quadtree partitioning. Adaptive predictors that were designed for each region (irregular subregion or regular subblock) based on least square (LS). Only encoding time metric has been applied for evaluating the proposed model performance. Moreover, results of the proposed model have been compared with other models called edge director prediction (EDP). Practically, the proposed model has resulted in encoding time about (1–3 s) while EDP has consumed about (1–2 s). Several CT and MRI images have been used as evaluation samples. The images have been taken from the Mallinckrodt Institute of Radiology Image Processing Laboratory (available at CIPR) and Computer Vision Group of the University of Granada. The best obtained result is about 1 s. of encoding time. Although the proposed model has achieved high scores, the performance metrics were lacking for computation of CR. Furthermore, the encoding time of EDP model has outperformed the proposed model. Therefore, the proposed model is considered to be unclear in terms of accurate performance.

Technically, suitable size with high quality was the main goal for Kumar et al. [21] that have discussed the problem of large sizes for medical images, especially CT images representing an obstacle for efficient storage and transmission. This paper has proposed a lossless compression algorithm based on prediction using least square technique. Initially, the processing has been performed using neutrosophic median filter. Next, prediction coefficients have been determined by the gradient adjusted prediction method. Then, the selection of optimal coefficients has been applied by

polynomial least square fitting scheme. Finally, the prediction coefficients results have been encoded using Huffman coder. In order to check the proposed model efficiency, PSNR and CR have been measured. Moreover, the results of NS-LS model (proposed model) have been compared with three other models called: bat optimization-based vector quantization (BAT-VQ), JPEG lossy, and JPEG lossless. Experimentally, PSNR have reached (53–60) for NS-LS while other models (33–35), (30–36), and (35–40) for BAT-VQ, JPEG lossy, and JPEG lossless, respectively. Meanwhile, NS-LS has been resulted in CR about (5–8), whereas other models (3), (8–9) and (6–7) for BAT-VQ, JPEG lossy, and JPEG lossless, respectively. Four datasets consist of CT images from Metro Scans and Research Laboratory, Thiruvananthapuram have been used for evaluated and testing intentions. The image's size was 512×512 . PSNR about 60, CR about 8 have been shown as best result. Technically, high obtained results have been achieved using NS-LS model. However, execution time was not computed. Furthermore, the size of image samples was very little. Therefore, NS-LS performance stays ambiguous.

3.3 Other Lossless Approaches

There are several techniques used by researchers to compress the images without any loss in reconstructed image. Geetha et al. [22] have addressed the problem of the large sizes of medical images causing communication obstacles. Moreover, keeping the fine details of medical images is a big challenge. This paper has presented a model based on Linde–Buzo–Gray (LBG) algorithm that commonly used vector quantization (VQ) which is a popular image compression method. This algorithm constructs a local optimal codebook to compress image. Construction of VQ codebook is an optimization problem as L2-LBG has been proposed using lion optimization algorithm (LOA) for the codebook construction. Technically, Lempel–Ziv–Markov chain algorithm (LZMA) has been applied to compress index table in addition to improving LOA compression performance. Two types of metrics have been applied to validate the proposed method performance. First type aim to validate compression efficiency such as CR, CF, and bitrate. Second type aims to validate image quality such as MSE, RMSE, and PSNR. Furthermore, L2-LBG has been evaluated in comparison with cuckoo search-based LBG (CS-LBG), firefly-based LBG (FF-LBG), and JPEG 2000. Empirically, L2-LBG has resulted in CR around 0.14–0.58 while other comparison models have resulted in CR around 0.17–0.95. Similarly, L2-LBG has resulted in CF around 1.6–6.9 while other models have resulted in CF around 1.04–5.8. Evidently, L2-LBG has shown less bitrate (1.14–4.87) in comparison with other models (1.36–7.92). On the other hand, L2-LBG has achieved better MSE (0.17–0.76), RMSE (0.41–0.87), and PSNR (49.32–55.82) than other models MSE (0.22–2.34), RMSE (0.46–1.52), and PSNR (44.43–54.70). Eight different benchmark medical images have been applied using three datasets: diabetic retinopathy (<https://www.kaggle.com/c/diabetic-retinopathy-detection/data>), mammography (<https://peipa.essex.ac.uk/info/mias.html>), and brain tumor (<https://www.aboutcancer.com/mri-gbm.htm>).

The best average results achieved for CR was about 0.34 and for PSNR was about 52.62. It is clear that the behavior of the proposed system is not persistent as the largest size of image samples did not reflect the highest CF, although their information redundancies are quite clear. Moreover, processing time and complexity are missing from the evaluation as they are essential for medical applications.

Haouam et al. [23] have proposed a hybrid algorithm combining geometric active contour model and biorthogonal wavelet transform as an attempt to solve the problem of large medical image sizes through reducing them without losing their quality that is crucial for medical diagnosis. This model requires to identify region of interest (ROI), and therefore level set technique has been applied. Then, lifting scheme biorthogonal CDF (biorthogonal lifting scheme CDF 9/7, Gall 5/3 and FB) combined with the set partitioning in hierarchical trees algorithm (SPIHT) are applied. Two metrics have been used for analysis purposes in order to measure model's performance with PSNR and mean structural similarity (MSSIM). Moreover, tree algorithms presented in this paper are compared with each other by using segmentation technique (level set) and without segmentation. The obtained results have shown CDF 9/7 (lifting) in the presence of segmentation technique is the best as it scores the highest PSNR (34–56) and MSSIM (0.78–0.99). Furthermore, GALL 5/3 (lifting) and filter bank have resulted in (PSNR 30–54, MSSIM 0.74–0.99) and (PSNR 27–51, MSSIM 0.64–0.98), respectively. On the other hand, GALL 5/3 (lifting) without segmentation has outperformed other models with (PSNR 25–52, MSSIM 0.76–0.99), while CDF 9/7 (lifting) without segmentation has resulted in (PSNR 23–49, MSSIM 0.59–0.98). Different grayscale MRI medical images of size 512×512 (8-bit per pixel) have been used for models evaluation. This paper presented PSNR about (56) and MSSIM about (0.99) as best results. Despite the high results for PSNR in this article, encoding time and compression ratio are missing that led to insufficient performance analysis.

On the other hand, Badshah et al. [24] have discussed the problem of heavy payload watermarking of medical images which effects the deterioration of the perceptual image that directly effects medical diagnostics. They have attempted to make the payload of watermark suitable for an image with maintained the image quality. This paper has proposed Lempel—Ziv—Welch (LZW) compression technique to reduce watermarking payload without data loss. The watermark consists of combine region of interest (ROI) of an image and secret key of watermark. In order to check the performance of the proposed method, two metrics have been used: PSNR and CR. CR results have been compared with other models, namely PNG, GIF, and JPEG2000. LZW has resulted in PSNR from (51–56) of watermarked image and the same value shown for the recovered image. On the other hand, LZW has CR results (0.02–0.08) while other models (0.2–0.5), (0.2–0.9), (0.2–0.4), respectively. Six different ultrasound medical images have been used for testing and evaluation. The highest obtained results for PSNR are about 56 and CR is about 0.08 for the model. Although the proposed method has shown significant PSNR for image watermarked and the same value for the retrieved image, CR is considered to be very low. Furthermore, the time required for both encoding and decoding of an image has not been discussed in this paper which made the conditions of the model efficiency is insufficient.

In order to reduce images size without any impact on the quality, Kumar et al. [25] have discussed the problem of telemedicine when the medical images have large amount of sizes which playing essential role in the storage and transmission. This paper has produced a compression algorithm for CT images based on contextual vector quantization (CVQ) with optimized codebook using simulated annealing (SA). This algorithm was based on the idea of separating images into region of interest, foreground (ROI) and non-region of interest, background (Non-ROI). The separation process has been applied using region growing algorithm. Then, ROI has been compressed with low CR and high bit rate, while the background was compressed in reverse order. Furthermore, the codebook has been generated from the two parts—foreground and background—then merged and optimized using simulated annealing algorithm. In order to evaluate the proposed model (CVQ-SA) performance, two metrics have been used: PSNR and CR. Moreover, the CVQ-SA results have been compared with other models named: JPEG—lossy, JPEG—lossless, VQ, and CVQ. The CVQ-SA has resulted in PSNR about (39–40) while other models have reached (35–37), (29–31), (33–35), and (36–38) for JPEG—lossy, JPEG—lossless, VQ, and CVQ, respectively. On the other hand, resultant CR for CVQ-SA is (6), whereas other models have obtained (5, 4, 5, and 4) for JPEG—lossy, JPEG—lossless, VQ, and CVQ, respectively. Many CT images have been applied for experimentation and testing objectives. The best obtained results are: PSNR about 40 and CR about 6. Although the high results have been obtained using CVQ-SA model, time complexity was missing from this paper completely. Therefore, the evaluation metrics are insufficient. Furthermore, CRs have the same values for all samples applied by comparison models. It was not clarified anywhere why all comparison models have the same CR for all CT samples.

UmaMaheswari et al. [26] have aimed to develop a technique capable to reduce size and maintain high quality by addressed the problem of large amount of medical images size representing a major challenge for both storage and transmission issue. This paper has proposed tetrolet transform that represent a development of Haar model using the tile matching and rearrangement. This technique has involved dividing the image into 4×4 blocks. Quadrat fraction has been applied for each block and is updated according to the image geometry. Then, each four equal size sequence have joined together with at least one square along the edge. In order to get normal quadrant matching rearrangement, Haar transformation has been developed for both rearrangement and subsequent. Finally, low pass image procedure has been performed for all 4×4 blocks. Moreover, sparest covering of each part has been stored in the wavelet basis function as non-redundancy element. The proposed model has analyzed and evaluated using three main metrics: PSNR, CR, and execution time. Furthermore, CR and execution time results for the proposed model have been compared with other models named: Haar (kadam and rathod) and FQT (kadam and rathod). Technically, tetrolet has resulted in CR about (3–4) while other models about (7) and (3–4) for Haar (kadam and rathod) and FQT (kadam and rathod), respectively. Similarly, execution time has consumed about (6–7 s) for the tetrolet model. On the other hand, other models have consumed execution time less than the proposed model (5–6 s) and (2–4 s) for Haar (kadam and rathod) and FQT (kadam and rathod).

and rathod), respectively. Finally, tetrolet has achieved PSNR values started from 12 to 19. Three different type images have been applied for evaluation and analysis purposes. CR about 4 and processing time about 6 s. have been obtained as best results. CR and processing time have shown a high efficiency of tetrolet model. However, other models results were better than tetrolet model. On the other hand, three samples of size 256×256 were very few in order to analyze the model performance. Moreover, the model was customized for medical images while a normal image has been used as an evaluation sample. Therefore, the efficiency potential is inaccurate.

Nirmalraj et al. [27] have presented a lossless compressive technique after discussed the problem of large amount of medical images size caused several challenges especially in terms of telemedicine applications and storage devices. The researchers have aimed to minimize the images size with attempt for keeping the quality. Initially, impulse noise has been filtered from the biomedical images using fuzzy transform. Then, deterministic binary compressive sensing matrix has been applied to compress images and orthogonal matching pursuit (OMP) to recover them. In order to test the proposed model performance, PSNR, CR, and processing time have been performed as a main evaluation metrics. Furthermore, there is a comparison between the proposed model and other models named: set partitioning in hierachal trees (SPIHT), fractal coding, and CS using Gaussian matrix. Practically, PSNR has reached about (35–37) for the proposed model while other models have obtained about (33–36), (24–30), and (34–36) for SPIHT, fractal coding, and CS using Gaussian matrix, respectively. Moreover, the proposed model has resulted in CR about 5, whereas other models have achieved about (2–4), (2–4), and (4–5) for SPIHT, fractal coding, and CS using Gaussian matrix, respectively. Finally, the proposed model has consumed about (0.5–0.6 s) of processing time. Various biomedical images such as CT scan and PET images have been used for experimentation purposes. PSNR about 37, CR about 5, and consumed time about 0.5 s. have been achieved as best result. Despite the significant results have been obtained using the proposed system, the number and the size of evaluation samples were missing made the behavior of the proposed compression model is unrecognizable.

Another approach by Ahilan et al. [28] that have aimed to solve the problem of large sizes of medical images—where the obstacles of the storage and the transmission are inevitably—in the way of reducing images size with preserving high quality. This paper has proposed a lossless compression method. Particle swarm optimization (PSO), Darwinian particle swarm optimization (DPSO), and fractional-order Darwinian particle swarm optimization (FODPSO) have been applied to estimate the threshold value. Then, lossless compression algorithm based on the classification and blending prediction (CDP) has been performed. The proposed model has been evaluated using three metrics: (PSNR, CR, and encoding time). Furthermore, the result of PSNR for the proposed model has been compared with other models named: JPEG lossy and JPEG lossless. Practically, PSNR have reached about (25–30) for CBP model while other models have obtained (34–35) and (28–30) for JPEG lossy and JPEG lossless, respectively. Furthermore, CBP model has resulted in CR about 2. Finally, the proposed model has consumed about (7–8 s) of execution time.

Seven CT abdomen datasets for segmentation and six CT abdomen datasets for analysis have been used. The images were obtained from Metro Scans and Research Laboratory, Thiruvananthapuram. The image size was 512×512 . PSNR about 30, CR about 2 and execution time about 7 s have been obtained as best result. The proposed model has achieved significant results. However, the comparison between the proposed technique and other models in terms of CR and encoding time were missing. Furthermore, the results of other models have outperformed the proposed model. Finally, the size of the image samples was very little. Therefore, the efficiency of the model is considered to be unsure.

As neural networks are used to compress images in a lossy manner, they can be used to compress images without losing data (reversible manner) [3]. Balasubramani et al. [29] have addressed the problem of large sizes of medical images which represent a communication and storage bottleneck with maintained image quality that represent a critical issue for medical diagnosis. They have proposed neural network radial basis function (NN-RBF) based on function approximation. Proposed model works by adding neurons to the hidden layer of a radial basis network until required mean squared error is found, function is determined, and required neurons are reached. Five metrics: CR, PSNR, BPP, MSE, and encoding time have been applied to measure performance for NN-RBF algorithm. Moreover, results have been compared with other compression techniques (Huffman, fractal, ANN-BP). Empirically, ANN-RBF has resulted in PSNR from 29 to 58, while other models PSNR (24–31), (39–43), (44–108) for Huffman, fractal, and ANN-BP, respectively. Furthermore, ANN-RBF has achieved CR from 0.79 to 1.07, while other models CR (31–40), (1.8–10.9), (1.02–108) for Huffman, fractal, and ANN-BP, respectively. On the other hand, the proposed model has consumed 265 Ms–515Ms time, while other models have consumed (180–240 Ms), (540–840 Ms), (240–1260 Ms) processing time for Huffman, fractal, and ANN-BP, respectively. At the same time, ANN-BRF has produced MSE from 0.34 to 986.7, while other models MSE (6.72–20.11), (2.78–8.09), (0.16–8.7) for Huffman, fractal, and ANN-BP, respectively. Finally, BPP for the proposed model is about (7.45–10.11 bpp), while other models bpp (1.15–1.52), (1.36–1.89), (7.38–7.83) for Huffman, fractal, and ANN-BP, respectively. In order to evaluate the performance of ANN-RBF model, a set of different medical images such as MRI and CT of size 512×512 have been applied in this paper. ANN-RBF best results for CR, PSNR, and encoding time are 1.07, 58, 265 Ms, respectively. ANN-RBF has achieved higher PSNR and relatively little processing time. However, CR was very low. Furthermore, all the applied samples for evaluation have the same resolution 512×512 that is not diversified to get better analysis about model behavior.

4 Analysis and Evaluation

This paper has presented twenty-five models for lossy and lossless approaches of medical image compression techniques. The analysis process has relied on the

extracted results of CR and PSNR from all papers in order to evaluate models efficiency.

Table 1 shows the best results of CR and PSNR for lossy medical image compression models distributed into four groups (fractals, wavelet, ROI and Non-ROI, and other approaches). ROI and Non-ROI-based models have outperformed other approaches in terms of CR. Empirically, wavelet models have shown higher results of PSNR than other models. Furthermore, Table 2 illustrates the best resultant CR and PSNR for the lossless medical image compression models distributed into three groups (adaptive block, least square, and other approaches). Evidently, least square models have shown higher value for CR than other approaches. Moreover, adaptive block and least square models were superior to other approaches in terms of PSNR.

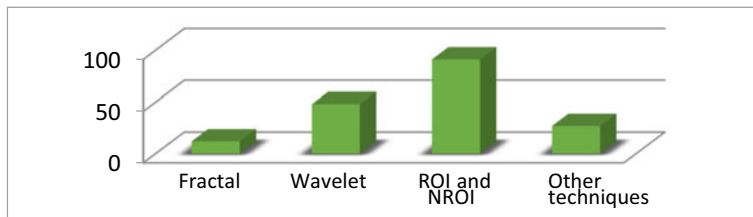
Finally, with the aim to provide clear and an accurate comparison vision, obtained results in Tables 1 and 2 are expressed visually in bar chart figures. Figures 1 and 3 show the comparison results of CR for lossy and lossless medical image compression models, respectively. Figures 2 and 4 state the comparison results of PSNR for lossy and lossless medical image compression methods. Moreover, average CR for

Table 1 Best compression ratio and best PSNR for lossy approaches for medical images

Category	Models	Metrics	
		Best CR	Best PSNR
Fractal	Fractal + neural network [4]	10	36
	Parallel fractal texture identification [5]	2	42
	Oscillation concept + quasi-fractal [6]	24	33
Wavelet	Contourlet transform and binary array [7]	6	101
	Wavelet transform and vector quantization [8]	91	60
Based on concepts ROI and Non-ROI	DWT and RNN [9]	23	35
	Contourlet transform with PSO optimization [10]	144	40
	Lempel–ZIV–Welch and clipped histogram equalization [11]	94	56
	Brain image compression based on the tumor location [12]	37	31
	Segmentation using visual saliency [13]	160	39
Other approaches	High bit-depth with HEVC [14]	50	62
	Matrix completion technique [15]	5	26
	Restoration of JPEG using cross-domain neural network [17]	–	37
	Enhanced ripplet transform [16]	–	37

Table 2 Best compression ratio and best PSNR for lossless approaches for medical images

Category	Models	Metrics	
		Best CR	Best PSNR
Adaptive block	A block adaptive near-lossless algorithm [18]	–	60
	Adaptive block-based spatial prediction [19]	–	59
Least square	Geometry-adaptive partitioning and LS [20]	–	–
	An improved predictive scheme [21]	8	60
Other approaches	Lion optimization algorithm [22]	0.34	52
	Neural network radial basis function [29]	1.07	58
	Level set method and biorthogonal CDF wavelet based on lifting scheme [23]	-	56
	Watermark compression using Lempel–ZIV–Welch (LZW) [24]	0.08	56
	Contextual vector quantization with simulated annealing [25]	6	40
	Tetrolet transformation [26]	4	–
	Fuzzy transform and deterministic binary compression sensing matrix [27]	5	37
	Segmentation by fractional-order DPSO [28]	2	30

**Fig. 1** Compression ratio for lossy medical image compression

each recognized group is calculated. Figure 5 shows the average CR for all lossy and lossless compression models according to their group. Technically, ROI and Non-ROI-based approaches outperformed other models (lossy and lossless) with a CR up to 91. The next best average CR is for wavelet-based approaches with 48 CR. Lossless least square-based approaches show an average CR about 8 that higher than some lossy approaches. This fact shows the potential of the customized compression models for medical image compression. Furthermore, average PSNR is computed for each group of compression models. Figure 6 shows the average PSNR for all lossy and lossless compression models according to their group. Surprisingly, lossy wavelet-based compression approaches outperformed all other lossy and lossless approaches. Although lossless approaches are expected to have infinity PSNR, lossless approaches recorded moderate PSNR values as a result of the image quality

adjusting for the medical remote imaging system. Except for wavelet, lossless adaptive block, and least square-based approaches in addition to other lossless approaches group have shown the best average PSNR in comparison with other models with values about 60, 60, and 47, respectively.

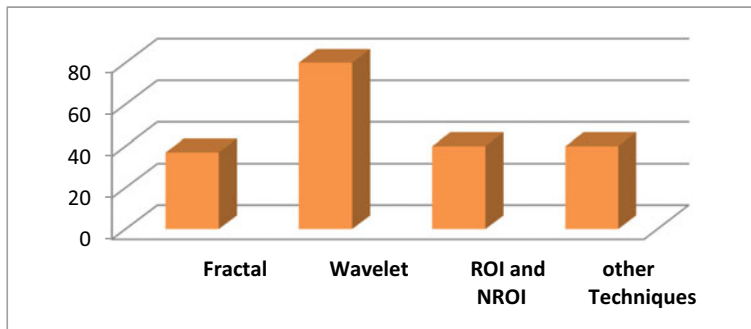


Fig. 2 PSNR for lossy medical image compression models

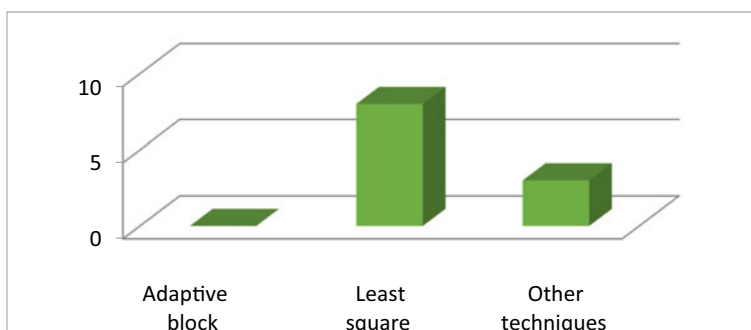


Fig. 3 Compression ratio for lossless medical image compression models

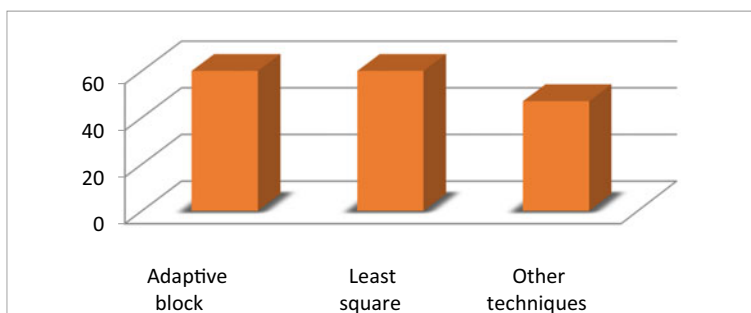


Fig. 4 PSNR for lossless medical image compression models

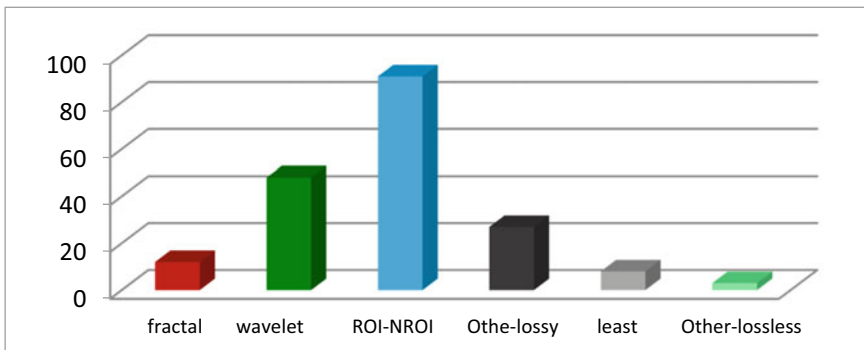


Fig. 5 Compression ratio for lossy and lossless medical image compression models

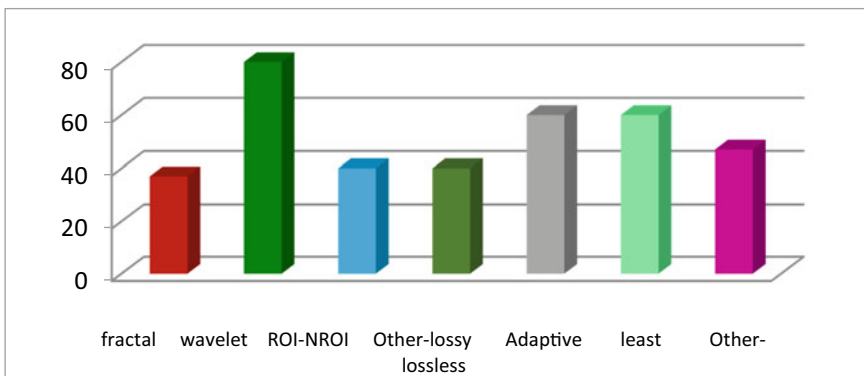


Fig. 6 PSNR for lossy and lossless medical image compression models

5 Conclusion

In conclusion, this paper has presented twenty-five compression models grouped into lossy and lossless medical image compression. Lossy medical image approaches are grouped into fractals, wavelet, ROI and Non-ROI, and other approaches. Lossless approaches are grouped into adaptive block, least square, and other lossless approaches. Technically, CR and PSNR are targeted and extracted from the literature of the included models in order to evaluate approaches efficiency. Average CR and average PSNR are calculated for all groups and compared with each other. ROI and Non-ROI-based compression outperformed other lossy approaches in terms of CR while wavelet achieved the best PSNR. Least square-based approaches outperformed other lossless approaches for both CR and PSNR. With the comparison for all models groups in terms of average CR and average PSNR, ROI and Non-ROI, and wavelet-based approaches have shown the best CR and PSNR, respectively.

References

1. Al-Shammary D (2013) Enhanced web services performance by compression and similarity-based aggregation of SOAP traffic
2. Al-Nassrawy KK, Al-Shammary D, Idrees AK (2020) High performance fractal compression for EEG health network traffic. *Procedia Comput Sci* 167
3. Al-Shammary D, Khalil I, Tari Z, Zomaya AY (2013) Fractal self-similarity measurements based clustering technique for SOAP Web messages. *J Parall Distrib Comput* 73(5)
4. Maha Lakshmi GV Implementation of image compression using Fractal Image Compression and neural networks for MRI images. In: 2016 international conference on information science (ICIS), Kochi, 2016, pp 60–64.
5. Suresh Kumar R, Manimegalai P (2020) Near lossless image compression using parallel fractal texture identification. *Biomed Signal Process Control* 58:101862.
6. Magar SS, Sridharan B (2020) Hybrid image compression technique using oscillation concept & quasi fractal. *Health Technol.* 10:313–320
7. Uma Vetri Selvi G, Nadarajan R (2017) CT and MRI image compression using wavelet-based contourlet transform and binary array technique. *J Real-Time Image Proc* 13:261–272
8. Ammah PNT, Owusu E (2019) Robust medical image compression based on wavelet transform and vector quantization. *Inf Med Unlocked* 15
9. Sabbavarapu SR, Gottapu SR, Bhima PR (2020) A discrete wavelet transform and recurrent neural network based medical image compression for MRI and CT images. *J Ambient Intell Human Comput*
10. Eben Sophia P, Anitha J (2017) A hybrid contextual compression technique using wavelet and contourlet transforms with PSO optimized prediction. *Int J Imag Syst Technol*
11. Manimekalai MAP, Vasanthi NA (2019) Hybrid Lempel-Ziv-Welch and clipped histogram equalization based medical image compression. *Cluster Comput* 22:12805–12816
12. Kumarganesh S, Suganthi M (2016) An efficient approach for brain image (tissue) compression based on the position of the brain tumor. *Int J Imaging Syst Technol* 26:237–242
13. Sran PK, Gupta S, Singh S (2020) Segmentation based image compression of brain magnetic resonance images using visual saliency. *Biomed Signal Process Control* 62
14. Parikh S, Ruiz D, Kalva H, Fernández-Escribano G, Adzic V (2018) High bit-depth medical image compression with HEVC. *IEEE J Biomed Health Inform* 22:552–560
15. Kumar R, Patbhaje U, Kumar A (2019) An efficient technique for image compression and quality retrieval using matrix completion. *J King Saud Univ—Comput Inf Sci*
16. Anitha J, Eben Sophia P, Son LH, Hugo V, de Albuquerque C (2019) Performance enhanced ripples transform based compression method for medical images. *Measurement* 144
17. Chung KJ, Souza R, Frayne R (2020) Restoration of Lossy JPEG-compressed brain MR images using cross-domain neural networks. *IEEE Signal Process Lett* 27:141–145
18. Sharma U, Sood M, Puthooran E (2020) A block adaptive near-lossless compression algorithm for medical image sequences and diagnostic quality assessment. *J Digit Imaging* 33:516–530
19. Song X, Huang Q, Chang S et al (2016) Novel near-lossless compression algorithm for medical sequence images with adaptive block-based spatial prediction. *J Digit Imaging* 29:706–715
20. Song X, Huang Q, Chang S et al Lossless medical image compression using geometry-adaptive partitioning and least square-based prediction. *Med Biol Eng Comput* 56:957–966 (2018).
21. Kumar SN, Fred AL, Kumar HA et al (2020) Lossless compression of CT images by an improved prediction scheme using least square algorithm. *Circuits Syst Signal Process* 39:522–542
22. Geetha, K, Anitha, V, Elhoseny, M, Kathiresan, S, Shamsolmoali, P, Selim, MM (2020) An evolutionary lion optimization algorithm-based image compression technique for biomedical applications. *Expert Systems*
23. Haouam I, Beladgham M, Bendjillali RI, Yassine H MRI image compression using level set method and biorthogonal CDF wavelet based on lifting scheme. In 2018 international conference on signal, image, vision and their applications (SIVA), Guelma, Algeria, 2018

24. Badshah G, Liew S, Zain JM et al (2016) Watermark compression in medical image watermarking using Lempel-Ziv-Welch (LZW) lossless compression technique. *J Digit Imaging* 29:216–225
25. Kumar SN, Lenin Fred A, Sebastin Varghese P (2018) Compression of CT images using contextual vector quantization with simulated annealing for telemedicine application. *J Med Syst* 42:218
26. UmaMaheswari S, SrinivasaRaghavan V (2020) Lossless medical image compression algorithm using tetrolet transformation. *J Ambient Intell Human Comput*
27. Nirmalraj S, Nagarajan G (2020) Biomedical image compression using fuzzy transform and deterministic binary compressive sensing matrix. *J Ambient Intell Human Comput.*
28. Ahilan A et al (2019) Segmentation by fractional order Darwinian particle swarm optimization based multilevel thresholding and improved lossless prediction based compression algorithm for medical images. *IEEE Access* 7:89570–89580
29. Balasubramani P, Murugan PR (2015) Efficient image compression techniques for compressing multimodal medical images using neural network radial basis function approach. *Int. J Imaging Syst, Technol*

Performance Evaluation of SEIG Under Unbalanced Load Operations Using Genetic Algorithm



Yatender Chaturvedi, Varun Gupta, Arunesh Chandra, and Ankit Goel

Abstract In the current world, superiority of nonconventional over conventional power sources is rapidly increasing in the area of powerful production. In this paper, the modeling of three-phase induction generator was done which turns into an objective function that has been solved for their variables using genetic algorithm as optimization tool in MATLAB. The program has been written in MATLAB and being called in GA optimization window by setting limits to its variables. The methodology as discussed has been adopted to analyze the performance of a 15 KW induction machine in terms of voltage unbalanced factor, power output, losses and efficiency of machine under different power factor loading.

Keywords Self-excited induction generator (SEIG) · Nonconventional power source · Genetic algorithm (GA) · Wind power · Unbalanced loading

1 Introduction

Since past decades, electric power has been the dynamic force for the growth of any nation. Today, most of the conventional energy resources are hazardous for environment and humanity as well. A fast decline of these energy sources and green environment bound the researchers to adopt other energy options. Rapid depletion of fossil fuels, terrific boost in the fuel cost and ongoing energy failure have paid attention to scientists toward renewable energy like wind power, solar and biomass,

Y. Chaturvedi (✉) · V. Gupta · A. Chandra · A. Goel
KIET Group of Institutions, Ghaziabad, Uttar Pradesh 201206, India
e-mail: yatendra.chaturvedi@kiet.edu

V. Gupta
e-mail: varun.gupta@kiet.edu

A. Chandra
e-mail: arunesh.chandra@kiet.edu

A. Goel
e-mail: ankit.goel@kiet.edu

etc. Electricity generation via renewable energy is growing sharply and out of other renewable sources wind power shares most important part.

It is the induction generators which have the great capability of power generation at unstable speed. These machines are being utilized in wind power systems with varying nature of wind. Out of wound rotor and squirrel cage, later one is quite simple, rough in construction and having less capital cost as compared to synchronous generators with same rating. Its other features like effortlessness, nonappearance of DC excitation, non-requirement of synchronization, etc. have lead to utilize such machines in self-excited mode. Performance at steady-state conditions of self-excited induction generators may be computed from per-phase equivalent circuit of self-excited induction generator. References [1, 2] analyzed the performance by applying the loop impedance and nodal admittance approach. The importance and necessity of excitation requirement in cut off mode of SEIG were discussed for its thriving operation in [3] while [4] offered a swot on the restrictions on the performance of three-phase SEIG.

The research work as presented by the researchers leads to quite bulky expression which requires time to solve it. In this direction, TF Chan [5] projected an iterative procedure which reduces the computational hard work and turns the analysis of these induction generators quite effortless. A new approach to analyze the operation of SEIG was presented [6] which consequences in only quadratic equation involving slip with supplementary parameters. The interesting conclusion was the maximum probable slip for SEIG which was the ratio of useful rotor resistance to useful rotor reactance. The study carried from work related to performance of SEIG [1–6] results to extensive and extremely nonlinear equations which are quite complicated to resolve. Nowadays, attentions of research persons are focused toward the soft computing techniques for the probable solutions to these nonlinear equations. Continuing in this area, genetic algorithm was taken care for the result of the nonlinear equations as shaped in the procedure of performance examination of SEIG [7]. A move toward minimization of the admittance of self-excited induction generators [8] was made using DIRECT algorithm which includes both real and imaginary functions. In this direction, [9] adopted an optimization techniques under balanced conditions of SEIG and [10] focused on whale optimization technique to find out the variables associated with the objective function. A PSO optimization technique was adopted [11] for selection of SEIG parameters to obtain maximum allowable operating range under unbalanced operations.

In the research work, an effort has been made to evaluate the performance of self-excited induction generator under unbalanced load using genetic algorithm as an optimization tool in MATLAB.

The research work as presented in the paper is organized as in the following. Section 2 consists of machine modeling made by adopting nodal admittance approach. An objective function has been formed that contains per unit values of generated frequency(a), magnetizing reactance of both the sequence networks (X_{mp} , X_{mn}) and the voltage unbalanced factor(k). Section 3 is enriching with a brief overview of genetic algorithms. The equations related to performance evaluation of SEIG are well structured in Sect. 4. Simulated results showing effect of load power

factor on power output, losses, efficiency, and voltage unbalanced factor has been described in Sect. 5. Lastly, the conclusion has been framed in Sect. 6.

Main contribution of the paper

- An objective function containing four variables has been prepared from model of SEIG and the same has been evaluated for all four variables using genetic algorithm as optimization tool in MATLAB.
- Performance of SEIG has been estimated under different power factor loadings.

2 Machine Modeling

A delta connected load which is powered by a three-phase self-excited induction generator is as shown in Fig. 1. Voltage and current in different phases of SEIG are V_a, V_b, V_c and I_a, I_b, I_c correspondingly. Admittances offered by each group of load and excitation capacitance are Y_{al}, Y_{bl}, Y_{cl} correspondingly.

Submission of KCL at nodes of delta connected load and involvement of symmetrical component theory leads into a second-order expression in voltage unbalance factor as:

$$f_1(K^2(K_z Y_1) + K(Y_0 K_z - Y_0) - Y_2) = 0 \quad (1)$$

where

$$Y_0 = \frac{1}{3}[Y_{ab} + Y_{bc} + Y_{ca}] \quad (2)$$

$$Y_1 = -\frac{1}{3}[aY_{ab} + Y_{bc} + a^2Y_{ca}] \quad (3)$$

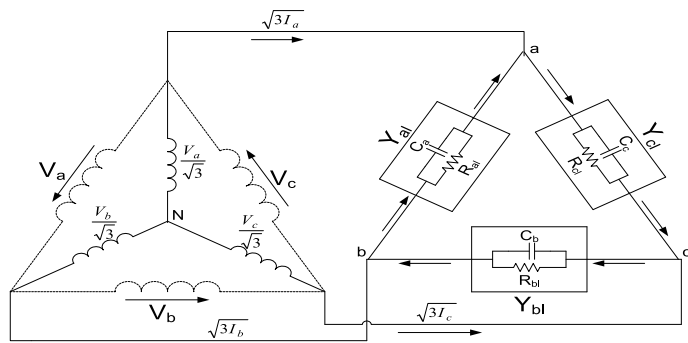


Fig. 1 Three-phase self-excited induction generator

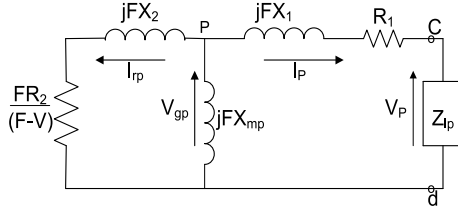


Fig. 2 Positive sequence circuit of SEIG

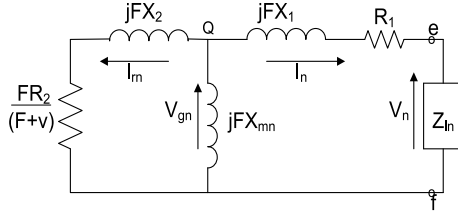


Fig. 3 Negative sequence circuit of SEIG

$$Y_2 = -\frac{1}{3} [a^2 Y_{ab} + Y_{bc} + a Y_{ca}] \quad (4)$$

Submission of loop analysis in positive and negative sequence circuits of SEIG as shown in Figs. 2 and 3 leads to the following expressions:

$$f_2(Z_{rmp} + Z_1 + Z_{lp}) = 0 \quad (5)$$

$$f_3(Z_{rmn} + Z_1 + Z_{ln}) = 0 \quad (6)$$

Instantaneous solution to Eqs. (1), (5) and (6), for an induction generator serving at a given speed and impedances across the stator, will lead to variables voltage unbalanced factor, generated frequency (p.u) and reactance of both the sequence networks.

3 Genetic Algorithm as an Optimization Tool

From last decades, the researchers are doing work toward the soft-coded algorithms for the solution optimization problems. These optimization problems consist of many variables so it needs a powerful algorithm for solution to these variables. Genetic algorithm [7] as an optimization tool is very impressive tool in order to solve the nonlinear equations. It fundamentally manipulates the number of strings in form of binary digits and evaluates each with a significant fitness value. Genetic algorithm

optimization tool has the benefit of parallel and stochastic search in the direction to finest solution. The algorithm contains three operators named reproduction, crossover and mutation on which appropriate solution to problem may be achieved.

Solution of objective functions as in Eqs. (1), (5) and (6) as demonstrated in Sect. 2 may be achieved by use of genetic algorithm as an optimization tool in MATLAB. The objective functions have been programmed in MATLAB and being called in MATLAB window GA optimization toolbox. Here, the minimization of objective functions takes place by setting upper and lower limits to all variables, and finally, optimized values corresponding to these variables may be obtained.

4 Performance Equations

The performance of any three-phase self-excited induction generators may be computed from the following equations:

$$K = \frac{V_n}{V_p} \quad (7)$$

$$P_{\text{out}} = I_{ab}^2 R_{ab} + I_{bc}^2 R_{bc} + I_{ca}^2 R_{ca} \quad (8)$$

$$P_{\text{loss}} = 3[I_p^2 R_1 + I_n^2 R_1 + I_{rp}^2 R_2 + I_{rn}^2 R_2] \quad (9)$$

$$\% \text{efficiency} = \frac{P_{\text{out}}}{P_{\text{input}}} \times 100 \quad (10)$$

5 Results and Discussion

The three-phase model of self-excited induction generator as discussed in Sect. 3 has been tested on a four-pole, three-phase, 15 KW, 50 Hz, 415 V, 30 A induction machine whose windings are connected in delta. Machine per-phase parameters in per unit are $R_1 = 0.029$, $R_2 = 0.03$, $X_1 = X_2 = 0.1455$. The air gap voltage of machine is expressed as $E = 0.49 + 0.82X_m - 0.3022X_m^2$. Under pure resistive loading, the machine is supposed to operate at their rated values of voltage and current by putting load of 1.58 per unit and value of capacitor across each phase to 0.775 per unit. The speed of induction generator is kept fixed at 1.02 per unit.

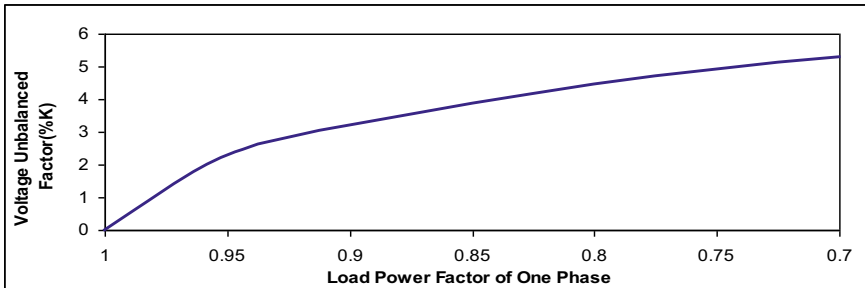


Fig. 4 Effect of load power factor of one phase on voltage unbalanced factor

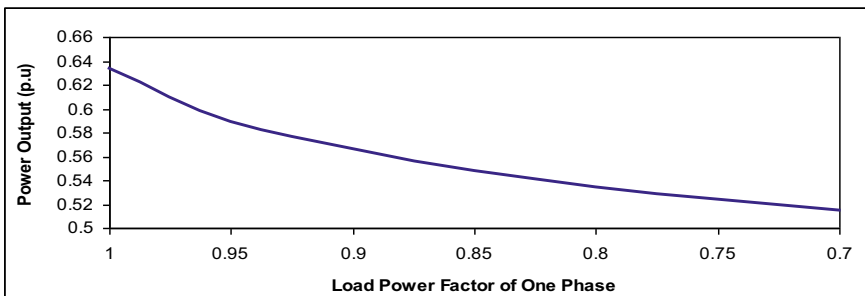


Fig. 5 Effect of load power factor of one phase on power output

5.1 *Effect on SEIG Under Variation in Load Power Factor of One Phase*

In this segment, performance of machine has been evaluated under load power factor of one phase only while the other two phases serve for a constant load power factor. The results in terms of voltage unbalanced factor, power output, power losses and efficiency of the machine are shown in Figs. 4, 5, 6 and 7. The operation of generator was kept fixed at a speed of 1.02 per unit during the simulation process.

5.2 *Effect on SEIG Under Variation in Load Power Factor of Two Phases*

In this segment, performance of machine has been evaluated under load power factor of two phases simultaneously while the remaining one phase serves for a constant load power factor. The results in terms of voltage unbalanced factor, power output, power losses and efficiency of the machine are shown in Figs. 8, 9, 10 and 11. The

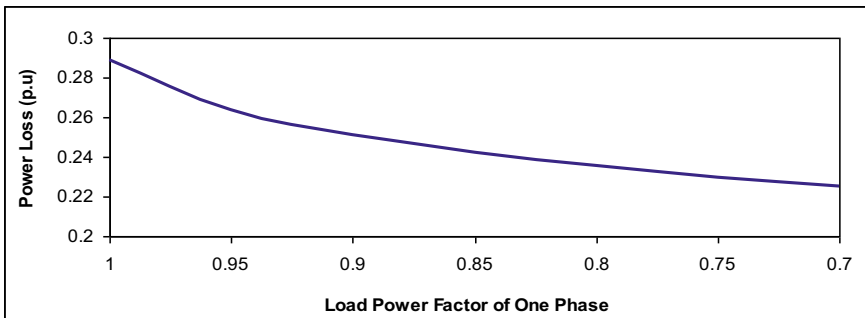


Fig. 6 Effect of load power factor of one phase on power loss

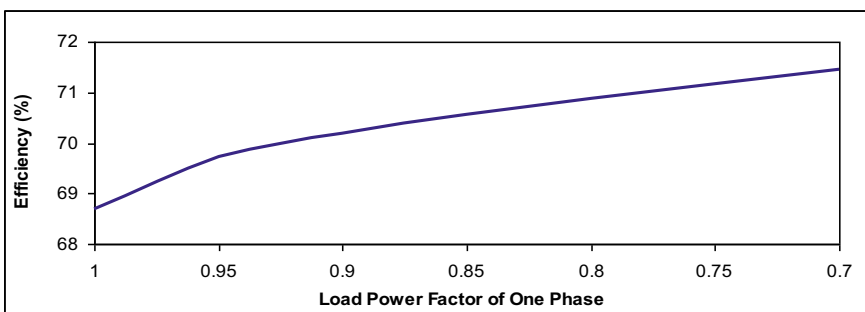


Fig. 7 Effect of load power factor of one phase on efficiency

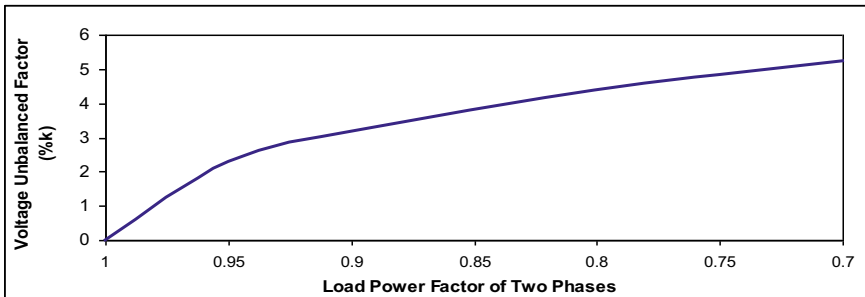


Fig. 8 Effect of load power factor of two phases on voltage unbalanced factor

operation of generator was kept fixed at a speed of 1.02 per unit during the simulation process.

Figures 4, 5, 6, 7, 8, 9, 10 and 11 represent the effects of load power factor of one phase and two phases simultaneously on the performance of SEIG. The explanations made from these graphs are listed as:

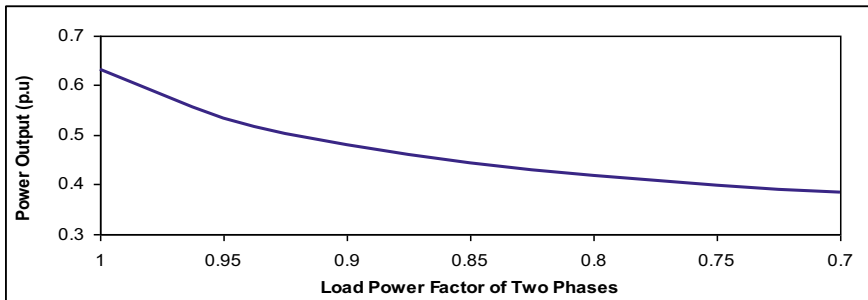


Fig. 9 Effect of load power factor of two phases on power output

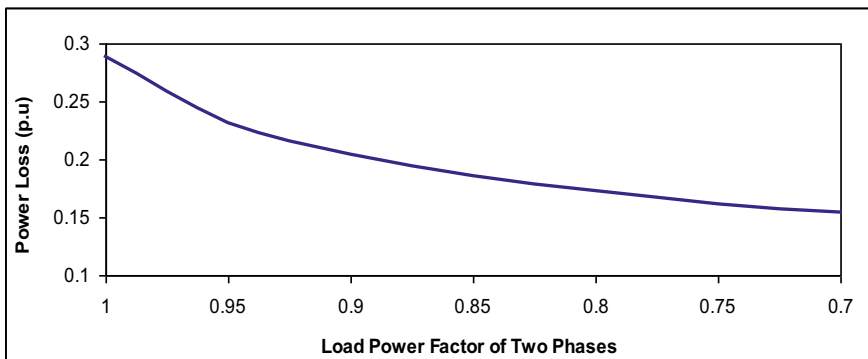


Fig. 10 Effect of load power factor of two phases on power loss

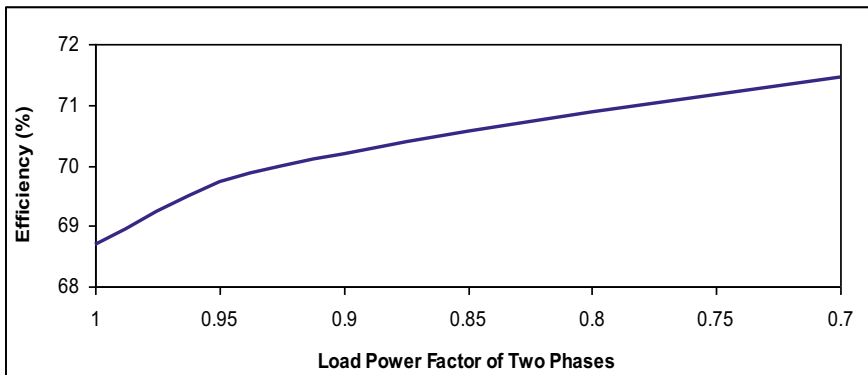


Fig. 11 Effect of load power factor of two phases on Efficiency

- Effect of load power factor of one phase only fallout to unbalancing of the generator which reflects in terms of voltage unbalanced factor. There is considerable increment in voltage unbalanced factor as power factor of load starts decreases. On the other hand, effect of load power factor of two phases shows a very small reduction in voltage unbalanced factor to that due to one phase only.
- There is considerable reduction in power output and power losses in the generator under load power factor of two phases as compared to one phase only.
- There is considerable increment in the efficiency of generator under load power factor of two phases as compared to one phase only.

6 Conclusion

The equivalent circuit of three-phase SEIG as presented in the research paper turns into an objective function that has been solved for performance estimation of self-excited induction generator using genetic algorithm as an optimization tool in MATLAB. The results as obtained from simulation may be incorporated in order to operate the generator with in a specific range of voltage unbalanced factor. In addition to it, the same generator may also be employed for gaining the higher efficiency with respect to change in the power factor of the load of one and two phases simultaneously.

References

1. Murthy SS, Malik OP, Tandon AK (1982) Analysis of self-excited induction generators. IEEE Proc Gener, Distrib, Trans, 129(6):260–265
2. Quazene L, McPherson G (1983) Analysis of self-excited induction generator. IEEE Trans Power App Syst PAS-102(8):2793–2798
3. Malik NH, Mazi AA (1987) Capacitance requirements for isolated self excited induction generators. IEEE Trans Energy Convers EC-2(1):62–67
4. Al Jabri AK, Alolah (1990) Limits on performance of the three-phase self-excited induction generators. IEEE Trans Energy Convers, 5(2):350–356
5. Chan TF (1995) Analysis of self-excited induction generators using an iterative method. IEEE Trans Energy Convers 10(3):502–507
6. Sandhu KS, Jain SK (1990) Operational aspects of self-excited induction generator using a new model. Electr Mach Power Syst 27(2):169–180
7. Joshi D, Sandhu KS, Soni MK (2006) Constant voltage constant frequency operation for a self-excited induction generator. IEEE Trans Energy Convers 21(1):228–234
8. Kheldoun A, Refoufi L, Khodja DE (2011) Analysis of self-excited induction generator steady state performance using a new efficient algorithm. Electric Power Syst Res 86:61–67
9. Saha SK, Sandhu KS (2017) Optimization techniques for the analysis of self-excited induction generator. In: Procedia of 6th international conference on smart computing and communications, ICSCC, pp 405–411

10. Chaturvedi Y, Kumar S, Gupta V (2020) Capacitance requirement for rated current and rated voltage operation of SEIG using Whale optimization algorithm. In: International conference on computational intelligence and date science (ICCIDDS 2019), Procedia computer science, vol 167, pp 2581–2589
11. Chaturvedi Y, Kumar S (2020) Selection of stand-alone self-excited induction generator parameters to obtain maximum allowable operating range under unbalanced operations using particle swarm optimization. *Int J Syst Assur Eng Manag* 11(3):677–689

Suppliers Selection Using Fuzzy AHP and Fuzzy TOPSIS Method—A Case Study of a Bearing Manufacturing Company



Ramesh Karwal, Pradeep Kumar, Manish Bhandari, and M. L. Mittal

Abstract Supplier selection is one of the most important activities of an industry. The goal of present paper is to exhibit key elements of supplier selection and ranking of potential suppliers. A bearing manufacturing company was considering two criteria of suppliers selection, i.e., quality rating and service rating. In the current paper, six criteria have been considered instead of two for improving the supplier's selection process which are product quality, product cost, location, delivery time, information system and service rating. First of all, the key factors involved in supplier selection have been identified, a survey has been conducted for data collection from purchase department in the company. Fuzzy AHP method and fuzzy TOPSIS method are used to calculate the criteria weights for the suppliers' selection and to determine the ranking of the suppliers. The contribution of this study is to give improved suppliers' selection process to the company.

Keywords Fuzzy · AHP · Suppliers · Selection

1 Introduction

Supplier selection which contains multiple conflicting objectives is explained as a process of identifying the appropriate suppliers with a combination of optimum quality, price and at right time and right quantities. The real challenge of supplier evaluation lies in constructing this trade-off between price and lead time in a way that perfectly reflects the buyer's preferences [1]. There are two areas of research in supplier selection. One is the factors or criteria that are important and should be considered, and the other is the process or methodology applied to rank the suppliers.

R. Karwal

Water Resources Department, Jaipur, Rajasthan 323001, India

P. Kumar (✉) · M. Bhandari

Department of Mechanical Engineering, MBM Engineering College, J.N.V University, Jodhpur 342003, India

M. L. Mittal

Department of Mechanical Engineering, MNIT, Jaipur 302017, India

Supplier selection has a major impact on proper functioning of supply chain as well as product quality. For the case of just in time (JIT) manufacturing, supplier selection is the most important. The purchasing function has got dominance in supply chain due to globalization and technological changes. Purchasing includes buying raw materials and supplying components to the organizations. The most important process of purchasing function is the selection of suppliers. The desired outcome of process of selection of supplier is to reduce risk and maximization of value for the buyer involving a no. of strategic variables [2]. There are no. of factors which affect supplier selection and the weights assigned [3]. It is imperative to have a trade-off among all factors, to choose the optimum suppliers. In single sourcing type, needs of all the buyers are satisfied by one supplier while in multiple sourcing type no supplier can satisfy all the requirements of all the buyer's [4]. Fuzzy DEMATEL (decision-making trial and evaluation laboratory) has been used to solve multi-criteria problems in which triangular type-1 fuzzy sets are used to define linguistic evaluation [5, 6].

In the present paper, methodology is developed to evaluate suppliers in supply chain cycle with the use of TOPSIS (Technique for Order Preference by Similarity to Ideal Solution method). In the current paper, six criteria have been considered instead of two for improving the supplier's selection process which are product quality, product cost, location, delivery time, information system and service rating. The contribution of this study is to give improved suppliers' selection process to the company.

2 Methodology: Fuzzy Logic Approach

In the method of fuzzy logic, ratings and weights are assessed by linguistic values for various factors which are then expressed in trapezoidal or triangular fuzzy numbers. The ratings and weightages of the criteria in the problem are estimated by variables related to linguistic since human judgments cannot prioritize with exact numerical value. The decision matrix is transformed into a weighted-normalized fuzzy decision matrix and a closeness coefficient of each option is estimated to rank all options.

2.1 Fuzzy Set-Theory

F-AHP (Fuzzy Analytic Hierarchy Process) connects the fuzzy theory to basic AHP (Analytic Hierarchy Process). AHP is used to compare pair-wise alternatives subject to various criteria. It is a decision support tool for multi-criteria decision problems. The goal of AHP tool is in the first level, and the criteria and subcriteria are in the II and III levels, respectively. The alternatives are found in the final or fourth level. In F-AHP, the triangular membership functions are defined for the pair-wise comparisons. Fuzzy set theory was first introduced by Zadeh [7] which is used for manipulation of data and information subject to non-statistical uncertainties. Some

basic definitions of fuzzy sets, fuzzy numbers and linguistic variables are reviewed by Zadeh [8], Buckley [9], Kaufmann and Gupta [10]. Kumari et al. [11] proposed some new designs with fuzzy [12] and neuro-fuzzy systems [13]. Compared to binary logic, fuzzy logic variables may have a truth value that ranges in degree between 0 and 1.

2.2 Definitions of Fuzzy Sets

A fuzzy set ‘A’ in universe of discourse ‘X’ is characterized by a function of membership ‘ $\mu_A(x)$ ’ which is associated with each element ‘x’ in ‘X’, a real number in the interval (0, 1), the function value is the term of grade of membership of ‘x’ in ‘A’ [10]. A fuzzy set ‘A’ in universe of discourse ‘X’ is convex if and only if

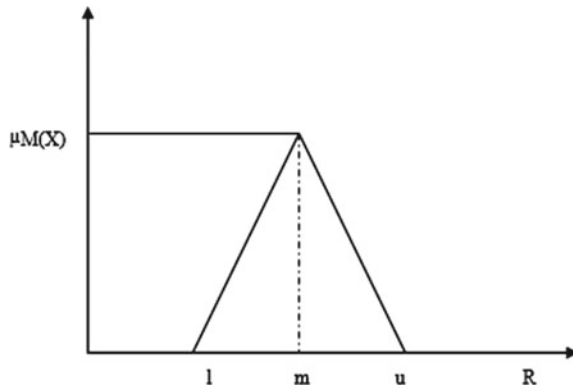
$$\mu_A(\lambda + (1 - \lambda)) \min(\mu_A(x_1), \mu_A(x_2))$$

For all ‘X’ and all ‘ λ ’ [0, 1], where min denotes the minimum operator [14].

A triangular fuzzy number \tilde{A} is represented by (l, m, u) that is shown in Fig. 1 such that $l \leq m \leq u$.

where ‘ l ’ is the smallest possible value, ‘ m ’ is the most promising value, and ‘ u ’ is the largest possible value.

Fig. 1 Membership function of a TFN [5]



3 Case Study

3.1 *Introduction of the Company*

NBC Bearings is founded in 1946 by the great industrialist late ‘Shri B.M.Birla.’ NBC produces over 100 million bearings each year in more than 1000 sizes. The products of NBC are ball bearings, tapered roller bearings and double-row angular contact (DRAC) bearings, cylindrical and spherical roller bearings.

The present procedure is applicable to the following category of supplier:

- Raw material (tubes, bars, wires, forged rings)
- Semi-finish product
- Product packing material.

3.2 *Current Supplier Selection Method*

The present procedure of the supplier selection in NBC Company is based on the quality rating and service rating factor, but there are more than two factors important like product price, information system, location, etc. Therefore, in this thesis we consider the six factors such as product price, service rating, information system, location, products quality and delivery time. In this thesis, six criteria and eight potential suppliers are determined as a result of negotiations held with decision makers.

3.3 *Supplier Selection Criteria Description*

There are a number of supplier selection criteria. In this work, six criteria are considered which are cost, product quality, location, price, information system and service rating. These six criteria are explained below [15–17].

3.3.1 Cost/Price

The cost/ price dimensions are: total cost, payment procedures, competitive pricing, quantity discounts and payment terms.

3.3.2 Quality

Selection criteria involve quality control methods, handling of complaints, quality manuals and internal rating and reporting systems.

3.3.3 Service Rating

Service rating is the flexibility in the implementing changes in delivery, design, etc. Service rating is a very important factor in supplier selection criteria. Service rating includes following parameters:

- Cooperativeness and readiness to help in emergencies.
- Response on quality complaints including replacement of rejected materials.
- Flexibility in implementing changes in delivery, design, etc.
- Promptness in reply.
- Compatibility to bill payment terms.

Service rating (SR) on overall basis is to be assigned by a committee consisting of representatives from purchase department and planning department. The final service rating for a given vendor will be the average of rating assigned by all members of the committee. The service rating shall be once a year for a given vendor and shall be completed well before the tendering action for the next year's requirement, based on the experiment from the supplier for the previous year.

3.3.4 Delivery Time

The delivery dimensions are: ability to expedite an order, time taken for delivery of the supplies, upcoming delivery commitments, transportation safety and security and transportation modes.

3.3.5 Location of Supplier

Location is also important criteria for supplier selection. If supplier locates near the organization, then it is better for organization. Supplier location is also impact on supplier selection.

3.3.6 Information System

Supplier should be fully integrated with information and communication technology. There is a trade-off between the ease of implementing a system and the system's level of complexity.

3.4 Solution of Supplier Selection Problem Using FUZZY AHP and FUZZY TOPSIS Method

In this section, the evaluation methodology is followed which is described in previous section. The eight supplier alternatives and six criteria (Product Quality, Service Quality, Delivery Time, Price, Location and Information System) are selected. Figure 2 shows the flow chart for evaluation of supplier selection.

Step 1: The supplier alternative rating is given according to the supplier criteria in terms of linguistic values. The selection criteria of supplier and alternatives of supplier are transformed into linguistic variables which are given in Table 1. Table 1 gives the linguistic values in terms of fuzzy number.

Step 2: The fundamental relational scale is adopted for pair-wise comparisons in which intensity of importance on an absolute scale in between 1 and 9. If absolute scale is 1, then it means two activities contribute equally to the objective. If absolute scale is 2, then it means weak importance which in turn means past experience slightly favor one activity and it represented in the scale of fuzzy number as (1, 2, 3). The fundamental relational scale which follows in this work is shown in Table 2.

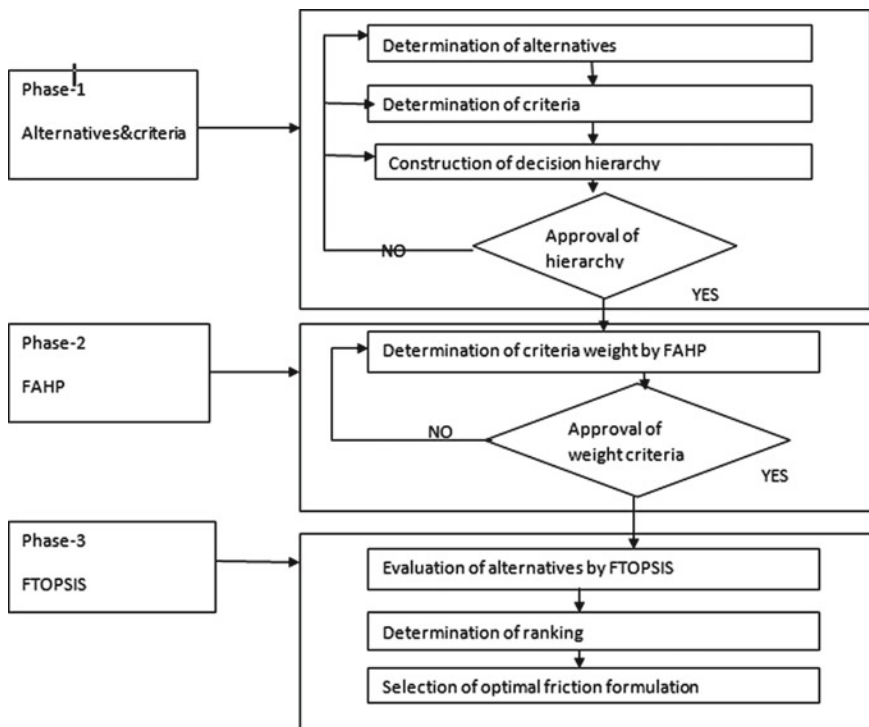


Fig. 2 Evaluation methodology of supplier selection

Table 1 Linguistic values and fuzzy numbers [18]

Linguistic values	Fuzzy numbers
Very low (VL)	(0, 0.10, 0.25)
Low (L)	(0.15, 0.30, 0.45)
Medium (M)	(0.35, 0.50, 0.65)
High (H)	(0.55, 0.70, 0.85)
Very high (VH)	(0.75, 0.90, 1)

Table 2 Relational scale

Intensity of importance on an absolute scale	Definition	Explanation	Scale of FUZZY numbers
1	Equal importance	Equal contribution by two activities	(1, 1, 1)
2	Weak importance	Slight favor of one activity due to past experience	(1, 2, 3)
3	Moderate importance	Moderate favor of one activity due to past experience	(2, 3, 4)
4	Preferable	Strong favor of one activity due to past experience	(3, 4, 5)
5	Essential or strong importance	Strong favor of one activity due to past experience	(4, 5, 6)
6	Fairly good importance	Strong favor of one activity due to past experience	(5, 6, 7)
7	Very strong importance	An activity is dominating in practice	(6, 7, 8)
8	Absolute	An activity is absolutely favored	(7, 8, 9)
9	Extreme importance	The favor of one activity is of the highest possible order of affirmation	(8, 9, 10)

Step 4: Table 2 is used in the pair-wise comparison. From the survey in purchase department and brainstorming, the comparison matrix is constructed. In the product quality row and service rating column value is 2 which means product quality is two times weighting than service rating. Similarly, in product quality row and delivery time column value is 3 means product quality is 3 time important than delivery time. All the criteria values corresponding other criteria are shown in Table 3.

Table 3 Pair-wise comparison matrix

	Product quality	Service rating	Delivery time	Price	Location	Information system
Product quality	1	2	3	2	2	2
Service rating	0.5	1	2	1	3	3
Delivery time	0.333	0.5	1	3	2	2
Price	0.5	1	0.333	1	2	2
Location	0.5	0.333	0.5	0.5	1	0.5
Information system	0.5	0.333	0.5	0.5	2	1

In the pair-wise comparison matrix, decision makers decided the importance of one criterion to other criteria. After the making of pair-wise matrix, we find the consistency index (CI) value by the use of software CGI.CGI software gives the following results:

$$\text{Max. eigenvalue} = 6.46843 \quad \text{C.I.} = 0.0936856$$

$$\text{Weights (eigenvector)} \quad \text{Product quality} = 0.291707$$

$$\text{Service rating} = 0.213817 \quad \text{Delivery time} = 0.178594$$

$$\text{Product price} = 0.140721$$

$$\text{Supplier location} = 0.0778034$$

$$\text{Information system} = 0.0973571.$$

Where consistency index value measures the consistency of the pair wise comparison. The CI value is defined as

$$\text{CI} = (\lambda_{\max} - 1)/(n - 1).$$

where λ_{\max} is largest (principal) eigenvalue and n is pairwise comparison order (size of matrix). A comparison matrix can be thought to be consistent if its CI value is less than 0.10.

Step 5: After making the pair-wise comparison, this matrix is converted in terms of fuzzy number which is shown in Table 4.

Step 6: After converting the pair-wise comparison matrix in fuzzy number terms, the individual weights of each criteria or attribute are calculated. In this result, we multiply the first fuzzy number in each row and then give the power 1/6. Further use this process for second fuzzy numbers in first row and similarly for third numbers (l_1, m_1, n_1). We use similar calculation for every row. Then, sum the all rows first fuzzy numbers, second fuzzy numbers and third fuzzy numbers (l_2, m_2, n_2). Then, we use the formula for individual row as $[(l_1/n_2), (m_1/m_2), (n_1/l_2)]$. Finally, we get the individual criteria weight in fuzzy terms which is shown in Table 5.

Step 7: After weighting the criteria, the linguistic scale value for supplier alternatives from purchase department of NBC Company for each criterion are collected.

Table 4 Pair-wise comparison matrix in terms of fuzzy numbers

	Product quality	Service rating	Delivery time	Price	Location	Information system
Product quality	(1, 1, 1)	(1, 2, 3)	(2, 3, 4)	(1, 2, 3)	(1, 2, 3)	(1, 2, 3)
Service rating	(0.333, 0.5, 1)	(1, 1, 1)	(1, 2, 3)	(1, 1, 1)	(2, 3, 4)	(2, 3, 4)
Delivery time	(0.25, 0.333, 0.5)	(0.333, 0.5, 1)	(1, 1, 1)	(2, 3, 4)	(1, 2, 3)	(1, 2, 3)
Price	(0.333, 0.5, 1)	(1, 1, 1)	(0.25, 0.333, 0.5)	(1, 1, 1)	(1, 2, 3)	(1, 2, 3)
Location	(0.333, 0.5, 1)	(0.25, 0.333, 0.5)	(0.333, 0.5, 1)	(0.333, 0.5, 1)	(1, 1, 1)	(0.333, 0.5, 1)
Information system	(0.333, 0.5, 1)	(0.25, 0.333, 0.5)	(0.333, 0.5, 1)	(0.333, 0.5, 1)	(1, 2, 3)	(1, 1, 1)

Table 5 Result of comparison matrix (FAHP)

Attribute	Fuzzy weight criteria
Product quality	(0.11948, 0.289230, 0.59374)
Service quality	(0.1116968, 0.218819, 0.43200)
Delivery time	(0.07899, 0.17032, 0.3668)
Price	(0.07035, 0.1417927, 0.29115)
Location	(0.04060, 0.07957, 0.20187)
Information system	(0.048772, 0.100273, 0.24245)

The linguistic values consist of five values such as very low (VL), low (V), medium (M), high (H), very high (VH). Table 6 shows the linguistic fuzzy evaluation matrix for the supplier alternatives.

Table 6 Linguistic fuzzy evaluation matrix for the ranking of alternatives

	Product quality	Service rating	Delivery time	Price	Location	Information system
VINAYAK	VH	VH	H	H	H	M
CHANDRA	M	VH	M	VH	VH	H
WIRE RINGS	M	VH	VH	M	M	VH
ADITYA	VH	H	M	VL	H	H
TASHI	M	M	L	M	M	VH
HARSHA	VH	VH	M	M	H	H
MANU	VH	M	L	L	M	M
AGARSEN	VL	M	H	M	H	M

Table 7 Linguistic fuzzy evaluation matrix

	Product quality	Service rating	Delivery time	Price	Location	Information system
VINAYAK	(0.75, 0.90, 1)	(0.75, 0.90, 1)	(0.55, 0.70, 0.85)	(0.55, 0.70, 0.85)	(0.55, 0.70, 0.85)	(0.35, 0.50, 0.65)
CHANDRA	(0.35, 0.50, 0.65)	(0.75, 0.90, 1)	(0.35, 0.50, 0.65)	(0.75, 0.90, 1)	(0.75, 0.90, 1)	(0.55, 0.70, 0.85)
WIRE RINGS	(0.35, 0.50, 0.65)	(0.75, 0.90, 1)	(0.75, 0.90, 1)	(0.35, 0.50, 0.65)	(0.35, 0.50, 0.65)	(0.75, 0.90, 1)
ADITYA	(0.75, 0.90, 1)	(0.55, 0.70, 0.85)	(0.35, 0.50, 0.65)	(0.10, 0.25)	(0.55, 0.70, 0.85)	(0.55, 0.70, 0.85)
TASHI	(0.35, 0.50, 0.65)	(0.35, 0.50, 0.65)	(0.15, 0.30, 0.45)	(0.35, 0.50, 0.65)	(0.35, 0.50, 0.65)	(0.75, 0.90, 1)
HARSHA	(0.75, 0.90, 1)	(0.75, 0.90, 1)	(0.35, 0.50, 0.65)	(0.35, 0.50, 0.65)	(0.55, 0.70, 0.85)	(0.55, 0.70, 0.85)
MAV	(0.75, 0.90, 1)	(0.35, 0.50, 0.65)	(0.15, 0.30, 0.45)	(0.15, 0.30, 0.45)	(0.35, 0.50, 0.65)	(0.35, 0.50, 0.65)
AGARSEN	(0, 0.10, 0.25)	(0.35, 0.50, 0.65)	(0.55, 0.70, 0.85)	(0.35, 0.50, 0.65)	(0.55, 0.70, 0.85)	(0.35, 0.50, 0.65)
Weight criteria	(0.1194, 0.2892, 0.5937)	(0.1116, 0.2188, 0.4320)	(0.0789, 0.1703, 0.3668)	(0.0703, 0.1417, 0.29115)	(0.0406, 0.0795, 0.20187)	(0.0487, 0.1002, 0.2424)

Step 8: The linguistic fuzzy evaluation matrix is created by decision maker and purchase department. According to the scale, we convert this linguistic value into the fuzzy number by the use of scale as shown in Table 1. This Table 1 is followed by most of the journals which is related to linguistic values and fuzzy number. We convert the linguistic values as VL = (0, 0.10, 0.25), L = (0.15, 0.30, 0.45), M = (0.35, 0.50, 0.65), H = (0.55, 0.70, 0.85) and VH = (0.75, 0.90, 1) which is presented in Table 7.

Step 9: In Table 8, fuzzy weighted evaluation matrix is presented. From the help of Table 8, we multiplying weighted criteria in each row corresponding to criteria. For example supplier alternative VINAYAK the product quality weighting criteria (from Table 5) is (0.1194, 0.2892, 0.5937) and Vinayak product quality value in terms of fuzzy is (from Table 7) (0.75, 0.90, 1) then the value of fuzzy weighted evaluation matrix for Vinayak is calculated as [(0.75 × 0.1194), (0.90 × 0.2892), (1 × 0.5937)]. The value for Vinayak is [0.089, 0.260, 0.593]. Similar calculation is done for other supplier alternatives, and we get the above fuzzy weighted evaluation matrix as shown in Table 8.

Step 10: The fuzzy positive ideal and fuzzy negative ideal solution for given criteria is shown in Table 9.

Step 11: In Table 8, the given element is normalized to TFN and their ranges are close to interval [0, 1]. We consider fuzzy positive ideal solution as (1, 1, 1) and (0,

Table 8 Fuzzy weighted evaluation matrix

	Product quality	Service rating	Delivery time	Price	Location	Information system
VINAYAK	(0.089, 0.260, 0.593)	(0.083, 0.196, 0.432)	(0.043, 0.119, 0.311)	(0.038, 0.099, 0.247)	(0.022, 0.055, 0.171)	(0.017, 0.050, 0.157)
CHANDRA	(0.418, 0.144, 0.385)	(0.083, 0.196, 0.432)	(0.027, 0.085, 0.238)	(0.052, 0.127, 0.291)	(0.030, 0.071, 0.210)	(0.026, 0.070, 0.206)
WIRE RINGS	(0.418, 0.144, 0.385)	(0.083, 0.196, 0.432)	(0.059, 0.153, 0.366)	(0.024, 0.070, 0.189)	(0.014, 0.039, 0.131)	(0.036, 0.090, 0.242)
ADITYA	(0.089, 0.260, 0.593)	(0.061, 0.153, 0.367)	(0.027, 0.085, 0.238)	(0, 0.014, 0.072)	(0.022, 0.055, 0.171)	(0.026, 0.070, 0.206)
TASHI	(0.418, 0.144, 0.385)	(0.039, 0.109, 0.280)	(0.011, 0.051, 0.165)	(0.024, 0.070, 0.189)	(0.014, 0.039, 0.131)	(0.036, 0.090, 0.242)
HARSHA	(0.089, 0.260, 0.593)	(0.083, 0.196, 0.432)	(0.027, 0.085, 0.238)	(0.024, 0.070, 0.189)	(0.022, 0.055, 0.171)	(0.026, 0.070, 0.206)
MANU	(0.089, 0.260, 0.593)	(0.039, 0.109, 0.280)	(0.011, 0.051, 0.165)	(0.010, 0.0425, 0.131)	(0.014, 0.039, 0.131)	(0.017, 0.050, 0.157)
AGARSEN	(0, 0.028, 0.148)	(0.039, 0.109, 0.280)	(0.043, 0.119, 0.311)	(0.024, 0.070, 0.189)	(0.022, 0.055, 0.171)	(0.017, 0.050, 0.157)

Table 9 Fuzzy ideal solution

Product quality	Service rating	Delivery time	Price	Location	Information system
(1, 1, 1)	(1, 1, 1)	(0, 0, 0)	(0, 0, 0)	(0, 0, 0)	(1, 1, 1)
(0, 0, 0)	(0, 0, 0)	(1, 1, 1)	(1, 1, 1)	(1, 1, 1)	(0, 0, 0)

Table 10 Fuzzy closeness index and ranking of supplier alternatives

Supplier	Euclidian distance (fuzzy positive)	Euclidian distances (fuzzy negative)	Fuzzy closeness index	Ranking
VINAYAK	5.065	1.202	0.808	2
CHANDRA	5.005	1.203	0.806	3
WIRE RINGS	4.856	1.372	0.779	6
ADITYA	5.024	1.028	0.830	1
TASHI	5.024	1.261	0.799	4
HARSHA	5.110	1.418	0.782	5
MANU	5.313	1.905	0.736	8
AGARSEN	5.212	1.770	0.746	7

0, 0) for benefit criteria and fuzzy negative ideal solution as (1, 1, 1) and (0, 0, 0) for cost criteria. The value of closeness index is given in Table 10.

The fuzzy closeness index of the supplier alternatives is calculated which is shown in Table 10. According to the closeness index, the ranking of supplier alternatives in descending order is ADITYA, VINAYAK, CHANDRA, TASHI, HARSHA, WIRE RINGS, AGARSEN and MANU. The final result of supplier selection alternatives is shown in Table 10 which shows the final ranking for suppliers alternatives, which is based on closeness index. The supplier ADITYA is selected as the best one for the NBC Company.

4 Conclusion

Supplier selection is an important task in the whole purchasing process. It has a great impact over the expenditure and organization objective. Generally, there are many suppliers for single items with varying capabilities. Organization generally faces a problem of selection of a supplier for an item fulfilling the organizational objectives. This requires a systematic approach. The literature related to this is reviewed in this paper which falls into two categories: the criteria to be used and the methodology for the ranking of the suppliers based on the company requirements and the supplier capabilities. The most important criteria include price, quality, service rating, delivery time, and location and information system. A case study is presented in this dissertation in which a private sector company, NBC, is considered as the case company.

Existing supplier selection process in the company is first reviewed, and the weaknesses are identified. In order to overcome these weaknesses, a supplier selection process is proposed. Four factors which have not been used by the company earlier are suggested for use. In this research work, we have used fuzzy AHP for weighting the selection criteria and fuzzy TOPSIS method for the ranking of supplier alternatives. The initial response of the company executives is very good for the new process, and it is hoped that company will be benefited to a great extent by the new supplier selection process.

Acknowledgements We acknowledge 'NBC Bearings, Jaipur' where ample opportunities and useful insights have been provided for the current case study.

References

1. Bello MJS (2003) A case study approach to the supplier selection process. Doctoral dissertation, University Of Puerto Rico Mayagüez Campus
2. Bhutta MKS (2003) Supplier selection problem: methodology literature review. *Journal of International Information Management* 12(2):5
3. Sonmez M (2006) Review and critique of supplier selection process and practices. © Loughborough University
4. Ho W, Xu X, Dey PK (2010) Multi-criteria decision making approaches for supplier evaluation and selection: a literature review. *Eur J Oper Res* 202(1):16–24
5. Abdullah L (2018) Zulkifli N A new DEMATEL method based on interval type-2 fuzzy sets for developing causal relationship of knowledge management criteria. *Neural Comput Appl* 31:1–17
6. Ayodele TR, Ogunjuyigbe ASO, Odigie O (2018) Munda JL A multi-criteria GIS based model for wind farm site selection using interval type-2 fuzzy analytic hierarchy process: the case study of Nigeria. *Appl Energy* 228:1853–1869
7. Zadeh LA (1965) Fuzzy sets. *Inf Control* 8(3):338–353
8. Zadeh LA (1975) The concept of a linguistic variable and its application to approximate reasoning—I. *Inf Sci* 8(3):199–249
9. Buckley RC (1985) Distinguishing the effects of area and habitat type on island plant species richness by separating floristic elements and substrate types and controlling for island isolation. *J Biogeogr* 527–535
10. Kaufmann A, Gupta MM (1991) Introduction to fuzzy arithmetic: theory and applications. Arden Shakespeare
11. Kumari R, Kumar S, Sharma VK (2015) Fuzzified expert system for employability assessment. *Procedia Comput Sci* 62:99–106
12. Kumari R, Kumar S, Sharma VK (2014). Air conditioning system with fuzzy logic and neuro-fuzzy algorithm. In: Proceedings of the second international conference on soft computing for problem solving (SocProS 2012), December 28–30, 2012. Springer, New Delhi, pp 233–242
13. Kumari R, Sharma VK, Kumar S (2014) adaptive neural fuzzy inference system for employability assessment. *Int J Comput Appl Technol Res* 3(3):159–164
14. Yuan Y, Shaw MJ (1995) Induction of fuzzy decision trees. *Fuzzy Sets Syst* 69(2):125–139
15. De Boer L, van der Wegen L, Telgen J (1998) Outranking methods in support of supplier selection. *Eur J Purchasing Supply Manag* 4(2):109–118
16. De Boer L, Van der Wegen LLM (2003) Practice and promise of formal supplier selection: a study of four empirical cases. *J Purch Supply Manag* 9(3):109–118

17. Keskar HS (2004) Supplier selection metrics and methodology. Doctoral dissertation, University of Cincinnati
18. Kilincci O, Onal SA (2011) Fuzzy AHP approach for supplier selection in a washing machine company. *Expert Syst Appl* 38(8):9656–9664

A New Approach to Classify the Boolean Functions Based on Heuristic Technique



Rajni Goyal and Harshit Grewal

Abstract Classification of the Boolean functions still remains an open problem for theoretical cryptographers. In this paper, one method is introduced for systematic classification of Boolean functions for n -variables. Our classification method is an evolutionary approach based on nonlinearity. In the method, we started with 1-variable functions and found the classification formula for n -variables.

Keywords Classification · NSGA-II · Boolean functions · Cryptography

1 Introduction

Any new technique of systematic classification of Boolean functions is always an area of interest for theoretical cryptographers. Classification methods are always welcomed because it makes representation of Boolean functions extremely easy, and Boolean function that belongs to same class will have same properties. In [1], authors have mentioned mainly three criteria to classify the set of n -input functions: cardinality of functions in each class, the cardinality of classes and the cardinality of NPN classes. In [2], authors partitioned the set of Boolean functions into equivalence classes based on permutation and combination. They have given the formula to find number of classes based on this approach. In [3], the selection procedure of the representative from each class has been highlighted. Moreover in [4], set of Boolean functions has been divided into two groups: linear and affine, and an algorithm has been given to find the count of Boolean functions in each group. Some author partitioned the classes based on properties like autocorrelation, resiliency, etc. Some methods listed in [5, 6] are based on above properties. In [7], Rout et al. gave two new approaches, recursive and nonrecursive. They have partitioned the whole set of Boolean functions in such a way exactly one affine function is representative of each

R. Goyal (✉) · H. Grewal
Amity University, Noida, UP 201313, India
e-mail: rgoyal1@amity.edu

H. Grewal
e-mail: harshit.grewal@s.amity.edu

class. This method was based on concatenation and recursive approach. In [8], two approaches are given: One is based on Hamming distance and another on recursive. Above all, selection of representative is also an important task. In [3], Golomb has also highlighted the procedure of selection of a representative function, with one member from each equivalence class.

After analyzing all the work above, we formulated an evolutionary approach. In our approach, we started with 1-variable functions and went up to n -variables. We applied NSGA-II and observed better results than previously listed results.

We have arranged our paper as follows: Related definitions (taken from the literature) have been given in Sect. 2. A brief description of evolutionary approach that is based on heuristic technique (NSGA) has been given in Sect. 3. Our developed approach and classification method for n -variable Boolean functions have been described in Sect. 4. Results and discussion has been described in Sect. 4. In Sect. 5, our work has been concluded.

2 Related Definitions

2.1 Boolean Function

\mathbb{F}_2 is a field of two elements and \mathbb{F}_2^n is a n -dimensional vector space over \mathbb{F}_2 . Boolean function $f(x_1, \dots, x_n)$ is a mapping from a set of all possible bit string of \mathbb{F}_2^n to \mathbb{F}_2 . Collection of all possible Boolean function can be denoted by F_n , and cardinality of this set is 2^{2^n} .

Number of 1's present in the string of $f(x_1, \dots, x_n)$ is called weight of Boolean function. If number of 1's is equal to the number of 0's in the string of $f(x_1, \dots, x_n)$, then Boolean function is called balanced Boolean function.

An affine function is a Boolean function with algebraic degree one (at most). The n -variable affine function can be represented by

$$f_{\text{affine}}(x) = a_1.x_1 \oplus a_2.x_2 \oplus a_3.x_3 \oplus \dots \oplus a_n.x_n \oplus c,$$

where a_i and $c \in \mathbb{F}_2$. For $c = 0$, above function is called linear.

2.2 Hamming Distance

The Hamming distance between two functions f_1 and f_2 can be defined as the number of truth table positions in which the functions f_1 and f_2 are distinct, and we denote Hamming distance by $\text{hd}(f_1, f_2)$. So,

$$\text{hd}(f_1, f_2) = |\{x : f_1(x) \neq f_2(x)\}|,$$

where $|\cdot|$ represents the cardinality of the set.

2.3 Walsh–Hadamard Transform

By Walsh–Hadamard transform W_{HT} , we represent a Boolean function with a different manner. For a given $t \in \mathbb{F}_2^n$, the W_{HT} of a f (Boolean functions) can be represented by $W_f(t)$ and defined by

$$W_f(t) = \sum_{x \in \mathbb{F}_2^n} (-1)^{f(x)+t \cdot x}.$$

2.4 Nonlinearity of Boolean Function (f)

Nonlinearity of a Boolean function (f) is the minimum Hamming distance from set of all affine functions, which is called nonlinearity of that functions. It can be represented by the following mathematical formula:

$$Nl(f) = \binom{1}{2} * (2^n - \max_{\lambda \in \mathbb{F}_2^n} |W_f(t)|)$$

3 Our Approach for Classification

In this approach, we have described the developed method for classification. Our developed method can be explained into two parts: (i) formulation of objective function and (ii) applications (non-dominating sorting genetic algorithms-II) [9].

- (i) Formulation of objective function: We have used criteria of nonlinearity to classify the Boolean functions.

We know that for n -variable Boolean function the highest limit of nonlinearity can be given by

$$Nl(f) = \left(\frac{1}{2}\right) * \left(2^n - 2^{\frac{n}{2}-1}\right).$$

and lowest is zero. As there are total 2^{2^n} Boolean functions for n -variable, hence these functions attain nonlinearity between zero and $(2^n - 2^{\frac{n}{2}-1})$. So, we classified set of all Boolean functions based on their nonlinearity and found interesting results. Firstly, we formulated an objective function and then applied NSGA-II on this with proper parameter. Obtained results are listed in Tables 1, 2 and 3.

As per def (2.3), value of Walsh–Hadamard transform can be given by the following formula:

$$W_f(\lambda) = \sum_{x \in \mathbb{F}_2^n} (-1)^{f(x)+\lambda \cdot x}.$$

and nonlinearity of Boolean function for n -variable can be given by

$$Nl(f) = \left(\frac{1}{2}\right) * \left(2^n - \max_{\lambda \in \mathbb{F}_2^n} |\sum_{x \in \mathbb{F}_2^n} (-1)^{f(x)+\lambda \cdot x}| \right).$$

Table 1 Obtained results for 1-variables

Nonlinearity	Boolean function (class) results by NSGA-II
0	00, 01, 10, 11

Table 2 Obtained results for 2-variables

Nonlinearity	Boolean function (class) results by NSGA-II
0	0000, 0011, 1100, 1010, 0110, 0101, 1111, 1001
1	0001, 0111, 1110, 1000, 0100, 0010, 0001, 1101

Table 3 Obtained results for 3-variables

Nonlinearity	Boolean function (class) results by NSGA-II
0	Total 16 functions of even weight (0 and 4) with symmetrical patterns like 00000000, 11111111, 10101010, 01010101, 01011010, 10100101, 01100110, 10011001, 10010110, 01101001, 11110000, 00001111, 11001100, 00110011, 00111100, 11000011
1	128 (functions all the Boolean functions of odd weight)
2	Total 112 functions of even weight (2, 4 and 6) with asymmetrical patterns (11101000, 11011000, 10111000, 01111000, 11100100, 11010100, 01110100, 10101100)

We assign f_1 equal to nonlinearity and take as our objective function,

$$f_1 = NL(f),$$

$$f_1 = NL(f) = \left(\frac{1}{2}\right) * (2^n - \max_{\lambda \in F_2^n} |\sum_{x \in F_2^n} (-1)^{f(x)+\lambda \cdot x}|),$$

To optimize the above objective function, we have applied optimization technique (NSGA-II).

- (ii) Application of optimization technique: After forming the objective function (f_1), we have applied optimization technique at f_1 . With the help of proper parameters, we have found some desired results (f') and these results are shown in Sect. 5. The proper parameters that we have taken for our optimization technique are listed in Tables 4, 5 and 6. For 1-variable, there are a total of 4 Boolean functions. When we have applied NSGA-II on our objective function, we got zero value of nonlinearity for all four Boolean functions; hence, we have placed all functions in one class. So, there is only one class for one-variable functions.

When we applied NSGA-II on objective function for 2-variable Boolean functions, we got two values of nonlinearity: zero and one. So, we placed all Boolean functions

Table 4 Parameters (for 1-variables)

Count of generations	100
Count of population	16
probability1 (of C_R)	0.777
probability2 (of M_T)	0.1181
SRN*	0.9999
Total number of bits (for each variable)	1
Total objective functions	1
Constraints	0

* Related to NSGA-II

Table 5 Parameters (for 2-variables)

Count of generations	500
Count of population	256
probability1 (of C_R)	0.776
probability2 (of M_T)	0.1182
SRN*	0.9998
Total number of bits (for each variable)	1
Total objective functions	1
Constraints	0

* Related to NSGA-II

Table 6 Parameters (for 3-variables)

Count of generations	2000
Count of population	256
probability1 (of C_R)	0.811
probability2 (of M_T)	0.1180
SRN*	0.9877
Total number of bits (for each variable)	1
Total objective functions	1
Constraints	0

* Related to NSGA-II

in two classes. Boolean functions belonging to a single class have same nonlinearity. We have observed few similarities among the functions of a class, such as all odd weight functions belonged to one class whereas even weight functions belonged to another class. Another observation is that both classes have same number of Boolean functions. Similarly, we can classify Boolean functions for higher variables as well. Main feature of this method is that, corresponding to a value of nonlinearity, we found all possible Boolean functions in a single run with the help of proper parameters. In Tables 7, 8 and 9, we have shown subclassification of classes for all three variables.

The inferences drawn from the above classification method are as follows:

1. Functions that belong to a class have same nonlinearity.
2. No. of classes are very less.
3. Cardinality of each class is not necessarily same.
4. Functions that belong to same class have similar pattern of bits.

Table 7 Subclassification of class-I for 1-variable functions

No. of Boolean function	Hamming distance (from the base Boolean function 00000000)	Weight
1	0	0
2	1	1
1	2	2

Table 8 Subclassification of class-I of 2-variable functions

No. of Boolean function	Hamming distance (from the base Boolean function 00000000)	Weight
1	0	0
6	2	2
1	6	6

Table 9 Subclassification of class-I of 3-variable functions

No. of Boolean function	Hamming distance (from the base Boolean function 00000000)	Weight
8	1	1
56	3	3
56	5	5
8	7	7

4 Results and Discussion

After applying the method developed in Sect. 4 and in Sect. 5, we classified the Boolean functions. These functions belong to different classes, and same class functions have symmetry among them. The parameters taken to classify functions (by NSGA-II) for 1-, 2- and 3-variables are listed in Tables 4, 5 and 6, respectively. Our methods are new and with less complexity as compared to [2, 3, 7, 8].

5 Conclusion

In this piece of work, we have partitioned the set of n -variable Boolean functions into equivalence classes of same size. Main characteristic of our first method is that we need only one member of previous class to define whole class. Classification has been done by two different approaches. Our methods are efficient and less complicated. In evolutionary approach method, we have found all possible results in single run (for each n -variable) only. This is the main characteristic of this method.

Acknowledgements The authors are thankful to the Amity University, Noida, and Gopisoft Private Limited of India, for financial and technical assistance.

References

1. Correia VP, Reis AI (2001) Classifying n -input Boolean functions. In: Proceedings of the 7th workshop IBERCHIP (IWS'01), Montevideo, Uruguay, p 5866
2. Slepian D On the number of symmetric types of Boolean functions of n variables. Soc Ind Math 05(02):185–193
3. Golomb SW (1959) On the classification of Boolean functions. IRE Trans Circuit Theory 6(5):
4. Harrison MA, On the classification of Boolean functions by the general linear and affine groups. J Soc Ind Appl Math 12(2):285–299
5. Braeken A, Borissov Y, Nikova S, Preneel B.: Classification of Boolean Functions of 6 variables or less with respect to cryptographic properties. In: Sixth international scientific conference FMNS2015, At Blagoevgrad, vol 1, 2015

6. Shtrakov S, Damyanov I (2015) On the classification of Boolean functions. In: Proceedings of the sixth international scientific conference FMNS2015, vol 1, pp 124–130
7. Rout RK, Chaudhary PP, Sahoo S Classification of Boolean functions where affine functions are uniformly distributed. *J Discrete Math*, vol 2013. Artical ID 270424
8. Das JK, Choudhury PP, Classification of n -variable Boolean functions through Hamming distance and their application in system biology. *Int J Comput Appl (IJCA)*, (0975 8887), NCWBCB-2014, 11
9. Deb K, Pratap A, Agarwal S, Meyarivan T (2002) A fast and elitist multiobjective genetic algorithm. *IEEE Trans Evol Comput* 6(2):182–197

Influence of Object-Oriented Software Design Measures on Reliability: Fuzzy Inference System Perspective



Syed Wajahat Abbas Rizvi

Abstract Looking at the lifestyle that everyone of us is living, it can be easily noticed that the impact of information technology is growing exponentially. Whether it is urban or rural area, everyone is heavily dependent on software directly or indirectly. This dependence on software has been creating a pressure on the information technology industry to meet this exponential demand. At the same time, various software quality attributes have been gaining its importance. The roots of a reliable software lie in the careful and informed implementation of design stage. Therefore, author has focused on the design stage and identified some object-oriented design measures and further analyzed the impact of these measures on the identified quality attribute that is reliability of application software using the fuzzy inference system.

Keywords Object-oriented metrics · Software design · Software reliability · Fuzzy inference system

1 Introduction

Although there are numerous definitions of the software reliability but the most balanced way to describe the software reliability is the probability of failure-free software operation for a particular duration in a given environment [1]. As it could be perceived that such a huge rise in the demand of software-based applications has put together the entire planet, as long as knowledge sharing is concerned. All the vertical markets like telecom, retail, banking, forex trade, stock markets, education and transportation have been dependent on the software applications [2, 3]. The reliability of these application is of big concern. Such dependence is forcing the software developers to develop more software to encounter the growing user demand. It has been creating more and more burden on developers to market their software applications in lesser time; consequently, some of the applications developed under this situation are not meeting the criteria as far as their reliability is concerned [4].

S. W. A. Rizvi (✉)

Department of Computer Science and Engineering, Amity University, Uttar Pradesh, Lucknow, India

e-mail: swarizvi@lko.amity.edu

After noticing the criticality of reliability, its timely prediction, estimation or quantification needs to be done on priority basis. The more accurately it is quantified, the more successful will be the software application in its operational life. As far as SDLC is concerned, it is advantageous to arrest the factor as early as possible, those are having any negative impact on the subject that how much reliable is the software that is being developed. A significant quantity of unpleasant events had already occurred because of unreliability of software belonging to a variety of domains [4]. It is generally observed that various faults creep into the software in the requirements and design levels of software development life cycle [5]. And these are the phases of SD life cycle those had not been given required focus while estimating the software reliability. So, there is an emerging requirement that the measures from design stage need to be investigated for their influence that they have on the reliability of the finally delivered software. The remaining paper is organized as follows: Sect. 2 presents the state of the art on how object-oriented design level measures play a key role in quantifying the reliability of developing software. Section 3 focuses on some of the reliability-relevant software design metrics. Section 4 quantitatively analyzed as well as shortlisted design level measures along with their sensitivity analysis, and at last the study concludes in Sect. 5.

2 Related Work

Appropriate review of the literature regarding reliability-related research studies has revealed the actual scenario rolled-out in past three decades, and it highlights that reliability of the application is a key focused research area for the prediction of quality attributes of software applications [6–16]. During the earlier studies also, the researcher has critically studied a good number of efforts [4, 17, 18]. As the researcher has gone thoroughly to a significant studies, it has been inferred that a large spectrum of early stage software measures has been utilized in quantifying the software defects. But in most of the cases, the metrics belong to either object-oriented or product metrics. Saini et al. [19] performed study of related literature, and Sharma et al. [20] discussed specific software development approach. In a research study [21], author has suggested that appropriate selection of metrics is an issue that should not be ignored at any cost, because this becomes as a foundation for a reliability prediction model having higher accuracy.

3 Object-Oriented Design Measures

Researcher has observed that during the period of past twenty years, lot of researchers have focused on and used various object-oriented design measures in their studies. In this study, the author has gone through a significant number of studies to identify a set of design metrics those have proved to be very effective while modeling or

Table 1 Object-oriented design measures

S. No.	Design metrics
1	Lack of cohesion in methods (LCOM)
2	Inheritance metric complexity perspective (IMc)
3	Number of children (NOC)
4	Cohesion metric complexity perspective (CoMc)
5	Weighted method per class (WMC)
6	Response for a class (RFC)
7	Attribute hiding factor (AHF)
8	Message pass coupling (MPC)
9	Depth of inheritance (DIT)
10	Encapsulation metric complexity perspective (EMc)
11	Coupling metric complexity perspective (CMc)
12	Coupling between objects (CBO)
13	Data abstraction coupling (DAC)
14	Attribute inheritance factor (AIF)

predicting the reliability of software applications. After reviewing a good number of software metrics, the set of metrics listed in Table 1 has been chosen in the first round of this work. These measures have been proposed to predicting or estimating the reliability of the software. Researchers have proposed these metrics at various stages of software development like requirements, design and coding. Besides it a good number of reliability prediction models based on these software measures that have been published in last two decades. All these models are predicting or estimating the reliability by incorporating a considerable number of software metrics. These metrics are categorized as traditional, object-oriented and process metrics. However, looking at the existing literature, it does not seem appropriate to consider all types of reliability-relevant metrics in order to predict the corresponding software quality attributes.

It could be inferred in the literature that the root cause of most of the reliability-related issues is based on the faulty design of the application software being developed. Therefore, the researcher has focused in this study only on the design metrics. In order to cover the key aspects of object-oriented paradigm, researcher has shortlisted the four design metrics as inheritance metric (IMc), encapsulation metric (EMc), cohesion metric (CoMc) and coupling metric (CMc).

3.1 *Inheritance Metrics (IMc)*

It is an inheritance metric which gives the general complexity of a design in a class diagram hierarchy, comprised of various member functions as well as member variables or attributes [22].

$$IM = \text{Avarage of}\{IMClass\}$$

where

$$IMClass = (IClass)/(TClass)$$

High Value of Inheritance => Low Reliability.

3.2 Encapsulation Metric (EM)

This is the metric that computes the level of encapsulation with respect to complexity and focuses on the design level complexity through the numerous encapsulated methods as well as member variables of every class in the given class diagram [23].

$$EM = \text{Avarage of}\{EMClass\}$$

where

$$EMClass = (EClass)/(TClass)$$

High Value of Encapsulation => High Reliability.

3.3 Cohesion Metric (CoMc)

This is the metric that computes the level of cohesion with respect to complexity and focuses on design level complexity through various methods as well as member variables of every class in the given class diagram. Here the computation of this metric is defined as the average as specified below [24].

$$CoMc = \text{Avg}\{CoMc_Class\}$$

where

$$CoMc_Class = \text{Avarage of}(LCClass \text{ and } HCClass)$$

$$LCClass = (DUDM)/NDIC$$

$$HCClass = \sum(DUDM, IDUM)/NDIC$$

High Value of Cohesion => High Reliability.

Therefore, briefly we can show how the four identified design stage measures are associated with reliability

$$\begin{aligned} \text{IMc} &\propto 1/\text{Reliability}; \text{ CMc} \propto 1/\text{Reliability}; \\ \text{CoMc} &\propto \text{Reliability}; \text{ EMc} \propto \text{Reliability} \end{aligned}$$

4 Analysis Phase

Under this section of the article, the researcher is going to analyze that how identified object-oriented design metrics are impacting the software reliability at the end of design stage. The primary data used in this analysis is collected by the investigator from reputed software companies. Subsequently, it is fed into the MATLAB (Table 2).

4.1 Sensitivity Analysis

To accomplish the comprehensive scrutiny of the identified design level metrics on software reliability, the author has done the sensitivity analysis. Where the impact of the different combinations of these four design level metrics on the single variable is design level reliability (DLR), it is the output variable in fuzzy inference system that has been analyzed.

As the value of DLR depends on four design stage metrics IMc, EMc, CoMc and CM, so to control the reliability before the coding, more proactively it is better to

Table 2 DLR with respect to EM

CoM = 0%		CoM = 25%		CoM = 50%		CoM = 75%		CoM = 100%	
IM = 0%		IM = 25%		IM = 50%		IM = 75%		IM = 100%	
CM = 0%		CM = 25%		CM = 50%		CM = 75%		CM = 100%	
RLR = 0%		RLR = 25%		RLR = 50%		RLR = 75%		RLR = 100%	
EM	DLR	EM	DLR	EM	DLR	EM	DLR	EM	DLR
0.0	0.350	0.0	0.350	0.0	0.550	0.0	0.450	0.0	0.750
0.2	0.350	0.2	0.350	0.2	0.550	0.2	0.450	0.2	0.750
0.4	0.350	0.4	0.350	0.4	0.550	0.4	0.550	0.4	0.750
0.6	0.350	0.6	0.350	0.6	0.550	0.6	0.550	0.6	0.750
0.8	0.550	0.8	0.550	0.8	0.650	0.8	0.650	0.8	0.750
1.0	0.550	1.0	0.550	1.0	0.650	1.0	0.650	1.0	0.750

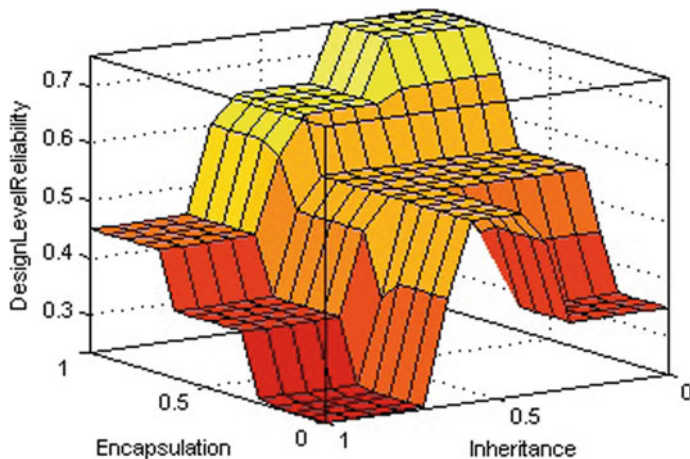


Fig. 1 Design level reliability versus encapsulation and inheritance

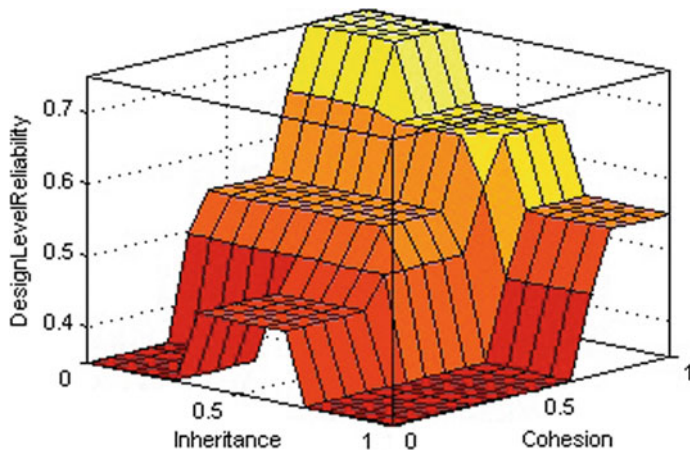


Fig. 2 Design level reliability versus inheritance and cohesion

know its impact. Figures 1, 2, 3 and 4 are depicting the outcome of the sensitivity of DLR with respect to these four design metrics.

4.2 Design Metrics Analysis

As per the various quantitative results obtained through fuzzy logic toolbox in MATLAB, it may be inferred easily that the level of design level reliability (DLR) is

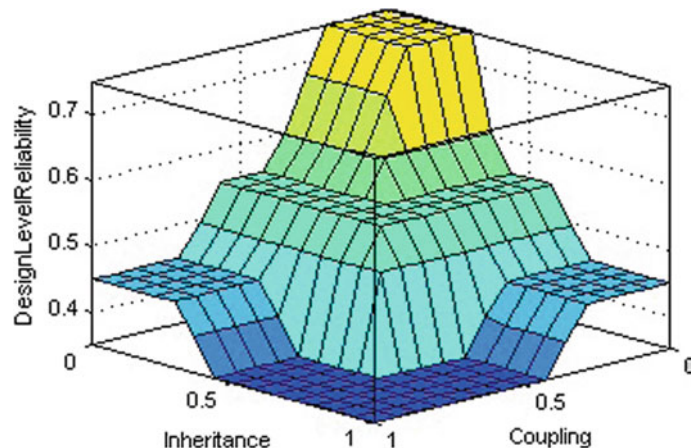


Fig. 3 Design level reliability versus inheritance and coupling

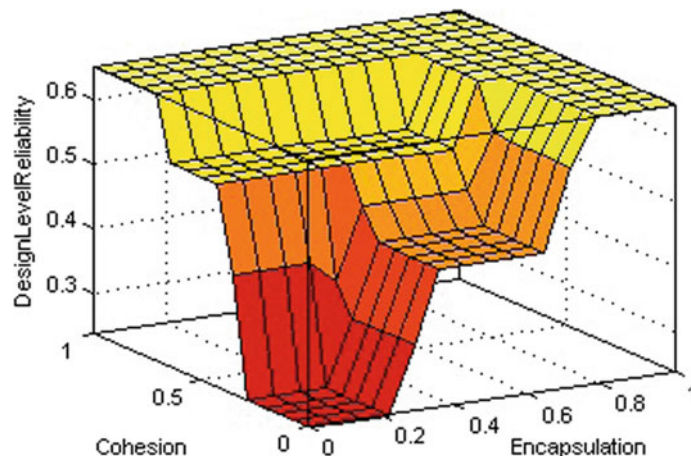


Fig. 4 Design level reliability versus encapsulation and cohesion

varying with the variation of values of four design level measure, and subsequently the researcher has noticed the following observations:

Individual Variation. Carefully looking at the values of encapsulation metric in Table 3, it can be noticed that as metric proceeds toward 1, the value of DLR also increases, As the value of encapsulation metric approaches 0 design level reliability also decreases, Similarly Table 4 presents that, as the value of cohesion metric starts from lower value 0 and move toward 1, the value of DLR also increases.

Spotting the values from Table 5, when value of IM progresses from 1 to 0, the value of design level reliability moves from 0 to 1; similarly when inheritance metrics

Table 3 DLR with respect to EM and IM

RLR = 0%		RLR = 25%		RLR = 50%		RLR = 75%		RLR = 100%	
CM = 0%		CM = 25%		CM = 50%		CM = 75%		CM = 100%	
CoM = 0%		CoM = 25%		CoM = 50%		CoM = 75%		CoM = 100%	
EM, IM	DLR	EM, IM	DLR	EM, IM	DLR	EM, IM	DLR	EM, IM	DLR
0.0	0.350	0.0	0.350	0.0	0.350	0.0	0.550	0.0	0.750
0.2	0.350	0.2	0.350	0.2	0.350	0.2	0.550	0.2	0.750
0.4	0.114	0.4	0.127	0.4	0.550	0.4	0.650	0.4	0.750
0.6	0.114	0.6	0.127	0.6	0.550	0.6	0.650	0.6	0.750
0.8	0.350	0.8	0.350	0.8	0.450	0.8	0.650	0.8	0.750
1.0	0.350	1.0	0.350	1.0	0.450	1.0	0.650	1.0	0.750

Table 4 DLR with respect to CoM

EM = 0%		EM = 25%		EM = 50%		EM = 75%		EM = 100%	
IM = 0%		IM = 25%		IM = 50%		IM = 75%		IM = 100%	
CM = 0%		CM = 25%		CM = 50%		CM = 75%		CM = 100%	
RLR = 0%		RLR = 25%		RLR = 50%		RLR = 75%		RLR = 100%	
CoM	DLR	CoM	DLR	CoM	DLR	CoM	DLR	CoM	DLR
0.0	0.350	0.0	0.350	0.0	0.450	0.0	0.450	0.0	0.550
0.2	0.350	0.2	0.350	0.2	0.450	0.2	0.450	0.2	0.550
0.4	0.350	0.4	0.350	0.4	0.550	0.4	0.550	0.4	0.750
0.6	0.350	0.6	0.350	0.6	0.550	0.6	0.550	0.6	0.750
0.8	0.550	0.8	0.550	0.8	0.650	0.8	0.650	0.8	0.750
1.0	0.550	1.0	0.550	1.0	0.650	1.0	0.650	1.0	0.750

Table 5 DLR with respect to IM

EM = 0%		EM = 25%		EM = 50%		EM = 75%		EM = 100%	
CoM = 0%		CoM = 25%		CoM = 50%		CoM = 75%		CoM = 100%	
CM = 0%		CM = 25%		CM = 50%		CM = 75%		CM = 100%	
RLR = 0%		RLR = 25%		RLR = 50%		RLR = 75%		RLR = 100%	
IM	DLR	IM	DLR	IM	DLR	IM	DLR	IM	DLR
0.0	0.350	0.0	0.350	0.0	0.550	0.0	0.750	0.0	0.937
0.2	0.350	0.2	0.350	0.2	0.550	0.2	0.750	0.2	0.925
0.4	0.350	0.4	0.350	0.4	0.550	0.4	0.650	0.4	0.925
0.6	0.350	0.6	0.350	0.6	0.550	0.6	0.650	0.6	0.925
0.8	0.114	0.8	0.127	0.8	0.350	0.8	0.650	0.8	0.750
1.0	0.096	1.0	0.127	1.0	0.350	1.0	0.650	1.0	0.750

Table 6 DLR with respect to CM

EM = 0%		EM = 25%		EM = 50%		EM = 75%		EM = 100%	
IM = 0%		IM = 25%		IM = 50%		IM = 75%		IM = 100%	
CoM = 0%		CoM = 25%		CoM = 50%		CoM = 75%		CoM = 100%	
RLR = 0%		RLR = 25%		RLR = 50%		RLR = 75%		RLR = 100%	
CM	DLR	CM	DLR	CM	DLR	CM	DLR	CM	DLR
0.0	0.350	0.0	0.350	0.0	0.550	0.0	0.650	0.0	0.937
0.2	0.350	0.2	0.350	0.2	0.550	0.2	0.650	0.2	0.925
0.4	0.109	0.4	0.127	0.4	0.550	0.4	0.650	0.4	0.928
0.6	0.114	0.6	0.127	0.6	0.550	0.6	0.650	0.6	0.925
0.8	0.114	0.8	0.127	0.8	0.350	0.8	0.650	0.8	0.750
1.0	0.096	1.0	0.127	1.0	0.350	1.0	0.650	1.0	0.750

moves in reverse direction that is from 0 to 1, subsequently design level reliability goes downward from 1 to 0. Looking at the outcomes of Table 6, as coupling has been increased in a class diagram, values of design level reliability also move inversely proportional that it decreases.

Combinational Variation. Observing carefully Fig. 4 that highlights the impact of encapsulation along with cohesion on the design level reliability, till now we have impact of one object-oriented measure on DLR at a time that is keeping all the three measures constant, now we are observing the impact of various combinations of these four object-oriented measures on design level reliability. Now noticing the values displayed in the tables as well as figures, it is quite apparent that when encapsulation and cohesion increase, DLR also moves in the same direction.

Similarly, as the value inheritance along with coupling decreases, the movement of DLR is in opposite direction that is while IM and CM approach 0, the design level reliability goes toward 1. Again, noticing the encapsulation and coupling measures, they do not have any substantial impact on DLR, that is design level reliability neither increases nor decreases when encapsulation and coupling approach 0 or 1. The same case is with coupling and cohesion, while keeping inheritance and encapsulation, that is, as they have neither positive nor negative impact on DLR.

Now after scrutinizing individual as well as combinational impact of these four identified object-oriented design measures on design level reliability, it could be concluded that higher the coupling lesser the DLR, higher the encapsulation in the class diagram higher the reliability of the design. Lesser the inheritance, less reliable the object-oriented design is.

Now if have a close look on Table 2, then anyone could easily conclude that keeping the three measures constant encapsulation is directly proportional to design level reliability. The same we can state using different words that we should focus more on encapsulated classes in the object-oriented design as it may lead to a more better as well as reliable object-oriented design.

Similarly observing the data in other tables, one may deduce that while keeping other metrics constant, and some metrics combinations have a positive or negative effect that is either they are directly proportional or inversely proportional. Besides it some pairs of object-oriented measure are reflecting even natural also, like encapsulation and inheritance.

Just have a look on Table 4, we may notice that cohesion which is one of the key components of OOPs has a direct relation with the design reliability. Because while keeping encapsulation, inheritance and coupling constant, the values of DLR are moving in the same direction as the cohesion is moving. Therefore, in order to make the design more and more reliable, cohesion should be on the higher side.

Again, focusing on the numbers appearing in Table 5, we could interpret that while the levels of EM (encapsulation), CM (coupling) and CoM (cohesion) are not changing, the inheritance metric is behaving inversely with respect to the DLR. Therefore, the software application where design has inheritance on higher end will lead toward lesser level of software reliability.

Noticing the data present in Table 6, it could be interpreted that keeping constant values for encapsulation, inheritance and cohesion, the coupling is impacting negatively on the design level reliability. In other words, as the value of coupling increases from 0 toward 1, then DLR goes down from 1 toward 0. So, the higher coupling in the object-oriented design will lead to a design which will result in a low reliable software.

If you look carefully at Fig. 2, you may appreciate that inheritance along with cohesion does not have any substantial impact on the reliability level of the developing software at this design stage, while the other two object-oriented measures coupling and encapsulation are not varying.

Observing Fig. 3, anyone could easily notice that as the values of coupling and inheritance are going toward higher end that is 1, the level of design level reliability is going down toward 0. Therefore, we can interpret it as while encapsulation and cohesion are constant, the coupling and inheritance have adverse impact on DLR.

Finally analyzing another combination and its impact on design level reliability in Fig. 4, it could be noticed that encapsulation along with cohesion has a direct relation with the movement of values of DLR. In other words, we can interpret it while keeping inheritance and coupling constant, high cohesion as well as high encapsulation results in an object-oriented design that may result to software application possessing a high level of reliability.

5 Conclusion

The current study has focused the criticality and significance of object-oriented design measures in the prediction or estimation of software reliability before the coding starts to finally shape the software. The state of the art as mentioned in Sect. 2 specifies that these measures did not get the required attention as far as the early stage reliability quantification is concerned. This work has not only focused exclusively

on early phase measures but also analyzed them using the primary data by the fuzzy toolbox. The outcome of the investigation has been discussed in the form of critical findings. Therefore, these identified object-oriented design metrics will definitely assist the researchers to perform their early prediction of software reliability on the basis of these measures. Such early prediction not only minimizes future efforts, but also reducing various inevitable rework to be done in future in order to develop a quality product.

References

1. Dalal SR, Lyu MR, Mallows CL (2014) Software reliability. Wiley
2. Lyu MR (1996) Handbook of software reliability engineering. IEEE CS Press, California
3. Rizvi SWA, Raees AK (2010) Maintainability estimation model for object-oriented software in design phase. *J Comput* 2(4):26–32
4. Rizvi SWA, Vivek KS, Khan RA (2016) The state of the art in software reliability prediction: software metrics and fuzzy logic perspective. *Adv Intell Syst Comput* 433:629–637
5. Tanasijevic M, Jovancic P, Ivezic D, Bugaric U, Djuric R (2019) A fuzzy-based decision support model for effectiveness evaluation—a case study of examination of bulldozers. *Int J Ind Eng Theory* 26(6):878–897
6. Ross TJ (2010) Fuzzy logic with engineering applications, 3rd edn. Wiley
7. Kraidi L, Shah R, Matipa W, Borthwick F (2020) Using stakeholders' judgement and fuzzy logic theory to analyze the risk factors in oil and gas pipeline projects: case study in Iraq, Stage II. *Int J Crit Infrastruct Prot* 28:100337
8. Radjenovic D, Hericko M, Torkar R, Zivkovic A (2013) Software fault prediction metrics: a systematic literature review. *Inf Softw Technol* 55(8):1397–1418
9. Rizvi SWA, Raees AK (2009) A critical review on software maintainability models. In: Proceedings of the conference on cutting edge computer and electronics technologies, pp 144–148
10. Chandima RM, Antosz K (2017) Development of a risk matrix and extending the risk-based maintenance analysis with fuzzy logic. *Procedia Eng* 182:602–610
11. Zhao L, Zhang J, Yang J, Chu Y (2010) Software rel. growth based on fuzzy wavelet neural Network. In: 2nd International conference on future computer and communication (ICFCC). IEEE, Wuhan, pp 664–668
12. Jaderi F, Ibrahim ZZ, Zahiri RZ (2019) Criticality analysis of petrochemical assets using risk based maintenance and the fuzzy inference system. *Saf Environ Prot* 121:312–325
13. Chang Y, Wu Y, Chen G, Chen B, Xu L, Yin Z, Ren K (2018) Comprehensive risk assessment of drilling riser using fuzzy Petrinet. *Process Saf Environ Prot* 117:483–497
14. Singh Y, Kaur A, Malhotra R (2009) Empirical validation of object-oriented metrics for predicting fault proneness models. *J Softw Qual Control* 18(1):3–35
15. Mohanty R, Ravi V, Patra MR (2013) Hybrid intelligent systems for predicting software reliability. *Appl Soft Comput* 13(1):189–200
16. Rizvi SWA, Khan RA (2013) Improving software requirements through formal methods. *Int J Inf Comput Technol* 3(11):1217–1223
17. Rizvi SWA, Vivek K, Khan RA (2016) Fuzzy logic based software reliability quantification framework: early stage perspective (FL -SRQF). *Procedia-Comput Sci* 89:359–368
18. Rizvi SWA, Singh VK, Khan RA (2016) Software reliability prediction using fuzzy inference system: early stage perspective. *Int J Comput Appl* 145(10):16–23
19. Saini GL, Panwar D, Kumar S, Singh V (2020) A systematic literature review and comparative study of different software quality models. *J Discrete Math Sci Cryptogr* 23(2):585–593

20. Sharma MM, Agrawal A, Deore H, Kumar S, Kumari R (2020) Revisiting agile software development process based on latest software industry trends. *J Inf Optim Sci* 41(2):533–541
21. Lo JH (2009) The implementation of artificial neural networks applying to software reliability modeling. In: Control and decision conference, Chinese, pp 4349–4354
22. Yadav A, Khan RA (2012) Development of encapsulated class complexity metric. *Procedia Technol* 754–760. In: International conference on computer, control and information technology
23. Yadav A, Khan RA (2011) Class complexity metric (C3M). In: Proceedings of international conference on computer and communication technology, pp 353–366
24. Yadav A, Khan RA (2009) Measuring design complexity—an inherited method perspective. *ACM Softw Eng Notes* 34(4):1–5

Test Case Prioritization Based on Requirement



Amrita and Prateek Gupta

Abstract In the software development process, the main concern of the developer is to develop a quality product and optimizing time and cost. Maintenance of the software is considered a costly activity. Regression testing is performed to test the modified software in the maintenance phase. In order to minimize the total time and cost, we can arrange test cases according to the different requirements proposed in the starting phase of the development. We can prioritize the test cases in such a manner that the higher priority test cases will execute before the lower priority test cases. This paper presents an approach to prioritize regression test cases based on requirements. Firstly, we have selected some requirement factors; based on these requirements, the weight for each specific requirement will be calculated. Further, we will map the test cases to the requirements and calculate a parameter based on the mapping, known as Test Case Weight (TCW) to the set of requirements. The higher TCW will be executed first. We have compared our proposed work with other prioritization techniques and found better results.

Keywords Software testing · Regression testing · Test cases · Test case weights · Test case prioritization

1 Introduction

Developing a test suite is an expensive operation. If a product with 30,000 lines of coding is to run the whole test suite for several weeks [1], it is also unworkable to run the whole test package. Researchers suggest several test suite minimization strategies to reduce costs [2]. We minimize the test suite and negotiate the identification of defects. The priority of test cases based on such requirements such as code coverage etc. is also an approach to test improvement. The principle of prioritizing the test case is to first pick the high-priority test cases and then the low-priority test cases

Amrita
Banasthali Vidyapith, Vanasthali, Rajasthan, India

P. Gupta (✉)
UPES, Dehradun, India

[3]. The concept in this strategy is to priority the test cases rather than to discard them, so that the disadvantages of the minimization method in the test case can also be removed. Such conditions exist for a good project such as (a) minimization of the cost and time of the project, and (b) maximization of product quality. These can be achieved by successful software testing techniques [4, 5]. This paper proposes a system-level prioritizing strategy for new and back-up test cases. We plan to establish a priority test case scheme for product quality changes and earlier detections of faults. With this concept, the suggested priority strategy is considered by some of the necessary faculty. These considerations include preference for consumers, difficulty of implementation of developer-perceived code, changes in specifications, failure, and usability and application flow. In Sect. 2 a short introduction has been given to the test case priority. The first three considerations are new test cases, and the remainder is linked to reusable test cases. Section 3 addresses the proposed technique of prioritization. Section 4 describes the findings of the suggested priority setting technique. The conclusion is outlined in Sect. 5.

2 Test Case Prioritization

The key purpose of the priority regression test case is to ensure later completion of the first and secondary priority trials. The priority can be dictated by certain performance criteria. In [6–8] the question of the test case priority is specified as follows: since T is the test suite, PT is a permutation set for T and f is a PT -to-true number function. The Test Case Issue Priority The problem is that the T' belonging to PT , so T'' , T'' and ($t'' \neq T'$) [$f(T') \geq f(T'')$]. In the above description, PT refers to the set of any prioritization or order of T , f is the function used for each order and returns the award value. A variety of potential targets can be defined to prioritize test cases. The goal of this study is to establish a test case priority method that prioritizes regression test cases on the basis of a maximum test case requirement coverage [9].

3 Proposed Methodology

This section proposes a description of our proposed methodology. The idea is to prioritize the test cases based on some criteria for example requirement weight and its associated test case. Also, we are prioritizing the test cases and not removing any test case from the suit therefore it is overcoming the disadvantage of test case reduction also. It has been observed from the past studies [1–3] that requirements identified in SRS could be further optimized based on their weights; therefore our focus is to optimize the requirements. For example, there are total m requirements and we could represent these as $R = \{n_1, n_2, n_3, \dots, n_m\}$. Also, suppose we have a set of test cases T containing p test cases and we can represent them as $T = \{t_1, t_2, t_3, \dots, t_p\}$. Now, let's say n_1 and n_2 are the requirements that have the highest

weights and t_1 is the test case that can cover these two requirements. t_2 is the test case that can cover n_1 , n_2 , and n_3 . However, we are assuming that n_3 has the smallest weights, so we will prefer to test t_1 first, and this is the main concept that has been employed in the proposed methodology in this paper. The proposed methodology is based on three steps: First, we will identify all the requirements and the test cases. Second, we will calculate the requirement weight and test case weight. Third, we will prioritize the test cases based on the test case weight in descending order. The proposed method adapts six prioritizing parameters for the proposed approach.

For the proposed approach we are considering nine parameters. As we know that the test case prioritization is based on the requirements, therefore we have identified some factors whose weight can vary for different requirements. Following are the factors that are considered in our proposed approach: (a) customer priority of requirements (CP), (b) implementation complexity (IP), (c) requirement changes (RC), (d) fault impact of requirements (FI), (e) completeness (CO), (f) traceability (TR), (g) implementation delay, (h) occurrence probability, and (i) severity.

Let us discuss the parameters in detail [10]:

1. Customer-assigned priority (CP): Inclusion of customer's view can increase the reliability as he is the person who is intended to use the product. The priority is decided by the customer and it is provided a range from 1 to 10 where 10 show the highest priority.
2. Implementation complexity (IC): At the initial stage of the development, it has been assured by a group of people about its feasibility, and it contains three different type of feasibility. In that phase it is also checked to measure the implementation complexity subjectively.
3. Requirement changes (RC): How many numbers of times, a particular requirement is changed, we want to keep this information, so that unpredictability of any requirement can be calculated. We can scale it from 1 to 10, to define the frequency of changes.
4. Completeness (CO): This is required to further increase customer satisfaction in terms of quick response. It can include the various functions that have to be implemented, the environment in which the system will be used, and any other constraint that can influence the system can be presented here.
5. Traceability (TR): It is useful when the prerequisite can be considered for the reuse. We can scale it from 1 to 10. We can improve the quality of the software by considering the traceability of the requirement.
6. Implementation delay (ID): It is related to the implementation complexity of any system. The more complex system is, the more time it will take to complete it.
7. Fault impact of requirements (FI): It is related to an error that has been occurred in a released product. It can be helpful to consider this parameter to improve the quality as well as customer satisfaction.
8. Occurrence probability (OP): It is related to the number of times, a particular function is used by the user. The idea is to prioritize those functions having high usage as defined by the customers.

9. Severity: It is related to the criticality of the functions present in the system. For a system, consisting of n functions, it is not necessary that all n functions will be severe. Therefore, out of all, the function with high severity can be chosen.

Step by Step Process for the Proposed Test Case Prioritization methodology

Step 1: Initially set of requirements are accepted by the system and then the set of test cases. The set of requirements are given by,

$$R = \{r_1, r_2, r_3, \dots, r_m\}, \text{ where } m \text{ is the total number of requirements.}$$

Now the set of test cases are given as

$$T = \{t_1, t_2, t_3, \dots, t_n\}, \text{ where } n \text{ is the total number of test cases.}$$

Step 2: Calculate the requirement factor weight for each requirement

$$\sum_{rf=1}^m \text{ReqFactorWeight}_{rf},$$

where rf denotes the different factors and m represents the total requirements.

Step 3: Calculate weight for each requirement

$$\text{Reqweight}(i) = \sum_{rf=1}^m (\text{ReqFactorValue}_{irf} * \text{ReqFactorWeight}_{rf})$$

Step 4: Compute Test Case Weight (TCW)

$$\text{TCW}(tc) = \frac{\text{Reqatisfied}(tc)}{\text{Test case cost}(tc)}$$

Step 5: Prioritize test cases in order of decreasing TCW.

4 Results and Validation

This segment addresses the outcome of our proposed approach for priority test cases. The procedure has been tested on the basis of the mapping of the expense of the test case. The five criteria and various requirement factors are shown in Table 1. Each factor in need is assigned a value on a 10-point scale for the purposes of analysis [10]. We measure ReqFactorWeight_{rf} and Reqweight on the basis of these values. Now we have test case costs from historical records which is shown in Table 2. Test Case Weight (TCW), as shown in Table 3, is determined based on the weight of the test case and its expense. We assume that the maximum TCW is first performed for the proposed technique. When there is a case with the same TCW, the test case will

Table 1 Factors based on requirements

Heading level	CP	IC	RC	CO	TR	ID	FI	OP	S
R1	9	8	5	2	7	6	2	5	8
R2	8	7	4	1	5	5	4	5	7
R3	9	7	3	2	6	7	3	4	7
R4	6	6	3	1	8	5	2	4	6
R5	7	5	2	2	7	5	1	4	5

Table 2 Test case cost

Heading level	R1	R2	R3	R4	R5	Cost
T1	0	0	1	1	0	2
T2	1	1	1	0	0	3
T3	0	1	1	0	0	2
T4	1	0	1	0	1	3

Table 3 Test case weight

Test case weight number	Test case weight
TCW ₁	0.1895
TCW ₂	0.21839
TCW ₃	0.20689
TCW ₄	0.2241

be chosen to satisfy a higher number of requirements. Our sample of data is taken from here [10]. The larger the TCW, the more it is given in Table 3. It's thus obvious that TCW's TCW₄ > TCW₂ > TCW₃ > TCW₁ will be the order of TCW specified test cases. We want to define a relation between the coverage of requirements and the test case costs using the proposed methodology. During the regression testing this helps increase commitment. The soft computing methods can be further optimized. We also validated the proposed technique by measuring the ReqSat metric for the proposed method and the random order method and found that our methodology's efficiency is higher than the average order technique.

5 Conclusion

We basically require test case prioritization in the regression testing. We know that regression testing is performed in order to test the product several number of times. We do not want to reduce the test suit and therefore we proposed the methodology which prioritizes the test cases according to its mapping with the requirements. It can improve the quality of the product. We took requirement coverage by the test

cases and test case cost as the parameter for the prioritization. It will also be helpful in increasing the customer satisfaction.

References

1. Elbaum S, Malishevsky A, Rothermel G (2000) Prioritizing test cases for regression testing. In: Proceedings of the 2000 ACM SIGSOFT International Symposium on Software Testing and Analysis, Portland, Oregon, USA, pp 102–112
2. Kavitha R, Sureshkumar N (2010) Test case prioritization for regression testing based on severity of fault. *Int J Comput Sci Eng* 02(05):1462–1466
3. Tahviliy S, Saadatmand M, Bohlin M (2015) Multi-criteria test case prioritization using fuzzy analytic hierarchy process. In: ICSEA 2015: The tenth international conference on software engineering advances
4. Amrita, Yadav DK (2015) A novel method for software test case allocation. In: Proceeding of international conference on recent trends in computing
5. Krishnamoorthi R, Mary SSA (2009) Factor oriented requirement coverage based system test case prioritization of new and regression test cases. *Inf Softw Technol* 51(4):799–808
6. Do H, Mirarab S, Tahvildari L, Rothermel G (2010) The effects of time constraints on test case prioritization: a series of controlled experiments. *IEEE Trans Softw Eng* 36(5):593–617
7. Kayes ML (2011) Test case prioritization for regression testing based on fault dependency. In: Proceedings of 3rd international conference in electronics computer technology (ICECT), vol 5, pp 48–52
8. Mei H, Hao D, Zhang L, Zhou J, Rothermel G (2012) A static approach to prioritizing junit test cases. *IEEE Trans Software Eng* 38(6):1258–1275
9. Sampath S, Bryce R, Memon AM (2013) A uniform representation of hybrid criteria for regression testing. *IEEE Trans Software Eng* 39(10):1326–1344
10. Reddy V, Reddy D, Mohan AR (2016) An approach for fault detection in software testing through optimized test case prioritization. *Int J Appl Eng Res*. 11(1):57–63. ISSN 0973-4562

Mining and Predicting No-Show Medical Appointments: Using Hybrid Sampling Technique



Albtool Alaidah, Eman Alamoudi, Dauaa Shalabi, Malak AlQahtani, Hajar Alnamshan, and Nirase Fathima Abubacker

Abstract Clinics use scheduling systems for patients' appointments. However, no-shows are frequent in both general medical practices and specialties, and they can be quite costly and disruptive. This problem has become more severe because of COVID-19. The primary purpose of this study is to develop machine learning algorithms to predict if patients will keep their next appointment, which would help with rescheduling appointments. The main objective in addressing the no-show problem is to reduce the false negative rate (i.e., Type II error). That occurs when the model incorrectly predicts that the patients will show up for an appointment, but they do not. Moreover, the dataset encounters an imbalance issue, and this paper addresses that issue with a new and effective hybrid sampling method: ALL K-NN and adaptive synthetic (ADASYN) yield a 0% false negative rate through machine learning models. This paper also investigates the leading factors that affect the no-show rates for different specialties. The SHapley Additive exPlanation (SHAP) method reveals several patterns to identify the target feature (patient no-shows). It determined that a patient's history of missed appointments was one of the leading indicators. It was also found that greater lead times between booking the appointment and the appointment date were associated with more no-show behavior.

Keywords Predicting no-shows · Imbalanced data · Data mining · Health care · Feature engineering · Machine learning

A. Alaidah (✉) · E. Alamoudi · D. Shalabi · M. AlQahtani · H. Alnamshan · N. F. Abubacker
School of Computing, Dublin City University, Dublin, Ireland

E. Alamoudi
e-mail: eman.alamoudi@tu.edu.sa

H. Alnamshan
e-mail: hajar.alnamshan2@mail.dcu.ie

E. Alamoudi
Taif University, Taif, Saudi Arabia

1 Introduction

Hospitals face many issues that have a wide range of consequences for their services. One big issue confronting the healthcare sector and its scheduling systems is that patients miss their arranged healthcare appointments, an outcome called a no-show. The problem has a huge negative impact on a hospital's operation system and on other patients [1]. Scheduling appointments requires an allocation of time, medical supplies, rooms, and other care providers. Furthermore, hospitals have limited funds, tools, beds, and medical staff [2]. Therefore, a higher no-show ratio also may lead to severe abuse of resources that are already restricted. On the other hand, repeated no-shows can affect the quality of patient care as many of those who need emergent interventions might be putting their lives at risk as they lose the opportunity to receive enough treatment. Moreover, the severity of the problem has increased with the appearance of COVID-19. Barone et al. [3] performed a study in Brazilian hospital using data on 1701 patients and found that 38.4% of the individuals postponed their medical appointments and/or examinations because of COVID-19.

No-shows are a serious global issue, and they occur at different levels in different places: Asia (25.1%), the African continent (43.0%), South America (27.8%), North America (23.5%), and Europe (19.3%) [4]. The failure of patients to attend scheduled hospital appointments disturbs clinical management and wastes resources estimated at £1 billion each year in the United Kingdom National Health sector alone [4]. Therefore, this research aimed at developing models to predict if patients will show for their appointments, using machine learning algorithms on a dataset collected at a hospital in Brazil in May and June 2016. Such models could help healthcare providers identify efficient techniques to minimize no-shows. One of those techniques is overbooking for a predicted missed appointments day [5]. The dataset used in this study suffered from an imbalance because of a notable difference in the ratio between the two cases (shows and no-shows) of the target class. Consequently, that problem also is addressed in the suggested approach.

The rest of this paper is structured as follows: The section of the related work discusses recent field works. The section of methodology discusses the data used in this paper, the data preprocessing approaches, an overview of the sampling techniques, and outline the prediction models and evaluation criteria applied in this research. Section of experiment and results describes the experimental settings, results analysis, and interpretation. Finally, the conclusions provide a summary of workflow and achievements.

2 Related Work

In this section, we present the studies that use machine learning models to predict medical appointment no-shows. Moreover, we review studies that experiment the sampling methods to deal with imbalanced data.

2.1 Machine Learning Methods to Predict Medical Appointment No-Shows

In this section, we discuss the machine learning models used in related studies with an emphasis on the leading causes of no-show behavior. Researchers in [6] considered three main groups of features: patient demographics, appointment characteristics, and appointment history. They used logistic regression for the classification task to anticipate the patient no-shows. They found that when the lead time was rather large, the chances the patient might not show rose. However, when a patient had multiple appointments on the same day, the possibility of reverting to the booking was much higher. Another study aimed to predict clinical appointment no-shows among diabetic patients, which can disrupt the patient's treatment [7]. The researchers used logistic regression, multilayer perception, and Naïve Bayes machine learning models to classify patients. They found that age had a considerable impact on no-show behavior. So, the researchers engineered the features that improved the performance of their model such as lead time, prior no-show rate, and days since the last booking date. In [8], the researcher introduced engineered features such as the day of the week and the patient's compliance with the treatment schedule. The researcher eliminated canceled or rescheduled appointment records from the dataset and used a logistic regression model with precision, recall, and area under the receiver operating characteristic curve (AUC) as the evaluation metrics. In [4], the researchers experimented with 81 features, including some of the variables used in previous studies. The models used were logistic regression, support vector machines, random forest, and a gradient boosting machine. They focused on higher AUC and precision. One of their suggestions for future work was to use a grid search. Alshaya et al. [9] proposed building a predictive model to predict no-show patients to reduce the negative consequences. They used the same dataset used in this study, and they used logistic regression, random forest, support vector machines, stochastic gradient descent, and K-nearest neighbor for prediction. Support vector classifier and stochastic gradient descent models had the best results compared to the other models. Last, most of the previously mentioned studies ignored experimenting techniques for imbalanced data for the medical appointment no-show problem. However, it is considered in this study as a limitation that we want to overcome.

2.2 Methods Used for the Problem of Imbalanced Data

Class imbalance is very common in real-life datasets [10]. In our situation, the number of patients in the class of no-shows was much less than patients in the class who showed up. An imbalanced dataset can create a big challenge for classifiers in machine learning and deep learning. Smaller classes are often more valuable, but the classifiers usually consider the big classes and ignore the smaller ones [10]. Thus, an imbalanced dataset can reduce the accuracy of the model's prediction and increase the

error rate [11]. The challenge is to reduce the effects of the imbalance ratio to enhance the abilities of the classification algorithm to be more sensitive to the minority class because the minority classes are usually the reason for the predictions. Researchers have been devising ways to reduce the effects of class imbalance and improve the predictive performance of classification algorithms [12]. Sampling technique is one of the ways to handle class imbalance, such as oversampling, undersampling, or a hybrid of the two.

Oversampling techniques were made popular by the pioneering work of [13] through a process called the synthetic minority oversampling technique (SMOTE). SMOTE oversampled the minority class by creating synthetic examples rather than with replacement. The K-nearest positive neighbors of all positive instances were identified, and synthetic positive examples were created and placed randomly along the line segments joining the K-minority class nearest neighbors [14]. The researchers in [11] demonstrated the ability of SMOTE and ensemble, a machine learning method to improve the prediction of diabetes using cardiorespiratory fitness data. The dataset comprised diabetics and non-diabetics patients, but the diabetics represented only 15.7% of the subjects. This illustrated the imbalance of the dataset. The SMOTE method was applied to solve the imbalanced dataset by increasing the diabetic cases in three different proportions: 100%, 200%, and 300%. This gradually increased the minority class from 15.7% in the original dataset to 47% in the SMOTE with a 300% increase. Thus, it is considered an oversampling technique. Better results have been obtained by voting methods with three decision trees (Naïve Bayes tree, random forest, and logistic model tree) with 0.92 AUC. The researchers in [15] used another oversampling technique called adaptive synthetic sampling (ADASYN). The basic idea behind ADASYN is to use a weighted distribution for different minority class instances based on their classification difficulties. The most synthetic data are generated for minority class instances that are more difficult to classify when compared to minority class instances that are easier to classify [16]. Wang et al. [17] relied on ADASYN to minimize the effect of class imbalance on prediction performance in the diabetes dataset. They found that predicting diabetes using the random forest model had an accuracy of 87.10%.

The opposite of oversampling is undersampling, which reduces the number of majority class data from the original dataset. The researchers in [15] used a method called random undersampling, one of the simplest methods of handling imbalanced data in a dataset. It works by randomly deleting cases from the majority classes to decrease their total number. Another undersampling technique is ALL K-NN. It works by using the nearest neighbors to remove instances from the majority class without noisy data [18].

There are positive and negative aspects to both undersampling and oversampling [19]. Therefore, a combination of oversampling and undersampling algorithms, or hybrid sampling, has been proposed to get reliable outcomes in data processing. The basic principle of hybrid sampling is to increase the minority samples and decrease the majority samples to make a balanced dataset. In 2014, Cateni et al. [20] proposed a method for rebalancing the real-world problems dataset called similarity-based undersampling and normal distribution-based oversampling (SUNDO). It combined

oversampling and undersampling approaches. Two subsets of data were generated from the original training set. One representing the minority class for which the oversampling approach was used and the other representing the majority class on which the undersampling approach was applied. Then the two subsets were merged to create a new training set to train the selected classifier. Xu et al. [21] proposed an algorithm to combine misclassification-oriented synthetic minority oversampling technique (M-SMOTE) and edited nearest neighbor (ENN) based on random forest for imbalanced medical data. By replacing the sample imbalance rate with the misclassification rate of the sample, a balanced dataset was generated by hybrid sampling using M-SMOTE and ENN. The minority class was increased by applying M-SMOTE, where the random forest misclassification rate considered the M-SMOTE oversampling rate. ENN also was applied to eliminate noise from most samples. Recall achieved 99.2% with a random forest algorithm to perform classification predictions for samples after hybrid sampling. Alshaya et al. in [9] demonstrate the effectiveness of various sampling methods on no-shows medical appointment issue. They found desirable results when different machine learning models are combined with the following sampling methods: ADASYN, SMOTE, random oversampling, random undersampling, ALL K-NN, SMOTEEENN, and SMORETomek.

We have identified that there are no enough satisfactory studies have been done on no-show problem that are related to solving the imbalance dataset. Most of the prior similar studies focused only on machine learning models. That is why our proposed study will fill this research gap. The focus of this paper is to develop a special framework that helps the hospitals in an efficient manner to design a reliable and accurate predictive model. We compare the results of our proposed method with similar studies. In addition, a newly proposed sampling method will be implemented as a solution for imbalanced dataset.

3 Methodology

In this section, we present the general framework that we implemented in our effort to build efficient and effective predictive models for appointment no-shows. The structure for constructing the proposed solution is shown in Fig. 1. Different methods were implemented at each stage to obtain various technique combinations and achieve desirable outcomes. The objectives of each phase and the descriptions of the techniques are presented in the following sections.

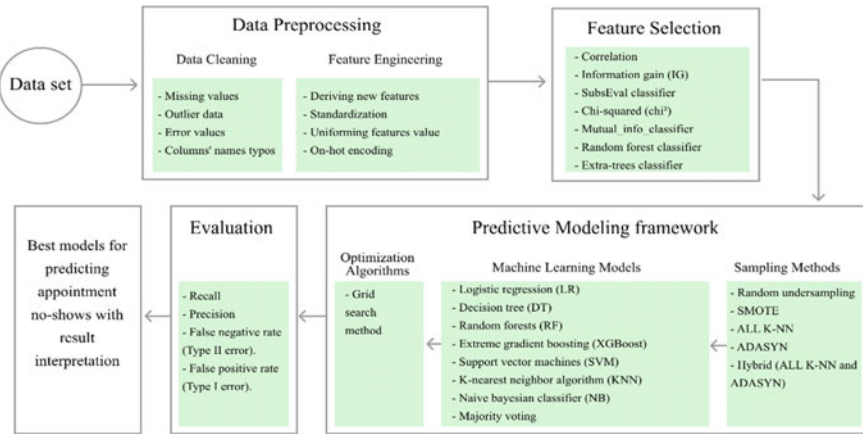


Fig. 1 Methodology framework

3.1 Data Description

The data for this research were obtained from the Kaggle Web site,¹ and it was collected from the medical public sector in Brazil. The dataset contained 110,527 records, and it had 14 features: 13 descriptive features and one target feature (no-shows). The data types involve numerical, categorical, and datetime data which are described in Table 1.

3.2 Data Preprocessing

In this section, we present the techniques used to transform the raw data in a suitable and efficient format for machine learning models. The technical details of each phase are presented in the following sections.

Data Cleaning. The common issues in this phase are missing values, outliers, and error values. The current dataset was free of missing values. Outliers are values that stand away from a feature's central tendency. The outliers in the dataset were identified by examining the minimum and maximum values of the numerical features. The age column showed some out-of-average values, but they were accepted because they reflect a group of elderly patients. Ages less than zero were omitted as they were error values. Typographical errors in column names were corrected.

Data Analysis. The exploratory data analysis (EDA) approach was applied to understand the data and summarize its chief characteristics. The first exploration of the

¹<https://www.kaggle.com/joniarroba/noshowappointments>.

Table 1 Features of the dataset used in this research

Feature name	Description	Data type
Patient ID	Identity number of a patient	Numerical
Appointment ID	Identity number of an appointment	Numerical
Gender	The patient is male or female	Categorical
Scheduled day	Date and time the appointment was booked	Datetime
Appointment day	Date and time of the appointment	Datetime
Age	Age of the patient	Numerical
Neighborhood	Place of the appointment	Categorical
Scholarship	The patient is enrolled in a program supporting (yes or no)	Categorical
Hypertension	Does the patient have hypertension (yes or no)	Categorical
Diabetes	Does the patient have diabetes (yes or no)	Categorical
Alcoholism	The patient is an alcoholic (yes or no)	Categorical
Handicap	Number of disabilities (0 or 1 or 2 or 3 or 4)	Categorical
SMS received	Did the patient receive SMS messages for appointments? (yes or no)	Categorical
No-show	Did the patient miss this appointment ?(yes or no)	Categorical

data showed that there was no balance between show (negative) and no-show (positive) cases, where the showing up category had a value of about 80%. The ages were distributed between 0 and 115, with an average of 37. The cases of no-shows declined as age increased. Most of the appointments that were scheduled on the same day had a higher percentage of patient attendance, whereas for long waiting days (i.e., appointments made far in advance), the probability of missing the appointment increased. Absenteeism did not occur often when the waiting days were less than a week. Females represented approximately 65% of the patients. Less than 10% of the patients had a scholarship, but both categories had instances of no-shows. Most patients did not suffer from diseases. Only 7% had diabetes, 20% had hypertension, 3% had alcoholism, and 11% had a handicap. Health status did not have a great impact on keeping patients from attending their appointments. There were 81 unique neighborhoods with different distributions of show and no-show instances, Jardim Camburi had the highest number of patients at 7,717, and 1,465 of them were no-shows.

Feature Engineering. Many new features can be derived from the raw features that are valuable for prediction models [22]. Selecting the best feature engineering methods depends on the model used and the most accurate outcomes [22]. For the proposed approach, several new features were extracted. One important new feature was the number of waiting days. In [23], waiting days had a significant role in the prediction models. Waiting days indicate the number of days between the scheduled and appointment date. The day of the week of each appointment was extracted from the appointment date. Furthermore, the most significant predictor of no-shows

was a history of being a no-show. Thus, if a patient missed previous appointments, then that past behavior could reflect future behavior. To ensure there was no data leakage, appointments were carefully grouped and sorted to calculate the number of missed appointments for each patient and calculated the total number of all previous appointments. Then we split waiting days into different categories for more investigation. Equal width binning was applied on age, which resulted in nine age groups to capture how generational variance affected not keeping an appointment. In that phase, the data were also prepared for use in machine learning prediction models, and feature scaling was a common requirement for many machine learning models [24]. Thus, a min-max scaling approach was applied to continuous features because they were not normally distributed. Furthermore, to make all features' values uniform, responses like Yes/No and Male/Female were converted to (1, 0), and a separate variable for each subcategory of a variable was created by performing one-hot encoding in order to make the dataset applicable for machine learning models. By creating additional features, an excess of variables was added to the data. After standardizing the continued features and encoding categorical features, there were 34 unique predictors to consider (see Table 2).

Feature Selection. This is the process of picking out the most informative features to create an accurate and fast predictive model [25]. Feature selection was implemented using various techniques namely, correlation, information gain (IG) [25], CfsSubsetEval [26], chi-squared (χ^2) [27], and ensemble learning methods (i.e.,

Table 2 Features in engineering and selection phases

Original features	New engineered features	Final selected features
Patient ID	Previous appointment	Previous appointment
Appointment ID	Missed previous appointments	Missed previous appointments
Scheduled day	Waiting days categories [waiting days: 0, week: 1–7, month: 8–30, quarter: 31–90, or a long period of time: >91]	Waiting days categories [waiting days: 0, week: 1–7, month: 8–30, quarter: 31–90 or a long period of time: >91]
Appointment day	Day of week [0, 2, 3, 4, or 5]	Day of week [0, 4 or 5]
Age	Age bin [baby, children, teenager, young, young–adult, adult, adult-II, senior, or old]	Age bin [baby, children, teenager, young, young–adult, adult, senior or old]
Handicap	Handicap [0, 1, 2, 3, or 4]	Handicap [1]
Gender	Gender [M or F]	Gender [M]
Hypertension		Hypertension
Diabetes		Diabetes
Scholarship		Scholarship
SMS received		SMS received
Alcoholism		
Neighborhood		

mutual info classifier, random forest classifier, and an extra trees classifier) [28]. Seven different experiments were applied, as each previously mentioned technique was applied independently to the data. In the first experiment, the results of the correlation showed which features were connected to the target feature. The other six experiments had similar results, with slight differences in the order of features. The first 24 features in the results of each of the seven experiments were similar, so they were entered into the prediction models because they got the highest scores. Furthermore, the derived features had a stronger relationship to the target feature than the raw features (see Table 2).

3.3 Predictive Modeling Framework

In previous sections, we transformed the data to make it ready for the next phase. In this section, we describe the method used for the experimentations in a predictive modeling framework.

Sampling Methods. As noted earlier, the class of no-shows was a minority, making the dataset imbalanced. The techniques explored in this paper were undersampling methods (random undersampling and ALL K-NN), oversampling methods (SMOTE and adaptive synthetic (ADASYN), and a hybrid technique (ALL K-NN with ADASYN). In our hybrid method, ALL K-NN was used to undersample the majority class, while ADASYN was used to oversample the minority class. By merging oversampling and undersampling methods, the dataset achieved a balancing state. It neither lost too much information nor did it suffer from overfitting caused by having a class that was too heavily oversampled [14].

Machine Learning Models. In this research, a variety of well-known supervised machine learning models was used to compare their performances based on selected evaluation criteria. The following are the predictive models used for the classification problem. Logistic regression (LR) is the probability of converting the dependent variable into a logistic variable by passing a linear regression into the sigmoid function [29]. Support vector machines (SVM) are based on the concept of optimizing the margin of a hyperplane that helps to find support vectors for dividing different classes [29]. K-nearest neighbor (KNN) is a nonparametric method that stores all available instances and then classifies them according to most neighbor's similarities [30]. Naïve Bayesian (NB) is a probabilistic machine based on the theorem of Bayes with the assumptions of independence among predictors [29]. Decision tree (DT) divides the decision nodes into leaves according to specific parameters, and the shortest decision tree is set by entropy and calculating information gain [29].

On the other side, the following are the models used in the ensemble learning category. Random forest (RF) uses an aggregation and bootstrap approach to build multiple independent decision trees [29]. Extreme gradient boosting (XGBoost) is a boosting machine that uses the core of gradient boosting machines for multiple dependent decision trees as a base [31]. Majority voting is another ensemble classifier

wherein the prediction depends on the majority vote by using more than one algorithm independently [32]. In this research, logistic regression, decision tree, and random forest were used as a majority voting model.

To enhance the model's performance, grid search optimization was used. This method fine-tunes a model by testing it against different hyperparameters [33]. A grid search method used with cross-validation is a powerful preventative technique against the overfitting problem, so it results in a less biased estimation [34].

Evaluation Criteria. To evaluate the results from the models and nominate the best model, a wide variety of prominent evaluation metrics was used. Based on the problem of detecting the positive class (i.e., the no-shows), we focused more on recall and precision. Furthermore, a comprehensive assessment was carried out by analyzing false negative and false positive rates, which were calculated from the confusion matrix.

Recall. This is the ratio of correctly predicted positive observations to all the observations in the actual class. Of all the patients that truly did not show, how many were labeled correctly? [35]. The equation for recall is as follows:

$$\text{Recall} = \frac{\text{True Positive}}{\text{False Negative} + \text{True Positive}} \quad (1)$$

Precision. This is the ratio of correctly predicted positive observations to all the predicted positive observations. Of all patients that were labeled as no-shows, how many actually did not show? [35]. The equation for precision is as follows:

$$\text{Precision} = \frac{\text{True Positive}}{\text{False Positive} + \text{True Positive}} \quad (2)$$

False Positive Rate (FPR). Also known as Type I error is the probability of a false alarm. A false positive occurs when the prediction is that a patient will not show, but the patient eventually attends [35]. The equation for FPR is as follows:

$$\text{FPR} = \frac{\text{False Positive}}{\text{False Positive} + \text{True Negative}} \quad (3)$$

False Negative Rate (FNR). Also known as Type II error is the probability of missing the true positive class. A false negative occurs with an incorrect prediction that the patient will show up for an appointment, but eventually they do not attend [35]. The most expensive error in the no-show medical appointment problem is a false negative rate. The equation for FNR is as follows:

$$\text{FNR} = \frac{\text{False Negative}}{\text{False Negative} + \text{True Positive}} \quad (4)$$

4 Experiment and Results

In this section, we experiment with a special framework that is designed to select the best predictive model for the research problem. Moreover, we present the results of the experiments and analyze them based on technical and business perspectives.

4.1 Experiment Setting

The imbalanced dataset contained fewer patients in the class of no-shows, so we needed to ensure that our method would develop models that could discover those patients with high recall and a lower false negative rate (i.e., Type II error). Accordingly, we had to balance the data where the models learn both classes (show and no-show) in an approximately equal way so future performance is better. However, we needed to create a reliable framework in selecting a better-balanced training dataset (i.e., sampling techniques) and predictive (i.e., machine learning) models. The framework is shown in Fig. 2, and it was designed to help the hospitals to reduce the time needed to choose and analyze the appropriate approach for forecasting.

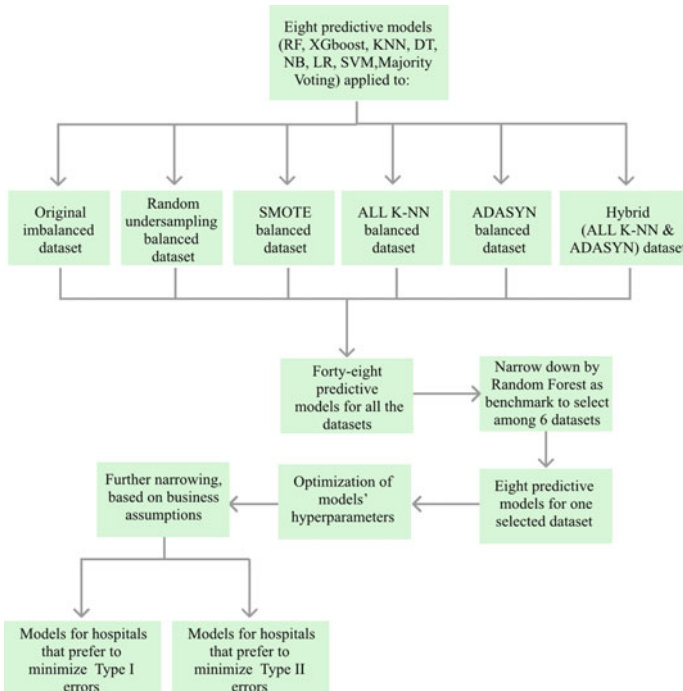


Fig. 2 Detailed predictive modeling framework for model selection experiment

First, we developed all eight algorithms that were mentioned in the proposed model section to six different datasets. Those datasets were created based on sampling techniques: the original imbalanced dataset, a random undersampling balanced dataset, the SMOTE balanced dataset, the ALL K-NN balanced dataset, the ADASYN balanced dataset, and the hybrid (ALL K-NN and ADASYN) balanced dataset. The reason for choosing ALL K-NN and ADASYN for the hybrid method was that those sampling techniques revealed the best results in most of the predictive models in terms of a reduced false negative rate. All sampling methods balanced the dataset for both show and no-show classes into approximate 50:50 ratios. In the hybrid sampling method, ALL K-NN reduced the show class from 70,000 to 64,000, and ADASYN generated new instances for the minority by growing the no-show class from 18,000 to 63,000.

In the experiment, we divided all the datasets into an 80:20 ratio for training and testing. Thus, we had 48 different models. However, it was inefficient, and it would cause confusion for the business domain to select from such a large number of models. Therefore, our proposed method helps the hospitals in an efficient manner to design an accurate predictive model with reducing the cost of the experimental phase.

A random forest (RF) classifier was selected as the benchmark model to choose among six datasets. RF was selected for two reasons. First, it is a nonparametric ensemble method that makes no a priori assumptions and gives a robust first pass attempt to model the relationship [36]. Furthermore, researchers in [37] showed that RF was efficient as a benchmark; it outperformed in approximately 69% of 243 datasets. Second, RF showed a better result in the original dataset and most of the balanced datasets. As a result, it was evident by RF that the hybrid sampling (ALL K-NN and ADASYN) dataset outperformed in helping the models to determine a more distinguishable decision boundary for the minority class of no-show appointments. The recall of RF with the original imbalanced dataset was 73.65%. However, when applying sampling techniques, the higher result for recall was obtained by the hybrid method, where it increased to 100%. On the other side, we ensured that precision also increased, so the positive predicted values were truly predicted, and we could consider such improvements. Accordingly, the hybrid (ALL K-NN and ADASYN) balanced dataset was selected, and the number of models was reduced from 48 to 8.

For further enhancement, a hyperparameter tuning technique was used. It is a grid search optimization method to enhance the performance of all eight models. The best hyperparameters are given in Table 3.

4.2 Experiment Results

The evaluation metrics were applied to the selected models in the second stage of Fig. 2. Results were measured on the test (unseen) dataset to ensure its applicability in the future. Furthermore, the results of the evaluation on the training dataset showed results similar to those of the test dataset. Hence, it was evident that the models did

Table 3 Results of a grid search of the selected machine learning models

Model	Selected hyperparameters
RF	{‘bootstrap’: True, ‘criterion’: ‘gini’, ‘max_depth’: 3, ‘n_estimators’: 300}
XGboost	{‘booster’: ‘gbtree’, ‘max_depth’: 10}
KNN	{‘algorithm’: ‘brute’, ‘n_neighbors’: 17}
DT	{‘criterion’: ‘gini’, ‘max_depth’: 16}
NB	{‘priors’ = None, ‘var_smoothing’ = 1e-09}
LR	{‘C’: 1.0, ‘penalty’: ‘l2’}
SVM	{‘C’: 10, ‘kernel’: ‘poly’}

not overfit. As shown in Fig. 3, higher results for the total of recall and precision were obtained by RF, DT, XGBoost, LR, and the majority voting model; whereas, low results were shown by KNN, NB, and SVM. Some justification for the low performance was that SVM negatively affected because the dimensionality of the data was high, and NB was naively biased toward positive class with a huge precision loss for the real predicted positive class. Moreover, K-NN did not do bad work, but it had the lowest average among the good models. Generally, ensemble models have promising results on this dataset. As a result, we could outperform the researchers in [9] by using our designed method, from selecting the features to selecting the appropriate sampling techniques. Their highest recall was 92%, and their highest precision was 62%.

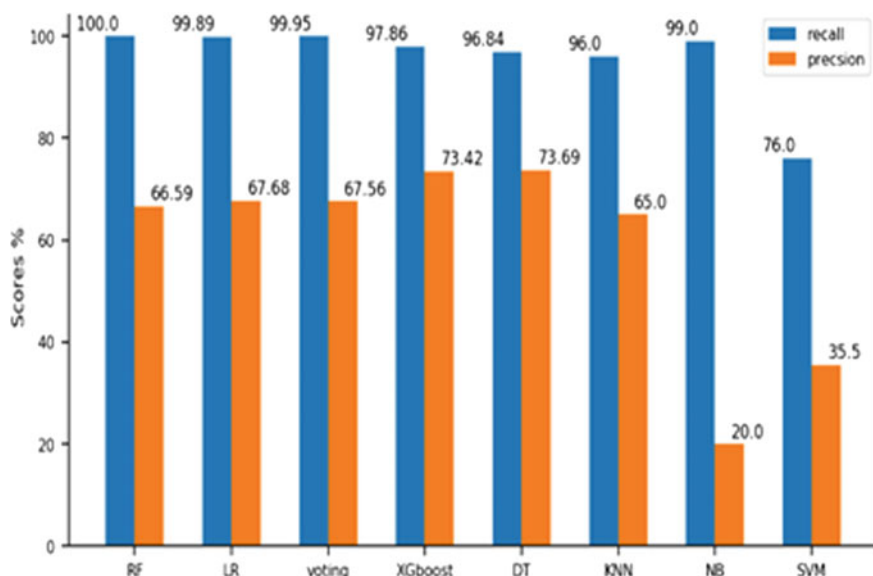
**Fig. 3** Recall and precision results for machine learning models with a hybrid sampling approach

Table 4 Confusion matrix for the selected machine learning models with a hybrid approach

		<i>Random forest forecasts</i>			
Real values			Show	No-show	Error %
	Show		15,454	2222	12.5%
	No-show		0	4429	0%
<i>Logistic regression forecasts</i>					
Real values			Show	No-show	Error %
	Show		15,563	2113	12%
	No-show		5	4424	0.11%
<i>Majority Voting forecasts</i>					
Real values			Show	No-show	Error %
	Show		15,550	2126	12%
	No-show		2	4427	0.04%
<i>XGboost forecasts</i>					
Real values			Show	No-show	Error %
	Show		16,107	1569	9%
	No-show		95	4334	2%
<i>Decision tree forecasts</i>					
Real values			Show	No-show	Error %
	Show		16,145	1531	9%
	No-show		140	4289	3%

Therefore, additional analysis was done by assigning the appropriate algorithm for each business assumption based on Type I or Type II errors from the confusion matrix, as shown in Table 4.

Our focus was on having a low false negative rate (Type II error) and reducing the chance of not capturing the possible patients with no-show. Hence, the positive cases (no-shows) were the targets to be captured by the effective model. However, some hospitals prefer having lower false negative rates while giving more importance to models with lower false positive rates (Type I) and reducing the false alerts of the positive cases.

As a result, we formulated two hypotheses. The first was for hospitals that focused more on minimizing Type II, which was our focus in this study. In this hypothesis, we assumed that the hospitals had enough resources and ability to overbook patients, as that was applied in the case study in [38]. The best choice would be RF, LR, and majority voting algorithms where the false negative rate equaled zero. Furthermore, if the hospital considered sustainability and opted for less energy and computing consumption, LR was the best option since it requires less run time.

Second, some hospitals wanted fewer Type II errors, but they were also concerned about minimizing Type I errors because of their limited resources for covering the false alerts. Hence, the best choice would be DT and XGBoost where the error rate

for Type I was 9%, which was less than LR, RF, and the majority voting algorithms. For sustainability, DT was the best option since it required less run time.

4.3 Experiment Interpretation

In this section, we interpret the results of best-performing predictive models to gain some insights into the functionality of the models. Model interpretation phase enables the hospitals to understand better the model decision-making rules. Moreover, this is to enable transparency and confidence to use predictive models in real-world problems. Mainly, we dive further into the factors with a significant impact on detecting patient no-show behavior. Besides, we draw policies to help the hospitals in improving their decision-making system. The SHapley Additive exPlanation (SHAP) is a powerful interpretation tool for ensemble classifiers and deep learning [39]. Thus, SHAP was used in this research as a tool to explain how the complex classifier with significant results functioned. SHAP works by agnostically determining the importance of predictive features in assigning the target feature. For the straightforward models, coefficient listing was used to interpret the models better.

Random Forest. SHAP was used to understand better the factors that drive random forest functionality. In Fig. 4, the influence of the features is sorted from top to bottom in order of overall importance. The model leading features are the total number of previously missed appointments for each patient, the total number of previous appointments, and waiting days between the schedule date and the appointment date. The extracted information by SHAP can help the hospital to monitor those features and make a decision. When the hospital is aware that the patient has missed a prior appointment, the likelihood of no-show is high. Therefore, the hospital can charge no-show fees after missing a couple of appointments. This may discourage the patient from missing the next appointments. The controlling actions can be applied in a small section for close monitoring and refining of calculations refinement. An additional conclusion was that we could see from the waiting days that when a patient reserves an appointment within the same day (i.e., `waiting_days_categories_no waiting days: 0`), the likelihood of patient attendance was rather high in contrast with other categories of waiting days. Thus, sending the reminder calls for the patients with long waiting days will most likely support keeping or canceling the appointment.

XGBoost. Figure 5 shows from using SHAP that the three most dominant predictors were the same as for random forest. However, the subsequent predictors revealed a new understanding of patient behavior. It appears that patients with no medical insurance coverage (i.e., scholarship) are more reluctant to miss a medical appointment and that the youngest age group was the largest group to miss appointments. Thus, non-paying patients are taking the hospital service for granted. Therefore, including a cancellation fee for those with medical insurance may raise the appointment keeping.

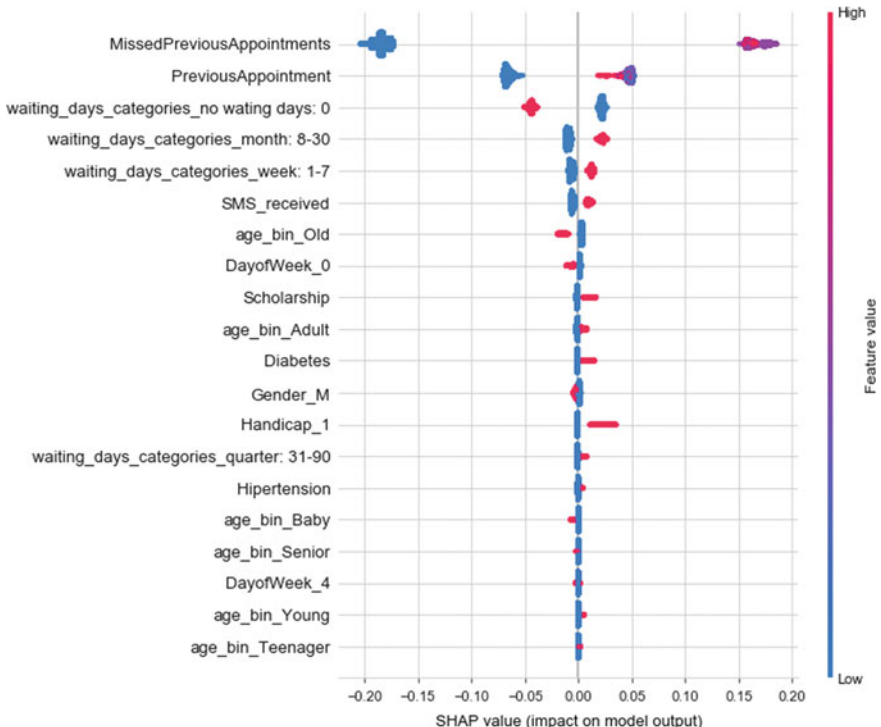


Fig. 4 SHAP graph for random forest model

Logistic Regression. Listing the value of each predictors' coefficients indicated the degree that the predictor influences the target feature. The most prominent predicting feature was prior behavior in missing an appointment with a value of (97.948719), and it is the first leading factor in most of the predictive models. It was followed by the handicap status of the patient (0.380118) and then medical insurance coverage (0.221843), which is a common leading factor between multiple models. It is worth mentioning that this algorithm identified the difficulties handicapped patients may encounter while attempting to attend their appointments. Therefore, the hospital can send a reminder to the patients' caregiver or family member to reduce no-show ratio for the patients with handicaps.

5 Conclusion

The purpose of this paper has been achieved by predicting whether patients will show up for their next appointments and by performing an analysis to understand patients' no-show behavior. We used a dataset containing approximately 100,000 appointments that had an issue with the patient's attendance. Heavy feature engineering was

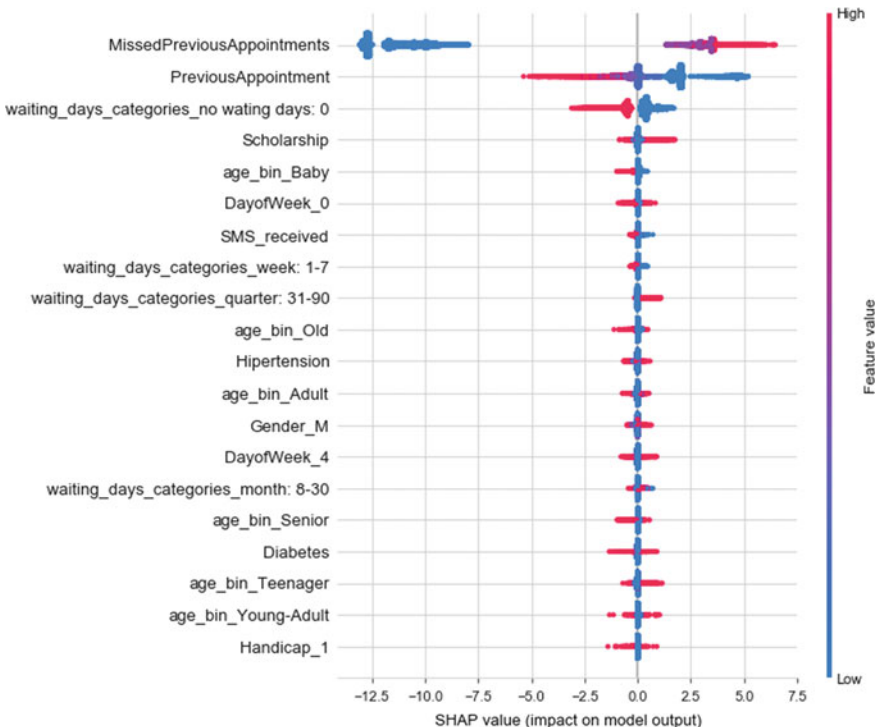


Fig. 5 SHAP graph for the XGBoost model

carried out, and new features were identified and considered as significant predictors. These included lead time and previous missed appointments. In addition, machine learning models were developed to predict when patients might not show up for a medical appointment. The proposed predictive modeling framework of using random forest as a benchmark will help the hospitals to reduce the costs of the experimental stage. Moreover, we showed that it is good practice to merge oversampling and undersampling techniques to achieve outstanding performance. This was validated by our study that a hybrid sampling method (ALL K-NN and ADASYN) gave a more balanced dataset when combined with the proposed predictive models. However, the results cannot be generalized without experimenting with this approach on many other datasets. Furthermore, the implications of these findings may be used to design new interventions to improve the scheduling process and to develop other policies and practices for better and timelier access to care. It was suggested that operations and policies be redesigned, from scheduling practices to reminder systems, since the feature of receiving an SMS plays a role in no-show behavior. Also, hospitals can check the reservation of an appointment when the patient has a high probability of missing it. As for future work, techniques to reduce dimensionality further should be explored. This includes multiple correspondence analysis (MCA) and principal component analysis (PCA) to expedite the models' performance if interpreting the

model is not required. Moreover, deep learning models can be used when a facility has big data and enough computing resources. However, for smaller facilities or facilities with less robust technology, machine learning models are efficient. Finally, it may be important for some healthcare facilities to determine a risk score for each appointment, perhaps using regression models.

References

1. Mallor F, Azcárate C (2016) Control problems and management policies in health systems: application to intensive care units. *Flex Serv Manuf J* 28(1–2):62–89
2. Belciug S, Gorunescu F (2015) Improving hospital bed occupancy and resource utilization through queuing modeling and evolutionary computation. *J Biomed Inform* 53:261–269
3. Barone MT, Ugliara T et al (2020) The impact of COVID-19 on people with diabetes in Brazil. *Diabetes Res Clin Pract* 166:108304
4. Nelson A, Herron D, Rees G, Nachev P (2019) Predicting scheduled hospital attendance with artificial intelligence. *NPJ Digit Med* 29(1):1–7
5. Huang Y, Zuniga P (2012) Dynamic overbooking scheduling system to improve patient access. *J Oper Res Soc* 63(6):810–820
6. Goffman RM et al (2017) Modeling patient no-show history and predicting future outpatient appointment behavior in the Veterans Health Administration. *Mil Med* 82(5–6):e1708–e1714
7. Mohammadi I, Wu H, Turkcan A, Toscos T, Doebling BN (2018) Data analytics and modeling for appointment no-show in community health Centers. *J Primary Care Community Health* 9:2150132718811692
8. Kurasawa H et al (2016) Machine-learning-based prediction of a missed scheduled clinical appointment by patients with diabetes. *J Diabetes Sci Technol* 10(3):730–736
9. Alshaya S, McCarren A, Al-Rasheed A (2019) Predicting no-show medical appointments using machine learning. In: International conference on computing. Springer, Cham, pp 211–223
10. Ramyachitra D, Manikandan P (2014) Imbalanced dataset classification and solutions: a review. *Int J Comput Bus Res* 5(4)
11. Alghamdi M, Al-Mallah M, Keteyian S, Brawner C, Ehrman J, Sakr S (2017) Predicting diabetes mellitus using SMOTE and ensemble machine learning approach: the Henry Ford Exercise Testing (FIT) project. *PLoS One* 12(7)
12. Ebenuwa S, Sharif M, Alazab M, Al-Nemrat A (2019) Variance ranking attributes selection techniques for binary classification problem in imbalance data. *IEEE Access* 7:24649–24666
13. Zheng X (2020) SMOTE variants for imbalanced binary classification: heart disease prediction. ProQuest
14. He H, Ma Y (2013) Imbalanced learning: foundations, algorithms, and applications. Wiley
15. Almutairi S, Shaiba H, Bezbradica M (2019) Predicting students' academic performance and main behavioral features using data mining techniques. In: Communications in computer and information science. Springer, Cham, pp 245–259
16. He H, Bai Y, Garcia E, Li S (2008) ADASYN: adaptive synthetic sampling approach for imbalanced learning. In: 2008 IEEE international joint conference on neural networks (IEEE world congress on computational intelligence). IEEE, pp 1322–1328
17. Wang Q, Cao W, Guo J, Ren J, Cheng Y, Davis DN (2019) DMP_MI: an effective diabetes mellitus classification algorithm on imbalanced data with missing values. *IEEE Access* 7:102232–102238
18. Tomek I (1976) An experiment with the edited nearest-neighbor rule. *IEEE Trans Syst Man Cybern Part C* 6
19. Prachuabsupakij W (2015) CLUS: a new hybrid sampling classification for imbalanced data. In: 12th International joint conference on computer science and software engineering (JCSSE). IEEE, pp 281–286

20. Cateni S, Colla V, Vannucci M (2014) A method for resampling imbalanced datasets in binary classification tasks for real-world problems. *Neurocomputing* 135:32–41
21. Xu Z, Shen D, Nie T, Kou Y (2020) A hybrid sampling algorithm combining M-SMOTE and ENN based on Random forest for medical imbalanced data. *J Biomed Inform* 103465
22. Zheng A, Casari A (2018) Feature engineering for machine learning: principles and techniques for data scientists, 1st edn. O'Reilly Media, Inc.
23. Dantas LF, Fleck JL, Oliveira FLC, Hamacher S (2018) No-shows in appointment scheduling—a systematic literature review. *Health Policy* 122(4):412–421
24. Singh BK, Verma K, Thoke AS (2015) Investigations on impact of feature normalization techniques on classifier's performance in breast tumor classification. *Int J Comput Appl* 116(19)
25. Alhaj TA, Siraj MM, Zainal A, Elshoush HT, Elhaj F (2016) Feature selection using information gain for improved structural-based alert correlation. *PLoS ONE* 11(11):e0166017
26. CfsSubsetEval. (Online). Available: <https://weka.sourceforge.net/doc.dev/index.html?weka/attributeSelection/CfsSubsetEval.html>. Accessed 10 June 2020
27. Sharpe D (2015) Your chi-square test is statistically significant: now what? *Pract Assess Res Eval* 20(1):8. (Online). Available: https://www.researchgate.net/publication/281962515_Your_chi-square_test_is_statistically_significant_Now_What. Accessed 10 June 2020
28. Wang J, Xu J, Zhao C, Peng Y, Wang H (2019) An ensemble feature selection method for high-dimensional data based on sort aggregation. *Syst Sci Control Eng* 7(2):32–39
29. Charoenpong J, Pimpunchat B, Amornsamankul S, Triampo W, Nuttavut N (2019) A comparison of machine learning algorithms and their applications. *Int J Simul-Syst Sci Technol* 20(4)
30. Saini I, Singh D, Khosla A (2013) QRS detection using K-Nearest Neighbor algorithm (KNN) and evaluation on standard ECG databases. *J Adv Res* 4(4):331–344
31. Chen T, He T, Benesty M, Khotilovich V, Tang Y (2015) Xgboost: extreme gradient boosting. R Packag Version 0.4-2, 1–4
32. Raza K (2019) Improving the prediction accuracy of heart disease with ensemble learning and majority voting rule. In: U-Healthcare Monitoring Systems, pp 179–196
33. Bergstra J, Yamins D, Cox D.: Making a science of model search: hyperparameter optimization in hundreds of dimensions for vision architectures. In International conference on machine learning, pp. 115–123
34. Arlot S, Celisse A (2010) A survey of cross-validation procedures for model selection. *Statistics Surv* 4:40–79
35. Hossin M, Sulaiman M (2015) A review on evaluation metrics for data classification evaluations. *Int J Data Mining Knowl Manage Process* 5(2):01–11
36. Biau G (2010) Analysis of a random forests model. *J Mach Learn Res* 13(1):1063–1095
37. Couronné R, Probst P, Boulesteix A-L (2018) Random forest versus logistic regression: a large-scale benchmark experiment. *BMC Bioinform* 19(1):270
38. Daggy J et al (2010) Using no-show modeling to improve clinic performance. *Health Inform J* 16(4):246–259
39. Lundberg SM, Lee S-I (2017) A unified approach to interpreting model predictions. In: Advances in neural information processing systems, pp 4765–4774

Adaptive Strategy for Environment Exploration in Search and Rescue Missions by Autonomous Robot



Rokas Semenas and Romualdas Bausys

Abstract In this research, a new adaptive strategy is proposed for the autonomous mobile robot, which explores the unknown search and rescue (SAR) environment. The robot, which implements the proposed strategy, operates on the frontier-based exploration approach and makes a decision of where to move next by applying a total of eight new strategies for candidate frontier assessment. The fuzzy logic controller is applied to determine the most suitable candidate frontier assessment strategy regarding the current robot state and the discovered environment information. The final decision of where to move next is made by the neutrosophic interval-valued multi-criteria decision-making method, namely WASPAS-IVNS, which enables the modelling of vagueness present in the initial sensor data. The proposed adaptive strategy is tested in the virtual Gazebo simulation. The obtained test results show the increased efficiency when comparing the proposed adaptive environment exploration strategy to the static environment exploration strategies and the standard greedy environment exploration approach.

Keywords Autonomous robot · Search and rescue · Fuzzy logic controller · Neutrosophic sets · WASPAS-IVNS

1 Introduction

The search and rescue (SAR) missions are complex and, often, dangerous operations in which the top priority of first responders is the search of human survivors that can be unconscious, trapped or heavily injured. In these missions, rescue teams can utilise the autonomous robots to collect the on-scene information about the human-inaccessible parts of the disaster site and the effects of the disaster without putting human personnel in danger. This approach can increase the awareness of

R. Semenas (✉) · R. Bausys

Department of Graphical Systems, Vilnius Gediminas Technical University, Vilnius, Lithuania
e-mail: rokus.semenas@vgtu.lt

R. Bausys

e-mail: romualdas.bausys@vgtu.lt

the responders, allowing them to determine high-risk areas that require additional safety precautions before accessing them [1]. As such, robots are expected not only to map the disaster site without the intervention of human operators but also to complete a set of tasks, for example, to find the human survivors and establish communication with them or to locate dangerous objects and events in the area [2]. And although autonomous robot decision-making and environment exploration abilities have notably improved over the years, the real-world SAR missions still provide many hard-to-solve challenges to the robot designers [3].

One of such challenges, in particular, is the modelling of the efficient unknown environment exploration strategy for the autonomous SAR robot. In general, the unknown environment exploration tasks are complex due to the lack of the initial information about the disaster site, meaning that the robot has to operate by iteratively discovering new information, adding it to the constructed environment representation model, and making a decision of where to move next based on this model. In other words, the robot operates by employing an on-line approach [4] in which the decisions of where to move next are made by evaluating the current state of the robot and the set of currently reachable candidate locations.

Considering the complexity of such environment exploration problem and the inherent complexity of real-world environments, it can be argued that an efficient SAR robot should be capable of switching between the rules that govern the autonomous environment exploration process rather than applying the same exact rules for each decision-making iteration, as it is common for state-of-the-art environment exploration strategies [5]. Therefore, in this research, we propose an adaptive SAR environment exploration approach which is driven by a multi-criteria decision-making (MCDM) method (which is used by the robot to make a decision of where to move next) and the fuzzy logic controller (which is used to determine the most suitable strategy for candidate frontier assessment). The novel contributions of this research are:

- The adaptive strategy is proposed for candidate frontier evaluation in search and rescue missions.
- The vagueness of the initial information in the proposed adaptive candidate frontier evaluation strategy is modelled by interval-valued neutrosophic multi-criteria decision-making method, namely WASPAS-IVNS.

This research paper is structured as follows. The related work is presented in Sect. 2. The original environment exploration approach, which is applied by the autonomous robot in search and rescue missions, and the novel strategy for candidate frontier assessment problem are presented in Sect. 3. Section 4 describes the experiments which were conducted in a simulated environment. The obtained results are also discussed in this section. The conclusions and future work are presented in Sect. 5.

2 Related Work

As the requirements and standards are constantly increasing for the complex, intelligent systems which have a direct impact to the well-being of humans when applied in real-life situations [6], the environment exploration problem for autonomous SAR robots continues to remain a prominent study subject. And although many state-of-the-art strategies directed at solving the environment exploration tasks were introduced over the years [5], a common and easy-to-implement approach that is a base for many environment exploration algorithms [7] is the frontier selection-based strategy [8].

In general, the frontier is defined as a region which is located at the boundary between the known (already explored) and the unknown (which is yet to be discovered) parts of the exploration environment. When the robot visits a frontier region, it obtains new information which is added to the partial environment map. Then, a decision of where to move next is made based on this new information. When all of the available frontiers are visited (including the ones that were discovered during the exploration), the environment is considered as explored.

In theory, the simple approach of leading the robot to the closest frontier would be sufficient in eventually covering the whole exploration space. However, as the complexity of the task increases, so does the complexity of the candidate frontier assessment. For example, in tasks where the exploration speed is an important condition for the overall success of the mission (such as in the case of search and rescue), the robot operators could prioritise visiting frontiers that are expected to provide more information about the environment while also minimising the time needed to reach the candidate frontier. In other words, multiple (and often competing) criteria can be applied to assess the utility of a candidate frontier. Therefore, this problem can be viewed as the multi-criteria decision-making problem, where each candidate is evaluated by combining a set of task-related criteria to determine the one with the highest utility. This candidate frontier is then chosen by the robot as a next-best location that is hoped to provide new information.

However, this decision-making process introduces two main issues—what strategy is applied for candidate frontier assessment and how the criteria are combined when determining the utility of a candidate frontier. Several papers tackle these problems by introducing varying strategies for the assessment of candidates. For example, González-Baños and Latombe [9] propose to select the frontier by assessing the estimated cost of reaching the frontier and the expected information that would be gained by the robot after reaching it. Makarenko et al. [10] propose to assess the candidate locations by summing up the results of three utilities, namely information gain utility (which is measured by estimating the amount of free grid-map cells around each candidate frontier), the navigation utility (which is estimated by the cost of driving from the robots current location to the candidate location) and the localisation utility (which defines the expected precision of robot localisation after reaching the candidate location). Gomez et al. [7] propose a cost-utility function that considers the geometric, semantic and topologic environment information.

The criteria combination problem is discussed by Tovar et al. [11], who propose a multiplicative criteria combination approach to estimate the utility of a candidate. Basilico and Amigoni [12] propose a multi-criteria decision-making approach which implements Choquet integral for criteria combination. Taillandier and Stinckwich [13] utilise the PROMETHEE II multi-criteria decision-making method to combine different criteria and conclude that this approach can allow obtaining better results than classic exploration strategies. Jeddissaravi et al. [14] propose to solve a time-limited environment coverage and exploration task by utilising ELECTRE I framework for path selection problem, and Bausys et al. [15] propose a new strategy for sustainability principle implementation in autonomous environment exploration task. However, these methods apply candidate frontier assessment strategies which follow predefined environment exploration rules, regardless of the current robot environment during the full length of the environment exploration process. Therefore, in this work, we argue that to better adapt to the complex SAR situations, the strategy which is applied by the autonomous robot to determine the candidate frontier with the highest utility score can be switched in each decision-making iteration by utilising the fuzzy logic controller.

Currently, fuzzy logic controllers are widely applied to solve autonomous robot navigation issues due to their ability to make robust decisions despite the imprecise input information [16]. Fuzzy logic is a powerful technique which has the capability of capturing human reasoning to solve complex nonlinear problems as it enables the mapping of input data to the output action by modelling the expert or domain knowledge in a linguistic manner which is based on a set of IF-THEN rules [17]. Due to the simplicity and versatility of this approach, this type of fuzzy linguistic rules has formed the basis for many robot controllers. For example, Omrane et al. [18] propose a fuzzy logic-based trajectory tracking controller for indoor environments. Chen et al. [19] present a fuzzy logic controller for a six-legged bionic robot to define obstacle avoidance and wall following behaviours. Singh and Thongam [20] reduce the robot travelling time by introducing a fuzzy strategy for avoiding obstacles in static environments, and Abiyev et al. [21] propose a fuzzy system to control the linear and angular speed of the omnidirectional soccer robots which are used in RoboCup competitions. Multiple robot application which implements a fuzzy controller was also discussed by Din et al. [22], and the latter approach tackles the SAR mission problems in an unknown environment. As the fuzzy logic application in robotic systems is a widely studied subject, some of the literature review efforts could also be mentioned. For example, Khurpade et al. [23] review the fuzzy systems employed in robotic manipulators, Hong et al. [16] review the fuzzy logic applications in autonomous robot navigation, and an in-depth review of fuzzy controlled humanoid robots is conducted by Kahraman et al. [24].

As the purpose of this research is to introduce an adaptive decision-making approach which allows for the possibility to adapt to the different situations in SAR missions, the fuzzy logic controller is applied before each decision-making process to determine which candidate frontier assessment strategy would best suit the current state of the robot. As the fuzzy logic is widely applied in modelling robot controllers due to their robustness in complex and nonlinear systems [17, 23], we argue that

this approach can help to deal with the inherent ambiguities of SAR missions and, thus, assist the robot in making better decisions during the unknown environment exploration. Next, we describe all of the components that were used to develop the proposed environment exploration strategy employed by our robot.

3 Methodology

3.1 Adaptive Environment Exploration Strategy

In this research, the search and rescue robot implements an on-line environment exploration strategy which is based on the iterative candidate frontier selection approach, in which each candidate frontier is assessed according to a set of task-related criteria. The proposed environment exploration strategy is developed by utilising ROS-provided packages [25] and employed by a virtual Pioneer 3-AT robot. Our robot uses laser range finder sensor as a primary environment perception device and the ROS-provided grid map [26] for localisation, frontier detection and object marking (in this research, we search for and mark the dangerous objects and the possible survivors).

The robot-utilised grid map is constructed from a set of 0.1 m resolution cells which are thresholded as unoccupied, occupied or unknown. Considering this approach, the frontiers can be defined as the chains of free cells that are adjacent to unknown cells. In this case, the centre point $p_f(x, y)$ of the frontier is considered as a goal that the robot can reach. In our approach, the robot explores the search and rescue environment by selecting and moving to the frontier with the highest utility score. The fuzzy logic controller is applied to determine the most suitable candidate frontier assessment strategy. In our approach, this decision is based on the common parameters of search and rescue mission, namely the danger around the robot (denoted by E_d) and the position of the detected survivors (denoted by E_s) [3]. The utility of a candidate frontier is determined by applying a multi-criteria decision-making method which is modelled under the interval-valued neutrosophic environment, namely WASPAS-IVNS [27].

When multi-criteria decision-making methods are applied in an autonomous environment exploration strategy, the decision of where to move next is made by selecting the candidate with the highest utility score. The utility U of each candidate frontier $p_f(x, y)$ is computed by referring to a set of problem-related criteria $C = \{c_1, c_2, \dots, c_n\}$ with their relative weights $W = \{w_1, w_2, \dots, w_n\}$. In this case, a set of m candidate frontiers denoted as $P = \{p_1, p_2, \dots, p_m\}$ is determined for each decision-making iteration. In our proposed system, this frontier detection and utility recalculation process is conducted by the ROS-controlled function, which is called at specific simulation-time intervals. This approach helps to reduce the number of needed computations and enables the robot to change the decision if a frontier with a higher utility is detected while moving to the selected frontier. During this evaluation

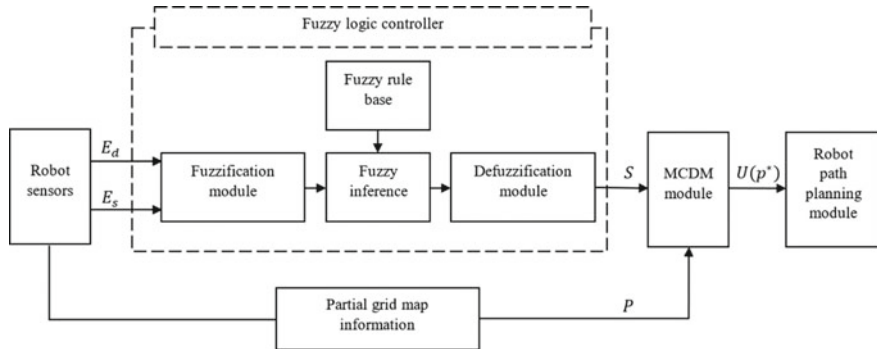


Fig. 1 Proposed adaptive candidate frontier assessment process

process, a vector of criteria values $c \in C$ is mapped to the candidate frontier p_i as $c_1(p_i), c_2(p_i), \dots, c_n(p_i)$. By applying the multi-criteria decision-making methods and referring to the criteria values and their relative weights, the utility $U(p_i)$ of a candidate frontier $p_i \in P$ is determined, and the one with the highest utility $U(p^*)$ is chosen as a next goal for the SAR robot.

However, as differently weighted criteria set can define a different candidate frontier assessment strategy, the general form of the proposed strategy set can be denoted as $ST = \{S_1(C_1, W_1), S_2(C_2, W_2), \dots, S_k(C_k, W_k)\}$, where ST is the set of candidate frontier evaluation strategies, $S_i(C_i, W_i)$ represents a single strategy which is defined by a set of problem-related criteria with differently modelled weights and k represents the number of elements in ST . As it was already discussed, in our approach, a decision of which strategy S to apply from the ST set for candidate frontier assessment is made by applying the fuzzy logic controller. This strategy is then applied by the multi-criteria decision-making module to determine the candidate frontier with the highest utility. The proposed adaptive candidate frontier assessment process, which is implemented by our robot, is schematically presented in Fig. 1.

After making a decision of where to move next, the robot applies the A^* path planning algorithm to determine the route $r = (p_r, wp_1, wp_2, \dots, wp_n, p_f)$ to the candidate frontier, where p_r is the current robot position on the constructed grid map, p_f is the candidate frontier and wp are the waypoints returned by the A^* path planning algorithm. If any new information about the environment is obtained during the movement process, the robot re-evaluates the partial map information and recalculates utility values for all available candidate frontiers. This process is repeated until the termination condition is met (in our case, there are no more frontiers that are considered reachable by the robot).

Next, we describe the criteria that define the proposed candidate frontier assessment strategies, and the fuzzy logic controller, which are applied in our approach.

3.2 Candidate Frontier Assessment Strategy

In the proposed environment exploration approach for SAR missions, candidate frontiers are evaluated according to the seven criteria, which are presented in Table 1. The core of the criteria set is constructed by referencing the common utility estimation strategies found in the literature [9, 12, 13] and by introducing two additional criteria, namely the *estimated survivor hypothesis confirmation* and the *estimated danger near the computed A* path*. The latter criteria are added to the proposed set as the common requirement in search and rescue missions is to safely reach and inspect the potential survivor to possibly confirm the survivor hypothesis [27–29], or to examine locations that are potentially hazardous to the survivors in the nearby area [30].

The c_1 and c_2 criterions, namely the *length of the frontier* and the *ratio between the number of unknown cells and the sample population size around the candidate frontier*, define the estimated amount of information that could be gained by reaching the candidate frontier. The c_1 criterion can provide an estimate of how much information can be acquired [7], as the short frontier may indicate frontiers near the corners and large frontiers may indicate wide open spaces or corridors. The c_2 criterion can be applied to determine if the frontier is surrounded by already explored space or if it borders the edge of the largely unexplored environment. In this research, the c_2 criterion value is estimated by sampling the grid-map cells around the candidate frontier in the radius of 4 m with the sample population of 880. If the cell is thresholded as unknown, it is added to the total sum of unknown cells, and the obtained result is divided by the total sample population. In this case, the criterion value is maximised to direct the robot to the candidate frontiers that are surrounded by mostly

Table 1 Proposed criteria for candidate frontier assessment

Criteria definition	Criteria name	Measurement	Estimated measurement variance
c_1	Length of the frontier	m	± 0.6 m
c_2	The ratio between the number of unknown cells and the sample population size around the candidate frontier	%	$\pm 3\%$
c_3	Distance from the robot to the candidate frontier	m	± 0.3 m
c_4	Estimated time for reaching the candidate frontier	s	± 1.2 s
c_5	Distance from the candidate frontier to the robot control station	m	± 0.3 m
c_6	Estimated danger near the computed A* path	rp	± 0.3 rp
c_7	Estimated survivor hypothesis confirmation	%	$\pm 5\%$

unknown space. As the utilised WASPAS-IVNS method enables the robot to evaluate the possible variations in the input data while making a decision, considering our setup, the estimated variance of c_1 and c_2 criteria are set to ± 0.6 m and $\pm 3\%$, respectively.

The c_3 criterion, namely the *distance from the robot to the candidate frontier*, is measured as the Euclidean distance between the robot's current position $p_r(x, y)$ and the candidate frontier $p_f(x, y)$. In our setup, the robot can stop at any given position within a radius of 0.3 m around the candidate frontier. Therefore, the estimated criterion value variance is set to be equal to this value. If the criterion is minimised, the robot is set to prioritise the closer located candidate frontiers, resulting in a more structured environment exploration. However, by following this approach, close frontiers that may be difficult to reach can be falsely considered as desirable candidates (e.g. consider the situation where the closest frontier is behind a wall). Therefore, the *estimated time for reaching the candidate frontier* (defined as c_4) is another minimised criterion proposed for candidate frontier assessment, as the robot should try to preserve as much energy as possible during the exploration process and prioritise frontiers that are reachable by short and straight paths. This criterion value is determined by applying the methodology described by Basilico and Amigoni [12] when the considered constant robot movement speed used in the calculations is equal to 0.25 m/s, and the constant rotation speed is equal to $20^\circ/\text{s}$.

The c_5 criterion, namely the *distance from the candidate frontier to the robot control station* is another important criterion in SAR missions which defines the robot's ability to transfer information after reaching the candidate frontier. The criterion value is measured as the Euclidean distance between the candidate frontier $p_f(x, y)$ and the robot control station $p_c(x, y)$, which is considered to be the robots starting position. As the communication stream between the robot and the control station should stay uninterrupted during the navigation process to provide the newest information [31] (e.g. the positions of the discovered survivors, dangerous obstacles or environment structures), this criterion should be minimised. However, it is worth to mention that the criterion can also be maximised in some specific situations where the robot is required to cover as much exploration space as possible. The estimated measurement variance of this criterion is set to ± 0.3 m due to the resolution of the robot-constructed grid map. The *estimated danger near the computed A* path* (defined as c_6) is a criterion which is introduced to support the robot self-preservation requirements. As the search and rescue environments can have objects that may pose a threat to the robot (e.g. fire or radiation sources), the robot should try to minimise the possible damages during the autonomous exploration [27]. In this case, dangerous obstacles are avoided while evaluating the global information, rather than the local [32]. The criterion value is estimated by the following equation:

$$rp = \sum_{j=1}^n \sum_{i=1}^m d_k(wp_i, o_j) \quad (1)$$

where $d_k(wp_i, o_j) = \begin{cases} 2 - d_d(wp_i, o_j); & \text{if } d_d(wp_i, o_j) < 2 \\ 0 & \text{otherwise} \end{cases}$

Here, the route penalty rp is estimated by summing the partial penalty denoted by d_k . The d_k values are estimated by inspecting the Euclidean distances d_d between each waypoint wp in a robot-computed A^* path r and all known dangerous objects in a set $O = (o_1, o_2, \dots, o_n)$. In our approach, it is considered that each dangerous object o_j can inflicting damage at a 2 m radius around its location. Therefore, if the distance between wp_i and o_j is 1.25 m, the robot is estimated to receive a penalty of 0.75 points. The estimated measurement variance for this criterion is set to $\pm 0.3 rp$.

The *estimated survivor hypothesis confirmation* is defined as c_7 and is an important criterion when considering autonomous search and rescue missions. The criterion is minimised to encourage the robot to choose a path to the frontier that is close to the object which is hypothesised (but not yet confirmed) as the survivor. This behaviour can help the robot to determine if the detected object is in fact a survivor that needs to be reached by the rescue team. However, as the human and dangerous object recognition introduces many problems that are out of the scope of this research, we assume that the robot can ideally recognise these objects when they are detected in the robot's field of view. However, the survivor confirmation rate is based on the distance between the robot and the hypothesised survivor and increases (with a constant estimated variation of $\pm 5\%$) as the robot approaches the detected object. The 100% confirmation rate is set when the distance between the robot and the survivor is less than 1.5 m [29].

Next, we describe the fuzzy logic controller, which is applied by the robot to select the candidate frontier assessment strategy, which is considered as the most suitable in the robots' current state.

3.3 Fuzzy Logic Controller for Selecting the Candidate Frontier Assessment Strategy

In general, fuzzy logic control systems include four elements: fuzzy rule base, fuzzification module, fuzzy inference machine and defuzzification module [17, 33]. Fuzzification is the process of mapping a set of crisp input values to the linguistic values (fuzzy sets) and determining the degree of membership of each set in the unit interval of $[0, 1]$ [17]. The inference module enables the controller to assess the obtained fuzzified input data by a set of fuzzy IF-THEN rules and connect it to the outputs. In this case, a fuzzy rule base represents the rules used by the inference system. As there may be multiple rules that are activated due to the overlaps in the fuzzy output, the defuzzification module converts the obtained results to a crisp output which can then be used for further application. The defuzzification process can be conducted by applying one of the many defuzzification methods, such as the centre of sums method, the centre of gravity method, or the mean of maxima, first of maxima and last of maxima membership methods, to name a few [34].

In this research, the search and rescue robot applies the fuzzy controller to determine which strategy should be used for candidate frontier evaluation. The proposed

fuzzy logic controller uses two inputs, namely the current distance from the robot to the visible hypothesised survivors E_s and the distance from the robot to the visible dangerous objects E_d , and provides one output, namely, the selected candidate frontier assessment strategy S (please refer to Sect. 3.1). In this case, the triangular membership functions are used for inputs which are presented in Figs. 2 and 3, and outputs which are presented in Fig. 4. The input membership functions for the distance between the robot and the hypothesised survivors are defined as Contact (SC), Near (SN), Medium (SM), Far (SF) and Very far (SVF). The input membership functions of the distance to the dangerous objects are defined as: Critical (DC), Very near (DVN), Near (DN), Medium (DM), Far (DF), Very far (DVF) and Safe to ignore (DSI).

In the proposed approach, the fuzzy controller output membership functions are mapped to the candidate frontier assessment strategies and are defined as danger avoidance strategy (DA) which prioritises the safety of the robot, the restrictive reach survivor strategy (RRS) which prioritises the safe exploration around the estimated survivor, the reach survivor strategy (RS), which prioritises candidate frontiers that

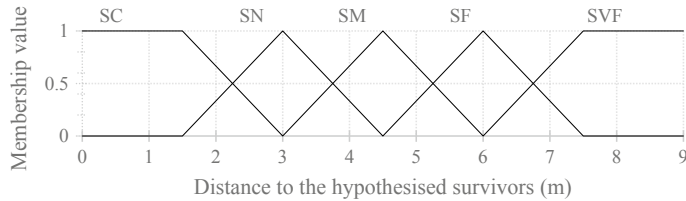


Fig. 2 Input membership function for the distance to the hypothesised survivors

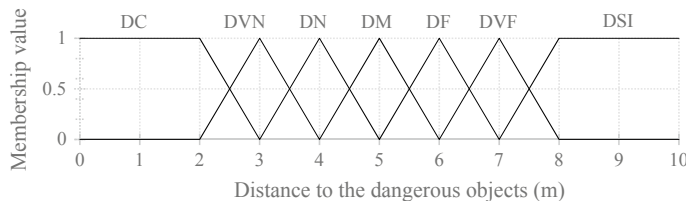


Fig. 3 Input membership function for the distance to the dangerous objects

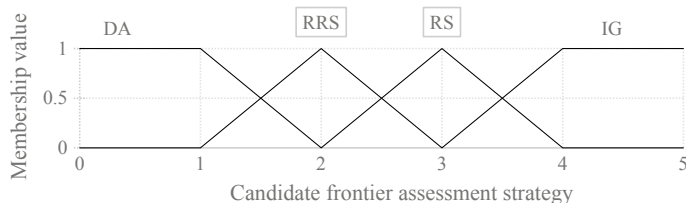


Fig. 4 Output membership function for candidate frontier assessment strategy selection

Table 2 Fuzzy rule base for candidate frontier assessment strategy selection

		E_d						
		DC	DVN	DN	DM	DF	DVF	DSI
E_s	SC	DA	RRS	RRS	RRS	RS	RS	RS
	SN	DA	RRS	RRS	RRS	RS	RS	RS
	SM	DA	DA	RRS	RRS	RS	RS	RS
	SF	DA	DA	DA	RRS	RS	IG	IG
	SVF	DA	DA	DA	DA	RS	IG	IG

are relatively close to the estimated survivor, and the information gain strategy (IG), which is modelled while considering the common greedy exploration strategies found in the literature [9, 12].

Since there are five membership functions for E_s and seven membership functions for E_d , the proposed fuzzy rule base is defined by 35 IF-THEN rules which are presented in Table 2. This fuzzy rule base is constructed referencing the partially successful autonomous environment exploration tests and the expert experience. The max-min composition is applied in fuzzy inference, and some of the example fuzzy rules used by the proposed fuzzy logic controller are defined as follows:

- IF E_s is SC AND E_d is DC THEN S is DA.
- IF E_s is SM AND E_d is DM THEN S is RRS.
- IF E_s is SN AND E_d is DF THEN S is RS.
- IF E_s is SVF AND E_d is DSI THEN S is IG.

To determine the crisp output value of the proposed fuzzy logic controller, the defuzzification step is conducted by applying the centre of sums method. This output is then mapped to the candidate frontier assessment strategies (which are presented in Table 3) according to the thresholded membership value. In this case, we use the obtained crisp value S to determine the membership to the candidate frontier selection strategy as weak or strong. The membership is determined as strong, and the selected candidate frontier assessment strategy uses the criteria weight set denoted as w_s when

Table 3 Proposed candidate frontier assessment strategies

C	DA			RRS			RS			IG		
	Op	w_s	w_v									
c_1	max	0.15	0.14	max	0.08	0.09	max	0.10	0.10	max	0.12	0.12
c_2	max	0.19	0.16	max	0.09	0.10	max	0.13	0.12	max	0.16	0.14
c_3	min	0.08	0.09	min	0.06	0.07	min	0.09	0.09	min	0.11	0.09
c_4	min	0.06	0.11	min	0.14	0.12	min	0.21	0.15	min	0.22	0.16
c_5	max	0.05	0.07	max	0.05	0.20	max	0.05	0.07	max	0.25	0.21
c_6	min	0.34	0.24	min	0.35	0.28	min	0.08	0.20	min	0.08	0.20
c_7	min	0.13	0.19	min	0.22	0.16	min	0.35	0.28	min	0.05	0.07

the obtained output value S fulfils the following rule:

$$w_s \text{ is true if } \begin{cases} S \leq x + 0.25 \\ S \geq x - 0.25 \end{cases} \quad (2)$$

where x is the integer value which is closest to the fuzzy controller output value S . Similarly, the weak membership is determined, and the selected candidate frontier assessment strategy uses the criteria weight set denoted as w_v when the obtained output value S fulfils the following rule:

$$w_v \text{ is true if } \begin{cases} S > x + 0.25 \\ S \leq x + 0.5 \end{cases} \quad \text{or} \quad \begin{cases} S < x - 0.25 \\ S \geq x - 0.5 \end{cases} \quad (3)$$

where x is the integer value which is closest to the fuzzy controller output value S . Next, in Table 3, we provide eight distinctive candidate frontier assessment strategies, which are modelled by addressing the expert-provided opinion on the criteria relative optimums Op and the weights which are relative to the strong membership w_s and weak membership w_v .

The final step in the proposed autonomous environment exploration strategy in search and rescue missions is the assessment of candidate frontier utility. In our approach, the robot decides where to move next by applying the WASPAS-IVNS method, which is described in detail by Semenas and Bausys [27]. As the details of this method can be easily traced to the original paper, in this paper, we do not provide an additional method explanation. Next, we discuss the results obtained by testing the proposed environment exploration strategy in a simulated search and rescue mission.

4 Simulation Results and Discussion

The proposed adaptive environment exploration strategy for search and rescue mission is tested in an indoor environment which is simulated in the Gazebo simulation software. The considered exploration space covers the 26 m by 18 m area and is presented in Fig. 5. The main task given to the robot is to explore the unknown SAR environment and mark all of the detected dangerous objects and survivors. In this environment, the red markers represent six dangerous objects with a 4 m diameter area-of-effect zone that the robot should try to avoid. The yellow markers represent the four survivors who should be detected, and preferably, visited by the exploring robot. It is assumed that both types of objects keep a constant position during the simulation. The robot always starts the exploration process from the position represented by the blue marker and explores the search and rescue environment until there are no frontiers left that are considered reachable by the autonomous robot.

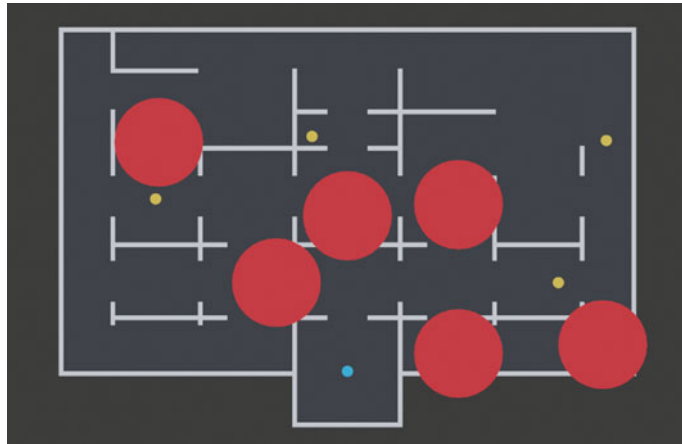


Fig. 5 Simulated indoor environment. The red markers represent the six dangerous objects that should be avoided by the robot, and the yellow markers represent four survivors that should be reached by the robot. The blue marker represents the robot starting position, which is constant in each test run

As the robot will not necessarily show the exact same behaviour and follow the same route in each simulation due to the movement speed variations and the allowed variations in path planning module, noise in the laser range scanner sensor and errors in the constructed grid map, which represents the exploration space, we conduct ten simulation runs for each individual strategy, when strong membership weights w_s are applied (please refer to Table 3). The average results obtained during these simulations are presented in Fig. 6. In this example, DA, RRS, RS and IG denote the results obtained by the robot when it applies only the specified individual strategy

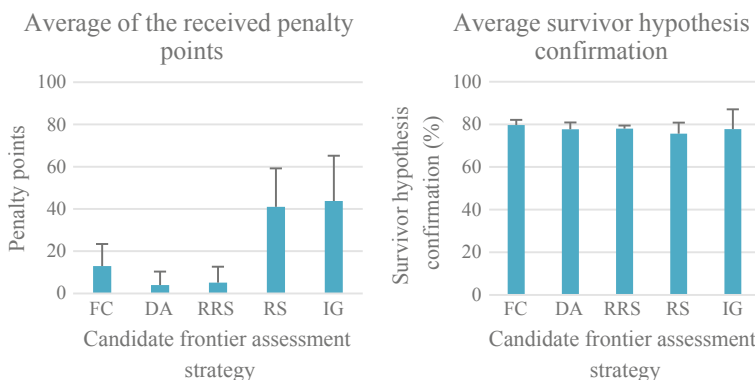


Fig. 6 Left—the average of penalty points received by the robot during the simulation. Right—the average percentage of the survivor hypothesis confirmation. The results obtained by the proposed adaptive environment exploration strategy are denoted by FC

for candidate frontier assessment. The results obtained by the proposed adaptive environment exploration strategy, which implement the fuzzy logic controller to determine the most suitable candidate frontier assessment strategy in each decision-making iteration, are denoted by FC.

The ANOVA test with the $\alpha = 0.5$ parameter was also conducted to evaluate the obtained results. The obtained p-values for each pair of the candidate frontier assessment strategies are presented in Table 4.

The obtained results show that the proposed environment exploration approach, which applies the fuzzy controller for adaptive candidate frontier assessment strategy selection during the SAR mission (denoted as FC), provides significantly different results when it is compared to the DA, RS and IG strategies and the average penalty received by the robot is considered. In this case, the robot which is operating by applying the proposed environment exploration approach receives an average of 13 penalty points. However, if the robot makes a decision of where to move next by applying the IG strategy (which corresponds to the greedy exploration strategy, modelled by referencing what is commonly done in the literature), it receives an average of 44 penalty points. Therefore, we conclude that the proposed adaptive environment exploration approach shows better performance when compared to the standard greedy approach.

However, the obtained results also indicate that there is no significant variation between the proposed adaptive environment exploration strategy FC and the DA, RRS and IG strategies when considering the average percentage of survivor confirmation hypothesis. In this case, the FC strategy obtains an average survivor confirmation rate of 80%, and DA, RRS and IG strategies obtain an average confirmation rate of 78%. The obtained result can be explained by considering the simulated exploration space. As the search and rescue environment is relatively small, the autonomous robot can cover the whole area in several minutes, meaning that every survivor will be found by the robot. However, in this case, the strong suit of the proposed fuzzy logic controller is that it tends to direct the robot away from dangerous areas (by applying the danger avoidance strategy—DA) and direct it to the frontiers that are close to the hypothesised survivors (by applying the restrictive reach survivor strategy—RRS).

To better illustrate how the adaptive candidate frontier assessment strategy selection works, we provide the example which showcases the distance sensor values and the decisions made by the fuzzy logic controller. In this case, Fig. 7 shows the robot movement trajectory and the E_d and E_s values obtained at the specific time of search and rescue mission are presented in Fig. 8.

The candidate frontier assessment strategy activation times by the proposed fuzzy logic controller are presented in Fig. 9. In this case, the value of zero indicates that the strategy is inactive, and the value of one indicates that the strategy is active, and the robot makes a decision of where to move next based on it.

As it is clear from the provided example, the fuzzy logic controller enables the robot to switch between the candidate frontier assessment strategies, based on its current state, for example, environment exploration is started by applying the information gain strategy IG. However, the robot identifies several dangerous objects around its current location as soon as it leaves the starting room. As such, the fuzzy

Table 4 *p*-values for each pair of the candidate frontier evaluation strategies, obtained by the ANOVA test, when $\alpha = 0.5$

p-values for the average of penalty points received by the robot					<i>p</i> -values for the average survivor hypothesis confirmation by the robot						
	DA	RRS	RS	IG		DA	RRS	RS	IG		
FC	0.03	0.07	0.00	0.00	FC			0.13	0.08	0.04	0.54
DA	–	0.73	0.00	0.00	DA			–	0.78	0.30	0.98
RRS	–	–	0.00	0.00	RRS			–	–	0.18	0.93
RS	–	–	–	0.76	RS			–	–	–	0.53

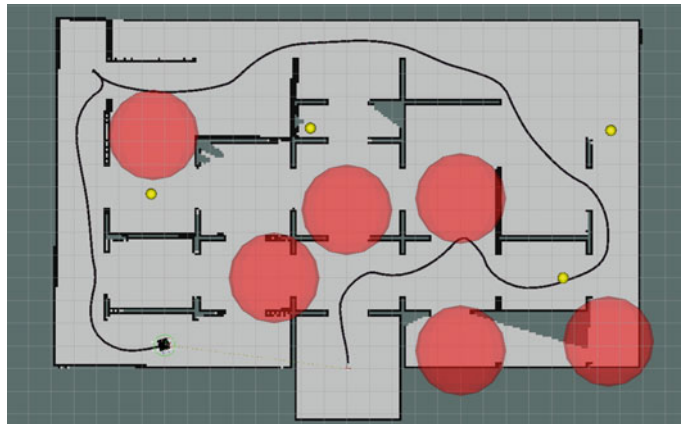


Fig. 7 Example of the robot movement trajectory by applying the proposed adaptive environment exploration strategy. Yellow markers indicate the detected survivors. Red markers represent dangerous objects with a 4 m diameter area-of-effect zone

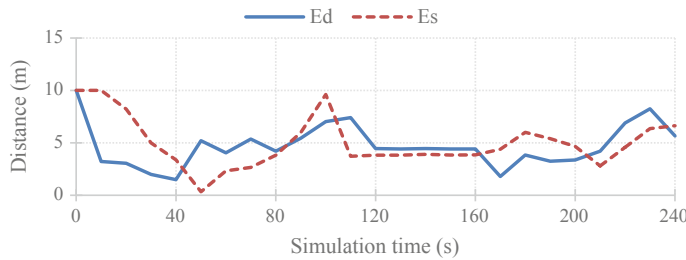


Fig. 8 E_d and E_s values obtained by the robot sensors at the specific simulation time

logic controller selects the danger avoidance strategy DA and operates by it until the first survivor is detected at the end of the right corridor. In this case, the candidate frontier assessment strategy is switched to the RRS, and the robot is directed to the frontiers which are closer to the detected survivor and also pose less danger to the robot.

5 Conclusions

In this research, we propose a new adaptive strategy for environment exploration by an autonomous search and rescue robot. A total of eight new strategies are proposed for candidate frontier assessment, and the fuzzy logic controller is introduced for selecting the most suitable strategy, depending on the current robot state. The decision of where to move next is made by applying the neutrosophic interval-valued

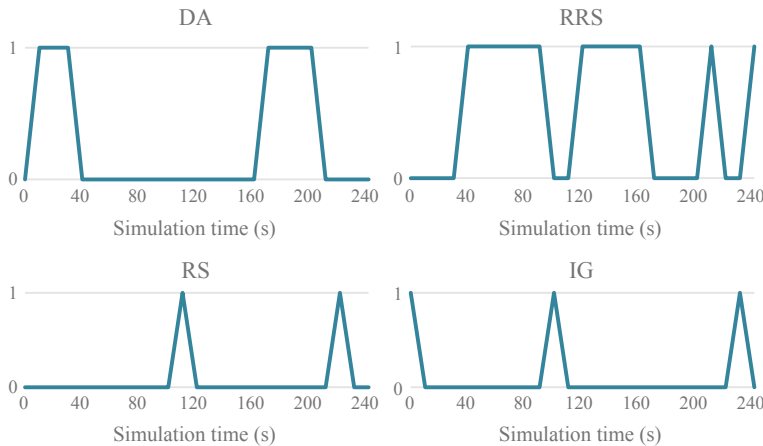


Fig. 9 Top left—the activation times of the danger avoidance strategy DA. Top right—the activation times of the restrictive reach survivor strategy RRS. Bottom left—the activation times of the reach survivor strategy RS. Bottom right—the activation times of the information gain strategy IG. The value of one indicates that the strategy is activated at the given time in the simulation

multi-criteria decision-making method, namely WASPAS-IVNS, which enables the modelling of vagueness present in the initial sensor information.

The results which were obtained by testing the proposed system in a simulated environment show that the proposed strategy introduces a clear improvement when it is compared to the standard greedy environment exploration approach and other non-adaptive strategies. The proposed approach enables the robot to switch between the candidate frontier assessment strategies based on the distance between the robot and dangerous objects and the detected survivors. The obtained simulation results indicate that the proposed strategy is suitable for search and rescue missions as it can effectively balance the information gain, danger avoidance and survivor detection strategies. The robot which implements the proposed adaptive environment exploration strategy receives an average of 13 penalty points during the autonomous exploration missions, whereas the robot, which has no ability to switch between the candidate frontier assessment strategies and, thus, operates only on the greedy information gain strategy, receives an average of 44 penalty points during the simulated test. However, no significant impact of the proposed strategy is observed when the average survivor hypothesis confirmation is considered. This can be explained by considering the size of the simulated environment. As the exploration space is relatively small, the autonomous robot is capable of covering most of the SAR environment in a reasonably short amount of time, and consequently, discover all of the survivors.

As the proposed fuzzy logic controller shows promise in autonomous environment exploration tasks, for future work, authors consider further improving the proposed adaptive environment exploration strategy by introducing an automated criteria

weight redistribution system, which could help to further increase the flexibility of the autonomous robot in SAR missions.

References

1. De Cubber G, Doroftei D, Rudin K, Berns K, Matos A, Serrano D, Sanchez J, Govindaraj S, Bedkowski J, Roda R, Silva E, Ourevitch S (2017) Introduction to the use of robotic tools for search and rescue. In: Search and rescue robotics—from theory to practice. InTech, pp 1–17
2. Jacoff A, Messina E, Weiss BA, Tadokoro S, Nakagawa Y (2003) Test arenas and performance metrics for urban search and rescue robots. IEEE Int Conf Intell Robot Syst 4:3396–3403. <https://doi.org/10.1109/iros.2003.1249681>
3. Sheh R, Schwertfeger S, Visser A (2016) 16 years of RoboCup Rescue. KI - Künstliche Intelligenz 30:267–277. <https://doi.org/10.1007/s13218-016-0444-x>
4. Choset H (2001) Coverage for robotics—a survey of recent results. Ann Math Artif Intell 31:113–126. <https://doi.org/10.1023/A:1016639210559>
5. Juliá M, Gil A, Reinoso O (2012) A comparison of path planning strategies for autonomous exploration and mapping of unknown environments. Auton Robots 33:427–444. <https://doi.org/10.1007/s10514-012-9298-8>
6. High-Level Independent Group on Artificial Intelligence (AI HLEG) (2019) Ethics guidelines for trustworthy AI. Eur Commun 1–39. <https://ec.europa.eu/digital-single-market/en/news/ethics-guidelines-trustworthy-ai>. Last accessed 2020/07/01
7. Gomez C, Hernandez AC, Barber R (2019) Topological frontier-based exploration and map-building using semantic information. Sensors (Switzerland) 19:1–20. <https://doi.org/10.3390/s19204595>
8. Yamauchi B (1997) A frontier-based approach for autonomous exploration. In: IEEE international symposium on computational intelligence in robotics and automation, Monterey, CA, pp 146–151
9. González-Baños HH, Latombe J (2002) Navigation strategies for exploring indoor environments. Int J Rob Res 21:829–848
10. Makarenko AA, Williams SB, Bourgault F, Durrant-Whyte HF (2002) An experiment in integrated exploration. IEEE Int Conf Intell Robot Syst 1:534–539. <https://doi.org/10.1109/irds.2002.1041445>
11. Tovar B, Muñoz-Gómez L, Murrieta-Cid R, Alencastre-Miranda M, Monroy R, Hutchinson S (2006) Planning exploration strategies for simultaneous localization and mapping. Rob Auton Syst 54:314–331. <https://doi.org/10.1016/j.robot.2005.11.006>
12. Basilico N, Amigoni F (2011) Exploration strategies based on multi-criteria decision making for searching environments in rescue operations. Auton Robots 31:401–417. <https://doi.org/10.1007/s10514-011-9249-9>
13. Taillandier P, Stinchwick S (2011) Using the PROMETHEE multi-criteria decision making method to define new exploration strategies for rescue robots. In: 9th IEEE international symposium on safety, security, and rescue robotics, SSRR 2011, pp 321–326. <https://doi.org/10.1109/SSRR.2011.6106747>
14. Jeddasaravi K, Alitappeh RJ, Luciano LC, Guimarães FG (2016) Multi-objective approach for robot motion planning in search tasks. Appl Intell 45:305–321. <https://doi.org/10.1007/s10489-015-0754-y>
15. Bausys R, Cavallaro F, Semenas R (2019) Application of sustainability principles for harsh environment exploration by autonomous robot. Sustainability 11:1–18. <https://doi.org/10.3390/su11092518>
16. Hong TS, Nakhaeinia D, Karasfi B (2012) Application of fuzzy logic in mobile robot navigation. In: Dadios E (ed) Fuzzy logic—controls, concepts, theories and applications. InTech, pp 21–36. <https://doi.org/10.5772/36358>

17. Klir G, Yuan B (1995) Fuzzy sets and fuzzy logic: theory and applications. Prentice Hall, New Jersey
18. Omrane H, Masmoudi MS, Masmoudi M (2016) Fuzzy logic based control for autonomous mobile robot navigation. *Comput Intell Neurosci* 2016. <https://doi.org/10.1155/2016/9548482>
19. Chen CH, Wang CC, Wang YT, Wang PT (2017) Fuzzy logic controller design for intelligent robots. *Math Probl Eng* 2017. <https://doi.org/10.1155/2017/8984713>
20. Singh NH, Thongam K (2018) Mobile robot navigation using fuzzy logic in static environments. *Procedia Comput Sci* 125:11–17. <https://doi.org/10.1016/j.procs.2017.12.004>
21. Abiyev RH, Günsel I, Akkaya N, Aytac E, Çağman A, Abizada S (2016) Robot soccer control using behaviour trees and fuzzy logic. *Procedia Comput Sci* 477–484. <https://doi.org/10.1016/j.procs.2016.09.430>
22. Din A, Jabeen M, Zia K, Khalid A, Saini DK (2018) Behavior-based swarm robotic search and rescue using fuzzy controller. *Comput Electr Eng* 70:53–65. <https://doi.org/10.1016/j.compeleceng.2018.06.003>
23. Khurpade JB, Dhami SS, Banwait S.S (2011) A review of fuzzy logic based control of robotic manipulators. In: ASME international mechanical engineering congress and exposition, IMECE 2011, vol 7, pp 241–257. <https://doi.org/10.1115/imece2011-64527>
24. Kahraman C, Deveci M, Boltürk E, Türk S (2020) Fuzzy controlled humanoid robots: a literature review. *Rob Auton Syst* 134:103643. <https://doi.org/10.1016/j.robot.2020.103643>
25. ROS, <https://www.ros.org/>. Last accessed 2020/09/12
26. ROS Gmapping, <https://wiki.ros.org/gmapping>. Last accessed 2020/09/12
27. Semenas R, Bausys R (2020) Modelling of autonomous search and rescue missions by interval-valued neutrosophic WASPAS Framework. *Symmetry (Basel)* 12. <https://doi.org/10.3390/SYM12010162>
28. Kohlbrecher S, Kunz F, Koert D, Rose C, Manns P, Daun K, Schubert J, Stumpf A, Van Stryk O (2015) Towards highly reliable autonomy for Urban Search and Rescue robots. *Lect Notes Artif Intell (Subseries Lect Notes Comput Sci)* 8992:118–129. https://doi.org/10.1007/978-3-319-18615-3_10
29. Aghababa FP, Kabiri A, Hughes J, Visser A, Amigoni F, Shimizu M (2019) RoboCup 2019 RoboCup rescue simulation league virtual robot competition rules document. Document version 1.0: 18 Apr 2019. <https://rescuesim.robocup.org/events/past-events/#2019>. Last accessed 2020/10/2
30. San Juan V, Santos M, Andújar JM (2018) Intelligent UAV map generation and discrete path planning for search and rescue operations. *Complexity* 2018:1–17. <https://doi.org/10.1155/2018/6879419>
31. Visser A, Slamet BA (2008) Including communication success in the estimation of information gain for multi-robot exploration. In: Proceedings of 6th international symposium on modeling and optimization in mobile, ad hoc, and wireless networks and workshops, WiOpt 2008, pp 680–687. <https://doi.org/10.1109/WIOPPT.2008.4586160>
32. Seraji H, Howard A (2002) Behavior-based robot navigation on challenging terrain: a fuzzy logic approach. *IEEE Trans Robot Autom* 18:308–321. <https://doi.org/10.1109/TRA.2002.1019461>
33. Novakovic B, Vranjes B, Novakovic D, Majetic D, Kasac J, Brezak D (2002) An adaptive fuzzy robot control without a fuzzy rule base. *IFAC Proc* 35:311–316. <https://doi.org/10.3182/20020721-6-es-1901.00864>
34. Sreekumar M (2016) A robot manipulator with adaptive fuzzy controller in obstacle avoidance. *J Inst Eng Ser C* 97:469–478. <https://doi.org/10.1007/s40032-015-0215-8>

Investigating the Effect of Lockdown During COVID-19 on Land Surface Temperature Using Machine Learning Technique by Google Earth Engine: Analysis of Rajasthan, India



Amita Jangid and Mukesh Kumar Gupta

Abstract The COVID-19 in India is part of the global coronavirus pandemic (COVID- 19) caused by severe acute breathing syndrome 2 (SERS-CoV-2). The first case of COVID-19 in India, which originated from China, was reported on January 30, 2020. This study analyzes the effects of lockdown during COVID-19 on land surface temperature for the six categories of water, wetland, bare land, forest, cropland, and urban. It is essential to examine the mean LST differences for each land cover type. This study uses the SR data from Landset8. All Landsat level 1 and level 2 data is directly available to Google Earth Engine, including top of atmosphere (TOA) and surface reflectance (SR). The process is a comparative analysis, so data of the same periods are analyzed for 2019 before lockdown and 2020. There are significant changes that have been seen in land surface temperature. Therefore, it is essential to incorporate an investigation regarding LST differences for each land cover type in various anthropogenic levels. So our results show mean LST differences between during and before the emergence of COVID-19 for each land cover type regarding lockdown policy in Rajasthan, India.

Keywords Land use land cover classification · Land surface temperature · Time series normalized difference vegetation index (NDVI) · Landsat8 · Machine learning · GEE

1 Introduction

The rapid spread of COVID-19 resulted in the Indian Government deciding to close India to prevent and monitor its space. This strategy was well established in Rajasthan with ‘Lockdown’ from March 25, 2020, until the next 20 days. Previous COVID-19 environmental studies were performed by Tobías et al. [1, 2]. Studies carried out by Liu et al. (2020) [2] show the meteorological factors somewhat contribute the shaping of COVID-19 transmittals that are likely to facilitate COVID-19 transmission

A. Jangid (✉) · M. K. Gupta

Department of CSE, Swami Keshvanand Institute of Technology Management & Gramothan, Jaipur, Rajasthan, India

in low humidity and moderate diurnal temperatures. Research by Tobías et al. (2020) has also shown improved quality air levels, as demonstrated that, reducing such contaminants like nitrogen dioxide (NO₂), black carbon (BC) and PM10 by two weeks after lockdown. According to the findings, we can say that COVID-19 has many implications for the climate.

The land surface temperature (LST) is another attractive environmental variable essential to investigate because of the emergence of COVID-19. LST plays an important role in various studies, including global change of climate, hydrological, agriculture based, urban use land and use land cover [3]. Moreover, LST has become a core problem for improving human life quality as continuous urbanization worldwide.

Earth observation, that includes LST measurement, is carried out by observation made by satellite in various ways with different spatial as well as temporal resolutions [3, 4] through the rapid development of remote-sensing technology. However, an imaging device with the capacity to acquire LST on a regular or weekly basis with comprehensive cover is required to track LST at a regional level for several years.

To comparing LST variance in Rajasthan as a result of implementing the lockdown policy in one summer weather cycle, it would be possible to determine if the differences were due to normal seasonal changes in overtime rather than the lockdown policy impact. Therefore, the analysis should compare the LST variation before and after the lockup phase in one year (i.e., March 2020–May 2020) and compare the LST variation in the prior year 2019 to render a situation before COVID-19 emerges. LST comparisons with LST from the previous year 2019, on the same date (i.e., the last one the year of 2019) at the time of emergence of COVID-19 (i.e., March 2020–May 2020), we can better understand the LST conditions while lockdown and prior to lockdown the emergence of COVID-19. However, anthropogenic activities various strengths during and before the emergence of COVID-19 could also lead to different LST values. Also, the severity of anthropogenic activities between and before lockdown will vary in built-up areas. Thus, it is essential to integrate investigations into LST differences at various anthropogenic levels for each land cover type. Based on the above arguments, this study utilized Landsat8 data, i.e., (1) to find out the medium LST differences between COVID-19 during emergence and the past year for the same dates, reflecting the pre-appearance of COVID-19, in Rajasthan, India; (2) to do space-temporal LST mean analysis in mid during and prior its emergence; and (3) to examine mean LST differences between during and before the emergence of COVID-19 for each land cover type with regards to lockdown policy in Rajasthan, India.

2 Methodology

2.1 Area of Study and Data

Figure 1 depicts Rajasthan's position as study areas with widespread land cover from land cover datasets Landsat8. We load images of Landsat and philter to the region and interest rates. Rajasthan, India, is located in India, with GPS coordinates of $27^{\circ} 23' 28.5972''$ N and $73^{\circ} 25' 57.4212''$ E in the group of states. Rajasthan, India's largest province, is located in India's northwestern part, right on Pakistan's frontier. It occupies 10% of the land and has a total area of around 132 000 square miles. The city of Jaipur, located in the northeastern part of the state, is Rajasthan's capital. Rajasthan has borders with five states of the country, Punjab, Haryana, Uttar Pradesh, Madhya Pradesh, and Gujarat as shown in Fig. 2. Known as the Land of Kings, the government is where the country's largest desert, the Great Indian Desert or the Thar Desert, is situated. Some part of the state is occupied by the Aravalli Mountain Range, with the top of Mount Abu being the country's highest point. There are also some green areas covered by fertile soils and natural preserves, mainly the northwestern thorn scrub forests, which are famous in India. A few rivers like the Luni River or the Ghaggar River are crossing the state from its eastern parts (with the higher elevation) to Rajasthan's southern or western parts.

Rajasthan has a tropical climate in the desert. It is freezing from October to February while that brings sun's heat starting from March to the end of September. Rainfall is scanty in Rajasthan that is drought. The Rajasthan summer starts in March.

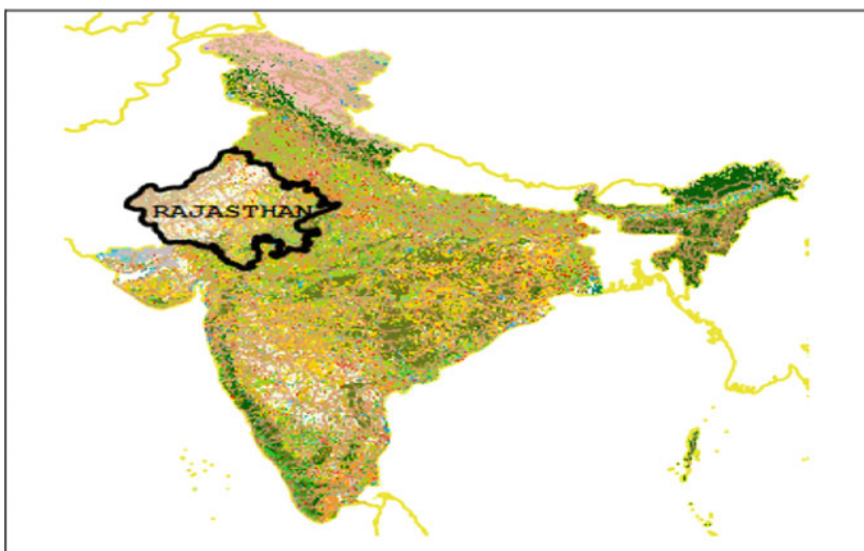


Fig. 1 Rajasthan the study area

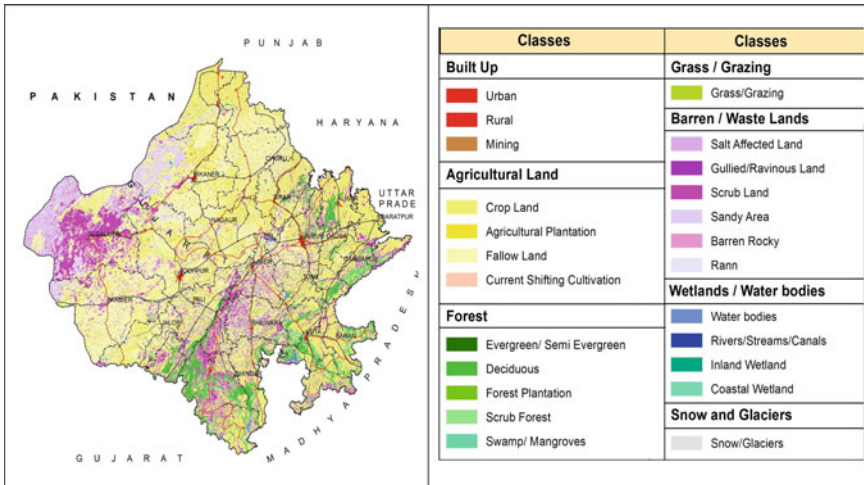


Fig. 2 LULC classification of Rajasthan by Landset8

In summer, the climate stays dry and hot, and in April, May, and June, the temperature steadily increases. The western part and the eastern part of Aravalli in Rajasthan have 40–45 °C in other regions, such as Bikaner, Jaisalmer, Phalodi, and Barmer. In summer, it also increases to the high temperature of 49 °C. January is coldest month in Rajasthan. Places such as Churu, Sikar, Pilani, and Bikaner have at least –2 °C at night and in winter. During winter, the wind blows over East, West, and North, making the sandy land cooler. These winds also have mild precipitation. In winter, the weather is always chilly. The northeast portion of the Jaisalmer has an yearly rainfall of less than ten centimeters, the Bikaner and Ganganagar have a rainfall of 20 cm, and Barmer areas have 30 cm of annual rainfall, while the Nagaur and Churu have an annual rainfall of 30 cm and Jodhpur, and Jalore regions have an average rainfall of 40 cm, with the annual precipitation of 40 cm in Jhunjhunun, Sikar, Pali, and the western Aravalli. Ajmer in Jhalawar gets 55 cm of annual precipitation to 102 cm which are located in the east of Aravalli.

Sirohi receives 163.8 cm of precipitation which is southwest part, the highest state rainfall. The monsoon starts in the last week of June until the middle of September. It is considered as the post-monsoon season, with the max temperature between 33 and 38 °C and the minimum temperature between 18 and 20 °C.

2.2 Data Processing Technique and Analysis

It is a comparative analysis of LST LULC shifts of two separate times during and before the appearance of COVID-19. During the advent of COVID-19, the period chosen was from March 2020 to May 2020. In March 2020, April 2020, and June

2020, it was a time when COVID-19, the lockdown was initiated and just a few weeks after the lockdown began in Rajasthan, respectively. The time will then be called “during COVID-19.” Similarly, before the advent of the COVID-19 tenure, which was subsequently named “before COVID-19,” it applied to an average LST for past year of 2019 on the same dates as the COVID-19 period (March to May). For example, in the first week of COVID-19 (March 2020), the LST for the last year was compared with the LST for March 2019. Minimum and maximum LST in between and prior COVID-19 cycles for each land cover from Figs. 4 and 5 were compared about Rajasthan during and before the lockdown. The land cover originally comprised 13 classes; then, classes are consolidated into six main land cover, i.e., water, wetland, urban, bare land, forest, and cropland. Land cover was derived from Landsat8.

Then, we removed the cloud cover that includes a cloud and snow masking algorithm that depends on every sensor pixel quality evaluation band. Snow, clouds, and their shadows are therefore excluded from all pictures in a series.

Chronological order steps are as follows:

1. Study area, time frame, and satellite sensor selection.
2. Application of the cloud mask algorithm to pre- and post-fire image collections.
3. Creation of cloud-free composites.
4. Evaluation of normal indexes (NDVI, NDWI) for the defined period (pre- and post-dates).
5. Subtraction of pre- and post-vegetation states and scaling factor information.

3 Result and Discussion

3.1 Mean LST Differences for Each Land Cover Type Between During and Before the Emergence of COVID-19 Concerning the Implementation of Lockdown Policy

Figure 4 shows time series of mean land surface temperature in the Rajasthan regions, for each six parts during the COVID-19 period. Figure 5 shows the time series of mean land surface temperature in six areas. For every six parts before the emergence of the COVID-19 period for each land cover type, as without and with lockdown policy implementation. Overall, the water body exhibited the most significant LST differences for both before and during lockdown policy performance. In Rajasthan, the lockdown start date is March 21, 2020. According to the results in the first week during the lockdown, the water cover land surface temperature was 2606.954 K and before lockdown in the same week of March 2019, Rajasthan’s water land surface temperature was 3060.926 K.

We can see the vast difference in the temperature of water land during and before the lockdown. The minimum cropland cover surface temperature of Rajasthan during (March 2020–May 2020) lockdown is 2361.264 K, and maximum cropland cover

surface temperature during lockdown is 3150.923 K. In Rajasthan, before the lockdown for the same months (March 2019–May 2019), the minimum cropland cover surface temperature was 2583.487 K, and maximum cropland cover surface temperature before lockdown was 3219.923 K. According to the results, the minimum and maximum temperatures are the smallest for forest land cover surface before and during the lockdown in Rajasthan, India. In Fig. 3, the minimum and maximum forest land cover surface temperatures during lockdown are 3040.544 K and 3085.36 K, respectively. In Fig. 4, the minimum and maximum forest land cover surface temperatures before lockdown are 3048.004 K and 3141.815 K, respectively. Rajasthan's minimum urban land cover surface temperature during lockdown is 3060.62 K, and maximum urban land cover surface temperature during lockdown is 3098.773 K. In

Methodological Framework within GEE

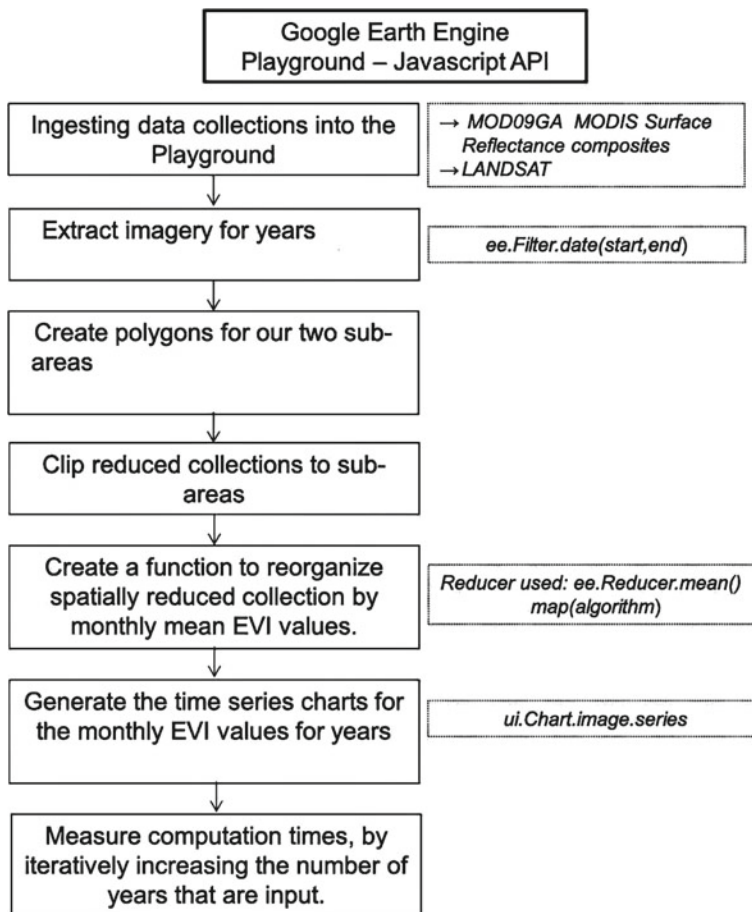


Fig. 3 Experimental Approach for LULC classification

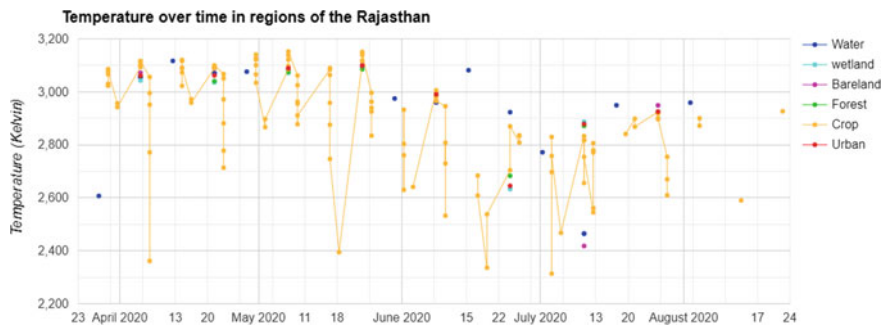


Fig. 4 Time series of mean land surface temperature in six regions during lockdown in Rajasthan

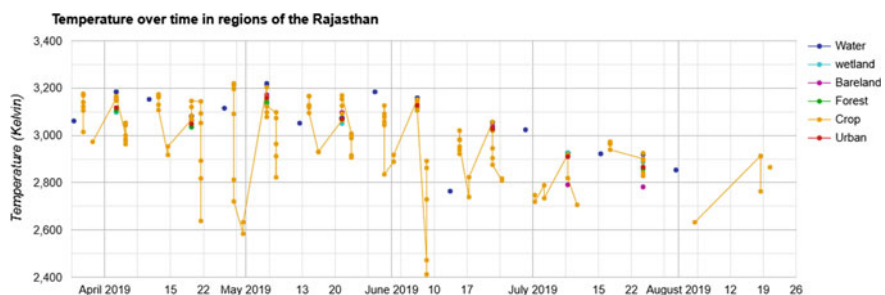


Fig. 5 Time series of mean land surface temperature in six regions before lockdown in Rajasthan

Rajasthan, before the lockdown for the same months (March 2019–May 2019), the minimum urban land cover surface temperature was 3117.238 K, and the maximum urban land cover surface temperature lockdown was 3158.773 K. Bare land cover surface temperature during lockdown in Rajasthan is 3072 K, and before lockdown, this temperature was 3171 K. In Figs. 3 and 4, maximum surface temperature variations are seen for the cropland cover surface. The results have analyzed that Rajasthan's land surface temperature is decreased during the lockdown period due to many atmospheric changes because the pollution was less from March 2020 to May 2020. According to Rajasthan, the land surface temperature was high before lockdown from March 2019 to May 2019 compared to during the lockdown period (March 2020 to May 2020).

3.2 Discussion

Previous studies have shown that generally speaking, LST continues to rise due to the change in land use, urban development, and an increase in the human population [5–7]. However, the study revealed significant findings that decrease the average

LST during opted time that may attribute to the decrease of anthropogenic activities. Study helps us to understand that the average LST applied to lockdown policies while the emergence of COVID 19, i.e., between March 2020 and May 2020 (Fig. 4) was comparatively lower than the average LST for six Rajasthan regions of the country prior to the emergence of COVID-19 as on the same dates (Fig. 5). Therefore, this study shows that LST does not always increase as built-up areas grow and the population increases. It may decrease with a particular tactic to suppress anthropogenic heat liberation, such as a lockdown policy.

Based on Landsat8 land coverage data with special resolution (Fig. 2), in general, the study indicates three types of agricultural vegetation's total variation, which show three types of crops. The group represented 44.32 percent of the total area defined by the report. Wastelands have been isolated from agriculture without crops in the present study by analyzing multiple time data from a part of the study field. Rajasthan has 22.84% wasteland. The seasonal river trace is current and is observed in Rajasthan as a water body. There is a much lower percentage of water in the total study area. Just 1.93% of the land in Rajasthan is filled with water. Urban land types include social housing and houses, transportation, water, vegetation, and empty lands within the precincts of this city, and all of them account for almost 1.77% of the geographical area. A comparison of detailed LULC data with various methods is shown in Fig. 6.

Forest and water bodies cover comparatively lower LST than built-up areas because of their capacity to carry water due to the purpose of evaporative cooling.

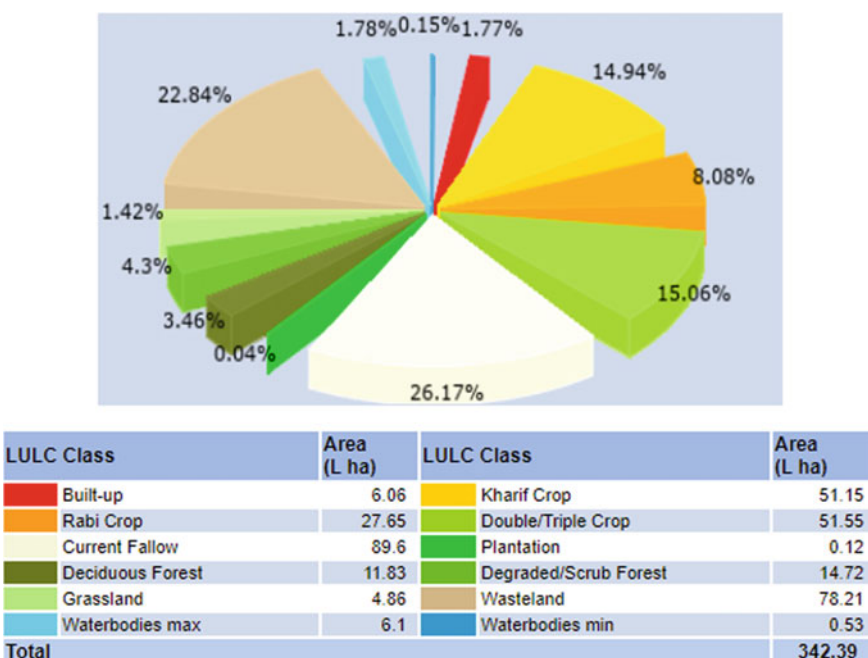


Fig. 6 LULC classifications (2019) of Rajasthan, India

Land coverings including moisture, like woods and water bodies, increase the amount of latent heat flux and transfer sensitive heat; in comparison, dry urban areas intensify sharp heat transfer and inhibit latent heat stream [8]. Moreover, due to its ability to control heat, the water body appears to have stable temperatures from time to time using the convection mechanism in any part of the water body [9]. The conditions described above may thus explain the lowest mean LST differences, irrespective of the severity of humans' lockdown activities, prior, during and post the appearance of COVID-19 in a water body, as illustrated in Fig. 6.

Before locking down, the average LST discrepancy between the emergence of COVID-19 and last year (2019) is described as a positive difference, indicating that during the creation of COVID-19 (2020), the average LST is lower than in 2019. The land cover classification for comparing both periods was developed using the Landsat8 dataset Google Earth engine. The grade is categorized based on the pixel (500 m) percentage and is divided into specified classes—the higher LST gap for inbuilt lands relative to previously built-up regions. Areas which are urban are the principal sources for anthropic heat release by production, transportation, and lighting, cooling, and heating facilities [10] about anthropogenic activities. Recently, Singh et al. [11], Bhatnagar et al. [12] and Kumari et al. [13] performed some studies on COVID-19 and predicted different parameters.

Consequently, before the lockdown the temperature is high in urban areas, are affected from covered land and human (anthropological) activities in specific areas. There is, therefore, a risk of LST decreasing in Rajasthan, India if social activities decrease during the lockdown time. Moreover, the ideas described previously could explain the most crucial difference in mean LST in built-in areas when the mean LST in built-up areas was less than the mean LST of built-up areas at the same time as COVID-19 with lockdown policies in Rajasthan than the mean LST of the previous year. In the meantime, the water soil differs greatest in LST as shown in Fig. 6.

4 Conclusions

This analysis compared the mean LST differences between the COVID-19 emergence, and the LST of 2019 for the same dates before COVID-19 in Rajasthan state, India, was found. Results showed that the mean LST during the advent of COVID-19 with a lockdown policy applied, in other words, from late March 2020 until early May 2020, was lower than the previous year's average LST in the same period. Built-in development was in type of medium and low size, because problems with urban geometry did not exist dominion in these areas. The LST level is higher in the city area due to high development areas in cities of Rajasthan because built-up areas produce high heat dispersion.

Regarding spatial distribution, the distribution of LST values throughout the Rajasthan state tends to be distributed irregularly. Moreover, parts of Rajasthan state were experienced during the entire period, i.e., water bodies and forest cover, at consistently low temperatures. This soil covers low temperatures in the study areas

due to preserving water for evaporative cooling. Furthermore, study has shown that among six land capping, i.e., water bodies, wetlands, urban areas, forests, cropland, and bare land, the LST mean for water areas was the most important in the span among COVID-19, with lockup policies implemented on the same dates as in previous years 2019.

Certain potential confounding variables related to the dynamics of the LST were not analyzed in this review. Further research should also concentrate on the assessment of LST in quarantined towns using higher spatial resolution data. In addition, we can do analyses of LST patterns for urban planning. These outcomes are required autocorrelation by transient correlation of LST patterns. In the future, the methodology used here can be used as a decision-making tool for urban planning.

References

1. Tobías A, Carnerero C, Reche C, Massagué J, Via M, Mingüillón MC, Querol X (2020) Changes in air quality during the lockdown in Barcelona (Spain) one month into the SARS-CoV-2 epidemic. *Sci Total Environ* 726:138540. <https://doi.org/10.1016/j.scitotenv.2020.138540>
2. Liu J, Zhou J, Yao J, Zhang X, Li L, Xu X, Zhang K (2020) Impact of meteorological factors on the COVID-19 transmission: a multi-city study in China. *Sci Total Environ* 726:138513. <https://doi.org/10.1016/j.scitotenv.2020.138513>
3. Ndossi MI, Avdan U (2016) Application of open source coding technologies in the production of land surface temperature (LST) maps from Landsat: a PyQGIS Plugin. *Remote Sens* 8(5). <https://doi.org/10.3390/rs8050413>
4. Jensen JR (2015) Introductory digital image processing: a remote sensing perspective. One Lake Street Prentice Hall, Upper Saddle River
5. Singh P, Kikon N, Verma P (2017) Impact of land use change and urbanization on urban heat island in Lucknow city, Central India. A remote sensing based estimate. *Sustain Urban Areas* 32:100–114. <https://doi.org/10.1016/j.scs.2017.02.018>
6. Walawender JP, Szymankowski M, Hajto MJ, Bokwa A (2014) Land surface temperature patterns in the urban agglomeration of Krakow (Poland) derived from Landsat-7/ETM+ Data. *Pure Appl Geophys* 171(6):913–940. <https://doi.org/10.1007/s00024-013-0685-7>
7. Wang Y, Zhan Q, Ouyang W (2017) Impact of urban climate landscape patterns on land surface temperature in Wuhan, China. *Sustainability* 9(10):1700. <https://doi.org/10.3390/su9101700>
8. Shahmohamadi P, Che-Ani AI, Maulud KNA, Tawil NM, Abdullah NAG (2011) The impact of anthropogenic heat on formation of urban heat island and energy consumption balance. *Urban Stud Res* 2011:1–9. <https://doi.org/10.1155/2011/497524>
9. Jensen JR (2014) Remote sensing of the environment: an earth resource perspective. Pearson, Essex
10. Gartland L (2011) Heat islands: understanding and mitigating heat in urban areas. Earthscan, London
11. Singh V, Poonia RC, Kumar S, Dass P, Agarwal P, Bhatnagar V, Raja L (2020) Prediction of COVID-19 corona virus pandemic based on time series data using Support Vector Machine. *J Discrete Math Sci Cryptogr* 23(8):1583–1597. <https://doi.org/10.1080/09720529.2020.1784535>
12. Bhatnagar V, Poonia RC, Nagar P, Kumar S, Singh V, Raja L, Dass P (2020) Descriptive analysis of COVID-19 patients in the context of India. *J Interdiscip Math* 1–16. <https://doi.org/10.1080/09720502.2020.1761635>
13. Kumari R, Kumar S, Poonia RC, Singh V, Raja L, Bhatnagar V, Agarwal P (2021) Analysis and predictions of spread, recovery, and death caused by COVID-19 in India. *Big Data Min Anal*. <https://doi.org/10.26599/BDMA.2020.9020013>

Emotion Distribution Profile for Movies Recommender Systems



Mala Saraswat and Shampa Chakraverty

Abstract Reviews, comments and feedbacks are user-generated content which comprises of insights regarding a given item or a thing and furthermore user' emotions. Various highlights of user-created content incorporate feelings, opinions and survey helpfulness that shows a promising research in the field of recommender systems. Reviews contain various words and sentences that show their natural passionate substance. Emotions are a significant component of human conduct. They enable us for decision making by generating a liking or disliking toward a particular item. This paper harnesses reviews as the content generated from user to exploit, emotion as a basis for generating recommendations. Through experiments conducted on real dataset, our proposed approach compares the performance with traditional item-based collaborative filtering approach. Experimental results show 173% increase in prediction accuracy for top 25 recommendations as compared to prediction accuracy based on rating-based item similarity.

Keywords User-generated content · Recommender systems · Reviews · Item-based collaborative filtering · Emotion-based distribution

1 Introduction

Emotions are one of the user-generated content used for recommendations. Emotions for recommendations are mostly used as one of the features for recommending items. This is so as most of the entertainment field such as books, television shows, books and movies intrigue our emotions. Our objective is to assess the effectiveness of emotions as a link for finding similarity between items of same domain. Collaborative filtering (CF)-based approaches in recommender system finds similarity of users or items to make recommendations. CF approaches recommend items based on users' or items' having similar taste or interest [1]. In this paper, emotions extracted from reviews

M. Saraswat (✉)
ABES Engineering College, Ghaziabad, U.P., India

S. Chakraverty
Netaji Subhas University of Technology, Delhi, India

using both content-based filtering where reviews are the content and collaborative filtering-based approaches where ratings are used for CF for recommending items are used. Next, an emotion distribution of item and user is generated to build and emotion-based recommender system. This approach uses six basic emotions extracted using emotion lexicon from reviews of item as content features and then using model-based collaborative filtering to recommend items from a single domain. We use movies dataset to validate our contention of using emotion as a feature to generate item and user emotion profile for computing similarity for recommending items from various entertainment fields. We also compare item-based collaborative filtering approach that uses item ratings as similarity and also user-based collaborative approach.

2 Related Work

Emotions are an important component of human behavior. Recently, emotions have been utilized in different ways for recommendations [2–4]. Shi et al. proposed movie recommendation using a contextual mood-specific movie similarity using joint matrix factorization model [2]. Authors in [3] suggest movies of different genres by analyzing different user's mood. In their work, Baldoni et al. [4] harnessed emotions from item annotations in social tagging systems. Most of these works separate emotions from tags commented on by users. Tags however are minimized depictions and limit users from picking terms openly. In this way, they do not catch emotions as viably as reviews. While composing reviews after watching a movie, users openly pen down their contemplations and feelings. Consequently, reviews give a more extravagant wellspring of feelings and emotions compared to tags. Some recent study performed by Munjal et al. [5] considered sentiment analysis [6] and opinion mining [7].

Saraswat et al. [8] in their approach discussed about latent topic-based distribution profile extracted from the reviews of items for movies and book recommender system. In this paper, we investigate how we can use emotions to generate emotion-based distribution profiles from reviews of items for movies recommender system. Our approach uses both CF and CB for recommending items. CB uses reviews from where emotions are extracted, and then, CF is done based on similar items and user preferences in the form of ratings. In this chapter, we introduce a new dimension of using emotions for recommendations. Evaluation on emotion-based item prediction further verifies the effectiveness of the proposed model in comparison to traditional item-based CF model for recommendation. The top 10 recommendations using emotion distribution profile for movies recommender system provide 111.76% higher accuracy compared to item-based collaborative filtering.

3 Emotion Distribution-Based Profile Approach

Block diagram in Fig. 1 illustrates the proposed emotion distribution profile for movies recommender system.

3.1 Data Preparation Model

This module collects and prepares the data by extracting the ratings from the movies dataset and item review corpus from *imdb* website. We use *Ratings* from MovieLens dataset for movies domain for implementing our proposed approach [9]. The dataset is composed of 1682 movie ratings given by 943 users.

3.2 Preprocessing

People write informally mostly freestyle, while writing reviews leading to spelling mistakes and noise. Therefore, before extracting emotions from the textual corpora the extraneous content are filtered in this module. Steps for preprocessing and preparation of review include:

1. *Stop word removal* such as “like,” “the,” “is,” “am” as they are irrelevant for recommendation.
2. *Removal of numeric characters*: only alphabets are retained.
3. *Compression of words*: Extra elongated words using triple or more number of same alphabets are compressed such as *cuteeeee* to *cute*.

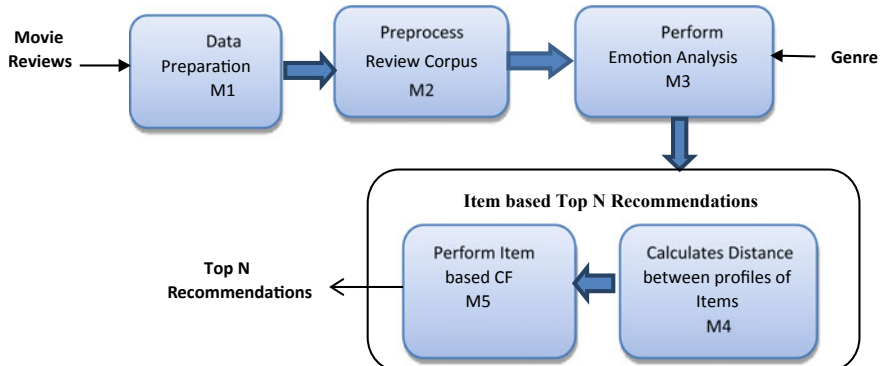


Fig. 1 Framework for emotion distribution-based recommender system

3.3 Emotion Analysis

The emotion profile of an item extracted from reviews indicates the various emotions that users might have felt while watching a movie or reading a movie. The emotion distribution profile provides the prevalence of different emotions that users express through their reviews. The emotion profiling process builds an emotion profile for each item in the given domain. The emotion distribution profile of an item or a user is represented as:

$$E = [e_1 e_2 e_3 e_4 e_5 e_6].$$

where e_i ($i \in 1, 2, \dots, 6$) represents the six basic emotions “*love, joy, surprise, anger, sadness* and *fear*; respectively.” The strength of the emotion k for an item l is represented by $e(k, l)$.

3.3.1 Emotion Lexicon

In their paper, Chakraverty et al. provided an entire set of lexicon for each basic emotion [10]. The lexicon is prepared using W. Parrott’s list of emotions. This list consists of hierarchical model for emotion classification having three levels viz. primary level, secondary level and tertiary level. In various areas of NLP such as emotion detection in tweets [11] and emails [12], Parrot’s list of emotions has been used.

3.3.2 Generating Emotion Profile of Movie Items

Emotions are extracted from the movie reviews in websites. Movie reviews are raw text that convey a mix of emotions of various intensity or strength. In the module M3, the emotion profiles of movie items are generated. This module generates the emotion distribution profile of movie l viz. $E(l)$:

$$E(l) = \{e(1, l), e(2, l), e(3, l), e(4, l), e(5, l), e(6, l)\} \quad (1)$$

where $e(k, l)$ is the k th emotion of the l th item in the movie domain M . $E(l)$ carries information about the level of different emotions in movie l .

3.4 Emotion Based Item Similarity

For finding the similarity of emotion distribution profile of items, our proposed approach computes Kullback-Leibler Divergence (KLD). KLD is a measure of “*how a probability distribution say Q diverges from another probability distribution P*,” KLD is also known as the relative entropy. However, KLD is not a symmetric distance. We use the symmetric KLD divergence as the similarity between two emotion distribution profiles must be symmetric to reflect its true distance [13]. Let the parameter $\Delta_{x,y}$ denotes the symmetric KLD between the emotion distributions of movie items M_x and M_y . Then, given their pmf(.) over the six basic emotions, $\Delta_{x,y}$ is given by:

$$\begin{aligned}\Delta_{x,y} &= KLD(pmf(ew^M(x)), pmf(er^M(y))) \\ &= \sum_{k=1}^6 (p(ew^M(k, x)) - p(ew^M(k, y))) \ln \frac{p(er^M(k, x))}{p(er^M(k, y))}\end{aligned}\quad (2)$$

The smaller the divergence $\Delta_{x,y}$ between two items x and y the more similar they are.

3.5 Generating Top-N Recommendation

Module $M5$ builds a recommendation model by analyzing the similarity based on KLD between the various items discussed in module $M4$. Using this similarity between items, $M5$ identify the set of top-N items with least KLD divergence to be recommended to a user as is done in [14].

4 Implementation and Results

This section experimentally evaluates the performance of our proposed review-based emotion distribution profile for top-N recommendation. We compare it with the item-based CF recommendation approach [15] using real-world dataset for movies, i.e., MovieLens as discussed in Sect. 3.1.

Further, we measure the performance of our emotion-based recommender system in movie domain using emotion distribution as features using various classifiers.

4.1 Comparison with Item-Based CF Approach

Table 1 shows a sample of some movies with their emotion distribution profile. For evaluating our proposed approach using performance metrics as accuracy, with tenfold cross-validation for prediction, we split the MovieLens dataset into training and testing datasets. Tenfold cross-validation approach leads to less biased estimate of model compared to simple train/test split. Here, the dataset is split into ten groups taking one group as test dataset and other nine as training datasets. Such type of grouping is repeated after shuffling the dataset. For each such group, the model is evaluated on test dataset.

The experimental analysis showing prediction accuracy of top-N recommendations for $N = 10, 15, 20$ and 25 is presented in Table 2. The table clearly shows that the prediction accuracy of emotion distribution profile of movies items for top-N recommendation algorithm performs better than item-based CF. For top 10 recommendations, emotion distribution-based approach provides 11.17% increase in prediction accuracy as compared to prediction accuracy for item-based CF approach. Similarly, top 15 recommendation approach provides around 135% increase in prediction accuracy, top 20 recommendation provides 161%, and top 25 provides around 173% increase in prediction accuracy as compared to prediction accuracy based on rating-based item similarity. This proves that emotion extracted from reviews for generating emotion profile distribution provides more accurate results for recommendation compared to item-based CF approach.

Figure 2 depicts the accuracy of both approaches viz. item-based CF and emotion distribution-based profile for MovieLens dataset. With increase in N , accuracy

Table 1 Snapshot of emotion distribution of six basic emotions for different movies

S. No.	Movie name	Joy	Love	Sad	Anger	Fear	Surprise
1	A family thing	0.502	0.113	0.116	0.129	0.120	0.11
2	A farewell to arms	0.486	0.356	0.064	0.034	0.046	0.014
3	Basic instinct	0.655	0.207	0.015	0.079	0.032	0.012
4	Zeus and Roxanne	0.214	0.642	0.022	0.080	0.034	0.018
5	Higher learning	0.387	0.120	0.145	0.193	0.129	0.026

Table 2 Performance of top-N recommendations

Top-N recommendations	Accuracy for item-based CF	Accuracy for emotion based movies recommender system
Top 10	0.289	0.612
Top 15	0.268	0.631
Top 20	0.250	0.653
Top 25	0.246	0.671

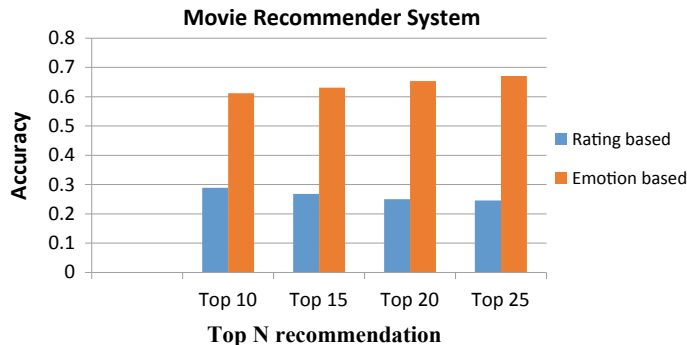


Fig. 2 Variation of accuracy with N for top- N recommendation

decreases slightly for item-based CF approach. On the contrary for emotion distribution profile for recommender systems, accuracy slightly increases. This increase in prediction accuracy is because as N increases, the item list will have more common items.

4.2 Evaluating the Performance of Emotion Distribution Profile of Movies Recommender System

The performance of emotion distribution profile of movies recommender system using various classification models such as classifiers such as KNN, random forest, decision trees and Bayes classifiers is evaluated here. For evaluating using different machine learning algorithms, the ratings of movies are classified into two classes: *like* and *dislike*. Ratings for movies greater than 3 were classified in *like* class, and those movies that get less than 3 ratings by users were classified as *dislike*. Movies that get 3 ratings are ambiguous so are not considered. Using emotion distribution profile and using six emotion features of the rated movies, different classifiers in Python are trained using Gensim toolkit. We evaluated our approach using various performance metrics viz. precision, recall, F-measure and accuracy with tenfold cross-validation for predicting the classes of test cases. Table 3 shows the various performance metrics such as precision, recall, F-measure and accuracy using different classifiers in movie

Table 3 Performance of emotion distribution in movies

S. No.	Precision	Recall	F-measure	Accuracy
KNN	0.62	0.60	0.61	0.62
Random forest	0.60	0.62	0.61	0.62
Decision tree	0.61	0.65	0.63	0.63
Bayes classifier	0.52	0.94	0.67	0.52

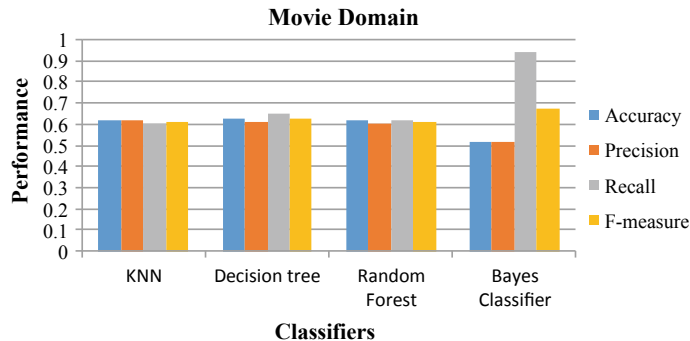


Fig. 3 Performance measures for review-based emotion distribution profile for movies recommender

domain using emotion distribution of the six basic emotions as features. Figure 3 depicts the result graphically. It can be seen from the results that Bayes classifier has the best F-measure 67% compared to all other classifiers. It is followed by decision trees with 63% *F*-measure, KNN and random forest both with 61% *F*-measure.

The accuracy for top 10 recommendations using emotion-based similarity is twofold higher compared to rating-based similarity. This is because the item-to-item similarities based on ratings does not provide a sufficient degree of personalization in items. We also compared the efficacy of different classifiers in predicting the recommendations and found that the Bayes classifier yields the best *F*-measure of 0.67 compared to other classifiers. In the future, we may extract emotions not only from reviews but also from images for providing recommendations in different domains also.

5 Conclusions

In this paper, we present an emotion distribution profile extracted from reviews for movies recommender system. We then analyze emotion distribution-based top-N recommendation model extracted from reviews of the items in movie domain and compare this with our item-based CF model. Experimental results show that emotion distribution-based item similarity using symmetric KLD metric provides prediction accuracy of more than 173% as compared to item-based CF model for top 25 recommendation.

References

1. Adomavicius G, Tuzhilin A (2005) Toward the next generation of recommender systems: a survey of the state-of-the-art and possible extensions. *IEEE Trans Knowl Data Eng* 6:734–749
2. Shi Y, Larson M, Hanjalic A (2010) Mining mood-specific movie similarity with matrix factorization for context-aware recommendation. In: Proceedings of the workshop on context-aware movie recommendation. ACM, pp 34–40
3. Winoto P, Tang TY (2010) The role of user mood in movie recommendations. *Expert Syst Appl*
4. Baldoni M, Baroglio C, Patti V, Rena P (2012) From tags to emotions: ontology-driven sentiment analysis in the social semantic web. *Intell Artif* 6(1):41–54
5. Munjal P, Kumar S, Kumar L, Banati A (2017) Opinion dynamics through natural phenomenon of grain growth and population migration. In: Hybrid intelligence for social networks. Springer, Cham, pp 161–175
6. Munjal P, Narula M, Kumar S, Banati H (2018) Twitter sentiments based suggestive framework to predict trends. *J Stat Manag Syst* 21(4):685–693
7. Munjal P, Kumar L, Kumar S, Banati H (2019) Evidence of Ostwald Ripening in opinion driven dynamics of mutually competitive social networks. *Phys A* 522:182–194
8. Saraswat M, Chakraverty S, Sharma A (2020) Based topic distribution profile for recommender systems. In: Advances in data sciences, security and applications. Springer, Singapore, pp 433–443
9. Harper FM, Konstan JA (2016) The movielens datasets: history and context. *ACM Trans Interact Intell Syst (Tiis)* 5(4):19
10. Chakraverty S, Saraswat M (2017) Review based emotion profiles for cross domain recommendation. *Multim Tools Appl* 76(24):25827–25850
11. Chakraverty S, Sharma S, Bhalla I (2015) Emotion–location mapping and analysis using twitter. *J Inf Knowl Manag* 14(03):1550022
12. Karthik K, Ponnusamy R (2011) Adaptive machine learning approach for emotional email classification. In: International conference on human-computer interaction. Springer, Berlin, pp 552–558
13. Johnson D, Sinanovic S (2001) Symmetrizing the Kullback-Leibler distance. *IEEE Trans Inf Theory*
14. Saraswat M, Chakraverty S, Kala A (2020) Analyzing emotion based movie recommender system using fuzzy emotion features. *Int J Inf Technol* 1–6
15. Karypis G (2001) Evaluation of item-based top-N recommendation algorithms. In: Proceedings of the tenth international conference on information and knowledge management. ACM, pp 247–254

Prediction of Modulus of Subgrade Reaction Using Machine Language Framework



K. S. Grover, Jitendra Khatti, and Amit Kumar Jangid

Abstract The modulus of subgrade reaction test is also known as k_s value test, and it is essentially a plate bearing test. This test is generally used in the design of rigid pavements and raft foundations. In the present research work, the modulus of subgrade reaction has been predicted by an artificial neural network and principle component analysis. For the prediction of k_s value, the neural network (NN) models of the different number of hidden layers and nodes have been developed in MATLAB R2016b. The range of the number of hidden layers has been selected from one to five, and for each hidden layer, the range of the number of nodes has been selected from two to eleven. Based on the training and validation performance of NN models, the best architectural neural network model is selected. In the present work, the neural network model of two hidden layers with eleven nodes on each hidden layer has been selected as the best architectural neural network. The best architectural neural network has been compared with principle component analysis. From the comparison, it has been concluded that the principle component analysis has predicted modulus of subgrade (k_s value) with 86.4% accuracy, which is ≈ 1.11 (1.105) times less than the accuracy of the neural network model.

Keywords Artificial neural network · Modulus of subgrade · Principle component analysis · Rigid pavement

1 Introduction

The relation between soil pressure and deflection of subgrade (soil) is known as modulus of subgrade reaction. The modulus of subgrade reaction test is also known as k_s value test. The modulus of subgrade reaction is determined for the continuous footing, mats, various types of piling and pavements. The Winkler model is the most popular model for determining the modulus of subgrade reaction [1]. According to this model, the soil is assumed to behave like infinite number of linear elastic springs, and the stiffness of springs is known as modulus of subgrade reaction. The modulus

K. S. Grover · J. Khatti (✉) · A. K. Jangid
Rajasthan Technical University, Kota, Rajasthan 324010, India

of subgrade reaction is affected by type of soil, size and shape of soil, depth and type of foundation or pavement. Iancu et al. [2] in 2009 carried out plate load tests with plates of various sizes to find out effect of size of plate on the settlement along with numerical simulation to check the size effect on settlement. The results are compared with results of FEM model using Mohr–Coulomb soil model. From the determined numerical value, it was observed that the modulus of subgrade reaction depends on the size of area of loading and magnitude of loading [2]. The Young's modulus of footing on cohesionless soil was determined by Elasmny et al. in 2010 using plate load test [10]. For the determination of compaction quality of railway subgrade, the plate load test was performed in 2011 by Dae and Seong [3]. The unrepeatitive plate load test and repetitive plate load test methods were selected in this research work. From the unrepeatitive plate load test and repetitive plate load test, the modulus of subgrade reaction (K) and strain modulus (E_v) is determined [3]. Biot [4], Terzaghi [5], Vesic [6] and Bowles [7] investigated the factors affecting the modulus of subgrade reaction. In 1937, Biot solved the problem for infinite beam with concentrated load resting on three-dimensional elastic soil continuum. From the investigation, the correlation of the continuum elastic theory and Winkler model was found.

2 Artificial Neural Network

The artificial intelligence or machine language/learning is an advanced technology of twenty-first century. The artificial intelligence (AI) or machine language/learning (ML) is consisting of two technologies, i.e., artificial neural network and convolutional neural network [8]. Presently, the artificial neural network has been more in use in medical science, space science as well as in engineering field. In engineering field, the artificial neural network is used for the prediction of engineering or mechanical properties of materials. The artificial neural network is consisting of three layers, i.e., input layer, hidden layer(s) and output layer. These layers are interconnected with neurons, and the initial and ending point of neurons is known as nodes. The input layer is consisting of input vectors or parameters, and the final predicted results are determined or obtained at output layer. These neural networks are consisting of different types of class, i.e., recurrent neural network (RNN) class and multilayer perceptron (MLP) neural network class. In present research work, multilayer perceptron class neural network has been developed in MATLAB R2016b with different parameters. The simple multilayer perceptron neural network model is shown in Fig. 1.

In present research work, the input and output parameters have been normalized by min–max normalizing function and log normalizing function, respectively. Since the output parameter, modulus of subgrade reaction gets affected by particle size of soil. Hence, for the prediction of modulus of subgrade reaction, the percent of fine particles and sand particles have been used as input parameters. In this work, the fifty-nine datasets of soil specimen have been used. These data sets have been

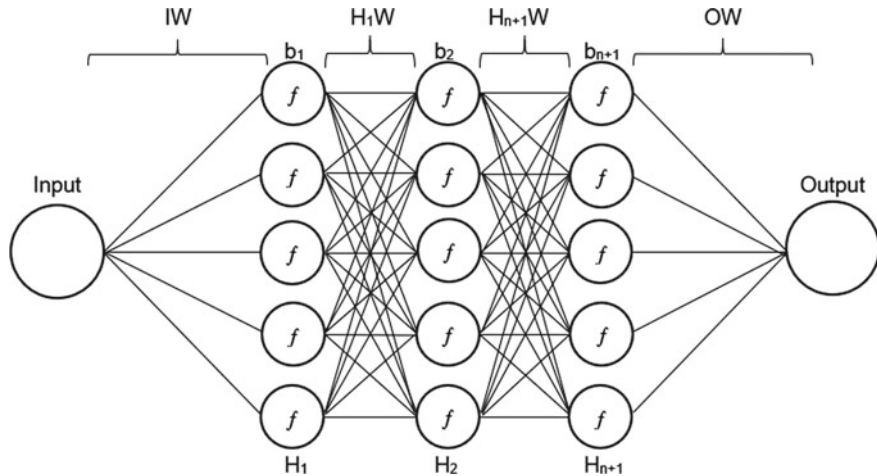


Fig. 1 Simple multilayer perceptron class neural network

divided as forty for training of neural network models and nineteen for testing of neural network models. Out of the forty data sets of soil available, 28 have been used for training and 12 data sets have been used for validation of models.

The most important part of every neural network is hidden layer(s). The hidden layer is consisting of sum of weight * input and activation function. The activation functions increase the accuracy of prediction. These activation functions are linear activation function, nonlinear activation function and binary activation function. In this work, the both linear and nonlinear activation functions have been used for the prediction of modulus of subgrade reaction. The sigmoid nonlinear activation function has been used on each hidden layer, and linear activation function has been used on output layer. For the determination of error in prediction by neural network models, the following performance matrixes have been used:

$$\text{RMSE} = \sqrt{\frac{1}{N} \sum_{i=1}^N (T_i - P_i)^2}$$

$$\text{MAE} = \frac{1}{N} \left(\sum_{i=1}^N \text{abs}(T_i - P_i) \right)$$

$$R = \frac{\sum_{i=1}^N (T_i - \bar{T})(P_i - \bar{P})}{\sqrt{\sum_{i=1}^N (T_i - \bar{T})^2 \sum_{i=1}^N (P_i - \bar{P})^2}}$$

For the distribution of error, the Levenberg–Marquardt algorithm has been used for the backpropagation process. The flowchart of proposed neural network is shown in Fig. 2.

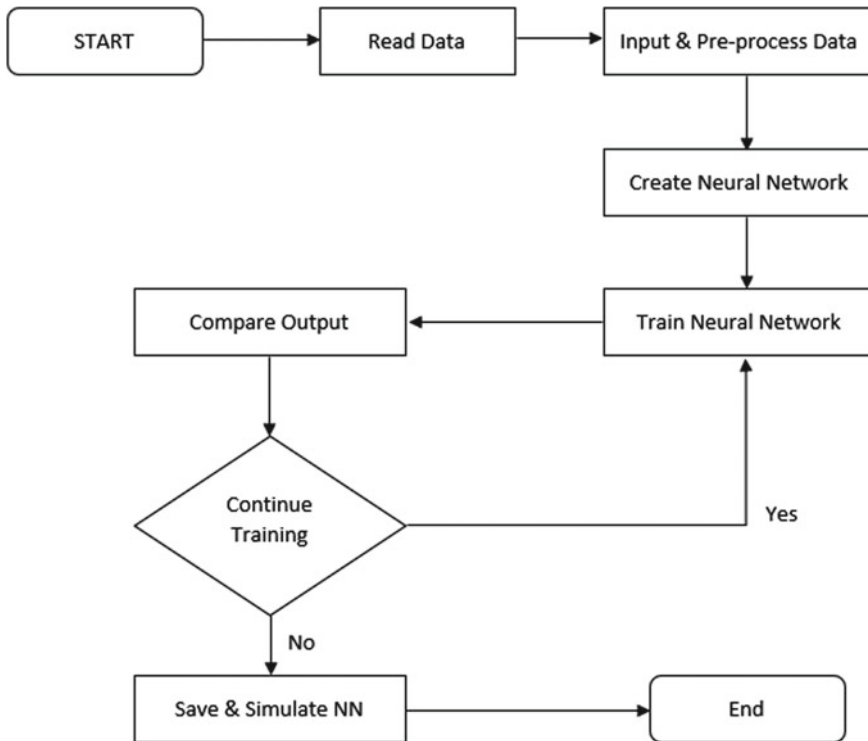


Fig. 2 Flowchart of proposed neural network

3 Principle Component Analysis

The regression analysis is known as principle component analysis, and it is the most powerful method/analysis of statistic for the prediction or forecasting of values/numbers. The most adopting methods of regression analysis are two types, i.e., linear regression method and nonlinear regression method. In present research work, multilinear regression analysis has been done for the prediction of modulus of subgrade reaction. The percentage of fine grained and sand has been selected as input parameters, and modulus of subgrade reaction has been selected as output parameter in regression analysis.

The multilinear regression (MLR) model has been developed in Microsoft Excel. For the training and validation of MLR model, forty data sets of soil have been used. The MLR model has been tested by nineteen data sets of soil. From the regression analysis, the following equation has been developed for the prediction of modulus of subgrade reaction.

$$k'_s = 31.867 - 0.1662 * FG + 0.0951S \quad (1)$$

Table 1 Architecture of artificial neural network models

Number of hidden layers				
One	Two	Three	Four	Five
ANN_ks_2H1	ANN_ks_2H2	ANN_ks_2H3	ANN_ks_2H4	ANN_ks_2H5
ANN_ks_3H1	ANN_ks_3H2	ANN_ks_3H3	ANN_ks_3H4	ANN_ks_3H5
ANN_ks_4H1	ANN_ks_4H2	ANN_ks_4H3	ANN_ks_4H4	ANN_ks_4H5
ANN_ks_5H1	ANN_ks_5H2	ANN_ks_5H3	ANN_ks_5H4	ANN_ks_5H5
ANN_ks_6H1	ANN_ks_6H2	ANN_ks_6H3	ANN_ks_6H4	ANN_ks_6H5
ANN_ks_7H1	ANN_ks_7H2	ANN_ks_7H3	ANN_ks_7H4	ANN_ks_7H5
ANN_ks_8H1	ANN_ks_8H2	ANN_ks_8H3	ANN_ks_8H4	ANN_ks_8H5
ANN_ks_9H1	ANN_ks_9H2	ANN_ks_9H3	ANN_ks_9H4	ANN_ks_9H5
ANN_ks_10H1	ANN_ks_10H2	ANN_ks_10H3	ANN_ks_10H4	ANN_ks_10H5
ANN_ks_11H1	ANN_ks_11H2	ANN_ks_11H3	ANN_ks_11H4	ANN_ks_11H5

where

k'_s is the predicted modulus of subgrade reaction ($\text{kN}/\text{m}^2/\text{m}$).

FG is the fine grained (in percentage).

S is the sand (in percentage).

Equation (1) has been used for the prediction of modulus of subgrade reaction for nineteen data set of soil.

4 Model Architecture and Data Statistics

The artificial neural network has been developed in MATLAB R2016b with different number of hidden layers and nodes. The range of number of hidden layers has been selected from one to five, and for each hidden layer, the range of number of nodes has been selected from two to eleven [9]. The architecture of artificial neural network is shown in Table 1 for different models of modulus of subgrade reaction.

The architecture of regression model is presented by MLR_ks. The given model in Table 1 has been trained and validated by forty data set and tested by nineteen data sets of soil. The statistics of fifty-nine data sets of soil are given in Table 2.

5 Results and Discussion

In this section, the performance, accuracy, error in prediction, confidence and prediction interval of neural network models and regression model has been given, and the

Table 2 Statistics of data sets of soil

Particulars	Gravel (%)	Sand (%)	Silt (%)	Clay (%)	Pan (%)	FG (%)	k_s (kN/m ² /m)
Minimum	0.00	0.00	0.00	0.00	0.00	0.00	7.93
Maximum	74.00	100.00	82.00	87.00	60.00	100.00	48.59
Mean	12.07	54.50	10.66	17.79	4.98	33.44	31.17
Standard deviation	17.81	31.09	15.52	21.38	13.23	31.44	9.93
Confidence level (95%)	4.64	8.10	4.04	5.57	3.45	8.19	2.59

discussion on the results of modulus of subgrade reaction (k_s) of nineteen data sets of soils has also been made.

5.1 Training and Validation Performance of Models

During the training of artificial neural network model of one, two, three, four and five hidden layers, the training and validation performance of neural network models have been observed. The neural network models have been trained and validated by twenty-eight and twelve data sets of soils, respectively. The training and validation performance of one, two, three, four and five hidden layers with different number of nodes is given in Tables 3, 4, 5, 6 and 7, respectively.

For the determination of the best architecture neural network model having one hidden layer, the range of nodes have been selected from two to eleven. From Table 3, the best architecture neural network model of one hidden layer has been determined as ANN_ks_5H1 NN model having five nodes. The ANN_ks_5H1 neural network

Table 3 Training and validation performance of one hidden layer NN model

Model architecture	Training performance			Validation performance		
	RMSE	R	MAE	RMSE	R	MAE
ANN_ks_2H1	0.11839	0.94022	0.07178	0.20833	0.61098	0.10050
ANN_ks_3H1	0.18427	0.87032	0.04572	0.23568	0.63286	0.07956
ANN_ks_4H1	0.21898	0.78760	0.07233	0.21752	0.81231	0.09294
ANN_ks_5H1	0.16586	0.84316	0.06144	0.14391	0.91200	0.08396
ANN_ks_6H1	0.14181	0.90314	0.07007	0.18449	0.73313	0.09857
ANN_ks_7H1	0.14391	0.89483	0.06012	0.15248	0.87883	0.09899
ANN_ks_8H1	0.11623	0.93275	0.19190	0.20501	0.72350	0.22580
ANN_ks_9H1	0.16722	0.88158	0.26900	0.20632	0.86847	0.30710
ANN_ks_10H1	0.08900	0.96237	0.05293	0.27038	0.39209	0.11790
ANN_ks_11H1	0.17169	0.89858	0.04048	0.23563	0.74705	0.10080

Table 4 Training and validation performance of two hidden layer NN model

Model architecture	Training performance			Validation performance		
	RMSE	R	MAE	RMSE	R	MAE
ANN_ks_2H2	0.15246	0.88696	0.02830	0.15504	0.76948	0.03666
ANN_ks_3H2	0.20355	0.76981	0.12020	0.16093	0.85806	0.11250
ANN_ks_4H2	0.14567	0.88438	0.04979	0.17251	0.85993	0.06203
ANN_ks_5H2	0.13998	0.89895	0.05473	0.13677	0.91711	0.04844
ANN_ks_6H2	0.12483	0.92726	0.03894	0.20069	0.55576	0.06885
ANN_ks_7H2	0.30182	0.78014	0.12120	0.24978	0.69308	0.21560
ANN_ks_8H2	0.28365	0.87197	0.07172	0.24458	0.69903	0.13140
ANN_ks_9H2	0.09345	0.96915	0.07758	0.25539	0.65320	0.15280
ANN_ks_10H2	0.00381	0.99992	0.00836	0.15899	0.90843	0.04074
ANN_ks_11H2	0.16583	0.85407	0.21490	0.08759	0.96082	0.22720

Table 5 Training and validation performance of three hidden layer NN model

Model architecture	Training performance			Validation performance		
	RMSE	R	MAE	RMSE	R	MAE
ANN_ks_2H3	0.23217	0.64645	0.07458	0.19700	0.89177	0.07921
ANN_ks_3H3	0.14537	0.90555	0.06701	0.25197	0.55268	0.09484
ANN_ks_4H3	0.16091	0.87830	0.03977	0.13079	0.92497	0.03592
ANN_ks_5H3	0.15421	0.85875	0.03503	0.16559	0.91923	0.04977
ANN_ks_6H3	0.29860	0.55635	0.07241	0.21079	0.84349	0.10490
ANN_ks_7H3	0.15488	0.85679	0.10100	0.15119	0.93970	0.18090
ANN_ks_8H3	0.07420	0.97256	0.07328	0.27536	0.65553	0.14100
ANN_ks_9H3	0.14495	0.89911	0.04229	0.13475	0.90127	0.04106
ANN_ks_10H3	0.21730	0.90421	0.19260	0.26255	0.64059	0.30670
ANN_ks_11H3	0.10935	0.94334	0.11320	0.11253	0.93014	0.09948

model has 91.20% performance achieved, and error in prediction (RMSE) has been reduced up to 0.14391 kN/m²/m. The graphical presentation of training and validation performance of one hidden layer neural network models is shown in Fig. 3.

In the case of two hidden layers, the best architecture neural network has been determined with eleven nodes on each hidden layer. From Table 4, it has been observed that the best architectural ANN_ks_11H2 neural network model having eleven nodes has 96.08% performance achieved, and the error in prediction (RMSE) has been reduced up to 0.08759 kN/m²/m. The graphical presentation of the training and validation performance of two hidden layer neural network model is shown in Fig. 4.

Similarly, based on the performance of the neural network, the best architecture neural network model has been determined as ANN_ks_11H3. The best architectural

Table 6 Training and validation performance of four hidden layer NN model

Model architecture	Training performance			Validation performance		
	RMSE	R	MAE	RMSE	R	MAE
ANN_ks_2H4	0.15114	0.85208	0.03094	0.19480	0.85280	0.05977
ANN_ks_3H4	0.15226	0.89580	0.04581	0.14245	0.83552	0.05655
ANN_ks_4H4	0.17582	0.85150	0.05765	0.14497	0.91234	0.05548
ANN_ks_5H4	0.19804	0.84035	0.06975	0.22210	0.61442	0.08424
ANN_ks_6H4	0.16534	0.86482	0.30680	0.16951	0.84213	0.32780
ANN_ks_7H4	0.16059	0.86564	0.08593	0.22448	0.73941	0.12200
ANN_ks_8H4	0.13535	0.90340	0.10510	0.17195	0.89659	0.11750
ANN_ks_9H4	0.14078	0.90378	0.17040	0.19045	0.68919	0.23580
ANN_ks_10H4	0.20686	0.77887	0.14220	0.24932	0.83958	0.19160
ANN_ks_11H4	0.18321	0.84538	0.04480	0.19315	0.70874	0.07286

Table 7 Training and validation performance of five hidden layer NN model

Model architecture	Training performance			Validation performance		
	RMSE	R	MAE	RMSE	R	MAE
ANN_ks_2H5	0.13424	0.91170	0.04990	0.17970	0.81655	0.06602
ANN_ks_3H5	0.14969	0.87928	0.03720	0.16987	0.85140	0.05173
ANN_ks_4H5	0.15395	0.87754	0.05365	0.21536	0.73903	0.08292
ANN_ks_5H5	0.13389	0.91777	0.03087	0.18906	0.75748	0.04547
ANN_ks_6H5	0.11503	0.93524	0.06513	0.20826	0.72056	0.07681
ANN_ks_7H5	0.10741	0.94861	0.09051	0.25908	0.72258	0.13700
ANN_ks_8H5	0.14230	0.91401	0.10680	0.21650	0.73882	0.12670
ANN_ks_9H5	0.20732	0.85931	0.20710	0.18354	0.83788	0.22130
ANN_ks_10H5	0.16447	0.87034	0.03922	0.20217	0.82588	0.10800
ANN_ks_11H5	0.22582	0.81915	0.04543	0.28238	0.48753	0.13960

neural network model ANN_ks_11H3 having eleven nodes has 93.01% performance achieved, and error in prediction has been reduced up to 0.11253 kN/m²/m. The graphical presentation of training and validation performance of all neural network models of three hidden layers is shown in Fig. 5.

The best architecture neural network models of four hidden layers models have been determined with three nodes on each hidden layer. The ANN_ks_3H4 neural network models having three nodes have been selected as the best architecture neural network model. This neural network model has 93.55% performance achieved, and error in prediction has been reduced up to 0.14245 kN/m²/m. The graphical presentation of all neural networks of four hidden layers is shown in Fig. 6.

In the case of five hidden layer models, the best architecture neural network model has been determined as ANN_K_3H5 neural network models. The ANN_ks_3H5

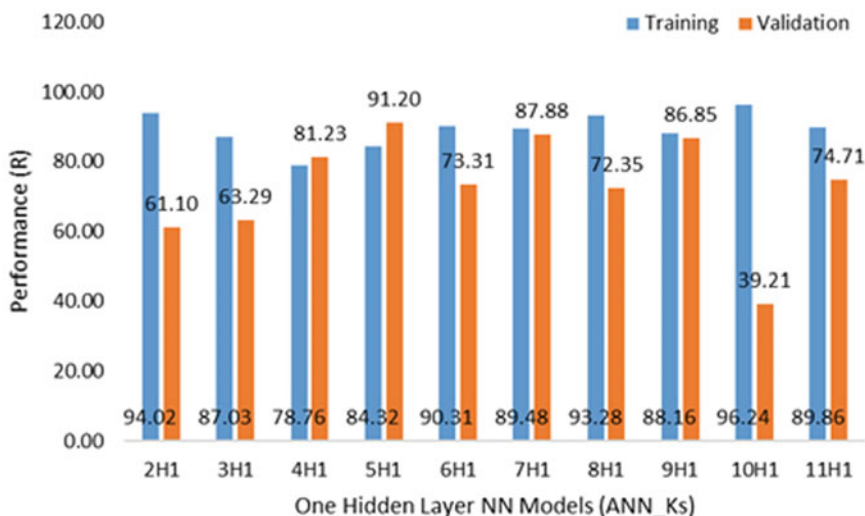


Fig. 3 Training and validation performance of one hidden layer NN models

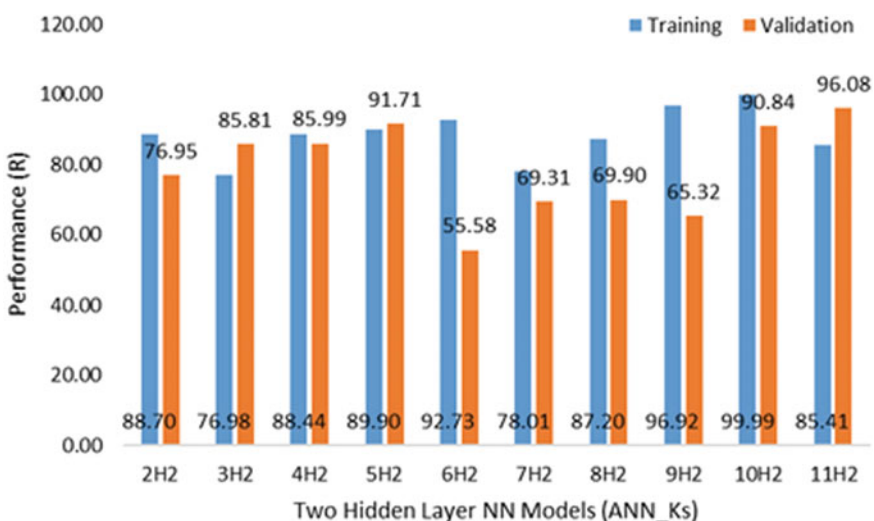


Fig. 4 Training and validation performance of two hidden layer NN models

neural network model having three nodes has 85.14% performance achieved, and error in prediction (RMSE) has been reduced up to $0.16987 \text{ kN/m}^2/\text{m}$. The graphical presentation of the performance of five hidden layer neural network models is shown in Fig. 7.

For the prediction of modulus of subgrade reaction of nineteen data set of soil, the multilinear regression (MLR) analysis has been done. During the training of MLR

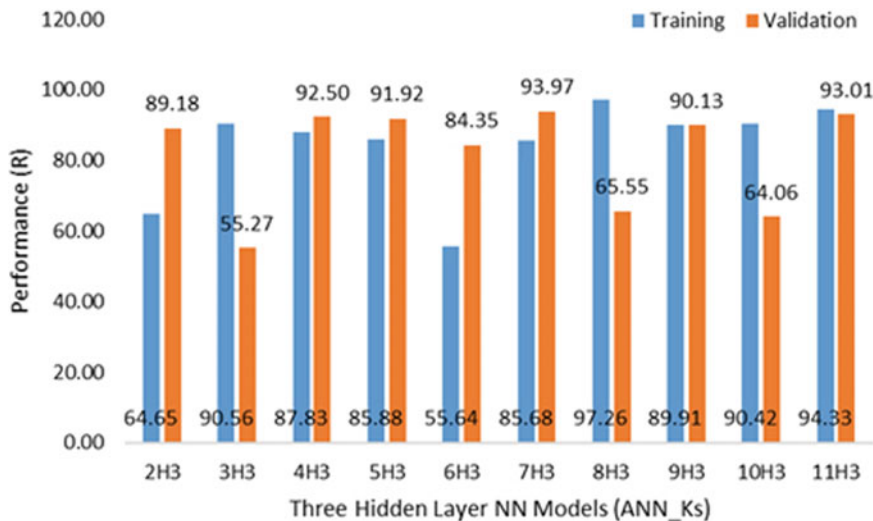


Fig. 5 Training and validation performance of three hidden layer NN models

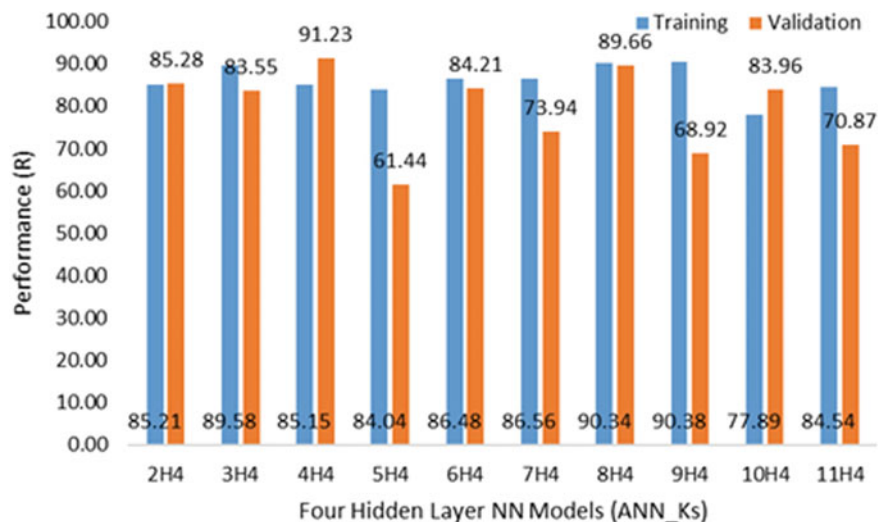


Fig. 6 Training and validation performance of four hidden layer NN models

model, the training and validation performance of MLR model has been determined, and it has been shown in Table 8.

From Table 8, it has been observed that the MLR_{*k*_s} model has 92.53% performance achieved, and error in prediction (RMSE) has been reduced to 3.22 kN/m²/m.

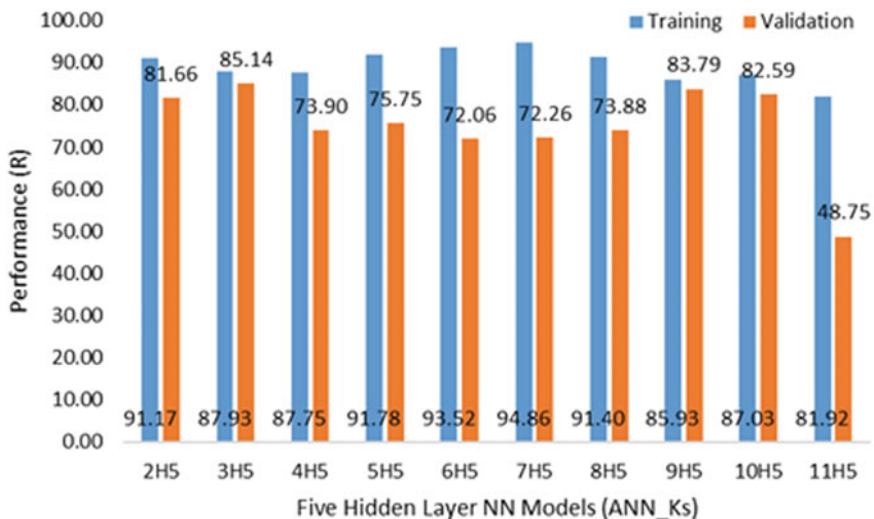


Fig. 7 Training and validation performance of five hidden layer NN models

Table 8 Training and validation performance of MLR model

Model architecture	Training performance			Validation performance		
	RMSE	R	MAE	RMSE	R	MAE
MLR_ks	5.45957	0.81444	4.25225	3.21527	0.92527	2.48957

Comparison of performance of models

From the training and validation performance of one, two, three, four and five hidden layers neural network model, it has been observed that the performance of NN model has been affected by number of nodes as well as by the number of hidden layers. Based on the training and validation performance, the ANN_ks_5H1, ANN_ks_11H2, ANN_ks_11H3, ANN_ks_3H4 and ANN_ks_3H5 neural network models have been selected as best architecture neural network model. The performance of best architecture neural network models and MLR model is given in Table 9.

From the comparison of the performance of the neural network model and MLR model, it has been observed that the ANN_ks_11H2 neural network model has been achieved maximum performance.

Table 9 Comparison of performance of models

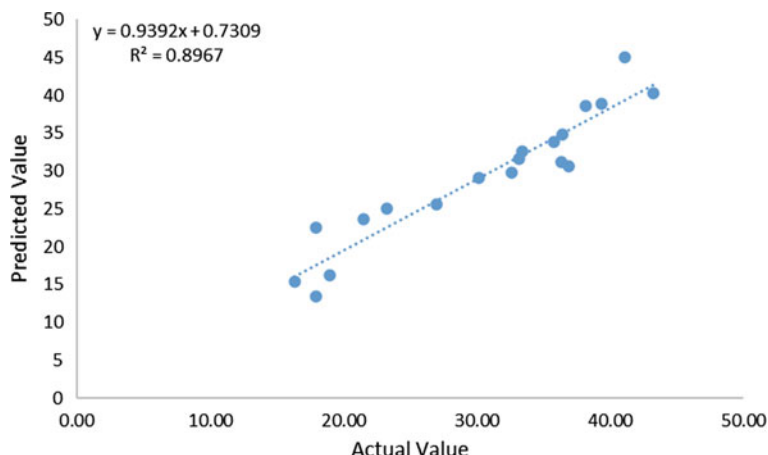
Model architecture	Training performance			Validation performance		
	RMSE	R	MAE	RMSE	R	MAE
ANN_ks_5H1	0.16586	0.84316	0.06144	0.14391	0.91200	0.08396
ANN_ks_11H2	0.16583	0.85407	0.21490	0.08759	0.96082	0.22720
ANN_ks_11H3	0.10935	0.94334	0.11320	0.11253	0.93014	0.09948
ANN_ks_3H4	0.15226	0.89580	0.04581	0.14245	0.83552	0.05655
ANN_ks_3H5	0.14969	0.87928	0.03720	0.16987	0.85140	0.05173
MLR_ks	5.45957	0.81444	4.25225	3.21527	0.92527	2.48957

5.2 Accuracy of Models for Prediction of k_s Value

The best architecture ANN_ks_5H1, ANN_ks_11H2, ANN_ks_11H3, ANN_ks_3H4 and ANN_ks_3H5 neural network models and MLR_ks model have been used for prediction of modulus of subgrade reaction of nineteen data sets of soil. For the determination of the accuracy of ANN_ks_5H1 neural network model, the correlation between actual (test) value and the predicted value of modulus of subgrade reaction has been plotted in a graph as shown in Fig. 8.

From Fig. 8, it has been observed that the ANN_ks_5H1 neural network model having five nodes has predicted modulus of subgrade reaction with 89.67% accuracy. Similarly, the accuracy of ANN_ks_11H2 neural network model has been plotted in a graph as shown in Fig. 9.

From Fig. 9, it has been observed that the ANN_ks_11H2 neural network model having eleven nodes has been predicted modulus of subgrade reaction with 95.51% accuracy. From the accuracy of ANN_ks_5H1 and ANN_ks_11H2 neural network

**Fig. 8** Accuracy of ANN_ks_5H1 NN model

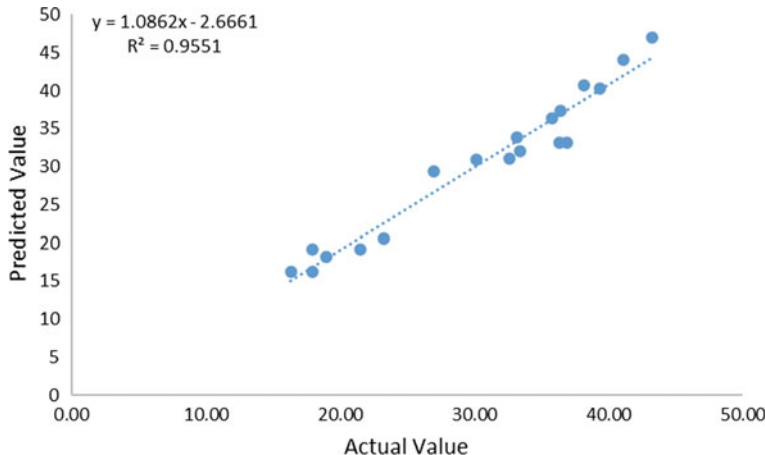


Fig. 9 Accuracy of ANN_k_s_11H2 NN model

model, it has also been observed that the accuracy has increased with increasing the number of hidden layers. In the case of three hidden layers, the ANN_k_s_11H3 neural network model has also been plotted with 91.36% accuracy as shown in Fig. 10.

From Fig. 9, it has been observed that the ANN_k_s_11H3 neural network model has been accuracy achieved as 91.36%, and it has also been observed that the accuracy has decreased with increasing the number of hidden layers. Similarly, the accuracy of ANN_k_s_3H4 neural network has been plotted in a graph as shown in Fig. 11.

From Fig. 10, it has been observed that the ANN_k_s_3H4 neural network model has predicted modulus of subgrade reaction with 81.04% accuracy. Similarly, the

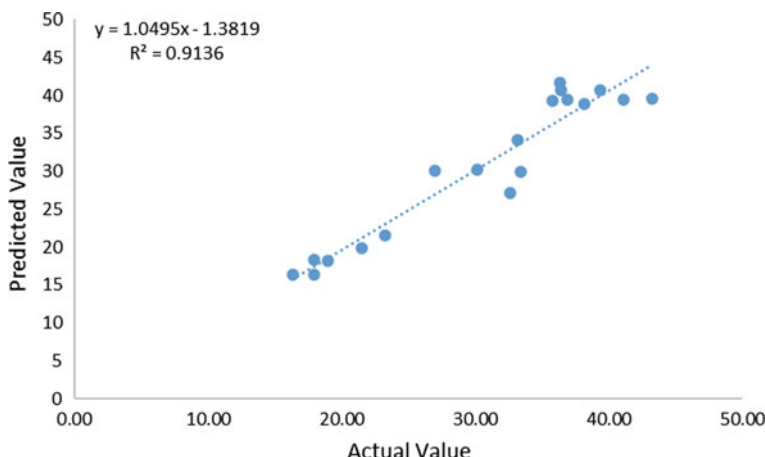


Fig. 10 Accuracy of ANN_k_s_11H3 NN model

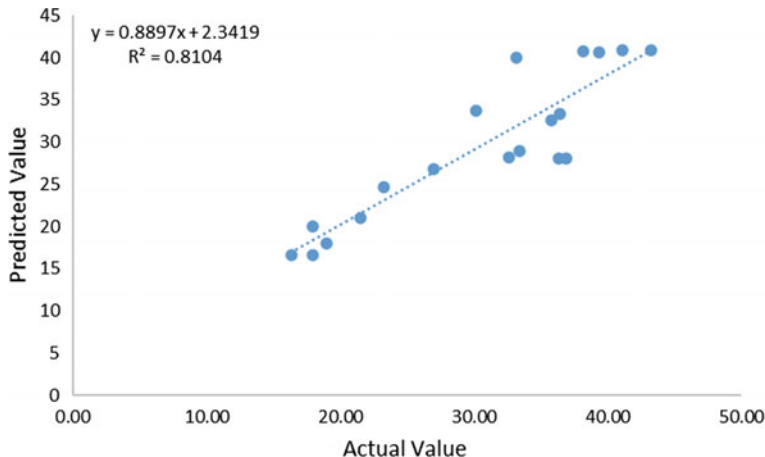


Fig. 11 Accuracy of ANN_{k_s}_3H4 NN model

accuracy of ANN_{k_s}_3H5 neural network has been plotted in a graph as shown in Fig. 12.

From Fig. 11, it has been observed that the ANN_{k_s}_3H5 neural network model has been predicted modulus of subgrade reaction of nineteen data sets of soil with 87.84% accuracy. The accuracy of best architecture neural network models has been compared with the accuracy of MLR_{k_s} model. The graphical presentation of accuracy of MLR_{k_s} model is plotted in a graph as shown in Fig. 13.

After the drawing correlation between predicted and test value of modulus of subgrade reaction, it has been observed that the MLR_{k_s} model has predicted modulus of subgrade reaction of nineteen data set with 86.4% accuracy.

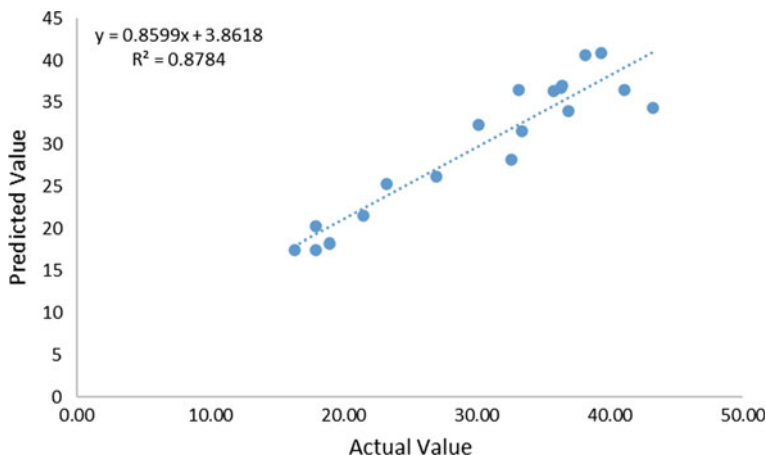


Fig. 12 Accuracy of ANN_{k_s}_3H5 NN model

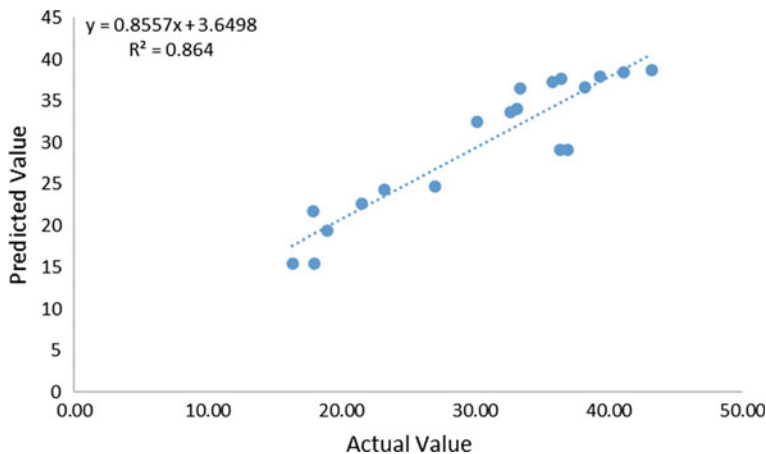


Fig. 13 Accuracy of MLR_{k_s} model

Table 10 Comparison of accuracy of models and P/A relationship

Model architecture	Performance (%)	Accuracy (%)	P/A relation
ANN _{k_s} _5H1	91.20	89.67	1.017
ANN _{k_s} _11H2	96.08	95.51	1.006
ANN _{k_s} _11H3	93.01	91.36	1.018
ANN _{k_s} _3H4	83.55	81.04	1.031
ANN _{k_s} _3H5	85.14	87.84	0.969
MLR _{k_s}	92.53	86.40	1.071

Comparison of accuracy of models and performance accuracy (P/A) relationship

The accuracies of best architecture neural network models and MLR model are shown in Table 10. From Table 10, it has been observed that the maximum accuracy has been achieved by ANN_{k_s}_11H2 neural network model.

The relationship has been determined between performance and accuracy. From the results, it has been observed that the ANN_{k_s}_11H2 neural network model has P/A relationship approximately equal to 1. Hence, the ANN_{k_s}_11H2 neural network model can be used for the prediction of modulus of subgrade reaction.

5.3 Prediction of K Value by Optimal Architecture Model

From the performance and accuracy of the neural network and MLR models, the ANN_{k_s}_11H2 neural network model having eleven nodes has been determined as

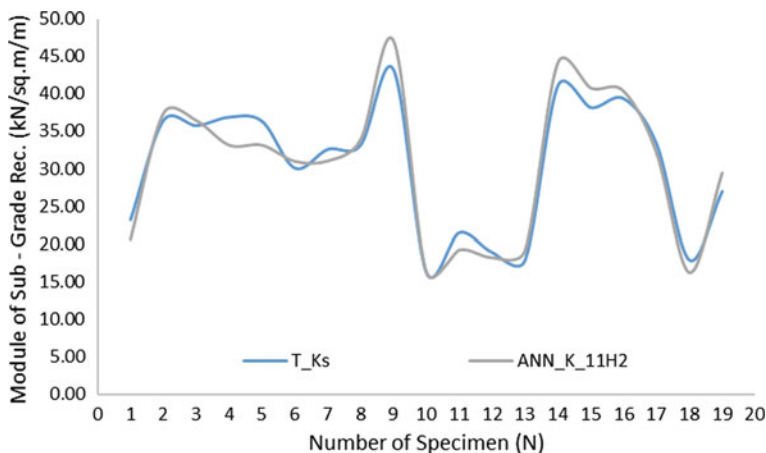


Fig. 14 Test and predicted modulus of subgrade reaction

the optimal architecture neural network model. The modulus of subgrade reaction of nineteen data sets of soil has been predicted by ANN_{k_s}_11H2 neural network model. The field test (T_{k_s}) and predicted value of modulus of subgrade reaction are shown in Fig. 14.

From Fig. 13, it has been observed that ANN_{k_s}_11H2 neural network model has predicted modulus of subgrade reaction approximately equal to field test value of modulus of subgrade reaction.

5.4 Confidence Interval of Predicted K Value by Model

From the result of modulus of subgrade reaction, the ANN_{k_s}_11H2 NN model has been determined as optimal architecture neural network model. The confidence interval of predicted modulus of subgrade reaction has been plotted in a graph as shown in Fig. 15.

From Fig. 14, it has been observed that the ANN_{k_s}_11H2 neural network model has predicted modulus of subgrade reaction with 1.68% confidence interval, and it has also been observed that the upper confidence level (UCL) and lower confidence level (LCL) of predicted modulus of subgrade have been closely plotted. The less distance between the upper confidence level and the lower confidence level shows that the predicted values are very close to the test values.

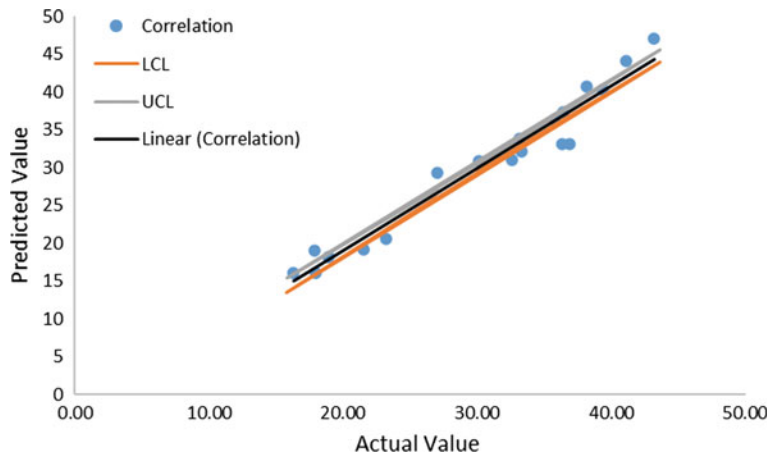


Fig. 15 Confidence interval of predicted modulus of subgrade reaction

5.5 Prediction Interval of Predicted k_s Value by Models

The ANN_ks_11H2 neural network model has predicted modulus of subgrade reaction of nineteen data sets of soil with 95.51% accuracy. The predicted modulus of subgrade reaction has been validated by plotting a graph of prediction interval as shown in Fig. 16.

From Fig. 15, it has been observed that the ANN_ks_11H2 neural network model has predicted modulus of subgrade modulus with 4.39% prediction interval, and it has also been observed that the predicted modulus of subgrade reaction of nineteen data

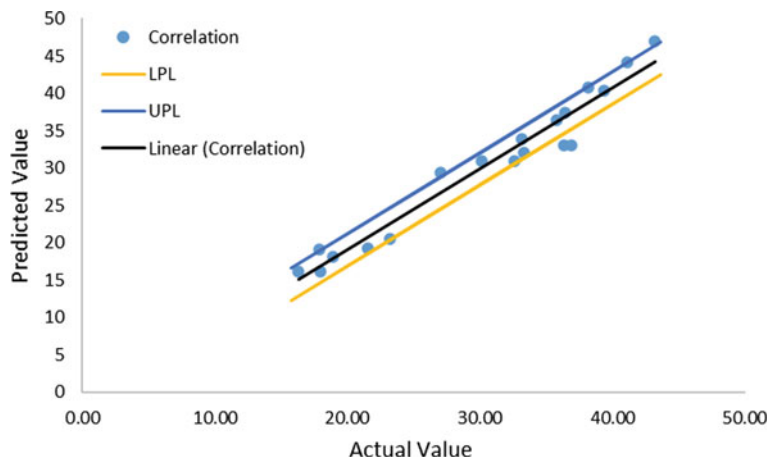


Fig. 16 Prediction interval of predicted modulus of subgrade reaction

sets of soil has found between upper prediction level (UPL) and lower prediction level (LPL). It has also been observed that the upper prediction level and lower prediction level have been closely plotted, which shows the high degree of prediction of modulus of subgrade reaction by ANN_{*k_s*}_11H2 neural network model.

6 Conclusions

In this research work, the performance and accuracy of the best architecture neural network models with different numbers of the hidden layers have been compared with regression model. From the comparison, the optimal neural network has been used for the prediction of modulus of subgrade reaction of nineteen data sets of soil. From the training and validation performance of neural network models, the ANN_{*k_s*}_5H1, ANN_{*k_s*}_11H2, ANN_{*k_s*}_11H3, ANN_{*k_s*}_3H4 and ANN_{*k_s*}_3H5 neural network models have been identified as the better performing architecture neural network models when hidden layers are increased from 1 to 5 with 2 to 11 nodes. The ANN_{*k_s*}_5H1, ANN_{*k_s*}_11H2, ANN_{*k_s*}_11H3, ANN_{*k_s*}_3H4 and ANN_{*k_s*}_3H5 neural network models have 91.20%, 96.08%, 93.01%, 83.55% and 85.14% performance achieved, respectively. The performance of the best architecture neural network models has been compared with the performance of the MLR_{*k_s*} model, and it has been observed that the neural network models have better performance. The ANN_{*k_s*}_11H2 neural network model has been determined as the optimal architecture neural network model.

The ANN_{*k_s*}_11H2 neural network model has 95.51% accuracy achieved, and the relationship of performance and accuracy for ANN_{*k_s*}_11H2 NN model has been determined as 1.006 which is approximately equal to 1. The modulus of subgrade reaction of nineteen data sets of soil has been predicted with 1.69% confidence interval and 4.69% prediction interval by ANN_{*k_s*}_11H2 neural network model. From the above, it may be concluded that the ANN_{*k_s*}_11H2 neural network model can be used for the prediction of modulus of subgrade reaction for the design of different types of foundations and rigid pavements.

References

1. Winkler E (1987) On elasticity and fixity. Praguc, p 182
2. Iancu BT, Ionut OT (2009) Numerical analyses of plate loading test numerical analyses of plat loading test. Buletinul Institutului Politehnic Din IASI Publicat de Universitatea Tehnica, Gheorghe Asachi, Tomul LV (LIX), Fasc. 1, Sectia Construct II. Arhitectura (Iancu – Bogdan Teodoru and Ionut – Ovidiu Toma), pp 57–65
3. Dae SK, Seong YP (2011) Relationship between the subgrade reaction modulus and the strain modulus obtained using a plate loading test. In: 9th WCRR Lille World Congress
4. Biot MA (1937) Bending of infinite beams on an elastic foundation. J Appl Mech Trans Am Soc Mech Eng 59:A1–A7

5. Terzaghi K (1955) Evaluation of coefficients of subgrade reaction. *Geotechnique* 5(4):297–326
6. Vesic AB (1961) Beam of elastic subgrade and Winkler's hypothesis. In: Proceedings of the 5th international conference on soil mechanics and foundation engineering, Paris, pp 845–850
7. Bowles JE (1998) Foundation analysis and design, 6th edn. McGraw-Hill International Press, New York
8. Zurada JM (2012) Introduction of artificial neural network. West Publishing Company, USA
9. Khatti J, Grover KS (2020) Determination of permeability of soils for international soil classification system using artificial neural network technique. In: 1st international conference on recent innovation in science, engineering and technology, 11–12 Sept, Invertis University, Bareilly, Utter Pradesh, India
10. Elsamny MK, Elsadeek MB, Abd Elsamee WN (2010) Effect of depth of foundation on modulus of elasticity 'Es' for cohesionless soil. *Civ Eng Res Mag Al-Azhar Univ* 32(3):938

Enyo: A Multistage Partition and Transposition Based Cipher



Apratim Shukla, Mayank K. Tolani, Dipan Polley,
Abhishek Thazhethe Kalathil, and N. Subhashini

Abstract The increase in demand for information security has made cryptography a basic need for protecting data from unauthorized access. In this paper, a computationally inexpensive Enyo block cipher has been presented. This multi-layered algorithm provides a promising solution to safeguard user's information. The cipher works on the same line as the Feistel-based network with the symmetric structure and operates on 8-bit ASCII characters. Using 6-bit custom encoding, a secret key generates 6-bit encrypted text. This cipher modeled using undemanding operations utilizes partitioned key-based encryption with unique mapping followed by various bitwise swaps, a shifted modulo encryption, and using a transposition matrix. The proposed cipher is highly customizable as per user demands and necessities that make it more dependent on user inputs. Enyo cipher is faster in encryption and decryption than the Playfair cipher and shows comparable performance with XOR encryption. Enyo cipher demonstrates good resistance to a brute-force attack. It is well suited for small-scale applications where the computational power is a bottleneck. A comparison is also made that shows the impact of the proposed cipher to commonly available classical ciphers.

Keywords Cryptography · Encryption · XOR cipher · Transposition cipher · URL safe encryption

1 Introduction

In the virtual world, it is vital to secure the messages transmitted electronically. Data sent through the URL of a Web application could be sensitive, and exposure of this data can be devastating for governments, companies, and individuals [1]. Cryptography secures websites and ensures safe transmission; it deals with the mechanisms for ensuring integrity, techniques for exchanging keys, and protocols for authentication of users [2]. Encryption is the principal application of cryptography; it makes

A. Shukla · M. K. Tolani · D. Polley · A. T. Kalathil · N. Subhashini (✉)
Vellore Institute of Technology, Chennai, Tamil Nadu 600127, India
e-mail: subhashini.n@vit.ac.in

data incomprehensible to ensure its confidentiality. Encryption uses an algorithm called a cipher along with a secret value called the key; if one does not know the classified key, he/she cannot decrypt, nor can learn any bit of information on the encrypted message—and neither can any attacker [3].

Encryption may use some substitution techniques, shifting techniques, or mathematical operations [4]. In this paper, a simple encryption technique using several layers of protection has been proposed. The sender and the receiver agree on a secret (shared) key. This secret key is used to encrypt and decrypt their message [5]. Section 2 describes the cryptographic techniques available in the literature. Section 3 discusses the proposed Enyo block cipher. The implementation of the encryption and decryption technique is discussed in Sect. 4, and Sect. 5 analyzes the performance of the technique with the existing cipher techniques. Section 6 concludes the paper.

2 Literature Survey

There are several ciphering techniques available in the literature. Feistel cipher is a structure used to design block ciphers. The symmetric design of these ciphers makes encryption and decryption very similar operations. The network consists of a function known as the round function [6]. It is then run on half of the data to be encrypted. The output is XORed with the other half of the data. The XOR cipher is one of the simplest encryption algorithms. It utilizes the XOR operation (also known as exclusive disjunction or modulo two addition) to encrypt data [7]. In the XOR operation, the output is 1 when the inputs differ. A secret key generates encrypted data from plaintext by a bitwise XOR operation. Decryption in the XOR cipher involves XOR operation again with the encrypted data using the same key. Since the cipher uses the same key for both encryption and decryption, it is known as symmetric encryption.

Transposition ciphers serve as the building blocks for the construction of modern block ciphers. In a transposition cipher, the plaintext essentially remains the same, and shuffling of character order occurs. The columnar transposition involves writing the plaintext in rows of fixed length and then reading it column by column. Column choosing in a scrambled order based on a secret key is a crucial aspect of these ciphers [8].

Some prominent Feistel ciphers are Blowfish [9], Twofish [10], and DES [11]. The Blowfish cipher is a symmetric block cipher with a block length of 64 bits and variable key length [9]. It applies padding to the message if its length is not divisible by eight. Twofish is another symmetric block cipher with a block size of 128 bits and a key length up to 256 bits. It is fast and flexible and consequently useful for applications with minimal RAM and ROM [10]. The DES algorithm also operates on 64-bit blocks like the Blowfish cipher. However, the DES algorithm uses a fixed key of length 56 bits [11].

3 Proposed Method

There exist many ciphers for encryption where one of the prominent ciphers is a Feistel cipher [7]. The cipher proposed in this paper is a balanced symmetric Feistel cipher consisting of modular arithmetic and transposition stages. Symmetrical cipher uses the same key for both encryptions as well as decryption [12]. The given text input and the key in the ASCII system, which is an 8-bit character set, are encoded to a character set with 6 bits. Thus, the algorithm proposed in this paper works on custom base64 encoded text. The base64 character set design ensures that the encrypted text is always URL safe [13]. Following the encoding stage are the encryption stages. The text and the key are taken as input from the user and converted to custom base64. The first step of the algorithm is a character set modifier. Familiarity with Caesar cipher ensures that this step is a piece of cake. This step calculates the character sum of the key according to the character set and then takes modulus 16. The result then shifts the character set cyclically. It is not a sturdy encryption stage but still offers some security as it is dependent on the key. The simplicity and efficiency this step provides are justifying its addition as one of the encryption stages. In the next stage, character-by-character encryption is done. The value corresponding to each character in the modified character set is taken, and it is divided by 16. Dividing the value by 16 gives a remainder between 0 and 15 and a quotient between 0 and 3. Through this stage, the balance consists of 4 bits and a quotient of 3 bits. These resultant 4 bits obtained by modulus attached with the 2 bits yielded by the division give a unique set of 6 bits, the character corresponding to this 6-bit value is the result. The aforementioned stage does not qualify as encryption but contributes to a secure encoding stage.

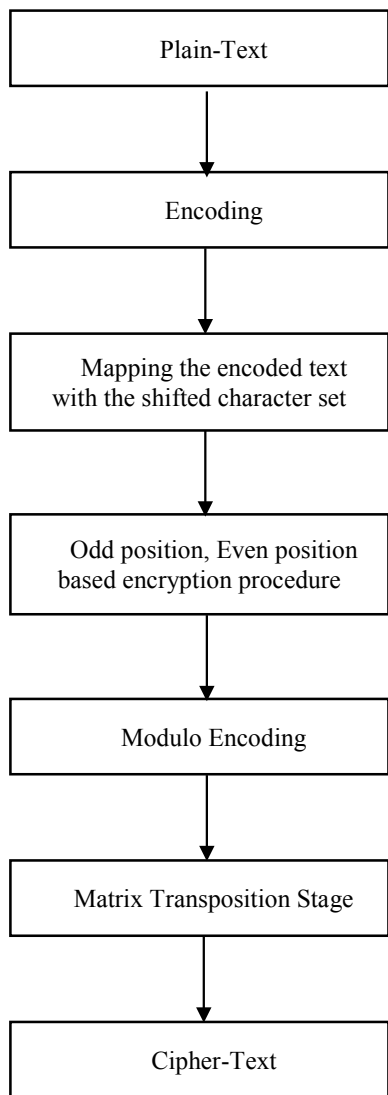
Enyo's similarity with the Feistel ciphers [7] establishes in this step. The XOR of the characters between the text and the key is done. Before performing the XOR operation, the partitioning of the key is vital to help achieve the advantageous avalanche effect. The Avalanche effect is a desirable property of most of the ciphers which says that if the input is changed slightly, the output should change significantly [14]. The characters are then repeatedly XORed with the partitioned key, resulting in the encrypted product. Figure 1 shows the different stages of the Enyo cipher.

The Enyo cipher takes 8-bit ASCII characters as input. Therefore, before the encryption stage, both the secret key and data are encoded. This encoding is crucial because the encryption algorithm deals with 6-bit characters. The encoding utilized in the Enyo cipher is quite similar to base64 [14]. The Enyo encoding scheme consists of two sets, the character set and the numeric set, that is shown in Table 1.

The numeric set consists of integer values mapped to the characters from the table and vice-a-versa in the character set. The reason for choosing this custom encoding scheme is to make the output URL safe [15]. A workflow of the encoding stage is shown in Fig. 2.

After the encoding of the characters of the secret key into corresponding 6-bit characters, the next stage is key partitioning. An important point to consider before partitioning is that the number of partitions should be less than the length of the

Fig. 1 Encoding and encryption stages in the Enyo cipher



secret key. Enyo cipher adopts the two partition approach by default. An appropriate security-performance tradeoff can decide the number of partitions if required.

The partitioning algorithm ensures that the secret key can be divided into the desired number of parts of equal length. It accomplishes this using the following logic.

Table 1 Enyo encoding scheme

A	B	C	D	E	F	G	H	I	J	K	L	M	N	O	P
0	1	2	3	4	5	6	7	8	9	10	11	12	13	14	15
Q	R	S	T	U	V	W	X	Y	Z	a	b	c	d	e	f
16	17	18	19	20	21	22	23	24	25	26	27	28	29	30	31
g	h	i	j	k	l	m	n	o	p	q	r	s	t	u	v
32	33	34	35	36	37	38	39	40	41	42	43	44	45	46	47
w	x	y	z	0	1	2	3	4	5	6	7	8	9	-	-
48	49	50	51	52	53	54	55	56	57	58	59	60	61	62	63

```

i = length_of_key % number_of_partitions
while(length_of_key % number_of_partitions !=0)
    key = key+key[i]
    i = i + 1

```

The next shifting stage uses the concept of Caesar's cipher (also known as the shift cipher) to transform the character set according to the secret key. It shifts the character set values circularly by an amount equal to the sum of the encoded secret key characters modulo sixteen.

The encryption of data using the secret key occurs in the encryption stage. The number of partitions decides the number of iterations for encryption. This stage extends the XOR cipher algorithm by applying it repeatedly. First, the character index is checked. A character in an odd position is XORed with the corresponding character at the same index in the first partition. The result of this is then XORed with the corresponding character at the same index in the second partition. This process is repeated until it has been XORed with all appropriate values in the entire key partition array.

The logic applied to characters at even indices differs slightly. A new swapping stage is the highlight of this part. Once the encoded text character has been XORed with the corresponding value in the first partition, the swapping stage begins. In this stage, the 6 bits are divided into two blocks of 3 bits from MSB to LSB. Further, these two blocks are swapped to obtain a new result. This result is then XORed with the corresponding character at the same index from the second partition. This process is continued for the entire key partition array. Figure 3 shows the encryption stage elaborately.

After this, modulo encoding re-encodes the output from the previous stage using a simple algorithm. This stage adds prospects for improvement and shows the possibility for conversion into a simple encryption stage in the future. The algorithm divides the 6-bit binary value with 16 for each character. The maximum quotient and remainder values are 3 and 15. Since the quotient and remainder accommodate in 6 bits, therefore 16 is used.

The transposition stage is optional in Enyo cipher and disabled by default. The reason for this is its high computational cost. Columnar transposition enhances the

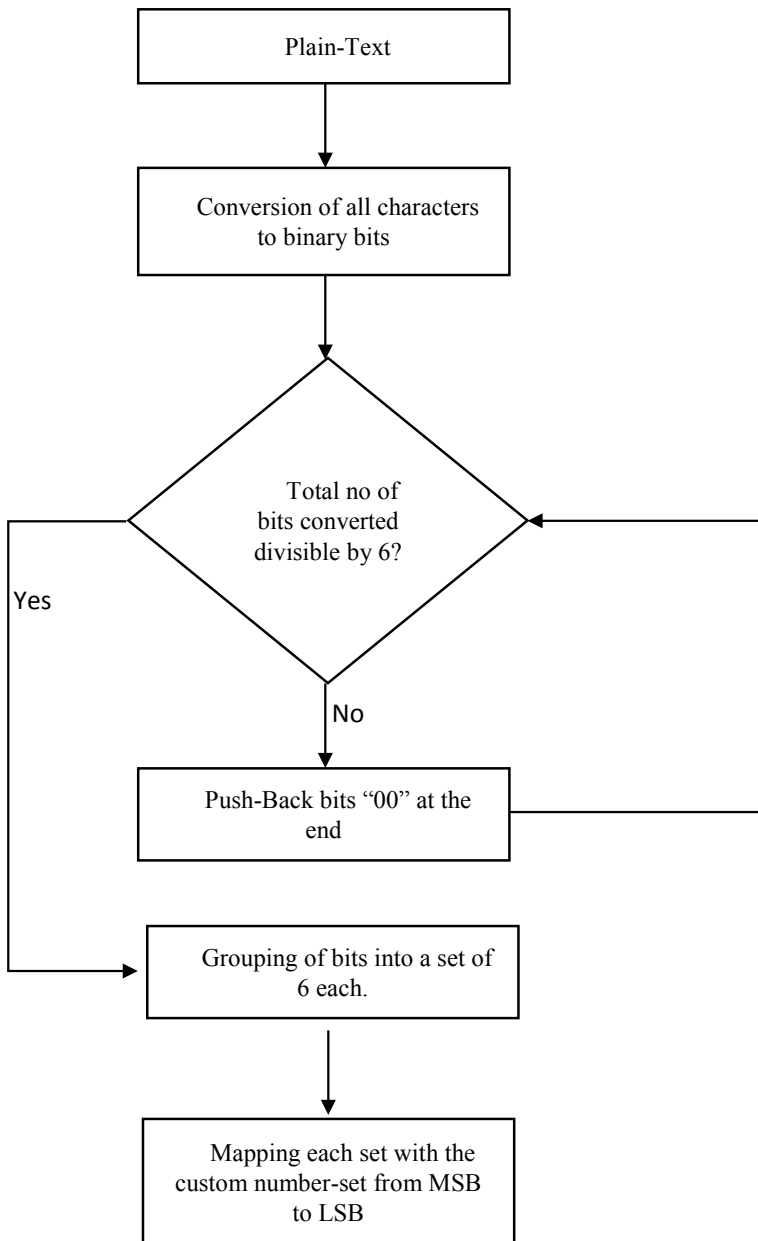


Fig. 2 Workflow of the encoding stage

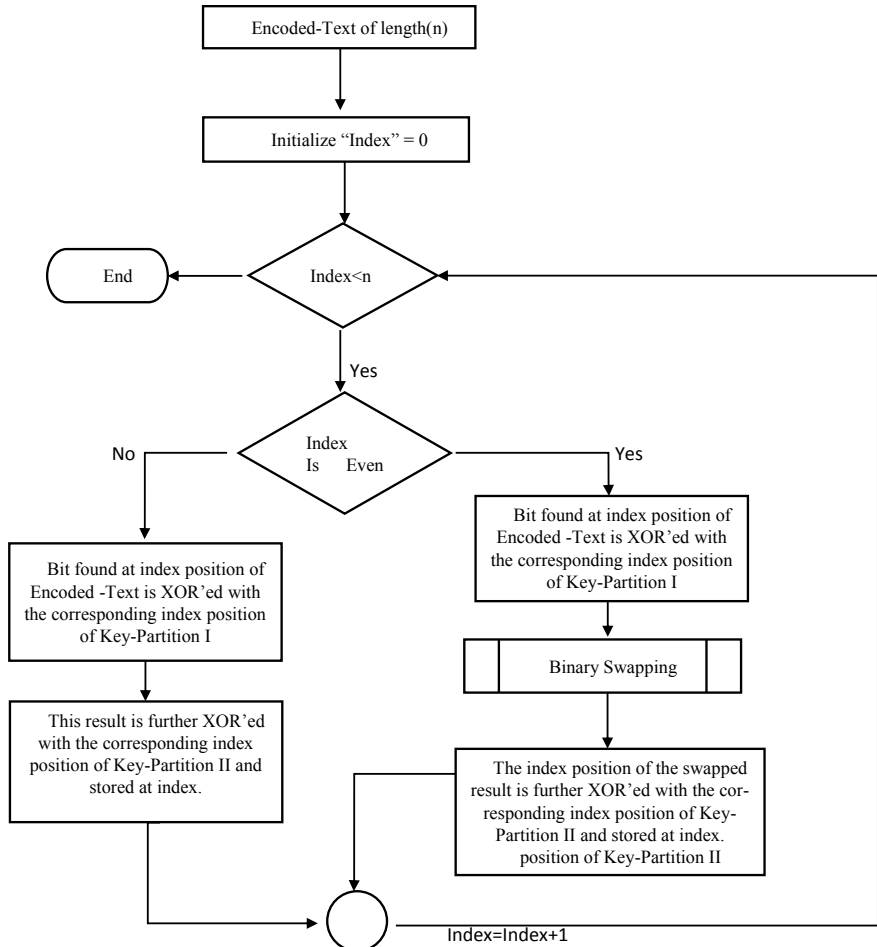


Fig. 3 Workflow of the encryption stage

security of the Enyo cipher, provided the secret key is strong enough. The result from the previous stage is written row-wise, and then, the output is obtained column-wise. Priority-based selection of columns occurs. Because the secret key consists of two or more partitions, therefore, the transposition is also multi-staged. The transposition stage involves the following sequence of steps. Computation of the matrix size for the columnar transposition occurs first. It is the minimum of the length of the secret key partition and the floored square root of the length of modulo encoded output. The output from the previous stage is written row-wise in the matrix of the defined dimension. The columns are chosen according to the priority. The first column which is selected is the one with the lowest value. Then, the column with the second minimum value, then third, and so on is selected. The lower priority is assigned to the column

on the left if two columns have the same numeric value according to the first part of the secret key. The output obtained from the previous step is written in a new matrix. Now repeat this process for the next part of the secret key. This multistage columnar transposition continues until the entire text is covered.

In decryption, the sequence generator outputs the indices of the columns in which encrypted text characters will be placed column-wise. The last key value in the array will be used first, as it was the last one at the time of encryption. The sequence is then generated. This sequence is the index values of the characters according to their mapped values when arranged in ascending order. The matrix is formed column-wise. The row-wise scanned output of this matrix will do the de-shuffling. This process continues up to the first partition of the key. The de-shuffled decrypted value is the result of this stage.

The next stage is modulo decoding. Each character is converted into 6 bits whose first 4 bits represent a remainder and the last 2 bits a quotient. The dividend is calculated by selecting the divisor as 16. This number maps to a character in the new charset, and it is the result. Repeating the process for every character gives the modulo decoded text.

Now trace back the steps in the encryption stage. The first character from the last key is selected. XOR operation is performed with the binary values of this and the first character of the decoded text from the previous stage. If the index of the character is even, perform a binary swap. Ignore binary swapping if the index is odd. The result so obtained is again XORed with the first character of the previous key. This binary result is converted to its decimal value. Mapping it to the character set gives us the decrypted value.

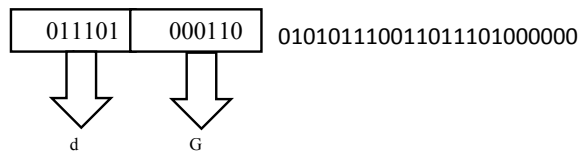
The decrypted text formed needs to be decoded where conversion of the text to decimal value based on its ASCII value is done to obtain a concatenated result of binary numbers. Starting from the MSB, 8 bits are chosen and converted to the corresponding decimal value. The corresponding ASCII character represents the decoded text. This process is repeated until the entire text is decrypted.

4 Implementation

Let us consider the plaintext “test.” The word “test” is 011101000110010101110011011101000000 in binary after the addition of sufficient 00s at the end to make the binary string length divisible by 6. The encoded string results from taking 6 bits at a time and mapping it with the corresponding numeric set value. Figure 4 shows the encoded string of the plaintext “test.” Therefore, the word “test” encoded in this custom encoding is “dGVzdA.”

Consider the text “secret key” as the key. Encoding the key transforms it into “c2VjcmV0a2V5.” In case of the default number of partitions that are two, no change will occur because the length of the encoded key is 12, and 12 is exactly divisible by 2.

Fig. 4 Encoding the binary string of the plaintext “test”



Continuing the former example of two partitions on text “secretkey” gives two parts “c2Vjcm” and “V0a2V5.” Now, these two parts will be utilized for the encryption algorithm.

Considering the same key “secretkey,” the shifted character and number sets are found. After encoding and adding the values mapping from the initial character set, sum 435 is obtained. 435 modulo 16 yields 3. Therefore, character and number sets are shifted circularly by 3. The new character and number sets are shown in Table 2.

Considering the same parameters for encryption, the encoded plaintext is “dGVzdA.” The encoded key is then “c2VjcmV0a2V5.” The partitioned key is “c2Vjcm” and “V0a2V5” assuming that the default number of partitions is 2. The encoded binary text string obtained after the character set transformation is 100000 001001 011000 110110 100000 000011. The encoded binary key strings obtained after character set transformation are 011111 111001 011000 100110 011111 101001 and 011000 110111 011101 111001 011000 111100.

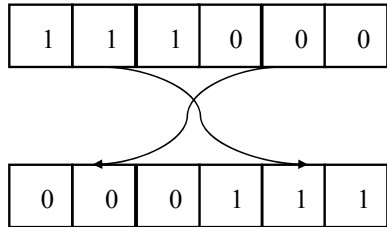
Since the character d lies at even index, hence even logic encrypts it. Let $P(x)$ denotes the output, where x is the stage number. $P(0) = 100000 \text{ XOR } 011111 = 111111$. Next is the binary swapping stage. Let $B(x)$ denotes the output, where x is the input binary string. Figure 5 shows the binary swapping stage on 111000.

In the case of the example, $B(111111) = 111111$. The output from the previous step will be XORED with the next part. $P(1) = 111111 \text{ XOR } 011000 = 100111$. Since 100111 in binary is equal to 39 in decimal. Let $T(x)$ denotes the character corresponding to the integer value x in the transformed character set, then, $T(39) = k$. Repeating the above steps for the remaining characters, the output string after the encryption stages is “kEamkT.” No binary swapping because the character lies at an odd index. The modulo encoding and transposition encryption are applied to the

Table 2 Modified character and number set

A	B	C	D	E	F	G	H	I	J	K	L	M	N	O	P
3	4	5	6	7	8	9	10	11	12	13	14	15	16	17	18
Q	R	S	T	U	V	W	X	Y	Z	a	b	c	d	e	f
19	20	21	22	23	24	25	26	27	28	29	30	31	32	33	34
g	h	i	j	k	l	m	n	o	p	q	r	s	t	u	v
35	36	37	38	39	40	41	42	43	44	45	46	47	48	49	50
w	x	y	z	0	1	2	3	4	5	6	7	8	9	-	-
51	52	53	54	55	56	57	58	59	60	61	62	63	0	1	2

Fig. 5 Binary swapping stage applied on 111000



same parameters. The output after modulo encoding is obtained as “SqpaSN,” and the output after the transposition stage is obtained as “SaSQpN.”

The above result “SaSQpN” is decrypted using the same key “secretkey.” Sequence generator output for “V0a2V5” is [0, 3, 2, 4, 1, 5]. Output after transposition decryption stage is “SqpaSN.” Output after the modulo encoding stage is “kEamkT.” Output after the decryption stage is obtained as “dGVzdA.” Converting each letter to its binary results in 011101000110010101110011011101000000 followed by choosing 8 bits at a time from the beginning for the decoding stage. The output of the decoding stage is “test” which was the original message that was traced back using the same key.

5 Performance Analysis

The Enyo cipher ensures to provide a perfect balance between the complexity of ciphertext and the computational time. The algorithm is implemented and is available at PyPi [16]. Table 3 depicts the comparison between Enyo and other commonly used classical ciphers. The computational time taken depicted in Table 1 is represented in

Table 3 Time taken by cipher algorithms

Cipher name		0.5 MB	1 MB	5 MB	10 MB
Enyo (no transposition stage)	Encryption	2.30	4.62	23.82	47.82
	Decryption	2.34	4.61	23.81	49.33
Enyo (with transposition stage)	Encryption	168.45	380.31	197.03	TLE
	Decryption	170.41	387.89	194.56	TLE
XOR cipher	Encryption	0.11	0.23	1.23	2.53
	Decryption	0.12	0.23	1.23	2.56
Playfair cipher	Encryption	3.17	7.19	165.77	TLE
	Decryption	5.36	10.89	88.74	TLE
Caesar cipher	Encryption	1.93×10^{-5}	1.97×10^{-5}	1.93×10^{-5}	2.24×10^{-5}
	Decryption	3.12	6.19	32.79	66.76

TLE means time limit exceeded

seconds. It is tested using the Enyo library for Python. The Enyo module allows the user to customize based on their need for the security level. The transposition stage with shuffling techniques removes any pattern. As a result, it forms a fewer number of comparable trigraphs and digraphs. But the shuffling algorithm is complex and thus requires more computational time. Figures 6 and 7 show a graphical comparison between Enyo and other commonly used classical ciphers in terms of encryption and decryption time (in seconds), respectively.

The Enyo cipher with no transposition stage adds more security than any other mono-alphabetic substitution ciphers. Comparing it with the Playfair [17] cipher, it takes lesser computational time in encrypting and decrypting. The XOR cipher is also monolayered, for which its computation speed is very high. In contrast to Enyo, it is more vulnerable to frequency analysis and other attacks. Thus, this showcases the advancement of the Enyo cipher over Playfair, XOR, and other mono-alphabetic [18, 19] substitution ciphers.

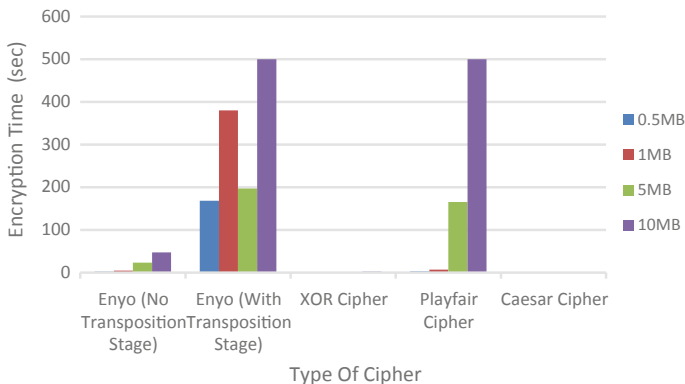


Fig. 6 Encryption time comparison between Enyo and other commonly used classical ciphers

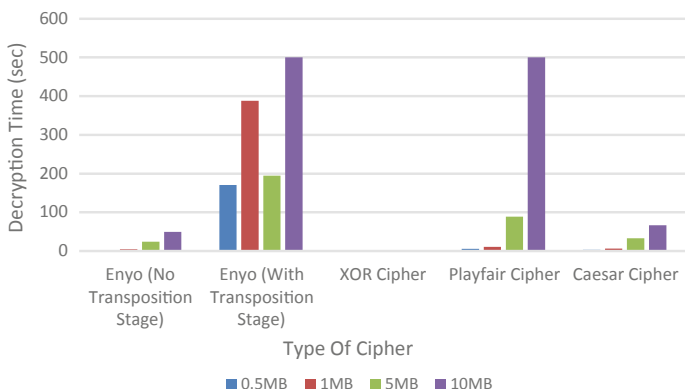


Fig. 7 Decryption time comparison between Enyo and other commonly used classical ciphers

6 Conclusion

Since the algorithm uses the Feistel network, the main advantage is that it assures that the entire operation is invertible. The encryption and decryption follow the same methodologies, so it makes the implementation of the algorithm easier since decryption is just the reversal of encryption. A Feistel network provides structural reusability. The Feistel approach used in the algorithm follows a balanced Feistel structure, wherein the lengths of the partitioned key are equal. The XOR operation used inside the Feistel structure has some advantages and disadvantages too. The most prominent benefit is simplicity. It allows easy encryption and decryption of a string that other logical operations do not. However, one obvious concern regarding the XOR operation is that it is easily reversible. Another setback of using the XOR operation is that for a palindromic key, the encrypted text will consist of repeated substrings.

One disadvantage of Feistel ciphers is that their ability to be parallelized is less as compared to other ciphers. In other ciphers, the entire internal state of the cipher changes with each round, while Feistel ciphers only change part of the internal state each round.

Though the transposition stage used in the algorithm is computationally expensive, the high security that comes along with it overshadows the underlying disadvantages. The transposition stage increases the complexity of the algorithm and makes the cipher more laborious and more error prone. For this reason, the transposition stage is optional and is the sole choice of the user whether he/she wants to add it or not. Another downside is that it only jumbles up the existing characters while generating the encrypted text and creates no new characters. Deciphering small messages can also be done quickly. The jumbling of characters is treated as an advantage because it has a better mixing up of characters than some ciphers like the Rail Fence cipher [20].

The proposed cipher strikes a balance between speed and security. Through the performance analysis, it is found that Enyo is faster and more secure than most primitive ciphers. The cipher's flexibility of increasing complexity as stipulated makes it an ideal choice for small-scale applications like making URLs safe for transit, in chat applications, and even in digital signatures.

References

1. Osman M, Johansson A (2017) A comparison of encryption algorithms for protecting data passed through a URL. Dissertation
2. Katz J, Lindell Y (2015) Introduction to modern cryptography, 2nd edn. CRC Press, Boca Raton
3. Aumasson J-P (2018) Serious cryptography: a practical introduction to modern encryption. No Starch Press, USA
4. Thambiraja E, Ramesh G, Umarani R (2012) A survey on various most common encryption techniques. Int J Adv Res Comput Sci Softw Eng 226–233

5. Al Tamimi A-K (2006) Performance analysis of data encryption algorithms. IJSART 2(12)
6. Knudsen LR (1994) Practically secure Feistel ciphers. In: Anderson R (ed) Fast software encryption. FSE 1993. Lecture notes in computer science, vol 809. Springer, Berlin. https://doi.org/10.1007/3-540-58108-1_26
7. Sravan Kumar D, Suneetha CH, Chandrasekhar A (2011) A block cipher using rotation and logical XOR operations. IJCSI Int J Comput Sci Issues 8(6):1
8. Mishra A (2013) Enhancing security of Caesar cipher using different methods. Int J Res Eng Technol 2(9):327–332
9. NehaKhatri-Valmik M, Kshirsagar VK (2014) Blowfish algorithm. OSR J Comput Eng 16(2)
10. Schneier B, Kelsey J, Whiting D, Wagner D, Hall C, Ferguson N (1999) The Twofish Encryption Algorithm: A 128-Bit Block Cipher. New York City: John Wiley & Sons. ISBN 0-471-35381-7
11. Kaur N, Sodhi S (2016) Data encryption standard algorithm (DES) for secure data transmission. IJCA Proceedings on International Conference on Advances in Emerging Technology ICAET 2016 (2):31–37, September 2016
12. Stalling W (2004) Network security essentials (applications and standards). Pearson Education, Fayetteville
13. Josefsson S (2006) The base16, base32, and base64 data encodings. RFC, 4648, 1–18
14. Ramanujam S, Karuppiah M (2011) Designing an algorithm with high Avalanche effect. Int J Comput Sci Netw Secur 11(1)
15. Berners-Lee T, Fielding R, Masinter L (2005) Uniform resource identifier (URI): generic syntax. <https://tools.ietf.org/html/rfc3986>
16. PyPi Enyo. <https://pypi.org/project/enyo/>. Last accessed 2020/10/24
17. Deepthi R (2017) A survey on playfair cipher and its variants. Int Res J Eng Technol 04(04)
18. Jain S, Chhibber N, Kandi S (2018) Cryptanalysis of mono-alphabetic substitution ciphers using genetic algorithms and simulated annealing. IARS Int Res J 08(01)
19. Hilton R (2012) Automated cryptanalysis of monoalphabetic substitution ciphers using stochastic optimization algorithms. Ph.D. thesis, Department of Computer Science and Engineering, University of Colorado, Denver
20. Siahaan APU (2016) Rail fence cryptography in securing information. Int J Sci Eng Res 7(7)

Exploring Cognitive Process in Extended Data Mining



Zexi Xing and Zhengxin Chen

Abstract With the growing popularity of big data and data mining research, the relationship between human cognition and data mining deserves a lot of attention, and it is an important aspect of technology on a human scale. In this paper, we examine this interesting issue. We first provide a brief review on selected work related to this topic and point out that there are several different aspects involved. The focus of this paper is on the human cognitive activities in the process of identifying and acquiring additional online resources for effective data mining (which is referred to as extended data mining). We present a detailed case study and report what we have learned from this process. Our experimental study shows that cognitive process in data mining is a rich research area to explore, and such kind of study will not only enhance the future practice of data mining, but also serve as an important step toward better understanding of man–machine symbiosis.

Keywords Cognition · Cognitive process · Extended data mining · Critical thinking · Man–machine symbiosis

1 Introduction

With the growing popularity of big data and data mining research, the relationship between human cognition and data mining deserves a lot of attention, and it is an important aspect of technology on a human scale. In general, cognitive science refers to study of mind. According to Oxford Dictionary [1], cognition is the process by which knowledge and understanding are developed in the mind. Britanica.com defines cognition as the states and processes involved in knowing, which in their completeness includes perception and judgment. As to be explained in Sect. 2, there are quite a few cognitive aspects related to data mining. The focus of this paper is on

Z. Xing (✉) · Z. Chen
College of IS&T, University of Nebraska, Omaha, NE 68182, USA
e-mail: zxing@unomaha.edu

Z. Chen
e-mail: zchen@unomaha.edu

the human cognitive activities in the process of identifying and acquiring additional online resources for effective data mining (which is referred to as extended data mining), rather than the data mining process itself.

The organization of the rest of this paper is as follows. In Sect. 2, we review various cognitive aspects related to data mining and explain the scope of this paper. In Sect. 3, we discuss cognitive processes in data mining. Based on this discussion, in Sect. 4, we present a detailed case study on student debts, describing the cognitive activities involved, and examine what we have learned. We conclude our work in Sect. 5.

2 Cognitive Aspects Related to Data Mining

Various cognitive aspects have been discussed in data mining literature. Here we present a brief survey of selected work.

1. **Data mining for cognitive science.** Because data mining has been successful in many applications, computer science educators have made a good effort to apply data mining techniques to improve education at all levels. An example is on improving learning efficiency with the cognitive tutor through educational data mining [2]. A new journal is devoted to educational data mining (JEDM). As noted at the journal's Web site [3], educational data mining is an emerging discipline, concerned with developing methods for exploring the unique types of data that come from educational settings, and using those methods to better understand students, and the settings in which they learn. In particular, one of the topics to be investigated is improving understanding of learners' domain representations and improving assessment of learners' engagement in the learning tasks. Daniel [4] studied the challenges of engaging with big data research in education and identified a wide range of critical issues that researchers need to consider, including diversity in the conception and meaning of big, as well as the use of innovative technologies for capturing, storing, distributing, managing and analyzing large and heterogeneous data sets. However, we should also note that although applying data mining techniques to cognitive science is important, the relationship between data mining and cognitive science goes far beyond education, as to be explained below.
2. **Theoretical and experimental exploration on the fundamental relationship between cognitive mining and data mining.** Khabaza [5] hypothesized that data mining is a kind of intelligence amplifier and suggested that machine learning algorithms inspired by ideas from cognitive science have contributed significantly to the field of data mining. In fact, there are many unknown things in this relationship which are yet to be studied. For example, it has been noted that humans have knowledge they cannot verbalize and such knowledge has to be acquired through non-conscious information acquisition and processing. As Thomas Hill put it, "humans can acquire complex advanced expertise that they

- cannot verbalize” [6]. An important remark is that “exposure to complex and rich stimuli, consisting of large numbers of sensory inputs and high-order interactions between the presence or absence of specific features, will stimulate the acquisition of complex procedural knowledge without the learners’ conscious awareness. Hence the acquisition of such knowledge is best characterized as non-conscious information acquisition and processing.” In addition, Lumosity (an online program consisting of games claiming to improve memory, attention, flexibility, speed of processing and problem solving) has launched a research project on data mining for human cognition in 2013 which is intended to advance the study of human cognition with a new project that will leverage big data collected from its popular Web site. The human cognition project should mine data collected from 40 million Lumosity users over the past six years, with the goal of conducting scientific studies on brain development and learning theory that would be difficult to undertake in the laboratory [7].
3. **Cognitive computing.** Related to the aspect discussed above but taking an engineering approach, the concept of cognitive computing has been proposed. It is noted that in order to face challenges of big data, there is a need for incorporating “cognitive machines mimicking human intelligence” [8]. The rationale of having cognitive computing is due to the fact that the analysis of data by humans can be a time-consuming activity and thus use of sophisticated cognitive systems can be utilized to crunch this enormous amount of data [9, 10]. Cognitive computing is an AI-based system that enables it to interact with humans like a fellow human, interpret the contextual meaning, analyze the past record of the user and draw deductions based on that interactive session. Cognitive computing helps humans in decision making, whereas AI-based systems work on the concept that machines are capable of making better decisions on the human’s behalf. Cognitive computing is a subset of AI and anything that is cognitive is also AI [9]. The goal of cognitive computing is to build a rationale, combined and collective mechanism motivated by the capability of the human mind [11]. We may view cognitive computing as incorporating an intelligent machine partner to the traditional notion of man-machine symbiosis, a concept originally rooted in cybernetics [12], at the new era of big data. Apparently, this is an idea endorsed by DARPA, as shown in the title of a recent report: “The merging of humans and machines is happening now” [13].
4. **Cognitive process in data mining.** Complementary to cognitive computing which is aimed to mimic human intelligence in the man-machine symbiosis, there is another side of this symbiosis; that is, exploring human cognitive activities involved in actual data mining practice. This is not a commonly explored issue and is the main topic of this current paper. Below we will take a look at this issue.

3 Cognitive Process in Extended Data Mining

In order to examine the overall cognitive process in data mining, in this section we will start with a brief note on the interaction of users and data mining. As we can see from this discussion, the topic of cognitive process in data mining goes far beyond human–computer interface. We will then introduce two important concepts, namely behavior mining and extended data mining, to conduct research on the various aspects of cognitive process in extended data mining. Finally, we also point out the importance of critical thinking in the process of our examination.

3.1 *Interaction of Users and Data Mining*

When talking about interaction of users and the data mining process, the first thing to consider is, of course, user interface. According to Han et al. [14], user interface is an important component in the architecture of data mining systems. The user plays an important role in the data mining process. Interesting areas of research include how to interact with a data mining system, how to incorporate a user’s background knowledge in mining and how to visualize and comprehend data mining results. Note the second edition of Han [14] contains specific data mining methods involving users, such as user-constrained cluster analysis and multi-relational clustering with user guidance (including user guidance in the form of a simple query). However, interaction of users and data mining is not restricted to user interface in the conventional sense. Below we focus on human cognitive activities in the process of identifying and acquiring additional online resources for effective data mining. Since this discussion is rooted in the concept of behavior mining, below we review this concept first.

3.2 *Behavior Mining and Extended Data Mining*

The term *behavior mining* was proposed more than a decade ago to emphasize the need for studying the underlying process which produced the final observable surface data, rather than just mining the surface data alone [15]. Note the term behavior has a broad sense of meaning and is not restricted to user or customer behavior. The motivation was based on the fact that one common misunderstanding of data mining is as follows: Give me the data set, and data mining tools will show me the hidden knowledge. However, this thinking is quite naive and is not realistic in many real-world applications. So far, the experimental work to best demonstrate the main idea of behavior mining is from a project named SONCA [13], even though it is not under the umbrella of behavior mining.

In order to fully understand the original data, there may be a need to acquire more related data, and this can be done through Web crawling. To emphasize the technical aspects when implementing behavior mining, the concept of *extended data mining* has been proposed, which has the ultimate goal of (semi)automatically collecting additional data when needed for effective data mining [16].

3.3 *Cognitive Aspects in Extended Data Mining*

We can now take a look at cognitive aspects in extended data mining. But first of all, what does cognitive process in extended data mining mean? Since extended data mining is concerned with questions such as what (what to mine), where (where to find the needed data) and how (how to acquire the additional data), cognitive aspects could involve dynamically adjusted goal, dynamically adjusted depth or breadth, along with a number of other important aspects. As an example, we can consider an existing work on critical thinking for behavior mining. It has been noted [17] that critical thinking offers useful hindsight and effective principles to face the challenges of volume, velocity, variety and veracity of big data, and critical thinking is an important cognitive process in extended data mining.

4 A Case Study

Below we present a case study which exemplifies a semiautomatic data mining process in which human cognitive activities play a very important role.

4.1 *Student Debt: The Case Study*

With the general objective of exploring the human cognitive process in mind, we have to select a specific topic and identify appropriate tools. After numerous efforts, we have decided to select Web site Statista (<https://www.statista.com/>) as our experiment object to analyze because it has fewer dead links and almost all of the extracted URLs from Statista contain tables. Additionally, since it asks university credentials to access its data set, the information inside of the Statista is somewhat authenticated and trustworthy. Through numerous trials, we have also decided to pick WebCopy (<https://www.cyotek.com/cyotek-webcopy>) as the primary tool to process Statista Web sites tables.

Since student debts have become an urgent topic demanding public attention, we decide to select “student debt” as the initial keyword to perform Web crawling on Statista. Our objective is to discover important hidden knowledge related to student debt from data sets publicly available on line. In order to achieve this goal, we

use Data Miner (a live data collector, which is a Google Chrome-based application also known as DataScraper, <https://chrome.google.com/webstore/detail/data-scraper-easy-web-scr/nndknusepjnlbdbepjfgmncbgmopgden?hl=en-US>) as the tool to start crawling on the starting (root) page (referred to as level 1) and use WebCopy to accomplish the crawling for the levels beyond. Starting at level 1, the usefulness of the new URLs acquired from the tools is determined by human users; the URLs deemed to be relevant to our goal are used for the next level of crawling, and tables extracted from these URLs are combined with previously acquired information so that integrated tables can be constructed. This kind of process can continue until user satisfaction is reached or a significant number of URLs become seemingly irrelevant to the initial interest (we will get back to this issue later; see Sect. 4.3). The total number of levels of crawling for this case study is 3. Because the result that we could retrieve from Data Miner and Webcopy is a set of URLs that contain tables, so as long as the new URL or this URL's description has the keyword, we will retrieve it and analyze manually. Here, the reason for manually analyzing tables is because most of the tables we have found are too small and most columns and rows are irrelevance even though they all describe "student debt."

In order to effectively conduct data mining, it is very important to determine data mining functionalities (or tasks), which are used to specify the kinds of patterns to be found in data mining tasks. These include characterization and discrimination, the mining of frequent patterns, associations, correlations, classification and regression, clustering analysis, outlier analysis, etc. Usually, one or two specific functionalities are determined at the very beginning when data mining gets started. However, in this study, since at the starting point we had very little knowledge about student loans, we are interested in all possible aspects related to student debt. Since we are exploring an uncharted territory, we decide to leave the functionalities open. This allows us to freely explore any new issues on the fly—guided by human users. For example, the functionality may be characterization and discrimination: What characterizes the students which have loans, and what are the different features for students to have high amount loans versus others? The functionality could also be related to association: Are there other common activities associated with student loans? Are there any general patterns or trends for those students with loans as time goes by? An advantage of this choice is that we can maximize human guidance in the overall process.

After using Data Miner to collect first level URLs, more than 200 URLs were returned for the keyword "student debt." We have identified about 150 URLs which are valid for our searching keywords "student debt." However, not every URL contains new tables or data that can be used for generated new tables, because some URLs contain some duplicated information or attributes. Hence, inside of these valid URLs, we want to pick non-duplicated (contains new data instead of similar data we have already taken) URLs and "tabled" URL (contain table format information, not just image, graph or some other data) to see if those tables can be used for deriving new data set, so manually picking and sorting are necessary. Eventually we have identified 47 useful URLs that might help us to generate new data sets, so we use XMind (<https://www.xmind.net/>) to show the relationship between different URLs

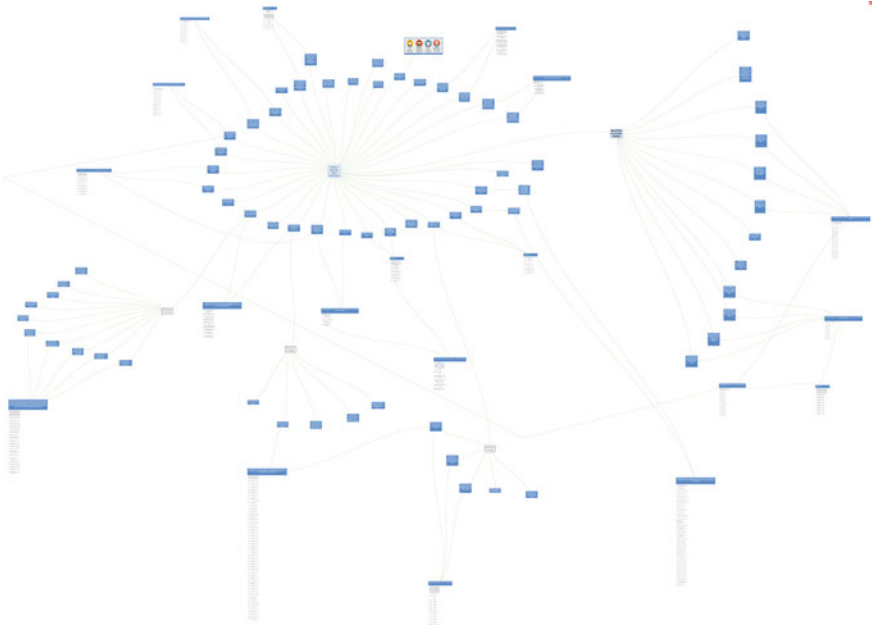


Fig. 1 Overview of the relationship between crawled web sites topics on the second and third level and manually generated tables

in the second level of crawling and generated 17 new tables. XMind is claimed as a full-featured mind mapping and brainstorming tool, designed to generate ideas and inspire creativity, and thus becomes our companion in conducting extended data mining. Then we picked seven URLs from the second level of depth, to further conduct web crawling using WebCopy to get new results on the third level of depth. Figure 1 is the resulting overview of three-level crawling screenshots from Xmind. Note that the image shown in Fig. 1 might be hard to recognize because it contains numerous links and nodes, so readers are encouraged to expand the editor view of the soft copy or use XMind to open the original files.

In Fig. 1, the node in the very middle is where we have started on “student debt” exploration (i.e., level 1 in depth). Those nodes directly connected to the middle node are the second-level depth which contains 37 related URLs, as shown in Fig. 2.

In Fig. 2, there are 37 direct links from “student debt keyword searching.” Here we pick a specific branch to demonstrate the involved human cognitive process. Based on the second-level crawling result from Data Miner, we have generated a bunch of ramifications from “student debt.” Some of these tables are closely related, even though they come with different URLs. For example, there are two tables with topics “The 20 richest colleges in the United States in FY 2018, by endowment funds market value” and “Most affordable colleges in the United States in 2012, showing attendance cost,” respectively. According to the titles, we could not find anything in common except for the relationship with “student debt.” However, we can easily

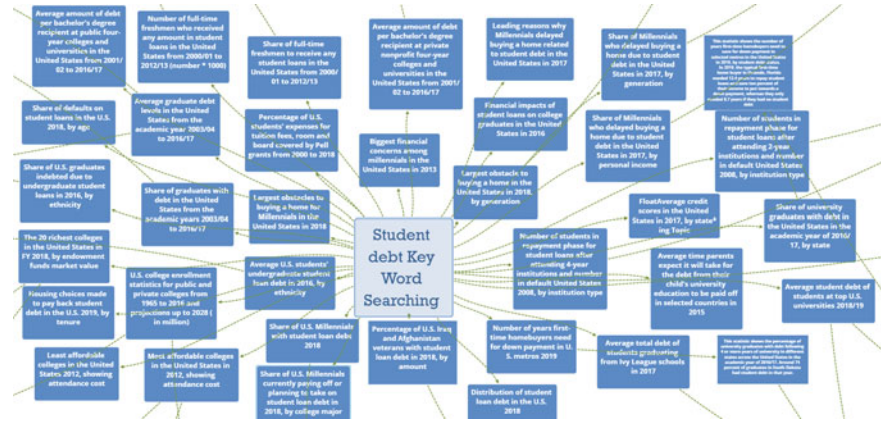


Fig. 2 Thirty-seven URL titles from second-level crawling (Every single topic contains a different table)

extract information from both tables and combine them into one integrated table. Table 1 shows the result of our human cognitive process.

Continuing our work at the third-level crawling using Webcopy, we have noted that a table named as “The 20 richest colleges in the United States in FY 2018, by endowment funds market value” becomes the best choice, because it contains contemporary data that researchers would like to know. Crawling data on the third level returns 10 more tables that are connected to “student debt.” Figure 3 is the screenshot of topics indicating which aspects of information we have extracted from third crawling.

Note that on the right-hand side of Fig. 3 (Table 2 which has not been included in Fig. 3) is a big table which is an elaboration of the procedure related to the manual construction of the table by using cognitive learning process. The topic of those five third depth URLs that Fig. 2 has shown is listed below:

1. Forbes ranking of the best colleges in the USA in 2019, by tuition cost and average debt
2. Universities in the USA ranked by number of Forbes 500 member alumni in 2019
3. 2019 Academic Ranking of World Universities (ARWU) by Shanghai Ranking Consultancy
4. US universities that produced the most ultra-high net worth individuals in 2019
5. Average early career salary of Ivy League attendees in 2019 (in US dollars).

Since those five nodes that link to the right tables contain valid data that are all in the same time period, they are combined manually, ready for further analysis. Table 2 explains seven categorized columns’ information regarding university rank, university members in Forbes, college’s awards, students’ salary and college investment. Additionally, there still are some universities that have not been listed in Table 2 because several information pieces of those universities are missing. For example,

Table 1 Combined tables of “The 20 richest colleges in the United States in FY 2018, by endowment funds market value” and “Most affordable colleges in the United States in 2012, showing attendance cost”

University	Endowment fund value in billion US dollars	University rank in USA with state	Amount in US dollars for attendance on average
Harvard University, MA	38.3	(5) Harvard University, Massachusetts	\$56,000
Yale University, CT	29.35	(14) Yale University, Connecticut	\$58,250
Stanford University, CA	26.46	(9) Stanford University, California	\$57,755
Princeton University, NJ	25.92	(2) Princeton University, New Jersey	\$53,934
Massachusetts Institute of Technology, MA	16.53	(1) Massachusetts Institute of Technology, Massachusetts	\$55,270
The Texas A&M University System, TX	13.52	(22) Texas A&M University, Texas	\$20,723
Northwestern University, IL	11.09	(6) Northeastern Illinois University, Illinois	\$17,802
University of California, CA	11.01	(21) University of California Berkeley, California	\$32,632

Massachusetts Institute of Technology does not have both “Number of Forbes 500 member alumni information” and “Average Early career salary in US dollars.” As a result, we have not included those incomplete universities’ information in the table below.

4.2 Examination of Cognitive Process in the Case Study

An examination of the cognitive process in this case study can offer the following observations:

1. As indicated earlier, at the beginning, we purposely leave the data mining functionalities open so we can explore the role of human cognitive activities in guiding the data mining process. Therefore, it is important for the human users in identifying data mining functionalities while acquiring new data sets (even the detailed steps of performing actual data mining are not in the scope of this paper). In our case study, we can identify data mining functionalities such as

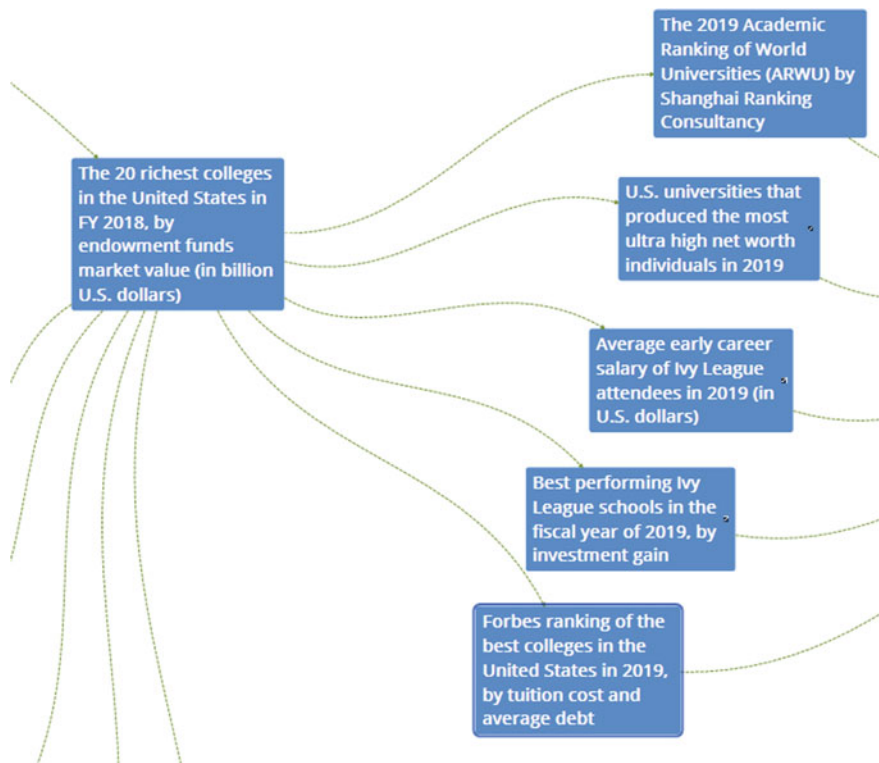


Fig. 3 Third-level URL titles crawled from one second depth URL, the second depth URL's topic is “The 20 richest colleges in the United States in FY 2018, by endowment funds market value”

association between student loans and ranks of universities, characterization of students with large amount of loans, discrimination of students with loans among different states, analysis of trends for students paying off loans, etc. Cognitive activities include conceptualizing potential new specific topics or subtopics to be further mined, matching newly acquired data versus existing data, discard (or table) uninteresting data, etc.

2. Data sets used in the research as reported in this paper are not large data sets, mainly due to the fact that we only want to study publicly available data sets, while many large data sets are proprietary data or of limited research interest. Even the data sets are not big, they are sufficient to demonstrate the main idea of extended data mining and thus complement experiments involving larger data sets such as in the SONCA project.
3. It is interesting for Gupta to note that the characteristics of cognitive computing can be mapped to the five Vs of big data, where cognitive computing is mapped onto big data, observation is mapped to volume, interpretation is mapped onto variety, evaluation is mapped to velocity, and decision is mapped to veracity. Even the observations (in our case, data sets) involved in our case study are not

Table 2 Combined result from five existing tables retrieved from third-level webpages

University	Tuition cost in US dollars	Average debt	Number of Forbes 500 member alumni	Ranking scores of World Universities (ARWU) by Shanghai Ranking Consultancy	Average early career salary in US dollars	Number of degrees awarded to today's billionaires
Harvard University (Massachusetts)	69,600	7372	3	100	74,800	1830
Yale University (Connecticut)	71,290	4962	2	50.8	70,300	358
Princeton University (New Jersey)	66,150	4451	2	60	75,200	309
University of Pennsylvania (Pennsylvania)	71,715	7733	2	47.3	72,800	744
Cornell University (New York)	70,321	8107	3	49.8	70,100	299
Columbia University (New York)	74,199	10,740	1	59.1	71,400	516

big, and the rest of mapping described above still makes sense. For example, interpretation of the newly acquired data sets is very diverse, evaluation changes since the meaning of data is changing, and the decision of which direction to expand could be controversial.

4.3 What We Have Learned in the Case Study

Below are some interesting things we have learned, which illustrates the importance of critical thinking in extended data mining. Although they are case study specific, we believe they may have general indications.

1. Depth versus breadth: Initially, we have expected that when we increase the depth, we should always get some new data. But in reality, it is not true, because it is not uncommon that the seemingly newly acquired data is actually among the data we have already acquired in previous depths. Cognitively, this suggests us thinking about the relationship between depth and breadth in extended data mining. A better Web crawler may reduce this kind of problem, but again this

problem illustrates the importance of human guidance in conducting extended data mining.

2. Dealing with newly acquired data which is beyond originally defined scope: A simple solution could be discarding such kind of data, and a better Web crawler could reduce this kind of data. However, chances are a new research horizon may emerge, and this scenario could be another example involved in human cognitive activity: Instead of throwing it away as a piece of garbage, we may view it as a new, valuable token leading us to new research territory. For example, in our case study, take a look at an example from the crawling result which is “Percentage of US Iraq and Afghanistan veterans with student loan debt in 2018, by amount.” When we are doing third-level crawling, we exploit eight more links that contain information which might not be related to the research topic “student debt,” but it can be thought as useful for other aspects of researching areas. See Fig. 4 for details.

Above image shows numerous aspects of the US Iraq and Afghanistan veterans’ conditions. Although there are a couple of tables connecting debts of students and their families, most of the tables are seemingly not directly related to student loans. However, these resources may provide some unexpected, yet important data which

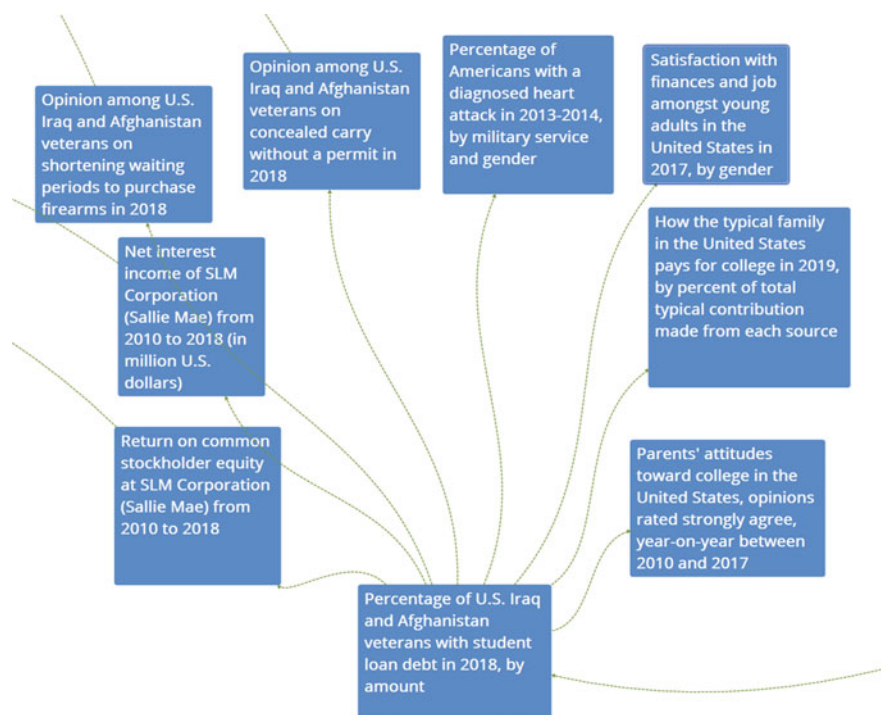


Fig. 4 Eight third-level URL topics crawled from a second-level URL in which the topic is “Percentage of US Iraq and Afghanistan veterans with student loan debt in 2018, by amount.”

might be ignored and valuable for future exploring, such as veterans' (who have student loans) abnormal behaviors.

5 Conclusion

In this paper, we started with a brief review on selected work related to human cognition and data mining. This review is not intended to be complete, but it is sufficient to show that this is a rich research area and there are different aspects related to cognition and data mining. We then presented our work on the human cognitive activities in the process of identifying and acquiring additional online resources for effective data mining. Of course, a lot of work in this direction of study is yet to be done. Similar to Daniel [4], the goal of this paper is to raise awareness on these issues and initiate a dialog.

We conclude this paper with the following two critical remarks:

1. There are multiple aspects of cognitive aspects related to data mining as discussed in Sect. 2. Among these aspects, human cognition in the process of data mining is a somewhat overlooked issue, but it has rich contents, so should be studied carefully.
2. In addition, as shown in extended data mining, cognitive aspects in the data mining process are not restricted to data mining functionalities, but it is also related to identifying additional resources beyond given data.

We have summarized interesting things we have learned, which illustrates the importance of critical thinking in extended data mining. Although out of the scope of this paper, critical thinking (and cognitive process in general) plays an important role in data mining functionalities (or tasks) as well.

Our experimental study shows that cognitive process in data mining is a rich research area to explore, and such kind of study will not only enhance the future practice of data mining, but also serve as an important step toward better understanding of man-machine symbiosis. Finally, we would like to note that our work is also related to recent progress in brain informatics (BI) and brain-computer interface (BCI), but due to space limitation, no details will be presented here.

References

1. Oxford Learner Dictionaries. <https://www.oxfordlearnersdictionaries.com/us/definition/english/cognition>. Last accessed 2020/10/20
2. Cen H, Koedinger K, Junker B (2007) Is over practice necessary? Improving learning efficiency with the cognitive tutor through educational data mining. https://www.researchgate.net/publication/221297263_Is_Over_Practice_Necessary_-_Improving_Learning_Efficiency_with_the_Cognitive_Tutor_through_Educational_Data_Mining

3. Educational Data Mining Organization. <https://educationaldatamining.org/>. Last accessed 2020/10/20
4. Daniel BK (2019) Big data and data science: a critical review of issues for educational research. *Br J Educ Technol.* <https://doi.org/10.1111/bjet.12595>, Vol50No1
5. Khabaza T (2011) From cognitive science to data mining: the first intelligence amplifier. In: From animals to robots and back
6. Piatetsky G (2013) Exclusive: cognitive mining, data mining, and statsoft—interview with Dr. Thomas Hill. <https://www.kdnuggets.com/2013/10/cognitive-mining-data-mining-interview-statsoft-thomas-hill.html>
7. Woodie A (2013) Data mining for human cognition. Datanami. https://www.datanami.com/2013/07/09/data_mining_for_human_cognition/
8. Chen M (2017) Welcome to the new interdisciplinary journal combining big data and cognitive computing. *Big Data Cogn Comput* 1(1):1. <https://doi.org/10.3390/bdcc1010001>
9. Gupta S, Kar AK, Baabdullah A, Al-Khowaiter WAA (2018) Big data with cognitive computing: a review for the future. *Int J Info Manag* 42:78–89
10. Kim HW, Chan HC, Gupta S (2016) Examining information systems infusion from a user commitment perspective. *Inf Technol People* 29(1):173–199
11. Kwon O, Lee N, Shin B (2014) Data quality management, data usage experience and acquisition intention of big data analytics. *Int J Inf Manage* 34(3):387–394
12. Wiener N (1965) Cybernetics, or control and communication in the animal and the machine. MIT Press, USA
13. Szczuka M, Slezak D (2013) How deep data becomes big data. In: IFSA/NAFIPS 2013, pp 579–584
14. Han J, Kamper M, Pei J (2012) Data mining: concepts and techniques, 3rd edn. Morgan Kaufmann, USA (Han J, Kamper M, 2nd edn., 2006)
15. Chen Z (2017) Understand what happened under the surface: tracing dynamic deep data. In: Proceedings of INCISCOS
16. Kaspa LP, Akella VNSS, Chen Z, and Shi Y (2018) Towards extended data mining: an examination of technical aspects. In: Proc of International Conf on Computer Science, vol 139, pp 49–55
17. Chen Z (2014) Behavior mining for big data: promoting critical thinking in data science education. In: Proceedings of FEC, pp 337–341

Sentiment Analysis from Bangla Text Review Using Feedback Recurrent Neural Network Model



Pratim Saha and Naznin Sultana

Abstract Sentiment analysis is one of the most discussed topics in natural language processing. A number of researches have already been made on sentiment analysis, and most of the works are on English language text. There are only a few works that have been found on sentiment analysis from Bangla text. Bangla is the seventh most communicated language in the world, so sentiment analysis on Bangla text plays an important role in detecting the opinion and sentiment of Bengali-spoken people about some products, services, or business. There are lots of microblogging sites and social networks where Bengali-spoken people write comments in Bangla texts. In our paper, we have proposed a special version of recurrent neural network (RNN) model, called long short-term memory (LSTM) to detect the sentiment from the text review dataset. In this regard, we have collected a total of 4000 comments from different online repositories. Our proposed model can successfully classify positive and negative sentiments from Bangla text with an accuracy of 84% and precision of 85%.

Keywords Sentiment analysis · Bangla text · Recurrent neural network · Long short-term memory

1 Introduction

Bangla being an Indo-Arabian language which is most widely spoken language in Bangladesh. This language is the second most widely communicated language in India. At present, approximately 228 million native speakers and about 37 million

¹https://en.wikipedia.org/wiki/Bengali_language.

P. Saha · N. Sultana (✉)
Daffodil International University, Dhaka, Bangladesh
e-mail: naznin.cse@diu.edu.bd

P. Saha
e-mail: shahapratim@gmail.com

people speak in Bangla as their second language.¹ With the advancement of technology, people can comment on different online platforms in Bangla language, like people express their emotions about a new movie, about a new product launched into the market, about any government's decisions or else. The comments can be used to analyze people's reaction about different topics to take decision about any matter. But, analyzing a vast amount of comments for human is a tedious work, so an automated approach can possibly solve the problem to a great extent.

A number of approaches have already been done for sentiment analysis. Most of the work is done on English text [1, 2]. Various machine learning algorithms [2, 3] have been used for sentiment analysis. In this paper, we have used a deep learning RNN model called long short-term memory to train our model to automatically detect whether a text reflects a positive sentiment or negative sentiment. The reminder of the paper is arranged as follows:

Section 2 contains the discussion on related works, Sect. 3 contains our proposed methodology, Sect. 4 discusses the experimental results, and finally, we conclude with future works in Sect. 5.

2 Related Works

A number of researchers have worked on sentiment analysis. In this section, we will be highlighting the contributions of some researchers' in this field found in the literature. It has been found that most of the research works on sentiment analysis done so far were based on English language, and a very few works have been found that worked on extracting sentiment from Bangla text found on different microblog posts, social networks, or e-commerce sites. In this section, we briefly overview the research works carried out on both English and Bangla languages found in the literature. Authors in [4] used SVM, maximum entropy, and naïve Bayes algorithms to train their model. Applying emoticons to train the corpus, they obtained 80% accuracy from their experiment. The authors in [5] used twitter data for sentiment classification and used hashtags and emoticons to determine sentiment label. Using K-nearest neighbors (KNN) algorithm and multi-class classification, the average precision obtained was 0.75. The authors in [6] manually developed a sentiment lexicon consisting of two sentiment bearing words (i.e., positive and negative sentiments) and used a set of rules to identify sentiment from unknown samples. Naive Bayes and SVM models were employed by Banik and Hasan Hafizur Rahman [7] to classify movie reviews in Bangla, and it achieved an overall precision and recall of 0.86 from their model using SVM. N-gram-based sentiment analysis from Bangla text using SVM was proposed by Abu Taher et al. [8]. They used both linear and nonlinear SVM to compare the performance of the model for text classification. The authors in [9] proposed LSTM-based model for multilabel sentiment and emotion detection from Bangla YouTube comments. Their approach achieved an accuracy of 65.97% for a three-label dataset and 54.24% for a five-label dataset. Another work on sentiment classification using SVM was proposed by Arafin Mahtab et al. [10]. They used multi-label dataset

consisting of three classes, positive, negative, and neutral. Using count vectorization and TF-IDF, they achieved an accuracy of 64.596% and 73.49% for two different Bangla datasets.

From the literature, it has been clear that the main cause of being held behind of Bangla natural language processing is due to insufficient Bangla text dataset. Moreover, deep learning models require even more data as they perform feature extraction automatically based on training data samples [11]. So, classification using deep learning neural network-based model is very difficult with the small quantity of Bangla text data available. This paper centers around two-level sentiment classification (i.e., positive and negative) of Bangla text reviews using deep learning neural network model.

3 Methodology

This section contains the methodology we have adapted for sentiment analysis. Figure 1 represents the block diagram of our proposed model. Though a wide variety of machine learning and deep learning algorithms can be applied for sentiment analysis, but most of the time the performance of the model varies depending on the dataset. During this research, traditional machine learning algorithms such as logistic regression (LR), stochastic gradient descent (SGD), support vector machine (SVM), naïve Bayes (NB), decision tree, and random forest were used in order to compare the outcome with our proposed neural network-based LSTM model.

The following sections describe the different steps of our proposed framework:

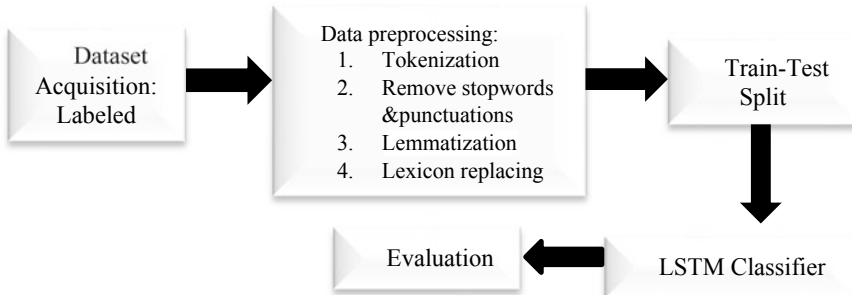


Fig. 1 Block diagram of our proposed model

3.1 Dataset Preprocessing

Tokenization—The first step of text processing is tokenization. Tokenization means making tokens of individual words as token. We separate the text based on space between words.

Original text: 'ক্রিকেট আমার এবং আমার বন্ধুর প্রিয় খেলা'

Tokenized text: 'ক্রিকেট', 'আমার', 'এবং', 'আমার', 'বন্ধুর', 'প্রিয়', 'খেলা'

Remove stopwords and punctuations—There are multiple words in the text which contains less information about the sentiment of the text. We call these words as stopwords. So, after tokenization, we removed the stopwords from the text. For this purpose, we listed a total of 398 words as stopwords.

Original text: 'ক্রিকেট আমার, এবং আমার বন্ধুর প্রিয় খেলা।'

After removing stopwords and punctuations: ক্রিকেট বন্ধুর প্রিয় খেলা

Lemmatizing—When we write a text, we use different forms of a word depending on the tense, place of living, ascent of different regional people. For example, করিতেছে, কর, করা, করতেছিলাম, all of these words have same meaning just in different forms. Lemmatizing transforms different conjugational form of a word into its basic form.

Lexicon replacing—We have collected a list of positive lexicon and negative lexicon from different online sources. Lexicons are used to find the words present in the dataset. In our review dataset, if words in the texts matched with positive lexicon, the word was replaced with the word “positive,” similarly if text contained any negative lexicon, the word was replaced with the word ‘negative.’

Original text: ক্রিকেট আমার, এবং আমার বন্ধুর প্রিয় খেলা।

Lexicon replaced text: ক্রিকেট আমার, এবং আমার বন্ধুর positive খেলা।

3.2 Splitting into Training and Testing Dataset

We splitted our dataset into 80:20 ratio; i.e., 80% of the total dataset was used for training the model, and the rest 20% was used for testing the model. At first, we trained our model using our dataset, and after the training process, the test dataset was applied to the trained classifier so that any unknown text reviews are classified as positive or negative based on the trained result. For the comparison purpose, we have experimented with eight different machine learning algorithms along with our proposed LSTM algorithm.

3.3 Preparation of the LSTM Model

We have loaded a pre-trained vector from Google news and set the embed size to 300, with number of filters to 64 and set the number of epochs to 20. We set the

Table 1 Sample Bangla review with sentiment label of our dataset

Text Review	Label
ভাই সব আপনাদের খুব ভাল লাগছে	Positive
বিজ্ঞান কোথায় যাচ্ছে বিজ্ঞানের জয়রथ আরো এগিয়ে যাক	Positive
যাও গিয়ে জিতে এসো। শুভকামনা থাকলো।	Positive
ক্লিনিকের মালিককে গণদোলাই দেওয়া দরকার	Negative
মেসি হল বার্সেলোনার কিনিত গোলাম	Negative
তা নিয়া তোমার দরকার নেই হারামজাদ	Negative

checkpoint using Keras built-in function model checkpoint in order to save the best model. Finally, we created a sequential LSTM model and fitted our dataset into the model.

4 Experimental Result and Evaluation

This section describes the dataset we have used in our experiment and the details of the experimental results we conducted in our research work. Furthermore, a comparison with other existing works is also portrayed in this section.

4.1 Dataset Description

We have collected labeled dataset containing 2000 positively labeled comments and 2000 negatively labeled comments from online repository. Table 1 describes some sample data of our dataset with their corresponding label. Figure 2 describes the number of comments belonging to each label in the dataset where 0 indicates negative and 1 indicates positive sentiment.

4.2 Result Analysis

It has been found that the size and lack of properly labeled dataset affects the performance of the model. As the size of our dataset was only 4k, so in order to improve the performance, we set 20 epochs to train our model and experimented with different hyperparameter settings. Table 2 shows the accuracy, precision, recall, and $f - 1$ score found from our proposed LSTM model. We achieved a maximum accuracy of 84.25% with a precision of 85.02%. Figure 3 shows the training accuracy and loss of the model. The best validation accuracy we obtained from our model was at 4th

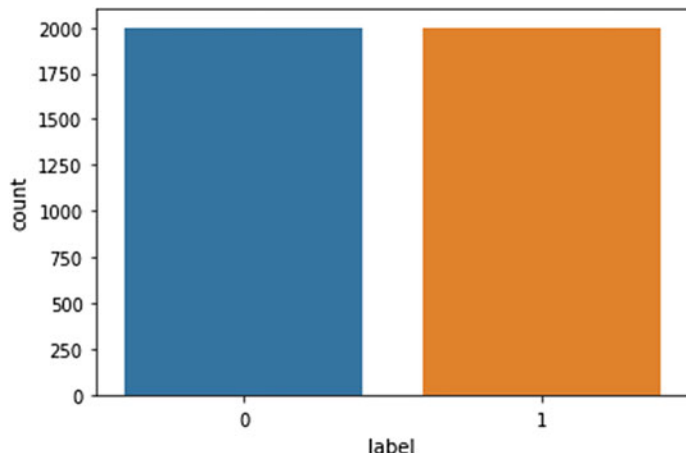


Fig. 2 Number of comments per label in the dataset

Table 2 Various evaluation measures (LSTM model)

Accuracy	Precision	Recall	<i>F</i> -1 score
84.25%	85.04%	82.44%	84.24%

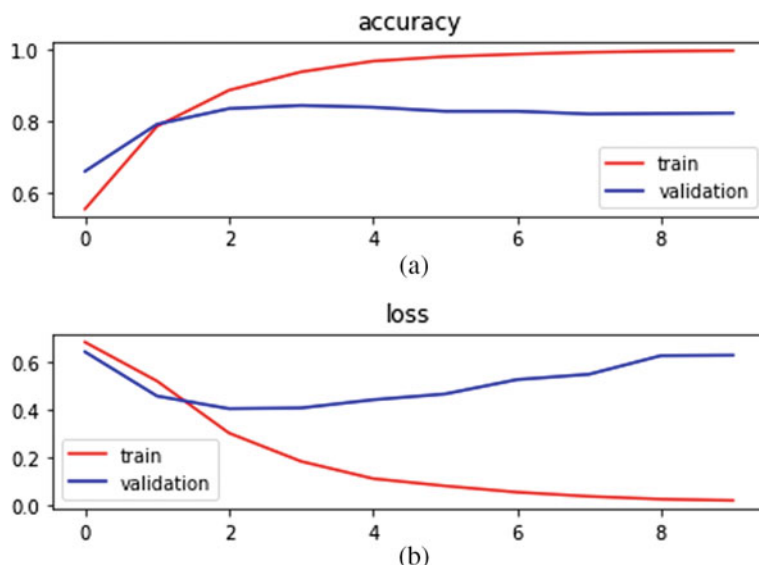


Fig. 3 **a** Training accuracy (LSTM model); **b** training loss (LSTM model)

epoch. We used callback function to save the weight of the epoch which generates the highest accuracy. Figure 4 shows the confusion matrix of the model where true negative, false negative, true positive, false positive counts are 235, 44, 271, and 50, respectively. Figures 5 and 6 show the ROC-AUC curve and the validation accuracy of the model at different epochs.

In order to compare the result of our proposed LSTM-based sentiment classification model from Bangla text review, we have selected eight different classic machine learning algorithms and computed the performance of these algorithms in classifying sentiment for the same dataset. Tables 3 and 4 show the various evaluation matrices

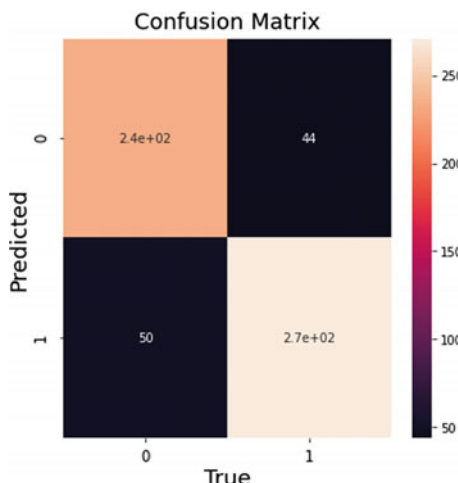


Fig. 4 Confusion matrix (LSTM model)

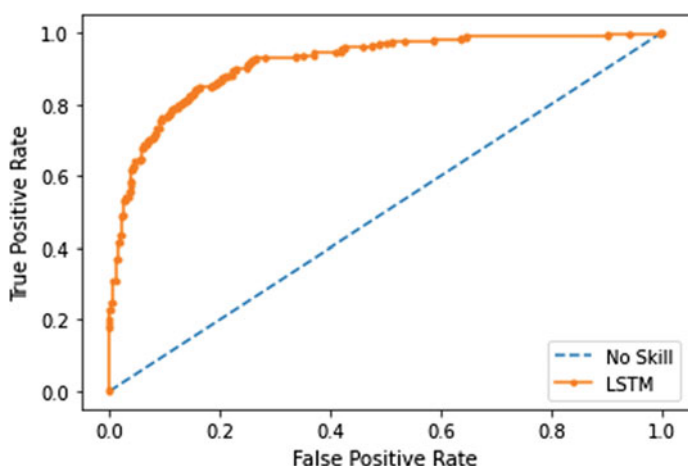


Fig. 5 ROC-AUC curve (LSTM model)

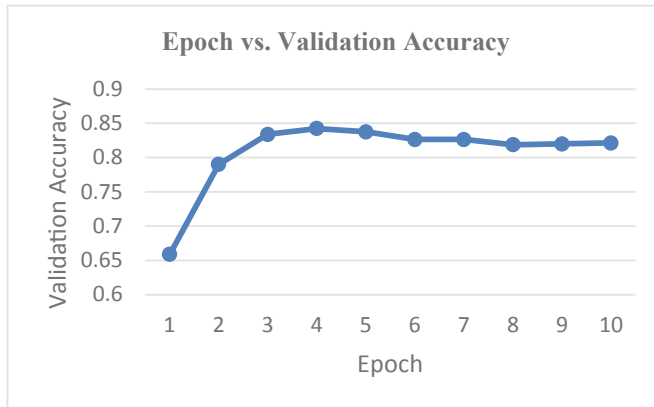


Fig. 6 Validation accuracy of LSTM model during training phase

Table 3 Various evaluation measures for different machine learning algorithms (count vectorizer)

Models	Count vectorizer	Accuracy	Precision	Recall	F-1 score	Kappa score	ROC-AUC score
LR	N-gram (1,3)	0.801	0.816	0.781	0.801	0.60	0.801
SGD	N-gram (1,3)	0.786	0.815	0.744	0.785	0.57	0.786
Linear SVM	N-gram (1,3)	0.763	0.771	0.754	0.763	0.53	0.763
Multinomial NB	N-gram (1,3)	0.800	0.780	0.838	0.799	0.60	0.799
Bernoulli NB	N-gram (1,3)	0.673	0.612	0.957	0.644	0.34	0.671
SVM	N-gram (1,3)	0.741	0.835	0.605	0.736	0.48	0.743
Decision tree	N-gram (1,3)	0.725	0.737	0.704	0.724	0.45	0.725
RF	N-gram (1,3)	0.783	0.794	0.769	0.783	0.57	0.783

of these algorithms using count vectorizer and TF-IDF as the feature extraction techniques, respectively. Furthermore, in the tables, it has been also shown that we have conducted our experiment for n-gram feature extractions in the range between 1 and 3, i.e., for unigram, bi-gram, and tri-gram. The evaluation matrices of these algorithms suggest that count vectorizer performs slightly better than TF-IDF as the feature selection method for our dataset.

The highest accuracy obtained from these algorithms using our dataset is from logistic regression and multinomial naïve Bayes algorithms, and it is 80%, whereas

Table 4 Various evaluation measures for different machine learning algorithms (TF-IDF)

Models	TF-IDF	Accuracy	Precision	Recall	F-1 score	Kappa score	ROC-AUC score
LR	N-gram (1,3)	0.788	0.819	0.724	0.787	0.58	0.787
SGD	N-gram (1,3)	0.790	0.818	0.730	0.789	0.58	0.788
Linear SVM	N-gram (1,3)	0.797	0.821	0.745	0.796	0.59	0.796
Multinomial NB	N-gram (1,3)	0.791	0.760	0.832	0.791	0.58	0.792
Bernoulli NB	N-gram (1,3)	0.647	0.583	0.964	0.612	0.31	0.656
SVM	N-gram (1,3)	0.787	0.832	0.704	0.785	0.57	0.785
Decision tree	N-gram (1,3)	0.728	0.726	0.709	0.728	0.46	0.728
RF	N-gram (1,3)	0.768	0.811	0.683	0.766	0.54	0.766

the accuracy obtained from LSTM model was 84.25% which is far better than this result. Comparing the results of LSTM model in Table 2 with Tables 3 and 4, it has been found that LSTM model outperforms in all evaluation matrices than the other algorithms we have employed in our experiment. Furthermore, we compared the results of our LSTM-based model with the state-of-the-art research work in Bangla text data for sentiment analysis. The details of the existing research works are summarized in Table 5. Though most of the researchers obtained best accuracy for support vector machine, but according to our experiment, LSTM achieves best performance in terms of accuracy and other evaluation matrices than the other traditional machine learning algorithms. As the size of our dataset was only 4k which is not enough for getting good results using deep learning model, so for further development of this work, more data samples need to be added to enhance the dataset. And, it is obvious that for a large amount of labeled dataset, we can achieve more better performance using the same LSTM model.

So, from the above discussion, it has been found that there are a very few works that have been done on public sentiment or emotion detection from Bangla text and the accuracy of the results found so far using different machine learning and deep learning algorithms is much less than the accuracy we found in our experiment.

Table 5 State-of-the-art works

Authors	Algorithms used	Accuracy					
Chowdhury et al. [12]	SVM	88.90%					
	LSTM	82.42%					
Hassan et al. [13]	LSTM	78%					
Sazzed and Jayarathna [14]	Algorithms used	Cricket dataset	Cricket dataset (balanced)	Drama review			
	Logistic regression	70.9/72.2	54.2/65.8	64.2/68.2			
	Ridge regression	69.6/72.7	54.4/66.6	65/70			
	SVM	70.1/73.2	53.3/67.2	65.4/70.1			
	Random forest	69.1/72.1	59.8/71.6	63/61.7			
	Extra randomized tree	68.3/72.6	59.9/71.3	63/64.6			
	LSTM	59.0/72.2	45.5/47.9	58.2/64.2			
	Algorithms used	Multi-class		Binary class			
Rahman et al. [15]		F-1	Precision	Recall	F-1	Precision	Recall
	CNN	0.4819	0.4863	0.4819	0.7557	0.7598	0.7530
	LSTM	0.4658	0.4617	0.4658	0.7117	0.7093	0.7168
	DNN	0.4236	0.4319	0.4236	0.6867	0.6862	0.7048

5 Conclusion and Future Work

Sentiment analysis is a very important and urgent issue in the field of natural language processing. Detecting sentiment from Bangla texts is a must since a large number of people posts, comments in different online blogs and social media's in Bangla language. In this paper, we proposed an LSTM-based neural network model to detect sentiment of people from their comments on different online platforms. We first preprocessed our entire dataset to make it suitable for the model to predict sentiment. Our proposed model generates an accuracy of 84.25%. Although the accuracy is not quite satisfactory compared to sentiment analysis on English text, but the accuracy we achieved is higher than most other works done on Bangla texts. The reason behind low accuracy of the model on Bangla text is the lack of properly labeled dataset, lack of stopwords, lexicons, and lemmatizing utilities. In this paper, we have only classified sentiment as positive and negative. As a future extension of this work, we have planned to focus on multilabel sentiment analysis. The use of some other recurrent neural network architecture or the integration of knowledge-driven methodology can be a further extension of this work. Furthermore, unsupervised- or semi-supervised-based approach can be another dimension to work with in the future.

References

1. Neethu MS, Rajasree R et al (2013) Sentiment analysis in twitter using machine learning techniques. [ieeexplore.ieee.org](https://ieeexplore.ieee.org/abstract/document/6726818#sec4). Published on 2013, available: <https://ieeexplore.ieee.org/abstract/document/6726818#sec4>
2. Yang CC et al (2010) Understanding online consumer review opinions with sentiment analysis using machine learning. *AIS J* 2(3). Available: <https://aisel.aisnet.org/pajais/vol2/iss3/7/>
3. Hemalatha et al (2010) Sentiment analysis tool using machine learning algorithms. *Elixir Comp Sci Eng* 58(2013):14791–14794. Available: www.elixirpublishers.com
4. Go A, Bhayani R, Huang L (2009) Twitter sentiment classification using distant supervision. Technical report, Stanford Digital Library Technologies Project
5. Davidiv D, Tsur O, Rappoport A (2010) Enhanced sentiment learning using twitter hash-tags and smileys. In: Proceedings of the 23rd international conference on computational linguistics: posters, COLING '10. Association for Computational Linguistics, Stroudsburg, PA, pp 241–249
6. Maynard D, Funk A (2012) Automatic detection of political opinions in tweets. In: Garcia-Castro R, Fensel D, Antoniou G (eds) The semantic web: ESWC 2011 workshops. Lecture notes in computer science, vol 7117. Springer, Berlin, pp. 88–99
7. Banik N, Hasan Hafizur Rahman M (2018) Evaluation of Naïve Bayes and support vector machines on Bangla textual movie reviews. In: 2018 international conference on Bangla speech and language processing (ICBSLP), Sept 2018, pp 1–6
8. Abu Taher S, Afsana Akhter K, Azharul Hasan KM (2018) N-gram based sentiment mining for Bangla text using support vector machine. In: 2018 international conference on Bangla speech and language processing (ICBSLP), Sept 2018, pp 1–5
9. Irtiza Tripto N, Eunus Ali M (2018) Detecting multilabel sentiment and emotions from Bangla Youtube comments. In: 2018 international conference on Bangla speech and language processing (ICBSLP), Sept 2018, pp 1–6

10. Arafin Mahtab S, Islam N, Mahfuzur Rahaman M (2018) Sentiment analysis on Bangladesh cricket with support vector machine. In: 2018 international conference on Bangla speech and language processing (ICBSLP), Sept 2018, pp 1–4
11. Sagina IJ (2018) Why go large with data for deep learning? April 2018 [Online]. Available: <https://towardsdatascience.com/whygo-large-with-data-for-deep-learning-12eee16f708>
12. Chowdhury RR et al (2019) Analyzing sentiment of movie reviews in Bangla by applying machine learning techniques. In: International conference on Bangla speech and language processing (ICBSLP), 27–28 Sept 2019
13. Hassan A et al. Sentiment analysis on Bangla and Romanized Bangla text (BRBT) using deep recurrent models. Available: https://www.researchgate.net/publication/308831680_Sentiment_Analysis_on_Bangla_and_Romanized_Bangla_Text_BRBT_using_Deep_Recurrent_models
14. Sazzed S, Jayarathna S (2019) A sentiment classification in Bengali and machine translated English corpus. In: 2019 IEEE 20th conference on information reuse and integration for data science (IRI)
15. Rahman M et al (2020) Identifying and categorizing opinions expressed in Bangla sentences using deep learning techniques. Int J Comput Appl (0975–8887) 176(17)

Improved Vehicle Detection and Tracking Using YOLO and CSRT



I. C. Amitha  and N. K. Narayanan

Abstract Vehicle detection and tracking plays an important role in Intelligent Transportation Systems (ITS). This paper reports an improved vehicle detection and tracking performance of combined You Only Look Once (YOLO) and Discriminative Correlation Filter (with Channel and Spatial Reliability) (CSRT). CSRT is mainly used for face prediction and moving object detection. The proposed system uses CSRT for vehicle tracking, particularly for cars, buses, and trucks. To perform the vehicle detection task, we have used the YOLO v3 pre-trained model. The accuracy and effectiveness of our vehicle detection and tracking system are tested with 8 different commonly available trackers in various publicly available traffic videos. Experimental results show that the CSRT gives the best performance among all the other trackers. CSRT gives 100% accuracy in all the four publicly available traffic videos even though vehicles with poor lighting conditions.

Keywords Vehicle detection · Vehicle tracking · YOLO · CSRT

1 Introduction

Traffic monitoring and management is a tedious task with different phases such as capturing the traffic, process the traffic image or video, and control the traffic system according to the processed signal. To process the input from the traffic, we need to process the video either using some conventional approaches or a machine learning-based approach. For intelligent traffic monitoring and management, deep learning-based approaches are best suited [1]. A new and easy approach toward object detection explained in [2] is best suited for vehicles and pedestrian's detection in road traffic. The normal working of traffic signals is based on a preset timer, according

I. C. Amitha 

Department of Information Technology, Kannur University, Kannur, Kerala, India
e-mail: amithaic@sngcet.org

N. K. Narayanan

Indian Institute of Information Technology Kottayam, Kottayam, Kerala, India
e-mail: nknarayanan@iiitkottayam.ac.in

to the settled time, and it allows the vehicles to pass over a particular lane in the traffic junctions. In this study, we are incorporating machine intelligence into traffic monitoring and management to get a hassle-free road traffic system.

The normal task of vehicle counting and classification can be done either through software solutions or hardware solutions. Hardware solutions for traffic monitoring and management are much expensive than software solutions. Some kinds of sensors were used in the earlier days as hardware solutions. With the rapid developments in computer vision and object detection, software solutions can perform scene analysis and object detection very easily. Different software solutions being used traffic monitoring nowadays are based on deep learning approaches. Several approaches are available for object detection and retrieval in both conventional and machine learning approaches. The conventional approach is purely based on some handcrafted algorithms; on the other hand, convolutional neural network is the heart of the machine learning approach [2, 3].

The proposed system uses the YOLO framework for image recognition and object detection from the video input. After the vehicle detection from the scene, our counting setup will count the number of vehicles in each lane. Checkpoints are fixed in the traffic video to count how many vehicles are passing through the points. To check the tracker performance, our system was tested with eight different trackers in various traffic videos. The analyses show that, with adequate surrounding light, the proposed framework can arrive at high counting precision [2, 4].

The rest of the paper is formulated as follows. Related works their strength and weaknesses are discussed in Sect. 2. Section 3 explains the proposed architecture of vehicle detection, tracking, and tracker performance. Experimental results and identification of the best tracker are done in Sect. 4. Section 5 concludes the work.

2 Related Work

Vehicle detection and tracking in road traffic is an inevitable stage in the intelligent transport system. This section has been discussed various vehicle detection, tracking, and counting methods. Redmon et al. [2] have presented YOLO, a bound together model for object detection. Their model is easy to build and can be trained straightforwardly on full images. Fast YOLO is the fastest object detector in real-time object detection. In [3], Lin and Sun have proposed a framework to get the vehicles to count by using basic distance calculation with an updated YOLO model. The framework structure comprises a detector, buffer, and counter. By trying with two different videos, they have illustrated the accuracy of the proposed system. Asha and Narasimhadhan [4] have proposed a vehicle detection and counting framework in a diverse traffic environment. They have utilized the YOLO framework for detection and correlation filters for tracking.

Zaatouri and Ezzedine [5] have explained a method, and its objective is to improve ITS by building up a self-versatile procedure to control road traffic dependent on deep learning. In [6], Huang et al. presented a system that can perform vehicle analysis and counting for two-way roads. They have considered various attributes of input

videos, to categorize the vehicles as bike or car. They can achieve a classification accuracy of 96.4 and 92.7 for cars and bikes, respectively. Liu et al. [7] have explained a moving object detection and tracking based on a combination of Gaussian model and Kalman filter, respectively. In [8], Lai et al. suggested a method to extract the vehicle regions through a combined background subtraction procedure along with the shadow removal method. They have classified the vehicles into three categories such as truck, car, and bus based on their compactness and aspect ratio.

Song et al. [9] have addressed two challenges such as the detection of vehicles in different sizes and accuracy in vehicle counting. Gao and Li [10] have proposed another convolutional neural network dependent on SSD for vehicle detection, which applies feature combination and batch normalization on it. They have used a combination layer which is intended for getting more data by connecting feature highlights at various levels. Dai et al. [11] have proposed a vehicle counting structure dependent on video scenes. The outcomes show that the detection technique utilizing YOLO v3 with their dataset is high, reaching 87.6%, regardless of whether the traffic condition is very unpredictable. In [12], Fang et al. have proposed a vehicle tracking strategy based on particle filtering. The proposed model consolidates a part-based system with a particle filter. Scheel and Dietmayer [13] have used a variational radar model to track multiple vehicles. Zhang et al. [14] have suggested a vehicle tracking system dependent on vehicle detection and velocity estimation. In their system, they have achieved the detection process through color faster R-CNN and tracking is performed through Kalman filter. In [15], Amitha and Narayanan proposed an object retrieval method in images using SIFT and R-CNN. They have tested their method both in the oxford building dataset as well as in the customized dataset. From the above study, it is found that the YOLO framework provides the best vehicle detection accuracy.

Farhodov et al. [16] have proposed a vehicle detection and tracking method in that vehicle detection is performed by faster R-CNN and tracking is done through OpenCV CSRT. In [17] Emami et al. have implemented one tracking algorithm using open-source computer vision (open cv) and evaluated the efficiency with Continuously Adaptive Mean-Shift (CAMSHIFT) tracker with failure detection and correction. Henriques et al. [18] have derived a new kernelized correlation filter (KCF). Many beneficial algorithms can also additionally be acquired from the study of circulant information together with classical filters. In [19], Liu et al. proposed a tracker with multiple features. Most importantly they have found an upper bound boosting error in a sub-training framework. The stable principle helps, and convincible empirical results exhibit that the prospective tracker is promising error-free tracking.

In [20], Bolme et al. have explained a new variety of correlation filters named minimum output sum of squared error (MOSSE) filter, used for object detection and tracking. Their filter is robust in various lighting conditions and pose. Babenko et al. [21] have addressed a specific problem in object tracking. Specifically, they have explained about tracking by detection, and this is achieved by a novel technique multiple instance learning (MIL). Jia et al. [22] they have modified the conventional tracking learning detection (TLD) method. The updated TLD shows improved accuracy rate and robustness in the tracking process. In [23], Varfolomeiev and Lysenko have described an improved version of the median flow algorithm for object tracking in visual scenes. The proposed method is implemented using OpenCV. In

this section, we have studied different trackers and their tracking accuracy in visual object tracking.

3 Vehicle Detection and Tracking

A real-time intelligent traffic monitoring system is depicted in Fig. 1. In our previous work, we have implemented a similar system and the performance was tested with three different trackers such as CAMSHIFT, KCF, and CSRT. In this paper, we have studied different object detection techniques and various tracking methodologies to get a better vehicle detector and tracker. In this paper, we have proposed an efficient vehicle detection and tracking system. Vehicle detection is performed by the YOLO

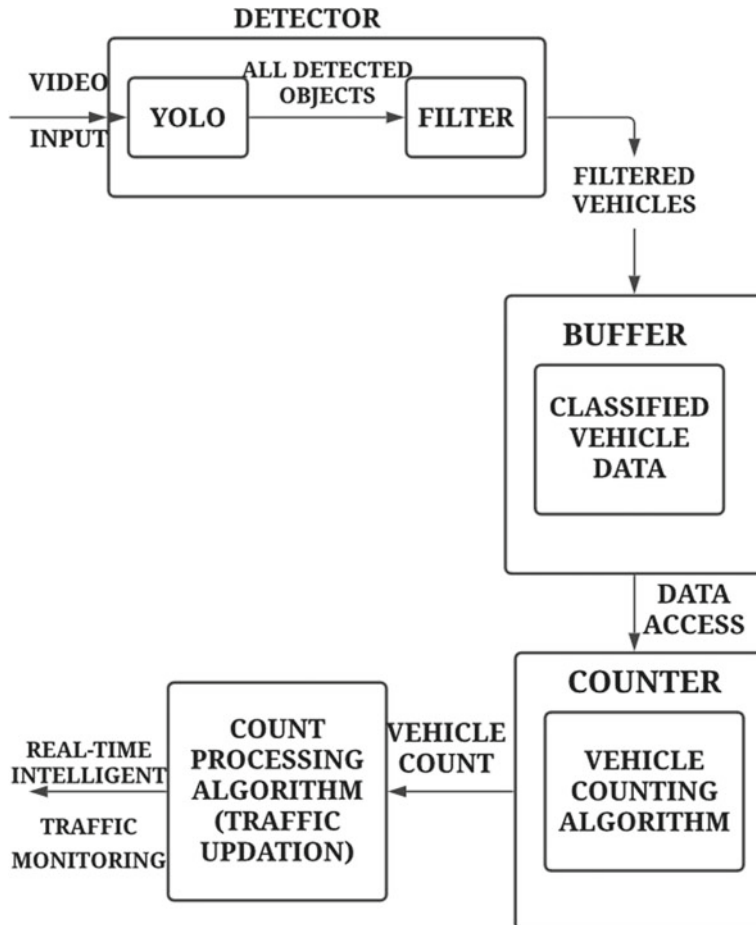


Fig. 1 Vehicle detection and tracking architecture

v3 pre-trained model, and this can detect 80 objects in the real world. In our proposed system is designed in such a way that to detect only three vehicle classes. Three filtered classes for our intelligent transport system are car, bus, and truck. Table 1 gives a summary of the proposed method.

Our present work mainly focuses on the identification of the best tracker from a set of available trackers and applies the system to a real-time vehicle detection and tracking process. Most of the trackers are available in Open CV. In the first step, feed the input video to the YOLO framework. In this, we are using a pre-trained YOLO v3 framework to detect the vehicles in the video input. In the next stage, filtered vehicles are passed to a buffer which is kept to store the classified vehicles by the YOLO framework. After completing the detection task using YOLO,

Table 1 Algorithm

Step 1: Input: Feed input video to YOLO framework
2: Filter the vehicles of our interest: bus, car, and truck.
3: Classified vehicles are kept in the buffer for further process
4: Perform the tracking process using the following trackers:
a. CSRT
b. CAMSHIFT
c. KCF
d. BOOSTING
e. MIL
f. TLD
g. MEDIAN FLOW
h. MOSSE
5: Apply the vehicle counting algorithm:
a. Arrange two fixed points or lines before recording the traffic video.
b. Take the number of vehicles between the fixed area.
6: Apply the count processing algorithm to control the traffic lights.
a. Take the number of vehicles in each lane.
b. Give the highest priority to the lane with maximum number of vehicles.
c. Turn the traffic signal from red to green.

Table 2 Video 1 with 325 frames

TRACKER	Y_TRUE	Y_PREDICTED	ACCURACY
CSRT	4	4	100
KCF	4	4	100
BOOSTING	4	4	100
MOSSE	4	4	100
TLD	4	3	75
MIL	4	4	100
MEDIAN FLOW	4	4	100
CAMSHIFT	4	2	50

Table 3 Video 2 with 400 frames

TRACKER	Y_TRUE	Y_PREDICTED	ACCURACY
CSRT	8	8	100
KCF	8	8	100
BOOSTING	8	8	100
MOSSE	8	8	100
TLD	8	7	87.50
MIL	8	8	100
MEDIAN FLOW	8	8	100
CAMSHIFT	8	4	50

perform the tracking operation in the following trackers: CSRT, CAMSHIFT, KCF, BOOSTING, MIL, TLD, MEDIAN FLOW, and MOSSE. After tracking, apply the vehicle counting algorithm, according to the vehicle count control the traffic lights.

4 Experimental Results and Discussions

Improved Vehicle Detection and Tracking using YOLO and CSRT is implemented in Python code. For experimental setup, YOLO v3 and specified trackers are selected. In our experimental study, it is found that YOLO v3 gives best detection and CSRT gives proper tracking too. Our method uses four publicly available traffic video as dataset. All trackers are tested with four different video inputs with different vehicles, various poses, different velocities, and different lighting conditions. Three videos have 1920×1080 , and one has 1280×720 resolution in RGB. These videos contain background scenes and road vehicles. To perform the vehicle counting, checkpoints are assigned manually on the roads in the videos. Tables 2, 3, 4, and 5 show the tracking performance of various trackers in different road traffic videos. Video 1 is a 13-s duration with 325 frames, video 2 is a 16-s duration with 400 frames, video 3 is a 26-s duration with 780

Table 4 Video 3 with 780 frames

TRACKER	Y_TRUE	Y_PREDICTED	ACCURACY
CSRT	14	14	100
KCF	14	13	92.85
TLD	14	12	85.71
MOSSE	14	12	85.71
BOOSTING	14	10	71.42
MEDIAN FLOW	14	10	71.42
MIL	14	9	64.28
CAMSHIFT	14	4	28.57

Table 5 Video 4 with 2100 frames

TRACKER	Y_TRUE	Y_PREDICTED	TRACKING ACCURACY
CSRT	19	19	100
KCF	19	19	100
BOOSTING	19	18	94.73
TLD	19	17	89.47
MOSSE	19	15	78.94
MIL	19	13	68.42
MEDIAN FLOW	19	1	05.26
CAMSHIFT	19	0	00.00

frames, and video 4 is a 42 s with 2100 frames. All the input videos have a different number of frames according to their duration and number of frames per second. The experimental results are shown in the following tables.

From our experimental results, it is clear that CSRT gave the best performance in all the four input cases. CSRT can detect all the vehicles in various lighting conditions. KCF, BOOSTING, and TLD also show better performance than the remaining trackers. Table 6 gives the best 4 vehicle detection and tracking results. To analyze the proposed method quantitatively, calculate Precision (P), Recall (R), F -score (F), and Counting Accuracy (CA). The calculations are done as follows in Eqs. (1), (2), (3), and (4), respectively. The sample screenshot of vehicle detection, tracking, and counting of

$$P = \frac{\text{No of Correctly detected vehicle bounding box}}{\text{No of vehicles in ground-truth}} \quad (1)$$

$$R = \frac{\text{No of Correctly detected vehicle bounding box}}{\text{No of detected vehicles}} \quad (2)$$

$$F = \frac{2PR}{P + R} \quad (3)$$

Table 6 Result of vehicle detection, tracking, and counting using CSRT tracker for all videos

Video sequence	No of frames	Total no. of vehicles in the ground-truth	Total no of vehicles detected using the proposed method	Missing/ multiple detection/ error	Precision %	Recall %	F-score	Counting accuracy %
1	325	4	4	0/0/0	100	100	100	100
2	400	8	8	0/0/0	100	100	100	100
3	780	14	14	0/0/0	100	100	100	100
4	2100	19	19	0/0/0	100	100	100	100

$$CA = \frac{\text{No of Correct detection}}{\text{No of ground truth detection}} \quad (4)$$

CSRT, CAMSHIFT, and KCF trackers are shown in Fig. 2. Tables 6 and 7 give the performance of CSRT and KCF trackers. The performance of the CSRT tracker is shown in Fig. 3.

Some other trackers shown best results in our proposed method are KCF, MOSSE, and TLD. The performance of the KCF tracker is shown in Fig. 4, for video sequence 3 KCF tracker cannot achieve 100% accuracy. Out of 14 vehicles, it can detect, track, and count 13 vehicles. Figure 5 shows the final vehicle counting and traffic signal generation. Once the vehicle count is identified from each lane, the signal is generated, depending on the number of vehicles in each lane. Take an instance from Fig. 5, [27, 58, 36, 77] is the number of vehicles in the four lanes, respectively. The maximum number of vehicles is in lane 4, so give priority to the lane 4 and the signal is changed from red to green.

5 Conclusions

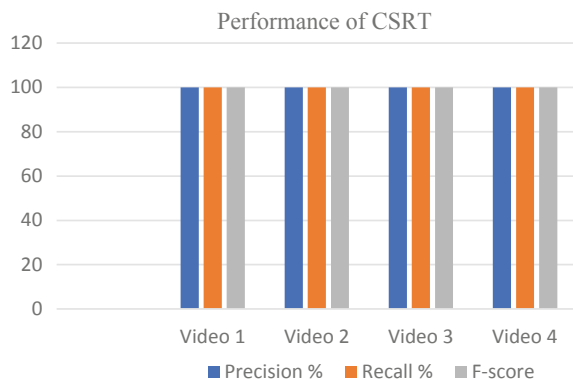
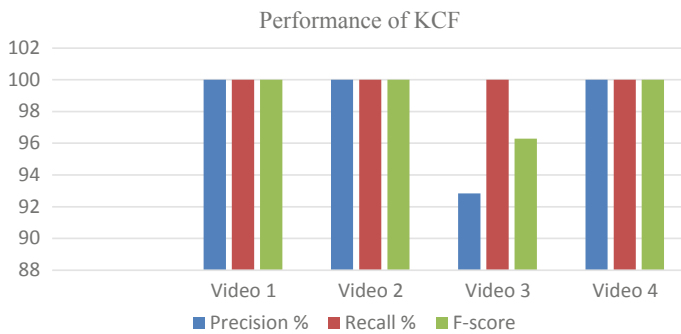
The proposed system exploited the YOLO v3 framework for object detection, and various OpenCV trackers are used for tracking. The system performance is evaluated with four different video sequences. Among the eight trackers, CSRT has the best performance, and it can detect all the vehicles which are in the ground-truth set. Our combined YOLO v3 and CSRT achieved 100% vehicle detection and tracking with the four publicly available road traffic videos, BOOSTING, and TLD also show some better performance when comparing with MOSSE, MIL, MEDIAN FLOW, and CAMSHIFT. In our study, it is found that the detection accuracy is influenced by the efficiency of the tracker, input duration, lighting conditions of the video, frequency of vehicles in the traffic, the distance between vehicles.



Fig. 2 Sample vehicle detection and tracking snapshots of CSRT, CAMSHIFT, and KCF

Table 7 Result of vehicle detection, tracking, and counting using KCF tracker for all videos

Video sequence	No of frames	Total no. of vehicles in the ground-truth	Total no of vehicles detected using the proposed method	Missing/multiple detection/error	Precision %	Recall %	F-score	Counting accuracy %
1	325	4	4	0/0/0	100	100	100	100
2	400	8	8	0/0/0	100	100	100	100
3	780	14	13	1/0/0	92.85	100	96.29	93.7
4	2100	19	19	0/0/0	100	100	100	100

**Fig. 3** Performance of CSRT tracker**Fig. 4** Performance of KCF tracker

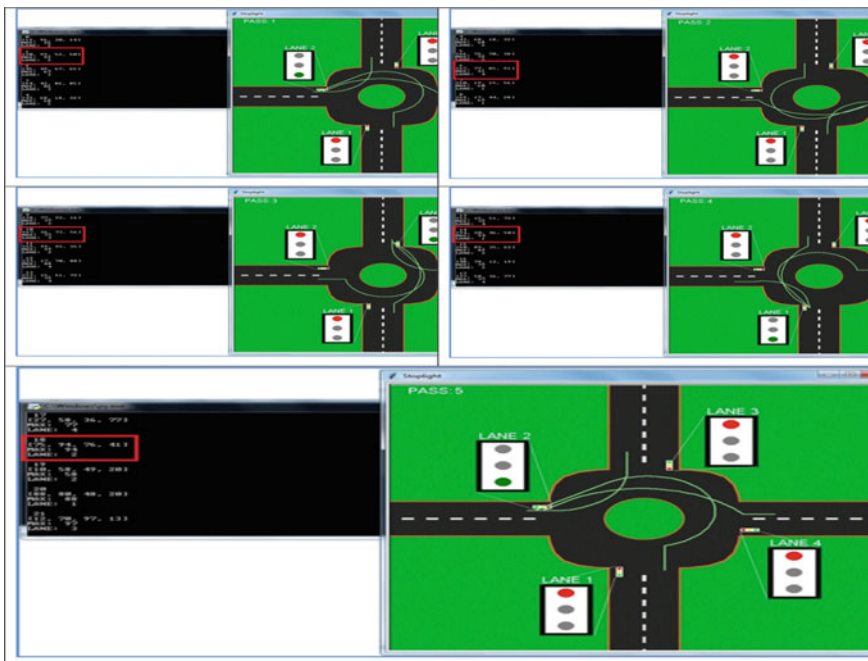


Fig. 5 Count processing and traffic signal generation

References

- Olariu S, Weigle MC (eds) (2009) Vehicular networks: from theory to practice. CRC Press, Boca Raton
- Redmon J, Divvala S, Girshick R, Farhadi A (2016) You only look once: unified, real-time object detection. In: Proceedings of the IEEE conference on computer vision and pattern recognition, pp 779–788
- Lin J-P, Sun M-T (2018) A YOLO-based traffic counting system. In: 2018 conference on technologies and applications of artificial intelligence (TAAI). IEEE, pp 82–85
- Asha CS, Narasimhadhan AV (2018) Vehicle counting for traffic management system using YOLO and correlation filter. In: 2018 IEEE international conference on electronics, computing and communication technologies (CONECCT). IEEE, pp 1–6
- Zaatouri K, Ezzedine T (2018) A self-adaptive traffic light control system based on YOLO. In: 2018 international conference on internet of things, embedded systems and communications (IINTEC). IEEE, pp 16–19
- Huang D-Y, Chen C-H, Wu-Chih Hu, Yi S-C, Lin Y-F (2012) Feature-based vehicle flow analysis and measurement for a real-time traffic surveillance system. *J Inf Hiding Multimedia Signal Process* 3(3):279–294
- Liu Y, Ai H, Xu G (2001) Moving object detection and tracking based on background subtraction. In: object detection, classification, and tracking technologies, vol 4554. International Society for Optics and Photonics, pp 62–66
- Lai J-C, Huang S-S, Tseng C-C (2010) Image-based vehicle tracking and classification on the highway. In: The 2010 international conference on green circuits and systems. IEEE, pp 666–670

9. Song H, Liang H, Li H, Dai Z, Xu Y (2019) Vision-based vehicle detection and counting system using deep learning in highway scenes. *Eur Transp Res Rev* 11(1):51
10. Gao H, Li X (2020) Vehicle detection in high resolution image based on deep learning. *Int Arch Photogrammetry Remote Sens Spat Inf Sci* 43:49–54
11. Dai Z, Song H, Wang X, Yong Fang Xu, Yun ZZ, Li H (2019) Video-based vehicle counting framework. *IEEE Access* 7:64460–64470
12. Fang Y, Wang C, Yao W, Zhao X, Zhao H, Zha H (2019) On-road vehicle tracking using part-based particle filter. *IEEE Trans Intell Transp Syst* 20(12):4538–4552
13. Scheel A, Dietmayer K (2018) Tracking multiple vehicles using a variational radar model. *IEEE Trans Intell Transp Syst* 20(10):3721–3736
14. Zhang Y, Song B, Xiaojiang Du, Guizani M (2018) Vehicle tracking using surveillance with multimodal data fusion. *IEEE Trans Intell Transp Syst* 19(7):2353–2361
15. Amitha IC, Narayanan NK (2020) Object retrieval in images using SIFT and R-CNN. In: 2020 international conference on innovative trends in information technology (ICITIIT). IEEE, pp 1–5
16. Farhodov X, Kwon O-H, Kang KW, Lee S-H, Kwon K-R (2019) Faster RCNN detection based openCV CSRT tracker using drone data. In: 2019 international conference on information science and communications technologies (ICISCT). IEEE, pp 1–3
17. Emami E, Fathy M, Kozegar E (2013) Online failure detection and correction for CAMShift tracking algorithm. In: 2013 8th Iranian conference on machine vision and image processing (MVIP). IEEE, pp 180–183
18. Henriques JF, Caseiro R, Martins P, Batista J (2014) High-speed tracking with kernelized correlation filters. *IEEE Trans Pattern Anal Mach Intell* 37(3):583–596
19. Liu R, Cheng J, Lu H (2009) A robust boosting tracker with minimum error bound in a co-training framework. In: 2009 IEEE 12th international conference on computer vision. IEEE, pp 1459–1466
20. Bolme DS, Ross Beveridge J, Draper BA, Lui YM (2010) Visual object tracking using adaptive correlation filters. In: 2010 IEEE computer society conference on computer vision and pattern recognition. IEEE, pp 2544–2550
21. Babenko B, Yang M-H, Belongie S (2009) Visual tracking with online multiple instance learning. In: 2009 IEEE conference on computer vision and pattern recognition. IEEE, pp 983–990
22. Jia C, Wang Z, Wu X, Cai B, Huang Z, Wang G, Zhang T, Tong D (2015) A tracking-learning-detection (TLD) method with local binary pattern improved. In: 2015 IEEE international conference on robotics and biomimetics (ROBIO). IEEE, pp 1625–1630
23. Varfolomieiev A, Lysenko O (2016) An improved algorithm of median flow for visual object tracking and its implementation on ARM platform. *J Real-Time Image Proc* 11(3):527–534

A Comparative Analysis of Japan and India COVID-19 News Using Topic Modeling Approach



Piyush Ghasiya and Koji Okamura

Abstract Severe acute respiratory syndrome coronavirus 2 (SARS-CoV-2) is wreaking havoc. This virus has infected more than 62.01 million and killed around 1.44 million people worldwide in less than a year. For the past 11 months, this is the most critical issue that the world is dealing with. Hence, there is a rapid accumulation of coronavirus-related news. Natural language processing (NLP) and machine learning (ML) methods such as topic modeling receive much attention because of their ability to discover hidden themes and issues from large unstructured text data. We collected 63,424 COVID-19/coronavirus themed news articles from Japanese and Indian English newspapers and applied the recently proposed Top2Vec model to analyze and extract major topics. Our research finds out that both countries' media reported heavily about the problems that arise due to coronavirus in sports, education, and entertainment sectors. Our findings also point out that Indian media gave very little space to the issues such as unemployment and the migrant crisis that impacted millions during this period. This research can be used as a template to understand and analyze how this pandemic impacted other countries. It also brought to our attention the media's failure to prioritize critical importance issues for society (migrant crisis) and focused on trivial news (celebrities social media posts).

Keywords Topic Modeling · Top2Vec · COVID-19 · Coronavirus · NLP

1 Introduction

On December 31, 2019, Chinese health officials informed the World Health Organization (WHO) about the cluster of 41 patients with pneumonia, and most of them are connected to Huanan Seafood Wholesale Market [1]. However, as the scientists are trying to map the early transmission of COVID-19, the Chinese government data shows that the 55-year-old lady from Hubei Province can be the first person to have contracted COVID-19 on November 17, 2019 [2]. On January 11, 2020, China recorded the first death due to COVID-19, and this virus and disease have spread all

P. Ghasiya (✉) · K. Okamura
Kyushu University, Fukuoka 819-0395, Japan

over the world (218 countries) like wildfire infecting more than 62.01 million and killing more than 1.44 million people till the time of writing this paper. With around 13.45 million infected people and 271,029 deaths, the USA is the most severely affected country [3]. On January 30, 2020, WHO declared it a Public Health Emergency of International Concern (PHEIC), and on March 11, 2020, the WHO director characterized COVID-19 as a pandemic [4]. The healthcare system in many worst affected countries is going through extreme challenges to handle this pandemic.

Other than the loss of life, this pandemic has brought many collateral damages in several countries. The biggest damages in the sporting world came from Japan (139,491 infected and 2051 deaths) in the form of postponement of the Tokyo 2020 Olympics and Paralympics Games till next year [5]. On the other hand, India (the second worst affected country with 9.35 million infected and 136,238 deaths till November 28, 2020)—a country with 1.3 billion people—was under complete lockdown for 68 days starting from March 25, 2020, till May 31, 2020, to contain the infection. However, this sudden lockdown (declaration came only 4 h before) had a huge social and economic impact on millions of daily wage workers as they were thrown out of work. Migrant workers packed to go home in busses and trains, and as all the transport options available due to lockdown, many in Delhi, Mumbai, and other big cities walked hundreds of kilometers to their villages [6].

As the world is in the grip of this pandemic, newspapers (both print and digital) all over the world are full of COVID-19/coronavirus-related news, articles, and stories. Making sense of this data is a challenge but a challenge worth doing. Topic modeling is an approach used for automatic comprehension and classification of data in a variety of settings. We will use the recently proposed Top2Vec model of the topic model—in understanding COVID-19-related news in Japan and India. In machine learning (ML) and natural language preprocessing (NLP), the topic model is a statistical model for discovering abstract topics in a corpus. In this research, we have collected 63,424 COVID-19/coronavirus-related news articles (till September 30, 2020) from major newspapers (digital version) such as The Japan Times, Asahi Shimbun, Mainichi Shimbun, Hindustan Times, and The Indian Express and tried to analyze them using the topic modeling approach. This research aims to identify various topics (hence issues) in the COVID-19/coronavirus themed news articles from both countries, which will help us in decluttering this large dataset.

The rest of the paper is systemized as follows: Literature review of the work related to topic modeling and methodology of this paper would be presented in Sects. 2 and 3, respectively. Topic modeling results and analysis would be discussed in Sect. 4. Section 5 would present a comparative analysis and consideration. Lastly, Sects. 6 and 7 would present various limitations and conclusions of this research, respectively.

2 Literature Review

An early topic model is proposed by Papadimitriou, C.H., Raghavan, P., Tamaki, H., and Vempala, S. in the paper “Latent semantic indexing: A probabilistic analysis”

where they introduced latent semantic indexing (LSI) as an information retrieval technique based on the spectral analysis of the term–document matrix [7]. After that, many new methods were developed, and latent Dirichlet allocation (LDA) is one such method that is the most common topic model method currently in use. Blei, D.M., Ng, A.Y., and Jordan, M.I. published their seminal research in the paper “Latent dirichlet allocation” in 2003 [8]. They introduced Dirichlet prior distributions over document–topic and topic–word distributions. Non-negative matrix factorization (NMF) for topic modeling was proposed by Arora, S., Ge, R. and Moitra, A. in 2012 in the paper “Learning Topic Models—Going Beyond SVD” which is another method for topic modeling. NMF approach is analogous to SVD, where all vectors are non-negative [9]. The most recent entry into topic modeling methods is the Top2Vec method. Dimo Angelov proposed in the paper titled “Top2Vec: Distributed Representations of Topics” in August 2020. Unlike other methods, this does not require a stop words list, stemming, and lemmatization. It leverages the joint document and word semantic embeddings to find topic vectors. The resulting topic vectors are jointly embedded with the document and word vectors, with the distance between them representing semantic similarity [10]. Some other studies related to COVID-19 spread are conducted by Singh et al. [11], Bhatnagar et al. [12], and Kumari et al. [13].

3 Research Methodology

This research can be divided into two steps: (1) data acquisition and (2) topic modeling and Top2Vec.

3.1 Data Acquisition

For data collection, we used “COVID-19”/“coronavirus” as keywords. Newspapers articles with these keywords from five newspapers’ Web sites (English version) of Japan and India were collected using web-scraping methods and collected 63,424 articles from January till September 30, 2020. Below is Table 1, which shows the collected data.

Table 1 Collected COVID-19/coronavirus newspaper source and number

Country	Newspapers	No. of Articles
Japan	The Japan Times, Asahi Shimbun, Mainichi Shimbun	18,846
India	Hindustan Times, The Indian Express	44,578
Total		63,424

3.2 Topic Modeling and Top2Vec

In NLP, a universal problem is organizing, searching, and summarizing a large volume of text. Topic modeling is used when a large corpus of text cannot be judiciously read and sorted through by a person. A topic model can discover the latent semantic structure or topics present in the corpus. Traditional topic modeling methods use bag-of-words (BOW) representations of documents that ignore word semantics. For example, BOW represents the words “India” and “Indian” as different words despite their semantic similarity. Further, in these methods, stemming and lemmatization (preprocessing of data) are also required, which do not identify the similarity between the words small and short. Finally, the biggest drawback of these methods is that for the best results, you need to know the number of topics in the corpus beforehand [10].

Word2Vec introduced distributed word representations that capture semantic word relationships [14], and Doc2Vec can learn distributed representations of varying text lengths, from sentences to documents [15]. The newly proposed Top2Vec model takes the Word2Vec and Doc2Vec idea further. Top2Vec works on the assumption that many semantically similar documents are indicative of the underlying topic. It produces jointly embedded topic, document, and word vectors such that the distance between them represents semantic similarity. Further, it does not require removing stop words, stemming, and lemmatization of text, and there is no need to have prior knowledge of the existing topics to produce a good topic model.

Figure 1 shows the working of the Top2Vec algorithm. In the first step, jointly embedded document and word vectors are created using Doc2Vec. This step will place documents close to other similar documents and the most distinguished words. The next step will use UMAP [16] to create a lower-dimensional embedding of document vectors. As document vectors in high-dimensional space are very sparse, dimension reduction helps find dense areas. In this, each point is a document vector. The third step would find dense areas of documents using HDBSCAN [17]. Here, the colored areas are the dense areas of documents, and red points are outliers that do not belong to a specific cluster. Finally, each dense area calculates the centroid of document vectors in the original dimension, the topic vector. The purple points are document vectors that belong to a dense area, from which the topic vector is calculated (red points are not used for calculating the topic vector) [18].

4 News, Topic Modeling, and Analysis

News media’s practice of gathering information about issues and events, wrapping them into discrete news stories, and circulating them through various mediums such as print, broadcast, and online can be referred to as newsmaking. This practice of newsmaking is informed by a variety of cultural beliefs and ideological assumptions

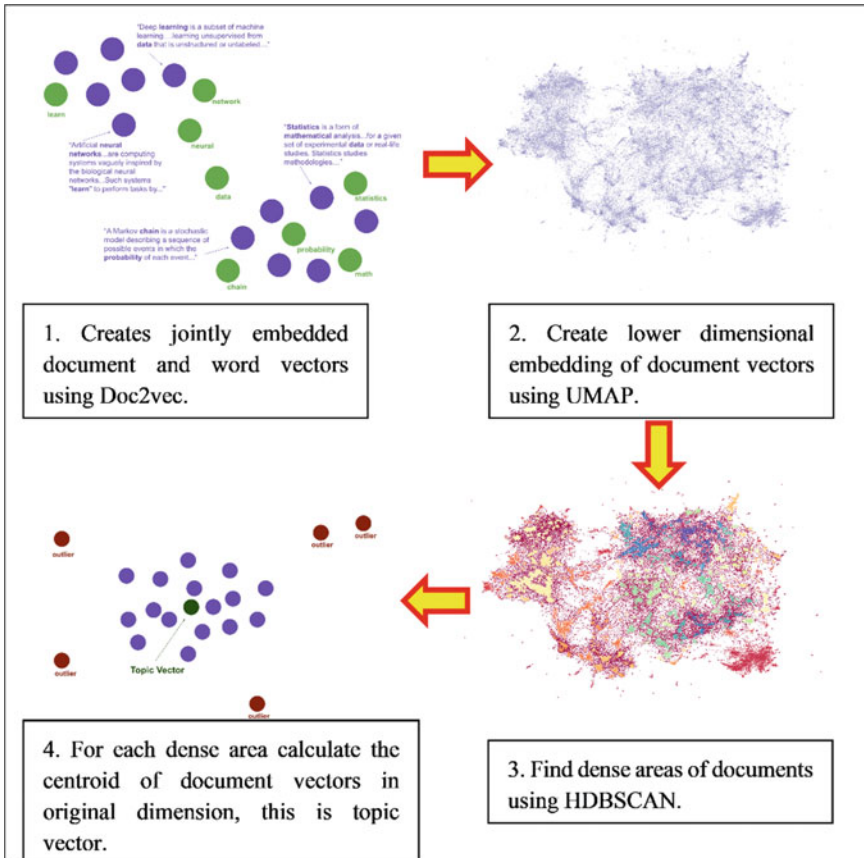


Fig. 1 Collection of images showing four working steps of the Top2Vec algorithm

[19]. Thus, the product of newsmaking—news—is a social text, symbolically incorporating and recirculating those assumptions and beliefs and thereby reproducing social reality.

Topic modeling revealed what (issues, ideologies, events, nations) or who (institutions, individuals) dominated the discourse and what and who was marginalized. Section 4.1 and 4.2 will analyze in detail the results of each country's topic model individually.

4.1 Topic Modeling—Japan

The first case of COVID-19 appeared in Japan on January 16, 2020 [20]. Initially, Japan saw very few infections till March 23, but then there was a rise in infection,

and it continued until the first week of May. Then the second wave hit Japan around the last week of June. The second wave peaked in mid-August, and right now, Japan is going through the third wave with more than 2000 cases every day. At present, the tally of infected people in Japan reached 139,491, with 2051 deaths (till November 28, 2020) [21]. Figure 2 shows daily new cases in Japan.

When we trained our Japan's dataset on the Top2Vec model with the "deep learn" parameter, it took five hours and came up with 238 topics. The largest topic consists of 500 articles, and it is about "postponement of Tokyo 2020 Games." Three topics—"South Korea's parliament elections," "Japan's tennis star Kei Nishikori tested positive for Coronavirus," and "the political unrest in Belarus"—with 22 articles are the smallest topics in Japan's data. Table 2 shows the top ten topics with topic size (number of articles), top keywords, and topic labels. (The topic label is not provided by the model. It has been given based on top words by the authors of this paper.)

Out of the top ten topics, topics 3 and 5 are about the stock market. Japan is a mercantile state, and its focus is always on economic issues. The presence of stock market news on top confirms this nature of the Japanese state. The Japanese government has viewed The Tokyo 2020 Games as a huge opportunity to jump-start its declining economic growth. However, due to the coronavirus pandemic, these games were postponed, which was a huge setback for Japan. This explains the reason for the postponement of the Tokyo 2020 Games as the top topic very clearly. This pandemic has a severe impact on both global and individual country economies. Japan's economy was already facing trouble even before the pandemic due to various sociopolitical issues.

Other than the pre-WWII historical connections, Japan has geo-political interests with both South and North Korea. While North Korea is perceived as a security threat, South Korea is an ally. From that perspective, Japan keeps a close eye on both countries in the Korean peninsula. This is visible in topics 6 and 8. While topic 6

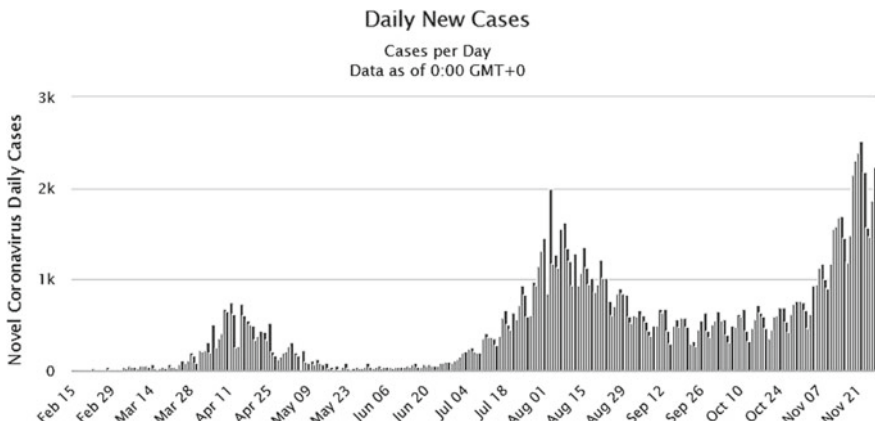


Fig. 2 Daily new infections in Japan [21]

Table 2 Top ten topics with size, top keywords, and label in Japan's data

No	Topic Size	Top keywords	Label
1	500	IOC, Athletes, Olympic, Olympics, Bach, Paralympics, Postponement, Games, Paralympics, Federations	Postponement of Tokyo 2020 Games
2	456	League, Bundesliga, Soccer, Club, Bayern, Matches, Murai, Champions, Stadiums, Relegation	Soccer News
3	302	Decliners, Section, Advancers, Brokers, Fetched, Yen, Shares, Issues, Outnumbered, Investors	Stock Market (especially Nikkei) News
4	298	Eiju, Inpatients, Outpatients, Taito, Hospital, Kanagawa, Hospitalized, Patients, Saitama, Resting	Infections in Japan's Prefectures
5	278	Stocks, Dow, Nasdaq, Investors, Gains, Benchmark, Composite, Markets, Wall, Indexes	Stock Exchanges around the World
6	260	KCDC, Eun, Seoul, Kyeong, Kwon, Sye, Daegu, Kyun, Jeong, Itaewon	South Korea's Coronavirus News
7	255	Prefectures, Declaration, Hyogo, Hirofumi, Emergency, Governors, Kanagawa, Saitama, Nishimura, Yoshimura	Prefectures News
8	233	Pyongyang, Kim, Jong, Un, North, KCNA, Korean, Kaesong, Koreas, Yo	North Korea News
9	206	Elementary, Education, School, Academic, Schools, Hagiuda, Boards, Junior, Classes, Teachers	Impact of the Pandemic on Education
10	197	Music, Artists, Performances, Musical, Band, Musicians, Orchestra, Theater, Album, Concert	Music and Theater in the Time of the Pandemic

is about pandemic-related news in South Korea, topic 8 focused on North Korean defense and security-related news.

Education and Art (Cinema, Music and theater) industries are among the most severely affected sectors during this pandemic worldwide. Both sectors are trying to find a new way if they want to survive this pandemic. Topics 9 and 10 show that in Japan, these sectors are also given a large space. Topic 9 is about the pandemic's impact on education, teaching methods, and parents' concern about the kid's education and well-being. Topic 10 is especially about various news related to Japan's music industry. J-POP stars have a huge following in Japan and other Asian countries, and their concert attracts a large crowd. However, the pandemic put a full stop to these events.

Other top topics are about soccer leagues and infections and situations in various prefectures in Japan.

4.2 Topic Modeling—India

The first case of Coronavirus infection appeared in India on January 30, 2020. However, till March end, there were very few cases reported. After that, India saw a gradual rise in new cases and peaked in the second–third week of September. At its peak, India had around 98,000 new infections every day. Since then, there has been a decline in new cases, but India is still clocking an average of 43,000 cases every day [22]. Figure 3 shows daily new cases in India.

Since the Indian dataset is larger than the Japanese one, it took around 10 h to train our Top2Vec model with the “deep learn” parameter. The model came up with 379 topics. The biggest topic with 1245 articles is “cricket, especially postponement of Indian Premier League (IPL).” “Locust attack” and “Charted Accountant (CA) exam” related topics were the smallest with 20 articles each. Table 3 shows the top ten topics, top keywords, and topic labels in the Indian dataset.

Cricket is the most popular sport in India, and IPL (20–20 format) since its inception in 2008 has achieved tremendous commercial success in India. Just like Soccer leagues or Baseball leagues, people in India look forward to the IPL. However, due to the coronavirus pandemic, it was postponed (presently in progress in UAE). IPL popularity can be verified by the top spot it achieved in the Indian dataset. Though on-ground soccer is comparatively less popular than cricket, however, the viewership of several soccer leagues in India is very high, and that is why media gave it a large space in the sports section. However, its position as the third top topic is unexpected.

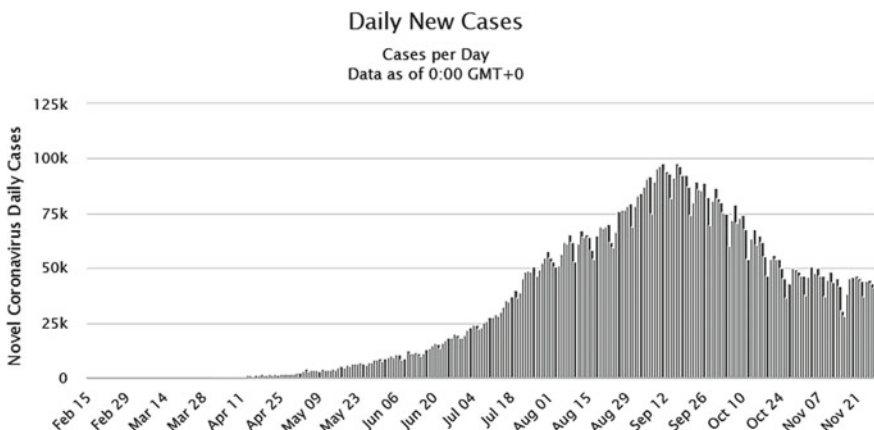


Fig. 3 Daily new infections in India [22]

Table 3 Top ten topics with size, top keywords, and label in India's data

No	Topic size	Top keywords	Label
1	1245	Cricket, ODI, Espnccrinfo, I.P.L., ODI's Cricketing, Batsman, Cricketers, Pacer, Overs	IPL and cricket related
2	617	Faridkot, Jalandhar, Ludhiana, Gurdaspur, Sangrur, Hoshiarpur, Surgeon, Patiala, Moga, Kapurthala	Punjab News
3	563	Relegation, Midfielder, Club, League, Bundesliga, Europa, Guardiola, Champions, Defender, Juventus	Soccer league (especially UEFA)
4	467	Vaccine, AstraZeneca, Vaccines, Oxford, Doses, Moderna, Trials, Pfizer, Biontech, Preclinical	Vaccine development
5	417	ICMR, PCR, RT, Diagnostic, Rapid, Polymerase, Laboratories, Testing, Antibody, Antigen	ICMR and Testing
6	416	Pdt, Apr, Feels, Enjoying, Myself, Adds, Asserts, Feel, Things, Negativity	Celebrities at Home
7	408	Classes, Teachers, Learning, Classroom, Teaching, Worksheets, Curriculum, Syllabus, Schools, School	Education during pandemic
8	406	Kejriwal, Baijal, Satyendar, Arvind, Sisodia, DDMA, LNJP, Lieutenant, Beds, Delhiites	Delhi related
9	396	Cuomo, York, Arizona, Americans, Florida, Governors, Pence, Trump, Democrat, Republican	US (especially New York) related news
10	396	PIL, Petitioner, Bench, Advocate, Petition, Hearing, Litigation, Petitioners, HC, Submissions	Petition in Bombay High Court

Many nations, multinational pharmaceutical companies, and research institutes are currently working tirelessly to develop effective vaccines against COVID-19. India is not only a very big market but also has a world-renowned pharmaceutical industry. Keeping that in mind, news related to vaccine development for COVID-19 is understandable. Indian Council of Medical Research (ICMR) is the government body handling the medical research aspect of this pandemic in India, and it is responsible for testing. At the starting of India's COVID-19 timeline, there was criticism of ICMR for low testing. Availability of personal protective equipment (PPE) kit for frontline warrior was also an issue that led to the criticism of ICMR. ICMR and testing-related news was on number 5 in the Indian dataset.

Education is one of the most severely impacted sectors all over the world. This pandemic has forced the world to change the ways to impart education. While online education (just like work from home) opened the door for imparting education for

some sections of society, online education is inaccessible for many in villages and poor students in cities. Completion of the curriculum before the exam also became a critical issue. Topic 7 is one of the topics that show the impact of the pandemic on education in India.

News about infections in the USA, especially New York, celebrities during the lockdown, various petition filed in Bombay High Court, and Delhi and Punjab related are also featured in the top 10 topics.

5 Comparative Analysis and Consideration

After describing the topic model results for individual countries in Sects. 4.1 and 4.2, this section would provide a comparative analysis of Japan and India topic models. It would be fascinating to study what are common and different themes in both countries. Further, the applicability and benefits of NLP especially topic modeling in deciphering large dataset are provided in consideration.

5.1 Comparative Analysis of Japan and India Topic Models

Tables 2 and 3 shows that in both countries, the biggest topic is sports related. For Japan, it is the postponement of the Tokyo 2020 Games (topic size—500 articles), and for India, it is the postponement of IPL (topic size—1245 articles). Olympics are the biggest sporting event, and organizing it is considered an honor. Moreover, it brings an opportunity for the host nation and city economic benefits. This makes “the postponement of Tokyo 2020” the biggest news for Japan. On the other hand, “Cricket is a religion in India.” IPL has seen exponential growth in the past decade. A huge amount of money is involved in it, so it became the biggest sporting casualty for India. Other sports-related topics are also present. Topic no. 2 with 456 articles in Table 2 and topic no. 3 with 563 articles in Table 3 both show soccer-related news in both countries’ dataset. These topics show that sports are a very widely covered section in Japan and India, even during pandemic times.

Another common topic between the two countries is “Education.” Topic no. 9 in Table 2 with 206 articles and topic no. 7 in Table 3 with 406 articles show the “impact of the pandemic on education” in both Japan and India, respectively. Till now, school education is provided face to face. However, the nature of this pandemic (easily spreadable) makes this extremely dangerous. Hence, education is another severely impacted sector across the world. The presence of education in top topics in both countries verified this. This pandemic forced the world to adapt to online learning methods, which was restricted to higher education only in the form of massive open online courses (MOOC). Currently, even primary school kids have online classes every day.

Table 4 Issues that have an impact on millions but got less attention in the Indian dataset

Topic No	Topic size	Top keywords	Label
29	275	Kuan, UPSRTC, Migrants, Busses, Hometowns, Migrant, Bus, ISBT, Ferrying, Laborers	Exodus of Migrants
205	85	Skill, Employment, Skilled, Opportunities, Unskilled, Jobs, Seekers, Mapping, Job, Employers	Employment-related

Entertainment (movies, music, or theater) has a special place in human society. Whether watching movies in the cinema halls, attending music festivals, or going to the theaters are social activities. This pandemic put a full stop on every social activity. Because of this, the entertainment industry is also affected tremendously. Hence, the last common topic is entertainment or art related. Topic no. 10 with 197 articles in Table 2 is related to the pandemic's impact on music concerts and theaters in Japan. While topic no. 6 with 416 articles in Table 3 is focused on celebrities and their activities on social media. In Japan, J-POP stars are very popular, and thousands of people attend their concerts. At the same time, Bollywood celebrities have a special place in Indian society. This explains the presence of entertainment industry-related news as one of the most talked-about topics in both countries.

As explained in the above paragraphs, in both countries, sporting events, education, and entertainment are critical sectors where the coronavirus pandemic's impact is felt. However, from a socioeconomic point of view, there are some other critical issues also. For a mercantile nation like Japan, economics and trade (represented by the stock market) are high priority issues. The presence of stock market-related news (topic no. 3 and 4 in Table 2) in Japan's top topics can be justified from this perspective.

In India, the “Exodus of Migrants workers” was one of the biggest humanitarian crises in recent memory. However, this issue came in the 29th position with only 275 articles. “Unemployment” or “Job loss” is another critical issue that impacted millions of Indians, but this issue came up in the 205th position. This shows that Indian media has given less space to the issues that have a large socioeconomic impact on millions of people in India. Table 4 shows the two topics mentioned above, with the topic no., size, keywords, and labels.

5.2 Consideration

Our research utilizes a topic modeling approach to comprehend a large volume of COVID-19 themed news articles and presented the results in the comparative analysis section. In this way, we found the hidden patterns and themes in our dataset and know what topics or issues are prioritized and which are not. The task of this nature would have taken extensive human resources and a significant amount of time without using

NLP and ML techniques such as topic modeling. Moreover, by using these tools, we can also keep subjectivity out of the way from influencing the results.

Further, our research presents one method to comprehend the impact of coronavirus pandemic on different societies. This pandemic has influenced almost every aspect of human society, such as health, politics, economic, entertainment, sports, and education. To understand this, media, especially newspapers, are a very critical source. Newspapers are not just the source of disseminating information, but they have the power to help in the emergence of public opinion. Our research provides two crucial findings. One finding helps us understand various hidden themes and issues in both countries. The other finding is about the media's negligence or failure to prioritize issues of grave concern (unemployment and migrant crisis) and concentrate on trivial news (celebrities' everyday lives).

6 Limitations

Newsmaking and news are dependent on various commercial and ideological interests of the media organization. Each news agency or newspaper company has a targeted audience, and its news tries to cater to this audience. For example, in Japan, where the English-speaking population is very limited, English newspapers (both print and online) target foreign citizens living in Japan. In India, the English language newspaper's targeted audience is the middle class in cities. In this way, many critical stories or issues did not find space in these newspapers. Though the newspapers from where data is collected are national level and reputed, the collected data cannot be termed representative of the whole nation, especially in big countries such as India. These are some limitations of this research.

7 Conclusion

The coronavirus pandemic is still wreaking havoc worldwide even after nine months since the first reported case. Many nations shut down all the activities to stop or prevent the spread of the SARS-CoV-2 virus in a large population. Because of this reason, the socioeconomic impact of this pandemic is also very huge. From the analyses of COVID-19 themed news articles by using topic modeling Top2Vec model, we discovered issues and themes critical for Japan and India. The reasons for choosing Top2Vec are numerous. Compared to traditional topic models, Top2Vec does not require stemming and lemmatization and creates the joint document and word semantic embedding to find topic vectors. Moreover, it also discovers the number of topics automatically. Our topic models result shows that socioeconomic issues that impact Japan (postponement of Tokyo 2020 Games, Education, and Entertainment) is very well covered. The Indian media also covered some critical issues (education, vaccine development, and ICMR and testing). The comparative analysis

shows that both countries have common topics such as sporting events postponement, education, and entertainment. Japanese media also gave priority to stock market news because of its criticality for Japan. However, Indian media gave very little space to the migrant crises and unemployment that impacted millions. In this way, by using topic modeling on COVID-19 news articles, our research provides a complete comparative analysis of the coronavirus pandemic's socioeconomic-political impact on Japan and India. Achieving unbiased results with minimal human resources in significantly less time could not be possible without the NLP techniques such as topic modeling.

References

1. WHO. Novel Coronavirus (2019-nCoV). <https://web.archive.org/web/20200202151307/https://www.who.int/westernpacific/emergencies/novel-coronavirus/>, Last accessed 2020/10/13
2. Ma J. Coronavirus: China's first confirmed Covid-19 case traced back to November 17, South China Morning Post. <https://www.scmp.com/news/china/society/article/3074991/coronavirus-chinas-first-confirmed-covid-19-case-traced-back>. last accessed 2020/10/13
3. Worldometers Coronavirus. <https://www.worldometers.info/coronavirus/>. Last accessed 2020/11/28
4. WHO. Coronavirus disease (COVID-19) outbreak. <https://www.who.int/westernpacific/emergencies/covid-19>. Last accessed 2020/11/28
5. Tokyo 2020. Olympic Games postponed to 2021. <https://tokyo2020.org/en/news/joint-statement-from-international-olympic-committee-and-tokyo2020>. Last accessed 2020/10/13
6. Chandrashekhar V. 1.3 billion people. A 21-day lockdown. Can in India curb the Coronavirus? Science. <https://www.sciencemag.org/news/2020/03/13-billion-people-21-day-lockdown-can-india-curb-coronavirus>. Last accessed 2020/10/13
7. Papadimitriou CH et al (2000) Latent semantic indexing: a probabilistic analysis. *J Comput Syst Sci* 61(2):217–235
8. Blei DM, Ng AY, Jordan MI (2003) Latent dirichlet allocation. *J Mach Learn Res* 3(Jan):993–1022
9. Arora S, Ge R, Moitra A (2012) Learning topic models—going beyond SVD. In: 2012 IEEE 53rd annual symposium on foundations of computer science, IEEE
10. Angelov D (2020) Top2Vec: distributed representations of topics. arXiv preprint [arXiv:2008.09470](https://arxiv.org/abs/2008.09470)
11. Singh V, Poonia RC, Kumar S, Dass P, Agarwal P, Bhatnagar V, Raja L (2020) Prediction of COVID-19 corona virus pandemic based on time series data using Support Vector Machine. *J Discrete Math Sci Cryptography* 23(8):1583–1597. <https://doi.org/10.1080/09720529.2020.1784535>
12. Bhatnagar V, Poonia RC, Nagar P, Kumar S, Singh V, Raja L, Dass P (2020) Descriptive analysis of COVID-19 patients in the context of India. *J Interdisc Math* 1-16. <https://doi.org/10.1080/09720502.2020.1761635>
13. Kumari R, Kumar S, Poonia RC, Singh V, Raja L, Bhatnagar V, Agarwal P. Analysis and predictions of spread, recovery, and death caused by COVID-19 in India. In: Big data mining and analytics. <https://doi.org/10.26599/BDMA.2020.9020013>
14. Mikolov T et al (2013) Efficient estimation of word representations on vector space. arXiv preprint [arXiv:1301.3781](https://arxiv.org/abs/1301.3781)
15. Le Q, Mikolov T (2014) Distributed representations of sentences and documents. In: International conference on machine learning
16. McInnes L, Healy J, Melville J. Umap: uniform manifold approximation and projection for dimension reduction. arXiv preprint [arXiv:1802.03426](https://arxiv.org/abs/1802.03426)

17. McInnes L, Healy J (2017) Accelerated hierarchical density based clustering. In: 2017 IEEE International Conference on Data Mining Workshops (ICDMW), IEEE, pp 33–42
18. Angelov D. <https://github.com/ddangelov/Top2Vec>. Last accessed 2020/10/14
19. Reese SD (2001) Prologue—framing public life. In: Reese SD, Gandy Jr OH, Grant AH (eds) *Framing public life*. Lawrence Erlbaum, Mahweh, NJ, pp 7–31
20. WHO. Novel Coronavirus—Japan (ex-China). <https://www.who.int/csr/don/16-january-2020-novel-coronavirus-japan-ex-china/en/>. Last accessed 2020/10/14
21. Worldometers Coronavirus. <https://www.worldometers.info/coronavirus/country/japan/>. Last accessed 2020/11/28
22. Worldometers Coronavirus. <https://www.worldometers.info/coronavirus/country/india/>. Last accessed 2020/11/28

Double-Sided Split Ring Resonator-Based Probe Feed Patch Antenna with Enhanced Bandwidth for 5G and Ku Band Applications



E. Kusuma Kumari , M. Vinod Kumar, Purnima K. Sharma , and S. Murugan

Abstract This paper discusses the enhancement of bandwidth in coaxial probe feed antenna achieved with double-sided complementary split ring resonator (CSRR). The split ring resonator loaded antenna is designed on an RT/duroid 5880 dielectric substrate with the relative permittivity of 2.2 and the thickness of 1.6 mm. The length and width of the substrate and antennas are 200 mm × 180 mm and 40 mm × 30 mm, respectively. The dimensions of SRR were chosen to achieve the maximum bandwidth. To determine the features expansion, a conventional antenna without complementary split ring resonator is designed using the substrate to operate at the same resonant frequency 2.4 GHz. Antenna structures like simple probe feed, single-sided SRR loaded on substrate, and double-sided SRR structures were designed, and characteristics of all structures are compared each other in terms of, return loss, VSWR, gain, and radiation pattern. From the designed antenna result, it is shown that the implementation of double-sided split ring resonators on substrate and ground can achieve the bandwidth enhancement was achieved compared to conventional simple probe feed antenna from 30 MHz to 11 GHz.

Keywords UWB antennas · SRR · Millimeter wave · 5G Communications · Metamaterials

1 Introduction

Microstrip antennas (MSAs) have been extensively used in high performance millimeter wave, 5G, satellite, and wireless communication applications with their exclusive features such as low cost, low profile, light weight, simplicity of fabrication, and compatibility to incorporate with circuit technology. Compactness, good efficiency, and wide bandwidth are the essential requirements for such antennas. However, the latter wide frequency bandwidth is still an inherent problem and a point of challenge in design of these kind of antennas [1]. Increasing the height of

E. K. Kumari · M. V. Kumar · P. K. Sharma · S. Murugan
ECE Department, Sri Vasavi Engineering College, Tadepalligudem, Andhra Pradesh, India
e-mail: hod_ece@srivasaviengg.ac.in

the substrate, stacked patches or addition of parasitic elements and direct coupled patch elements [2] strip foam inverted patch can surely expand the bandwidth but they lead to low profile benefit of the antenna. Further, broad bandwidth can be reported from other types of designs such as inserting U-shaped and multi-U-shaped slots and arc-shaped slots E-shaped patch using air as the substrate. The recent advancements in antenna design and the communication devices are becoming smaller and supporting multiple operations. To fulfill the increasing need of wireless communication demands, broadband antennas with acceptable radiation characteristics are required. Metamaterial (MTM) can be used to improve the characteristics of antenna [3, 4]. The antenna performances can be improved with MTMs [5]. In the past decade, the metamaterial-based applications were widely investigated and presented due to their exciting unusual and attractive features [6]. Electrically small antenna designs have been realized with the well-known split ring resonators (SRRs) and their coequal, complementary split ring resonators (CSRRs). Metamaterials can be integrated as a part of the antenna design to decrease the size of antennas without effecting its performance. The most interesting technologies in the millimeter wave sub-6 GHz band are the sub-6-GHz Wi-Fi and sub-6 GHz 4G long-term evolution (LTE) due to the existence of continuous and broad spectrum in millimeter wave spectrum from 6 to 100 GHz (i.e., ~94 GHz).

2 Literature Survey

DGS, CSRR, Insertion of Vias and Varying the Vias Diameter are the different parameters by which the filter characteristics can be improved. The DGS and CSRR might improve the filter characteristics [7].

Michalis Nitas et al.—the potentiality of high-capacity wireless transmission of multi-gigabit-per-second (Gbps) data rates is offered by high-bandwidth underutilized millimeter wave (mmWave) [8].

W. Aditomo, N. Ismail, and W. Aditomo et al.—reduction in size, improvement in the gain, bandwidth enhancement, and also multiband operations can be achieved in the performance of antennas with metamaterial structures [13–15]. Therefore, depending on application, technical requirements, and metamaterials will be employed in the design of the antenna.

Adamu Y Iliyasu and Achmad Munir et al.—based on the design requirements, the resonant and non-resonant methods are used to design the MTM [9, 10].

Ade Saputra et al.—the split ring resonators (SRRs), complementary SRRs (CSRRs), electric field-coupled LC, etc., are coming under the resonant approach to design the left-handed material [11].

N. Ismail et al.—the resonant presences are narrow band obviously; therefore, the antenna should be properly unified with various design techniques to improve the performance [6, 12].

The metamaterial and complementary split ring resonator (CSRR)-based antennas have attracted the designers because of their unique features and extraordinary results.

More and more attention was focused on to improve the radiation characteristics and bandwidth enhancement which are highly essential requirements and became main key components in huge data rate applications.

Wide bandwidth and good radiation characteristics were achieved by SRR loading on the conventional unloaded monopole antennas. Further, the bandwidth was improved by realizing compact planar microstrip ultra-wideband (UWB) band-pass filter comprises the cascading structure of high-pass filter (HPF) and a low-pass filter (LPF) which uses complementary split ring resonator (CSRR). The presented band-pass filter has a wide bandwidth from 3.0 to 10.7 GHz. Another classical way to achieve wide bandwidth is microstrip antenna combined with a simple CSRRs structure that is cut from the ground plane along with two crossovers via bridges to the CSRRs structure supports impedance match to the basis over a broader bandwidth and maintains better radiation efficiency.

The bandwidth characteristics of CSRR were investigated by various positions of the split for standard rectangular patch applications and found that position of the split SRR can control the bandwidth from 3.2 to 31%.

In this paper, a double-sided split ring resonator-based coaxial probe feed patch antenna was designed and investigated the impact of incorporation of CSRR on both substrate and ground plane. The patch antenna loaded with CSRR has shown the improved performance in radiation characteristics, return loss, and also bandwidth was broadened.

3 Design Concepts of Proposed Antennas

3.1 Conventional Probe Feed Simple Patch Antenna

Initially, the conventional probe feed simple patch antenna was designed without any SRR loading on dielectric substrate of RT/duroid 5880 with the relative permittivity of 2.2 and the dimensions of 200 mm × 180 mm × 1.6 mm. The length and width of patch are 40 mm × 30 mm. Coaxial feed line of $50\ \Omega$ was connected along the orthogonal axis from the center of the patch. During the simulation, the feed location was adjusted to obtain impedance matching at the $50\ \Omega$ source. The center is same for both ground plane and patch as shown in Fig. 1. To validate the designs, structures are modeled by using HFSS Software tool (Figs. 2, 3 and 4).

3.2 Design of Patch Antenna with SRR Loading on Substrate

Displayed by observing the improvement in patch antenna performance after addition of composite SRR substrate in terms of gain, bandwidth, and multi-frequency operations. In this paper, the second antenna was proposed and designed with SRR

Fig. 1 Dimensions of substrate and patch

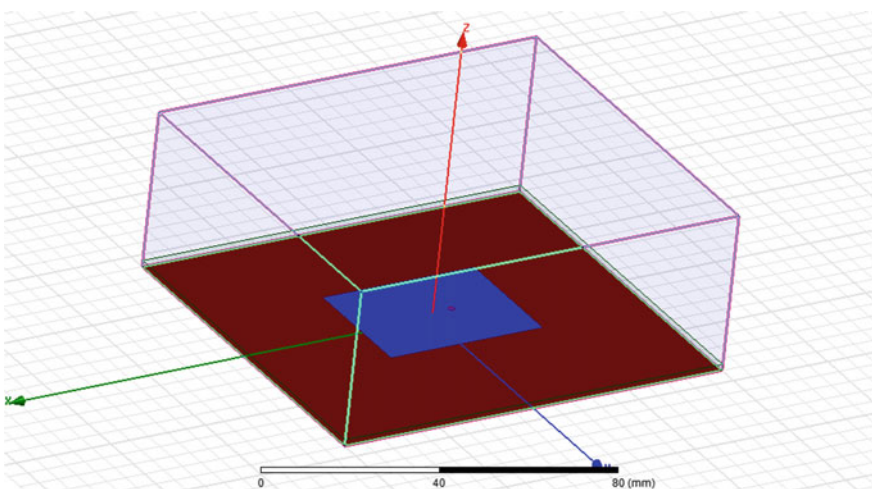
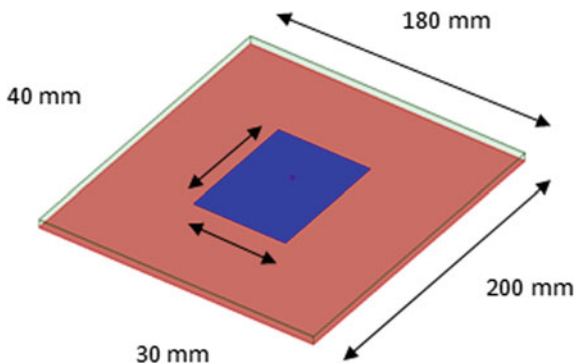


Fig. 2 Design of conventional coaxial feed patch in HFSS tool

loading on substrate with outer metallic square ring structure. The dimensions of square split ring resonator were shown in Table 1. The size and structure of the outer metallic square ring resonator were shown in Fig. 5. The designed antenna was simulated and observed the acceptable performance in terms of return loss, bandwidth, and VSWR compared to conventional probe feed patch antenna.

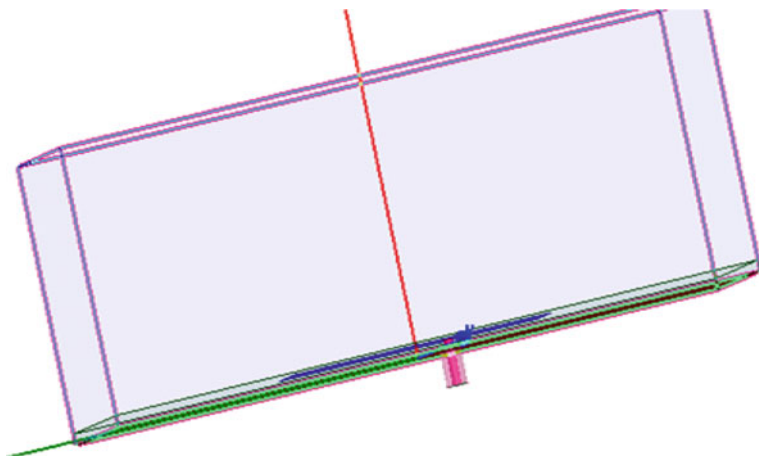


Fig. 3 Coaxial probe feed at the bottom of ground plane

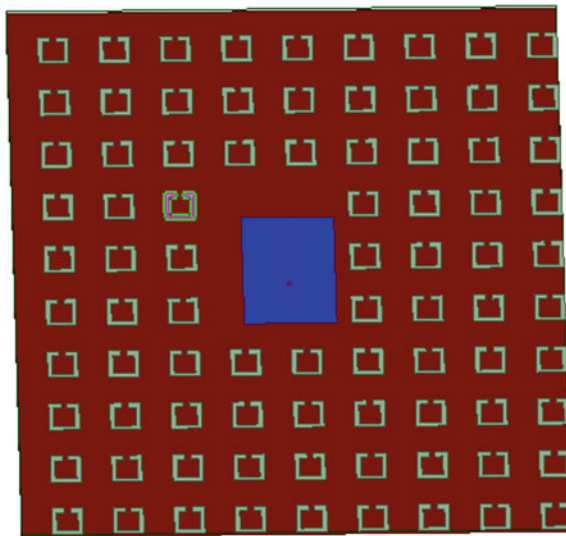


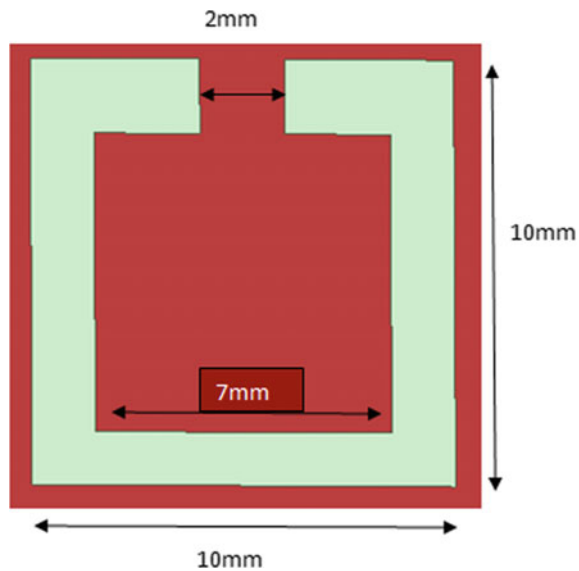
Fig. 4 Front view of antenna with outer square ring SRR loaded on substrate

3.3 Design of Patch Antenna with SRR Loading on Both Substrate and Ground

The third configuration of the antenna was proposed and designed with SRR loading on both substrate and ground. The below figure shows that the only back view of the proposed antenna, i.e., modified ground plane. The periodic outer square ring SRR structures were subtracted from the ground plane. Therefore, the miniaturization of

Table 1 Design parameters of proposed antennas

S. No.	Design parameter	Value in mm
1	Substrate length	200
2	Substrate width	180
3	Substrate height	1.6
4	Patch length	40
5	Patch width	30
6	CSRR outer ring	10×10
7	Outer ring split width	2
8	CSRR inner ring	5×5
9	Inner ring split width	1

Fig. 5 Dimensions of the outer square ring resonator

the antenna was obtained. After simulation, very good results were reported in terms of return loss and bandwidth (Fig. 6).

The below figure shows that two outer square ring resonators were mounted on both substrate and ground are complement to each other in their splits. Therefore, almost CSRR structure was obtained. Hence, the two square rings were separated by distance of substrate height of 1.6 mm. The resultant structure and dimensions are shown in below Fig. 7.

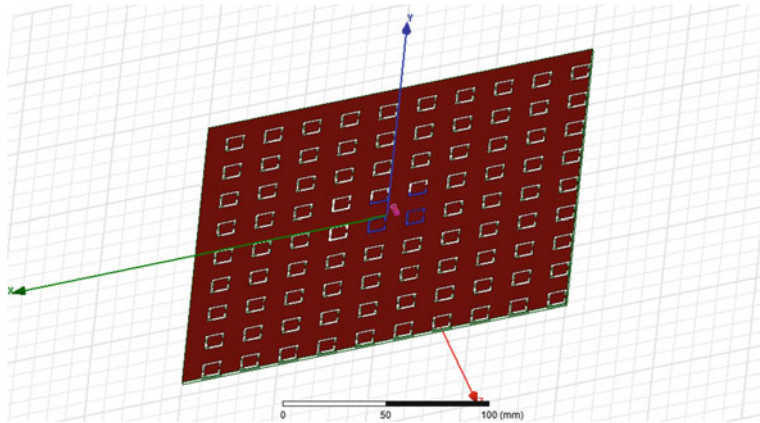


Fig. 6 Back view of antenna with outer square ring SRR loaded on ground

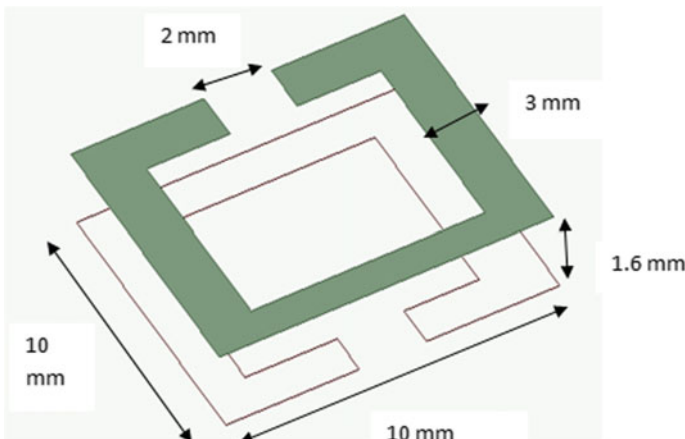


Fig. 7 Structure and dimensions of CSRR

3.4 Design of Patch Antenna with Dual Ring CSRR Loading on Both Substrate and Ground

Displayed finally the fourth configuration of the proposed antenna was designed with square-shaped dual complementary split ring resonators; i.e., outer ring and inner ring were mounted on both sides, i.e., on both substrate and ground plane. Further improvements in the results in terms of wide Bandwidth were observed after simulation using HFSS tool. The following two figures represent the front view and back view of an antenna with CSRR structures (Figs. 8, 9 and 10).

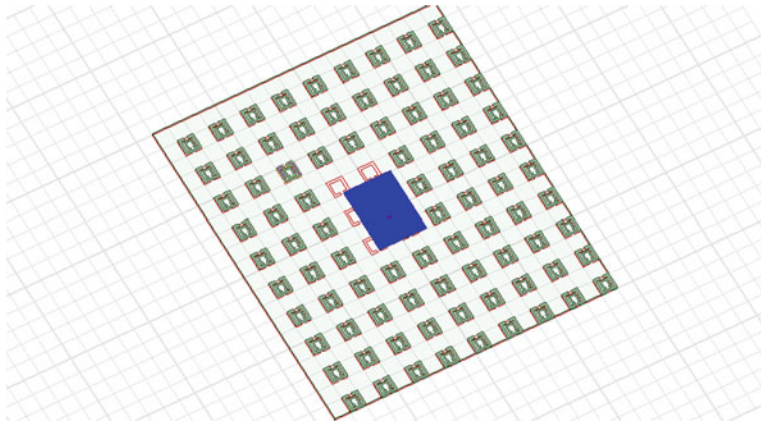


Fig. 8 Front view of antenna (substrate loaded with CSRR)

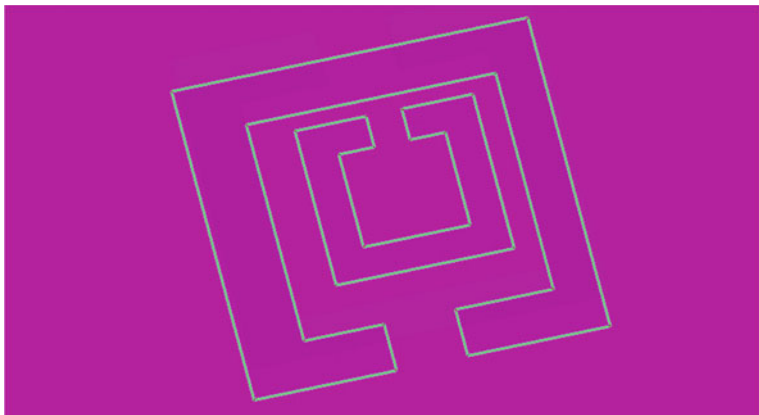


Fig. 9 Two square (outer and inner) split ring resonator

4 Results and Discussions

In this paper, complete antenna design and simulation are carried out with ANSYS HFSS, and it is an industry leading 3D electromagnetic (EM) simulation software tool for antenna design. Antenna was proposed and designed in four configurations. All the four structures were simulated and results in terms of return losses, VSWR, gain, and bandwidth were presented individually. The first configuration of antenna is simple coaxial probe feed patch antenna without any SRR loading. The simulated results are shown in below. The obtained return loss from first configuration is -14.14 dB with the 300 MHz bandwidth was reported along with 2.12 VSWR value.

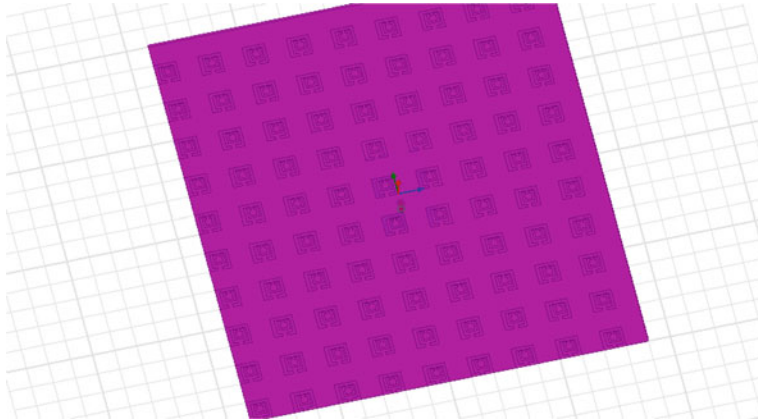


Fig. 10 Back view of antenna (ground plane loaded with CSRR)

The 3D polar plot of radiation pattern is also shown in figure with the high gain of 7.378 dB (Fig. 11).

Further the results of return loss and bandwidth were drastically improved with the application of SRR structure in the antenna design. Therefore, the second configuration of antenna is patch antenna loaded with SRR on substrate. The simulated results are shown in below. The obtained return loss from first configuration is –22 dB with the 10.13 GHz bandwidth was reported along with 2.09 VSWR value. The 3D polar plot of radiation pattern is also shown in figure with the high gain of 7.298 dB (Fig. 12).

The third configuration of antenna was designed in such a way that SRR structure was incorporated on both substrate and ground plane. Compared to earlier designs, the third configuration resultant structure reports a very good performance in terms of return loss, and also, the bandwidth was broadened. The simulation results are shown below. The obtained return loss characteristics from third configuration is –32 dB with the 11 GHz bandwidth was reported along with 2.02 VSWR value. The 3D polar plot of radiation pattern is also shown in figure with the high gain of 7.23 dB (Fig. 13).

The above two antenna configurations were designed with SRR loaded on substrate and ground plane, as the SRR characterized with only square-shaped outer ring. The fourth configuration of antenna was designed in such a way that SRR structure with square-shaped dual complementary split ring resonators were mounted on both sides, i.e., on both substrate and ground plane. Further improvements in the results in terms of wide Bandwidth were observed after simulation using HFSS tool. The simulation results are shown below. The obtained return loss characteristics from third configuration is –16 dB with the enhanced bandwidth of 13 GHz was reported along with 1.98 VSWR value. The 3D polar plot of radiation pattern is also shown in figure with the high gain of 7.203 dB. Compared to all earlier designs, the fourth

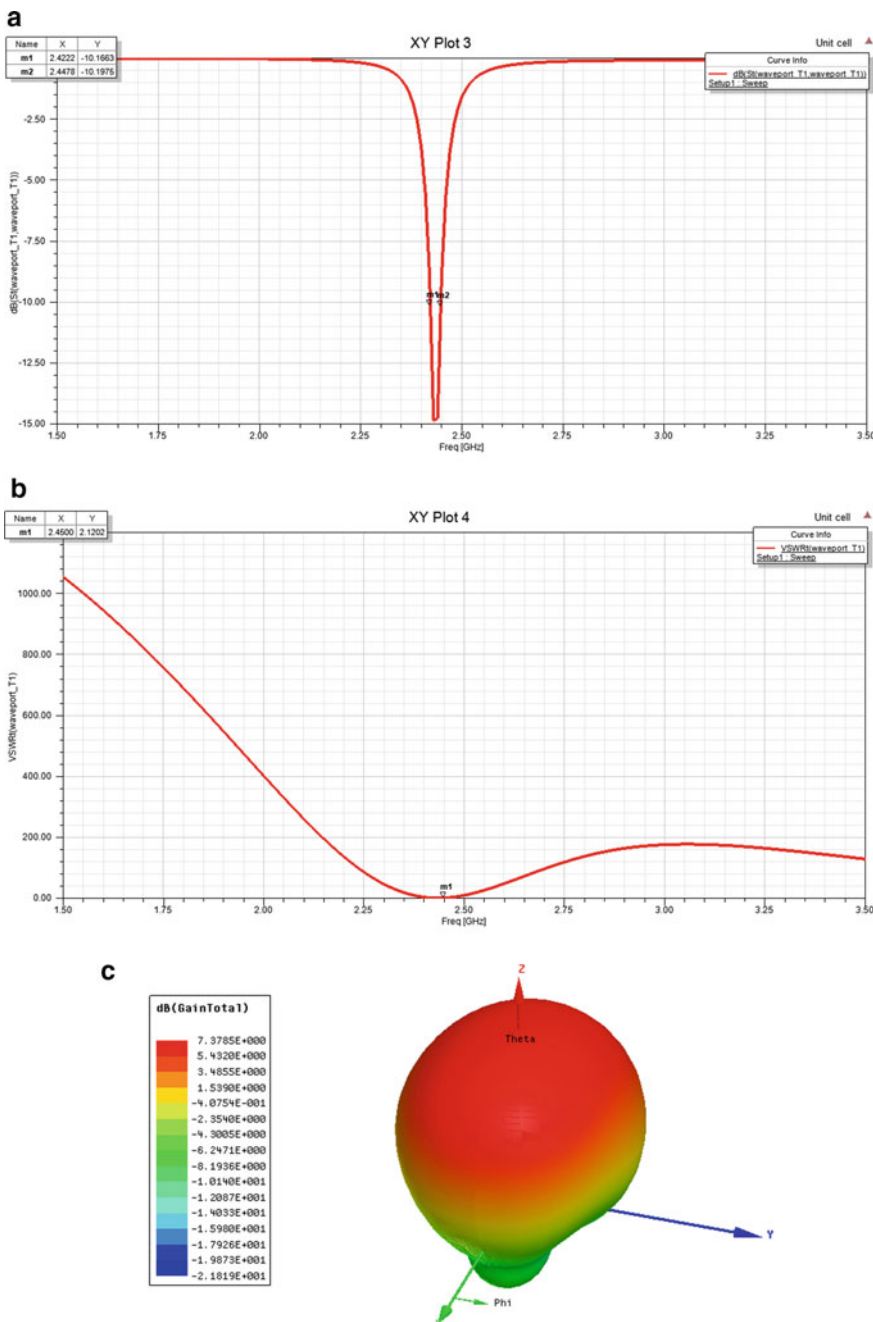


Fig. 11 Simulation results of conventional antenna **a** Return loss characteristics, **b** VSWR Plot, **c** Radiation pattern

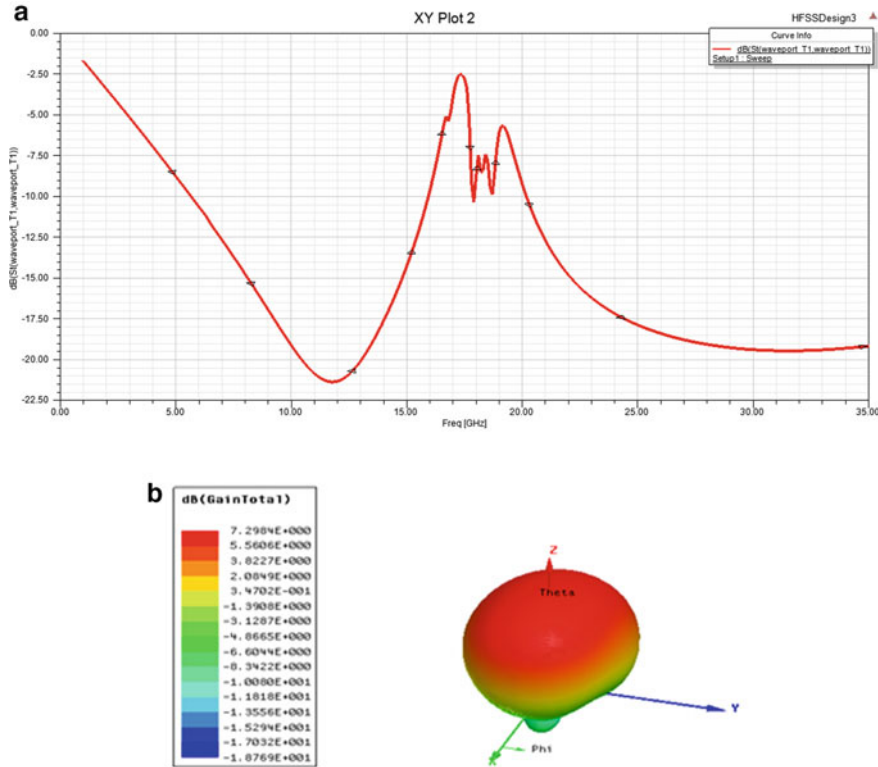


Fig. 12 Simulation results of antenna with SRR loaded on substrate only **a** Return loss characteristics, **b** Radiation pattern

configuration structure shows further better results, yet less return loss is observed as compared to the former cases (Fig. 14).

The reported results from all the four configurations were shown above, and all the performance parameters are comprehensively given and shown in Table 2.

From the above comparison table, it was clearly understood that the incorporation of SRR structure with single outer ring on substrate affects the antenna performance. Miniaturization of antenna size was achieved with third and fourth configurations of antenna with SRR and CSRR on both ground plane and substrates leads to further enhancement in bandwidth.

Results.

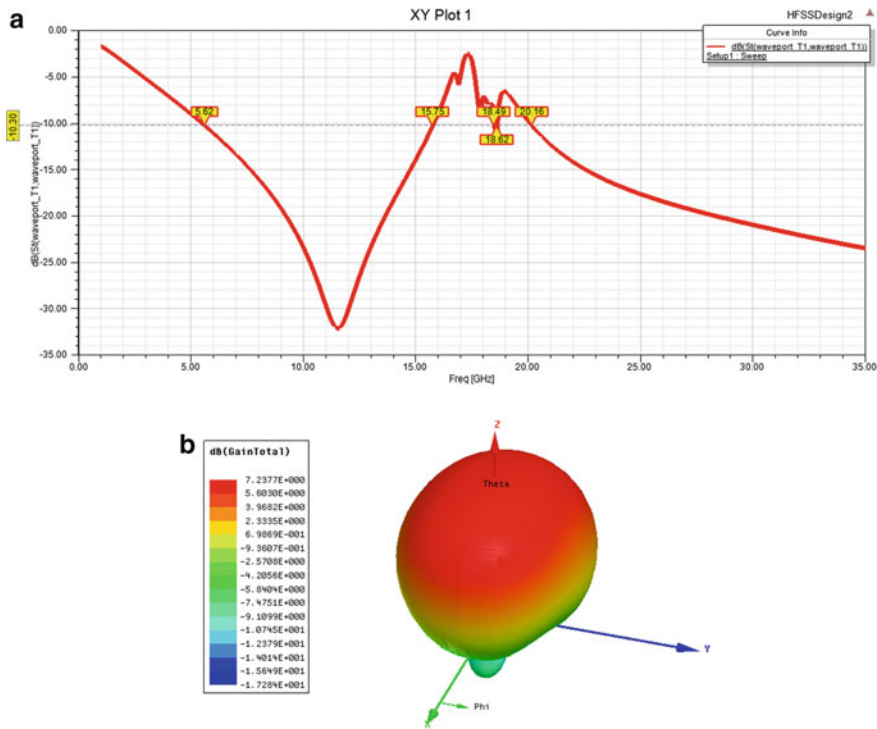


Fig. 13 Simulation results of antenna with SRR loaded on substrate and ground plane **a** Return loss characteristics, **b** Radiation Pattern

5 Conclusion

The bandwidth enhancement of an antenna by incorporating square-shaped CSRR into the substrate and ground plane has been statistically investigated. The proposed antennas with and without CSRR incorporation have been designed with a thickness of 1.6 mm, RT/duroid 5880 dielectric substrate can achieve the bandwidths of 10.13 GHz, 11 GHz, and 13 GHz, while the conventional antenna without CSRR has the bandwidth of 0.03 GHz with the peak gain of 7.37 dB.

The first configuration of antenna is to resonate at 2.4 GHz frequency suitable for WLAN application. From the result, the antenna can be utilized for WLAN application as well as with the broadened bandwidth designed antennas are suitable for millimeter wave applications without much affecting the peak gain of an antenna. Implementing the complementary split ring resonator, structure has hold an important role in effectively enhancing the characteristics of the antenna.

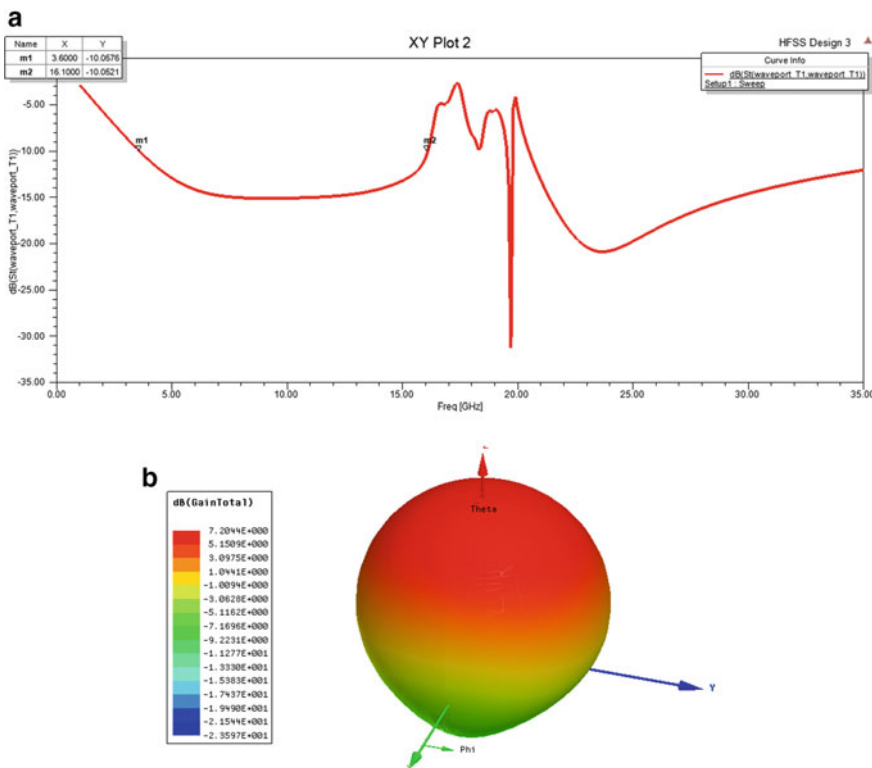


Fig. 14 Simulation results of antenna with dual ring CSRR loaded on substrate only **a** Return loss characteristics, **b** Radiation pattern

Table 2 Comparison of all performance parameters proposed antenna configurations

S. No.	Type of the Antenna configuration	Return loss	Gain	VSWR	Bandwidth
1	Simple probe feed patch antenna	-14.74 dB	7.378 dB	2.12	300 MHz
2	Patch antenna with outer SRR on substrate	-22 dB	7.290 dB	2.09	10.13 G Hz
3	Patch antenna with outer SRR on substrate and ground	-32 dB	7.23 dB	2.02	11 GHz
4	Patch antenna with double-sided SRR on substrate and ground	-16 dB	7.203 dB	1.98	13 GHz

References

- Mohammad A, Mohammad N, Moghadasi RA, Sadeghzadeh F (2015) Bandwidth and radiation specifications enhancement of monopole antennas loaded with split ring resonators. IET Microwaves Antennas Propag 2(5):99–110

2. Farzad A, Changiz G, Javad N, Rasoul Z (2014) Bandwidth enhancement of patch antennas loaded with complementary split-ring resonators. In: Symposium on telecommunications. IEEE
3. Muhammad S, Antonio DC. A compact CSRR Enabled UWB diversity antenna. In: IEEE antennas and wireless propagation letters
4. Michalis N, Savvas R, Vasilis S, Traianos V. Fully planar CSRR-SIW slot antennas of optimized gain and enhanced bandwidth for millimeter wave and 5G communications. In: Proceedings of 2018 IEEE international RF and microwave conference
5. Ismail N, Siregar RA, Nusantara H, Munir A (2018) Wideband substrate integrated-waveguide BPF incorporated with complimentary-split-ring-resonators. In: Progress in Electromagnetics Research Symposium (PIERS-Toyama), Toyama, Japan, pp 1134–1137, Aug 2018
6. Mishra CS, Nayyar A, Kumar S, Mahapatra B, Palai G (2019) FDTD approach to photonic based angular waveguide for wide range of sensing application. *Optik* 176:56–59
7. Ade S, Nanang I, Mochamad Y (2018) Split ring resonator miniaturization of 2.4GHz SIW antenna using complementary split ring resonator. IEEE
8. Ismail, R. Siregar A, Nusantara H, and Munir A. Wideband substrate integrated-waveguide BPF incorporated with complimentary-split-ring-resonators. In: Progress in Electromagnetics, Research Symposium (PIERS-Toyama), Toyama, Japan, pp 1134–1137, Aug. 2018
9. Magthelin Therase L, Jayanthi T. Design of high gain and wideband microstrip antenna using complementary split ring resonator on epoxy resin material. In: Proceedings of the third international conference on I-SMAC (IoT in Social, Mobile, Analytics and Cloud) (I-SMAC 2019) IEEE Xplore
10. Ismail N, Latip A, Hamidi EAZ, Munir A (2019) Defected ground structure for characteristic enhancement of CSRR-based substrate integrated waveguide BPF. In: Progress in Electromagnetics Research Symposium (PIERS), Rome, Italy, Jun (1–4)
11. Aditomo W, Munir A (2013) Bandwidth enhancement of ultra-wideband microstrip bandpass filter using defected ground structure. In: 13th International Conference on Quality in Research (QiR), Yogyakarta, Indonesia, Jun, pp 150–154
12. Aditomo W, Munir A (2013) Bandwidth enhancement of ultra-wideband microstrip bandpass filter using defected ground structure. In: 13th International Conference on Quality in Research (QiR), Yogyakarta, Indonesia, pp 150–154, Jun 2013

A Soft Computing Technique to Optimize Energy Consumption in Wireless Sensor Networks



Anupma Sangwan, Rishi Pal Singh, Garima Popli, and Anju Sangwan

Abstract Reduction in energy consumption is one of the significant issues in wireless sensor networks (WSNs). Optimization of energy consumption plays a significant role in achieving the longer lifetime of wireless sensor networks. In the process of optimization, energy model also plays an important role as it provides the analysis of energy consumption, which is the first step in direction of achieving maximum lifetime for the network. In the present work, an energy model based on the physical and MAC layer parameters is considered which is used to drive optimal transmit power for energy-efficient communication over AWGN channel. Then, a genetic algorithm is implemented to get a better optimal value of transmit power for BPSK modulation.

Keywords Energy optimization · Wireless sensor network · Energy consumption · Energy packet · Genetic algorithm · BPSK modulation

1 Introduction

A thousand of minute nodes, when accompanied in the physical environment in order to monitor objects, temperature and humidity, etc., is termed as wireless sensor network [1]. Energy consumption is the main concern for operation of wireless sensor networks. It is not possible to recharge batteries or replacing them in case nodes are deployed inaccessible manner. So, the lifetime of wireless sensor network is also limited due to the limited battery power of nodes. Therefore, there is a need to search out the alternatives to cope with this problem of limited power. Energy can be extracted from the environment. For example, solar cells can be used to extract energy from the environment. However, the amount of energy that can be extracted from the environment is still limited in nature. So, in order to support the longer lifetime of wireless sensor network, nodes should perform energy-efficient operations. Energy-efficient operations are the most important factor for the designing of wireless

A. Sangwan · R. P. Singh (✉) · G. Popli · A. Sangwan

Department of Computer Science and Engineering, Guru Jambheshwar University of Science and Technology, Hisar, Haryana, India

sensor networks [2]. Transceiver unit is the most significant component of wireless sensor nodes. It is the component, which consumes more energy as compared to the other components in the wireless sensor node. It offers the connection of node to the network. As transceiver consumes more power, so one of the major factors involved in the design of transceiver is low cost, energy-efficiency and low-duty-cycle radio circuits which is the most challenging task. Like the transceiver unit, sensor nodes also have limited processing and memory capabilities due to its size and cost. High computational power can be provided by the small processor [2]. Today, genetic algorithm, a soft computing paradigm, is a hot topic of attention for the researchers those who have an interdisciplinary approach to obtain best results. Genetic algorithms are basically search algorithms based upon the mechanics of natural selection or natural genetic. Genetic algorithms are based on “Survival of the fittest” concept (Darwin Theory) that means fittest generation will survive and reproduce. Successive generations became better and better as compared to the previous generations. Genetic algorithms mimic the process of evolution. Genetic algorithm developed by Prof. John Holland, his colleagues and students at the University of Michigan around 1975.

The rest of the paper is organized as follows: Sect. 2 presents a short review of the role of a genetic algorithm for optimization in WSNs. Section 3 proposes an energy model to derive out optimal energy consumption. Section 4 describes the role of genetic algorithm in the optimization of energy consumption. Section 5 gives the performance evaluation. Finally, Sect. 6 presents the conclusion as well as future scope.

2 Literature Review

Many researchers have advised soft computing paradigms for the optimization in WSNs. The authors in [3] have proposed an optimal energy-efficient clustering technique by making use of a multi-objective genetic algorithm in wireless sensor networks. This algorithm is divided into two levels. At the first level, the algorithm works with a goal of lifetime optimization using different delay values within clustering schemes. At the second level, it works to find out efficient topology to transfer data from sensor nodes to the cluster head. In the end, the results obtained revealed that the proposed algorithm is successful in obtaining efficient clustering scheme for energy optimization. The authors in [4] have discussed a genetic algorithm-based scheme to balance the energy consumption in heterogeneous WSNs. In comparison to the proposed scheme with five state-of-the-art methods, it is found that the proposed scheme greatly expands the life of network. And, the results obtained are improvement of 33.8% and 13% in the network life and average improvement, respectively, based on the first node die and last node die. Moreover, the selection of an optimal set of protocol for the deployment of wireless sensor nodes is a terrific task. The authors in [5] have presented a performance optimization system modeled as a linear formula

by making use of weight vectors as multiple assignment and metrics as obtained by simulations.

Further, genetic algorithms are used for offline optimization. The authors in [6] have given an energy management policy for a specific application without losing any network characteristic with an expansion in the network life span. The authors have used genetic algorithms as an optimization tool, and appropriate fitness functions are obtained for various aspects in order to monitor the network performance. By making the use of genetic algorithm system, the authors have optimized sensor nodes status, selection of cluster head as well as choice between two signal ranges. And, it is found that the proposed genetic algorithm-based system meets all the goals as specified by application specifics. The authors in [7] have used the genetic programming and genetic algorithm in node placement in sensor networks. In the presented work, genetic programming has played the role of a master, as it optimizes the deployment structures by making the use of hybrid technique, and the genetic algorithm has played the role of servant by doing actual node placement in the optimized structure. And, it is found that the use of a genetic algorithm in placement is much better than random deployment. The authors in [8] have studied the use of genetic algorithm on different performance parameters like network lifetime, energy consumption, etc., which impacts network performance greatly. In the presented survey, the authors have to dig out the improvement in all the operational stages of wireless sensor networks by making the use of genetic algorithms. In the end, based on genetic algorithm and simulations, fitness function was fixed, optimized for various operational stages of the network. Kumar et al. [9], Sagtani et al. [10] and Goyal et al. [11] carried out detailed study for WSN and optimized energy consumption.

3 Proposed Energy Model

Reduction in energy consumption is one of the significant issues in wireless sensor networks. Nodes in WSNs have a limited scope of energy budget. Recharging and replacement of the battery are not always possible, especially when nodes are deployed in an impractical environment and hostile environment. Moreover, large-scale deployment suffers from the limited stock of energy source. Optimization of energy consumption plays a significant role in achieving the longer lifetime of the wireless sensor network. Energy model plays important role in achieving the optimization of energy consumption. Because energy model considers all possible options of energy consumption concerning various scenarios taking place during the process of communication, which in turn used to make analysis of energy consumption in overall procedure. This is the primary step in the direction to achieve the goal of maximum lifetime of wireless sensor networks. Physical and MAC layers consumed more energy. Therefore, an energy model based on the parameters of the physical and MAC layer and channel model (AWGN channel) is proposed. The proposed model is used to derive the optimal transmit power for energy-efficient

communication over AWGN channel. The explanation of optimal transmit power in closed form is also proposed for the BPSK modulation scheme [12].

The proposed energy model is derived by analysis of the following:-

- Structure of packet in the communication system.
- Energy consumption of transceiver components.
- Energy consumption of MAC protocols.
- Energy consumption of SMAC protocols.

After the analysis of these energy consumption components, the energy model is being derived by taking into account parameters of these energy consumption components. Analysis of energy consumption components of wireless sensor networks leads to derive the energy consumption model which play a significant role in optimizing the energy consumption in wireless sensor networks. The proposed model used to derive optimal transmit power at which energy consumption can be minimized for communication over AWGN channels. Further, a closed-form expression for optimal transmit power for different modulation schemes is being derived [12]. Description of energy consumption of each component is described as follows:

3.1 General Structure of Packet in Communication Systems

General packet structure in communication systems at the physical and MAC layer is shown in Fig. 1. The packet consists of L_p as the total number of bits, N_p as the physical payload, header and O_p as physical payload. Physical payload became a data frame for the MAC layer which comprises of Mac overhead (O_M) and Mac payload (N_M) [12].

Relation between number of bits (L_p) and raw bit rate (D_r) [12]:

$$L_p = D_r T_p \quad (1)$$

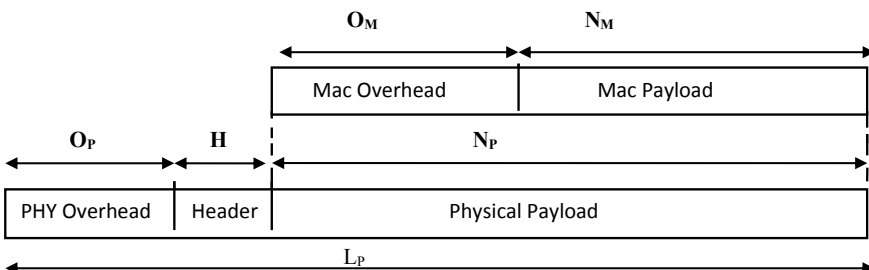


Fig. 1 Packet structure at physical and MAC layers

Relation between number of bits per packet (N_M) and bit rate (R_A) after removing header and overhead [12]:

$$R_A = (N_M/L_p) * D_r \quad (2)$$

Relation between data received per packet (N_S), data bits per packet (N_M) and total probability of success ($1-p_e$) [12]:

$$N_S = N_M(1 - p_e) \quad (3)$$

Energy Consumption of Transceiver Components

Energy consumed by transceiver during transmission and reception is given by T_{px} and R_{px} . At the transmission, side transceiver comprises of baseband digital circuit, analog transmitted circuit and power amplifier. At the receiver, side transceiver comprises of baseband digital circuit, analog receiver circuit and low noise amplifier [12].

Power consumption of components during transmission at transceiver is given by[12]:

$$T_{px} = p_{dct} + p_{act} + p_{amp} + T_p \quad (4)$$

where p_{dct} and p_{act} are power consumption of digital and analog circuit and P_{amp} is the power consumption of amplifier and T_p is transmitted power.

Or

$$T_{px}=T_{po} + (\alpha + 1)T_p \quad (5)$$

Equation (4) can be modeled as Eq. (5) where T_{po} and T_p are transmitted power and $\alpha = \frac{\varepsilon}{\eta} - 1$ where ε is the peak-to-average ratio and η being drain efficiency.

Power consumption of components during reception at transceiver is given by [12]:

$$R_{px}=p_{dcr} + p_{acr} + p_{lna} \quad (6)$$

where $p_{dcr}, p_{acr}, p_{lna}$ is the power consumption of analog and digital circuit and low noise amplifier at the receiver side.

Or

$$R_{px} = R_{po} \quad (7)$$

Equation (6) can be modeled as Eq. (7) where R_{po} is the power consumed during reception at transceiver.

3.2 Energy Consumption of MAC Protocol

This subsection provides an overview of the model for computing energy consumption of MAC protocols. During one data generation interval (T_{data}), sensor node senses the data and then conveys it to the next hop. Through normalized transmission (T_{tx}) and reception (T_{rx}), energy consumption of MAC protocol can be derived as follows[12]:

$$P = T_{\text{tx}}T_{\text{px}} + T_{\text{rx}}R_{\text{px}} + (1 - T_{\text{tx}} - T_{\text{rx}})p_{\text{sleep}} \quad (8)$$

where

T_{tx} and T_{rx} are normalized transmission, T_{px} and R_{px} are the transmitted and received power and p_{sleep} is the time consumed by the transceiver in sleep state.

3.3 Energy Consumption of SMAC Protocol

SMAC protocol is extensively used as energy upkeep protocol in WSNs. It overcomes the problem of idle listening. In SMAC protocol, each sensor nodes having two states namely sleep and active state. Each node shares its sleep schedules with their neighboring nodes using SYNC packets. When SMAC protocol starts to exchange packet carrier sense (CS) to avoid collision, communication between sensors nodes takes place. After that RTS and CTS packets are swapped for data transmission. Each transmission and reception is headed by radio start-up transient T_{sut} [12] (Fig. 2).

Normalized transmission (T_{tx}) and reception (R_{tx}) for transmitting nodes are [12]:

$$T_{\text{tx}} = (3T_{\text{sut}} + l_{\text{sync}}/D_r + l_{\text{rts}}/D_r + l_{\text{data}}/D_r) * 1/T_{\text{data}} \quad (9)$$

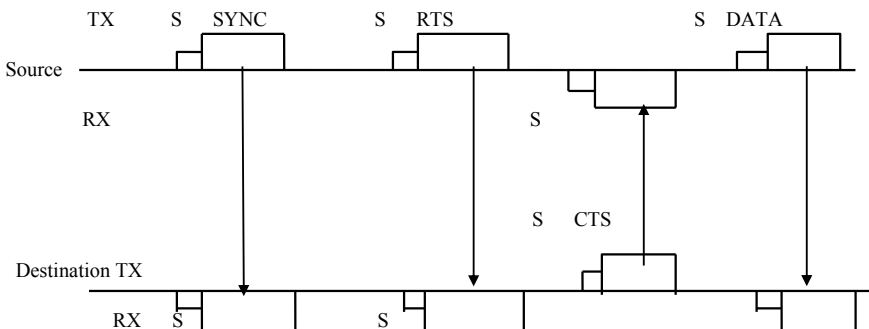


Fig. 2 Communication between nodes in SMAC

$$T_{rx} = (T_{sut} + l_{cts}/D_r) * 1/T_{data} \quad (10)$$

where l_{sync} , l_{rts} , l_{cts} and l_{data} are the length of sync, RTS, CTS and data packet, respectively.

3.4 Energy Model for Total Energy Consumption

Amount of energy consumption of transmitter in transmitting a frame per bit to the receiver can be expressed as follows [12]:

$$E_{bit} = P * T_{data}/(N_m * (1 - P_e)) \quad (11)$$

Energy consumption in terms of transmitted power can be derived by replacing P_e in Eq. (11) by [12]:

$$P_e = 1/2 * e^{(\text{for BPSK modulation})} \quad (12)$$

But SNR per bit is defined as

$$\gamma = p_r/2BN_0 \quad (13)$$

where p_r is received power, B is the signal bandwidth and N_0 is the spectral power density of AWGN channel.

$$\text{Also, } T_p/A_0d^\alpha = p_r \quad (14)$$

where A_0 is the parameter that depends on the transmitter and receiver antenna gain and transmission wavelength, d is the distance between transmitter and receiver and α is the path loss exponent.

By replacing p_r in Eq. (13) with Eq. 14 we get,

$$\gamma = T_p/A_0d^\alpha 2BN_0 \quad (15)$$

On putting Eq. (15) in Eq. (12) became

$$P_e = 1/2 * e^{-\gamma T_p/A_0d^\alpha 2BN_0} \quad (16)$$

By replacing P_e in Eq. (11) by (16) Equation of energy model became

$$E_{bit} = \frac{P * T_{DATA}}{\left(1 - Xe^{\frac{-\gamma T_p}{2Bd^\alpha A_0 N_0}}\right)} \quad (17)$$

For BPSK modulation $X = 0.5$ and $y = 1$.

In order to minimize E_{bit} with respect to T_p ,

$$\text{set } \frac{\partial E_{\text{bit}}}{\partial T_p} = 0$$

Which in turn give following equation:

$$[V + W(U + VT_p)]e^{(-CT_p)} = B/X$$

where

$$U = (T_{\text{tx}}T_{\text{po}} + T_{\text{rx}}T_{\text{po}} + (1 - T_{\text{tx}} - T_{\text{rx}})p_{\text{sleep}})T_{\text{data}}$$

$$V = (\alpha + 1)T_{\text{tx}}T_{\text{data}}$$

$$W = \frac{y}{2Bd^{\alpha}A_oN_o}$$

Closed form expression of optimal transmits power is given by [12] (Table 1):

$$T_p = \frac{1}{W} \ln \left(\frac{V + UW}{V/X} \right) \quad (18)$$

4 Genetic Algorithm(GA) for Optimization of Energy Model

A genetic algorithm is a randomized optimization process which is evolved with an inspiration of existence in variety of environments in natural systems. The initiation of GA takes place with randomly generated population, and with each iteration, a quality measurement is done on individual using a fitness function. The whole evolutionary process relies on three oprations—reproduction, crossover and mutation. In each successive iteration, the newly generated population is compared with previous one until a specified stopping criteria is met (Fig. 3).

In our work, a genetic algorithm is used to optimize the transmitted power model, so that energy consumption per bit can be minimized. Algorithm starts with randomized initial population of distance. Corresponding to each distance values, the optimal value of transmitted power is obtained.

Table1 System parameters and notations used

T_{po}	Constant
R_{po}	Constant
ε/η	Drain efficiency/peak-to-average ratio
H	Header length
O_{PHY}	Physical layer overhead
B	Signal bandwidth
D	Distance between transmitter and receiver
L_{RTS}	Length of RTS
p_{sleep}	Power consumed by sleep state
T_{data}	Data generation interval
D_r	Data rate
N_{PHY}	Physical payload bits
O_{MAC}	MAC overhead
N_o	Spectral power density of AWGN channel
l_{sync}	Length of sync
l_{CTS}	Length of CTS
l_{Data}	Length of data packet
T_{sut}	Radio start-up transient
A	Path loss exponent
A_o	Parameter that depends upon transmitter and receiver antenna gain and transmission wavelength

5 Performance Evaluation

5.1 Optimal Transmission Power for BPSK Modulation at Which Energy Consumption Is Minimized

Using Eq. (18), transmit power is described as follows:

$$T_p = \frac{1}{W} \ln \left(\frac{V + UW}{V/X} \right)$$

where

$$U = (T_{\text{tx}} T_{\text{po}} + T_{\text{rx}} T_{\text{po}} + (1 - T_{\text{tx}} - T_{\text{rx}}) p_{\text{sleep}}) T_{\text{data}}$$

$$V = (\alpha + 1) T_{\text{tx}} T_{\text{data}}$$

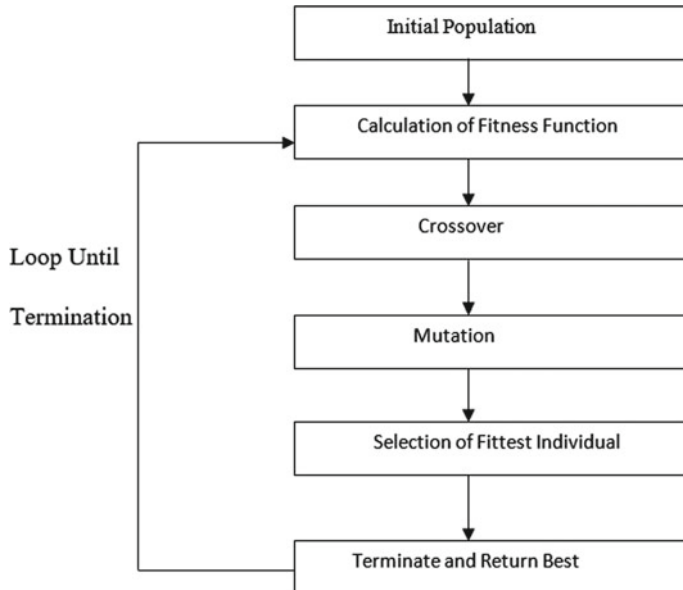


Fig. 3 Basic structure of genetic algorithm

$$W = \frac{y}{2Bd^\alpha A_o N_o}$$

Relation between transmit power and energy consumption per bit (Fig. 4):

$$E_{\text{bit}} = \frac{P * T_{\text{DATA}}}{\left(1 - X e^{\frac{-yT_p}{2Bd^\alpha A_o N_o}}\right)}$$

As shown in figure, optimal transmit power increases with increase in distance in order to minimize the energy consumption per bit [38] (Table 2).

5.2 Optimal Value of Transmit Power After Applying Genetic Algorithm

After applying the genetic algorithm, we get the best optimal value of power as compared to the previous original values of transmit power, which is obtained without applying a genetic algorithm. We get better optimal values of transmit power in the range 40–70. We get the best fit value of distance and transmit power as follows:

Best Distance = 68.6275 (Fig. 5; Table 3).

Optimal Value of Transmit Power = 0.0729.

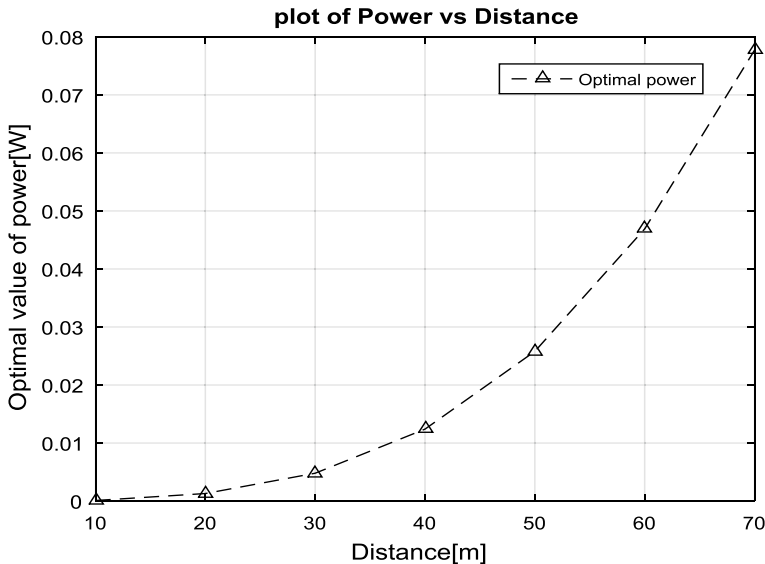


Fig. 4 Optimal transmit power versus distance before applying genetic algorithm

Table 2 Value of transmit power corresponding to each distance before applying genetic algorithm

Distance (in m)	Transmit power (in W)
10	0
20	0
30	0
40	0.02
50	0.025
60	0.045
70	0.079

6 Conclusion and Future Scope

Optimization of energy model using genetic algorithms is performed in existing work. Optimal transmit power values are obtained when a genetic algorithm is applied to the transmit power as a fitness function. Before applying genetic algorithm transmits power values are between ranges (0.02–0.07) Watt for distance values (40–70). After applying genetic algorithm, we get optimal value of transmit power (0.08–0.072) Watt for the distance range (40–70). In addition, we get an optimal value of transmit power corresponding to bandwidth. Before applying a genetic algorithm, we get transmission power values (1.3–4) Watt for bandwidth range (30–100) KHZ. After applying genetic algorithm, we get optimal transmits values (1.8–6) for bandwidth range (30–100) KHz. Optimal transmit power increases with increase in distance and

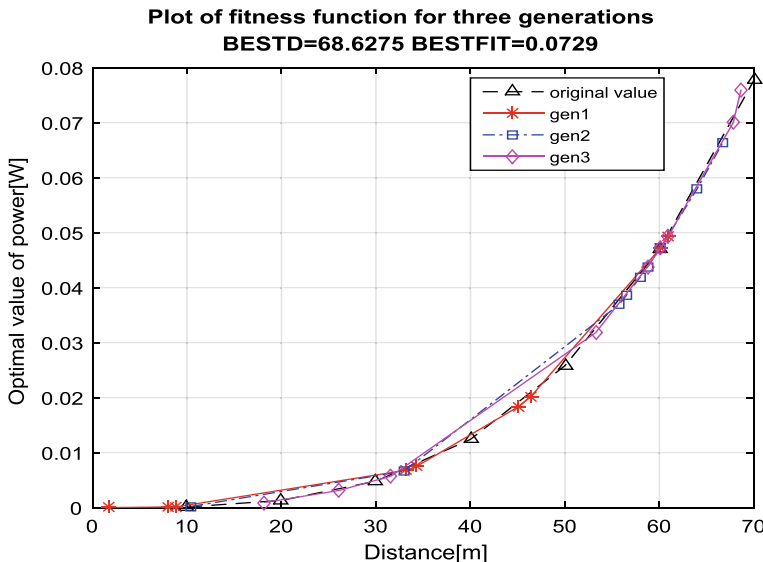


Fig. 5 Optimal transmit power vs distance after applying genetic algorithm

Table 3 Value of transmit power corresponding to each distance after applying genetic algorithm

Distance (in m)	Optimal value of transmit power (in W)
10	0
20	0
30	0
40	0.08 (Optimal value of power)
50	0.03 (Optimal value of power)
60	0.049 (Optimal value of power)
70	0.0729

bandwidth in order to decrease energy consumption per bit. Genetic algorithm plays a significant role in the optimization of energy model considering BPSK modulation. In future with same working manner, we can optimize the energy model using genetic algorithm considering various other modulation schemes like- M-PSK, M-QAM.

References

- Anastasi G, Conti M, Di Francesco M, Passarella A (2008) A survey on energy conservation in wireless sensor network. *Ad Hoc Netw* 7(3):537–568
- Akyildiz FI, Vuran CM (2010) Wireless sensor networks. Wiley, UK
- Peiravi A, Rajabi Mashhadi H, Hamed JS (2013) An optimal energy-efficient clustering method in wireless sensor networks using multi-objective genetic algorithm. *Int J Commun Syst* 26(1):114–126

4. Elhonseny M, Yuan X, Yu Z, Mao C (2014) Balancing energy consumption in heterogeneous wireless sensor networks using genetic algorithm. *IEEE Commun Lett* 19(12):1–1
5. Fan J, Parish DJ (2007) Using a genetic algorithm to optimize the performance of a wireless sensor network, 1–6
6. Ferentinos PK, Tsiligiannis AT (2007) Adaptive design optimization of wireless sensor networks using genetic algorithms. *Comput Netw* 51(4), 1031-1-51
7. Tripathi A, Gupta P, Trivedi A, Kala R (2011) Wireless sensor node placement using hybrid genetic programming and genetic algorithms. *Int J Intelligent Technol* 7(2):63–83
8. Norouzi A, Zaim HA (2014) Genetic algorithm application in optimization of wireless sensor networks. *Sci World J* 2014:1–15
9. Kumar S, Goyal M, Goyal D, Poonia RC (2017, December) Routing protocols and security issues in MANET. In: 2017 International Conference on Infocom Technologies and Unmanned Systems (Trends and Future Directions)(ICTUS). IEEE, pp 818–824
10. Sagtani VK, Kumar S (2014) Modern approach to enhance routing recitation in MANET. *Int J Emerging Technol Adv Eng* 4(7):265–270
11. Goyal M, Poonia SK, Goyal D (2017) Attacks finding and prevention techniques in MANET: a survey. *Adv Wireless Mobile Commun* 10(5):1185–1195
12. Abo-Zahhad M, Farrag M, Ali A, Amin O (2015) An energy consumption model for wireless sensor networks. In: IEEE: 5th international conference onenergy aware computing systems and applications, pp 1–4

Witty City—Smart City on an Intelligent Conway Grid



Prakash Hegade and Girish P. Mallya

Abstract The classics and contemporaries of a smart city design and deliberations demand a self-learning evolutionary model. While numerous models are proposed, implemented, evaluated, and critiqued, the unpredictable challenges inquire a model relevance. This paper proposes a self-learning cellular automaton model based on Conway's Game of Life rules to design a smart city—Witty City. A good city design must encompass the historical data, act upon it to learn, and incorporate future needs with ease. The proposed model uses contemporary data, historical data, and ideal data to predict the city design for time generation instances. Future generations learn and improve based on the predicted results. The tuple model designed on the grid provides a scope to inherit the foundational properties and improve over the environmental constraints. The paper presents the design, rules, tuple definition, and application of the model on a sample data. The basic algorithm procedures to implement the discussed model are also presented for future adaptations. Game of Life is turing complete, and the model promises to be a practical blueprint for building a smart city.

Keywords Cellular automaton · Game of Life · Self-learning · Smart city

P. Hegade (✉) · G. P. Mallya
KLE Technological University, Vidyanagar, Hubli, Karnataka, India
e-mail: prakash.hegade@kletech.ac.in

1 Introduction

‘All cities are mad: but the madness is gallant. All cities are beautiful, but the beauty is grim,’ quotes an American journalist, Christopher Morley [1]. Along with madness and beauty, humankind has also demarcated culture, rooting for dynamics to thrive. Amidst the game of coordination and competition, a city is identified with a multitude of dimensions. Cities are born; they grow and evolve based on human factors, natural factors, and human-made causes and effects. A city has put forth several challenges on the verge of being smart. To name a few, firstly, the factors contributing to the quality of life and livelihood, and their effective management. Secondly, business collaborations can provide cumulative benefits toward globalization—an operative technological portfolio investment for city evolution. Thirdly, to incubate diverse lifestyles and economic backgrounds. Fourthly, plan and design a progression model for various factors like population, climate change, economy, infrastructure, natural resource management, government bodies, and facilities.

Under the efforts of a smart city, several programs and initiatives have been designed to meet the said challenges. However, the ground rules to define a smart city are yet under revision [2]. The city structures have been analyzed, and research challenges are presented for a city as a laboratory for innovation [3]. Efforts have been made to design sustainable smart cities, and challenges have been discussed [4]. Smart cities have been studied with respect to technology and information system perspective [5]. In regards, smartness and intelligence have been argued and debated [6]. Methodological frameworks like SMART models have been recommended for the implementation of smart cities [7]. Cities like Singapore have been studied as case study to evaluate and comprehend the adapted methodologies [8]. The quest for new utopian cities has been modeled [9].

Not only positive growth, but a growing diverse city also has its negative aspects like informal development, population, traffic, waste management, and crime [10]. The research on smart cities has also been critiqued that they appear to be non-ideological, common-sensical, and pragmatic [11]. Though smart cities are intended to assure the quality of life, contemporary disputes demand evolving solutions [12]. This paper attempts to address the gaps of smart cities using Conway’s Game of Life model. Game of Life is a cellular automaton model devised by John Conway in 1970 [13].

This paper is further divided into the following sections. Section 2 presents the literature survey. Section 3 presents our design principles, model, and algorithms. Section 4 deliberates the results and discussion. Section 5 concludes with the conclusion and future scope.

2 Literature Survey

This section presents the literature survey from classics to state-of-the-art smart city innovations and advancements. According to Google Trends, there is a significant increase in web search traffic for the term ‘smart city’ [14]. With an evolving timeline, various aspects associated with the definition of a smart city have been uncovered. It has been a study of interest for institutes and industries. There has also been a prominent focus on interdisciplinary integrations emerging across the domains, exhibiting new façades.

Smart cities have been discussed in the 1970s [15] and also well before that. The smart city vision includes providing a safe and secure environment, green and efficient structures designed, constructed, and maintained using advanced technology [16]. Over a period of time, integrated materials, sensors, the Internet of things, cyber-physical systems have been integral part of this vision. In this regard, the relationship between city growth and human capital has been explored [17]. Designs have been researched and recommended for liveable cities under smart development [18]. The digital divide issues have been put forth for argument [19].

With the recent advancements in the technology and as applied to various domains, smart cities have been principled with domain-specific perspectives. Blockchain-based hybrid network architectures have been devised [20]. Quality-of-experience-driven big data architectures have been designed considering its growing omnipresent presence [21]. Smart city ontologies have been developed, formally addressing the effectiveness of smart city applications [22]. Internet of things for smart cities has been proposed considering the heterogeneous platforms and developments [23]. Additionally, smart cities have also been designed on the Internet of things platform with micro-service architecture [24], where cloud services have been used for optimal service design.

The policies created for smart cities have been questioned if leading to sustainability [25]. Smart cities have been conceptualized and benchmarked using various models, to name one, a Unified Smart City Model [26]. Culture, metabolism, and governance have been studied, and smart cities have been redefined accordingly [27]. The blurry picture of smart city policies on urban innovation has been discoursed [28]. Information technology research and opportunities with respect to smart cities have been reviewed and laid out [29].

Security and privacy in smart cities have always been a challenge [30]. Though approaches and challenges to enable cognitive smart cities using big data and machine learning have been proposed [31], there are still substantial gaps that need to be worked on. Even with artificial intelligence enabled micro-grid framework, there have been several challenges that need immediate addressing [32]. The challenges mentioned in the introduction section still demand completeness, despite the humongous amount of research on smart cities. Hence, this paper presents a self-learning model using Conway’s grid, which attempts to provide a formally verified city design.

3 Witty City—Model Design and Deliberations

Witty is wise with decent judgment skills. We hence prefix our city with witty aiming to build that ability over time. Essentially, a self-learning model is to understand the past and present, comprehended, and analyze for the future. We present the model details in this section. We present the Game of Life rules and its application to our model, the data considerations, the model design, the formal components of the model and the algorithms.

3.1 *Game of Life—Rules*

Using the Game of Life model, we set up a city on a two-dimensional grid, where each cell is of the uniform area. Uniformity is, however, a pictorial representation concern only. Each cell has two possible states of being active or inactive (also, dead or alive). Every cell apart from the one present in the boundaries has eight neighbors. We use the term ‘generation’ to represent a time tick or an iteration. Game of Life is a rule-based model which works on the following rules [33].

- Rule 1: An active cell with less than three active neighbors becomes inactive because of underpopulation.
- Rule 2: An active cell with two or three active neighbors gets to live for the next generation.
- Rule 3: An active cell with more than three active neighbors becomes inactive because of overpopulation.
- Rule 4: An inactive cell with three active neighbors becomes active because of reproduction.

We map a city on to a grid, where each cell represents an infrastructure or component of a city. The first rule prevents a construction from being isolated with the city hub, which is undesirable—no part of the city must be underdeveloped or lack in infrastructure or planning. The second rule is helpful to identify the possible directions the future buildings can be constructed, also determining the possibilities for new constructions so that it does not overpopulate or under populate a specific region. The third rule works to prevent specific areas of the city being overpopulated or overcrowded, which is again, not desirable. The last rule maps to growth of cities sub-components or an extended infrastructure. The rules, when applied, systematize the process of construction and coordinate the predictable structure.

3.2 Data Considerations

We classify our data into three categories in Witty City model: contemporary data, historic data and ideal data.

Historic Data. This is data of the city from past N years. When the time lapses to a new generation, the previous generation data becomes historic data.

Contemporary Data. This is the data that the model observes to build or generate recommendations for a new building based on the rules specified. Basically, the data that is currently existing on the Conway grid.

Ideal Data. This is the data of the ideal city we would like to achieve; this is a hypothetical data which the model refers to while operating on the contemporary data. The constraints of the city are designed and added in this data set.

3.3 The Grid Model

The model is designed to incorporate the challenges and design decisions as discussed in the introduction. The model can be seen below (see Fig. 1). The model predicts for time t using the data components as mentioned in the model: accumulating its learning's from the historical data, operating on the current data and working toward the ideal data. The model learns by analyzing all the existing data to propose the recommendations of the future buildings. The rule model applies and builds by generating and applying all the rules on the grid model.

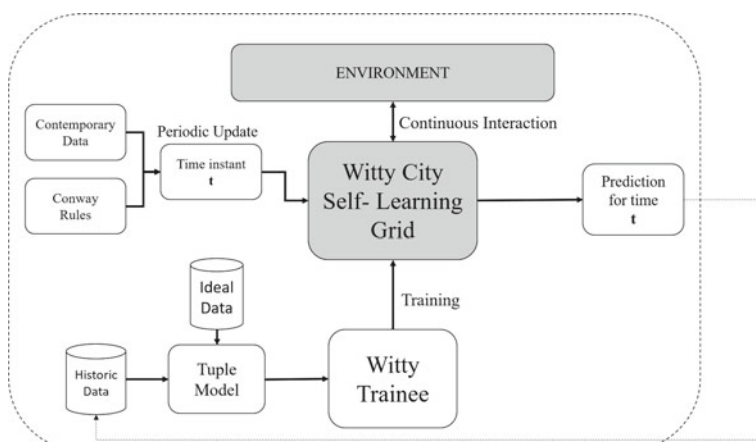


Fig. 1 Witty City model

Table 1 City tuple definition

Tuple	Name	Description
Q	States	The city infrastructure: this could be flyovers, roads, railway tracks, houses, malls, restaurants, hospitals etc
Δ	House Operator	The possible transitions by people who control the development of the city like corporations, mayor, community, government. Basically, the rules on states. Also, the four rules
δ	Transition Function	The transition that happens in the Conway grid at an instant of time t , the rule behavior. $\delta = (\text{value} + 1) \% 2$, where value = 0 or 1, the active or inactive cell state
Q_0	Initial State	An initial state which represents the Conway grid representing the current data (or historical) of the buildings. Initial Grid G_0 with N live cells
F	Final State	A utopian city model, result of the city game. Final state, when G_n and G_{n+1} are the same

The rules that meet the criteria are retained and other rules are discarded. The rules are validated based on the data sets and the constraints generated by the ideal city model. The growth model is part of the rule-based system that controls the model behavior. The prediction of time t , acts as feedback for time $t + 1$, by which the model also self learns to improve the future predictions. The city environment is used as a hook to act on the constraints. The dynamics of the city are governed and controlled through the environment.

3.4 Tuple Definition

We represent a city at time t using a five tuple definition $C = (Q, \Delta, \delta, Q_0, F)$. The tuples are explained in Table 1.

3.5 Algorithms

This section presents the generic algorithms of the rules implementation from the Game of Life for the Witty City. The conventions used are G_n is the grid of size n and x and y are its coordinates. The algorithms describe the process to check if a cell is valid in the grid, to find the sum of neighbors in the grid where apart of boundary conditions each cell has eight neighbors, to update the board based on identified coordinates, to run the iterations of the game, and to finally run the game.

```

ALGORITHM isValidCell (x, y)
// Checks if the supplied input co-ordinates are present on the grid or not
if x-1 < 0 || x+1 > N || y-1 < 0 || y+1 > N
    return false
else
    return true

ALGORITHM sumOfNeighbors ( Gn, x, y)
// Returns the sum of eight neighboring cells
sum ← 0
neighbors = ( [x-1, y], [x+1, y], [x, y-1], [x, y+1], [x-1, y+1], [x-1, y-1], [x+1, y+1],
               [x+1, y-1] )
for each neighbor in neighbors
    if isValidCell ( neighbor[0], neighbor[1] ) == true
        sum = sum + Gn [ neighbor[0] ] [neighbor[1] ]
return sum

ALGORITHM runIteration( Gn)
// Applies the defined rules to the grid
coordinates_to_change ← Ø
for each x, y in Gn
    if Gn[x][y] == 1 && sumOfNeighbors(Gn[x],Gn[y]) != 1
        coordinates_to_change ← coordinates_to_change U Gn[x][y]
    if Gn[x][y] == 0 && sumOfNeighbors(Gn[x],Gn[y]) == 3
        coordinates_to_change ← coordinates_to_change U Gn[x][y]
updated_board = updateBoard(Gn, coordinates_to_change)
return updated_board

ALGORITHM updateBoard (Gn, coordinates_to_change)
// Updates the grid with the coordinates identified in runIteration
for each x,y in coordinates_to_change
    Gn[x][y] ← (Gn[x][y] + 1) % 2
return Gn

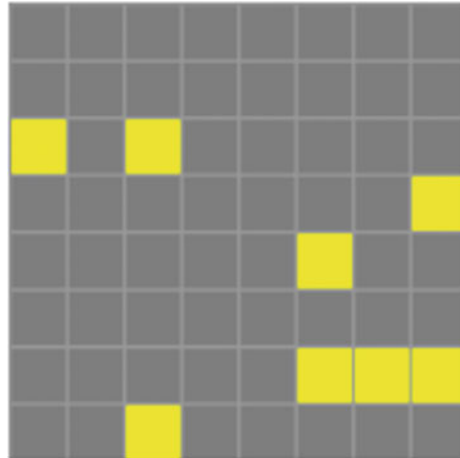
ALGORITHM runGame (Gn, Gn+1)
// The main program
while Gn+1 != Gn:
    Gn+1 ← runIteration(Gn)
    runGame(Gn, Gn+1)

```

4 Results and Discussion

The implementation of Conway grid was simulated in Python. The two key components to this model are the grid and the cells. A Boolean two-dimensional list of a finite size $N \times N$ is the data structure used in this implementation. The $N \times N$ list acts as a grid, and each element within the grid acts as a cell. The Boolean value of each cell is used to indicate the status of the cell, i.e.,—0 for dead state and 1 for alive state.

Fig. 2 Sample matrix representation



A sample implementation with a grid size of 8×8 and results is discussed below. The grid is initially populated with random live cells. This initial grid with random live cells is the Q_0 tuple from Table 1. Each cell has a probability of $1/N^2$ to be a live cell. A sample initialized matrix for an 8×8 grid can be seen below. For ease of understanding, the matrices presentation is adapted and visualized on playgameoflife [34]. The yellow box indicates cells with value 1, and gray indicates cells with value 0 (Fig. 2).

On the basis of the 5 tuples defined in Table 1, Q can be flyovers, trees, or buildings. There will be a Conway grid for each of these states. In this implementation, we have considered only the buildings as entities in the city. Of the five major algorithms presented, the first is `isValidCell()`, which takes coordinates on the grid as input and checks if they are valid points on the grid. Second is `sumOfNeighbors` which takes the grid and x, y coordinates of an element in the grid as inputs and returns the sum of neighboring 8 elements which implies the number of live cells neighboring the input cell.

The next algorithm is `runIteration`, and this is the procedure where the house operator Δ is applied. These rules are defined based on an ideal state for the city and can be altered accordingly. This is the key tenet that makes a city smart, the Δ can be defined according to one's definition of smart city. The `runIteration` procedure loops over each element in the grid at time t_n , calculates the sum of neighbors of said element, and applies the Δ , which in this implementation are the four rules defined in Sect. 3.1.

Once the rules are applied, we identify the cells which need a state change for the next generation and store the coordinates of these cells in a separate array. This step is important because we cannot immediately update the states of the cells as it affects the sum calculations in the current iteration. The final algorithm is the `updateGrid` procedure which reads from the aforementioned list of coordinates and updates their states according to the defined transition function δ to alive if dead and vice versa. δ

is computed as shown in Eq. 1.

$$\delta = (k + 1\%2) \quad (1)$$

where k is the value on the grid for any given coordinates. The output of this procedure is the next generation of the grid. The five procedures are called in an infinite loop recursively and updated consistently with the set of rules defined. The recursive call of the function is terminated when there can be no more state changes possible, i.e., when the grid at time t_n is the same as the grid at t_{n+1} .

It is at this state that we can say the final state \mathbf{F} is achieved for the entity in \mathbf{Q} . These state transitions are stored as the historical data that can be input to the model for the next entity.

Below is a sample prediction generated by the model. Data was collected from Google Maps [35] for Bharat Education Society (BES) campus in, 32nd E Cross Rd, Jayanagar, Bangalore (see Fig. 3).

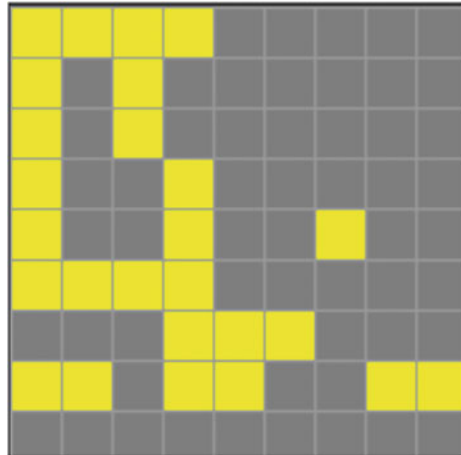
The buildings in the campus are represented by 1 in the matrix, the 0 represents empty spaces on campus. An approximated representation of the campus in the matrix form is shown below (see Fig. 4).

Let us assume the campus wants to construct a new hostel for its students, the best location for this will be demonstrated by running the model against this matrix. The

Fig. 3 Sample data map considered from BES educational institutes



Fig. 4 Matrix representation of the sample data



cells which in the previous iteration were 0, but became 1 are the suggested locations to construct the new building. The recommendations are based on the rules, as implied by the active neighbors (cells with 3 active neighbors; see Fig. 5).

The model can have applications in multiple facets of the city construction. Let us say the campus wants to plant trees around each building. This can be achieved by modifying the house operator, Δ with following conditions: Every dead cell around a living cell becomes alive and every live cell that has more than five live cells becomes dead (to prevent overpopulation). The presentation is marked in below matrix with 0, 1. For ease of visualization, we have represented (see Fig. 6) the output of this new rule with green color, to indicate suggested locations for the trees.

If the campus administration wants to construct roads across the campus to connect the different departments, the house operator would be modified to guarantee that

Fig. 5 Predictions of new buildings

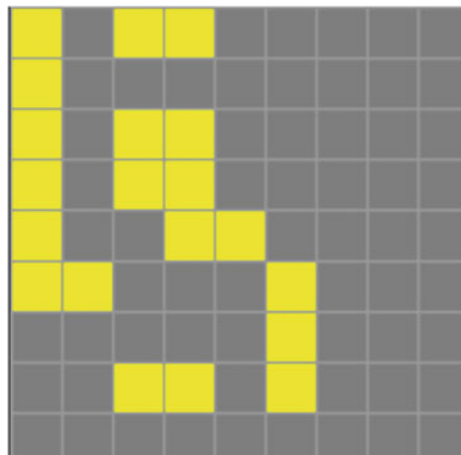
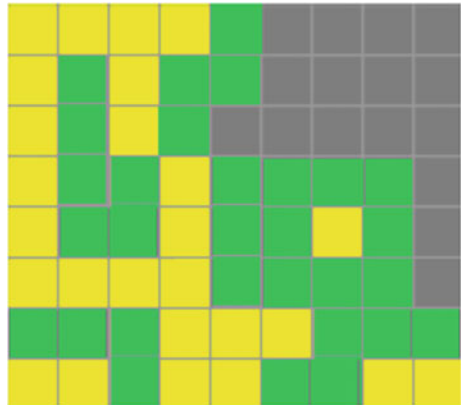


Fig. 6 Prediction on where to plant trees on campus

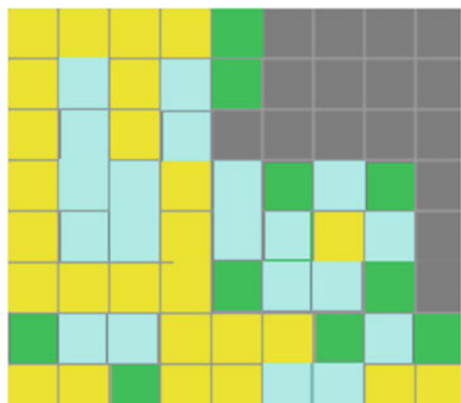


buildings are not completely surrounded by trees. So, the following rule would be added: If any tree is surrounded on diametrically opposite sides (left and right or above and below) by trees, it becomes a dead cell. The representation of this new rule is shown below (see Fig. 7). For ease of visualization, the suggested locations for road connectivity across campus are displayed in aqua color.

In the above matrix, we can see that no buildings are completely blocked out by trees and there is a possibility to connect all buildings by road. Similar kinds of simulations were performed by adding several city conditions and accordingly modifying the rules input to the model. Following are the prominent points to be considered:

- The model can be used for intelligent construction predictions.
- The model can predict the near future over-crowds.
- The model can help in planning a proper smart city design.
- The model learns and evolves with past, present, and future data.

Fig. 7 Prediction of road connectivity across campus



- The model adheres to the computational thinking features of decomposition, pattern recognition, and abstraction.

5 Conclusion and Future Scope

A city is not a smart city only by a technology adaptation. A city must also consider several factors like population, economy, culture, social characteristics, weather, resources, infrastructure, technology usage, digital divide, and geographical conditions. All the conditions can be mapped to a grid and converted into rules and constraints. The Conway's self-learning grid promises to be an effective model to enterprise cities. The model presented considered the historic data, built an environment of constraints, and worked according to the established ideal city protocols. The paper presented the model abstraction and design components along with a possible implementation giving scope to future design and improvements.

The paper presented the basic model, and as Game of Life is turing complete, any future city problem can be mapped into the intelligent grid, analyzed, and solved. With tuple definition and transition functions, the model can be verified for safety, correctness, and liveness properties which are a foremost part of the future scope.

Acknowledgements We would like to thank Knit Arena Software Research and Services Private Limited for guidance and supporting this work. The model is further being improvised in the company by refining the house operator and the transition function.

References

1. Rohrmeier K, Starrs P (2014) The paradoxical black rock city: all cities are mad. *Geogr Rev* 104(2):153–173
2. Albino V, Berardi U, Dangelico R (2015) Smart cities: definitions, dimensions, performance, and initiatives. *J Urban Technol* 22(1):3–21
3. Batty M, Axhausen K, Giannotti F, Pozdnoukhov A, Bazzani A, Wachowicz M, Ouzounis G, Portugali Y (2012) Smart cities of the future. *Eur Phys J Special Topics* 214:481–518
4. Silva B, Khan M, Han K (2018) Towards sustainable smart cities: a review of trends, architectures, components, and open challenges in smart cities. *Sustain Urban Areas* 38:697–713
5. Ismagilova E, Hughes L, Dwivedi Y, Raman K (2019) Smart cities: advances in research—an information systems perspective. *Int J Inf Manage* 47:88–100
6. Deakin M, Al Waer H (2011) From intelligent to smart cities. *Intelligent Build Int* 3:140–152
7. Ben Letaifa S (2015) How to strategize smart cities: revealing the SMART model. *J Bus Res* 68:1414–1419
8. Mahiznan A (1999) Smart cities: the Singapore case. *Cities* 16:13–18
9. Townsend A (2013) SMART CITIES: big data, civic hackers, and the quest for a New Utopia. W. W. Norton & Company
10. Harrison C, Donnelly IA (2011) A theory of smart cities. In: Proceedings of the 55th annual meeting of the ISSS—2011, Hull, UK. 55, 1
11. Kitchin R (2014) Making sense of smart cities: addressing present shortcomings. *Camb J Reg Econ Soc* 8:131–136

12. Kumar N, Goel S, Mallick P (2018) Smart cities in India: features, policies, current status, and challenges. In: 2018 Technologies for Smart-City Energy Security and Power (ICSESP), pp pp 1–4
13. Gardner M (1970) Mathematical games—the fantastic combination of John Conway's new solitaire game of life. *Sci Am* 223:120–123
14. Google Trends. Keyword search for smart city, link: <https://trends.google.com/trends/explore?date=all&q=smart%20city>. Last accessed 2020/12/05
15. Legget RF (1973) Cities and geology. McGraw-Hill, New York
16. Hall RE, Bowerman B, Braverman J, Taylor J, Todosow H, Von Wimmersperg U (2000) The vision of a smart city. Brookhaven National Lab, Upton, NY (US)
17. Shapiro J (2003) Smart Cities: explaining the relationship between city growth and human capital. *SSRN Electronic J*
18. Geller A (2003) Smart growth: a prescription for livable cities. *Am J Public Health* 93:1410–1415
19. Partridge HL (2004) Developing a human perspective to the digital divide in the smart city
20. Sharma P, Park J (2018) Blockchain based hybrid network architecture for the smart city. *Futur Gener Comput Syst* 86:650–655
21. He X, Wang K, Huang H, Liu B (2018) QoE-driven big data architecture for smart city. *IEEE Commun Mag* 56(2):88–93
22. Komninos N, Bratsas C, Kakderi C, Tsarchopoulos P (2016) Smart city ontologies: Improving the effectiveness of smart city applications. *J Smart Cities* 1
23. Zanella A, Bui N, Castellani A, Vangelista L, Zorzi M (2014) Internet of things for smart cities. *IEEE Internet Things J* 1:22–32
24. Krylovskiy A, Jahn M, Patti E (2015) Designing a smart city internet of things platform with microservice architecture. In: 2015 3rd international conference on future internet of things and cloud, pp 25–30
25. Yigitcanlar T, Kamruzzaman M (2018) Does smart city policy lead to sustainability of cities? *Land Use Policy* 73:49–58
26. Anthopoulos L, Janssen M, Weerakkody V (2016) A Unified Smart City Model (USCM) for smart city conceptualization and benchmarking. *Int J Electronic Government Res* 12:77–93
27. Allam Z, Newman P (2018) Redefining the smart city: culture, metabolism and governance. *Smart Cities* 1:4–25
28. Caragliu A, Del Bo C (2019) Smart innovative cities: the impact of Smart City policies on urban innovation. *Technol Forecast Soc Chang* 142:373–383
29. Kumar A, Singh Rattan J (2020) A journey from conventional cities to smart cities. In: Smart cities and construction technologies, pp 84–94
30. Braun T, Fung B, Iqbal F, Shah B (2018) Security and privacy challenges in smart cities. *Sustain Urban Areas* 39:499–507
31. Mohammadi M, Al-Fuqaha A (2018) Enabling cognitive smart cities using big data and machine learning: approaches and challenges. *IEEE Commun Mag* 56:94–101
32. Khan S, Paul D, Momtahan P, Aloqaily M (2018) Artificial intelligence framework for smart city microgrids: State of the art, challenges, and opportunities. In: 2018 third international conference on Fog and Mobile Edge Computing (FMEC), pp 283–288
33. Conway's Game of Life. https://www.conwaylife.com/wiki/Conway's_Game_of_Life. Last accessed 2020/12/05
34. Play John Conway's Game of Life. <https://playgameoflife.com/>. Accessed 23 Oct 2020
35. Google Maps, BES Educational Institutions. <https://goo.gl/maps/prp8XDusR1qwf2ip7>. Last accessed 2020/12/05

Reinforcement Learning-Based Clustering Algorithm for Cognitive Wireless Sensor Networks



Anu Maria Joykutty and B. Baranidharan

Abstract As the number of wireless devices is increasing rapidly, there is a huge demand for radio spectrum. Recent advancements in cognitive radio (CR) technology enable opportunistic spectrum access so that unused spectrum can be utilized efficiently without hindering the licensed users. Cognitive wireless sensor networks (CWSNs) make use of CR technology for organizing and managing the sensor nodes. Clustering of sensor nodes in CWSNs helps to improve the network lifetime, stability, etc. In recent years, lot of clustering algorithms based on reinforcement learning was proposed for C-WSN, and it improved the overall functionality of C-WSN to certain extent. This study proposes an improved reinforcement learning-based clustering mechanism. The proposed clustering algorithm achieves improved network lifetime, stability and mitigates channel interference.

Keywords Cognitive radio · Wireless sensor networks · Reinforcement learning

1 Introduction

The present era belongs to mobile and wireless. The explosive rate at which the number of mobile phones, smartphones and other wireless devices is increasing worldwide is unlike any other products. Studies and statistics show that for every person in the world there will be 3.6 networked devices by 2023 [1]. The reason for this tremendous speed of increase is the facilities offered by these devices and also the advancement in wireless technology. People are becoming more and more dependent on such devices; hence, the demand is ever growing. Also, new and innovative products are entering the market, thereby propelling the growth further.

A. M. Joykutty (✉)

Rajagiri School of Engineering and Technology, Kerala, India
e-mail: anumj@rajagiritech.edu.in

B. Baranidharan

SRM Institute of Science and Technology, Tamil Nadu, India

Wireless devices operate in the radio spectrum which is a part of the electromagnetic spectrum. The frequencies in the radio spectrum range from 3 kHz to 300 GHz. This is commonly known as the radio frequency (RF) spectrum or simply the radio spectrum. The allocation of the radio spectrum to various services is regulated by the International Telecommunication Union (ITU). Parts of the spectrum are licensed to users for exclusive usage, and only those licensed users are permitted to operate in that specified frequency range. This method of static allocation of the radio spectrum has turned out to be highly inefficient as certain parts of the spectrum are heavily used, whereas there are many parts of the spectrum that are rarely or not used at all. This has resulted in spectrum scarcity wherein there is unavailability of spectrum for a lot of services especially for the non-licensed users. The ever-increasing number of wireless devices has only added to this challenge of spectrum scarcity. In order to overcome this problem of limited spectrum availability, a lot of novel technologies such as frequency reuse and dynamic spectrum management are used. Cognitive radio (CR) is one such technology that aims to improve the spectrum utilization by providing opportunistic spectrum access to non-licensed users. This usage of spectrum resources is greatly improved by the emergence and advancement in the cognitive radio technology.

Because of these reasons, CR technology has become popular over the years, and various research works are being carried out based on the same. CR has also found application in areas like wireless sensor networks (WSNs). The highly dynamic nature of WSNs makes it a suitable candidate for utilizing CR technology. This study proposes how efficiently reinforcement learning technique can be used for clustering in WSNs.

2 Cognitive Radio

Cognitive radio technology involves the addition of cognition or intelligence into the process of spectrum access or management. It is built based on the principles of a software-defined radio (SDR) with additional capability to sense the environment, do analysis and perform actions based on the analysis [2]. The basic operating principle of a cognitive radio is to sense or detect the presence of unused spectrum (or channels). The licensed users are known as primary users (PU). The unlicensed users known as secondary users (SUs) can opportunistically access these channels without causing any kind of interference to the PUs, i.e., when the channels are not being used by the PU, then it can be utilized by the SUs for transmission. This kind of spectrum access enables the unlicensed users also to utilize the spectrum, thereby solving the problem of spectrum unavailability. Cognitive radio uses intelligent methods to interact with the environment and collect information about the environment. It then uses this information, selects the best channel for transmission and modifies its parameters so that it can transmit using that channel. If the PU is returning to the channel, then the SU has to leave it so that it does not interfere with the operation of the PU. The

Federal Communications Commission (FCC) in the USA has allowed the utilization on unused spectrum known as white spaces by unlicensed users [3].

2.1 Cognitive Cycle

For a CR device to opportunistically access the spectrum, it has to first scan the spectrum and detect the presence of unused channels. This phase is known as the sensing phase. After the sensing phase is done, the sensed results have to be analyzed so as to decide whether to use the channel or not for transmission. This is known as the analyzing phase. Once the sensing and analysis phases are complete, the CR device decides which of these channels to use and then adapts its operating parameters so as to use that channel. The CR device or the SU has the capability to configure its operating parameters such as the frequency range, modulation type, output power in a dynamic manner so that optimal performance can be achieved.

The primary user will always have priority for spectrum usage. The secondary user can only access the licensed channel only when it is not used by the PU or if it is a vacant channel, i.e., in the absence of the PU. When a secondary user is using a channel for transmission in the absence of a PU, but if the PU is reclaiming the channel, then the SU has to immediately vacate the channel. So, the SU has to consistently monitor or scan the spectrum for reappearance of the PU. For performing the channel sensing and detecting the presence of PUs, detection techniques such as energy detection, matched filer technique and cyclostationarity technique are used by CR. In all these sensing methods, a single SU is performing the sensing, and hence, the detection performance will be limited because of noise, multipath fading effect, etc. To overcome these limitations and to improve the performance, spectrum sensing can be done in a cooperative manner. This is known as cooperative spectrum sensing (CSS).

2.2 Cooperative Spectrum Sensing

In CSS, the sensing results of different SUs will be collected together by fusion center (FC). The FC makes a decision about the presence or absence of a PU based on the sensing results it has received from the participating SUs. The decision taken by the FC is then broadcasted to the SUs. CSS improves the detection performance, but it comes with the cost of additional energy consumption. Energy is consumed during channel sensing by the SUs. In the case of CSS, energy is also consumed when the SUs have to relay these sensing results to FCs. This is known as reporting phase. The energy consumption in the reporting phase is proportional to the distance between the FC and the SUs. In the case of wireless devices, energy usage should be regulated as these devices are restricted by the capacity of the battery. Hence, various methods are used to reduce the energy usage during cooperative spectrum

sensing. Clustering of the SUs is one such method which can increase the energy efficiency while performing CSS. Over the years, different techniques were proposed for clustering in cognitive radio networks. In the following section, a few of the recent works related to clustering mechanisms in cooperative spectrum sensing in CRNs will be discussed.

3 Clustering in CRN

Clustering is used in CRNS for increasing the energy efficiency and also to achieve network stability, thereby improving the lifetime of the network [4]. Clustering also helps to perform cooperative tasks like cooperative spectrum sensing and spectrum access in an even efficient manner. Clustering is a mechanism for managing the topology in networks by logically organizing the members of the networks (known as nodes) into different clusters. There will be a cluster head (CH) for every cluster that will be selected based on some criteria. Because of the specific characteristic of CRNs, the traditional clustering algorithms might not be suitable, and hence, many novel clustering algorithms have been proposed over the years.

In [5], a spectrum-aware clustering algorithm is proposed for cognitive radio sensor network which is based on a weighted clustering metric. There are three important factors that affect the metric: the residual energy, temporal and spatial correlation and the sensing confidence. The temporal correlation indicates that neighboring nodes have more idle channels in common and then can be grouped into a single cluster. Spatial correlation indicates the geographical closeness of nodes. Each node calculates the metric and broadcasts to others so as to elect the CH. If a node has a higher metric value than the others received, then it appoints itself as a CH. Else it will join a cluster at a one-hop distance where the CH has the maximum value of the metric. The optimal number of clusters is determined by finding the similarity within the cluster (intra-cluster) and also between the clusters (inter-cluster). Once the clustering is done, and there only the CHs perform the sensing, thereby conserving energy of the member nodes, achieving energy efficiency and also enhancing the stability of the network. The transmission can be done by the member nodes which also improves the throughput of the network. Once the CH realizes that the number of common channels is less than a particular threshold value, then it results in re-clustering. The experimental results show that the proposed algorithm greatly improves the network performance in terms of transmission and also reduces the energy consumption.

DMS Bhatti et al. [6] proposed a method for collaborative sensing by a set of selected SUs that are organized into clusters. This novel clustering technique reduces the high energy consumption that occurs when all the SUs perform the sensing. Only limited number of SUs from the whole network is selected, and those nodes will be grouped into clusters. This method of using an optimal number of SUs for sensing will conserve energy. The cluster formation and CH election are performed using the affinity propagation (AP) algorithm. This algorithm works by exchanging messages between the users. Moreover, it is not needed to determine the number

of clusters before the starting of the algorithm. This method is shown to improve network performance in terms of energy efficiency of the network as well as the throughput of the network.

In [7], Wenli Ning et al. proposed a method for cooperative spectrum sensing in CRNs by making use of reinforcement learning (RL). In this proposal, an order in which the various channels are to be scanned is determined by each SU by making use of RL. This is done by using Q-learning to understand how the various channels will be occupied by PUs and then using this information to develop a dynamic channel scanning order. Also, in this method, each SU selects a potential partner for channel scanning in the CSS. Each SU will learn about the detection probability of all its neighbors and selects the one neighbor with the highest probability as its partner. Using this method of determining, the partner is shown to improve the detection efficiency. Overall simulation results for the proposed CSS mechanism based on RL demonstrate substantial improvement in performance over the traditional algorithms in terms of access delay, overhead for scanning and detection efficiency.

Liu et al. in [8] proposed a clustering method based on Bayesian learning to improve the performance of sensing in the case of both perfect and imperfect sensing reports. There are two types of cooperative sensing happening here: One is within the cluster (intra-cluster), and second is between the clusters (inter-cluster). A sensing threshold value for intracluster cooperative sensing is obtained by minimizing the total Bayesian cost. Bayesian fusion is being made use to determine the detection probability and false alarm probability in the case of inter-cluster cooperative sensing. This study uses k-means algorithm for clustering and cluster head selection. When compared with other methods, the proposed method of CSS based on clustering is shown to perform much better than the existing algorithms or methods. This method is shown to improve the sensing performance and also to reduce the time overhead that occurs in CSS when compared with other traditional clustering techniques.

Rashad et al. [9] proposed the CogLeach algorithm as an improvement to the Leach algorithm [10]. This study proposes a spectrum-aware clustering protocol for cognitive radio sensor networks. The parameter that is being considered here is the number of vacant channels available at each node. This factor is taken as the weight and used while calculating the probability of a particular node to be selected as the cluster head.

Alvin et al. [11] discuss the various clustering techniques available specifically for cognitive radio networks. These methods are classified based on the objective of the clustering and also the number of node hops. The complexity analysis and the improvements in terms of performance for each method, the disadvantages, etc., are discussed in this study.

4 Reinforcement Learning Based Clustering in CRN

Over the years, machine learning techniques have been widely used in the area of cognitive radio. Supervised and unsupervised machine learning techniques have lot

of applications in networking domain, especially in optimizing the network performance [12]. Over the recent years, reinforcement learning (RL) techniques have also become popular among researchers in the networking domain. Reinforcement learning is quite different from both supervised and unsupervised learning. In the case of reinforcement learning, there will be an agent which tries to learn by itself based on the interactions it has with the environment. The agent takes an action which results in the transition from present state to another state and also gives a reward. The agent tries to find a suitable action that will maximize the cumulative reward. If the action taken by the agent is not suitable, then it can result in a negative reward.

RL-based techniques are highly suitable for cognitive wireless sensor networks owing to their dynamic nature and changes in spectrum usage. Model-free RL method such as Q-learning can be used for evaluating the quality of the channel, and this can be utilized while performing spectrum sensing. In [13], a clustering mechanism is proposed for cognitive radio ad-hoc networks. This method is based on reinforcement learning that uses Q-learning algorithm for cluster formation. The quality of each channel is determined by finding its corresponding Q-value.

In this proposal, a reinforcement learning-based clustering scheme is proposed for cognitive wireless sensor networks. *Q*-learning algorithm is used to determine the *Q* value of the channels associated with the SUs. The initial *Q*-value of each channel is determined, and it gets updated based on the past value and the expected rewards. If $Q(su_s, ch_c)$ is the *Q*-value of channel ch_c of su_s . Then, the channel *Q*-values are updated as shown below:

$$Q(su_s, ch_c) = Q(su_s, ch_c) + \alpha[r_{su_s}^{ch_c} + \gamma \cdot \max_{ch_c} Q(su_s, ch_c) - Q(su_s, ch_c)] \quad (1)$$

where the reward $r_{su_s}^{ch_c}$ is the total idle time of the channel.

The SU with the channel having the highest *Q* value is selected as CH. The channel having the highest *Q* value is used for transmission between the nodes and the CH and also between the CH to the FC. Since this channel is having the *Q* value which is in turn based on the total idle time available, the chances of a PU returning to the channel are very less. This ensures that channel switching will not happen frequently, thereby improving the quality of SU transmission.

5 Experimental Setup and Results

The existing algorithm and the proposed algorithm are simulated using MATLAB. The experiment was conducted with 50, 75 and 100 wireless sensor nodes as secondary users, and the number of primary users is 4. The nodes are scattered in the 100×100 m area. Figure 1 depicts the deployment of secondary nodes and primary nodes in the field. The transmission range of each secondary user or wireless sensor node is varied from 25 to 50 m. The proposed reinforcement learning-based algorithm selects best channel for transmission between member node to CH and CH

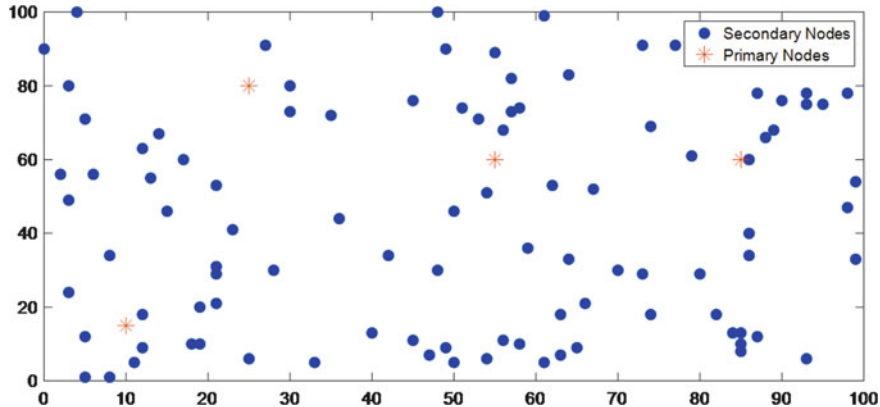


Fig. 1 Random distributions of SUs and PUs

to BS. In the proposed algorithm, there was not even a single retransmission due to channel loss by the secondary nodes to primary nodes. This is achieved by selecting the channel which is having highest continuous idle time for transmission.

Figure 2 shows the number of clusters for the proposed algorithm in different range from 25 to 50 m. It is observed that when the transmission range of the secondary nodes increases the number of clusters decreases since it enables the formation of big clusters. Also, Fig. 3 shows the increase of average number of member nodes in a cluster when the transmission range of secondary node increases.

Figures 4, 5 and 6 depict the average energy consumption per cluster during a fixed transmission slot and correspond to 50, 75 and 100 sensor nodes. In the experimental setup, it is simulated in such a way that a transmission slot is equal to 10 rounds of data transmission from member nodes to its cluster heads. In [14], a multi-channel-based clustering (MCBC) mechanism is proposed for CRNS. In this method, the cluster head selection is performed based on the number of nodes on each available

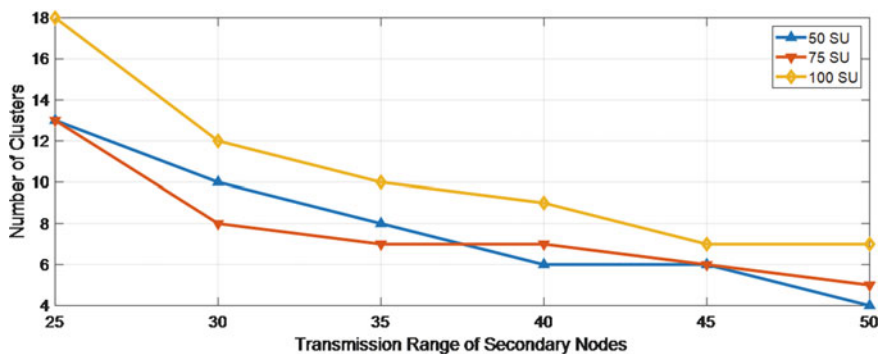


Fig. 2 Number of clusters versus transmission range of SUs

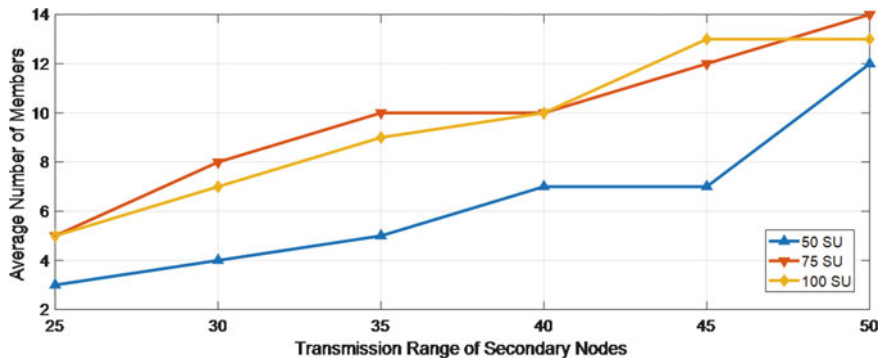


Fig. 3 Average number of members in a cluster versus transmission range of SUs

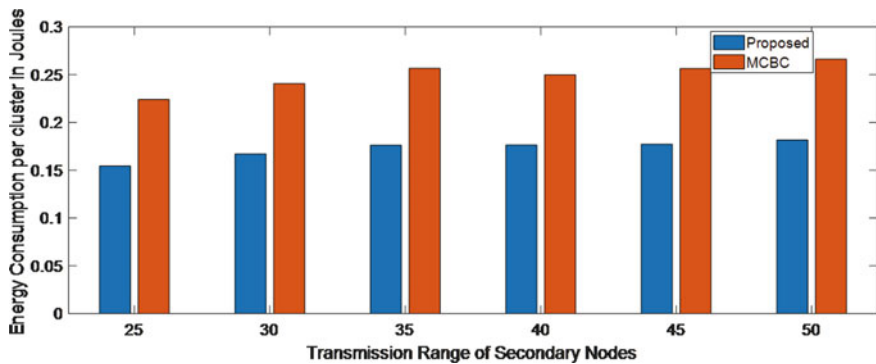


Fig. 4 Energy consumption per cluster versus transmission range of SUs (50 SUs)

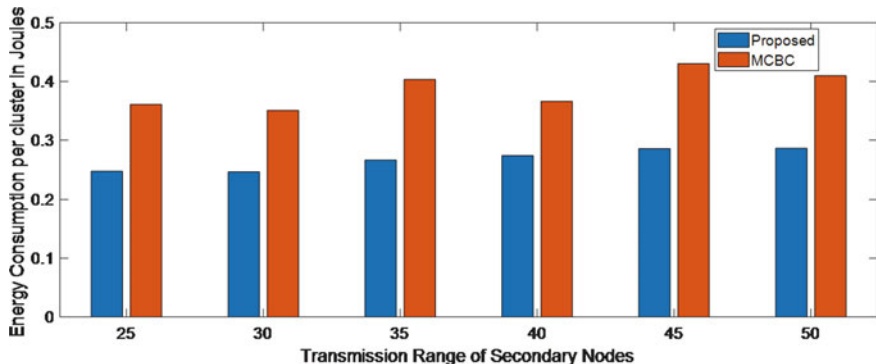


Fig. 5 Energy consumption per cluster versus transmission range of SUs (75 SUs)

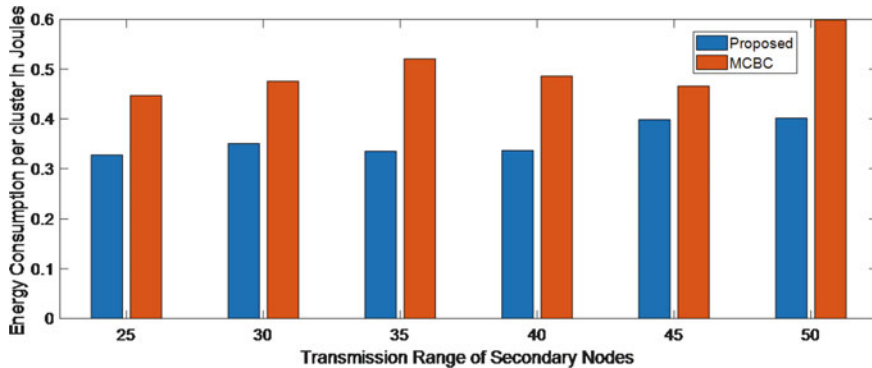


Fig. 6 Energy consumption per cluster versus transmission range of SUs (100 SUs)

channel, which is considered as the node degree. The node with the highest degree is elected as the cluster head. The proposed work is compared with MCBC algorithm. The experimental results show that the proposed algorithm spends less energy in all the transmission ranges than MCBC because of the proper channel selection. But in the case of MCBC when there is an interrupt from primary nodes, channel switching occurs. This leads to increased energy consumption due to the frequent retransmissions. Also, it is observed that when the transmission radius increases, SUs is more prone to interruption from PUs and further increases frequency of channel switching. This does not happen in the case of the proposed algorithm. The proposed algorithm is based on the Q -value, and hence, it is shown to improve the network lifetime by reducing the number of retransmissions.

6 Conclusion

Cognitive radio technology is growing in a very rapid manner owing to its importance in the field of dynamic radio spectrum management. Machine learning techniques are widely applied in the area of CR especially for spectrum sensing and allocation. The proposed method makes use of reinforcement learning technique for clustering in cognitive wireless sensor networks (CWSNs). It uses the Q -learning algorithm to determine the Q -value of the channels. The cluster head selection is also done on the basis of the Q -value which greatly improves the network stability and also avoids retramsmissions. The proposed method is compared with other existing technique such as MCBC. Experimental results indicate that this method shows substantial improvement over existing methods in terms of quality of transmission as well as energy consumption.

References

1. CISCO Annual Internet Report (2018–2023) White Paper. <https://www.cisco.com/c/en/us/solutions/collateral/executive-perspectives/annual-internet-report/white-paper-c11-741490.html>. Last accessed 2020/10/20
2. Jondral FK (2005) Software-defined radio—basics and evolution to cognitive radio. *J Wireless Com Netw* 2005:652784. <https://doi.org/10.1155/WCN.2005.275>
3. FCC White Spaces. <https://www.fcc.gov/general/white-space>. Last accessed 2020/10/20
4. Ponrajakumari M, Rajendran, Vimala Devi, Subramaniam M (2020) A survey on clustering algorithms in cognitive radio networks. *J Critical Rev* 7:722–729. <https://doi.org/10.31838/jcr.07.19.88>
5. Wang T, Guan X, Wan X, Shen H, Zhu X (2019) A spectrum-aware clustering algorithm based on weighted clustering metric in cognitive radio sensor networks. *IEEE Access* 7:109555–109565. <https://doi.org/10.1109/ACCESS.2019.2929574>
6. Saqib Bhatti DM, Ahmed S, Chan AS, Saleem K (2019) Clustering formation in cognitive radio networks using machine learning. *Int J Electronics Commun.* <https://doi.org/10.1016/j.aeue.2019.152994>
7. Ning W, Huang X, Yang K, Wu F, Leng S (2020) Reinforcement learning enabled cooperative spectrum sensing in cognitive radio networks. *J Commun Netw* 22(1):12–22. <https://doi.org/10.1109/JCN.2019.000052>
8. Liu X, Zhang X, Ding H, Peng B (2019) Intelligent clustering cooperative spectrum sensing based on Bayesian learning for cognitive radio network. *Ad Hoc Netw* 94, 101968. ISSN 1570-8705, <https://doi.org/10.1016/j.adhoc.2019.101968>
9. Eletreby RM, Elsayed HM, Khairy MM (2014) CogLEACH: a spectrum aware clustering protocol for cognitive radio sensor networks. In: 2014 9th International Conference on Cognitive Radio Oriented Wireless Networks and Communications (CROWNCOM). IEEE, pp 179–184
10. Palan NG, Barbadekar BV, Patil S (2017) Low energy adaptive clustering hierarchy (LEACH) protocol: a retrospective analysis. In: 2017 International Conference on Inventive Systems and Control (ICISC), Coimbatore, pp 1–12. <https://doi.org/10.1109/ICISC.2017.8068715>
11. Alvin Yau K-L, Ramli N, Hashim W, Mohamad H (2014) Clustering algorithms for Cognitive Radio networks: a survey. *J Netw Comput Appl* 45:79–95. ISSN 1084-8045. <https://doi.org/10.1016/j.jnca.2014.07.020>
12. Usama M et al (2019) Unsupervised machine learning for networking: techniques, applications and research challenges. *IEEE Access* 7:65579–65615. <https://doi.org/10.1109/ACCESS.2019.2916648>
13. Hossen MA, Yoo S (2019) Q-learning based multi-objective clustering algorithm for cognitive radio Ad Hoc networks. *IEEE Access* 7:181959–181971. <https://doi.org/10.1109/ACCESS.2019.2959313>
14. Kumar Berwer R, Kumar S (2017) Multi channel-based clustering in cognitive radio networks. In: 2017 international conference on smart technologies for Smart Nation (SmartTechCon), Bangalore, pp 665–670. <https://doi.org/10.1109/SmartTechCon.2017.8358455>

An Exploratory Analysis and Prediction of Factors Influencing the Debugging Behavior of Computer Science Students



Sherna Mohan and E. R. Vimina

Abstract In recent years, most of the students registered in computer science courses are confronted with the difficulty in computer programming. This is a serious concern for educators and the students. So there is a critical need to analyze the factors influencing the same. Meanwhile, many investigations have been conducted in analyzing the programming skill, and more importantly, their studies focused on marks secured in various science subjects, prior programming experience, reasoning ability, etc. But the analysis of programming behavior in the current study is focused mainly on patterns generated by the students after the compilation. Furthermore, the relationship between debugging capability and hit rate with academic performance was analyzed. Methods like correlation and regression are adopted for analyzing these factors. It is observed that the debugging skill of the students and their hit rate has an upper hand in determining the programming skill compared to the marks secured in the examinations.

Keywords Programming skill · Performance · Behavior · Correlation · Goodness of fit · R square · Adjusted R square · Debugging · Regression

1 Introduction

According to programming pedagogy, programming is a sophisticated task for the novice programmers, especially for those from non-computer science background. Programming is an arduous task to learn. Many students lack the proficiency to learn programming because of the nature of the subject. This leads to high dropout rates in programming courses. In the current study, the investigator analyzed the enormous problems faced by the novice programmers, does not carry out to be the

S. Mohan (✉) · E. R. Vimina

Department of Computer Science and IT, Amrita School of Arts and Sciences, Amrita Vishwa Vidyapeetham, Kochi Campus, Kochi, India
e-mail: sherna.mohan@gmail.com

E. R. Vimina

e-mail: viminaer@asas.kh.amrita.edu

understanding of programming concepts, but rather figuring out how they react to programming exercises assigned by the educators. We started seeing exploration concerning the use of debugging behavior and programming performance benefited for novice programmers. The present research on the debugging behavior of first-year students deals with the study of interactions with the compiler during the learning process. That is, study concentrates more on the patterns generated by the students after the compilation.

Over the years, several investigations have been conducted to recognize the factors such as prior experience [1, 2], high school grade point [3], the marks obtained in language and science subjects [2, 4], etc., that influence the student's performance. But not many researches have been focused on the coding patterns generated by the students after the compilation. So this research concentrates more on the analysis of coding patterns to predict the programming skill and debugging behavior of the students. The main intention of this research work is to explore the various factors that can be used to determine the programming skill of the students. To predict the programming behavior, some techniques are employed for recognizing the hidden relationship among the attributes of the data set. The study concentrates on the following objectives:

- To determine the effect of marks scored in qualifying examination, especially in mathematics in analyzing the programming skill of a student.
- To investigate various compile time errors that are often generated by the students.
- To analyze the debugging behavior and programming skill by considering the coding pattern generated by the students after the compilations in each level (easy, medium, and hard).
- To predict the programming performance of the student based on programming assignments, which are analyzed through debugging capability and by evaluating the hit rate.

This paper is organized as follows. The background work is described in Sect. 2 and proposed approach in Sect. 3. Section 4 deals with the methodology used; evaluation and interpretation of prediction are discussed in Sect. 5. In Sect. 6, results and discussions are analyzed, and finally, in Sect. 7, the conclusions and future scope are explained.

2 Related Works

Earlier the researchers have identified numerous valuable information about novice programmers and distinguished great and terrible components of the present programming systems, both visual and textual. In [5], collected the data using freely available Java compiler called Jikes in which the students are able to update the coding part of this compiler. In 2006, the Department of Information Systems and Computer Science has been utilizing an instrumented form called BlueJ, an integrated development environment (IDE) for Java (Kolling and Rosenberg 1996). To

empower us to get to the compilation logs rapidly and effectively, and to produce reports of programs, the BlueJ browser is updated [6]. The compilations produced by the student, error quotient [7], and confusion rates [8] were accessed using the BlueJ browser. To investigate potential predictors of accomplishment, programming behavior was analyzed using BlueJ IDE [9].

Another research [9, 10] discovered some syntax and logical errors such as missing comma, variable out of scope, mistakenly change the operator ($i++$ becomes $++i$), cannot find symbol, escape sequences outside the quotes, use ‘=’ operator instead of ‘==’ operator, misplacement of the ‘return’ keyword, wrong initialization, etc. The study [9] analyzed a fragment of compilation log information from novice programmers based on a quantitative and qualitative manner. The data used for this study include high school marks, compilation logs, midterm grades, test scores of Java programming, etc. Another study [11] consolidated the source code snapshot information by implementing machine learning methods that are collected from students’ programming process, capable of recognizing high and low-performing students with greater accuracy in the first-year introductory programming course. The various characteristics that influence this programming performance include gender, academic performance, prior programming experience, midterm score, source code snapshots, etc., from a total of 86 students. In [12], some discovered parameters that influence the programming performance of the students in the introductory course and expect to find a correlation between different assessment methods, student’s interest, and their final performance are estimated. Another research [1] also assessed the performance of students in such environments.

In [3], predict the student’s academic performance in the final exam by comparing the linear regression method and multilayer perceptron method in the Weka tool. Various attributes in student’s environment such as demographics (place, hobby, family size employment, education of parents), students behavior, students information (name, age, gender, address, admission ID), psychological (mindset, behavior, and inspiration), and socioeconomic (socioeconomic history of the student as well as their academic background) aspects have been studied. One of the issues encountered in the introductory programming courses is the high failure rate in most of the universities. To address this issue, a study was conducted [4], which presents a clear understanding of the effect of sex and former programming knowledge in introductory programming courses. To analyze the programming solutions or reducing the failure rate attempted by the students, [13] implemented a continuous assessment methodology upheld by an automatic judgment tool applied to the programming practices (online judge) performed by 108 students in the laboratory. In [14] concentrates on run time semantics and logical errors. Here educators assign 8 programming questions and students attempted these questions in an online C++ shell. The majority of the students in the introductory programming course fall in common bugs such as array index out of bounds, division by an integer, condition variable not updated, use ‘=’ instead of ‘==’ etc. As a solution, this work proposes, students with more expertise in programming require less debugging time. Shortly, experience in programming is one such significant factors in debugging skills.

3 Proposed Approach

Many investigations have been performed to recognize the factors that influence the student's performance based on marks [1, 13], but not many studies have come out with compiler (coding) pattern analysis generated by the students. Hence, this study concentrates more on coding patterns during compilation. In this connection, the programming performance model has two stages of processes.

- i. Identifying the best predictive factors among the set of parameters used in our study by applying different correlation methods.
- ii. Prediction of programming performance using the regression model.

3.1 Data Set Collection and Preparation

The study was carried out among the students of first-year computer science programming course, and one hundred and eight students took part in it. Seventy-three of the participants were females, and thirty-five were males. The students fall in wide range of educational backgrounds. Here, the research analyzed the programming skill and debugging behavior of students which deals with the study of interactions with the programming assignments and compiler during the learning process. When the study focused on the learning environment, computer science and non-computer science students engaged in an 'edit-compile-execute' recurrent cycle while learning to program. It is common for novices to take part in these recurrent programming cycles. To explore this cycle, beginners instrumented Java [6, 7], a high-level programming language as the learning program platform since Java is included in their first-year academic curriculum.

Here, the educators assigned some programming questions or assignments to the students in the computer laboratory, and they were broadly classified into three difficulty levels—easy (E), medium (M), and hard (H). The point of this analysis is to find out that whether, for a particular question and difficulty level (E, M, and H), the students will reach the output within a stipulated period of time which is assigned by the teachers. If a brilliant student performs well in solving the questions than other students, then it infers that solved count does reflect a student's programming capability. To analyze it, the educators collect the compilation output of each student.

The compilation pattern is like unstructured data, and we have to extract the information from it. The sample output is depicted in Fig. 1. To analyze the unstructured data from the output screen, some text analysis methods are used. Within a text, the most relevant keywords can be extracted. From the output screen, the type and number of errors in each compilation, number of error occurrences in the penultimate compilation, number of compilation attempts, time taken to debug a program, etc., were assessed. Different types of errors like run time errors, compiler errors, etc., were also extracted from the output through the text analysis process. From Fig. 1, it is noticeable that the relevant keyword 'error' is repeated 3 times in Fig. 1a and 11

```

user@user-To-be-filled-by-O-E-M:~$ javac qm5.java || date
qm5.java:7: error: cannot find symbol
display(data);
^
symbol: variable data
location: class qm5
qm5.java:8: error: cannot find symbol
sort(data);
^
symbol: variable data
location: class qm5
qm5.java:10: error: cannot find symbol
display(data);
^
symbol: variable data
location: class qm5
3 errors
Wed Jun 12 14:19:09 IST 2019
user@user-To-be-filled-by-O-E-M:~$ java qm5
Error: Could not find or load main class qm5
user@user-To-be-filled-by-O-E-M:~$ javac qm5.java || date
user@user-To-be-filled-by-O-E-M:~$ java qm5
Unsorted List is :
9 5 1 3 2 5
Sorted List is :
1 2 3 5 5 9 user@user-To-be-filled-by-O-E-M:~$
```

(a)


```

user103@user103-H81M-S:~$ cd 3sd
user103@user103-H81M-S:~/3sd$ javac qm4.java ||date
qm4.java:8: error: ';' expected
int a[2][2],i,j,d;
^
qm4.java:8: error: illegal start of expression
int a[2][2],i,j,d;
^
qm4.java:8: error: ';' expected
int a[2][2],i,j,d;
^
qm4.java:8: error: not a statement
int a[2][2],i,j,d;
^
qm4.java:8: error: ';' expected
int a[2][2],i,j,d;
^
qm4.java:8: error: not a statement
int a[2][2],i,j,d;
^
qm4.java:8: error: ';' expected
int a[2][2],i,j,d;
^
qm4.java:8: error: not a statement
int a[2][2],i,j,d;
^
qm4.java:17: error: reached end of file while parsing
}
^
11 errors
Tue Jun 11 15:32:28 IST 2019.
```

(b)

Fig. 1 Sample output

times in Fig. 1b. So that we can identify the total number of errors that occurred in each compilation. Through compilation, by analyzing the keyword ‘javac,’ the study calculated the count of compiling attempts. The date and time can also be assessed by providing pipe symbol ‘||’ along with compilation in the command line, and it can be assessed using the text analysis process.

Students commit numerous compilation errors like syntactical errors, run time errors, etc., while compiling a program. Figure 2 depicts the percentage of errors in each level (E, M, and H) when participants try to solve the programming exercises, and it is categorized into compile time errors, run time errors, and no output. The hard level shows the increased number of errors compared to medium and easy levels. In this research, quantitative types of data were collected from the students, and it is normalized to rescale the values from 0 to 1 without losing information.

The syntax errors or compiler errors in easy level are 16.67% which is very much less compared to hard level errors (37.04%). That is, error increases as the difficulty level of programming exercises increases. After compiling, the compiler generates some compilation logs containing error messages or it enters the executable mode directly.

When compiling the Java program, the user inputs the ‘time’ command along with the ‘javac’ command to create a time stamp. This time stamp gives more information to the educators that help them to identify the time spent by the students during the compilation. For each student, the study records the time spent in each compilation and then normalizes the time compared to the average time the student has spent while programming at three difficulty levels. By capturing the time stamp, the time taken

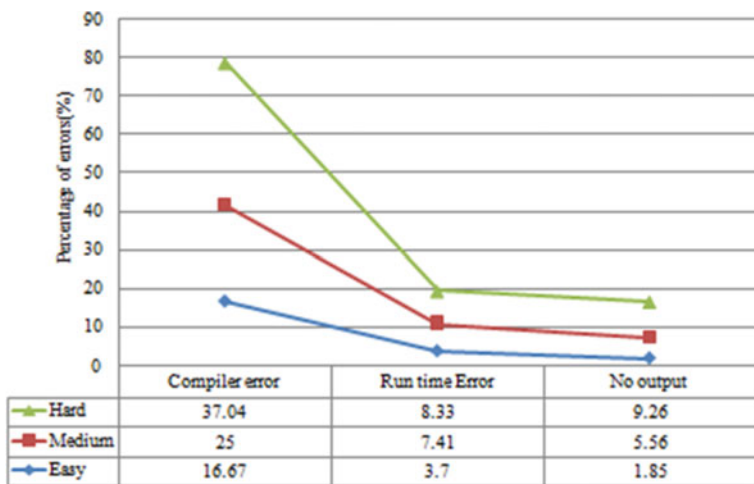


Fig. 2 Percentage of errors in each levels

to complete the program, time interval taken between the compilations, etc., can be analyzed. The simplest approach to finding the timing between each compilation is to compute the difference between the time stamps of the first and second compilations. Like this, we can compute the total compilation time taken to execute the program at all levels. The time is measured in seconds. Meanwhile, we can calculate the average time taken to debug the programs in easy, medium, and hard levels. That is, our normalization or standardization is based on the average time spent by the students while programming.

The goal of this study is to analyze the programming skill and how it gets reflected in academic performances. The final marks of 108 students were analyzed across various sessional exams. The assessment of these exams is based on the coding tests consisting of laboratory tests and viva voce. This will help in gaining a better knowledge of the programming course. This assessment method was used to assess the student's cooperation and progress in writing computer programs in the current programming course.

4 Methodology

As mentioned in the previous section, the primary aim of this work is to predict the programming performance of the students by analyzing the coding pattern after the compilation and examine various parameters that affect this performance. A subjective strategy of data preparation was endorsed to determine the student's perception of the factors.

4.1 Factors Influencing Programming Skill

The goal of this study is to recognize the factors that affect the achievement in an introductory programming course. Over several years, many researchers and teachers have carried out various investigations to identify the factors that affect student's success in their programming path. In this paper, we used a hypothesis way to determine the failure rates in these courses. Several problems that affect the programming courses have been identified by the previous studies. Some of them are insufficient program planning, inadequate problem-solving skills, lack of program logic, lack of identifying compiler errors as well as run time errors, etc. Different studies demonstrate various factors such as demographics profiles [3, 4], entry qualifications and prior programming experience [2], prior marks obtained in various science subjects [2], etc. But the current study deals with some programming performance measures rather than prior experience as well as demographics.

Academic context factors play an important role in influencing the academic progress of the students. To predict the success in an introductory programming course, the current study deals with mathematics marks [4, 15], final marks secured in qualifying examinations (one should be eligible to take part in the next course), and final marks obtained in the current programming course.

Measuring Debugging Capability and Hit Rate

One of the hardest situations for the novices is that they need to understand the working of the program and execution of the buggy program and must be aware of an application domain, errors, debugging methods, and the programming language. Therefore, teachers must take ample care of students who make the same mistakes, a frustrating number of attempts to understand error messages and correct their code, and waste hours for correcting errors, etc. By considering these issues, the current study analyzed the debugging behavior using some quantitative measurement called debugging capability (DC). While the students compiled the source code, the compiler generates some syntax errors, run time or exception errors, etc., and for each difficulty level, the programmers need to identify the errors that occurred after the compilation. To compute DC, the utmost number of errors obtained and penultimate compilation error values are captured from the compilation pattern during the compilation process. In this manner, we compute the debugging capability of the students in three levels (E, M, and H), and the numerical values should be normalized within the range from 0 to 1. To quantify the debugging capability, the compilation attempts and errors that occurred during the debugging stage were used.

The formula for calculating debugging capability is given as

$$DC_{s1} = 1 - \left(\frac{PCE_{\max} - PCE_{\min}}{CA} \right) \quad (1)$$

where

- DC_{s1} = debugging capability of individual student

- PCE_{max} = maximum number of errors occurred while debugging a single program in the compilation
- PCE_{min} = number of errors occurred in the penultimate position while debugging a single program in the compilation
- CA = total number of compilation attempts made by the student to reach the programming output

From Eq. (1), the quantified DC value is used to measure the debugging behavior of novice programmers. Later, we analyze how this behavior reflects the academic performance of a student. Based on the compilation pattern, one can understand how students identify the right solutions from the compilation effort that they have made so far. That is, how the rate of success of students in solving programming assignments can be measured. This rate (called as hit rate) represents the percentage of true solutions in terms of programming attempts. It is very significant to understand how many programming shots or attempts have been carried out by the students to determine the programming exercises.

$$\text{Hit Rate} = \left(\frac{\text{TS}_{s1}}{\text{PA}} \right) \times 100 \quad (2)$$

where

- TS_{s1} = average number of true solutions made by the student
- PA = average number of programming attempts made by the student

In particular, the 100% hit rate means every program done by the student was treated as a true solution. On the adverse, a hit rate of 0% indicates that all the programs done by a student were deemed solutions with errors. In such a way, the researchers can evaluate the progression of the students from the date the assignment exercises were proposed. This acknowledges the number of programming attempts required by the students to reach the final solution. The hit rate can be treated as a substantive manner to assess the connection between the students and the programming assignment solution. Some students may arrive at correct solutions and some others at errors.

From Fig. 3, the frequency of programming solutions indicates that the count of incorrect solutions was always higher than the correct solutions in medium and hard levels. But at the easy level, it can be seen that the incorrect solutions are less than the correct solutions.

To answer the question: What is the relationship between the hit rate and academic performance of a student? Or, how the hit rate is reflected in academic performance? For this, some statistical or analytical tests were performed to identify correlations between the variables. In this study, the student's academic performance was determined according to the final score obtained in the examination. Therefore, the study only addresses the relationship between hit rate and academic performance, and it will be explained in the next section.

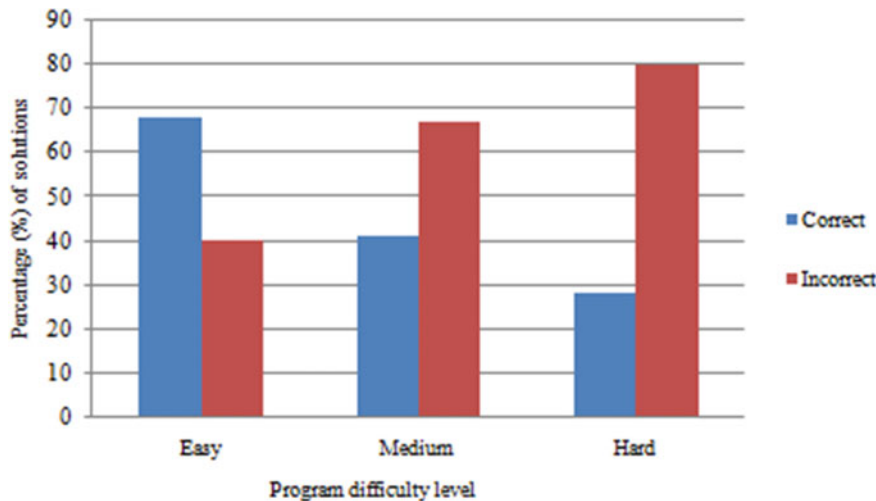


Fig. 3 Percentage of correct and incorrect solutions

Correlation analysis of Debugging Capability, Hit Rate, and Academic Performance

Our study investigated that there are some groups of students who have a reasonable knowledge of programming and that they could achieve very good marks in the final examination, while some others were not able to correct all the errors because of a lack of programming knowledge. That is, they are unsuccessful in finding the errors and, hence, lack the capability of program implementation. Taking this into consideration, the present study conducts some statistical tests to analyze the debugging behavior and programming skill. To correlate the dependency between various factors, Pearson correlation plays an essential role in identifying the relationship between them, and it is used to quantify the association between two continuous variables. In this segment, we make a correlation analysis between the following:

- Debugging capability (DC) of a student with marks obtained in the qualifying examination and the final examination of the current programming course.
- Hit rate of a student with final marks obtained in the examination of the current programming course.

By definition, the coefficient of correlation assumes any values in the interval between -1 and $+1$, and it is calculated as

$$r = \frac{n(\sum xy) - (\sum x)(\sum y)}{\sqrt{[n \sum x^2 - (\sum x)^2][n \sum y^2 - (\sum y)^2]}} \quad (3)$$

where

- n = the number of students
- x and y = the marks obtained in the qualifying examination and the final examination.

To find (a), refine the programming methods by considering the compiler errors and logical errors from the students. As part of this, the study needs to measure the debugging behavior using the debugging capability (DC) a quantified value in each level and the marks scored in the qualifying examination and the final examination of the current course, that is, how debugging skills are reflected in academic performance. The study also analyzes the effect of marks [4, 15] secured for Mathematics in the qualifying examination. The statistical correlation values between the above attributes are shown in Table 1. It is pointed out that the programming behavior of a student is weakly correlated with marks secured in the qualifying examination. The correlation coefficients of marks obtained for Mathematics and the final mark (0.21) are very less correlated, and the final marks in the qualifying examination (0.35) are also rather weak. Table 1 shows the strong positive association between the marks obtained in the final examination and the debugging capability of students at different levels (easy, medium, and hard). The correlation coefficients (0.83, 0.92, 0.89) at each level among them are highly correlated. From this, it is pointed out that the debugging skill of the student has an upper hand in determining the programming skill compared to the marks secured in the examination.

To find (b), some statistical or numerical tests were conducted to analyze the association between hit rate and programming performance in each level. To perform this test, the investigator had to use three factors—the number of true solutions attempted by the student, the number of programming attempts, and the marks scored in the final examination of the current programming course. Hit rate is measured using Eq. (2). Table 2 depicted the correlation analysis between the above factors. The results indicate that the students who score high marks in programming assignments are those who have made the least number of programming attempts with the right

Table 1 Results obtained by the correlation analysis of debugging capability

Performance criteria	Marks obtained for mathematics in qualifying examination	Final marks secured in the qualifying examination	Debugging capability (easy level)	Debugging capability (medium level)	Debugging capability (hard level)
Final marks secured in the examination	0.21	0.35	0.83	0.92	0.89

Table 2 Results obtained by correlation analysis of hit rate

Performance criteria	Hit rate (easy level)	Hit rate (medium level)	Hit rate (hard level)
Final marks secured in the examination	0.84	0.88	0.87

solutions (high hit rate). This table depicts the correlation analysis, which shows that there is a strong positive association between the hit rate of the students at each level (0.84, 0.88, 0.87) with marks secured in the final examination. This result intensified the outcomes of programming solutions received by the students, that is, the relationship established between hit rate and final marks empowers to theorize that the students with better hit rates are the individuals who make speculative programming attempts to solve the problem. In short, it is to be noted that they are very careful in eliminating the trial and error approach.

5 Evaluation and Interpretation of Prediction

Predicting the programming performance of students has consistently been a keen area of enthusiasm for many analysts. There have been numerous findings accomplished to predict students programming performance through various data mining techniques [15, 16]. The rationale behind the perception that data mining is an extensively popular tool used for evaluating a learner's programming efficiency comes from the fact that it offers various mechanisms to scrutinize the data and subsequently assists in investigating new trends and associations. In this work, supervised machine learning technique is used for analyzing the programming performance of the participants. The teachers will get an opportunity to recognize the student's performance from these predictions. This study implemented a method called multiple linear regression (MLR) which is a statistical methodology used for numerical prediction. The conventional measures such as R^2 and mean square error (MSE) are used to evaluate the MLR and to examine the goodness of fit of the regression models. In this study, we evaluated the goodness of fit of the regression model with some measured factors like debugging capability (DC) and hit rate to determine the predictive performance of the regression models, thus enabling educators to evaluate the prediction accuracy. The formula for calculating MAE, MSE, and RMSE is shown below.

$$\text{MAE} = \frac{1}{n} \sum_{j=1}^n |y_j - y'_j| \quad (4)$$

$$\text{MSE} = \frac{1}{n} \sum_{j=1}^n (y_j - y'_j)^2 \quad (5)$$

$$\text{RMSE} = \sqrt{\frac{1}{n} \sum_{j=1}^n (y_j - y'_j)^2} \quad (6)$$

To evaluate the benefit of fitting a parametric linear regression model, it is quite common to compute the coefficient of determination R square, which can be rendered

in terms of the percentage of variance stated by the model. If the number of parameters is large compared to the number of observations, R square can be increased systematically and artificially. A higher R^2 value indicates higher explanatory power for the model. This value increases when more factors are applied. That is why R square is supplemented with another coefficient called ‘adjusted R^2 ’ which does not affect this inflation problem.

The quantified value of debugging capability (DC) which is clearly shown in Eq. (1) can be employed to predict the programming behavior of the students. Using regression methodology, the result is shown below.

$$Y = 0.405 - (0.011 * DC_E) + (0.465 * DC_M) + (0.11 * DC_H) \quad (7)$$

where the independent variables DC_E , DC_M , and DC_H determine the debugging capability of each student at different levels (easy, medium, hard), and the computation is shown in Eq. (1). Y is the dependent or targeted variable which characterizes the marks secured in the final examination of the current course.

By considering the regression model, the R^2 value is 0.81, and evaluation metric values MAE and RMSE have very few residual values (from Table 3) which produces a better prediction. In addition to evaluating the goodness of fit of a regression model with R^2 and MSE, the distribution of residuals for the regression model must be examined. For this, a scatter plot is used for considering the hypothesis which is shown in Fig. 4. From this figure, it is analyzed that the regression line minimizes or reduces the squared sum of errors. Then the prediction will be more accurate. From the above analysis, it can be predicted that programming behavior is strongly correlated with final marks in the examination than marks obtained in the qualifying examination. It is pointed out that the debugging skill of the student has an upper hand in determining the programming skill compared to the marks secured in the examination.

Moreover, to assess the solutions of programming exercises done by the students, we have to evaluate the student’s hit rate. It is very significant to learn how many programming attempts were made by the students to determine the programming exercises. Hit rate calculation is shown in Eq. (2). By considering the factors such as the number of true solutions attempted by the student, the number of programming attempts, and the marks scored in the final examination of the current programming course, some analytical or statistical tests were conducted to recognize the relationships among them. Using regression methodology, the result is shown below

Table 3 Results of regression model based on debugging capability

Feature affecting the programming skill	Coefficient of determination (R^2)	Mean absolute error (MAE)	Mean-squared error (MSE)	Root mean-squared error (RMSE)
Debugging capability	0.81	0.047	0.0033	0.218

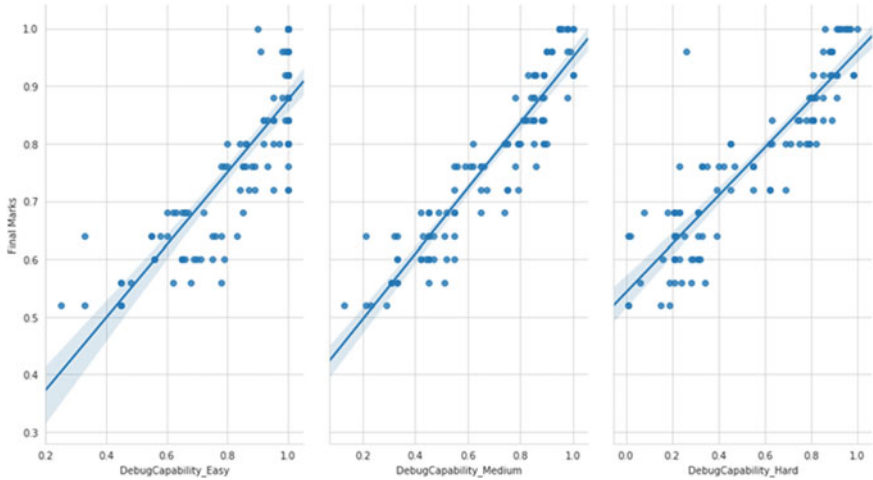


Fig. 4 Correlation between the debugging capability of each levels and the final marks

$$Y = 0.392 + 0.068 * \text{HitRate}_E + 0.352 * \text{HitRate}_M + 0.16 * \text{HitRate}_H \quad (8)$$

where the independent variables HitRate_E , HitRate_M , and HitRate_H deal with the average hit rate of each student at different levels (E, M, and H), and Y determines the academic score of the current programming course. To visualize the prediction of programming performance, a scatter plot was constructed based on the hit rate. This representation is illustrated in Fig. 5.

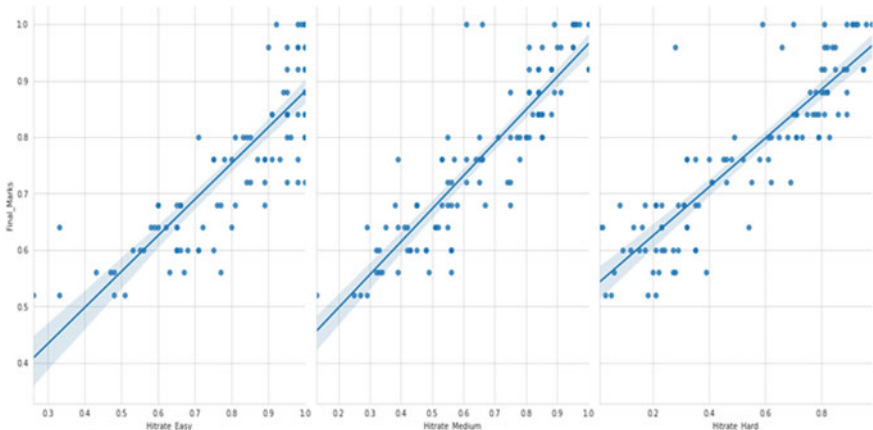


Fig. 5 Correlation between the hit rate of each levels and the final marks

Moreover, this investigation requires some validation measurement to determine the benefit of fitting in the regression analysis. R square test is used for better prediction. The closer the R -squared value to 1, the better the model is. But when the number of parameters is added to the model, the value of r-squared always increases, no matter whether the newly added parameters have a positive impact or not. The adjusted R square score is therefore used to penalize when additional parameters are added to our model. To evaluate the goodness of the fit, one usually compares the predicted values (\hat{Y}) with the observed values (Y) using R^2 and adjusted R^2 , and their formulas are given below

$$R^2 = 1 - \frac{SS_{\text{res}}}{SS_{\text{tot}}} \quad (9)$$

$$R_{\text{adj}}^2 = 1 - \frac{(1 - R^2)(n - 1)}{n - m - 1} \quad (10)$$

such that $R_{\text{adj}}^2 \leq R^2$. Here n is the number of data points, and m is the number of regressors. From the above equations, R^2 describes the ratio of the variances for a dependent variable (final marks) which is explained by to what extent the variance of one variable explains the variance of the second variable.

$SS_{\text{res}} = \sum (Y_i - \hat{Y})^2$ which is termed as sum of squared residuals and $SS_{\text{tot}} = \sum (Y_i - \bar{Y})^2$ termed as sum of total and $\bar{Y} = \sum \frac{Y_i}{n}$.

In contrast to the above equations, multiple linear regression simultaneously thinks about the impact of different explanatory variables on one response variable Y . In other words, it allows us to evaluate the effect of the dependent variable on multiple independent variables. Although multiple regression parameters can be calculated, this is challenging because it involves a large amount of mathematical algebra and the use of matrices. Debugging capability and hit rate at each level are considered as the predictor variables and final marks secured in the examination are targeted as dependent variables. While adding more independent variables, the regression equation becomes

$$\begin{aligned} Y = & 0.409 - 0.087 * \text{HitRate}_E + 0.067 * \text{HitRate}_M + 0.012 * \text{HitRate}_H \\ & + 0.051 * \text{DC}_E + 0.410 * \text{DC}_M + 0.106 * \text{DC}_H \end{aligned} \quad (11)$$

In this model consisting of six predictor variables, each predictor variable has its own coefficients. Again, the study does not permit causal conclusions, but it does allow us to investigate how a set of explanatory variables correlates with the response variable of interest. By validating the regression analysis, the goodness of fit (R square) is measured as 0.845 which indicates the better model. To penalize the explanatory variables, adjusted R square is 0.8357.

Significance of goodness of fit

One can see that multiple linear regression in this research can be used for predicting the debugging behavior and programming performance of the students. The summary of multiple linear regression using the ordinary least square method is given in Tables 5 and 6, and it has been found that this approach is having the highest value of R square which predicts the better model. Here the null hypothesis $H_0: \beta_1 = 0$ which indicates that there is no relationship between independent and dependent variables. If a model has $R > 0.7$ and the RMSE and MAE values are the lowest, then there is a strong correlation between the predicted values and the measured values based on a logical assumption. It can be noted from Tables 3 and 4 that the RMSE (0.218 and 0.211) and MAE (0.047 and 0.44) values were lower in the model predicted by the MLR, and they could predict acceptable levels of target values. While combining all the independent variables, the study assured the significance of the goodness of fit. The independent variables are really independent, but not collinear. There are various statistical tests used to evaluate the residual distribution. The statistical test results based on OLS regression are shown in Tables 5 and 6.

In this study, we use t-test to measure the null hypothesis that the coefficient of a regressor variable is zero, suggesting that the given regressor has no obvious

Table 4 Results of regression model using hit rate

Feature affecting the programming skill	Mean absolute error (MAE)	Root mean-squared error (RMSE)	R-squared	Adjusted R-squared
Hit rate	0.044	0.211	0.796	0.791

Table 5 OLS regression results

	HtRate_E	HitRate_M	HitRate_H	DC_E	DC_M	DC_H
Coef.	0.7240	0.3473	-0.1294	0.6504	0.4515	-0.1665
Std. err	0.063	0.091	0.053	0.069	0.113	0.062
$P > t $	0.000	0.000	0.017	0.000	0.000	0.009

Table 6 Statistical test values

Statistical tests	HitRate at 3 levels (E, M, H)	DC at 3 levels (E, M, H)	Combining all independent variables
Prob (omnibus)	0.007	0.000	0.574
Skew	0.568	0.738	0.185
Kurtosis	4.066	4.547	3.161
Durbin-Watson	1.697	1.669	1.791
Jarque-Bera (JB)	10.931	0.570	0.731
Cond. No.	16.1	20.2	30.4

impact on the response variable. The alternative hypothesis determines the predictor does contribute to the response. F -statistic can also be measured to determine how significant the fit is. In this testing, the threshold value is $\alpha = 0.05$ and $P(|t|) = 0.000 < \alpha$, so we can reject the null hypothesis. The t-test permits us to judge the significance of various regressors accepting that the residuals of the model are typically circulated around zero. So it is indicated that there is a relationship between the independent and response variable and the study accepted the alternate hypothesis. From Table 5, the probabilities of F -statistic based on three columns are 6.28e–100, 1.06e–99, and 3.82e–10.

6 Discussion

In this study, the various factors that affect the programming performance of the introductory programming courses are analyzed. In addition to identifying factors, the study also analyzed how debugging behavior and programming skills are reflected in the academic performance. The association between the students and the computer programming was concentrated through subjective analyses. Additionally, the student's performance toward the programming skill was determined through live programming assignments which was executed in the laboratory.

The marks obtained in the programming papers rely on the type of programming assignments the efforts exhibited by the students in the laboratory. The correlation coefficients from Table 1 (0.83, 0.92, 0.89) at each level (easy, medium, and hard) between the academic performance and debugging capability are highly correlated. From this, it is pointed out that the debugging skill of the student has an upper hand in determining the programming skill compared to the marks secured in the examination. That is, the analytic work done by the students and the laboratory assignments revealed that the number of attempts of programming errors is very much proportional to the marks scored in the final examination. Our study explores the significance of practical experience of computer science programming concepts, as it demonstrates that students with better programming aptitudes acquire better-paying jobs than students who are simply centered around the theoretical knowledge.

Table 2 depicts the correlation analysis, which shows that there is a strong positive association between the hit rate of the students at each level (0.84, 0.88, 0.87) with marks secured in the final examination. This result intensified the outcomes of programming solutions received by the students. Multiple linear regression (MLR) is used to predict the measured value of dependent variables that fit into historical data. By considering the regression model, the R^2 value is 0.81, and evaluation metric values MAE and RMSE have very few residual values (from Table 3) which produces a better prediction. From the analysis, it can be predicted that programming behavior is strongly correlated with final marks in the examination than marks obtained in the qualifying examination. Also from this, we can derive that the accuracy indicates the

difficulty level of the problem, and the number of programming questions successfully solved by the participants is two principle factors that impact the outcome irrespective of the platform that the student is taken part in.

The results of Table 4 suggest that the relationship between hit rate and final marks empowers to theorize that the students with better hit rates are the individuals who make speculative programming attempts to solve the problem. To visualize the prediction of programming performance, a scatter plot was constructed based on the hit rate which is depicted in Fig. 5. From Table 4, it is shown that the R square test is used for better prediction. The closer the R-squared value to 1, the better the model is (0.796). For a particular student, his or her previous programming history and assigned problem may predict that the problem will not be solved properly, but if the student tests the problem successfully, this may indicate that the student has improved the problem domain. Moreover, it was discovered that there is a linear association between hit rate and academic performance within the context of programming assignments. This recommends that students who see better the problems prior formulating and submitting possible solution for assessment require lesser attempts to find out the correct solution, and they also have good academic achievement. It indicates that the educators should try to implement some strategies to understand the problems for the students.

However, besides the above factors, some more parameters were considered for analyzing the programming skills and debugging behavior. The time taken to compile and the number of attempts made to compile a program were considered for each student to analyze whether there was any relationship between these parameters at each level. When students make programming assignments at an easy level, the value ($r = 0.436$) is moderately positive. That is, the amount of time spent on the easy level programming questions during debugging was significantly lower compared to the medium ($r = 0.594$) and hard level ($r = 0.688$) questions. Due to the complexity of the programs at the medium and hard levels, the time and compilation efforts are greatly augmented.

To evaluate the nature of debugging, students' errors in programming assignments based on time intervals were also analyzed. For each programming exercise, the number and type of errors were collected. The percentage of students making such errors was calculated to ensure that the archived data were significant. Results show that there is a strong positive correlation between the number of errors and the time taken to debug a program. The results suggest that, on the easy level, it is 0.396, the middle level is 0.494, and the hard level is 0.634. That is, even if the number of errors is high, a student who takes less time to debug the program should be greatly appreciated. However, the correlation between the average time spent on debugging and the average number of errors is positively correlated.

7 Conclusion and Future Scope

Depending on the goodness of fit and residual analysis results for the established regression model, multiple linear regression is suitable for constructing a student programming performance prediction model. In addition to predicting the student's programming performance using regression, analyses were conducted to understand the key factors influencing student programming behavior. The debugging capability of novice programmers with which they perform in the laboratory and the number of attempts they make in programming assignments are important features that influence the prediction. The results indicate that the student's skill set is the factor that contributes to the student's progress. Besides, it has been discovered that there is a linear relationship between academic score and achievement (or success) rate in the system of programming exercises. This desires that students who comprehend the problems well before submitting a solution for assessment need less effort and have better academic performance. Solutions offered by students with excellent academic performance and high success rates are essentially the right solutions.

The study exhibits a high correlation between debugging capability, rate of success, and student academic performance. The current research tends to the significance of practical knowledge of computer science programming ideas as it demonstrates that the students with better programming aptitudes receive better-paying occupation over students who focus solely on theoretical knowledge. In this implementation, the academic performance and debugging pattern of a student are considered. In the future, planning to execute a similar study is by investigating some other success factors such as learning strategy and motivation and also planning to build some automated assessment tools to determine what methods are most successful in teaching the debugging skills.

References

1. Sagar M, Gupta A, Kaushal R (2016) Performance prediction and behavioral analysis of student programming ability. In: 2016 International conference on advances in computing, communications and informatics (ICACCI), pp 1039–1045. IEEE
2. Amoako PYO, Adu-manu Sarpong K, Arthur JK, Adjetey C (2013) Performance of students in computer programming: background, field of study and learning approach paradigm. *Int J Comput Appl* 77(12)
3. Widyahastuti F, Tjhin VU (2017) Predicting students performance in final examination using linear regression and multilayer perceptron. In: 2017 10th International conference on human system interactions (HSI). IEEE, pp 188–192
4. Ayalew Y, Tshukudu E, Lefoane M (2018) Factors affecting programming performance of first year students at a university in Botswana. *Afr J Res Math Sci Technol Educ* 22(3):363–373
5. Ahmadzadeh M, Elliman D, Higgins C (2005) An analysis of patterns of debugging among novice computer science students. In: Proceedings of the 10th annual SIGCSE conference on Innovation and technology in computer science education, pp 84–88
6. Rodrigo MMT, Tabanao E, Lahoz MBE, Jadud MC (2009) Analyzing online protocols to characterize novice java programmers. *Philippine J Sci* 138(2):177–190

7. Jadud MC (2006) Methods and tools for exploring novice compilation behaviour. In: Proceedings of the second international workshop on computing education research, pp 73–84
8. Lee DMC, Rodrigo MMT, Baker RSJ, Sugay JO, Coronel A (2011) Exploring the relationship between novice programmer confusion and achievement. In: International conference on affective computing and intelligent interaction, pp 175–184. Springer, Berlin
9. Rodrigo MMT, Andallaza TCS, Castro FEVG, Armenta MLV, Dy TT, Jadud MC (2013) An analysis of java programming behaviors, affect, perceptions, and syntax errors among low-achieving, average, and high-achieving novice programmers. *J Educ Comput Res* 49(3):293–325
10. Kiran ELN, Moudgalya KM (2015) Evaluation of programming competency using student error patterns. In: 2015 International conference on learning and teaching in computing and engineering. IEEE, pp 34–41
11. Ahadi A, Lister R, Haapala H, Vihavainen A (2015) Exploring machine learning methods to automatically identify students in need of assistance. In: Proceedings of the eleventh annual international conference on international computing education research, pp 121–130
12. Alturki RA (2016) Measuring and improving student performance in an introductory programming course. *Inf Educ Int J* 15(2):183–204
13. Restrepo-Calle F, Ramírez Echeverry JJ, González FA (2019) Continuous assessment in a computer programming course supported by a software tool. *Comput Appl Eng Educ* 27(1):80–89
14. Alqadi BS, Maletic JI (2017) An empirical study of debugging patterns among novices programmers. In: Proceedings of the 2017 ACM SIGCSE Technical Symposium on Computer Science Education, pp. 15–20
15. Yang SJH, Lu OHT, Huang AYQ, Huang JCH, Ogata H, Lin AJQ (2018) Predicting students' academic performance using multiple linear regression and principal component analysis. *J Inf Process* 26:170–176
16. Bringula RP, Aviles ADV, Ma Batalla CY, Ma Borebor FT, Uy MAD, San Diego BE (2017) Factors affecting failing the programming skill examination of computing students. *Int J Mod Educ Comput Sci* 9(5)

Automated Short Video Caption Generation Using Video Features and Audio Content



Shubhra Choudhary, Yogesh Kumar Ahuja, Nishkarsh Makhija,
Srihitha Tangudu, and B. Rajitha

Abstract This paper presents a method to automatically generate caption for short videos using video features and audio content. Main aim is to generate one line captions for videos in natural language (i.e., English) which will describe the video according to its content. To accomplish this task first, audio content is extracted from video so that both the works can be performed separately. Firstly, captions are generated on video features, by creating a fixed length vector to represent the features extracted from each video frame using convolution neural network (CNN), and then it is decoded using long short-term memory (LSTM) model into a sequence of words composing the description of the video. Secondly, audio content is considered for generating captions. Audio content from the video file is extracted transcribed, and used as an input to sequence-to-sequence model, with an added attention layer. Once the captions are generated from both the video as well as audio content, then they are merged to generate final caption. The proposed method had been compared with existing approaches and found to be the best with a bilingual evaluation understudy (BLEU) score of 77.0.

Keywords Video caption generation · Information retrieval · CNN · VGG

1 Introduction

The video content on any search engine needs to be retrieved in less time and also the most relevant as per the query. To make any video retrieval faster or to understand the video content in less time, captioning the video will be helpful. There are many reasons to add/generate the captions to the videos such as: to improve the marketing strategy, faster accessibility, better indexing of the videos, improving the user viewing experience, to make video understandable to non-native speaker of the original video content, average watching time can be reduced as per the requirement of the user. Most importantly, it will be more beneficial to the deaf and dumb people who can read

S. Choudhary · Y. K. Ahuja · N. Makhija (✉) · S. Tangudu · B. Rajitha
Department of Computer Science and Engineering, Motilal Nehru National Institute of
Technology Allahabad, Uttar Pradesh, Prayagraj, India

and understand the natural language. So, video captioning in their native language can help such people to understand the speaker and video content as well. As per a survey, at least 5% population in the world faces such hearing issues [1]. Thus, video captioning can increase the video viewable in multiple languages and environments.

Video captioning is the process of generating textual description of a video. It is a trivial task for humans to caption a short video, but it is a difficult task for machines. This problem connects computer vision and natural language processing in the field of artificial intelligence. Getting to know the main content of video, especially when the videos are of large size, it is a tiresome and time-consuming process. It is still easy for humans to watch a video to know about its content, but it is challenging task for a machine to be able to successfully identify the video content and describe it. Thus, this paper tries to take this work which not only requires recognizing objects but also other visual elements such as actions and attributes. Later, construct a fluent sentence describing how objects, actions and attributes are related in a video. In other words, it is intended to generate a single line caption describing the events in the video.

This work concerns with “automated short video caption generation using video features and audio content.” This paper is aimed to generate one line captions for videos in natural language (English). This application bridges the gap between the vision and natural language. Pretrained networks of existing architectures are used for features extraction from the video’s frames. To accomplish the desired task, the concept of transfer learning is used to generate the video feature representation. The whole task of this paper is divided into two modules. One uses video features and other uses audio features to extract information and generate caption. Later, the model is tested on Microsoft video description corpus (MSVD) data-set which is the largest data-set of videos and sentence pair. For performance evaluation, a bilingual evaluation understudy (BLEU) score is used. BLEU is a metric for evaluating a generated sentence to a reference sentence.

The paper is organized as follows: Sect. 2 describes the literature articles pros and cons; Sect. 3 presents the methodology of the proposed approach. Section 4 describes the experimental setup and result analysis. Finally, Sect. 5 presents the conclusion of the paper.

2 Literature Survey

Many different methods for getting information from videos and captioning it as a natural language text has been proposed by researchers. Most of the work in this field can be divided into two approaches, namely template-based approach and encoder-decoder approach. In template-based approaches, first some specific semantics for language grammar which act as template will be defined. Then, a parser forms a sentence by finding specific components of a semantic such as subject, verb, and object. These components are combined to form a natural language sentence. Secondly, encoder-decoder approach is a two-step process. In that the first step, a

fixed length vector representation of video is generated by extracting features from a neural network. In the second step, a long short-term memory (LSTM) network is used to generate sequence of words composing the description of the video from the extracted features. It was first proposed in [2]. Many researchers take inspiration from encoder-decoder model and modified it to make it better. To evaluate the performance of the model bilingual evaluation understudy (BLEU) score is used.

Neural networks, as its name suggests, is a machine learning technique which process information in a similar way the human brain does. Neural nets are a means in which a computer analyzes training examples to learn to perform some task. A neural net consists of a large number of basic processing nodes that are densely interconnected. Most of neural networks that are created nowadays are organized into layers of nodes, and they are “feed-forward” so that the data move through them in only one direction. There can be a large number of layers in neural networks. While training a neural net, its weights and thresholds are initialized with random values or zeros values. Training data is fed to the input layer and it then passes through the succeeding layers where it will get transformed in complex ways, till it reaches the output layer where it is radically transformed. During training, the weights and thresholds are continually adjusted with backpropagation method until training data with the same labels consistently yield similar outputs.

A convolutional neural network (ConvNet or CNN) stands for class of deep, feed-forward artificial neural networks with its application in analysis of visual imagery. Connectivity pattern between different neurons is inspired from animal visual cortex. They are made up of neurons that have weights and biases that could be adjusted while learning. Each neuron in a CNN receives inputs, performs a dot product and follows it with a nonlinearity optionally. The entire network still expresses one single differentiable score function and they have a loss function (example—SVM/softmax) on the last (fully connected) layer. Their learning is the same as that in neural networks.

Recurrent neural network, popularly called RNN, is an artificial neural network architecture, having internal memory and in which the connections between different units form a directed graph along a sequence. This renders it to exhibit a dynamic temporal behavior for a time sequence. RNNs use their internal state called memory to process sequence of inputs unlike feed-forward neural networks. Long short-term memory networks (LSTMs) are a special kind of RNN, specially designed to avoid the long-term dependency problem. This problem arises when the next word which needs to be generated is dependent on the word generated way before it. Thankfully, remembering information for long periods of time is practically LSTM default behavior, something they are designed to learn.

In [3], the author devised a model which uses play-and-plug PICKNet in encoding phase and a gated recurrent unit (GRU), a simplified version of LSTM in decoding phase. It has a BLEU score of 46.1. In [4], author proposed a model which uses pretrained CNN models in first step and fused multi-model information LSTM for the second step. It also uses memory modeling techniques to increase the ability of CNN. It has a BLEU score of 52.82.

Researchers modified encoder-decoder architecture to make it more beneficial. In [5], author proposed a novel recurring neural network (RecNet) with the encoder-decoder-reconstruction architecture. In this model, re-constructor is to build on top of encoder-decoder architecture to enhance the relationships between the input video sequence and the caption. It has a BLEU score of 52.3. In [6], author modifies encoder-decoder architecture by using temporal segmentation, i.e., they first segment video into ‘S’ number of clips of equal time intervals, and then encode it using encoder. It uses pretrained ResNet model for encoding. It has a BLEU score of 51.7.

The method of this paper is inspired from encoder-decoder architecture and tried to build a modified model over it. Although many models has been proposed in literature, but their BLEU score was less than 60. Along with it they were not focused on important part of video content which is audio associated with it. Most of the times only video frames may not be enough to justify information in video. Thus, our approach uses both, i.e., information from video frames and audio, to generate caption.

3 Proposed Model

In the proposed model of this paper, captions are generated considering both the video features and audio content of the video. Firstly, caption is generated based on video features, for which, we extract features from the video frames using CNN and generate a fixed length vector representation of it, then this vector is used in decoding phase to compose a sequence of words, describing the video using LSTM. The CNN used in the paper is pretrained VGG model; the advantage of using a pretrained network with transfer learning is that it is typically much easier and faster than training a network. It allows us to build an accurate model in less time and computationally saving. Secondly, audio content of videos is considered to generate a caption. Audio content from video is extracted and transcribed, and used as input to sequence-to-sequence model, with an added attention layer.

The proposed model is divided into two modules, **module-1: captioning via video features** and **module-2: captioning via audio content of video**. Here, the intention is to present the results from both the modules, so that it can handle videos with audio in different languages and muted videos as well. Moreover, in case video and audio contents are unrelated, in that case having both the captions help in better understanding the video. The complete process of the paper is shown in Fig. 1.

3.1 Module-1: Captioning via Video Features

Video Preprocessing. The input videos are used to generate a fixed length vector representation of the same which is obtained after running a forward pass till the penultimate layer, i.e., the FC7 (fully connected) layer, after applying the rectified

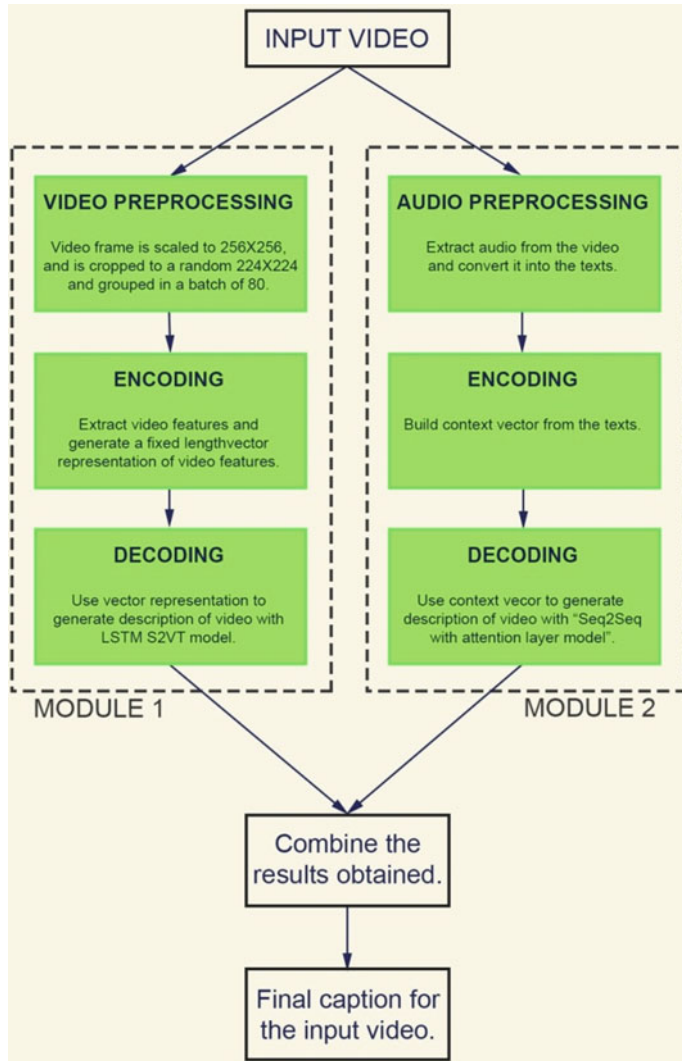


Fig. 1 Proposed model

linear unit (ReLU) nonlinearity of VGG-19 model. The input frames were grouped in batches of 80 frames and fed to VGG-19 CNN, in which the last fully connected layer is removed. Here, a pretrained VGG model is used, which is trained on 1.2 M image ILSVRC-2012 object classification subset of the ImageNet data-set [7], publicly available via the Caffe ModelZoo. Each input video frame is scaled to 256×256 and is cropped to 224×224 size randomly, and it is then grouped in batch size of 80 to input in the CNN to get the embedding. The original last fully connected classification layer of the CNN is removed.

Text Representation. Vector encoding is used to represent the final output which is sequence of words (1-of- N coding, where N is the size of the vocabulary). These vectors obtained from CNN are combined with first LSTM output h_i . Later, they are sent as an input to second LSTM.

Caption Generation. The input video and text are processed to input them to the LSTM stack. For video caption generation, an approach similar to S2VT as proposed in the paper [8], which is a sequence-to-sequence model for video description, is used. The input is going to be a variable length sequence of video frames (x_1, \dots, x_n), with the required output as a sequence of words (y_1, \dots, y_m), where for this sequence-to-sequence problem, and an LSTM recurrent neural network (RNN) is used in training module. A stack of two LSTMs with 1000 hidden units each is used; the input (x_i) of the second LSTM is taken from the hidden representation (h_i) of the first LSTM layer. Video frames are modeled using the top LSTM and the output sequence of word is modeled by the other. The same LSTM is used for encoding and decoding stage, which helps in parameters sharing.

During training stage, the top LSTM gets as input the video frames features, in batches of 80, while the second LSTM layer receives its input from the hidden representation h_i . It concatenates it with null padded input words (zeros) and then encodes it. The decoding stage starts when all the input video frame exhausts in which the input to the first LSTM layer is padding input which simply a vector of zeros is. So in the encoding phase, a sequence of hidden states (h_1, \dots, h_n) is computed by first LSTM given an input sequence X (x_1, \dots, x_n). During the decoding phase, distribution over the output sequence $Y(y_1, \dots, y_m)$ given the input sequence X is defined as follows:

$$(y_1, \dots, y_m | x_1, \dots, x_n) = \prod_{i=1}^m p(y_i | h_{n+i-1}, y_{i-1}) \quad (1)$$

where the distribution of $p(y_i | h_{n+i})$ is given by a softmax over all of the words in the vocabulary. The model is maximized for the log-likelihood of the predicted output sentence given the previous words it has seen, and the hidden representation of the visual frame sequence, using stochastic gradient descent. The loss for the decoding stage is only computed. From Eq. 1, for a model with output sequence $Y = (y_1, \dots, y_m)$ and parameters θ , this is calculated as:

$$\theta^* = \arg \max_{\theta} \sum_{i=1}^m p(y_i | h_{n+i-1} | y_{i-1}, \theta) x e^{-x^2} \quad (2)$$

Softmax function is applied on the output z_i of the second LSTM layer to get the probabilistic distribution over the words y_0 in the vocabulary V to get the emitted word (y).

$$p(y | z_i) = \frac{\exp(W_y * z_i)}{\sum_{y' \in V} \exp(W_y * z_i)} \quad (3)$$

The use of TensorFlow allows to save and restore the session later, which had helped to share weights and biases learnt in training and also during the testing phase.

3.2 *Module-2: Captioning via Audio Content*

Video Preprocessing. In order to obtain the audio content from the videos, first the audio is recorded from mp4 video files and then with obtained mp3 from videos, and text is transcribed using Google speech to text API as supported by “speech recognition” library in Python. As the videos could have large audio content, splitting method has been used for audio based on silence so that correct and complete transcribed text corresponding to audio in videos is extracted.

Text Representation. A comma separated files having video id, summary, and text is generated first to train and test the output of the proposed approach. The text is obtained by transcribing the video files. The texts and captions are cleaned so as to expand short forms, remove HTML tags, punctuations, parenthesis, stop words, and to have them entirely in lower case. The summaries are added with starting and ending tokens to mark their start and end. To create a vocabulary, a tokenizer is used which can build the vocabulary having words with frequency more than a threshold in the input text or summary and converts their word sequence to an integer sequence.

Caption Generation. An abstract summary is created for all the videos using sequence-to-sequence (Seq2Seq) modeling [9] with attention layer that generates output (T_y) of different length from input of length (T_x), this architecture being called encoder-decoder architecture. Here, an attention layer has been added to improve the results. In the first step, encoder RNN produces a sequence of encoder hidden states by reading the source text word-by-word. Once the entire source text has been read by the encoder, the decoder begins to extract the sequence of words that should form the caption. In each step, the decoder updates its hidden state depending on the previous word of the summary received as input. On the first step, a special “sostok” token is used to signal the beginning of writing. This is used to calculate the probability distribution over the words in the source text. It helps the network to look selectively to produce the next word. In Fig. 2, the complete process of encoder and decoders for both modules has been depicted in detail. After that, this probability distribution is used to generate a weighted sum of the hidden encoder states, known as context vectors. The context vector can be considered as knowledge of “what has been learned from the source text” on this step of the decoder. Finally, the decoder hidden states and the context vectors are used to calculate the probabilistic distribution of the words in a huge fixed vocabulary. The word with the largest probability is selected as output, and the decoder moves on to the next step. The decoder’s ability to freely produce words in any order (including words that do not appear in the source text) makes the sequence-to-sequence model a powerful solution to abstract summary. A stacked LSTM is used which is known to learn problems with long range temporal

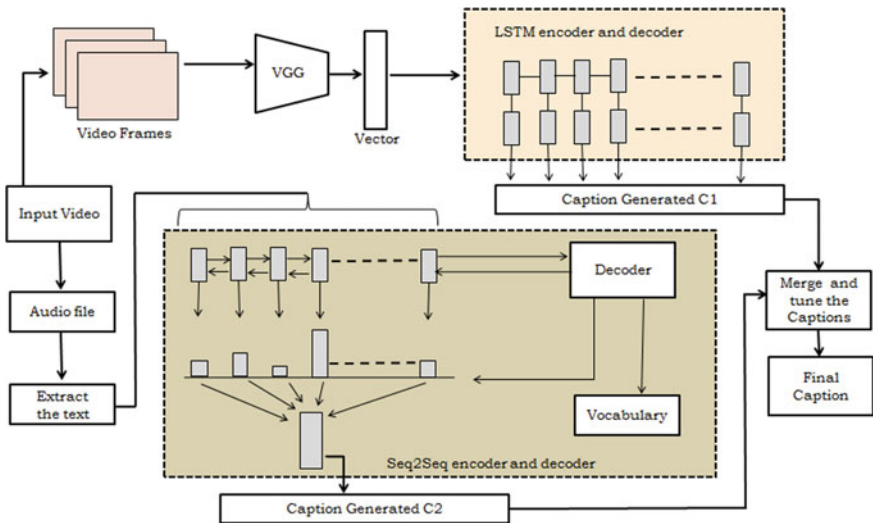


Fig. 2 Complete process of LSTM and Seq2Seq models

dependencies that has multiple layers of LSTM stacked on top of each other leading to a better representation of the sequence.

4 Results Analysis of Modules

The results are shown for both the modules individually in the following sub-sections.

4.1 Module-1

Data-set: Microsoft video description corpus (MSVD) data-set [10] has been used which is based on small parts of YouTube video clips and each having human annotated sentences, related to that part only. For the video clips, since a large number of them are not available at YouTube now, another data-set tarball provided at [8] has been added for training and testing. It provides the video description corpus. The original corpus has multilingual descriptions, but for this paper uses only English descriptions. The video clips depict a single, unambiguous action or event. The data-set was then divided into train and test sets in the ratio of 0.9. The input video specifies what part of video is taken for captioning as start and end time in seconds.

Results: The input video specify what part of video is taken for captioning as start and end time carried out in seconds. We were able to generate the video features,

which was result of application of VGG-19. The vocabulary was successfully generated, based on words present in captions so that it can be used to train the model, and the captions were encoded in size of vocabulary. With the access of Google Colab GPU, module-1 trained the model for 500 epochs and generated full sentences. Most of the sentences are found to convey sense and not distorted the idea of original content of the video. The output for the real-time video present at this link <https://www.youtube.com/watch?v=UgUFP5baQ9Y>, was tested on the proposed model and it generated the caption as “three women are dancing.” The same is shown in Figs. 3 and 4.

The main aim in training step was to minimize the cross-entropy loss of the true distribution and the estimated distribution of encoded text. The loss ranged from 38.261257 at the end of epoch 1 to 7.607178 at the end of epoch 500. For measuring the performance of the proposed approach, the BLEU score is calculated in the result obtained, which is found to be 77.95. The comparative analysis of proposed approach and previous methods [3, 5, 6, 11–20] is shown in Table 1.

```

preprocess.ipynb
File Edit View Insert Runtime Tools Help
CODE TEXT CELL CELL
> / 01DJG0q9j_K_1_24.avi
[ ] 8 0lh_UWF9ZP4_50_60.avi
     9 0I4VKj4d0WI_24_40.avi
C 10 0lh_UWF9ZP4_38_46.avi
    11 _txL57SS_0A_13_23.avi
    12 0lh_UWF9ZP4_27_31.avi
    13 _QJbjKkfdcs_52_57.avi
    14 0hyZ_3YhZc_279_283.avi
    15 _09kW8nuRU_77_81.avi
    16 0hyZ_3YhZc_352_356.avi
    17 0lh_UWF9ZP4_21_26.avi
    18 _xf24TYgbuY_14_20.avi
    19 00jrXRMlZOY_0_10.avi
    20 _60TzzK7t9Y_73_78.avi
    21 _UqnTFs1BLC_23_27.avi
    22 _ZnwKOzpt2I_69_76.avi
    23 _pBeOAMjGm8_1_18.avi
    24 _pj2Nutu5v8_1_8.avi
    25 _hbPLsZvvo_323_328.avi
    26 _aaMGK6GGw_57_61.avi
    27 _o1UXSxTjfo_68_80.avi
    28 _9iGSge01PM_3_11.avi
    29 _0nX-El-ySo_83_93.avi

```

Fig. 3 Video features extracted

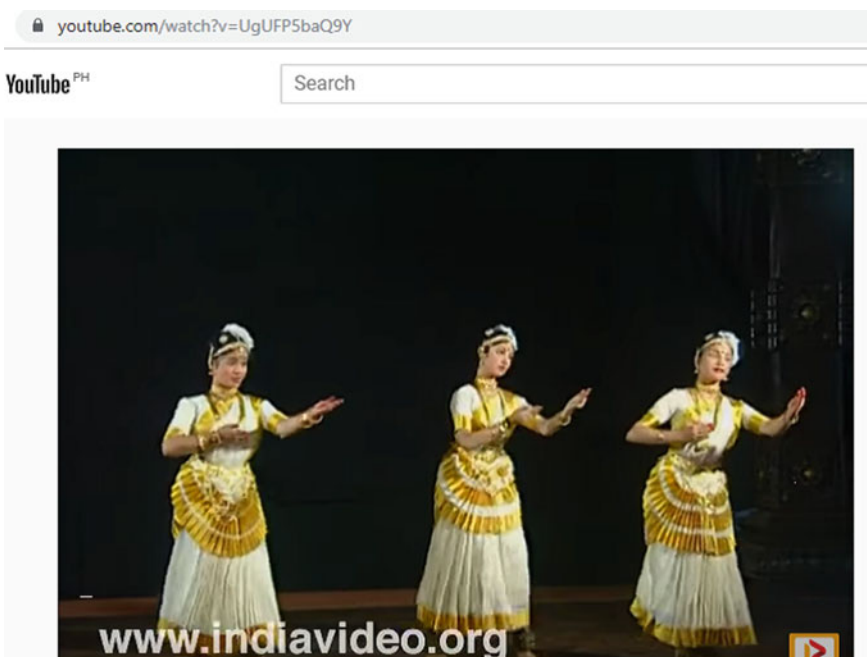


Fig. 4 Video screenshot captioned as “three women are dancing”

Table 1 Comparison between the proposed approach and literature approaches using BLEU score on MSVD data-set

Techniques/models/methods	BLEU score
h-RNN	49.9
MM-VDN	37.6
Glove + Deep Fusion Enable	42.1
HRNE	43.8
GRU-RCN	43.3
LSTM-E	45.3
SCN-LSTM	51.1
LSTM-TSA	52.8
TDDF	45.8
BAE	42.5
PickNet	46.1
M3- IC	52.8
RecNetlocal	52.3
TSA-ED	51.7
S2VT(VGG), ours	77.9

4.2 **Module-2**

Data-set and results: A number of videos have been downloaded from different domains, namely of wildlife, sports, cooking, etc. First, their audio content is obtained as spoken in the video. Then, using Google speech to text API as supported speech recognition library a feature file is created containing corresponding text and summary. Later, an architecture called as encoder-decoder, i.e., a Seq2Seq architecture with attention layer is added. The performance is measured using the BLEU score and ID found to be 0.92.

5 Conclusion

This paper is mainly aimed to generate an automated video caption for any video which is audio-based or a muted video. For this task, the present paper work has been divided into two modules, first, the video caption generation using the frames, and second, the caption generation using the audio content of the video. The performance of the proposed method was measured using BLEU score. Based on the analysis and the comparative measures, it is found that the proposed method is better than the literature methods. The proposed method had various applications such as business publicity/growth, improve marketing strategy, faster accessibility, better indexing of the videos, improving the user viewing experience, to make video understandable to non-native speaker of the original video content, beneficial to the deaf and dumb people. The proposed model currently stick to only English language, but, in future, it can be further extended to other native languages for even better accessibility.

References

1. Deafness and hearing loss. <https://www.who.int/news-room/fact-sheets/detail/deafness-and-hearing-loss>. Accessed 27 Nov 2020
2. Venugopalan S, Xu H, Donahue J, Rohrbach M, Mooney RJ, Saenko K (2014) Translating videos to natural language using deep recurrent neural networks. CoRR, abs/1412.4729 (2014)
3. Chen Y, Wang S, Zhang W, Huang Q (2018) Less is more: picking informative frames for video captioning. CoRR, abs/1803.01457
4. Wang J, Wang W, Huang Y, Wang L, Tan T (2016) Multimodal memory modelling for video captioning. CoRR, abs/1611.05592
5. Wang B, Ma L, Zhang W, Liu W (2018) Reconstruction network for video captioning. CoRR, abs/1803.11438
6. Wu X, Li G, Cao Q, Ji Q, Lin L (2018) Interpretable video captioning via trajectory structured localization. In: 2018 IEEE/CVF conference on computer vision and pattern recognition, pp 6829–6837
7. Imagenet. <https://www.image-net.org> (2020). Accessed 27 Nov 2020
8. Venugopalan S, Rohrbach M, Donahue J, Mooney R, Darrell T, Saenko K (2015) Sequence to sequence—video to text. In: 2015 IEEE international conference on computer vision (ICCV), Dec 2015

9. Sutskever I, Vinyals O, Le QV (2014) Sequence to sequence learning with neural networks
10. Collecting multilingual parallel video descriptions using mechanical Turk. <https://www.cs.ute.xas.edu/users/ml/clamp/videoDescription>. Accessed 27 Nov 2020
11. Chen D, Dolan W (2011) Collecting highly parallel data for paraphrase evaluation. In: Proceedings of the 49th Annual Meeting of the Association for Computational Linguistics: Human Language Technologies, pp. 190–200, Portland, Oregon, USA, June 2011. Association for Computational Linguistics
12. Erkan G, Radev DR (2004) Lexrank: graph-based lexical centrality as salience in text summarization. ArXiv, abs/1109.2128 (2004)
13. Graves A, Liwicki M, Fernández S, Bertolami R, Bunke H, Schmidhuber J (2009) A novel connectionist system for unconstrained handwriting recognition. IEEE Trans Pattern Anal Mach Intell 31(5):855–868 (2009)
14. Li X, Zhao B, Lu X (2017) MAM-RNN: Multi-level attention model based rnn for video captioning. In: Proceedings of the Twenty-Sixth International Joint Conference on Artificial Intelligence, IJCAI-17, pp 2208–2214 (2017)
15. Mehta N, Pai S, Singh S (2020) Automated 3d sign language caption generation for video. Univ Access Inf Soc 19:725–738
16. Nenkova A, Vanderwende L, McKeown K (2006) A compositional context sensitive multi-document summarizer: exploring the factors that influence summarization. In: Proceedings of the 29th Annual International ACM SIGIR conference on research and development in information retrieval, pp 573–580 (2006)
17. Olivastri S, Singh G, Cuzzolin F (2019) End-to-end video captioning. In: Proceedings of the IEEE/CVF international conference on computer vision (ICCV) Workshops, Oct 2019
18. Sak H, Senior A, Beaufays F (2014) Long short-term memory recurrent neural network architectures for large scale acoustic modeling. In: Proceedings of the annual conference of international speech communication association (INTER-SPEECH)
19. Shen Z, Li J, Su Z, Li M, Chen Y, Jiang Y-G, Xue X (2017) Weakly supervised dense video captioning. In: 2017 IEEE conference on computer vision and pattern recognition (CVPR), July 2017
20. Wang X, Chen W, Wu J, Wang Y-F, Wang WY (2018) Video captioning via hierarchical reinforcement learning. In: Proceedings of the IEEE conference on computer vision and pattern recognition (CVPR), June 2018

A Method of Polytexture Modeling in 3D Anatomy Simulators



Alexandr Kolsanov , Sergey Chaplygin , Aikush Nazaryan , and Anton Ivaschenko

Abstract The paper presents a problem of computational complexity balancing of 3D models of human body parts in order to provide universal access to the knowledge based on highly realistic anatomy models from the devices of high and low performance. There is presented an innovative method of polytexture modeling that provides adaptive complication of 3D anatomy scenes capable of solving the problem of visualization using various client devices. The proposed method is based on the modern advances in computational anatomy—a new scientific direction that develops the capabilities of simulation learning technologies in the three-dimensional space of virtual reality. Research results are illustrated by application of 3D anatomy simulation technologies in medical universities in Russia.

Keywords Simulation · 3D models · Anatomy · Computing

1 Introduction

Human anatomy is one of the most important disciplines in higher medical education. At the same time, there is a tendency to reduce the number of classroom hours for the study of anatomy with an increase in the volume of extracurricular and independent work of students. Taking into account the high role of visual methodological material necessary in the study of this discipline, it is important to provide students with access to high-quality and visually attractive visual content of 3D anatomy simulators.

Realistic simulation of anatomy scenes is a complex technical problem. Modern applications including surgery training suites and 3D atlases provide sufficiently detailed educational material good enough for educational purpose. Nevertheless, their practical use remains yet challenging due to the problems with their visualization using low-power devices including tablets and smartphones. High quality of 3D scenes requires high performance computers equipped with modern graphic

A. Kolsanov · S. Chaplygin · A. Nazaryan
Samara State Medical University, 89 Chapayevskaya st., Samara, Russia

A. Ivaschenko ()
Samara State Technical University, 244 Molodogvardeyskaya st., Samara, Russia

processors. Simplification of the models leads to degradation of image quality and detail.

In this paper, we present an innovative method of polytexture modeling that provides adaptive complication of 3D anatomy scenes capable of solving the problem of visualization using low-performance devices.

2 Existing Technologies Overview

The growing prevalence of mobile technologies increases the educational perspectives of medical simulating applications [1]. This review describes the applications most useful to anatomical educators in clinical, academic and educational settings. New applications such as Visible Body, 3D4Medical and Pocket Anatomy allow students to visualize and manipulate complex anatomical structures using detailed 3D models. They often contain complementary content, including a wide range of media, from instructional videos to interactive questionnaires.

It is noted that mobile devices allow presenting anatomical information to the user in the most appropriate way, taking into account his learning individualities. However, there is a problem of ensuring the level of detail and accuracy of the generated images required in higher medical education.

A rather interesting overview of imaging techniques used in teaching anatomy is presented in [2]. In addition to individual techniques, the implementation of virtual anatomy is considered. It is pointed out that Web systems play a critical role in enabling independent learning anytime. This examines the educational background, underlying data, model generation features and the inclusion of text components such as labels and explanations. Finally, stereoscopic devices and the first immersive VR solutions are discussed.

With the proliferation of tablets and three-dimensional (3D) applications, medical students are increasingly using 3D atlas to study anatomy. A study [3] investigating the effectiveness of a 3D simulation in providing students with an understanding of general anatomy analyzed the relationship between the use of a 3D atlas and learning outcomes in anatomy and embryology courses. Despite high educational efficiency, the problems are indicated that the described solution does not provide in-depth anatomical knowledge or memorization of the location of anatomical structures.

The study [4] presents the effectiveness of the use of three-dimensional models in teaching 67 medical students with a different spatial intelligence. The performance of students using 3D models in general, and the time spent on tasks was reduced. Ninety-seven percent of students reported that teaching using 3D technology is an effective teaching tool.

In [5], a critical assessment of the role and applicability of 3D technologies in medical education is made, in particular, taking into account the reliability of these models and assessment methods in simulation training in surgery. Very few studies have provided evidence of the correctness of the model or the estimation methods used. As a conclusion, the problem of ensuring the effectiveness of the application of

three-dimensional technologies in practice is raised, which is fixed despite the high potential of simulation technologies.

One of the methods for solving the problem of reducing the computational load in the study of 3D anatomical images proposes unloading data in files of common formats [6]. This once again underlines the importance of a systemic solution to the problem of load balancing.

Modern 3D applications for teaching anatomy are in different niches in the market and are focused on providing a certain range of advantages with acceptable disadvantages. All of this necessitates finding a balance between performance and visibility. This task can be solved in a single application by implementing dynamic adaptive loading of models using cloud technologies.

A systematic comparative analysis of mobile and Internet applications for the study of anatomy is presented in [7]. These studies were obtained on the basis of a comparative system analysis of 3D models, aspects of software and software functionality. Research results demonstrate the complexity of the task of choosing an effective solution, despite the large number of available electronic applications.

A successful solution to this problem is seen in the processing of three-dimensional anatomy models in order to ensure partial processing and loading. Selecting fragments and parts and ensuring autonomous work with them will allow balancing the computational load and ensuring the implementation of cloud technologies.

Modern advances in computational anatomy can solve this problem. This is a new scientific direction that develops the capabilities of simulation learning technologies in the three-dimensional space of virtual reality [8–10]. To control the formed three-dimensional picture modern methods and means of adaptive visualization allow tracking the feedback, analysis of behavior and fluctuations in the level of attention of the user, and building a system for adaptive control of visualization of the anatomical picture to adjust to a specific type of user and personalize the interface.

3 Scenario Ontology of 3D Anatomy

The preliminary stage of the method description is introduction of the specialized ontology acting as a knowledge base and forming the informational basis of the solution. Scenario ontology is proposed as a model for the distribution of computations for load balancing in multiuser remote access to the contents of a three-dimensional anatomy simulator. This ontology is required as a knowledge base for generation of various 3D scenes using compatible terminology, topology and semantics of the models of human body parts.

The scenario ontology of 3D anatomy contains a formalized description of human organs, and the interaction of which is described by their mutual arrangement in three-dimensional space. In this case, the bodies are also combined according to their functional purpose. The current state of organs and their relative position is described using a three-dimensional scene that simulates the physical and logical representation of the contents of a three-dimensional atlas. The physical representation describes

the real and possible behavior of an object. In the context of a simulator, this is a change in the location and/or configuration of an organ (position and orientation) in space.

Since the physical representation requires a fairly large amount of computation, it is proposed to store and process its data in the cloud. The physical representation of a scene object is determined by the properties of the object and the context in which it is used. One organ representation can be simulated in several different scenes. To implement a physical representation within the framework of a scenario ontology, its graphical representation (three-dimensional model) and a physical model (if necessary) are developed that describe possible reactions to the impact. This approach allows one to describe a change in the geometric state, for example, deformation.

A logical view contains a description of the relationships between objects in a scene that arise in the course of considering its functional or behavioral aspects. For example, it can be the entry of organs into one system or their change as a result of a disease. The logical representation models the reaction of an object to an impact, formalized as a chain of interrelated events.

It is proposed to separate the processing of logical views and partially process them in the cloud, and partially on client devices. This will ensure the required performance of simulation and high usability.

By a three-dimensional scene, we mean a set of physical and logical representations of objects, which are defined in accordance with the requirements of the anatomical picture formed by the atlas. The transition between the states of the scene is carried out when events occur: external (signaling the user's actions) and internal (arising during the simulation). Recording and processing of events are carried out on the user's terminal: a smartphone or tablet.

4 A Method of Polytexture Modeling

To ensure high realism of three-dimensional anatomical atlases, separate textures are developed for different organs. When superimposed on the surface of each organ, taking into account their relative position in space and model illumination, a picture is formed, which is usually observed in the educational process when familiarizing with human anatomy, or in surgical simulators when practicing the required skills of surgical intervention.

Requirements for textures differ depending on the application. In anatomical atlases, higher contrast and differentiation are required, in contrast to simulators, which require high realism. In addition, the textures of different elements and parts of the surface of one organ may differ.

Also, the requirements for textures are limited by the computational capabilities of the hardware and software of three-dimensional atlases, if necessary, provide the dynamic characteristics of organs in real time.

To solve this problem, an original approach based on polytextural modeling is proposed, which differs from analogs in the ability to optimize organ textures in conditions of a given realism and performance.

The processing of three-dimensional models based on polytextural modeling will make it possible to display interactive content of three-dimensional anatomical simulators, including with the help of devices with reduced performance.

In accordance with the principles selected above, this solution will implement two options for transferring the formation of anatomical scenes and displaying them on users' client devices. Switching between these options should be hidden from the user, taking into account the requirements of the cloud infrastructure, working with three-dimensional models for him looks like a single process of loading and refining the appearance of three-dimensional scenes.

The first option is to download ready-made 3D models adapted for display on a mobile device. These are, as a rule, simple models and lightweight textures that do not contain detailed details and do not provide high realism of the formed picture. For such organs and systems, simple operations are envisaged (changing the position in space, imposing a simple texture and a simple incision in the case of a homogeneous organ structure).

The second option is to execute a complex graphical query to the simulator, when a complex arrangement of atlas objects in space is performed on a mobile device or in a browser application, combining a large number of organs and systems and imposing complex highly realistic structures. In this case, the user operates in the preview mode with mock-ups of organs can perform cuts and sections, select and place organs on the stage. In this mode, the atlas objects are displayed in a semi-transparent form, and their borders are displayed with black lines.

When ready, this graphic request is sent to the server, where it is processed using the resources of the cloud information and computing infrastructure. Here, the required shaders are calculated, scaled and superimposed, which ensures high realism and reliability of the anatomical picture. The resulting images can undergo automated verification, as well as visual verification by experts for correctness. The resulting picture is returned to the mobile device in asynchronous mode and can be further used in training.

5 Implementation

Human organs were modeled in the Autodesk 3ds Max, which is a professional 3D modeling, animation and rendering design software. Distinctive features of the environment, which determine the main advantages, include extensive functionality for the development of complex highly realistic 3D models. As part of the chosen approach, the 3ds Max environment allows you to build new models with a complex structure based on standard objects. The use of primitives in combination with each other as elementary parts of composite objects allows you to connect different objects and provide an increase in the complexity of the constructed scenes.

The assembly of models is a collection of 3ds Max files and files of diffuse, normal, specular and special textures (alfa-channel in diffuse, emission, detail albedo, detail normal) on those objects where they are needed, or a collection of files in the Unity Package format containing required set of mesh models, materials and texture files. The assembly of models should contain files for all systems of both sexes, files for all additional scenes, files for all used textures. In the assembly of models, the presence of files of unused textures is unacceptable.

A model assembly version is a unique identifier for a model assembly, consisting of two digits separated by a dot. Modifications to 3ds Max files, Unity Package files or texture files must assign a new version number to the model assembly. The digit in the version number to the left of the dot should change if there is a large amount of change. The digit in the version number, located to the right of the dot, should be changed in case of corrections, or minor changes.

A model assembly change description file is a text file in a special format, which should describe all changes made to the model assembly version, the new assembly version number and the assembly version number relative to which the change file is maintained. An assembly for marking normal anatomy spots with textures is a collection of id texture files, files with names and descriptions of objects on textures, files for binding objects on textures to 3D models. The assembly for marking with textures must contain all the files necessary for the correct display in the atlas of texture marking of objects. In the assembly for marking with textures, it is not allowed to have files of unused textures, unused files with the names of texture markings and unused files for binding objects to 3D models.

An assembly for marking muscle attachment points with textures is a set of texture files and a text file with a list of all attachment points for muscle 3D models to bone 3D models. The assembly must contain all the files necessary for the correct display of muscle attachment points in the atlas. The assembly does not allow the presence of files of unused textures, as well as elements of the list of model mountings that are not associated with markings on textures.

Implementation results are shown in Figs. 1, 2 and 3. As a result, an interface design has been developed that allows users to provide a convenient user experience with the content of a three-dimensional anatomical atlas using low-performance client devices with a relatively small screen size.

The textured version of the assembly is a unique identifier for the models, consisting of two numbers separated by a dot symbol. When changing id texture files, files with names and descriptions of objects on textures, files of binding objects on textures to 3D models of the assembly version and a new number must be assigned for marking with textures.

The digit in the version number to the left of the dot should change if there is a large amount of change. The digit in the version number, located to the right of the dot, should be changed in case of corrections, or minor changes.

The proposed method and architecture of its software implementation provides an access to anatomy simulating technologies using low-power computers and mobile devices, which significantly expands their scope of application in higher medical education.

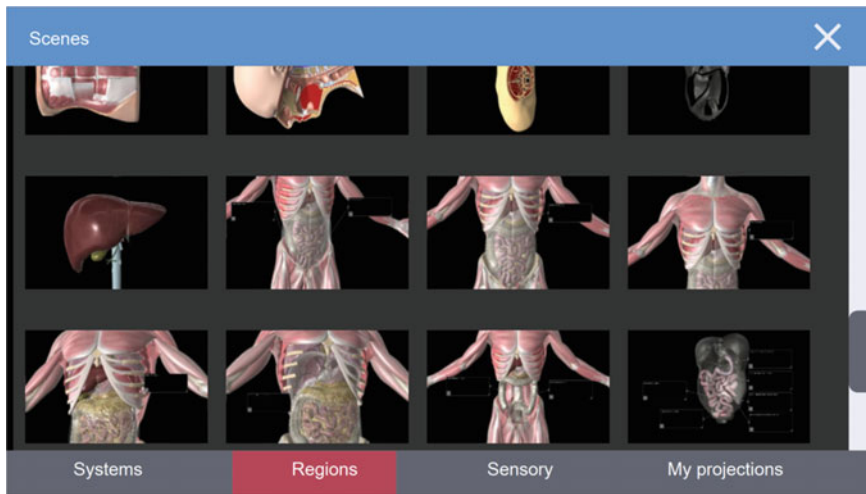


Fig. 1 Various scenes with different complexity

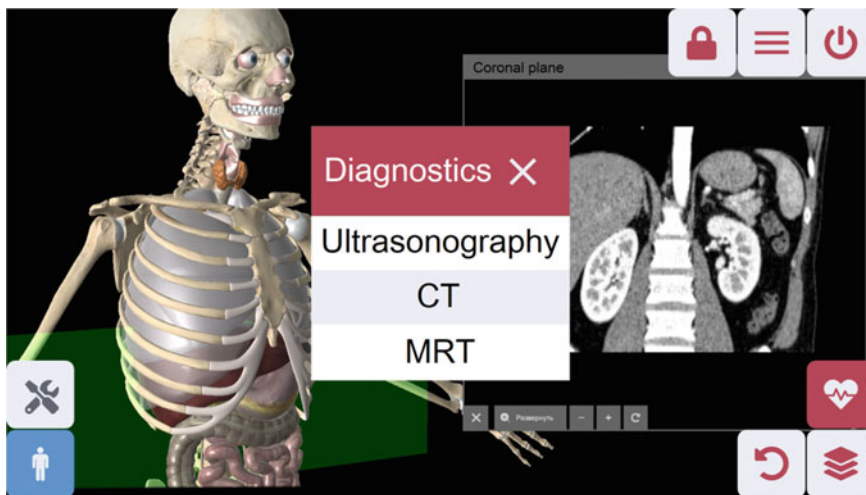


Fig. 2 Extension of the simple model with the results of KT diagnostics

6 Human Anatomy Simulation Application in Higher Medical Education

The introduced solution was used to develop series of simulation products for medical higher education. The doctor's knowledge of the individual anatomy from the stand-point of the three-dimensional topography of the organ structures of each patient

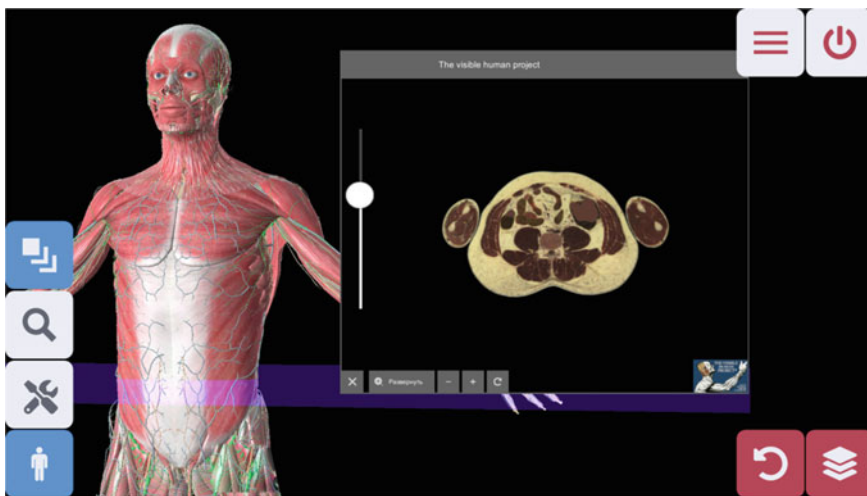


Fig. 3 Visualization of a medical cut

is becoming a leading task on the way to solving the issues of high-quality care provided by modern medical practice.

Human morphology, which studies the macro- and microscopic structure of the human body, is a fundamental discipline in medical universities and contains a huge amount of material that requires orderly study and detailed assimilation. The growing number of textbooks and atlases on human anatomy, unfortunately, does not improve the quality of students' knowledge. Often, even the style of presentation interferes with the correct perception of the studied area or an individual organ, and the illustrative material does not provide the necessary location and scale of the anatomical object.

The details of the structure and position of the organ, its shape and the relationship of organs are studied poorly by even quite successful students, and the bulk of students simply stop learning. Future doctors ultimately have a narrow mind without making significant efforts in a detailed study of the human body and make mistakes in the interpretation of the patient's health status, diagnosis and subsequent treatment. The considerable complexity of the study of anatomical disciplines and, at the same time, obtaining vital information about the structure of the human body, which is so necessary in clinical practice, can be compensated in the process of dissection of the human body. However, the current state of legislation puts medical universities in an extremely difficult position in the legal registration of cadaveric material, and its quality does not allow for full dissection of a large contingent of students.

The rapid process of digitalization of all spheres of human activity in general and medicine in particular is increasingly raising the issue of introducing modern teaching methods and computer simulators into the educational process, creating new forms of education associated with replacing traditional technologies by IT-based techniques. The translation of the mass of teaching aids into digital format of

the text only makes it accessible to a wide range of students, but does not solve the issue of both the long time that will be spent on its study and the lack of visualization of anatomical objects.

Introduction of modern simulation technologies to practice including the method of polytexture modeling allows developing a new branch of morphology, where a virtual person with characteristic proportional ratios and anatomical reliability of a living person with a full volume of images of macroscopic and microscopic anatomy of the male and female body, named computational anatomy, or *anatomia in silico*.

The proposed approach allowed creating a highly realistic low-poly model of the human body at the department of operative surgery, clinical anatomy with a course of innovative technologies at Samara State Medical University. The developed models made it possible to build a software and hardware complex for virtual work with a three-dimensional model of the human body—an interactive anatomical table “Pirogov”.

The new product has significantly expanded the scope of educational material from visual acquaintance with anatomy and obtaining textual information to checking the quality of the knowledge gained and automatic processing of results. In addition to the macroscopic structure of the human body, it is possible to go to the microscopic level, and it is also possible to compare various anatomical objects with each other (including norm and pathology), study additional diagnostic materials (CT, MRI, ultrasound (US)). The possibility to visualize not only the norm, but also pathologies and diagnostic data at the microscopic level distinguishes this educational product from analog developments.

7 Discussion

The solution was tested in practical classes in clinical anatomy for 3–4 year students and students of the faculty of advanced training of surgeons. Then, the database on anatomical objects was expanded and detailed, taking into account the requirements for the discipline “anatomy,” which not only made it possible to use the interactive atlas at the stage of completing the study of classical anatomy, but also made it possible to use it from the very first lessons in this discipline.

Given the complexity and volume of educational material on anatomy, which underlies the study of clinical anatomy, pathological anatomy, forensic medicine and other clinical disciplines, teachers have to use mainly an analytical teaching method. As a result, the whole human body is divided into systems, and then into individual organs. Clinical anatomy, like other clinical disciplines, needs a synergistic perception of certain areas of the human body, in which various organ systems are involved, interacting in a living organism precisely in a complex (synergistic) manner in their origin, development and functioning, and not in isolation. Such perception of the studied material is provided by a three-dimensional anatomical atlas, which includes four modes of operation.

Thus, the interactive anatomical table “Pirogov” allows transfer the study of anatomical disciplines to a new direction, as it helps students to better imagine the complex spatio-temporal organization of organ systems, heterogeneity, individuality and mobility of almost all levels of the living human body. It allows manipulations with a virtual person in space and time, becomes a reasonable alternative to traditional preparation, because it makes it possible to repeatedly remove and restore the volumetric layers of the human body and the relationship of organo-vascular-nervous formations. The interactive atlas provides a full cycle of studying anatomical disciplines—from visualizing anatomical objects to checking the quality of the information received, followed by automatic processing of test results.

The accuracy of the structure of the human body, the structuredness of a huge array of anatomical information, its storage, as well as the rapid search and quality of pathological samples make the developed solution unique in terms of anatomical, topographic and clinical content. Computational anatomy data are used not only in the educational process, but also in clinical practice, rehabilitation and research work. Strong assimilation of anatomical knowledge makes it possible to apply them in practice with a correct and adequate effect on the human body in the process of treatment, which is necessary for a quick return of a person to conditions of a favorable and harmonious life.

8 Conclusion

The proposed method extends an access to 3D content of simulated anatomy for the students of medical universities and training centers, medical specialists and employees of medical institutions, employees of sports organizations and rehabilitation centers, athletes (when developing individual training programs), etc. Implementation of the digital platform on its basis provides access to simulating technologies using low-power computers, which significantly expands its scope, especially under the conditions of distant education. It also allows realizing a personalized approach by taking into account the individual characteristics of the students' educational trajectories.

References

1. Lewis T, Burnett B, Tunstall R, Abrahams P (2014) Completing anatomy education using three-dimensional anatomy mobile software applications on tablet computers. *Clin Anat* (New York, N.Y.) 27. <https://doi.org/10.1002/ca.22256>
2. Preim B, Saalfeld P (2018) A survey of virtual human anatomy education systems. *Comput Graph* 71. <https://doi.org/10.1016/j.cag.2018.01.005>
3. Par S, Kim Y, Park S, Shin J-A (2019) The impacts of three-dimensional anatomical atlas on learning anatomy. *Anat Cell Biol* 52:76–81. <https://doi.org/10.5115/acb.2019.52.1.76>

4. Jamil Z, Saeed A, Madhani S, Baig S, Cheema Z, Fatima SS (2018) Three-dimensional visualization software assists learning in students with diverse spatial intelligence in medical education: anatomical sciences education. *Anat Sci Educ* 12. <https://doi.org/10.1002/ase.1828>
5. Kostusiak M, Hart M, Barone DG, Hofmann R, Kirollis R, Santarius T, Trivedi R (2017) Methodological shortcomings in the literature evaluating the role and applications of 3D training for surgical trainees. *Med Teach* 39:1–6
6. Park JS, Chung BS, Chung MS (2017) Digital anatomy using the surface models in portable document format file for self-learning and evaluation. *Digit Med* 3:133. https://doi.org/10.4103/digm.digm_29_17
7. Zilverschoon M, Kotte E, Esch B, ten Cate O, Custers E, Bleys R (2018) Comparing the critical features of e-applications for three-dimensional anatomy education. *Ann Anat Anatomischer Anzeiger* 222. <https://doi.org/10.1016/j.aanat.2018.11.001>
8. Ivaschenko A, Gorbachenko N, Kolsanov A, Nazaryan A, Kuzmin A (2016) 3D scene modelling in human anatomy simulators. In: Proceedings of the European simulation and modeling conference 2016, pp 307–314
9. Ivaschenko A, Gorbachenko N, Kolsanov A, Nazaryan A (2017) Adaptive human visualization in medical applications. In: Proceedings of SCIFI-IT 2017 conference, pp 59–64
10. Ivaschenko A, Kolsanov A, Chaplygin S, Nazaryan A (2019) Multi-agent approximation of user behavior for AR surgery assistant. *Smart Innov Syst Technol* 107:361–368

An Impact of Different Uncertainties and Attacks on the Performance Metrics and Stability of Industrial Control System



Brijraj Singh Solanki , Renu Kumawat , and Seshadhri Srinivasan

Abstract The revolutionized growth in the networked control system has made the system more vulnerable to different types of threats such as delays, packet losses, and attacks. Such uncertainties in the control system may be introduced in the forward and/or feedback direction by the intended attackers while transmitting the signal. Herein, the system is estimated by modeling different parameters along with the knowledge about the actual system while considering the delay, packet loss rate, etc., using system identification and True-Time tool. Also, the particle swarm optimization (PSO) algorithm is used for modeling the system and estimation of controller parameters. The efficacy of the estimated model is shown by evaluating the various performance measures along with the introduction of design of a model of attacks based on the estimated system parameters to compromise the actual network control performance. In the absence of attacks, the estimated model used here shows above 94% fit to the estimation data which indicate the efficacy of the estimated model. Later, different rates of packet loss such as 0, 5, 15, and 25% are introduced for estimating the system model. For each case, the attack is simulated to show the impact of service degradation attack on the performance metrics of the networked control system. The overshoots are 15.698% for 0% packet loss, 17.4% for 5% packet loss, 17.9% for 15% packet loss, and 17.5% for 25% packet loss along with modeled attack. The other metrics such as rise time, settling time, and peak time increase substantially, whereas root mean square value decreases, and the cost function increases for estimated system with different packet loss rate and attack, which is an indication of a compromised system.

B. S. Solanki (

Poornima College of Engineering, Jaipur, India
e-mail: brijraj@poornima.org

B. S. Solanki · R. Kumawat

Manipal University Jaipur, Jaipur, India
e-mail: renu.kumawat@jaipur.manipal.edu

S. Srinivasan

Karasalingam Academy of Research and Education, Krishnankoil, Tamil Nadu, India
e-mail: seshadri@klu.ac.in

Keywords Networked control system (NCS) · Particle swarm optimization (PSO) · Delay · Packet loss

1 Introduction

The networked connected control systems are characterized as a system where physical components are coupled together with closed control loop using communication network, while increasing the complexity of the system. Nowadays, networked control systems are being used in many applications such as industrial processes control, robotics control, medical field, and aircraft systems. The upgradation in technology is becoming the solution for faithfully transmitting the packets/signals and overcoming the problem of time delay in the networked connected control systems. The delays and packet losses in the networked control system worsen the response/performance of the physical process and try to fetch the system to the verge of instability. Therefore, estimation of delays, packet losses, and bandwidth are the key factors in stabilizing the physical process. These systems are also more vulnerable to malicious attacks. Thus, it is necessary to stabilize the system against the introduction of the attacks.

The networked control system may be fetched to the verge of instability by introduction of the attacks into the communication system that may be in the forward and/or backward stream. The main broad category of intervention may be service degradation, denial of service, etc., as have been reported in the literature. In this paper, the impact of these attacks on performance of the networked control system is presented.

The rest organizational flow of the paper is described as follows: The literature work is briefly described in the Sect. 2. Section 3 presents the problem formulation, and it also discusses the performance parameters for degradation of networked control system (NCS). The responses of the estimated system on the proposed methodology are summarized in Sect. 4. At the last, in Sect. 5, the conclusive remarks and future work are presented.

2 Background Work

In the networked control system, uncertain delays and packet losses are the key parameters to investigate the stability, where packet losses are designed using Bernoulli process. Some stability conditions have been derived to show the quality of measure of the defined method [1].

The predictive controller is designed to elaborate the response of the designed method for the controlled system. This may be affected by transmitting data due to insertion of denial of service attack [2, 3]. The introduced attacks are calculated

for the wireless connected networked control systems using the intrusion detection system, and authors have also validated the proposed method to be stable [4].

The delay estimation in the communication system is very important to design a controller for the networked control system, and it is estimated using Markov chain Monte Carlo method and from MODBUS over TCP/IP [5]. It has been observed that designed regulator performs better under the consideration of delay [6]. The stochastic optimal control system is designed to estimate the network delay dynamics, which showed the upgraded performance parameter of the control system [7].

The time delay attacks on the linear system are described in [8]. It is revealed that cryptography free time delay switch method showed the improved stability under delayed attack system. The networked motion control is simulated using the True-Time tool box, and it has been shown that the speed of the motor is not much affected by sudden change in the load [9]. The stability of the system also verified using the dynamical model of the said system by considering the parameter of network nodes. The better communication among the control devices and stability is achieved by the evaluated simulated system along with vehicle ad hoc network [10].

In this paper, the True-Time toolbox is used for developing the model of control system. It has been shown that the proposed method gives consensus along with the performance of the communication system while considering the delay. The improved performance for networked control system against service degradation, denial of service, and system identification attack was demonstrated in [11–13]. The optimized coefficients of plant and controller are estimated using system identification tool and BSA algorithm which shows the better performance while inducing such attacks.

The messaging data traveling from sensor to controller and from controller to actuator can be corrupted using different attacking techniques such as denial of service and replay attacks. The receding horizon control law and exponential stability are proposed to derive the stability condition for analyzing the performance [14, 15]. The improved performance of the control system for the distribution network control is addressed in [16]. The scheduling mechanism and strategy are used to show the efficacy of the system employed. The effect of delay, jitter, and loss of data packet in the transmission which is the key factor of instability of system is also discussed.

The performance of the control system is enhanced using the equivalent input disturbance estimator by rejection of the disturbances. Author also discussed the sufficient condition of the stability using linear matrix inequality tool to estimate the gain of state feedback controller. The system stability and performance can also be improved by using Smith predictor which compensates the delay [17]. The wireless communication system is used to model the distributed plant along with the True-Time MATLAB-based toolbox. Moreover, in [18, 19] author used PLEC block set for modeling the electrical system. In this, a wireless communication network link is used to control the active power and generator plant. The communication is the key issue between connected devices.

The general regression neural network (NN) is presented to model the delays, which affects the control system performance adversely and tries to fetch the system to the verge of instability. The genetic algorithm is used to get the best estimate

of the parameter which minimizes the error factor used for designing the proposed controlled system. It is shown that approximated delay compensation control scheme achieves good results than the methods reported in literature [20]. The effects of the delay and jitter on control system are discussed in [21–24] and also evaluated the parameters as solution for designing the control system. In this linear quadratic regulator, genetic algorithm is used to solve the optimization problem as well as to synthesize the performance and stability of the control system.

The packet lost and time delay problems are investigated to show the improved NCS performance by introducing switched model based on effective sensor packet and stabilizing condition which are also derived using linear matrix inequality [25]. The real-time networked control systems are simulated using the True-Time toolbox with different network protocols and scheduling strategies [26–31]. It has been shown that the simulated system can be imitated to show the performance under different attack scenario. The stability condition, considering packet loss probability for stabilizing the wireless networked control system using linear matrix inequality (LMI), and Markov jump linear system are proposed for designing the suitable controller so that improved performance of the system could be estimated [32]. The anomaly detection in cyber-physical system is discussed with the use of neural network technique and showed the efficacy of the proposed method [33]. The model of actual system can be estimated using the system identification tool by exploiting the knowledge of output and input data given to the system [34]. The estimated model is used to degrade the performance metrics of the system. The predictive control method based on the input/output data of system is used to compensate the packet loss, which showed the improved system performance [35]. To overcome the delay constraints, an optimized proportional gain, integral, and derivative controller gains are computed by employing the evolutionary algorithm for the given control problem and improved performance verified/validated using True-Time and UPPAAL [36]. To identify the intruder activity and securing the networked physical control system devices, honeypots of self-configuring nature were implemented in [37]. The stability condition for networked connected control system with Kalman filter and linear quadratic Gaussian (LQG) controller discussed to analyze the effects of attack and noise on the stability of networked control system [38].

It has been observed in the literature that there are some key factors which affect the performance of the networked control system such as delay, noise, packets loss, denial of service, and service degradation attacks. Hence, it is necessary to secure the control system mechanism against abovementioned parameters. In literature, it is also observed that the estimation of the model while considering uncertainties (such as delay, packet loss, and modeled attacks altogether) has not been addressed to show the performance measure degradation of the compromised system. This motivates to emphasize on designing of networked control system considering the factors as illustrated.

3 Problem Formulation

3.1 Description of the System:

The basic block diagram of the networked connected control system is presented in Fig. 1. Here, the output/response of the plant is sampled through the sensor and is directed toward the controller via the communication network which may be wire/wireless. The controller computes the control signal according to the sampled signal and reference signal using algorithm designed for the control purpose. The computed signal travels toward the actuator side through the communication channel to operate the plant following the targeted output. Herein, the dynamics of the process model are considered linear time invariant. In different literature, it has been observed that the attacker may interfere in any direction (i.e., forward and/or feedback) of the control system to degrade the control performance of plant.

The continuous time transfer function of the plant in Laplace domain is described as $G_p = 1.28/(0.002691s^2 + 0.2484s + 1.671)$.

The sampling time is taken as 0.02 s. The discrete form of plant $G_p(z)$ and controller $G_c(z)$ transfer function is represented as

$$G_p(z) = (0.05504z + 0.03005)/(z^2 - 1.047z + 0.1578) \quad (1)$$

$$G_c(z) = (14.73z - 12.63)/(z - 1) \quad (2)$$

The difference equation for control system is obtained as

$$\begin{aligned} y(k) = & 1.047y(k-1) - 0.1578y(k-2) + 0.05504u(k-1) \\ & + 0.3005u(k-2) \end{aligned} \quad (3)$$

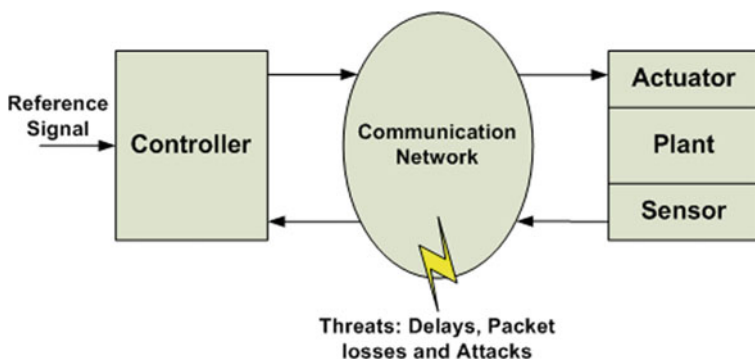


Fig. 1 Different types of uncertainty in NCS

$$u(k) = u(k-1) + 14.73e(k) - 0.1701e(k-1) \quad (4)$$

$$e(k) = r(k) - y(k) \quad (5)$$

In the above equations, ‘y’ represents the response of the plant; ‘u’ represents the control signal; ‘e’ denotes the error input to controller; the unit reference input is defined by ‘r’. The time response for this case under normal condition, i.e., without considering delay factor and intrusion is as follows: rise time $t_r = 0.0198$ s, peak overshoot $M_p = 15.4\%$, setting time $t_s = 0.0964$ s, and cost function value is $4.3369e-04$.

3.2 Uncertain Delay Dynamics

The sampled response taken by sensor is routed to controller through the communication channel, and controller generated control signal is sent toward the actuator through the communication network. Hence, there are delays from sensor toward controller and controller toward actuator signal, i.e., t_{sc} and t_{ca} , respectively. There are also processing delays which are very small in magnitude that can be neglected as compared to t_{sc} and t_{ca} . This random delay dynamics are dependent on the communication network length, bandwidth, etc. To predict the desired response, it is necessary to estimate the time delay very precisely and accurately.

The stochastic nature of the delay disturbance makes the system approach to instability. So, it is required to include the delay dynamics in modeling the system and designing controller. The time delay can be modeled using different approaches as reported in literature [24].

To transfer the packet effectively, the sampling time τ_s must follow the below-mentioned criterion:

$$\tau_s > t_{sc} + t_{ca} + (\text{processing delay}) \quad (6)$$

3.3 Random Packet Dropout

The sampled sensor signal travels to the controller and from controller toward the actuator to actuate the process. Hence, there is probability of packet dropout while traveling through the communication network. The problem of packet dropout may be present in both directions, i.e., forward and feedback. The packet dropout may be modeled by considering the following distribution function as follows:

$$p(\gamma_k) = \begin{cases} p, & \text{if } \gamma_k = 1 \\ 1 - p, & \text{if } \gamma_k = 0 \end{cases} \quad (7)$$

where $p \in [0, 1]$ represents the packet loss rate. If packet is lost at an instant k , then $\gamma_k = 0$, and when packet is arrived successfully at an instant k , then $\gamma_k = 1$. The time stamp theory is used for packet transmission, and packet is stored in buffer with time stamp. The linear time-invariant (LTI) system with networked delay τ_s and packet loss is represented as follows:

$$x(k+1) = Ax(k) + \gamma_k Bu(k - \tau_s) \quad (8)$$

$$y(k) = Cx(k) \quad (9)$$

where the state vector and the control vector are $x(k)$ and $u(k)$, respectively. The output signal is $y(k)$, and A, B, C are matrices with appropriate dimensions.

It is also considered that the sum of the total delay is less than that of the sampling interval. The above equation for a sampling interval $[kT_s, (k+1)T_s] \forall k$ can be expressed as follows:

$$x_{(k+1)} = A_o + \sum_{i=0}^{\eta-1} \gamma_{(k-i)} B_i^k u_{(k-i)} \quad (10)$$

where η is the delay bound and $i = 0, 1, 2 \dots \eta - 1$. Now $x_{(k)} = x(kT_s)$, $y(k) = y(kT_s)$, and $A_o = e^{AT_s}$. Here based on above equation, new state variable is defined as $h_k = \left[x_k^T \ u_{k-1}^T \ \dots \ u_{k-\eta}^T \right]^T$ such that the equation becomes $h_{(k+1)} = A_{h_k} + B_{h_k} u_k$.

Now, the matrices are converted to

$$A_{h_k} = \begin{bmatrix} A_0 & \gamma_{k-1} B_1^k & \dots & \gamma_{k-i} B_i^k & \dots & \gamma_{k-\eta} B_\eta^k \\ 0 & 0 & \dots & \dots & \dots & 0 \\ 0 & I_m & \dots & \dots & 0 & 0 \\ \vdots & 0 & I_m & \dots & \dots & 0 \\ \vdots & \vdots & \vdots & \ddots & \vdots & \vdots \\ 0 & 0 & \dots & \dots & I_m & 0 \end{bmatrix},$$

$$B_{h_k} = \begin{bmatrix} \gamma_k B_0^k \\ I_m \\ 0 \\ 0 \\ \vdots \\ 0 \end{bmatrix}$$

The controller minimizes the cost function:

$$J_o = \int_0^{\infty} [x^T Q_o x + u^T R_o u] dt \quad (11)$$

where Q_o is symmetric, square weighting matrix, and R_o is symmetric, square control cost matrix.

3.4 System Modeling

In networked control system, the performance of the plant can be degraded by introduction of large time delay, packet loss, and injecting the attack. These issues may arise in the feed-forward and/or feedback direction. There are different types of attacks that have been reported in the literature which are the key factors of the degradation of the system performance. Some of the most common attacks are service degradation and denial of service attacks. The denial of service attack is intended to interrupt the processing of the plant which makes the process unstable. The service degradation attack is intended to reduce the response of the process which costs to efficiency. The attacks may be designed by the intruder based on the knowledge of the system acquired through eavesdropping. The system can be modeled if the output of system and input to the system are known. The system can also be modeled if the plant transfer function coefficients are known.

In this paper, particle swarm optimization (PSO) algorithm is used to estimate the coefficients of the plant transfer function. These coefficients are determined by minimizing the cost function as used herein. The PSO is a meta-heuristic, swarm-based optimization algorithm which uses large search space to find optimized solution to the given problem. The size of population used here is 100, and maximum iteration used is 100 with a search space of $[-1, 1]$. The dynamics of the system model of networked control system are also estimated using MATLAB system identification toolbox/Simulink. To identify the continuous and discrete time model, it is required to use time and frequency domain input and output data. So, if the attacker is having the knowledge about input and output data of the system, the model of the system can be estimated for designing the intended attack. The block diagram representation for model estimation from the real-time system is shown in Fig. 2.

In this section, performance measures without attack and packet loss of actual as well as estimated models obtained using system identification tool as well as particle swarm optimization algorithm are shown in Figs. 3, 4, 5, and 6. The performance measures used here are rise time, settling time, overshoot, mean value, and cost function. The estimated model used here shows that above 94% fit to estimation data which indicate the efficacy of the estimated model. The rise time for actual and estimated model using system identification and PSO are 0.0198 s, 0.02558 s, and 0.07345 s, respectively, which are close to each other as indicated in Fig. 3.

Similarly, in Fig. 4, the overshoots for actual and estimated systems are 15.69, 8.152, and 6.989% which is close to actual system value. The mean value as shown

Fig. 2 Estimation of model from real-time system

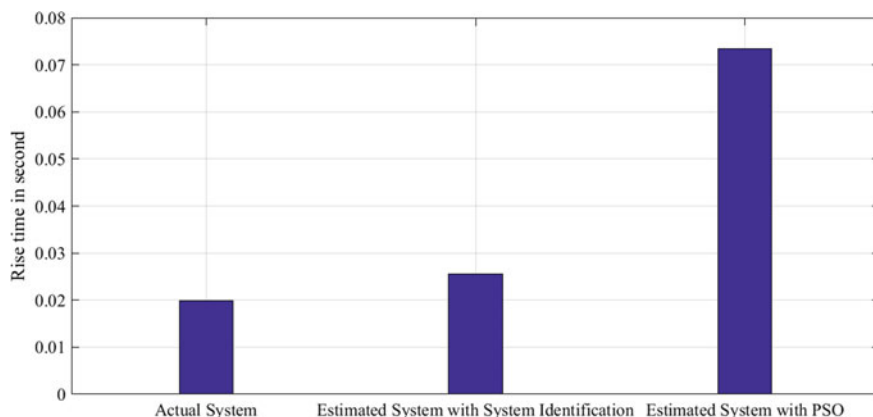
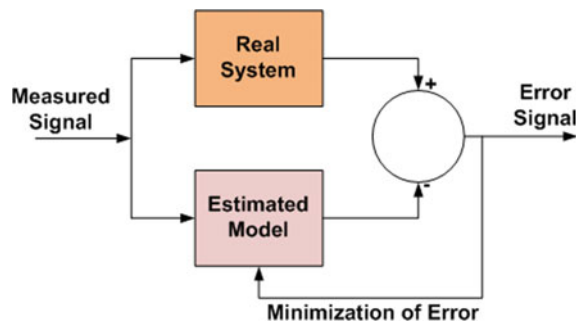


Fig. 3 Rise time for actual and estimated system

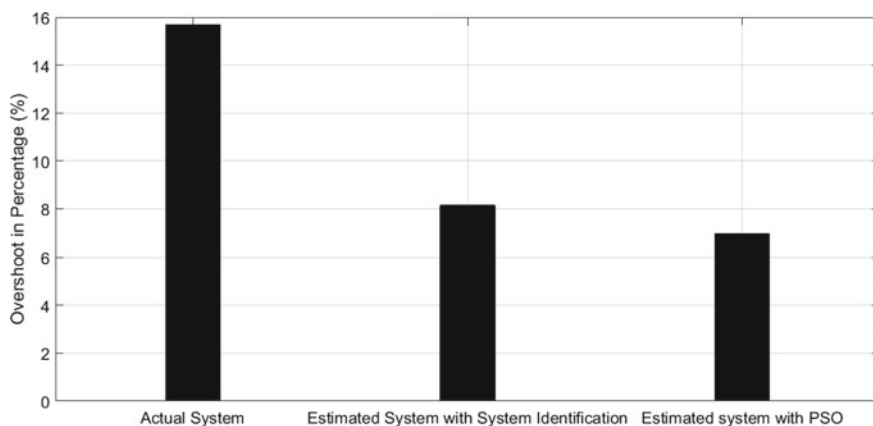


Fig. 4 Overshoot for actual and estimated system

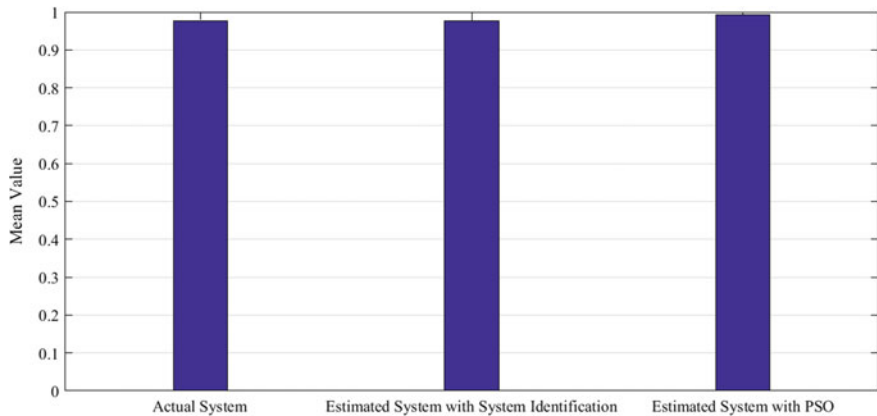


Fig. 5 Mean value for actual and estimated system

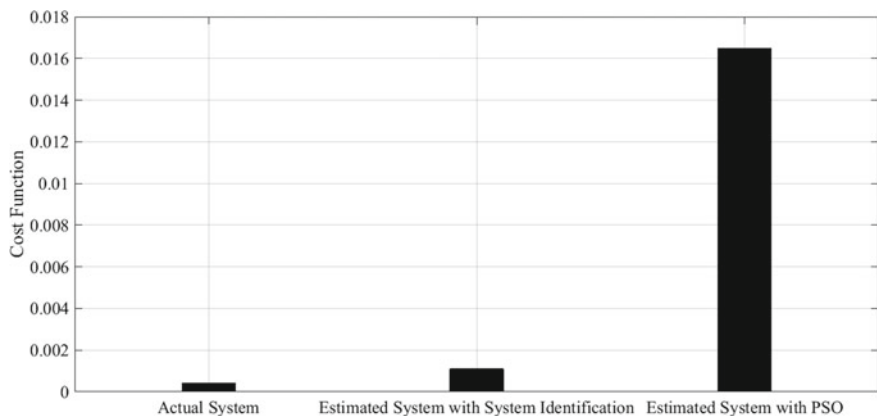


Fig. 6 Cost function for actual and estimated system

in Fig. 5 for all system is approximately equal which shows that estimated system shows the better performance measure compared to actual system. In Fig. 6, the cost function for actual system and estimated model also shows same pattern.

This parameter comparison shows the efficacy of the estimated model which can be used by attacker to compromise the actual system performance measure. These performance metrics are also evaluated in Sect. 4 for different cases of packet loss and attacks, modeled based on estimated parameters of the system, to show the networked control system performance degradation.

3.5 Controller Configuration

In this paper, to simulate the control signal, proportional–integral–derivative control elements are used. The control signal is estimated based on the error signal which is the difference of reference and sensor signal received through communication network. The control algorithm for proportional–integral–derivative action is shown below:

$$u_c(t) = K_c \left(e(t) + \frac{1}{T_r} \int_0^t e(t) dt + T_d \frac{de}{dt} \right) \quad (12)$$

where $u_c(t)$ is the signal computed by controller, K_c is gain of proportional controller, $e(t)$ is error signal which is the difference between reference and sensor signal received through communication network, T_d is derivative time, T_r is reset time required due to integral type control action to just equal the output response due to proportional action following a change in error. Equation (12) can also be shown in Laplace domain as transfer function of controller model:

$$G_c(s) = P_c + I_c \frac{1}{s} + D_c s \quad (13)$$

where $G_c(s)$ is overall gain of the controller in Laplace domain, P_c is gain for proportional action, I_c is gain for integral action, and D_c is controller gain for derivative action. The performance measure taken herein as a cost function is the integral time absolute error (ITAE). The minimizing integral time absolute error value reduces the error by adjusting the parameters of the system.

It also reduces the rise time which limits the effect of initial errors and reduces peak overshoots and settling time which limits effects of small errors presenting for a long time.

$$J_c = \int_0^t t |e(t)| dt \quad (14)$$

where J_c is the cost function, and $|e(t)|$ is absolute error which is the difference between reference and sensor signal received through communication network.

4 Performance Measures with Modeled Attacks

In this section, different performance measures are computed while considering the attack scenario and different packet loss probabilities.

The networked control systems are vulnerable to different uncertainties which may be encountered in any direction (i.e., feed-forward and/or feedback direction) in the control system. The computational delay and different rate of packet loss are also considered here to estimate the model of the actual system. For estimating the system transfer function with different rate of packet loss MATLAB/Simulink system identification, True-Time tool and particle swarm optimization (PSO) algorithm are used.

The various performance measure parameters of the networked control system for actual and estimated system are shown graphically from Figs. 7, 8, 9, 10, 11, 12, 13, and 14.

Here, different rates of packet loss such as 0, 5, 15, and 25% are used for estimating the system model. For each case, the attack is simulated based on the parameters of the estimated system to show the impact of service degradation attack on the

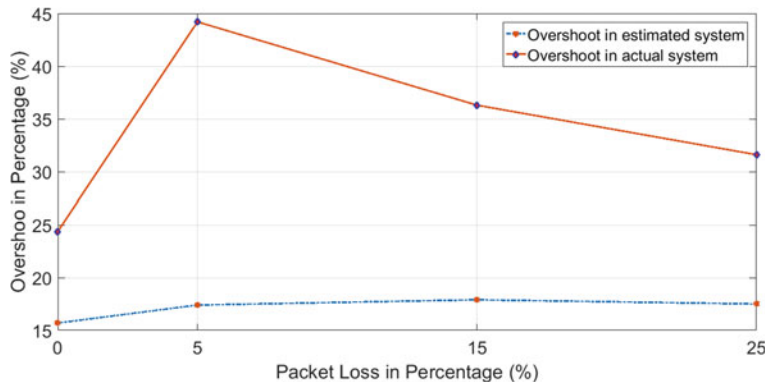


Fig. 7 Overshoot for actual and estimated system with different packet loss and attack

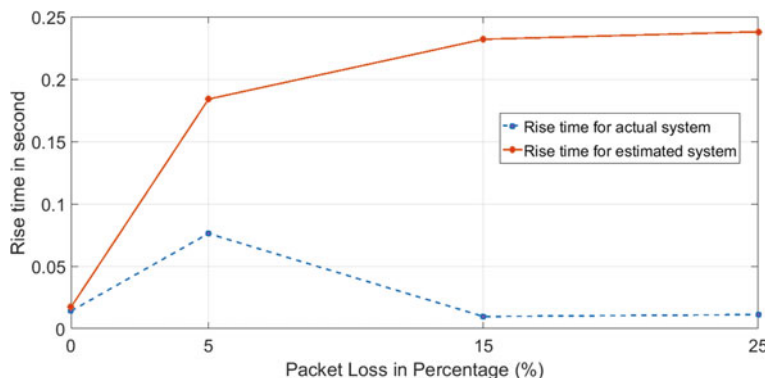


Fig. 8 Rise time for actual and estimated system with different packet loss and attack

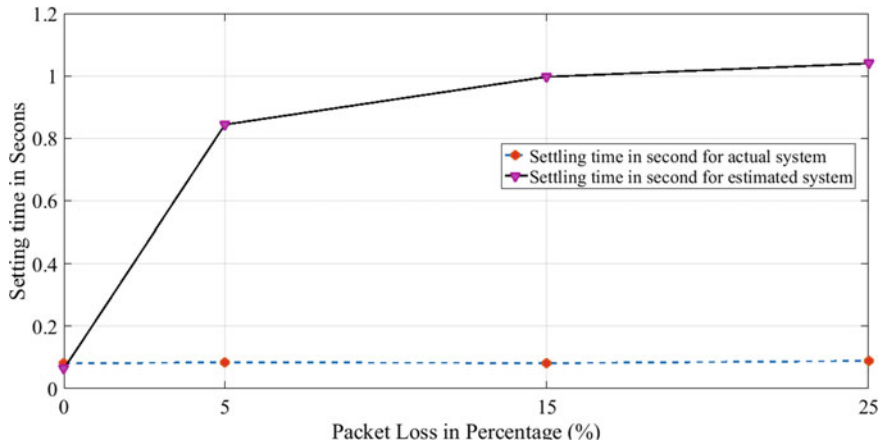


Fig. 9 Settling time for actual and estimated system with different packet loss and attack

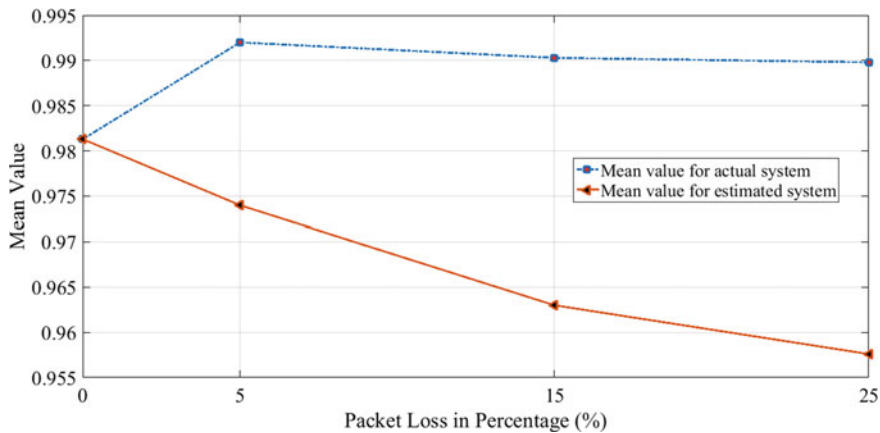


Fig. 10 Mean value for actual and estimated system with different packet loss and attack

performance metrics of the networked control system. The attack is modeled to show the consistency of overshoot in the estimated model of the actual system.

The overshoots are of same order for all cases of the packet loss probability. The overshoots are 15.698% for 0% packet loss, 17.4% for 5% packet loss, 17.9% for 15% packet loss, and 17.5% for 25% packet loss along with modeled attack.

Figure 7 shows that performance of networked control system can be compromised using service degradation attacks with model identification process. Figure 8 plots the rise time for both actual and estimated system for each case of packets loss and modeled attack. The rise time increases for estimated system.

Similarly in Fig. 9, the settling time for actual system is near about the same magnitude, whereas in estimated system the settling time increases much more than

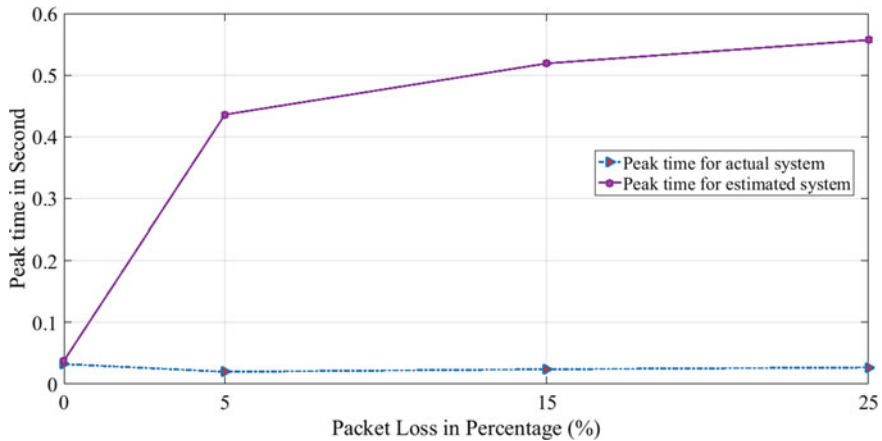


Fig. 11 Peak time for actual and estimated system with different packet loss and attack

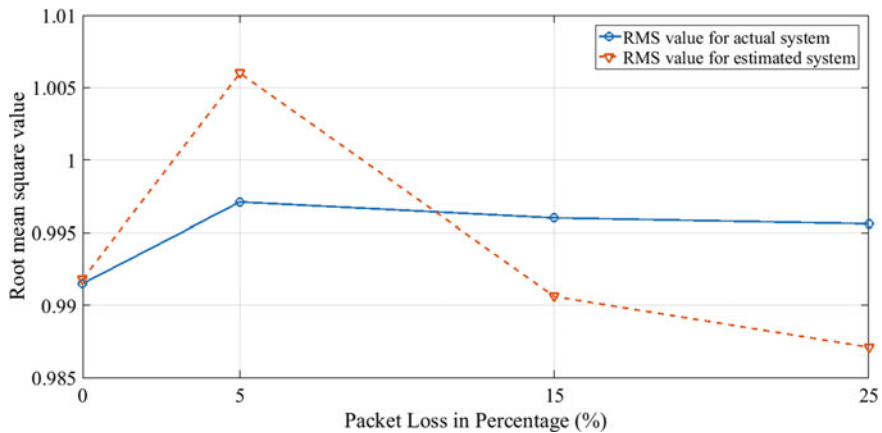


Fig. 12 Root mean square value for actual and estimated system with different packet loss and attack

actual system which is the indication of compromised system performance due to service degradation attack.

The mean value of the response for each case of packet loss and attack is shown in Fig. 10. The mean value is of the same order in each case which shows the effectiveness of compromised system involving estimation of the system using system identification. Figure 11 shows that the peak time to response for actual system under various packet loss and attack scenario is of the same pattern, whereas for estimated system it increases under the same condition.

The pattern of root mean square value as shown in Fig. 12 is same of order as in the case of actual system performance for different types of packet losses and attack

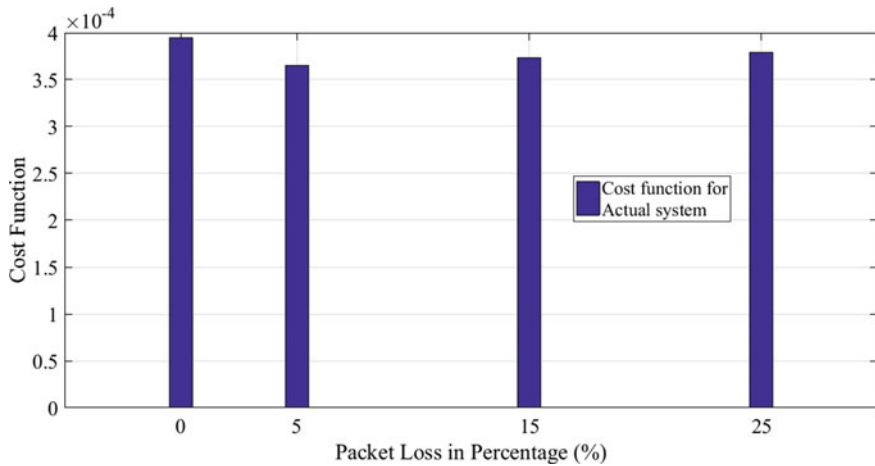


Fig. 13 Cost function for actual system with different packet loss and attack

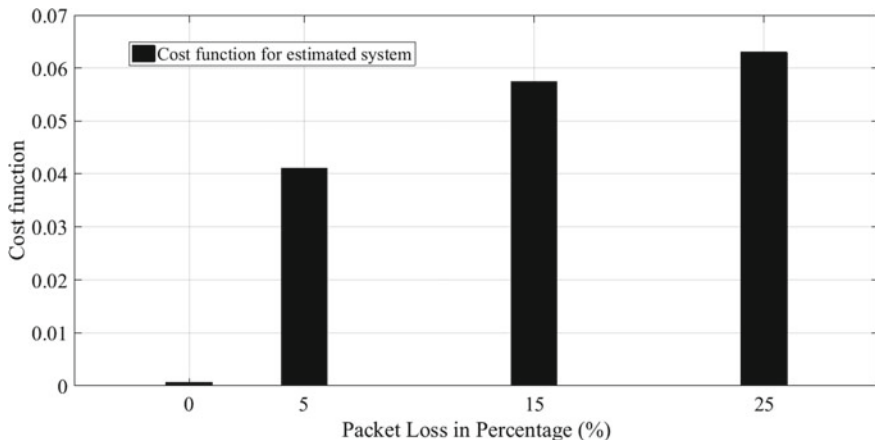


Fig. 14 Cost function for estimated system with different packet loss and attack

scenarios. However, in the estimated system, it is slightly decreasing which shows the compromised degradation of the system performance. The cost function value for actual system shows the same magnitude pattern for different rate of packet loss and attack as presented in Fig. 13. Similarly, Fig. 14 shows that cost function value increases with increase in the rate of packet loss and attack.

To summarize, it has been shown that the networked control system performance decreases due to uncertainties which may be encountered in the form of delay, packet loss and attacks modeled to perform denial of service attacks. Here, various performance metrics are presented for the better understanding of networked control system degradation under various rates of packet loss and attacks.

5 Conclusion and Future Work

The conclusive remarks over the performance metrics of networked control system under different uncertain conditions are presented in this section. It has been shown that system can be modeled efficiently if the attacker is having the basic knowledge of the output and the input to the system. To simulate the estimated model from the actual system, MATLAB/Simulink system identification and True-Time tool along with particle swarm optimization algorithm are used. The various performance metrics, i.e., overshoots, rise time, peak time, mean value, root mean square value, and cost function value are computed under delay, different rate of packet loss (i.e., 0, 5, 15, 25%), and modeled attacks. From Figs. 6, 7, 8, 9, 10, 11, 12, 13, and 14, the simulation result shows that the system can be compromised by estimation of modeled system from actual system and designing the attacks.

The overshoot, in each case of different packet loss, maintained approximately in between 15 and 17.9% which show the efficacy of the estimated system. The other metrics such as rise time, settling time, and peak time increase substantially, whereas root mean square value decreases, and also the cost function increases for estimated system with different packet loss rate and attack, which is an indication of a compromised system.

The networked control system performance metrics can be improved by suitably designing control system considering the delay, packet loss, and different attacks. The aforementioned uncertainties have also left the future scope in designing optimal control algorithm to mitigate these imperfections quickly such that performance metrics show better result.

References

1. Guo YF, Li SY (2010) Transmission probability condition for stabilisability of networked control systems. *IET Control Theory Appl* 4(4):672–682
2. Pang ZH, Liu GP (2012) Design and implementation of secure networked predictive control systems under deception attacks. *IEEE Trans Control Syst Technol* 20(5):1334–1342
3. Xia Y, Chen J, Zhou L (2007) Networked control systems with different control inputs. In: Proceedings of 26th Chinese control conference, CCC 2007, no. 6, pp 539–543
4. Al-Dabbagh AW, Li Y, Chen T (2018) An intrusion detection system for cyber attacks in wireless networked control systems. *IEEE Trans Circuits Syst II Express Briefs* 65(8):1049–1053
5. Seshadri S, Ayyagari R (2011) Dynamic controller for Network Control Systems with random communication delay. *Int J Syst Control Commun* 3(2):178–193
6. Srinivasan S, Vallabhan M, Ramaswamy S, Kotta Ü (2013) Adaptive regulator for networked control systems: MATLAB and true time implementation. In: 2013 25th Chinese control decision conference, CCDC 2013, pp 2551–2555
7. Bi S, Zawodniok M (2017) PDF-based tuning of stochastic optimal controller design for cyber-physical systems with uncertain delay dynamics. *IET Cyber-Phys Syst Theory Appl* 2(1):1–9
8. Sargolzaei A, Yen KK, Abdelghani MN, Sargolzaei S, Carbunar B (2017) Resilient design of networked control systems under time delay switch attacks, application in smart grid. *IEEE Access* 5:15901–15912

9. Wang C, He F (2017) Simulation technology for networked motion control system. In: Proceedings of 29th Chinese control decision conference, CCDC 2017, pp 6419–6424
10. Garcia-Santiago A, Castaneda-Camacho J, Guerrero-Castellanos JF, Mino-Aguilar G, Ponce-Hinestroza VY (2018) Simulation platform for a VANET using the TrueTime toolbox: further result toward cyber-physical vehicle systems. In: IEEE Vehicular Technology Conference, vol 2018, Aug 2018
11. De Sá AO, Carmo LFRDC, Machado RCS (2017) Covert attacks in cyber-physical control systems. *IEEE Trans Ind Inf* 13(4):1641–1651
12. Amin S, Cárdenas AA, Sastry SS (2009) Safe and secure networked control systems under denial-of-service attacks. In: Lecture notes in computer sciences (including Subseries Lecture notes in artificial intelligence, Lecture notes in bioinformatics), vol 5469, no 1, pp 31–45
13. Han S, Xie M, Chen HH, Ling Y (2014) Intrusion detection in cyber-physical systems: techniques and challenges. *IEEE Syst J* 8(4):1052–1062
14. Zhu M, Martinez S (2014) On the performance analysis of resilient networked control systems under replay attacks. *IEEE Trans Automat Contr* 59(3):804–808
15. Miao KL, Zhu JW, Zhang WA (2018) Distributed guaranteed cost control of networked interconnected systems under denial-of-service attacks: a switched system approach. In: Proceedings, 2018 33rd Youth Academic annual conference of Chinese association of automation, YAC 2018, pp 911–915
16. Liang Z, Guo Y, Yang Y, Chen G (2019) Distribution network control system scheduling strategy. In: Proceedings 2019 IEEE 3rd information technology, networking, electronic and automation control conference. ITNEC 2019, no. Itnec, pp 1424–1428
17. Li M et al (2019) Suppression of disturbances in networked control systems with time-varying delay based on equivalent-input-disturbance approach. In: IECON Proceedings (Industrial Electronics Conference), vol 2019, Oct 2019, pp 6957–6960
18. Dias JA, Liberado EV, Serni PJA, Marafao FP, Godoy EP (2016) Simulation of a distributed generator with wireless communication using TrueTime and PLECS. In: 2015 IEEE PES Innovative Smart Grid Technologies Latin America. ISGT LATAM 2015, pp 624–628
19. Ma J, Liu K, Sun S, Yang G (2018) Design and simulation of large delay wireless network control system. In: Proceedings of 8th International Conference on Instrumentation and Measurement, Computer, Communication and Control. IMCCC 2018, pp 217–220
20. Gnana Sambandam K, Kamalanabhan E (2016) Proceedings of the international conference on soft computing systems. Advances in Intelligent Systems and Computing, 398, pp 319–329
21. Srinivasan S, Buonopane F, Saravanan Kumar G, Subathra B, Ramaswamy S (2015) Modelling time-varying delays in networked automation systems with heterogeneous networks using machine learning techniques. *IEEE International Conf. Automation Science Engineering*, vol 2015, Oct 2015, pp 362–368
22. Srinivasan S, Buonopane F, Ramaswamy S, Vain J (2014) Verifying response times in networked automation systems using jitter bounds. In: Proceedings of IEEE 25th International Symposium on Software Reliability Engineering Work. ISSREW 2014, pp 47–50
23. Srinivasan S et al (2018) Adaptive controller for networked control systems subjected to random communication delays. *Adv Intell Syst Comput* 633(2):78–94
24. Seshadri S, Ayyagari R (2009) Hybrid controllers for systems with random communication delays. In: ARTCom 2009—International Conference on advances in recent technologies in communication and computing no. 1, pp 954–958
25. Li H, Chow MY, Sun Z (2009) State feedback stabilisation of networked control systems. *IET Control Theory Appl* 3(7):929–940
26. Irwin G (2005) Wireless networked control systems. *IEE Conference Publication*, no. 2005–10868, pp 43–55
27. Andersson M, Henriksson D, Cervin A, Årzén KE (2005) Simulation of wireless networked control systems. In: Proceedings of 44th IEEE conference on decision and control and European control conference. CDC-ECC '05, vol 2005, no. January 2006, pp 476–481 (2005)
28. Balasubramaniyan S, Subathra B, Hemesh RC, Gurusamy S, Srinivasan S (2016) On simulating processor schedules and network protocols within CPS using TrueTime. In: 2015 IEEE International conference on computational intelligence and computing research. ICCIC 2015

29. Henriksson D, Cervin A, Årzén KE (2002) TRUETIME: simulation of control loops under shared computer resources. *IFAC Proc* 15(1):417–422
30. Jithish J, Sankaran S (2018) Securing networked control systems: modeling attacks and defenses. In: 2017 IEEE International Conference on Consumer Electronics. ICCE-Asia 2017, vol 2018, Jan 2018, pp 7–11
31. Ding P, Wang Y, Yan G, Li W (2017) DoS attacks in electrical cyber-physical systems: a case study using TrueTime simulation tool. In: Proceedings of 2017 Chinese Automation Congress. CAC 2017, vol 2017, Jan 2017, no. 2015, pp 6392–6396
32. Qu FL, Guan ZH, Li T, Yuan FS (2012) Stabilisation of wireless networked control systems with packet loss. *IET Control Theory Appl* 6(15):2362–2366
33. Goh J, Adepu S, Tan M, Lee ZS (2017) Anomaly detection in cyber physical systems using recurrent neural networks. In: Proceedings of IEEE international symposium on high assurance systems engineering, pp 140–145
34. Naung Y, Schagin A, Oo HL, Ye KZ, Khaing ZM (2018) Implementation of data driven control system of DC motor by using system identification process. In: Proceedings of 2018 IEEE conference of Russian young researchers in electrical and electronic engineering. ElConRus 2018, vol 2018, Jan 2018, pp 1801–1804
35. Zhen S, Hou Z, Yin C (2017) A novel data-driven predictive control for networked control systems with random packet dropouts. In: Proceedings of 2017 IEEE 6th data driven control and learning systems conference. DDCLS 2017, pp 335–340
36. Balasubramaniyan S, Srinivasan S, Buonopane F, Subathra B, Vain J, Ramaswamy S (2016) Design and verification of Cyber-Physical Systems using TrueTime, evolutionary optimization and UPPAAL. *Microprocess Microsyst* 42:37–48
37. Vollmer T, Manic M (2014) Cyber-physical system security with deceptive virtual hosts for industrial control networks. *IEEE Trans Ind Inf* 10(2):1337–1347
38. Solanki BS, Renu K, Srinivasan S (2019) Stability and security analysis with identification of attack on industrial networked control system: an overview. *Internetw Indones J* 11(2):3–8

Parallel Matrix Sort Using MPI and CUDA



Priyanka Ojha, Pratibha Singh, Gopalakrishna N. Kini, B. Ashwath Rao, and Shwetha Rai

Abstract Sorted data is essential. Apart from information presentation or manual retrieval of information, sorted data is beneficial even when using machines' computational power. In many science and engineering fields, the sorting of extensive dataset is essential in matrix form. Matrix sort is an algorithm, which can sort a large amount of data in matrix form efficiently. In this paper, parallel algorithms are developed for the Matrix Sort algorithm (designed by S. Kavitha et al. Int J Comput Appl 143(9):1–6, 2016) [1]. This algorithm sorts the matrix rows and columns in parallel, subsequently applying the further procedure on resultant data. The implementations of parallel algorithms have been discussed by comparing the execution time results obtained in sequential and parallel form.

Keywords Matrix sort algorithm · Message passing interface programming · CUDA programming · Time complexity

1 Introduction

Sorting refers to ordering the data to increase or decrease fashion according to some linear relationship among data items. Sorting is required in a variety of computer applications and plays a vital role in solving computational problems.

The science and engineering field often needs to store and sort a large amount of data in matrix form like in electrical circuits, electronic networks, chemical engineering, hospitals, encrypting messages, robotics, automation, storing and analyzing user information companies, and so on. So an efficient sorting algorithm, which can sort matrix data faster, is needed. To make any algorithm efficient, we can parallelize it.

P. Ojha (✉) · P. Singh · G. N. Kini · B. A. Rao · S. Rai

Department of Computer Science and Engineering, Manipal Institute of Higher Education, Manipal, Karnataka 576104, India

G. N. Kini
e-mail: ng.kini@manipal.edu

There are numerous techniques which are based on different kinds of sorting algorithm. All these sequential algorithms work well for the limited data size. One such sorting algorithm is named Matrix Sort, whose time complexity is improved ($n\sqrt{n}\log\sqrt{n}$) for average case [1] while comparing the time complexity of other existing sorting algorithms.

2 Literature Survey

Many applications, which have a vast amount of data require sorting in matrix form. To sort extensive data in matrix form many sorting algorithms [2] are known. Some of them are merge sort, quicksort, Tim sort and, others. Merge sort [3] is a sorting algorithm, and it takes $O(n\log n)$ time to sort data.

Quicksort [4] is also a good sorting algorithm and its time complexity is $O(n\log n)$ in the best case but its worst-case time complexity is $O(n^2)$. Tim sort [5] is derived from insertion sort and merge sort, the time complexity of Tim sort is $O(n\log n)$, but the problem with this algorithm is that it works best for almost sorted data. For random data, Tim sort does not work well.

Durad et al. discussed the performance measure of many sorting algorithms such as odd–even sort, radix sort, quick sort, merge sort, and binary sort. Based on various parameters such as execution time versus no. of processing elements, sorting time versus the number of data items, timing analysis on virtue system, they have concluded an overall reduction in execution time with an increase in the number of processing elements [6].

Valerievich et al. paper shows how to do parallel sorting of data in the CUDA platform with Quicksort and shell sort. For Quicksort, the number of pivot element is chosen by dividing the vast series of elements into parts and applied quicksort independently on each part. The parallel quicksort and shell sort may not give the efficient result for the small size input because of transferring data to the graphic accelerator. If we increase the input size, a noticeable improvement can be observed [7].

Neetu et al. have proposed the parallelization of bubble sort algorithm using CUDA hardware and calculated the speedup for the same. The paper has shown the parallel algorithm's improved time complexities with respect to the sequential algorithm in various scenarios [8].

Similarly, we will be parallelizing an algorithm known as Matrix Sort using both MPI and CUDA separately in this paper. And will compute the speedups for the same with respect to the sequential algorithm of Matrix Sort.

3 Methodology

The Matrix sort algorithm's core operation is called top-down approach, in which it compares every element in the second half of a row with the element in the first half of its previous row [1].

Matrix sort [1] is a sorting algorithm used to sort data stored in matrix form by parallelly sorting its row and column, and then it uses a top-down approach to increase its efficiency. To sort row and column in the Matrix sort, merge sort algorithm is used because merge sort time complexity is better than most of the sorting algorithms. A top-down approach performs the row sort and column sort function first and then applies a function for data comparison between two consecutive rows. If the algorithm does sorting of rows and columns of data independently and parallelly, it will increase algorithm performance.

Message passing interface [9] is nothing but a communication protocol used for parallel computer programming. The main goal of MPI is to give high performance. MPI provides a programming language with independent, flexible, portable, and efficient standards for message passing. MPI programs work with many processes in a parallel manner; they provide communication between those processes by message passing and synchronize them. To process data concurrently, MPI is used. Implementing algorithms using MPI in which data can be processed parallelly will indeed reduce its processing time.

When you need to apply the same logic to massive amounts of data, parallel computing comes in to picture. When the amount of data is large, then you can utilize GPU power to perform parallelism. CUDA [10] is a parallel computing platform to work on GPUs. CUDA enables developers to speed up computer applications by utilizing GPU's power for a parallelizable part of the computation.

The programming language, data, and system configuration used for this project are as follow:

- Programming Language: MPI in C, CUDA
- Data: Randomly generated integers
- System Configuration: Host and Device configurations are shown in Tables 1 and 2.

Table 1 Host configuration

CPU	Intel Xeon X5550 2.67 GHz × 16
Main memory	47.2 GB

Table 2 Device configuration

GPU	GeForce GTX 1050 Ti
Global memory size	4 GB
GPU clock rate	1.62 GHz
Constant memory size	64 KB
Maximum thread per block	1024

3.1 Working in Sequential Form [1]

Matrix sort works in sequential form as follows:

1. The algorithm takes a 2D array of elements and sorts them in increasing order.
2. Rows of the matrix are sorted first.
3. Then columns of the matrix are sorted.
4. Then top-down operation is performed ' $n - 1$ ' times on all the rows of the matrix.
 - Every j th element in the first half of the current row i th is compared with the $(n - j - 1)$ th element in the previous row $(i - 1)$ th.
 - If the order is opposite to the desired order, then the elements are swapped.
 - Rows of the matrix are sorted.

After row sort and column sort, the row's largest element can be smaller than the smallest element in its next row. To remove this inconsistency, we perform a top-down operation.

A numerical example is taken to know how the working of matrix sort is discussed in [1].

3.1.1 Working in MPI

Matrix sort implementation using MPI works as follows:

5. The algorithm takes a 2D matrix as an input of size $n * n$ here n is the row size.
6. Matrix is divided row-wise and equally distributed between processes.
7. Each process sorts row using merge sort.
8. Each process returns a sorted row to the root process to form a matrix of $n * n$. This matrix will have each row sorted individually and refer to as a row sorted matrix.
9. Each column of the row sorted matrix is divided column-wise, and then the columns are equally distributed between processes.
10. Each process sorts the data it has using merge sort.
11. Then each process sends the data back to the root process to form a matrix of $n * n$. this matrix will have each column sorted as well.
12. After sorting row and column of the matrix parallelly, a top-down approach [1] will be applied on the matrix n times, where n is no of rows in the matrix.
13. The top-down approach is performed $n - 1$ times. Here, first half of the current row is compared with second half of the previous row if elements are in the wrong order means if current row elements are less than previous row elements, then swap them, otherwise do nothing.
14. Now perform row sort (i.e., step 2, step 3, step 4)
15. Perform step 9 and step 10 until swapping occurs, otherwise, stop and get the final sorted matrix.

3.1.2 Working in CUDA

Matrix sort implementation using CUDA works as follows:

1. It takes a 2D matrix as input.
2. The kernel will have the following configuration of grid size and block size.
Grid_size(1, no of rows) and
Block_size(1,1).
3. Each thread will sort the row associated with it using merge sort. We can refer to this as row sort.
4. Similarly, with the same grid and block size, each thread will sort a column associated with it using merge sort. We can refer to this as column sort.
5. Apply the top-down approach for n rows. The top-down approach is performed $n - 1$ times. Here, first half of the current row is compared with the second half of the previous row. If elements are in the wrong order, i.e., if current row elements are less than previous row elements, then swap them, otherwise do nothing.
6. Now perform row sort (i.e., step 3)
7. Perform step 5 and step 6 until swapping occurs, otherwise, stop and get the final sorted matrix.

3.1.3 Top-down Operation Pseudocode

Procedure: Top-down (n, Arr).

- Input: Matrix and no. of rows.
- Output: Matrix.

Algorithm:

The matrix sort algorithm to sort matrix is as,

Var $i, j, flag$;

Begin

- Take each row in using outer for loop from 1 to $n - 1$.
- Compare its elements with the respective second half row elements of the previous row by taking inner for loop from 0 to $n/2$.
- Compare $M[i][j] < M[i - 1][n - j - 1]$ then swapping between these two elements is done. This is performed on $n/2$ elements.
- If elements are swapped, the $flag$ value will toggle from zero to one.
- If $flag$ is 1, function returns 0.
- If $flag$ is 0, function returns 1.

End

4 Analysis of Matrix Sort

Consider n number of elements in a given matrix and assume that the matrix is a perfect square matrix. Each row and column will have \sqrt{n} elements, and we are using merge sort for sorting individual row and column. Therefore, the time complexity [8] for row sort is $\sqrt{n} \log \sqrt{n}$, and for column sort is $\sqrt{n} \log \sqrt{n}$. so the total time complexity is given as,

$$T_1(n) = \sqrt{n} \log \sqrt{n} + \sqrt{n} \log \sqrt{n} \quad (1)$$

$$T_1(n) = 2\sqrt{n} \log \sqrt{n}. \quad (2)$$

Expression (2) is the time taken for sorting the rows and columns initially. After that, a top-down operation is performed.

The top-down operation requires $n\sqrt{n}/2$ number of comparisons [1]. Each call of top-down is followed by row sort. As top-down is called \sqrt{n} times, row sort will also be called \sqrt{n} times. Therefore, the total number of comparisons in row sort will become $n \log \sqrt{n}$.

For top-down operation, the time complexity is,

$$T_2(n) = n \log \sqrt{n} + n\sqrt{n}/2. \quad (3)$$

The final expression for time complexity is,

$$\begin{aligned} T(n) &= T_1(n) + T_2(n) \\ T(n) &= 2\sqrt{n} \log \sqrt{n} + n \log \sqrt{n} + n\sqrt{n}/2. \end{aligned} \quad (4)$$

$$T(n) = O(n\sqrt{n}/2). \quad (5)$$

Therefore, time complexity is in the order of $O(n\sqrt{n}/2)$.

The time complexity of Matrix Sort in the sequential algorithm is $O(n\sqrt{n} \log \sqrt{n})$ [1], and for parallel algorithms, the time complexity is $O(n\sqrt{n}/2)$. This shows that the time complexity of sequential Matrix Sort is improved.

Table 3 gives the comparison of the time taken by Matrix Sort in Sequential execution, MPI implementation as well as CUDA implementation. As the size of the data increases, the execution time for Sort Matrix drastically reduced, as seen in Fig. 1.

Suppose we take $n = 250,000$ input size matrix by applying Sequential Matrix sort for average case time complexity, i.e., Eq. (1). We get the number of basic operations (comparisons) 674,742,500, and for the same number of input elements by applying Eq. (5), we get the number of basic operations (comparisons) 62,500,000. Therefore, theoretical speedup gained by Parallel Matrix sort with respect to Sequential Matrix sort is 10.79 for $n = 250,000$ input size matrix. And we have got 68.45

Table 3 Comparison of time taken by matrix sort in sequential execution, MPI implementation, and CUDA implementation

Size of input data (number of elements)	Time taken by sequential algorithm (ms)	Time taken using MPI (ms)	Time taken using CUDA (m)
100	0.214	146.1	0.29
2500	37.00	330	2.262
10,000	224.20	747	10.105
40,000	1650	1960	46.909
90,000	5660	7340	112.786
160,000	13,910	8740	228.61
250,000	27,650	16,285.5	403.90

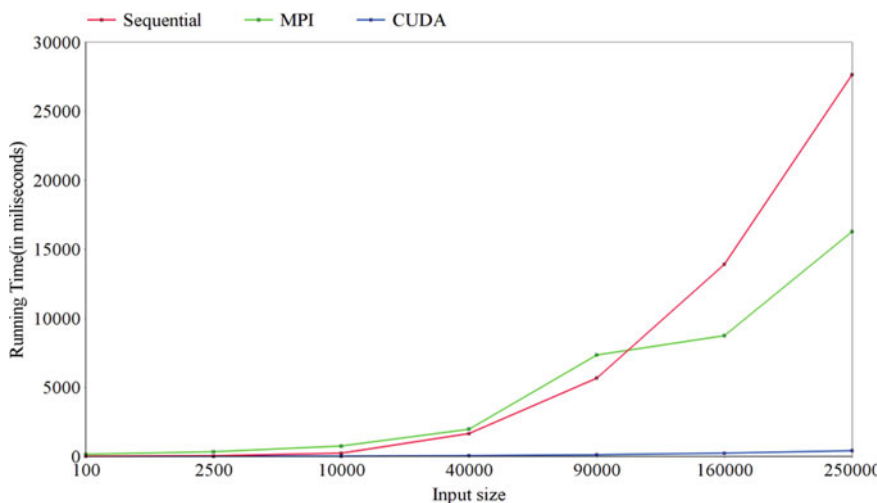


Fig. 1 Comparison between sequential, MPI and CUDA implementations

Speedup for real-time implementation in Parallel Matrix sort. Similarly, if we take $n = 40,000$ input size matrix then by applying Sequential Matrix sort for average case time complexity, i.e., Eq. (1), we get the number of basic operations (comparisons) 18,408,240. For the same number of input elements, by applying Eq. (5), we get the number of basic operations (comparisons) 4,000,000. Therefore, theoretical speedup gained by Parallel Matrix sort with respect to Sequential Matrix sort is 4.6 for $n = 40,000$ input size matrix. And we have got 35.17 Speedup for real-time implementation in Parallel Matrix sort.

A comparison of Real-Time Speedup of MPI and CUDA with respect to the sequential execution time is shown in Table 4. Figure 2 has proven that with CUDA,

Table 4 Speedups for MPI and CUDA algorithms with respect to sequential algorithm

Size of input data (number of elements)	MPI	CUDA
40,000	0.841	35.174
90,000	0.7741	50.18
160,000	1.591	60.84
250,000	1.6978	68.45

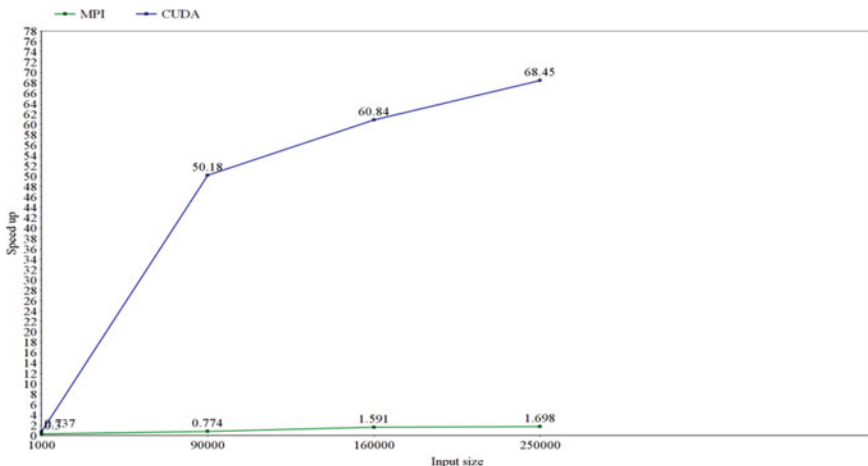


Fig. 2 Speedups for MPI and CUDA algorithm with respect to sequential algorithm

the Matrix Sort algorithm has given excellent performance compared to MPI as CUDA uses GPGPU for computation.

5 Conclusion

The Matrix sort is a sorting algorithm used to sort large data stored in the matrix from a parallelizing sorting technique [1]. Implementing matrix sort using MPI and CUDA will make it more efficient and reduce the time for a large dataset. The time required and working of Matrix Sort is already mentioned in the analysis section of the paper, which clearly shows the result obtained by MPI and CUDA implementations of Matrix sort algorithm is more advantageous.

Since the processing time requirement of this algorithm is $O(n\sqrt{(n/2)})$, clearly less than sequential Matrix sort algorithms, which takes $O(n\sqrt{n}\log\sqrt{n})$, it is useful in sorting large matrix data faster. As seen above, the time complexity of the parallel algorithm for matrix sort is less than many sorting algorithms, so this algorithm will reduce the time required by computers in performing sorting.

There is a vast scope of making algorithms efficient by making them parallel. Performance of Matrix sort can be further improved by using the hierarchy of memory of GPU for efficient parallel processing.

References

1. Kavitha S, Veerabadran V, Saketh A (2016) Matrix sort—a parallelizable sorting algorithm. *Int J Comput Appl* 143(9):1–6
2. Cormen T (2009) Introduction to algorithms. MIT Press, Cambridge
3. Khanna M (2021) Merge sort—GeeksforGeeks. GeeksforGeeks. Available: <https://www.geeksforgeeks.org/merge-sort/>
4. Jain P, Chaudhary U, Gupta I (2011) QuickSort—GeeksforGeeks. GeeksforGeeks. Available: <https://www.geeksforgeeks.org/quick-sort/>
5. Jain R, Kumar A (2021) TimSort—GeeksforGeeks. GeeksforGeeks. Available: <https://www.geeksforgeeks.org/timsort/>
6. Durad MH, Akhtar MN, Irfan-ul-Haq, Performance Analysis of Parallel Sorting Algorithms Using MPI. In: 2014 12th International conference on frontiers of information technology, Islamabad, 2014, pp 202–207
7. Valerievich BA, Anatolievna PT, Alekseevna BM, Vladimirovich SS (2017) The implementation on CUDA platform parallel algorithms sort the data. In: 2017 6th Mediterranean conference on embedded computing (MECO), Ba, pp 1–4r
8. Faujdar N, Ghrera SP (2017) A practical approach of GPU bubble sort with CUDA hardware. In: 2017 7th international conference on cloud computing, data science & engineering—confluence, Noida, pp 7–12
9. Gropp W, Lederman S, Lumsdaine A, Lusk E, Nitzberg B, Saphir W, Snir M (1999) MPI—the complete reference, vol 2, the MPI-2 extensions. *Comput Math Appl* 37(3):130
10. Kazennov A (2010) Basic concepts of CUDA technology. *Comput Res Model* 2(3):295–308

Experiences Involving Student Assistants in Interdisciplinary R&D Projects Using the Example of Aerospace Computing and Bioeconomics: The “HONEYCLOUD” Project



Alexander Hilgarth, Diego Gormaz-Lobos, Claudia Galarce-Miranda, and Sergio Montenegro

Abstract The Chair of Aerospace Information Technology at the University of Würzburg is working on a technology transfer project in the field of bioeconomics. The methods and tools of the aerospace industry will now be used in precision agriculture and in particular in precision beekeeping. Computer science students are actively involved in engineering activities. Students have the opportunity to work on a real project (Project-Based Learning), where the practical relevance goes clearly beyond purely academic exercises. In addition to methods and tools for coordinating cooperative work, students learn the difference between ideal and real systems in a laboratory for prototype construction. In cooperation with partner universities in Chile, a teaching and learning platform for Internet of Things (IoT) systems will be developed from the hardware and software components developed in the project. Donnelly and Fitzmaurice (Donnelly R, Fitzmaurice M (2005) Collaborative project-based learning and problem-based learning in higher education. In: O'Neill G, Moore S, McMullin B (eds) Emerging issues in the practice of university learning and teaching. AISHE/HEA, pp 87–98) define Project-Based Learning (PBL) as a learning method based on the principle problem-solving as a starting point for the acquisition and integration of knowledge and skills development. Considering the need to innovate in the way of learning, the authors of this work want to expose in this paper the: (1) the scientific arguments that support the PBL proposal in the Chair of Aerospace Information Technology and (2) a description of the case of PBL “HONEYCLOUD” at the University of Würzburg (Germany).

Keywords Beehive-monitoring · Precision farming · Technology transfer · Aerospace information technology · Project based learning in engineering

A. Hilgarth (✉) · S. Montenegro

Faculty of Mathematics and Computer Science, Julius Maximilians Universität Würzburg, Würzburg, Germany

e-mail: alexander.hilgarth@uni-wuerzburg.de

D. Gormaz-Lobos · C. Galarce-Miranda

Faculty of Engineering, International Center of Engineering Education, Universidad de Talca, Talca, Chile

1 Introduction

The HONEYCLOUD project is an ongoing research project at the University of Würzburg in the field of technology transfer from aerospace to terrestrial applications. Thematically, the project is in the field of bioeconomics and in particular in the field of precision agriculture and beekeeping. The project is set in the context of the worldwide bee mortality that has been observed for some time. In a two-year feasibility phase, it will be demonstrated that a hive monitoring system can be a potentially marketable product. In order to explain the motivation in more detail, the boundary conditions for beekeeping in Germany are presented below. In particular, the product concept focuses on the German honey market, which has some special features in a worldwide comparison. On the one hand, Germany is the country with the highest per capita consumption of honey, and on the other hand, 99% of German honey producers are private amateur beekeepers. Only a small part are professional beekeepers. After a steady decrease in the number of bee colonies observed since 1992, which continued until 2008, there was a change in the trend since 2009, which has increased the number of bee colonies.

One of the reasons could be the worldwide popularity of urban beekeepers during this period, which was not a short-term fashion, but a trend with great sustainability. In the course of this change, a shift in the demographics of German beekeepers could also be observed. Beekeeping in Germany was traditionally a geriatric and male hobby, so that about one-third of active beekeepers were men and over 65 years old. With the reversal of the trend, there was a clear rejuvenation. The new generation now comes from a much younger age cohort and is not recruited by retirement, as was previously usually the case. Another effect that can be observed, but not directly explained, is the significant increase in the proportion of female beekeepers. Currently, in 2019, the number of beekeepers in Germany is about 135,000 and the number of bee colonies about 900,000. The consideration of these boundary conditions was important, on the one hand, to evaluate the need for such a product and, on the other hand, to consider how to adapt it to target-specific groups. Finally, potential users directly and indirectly determine the selection of the technology to a large extent. For example, older people are often not technology-oriented and do not have a smartphone. The above analysis of the potential target group led to a focus on beekeepers under 65 years of age in urban and suburban areas.

The exploratory phase carried out before the project resulted in the system architecture shown in Fig. 1. The figure on the left shows a hive equipped with a weighing system and internal climate sensors (temperature, humidity, barometric pressure). Many of these hives can be placed next to each other and then connected via a wireless data link to a base station, which is located in close proximity of the hive. The base station is also equipped with climate sensors and therefore records the micro-climate outside the hives in the direct vicinity of the apiary. The base station collects data from all sensors located in the apiary and transmits it to a database via mobile Internet. The data is read from this database and displayed in a smartphone application or a browser window. Each hive is labeled with an individual QR code for easy

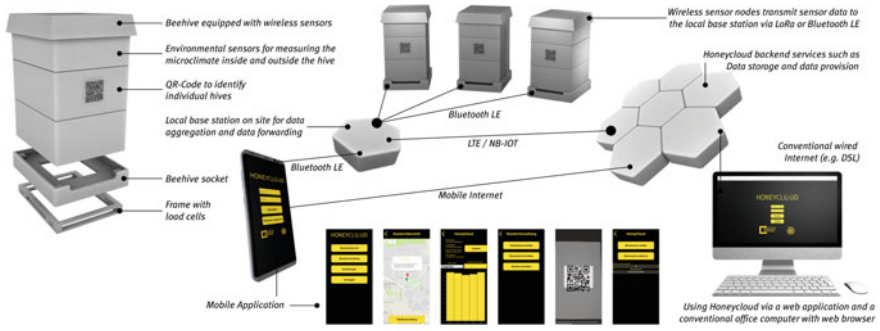


Fig. 1 Overview of the HONEYCLOUD platform

identification, so that the user of the smartphone application only has to scan this code to display the measured values of this hive. In the project, the computer science students must participate in the practical application of the concept, not only in the programming, but also in the engineering activities.

2 HONEYCLOUD: A Case of PBL in Engineering Education at University of Würzburg

2.1 PBL Definition and Characteristics

Compared to the typical teaching methodologies in engineering, Project-Based Learning (PBL) is believed to offer several advantages. Thus, PBL not only permits students to develop technical and methodological knowledge, gain confidence, and become more independent learners, but it also helps them to develop some relevant professional skills for their future professional performance, e.g. leadership, team working, planning competencies, decision-making abilities, time management, communication, among others. Donnelly and Fitzmaurice [1] define PBL as a learning method based on the principle problem-solving as a starting point for the acquisition and integration of knowledge and skills development. The fundamental characteristics of PBL are as follows: (a) learning as a student-centered process, (b) learning occurs in small groups, (c) teachers are facilitators or guides in this process, (d) problem solving is the focus and approach for learning organization and motivation, and (e) projects are a vehicle for developing resolution skills from problems [1].

In general, Project-Based Learning (PBL) can be understood as a teaching-learning strategy that organizes learning around projects. Behind this definition is a concept of learning that is important to note: learning as an “active process of investigation and creation based on the learners’ interest, curiosity, and experience and should result in expanded insights, knowledge and skills” [2]. A central aspect

of the PBL approach is the idea that learning is more effective when students put theory into practice activities: in other words, the conception of “learning by doing” from Dewey and Kilpatrick learning theory [3].

In Engineering Education, there is a general consensus that presented PBL as a teaching–learning strategy organized on project work, for the development of competences and skills of engineering students. The fundamental starting point of the PBL process is the problem (which the students wish and should solve) [4, 5]. Kolmos [6] considers the following key elements for PBL:

1. Ill-structured and complex questions based on real-world scenarios.
2. Student-centered active learning occurs.
3. Learning occurs in small groups, (teamwork) considering and reviewing solutions to open-ended problems.
4. The teacher becomes a facilitator.
5. Self-assessment increases efficacy.

The benefits PBL for student learning are presented in different scientific papers and empirical works related to Engineering Education. Some benefits that PBL offer are [7–9]:

- experience of authentic engineering problems and professional practices,
- experience of problem-solving and the design process,
- experience and development of a team and collaborative work,
- self-motivation and student ownership of the problem, solution, and learning,
- development of self-regulation, agency, commitment, time management, and another management competences,
- development of reflective skills,
- presentation of the multi-disciplinary and systemic nature of engineering problems,
- development of written, oral, and other communication skills, among others.

However, different authors warn that there are also risks by the implementation of PBL: (i) PBL needs effective learning environment, (ii) students must be trained to work in teams and for the collaborative work, (iii) before and during the project, students needs to be prepare for conflicts management between members of their team, (iv) for making group decisions, (v) for sharing out tasks, and (vi) for the necessary organizational preparations [7, 10].

2.2 *The HONEYCLOUD Project*

The Chair of Aerospace Information Technology at the University of Würzburg is mainly concerned with the programming of satellites and avionics systems. For this purpose, we develop and optimize our own tools developed by the research group. The most important tool in the field of software is our dependable real-time operating system (RODOS), which was developed by Sergio Montenegro at the German

Aerospace Center (Deutsches Zentrum für Luft- und Raumfahrt; DLR). RODOS is now being developed at his chair at the University of Würzburg. There are courses for the operating system, which are part of the curriculum of the master courses “Space-Master” and “SATEC.” The prerequisite for programming the operating system is knowledge of the programming language C++, which is also taught in the courses of the chair. Even if it is a computer science chair, embedded hardware systems are installed here as well. This is due to the fact that the aerospace field is interdisciplinary in nature and brings together knowledge from many different fields. Although there is no faculty of engineering at the University of Würzburg and although it is a chair of computer science, it is clear that engineering work is carried out here. Students are expected to acquire the necessary knowledge to work on projects independently. This includes, for example, becoming familiar with industry standard software packages such as “Altium-Designer”, a tool for the design of electronic circuits, or “Dassault SolidWorks,” a tool for mechanical design and simulation. In comparison to other German universities, a special feature of the “Aerospace” course at the University of Würzburg is the focus of the course through mathematics and computer science and not, as usual, through mechanical engineering. In this sense, students are already working in an interdisciplinary environment. Experience shows that interdisciplinary groups are very common in later professional life and preparation for them makes sense during their studies. It is only in very large companies that a high degree of specialization takes place in the workplace. Experience has shown that as the size of the company decreases, the requirement profile becomes broader and therefore also more interdisciplinary. This approach to knowledge transfer is relevant at the national level because Germany has a distinct structure of small- and medium-sized enterprises (“Mittelstand”) and graduates often begin their careers there.

The most important place for our interdisciplinary work is the laboratory for the construction of prototypes, which has been available for the first time since the beginning of the project. The laboratory is continuously being expanded, but since the beginning of the project it offers all important facilities for the realization of microelectronic projects. The laboratory for the construction of prototypes is divided into different workstations. The main working areas are “assembly and connection,” “optical inspection,” “repair,” “testing and commissioning,” “design and 3D printing,” as well as “RF and reliability testing.” In addition, workstations are reserved in the laboratory for students who can set up a fixed workstation here for the duration of their work. Almost all of the workstations include activities that go beyond the standard training of computer scientists and focus more on the area of engineering activities. Figure 2 illustrates the workstation for the assembly of the printed circuit boards. Students learn to operate this workstation in one day and have a routine in their use after only one week.

The following figure shows the working area of Surface Mount Technology (SMT) circuit boards. The assembly of the printed circuit board follows the following workflow:

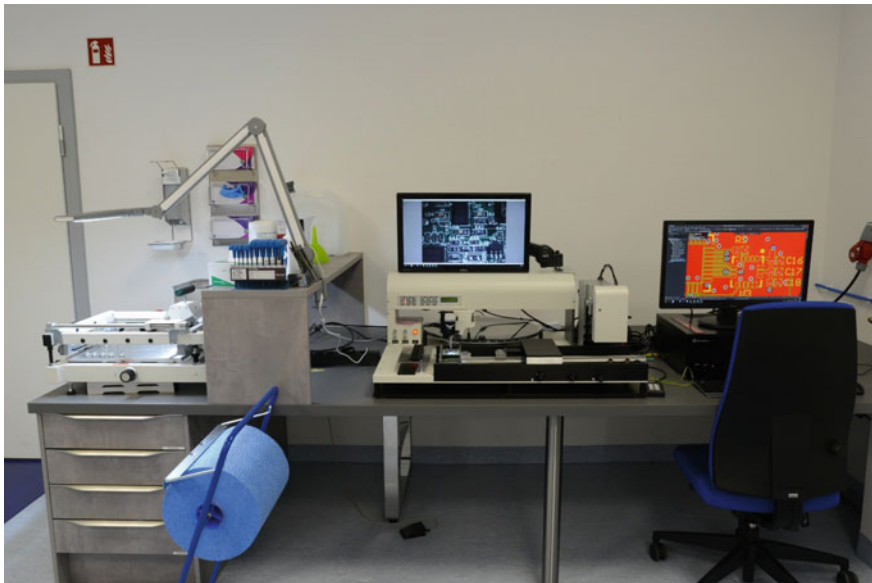


Fig. 2 Assembly and connection of printed circuits and conventional components, paste printer (left), assembly aid (center), design computer (right)

1. Computer-aided design of a board: creation of the circuit diagram, the board layout and the corresponding manufacturing data with an EDA tool (“Electronics Design Automation”), the program “Altium-Designer” is used for the beekeeping project.
2. Production of printed circuit boards according to these specifications by an external service provider and additional production of the so-called paste mask (here we cooperate with several service providers).
3. Paste printing: Use of the paste mask for paste printing, where the solder paste is applied at the intended places on the printed circuit board. The paste printer “Uniprint-M” from PBT-Works is used.
4. Assembly of the surface mounted components on the glued board. In this case, these components are placed in the correct position on the board with a micro-mechanical placement aid, without a fixed connection first.
5. Reflow soldering of the board: The solder paste on which the components and their contact surfaces or pins are placed is melted in the reflow oven and the desired mechanical and electrical connection between the component and the board is created.

Many of the circuit boards made in the project were assembled by the students themselves. The boards shown in Fig. 3 are the evaluation board and the wireless sensor boards derived from it.

Students usually work with pre-assembled evaluation boards, as is customary in the industry. Students are used to the fact that the hardware is already tested and

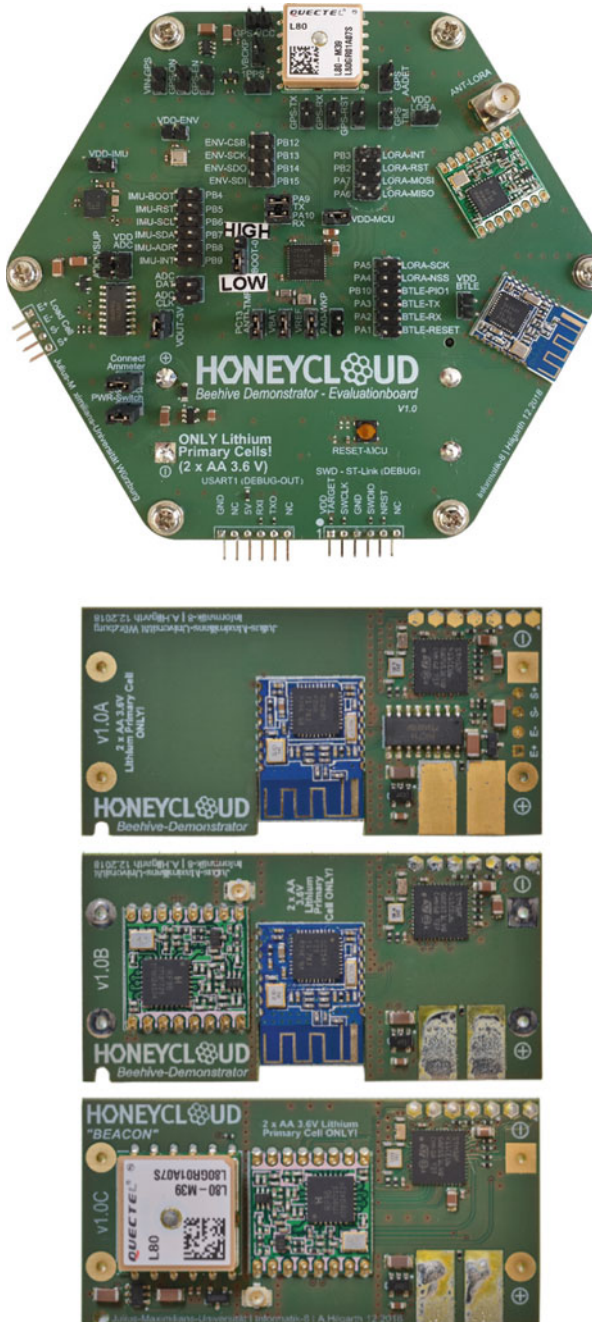


Fig. 3 “Evaluationsboard” (up) and several “Sensorboards” (down)

working. Errors often only appear as a total failure of the whole circuit. Students, as users of these ready-made development systems, can concentrate fully on software development, but often have the impression that the hardware always seems to be error-free and that therefore a malfunction of the circuit must be attributed to their own programming errors. The intensive occupation of hardware in our laboratory teaches computer students that they have had a rather idealized view of hardware and that real systems have many sources of error apart from self-written code. These include profane errors such as loose contacts and short circuits, but also “floating” inputs with no fixed potential and no interference on power or signal lines.

In joint discussions with different partner universities in Chile, it became clear that the platform created here should not necessarily be used only for beekeeping, but is also suitable for other areas. We aware that under the rubric of “digitalization” many digital innovations are already being incorporated in all areas of agriculture and that a significant change in the traditional job profile of farmers and agricultural technicians is to be expected in future. Digitalization is transforming traditional professional fields in many areas. University training in these professions must also follow this development, but not in a radical way, where farmers are replaced by computer scientists. The transformation must be carried out in such a way that future farmers and agricultural technicians can make use of the possibilities and tools of information technology without having a deep knowledge of programming. The approach we are discussing here is that of “low-code development,” the chances of which are particularly promising because of the special features of our choice of operating systems. In low-code development, the goal is to ensure that little or no programming is required and that professional software developers can be dispensed with as far as possible. The RODOS real-time operating system used in the project offers with its capabilities an approach for the creation of so-called software building blocks, so that software functions can be linked in a kit similar to assemblies.

2.3 Some Results of the HONEYCLOUD Project

The basic concept, system architecture and choice of technology were largely given to the students. This includes the evaluation cards and wireless sensor systems provided, which were completed by staff during the project period. This includes an evaluation board with a high-performance, energy-efficient microcontroller and its extensive sensors and communication peripherals. Several wireless sensor systems were derived from this evaluation board, each representing a subset of the evaluation board subsystems.

We have involved five international and six national computer science students in an ongoing project. The students were involved with different motivations, five of them did an internship, three worked on a thesis, and three were hired as student assistants. The average length of stay in the project was six months. The results of the practical work include hardware, software and mechanical designs. All the works were aimed at the realization of an IO platform. The students’ contributions focused

on programming. Design work and electronic circuit design were carried out by them to a lesser extent.

Despite the relatively small size of this work, it was important for the progress of the project. For the realization of the scale, the computer students received both a concrete construction specification and the necessary material. Although the computer students in Germany do not have to do a basic training as engineers, this work was carried out cleanly and correctly by them. The 3D molded parts had to be produced for the scale. These were housings for electronics as well as housings for housing facades. These parts were designed in the construction program “Autodesk Inventor” and printed with a 3D printer. In addition, numerous other functional housings were created especially for their use. The result shows that computer students can easily be used for non-specialized work due to their learned analytical approach, as here specifically in the field of mechanical engineering.

The project is not yet finished and is “in progress,” but the desire to use the components developed in the project to create a learning and teaching platform in cooperation with partner universities in Chile has already matured.

3 Conclusion

One of the strengths of PBL in Engineering Education is the central role of students at the teaching–learning process. Sometimes students take the solutions of their problems through a project much further than their teacher expects and manage to achieve much more in a very short time than the teacher ever anticipated. PBL is a methodology that is developed in a collaborative way that confronts students with situations that lead them to make proposals to confront certain engineering problems. The authors have observed along the semesters (not only through the evaluation of the students but also through their work and commitment) that the PBL has many effects in the development of personal, organizational, technical, and social competences of the students. Involving students in hands-on projects can be a great enrichment for both the project and the participating students. Students learn to formulate and work on issues in an international environment. Since this is not a mandatory event, but a voluntary participation in the project, student motivation is inherent and very high. However, it can be said that the first results of the work are very changeable at the beginning. The background to this is the initial motivation to satisfy one’s curiosity. In the following course, however, students realize that their work is not finished when their curiosity is satisfied, but only when the sub-task they have taken on is an executable system. Students learn that the time required for completion between a formally correct system and a reliably functioning system can be several times longer. In essence, this is the distinction between idealized models, as known from academic exercises, and real systems, as used in everyday industrial life. This helps students to be able to estimate the time investment more realistically. In handling information, both on a human level in communicating with project members and on a technical level in linking different systems and building blocks together, students

learn that interfaces are common causes of errors. The lesson learned from this is the importance of a complete specification at the time of delivery and a culture of “ask and repeat” to ensure consensus.

The project has not only benefited from the work time contributed by the students in processing the work packages. Joint discussions of practical interim results have resulted in many minor adjustments and, for example, a technological change in a web framework. The close involvement of the students directly influenced the idea of developing a learning and teaching platform based on HONEYLCLOUD. In the sense of a feedback loop, the students’ input could flow directly into the improvement of the teaching. The University of Würzburg, in cooperation with Universidad de Talca (University of Talca, Chile), wishes to continue the idea of a teaching and learning platform in future and to make it an open platform together with other partners.

References

1. Donnelly R, Fitzmaurice M (2005) Collaborative project-based learning and problem-based learning in higher education. In: O’Neill G, Moore S, McMullin B (eds) Emerging issues in the practice of university learning and teaching. AISHE/HEA, pp 87–98
2. Kolmos A (1996) Reflections on project work and problem based learning. *Eur J Eng Educ* 21(2):141–148
3. De Graaff E, Kolmos A (2007) Management of change; implementation of problem-based and project-based learning in engineering. Sense Publishers, Rotterdam
4. Gormaz-Lobos D, Galarce-Miranda C, Hortsch H, Kersten S (2019) The needs-oriented approach of the dresden school of engineering pedagogy and education. In: Auer M, Hortsch H, Sethakul P (eds) The impact of the 4th Industrial revolution on engineering education. ICL 2019. Advances in intelligent systems and computing, vol 1134, pp 589–600. Springer, Cham
5. Boud D (1985) Problem-based learning in perspective. In: Boud D (ed) Problem-based learning in education for the professions. Higher Education Research and Development Society of Australasia, Sydney
6. Kolmos A (2011) Problem based learning, tree—teaching and research in engineering in Europe (2007). In: Gavin K (2011) Case study of a project-based learning course in civil engineering design. *Eur J Eng Educ* 36(6):547–558
7. Frank M, Lavy I, Elata D (2003) Implementing the project-based learning approach in an academic engineering course. *Int J Technol Des Educ* 13(3):273–288
8. Mills JE, Treagust DF (2003) Engineering education—is problem based or project based learning the answer? *Australian J Eng Educ*
9. Helle L, Tynjälä P, Olkinuora E (2006) Project-based learning in post-secondary education—theory, practice and rubber sling shots. *High Educ* 51(2):287–314
10. Palmer S, Hall W (2011) An evaluation of a project-based learning initiative in engineering education. *Eur J Eng Educ* 36(4):357–365

Multidimensional Ensemble LSTM for Wind Speed Prediction



Ashapurna Marndi and G. K. Patra

Abstract Wind energy as an environmentally friendly energy resource plays a significant role in providing electricity to industrial as well as domestic consumers. Wind as a major source of green energy demands better prediction of wind speed with advancement of technique and technology. However, stochastic behavior of wind makes the accurate prediction challenging. Artificial intelligence techniques, especially deep learning algorithms, are recently been successful in addressing atmospheric prediction problems on time series data. In this paper, for wind speed prediction, a novel time series forecasting algorithm derived from deep learning approach has been proposed based on ensemble technique over distributing input dataset in multiple dimensions. Here, the input dataset is first distributed over time dimension and then over frequency dimension to build distinct varieties of dataset that are fed to individual LSTM, whose outputs are again inputted to ensemble LSTM to produce the final output. The potential efficiency of proposed approach has been demonstrated using wind speed data for multiple years and found the prediction results significantly improving over other AI-based models.

Keywords Deep learning · Long short-term memory · Ensemble forecasting · Multidimensional ensemble · Wind speed prediction

1 Introduction

Wind energy as one of the promising green energy resources has potential to change the power sector unprecedently. In tropical countries like India, with the help of windmills, wind energy can be very well utilized for energy generation by converting wind energy to electricity which is to be used for industrial and domestic use. In order to conduct proper energy planning, it is essential to have advance knowledge about

A. Marndi (✉) · G. K. Patra

Academy of Scientific and Innovative Research, Ghaziabad, Uttar Pradesh 201002, India
e-mail: asha@csir4pi.in

Council of Scientific and Industrial Research, Fourth Paradigm Institute, Bengaluru, Karnataka 560037, India

amount of wind energy needs to be generated. It is necessity to predict wind speed at the earliest with possible higher accuracy; however, it possesses a bigger challenge to predict wind speed accurately due to its stochastic behavior.

Generally, atmospheric variables like wind speed are predicted by numerical weather models which are complex mathematical models that in turn require large-scale computing power. In case of wind energy generation, it is essential to predict wind speed with more accuracy at the windmill location. Hence, it is essential to have a better method for such requirements.

Over the last few decades, various statistical methods such as Auto Regressive (AR), Autoregressive Integrated Moving Average (ARIMA) [1–3] have been used for wind speed prediction. However, most of the statistical approaches lack capability to analyze nonlinear time series data. With the recent trend of artificial intelligence to solve scientific problems having huge data and of varying veracity, many researchers attempted to use computational intelligence techniques, such as neural networks to solve wind speed problem [4]. Deep learning-based methods have been used successfully in several areas like image processing, video processing, audio processing, natural language processing, etc.

Few AI-based models are used to predict wind speed in different lead times such as short-term, medium-term and long-term. In this study [5], three local recurrent neural networks are used for long-term wind speed prediction. Later in one of the studies, three different neural networks are compared for prediction of wind speed with a lead time of one hour [6]. In [7, 8], recurrent neural network and feed-forward neural network have been used respectively to predict wind speed. Next, hybrid model based on neural network is used for wind speed prediction [9]. Wavelet transform with combination of deep belief network and spine quantile regression is used to predict wind speed [10]. Later on, combination of fuzzy logic and neural network is used for wind speed prediction [11]. In [12], it is proposed to decompose wind speed timeseries into sublayers of different frequencies using wavelet packet decomposing technique such as CNN for high frequency and LSTM for low-frequency sublayers. In [13], hybrid wind speed prediction system based on AI and double prediction approach is proposed. Later in [14], methodology for wind prediction is proposed based on ensemble technique where ensemble members are constructed by different time characteristics of the same input data. With all these techniques, though there have been improvements in the prediction capability over the last decade, there still exists sufficient scope for improvement in this direction.

In this paper, we have proposed a novel approach based on ensemble technique where two ensemble methods have been combined together to devise a new one. This has been demonstrated on wind speed data observed at Bengaluru, India, and found the result significantly better than existing other methods.

2 Methodology

For devising the method for solving multivariate prediction problem, following aspects need to be considered to bring domain context into the computational exercise.

- Selection of inputs
- Fixing range of prediction
- Designing of model.

2.1 *Selection of Inputs*

For solving time series prediction problem using statistical approach, usually data at previous timestamps are used to predict the data for future timestamps [15]. It is well known in the domain of climatology that wind speed is influenced by other weather parameters also such as temperature, humidity, pressure, rainfall, dew point, solar radiation, etc. However, temperature, humidity and pressure affect wind speed significantly more than other affecting parameters [16]. Hence, in order to build multivariate model only these three parameters apart from its own historical wind speed data are considered for predicting wind speed for future timestamps.

2.2 *Fixing Range of Prediction*

The next important aspect that needs to be considered is the time range of prediction. Some applications demand prediction to be made in few days or weeks in advance, i.e., long range, while some others need for next two to three hours in advance, i.e., short range.

Seven days ahead temperature prediction, i.e., medium-term prediction is useful in agriculture. Even extreme weather prediction at least five days advance will be helpful. One month ahead chlorophyll prediction, i.e., long-term prediction, is useful for identifying potential fishing zone. However, it is intuitive that longer the range, less accuracy in prediction. Having considered all these pros and cons, we have finally decided to work on short-range prediction of six hours in advance. This has potential application in wind energy estimation.

2.3 *Design of Model*

Selecting an existing model or designing a new model using existing model techniques fulfilling the requirement of the application is the most important step in this

whole experiment. Chance of obtaining better solution increases with selecting suitable base model which depends on type of data and problems to be solved. There are several models available based on numerical, statistical and artificial intelligence that are used to predict on time series data [17, 18]. However, observing the challenges faced in numerical as well as statistical methods and witnessing the latest developments in computational intelligence techniques such as deep learning technology, long short-term memory (LSTM), an especial algorithm in deep learning is considered for our studies as it is efficient to process time series data.

A typical LSTM network as shown in Fig. 1 has two states named as *cell state* and *hidden state* that are being updated in every timestamp and propagated to the next timestamp. The functionality of LSTM is performed through three *gates* such as *Forget gate*, *Input gate* and *Output gate*. The forget gate is responsible for removing unwanted information, whereas *Input gate* is for addition of new information to the cell state. The *Output gate*, which selects useful information from current cell, shows it as an output. More on the LSTM can be found at [19].

$$f_n = \sigma(W_f I_n + U_f h_{n-1} + b_f) \quad (1)$$

$$i_n = \sigma(W_i I_n + U_i h_{n-1} + b_i) \quad (2)$$

$$o_n = \sigma(W_o I_n + U_o h_{n-1} + b_o) \quad (3)$$

$$C_n = f_n * C_{n-1} + i_n * \tanh(W_c I_n + U_c h_{n-1} + b_c) \quad (4)$$

$$h_n = \tanh(C_n) * o_n \quad (5)$$

Weight matrices of current and previous timestamps are denoted by W_f , W_i , W_o , W_c and U_f , U_i , U_o , U_c respectively. The bias vectors corresponding to the gates f_n , i_n , o_n , c_n are represented by b_f , b_i , b_o , b_c respectively and current cell state is denoted

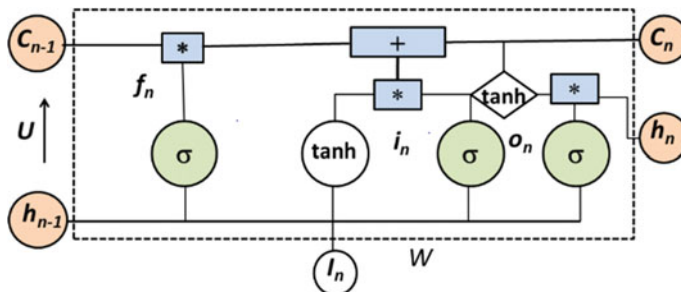


Fig. 1 Architectural block diagram of LSTM network

by C_n . Also, h_{n-1} is the hidden state of previous state, σ and $tanh$ are the sigmoid and hyperbolic tangent activation functions, respectively.

3 Proposed Solution: Multi-Dimensional Ensemble LSTM (MDE-LSTM)

We have proposed an enhanced model derived from basic LSTM by distributing input datasets with the intention to derive different inherent patterns from data. Main objective of ensemble method is to combine multiple hypothesis in order to reduce the variance and bias that lead to produce better prediction efficiency. Ensemble method consists of two significant steps: First one is to train the same model with different subsets of training data or different models with the whole training data. In second step, outputs of first level are combinedly fed into another model to build efficient model network. In the first step, we have followed the first approach where we divided the dataset into multiple subsets that are fed into separate LSTMs and then in second step, the outcomes of all these LSTMs are inputted into ensembled LSTM to bring out final results. In one of our earlier work [14], we had distributed the data into multiple ensembles based on difference in frequency of occurrences. This work has been enhanced further by adding another layer of distribution of inputs and thus made the ensembles of multi-dimensional. Based on its multi-dimensional characteristics of input distribution, the method is named as “Multi-Dimensional Ensemble LSTM” or in short MDE-LSTM. In our approach, the input data has been distributed based on time dimension and next on frequency dimension as discussed below.

3.1 Data Distribution Over Time Dimension (TD)

Whole dataset is distributed into multiple ensemble datasets in order to change the occurrence of patterns by resizing the training data. To begin with, a differential gap period is fixed which is nothing but a difference of period between two consecutive ensemble datasets. First ensemble window consists of whole training dataset. From second ensemble onward, for each window, starting time of input data shifts forward with lagging of differential gap period while keeping the end points same. In our case, as shown in Fig. 2, the training data is distributed into three ensemble datasets by considering differential gap of 1 year, such as data during 2010–2013, data during 2011–2013 and data during 2012–2013 with intention to have different initial conditions.

It has been observed that the training of a model gets impacted by the sequence of patterns. If certain patterns are found long back and other patterns are relatively recent having significant frequency, the new patterns may replace the older ones.

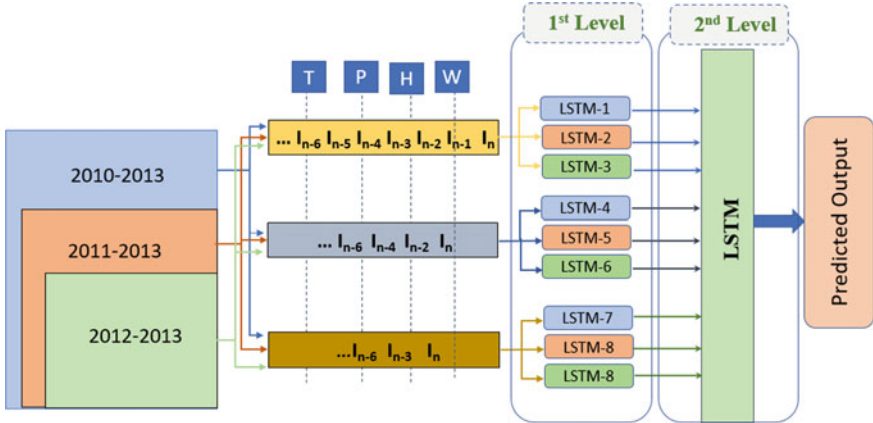


Fig. 2 Block diagram of Multi-Dimensional Ensemble LSTM (MDE-LSTM)

On the other hand, if same input pattern has two different outcomes, then the pair of input–output occurred at last may have chance to replace the other one. Thus, it is important to consider the start and end of a data sequence for a training model. This logic fits to design moving window of inputs in the model. However again, we found that the influence of long past dataset may incorrectly influence the future pattern and thus, it may be more rational to include data from last available period in all ensemble input datasets. Thus, we decided to move the starting period of the ensemble inputs but preferred to keep the end period fixed. Essentially, this approach creates varieties of data sequence that can train models differently. The differential gap period should be determined for ensuring there are couple of ensemble datasets with significant difference in sizes and the smallest dataset should be sufficient to train the model.

3.2 Data Distribution Over Frequency Dimension (FD)

Each ensemble member generated using above step is further distributed based on frequency of occurrences of input dataset, i.e., with difference of time gap between consecutive data. All the data points in an input sequence usually do not form significant patterns. Sometimes intermediate data points may be insignificant and can be ignored. This process may form new sequence of only important data. However, it may not be feasible to pick important data in a sequence beforehand and may not be logically justified for all cases. Thus, an attempt may be made to form few different unique data patterns from the input dataset by picking values at fixed positions. This overall concept was the baseline for building this approach to further distribute input data as done in [14].

For each ensemble input dataset devised from first step, all the input parameters, i.e., in this case four parameters: temperature (T), pressure (P), humidity (H) and wind speed (W) are consecutively placed to make one subsequence, i.e., $I = (T, P, H, W)$. Then subsequences corresponding to consecutive timestamps are placed one by one to form the input sequence. The input sequence can be expressed as

$$I^1 = I_n, I_{n-1}, I_{n-2}, \dots$$

The second type of sequence was formed by skipping values alternately from the original input sequence. The purpose is to make different interval values among subsequences leading to form a completely different input sequence. This input sequence can be expressed as

$$I^2 = I_n, I_{n-2}, I_{n-4}, \dots$$

The third type of sequence was formed by skipping two consecutive values at a time, and thus, it leads to another form of input sequence. This input sequence can be expressed as

$$I^3 = I_n, I_{n-3}, I_{n-6}, \dots$$

Each ensemble dataset devised in first step is further distributed into three second-level ensemble datasets as described above. In our experiment, while three ensemble datasets are carved out, each of them is further distributed to three ensembles and in total nine ensemble datasets are fed into individual LSTM making multidimensional ensemble. Individual LSTMs are optimally trained with their corresponding input ensemble dataset and then in second level, their outputs are fed into ensemble LSTM to derive final output.

4 Experiment

4.1 Data

To build an efficient predictive model for obtaining superior prediction, quality and accuracy of data play crucial role. The Council of Scientific and Industrial Research (CSIR), India, has established number of meteorological towers across India for collecting important meteorological parameters. For our studies, data during 2010–2014 are considered from a tower located in the city of Bengaluru (earlier called Bangalore), in South India. Four meteorological parameters such as temperature (T), pressure (P), humidity (H) and wind speed (W) available at 30 min averaged intervals, collected from tower of 20 m height have been used for this study.

4.2 Setup

As discussed in previous section, 2010–2013 have been considered as the training set and data during 2014 as the test set. As depicted in Fig. 2, data are distributed in time dimension (2010–2013) and frequency dimension, i.e., the frequency (or time interval) at which data are collected. All the LSTMs in first level are trained with 8 layers and 100 neurons at each layer. Training of model is started with 10 neurons at the first layer, and then, it was increased by 10 more neurons in the same layer until network perform satisfactorily. Once the number of neurons in the first layer was fixed, the network was tuned further by adding additional layer starting from second layer till network was optimized. Same procedure was followed to fix the hidden neurons and layers for LSTM at second level. Epoch, defined as number of times the training set is trained, affects the accuracy of the prediction system. The value of epoch is decided as 60 based on training validation loss. Since in this experiment multiple LSTMs are used, after close observation we found that all of them get optimized with similar hyperparameter counts and within small variations. Thus, the above same values were fixed for all ignoring those small variations among them.

The different modes of LSTM were implemented using Python, and different studies were conducted on intel(R) Xeon(R) CPU E3-1203 v3 @ 3.30 GHz with 8 cores and 32 GB RAM.

5 Result and Analysis

The experiment was conducted using existing well-known methods apart from our proposed algorithm to verify the accuracy level of this approach. Since this approach is based on LSTM, the whole dataset was trained and tested using normal LSTM also. Similarly, it was executed using convolutional neural network (CNN), artificial neural network (ANN) and extreme learning machine (ELM). The testing was also performed with only time division (TD) ensemble, i.e., first dimension of the proposed algorithm and similarly with only frequency division (FD) ensemble, i.e., second dimension.

Figure 3 shows prediction output for two days data using normal LSTM, CNN, ANN, ELM apart from the proposed approach, i.e., MDE-LSTM. It has been found that while outputs of normal LSTM, CNN, ANN are almost same, the ELM gives totally random outcome while MDE-LSTM provides prediction best among all. Wind speed depends on multiple parameters including known and unknown factors, and thus, it is very hard to predict wind speed accurately. In such situation, getting results with CC value 0.8 or above is a good solution and it can be useful in some applications.

We also compared results with other approaches such as Time Division Ensemble LSTM (TDE-LSTM) and Frequency Division Ensemble LSTM (FDE-LSTM). These two approaches are subpart of the proposed solution itself. However, the intention

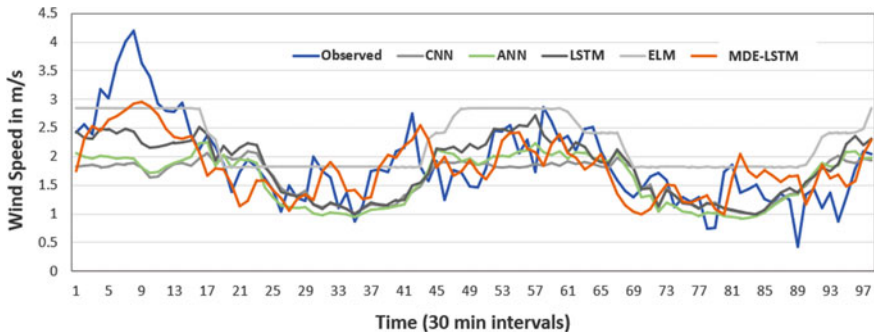


Fig. 3 Wind speed (m/s) (observed and predicted) using proposed model and traditional models

of comparing with them is that by combining both these approaches, we verified whether the model could really improve performance. From Fig. 4, it is evident that the combination performed better than individual approaches. While the outcome of TDE-LSTM and FDE-LSTM is surprisingly similar, the combination of these approaches, i.e., MDE-LSTM, has given some improvement over them. It might be noted that in some cases, the other two have outperformed the MDE-LSTM; however considering bigger time frame, the performance of MDE-LSTM is around 10% better than others based on their correlation coefficient (CC) values. This might be due to the fact that while either of them might not have covered all cases appropriately, the combination of both approaches might have been useful in covering more patterns and thus leads to better result.

Accuracy of the model is also evaluated by using few performance metrics such as mean absolute error (MAE), root mean square error (RMSE) and correlation coefficient (CC). The experimental outcomes in terms of these metrics are also presented in Table 1. All the performance metrics indicate the superiority of ensemble forecasting over non-ensemble methods, and further, MDE-LSTM is found to be best in the group of ensemble methods.

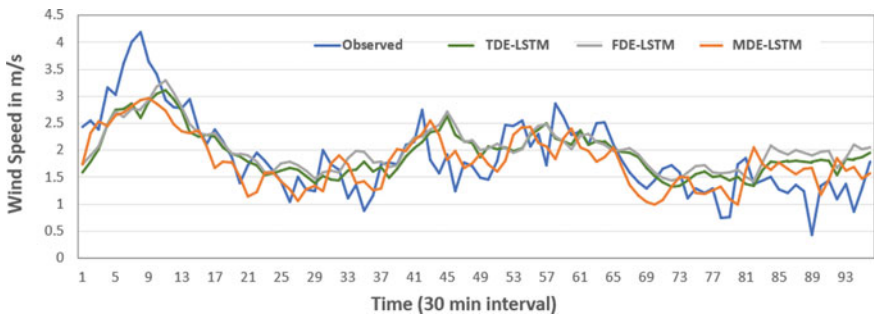


Fig. 4 Wind speed (m/s) (observed and predicted) using proposed model and its subparts

Table 1 Summary of performance metrics for predicted wind speed obtained from different models

Model	RMSE	MAE	CC
MDE-LSTM	0.827	0.595	0.839
FDE-LSTM	0.918	0.747	0.769
TDE-LSTM	0.926	0.764	0.767
CNN	1.148	0.962	0.647
LSTM	1.249	1.039	0.589
ANN	1.368	1.133	0.515
ELM	4.160	3.504	0.242

The performance was also evaluated based on how the predicted data were behaving in much wider scale. For various methods, especially the proposed model and its subpart models, i.e., TDE-LSTM and FDE-LSTM, and normal LSTM, the scatter plots were drawn on complete one-year test data which has 17,520 timestamps. As shown in Fig. 5, the slope of the trendline has improved significantly from normal LSTM and around 10% over TDE-LSTM and FDE-LSTM. From the improved coefficient of determination (R^2) values for MDE-LSTM, it indicates that more data points are within boundary of outliers and thus more points are considered to determine trend line, which indicates more predicted values are closer to the observed data. Thus, overall, the scatter plots show MDE-LSTM performed better than other methods.

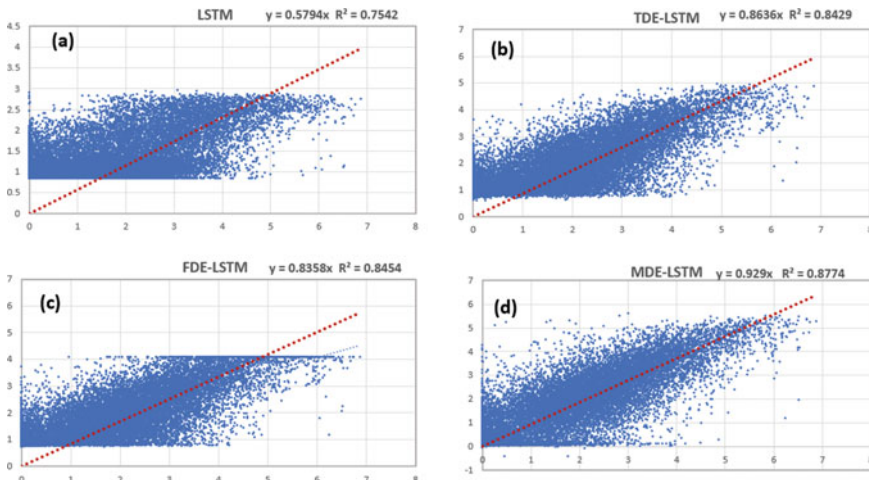


Fig. 5 Scatter plots of observed vs predicted wind speed in different approaches

6 Conclusion

Ensemble forecasting has gained significant popularity in solving various problems related to atmospheric studies. However, artificial intelligence (AI) technique-based ensemble forecasting for solving complex problems related to atmospheric science are relatively new. On top of that, multi-dimensional ensemble technique is a novel approach and can be applied in various problems across domains. The combination of distributing input data in two drastically different approaches was probably successful in fulfilling deficiency of each other and could make utilization of wide range of patterns in the input dataset. Also, various uncertainties in an AI based learning could be minimized by considering different ensembles and using them together. Multidimensional Ensemble LSTM can be used in different prediction problems with similar objective in various applications like oceanic chlorophyll, sea surface temperature, atmospheric temperature prediction, etc. The proposed model may have potential to improve prediction capability of other time series applications as well that may be interest to scientists and researchers.

References

1. Poggi P, Muselli M, Notton G, Cristofari C, Louche A (2003) Forecasting and simulating wind speed in Corsica by using an autoregressive model. *Energy Convers Manag* 44(20):3177–3196
2. Torres JL, García A, De Blas M, De Francisco A (2005) Forecast of hourly average wind speed with ARMA models in Navarre (Spain). *Solar Energy* 79(1):65–77
3. Erdem E, Shi J (2011) ARMA based approaches for forecasting the tuple of wind speed and direction. *Appl Energy* 88(4):1405–1414
4. Ühan U, Filik B, Filik T (2017) Wind speed prediction using artificial neural networks based on multiple local measurements in Eskisehir. <https://doi.org/10.1016/j.egypro.2016.12.147>
5. Barbounis TG, Theοcharis JB, Alexiadis MC, Dokopoulos PS (2006) Long-term wind speed and power forecasting using local recurrent neural network models. *IEEE Trans Energy Convers* 21(1):273–284. <https://doi.org/10.1109/TEC.2005.847954>
6. Gong L, Jing S (2010) On comparing three artificial neural networks for wind speed forecasting. *Appl Energy* 87(7):2313–2320. <https://doi.org/10.1016/j.apenergy.2009.12.013>
7. Qing C, Bradley E, Thompson T, Mark A (2012) Forecasting wind speed with recurrent neural networks. *Eur J Oper Res* 221(1):148–154. <https://doi.org/10.1016/j.ejor.2012.02.042>
8. Bhaskar K, Singh S (2012) AWNN-assisted wind power forecasting using feed-forward neural network. *IEEE Trans Sustain Energy* 3(2):306–315. <https://doi.org/10.1109/TSTE.2011.2182215>
9. Aditya G, Ashish K, Eric H (2015) A deep hybrid model for weather forecasting. In: Proceedings of the 21th ACM SIGKDD international conference on knowledge discovery and data mining, pp 379–386. <https://doi.org/10.1145/2783258.2783275>
10. Wang HZ, Wang GB, Li GQ, Peng JC, Liu YT (2016) Deep belief network based deterministic and probabilistic wind speed forecasting approach. *Appl Energy* 18:80–93
11. Ma X, Yu J, Qingli D (2017) A generalized dynamic fuzzy neural network based on singular spectrum analysis optimized by brain storm optimization for short-term wind speed forecasting. *Appl Soft Comput* 54:296–312
12. Liu H, Xiwei M, Yanfei L (2018) Smart deep learning based wind speed prediction model using wavelet packet decomposition, convolutional neural network and convolutional long short-term

- memory network. *Energy Convers Manag* 166:120–131. <https://doi.org/10.1016/j.enconman.2018.04.021>
- 13. Nie Y, Bo H, Zhang W, Zhang H (2020) Research on hybrid wind speed prediction system based on artificial intelligence and double prediction scheme, vol 2020
 - 14. Marndi A, Patra GK, Gouda KC (2020) Short-term forecasting of wind speed using time division ensemble of hierarchical deep neural networks. *Bull Atmos Sci Technol* 1:91–108. <https://doi.org/10.1007/s42865-020-00009-2>
 - 15. Andre Treiber N, Spath S, Heinermann J, von.Bremen L, Kramer O (2015) Comparison of numerical models and statistical learning for wind speed prediction. In: ESANN 2015 proceedings, European symposium on artificial neural networks, computational intelligence and machine learning
 - 16. Cadena E, Rivera W, Campos-Amezcua R, Heard C (2016) Wind speed prediction using a univariate ARIMA model and a multivariate NARX model. *Energy* MDPI
 - 17. Buhan S, Ozkazanc Y, Adirci IC (2016) Wind pattern recognition and reference wind mast data correlations with nwp for improved wind-electric power forecasts. *IEEE Trans Industr Inf* 12(3):991–1004
 - 18. Bianchi FM, Maiorino E, Kampffmeyer MC, Rizzi A, Jenssen R (2017) An overview and comparative analysis of recurrent neural networks for short term load forecasting
 - 19. Sepp H, Jürgen S (1997) Long short-term memory. *Neural Comput* 9(8):1735–1780. <https://doi.org/10.1162/neco.1997.9.8.1735>

A Novel Diagnosis System for Parkinson's Disease Using K-means Clustering and Decision Tree



L. Sherly Puspha Annabel , S. Sreenidhi, and N. Vishali

Abstract Parkinson's disease (PD) is an advanced neurological illness that causes tremor. As there is no particular system for the identification of PD, it is essential to design an automatic diagnostic system that assists the neurologists. In this work, we have established a new system that addresses PD diagnosis problems. This paper proposes an intelligent system named K-means clustering classification decision tree (k-CCDT) that makes use of unsupervised learning methods to accurately predict the disease. The system makes use of a K-means clustering algorithm to divide the data into classes, and the decision tree classification is performed to identify to which class the test data belong to. The PD dataset is categorized by 23 attributes based on the acoustic analysis of voice. Experimental results proved that the proposed system will act as a dominant method for diagnosing PD accurately for the test dataset with an accuracy of 95.56%.

Keywords Parkinson's disease · K-means clustering · Classification · Decision tree

1 Introduction

Parkinson's disease (PD) is a progressive nervous illness which is distinguished by tremor, muscular rigidity, and weary movement, mostly affecting elderly people. It occurs when nerve cells die in an area of the brain which controls movement. Because of this damage, the production of a neurotransmitter in our body called dopamine gets condensed. Also, it proceeds to damage of the nerve endings that produce norepinephrine which is also a neurotransmitter. The loss of these neurotransmitters helps in explaining some of parkinson's weary movement characteristics, like exhaustion, reduced food movement through the digestive tract, etc.

It is difficult to diagnose this disease, as it does not have a descriptive cause to indicate the stiffness or slow movement in the body. Also, symptoms are very subtle,

L. Sherly Puspha Annabel · S. Sreenidhi · N. Vishali
Department of Information Technology, St. Joseph's College of Engineering, Chennai 600119,
India

and the speed of progress varies from person to person. As of now, there are no testing procedures to give a conclusive result on PD. A neurologist can diagnose, only after observing the medical records or reviewing the symptoms of a person. Various other imaging scans such as ultrasound of the brain and PET scans are taken which yield an output with which the neurologist can eliminate false-positive people. However, it does not confirm whether the patient is having PD or not [1–10]. Hence, it is proposed to make the prediction by using a dataset that has been collected from acoustic analysis of voice which is used to identify the changes in voice parameters for predicting whether the patient has stiffness or trembling in the voice or not which in turn helps in identification of PD. The rest of the paper is ordered as follows: Sects. 2 and 3 explain the literature survey and proposed system. Sections 4 and 5 explain about the experimental results and conclusion.

2 Literature Survey

To detect the signs of PD, a deep brain stimulation (DBS) experiment was conducted by Defeng Wu et al. Implementation and comparison were made between traditional PSO-based radial basis function neural network (RBFNN) and RBFNN. A small decrease in efficiency but with a substantial decrease in computational overhead and accuracies of up to 89% has been obtained [1]. Sinziana Mazilu et al. did their experiment called freezing of gait (FoG) for patients with progressive PD. F1-measure of 56% in the pre-FoG class for patients was obtained during the implementation [2].

Reuben R. Shamir et al. have used deep brain stimulation (DBS) of the subthalamic region to detect the signs of PD. Here, they have implemented clinical decision support system (CDSS) that assists in optimization of the treatment which incorporates the patient's exact details. This system achieved 86% of the motor improvement scores with the help of combined ML algorithms [3]. Salim Lahmiri et al. assessed the efficiency of PD diagnostic strategies based on machine learning using dysphonia symptoms. They designed a medical support system using linear discriminant analysis (LDA), AdaBoost algorithm including support vector machine (SVM), etc. It is claimed that SVM is a successful approach built on dysphonia measurements to classify PD patients [4].

MusaPeker et al. applied a hybrid methodology where minimum redundancy maximum relevance (mRMR) algorithm is applied to identify the effective attributes. The resulting attributes after the conversion are introduced to the complex-valued artificial neural network (CVANN) as input data. For the diagnosis of PD in a relatively short time, they obtained a classification precision of 97.93% [5]. Resul Das, compared various types of classification for actual diagnosis of PD. Neural networks, decision tree, etc., are the classification schemas used for comparative study. Finally, neural network classifiers yielded 92.9% in the case of application scores [6].

To assist doctors in defining PD, an artificial neural network system with a back-propagation algorithm was used by Ramzi M. Sadek et. al. Prediction accuracy for smaller classes is reduced, and this design caused a significant increase of robustness

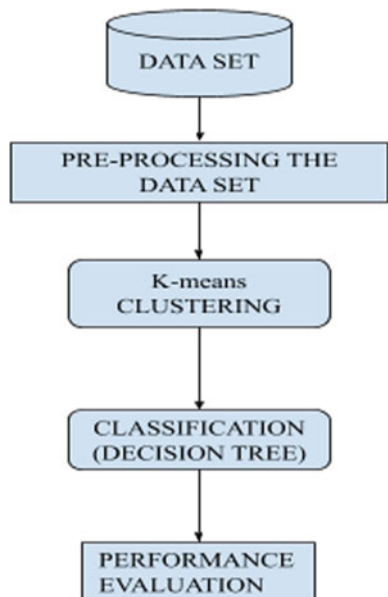
[7]. Srishti Grover et al. have proposed a methodology using deep neural networks (DNN) on UCI's Parkinson's telemonitoring voice datasets for the prediction of PD severity. They have implemented neural networks for predicting, and the accuracy that has been achieved is nearly 94.4% [8].

R. Prashantha et al. have tried to classify early PD subjects from normal using various classifiers like SVM, random forest, etc. The SVM classifier gave an accuracy of 96.40%, sensitivity of 97.03%, specificity 95.01, and 98.88% under receiver operating characteristic curve [9]. A new hybrid intelligent framework for PD progression prediction has been proposed by Mehrbakhsh Nilashi et al. where the prediction of PD progression is achieved by applying PCA, adaptive neuro-fuzzy inference system (ANFIS), and support vector regression (SVR) [10]. Shekhawat et al. [11] proposed a new approach for data transformation that leads to better classification.

3 Proposed System

In the proposed system named k-CCDT, the dataset is taken in a csv format and is preprocessed by removing all the unwanted or empty values. Then, clustering is performed that divides the data points into two subsets which help in performing the classification algorithm to easily identify to which class or category the data point will belong and after which the performance of the classification model is calculated. Figure 1 represents the architecture diagram of the k-CCDT system.

Fig. 1 Architecture diagram of the proposed k-CCDT system



Voice deterioration has been detected as the main symptoms of the PD. About 90% of people having PD are spotted with some kind of voice deterioration. Hence, voice measurement is used here in order to achieve great progress in the advancement of PD. Clustering is the technique which is used most profusely to get an intuition about the data structure. The clustering with K-means is a vector quantization method where the number of clusters, initialization of centroid, K data points selection, and centroid for the cluster will be computed.

The process of predicting the category of given data point is performed by decision tree classification algorithm. The decision tree is a nonlinear classifier and a model that uses a tree structure to demonstrate the relationships between the features. A decision tree classifier uses a branching decision structure, which provides a predicted final value. The tree is created in a top-down recursive manner of division and conquer. Classification trees are used where the target variable is categorical. From this tree, a confusion matrix is derived where the true values of the test data are known. Using this confusion matrix, the performance of the proposed system is calculated which describes the percentage of how efficient and effective predicted results are.

4 Experimental Results

R language is used for statistical software and data analysis development, and version 1.0.136 is used for our implementation. The dataset consists of 23 attributes including average, maximum, minimum vocal fundamental frequency, measures of variation in fundamental frequency, amplitude, measures ratio of noise to tonal components, status of the patient PD, dynamic complex measurement, etc.

Firstly, the dataset is cleaned, and then a clustering algorithm using the two key attributes is performed, i.e., HNR and spread2, where HNR is one of the measuring attributes of the noise-to-tonal part ratio in the voice and spread2 is one of the nonlinear measuring attributes of fundamental frequency variation. K-means clustering algorithm creates homogeneous subgroups where data points in the same group are similar to each other. These clusters are plotted using the plot function where the x-axis is HNR and spread2 lies on the y-axis. Centroid is plotted which acts as a representative of the entire cluster. Figure 2 represents the two clusters with each representing identical characteristics. Figure 3 represents the cluster with its centroids plotted in a graph.

Secondly, classification is performed to make it easy for the system to identify to which cluster the new data point will rely on. Classification is dividing or categorizing which means this algorithm uses divide and conquer methodology to achieve the goal of the system. Decision tree is a model used to represent the relationships between the attributes. To plot this tree, rpart function is loaded from the library. The dataset is split into a test and train set for which 77 and 23% of the dataset is assigned, respectively. The confusion matrix provides the classification model's output where the true values of the test data are known. It also provides a better understanding

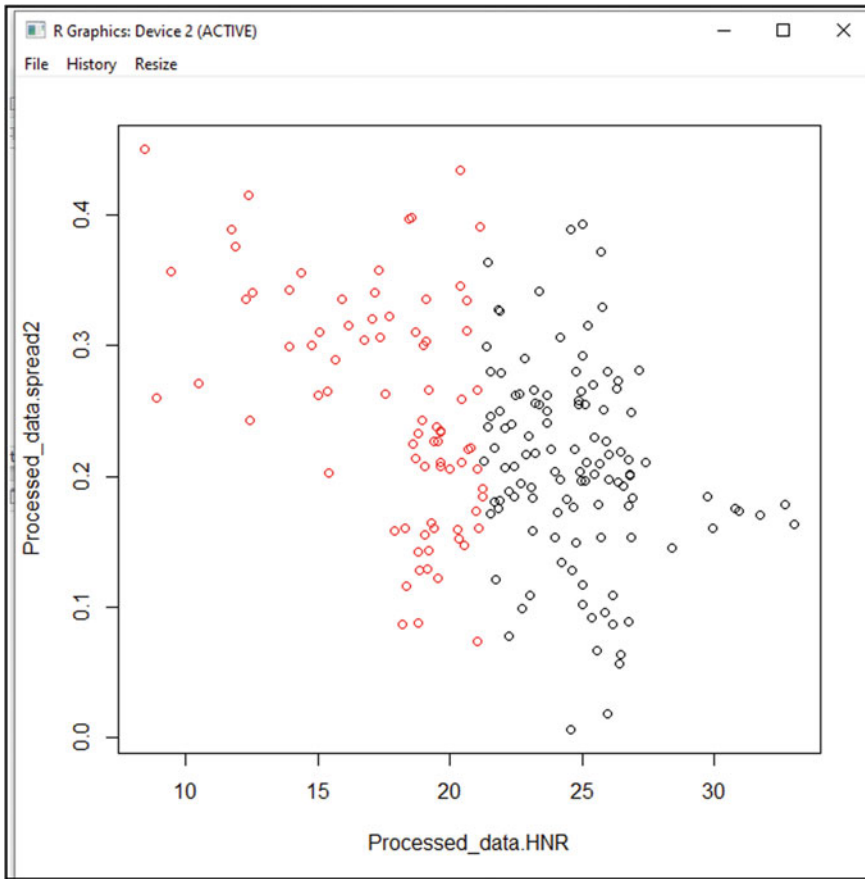


Fig. 2 Two clusters with each representing identical characteristics

about the correctness of the classification model. Figure 4 represents the probability of attaining accuracy using the decision tree.

In addition to accuracy, values for various other evaluation criteria are also computed. F-measure offers a way for both accuracy and recall to be integrated into a single measure that captures both properties. Precision is a metric of true positives out of the total positive class expected. Recall is an indicator of positive cases out of the total positive real instances. Specificity is a measure of negative instances out of the total actual negative instances. Table 1 describes the confusion matrix obtained for the proposed system k-CCDT.

It could be seen from the experiments that the proposed system k-CCDT produces a much better result when compared to the algorithms like RBFNN, TensorFlow DL, and CDSS. The following Fig. 5 shows the accuracy obtained through various algorithms to identify PD. The proposed system is compared with radial basis function neural network (RBFNN) that produces an accuracy of 89% [1]. Further decline is

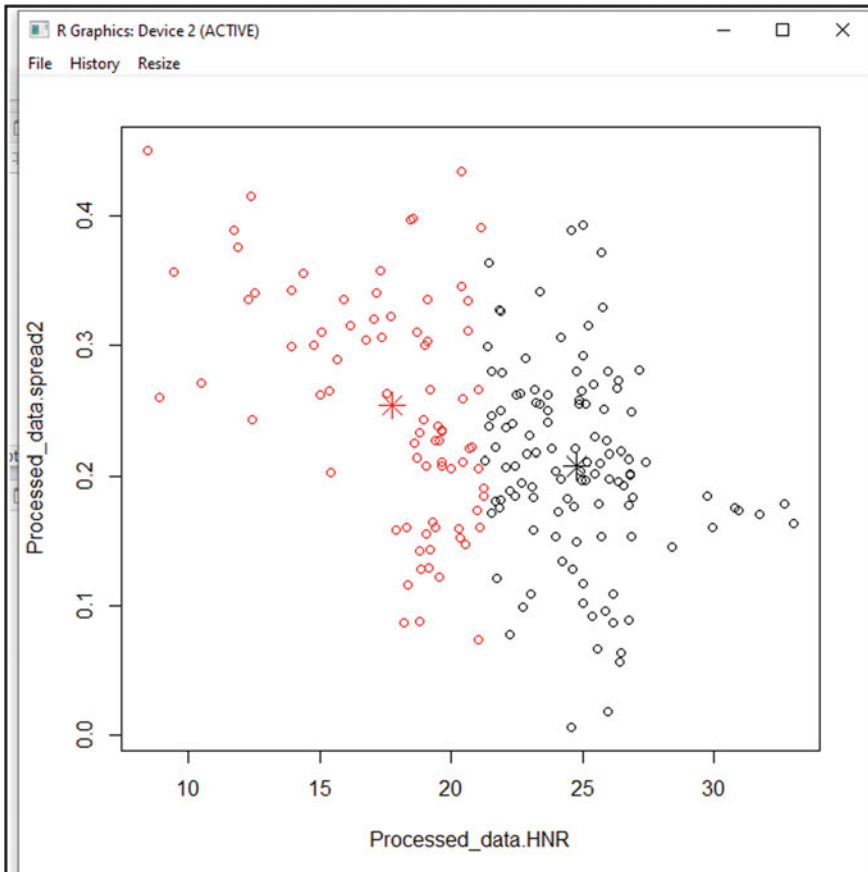


Fig. 3 Clusters with its centroids

seen in the clinical decision support system (CDSS) that shows an accuracy of 86% [3]. The proposed system is also compared with TensorFlow DL which achieves an accuracy of 94.4% [8]. Table 2 shows the values of all the performance evaluation parameters obtained from the implementation of the proposed system. It is clearly evident that the proposed system produces a better accuracy of 95.56% compared to that of the existing algorithms.

5 Conclusion

This paper presents a novel system named k-CCDT that helps the neurologist in diagnosing the PD. To recapitulate, the aim of the proposed system is to accurately identify how much test PD dataset is correctly identified using the acoustic vocal

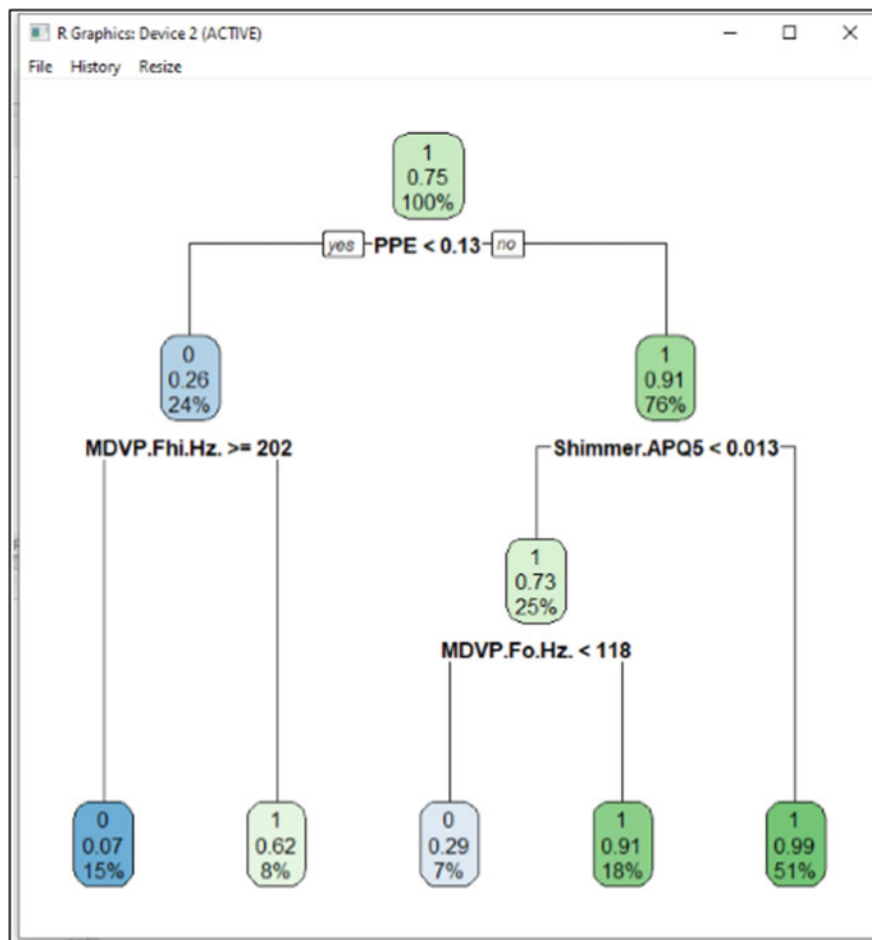


Fig. 4 Probability of attaining the accuracy by decision tree

Table 1 Confusion matrix obtained by k-CCDT

Actual value	Predicted value	
	Normal	PD
Normal	TRUE NEGATIVE (TN) = 9	FALSE POSITIVE (FP) = 2
	FALSE NEGATIVE (FN) = 0	TRUE POSITIVE (TP) = 34

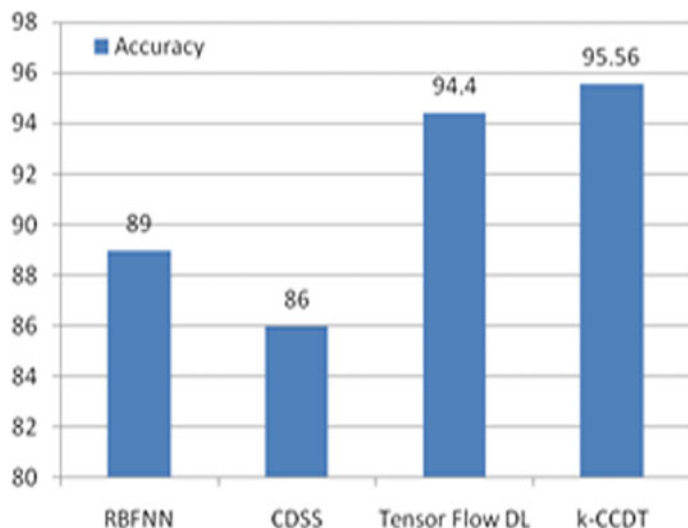


Fig. 5 Comparison of accuracy obtained by k-CCDT with existing algorithms

Table 2 Results achieved by k-CCDT according to the performance evaluation criteria

Performance criteria	Result	Result (%)
Accuracy	0.95556	95.5
Sensitivity or recall	1	100
Specificity	0.81818	81.8
Precision	0.94444	94.4
F-measure	0.97144	97.1

input. To achieve this, two algorithms are implemented. First, clustering is performed to split the data into two clusters, and then classification is performed after dividing the dataset into test and train sets. Decision tree is plotted with which a confusion matrix is generated. It is clearly evident from the experiment that the proposed system produces 95.56% of accuracy and outperforms various other existing algorithms in diagnosing the presence of PD. This could be further extended by connecting a hardware device to the input end, so that the data could be generated in real time and processed; thereby, the output generated in relation to the input is subsequently applied to the train dataset, making the system more efficient.

References

1. Wu D, Warwick K, Ma Zi, Gasson MN, Burgess JG, Pan S, Aziz TZ (2010) Prediction of Parkinson's disease tremor onset using a radial basis function neural network based on particle swarm optimization. *Int J Neural Syst* 20(02):109–116
2. Mazilu S, Calatroni A, Gazit E, Roggen D, Hausdorff JM, Tröster G (2013) Feature learning for detection and prediction of freezing of gait in Parkinson's disease. In: International workshop on machine learning and data mining in pattern Recognition. Springer, Berlin, Heidelberg, pp 144–158
3. Shamir RR, Dolber T, Noecker AM, Walter BL, McIntyre CC (2015) Machine learning approach to optimizing combined stimulation and medication therapies for Parkinson's disease. *Brain Stimul* 8(6):1025–1032
4. Lahmiri S, Ann Dawson D, Shmuel A (2018) Performance of machine learning methods in diagnosing Parkinson's disease based on dysphonia measures. *Biomed Eng Lett* 8(1):29–39
5. Peker M, Sen B, Delen D (2015) Computer-aided diagnosis of Parkinson's disease using complex-valued neural networks and mRMR feature selection algorithm. *J Healthc Eng* 6
6. Das R (2010) A comparison of multiple classification methods for diagnosis of Parkinson disease. *Expert Syst Appl* 37(2):1568–1572
7. Sadek RM, Mohammed SA, Abunbehian ARK, Abdul Ghattas AKH, Badawi MR, Mortaja MN, Abu-Nasser BS, Abu-Naser SS (2019) Parkinson's disease prediction using artificial neural network
8. Grover S, Bhartia S, Yadav A, Seeja KR (2018) Predicting severity of Parkinson's disease using deep learning. *Procedia Comput Sci* 132:1788–1794
9. Prashanth R, Dutta Roy S, Mandal PK, Ghosh S (2016) High-accuracy detection of early Parkinson's disease through multimodal features and machine learning. *Int J Med Inf* 90:13–21
10. Nilashi M, Ibrahim O, Ahani A (2016) Accuracy improvement for predicting Parkinson's disease progression. *Sci Rep* 6(1):1–18
11. Shekhawat SS, Sharma H, Kumar S, Nayyar A, Qureshi B (2021) bSSA: Binary salp swarm algorithm with hybrid data transformation for feature selection. IEEE Access. <https://doi.org/10.1109/ACCESS.2021.3049547>

An Investigation of Ground Barriers and Teachers' Attitude Towards Technology-Enabled Education in Schools



Gopal Datt and Naveen Tewari

Abstract Technology-Enabled Education integrates Information and Communication Technology in teaching–learning which is a global demand for global competency. In India, The National Mission on Education through Information and Communication Technology has been launched in 2009 as a landmark initiative for achieving the benefits of Technology-Enabled Education over traditional education. This study aims to investigate the ground barriers and attitudes of teachers towards Technology-Enabled Education in Schools of the Uttarakhand region. A survey questionnaire was distributed among school teachers of Uttarakhand state, using convenience-cum-random sampling basis. The data collected for this study through questionnaires were analysed using descriptive statistics and the results are discussed in detail. The survey was open for 30 days to fill by the participants where a total of 148 complete responses are received from the participants on time. The results indicate that the integration of Technology-Enabled Education in teaching–learning is a requisite step for future education. It was also found that the lack of infrastructure, i.e. Internet connection, Internet-enabled devices, etc., lack of training to implement technology-enabled education, lack of ICT skills, and lack of familiarity with technical tools are the key barriers to implement Technology-Enabled Education in the schools. For future studies, there is a need for considering the other stakeholder's opinions, i.e. students, parents/guardians, and school administrators for getting the full advantage of Technology-Enabled Education in schools.

Keywords Technology-enabled education (TEE) · Information and communication technology (ICT) · Online learning initiatives · NMEICT · MOOC

G. Datt (✉)

School of Vocational Studies, Uttarakhand Open University, Haldwani, India

N. Tewari

School of Computing, Graphic Era Hill University, Bhimtal, India

1 Introduction

Technology-Enabled Education is a buzzword in the twenty-first century. It used the applications of ICT to enhance the way of teaching–learning and also transforming the education and educational needs of twenty-first century learners. Technology-Enabled Learning provides the opportunity to access quality teaching–learning material beyond the physical boundaries. Integration of technology focusses on the increasing use of technology for teaching–learning purposes and to improve the effective use of technology to facilitate the learning needs of their aspirants. The inclusion of technology in education enables the teachers to enhance their way of teaching methodology. These technology-enabled methods of teaching are useful for the students to get the concept better, visually, and technically. This study is conducted to check the barriers and attitudes of teachers towards Technology-Enabled Education as without knowing the barriers and readiness to adopt new platforms; teacher's acceptance for Technology-Enabled Education cannot be evaluated.

In the age of the digital revolution, many developments have taken place in the education sector. Digitalization has completely changed the way of today's education in comparison to our traditional education system where the use of Information and Communication Technology (ICT) in teaching–learning is incorporated at a large scale to make education more accessible and effective. The digital advancements in education opened new doors of learning, i.e. OERs, MOOCs, Open Education, CourseWare, Digital Libraries, and Web-based e-content [1].

The use of ICT in education will assist teachers to fulfil the global requirements of facilitating technology-based teaching–learning. The Ministry of Education (Malaysia) considered ICT as one of the key elements in transforming the future development of the country. The use of ICT in teaching–learning will prepare an environment that will be more effective for both teachers and learners [2]. Shaikh et al. [3] experiment with higher education students and found that the student using technology for learning such as touch screens, sensors, etc. got the concepts much more easily than classroom learning. They also suggested the use of haptic technologies to support student learning [3]. Class-based teaching is converted to technology-enhanced learning with the development of technical hardware and software. The technical awareness between students and teachers also encourages technology-enabled learning to change with requirements [4]. In today's world, many countries are following the traditional education system whereas others are following a mixed-mode of education with the use of ICT for teaching–learning. There are many discrepancies in the non-digitized or traditional educational system, such as data backups and security. The data that is generated within an education system is in a huge amount and always vulnerable to external as well as internal sources. Usage of technology in the education system enables the system to get rid of these problems [5]. The purpose of this study is to identify and explore the various issues and the teacher's attitude towards incorporating Technology-Enabled Education in schools. In the light of the objectives of this study to get advantages of Technology-Enabled Education in schools, the necessary suggestions are recommended.

2 Survey of Literature

Information and Communication Technology (ICT) in education performs several roles, as-collaborative learning, resource sharing, planning, management, decision making, etc. ICT integration in school classrooms is focussed on upliftment in the learning capacity of the students, the reachability of quality educational resources to the end-user, etc. Technology can transform education but still challenge remains stands that how to effectively integrate technology in the curriculum [6]. Teachers' competence in ICT is a significant factor to effectively utilize ICT in teaching–learning as well teachers must have such opportunities to access ICT resources as when required [7]. The professional development of teachers is an important factor to adapt to periodic changes in the teaching sector. The effective professional development/training programs conducted for the teachers can enable to promote ICT utilization in education, especially in school education. Quality of teachers directly proportionate to the delivery; what they deliver to their students? The primary requirement of achieving Sustainable Development Goal (SDG) 4 is to develop/prepare quality teachers for the future. In such a situation, ICT has to perform a key role to develop quality among teachers in the form of increasing competency level, developing a student-centric education environment, adaptability, providing more flexible learning opportunities, etc. [8].

The use of ICT in education reveals the directions and forces affecting the globalization of education. There are too many challenges towards globalization of education where one should all set to face such challenges, as-adaptation to the latest techniques of teaching–learning, e-learning, and online education [9]. The ICT influences and constructivist learning environment in Malaysian schools have been noted where more emphasis on the integration of multimedia in learning [10]. The patterns of ICT integration in Ontario's publicly funded schools and their impacts on student academic achievement and empowerment as well as the role and importance of parent's awareness and involvement could be noted [11]. Technology-Enabled Active Learning (TEAL) is the most powerful and challenging which insights rethinking of learning pathways in Schools as well the TEAL can become a more attractive and engaging way of learning in schools [12]. In today's era, the technological competence of teachers can improve the quality of education simultaneously can invite innovations in teaching–learning, promote lifelong learning, and most important is the sharing of resources. In Israeli schools, the National ICT program was adapted in the year 2010 to prepare teachers for facing twenty-first century educational challenges and to identify possibilities of ICT in school education to strengthen the quality and access of education [13]. ICT performs a key role in developing education-related policy and also enables Technology-Enabled Education in schools, especially for quality access to education among the teaching–learning fraternity. To develop students for twenty-first century skills, the potential use of technology-enabled education in teaching–learning is today's demand [14]. The academic achievement and satisfaction regarding learner engagement are one of the important factors where

learner engagement tactics and identification of the most relevant constructs for learning in a blended learning environment are needed [15].

3 Statement of Problem

The National Mission on Education through Information and Communication Technology (NMEICT) has been launched by the Ministry of Education (MoE), Government of India (GoI) in the year 2009, for the sake of utilizing the potential of technology in teaching–learning. In the light of the NMEICT objectives access, equity, and quality of education should be achieved at all levels of teaching–learning. With the potential of technology, as we are transforming towards industry 4.0 called the industrial revolution, where the role of technology performs a key character in all aspects of our life. This study was designed to investigate the barriers, teachers' attitudes towards adapting and enabling Technology-Enabled Education in schools.

4 Objective

- To examine the usage of Information and Communication Technology (ICT) in schools, especially for teaching–learning purposes.
- To identify Internet accessibility and teachers' attitude towards enabling Technology-Enabled Education in the schools.
- To identify the barriers to implement Technology-Enabled Education in schools, especially in the state of Uttarakhand.
- Recommendations for policymakers/authorities to overcome the barriers which hinder the implementation of Technology-Enabled Education in schools.

5 Methodology

This study is descriptive research, and it has been carried out to examine the acceptance and the barriers of Technology-Enabled Education in context to schools in the state of Uttarakhand. The data required for this study was collected from primary sources. In the light of the objectives of the study, the information has been collected in the form of the questionnaire from the respondents, as school teachers either from government, semi-government or private schools in the state of Uttarakhand. And also reviewed several studies and research articles to identify the status of Technology-Enabled Education in the state. This research study follows a quantitative approach where the primary data is collected from the targeted participants to explore the infrastructural status, barriers, and teachers' attitude towards implementing Technology-Enabled Education in the state. Keeping in view the nature of

the study, the data drawn from various sources have been analysed with the help of mathematical and statistical tests as a simple percentage, averages, and standard deviation.

5.1 *The Questionnaire*

The questionnaire had some general questions, such as Gender, School Type, Location of the School, Teaching Subject, Teaching Section, etc. The questions are organized into two sections. Section one is about general questions and section two holds specific questions about the inclusion of technology, especially Information and Communication Technology (ICT) in teaching–learning, Barriers to implement Technology-Enabled Education in Schools, etc.

5.2 *Participants/Respondents*

The questionnaire for this study was sent through e-mail/WhatsApp/other social mediums and in the paper form, to the more than 200 participants (respondents) across the state Uttarakhand. The participants of this study are school teachers of the government, semi-government, and private schools. A total number of 148 complete responses are received from the participants on time. The survey was open to the participants to fill for 30 days. The selection of survey participants was based on convenience-cum-random sampling with the following criteria having in mind, the location of the school, teaching subjects, teaching sections, etc.

Table 1 presents the demographic profile of the participants. The gender-wise demography of the participants reveals more participation from the male participants (56.1%) in comparison to female participants (43.9%). In the case of school location-wise demography of the participants, 25.7% of participants belongs to the village or rural areas, 8.11% of participants belong to a small town, 18.2% of participants are belongs to the town, 37.2% of participants belong to the city, and 10.8% of participants belong to a large city. In the case of the teaching-section-wise demography of the participants, 8.8% of participants belong to the Pre-Primary section, 20.3% of participants belong to the Primary section, 27% of participants belong to the Secondary section, and 43.9% of participants belong to the Senior Secondary section. In the case of teaching subject-group wise demography of the participants, 10.8% of participants belong to Pre-Primary subjects group, 30.4% of participants are belongs to Science subjects group, 16.9% of participants are belongs to Social Science subjects group, 33.1% of participants are belongs to Language subjects group, and 8.8% of participants belong to Activity subjects group.

Table 1 Demographic profile of the respondents ($N = 148$)

Indicators	Contribution (%)
<i>Gender wise demography (1)</i>	
Male	56.1
Female	43.9
<i>School location wise demography (2)</i>	
A Village or Rural Area (fewer than 3000 people)	25.7
A Small Town (3000 to about 15,000 people)	8.11
A Town (15,000 to about 100,000 people)	18.2
A City (100,000 to about 10,00,000 people)	37.2
A Large City (over 10,00,000 people)	10.8
<i>Teaching section wise demography (3)</i>	
Pre-Primary (Play Group up to Class 2)	8.8
Primary (Class 3 up to Class 5)	20.3
Secondary (Class 6 up to Class 8)	27
Senior Secondary (Class 9 up to Class 12)	43.9
<i>Teaching subject-group wise demography (4)</i>	
Pre-Primary Subjects (Play Group to Class 2)	10.8
Science Subjects Group	30.4
Social Science Subjects Group	16.9
Language Subjects Group	33.1
Activity Subjects Group	8.8

Source Data compiled through questionnaire

6 Results and Discussion

This study has been carried out to examine the ground barriers and teachers' attitudes towards implementing Technology-Enabled Education in the Schools. In this study, the acceptance, barriers, and attitude of the teachers regarding Technology-Enabled Education are analysed in context to implement/introduce such efforts in teaching-learning at the schools. And also, how the barriers which hinder the implementation of Technology-Enabled Education in schools can be overcome has been analysed and discussed in detail.

Table 2 reveals that the majority of respondents having a poor or very poor skill set about introducing TEE in Schools. Only 27% of respondents had either excellent or good skill set regarding introducing TEE in the Schools, whereas 28.37% of respondents are having average digital skills regarding implementing TEE in Schools. In the case of the existing status of TEE in the Schools, the situation is not satisfactory,

Table 2 Status of digital literacy and Technology-Enabled Education in schools with future benefits ($N = 148$)

Indicators	Excellent (5)	Good (4)	Average (3)	Poor (2)	Very poor (1)	Mean	SD
Digital Skills towards Introducing Technology-Enabled Education in Schools	9	32	42	45	20	3	2.5
Status of Technology-Enabled Education in Schools	5	31	12	15	85	2	2
Future Benefits of Implementing Technology-Enabled Education in Schools	80	49	19	0	0	4	3.9

Source Data compiled through questionnaire

67.56% of respondents recorded their opinion as either poor or very poor, 8.1% of respondents are average, 20.94% of respondents recorded their opinion as Good, and only 3.37% of respondents recorded their opinion as to the excellent. It also has been observed that in the case of future benefits of implementing TEE in the Schools, the respondents recognized it as an outstanding step. Almost, 87% of respondents are in favour of future demands of such efforts in the teaching–learning in the schools.

Table 3 reveals the two sets of scenarios about Internet connectivity and accessibility at the school level: the first scenario about the number of devices connected to the Internet (refer to Table 3, part-A), and the second scenario about the percentage

Table 3 Status of Internet connectivity and accessibility at school and student's residence ($N = 148$)

Part-A: Number devices connected to the internet at school		Part-B: Percentage of your students having internet-enabled devices at their residence	
Indicators	Contribution (%)	Indicators	Contribution (%)
Up to 10	23.6	Up to 10%	25.0
Up to 20	8.8	Up to 20%	10.1
Up to 40	9.5	Up to 40%	11.5
Up to 60	8.1	Up to 60%	13.5
Up to 80	15.5	Up to 80%	16.2
Up to 100 And More	16.9	Up to 100%	15.3
No internet connection available	17.6	No internet enabled device(s) available	8.4

Source Data compiled through questionnaire

of students having Internet-enabled devices at their residence (refer to Table 3, part-B). It has been observed that 17.6% of respondents recorded their opinion as 'No Internet connectivity' is available at schools whereas 23.6% of respondents recorded that only up to 10 devices are connected to the Internet. In continuation of Internet connecting status in schools, 8.8% of respondents recorded that only up to 20 devices are connected to the Internet, 9.5% of respondents recorded that up to 40 devices are connected to the Internet, and so on (refer to Table 3, part-A). So, in the overall scenario, it seems to be an urgent need to facilitate Schools with the necessary infrastructure to develop such Schools as supportive to TEE in the future teaching-learning. In the case of assessing the students having Internet-enabled devices at their residence, the recorded responses present the actual picture of enabling TEE in Schools. During this study, it has been observed that 25% of respondents recorded their opinion that only up to 10% of their students having Internet facility for learning purposes at their home. In continuation of this study, it also has been observed that 10.1% of respondents recorded their opinion that up to 20% of their students having Internet facility at their home, and so on (refer to Table 3, Part-B).

Table 4 reveals the teachers' attitude towards enabling TEE in schools. It has been observed that 71.62% and 13.51% of respondents are, respectively, 'extremely agreed' and 'agreed' to facilitate computer facility to the school students for their learning enhancement, whereas 13.51% of respondents recorded their opinion as 'Neutral, neither agreed nor disagreed' to facilitate such facilities to the school students. In the case of assessing the necessity of Internet accessibility for the students to achieve global competitiveness and overall learning enhancements, 98.64% of respondents are recorded their opinion as either extremely agreed or agreed. For the skill enhancements of the teachers, 95.94% of respondents are recorded their opinion as either extremely agreed or agreed to frequently organize the workshops/hands-on-training programs, so that the teachers can achieve a higher level of skill set and definitely this newly adapted skill set will enhance the productivity of such teachers.

Table 5 reveals the teachers' attitude towards adapting TEE in schools. In the case of adapting TEE in the schools for teaching–learning purposes, 16.9% of respondents are unable to adapt TEE because of not comfortable operating the Internet, whereas 20.9% of respondents are unable to adapt TEE because of the unwillingness of school authorities to provide adequate facilities. The majority of the respondents (approximately 60%) recorded their opinion to adapt TEE in the schools without any condition, whereas only 2.7% of respondents are not in favour to adopt TEE in schools for teaching–learning purposes. Overall, 97% of respondents are in favour to adopt TEE in the schools but with resolving such practical hurdles that hinder the implementation of TEE in the schools. It has been observed that adequate facilities and hands-on training must be provided to the teachers on time to take the benefits of such new initiatives for teaching–learning purposes.

Table 6 reveals the barriers facing towards implementing TEE in the schools. During this study, the teachers' perception has been recorded and analysed towards the key barriers faced while TEE is proposed to implement at schools. It has been observed that 37.2% of respondents are facing lack of infrastructure (i.e. Internet connectivity, availability of resources, and trained/skilled human resource), 29.1%

Table 4 Teachers' attitude towards enabling technology-enabled education in schools ($N = 148$)

Indicators	Extremely Agree (5)	Agree (4)	Neutral (3)	Disagree (2)	Extremely Disagree (1)	Mean	SD
Computer facility should be available to the Students in Schools for Learning Enhancement	106	20	20	2	0	4.6	4.10
Internet Accessibility to the School Students is Necessary for Global Competitiveness and Overall Learning Enhancements in close Supervision to the Teachers/Parents	72	74	1	1	0	4.5	3.97
Training Programs should be Organized Frequently for the Skill Enhancements of the Teachers	61	81	5	1	0	4.4	3.88

Source Data compiled through questionnaire

Table 5 Teachers' attitude towards adapting Technology-Enabled Education in schools ($N = 148$)

Indicators	Contribution (%)
I am Interested, but I am not comfortable with operating computers/the Internet	16.9
I am interested in it, but the school authority(s) are unable to provide adequate facilities	20.9
I am not interested, it is time-consuming/shows an inferior approach to traditional teaching	2.7
I prefer to use Technology Enables Education	59.5

Source Data compiled through questionnaire

Table 6 Barriers facing towards implementing Technology-Enabled Education in schools

Indicators	Contribution (%)
Lack of infrastructure	37.2
Lack of training to implement technology in teaching–learning	29.1
Lack of ICT Skills	16.8
We cannot justify Technology-Enabled Education over Traditional Method of Teaching	16.9

Source Data compiled through questionnaire

of respondents are facing lack of training to implement TEE, 16.8% of respondents are either facing lack of ICT skills or they do not feel comfortable to work with Internet/computers, whereas 16.9% of respondents recorded their opinion that they cannot justify TEE over the traditional method of teaching. More or less, the above said barriers must be resolved on a prior basis to smooth implementation of TEE in the schools.

7 Suggestions and Future Scope

To accelerate the potential use of ICT in education, the policy formulation and distribution of quality learning resources are the two main challenges. The expansion of mobile technology makes TEE somehow easier to implement at the primary education level but still, there are too many challenges as observed during this study. TEE aims to increase access to quality teaching–learning among aspirants which also can overcome the shortage of quality teachers in the educational system. The development and growth of any country are directly aligned with technology expansion and inclusion for social wellness. In all such scenarios, educational inclusion and development is the real symbol of such type of growth. ICT in education makes the use of information delivery easier and also develops an accessible virtual learning environment. The TEE is transforming the classroom education beyond the physical limits and enhancing the quality, multi-mode, and accessible education for the aspirants. At the concluding phase of this study, the suggestions or the future recommendations are listed herewith to utilize the potential of Technology-Enabled Education for teaching–learning purposes–

- Proper awareness, importance, and benefits of TEE should be an urgent need to uplift the TEE status in the region.
- The infrastructural issues, i.e. Internet connectivity, electricity, and hardware infrastructure must be resolved on a prior basis.
- A dedicated ICT lab must be arranged by the school with adequate facilities for the overall learning enhancement of the students.
- Trained or expert teachers should be arranged for setting up TEE in the schools instead of enforcing existing teachers from different domains.

- School authorities must support (refer to Table 5) the TEE for the future learning enhancements of the students.
- Sufficient training/workshops (refer to Table 6) must be organized to implement TEE in schools.
- To develop ICT skills among teachers, the needful workshops should be organized from time to time.

References

1. Dubey HK, Singh A, Dubey S (2019) Education system in digitalised era. *Int J Adv Innov Res* 6(1):97–99
2. Ghavifekr S, Rosdy WAW (2015) Teaching and learning with technology: effectiveness of ICT integration in schools. *Int J Res Educ Sci* 1(2):175–191
3. Shaikh UAS, Magana AJ, Neri L et al (2017) Undergraduate students' conceptual interpretation and perceptions of haptic-enabled learning experiences. *Int J Educ Technol High Educ* 14(15). <https://doi.org/10.1186/s41239-017-0053-2>
4. Peng H, Ma S, Spector JM (2019) Personalized adaptive learning: an emerging pedagogical approach enabled by a smart learning environment. *Smart Learn Environ* 6(9). <https://doi.org/10.1186/s40561-019-0089-y>
5. Martins J, Branco F, Gonçalves R, Au-Yong-Oliveira M, Oliveira T, Naranjo-Zolotov M, Cruz-Jesus F (2019) Assessing the success behind the use of education management information systems in higher education. *Telemat Inf* 38:182–193
6. Padayachee K (2017) A snapshot survey of ICT integration in South African Schools. *South Afr Comput J* 29(2):36–65. <https://doi.org/10.18489/sacj.v29i2.463>
7. Aslan A, Zhu C (2018) Starting teachers' integration of ICT into their teaching practices in the lower secondary schools in Turkey. *Educ Sci Theory Pract* 18(1):23–45. <https://doi.org/10.12738/estp.2018.1.0431>
8. Li S, Yamaguchi S, Sukhbaatar J, Takada J (2019) The influence of teachers' professional development activities on the factors promoting ICT integration in primary schools in Mongolia. *Educ Sci* 9(78). <https://doi.org/10.3390/educsci9020078>
9. Rajesh M, Nair SP (2009) Indian school teachers' perspective on the globalization of education. *Turkish Online J Dist Educ TOJDE* 10(4):12–26. ISSN 1302-6488
10. Sultan WH, Woods PC, Koo AC (2011) A constructivist approach for digital learning: Malaysian schools case study. *J Educ Technol Soc* 14(4):149–163. <https://doi.org/10.2307/jedutechsoci.14.4.149>
11. Chen B (2015) Exploring the digital divide: the use of digital technologies in ontario public schools. *Can J Learn Technol (CJLT)* 41(3):1–23
12. Cinganotto L, Panzavolta S, Garista P, Guasti L, Dourmashkin P (2016) TEAL as an innovative teaching model (insights from educational avant-garde movement in Italy). *J e-Learn Knowl Soc* 12(2):115–126. ISSN: 1826-6223, eISSN: 1971-8829
13. Blau I, Inbal TS (2017) Digital competences and long-term ICT integration in school culture: the perspective of elementary school leaders. *Educ Inf Technol (The Official J IFIP Tech Committee Educ)* 22(3):769–787. <https://doi.org/10.1007/s10639-015-9456-7>
14. McCoy S, Marcus-Quinn A, Hourigan T (2019) The digital learning movement: how should irish schools respond? *Econ Soc Rev* 50(4):767–783
15. Halverson LR, Graham CR (2019) Learner engagement in blended learning environments: a conceptual framework. *Online Learn J* 23(2):145–178. <https://doi.org/10.24059/olj.v23i2.1481>

An Improved Ant Colony Optimization with Correlation and Gini Importance for Feature Selection



Tanvi Joshi, Ashwin Lahorkar, Gaurav Tikhe, Hrushikesh Bhosale, Aamod Sane, and Jayaraman K. Valadi

Abstract Accurate classification of examples depends upon identification of informative attributes and removal of redundant attributes. Attribute selection helps reduce the noise and increase classification accuracy. In computational biology and bioinformatics, feature selection facilitates identification of most relevant attributes thereby facilitating valuable domain information. In this project, we have employed a synergistic filter-wrapper methodology for simultaneous classification and attribute selection. Ant colony optimization employs correlation and Gini ranking information along with pheromone learning, for providing better and better attributes as iterations proceed. The robust random forest classifier employed classifies the data to maximize fivefold accuracy. We evaluated the performance of our algorithm with eight benchmark datasets.

Keywords Ant colony optimization · Feature-selection · Gini ranking · Correlation

1 Introduction

In the age of artificial intelligence, large volumes of data are generated day by day. Most of this data contains a large number of features. Some of these features have low or no predictive power and some of them are redundant as they are strongly correlated. Using such datasets for developing models not only increases computation burden but also causes a problem called the curse of dimensionality. Objective of feature selection (FS) is to eliminate such features and find a subset of features which are impactful and have good predictive power. Due to dimensionality reducing ability of FS methods, these methods have been an area of active research in different biology sub-domains and in bioinformatics. In order to find the optimal subset of features, the entire feature space needs to be searched.

T. Joshi · A. Lahorkar · G. Tikhe
Centre for Modeling and Simulation, SPPU, Pune, India

H. Bhosale · A. Sane · J. K. Valadi (✉)
Flame University, Pune, India

Different methods have been proposed for feature selection which are normally classified into three classes as filter methods, wrapper methods and hybrid approach [1]. Filter method ranks features by some metric and it rejects those features which are unable to achieve a threshold score. Some examples of metrics used for feature ranking are F-score, mutual information, information gain, etc. Filter methods are independent of the learning algorithm and may or may not find the optimal subset. These methods have high time efficiency but low accuracy. Advantages of filter methods include easy scalability for high-dimensional data, computationally simple. Disadvantages of filter methods are ignoring interaction with classifiers as well as ignoring feature dependencies [2]. Next class of methods is wrapper method which is dependent on selection of learning algorithms. Even though wrapper methods are known to have high accuracy, they also have high computational complexity. Advantages of wrapper method are: considering interaction between feature subset search and considering feature dependencies. Some pitfalls of this method include overfitting of data, possibility of computational intractability for a dataset with a large number of features. The last class of feature selection method is hybrid approach which attempts to take advantage of complementary features of filter and wrapper methods. This method involves using a learning algorithm for feature selection similar to wrapper method but it is less intensive compared to wrapper method. Some examples of hybrid approaches are LASSO and RIDGE regression, memetic algorithm, etc. Apart from these embedded methods are the fourth class of methods in which the classifier itself embeds feature selection. Random forest has two feature selection methods embedded in the algorithm itself.

Recently, different meta-heuristic methods have been used to tackle the problem of feature selection. Some popular ones include Genetic Algorithm [3], Ant colony optimization [4], particle swarm optimization [5], binary cuckoo search (bCS) [6], binary bat algorithm (bBA) [7], binary gravitational search algorithm (bGSA) [8], binary whale optimization with simulated annealing (bWOASA) [9], and binary gray wolf optimization (bGWO) [10], binary binomial cuckoo search (bBCS) [11], binary salp swarm algorithm (bSSA) [12], chaotic spider monkey optimization algorithm (CSMO) [13], exponential SMO [14], etc. The meta-heuristic methods are stochastic optimization techniques and are used due to suitability of their population characteristics for solving problems of feature selection. These techniques try to achieve better solutions by using feedback and heuristic information [15]. Exploration and exploitation are important features of meta-heuristics. Exploration is the ability to globally search the sample space which is associated with escaping the local optima entrapment. Exploitation is the ability to refine promising solutions which are found by exploration. To have a good performing model, a proper balance between both these features is required [16].

One of the popular techniques and is widely used for solving feature selection problems is ant colony optimization [4] which is a swarm-based method introduced by Dorigo in 1991. This algorithm is based on real-life foraging behavior of ants. The computational algorithms mimic the pheromone mediated search behavior of real-life ants. Our modified and improved algorithm employs a synergistic combination of Correlation and Random Forest Gini importance, probabilistically employed as

heuristics. The rest of the paper is structured as follows: Sect. 2 discusses the summary of ant colony optimization, its binary form and work done by different authors. Section 3 consists of methodology and algorithm proposed in this work. Section 4 discusses the experimental findings and the paper is concluded in Sect. 5.

2 Ant Colony Optimization

Ant colony optimization algorithm is a meta-heuristic method inspired from the real ant colonies and their traversal for food collection. When an isolated ant moves from the nest to the food source, it deposits some pheromone on its trail. Other ants in the neighborhood get attracted to the pheromone rich trail. They also deposit more pheromone, thereby increasing the pheromone strength of the trail. In this way more and more ants are attracted to this trail and the route to the food source from the nest and back is established. This autocatalytic pheromone-mediated search of real-life ants is mimicked by artificial ant algorithms for solving several real-life optimization problems.

2.1 Ant Colony Optimization for Feature-Selection

In the ant colony optimization technique for feature selection, features are considered as nodes of a graph with links connecting each node to each other node. Initially, random amounts of pheromone are deposited on all links. Apart from this, different algorithms employ appropriate heuristics in conjunction with pheromone deposition for determination of link weights for the selection of nodes from the current nodes. Algorithms mainly employ two processes, viz. exploration and exploitation for selection of the nodes from the current position. At every node, one of these processes is selected by a probability. This probability q_0 is fixed a priori. Ants start from a random node and move to the next node by exploitation with a probability q_0 and by exploration with a probability $(1 - q_0)$. If exploitation is selected, an ant moves to the feature whose link has maximum transition probability. If exploration is selected, it moves to the legally permitted connected node with a probability proportional to the transition probability of the links connected to current node. The transition probability is defined as a product of two terms composed of pheromone concentration and heuristics. This can be defined as follows:

$$P_{ij}^k(t) = \begin{cases} \frac{\tau_{ij}^\alpha \eta_{ij}^\beta}{\sum_l \tau_{il}^\alpha \eta_{il}^\beta} & \text{If } i \text{ and } j \text{ are admissible nodes} \\ 0 & \text{Otherwise} \end{cases} \quad (1)$$

2.2 Binary Ant Colony Optimization for Feature-Selection

In binary ant colony optimization, each attribute is assumed to have one of two states 0 and 1, hence the name binary ant colony optimization. State 1 indicates that the feature corresponding to that state is selected, while 0 indicates the feature is not selected. Now if we assume features as the nodes of a graph, between any two nodes four different types of links are possible. For example, say i and j are two nodes then, $i_0 - j_0$, $i_0 - j_1$, $i_1 - j_0$, and $i_1 - j_1$ are four different links representing different combinations of a selection of i and j . Unlike in classic ant colony optimization in this algorithm, ants traverse all the attributes. Finally, we get a vector of 1 and 0 s of length equal to the number of attributes along with a list of attributes in order of traversal.

3 Proposed Methodology and Algorithm

3.1 Approach Taken by Kashef and Nezamabadi-Pour

Recently, Kashef and Nezamabadi-pour [15] employed an advanced version of binary ant colony optimization incorporating correlation between features. They had developed a binary algorithm and judiciously used four different heuristic methods in conjunction with the pheromone mediated search. In our method, we had used the following three methods with certain modifications:

Method 1. This method employs the idea of minimum redundancy. The correlation coefficient (r_{ij}) represents the dependency of feature i with the rest of the features. Let's assume, the coefficient between the features i and j is high, which means those features are highly similar. Hence, either of them is sufficient to give us the desired results. If either of the features is selected, the probability of selecting/deselecting the other is $(1 - r_{ij})$ which has a low/high value. In case, either of the features is deselected, then there is no need of selecting the other feature as they both are similar. The below equations will give a better idea.

$$\eta_{i0,j0} = |r_{ij}| \quad (2)$$

$$\eta_{i0,j1} = 1 - |r_{ij}| \quad (3)$$

$$\eta_{i1,j0} = |r_{ij}| \quad (4)$$

$$\eta_{i1,j1} = 1 - |r_{ij}| \quad (5)$$

Method 2. The idea of max-relevance and min-dependency has been employed here [17]. Feature selection using max-relevance is likely to be rich in redundancy as it selects features with the highest relevance to the target class. To subside this effect, the component of minimum redundancy is included. Here, cls_corr_j represents the correlation between the feature j and the class. Closer the value of cls_corr_j is to 1, higher is the importance of the feature. In this case, η is the geometric mean of max-relevance and min-redundancy.

$$\eta_{i0,j0} = \sqrt{(|1 - |\text{cls_corr}_j|)(|r_{ij}|)} \quad (6)$$

$$\eta_{i0,j1} = \sqrt{(|\text{cls_corr}_j|)(1 - |r_{ij}|)} \quad (7)$$

$$\eta_{i1,j0} = \sqrt{((1 - |\text{cls_corr}_j|)(|r_{ij}|))} \quad (8)$$

$$\eta_{i1,j1} = \sqrt{((|\text{cls_corr}_j|)(1 - |r_{ij}|))} \quad (9)$$

Method 3. This method uses correlation between features while selecting a feature and correlation between feature and target class while deselecting a feature.

$$\eta_{i0,j0} = 1 - |\text{cls_corr}_j| \quad (10)$$

$$\eta_{i0,j1} = |\text{cls_corr}_j| \quad (11)$$

$$\eta_{i1,j0} = 1 - |r_{ij}| \quad (12)$$

$$\eta_{i1,j1} = |r_{ij}| \quad (13)$$

3.2 Our Methodology

This selection describes our approach. In the earlier algorithm, Kashef and Nezamabadi-pour [15] used four different heuristics independently and evaluated their performance. In our modified and improved algorithm, we employ a consolidated algorithm with a probabilistic combination of the above mentioned three of their heuristics. While we employ Pearson's correlation as used by earlier authors, for relevance vector and class correlation, we employ Gini importance measure. The algorithm is explained in detail below.

In this proposed algorithm, a modified version of binary ant colony optimization algorithm is developed for feature selection. Similar to binary ant colony optimization, there is a connected graph where the nodes represent the features and the edges between them represent the choice of the next feature and every node is associated with a binary vector that helps in selection or deselection of the feature. The ant traverses through the search space to select the next feature with a combination of exploration and exploitation. Probability of selection of link is computed as the product of pheromone and feature importance score, while the probability of non-selection link is computed as a product of pheromone and [1—feature importance score]. The feature importance score is calculated using the above three different methods [15]. While we employ Pearson Correlation as used by earlier authors, for relevance vector and class correlation we employ Gini importance measure. Additionally, in our consolidated algorithm we have probabilistically used all the three methods with a probability $P_1, P_2, P_3 = (1 - [P_1 + P_2])$ as heuristic information. This way of probabilistic selection makes the algorithm more stochastic and allows the algorithm to cross sub-optimal local optima. An Exploration–Exploitation parameter is set during initialization depending on which method to choose the next node and state is decided.

Exploitation. In case of exploitation, the link with highest transition probability is chosen as the next move for the Ant.

Exploration. In the case of exploration, the links are chosen with a probability proportional to the transition probability of the connected links to the current feature. The transition probability is defined as:

$$P_{ij}^k(t) = \begin{cases} \frac{\tau_{ij}^\alpha \eta_{ij}^\beta}{\sum_l \tau_{il}^\alpha \eta_{il}^\beta} & \text{If } 1 \text{ and } j \text{ are admissible nodes} \\ 0 & \text{Otherwise} \end{cases} \quad (14)$$

All the ants follow the same procedure and at the end each ant has its own solution vector in binary form, where 1 means feature is selected and 0 means deselected. Performance of these selected subsets of feature set is evaluated based on performance measure. The performance measure of the subset of selected features of a given ant is a function of CV accuracy of the subset given by the equation. It can be noted that this function penalizes a subset with more attributes and rewards subsets with lesser number of features. The ant with the best measure is determined. Only the best ant is allowed to increase the pheromone of the links visited with a quantity proportional to the quality of the tour. Pheromone levels of all links are evaporated with a certain percentage. This process is repeated for a certain number of iterations. The global best ant (i.e., ant with maximum performance measure) is determined, and the corresponding feature subset is declared as the chosen subset. Figure 1 represents the schematic of the proposed algorithm.

Random Forest Classifier. We employed a robust random forest ensemble classifier for evaluating the accuracy of selected subset of features selected by software ants.

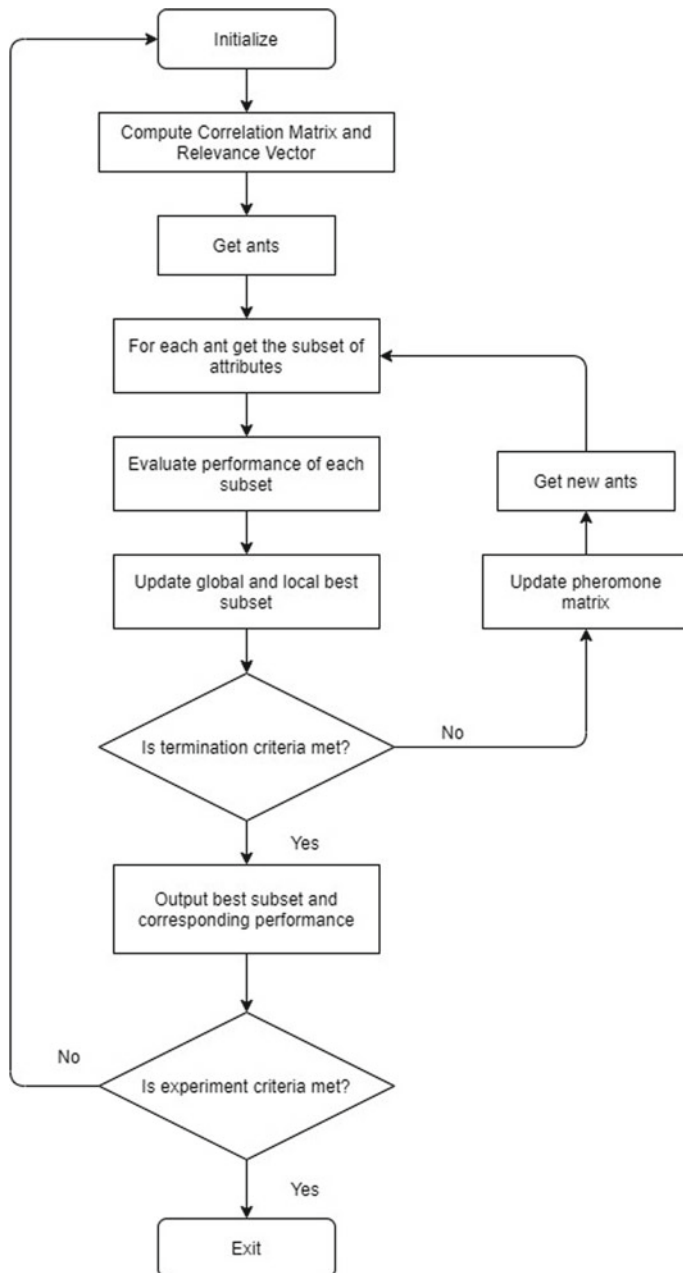


Fig. 1 Algorithm of the proposed method

Random forest (RF) is an ensemble of randomly constructed decision trees using bootstrap sampling technique. Randomness in RF is introduced in two ways: in the sample subset selected for growing trees and in choice of subset of attributes for node splitting. Once all the trees are grown, the performance measure of the ensemble is computed based on majority voting of individual tree measures. The algorithm has an embedded Gini importance feature ranking. We have used this measure as a relevance measure and class correlation measures in our heuristic information.

Performance Measure. The objective of employing feature selection is to get maximum classification accuracy with minimum number of features [9]. The objective function is defined as:

$$F(i) = \frac{\text{Accuracy}(i)}{1 + \lambda * n(i)} \quad (15)$$

where $F(i)$ is the performance measure of the i th ant, $\text{Accuracy}(i)$ is the fivefold cross-validation accuracy evaluated by Random Forest Classifier, classification accuracy, $n(i)$ is the length of selected features and λ is the weighing parameter. Increasing values of this parameters increasingly penalizes higher number of attributes.

Update of Pheromone Matrix. As the iterations for all ants are completed and the solution is determined, the pheromone values for the best ant are updated. At first, pheromone evaporation at all nodes is triggered. Then the ant with the best performance measure is rewarded with some amount of pheromone based on the classification accuracy. The rest of the ants will be punished by reducing their pheromone quantity. This will ensure increased probability of selecting the path with highest accuracy.

4 Experimental Studies and Results

To show effectiveness of the proposed methodology, the algorithm is applied on different datasets from different domains. For experimental studies, eight different datasets from different domain were taken. These datasets cover examples of different dimensions. The characteristics of these datasets are presented in following Table 1:

4.1 Parameter Setting

Different parameters involved in this work are number of ants, number of iterations, coefficient of pheromone evaporation (ρ), relative importance of pheromone (α), relative importance of visibility (β). Number of ants were set to 20, and number of iterations were set to 20. For each dataset, different values of the parameters α and β were tuned and optimum values were found in the range of (0.25, 1) and (0,

Table 1 Characteristics of datasets

Dataset	Number of classes	Number of features	Number of examples
Biodegradation	2	41	1055
Cardiotocography	3	21	2126
Dermatology	6	34	366
Wine	3	13	178
BreastEw	2	30	569
Heart	2	13	270
Ionosphere	2	33	351

1), respectively. The parameter λ is a weighting parameter and is varied as 0.001, 0.005, 0.01, 0.05. The parameter ρ was kept constant at 0.05. The probabilities for selection of method for calculating feature importance score were set as $P1 = P2 = P3 = 0.33$. The following table shows accuracy results of the experiments that were carried out (Tables 2 and 3).

Table 2 Accuracy results for different values of weighting parameter

Dataset	Mean accuracy			
	$\lambda = 0.001$	$\lambda = 0.005$	$\lambda = 0.01$	$\lambda = 0.05$
Biodegradation	86.20	85.48	85.17	84.53
Cardiotocography	88.41	87.70	86.50	84.80
Dermatology	98.20	96.40	96.70	95.20
Wine	99.20	98.20	98.20	95.20
BreastEw	96.52	96.27	96.42	93.43
Heart	84.78	84.02	83.56	82.40
Ionosphere	93.85	93.11	92.76	92.76

Table 3 Number of attributes selected for different values of weighting parameter

Dataset	Avg. attributes selected			
	$\lambda = 0.001$	$\lambda = 0.005$	$\lambda = 0.01$	$\lambda = 0.05$
Biodegradation	37.2	33.4	33.6	32.2
Cardiotocography	18.4	15.6	13.4	12.6
Dermatology	28.0	21.6	21.6	21.6
Wine	11.6	9.8	9.0	7.0
BreastEw	18.4	17.2	16.1	15
Heart	11.0	8.2	8.2	7.4
Ionosphere	24.0	23.4	23.0	23.2

To validate, these results are compared with the results from [17]. In the work [17], authors have combined binary ant colony optimization (BACO) with genetic algorithm (GA). This approach is called modified binary ant colony optimization with genetic algorithm (MBACO). Pheromone density model (PMBACO) and visibility density model (VMBACO) are two types of MBACO.

Pheromone density model (PMBACO). In this model, the effect of visibility density is ignored by setting $\beta = 0$. Relative importance for pheromone density is α which is set to 1. The solution obtained using GA is used for setting initial pheromone density. This is followed by the feature selection procedure using BACO and fittest ant replaces the solution obtained from GA, and GA is run again. In an alternate fashion, BACO and GA in turns run to reach termination criteria.

Visibility density model (VMBACO). In this model, effects of both pheromone density and visibility density are considered by setting $\alpha = 1$ and $\beta = 3$. Initial pheromone density is a random number ,and the solution of GA is used as visibility density. This is followed by the feature selection procedure using BACO, and fittest ant replaces the solution obtained from GA, and GA is run again. In an alternate fashion, BACO and GA in turns run to reach termination criteria. While a direct comparison is not possible due to different parameter settings, we can get an idea of the efficacy of our algorithm by looking at the earlier work.

We also compared our results with binary cuckoo search (bCS) [6], binary bat algorithm (bBA) [7], binary gravitational search algorithm (bGSA) [8], binary Whale optimization with simulated annealing (bWOASA) [9], and binary gray wolf optimization (bGWO)[10], binary binomial cuckoo search (bBCS) [11]. It can be seen that our results are quite good for all the datasets used in our simulations and comparable to earlier work. The results are represented in the following Tables 4 and 5.

5 Conclusion

Feature selection is very relevant and important in problems arising in the field of data science. In this paper, we have proposed a feature selection technique on the basis of the ant colony optimization algorithm using correlation and Gini importance synergistically as heuristic information. Performance of the proposed algorithm was evaluated using eight different datasets. These datasets are benchmark datasets in the different domains. As feature heuristic information is obtained using Random Forest Gini and Pearson's correlation, our algorithm can handle imbalanced dataset as well. The different parameters in the proposed algorithm were tuned, and their optimal values were found. Algorithm performance compares quite favorably with earlier developed algorithms. Detailed investigations on combination of various other available heuristics is an area of future research.

Table 4 Comparison of mean accuracy of selected subset of features

Dataset	Mean best accuracy of proposed method	PMBACO	VMBACO	bBCS	bWOASA	bCS	bGWO	bGSA	bBA
Biodegradation	86.20	76.82	78.22	—	—	—	—	—	—
Cardiotocography	88.41	85.64	86.24	—	—	—	—	—	—
Dermatology	98.20	94.64	95.16	—	—	—	—	—	—
Wine	99.20	98.70	99.10	99.21	93.65	93.25	97.89	97.54	85.08
BreastEw	96.52	—	—	10.52	97.23	95.42	97.05	92.89	93.81
Heart	84.78	—	—	5.05	80.04	81.24	77.02	77.91	86.85
Ionosphere	93.85	—	—	96.23	90.12	92.58	88.65	86.70	82.08

Table 5 Comparison of mean number of selected features

Dataset	Mean best accuracy of proposed method	PMBACO	VMBACO	bBCS	bWOASA	bCS	bGWO	bGSA	bBA
Biodegradation	37.2	9.70	7.85	—	—	—	—	—	—
Cardiotocography	18.4	5.30	4.40	—	—	—	—	—	—
Dermatology	28.0	11.30	10.45	—	—	—	—	—	—
Wine	11.6	5.30	5.15	5.82	5.85	5.25	8.95	6.48	4.78
BreastEw	18.4	—	—	10.52	13.46	15.25	15.61	14.93	11.77
Heart	11.0	—	—	5.05	5.31	7.25	6.61	6.85	5.35
Ionosphere	24.0	—	—	10.07	11.45	13.15	14.54	14.78	12.23

References

1. Liu H, Tu L (2004) Toward integrating feature selection algorithms for classification and clustering. *IEEE Trans Knowl Data Eng* 17(4):491–502
2. Beniwal S, Arora J (2012) Classification and feature selection techniques in data mining. *IJERT* 1(6)
3. Holland JH (1975) Adaptation in natural and artificial systems. University of Michigan Press, Ann Arbor
4. Dorigo M, Birattari M, Stutzle T (2006) Ant colony optimization. *IEEE Comput Intell Mag* 1:28–39
5. Eberhart R, Kennedy J (1995) A new optimizer using particle swarm theory. In: Proceedings of sixth international symposium micro machine human science, MHS 95, pp 39–43
6. Rodrigues D, Pereira LA, Almeida TN, Papa JP, Souza AN, Ramos CC, Yang XS (2013) BCS: a binary cuckoo search algorithm for feature selection. In: 2013 IEEE international symposium on circuits and systems (ISCAS). IEEE, pp 465–468
7. Rodrigues D, Pereira LA, Nakamura RY, Costa KA, Yang XS, Souza AN, Papa JP (2014) A wrapper approach for feature selection based on bat algorithm and optimum-path forest. *Exp Syst Appl* 41(5):2250–2258
8. Barani F, Mirhosseini M, Nezamabadi-Pour H (2017) Application of binary quantum-inspired gravitational search algorithm in feature subset selection. *Appl Intell* 47(2):304–318
9. Mafarja MM, Mirjalili S (2017) Hybrid whale optimization algorithm with simulated annealing for feature selection. *Neurocomputing* 18(260):302–312
10. Emary E, Zawbaa HM, Hassanien AE (2016) Binary grey wolf optimization approaches for feature selection. *Neurocomputing* 8(172):371–381
11. Pandey AC, Rajpoot DS, Saraswat M (2020) Feature selection method based on hybrid data transformation and binary binomial cuckoo search. *J Ambient Intel Human Comput* 11(2):719–738
12. Shekhawat SS, Sharma H, Kumar S, Nayyar A, Qureshi B (2021) bSSA: binary salp swarm algorithm with hybrid data transformation for feature selection. *IEEE Access*. <https://doi.org/10.1109/ACCESS.2021.3049547>
13. Kumar S, Sharma B, Sharma VK, Poonia RC (2018) Automated soil prediction using bag-of-features and chaotic spider monkey optimization algorithm. *Evol Intel* 1–12. <https://doi.org/10.1007/s12065-018-0186-9>
14. Kumar S, Sharma B, Sharma VK, Sharma H, Bansal JC (2018) Plant leaf disease identification using exponential spider monkey optimization. *Sustain Comput Inf Syst* 28. <https://doi.org/10.1016/j.suscom.2018.10.004>
15. Kashef S, Nezamabadi-pour H (2015) An advanced ACO algorithm for feature subset selection. *Neurocomputing* 147:271–279
16. Faramarzi A, Heidarinejad M, Stephens B, Mirjalili S (2020) Equilibrium optimizer: a novel optimization algorithm. *Knowl-Based Syst* 191:105190
17. Wan Y, Wang M, Ye Z, Lai X (2016) A feature selection method based on modified binary coded ant colony optimization algorithm. *Appl Soft Comput* 49:248–258

Automated Sleep Staging Using Convolution Neural Network Based on Single-Channel EEG Signal



Santosh Kumar Satapathy, S. Sharathkumar, and D. Loganathan

Abstract Sleep disorder diseases have one of the major health issues across the world. To handle this issue, the primary step taken by most of the sleep experts is the sleep staging classification. In this paper, we proposed an automated deep one-dimensional convolution neural network (1D-CNN) for multi-class sleep stages through polysomnographic signals. The proposed 1D-CNN model comprises eleven layers with learnable parameters: nine convolution layers and two-fully connected layers. The main objective of designing such a 1D-CNN model is to achieve higher classification accuracy for multiple sleep stage classifications with reduced learnable parameters. The proposed network architecture is tested on two different subgroups subject sleep recordings of ISRUC-Sleep datasets, namely ISRUC-Sleep subgroup-I (SG-I) and ISRUC-Sleep subgroup-III (SG-III). The proposed deep 1D-CNN model achieved the highest classification accuracy of 98.44, 99.03, 99.50, and 99.03% using the ISRUC-Sleep SG-I dataset and 98.51, 98.88, 98.76, and 98.67% using SG-III dataset for two to five sleep stage classification, respectively, with single channel of EEG signals. It has been observed that the obtained results from the proposed 1D-CNN model give the best classification accuracy performance on multiple sleep stage classifications incomparable to the existing literature works. The developed 1D-CNN deep learning architecture is ready for clinical usage with high PSG data.

Keywords Sleep stages analysis · Polysomnography signals · Convolution neural network · Deep learning

S. K. Satapathy (✉) · S. Sharathkumar · D. Loganathan
Department of CSE, Pondicherry Engineering College, Puducherry, India
e-mail: santosh.satapathy@pec.edu

S. Sharathkumar
e-mail: sharathkumar.s@pec.edu

D. Loganathan
e-mail: drloganathan@pec.edu

1 Introduction

Nowadays, it has been observed that the neurocognitive system directly decides the mental and cognitive performance in a particular task [1]. It's very difficult to determine the subjects neurocognitive performance (NCP) very accurately either numerically or any standard evaluation procedures. Currently, NCP is an open challenge in the medical domain concerning different diseases such as neurology disorder, rehabilitation, and psychology-related disorders. It's also very difficult to assess with a scenario of changes NCP with a known predictable manner. These types of diseases are more challenging concerning analysis and to get proper diagnosis solutions. Different sleep-related diseases are considered under these changes NCP cases since the brain-behavior changes according to different stages of sleep [1]. Sleep is one of the important ingredients for good human health and also responsible for maintaining the fitness and functioning of the different core systems of our body. It also puts an impact on our proper functioning of mental and cognitive systems.

For human life, a total of one-third of its duration is constituted of the sleep cycle. It has been observed from several studies that sleep deficiency causes so many consequences like inability to solve the problem, not able to make proper decisions, not controlling the emotions, and reflected several changes in people [2, 3]. Sometimes the improper quality of sleep influenced different types of sleep-related disorders such as sleep apnea, insomnia, depression, narcolepsy, hypersomnia, breathing-related disorders, and circadian rhythm disorders [4]. Sometimes it has been seen that sleep deprivation is considered as stress-related disorders or sleep pathology, which causes high risk in performing some common cognitive risks such as workplace incidents, road accidents happened [5]. According to a report of the National Highway Traffic Administration of USA, due to drowsiness, around one lakh car accidents happened, as consequences more than 1500 death cases resulted and injuries cases reported around 71,000 annually [6]. In this scenario, proper analysis of sleep stages is very important for identifying the sleep-related irregularities. So that it is very essential to analyze the sleep stage's behavior and accurate scoring of sleep states is a very crucial segment of the sleep staging process.

The polysomnography test is the primary step for any types of sleep-related disorders. It is a combination of a different physiological signal which is useful during analyzing the sleep patterns of an individual subject. Several polysomnographic recordings are included such as the electroencephalogram (EEG) signal, the electrooculogram (EOG) signal, and electromyogram (EMG) signals have tracked the changes in behavior muscle tone. The entire sleep staging process is generally conducted through visualizing the sleep patterns of the subject during sleep periods by well-trained sleep domain technicians according to the Rechtschaffen and Kales (R and K) [7] and the AASM sleep standards [8].

This traditional way of monitoring sleep stages methods has so many disadvantages such as requires more sleep experts to monitor the sleep recordings, time-consuming, and erroneous [9]. Due to more human interpretations during recording,

it may not report good classification accuracy in the diagnosis of sleep stage classification [10]. Based on the above-mentioned drawbacks, automated classification of sleep stages is introduced, which ultimately gives benefits for quick diagnosis and also reported with increases of high classification accuracy [11].

Sleep staging analysis and its scoring is a complicated procedure because of changes in sleep characteristics related to different sleep stages and also its non-stationary nature of the signal information.

2 Related Work

Most of the authors are proposed an automatic sleep stage classification system for identifying the sleep patterns and diagnosis of several types of sleep-related disorders [12–15]. In general sleep, staging procedures are conducted mainly on two strategies, one with single-channel input recording, and the other is multi-channel input recordings. In the first approach, only one channel is considered for extracting the informative features about the sleep characteristics of the subjects. There is a common approach taken by the different researchers during sleep staging as follows: (1) acquisitions of the signals, (2) signal pre-processing, (3) extraction of the properties, (4) feature reduction, and (5) classification [16]. The (3) feature extraction step is used for extracting the different characteristics parameter from preprocessed signal stage (2). These feature values can be extracted in frequency, time, time–frequency and nonlinear domains [17]. It has been seen that some of the ASSC system, one additional step used by authors that is feature reduction or dimensionality reduction stage. It is very helpful in screening the relevant features for the classification model. Currently, research on sleep staging plays an important role in NCP and human–machine interaction (HMI). There are several studies related to automated sleep staging using various physiological datasets and multimedia data, such as EEG, EMG, EOG, ECG, and audio, etc. One of the most popular contributions of sleep stage classification is the study of sleep behavior through human brain–computer interaction (BCI). We now look upon some of the recent contributions presented by different authors related to sleep staging using deep learning concepts.

2.1 *Polysomnography (PSG) Based Sleep Staging Using Deep Learning Approaches*

Nowadays, the researchers are majorly focused on deep learning techniques for sleep staging because of its robustness, scalability, and adaptability with related to handle large amounts of signal recordings and it's processing. Another important advantage related to deep learning models is no need to require any explicit features for

discriminating the subject's sleep behavior. In [18], the author used a deep convolution neural network for automated sleep staging with the input of single-channel EEG. The model achieved an overall accuracy of 74%. Sors et al. [19] presented automatic sleep stages scoring for five-sleep states based on one-channel of EEG using the CNN model, and the results reported for the proposed model are 87%. Chambon et al. [20] introduced a deep learning model with the concept of multi-variate signal analysis such as EEG, EOG, and EMG using KNN. The proposed model reached an overall accuracy of 80% with combinations of EEG + EOG + EMG. In [21] the authors obtained five-layer convolution layers for classifying the sleep stages based on two-channels of EEG and EOG signal and one-channel of EMG signal and achieved result for the model is 83%. Tripathy et al. [22] introduced a novel approach of sleep scoring based on coupling features of EEG data and RR time-series information using deep neural networks. The model resulted in an average accuracy of 95.71, 94.03, and 85.51% for the classification in between NREM versus REM, deep sleep versus light sleep, and sleep vs wake respectively. Cui et al. [23] proposed a sleep scoring system with input of 30 s multi-channel signal information based on CNN and fine-grained properties, the model reported an average accuracy of 92.2% with the ISRUUC-Sleep public dataset. Supra et al. [24] designed a system of sleep scoring through extracted time-invariant information using CNN and find sleep stages transition information from the bidirectional LSTM network. The reported classification accuracy performance reached to 86.2%. According to the existing contribution to sleep scoring, major challenges found that choosing the correct features which helps to distinguish the sleep stages. It has found that the maximum researchers extracted the time, frequency, and time-frequency features, then after finalizing the relevant features either manually or applied some conventional feature selection algorithm. In some cases, this selection algorithm increases the complexity factor and consumes more time. Another challenge related to feature selection is that some features are well fitted for some of the subjects but the same may not apply for another one. Sometimes this imbalance of sleep information may produce biased results with conventional machine learning algorithms.

Another limitation regarding selected features, some of the features well suitable for classification for some of the subject cases may be the same many not applicable for other categories of subjects. This may create a problem to achieve higher classification accuracy.

2.2 *Contribution*

The main contributions of our proposed research works are explained below:

1. We propose a 1D-CNN architecture for classifying multiple sleep classes based on multivariate signals using two different categories of subjects sleep recordings.

Table 1 Description of distribution of sleep stages

Subject category	Sleep states					Total epochs
	W	N1	N2	N3	REM (R)	
SG-I	1000	519	1215	589	427	3750
SG-III	791	648	1098	729	484	3750

2. The complete sleep staging process was analyzed with the input of single-channel EEG.
3. The proposed methodology uses fewer parameters for train the model and extracting the prominent features from the input signal data automatically, which supports achieving the high classification accuracy incomparable to the earlier contributions.

The remainder of the paper is organized as follows: Sect. 2 describes detailed on the proposed methodology including experimental data preparation, data preprocessing, feature extraction, and feature screening. Section 4 discusses the experimental results of the proposed methodology results. Section 5 presents the brief discussion about the proposed research work and makes result analysis with the state-of-the-art methods. Section 6 ends with concluding remarks with future work description.

3 Methodology

3.1 Experimental Data

In this paper, we used two different subgroups of sleep recordings, which were recorded during the sleep hours of the subjects under the direct supervision of the sleep experts of the Hospital of Coimbra University, Portugal. This dataset is called as ISRUC-Sleep dataset [25]. In the present work, two different categories (ISRUC-Sleep subgroup-I (SG-I) and ISRUC-Sleep subgroup-III (SG-III)) of the subjects considered for the purpose of experimental works, under SG-I, all the subjects were affected with the sleep diseases and SG-III, all the subjects were completely healthy category. The sleep epoch distributions among the different sleep stages are presented in Table 1.

3.2 Preprocessing

It has been better to remove the artifacts like muscle twitching, muscle movements, and eye blinks information for the better analysis the sleep behavior of the subjects. To

remove these irrelevant portions from the raw signal, we have applied a Butterworth bandpass filter with order 10 at the frequency ranges of 0.1–60 Hz.

3.3 CNN Model Architecture

The proposed 1D-CNN model comprises 20 layers: nine 1-D convolution layers (CONV-1 to CONV-9), nine max-pooling layers (Polling-1 to Polling-9), and one fully connected layer. Apart from these layers, the proposed model considered nine batch normalization and ReLU layers. The proposed 1D-CNN architecture is shown in Fig. 1.

The proposed network extracted hierarchical feature information automatically using a set of hidden layers. As we have mentioned earlier, the use of more FC layers may increase the computational overhead. Therefore in this research work, we have only considered one FC layer, and finally, the model resulted in a vector of size five corresponding to five different classes of sleep stages, and at last, a softmax activation function is applied in the FC layer to determine the final class label.

The main objective of designing such a custom model is to increase the classification accuracy compared to the preexisting trained model. The first convolution layer of the proposed model takes an input of preprocessed polysomnography signals of size 3000×1 sample points, and the first layer model convolves it with 16×8 filters and with four stride ratios to produce the resulting feature map of size 750×16 . The second layer of the proposed CNN model is the pooling layer; in this work, we have considered max-pooling techniques with filter size 2×2 and a stride 1 to produce a lower dimension size of output volume of size 375×16 . The BN layer and ReLU activation are applied over the output of each max-pooling layer of the models. Next, to the pooling layer, we have again applied the second convolution layer and it carried the previous convolution layer output information and convolves it with 32×3 kernel of size with two stride ratios; it provides the output volume of size 352×32 .

Finally, the output result of the convolution layer is fully connected to five neurons of a fully connected layer and applied softmax function to determine the probability distribution over each class label and finally, the output decided upon the neurons having the maximum probability score.

In this study, for model designing only three PSG signals and five sleep stages of the ISRUC-Sleep subgroup-I and subgroup-III dataset are used. Besides, both the subgroups datasets are split into 70% training data and 30% testing data.

4 Experiments and Results

The whole experiment was executed on the most popular and widely used ISRUC-Sleep subgroup-I and subgroup-III datasets. In this study, we have considered both

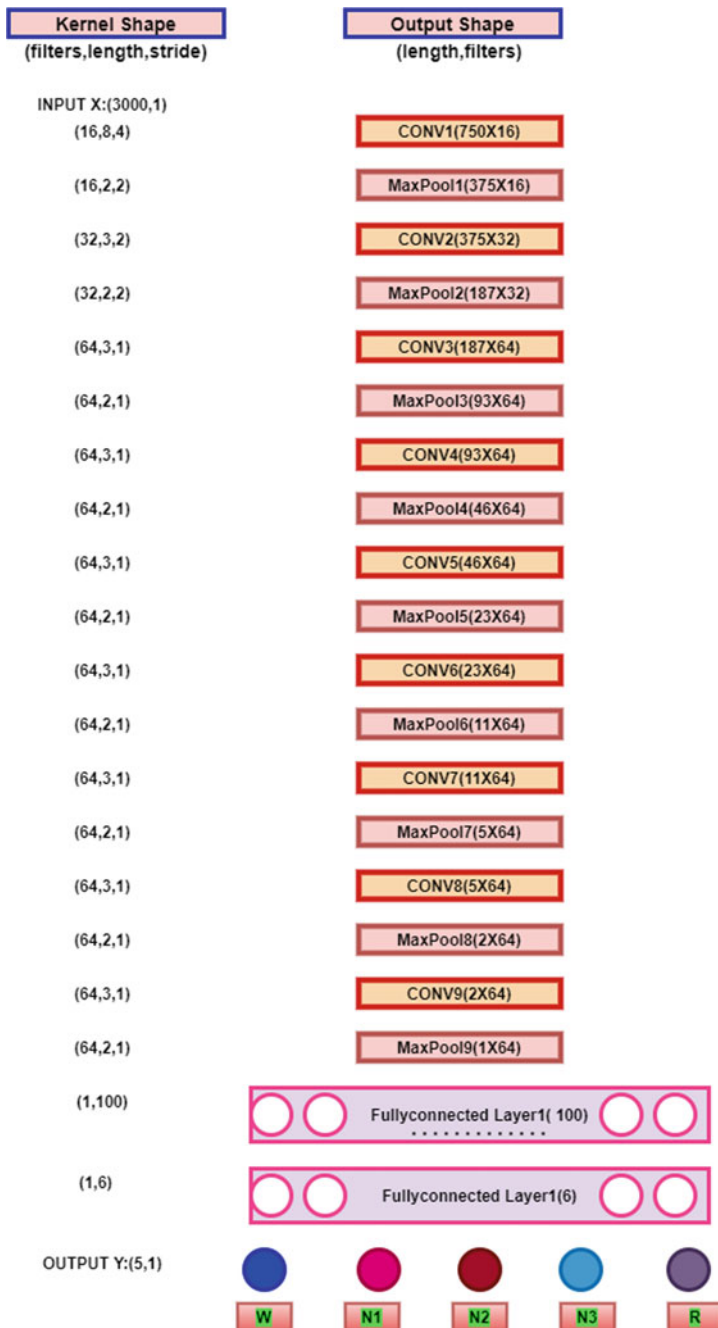


Fig. 1 Network architecture of the proposed one-dimensional convolution neural network for two-five sleep states classification task

Table 2 Hyperparameter values for the proposed model

Hyper parameter used	Value
Batch size	25
Number of epochs	100
Learning rate	0.0001
Optimizer	Adam

categories of subjects for sleep staging, (1) subjects affected with the sleep disorder and (2) healthy controlled subjects.

4.1 Experimental Setup

In this research study, we have considered EEG signals, and the collected EEG signals are segmented into a 30 s time frame. All the experiments of this proposed study executed using MATLAB software with system configuration Intel Xeon 2.4 Ghz CPU processor, 16 GB RAM, and used 4 GB GPU from NVIDIA Quadro K2200 platform running under Windows 10 operating system. The entire dataset was partitioned into training and testing parts. For training, we selected 70% recordings from the entire dataset, and the remaining 30% data were used for testing purposes.

The proposed 1D-CNN model recognizes the sleep behavior through learns high-level properties using several cyclic executions and to achieve consistent performance from the model, a set of hyperparameters are used during training and the detailed hyperparameter settings for this research work are described in Table 2. To evaluate the performance of the proposed 1D-CNN architecture, we considered confusion matrix outcome with subject to sleep scoring using multivariate signals. The confusion matrix four terms True Positive (TP), False Positive (FP), True Negative (TN), and False Negative (FN) are used for measuring the sensitivity [26], precision [27], F1 Score [28] and classification accuracy [29].

4.2 Results with the Input of ISRUC-Sleep Subgroup-I Dataset Using EEG Signal

In this experiment, we considered with single-channel C3-A2 of EEG signal recordings of five sleep-disordered subjects. For this experiment also, the ratio for training and testing is 70:30 with the same number of features are used. Table 3 presents the confusion-matrix generated from the training set and testing set for five-state sleep staging. The reported performance metrics results for the proposed methodology is presented in Table 4. The overall accuracy performance for two-five sleep states classification problems are presented in Table 5. The training and testing accuracy performance for 100 epoch iterations is shown in Figure 2.

Table 3 Confusion matrix of EEG for five state sleep staging

	W	N1	N2	N3	R
<i>C3-A2 channel/training samples (70%)</i>					
W	695	3	1	0	1
N1	5	305	3	0	4
N2	4	0	794	4	1
N3	1	0	5	408	0
R	1	0	10	0	380
<i>C3-A2 channel/testing samples (30%)</i>					
W	125	0	2	0	0
N1	1	193	5	0	0
N2	0	3	493	2	0
N3	0	1	3	194	0
R	0	0	1	0	102

Table 4 Reported results of the performance metrics

Classification problem	Sleep stages	Sensitivity (%)	Precision (%)	F1-Score (%)
Five class (training set)	Wake	99.29	98.44	98.86
	N1	96.21	99.03	97.60
	N2	98.88	99.50	99.19
	N3	98.55	99.03	98.79
	REM	97.19	98.45	97.81
Five class (Testing set)	Wake	98.43	99.21	98.81
	N1	96.98	97.97	97.47
	N2	99.00	99.60	99.30
	N3	97.98	98.98	98.48
	REM	99.03	99.05	99.51

The highest classification accuracy performance as 98.88% with training samples and 99.50% as testing samples.

The highest accuracy resulted for training set data as 98.88% and for testing set data as 99.50% for four sleep state classifications. Similarly, the performances of sensitivity, precision, and *F1*-score reported more than 96% for all the five sleep stages.

Results with the SG-III dataset

The experiment was conducted with the SG-III with same channel and the same training and testing samples. The same model layer parameters used with the previous dataset (SG-I dataset) were also applied for this dataset also (ISRUC-Sleep subgroup-III). The graphical representation of resulted accuracy from both training and testing

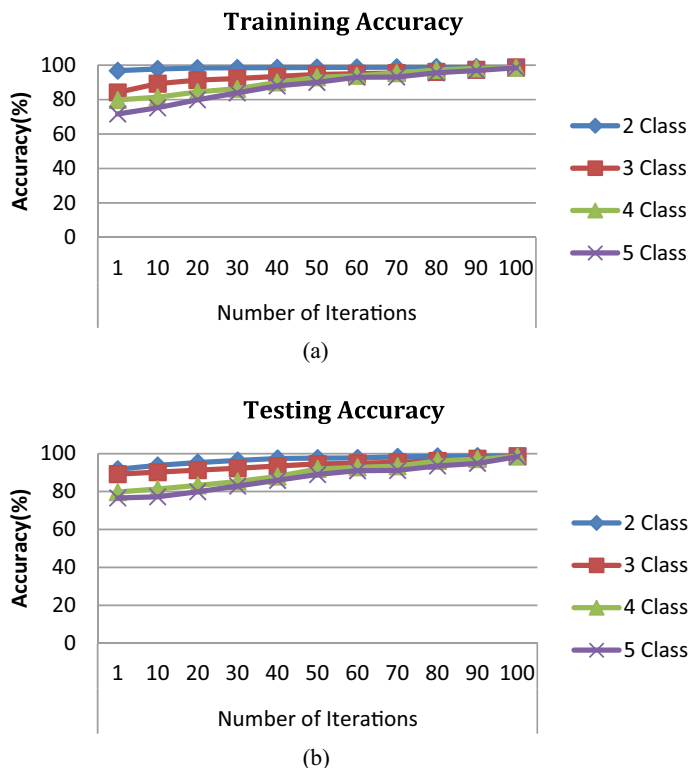


Fig. 2 Classification accuracy with the SG-I dataset: **a** training accuracy, **b** testing accuracy for the two-five sleep classes

Table 5 Reported results for two-five sleep class based on single-channel EEG using SG-I dataset

Model accuracy rate (%)		
Sleep classes	Training accuracy (%)	Testing accuracy (%)
Two	99.29	98.44
Three	96.21	99.03
Four	98.88	99.50
Five	98.55	99.03

data using single-channel EEG is shown in Fig. 3. The detailed accuracy results for two-five sleep states using SG-III dataset are given in Table 6.

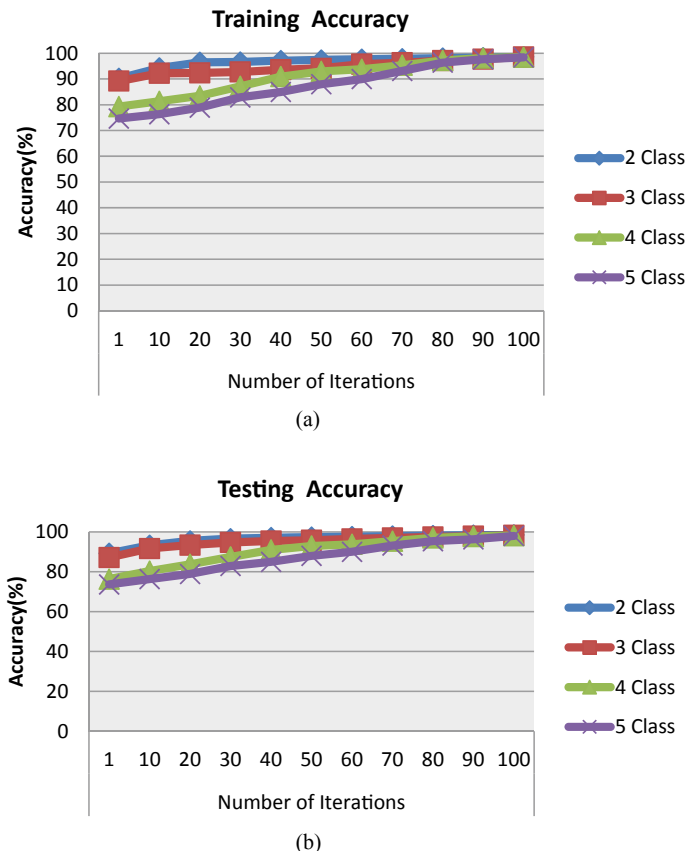


Fig. 3 Classification accuracy performance with SG-III data: **a** training accuracy, **b** testing accuracy for the two-five sleep classes

Table 6 Accuracy performances values for SG-III data

Model accuracy rate (%)		
Sleep classes	Training accuracy (%)	Testing accuracy (%)
Two	98.64	98.51
Three	98.61	98.31
Four	98.49	98.12
Five	98.4	97.96

Table 7 Accuracy performances values for ISRUC-Sleep subgroup-I/III data

Dataset	Input signals	Accuracy rate (%)			
		Sleep classes			
		Two class (%)	Three class (%)	Four class (%)	Five class (%)
SG-I	Single-channel EEG_Subgroup-I	98.44	99.03	99.50	99.03
SG-II	Single-channel EEG_Subgroup-III	98.51	98.31	98.12	97.96

4.3 Summary of Experimental Results

In the current research work, we have conducted sleep staging studies considering two subgroups of sleep recordings (Subgroup-I/Subgroup-III) of the Sleep-ISRUC dataset. For all the individual experiments, we used only the proposed 1D-CNN model and with the same training and testing dataset size (70:30). The proposed model is effective with subjects to sleep scoring without any manual feature extraction or feature screening. The reported summary results obtained from both the datasets with the input of single-channel EEG using the proposed 1D-CNN model presents in Table 7.

5 Discussion

Many similar research works have been conducted by different researchers on multiple sleep staging using different methodologies through machine learning techniques. Till now very few of the studies were conducted based on the 1D-CNN model with deep learning techniques. The proposed 1D-CNN architecture can automatically be learning high-level features from the input signals directly. The obtained results indicate that the proposed scheme achieved improved sleep stages classification accuracy compared to earlier similar contributed works using the deep learning (DL) approach. Table 8 presents the performance comparison results between the proposed methodology and the existing similar multiple sleep staging studies using different deep learning techniques. It has been found that the proposed framework achieved higher classification accuracies in comparison to the other state art of the contributions. The proposed 1D-CNN model results indicated that the model is performed excellently concerning two-five sleep stages classifications incomparable to the existing literature works. It has been seen that several similar works are completely based on handcrafted features and shallow classifiers. From this point, the proposed model completely differs from the rest of the work and provides good potential for sleep staging analysis. Despite the improved performance on classification accuracy, the proposed model reported some more advantages related to

Table 8 Performance comparisons in between the proposed sleep study and the existing state-of-the-art works

Study	Dataset	Number of channels/signals	Method	Accuracy Rates (%)			
				CT = 2	CT = 3	CT = 4	CT = 5
[18]	Sleep-EDF	1EEG	CNN	—	—	—	75%
[30]	Sleep-EDF	1EEG	1D-CNN	97.85%	94.23%	92.24%	90.48%
		1EOG	1D-CNN	98.06%	93.76%	91.88%	89.77%
		1EEG + 1EOG	1D-CNN	98.06%	93.76%	91.88%	89.77%
[31]	Sleep-EDF	1EEG	CNN + BLSTM	—	—	—	82%
[19]	SHHS-1	1EEG		—	—	—	87%
[32]	Sleep-EDF expanded	1EEG	CNN	—	—	—	91.97%
		2EEG		—	—	—	92.66%
		Ensemble		—	—	—	92.65%
[33]	Sleep-EDF	1EEG	PSD + CNN	—	89.8%	83.3%	—
[34]	Bonn Univ	1EEG	DL + LSTM	71.38%	—	—	—
[35]	ISRUC-Sleep	1EEG	DL + CNN	—	—	—	92.2%
[36]	Sleep-EDF	1EEG	DL + RNN + LSTM	—	—	—	86.7%
[37]	Sleep-EDF	1EEG	CNN	—	—	—	85.62%
[38]	ISRUC (Subgroup-I)	1EEG + 1EOG + 1EMG	Meta-learning + Transfer learning + CNN	—	—	—	68.74%
		1EEG + 1 EOG + 1EMG		—	—	—	73.89%
[39]	Sleep-EDF	1EEG	CNN	98.10%	96.86%	93.11%	92.95%
[40]	Sleep-EDF	1EEG	DNN	—	—	—	83.6%
Proposed	ISRUC-sleep subgroup-I	1EEG	1D-CNN	98.44%	99.03%	99.50%	99.03%
	ISRUC-sleep subgroup-III	1EEG	1D-CNN	98.51%	98.31%	98.12%	97.96%

the other works: (i) The proposed 1D-CNN model eliminates the traditional techniques for classification using multi-stage pipeline architecture, which creates a lot of complexity during execution and arises a lot of errors. (ii) The proposed model learned the features automatically from the polysomnography signals during the model training; therefore, it does not require any types of handcrafted features; (iii) the proposed model used less number of learnable parameters for training model incomparable to the existing some of the pre-trained DL models, (iv) with the same hyperparameter values, the sleep staging performance is significantly improved for two-five sleep states classification using both the subgroups of a dataset and

(v) the proposed architecture obtains higher classification accuracy performance in comparisons with the existing state-of-the-art works.

6 Conclusion

In this paper, we proposed a 1D-CNN model for automated sleep stage classification using polysomnography signals. The proposed architecture contains nine learnable layers, which helps to learn the features automatically from the single-channel EEG signals. The main objective of designing such architecture is to improve the classification accuracy results with better learnable parameters compared to the traditional shallow learning models. The proposed 1D-CNN architecture achieved the highest classification accuracy of 98.44, 99.07, 99.50, and 99.03% using the SG-I dataset; similarly, the same model reported accuracy using the SG-III dataset of 98.51, 98.88, 98.76, and 98.67% with single-channel EEG signals for two-five sleep stages classification. The proposed model not required any types of handcrafted features and shallow learning classification models for the classification of polysomnography signals, and it can assist clinicians during the sleep scoring. In future, we will collect the biomedical signals data from different medical institutes and test the efficiency of the model. Further, we also focus on several tasks which ranging from classification task to biomedical signal analysis. Furthermore, the proposed work to be extended for different types of sleep related diseases. We will also include the data augmentation techniques to overcome the data imbalance issues. Finally, it has been observed that the proposed framework improves the existing state of the art and achieves better classification results for the two-five sleep classification tasks. The proposed fully automated sleep staging classification systems could replace the traditional error-prone classification models.

References

1. Heyat MBB, Lai D, Khan FI, Zhang Y (2019) Sleep bruxism detection using decision tree method by the combination of C4-P4 and C4-A1 channels of scalp EEG. *IEEE Access* 7:102542–102553. <https://doi.org/10.1109/ACCESS.2019.2928020>
2. Chung MH, Kuo TB, Hsu N, Chu H, Chou KR, Yang CC (2009) Sleep and autonomic nervous system changes—enhanced cardiac sympathetic modulations during sleep in permanent night shift nurses. *Scand J Work Environ Health* 35(3):180–187. <https://doi.org/10.5271/sjweh.1324>
3. Aboalayon K, Faezipour M, Almuhammadi W, Moslehpoor S (2016) Sleep stage classification using EEG signal analysis: a comprehensive survey and new investigation. *Entropy* 18(9):272. <https://doi.org/10.3390/e18090272>
4. Reynolds CF, O’Hara R (2013) DSM-5 sleep-wake disorders classification: overview for use in clinical practice. *Am J Psychiatry* 170(10):1099–1101. <https://doi.org/10.1176/appi.ajp.2013.13010058>
5. Goel N, Rao H, Durmer J, Dinges D (2009) Neurocognitive consequences of sleep deprivation. *Semin Neurol* 29(04):320–339. <https://doi.org/10.1055/s-0029-1237117>

6. Garcés Correa A, Orosco L, Laciar E (2014) Automatic detection of drowsiness in EEG records based on multimodal analysis. *Med Eng Phys* 36(2):244–249. <https://doi.org/10.1016/j.medengphy.2013.07.011>
7. Kogure T, Shirakawa S, Shimokawa M, Hosokawa Y (2011) Automatic sleep/wake scoring from body motion in bed: validation of a newly developed sensor placed under a mattress. *J Physiol Anthropol* 30(3):103–109. <https://doi.org/10.2114/jpa2.30.103>
8. Rosenberg RS, Van Hout S (2013) The american academy of sleep medicine inter-scorer reliability program: sleep stage scoring. *J Clin Sleep Med* 9(1):81–87. <https://doi.org/10.5664/jcsm.2350>
9. Boashash B, Ouelha S (2016) Automatic signal abnormality detection using time-frequency features and machine learning: a newborn EEG seizure case study. *Knowl-Based Syst* 106:38–50. <https://doi.org/10.1016/j.knosys.2016.05.027>
10. Penzel T, Conradt R (2000) Computer based sleep recording and analysis. *Sleep Med Rev* 4(2):131–148. <https://doi.org/10.1053/smrv.1999.0087> PMID: 12531163
11. Li Y, Luo M-L, Li K (2016) A multiwavelet-based time-varying model identification approach for time-frequency analysis of EEG signals. *Neurocomputing* 193:106–114. <https://doi.org/10.1016/j.neucom.2016.01.062>
12. Holland JV, Dement WC, Raynal DM (1974) Polysomnography: a response to a need for improved communication. Presented at the 14th Annual Meeting Association Psychophysiology Study Sleep. [Online]
13. Acharya UR, Bhat S, Faust O, Adeli H, Chua EC-P, Lim WJE, Koh JEW (2015) Nonlinear dynamics measures for automated EEG-based sleep stage detection. *Eur Neurol* 74(5–6):268–287. <https://doi.org/10.1159/000441975>
14. Acharya UR, Oh SL, Hagiwara Y, Tan JH, Adeli H (2018) Deep convolutional neural network for the automated detection and diagnosis of seizure using EEG signals. *Comput Biol Med* 100:270–278. <https://doi.org/10.1016/j.combiomed.2017.09.017>
15. Acharya UR, Oh SL, Hagiwara Y, Tan JH, Adeli H, Subha DP (2018) Automated EEG-based screening of depression using deep convolutional neural network. *Comput Methods Prog Biomed* 161:103–113. <https://doi.org/10.1016/j.cmpb.2018.04.012>
16. Acharya UR, Vinitha Sree S, Swapna G, Martis RJ, Suri JS (2013) Automated EEG analysis of epilepsy: a review. *Knowl Based Syst* 45:147–165. <https://doi.org/10.1016/j.knosys.2013.02.014>
17. Ahmadlou M, Adeli H, Adeli A (2011) Fractality and a wavelet-chaos-methodology for EEG-based diagnosis of Alzheimer disease. *Alzheimer Dis Assoc Disord* 25(1):85–92. <https://doi.org/10.1097/WAD.0b013e3181ed1160>
18. Tsinalis O, Matthews PM, Guo Y, Zafeiriou S (2016) Automatic sleep stage scoring with single-channel eeg using convolutional neural networks; arXiv preprint [arXiv:1610.01683](https://arxiv.org/abs/1610.01683)
19. Sors A, Bonnet S, Mirek S, Vercueil L, Payen J-F (2018) A convolutional neural network for sleep stage scoring from raw single-channel eeg. *Biomed Signal Process Control* 42:107–114. <https://doi.org/10.1016/j.bspc.2017.12.001>
20. Chambon S, Galtier MN, Arnal PJ, Wainrib G, Gramfort A (2018) A deep learning architecture for temporal sleep stage classification using multivariate and multimodal time series. *IEEE Trans Neural Syst Rehabil Eng* 26(4):758–769. <https://doi.org/10.1109/TNSRE.2018.2813138>
21. Fernández-Varela I, Hernández-Pereira E, Moret-Bonillo V (2018) A convolutional network for the classification of sleep stages. *Proceedings* 2(18):1174. <https://doi.org/10.3390/proceedings2181174>
22. Tripathy RK, Rajendra Acharya U (2018) Use of features from RR-time series and EEG signals for automated classification of sleep stages in deep neural network framework. *Biocybern Biomed Eng*. <https://doi.org/10.1016/j.bbe.2018.05.005>
23. Cui Z, Zheng X, Shao X, Cui L (2018) Automatic sleep stage classification based on convolutional neural network and finegrained segments. *Hindawi Complex* 9248410. <https://doi.org/10.1155/2018/9248410>
24. Supratak A, Dong H, Wu C, Guo Y (2017) DeepSleepNet: a model for automatic sleep stage scoring based on raw single-channel EEG. *IEEE Trans Neural Syst Rehabil Eng* 25(11):1998–2008. <https://doi.org/10.1109/TNSRE.2017.2721116>

25. Khalighi S, Sousa T, Santos JM, Nunes U (2016) (2016) ISRUC-Sleep: a comprehensive public dataset for sleep researchers. *Comput Methods Programs Biomed* 124:180–192. <https://doi.org/10.1016/j.cmpb.2015.10.013>
26. Bajaj V, Pachori RB (2013) Automatic classification of sleep stages based on the time-frequency image of EEG signals. *Comput Methods Programs Biomed* 112(3):320–328. <https://doi.org/10.1016/j.cmpb.2013.07.006>
27. Yıldız A, Akin M, Poyraz M, Kirbas G (2009) Application of adaptive neuro-fuzzy inference system for vigilance level estimation by using wavelet-entropy feature extraction. *Expert Syst Appl* 36:7390–7399. <https://doi.org/10.1016/j.eswa.2008.09.003>
28. Sanders TH, McCurry M, Clements MA (2014) Sleep stage classification with cross frequency coupling. *Annu Int Conf IEEE Eng Med Biol Soc* 2014:4579–4582. <https://doi.org/10.1109/EMBC.2014.6944643>
29. Powers D, Ailab (2011) Evaluation: from precision, recall and F-measure to ROC, informedness, markedness and correlation. *J Mach Learn Technol* 2:2229–3981. <https://doi.org/10.9735/2229-3981>
30. Yıldırım O, Baloglu U, Acharya U (2019) A deep learning model for automated sleep stages classification using PSG signals. *Int J Environ Res Public Health* 16(4):599. <https://doi.org/10.3390/ijerph16040599>
31. Fernandez-Blanco E, Rivero D, Pazos A (2019) Convolutional neural networks for sleep stage scoring on a two-channel EEG signal. *Soft Comput*. <https://doi.org/10.1007/s00500-019-04174-1>
32. Ieracitano C, Mammone N, Bramanti A, Hussain A, Morabito F (2018) A convolutional neural network approach for classification of Dementia stages based on 2D-spectral representation of EEG recordings. *Neurocomputing* 323. <https://doi.org/10.1016/j.neucom.2018.09.071>
33. Nagabushanam P, Thomas George S, Radha S (2019) EEG signal classification using LSTM and improved neural network algorithms. *Soft Comput*. <https://doi.org/10.1007/s00500-019-04515-0>
34. Michielli N, Acharya UR, Molinari F (2019) Cascaded LSTM recurrent neural network for automated sleep stage classification using single-channel EEG signals. *Comput Biol Med* 106:71–81. <https://doi.org/10.1016/j.compbioemed.2019.01.013>
35. Li X, La R, Wang Y, Niu J, Zeng S, Sun S, Zhu J (2019) EEG-based mild depression recognition using convolutional neural network. *Med Biol Eng Comput*. <https://doi.org/10.1007/s11517-019-01959-2>
36. Banluesombatkul N, Ouppaphan P, Leelaarporn P, Lakan P, Chaitusaney B, Jaimchariyatam N, Chuangsawanich E, Chen W, Phan H, Dilokthanakul N, Wilairasitporn T (2020) MetaSleepLearner: a pilot study on fast adaptation of bio-signals-based sleep stage classifier to new individual subject using meta-learning
37. Mousavi Z, Yousefi Rezaii T, Sheykhanvand S, Farzamnia A, Razavi SN (2019) Deep convolutional neural network for classification of sleep stages from single-channel EEG signals. *J Neurosci Methods* 108312. <https://doi.org/10.1016/j.jneumeth.2019.108312>
38. Zhang X, Xu M, Li Y, Su M, Xu Z, Wang C, et al, (2020) Automated multi-model deep neural network for sleep stage scoring with unfiltered clinical data. *Sleep Breath*. <https://doi.org/10.1007/s11325-019-02008-w>
39. Nakamura T, Adjei T, Alqurashi Y, Looney D, Morrell MJ, Mandic DP (2017) Complexity science for sleep stage classification from EEG. In: 2017 international joint conference on neural networks (IJCNN). <https://doi.org/10.1109/ijcnn.2017.796641>
40. Hassan AR, Bhuiyan MIH (2017) Automated identification of sleep states from EEG signals by means of ensemble empirical mode decomposition and random under sampling boosting. *Comput Methods Programs Biomed* 140:201–210. <https://doi.org/10.1016/j.cmpb.2016.12.015>

Spark-Based FP-Growth Algorithm for Generating Association Rules from Big Data



D. K. Chandrashekhar, K. C. Srikantaiah, and K. R. Venugopal

Abstract Data mining is used to discover Business Intelligence Rules from large transactional database, frequent itemset mining and association rule mining are data mining techniques which are utilized for real-world applications using apriori algorithm as well as FP-Growth algorithm. To extract frequent itemset and association rules from the grocery store using traditional apriori algorithm takes time because it generates candidate key for each item in the dataset, whereas in FP-Tree without generating any candidate key it finds frequent items and association rules for the grocery dataset by constructing FP-Tree, and it is time consuming. To overcome this problem, we propose a method called MapReduce-based FP-Tree algorithm which generates frequent patterns and association rules by using parallel computations to reduce computational time. The experimental results show that time taken for generating frequent patterns and association rules for the grocery dataset is less.

Keywords Association rules · Big data · Data analytics · FP-growth · Frequent patterns · Hadoop · Map reduce

1 Introduction

Data is a fact, being computed, accumulated and described using graphs, images or by any other tools. And data can be of different types, namely text, numbers, and multimedia. In this digital world, the terabytes of data are generated per second. In day-to-day activities, huge amounts of data are generated, and as a result the volume of data is increasing dramatically, managing this huge amount of data has become a tedious work for the organizations, and it can be fulfilled by using big data management techniques. Mining information from this explosive growth of data has become one of the major challenges for data management and mining communities. Future trends and behaviors are estimated by data mining techniques

D. K. Chandrashekhar (✉) · K. C. Srikantaiah

Department of CSE, SJB Institute of Technology, Bengaluru, Karnataka 560060, India

K. R. Venugopal

Bangalore University, Bengaluru, Karnataka 560056, India

for allowing businesses to improve the practical knowledge and take good decisions. Finding frequent patterns and association rules in huge dataset is most important and expensive from past couple of years. There are many data mining algorithms to generate frequent itemset and association rules such as apriori and FP-Tree [1, 2]. Apriori algorithm generates a frequent itemset by grouping the itemset in single, pair and triplets, and also generates candidate key for all itemset in the given dataset. It generates an itemset in that some of the itemset may not be infrequent, and generating all those itemset is a complex thing. Because of these, the apriori takes more time to generate frequent itemset and association rules.

Big data is a term used for accumulation of huge and complex datasets, which is hard to reserve and process using available database management tools. And there are many challenges to handle the big data such as capturing, storing, searching, sharing, transferring, analyzing and visualization of data. The big data is described in Four V's, i.e., **Volume** which refers to the size of dataset might be greater than terabytes ad petabytes of data, **Velocity** refers to the speed of which data is generated and processed, **Variety** refers to the different types of data such as structured, unstructured and semi-structured, **Veracity** refers to the quality and trustworthiness of data.

The rest of the sections of this paper is as follows: Sect. 2 represents the detail study of related works, background study is discussed in Sect. 3, Sect. 4 defines the problem definition and Sect. 5 describes MapReduce FP-Growth, Sect. 6 discusses experimental details, and Sect. 7 concludes the paper.

2 Literature Survey

Zhang et al. [1] proposed an improved existing apriori algorithm, now it is called FP-Growth algorithm. This algorithm will overcome the problem of the two neck-bottle problems. The major reason to extend this apriori algorithm is to improve the mining efficiency in the given time and also the efficient usage of the memory and CPU utilization when comparison with the apriori, FP-Growth algorithm works better than previous apriori. Mansouri et al. [2] proposed an horizontal parallel-apriori algorithm to minimize the period of execution time during mining of frequent patterns. Mining data using single-node cluster is not possible since big data has huge complexity and scalability, and this problem is solved by using this HP-apriori algorithm. Lin et al. [3] proposed the improvised version of frequent pattern growth to find frequent itemsets. Improvised FP-Growth algorithm is better than normal FP-Growth algorithm in large dataset. FP-Growth algorithm has the main problem in time and space complexity as it adopts tree structure for storing information in longer run time. Rattanaopas et al. [4] designed frequently mined and maximum periodic patterns. The challenging task for much huge unstructured, raw and dynamic information extracted from various web server. Commonly big data requires two obtained more

essential information from this huge databases or different streams data. Many algorithms which are frequently used are more specific in calculating more important results, though it is much difficult applying on big data fields. UDDAG, SNTR like structure and formula which is expandable thus reduced in runtime comparing many steamers like DBSCAN and ECLAT. Agrawal et al. [5] proposed Apriori and Apriori Tid—these two algorithms are used to find all similar association rules in a transaction of large database. The problem is finding the association rules of itemsets in a large database. For solving this problem, two new algorithms are used, i.e., Apriori and Apriori Tid—these two algorithms are used to find all similar association rules in a transaction of large database.

Yu et al. [6] developed the enhancing performance of the MapReduce task by ignoring the network traffic generated at shuffling phase. MapReduce is programming model that simplifies the large amount of data by parallel processing tasks. Gao et al. [7] proposed a frequent pattern mining method for traffic prediction with spatiotemporal mode called frequent pattern mining matching. The data that are selected from the base stations are validated with different distribution and coefficients. The data are classified into test and training sets. Grahne et al. [8] proposed mining frequent itemset which is difficult for mining association rules. The author implemented using a pre-tree structure known as FP-Tree. To implement a FP-Tree, the author presented a technique called novel FP-Array.

3 Background

FP-Growth algorithm is best algorithm when compared with the apriori algorithm to generate frequent itemset and association rules. Apriori algorithm generates a candidate itemset in that some of the itemsets may be infrequent generating a frequent itemset in FP-Tree for every item; it consumes more execution time and high computational cost. To overcome this, the new MapReduce-based FP-Growth algorithm is proposed to generate frequent items and association rule by doing parallel computing. Finally, the generated association rules are stored in cloud for security purpose.

4 Problem Definition

Consider a log file ‘D’ of transactions and activities of Grocery store, and it is processed to extract required attributes, i.e., (I₁, I₂ ... I_n), where, I₁, I₂ I_n are required items for analysis. The objective of this work is to minimize the execution time and for generating frequent itemset and association rules using MapReduce-based FP-Growth algorithm in cloud-based big data environment.

5 MapReduce-Based FP-Growth

Phase-1: Parallelizing the Process of Finding Frequent Itemsets

Consider the dataset with 8 transactions T1...T8, with minimum support value $\text{min_sup} = 20\%$. The candidate extractor C1 extracts the each distinct item and gives the support count of each item, i.e., I1, I2, I3, I4, I5 as (2, 3, 5, 5, 6) from the dataset. All these distinct items are sorted in descending order to build FP-Tree. To construct FP-Tree, it creates a root node represented by null and consider the next transaction itemset count which is in descending order, any of the itemset of this transaction already present in any another branch in the tree which shares the common path or creates new path to reach the root. When item support count is increased, the normal node and new node count are also increased by 1 till the completion of all the transactions. Finally, the conditional FP-Tree is designed by counting each item in the path. In this example, the 4 items are selected such as I1, I2, I3, and I4 so parallelly 4 mappers are created. The mapper-1 finds the path from root node to reach item I1, if it has multiple paths to reach item I1 it considers all the paths and finds the support count of normal node to reach item I1. The support count of conditional FP-Tree for Item I1 is (I5:1, I4:1, I2:1), and set the path is I5 → I4 → I1 and new path I2 → I1 (Fig. 1).

The mapper-2 finds the path from root node to reach item I2, if it has multiple paths to reach item I2 it considers all the paths and finds the support count of normal node to reach item I2. The support count of conditional FP-Tree for Item I2 is (I5:2, I4:2), and set the path is I5 → I4 → I2 and other path is I5 → I4 → I3 → I2. The mapper-3 finds the path from root node to reach item I3. The support count of

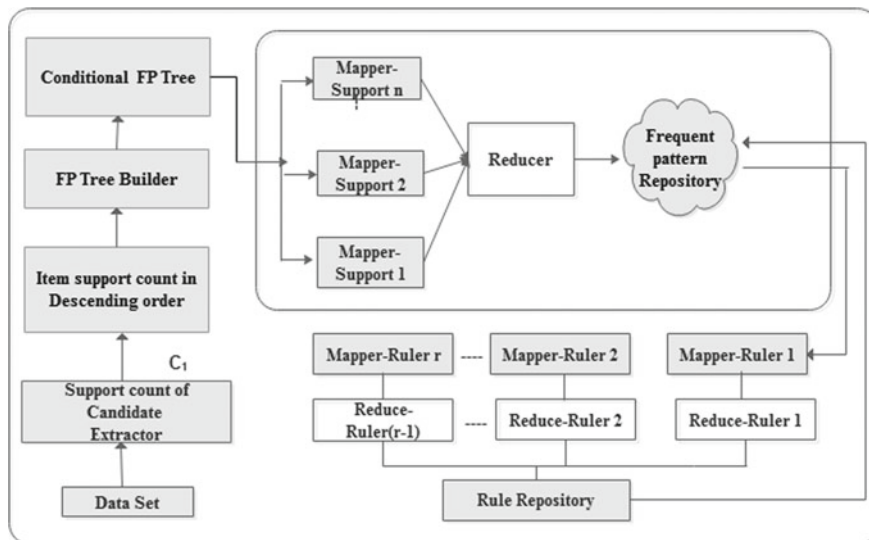


Fig. 1 Execution flow of an MR-FP

conditional FP-Tree for Item I3 is (I5:4, I4:2, I4:1) and set the path is $I5 \rightarrow I4 \rightarrow I3$, and new paths are $I5 \rightarrow I3$, $I4 \rightarrow I3$. The mapper-4 finds the path from root node to reach item I4. The all 4 mappers are working by doing parallel computation. Next, reducer receives each item support count and compares with minimum support count value. The support count of all the nodes to reach I1 is less than the minimum support value, i.e., (I5:1, I4:1, I2:1) so item I1 is not frequent. The support count of all the nodes to reach I2 is greater than or equal to minimum support value, i.e., (I5:2, I4:2) so item I2 is frequent, the generated frequent pattern is {I2, I4, I5:2}. So item I3 is frequent, and the generated frequent pattern is {I3, I4, I5:2}. The support count of all the nodes to reach I4 is greater than or equal to minimum support value, i.e., (I5:4) so item I4 is frequent, the generated frequent pattern is {I4, I5:4}.

Phase-2: Parallelizing the Process of Finding Association Rules

The association rules are generated by considering frequent itemset in larger to smaller order from the set L of frequent itemsets generated in phase-1, with threshold minimum confidence $\text{min_conf} = 60\%$, i.e., consider the largest frequent itemset {I2, I4, I5} in L, and generates all its subsets (except nullset and proper subset), i.e., $\{\{I2\}, \{I4\}, \{I5\}, \{I2, I4\}, \{I2, I5\}, \{I4, I5\}\}$. In our approach, we paralyze this process by using many mapper-ruler functions (as many as subsets). Mapper-ruler-1 takes the subset {I2} and computes the confidence using the equation 5 of the association rule $I2 \rightarrow \{I4, I5\}$, Mapper-ruler-2 takes the subset {I4} and computes the confidence of the association rule $I4 \rightarrow \{I2, I5\}$, and Mapper-ruler-3 takes the subset {I5} and computes the confidence of the association rule $I5 \rightarrow \{I2, I4\}$. This procedure is applied for all frequent items except frequent-1 itemsets in L to generate all possible rules shown in Table 1.

Table 1 All possible generated rules with confidence value

Frequent itemsets	Rule generated	Assigned to which mapper ruler	Confidence (in %)
<i>Subset of {I2, I4, I5}</i>			
{I2}	$I2 \rightarrow \{I4, I5\}$	Mapper-ruler-1	66.6
{I4}	$I4 \rightarrow \{I2, I5\}$	Mapper-ruler-2	40
{I5}	$I5 \rightarrow \{I2, I4\}$	Mapper-ruler-3	33.3
{I2, I4}	$\{I2, I4\} \rightarrow I5$	Mapper-ruler-4	100
{I2, I5}	$\{I2, I5\} \rightarrow I4$	Mapper-ruler-5	100
{I4, I5}	$\{I4, I5\} \rightarrow I2$	Mapper-ruler-6	50
<i>Subset of {I3, I4, I5}</i>			
{I3}	$I3 \rightarrow \{I4, I5\}$	Mapper-ruler-7	40
{I4}	$I4 \rightarrow \{I3, I5\}$	Mapper-ruler-8	40
{I5}	$I5 \rightarrow \{I3, I4\}$	Mapper-ruler-9	33.3
{I3, I4}	$\{I3, I4\} \rightarrow I5$	Mapper-ruler-10	66.6
{I3, I5}	$\{I3, I5\} \rightarrow I4$	Mapper-ruler-11	50
{I4, I5}	$\{I4, I5\} \rightarrow I3$	Mapper-ruler-12	50

Table 2 Generated association rules with confidence value

Frequent itemsets	Rule generated	Assigned to which mapper ruler	Confidence (in %)
<i>Subset of {I2, I4, I5}</i>			
{I2}	I2 → {I4, I5}	Mapper-ruler-1	66.6
{I2, I4}	{I2, I4} → I5	Mapper-ruler-4	100
{I2, I5}	{I2, I5} → I4	Mapper-ruler-5	100
<i>Subset of {I3, I4, I5}</i>			
{I3, I4}	{I3, I4} → I5	Mapper-ruler-10	66.6

Table 2 shows that the association rules of itemset $\{\{I2, I4, I5\}, \{I3, I4, I5\}\}$ is generated. Different rules are generated by different Mapper Rulers. The Reducer Rulers take rulers generated by Mapper Rulers as input. In the above example 4 different rules are generated having their confidence value greater than the minimum confidence value which is 60.

Algorithm 1: Map Reduce based FP-Growth

```

Map Reduce FP-Growth ( $D$ ,  $Min\_sup$ ,  $Min\_conf$ )
Input:  $D$ ,  $Min\_conf$  (0.60%),  $Min\_sup$ : (20%)
Output:  $F$ : Frequent itemsets, Rule set: Set of Association Rules.
Begin
    Preprocess ' $D$ ' and extracts Candidate one Itemset ( $C_1$ ) and computing
    support count
    Sort the item in  $C_1$  in descending order of their support count
    // Constructing FP –Tree
    For each transaction in  $d \in D$ 
        Item-name is identified by the node
        Counts the numbers of transactions of all the paths connecting to n
        the particular node.
        Node-link links to the next node and which carries the same item-
        name or if there is no item to link which means null.
    End for
    for each item  $c \in C_1$ 
        Set the path to reach the item and share the Common path to reach the
        root node In each path finds the item count
    End for
    Mapper_Support() // input:  $C_k$  -Candidate item
    {
        //output: Conditional FP Tree with Support( $S$ )
        for each item  $c_i \in C$  do
            Scan ' $D$ ' to find number of occurrences of  $C_i$ 
    }
}

```

```

Reducer( $C, S, Min\_Sup$ ) //input: Conditional FP Tree support( $S$ ),min_sup.
{
    // output:  $L$ -Large itemset
    for each item  $c \in C$  do
        if ( $S(c) \geq Min\_Sup$ ) then
             $L = L \cup C_i$ 
}
Mapper_Ruler ( $L_2, L_3, \dots, L_k$ ) //input: Large itemset  $L_2$  to  $L_k$ 
{
    // output: Rules
    for each large itemset  $j = 2$  to  $k$  do
        for each item  $l \in L_j$  do
            for each subset  $S \subseteq l$  do
                generate the Rule  $S \rightarrow l - S$  and
                compute its Confidence
                Rules= rules  $\cup S \rightarrow l - S$ 
}
Reducer_Ruler(Rules) //input: Rules
{
    //output: Ruleset
    for each rules  $r \in Rules$ 
        if ( $r.confidence \geq Min\_conf$ )
            Ruleset = Ruleset  $\cup r$ 
}

```

6 Experimental Details

6.1 Experimental Setup

The proposed model is executed in apache spark environment on a system having 2.30 GHz with 8 GB RAM having 64 bit OS. We recommend using 10 GB or higher network is the best way to make these applications run faster. It is necessary to possess at least 8–10 CPU cores per memory. This is implemented by using Python language and using pyspark API's. The model is trained with groceries dataset which is 0.5 GB in size.

6.2 Execution Time

In MapReduce-based FP algorithm, the support count of all the nodes which supports to set the path to reach the items are calculated using many mappers parallelly. Table 3 shows the execution time of FP-Growth and MapReduce-based FP-Growth for different dataset size with minimum support value is 0.01... In Fig. 2, X-axis represents the different dataset size and Y-axis represents the time taken in (ms), we conclude that MapReduce-based FP-Growth takes less execution time for generating frequent itemset and association rules.

Table 3 Runtime of FP-Growth and MapReduce-based FP-Growth algorithm

Dataset size (GB)	Time taken (ms)	
	FP	MR-FP
0.5	11.628	2.064
1	19.89	4.84
2	39.05	7.67
5	82.89	35.24

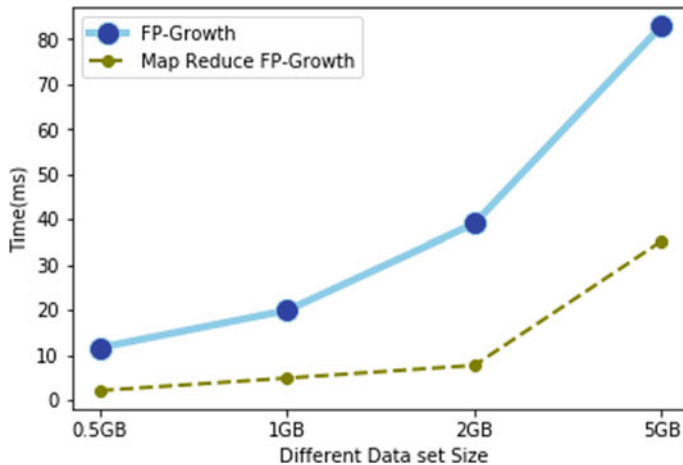


Fig. 2 Runtime of FP-Growth versus MapReduce-based FP-Growth algorithm

6.3 Execution Time of MapReduce Apriori Versus MapReduce FP-Growth

Generating frequent itemset and association rules using MapReduce FP-Growth takes less time compared with MapReduce Apriori algorithm. Table 4 shows that runtime of MapReduce Apriori versus MapReduce FP-Growth for the different dataset size with minimum support value 0.01 and minimum confidence value is 60%. Figure 3 shows that runtime of MapReduce Apriori versus MapReduce FP-Growth for different

Table 4 Runtime of MapReduce apriori versus MapReduce FP-Growth

Dataset size (GB)	Time taken (ms)	
	MR-apriori	MR-FP
0.5	10.62	2.064
1	18.89	4.84
2	36.05	7.67
5	154.89	35.24

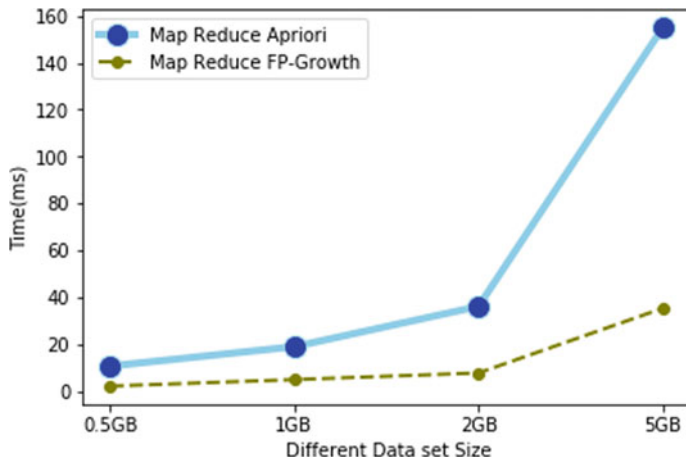


Fig. 3 Runtime of MapReduce apriori versus MapReduce FP-Growth

dataset size. X-axis represents different dataset size, and Y-axis represents the time taken for generating frequent itemset and association rules.

7 Conclusion

The conventional Apriori algorithm takes more time to generate frequent patterns and association rules by generating candidate key for each item in the dataset one by one. FP-Growth algorithm consumes more time for generating frequent itemset and association rules without generating candidate key for the item in the dataset. And generated frequent patterns by using FP-Tree construction step by step sequentially. This takes less time when compared to Apriori algorithm. Thus, to defeat the problem technique, the MapReduce-based FP-Growth algorithm is designed. This algorithm is executed in parallel for large dataset with different minimum support value. The results of convention FP-Growth algorithm and MapReduce FP-Growth algorithm are compared, and it shows that the processing time varies in terms of milliseconds. Therefore, the MapReduce FP-Growth algorithm proves fast generation of frequent itemset and association rules.

References

1. Zhang W, Liao H, Zhao N (2008) Research on the FP growth algorithm about association rule mining. In: 2008 international seminar on business and information management, vol 12(2). Wuhan, pp 315–318

2. Mansouri M, Nadimi-Shahraki M (2017) Hp-apriori: horizontal parallel-apriori algorithm for frequent itemset mining from big data. In: 2017 IEEE 2nd international conference on big data analysis (ICBDA), vol 30(18). Beijing, pp 286–290
3. Lin K-C, Liao I-E, Chen Z-S (2011) An improved frequent pattern growth method for mining association rules. *Exp Syst* 12(38):5154–5161
4. Rattanaopas K, Kaewkeeree S (2017) Improving Hadoop mapreduce performance with data compression: a study using wordcount job. In: 14th international conference on electrical engineering/electronics, computer, telecommunications and information technology (ECTI-CON), vol 31(12). Phuket, pp 564–567
5. Agrawal R, Srikant R (2000) Fast algorithms for mining association rules. In: Proceedings of the 20th international conference on very large data bases VLDB, vol 41(7), pp 1215–1221
6. Yu K, Lee M, Huang Y, Chen S (2014) An efficient frequent patterns mining algorithm based on MapReduce framework. In: International conference on software intelligence technologies and applications and international conference on frontiers of internet of things 2014. Hsinchu, vol 12(12), pp 1–5
7. Gao L, Zhang X, Wang W, Shen Q (2017) Spatiotemporal traffic modeling based on frequent pattern mining in wireless cellular network. In: 2017 IEEE international conference on internet of things (iThings) and IEEE green computing and communications (GreenCom) and IEEE cyber, physical and social computing (CPSCoM) and IEEE smart data (SmartData), exeter, vol 4(14), pp 60–67
8. Grahne G, Zhu J (2005) Fast algorithms for frequent itemset mining using FP-trees. *IEEE Trans Knowl Data Eng* 16(17):1347–1362

A Univariate Data Analysis Approach for Rainfall Forecasting



V. P. Tharun, Prakash Ramya, and S. Renuga Devi

Abstract Precipitation is instrumental for the existence of life forms on the globe. The agricultural sector, the economic mainstay of the country, etc., depend majorly on the rainfall. Hence, the rainfall forecasting models hold an unprecedented significance for the same. This work's main objective is to create an efficient, easy-to-implement rainfall forecast system that can promptly warn and alert the people of any unexpected downpours. As the attempt is to implement a simple system capable of giving noticeable results, the work starts with the assessment of rudimentary techniques like baseline/Naïve forecast, seasonal persistence algorithm, autoregression. The observed improvement in the performance as the complexity of models increased led to the evaluation of a comprehensive model like autoregressive integrated moving average (ARIMA) that imbibes some of the positive traits of the above models. This work does not present a novel forecasting technique but instead conducts a comparative study of univariate analysis using various statistical modeling techniques. The models are assessed on their performances using the root mean square error (RMSE) values calculated by comparing the predicted rainfall intensity values of the model with that of the actual rainfall intensity values present in the dataset. The research and analysis undertaken for this work are to predict the rainfall intensity of Coonoor in Nilgiris district, Tamil Nadu using a comprehensive statistical approach. Python was used as primary platform for the implementation of the above models. The prediction model developed using the ARIMA technique with an RMSE score of 11.9604 proved to be a better and more efficient model than the other statistical models considered in the paper (Toth in J Hydrol 239(1–4):132–147, 2000 [1]).

Keywords Univariate analysis · Baseline model · Seasonal persistence · Autoregression · ARIMA · Statistical model

V. P. Tharun
Wipro Ltd., Bengaluru, India

P. Ramya (✉)
British Telecom, Bengaluru, India

S. Renuga Devi
Vellore Institute of Technology University, Vellore, India

1 Introduction

Being a significant factor for supporting economy and human sustenance, rainfall forecasting has always been a matter of concern for the metrological department. The rainfall forecasts are vital information to support crops and for water and flood management. It directly influences the hydrological cycle, which, in turn, affects the monsoon season (June–August) of India, which is the most fecund time for agricultural practices [2]. It also has an indispensable part to execute in disaster management. Henceforth, a prior insight into possible rainfall can help lessen problems related to natural hazards like floods, droughts, and landslides [3].

Large-scale econometric models, which were prevalent for decades, used for structural estimation and forecasting, were supplanted with regression-based models that could better extract linear relationships in data [2]. However, the performance of the forecasting techniques can significantly vary in regard to the examined process, with the variations being more pronounced for precipitation in comparison to other metrological elements like temperature, wind speed, etc. [4].

The baseline of the work is to design and evaluate an effective and robust model using different variants of statistical modeling techniques for forecasting the daily rainfall for Coonoor in the Nilgiris district. Coonoor is a Taluk and a municipality in the Nilgiris district. There are approximately 14 rain gage stations in number near Coonoor, which record the received precipitation amount.

Rainfall data follows a time series pattern, which can be daily, monthly, or yearly, defined as the outcome of the interaction between several complex atmospheric processes [5], hence, being one of the most challenging elements of the hydrological cycle to forecast. The numerous uncertainties associated with rainfall occurrences affect the performance of both stochastic and deterministic rainfall prediction models [1]. Time series analysis (TSA), nonetheless, involves developing models that best capture or describe an optically canvassed time series to understand the underlying causes [6]. TSA techniques concerning intuitive, heuristic rainfall prediction approaches improve the forecasting accuracy even if the rainfall forecasting performance measures indicate only a weak to moderate relationship between forecasted and observed values [7]. One of the variants of TSA is univariate time series analysis; as the name suggests, it includes only one parameter for forecasting the rainfall and is quite handy for short-term demand forecasting as the forecasts accommodate for various periodic and seasonal cycles in the model specifications. With an approach that combines projections from multiple accurate forecasting methods, the sensibility of univariate analysis techniques to weather conditions and other seasonal trends is kept under check [8].

In the further sections, we will be focusing on the below-given methods to forecast the rainfall in Coonoor in Nilgiris District, Tamil Nadu:

1. Baseline algorithm/Naïve forecast
2. Seasonal persistence algorithm
3. Autoregression time series analysis
4. Autoregressive integrated moving average (ARIMA).

Considering only the rainfall intensity of Coonoor (univariate data), the predicted models are compared and evaluated based on the RMSE values.

2 Background Knowledge

A time series is a process observed over time in increments. The term ‘univariate time series’ refers to a quantitative analysis of one variable recorded sequentially over equal time increments.

2.1 Baseline/*Naïve* Method

It is the most widely recognized common technique for supervised machine learning. The outcome at time step ($t + 1$) is predicted using the observation at the previous time step ($t - 1$). This forecasting technique is one of the most convenient to implement and evaluate as the pattern of predictions is fixed. This technique is swift and repeatable and serves the purpose of a standard for assessing the results of other advanced modeling techniques.

2.2 Seasonal Persistence Algorithm

This algorithm engenders a better forecast than baseline due to the additional seasonal component, which persists the observation for the same time in the previous season. It is also a simple model because it uses a rudimentary function of the last few observations at the same time stamps in the previous seasonal cycles.

The sliding window concept is used to make forecasts. Within a sliding window, observations at the same time stamps in the previous season are collected, and the means of the observations are used to generate forecasts.

2.3 Autoregression Time Series

The autoregression models are built on the underlying assumption that there exists a dependency between the observations of the past and that of the future. The observations of the previous time stamps are fed into a regression equation fitted on the dataset to predict the values of the future time steps.

Autoregression can be explained as below:

$$Y = c_0 + c_1 * X \quad (1)$$

Here, Y is the prediction, $c0$ and $c1$ are coefficients found by optimizing the model on training data, and X is an input value. If the forecast is to be done for the next time step ($t + 1$) given the observations of the last two-time steps ($t - 1$) and ($t - 2$).

$$X(t + 1) = c0 + c1 * X(t - 1) + c2 * X(t - 2) \quad (2)$$

$X(t - 1)$ and $X(t - 2)$ are lag variables. As the regression model uses data from the same input variable at previous time steps, it is referred to as regression of self, i.e., autoregression. For the reason that the autoregressive approach relies only on the concerned variable, it is free from the effects of other dependent variables [2].

2.4 Autoregressive Integrated Moving Average

Autoregressive integrated moving average (ARIMA) is a popular and widely used statistical model which captures the key aspects discussed below:

Autoregression (AR)—a model that harnesses the correlation between an observation and any number of observations preceding it in terms of time stamps.

Integrated (I)—helps introduce stationarity in the time series by performing a difference operation on the observations.

Moving Average (MA)—a model that uses the dependency between an observation and a residual error from a moving average model applied to lagged observations.

A linear regression model is constructed considering the parameters, which removes the trend and seasonal structures that negatively affect the regression model. With the proper use of hyperparameters, the ARIMA model can be configured to perform the function of an ARMA model and even a simple AR, I, or MA model. Although ARIMA models are not efficient in modeling nonlinear time series data, they do quite well at developing linear forecasting models [9].

Performance measures of rainfall forecasting models using statistical modeling: Root Mean Square Error: RMSE reflects the deviation of the model prediction from the actual observations by calculating the average of the squared error between both.

$$\text{RMSE} = \sqrt{\frac{1}{n} \sum_{j=1}^n (y_j - \hat{y}_j)^2} \quad (3)$$

3 Dataset

Line plots (see Figs. 1 and 2), Histograms (see Fig. 3), density plots (see Fig. 4), box and whisker plots (see Figs. 7 and 8), lag plots (see Figs. 5 and 6), and autocorrelation plot (see Fig. 9) of the rainfall intensity values within various time ranges are generated to understand the distribution, seasonal trends, and linearity present in the dataset (Table 1).

Line, whisker, and lag plots have been plotted and visualized weekly as well as yearly. Density, histogram, and autocorrelation plots have been pictured for 10 years from 2004 to 2013. It shows the distribution of observations to provide valuable diagnostics of the univariate data to develop a better forecasting model. Major insights obtained from data visualization are as follows:

- There exist visible precipitation trends that repeat every year (see Figs. 1 and 2).
- The rainfall intensity value for most days lies in the range of 0–70 mm (see Figs. 3 and 4).
- There is no repeating trend when weekly data is considered (see Fig. 5).
- Mean of monthly and yearly rainfall data is confined in the range of 0–50 mm (see Figs. 7 and 8)
- The autocorrelation between daily rainfall data decreases as the number of lags increases (see Fig. 9).

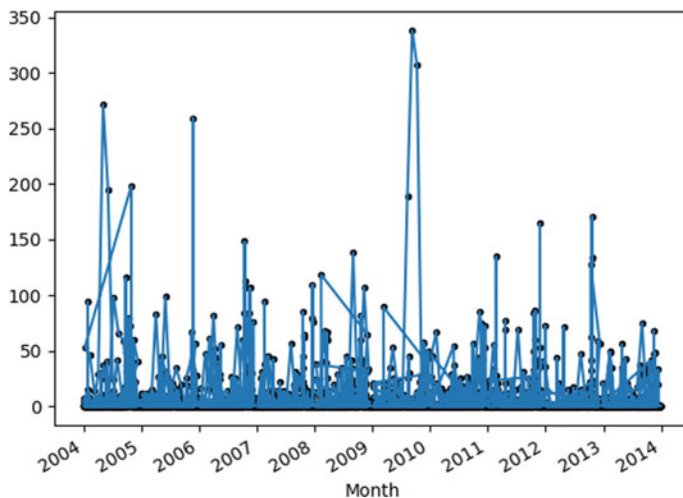


Fig. 1 Monthly series plot

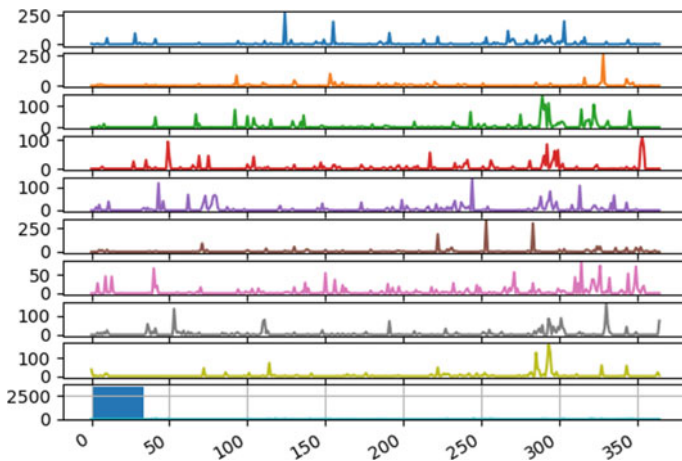


Fig. 2 Yearly series plot

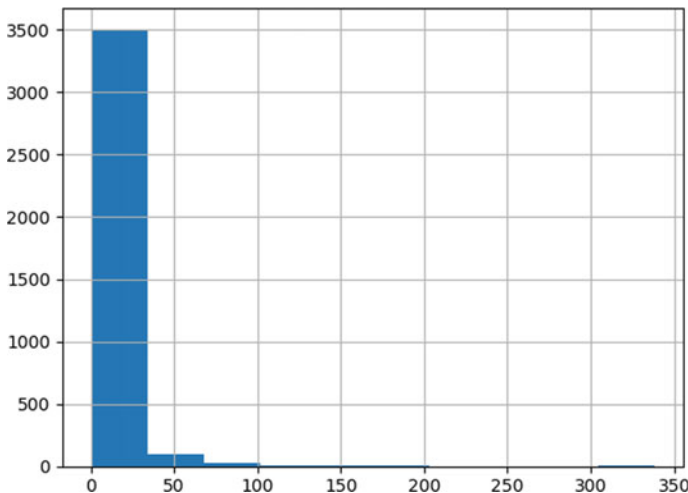


Fig. 3 Histogram plot

4 Results and Discussions

4.1 Baseline/*Naïve Forecast*

As discussed, this method acts as a reference to other modeling techniques. As shown in Table 2, the time step ($t - 1$) is used to forecast the rainfall amount of time step (t). This method is the baseline to all other forecasting methods. The expected and predicted amount of rainfall from 2004 to 2013 is plotted (see Figs. 10 and 11).

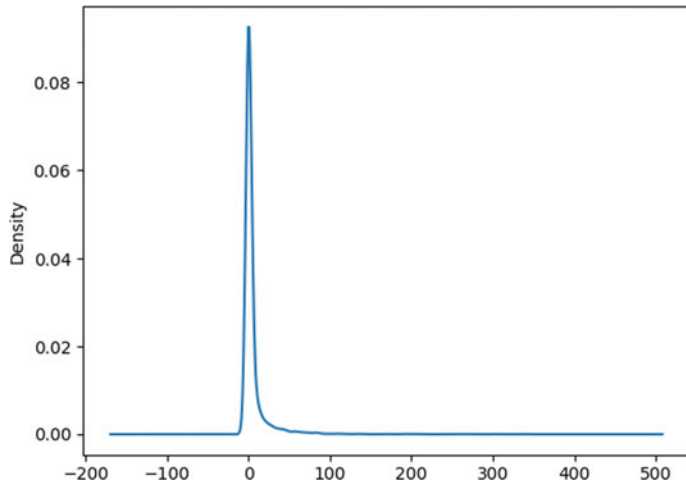


Fig. 4 Density plot

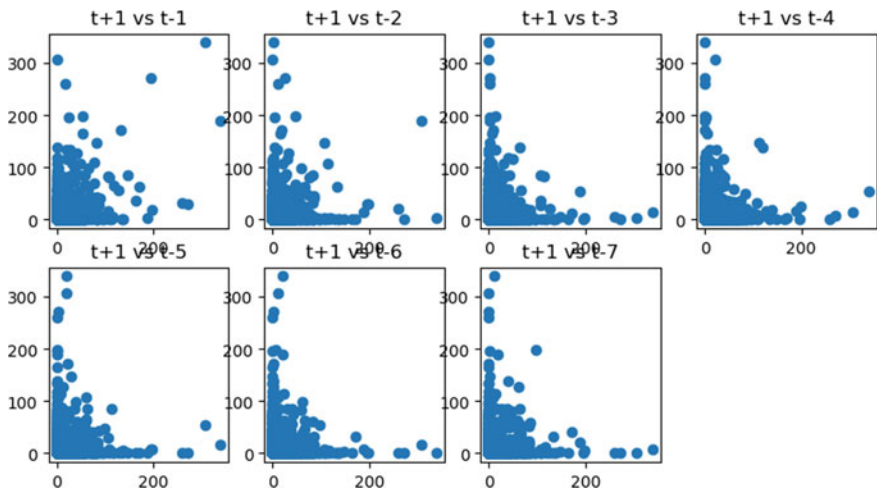


Fig. 5 Lag plot weekly

It can be inferred from Table 2 that the baseline model gives an RMSE value of 13.25 mm as per equation [3]. Only those models that outperform this baseline model in terms of RMSE score are considered for further implementations. Therefore, it helps to define a minimum performance standard that can be expected from the more advanced models. Any model that fails to meet this standard is deemed inefficient for practical implementation.

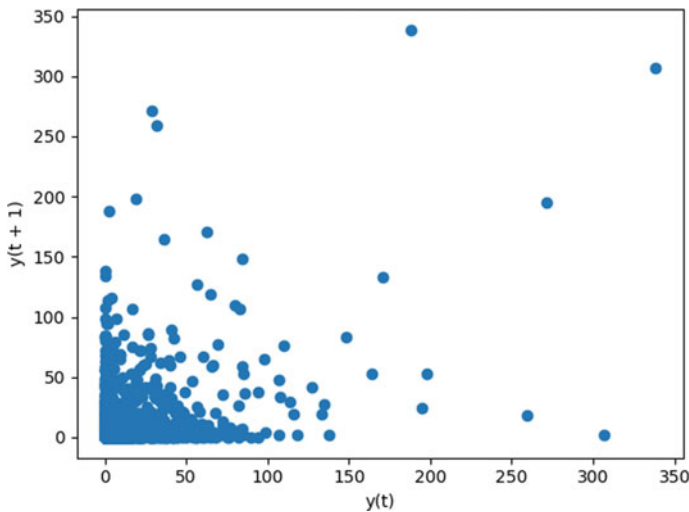


Fig. 6 Lag plot yearly

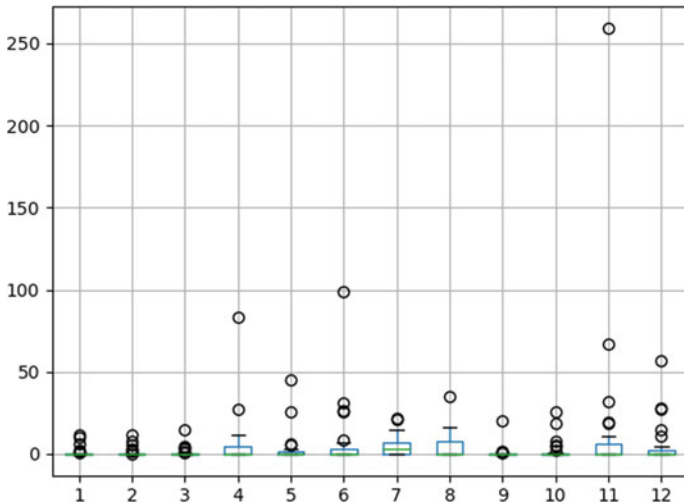


Fig. 7 Whiskers plot monthly

4.2 Seasonal Persistence Algorithm

Figure 12 shows the yearly seasonal variation of rainfall over 365–366 days (i.e., 12 months). As discussed in the previous section, observations simultaneously in the earlier seasons are aggregated for deriving a coherent prediction. Table 3 shows that to reach the minimal error point with the seasonal persistence

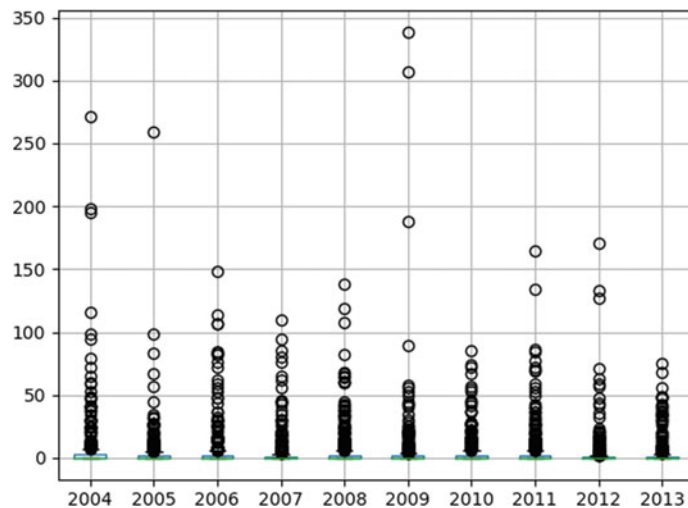


Fig. 8 Whiskers plot yearly

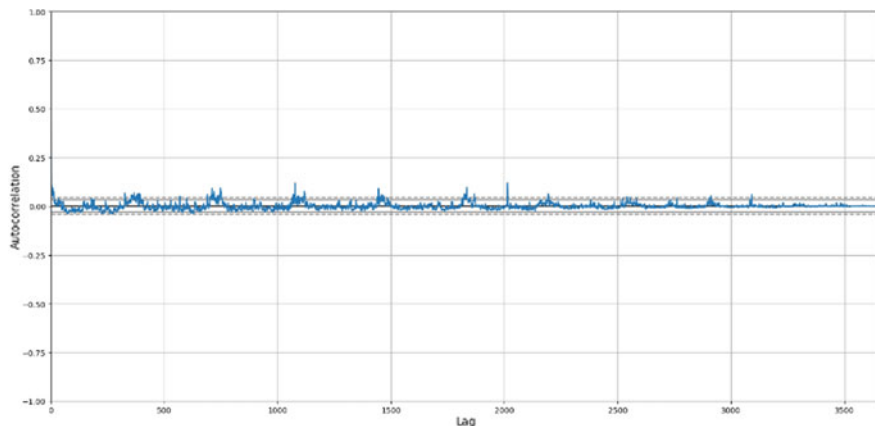


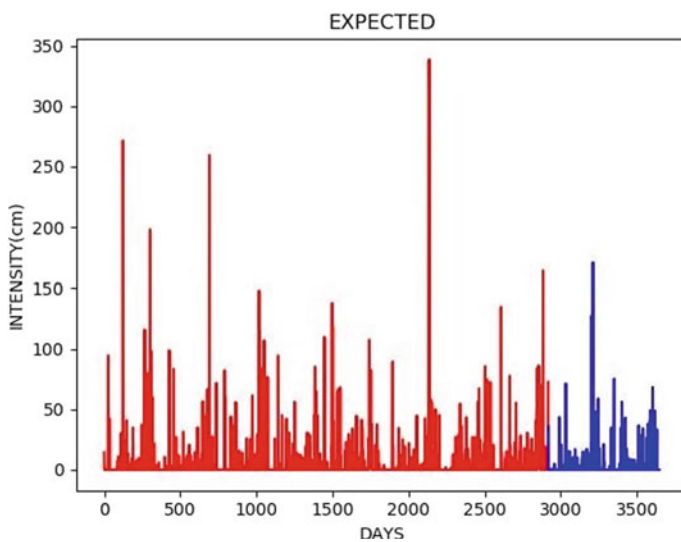
Fig. 9 Autocorrelation plot

Table 1 Meta-data of Coonoor dataset

Study area	Coonoor, Nilgiris, Tamil Nadu
Source of data	Indian Meteorological Department, Chennai Public Works Department, Nilgiris
Data acquisition period	10 years, i.e., 2004–2013
Input parameters	Rainfall intensity of nearby rain gage stations—Coonoor rain gage station, Coonoor railway station, and Runnymede
Output parameter	Rainfall (in mm)

Table 2 Actual versus expected rainfall (in mm)

Expected amount of rainfall	Predicted amount of rainfall	Expected amount of rainfall	Predicted amount of rainfall
72.6	35.8	0	0
35.8	0	0	0
0	0	0	0
0	0	0	0
0	0	0	0.3
0	0	0.3	0.4
0	0	0.4	0
0	0		

**Fig. 10** Expected rainfall intensity

technique, we have to consider the past 8 years of data for the dataset in hand. The reason that the day-wise seasonality model fails to produce an RMSE score that is below the standard set by the baseline model is why it is not chosen over the month-wise seasonality model that meets the standard.

Table 3 shows that the root mean square error value of daily rainfall decreases continuously throughout the training period of 8 years. In contrast, although the root mean square error initially increased for two years for the monthly rainfall period, it gradually decreased for the next five years. It can be concluded that (see Fig. 13), as the sliding window size in terms of the number of years increases for the seasonal persistence model, forecasting of rainfall can be done more accurately and precisely.

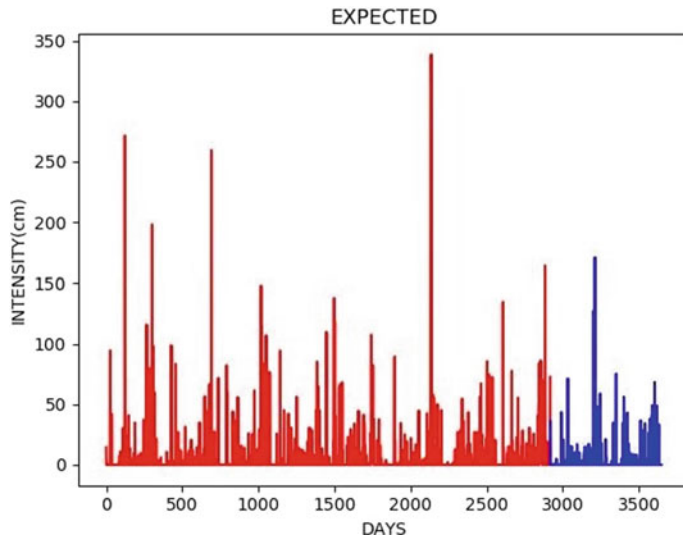


Fig. 11 Predicted rainfall intensity

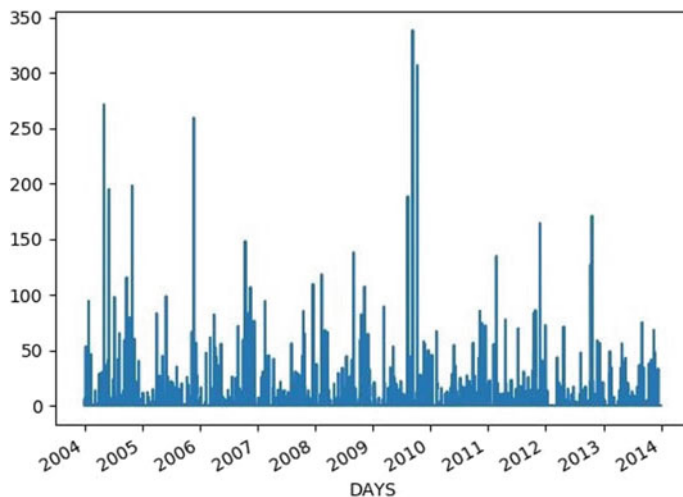


Fig. 12 Seasonal rainfall of variation (10 years)

Note that, even though a 1-year time-lag seems to produce a lesser RMSE value when a month-wise seasonality is considered, the day-wise score for the same is not creditable. It proves an inconsistency in the seasonal trend present when a lag of 1 year is taken. Besides, it could also be due to unexpected outliers present in the data. The above reasons fortify why an 8-year time lag, which gives the least RMSE score for both month-wise (next to 1-year time lag) and day-wise seasonality, is preferred.

Table 3 Root mean square error (monthly vs. daily rainfall)

Years	RMSE_M	RMSE_D
1	9.88026	19.2212
2	12.6957	16.5564
3	12.295	15.8951
4	11.2601	15.3252
5	11.4332	14.7592
6	10.8819	14.2212
7	10.196	13.8897
8	10.0673	13.6372

Bold values denotes the best result chosen from the table based on RMSE value

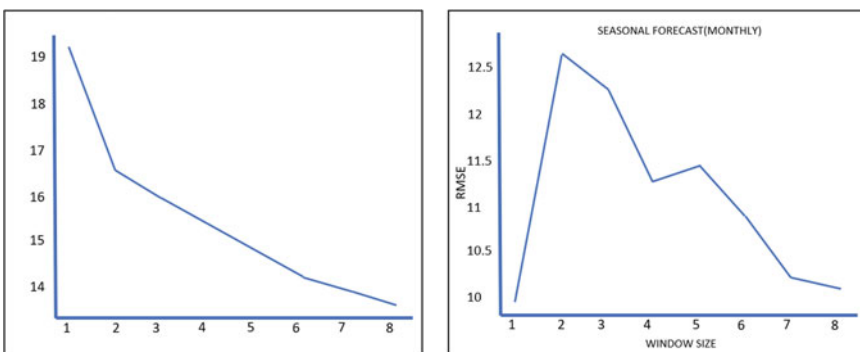


Fig. 13 Daily and monthly persistence model

4.3 Autoregression

As discussed in Sect. 2.3, the AR model feeds the generated regression equation with recorded observations of the past to obtain the rainfall values of the future time stamps. Figure 14 is a line plot that gives a more in-depth insight into the correlation between the rainfall intensity values of a day with that of the previous days in the same month.

Figure 14 helps to decide on the intensity values to be considered while formulating the regression equation. The decreasing trend shown by the line plots indicates very little correlation between the intensity values as we go behind in the number of days in a month.

Figure 15 is an all-inclusive autocorrelation plot that depicts the correlation maintained by the rainfall intensity value of any day with that of any other day within a span of 10 years in the dataset.

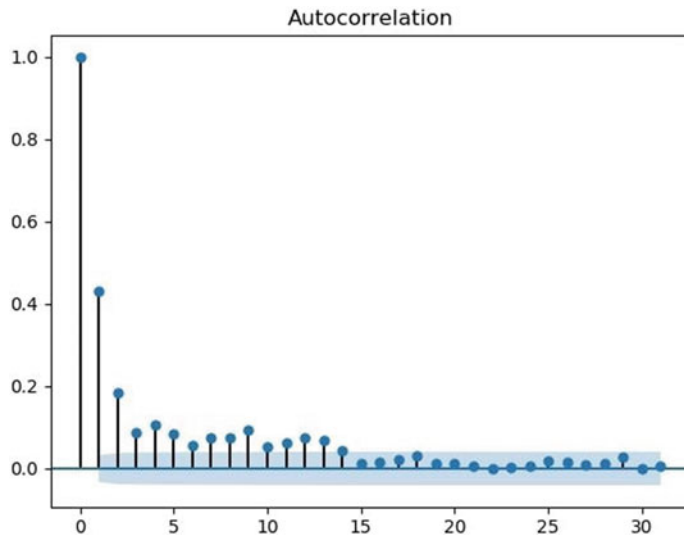


Fig. 14 Monthly autocorrelation plot

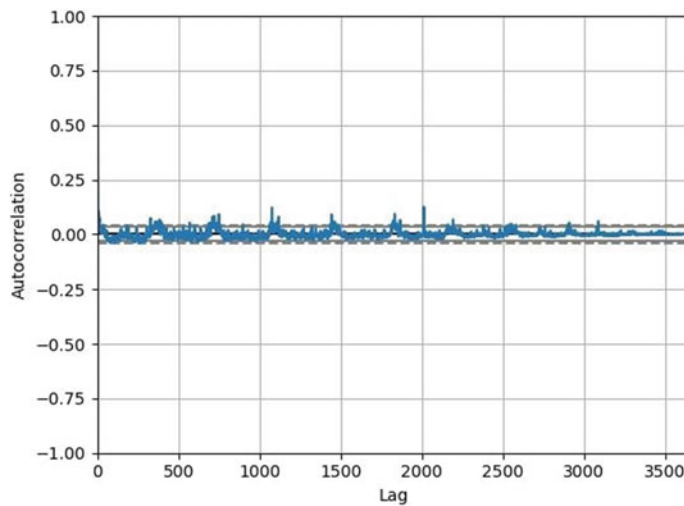


Fig. 15 Daily autocorrelation plot

Figure 15 gives an insight that the past year's data shows limited effects on the future rainfall intensity values as far as the development of the rainfall prediction model is considered.

Predictions become inaccurate over time in time series modeling. Hence, the walk-forward validation methodology is being used to retrain the data as it gets further

data points moving along the time series one-step at a time, making it a more realistic approach.

Figure 16 shows the results of the autoregression model with the inclusion of the walk-forward validation algorithm.

The model gives better results compared to the simple AR model (see Fig. 17). Here, the model's training is done with all samples available in the dataset, unlike

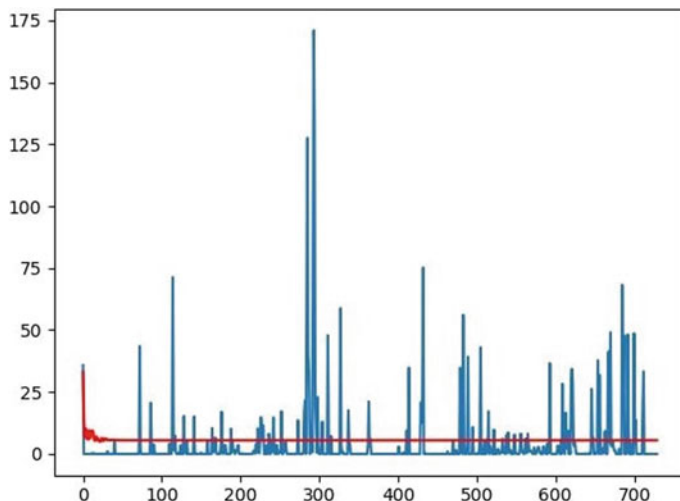


Fig. 16 Prediction using autoregression

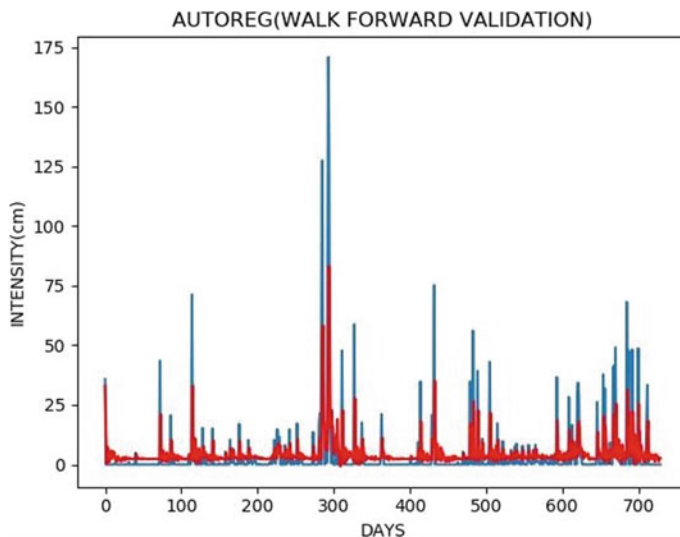


Fig. 17 Prediction using autoregression walk-forward validation algorithm

Table 4 Expected versus predicted rainfall intensity for autoregression model

Autoregression		Autoregression (walk forward validation)	
Expected amount	Predicted amount	Expected amount	Predicted amount
35.8	33.0599	35.8	33.0599
0	15.7632	0	16.9382
0	7.03883	0	0.245693
0	10.175	0	7.28758
0	9.49442	0	5.80882
0	5.95194	0	0.933555
0	7.82142	0	4.91533
0	5.85771	0	2.37111
0	9.52433	0	5.79746
0	6.42905	0	2.51351
RMSE = 13.347		RMSE = 12.024	

the simple autoregression model, where the model's training is done with samples present just in the training set (Table 4).

4.4 Autoregressive Integrated Moving Average

The regression model works best when the predictors are not correlated and independent of each other. This TSA model considers the number of lags to be used as predictors (p), the number of lagged forecast errors (q), and the minimum differencing required to make the time series stationary (d). ARIMA model is parameterized on p (lag order), q (size of moving average window), and d (degree of differencing) [10]. Table 5 shows the MSE values of the ARIMA model trained on different values of (p, q, d) .

It can be inferred from Table 5 that the best ARIMA model obtained from the sensitivity analysis is ARIMA (4, 0, 2) with $p = 4$, $q = 2$, $d = 0$ with the MSE value as 11.961.

Tables 6 and 7 show the rainfall intensity values of the previous timesteps, which are used for the formulation of the regression equation along with their respective coefficients in the equation.

The ' P ' value given in Table 7 corresponding to each coefficient describes how much influence each of them has in deciding the predicted result. The lesser the P -value, the more is the correlation of the parameter with the output (Fig. 18).

Table 8 shows the expected and predicted sample values from the trained model.

Figures 19, 20, and 21 show how the predicted rainfall value changes with the solver functions in python.

Table 5 ARIMA grid search results (p, d, q) versus MSE

ARIMA—grid search results			
ARIMA (p, d, q)	MSE	ARIMA (p, d, q)	MSE
(0, 0, 0)	13.337	(4, 0, 0)	12.050
(0, 0, 1)	12.226	(4, 0, 1)	11.992
(0, 0, 2)	12.048	(4, 0, 2)	11.961
(0, 1, 0)	14.305	(4, 1, 0)	12.898
(0, 1, 1)	12.851	(4, 1, 2)	12.013
(0, 1, 2)	12.150	(4, 2, 0)	15.814
(0, 2, 0)	23.222	(6, 0, 0)	12.050
(0, 2, 1)	14.311	(6, 0, 1)	12.077
(1, 0, 0)	12.024	(6, 0, 2)	11.999
(1, 0, 1)	12.029	(6, 1, 0)	12.493
(1, 0, 2)	12.049	(6, 1, 1)	12.050
(1, 1, 0)	13.679	(6, 1, 2)	12.082
(1, 1, 1)	12.043	(6, 2, 0)	15.192
(1, 1, 2)	12.047	(8, 0, 0)	11.996
(1, 2, 0)	19.045	(8, 1, 0)	12.299
(2, 0, 0)	12.028	(8, 1, 1)	11.997
(2, 0, 1)	12.019	(8, 1, 2)	12.034
(2, 0, 2)	11.975	(8, 2, 0)	14.125
(2, 1, 0)	13.365	(10, 1, 1)	12.009
(2, 2, 0)	17.469		

Bold values denotes the best result chosen from the table based on MSE value

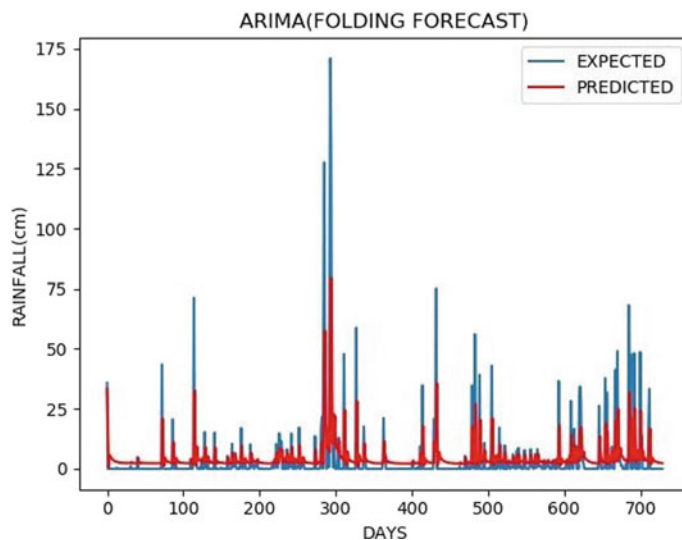
Table 6 Final ARIMA model results (1)

ARMA model results			
Dependent variable	Rainfall	No. of observations	3650
Model	ARIMA (4, 0, 2)	Log-likelihood	-15,304.116
Method	Css-mle	SD of innovations	16.022
AIC	30,624.233	BIC	30,673.853
Sample	01-01-2004	HQIC	30,641.904

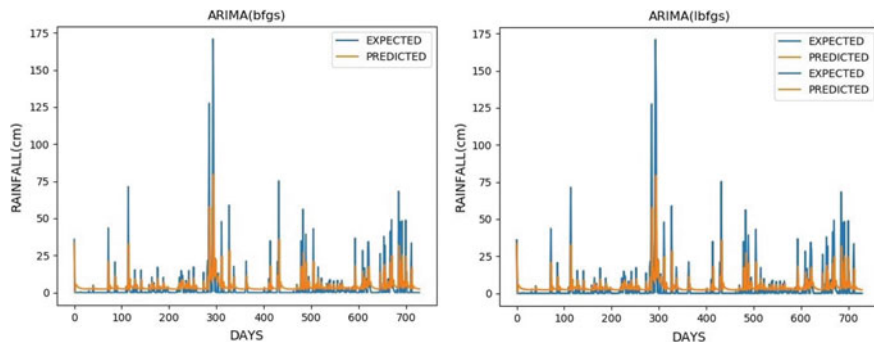
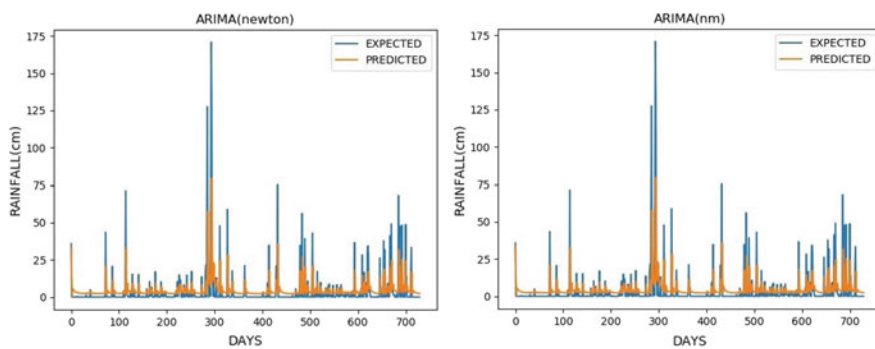
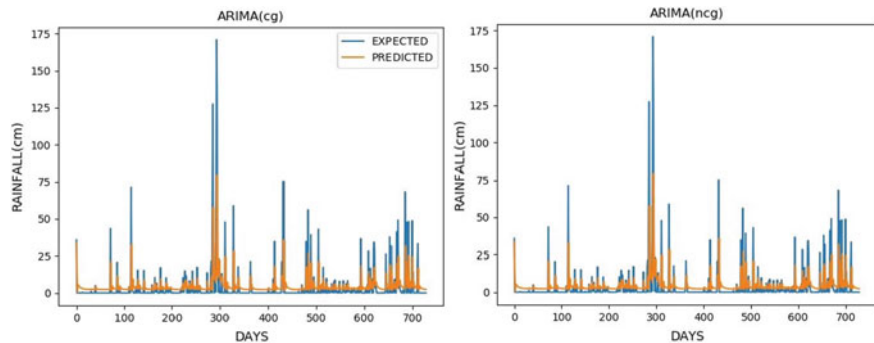
Figure 22 shows the comparison of RMSE values with different solver functions. The solver parameter defines the numerical optimization method used to fit the model's coefficient to the data. It can be observed that all the solver functions have very similar performance with respect to RMSE values.

Table 7 Basic ARIMA model results (II)

	Coeff	Std. err	Z	$ P > z$	[0.025	0.975]
Constant	5.51510	0.633	8.133	0.000	3.910	6.392
Ar.L1.RAINFALL	0.8612	0.163	5.269	0.000	0.541	1.181
Ar.L1.RAINFALL	0.1374	0.209	0.659	0.510	-0.271	0.546
Ar.L1.RAINFALL	-0.1598	0.065	-2.471	0.014	-0.287	-0.033
Ar.L1.RAINFALL	0.0643	0.018	3.551	0.000	0.029	0.100
Ar.L1.RAINFALL	-0.4375	0.163	-2.681	0.007	-0.757	-0.118
Ar.L1.RAINFALL	-0.3307	0.145	-2.278	0.023	-0.615	-0.046

**Fig. 18** ARIMA folding forecast prediction plot**Table 8** Expected versus predicted rainfall intensity of ARIMA

ARIMA folding forecast results	
Expected	Predicted
35.8	33.2715
0	16.9727
0	0.456497
0	5.56906
0	5.38867
0	4.63656
0	4.28323
0	3.89451
0	3.62006
0	3.37882

**Fig. 19** ARIMA lbfgs and bfgs**Fig. 20** ARIMA newton and nm**Fig. 21** ARIMA cg and ncg

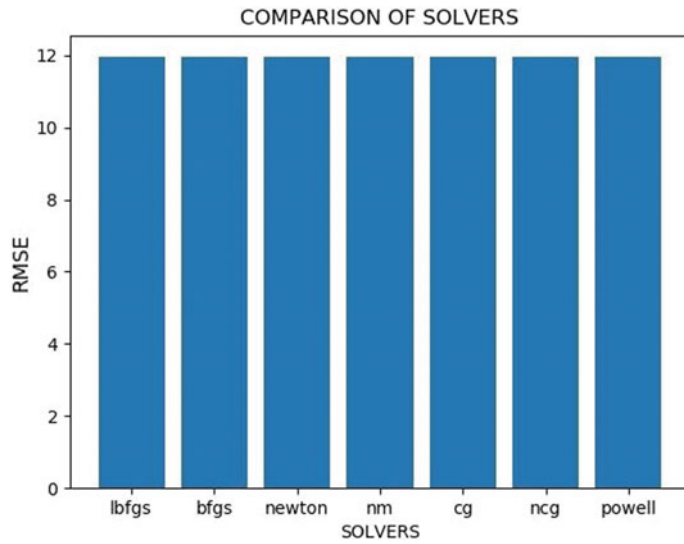


Fig. 22 Comparison of solvers

Figure 23 shows the comparison of execution time with varied solver functions. Although all the solver functions gave comparable results in terms of the RMSE value, the ‘NM’ function produces the results with lesser execution time. This insight is critical whenever a model has to be built for large datasets in the production

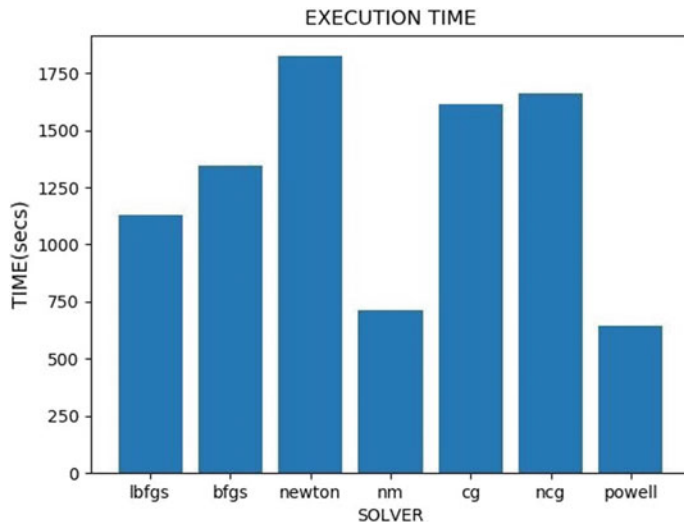


Fig. 23 Comparison of the execution time of each solver

Table 9 RMSE and execution time versus solvers

RMSE versus solvers		TIME versus solvers	
Lbfgs	11.96136	Lbfgs	1129.091
Bfgs	11.96155	Bfgs	1345.201
Newton	11.96136	Newton	1825.439
Nm	11.96074	Nm	710.3942
Cg	11.96151	Cg	1613.26
Ncg	11.96136	Ncg	1662.535
Powell	11.96092	Powell	646.4367

environments. Table 9 shows the quantitative results of the RMSE and execution time w.r.t to solver functions.

5 Conclusion

The paper presents a comparative study of the performances of some of the popular statistical modeling techniques in forecasting time series data (Rainfall). For the purpose of creating a ‘baseline’ for evaluating the performances of the considered models, a baseline/Naive forecast statistical model is used. It gives a reference RMSE score of 13.25 mm that is further taken as the cut-off score. Any model that failed to perform at par with or better than the baseline model in terms of RMSE score was ruled out. The seasonal persistence algorithm that successfully incorporated the rainfall data’s innate seasonal character furnishes an RMSE score of 10.06 mm for an 8-year time lag. The reason that this model showed a heavy dependence on the window size (lag) necessitated the need for a stabler model that has slim reliance on past data. Autoregression models, a model of the above kind, were expected to work equally well, even on the sparse dataset in hand. In contrast, the basic AR model failed to outperform even the Naive model. However, the AR model reinforced with the walk-forward validation technique produced a commendable RMSE score of 12.024. This is a clear validation for the claim that the data has got noticeable seasonal trends and that it shares a linear relationship with the past records. Finally, the more comprehensive ARIMA model, being a combination of the above, stand-alone models, achieved better accuracy and stability in terms of performance with an RMSE score of 11.9604. Though univariate modeling is a technique that is seldom used for metrological data, it is of considerable importance in works that are concerned with areas that are associated with a paucity of alternate predictor variables.

6 Future Work

The idea that the dataset is highly nonlinear gives a strong reason to consider nonlinear machine learning algorithms like neural networks for making forecasts. Adopting multivariate analysis techniques with the inclusion of other strongly correlated parameters like temperature, wind speed, and humidity should significantly improve the performance.

Acknowledgements We wish to extend our sincere gratitude to the Indian Meteorological Department (IMD), Chennai, and the Public Works Department of Coonoor for entrusting us with the data to carry out the research.

References

1. Toth E, Brath A, Montanari A (2000) Comparison of short-term rainfall prediction models for real-time flood forecasting. *J Hydrol* 239(1–4):132–147
2. Chattpadhyay S, Chattpadhyay G (2010) Univariate modelling of summer-monsoon rainfall time series: comparison between ARIMA and ARNN. *C R Geosci* 34(2):100–107
3. Box GEP, Jenkins GM, Reinsel GC, Ljung GM (2015) Time series analysis: forecasting and control. Wiley Publishers
4. Geoffrey Allen P, Morzuch BJ (2006) Twenty-five years of progress, problems, and conflicting evidence in econometric forecasting. What about the next 25 years? *Int J For* 22(3):475–492
5. Tharun VP, Ramya P, Renuga Devi S (2018) Prediction of rainfall using data mining techniques. In: 2018 2nd international conference on inventive communication and computational technologies (ICICCT). IEEE Xplore, Coimbatore, India
6. Mahmud I, Bari SH, Rahman MTU (2017) Monthly rainfall forecast of Bangladesh using autoregressive integrated moving average method. *Korean Soc Environ Eng* 22(2):162–168
7. Phan T-T-H, Caillault EP, Bigand A (2018) Comparative study on univariate forecasting methods for meteorological time series. In: 2018 26th European signal processing conference (EUSIPCO). IEEE, Rome, Italy
8. Caiado J (2010) Performance of combined double seasonal univariate time series models for forecasting water demand. *J Hydrol Eng ASCE* 15(3):215–222
9. Lee Y-S, Tong L-I (2011) Forecasting time series using a methodology based on autoregressive integrated moving average and genetic programming. In: Knowledge-based systems. Elsevier
10. Brockwell PJ, Davis RA, Fienberg SE (1990) Timer series: theory and methods. In: Springer time series: theory and methods, 2nd edn. Springer

Improved Adaboost Algorithm with Regression Imputation for Prediction of Chronic Type 2 Diabetes Mellitus



M. Dhilsath Fathima and S. Justin Samuel

Abstract Chronic type 2 diabetes mellitus is a type of diabetes which causes high blood glucose level in the human. Pancreatic insufficiency and elevated sugar level in blood are the conditions of getting diabetes mellitus. Type 2 diabetes mellitus (T2DM) affects the human metabolism such that a person with T2DM does not respond to the insulin released by the body, so glucose is not going into a cell in a normal and generates insulin resistance syndrome or metabolic syndrome. The consequences of diabetics are diabetic retinopathy, neuropathy, kidney damage, heart disease, slow healing and skin diseases. Hence, attention must be given to saving a person with T2DM by controlling the complications of T2DM. A predictive model is required to predict the T2DM effectively to reduce the severity of T2DM outcome. The main objective of this proposed work is to develop a T2DM prediction model using machine learning algorithms which act as a decision-making system to predict the type 2 diabetes in person. This model uses improved adaptive boosting algorithm (iABA) to develop the diabetic predictive model. This iABA model utilized Pima Indians diabetes dataset for building predictive model. Pima dataset contains many missing values which are imputed using regression imputation method. To examine the effectiveness of the proposed predictive model, the classifier performance measures are used. The iABA classifier outcomes are compared with a typical machine learning models. The output of the performance metric shows that an improved Adaboost algorithm achieves high accuracy of 78.3% than other machine learning classifiers. This model could be used to assist medical professionals to make prediction of type 2 diabetes and used to classify a person as a diabetic person and non-diabetic person.

Keywords Improved Adaboost algorithm · Type 2 diabetes mellitus prediction · Machine learning

M. Dhilsath Fathima (✉)

Sathyabama Institute of Science and Technology, Chennai, India

S. Justin Samuel

Department of Computer Science and Engineering, PSN Engineering College, Tirunelveli, India

1 Introduction

Diabetic mellitus is a cluster of metabolic disorder occurred due to high glucose level in blood. Type 2 diabetic mellitus (T2DM) is a type of diabetic mellitus and complicated chronic disease and very common type of diabetes, as 90% of people with diabetes have T2DM. Hyperglycemia is the concern of T2DM that is high blood sugar in the body and affects the people with different kind of diseases like neuropathy, diabetic retinopathy, a problem with blood vessels in the heart and kidneys. According to a survey given by [1] International Diabetes Federation (IDF) in the year 2019, almost 463 million adults are living with diabetic mellitus worldwide and one in two adults are living with diabetes is unknown. So, care should be taken to diagnose and predict the T2DM in middle-aged adult to avoiding the consequence of diabetic disease.

Some certain risk factors are associated with T2DM such as high body mass index (BMI), physical inactivity, insufficient exercise, genetic factors, high blood pressure, hypertension and low level of HDL cholesterol. Another significant risk factor of T2DM is gender, because the T2DM impact level for women is higher than for men [2], and women are more likely to transfer T2DM to their children [3]. Early prediction of T2DM can save human life, and T2DM can be avoided or delaying the complications related to diabetes by adopting a healthy lifestyle, increasing physical activity and improves quality of life. It is important to develop a decision-making system for medical professionals to an early prediction of T2DM using the diabetes risk factors. This proposed model is developed based on machine learning algorithm to predicts the presence of T2DM in a patient, and this current model will able to classify a patient is diabetes patient or non-diabetes patient.

This machine learning model uses improved Adaboost algorithm (iABA) for training and validating the pima diabetes dataset which contains diabetes risk factors. To clarify the potency of this proposed model, this model is compared with other machine learning classifiers. and the output of classifiers are assessed using classifier performance metrics. So, this proposed model could act as an effective T2DM decision-making system for diabetes prediction to support healthcare professionals and physicians in diabetes decision-making.

2 Related Work

A different decision support model for diabetic prediction based on machine learning classifiers was already proposed by many researchers in recent years. In [4], a research was carried using a support vector machine (SVM), a type of supervised classifier for the diagnosis of diabetic mellitus, they used radius basis function as a kernel trick in SVM and tenfold cross-validation to assess the model output. Experimental output from this study suggested that RBF kernel-based SVM provides 75.5% training accuracy on input data.

Sivakumar et al. [5] attempt to find solutions for diagnosing the diabetic disease through evaluating the useful patterns present in the input data to give the timely treatment to the patients using different machine learning models such as Naïve Bayes, KStar, ZeroR, oneR, random forest. They obtained a higher accuracy of 76.3% and 75.7% using the naïve Bayes algorithm and random forest algorithm, respectively, than other classifiers.

Adaptive neuro-fuzzy inference system (ANFIS) is a type of artificial neural network model used in [6] to predict and classify the patient into diabetic and non-diabetic using the Pima Indian women diabetes dataset and obtained 70.56% percent accuracy on the pima dataset. They have used MATLAB tool for building and training ANFIS model, and the trained mode is evaluated using k-fold cross-validation approach.

Authors of [7] utilized classification algorithms to develop a diabetic prediction model to diagnose diabetic at an initial stage. They used three machine learning models, namely support vector machine, decision tree, naïve Bayes algorithm on pima Indian Diabetes Dataset for building a diabetic prediction model. Performance of these three algorithms is evaluated using different measures as classifier accuracy, recall, precision, *F1*-score and receiver operating characteristic curve. The final results showed that naïve Bayes algorithm performs better than decision tree and support vector machine. An accuracy of Naïve Bayes algorithm is 76.3% which is higher than decision tree with 73.82% accuracy and support vector machine with 65.1% accuracy.

Another researcher [8] proposed a Type-2 diabetes decision support system which is built using radial basis function neural network classifier (RBFNN). RBFNN is a three-layer neural network, in which first layer used to process inputs of the model, the second layer is the hidden layer composed of number of nonlinear RBF activation units, last layer is the output layer of neural network classifier. Gaussian functions are used to implement activation functions in RBFNN. RBFNN uses pima Indian dataset for building diabetes prediction model which achieves 73.91% of accuracy, 81.33% of sensitivity and 60% of specificity.

We inferred from this related study that the pima Indian diabetes dataset (PID) is a general dataset for the development of a machine learning model to predict the progression of T2DM in a patient. We understood that machine learning and deep learning technique are giving equal contribution in predicting diabetes disease, and we analysed that many researchers are used Anaconda Environment with python 3.6 as an operating environment for analysis and visualization of machine learning and deep leaning environment. We have inspired by the related work analysis, proposed model (iABA classifier) is based on Adaboost algorithm with random forest classifier for training and tuning the iABA classifier. iABA uses Pima Indian diabetic (PID) dataset as an input dataset. From this proposed work, we ensure that final model will be act as an optimal decision support system for T2DM prediction.

3 Proposed Method

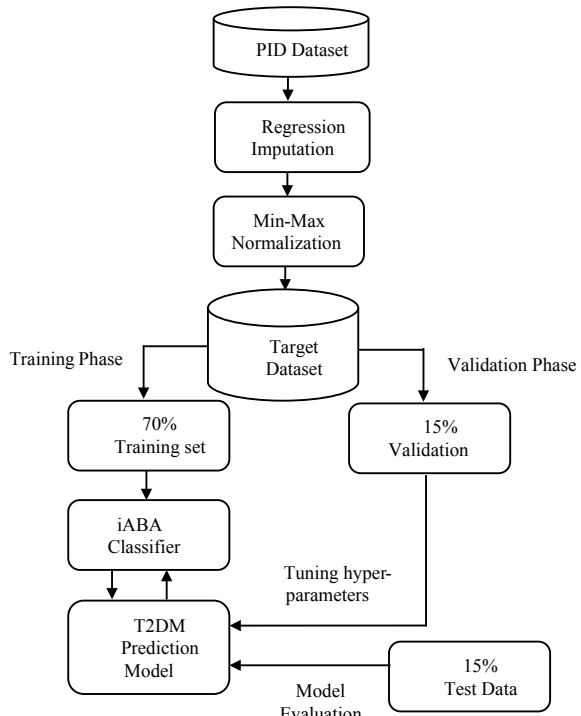
The proposed methodologies consist of primary phases, namely data collection, data pre-processing, development of a T2DM prediction model. In Fig. 1, the general diagram of the system being proposed is shown.

3.1 Dataset Description

The proposed model uses PID dataset [9] as an input for training and validating iABA classifier. The PID dataset is accessed from the UCI machine learning repository. The goal of this proposed work is to determine if a patient has type 2 diabetes mellitus based on risk factors for diabetes. In addition, all of the patients here are females of Pima Indian descent who are at least 21 of age.

This dataset consists of 768 samples, and eight attributes represent the diabetes diagnosis parameters with a single target class that defines the status of each person being examined, such as diabetes presence, diabetes absence. In this dataset, there are 268 positive instances tested, 500 negative instances tested.

Fig. 1 General Schematic diagram of the proposed method for predicting T2DM



3.2 Pre-processing Steps on PID Dataset

Data pre-processing is a technique which transform raw data and enables it suitable for a machine learning model. This is the first and essential step towards building a machine learning model as today's real-world data are extremely susceptible to noisy, inconsistent, incomplete data because of their typically large and also their probable source from different, heterogenous data sources [10].

Low-quality data may cause an inaccurate and poor prediction outcome. Data pre-processing techniques are therefore required to enhance the performance of the training and prediction outcomes. There are several types of data pre-processing techniques available for supervised machine learning [11] such as data cleaning, data normalization, feature extraction and selection of features. Data pre-processing methods are used to make our target dataset more accurate and meaningful for predicting T2DM. Following data pre-processing steps are applied to the PID dataset such as statistical analysis, regression imputation, min–max normalization. The first step in pre-processing is statistical analysis, the second stage in pre-processing is regression imputation and finally data normalization is used as the third step in pre-processing.

Statistical analysis is an approach to analyse the characteristics of PID dataset. This gives a clear insight into the missing data and a range of data values of each attribute. We observed more closely at the attributes of target dataset using statistical analysis and displayed the result in Table 3. It suggested the occurrence of missing values for the attribute's glucose, blood pressure, skin thickness, insulin, BMI as min value is zero for these attributes. According to clinical knowledge that these attributes cannot be a zero, so we conclude that some input values are missed for these attributes.

Missing values in a dataset may decrease the training and prediction results and can yield skewed results which leads to incorrect conclusions [12]. Numerous data imputations methods are proposed by many researchers to impute the missing value. This T2DM prediction model employs a probabilistic model called regression imputation strategy to predict the missing values, and this can beat the disadvantage of deletion method and mean imputation method. This method determines the missing values of an attribute from other attributes by finding relationship between dependent variable y (outcome variable) and independent variable $x = (x_1, x_2, \dots, x_n)$ (input variable). The generic regression imputation works as Algorithm 1.

Data normalization is another data pre-processing method, and the purpose of this normalization method is to alter the numeric column values in the dataset to a standard scale without altering differences in the value ranges; the imputed values therefore fall within a limited defined range of values such as $[0, 1]$ or $[-1, 1]$ after normalization. This will help accelerate the training phase and be useful for rapid convergence. We examined the statistical analysis which reveals data values of many input features are in large range. Therefore, data normalization is required to standardize the dataset. Three key types of data normalization [10] are available like z -score normalization, min–max normalization and decimal scaling normalization.

We used min–max normalization to standardize the dataset, and the mathematical model of min–max normalization is given in Eq. 1. Let X be a feature with n input values, x_1, x_2, \dots, x_N . This method performs linear transformation on the input data and maintains the relationship between the original values of data. Suppose that \min_x and \max_x are minimum and maximum values of a feature, X . Min–max normalization performs linear transformation on value, x_i of feature X to x'_i in the range of values between new_min_x and new_max_x by performing,

$$x'_i = \frac{x_i - \min_x}{\max_x - \min_x} (\text{new_max}_x - \text{new_min}_x) + \text{new_min}_x \quad (1)$$

Algorithm 1 Generic Regression Imputation Algorithm

1. *Input: Array of input variables*
 $x = (x_1, x_2, \dots, x_n)$
2. *Output: Imputation of missing values*
3. *Initialize and load the dataset*
4. *Determine the dependent variable (y_i) and independent variables (x_i)*
5. *Assign missing values as a dependent variable and remaining attribute (except target variable) as an independent variable.*
6. *Calculate line of best fit using the equation*
 - a. y_i : missing value
 - b. x_i : input value
 - c. w : Gradient
 - d. b : y-intercept
7. *Apply least square regression method to calculate Gradient and y-intercept*
8. *Compute Gradient (w) by*

$$w = \frac{N \sum (x_i y_i) - \sum x_i \sum y_i}{N \sum (x_i^2) - (\sum x_i)^2}$$

- $N \rightarrow$ Number of observations
9. *Compute y-intercept(b) by*
$$b = \frac{\sum y_i - w \sum x_i}{N}$$
 10. *Fit the values of w , b , x_i in Line of best fit equation.*

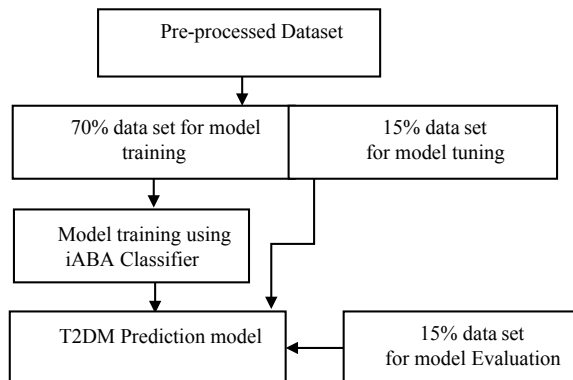
3.3 Classification Modelling Using iABA Algorithm

Classification modelling starts with a target set which is obtained after data pre-processing stage. The classification modelling is a two-step process, involving a training phase (where classifier is constructed to training and learning the parameter of the base classifier) and validation phase (where output of the training phase is evaluated then tuning the hyperparameter of base classifier to enhance the model accuracy). The classification modelling uses iABA classifier for training and validating the processed dataset. iABA is a type of ensemble learning algorithm used to build a strong hypothesis by combining multiple weak models together. The ensemble approach is a machine learning principle that is used to increase the effectiveness and accuracy of machine learning classifiers. In machine learning, there are 2 types of ensemble technique, namely bagging and boosting. Main purpose of these methods is reducing bias and variance from the trained model. iABA utilizes the power of both boosting and bagging by combining random forest as a base estimator in adaptive boosting (Adaboost) algorithm.

iABA is an improved Adaboost algorithm, and iABA enhances the efficiency of T2DM prediction model by tuning the Adaboost classifier and random forest classifier hyperparameters.

The classification modelling process is shown in Fig. 2. It begins with a pre-processed dataset that is obtained after pre-processing steps. The dataset is split into three sets, such as a training set, a validation set, a testing set or a hold-out set. In classification modelling, we have used 70% of the target set for training the classifier, 15% of the target set is used as a validation set which is used to tuning the hyperparameter of the classifiers. Final prediction model is assessed using remaining 15% of target set called test data which will be used when the classification model is completely trained and validated (using training set, validation set). The major focus of this test set is to calculate the actual performance of the diabetes prediction model

Fig. 2 Classification modelling process



to confirm the predictive ability of iABA classifier by comparing the outcomes of iABA classifier with other ML classifiers.

iABA Classifier

iABA classifier is called improved Adaptive boosting algorithm in which Adaboost algorithm is used as a main classifier with random forest classifier (RF Classifier) which is used as a base estimator in Adaboost algorithm. The iABA classifier is built using the training set in this proposed model and enhances the efficiency of the trained model by tuning Adaboost and RF classifier hyperparameters. iABA classifier uses the validation set to get an unbiased estimate of trained model and for tuning the algorithm's hyperparameters. Next, iABA classifier using 15% of test set for evaluating the output of final T2DM prediction model using classification performance metrics. iABA is an improved instance of Adaboost algorithm improves the accuracy of T2DM prediction model and minimize the misclassification of prediction model.

The suggested iABA classifier is built on the adaptive boosting algorithm (ABA), a common boosting technique used to develop predictive models in the type of an ensemble of weak classifiers or hypotheses, typically using decision tree [13]. iABA is mainly used for the purpose of improving prediction accuracy of the classifiers to minimizing a loss function or error rate by tuning the hyperparameters of the trained model. Fundamental idea of ABA classifier is to builds a metamodel in a frontward stage-wise manner by tweaking an arbitrary loss function to increase the power of the classifier or hypothesis, i.e., output of multiple weak models (decision tree) is ensembled to make strong predictive model. Loss function (misclassification rate) is used to evaluate the difference between predicted value and the actual value; having lower loss function in a model indicates our model is able to learn well on training dataset.

Default weak learner (base estimator) of ABA algorithm is decision tree but this proposed iABA classifier uses random forest as a base estimator in ABA algorithm which is found after tuning the hyperparameter of ABA algorithm. Probably have found the optimal parameters of ABA algorithm by checking ABA classifier with a range of decision trees, learning rate and random state for each tree node.

iABA classifier combines multiple random forest classifier (base estimator) with random selection of training set $\mathbf{x}_i = (\mathbf{x}_1, \mathbf{x}_2, \dots, \mathbf{x}_n)$ at each iteration using bootstrapping method, initial weight $w_i = 1/n$ where n is total number of samples in training samples and set of hyperparameters as learning rate (lr), maximum number of base estimators, number of trees in the random forest to get the good accuracy score in final voting. iABA classifier iteratively retrains the RF algorithm by selecting the random training samples and weight based on the classifier accuracy of the previous training. Figure 3 depicts the workflow of iABA classifier.

Tuning the parameters of Adaboost and RF classifier as follows, for each observation, if iABA classifier predicts response variable correctly then weight w_i and learning rate lr are decreased, otherwise w_i and lr are increased when iABA predicted response variable incorrectly. Train and tune the random forest classifier repeatedly using observation with adjusted weights and learning rate until observations predicted perfectly.

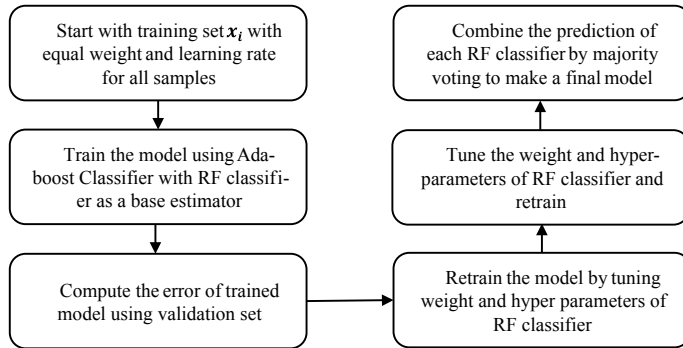


Fig. 3 Workflow of iABA classifier

Random forest [14] is an effective ensemble machine learning classification algorithm that delivers high accuracy due to its robust nature among many classifiers. It is an improved ensemble bagging method of decision tree algorithm to generate model with low variance. It improves the classifier accuracy by reducing the variance and minimize the overfitting issue by creating many single decision trees on the subset of training sample and bagging the output of all single decision trees by applying majority voting function. Random forest model provides good accuracy even there is a missing data in training samples. This classifier generating single decision tree from bootstrap subsampling method which is a statistical re-sampling technique involves random selection of data samples with replacement, and this technique is used for evaluate the uncertainty issue and reducing overfitting with machine learning model. Figure 4 depicts the workflow of random forest classifier.

Steps of random forest algorithm

Step 1

Apply bootstrap sampling method to partition training dataset D into m subset where $m < D$.

Step 2

For each subset m , construct a decision tree which uses Gini index as the attribute selection measure for optimally splitting the attributes to generating the decision tree. Gini index [10] is calculated for each attribute A of m and select the attribute with smallest Gini index to split the node to form a decision tree. Equation (2) defines the mathematical derivation of Gini index.

$$\Delta Gini(A) = Gini(m) - Gini_A(m) \quad (2)$$

where $Gini(A)$ is the Gini index of attribute A of m , $Gini(m)$ is the Gini index of subset sample m which consists of y class label and Eq. (3) expands the Gini index of m a

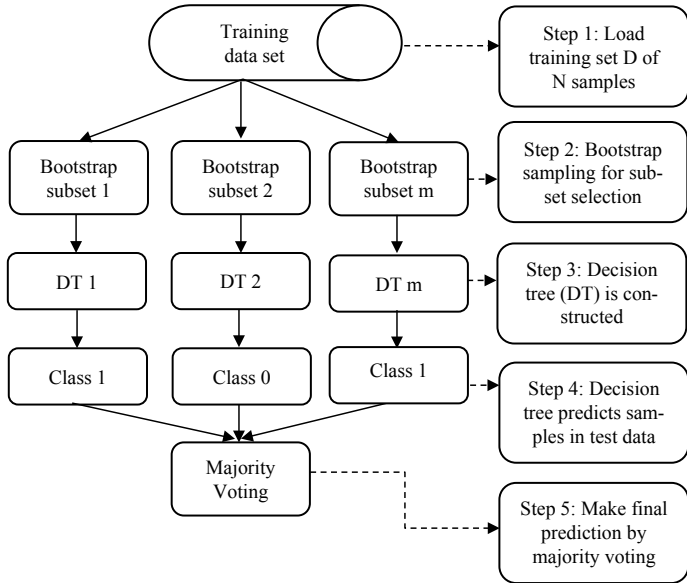


Fig. 4 Workflow of random forest classifier

$$Gini(\mathbf{m}) = 1 - \sum_{j=1}^y p_j^2 \quad (3)$$

where p_j is the relative probability of class j in \mathbf{m} which can be calculated as $p_j = \frac{|c_j, \mathbf{M}|}{|\mathbf{M}|}$ where $|\mathbf{M}|$ implies number of samples in subset \mathbf{m} and $|c_j, \mathbf{M}|$ is the number of class label in \mathbf{m} . If \mathbf{m} is split on attribute A into two subsets \mathbf{m}_1 and \mathbf{m}_2 , $Gini_A(\mathbf{m})$ is defined as in Eq. (4) as

$$Gini_A(\mathbf{m}) = \frac{|\mathbf{m}_1|}{|\mathbf{m}|} Gini(\mathbf{m}_1) + \frac{|\mathbf{m}_2|}{|\mathbf{m}|} Gini(\mathbf{m}_2) \quad (4)$$

n_estimator is the parameter of random forest classifier to determine the number of decision tree generated for each subset \mathbf{m} . Each decision tree is grown to the maximum extent possible without pruning.

Step 3

Individual decision tree predicts the sample in test data set, independently.

Step 4

Apply majority voting function to make final hypothesis on test dataset.

In this proposed iABA classifier, above-explained random forest algorithm is used as the base estimator (weak classifier) to classify and prediction of T2DM among person. In Algorithm 2, the steps of the iABA algorithm are explained in detail.

Algorithm 2 iABA Algorithm.

Input: Training set D which consist of N training samples $D = ((x_1, y_1), (x_2, y_2), \dots, (x_N, y_N))$ and $x_i \in X, y_i \in Y$ is a corresponding class labels or response vector of D associated with x_i . Value of $y \in \{1, 0\}$

Hyperparameters of iABA algorithm:

- **base_learner:** Weak learner used to train the Adaboost classifier. Random forest is selected as a base estimator.
- **n_est:** Count of weak learners to train iteratively.
- **est_rf :** Number of decision trees to be generated for each m .
- **lr_rate:** Setting learning rate of the classifier.
- **r:** Random Vector to construct a decision tree in random forest

Output: hyp_{op} is a final hypothesis with less error rate.

1. Load $D = ((x_1, y_1), (x_2, y_2), \dots, (x_N, y_N))$
2. Initialize weight of data sample: $w_1(i) = \frac{1}{N}$ for all $x_i, i = 1, 2, \dots, N$
3. for $est_ad = 1$ to range do.
4. for $est_rf = 1$ to range do.
5. Generate a vector r with initial weight $w_1(i)$
6. Apply bootstrap sampling on m called s_m
7. Generate decision Tree using $\Delta Gini(A)$ as in Eq. (2) called $dtc_m(s_m, r)$
8. make weak hypothesis hyp_{rf} using majority voting scheme.
9. end for est_{rf}
10. Get Weak hypothesis $hyp_{rf}(x_i) \rightarrow \{1, 0\}$ with $e_w = \frac{\sum(w_x(i)*error_x(i))}{\sum(w_x)}$
11. Calculate and Update the Weight $e_w : e_{w+1}(i)$

$$e_{w+1}(i) = \frac{e_w(i) \exp(-a_w y_i h_{yp_{rf}}(x_i))}{z_w}$$

- where z_w is the normalization constant and a_w is the parameter used to avoid overfitting and increase an algorithm's generalization; Assign $a_w = \frac{1}{2} \ln \left(\frac{1-e_w}{e_w} \right)$
12. end for est_{ad}
 13. Calculate $hyp_{op} = \sin(\sum_{w=1}^w a_w h_{yp_{rf}}(x))$

The iABA classifier tunes the hyperparameter of Adaboost and random forest classifier for improving the classifier prediction accuracy [15]. The hyperparameter of the iABA algorithm is shown in Table 1.

Table 1 Hyperparameter of iABA classifier with default parameter value and optimized parameter value

Proposed classifier	Algorithms used in iABA	Parameter name	Default hyperparameters value	Optimized hyperparameter value of iABA
iABA classifier	Random forest algorithm	<i>est-rf</i>	100	1000
		<i>splitting criterion</i>	Gini index, Entropy	Gini index
		<i>bootstrap</i>	True or False	True
		<i>random_state</i>	None	1
	Adaptive boosting algorithm	<i>base_learner</i>	None	Random forest algorithm
		<i>n_est</i>	50	1000
		<i>lr_rate</i>	1	0.05

4 Experimental Outcomes and Discussions

4.1 Characteristics of PID Dataset

The suggested iABA classifier uses PID dataset to develop T2DM prediction model. The characteristics of PID dataset are given in Table 2.

Table 2 PID dataset characteristics

Dataset	No. of attributes	No. of class label in the target attribute	No. of input samples	No. of missing values
Pima Indian diabetic dataset (PID dataset)	8	2	769	Yes

Table 3 Statistical analysis of PID dataset

Statistical properties	Attributes of PID dataset							
	Preg	Glu	BP	ST	Ins	BMI	Dbf	Age
Samples	768	768	768	768	768	768	768	768
Mean	3.84	120.9	69.10	20.53	79.79	31.99	0.47	33.24
SD	3.36	31.97	19.35	15.95	115.24	7.88	0.33	11.76
Min. val	0.00	0.00	0.00	0.0	0.0	0.00	0.078	21.00
25%	1.00	99.00	62.00	0.0	0.00	27.3	0.2	24.00
50%	3.00	117.0	72.0	23.00	30.5	32.00	0.37	29.00
75%	6.00	140.2	80.00	32.00	127.25	36.60	0.62	41.00
Max. val	17.00	199.0	122.0	99.00	846.0	67.10	2.42	81.00

The detail description of input attributes of PID dataset are as follows:

- Number of times of pregnancy (Preg)
- Plasma glucose concentration at 2 h in the oral glucose tolerance test (Glu)
- Diastolic blood pressure (BP)
- Triceps skin fold thickness (ST)
- Serum insulin for two hours (Ins)
- Body mass index (BMI)
- Diabetes pedigree function(dbf)
- Participant age (Age)
- Target class variable as either 0 or 1 (Outcome).

4.2 Experimental Result of Statistical Analysis

Table 3 shows an outcome of statistical analysis.

4.3 Experimental Result of Regression Imputation

PID dataset consists of 8 diabetic disease predictor attribute, and details are given in Table 1. Out of these 8 predictors, 5 predictors consist of missing values which are blood pressure, glucose, skin thickness, insulin, BMI. Table 4 describes the missing value details of predictor attribute of PID dataset and total count of missing value is 376. From the statistical analysis, we found PID dataset has more than 45% missing values. So, deleting missing rows is not a good method for handling the missing value as this may lead to a biased result.

This proposed T2DM prediction model uses generic regression imputation algorithm to handle these missing values for avoiding biased prediction and improving accuracy of the proposed classifier. The output of various machine learning algorithms is evaluated before applying regression imputation algorithm and after applying regression imputation algorithm to the PID dataset, the results are shown in Table 5.

Table 4 Missing value details of PID dataset

Predictor attribute	Count of missing value
Glucose	5
BP	35
ST	227
Ins	374
BMI	11

Table 5 Classifier accuracy of ML classifier on PID dataset before and after applying regression imputation

Machine learning algorithms	Before applying regression imputation	After applying regression imputation
Support vector machine	75	76
Logistic regression	74	76
Random forest	73	77
Gradient boosting	73	76

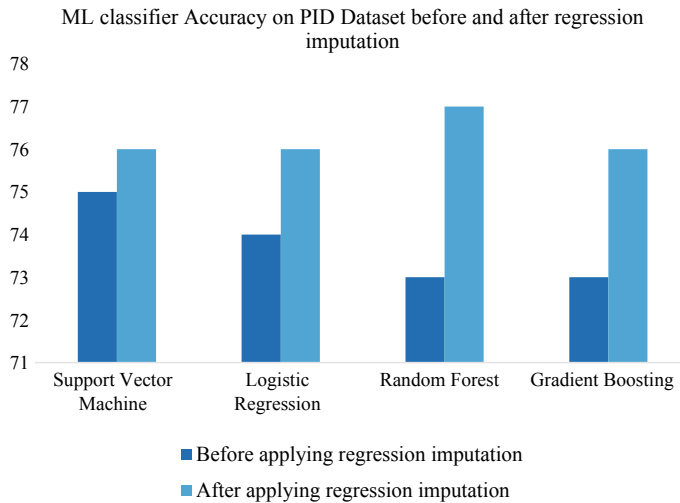


Fig. 5 Visual comparison of various ML classifier accuracy before and after applying regression imputation algorithm on PID dataset

The information present in above table is visually depicted in Fig. 5 to recognize the impact of regression imputation.

4.4 Experimental Result of iABA Classifier and Performance Comparison

Eight risk factors of diabetic disease (predictor attribute) and one binary target attribute (with 2 classes) of PID dataset are used as an input for the proposed iABA classifier after data pre-processing. Three-way split [16] is applied on pre-processed PID dataset for building T2DM prediction model, this method separate processed dataset into three subsets –70% of processed data is used for training the T2DM

Table 6 Performance evaluation metrics

Metrics	Definition	Formula
Acc	It is a ratio of the total number of correct predictions to the total number of input samples	$\text{Acc} = \frac{\text{Number of Accurate Predictions}}{\text{Overall input samples}}$
MCR	The ratio of the number of observations incorrectly to the total input samples	$\text{MCR} = 1 - \text{Classifier Accuracy}$
Sen	It is a ratio of the number of true positives to the total number of true positives and false positives	$\text{Sen} = \frac{\text{TP}}{\text{TP} + \text{FP}}$
Spe	It is a ratio of the number of true negatives to the total number of true negatives and false positives	$\text{Spe} = \frac{\text{TN}}{\text{TN} + \text{FP}}$
Pre	It is calculated from dividing true positives by the total true positives and total false positives	$\text{Pre} = \frac{\text{TP}}{\text{TP} + \text{FP}}$
ROC	This curve is plotted with True positive rate (TPR) against false positive rate (FPR)	$\text{TPR} = \frac{\text{Total True Positives}}{\text{Total positive samples}}$ $\text{FPR} = \frac{\text{Total False Positives}}{\text{Total negative samples}}$
F1	It is the average of the precision and recall. The range of F1 score is from 0 to 1	$\text{F1} = \frac{\text{Precision} * \text{Recall}}{\text{Precision} + \text{Recall}}$
MCC	It is used to measure the quality of prediction model using the given formula	$\text{MCC} = \frac{\text{TP} * \text{TN} - \text{FP} * \text{FN}}{\sqrt{(\text{TP} + \text{FP})(\text{TP} + \text{FN})(\text{TN} + \text{FP})(\text{TN} + \text{FN})}}$

TP—True positives samples; *TN*—True negative samples; *FP*—False positive samples; *FN*—False negative

model, 15% of processed data is used for validating and tuning the hyperparameters of iABA classifier and 15% of processed dataset called test dataset are used for evaluating the performance of final model. The output of final T2DM prediction model is evaluated using different classifier performance metrics and compared to existing machine learning models such as support vector machine, logistic regression, Adaboost algorithms and gradient boosting algorithms. The performance of the proposed method iABA classification algorithm is compared with various ML model on the basis of classifier performance metrics [17, 18].

The performance measures of iABA classifiers are defined in Table 6.

The outputs of the iABA classifier are shown in Table 7 and in Fig. 6.

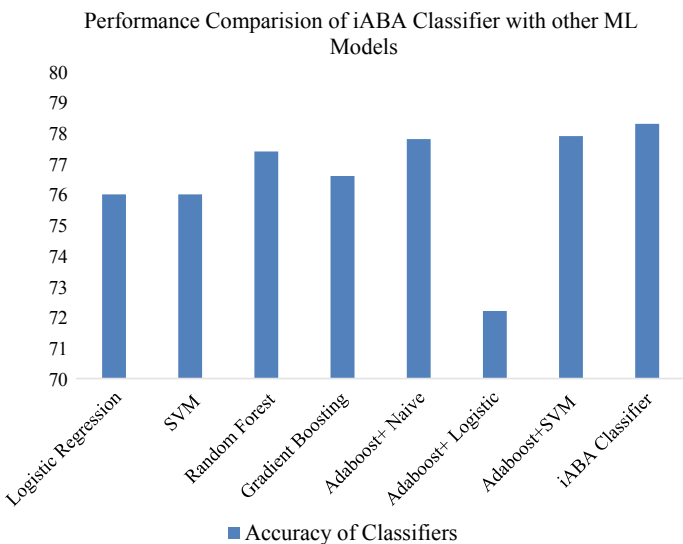
4.5 Analysis of Experimental Result

The proposed model iABA classifier is tested on diabetes datasets, namely Pima Indian Diabetes dataset. The output of this proposed classifier (iABA Classifier) is analysed using eight performance metrics as classifier accuracy, misclassification

Table 7 iABA Classifier performance compared on PID Dataset with other ML models

ML models	Acc	MCR	Sen	Spec	Prec	ROC	F1	MCC
LR	76	0.23	0.59	0.85	0.70	0.85	0.64	0.47
SVM	76	0.23	0.51	0.57	0.72	0.845	0.64	0.47
RF	77.4	0.22	0.65	0.84	0.70	0.84	0.67	0.50
GB	76.6	0.233	0.72	0.78	0.66	0.837	0.69	0.50
AB + NB	77.8	0.22	0.66	0.82	0.69	0.845	0.67	0.50
AB + LR	72.2	0.27	0.47	0.87	0.67	0.85	0.55	0.38
AB + SVM	77.9	0.22	0.58	0.89	0.75	0.852	0.65	0.50
iABA	78.3	0.21	0.64	0.86	0.72	0.87	0.68	0.52

Acc—Classifier Accuracy; *MCR*—Misclassification rate; *Sen*—Sensitivity; *Spe*—Specificity; *Prec*—Precision; *ROC*—Receiver operating characteristic curve; *F1*—F1 score; *MCC*—Matthew's correlation coefficient

**Fig. 6** Output comparison of iABA classifier with other ML models

rate, sensitivity, specificity, precision, ROC curve score, *F1* score, Matthew's correlation coefficient and comparative analysis is made with other ML models such as logistic regression, support vector machine, random forest, Gradient boosting algorithm, Adaboost with Naïve Bayes algorithm, Adaboost with logistic regression, Adaboost with support vector machine. From Table 7, we noticed that the proposed iABA classifier gives good accuracy score on training set and validation set than other ML classifiers on PID dataset in terms of various performance measures. Figure 6 is useful for visually understand the high accuracy of iABA classifier, and this score is compared with other ML algorithms. These findings are helpful in recognizing that

the proposed classifier capable of distinguishing positive and negative samples. But there is some type-I (False Positive), and type-II (False Negative) error exists in the proposed classifier.

Figure 6 shows an accuracy score of iABA classifier on PID dataset, and score is 78.3 which is higher than other compared ML models. This proposed model uses training data to learn the hyperparameter and used to train the model, utilizes validation set for tuning the hyperparameter of the built classifier and evaluates the functioning of the final T2DM model on new test dataset which is independent of training set. From Fig. 6, we conclude that the proposed classifier (iABA) has good accuracy score, MCC score than other classifier and well suited to classify the new diabetic disease data samples. From this classifier performance analysis, we propose that iABA classifier is able to well predict the occurrence of diabetic disease in a patient.

5 Conclusion

In this context, we have proposed an efficient automated diabetic disease diagnosis system for diagnosis of Type 2 diabetes mellitus (T2DM). Generic regression imputation algorithm is used for imputing the missing values in the PID dataset. Improved adaptive boosting Algorithm (iABA) was further suggested by combining the benefits of Adaboost classifier and the random forest classifier with hyperparameters tuning to increase the predictive accuracy of the diabetic prediction model. The result of the experiment illustrates that the suggested iABA model provides better result than other compared ML models on the PID dataset. This suggested approach achieves 78.3% model accuracy, 21% misclassification rate, 0.64 sensitivity, 0.86 specificity, 0.72 precision, 0.75 ROC, 0.68 F1-score and 0.52 MCC score. Sensitivity and specificity of this T2DM model are not strong, and this could be improved by implementing automated hyperparameter tuning algorithms such as grid search, random search [19] by expanding this proposed algorithm.

References

1. Accessed from the IDF diabetes atlas, 9th edn. Available <https://www.diabetesatlas.org/en/>
2. Juutilainen A, Kortelainen S, Lehto S, Rönnemaa T, Pyörälä K, Laakso M (2004) Gender difference in the impact of type 2 diabetes on coronary heart disease risk. *Diabetes Care* 27(12):2898–2904
3. Gale EA1, Gillespie KM (2001) Diabetes and gender. *Diabetologia* 44(1):3–15
4. Jegan C (2013) Classification of diabetes disease using support vector machine. *Int J Eng Res Appl* 3:1797–1801
5. Sivakumar S, Venkataraman S, Bwatiramba A (2020) Classification algorithm in predicting the diabetes in early stages. *J Comput Sci*

6. Motka R, Parmarl V, Kumar B, Verma AR (2013) Diabetes mellitus forecast using different data mining techniques. In: 2013 4th International conference on computer and communication technology (ICCCT), Allahabad, pp 99–103
7. Sisodia D, Sisodia DS (2018) Prediction of diabetes using classification algorithms. *Procedia Comput Sci* 132:1578–1585
8. Edla DR, Cheruku R (2017) Diabetes-finder: a bat optimized classification system for type-2 diabetes. *Procedia Comput Sci* 115:235–242
9. Blake CL, Merz CJ (1998) UCI Repository of machine learning databases. University of California: Irvine, CA. <https://www.ics.uci.edu/~mlearn/MLRepository.html>
10. Han J, Pei J, Kamber M (2011) Data mining: concepts and techniques. Elsevier
11. Kotsiantis SB, Kanellopoulos D, Pintelas PE (2006) Data preprocessing for supervised learning. *Int J Comput Sci* 1(2):111–117
12. Kang H (2013) The prevention and handling of the missing data. *Korean J Anesthesiol* 64(5):402
13. Freund Y, Schapire RE (1997) A decision-theoretic generalization of on-line learning and an application to boosting. *J Comput Syst Sci* 55(1):119–139
14. Breiman L (2001) Random forests. *Mach Learn* 45(1):5–32
15. Khan F, Kanwal S, Alamri S, Mumtaz B (2020) Hyper-parameter optimization of classifiers, using an artificial immune network and its application to software bug prediction. *IEEE Access* 8:20954–20964
16. Reitermanov'a Z (2010) Data splitting. In: WDS'10 Proceedings of contributed papers, Part I, pp 31–36. Copyright MatfyzPress
17. Hossin M, Sulaiman MN (2015) A review on evaluation metrics for data classification evaluations. *Int J Data Mining Knowl Manage Process* 5(2):1
18. Chicco D, Jurman G (2020) The advantages of the Matthews correlation coefficient (MCC) over *F1* score and accuracy in binary classification evaluation. *BMC Genom* 21(1):6
19. Feurer M, Hutter F (2019) Hyperparameter optimization. In: Automated machine learning. Springer, Cham, pp 3–33

Kardex: Platformer



Santiago Jones, Susana Flores, Claudia Torrero, Lamia Hamdan, Everardo Torrero, and Silvana Flores

Abstract The videogame industry has reported significant growth, generating worldwide sales of more than \$120 trillion in 2019. Starting from the point of view that developing a videogame industry can help the economic growth of a country a videogame was implemented. The methodologies on which the implementation was based were Chandler's four-step videogame creation methodology, the agile Scrum methodology and the Unified Process development. The development tools used were Blender and Unity in their free version. The use of these tools in conjunction with the methodologies allowed to achieve a first version of the videogame in the estimated time and at a low cost, with a small team.

Keywords Platformer videogame · Software engineering · Unity · Blender

1 Introduction

The videogame industry has significant growth worldwide, generating sales of \$120.1 trillion in 2019, of which \$64.4 trillion was spent on mobile gaming, \$29.6 trillion for PCs, and \$19.4 trillion to purchase console games [1]. Videogames have dabbled in daily life, finding applications for education, work, learning, socialization, fun, all thanks to the advancement of technology, which has allowed people like applications to be developed, as well as allowing them to make their own designs [2]. The twentieth century was the point that marks innovations in the way we make radio, music, film and television born the interactive industry in these entertainment companies, largely by the use of Information and Communications Technologies [3]. In this way, a videogame is narrative, interactivity and play [4].

S. Jones · S. Flores (✉) · C. Torrero · L. Hamdan · S. Flores
Tecnológico Nacional de México/Instituto Tecnológico de La Laguna, Torreón, Coah 27000,
México
e-mail: msfloresa@correo.itlaguna.edu.mx

E. Torrero
MAQTEC, Gómez Palacio, Dgo 35060, México

The existence of work structures, software tools to produce low-level computing code, and proprietary structures that enable you to manage visualization, physics, and artificial intelligence for different applications across multiple platforms and digital devices, enable videogame designers, artists, and programmers to realize their graphic design practices [5]. In the case of videogame construction, its development by small businesses and individual developers benefited from companies such as Epic Games, Unity and Crytek, among others, releasing their game building platforms at low prices and even for free; allowing small companies, students or individual developers to produce innovative, high quality videogames without investing large amounts of money and short time lapses [3, 5]. Since mid-2000, Unreal and Unity have monopolized the production of videogames made by professional or inexperienced teams, which Kirpatrick [6] cited in [5], criticizes, arguing that game engines conduct and standardize the craft of videogames, as well as containing “potentially disruptive or unwanted commercial uses of computer technologies” [5], in addition to which genres and games are linked to graphics engines. In the case of intellectual property Bogost [7] cited in [5] indicates that graphics engines are essentially intellectual property as owners of game extensions and materially as software tools. In contrast John Banks [8] quoted in [5] describes in his study of the SAGE machine, that graphic engines are “participate in parallel way in of creativity” and innovation.

2 Methodology

The making of a videogame unlike a traditional software application involves designers, story counters, graphic animators, artificial intelligence specialists, video producers, stage makers, sounds, marketing and salespeople, in addition to all these people, the staff who are in charge of the functional programming of the application [2, 4].

Videogames have been created using traditional Software Engineering methodologies, methodologies such as the Water Fall Process, the Rational Unified Process (UP), OpenUP, Team Software Process, Microsoft Solution Framework, have been analyzed; other researchers have modified Scrum to develop videogames and others report using Agile Methodologies for their construction [5, 8, 9, 10].

The wide range of professional actors involved in the development of a videogame, the digital revolution that has been embedded in the art industry, creating other forms of business models, value chain, distribution methods and in terms of creative processes the art form and consumption practices [6] creates a challenge to the traditional Software Engineering process. Some studies since 2010, conducted by Hendrick, Blitz Game Studio, McGrath, Chandler, and Ramadan and Widyani have proposed Game Development Software Engineering (GDSE); a videogame development process [2]. The life cycle of the GDSE process consists of three main moments: preproduction, production and postproduction (Fig. 1), which are approached differently by several videogame creators including: (a) Blitz game studios, which proposed six phases for the GDSE lifecycle: (1) initial design and game

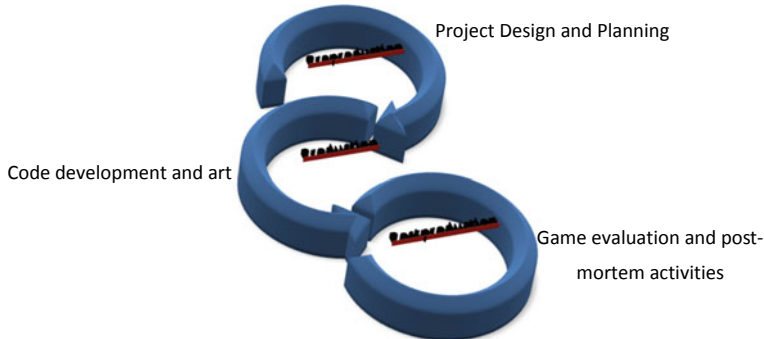


Fig. 1 Life cycle for the construction of a videogame

concept, (2) documentation of videogame design, (3) Implementation of the game concept, (4) internal game testing, (5) external testing, (6) game release; (b) Hendrick with five phases: (1) Initial prototype design, (2) Documentation, (3) Creation of assets, code and integral aspects, (4) user reception, (5) ready to play; (c) McGrath: (1) initial videogame documentation and design, (2) videogame development, (3) videogame evolution, (4) internal videogame testing, (5) external testing, (6) game release; (d) Chandler with four stages: (1) project design and planning, (2) code and art development, (3) game evaluation, (4) post mortem activities [2].

The decision was made to use the four stages established by Chandler, as it fits more into the development of the game, in addition to Evelin Espinal and Flor Huisa using it in the development of the videogame Vermillon, giving results in short times [3].

Chandler's proposal was complemented by Agile Methodologies, as, according to Casal Martínez, the adoption of Agile Methodologies in a software development team had a positive effect creating satisfaction both at the management level and in the team [6]. In another study presented by Flores et al., the quality and productivity of small working groups in the development of higher education projects were increased by using Agile Methodologies in particular Scrum for monitoring projects and reacting when they did not have adequate progress [11]. For the time of programming coding and to have a way to track it, the Unified Process development was used to document the programming part of the game.

3 Software Tools

Free open-source tools were used for the development of the game. One of them is Blender, a graphic engine to be used by small teams, but with enough tools to get high quality animations. It is a tool that its functionality can be modified and extended, although with the features that it has you can perform powerful simulations such as

bullets and water, it contains a basic and efficient video editor, a flexible interface and advanced rendering [12].

Major computer graphics engine companies such as Unity, Epic Game and Cryengine, among others, specializing in 2D, 3D, virtual reality and augmented reality, have released their applications, allowing individual developers and small groups to perform high quality applications in short times. Unity has a free app that can be used by students and personally developers. In the case of CryEngine, it allows the use of its graphics engine at no cost, applying 5% to royalties to the shipment of the project. The first \$5 K of annual royalties per project is free. Unreal Engine is completely free, only Epic Games charges 5% royalties for videogames that enter at least \$3,000.00 USD each quarter [13–15]. Unity has extensive tools that facilitate the development of console games, for mobile and computer, has the advantage of being aimed at people with small businesses and having an easy to adapt structure. For individual developers, for small companies and students, it has a free use version, being able to run on computers with minimum requirements of 4 core processors, 8 gigabyte memory, graphics card with Dx9, Windows operating systems from version 7 of 64 bit. In addition to being a company that does not charge royalties for the sale of products built with its graphics engine.

4 Results

Support in Chandler's methodology guided the work that was done. The steps Chandler proposes are described in this section, supported by Agile Methodologies and the Unified Process development.

4.1 *Preproduction*

One of the games that served as inspiration was Undertale. It is a game built by a single person, in the game you do not need to kill someone, each enemy can be defeated in a nonviolent way. The support points were (1) how to dodge enemy attacks, (2) the area and time when it dodges attacks, (3) the multiple routes and goals contained in the story. Another game that was inspired was Megamax's Super Max Adventure. This game is platform and was taken into account: (1) the introduction of the first level, (2) the ability to choose the level order (future work) (3) the character's actions (shoot, scale, dodge) [16, 17].

The story of the game focuses on a robot appearing and researching what is happening where it is. Its objective in each level is to overcome the obstacles that arise in the level. The robot counts for its survival with an energy bar, which can reach extremely low or very high temperatures; when reaching these temperature values, the game ends and returns to the last checkpoint.

Table 1 Backlog of the 1st Sprint

Pending	Priority
	Design
Story	High
Design the appropriate level	High
Level design	Medium
Plan the scenarios	Medium

4.2 Production

At this stage, Scrum and the Unified Process development were used to organize the construction of the game. The results obtained are presented in the following sections.

Sprint 1 To organize the first Sprint, several pending was identified: the design, characters and structure of the game, priorities were set, assignment of task managers, and review of task progress. Table 1 shows the estimate of the pending of the 1st Sprint.

Sprint 1 Results

As planned in Sprint 1, the following results were obtained.

History. You have a mysterious laboratory controlled by several people. The robot appears, ready to investigate and traverse the level, dodging the attacks, traps, and puzzles to which it will be subjected on the course.

Level design. Level 1 was performed on Blender. Figure 2 shows the level, which consists of a giant fan, pistons moving vertically, small spaces to pass, electric traps, climbing walls and a riddle that the player must guess to continue or end in the game.

Scenario planning. The game will be in two dimensions, with three-dimensional objects. It has obstacles that must be avoided with the functions of running and jumping, puzzles are used to advance on objects that stand in the way. The level

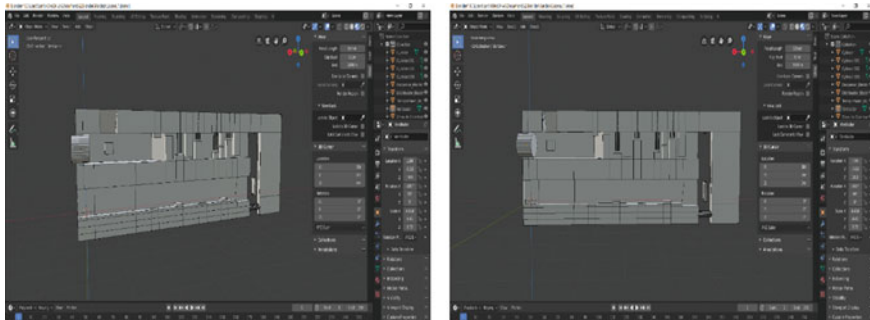


Fig. 2 Game scenario designed in Blender

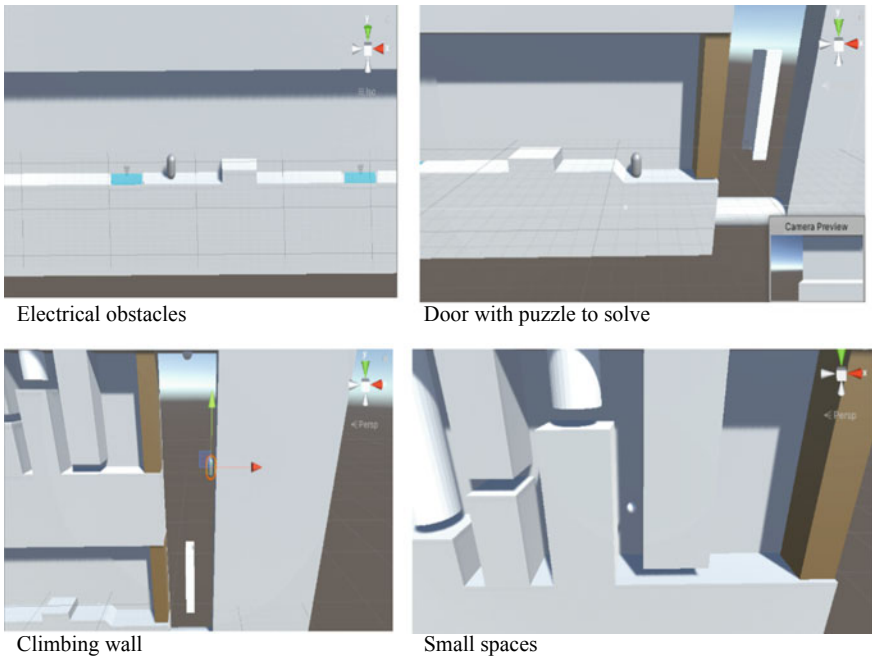


Fig. 3 Various obstacles

consists of two platforms, so to get to the second one you will have to scale. On the way to travel, you will find small spaces, so you will have to resize to be able to pass those places. A fan was introduced from which hot air emanates and to pass it you will have to change the temperature. Figure 3 shows some of these objects.

Position of the character at the beginning of the game. The avatar is located at the beginning of the level, without any obstacles around. Obstacles will appear until you perform the basic functions: run, jump, attack, become small, and change temperature.

Selection of the appropriate gender. A combination of action game, platform game and shooting game was selected.

Character control. The character was programmed horizontal movements to the right and left, vertical, in addition to wall scaling, ability to change size, temperature change to hot or cold mode, this change is associated with a temperature bar, which can indicate the temperature of the avatar.

Creating obstacles. Several obstacles were created: a ray of light (laser), sensors for the movement of platforms when pressed, electric traps which electrocute the player.

Sprint 2 Once level 1 design was completed, videogame programming began, where it was determined to use Unity, Visual Studio, and the Unified Process development to create flexible, clean, and easy to modify code.

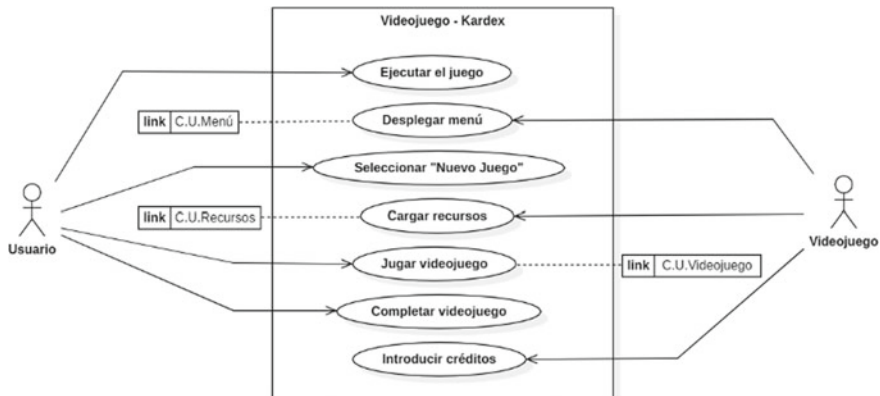


Fig. 4 Business use case diagram

Sprint 2 Results

In this sprint, the risks to complete the programming of the game code were analyzed and identified, pending only to avoid being hacked, its functionality, usability, reliability, performance, support, design and implementation and packaging was identified.

Unified Process. It is a case focused methodology, Fig. 4 shows the game use case diagram. In addition to this diagram and the detailed description of each use case, interaction, class, and application status diagrams were developed. Help was the organization of the classes that were in the development of the game.

5 Conclusions

The realization of a quality videogame, low cost and in a short time today, has become a less arduous task for those interested in this type of development, thanks to the release of graphics engines of large companies, such as Unity company; in the programming aspect, the Microsoft Visual Studio development environment; and for the design of 2D and 3D artifacts, the Blender application.

Another aspect to consider in order to come up with an attractive end product was the management and guidance of Chandler's videogame methodologies, the Scrum methodology, an agile methodology widely used in software creation houses, and the Unified Process development to document and organize application code programming.

Several remaining, related to the last stages pointed out by Chandler, which have had to be modified in view of the events of the pandemic by COVID and which have changed normality in society. However, actions are already being implemented to complete these stages.

References

1. Nielsen Company, «SUPERDATA,» Nielsen Company (2019) [En línea]. Available <https://www.superdataresearch.com/reports/2019-year-in-review>. Último acceso 03 Jan 2020.
2. Aleem S, Capretz y LF, Ahemed F (2016) Game development software engineering process life cycle: a systematic review. *J Softw Eng Res Dev* 4:1–30
3. Rabowsky B (2009) Interactive entertainment; a videogame industry guide. Radiosity Press, Oxnard, CA
4. Esposito N (2005) A short and simple definition of what a videogame is. In: de DIGRA 2005 changing views: WORLD IN PLAY 2005 international conference, Finlandia
5. Nicoli B (2018) Game engines: design, labour, and legality. In: de DIGRA international conference: the game is the message, Italy Turin
6. Kirkpatrick G (2013) Computer game and the social imaginary. Polity Press, Cambridge, UK
7. Bogost I (2010) Unit operations: an approach to videogame criticism. The MIT Press, Georgia, US
8. Banks J (2013) Co-creating videogames. Bloomsbury Publishing Pic, London
9. Torres C, Ferreyros MA, Festini Wendorff y PN, Juárez S (2016). Developing a videogame using unreal engine on a four stages methodology. In: de 2016 IEEE ANDESCON, Arequipa, Perú
10. Schwaber K (2004) Agile project management with scrum. Microsoftpress, USA
11. Flores S Torrero C, Torrero E, Hamdan y L, Flores S (2019) Software engineering methodologies for the evaluation and monitoring of projects of higher education. In: de Software engineering methodologies for the evaluation and monitoring of projects of higher education students. Springer, Saint Petersburg, Russia, pp 1–10
12. Blender. About [En línea]. Available <https://www.blender.org/about/>
13. CRYENGINE (2020) Achieve your vision. CRYtek [En línea]. Available <https://www.cryengine.com/#>. Último acceso 01 Sept 2020
14. Epic Game (2020) Unreal engine [En línea]. Available <https://www.cryengine.com/#>. Último acceso 01 Sept 2020
15. Unity Technologies (2020) Planes y precios [En línea]. Available https://store.unity.com/es/?_ga=2.27576700.1344036484.1603144153-1781157679.1592237123#plans-individual. . Último acceso 01 Sept 2020
16. Undertale, «Undertale,» Undertale, 2020. [En línea]. Available: <https://undertale.com/about/> . Último acceso 10 Jan 2020
17. AR (2020) APKPURE [En línea]. Available <https://apkpure.com/ar/super-max-adventure-action-platform-game/com.gamess.Super.max.boy.world>. [Último acceso: 12 01 2019].
18. Hallisey B (2012) Building a virtual world: the pipeline and process. *Computer* 45(12):90–92
19. Acerenza N, Coppes D, Mesa G, Viera A, Fernandez E, Laurenzo y T, Vallespir D (2009) Una Metodología para el Desarrollo de Videojuegos. In: de 38o JAIIO Simposio Argentino de software (ASSE 2009). BUenos Aires, Argentina
20. Morales Urrutia GA, NAva López CE, Fernández Martínez y LF, Rey Corral MA (2010). Procesos de Desarrollo para Videojuegos. In *CulCYT*, vol. 7, nº 36/37, pp 25–39
21. Casal Martínez J (2019) Implementación de Metodologías Ágiles en un Equipo de Desarrollo de Software. Universidad de Valladolid, Valladolid, España

Automatic Generation Control of Multi-area Multi-source Deregulated Power System Using Moth Flame Optimization Algorithm



**B. V. S. Acharyulu, Tulasichandra Sekhar Gorripotu, Ahmad Taher Azar,
Banaja Mohanty, Ramana Pilla, Sandeep Kumar, Fernando E. Serrano,
and Nashwa Ahmad Kamal**

Abstract In this paper, a novel nature motivated optimization technique known as moth flame optimization (MFO) technique is proposed for a multi-area interrelated power system with a deregulated state with multi-sources of generation. A three-area interrelated system with multi-sources in which the first area consists of the thermal and solar thermal unit; the second area consists of hydro and thermal units. The third area consists of gas and thermal units with AC/DC link. System performances

B. V. S. Acharyulu

Department of Electrical and Electronics Engineering, Lendi Institute of Technology and Management, Srikakulam, Andhra Pradesh 532402, India

T. S. Gorripotu

Department of Electrical and Electronics Engineering, Sri Sivani College of Engineering, Srikakulam, Andhra Pradesh 532402, India

A. T. Azar

College of Computer and Information Sciences, Prince Sultan University, Riyadh, Saudi Arabia

Faculty of Computers and Artificial Intelligence, Benha University, Banha, Egypt

A. T. Azar

e-mail: aazar@psu.edu.sa; ahmad.azar@fci.bu.edu.eg

B. Mohanty

Department of Electrical Engineering, Veer Surendra Sai University of Technology, Burla, Odisha 768018, India

R. Pilla

Department of Electrical and Electronics Engineering, GMR Institute of Technology, Rajam, Srikakulam, Andhra Pradesh 532127, India

e-mail: ramana.pilla@gmrit.edu.in

S. Kumar (✉)

CHRIST (Deemed to be University), Bangalore, Karnataka 560074, India

F. E. Serrano

Universidad Tecnologica Centroamericana (UNITEC), Tegucigalpa, Honduras

e-mail: feserrano@unitec.edu; serranofer@eclipso.eu

N. A. Kamal

Faculty of Engineering, Cairo University, Giza, Egypt

with various power system transactions under deregulation are studied. The dynamic system executions are compared with diverse techniques like particle swarm optimization (PSO) and differential evolution (DE) technique under poolco transaction with/without AC/DC link. It is found that the MFO tuned proportional-integral-derivative (PID) controller superior to other methods considered. Further, the system is also studied with the addition of physical constraints. The present analysis reveals that the proposed technique appears to be a potential optimization algorithm for AGC study under a deregulation environment.

Keywords Automatic generation control (AGC) · Generation rate constraint (GRC) · Moth flame optimization (MFO) · Proportional-integral-derivative controller (PID) · Disco participation matrix (DPM)

1 Introduction

Modern power systems are aimed at reformatting systems, and a deregulated promotion process is adopted. The deregulated power system has a generation corporation (GENCO), transmission corporation (TRANSCO), distribution corporation (DISCO), and an independent system operator (ISO). The ISO plays the role of providing secure and stable action of a power system, for which several auxiliary services are provided. One of the auxiliary examinations is the frequency regulation of the power system. Frequency regulation of a system is arising from the idea of load frequency control (LFC). The detailed discussions of LFC after deregulation are discussed in [1–3]. Many authors in the literature have reported LFC's problem under a deregulated environment [4–6], considering the thermal hydro scheme with an integral (I) controller optimized with various optimization techniques. In [7], the authors have presented a bacterial foraging optimization method to optimize the fractional-order PID controller for different area thermal schemes under the deregulated system. In [8], classical controllers are tuned with a minority charge carrier inspired (MCI) algorithm under the deregulation scheme with comparative analysis. In [9], the proportional-integral (PI) controller has been recommending a deregulated scheme with AC/DC link.

Foremost in the deregulated situation, multi-sources of generation are considered for AGC study [10]. In [11], the authors have proposed a hybrid differential evolution-pattern search (hDE-PS) optimized modified integral derivative (MID) controller for the deregulated system. Mohanty et al. have suggested fruit fly optimization (FOA)-based classical controllers tuned through under deregulation scenario with AC/DC link [12].

Recent studies [13–16] have suggested an AGC scheme integrating solar thermal power plant (STPP) in one area of the conventional AGC system. From the literature, it is observed that there is no much analysis on incorporating STPP in a deregulated AGC system. Hence, a deregulated system with multi-sources incorporating STPP

is analyzed. For improvement in system performances and to damp out oscillations, AC/DC link is included in the AGC system.

In AGC literature, different intelligent techniques are proposed for optimizing various controllers [17–20]. Mirjaili [21] recently developed a novel nature motivated intelligent optimization method called moth flame optimization (MFO). This technique depends upon the navigation scheme of the moth in the environment. Moths can travel in direct line for extended distances efficiently. The advantages of this technique are easy, simple to understand, and simplicity of execution. This technique cracks good demanding problems [22].

2 Investigated AGC in a Deregulated Environment with AC/DC Link

In a restructured power system, the intimation signals must pass from the DISCOs to the particular GENCOs to match the distribution and the generation of powers. It can be easily understood with the help of the disco partition matrix (DPM). In the DPM, the number of rows represents the quantity of GENCOs, and the number of columns represents the number of DISCOs of the scheme. The addition of all admissions of a column in the matrix is one.

To carry out the investigation, a three unequal area deregulated system is considered. Each area has 2 GENCOs and 2 DISCOs. Area 1 is having thermal, solar thermal, second area having hydrothermal, and while in third area gas-thermal GENCOs. The linearized three unequal areas model is represented in Fig. 1. The system DPM matrix is specified by

$$\text{DPM} = \begin{bmatrix} \text{cpf}_{11} & \text{cpf}_{12} & \text{cpf}_{13} & \text{cpf}_{14} & \text{cpf}_{15} & \text{cpf}_{16} \\ \text{cpf}_{21} & \text{cpf}_{22} & \text{cpf}_{23} & \text{cpf}_{24} & \text{cpf}_{25} & \text{cpf}_{26} \\ \text{cpf}_{31} & \text{cpf}_{32} & \text{cpf}_{33} & \text{cpf}_{34} & \text{cpf}_{35} & \text{cpf}_{36} \\ \text{cpf}_{41} & \text{cpf}_{42} & \text{cpf}_{43} & \text{cpf}_{44} & \text{cpf}_{45} & \text{cpf}_{46} \\ \text{cpf}_{51} & \text{cpf}_{52} & \text{cpf}_{53} & \text{cpf}_{54} & \text{cpf}_{55} & \text{cpf}_{56} \\ \text{cpf}_{61} & \text{cpf}_{62} & \text{cpf}_{63} & \text{cpf}_{64} & \text{cpf}_{65} & \text{cpf}_{66} \end{bmatrix} \quad (1)$$

“The cpf stands for a contract participation factor.”

The demand for power by individual DISCOs is explained in [12]. For the design of the PID controller, three main parameters, proportional gain (K_P), integral gain (K_I), and derivative gain (K_D), are determined. Different controllers are considered for different GENCOs, so parameters of the PID controller are $K_{P1}; K_{P2}; K_{P3}; K_{P4}; K_{P5}; K_{P6}; K_{I1}; K_{I2}; K_{I3}; K_{I4}; K_{I5}; K_{I6}$; and $K_{D1}; K_{D2}; K_{D3}; K_{D4}; K_{D5}; K_{D6}$.

In the present examination, the integral square error (ISE) is taken as the objective function represented as Eq. (2) as this objective function is considered in many works of literature [7, 12, 13]

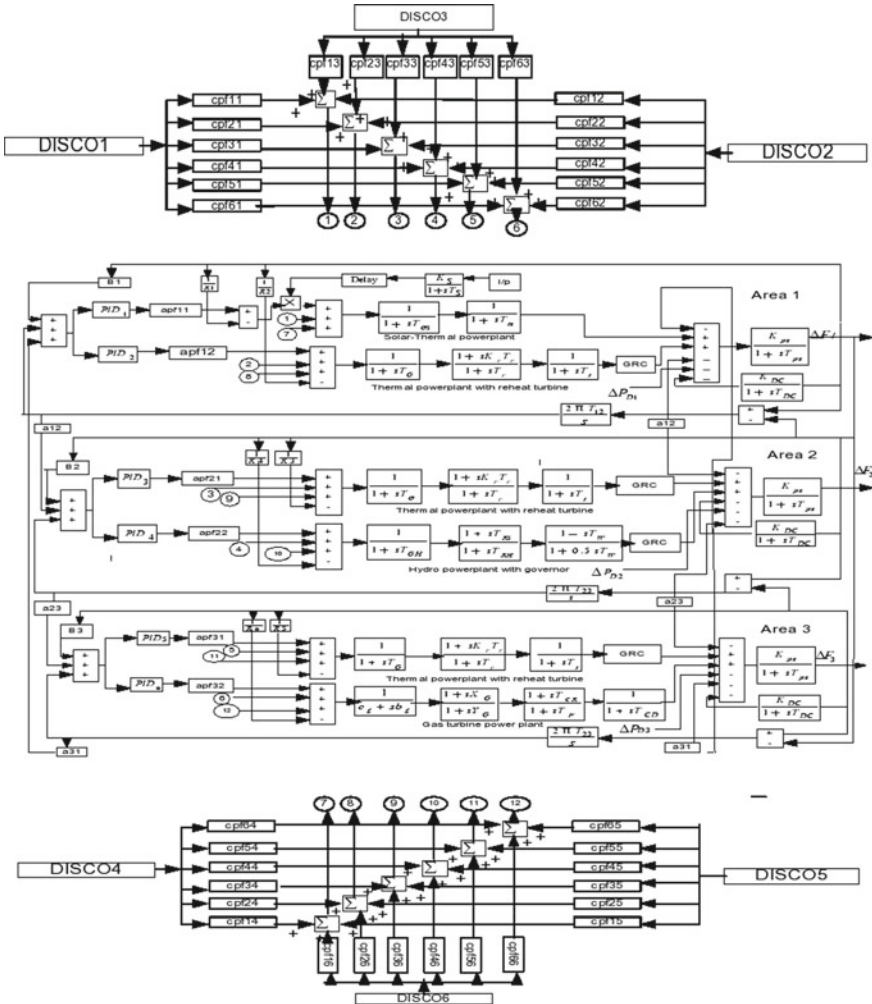


Fig. 1 Transfer function model of three area deregulated power system with AC/DC link

$$J = \text{ISE} = \int_0^{ts} (\Delta f_k^2 + \Delta P_{\text{tiek}-q, \text{error}}^2) dt \quad \text{where } k = 1, 2, 3 \quad (2)$$

where ts is the simulation time in seconds, and the problem limitations are the controller parameter limits. Therefore,

$$\text{Reduce } J \quad (3)$$

Subjected to

$$K_{P\min} \leq K_p \leq K_{P\max}; K_{I\min} \leq K_I \leq K_{I\max}; K_{D\min} \leq K_D \leq K_{D\max} \quad (4)$$

In that paper, MFO is compared with DE, PSO evolution strategy. The flowchart of the MFO algorithm is exposed in [19].

3 Simulation Results and Discussion

Implementation of MFO Algorithm

As shown in Fig. 1, the system model is designed in MATLAB/Simulink environment; PSO, DE, and MFO algorithms are written in .mfile. Different PID controllers are considered for each GENCOS, as different GENCOS are considered in each area. Initially, the PID controllers' gains and AC/DC link parameters are optimized with different optimization techniques under the poolco-based transaction. In present work, the PSO parameters are considered as: maximum iteration 100, size of population 50, $c_1 = 1.2$, $c_2 = 1.2$ and $w = 0.9$. Parameters of DE is considered as population size 50, maximum iteration 100, step size $F = 0.8$, and crossover probability of CR = 0.6. Parameters of MFO considered are mouths 30 and the maximum number of iterations 100.

3.1 CASE-1: Poolco Operation

In Poolco transaction, the DPM matrix is specified by

$$\text{DPM} = \begin{bmatrix} 0.5 & 0.5 & 0 & 0 & 0 & 0 \\ 0.5 & 0.5 & 0 & 0 & 0 & 0 \\ 0 & 0 & 0 & 0 & 0 & 0 \\ 0 & 0 & 0 & 0 & 0 & 0 \\ 0 & 0 & 0 & 0 & 0 & 0 \\ 0 & 0 & 0 & 0 & 0 & 0 \end{bmatrix}$$

All apf 's are specified as 0.5. The PID controllers' gains are optimized with PSO, DE, and MFO techniques without and with AC/DC Link and are given in Table 1.

The system performances for the PID controller without and with AC/DC link are specified in Table 2. The dynamic system results with a 2% step load change in area 1 are shown in Fig. 2a without AC/DC link and Fig. 2b with AC/DC link. Considering the numerical results of Table 2 and the system's dynamic results, the MFO tuned PID controller with AC/DC link performed better in requisites on minimum settling time,

Table 1 Tuned controller and AC/DC parameters under poolco transaction

Gains	Without AC/DC link			With AC/DC link		
	PSO	DE	MFO	PSO	DE	MFO
KP ₁	0.1514	0.3791	-0.3109	0.0313	0.2255	-0.5
KP ₂	0.0957	0.2508	-0.0581	0.1326	0.4163	0.5
KP ₃	0.4423	0.4288	-0.356	0.4432	-0.874	0.1131
KP ₄	0.1402	-0.212	0.241	-0.337	0.9817	-0.0642
KP ₅	-0.0508	0.4824	0.1199	0.9811	-0.7075	-0.0672
KP ₆	-0.1232	0.5	0.50	-0.3628	-0.875	-0.5
KI ₁	-0.4912	-0.1556	-0.2087	-0.6657	-0.0333	-0.5097
KI ₂	-0.2833	-0.4808	-0.50	0.5839	-0.754	0.5
KI ₃	-0.0568	-0.5	-0.5	-0.896	-0.9875	-0.4691
KI ₄	-0.1606	0.0405	0.2761	0.5838	0.6713	-0.2151
KI ₅	-0.3599	-0.0958	-0.50	0.7232	-0.7677	-0.85
KI ₆	-0.4116	-0.3467	0.0065	0.7871	-0.9942	-0.5
KD ₁	-0.4963	-0.2833	-0.4402	-0.6522	0.2381	-0.5
KD ₂	0.2977	-0.1195	-0.5	-0.9703	-1	0.5
KD ₃	-0.2063	-0.0507	-0.3541	-0.4287	1	0.1207
KD ₄	0.2114	0.3757	0.210	-0.9852	-0.2527	0.3007
KD ₅	-0.0565	0.0462	-0.1798	0.5240	0.1074	-0.408
KD ₆	-0.2039	-0.3169	0.03342	0.7598	0.538	-0.5
K _{DC}	-	-	-	0.7954	1	0.875
T _{DC}	-	-	-	0.2656	0.1054	0.1054

frequencies divergences, and tie-line power divergences, overshoot, and undershoot. Hence, for further analysis, MFO tuned PID controller is considered.

3.2 CASE-2: Bilateral Operation

For this bilateral operation case, the DPM A matrix is specified as.

$$DPM\ A = \begin{bmatrix} 0.2 & 0.25 & 0.6 & 0.2 & 0.1 & 0 \\ 0.2 & 0.15 & 0 & 0.2 & 0.1 & 0.2 \\ 0.1 & 0.15 & 0 & 0.2 & 0.2 & 0.2 \\ 0.2 & 0.15 & 0.4 & 0 & 0.2 & 0.3 \\ 0.2 & 0.15 & 0 & 0.2 & 0.2 & 0.2 \\ 0.1 & 0.15 & 0 & 0.2 & 0.2 & 0.1 \end{bmatrix}$$

Table 2 Performance analysis under poolco transaction with/without AC/DC link

Performance index	ISE	Without AC/DC link			With AC/DC link		
		PSO	DE	MFO	PSO	DE	MFO
		0.0048	0.0045	0.0044	3.703×10^{-4}	2.7614×10^{-4}	2.4363×10^{-4}
ΔF_1	ST	23.78	22.22	7.91	7.77	7.44	2.81
	OS	0.0130	0.0040	0.0039	0.0023	2.447×10^{-4}	7.03×10^{-5}
ΔF_2	ST	38.69	30.08	11.72	10.97	9.15	8.82
	OS	0.0143	0.0066	0.0022	0.0020	3.506×10^{-4}	6.96×10^{-5}
ΔF_3	ST	43.08	34.46	13.81	10.44	8.66	7.61
	OS	0.0146	0.0084	0.0044	4.947×10^{-4}	3.162×10^{-4}	7.1×10^{-5}
$\Delta P_{\text{tie}12}$	ST	17.54	18.75	15.82	12.28	15.69	11.96
	OS	0.0027	0.0017	0.0016	9.583×10^{-4}	6.761×10^{-4}	4.982×10^{-4}
$\Delta P_{\text{tie}23}$	ST	22.76	22.34	10.33	8.87	7.49	7.47
	OS	0.0027	0.0021	5.269×10^{-4}	5.5823×10^{-4}	2.542×10^{-4}	2.287×10^{-4}
$\Delta P_{\text{tie}31}$	ST	17.55	17.93	16.62	12.57	14.17	10.64
	OS	0.0087	0.0088	0.0087	0.0048	0.0033	0.0036

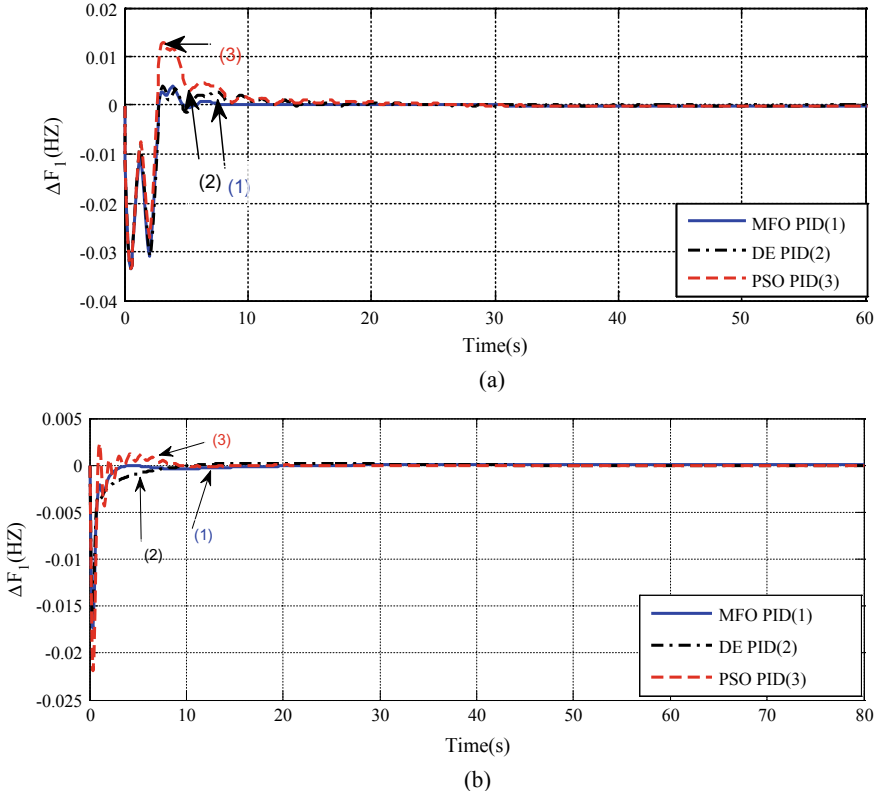


Fig. 2 Comparison of dynamic performances under poolco transaction **a** without AC/DC link ΔF_1 versus time **b** with AC/DC link ΔF_1 versus time

The load interruption in every DISCOs is measured as 0.01 puMw. The GENCOs ACE sharing estimated basing on generation insist in DPM matrix A as specified in [23]. So the resultant apf s are intended and specified as $apf_{11} = 0.6149$, $apf_{12} = 0.3851$, $apf_{21} = 0.4249$, $apf_{22} = 0.5751$, $apf_{31} = 0.56$, and $apf_{32} = 0.440$.

MFO tuned PID controller with and without AC/DC links are to examine the proper execution of the bilateral case operation. The optimal PID controller gains and AC/DC link parameters are given in Table 3. The results of the system are specified in Table 4. The dynamic results of the system are shown in Fig. 3. It is depicted from Fig. 3 that better dynamic results are attained with AC/DC link.

Table 3 Tuned controller parameters of AC/DC under bilateral and contract transaction

MFO tuned Gain values	Bilateral case		Contract violation case	
	Without AC/DC	With AC/DC	Without AC/DC	With AC/DC
KP ₁	-0.8468	0.8782	-0.153	0.0078
KP ₂	0.0477	0.1048	0.580	-0.2187
KP ₃	0.4117	-0.6306	0.3665	-0.2496
KP ₄	0.1142	-1	-0.065	1
KP ₅	-0.5544	-0.5602	0.9564	0.5856
KP ₆	0.8222	0.5643	1	0.1480
KI ₁	-0.2457	-0.3923	-0.434	-0.6859
KI ₂	-0.8388	0.199	-1	-0.8578
KI ₃	-0.5533	-0.9069	-1	-1
KI ₄	0.0696	-1	0.3141	-0.6107
KI ₅	-0.9295	0.3297	-0.4369	-0.1229
KI ₆	-0.0364	-0.7972	-1	-1
KD ₁	-1	-0.9752	-0.7263	-1
KD ₂	0.8926	0.4443	1	1
KD ₃	-0.1418	1	-0.5083	-0.4384
KD ₄	0.5969	0.6666	0.3570	-0.4308
KD ₅	-0.3159	0.3279	-1	0.00117
KD ₆	-0.5271	-1	-0.3854	-1
K _{DC}	—	1	—	1
T _{DC}	—	0.4561	—	0.02116

Table 4 Performance comparison of bilateral and contract violation transaction

Performance index	ISE	Without AC/DC link (bilateral)	With AC/DC link (bilateral)	Without AC/DC (CV)	With AC/DC (CV)
		0.0675	0.0015	0.11	0.0019
ΔF_1	ST	36.57	20.61	50.67	29.31
	OS	0.0036	4.505×10^{-4}	0.0579	0.0017
ΔF_2	ST	36.57	15.62	49.98	29.01
	OS	0.0043	3.747×10^{-4}	0.0672	0.0015
ΔF_3	ST	36.68	25.21	49.37	29.32
	OS	0.0049	4.886×10^{-4}	0.0629	0.0017
$\Delta P_{\text{tie}12}$	ST	27.34	17.43	33.75	16.31
	OS	0.0129	0.0042	0.0119	0.0023
$\Delta P_{\text{tie}23}$	ST	23.28	22.82	31.19	15.81
	OS	0.0018	0.0013	0.0021	0.0014
$\Delta P_{\text{tie}31}$	ST	25.89	22.11	39.58	8.32
	OS	0.0013	9.414×10^{-4}	0.0145	0.0012

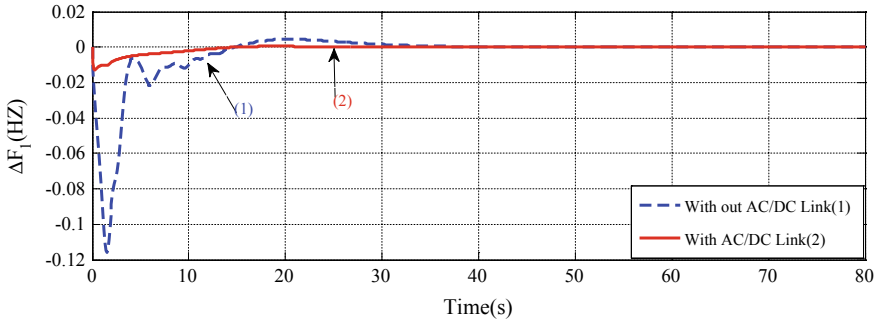


Fig. 3 Comparison of dynamic performances under bilateral transaction ΔF_1 versus time

3.3 CASE-3: Contract Violation

“In this case, DISCO may violet the agreement and demands extra power than that of the precise one. The GENCOs of the similar area contribute that power as the DISCOs. Let us consider DISCO1 demands 0.01 puMW of extra power, the local load of that area modifies, which is specified as

$$\begin{aligned}\Delta P_{L1}, \text{loc} &= \text{load of DISCO1}(0.01) + \text{load of DISCO2}(0.01) \\ &+ 0.01 = 0.03 \text{ puMW}\end{aligned}$$

The optimum values of parameters PID controller and AC/DC are given in Table 3. Numerical analysis of system performances is specified in Table 4, and the dynamic results of the system are exposed in Fig. 4. It reflects that system response also attains steady-state stability with uncontracted demand in both the cases, but results advance successfully with AC/DC link.

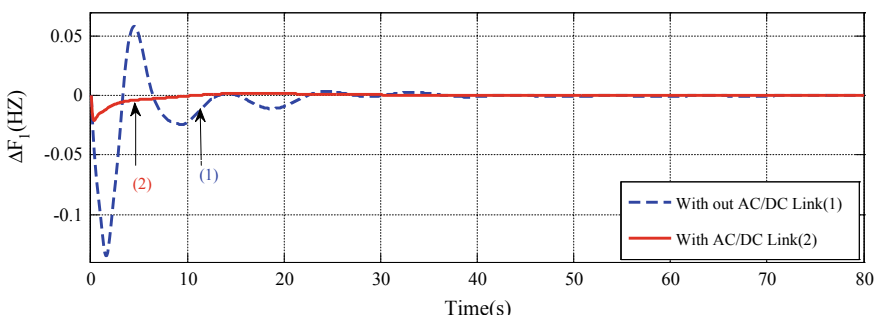


Fig. 4 Comparison of dynamic performances under contract violation transaction ΔF_1 versus time

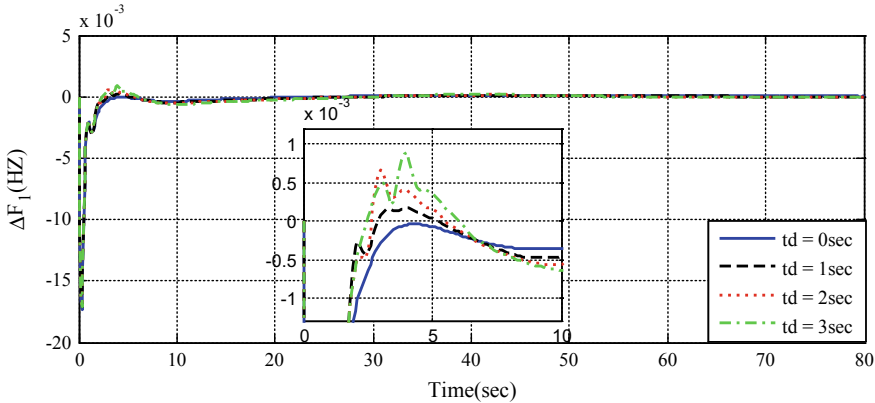


Fig. 5 Frequency deviation of area 1 versus time tie-line power deviation versus time

4 Physical Constraints

Primary physical constraints should be included in the system to analyze a realistic AGC system. The system imposes physical constraints such as governor-turbine, filters, communication channels, crossover elements in a thermal unit, and the penstocks' behavior in a hydraulic unit [22]. Typically, reheat turbine, GRC, governor dead band, and time delay are significant constraints that affect the system performances as a thermal system is considered, so reheat turbine is previously incorporated in the system under study. Further, GRC, GDB, and time delay are incorporated into the system to make the system more realistic. GDB's typical value is specified for steam turbines as 0.06% (0.036 Hz) [24]. Time delay is due to signal processing and data gathering unit, which must be incorporated in AGC system analysis. In the present analysis, the time delay is varied from 1 to 3 s. The system performances with the inclusion of GRC [12], GDB, and variation in time delay are shown in Fig. 5 under poolco transaction with the same optimized parameters obtained with AC/DC link. It is clear from Fig. 5, and the system performances almost remain the same with physical constraints. Hence, it can be finalized that the proposed methodology can also apply to realistic power systems.

5 Conclusion

A three-area interrelated model of power system consists of multi-sources is proposed for deregulated AGC system with AC/DC link. The MFO technique is established for tuning PID and has shown superior performance compared to PSO and DE techniques. System results are improved marginally with the inclusion of the AC/DC link. Further, to verify the robustness of the projected methodology, the system is

subjected to the addition of physical constraints in the system with equal tuned parameters attained during poolco operation. It can be concluded that the MFO-based PID controller can be successfully applied to a deregulated AGC system with diverse generation sources.

Appendix

$$\begin{aligned}
 B_K &= 0.425 \text{ puMW/Hz}; R_i = 2.4 \text{ Hz/pu}; K_S = 1.8; T_s = 1.8 \text{ s}; T_{TS} = 3; \\
 T_{GS} &= 1; T_{SG} = 0.08 \text{ s}; T_T = 0.3 \text{ s}; K_R = 0.3; T_R = 10 \text{ s}; K_{PSK} = 120 \text{ Hz/puMW}; \\
 T_{PSK} &= 20 \text{ s}; T_{12} = 0.545; a_{12} = -1; T_W = 1 \text{ s}; T_{RS} = 5 \text{ s}; \\
 T_{RH} &= 28.75 \text{ s}; T_{GH} = 0.2 \text{ s}; \\
 X_G &= 0.6 \text{ s}, Y_G = 1.1 \text{ s}, c_g = 1, b_g = 0.049 \text{ s}, T_F = 0.239 \text{ s}, \\
 T_{CR} &= 0.01 \text{ s}, T_{CD} = 0.2 \text{ s}.
 \end{aligned}$$

References

1. Donde V, Pai MA, Hiskens IA (2001) Simulation and optimization in an AGC system after deregulation. *IEEE Trans Power System* 16(3):481–489
2. Christie RD, Bose A (1996) Load frequency control issues in power system operation after deregulation. *IEEE Trans Power Syst* 11(3):1191–1200
3. Bekhouche N (2002) Automatic generation control before deregulation. In: Proceedings of the 34th Southeastern symposium on system theory, pp 321–323
4. Demiroren A, Zeynelgil HL (2007) GA application to optimization of AGC in three-area power system after deregulation. *Electr Power Energy Syst* 29:230–240
5. Ghoshal SP, Goswami SK (2003) Application of GA based optimal integral gains in fuzzy based active power frequency control of non reheat and reheat thermal generating systems. *Electr Power Energy Syst* 67:79–88
6. Bhatt P, Roy R, Ghoshal SP (2010) Optimized multi-area AGC simulation in restructured power systems. *Electr Power Energy Syst* 32(4):311–322
7. Debbarma S, Saikia LC, Sinha N (2013) AGC of a multi-area thermal system under a deregulated environment using a non-integer controller. *Electr Power Syst Res* 95:175–183
8. Nanda J, Sreedhar M, Dasgupta A (2015) A new technique in hydrothermal interconnected automatic generation control system using minority charged carrier inspired algorithm. *Electr Power Energy Syst* 68:259–268
9. Arya Y, Kumar N (2016) AGC of a multi-area multi-source hydrothermal power system interconnected via AC/DC parallel links under deregulated environment. *Electr Power Energy Syst* 75:127–138
10. Parmar KPS, Majhi S, Kothari DP (2014) LFC of an interconnected power system with multi-source power generation in deregulated power environment. *Electr Power Energy Syst* 57:277–286
11. Sahu RK, Gorripotu TS, Panda S (2015) A hybrid DE-PS algorithm for load frequency control under deregulated power system with UPFC and RFB. *Ain Shams Eng J* 6:893–911
12. Mohanty B, Hota PK (2015) Comparative performance analysis of fruit fly optimization algorithm for multi-area multi-source automatic generation control under deregulated environment. *IET Gener Trans Distrib* 9(14):1845–1855

13. Das DC, Sinha N, Roy AK (2012) GA based frequency controller for solar thermal–diesel–wind hybrid energy generation/energy storage system. *Electr Power Energy Syst* 43(1):262–279
14. Sharma Y, Saikia LC (2015) Automatic generation control of a multi-area ST-Thermal power system using Grey Wolf Optimizer algorithm based classical controllers. *Electr Power Energy Syst* 73:853–862
15. Dillip K, Rabindra KS, Tulasichandra Sekhar G, Sidhartha P (2019) Automatic generation control of power system in deregulated environment using hybrid TLBO and pattern search technique. *Ain Shams Eng J*:1–21
16. Acharyulu BVS, Mohanty B, Hota PK (2020) Analysis of moth flame optimization optimized cascade proportional-integral-proportional-derivative controller with filter for automatic generation control system incorporating solar thermal power plant. *Optim Control Appl Method*:1–16
17. Rahman A, Saikia LC, Sinha N (2015) Load frequency control of a hydrothermal system under deregulated environment using biogeography-based optimized three degree-of-freedom integral-derivative controller. *IET Gener Trans Distrib* 9(15):2284–2293
18. Bevrani H, Ghosh A, Ledwich G (2010) Renewable energy sources and frequency regulation: survey and new perspectives. *IET Renew Power Gener* 4(5):438–457
19. Banaja Mohanty BVS, Acharyulu PK (2017) Hota Moth-flame optimization algorithm optimized dual-mode controller for multi-area hybrid sources AGC system. *Optim Control Appl Method*:1–15
20. Mohanty B, Panda S, Hota PK (2014) Controller parameters tuning of differential evolution algorithm and its application to load frequency control of multi-source power system. *Electr Power Energy Syst* 54:77–85
21. Mirjalili S (2015) Moth-flame optimization algorithm: a novel nature-inspired heuristic paradigm. *Knowl-Based Syst* 89:228–249
22. Yamanya W, Fawzya M, Tharwath A, Hassaniend AE (2015) Moth-flame optimization for training multi-layer perceptrons. *IEEE*
23. Parida M, Nanda J (2005) Automatic generation control of a hydrothermal system in deregulated environment. In: Eighth international conference on electrical machines and systems, Nanjing, September, pp 942–947
24. Golpira H, Bevrani H, Golpira H (2011) Application of GA optimization for automatic generation control design in an interconnected power system. *Energy Convers Manage* 52:2247–2255

Spam Review Detection Using K-Means Artificial Bee Colony



Prateek Saini, Sakshi Shringi, Nirmala Sharma, and Harish Sharma

Abstract The current businesses which use Internet for marketing depend on online reviews, and these online reviews can direct a customer toward or away from a product and service. This effect of online reviews is the reason that business uses spam reviews to either benefit their business or hinder their rival's business. In this paper, a novel solution k-means artificial bee colony for feature selection and optimized clusters using artificial bee colony to detect spam reviews is presented. We report the testing of our novel method on three different datasets. The findings of our testing are encouraging and show a respectable performance on all three datasets.

Keywords Artificial bee colony algorithm · Metaheuristic method · Spam detection · Spam reviews · K-Means · Machine learning

1 Introduction

In the last two decades, the Internet had changed the way we communicate, interact with our peers, and do business in a good way [1]. All this is possible because of the reachability of the Internet and its ease of use. The one major boom we see in the last decade is in e-commerce or in other words we can say including the power of Internet to increase the pool of available customers. This is done by providing products and services online which directly impacts the pool of customers meaning now the limit of accessing any service or product is limited only by the reachability of the internet. In all this, new currency for these online businesses emerges which is called product review or simply review.

One thing we can notice in today's online business that reviews play a major role whether a service or product will be able to make its place in the market or not [2]. Any customer who wants to buy a product or use a service through the internet will first go through the reviews of the respective product and service. At this point, if reviews do not give him enough confidence in the authenticity and reliability of the

P. Saini (✉) · S. Shringi · N. Sharma · H. Sharma
Rajasthan Technical University, Kota, India

product, it is highly likely that he/she will not buy it and look for something else or somewhere else.

A scenario-like mentioned above had encouraged the online businesses to understand the experience of their customer and improve their product or services to better serve them in the future. To do so a new technology at the time help them achieve such a goal, namely opinion mining [3]. Opinion mining allows businesses to analyze their customers by finding out their attitude toward their product or service. To do so, the opinion mining techniques use the reviews given by customers and try to find about their attitude based on those reviews but there is an underlying assumption that is made by these techniques which is that all reviews are trustworthy and authentic. But sadly that is not the case because most of the time each product page on the web is affected by ‘spam reviews’ which do affect these opinion mining techniques in negative way and defeat the purpose of using them in the first place.

Jindal and Liu [4] had categorized the spam reviews into three categories which have varying degrees of effect on the customer’s decision to buy a product or not. ‘Positive spam reviews’ and ‘negative spam reviews’ are the most effective method to change a buyer’s decision on false information. As the name suggests, ‘positive spam review’ gives a positive review to a non-deserving product and ‘negative spam review’ gives a negative review to a non-deserving product.

Consider a situation in which a restaurant failed to provide a nice dining experience to one of its customers and as a result of that the customer gives a bad review about the restaurant’s bad hospitality on a site like Zomato or Yelp. As this can be bad for business, the restaurant hired someone to give positives reviews related to their dinning and mitigate the effect of that one honest review. These kinds of tactics cannot only be used to save your own skin but can also be used to destroy the business of your rivals. Spam reviews are designed to change the opinion of someone regarding something which is catastrophic.

In 2017, Rajamohana et al. [5] proposed a model using adaptive binary flower pollination algorithm for feature selection using naive Bayes classifier’s accuracy as the objective function and k-nearest neighbors as the classifier using selected features. In 2019, Pandey and Rajpoot [6] proposed a model using spiral cuckoo search to optimize k-means algorithm using sum squared error as the objective function. The available literature is a source of motivation to carry out the future work in the field.

The rest of the paper is structured as follows: the artificial bee colony algorithm is reviewed in Sect. 2. In Sect. 3, k-means clustering is reviewed. Proposed feature selection and cluster head optimization using artificial bee colony are mentioned in Sect. 4. Experimental results are discussed in Sect. 5. Finally, conclusion is given in Sect. 6.

2 Artificial Bee Colony Algorithm

Artificial bee colony algorithm is a swarm-based algorithm which mimics the intelligent foraging behavior of honeybees. They forage honey by coordinating with each by

exchanging the location of the food source, i.e., honey. To exchange the information, they dance in a particular area of hive called the dancing area and the dance itself is called waggle dance [7]. This exchange of the information about the location of food source allows them to work collectively and efficiently. Their gathering, exchanging of information, and collective working are called collective intelligence, and it is the reason why we mimics their behavior to solve complex problems. Recently, ABC algorithm modified for various application and successfully applied to get rid of complex problem [8–10].

To understand the implementation of foraging behavior of honeybee, the whole process can be divided into four phases as discuss below.

2.1 Initialization Phase

This is the first phase of the algorithm and will be implemented only once. In this phase, position of search agents is randomly initialized within the search space according to Eq. (1).

Once the position has been initialized, then the fitness of each search agent is calculated.

$$x_i^j = x_{\min}^j + \text{rand}(0, 1)(x_{\max}^j - x_{\min}^j), \forall j = 1, 2, \dots, D \quad (1)$$

2.2 Employed Bee Phase

This is the second phase of the algorithm, and it will be implemented for each iteration of the algorithm. In this phase, each search agent changes their current position and evaluates the fitness of the new position. If the new position's quality is better than the current position, then it keeps the new one otherwise the old one. The new position is selected using Eq. (2)

$$v_{ij} = x_{ij} + \phi_{ij}(x_{ij} - x_{kj}) \quad (2)$$

2.3 Onlooker Bee Phase

This is the third phase of the algorithm, and it will also be implemented for every iteration. In this phase, a search agent is selected based on probability, on its fitness according to Eq. (3).

$$p_i = \frac{\text{fitness}_i}{\sum_{i=1}^N} \quad (3)$$

Once a search agent has been selected, then the onlooker bee will change the current position and evaluate its fitness. If the new position is better than the current position, it will keep the new position otherwise the old one.

2.4 Scout Bee Phase

This is the fourth phase of the algorithm, and it will be implemented only when a search agent's position has not been changed for predetermined number of iterations. If any search agent enters this phase, it is now called a scout bee and it has to now find a new position. To do so, it is randomly initialized within the search space using Eq. (4).

$$x_i^j = x_{\min}^j + \text{rand}[0, 1](x_{\max}^j - x_{\min}^j), \forall j = 1, 2, \dots, D \quad (4)$$

3 K-Means Clustering

K-means clustering algorithm is designed to group similar things/samples/objects together or in other ways group them separately if they are dissimilar to each other in k distinct clusters. Their similarity and dissimilarity are evaluated based on what they are representing. If it is just numbers, then it can be their values or if it's a complex object like word and image, it can be their attributes.

From implementation point of view, k-means clustering can be represented in simple four steps implemented in sequence to achieve the goal.

1. Select k points either randomly or form the samples such that they are not too close to each other and within the boundaries of sample space. These k points will represent the centroid of k clusters.
2. Now assign each sample to a cluster centroid which is closest to it.
3. For each cluster, calculate its new centroid by taking the mean of all the samples within the cluster.
4. Repeat steps (2) and (3) till there is no change in the position of cluster centroid.

4 Proposed Method

This paper introduced a clustering method optimized with ABC to detect spam reviews. The proposed method is divided into following phases.

1. Preprocessing
2. Feature Extraction
3. Proposed feature selection using k-means ABC
4. Proposed Artificial Bee Colony Optimizer with k-Means
5. Testing (Fig. 1).

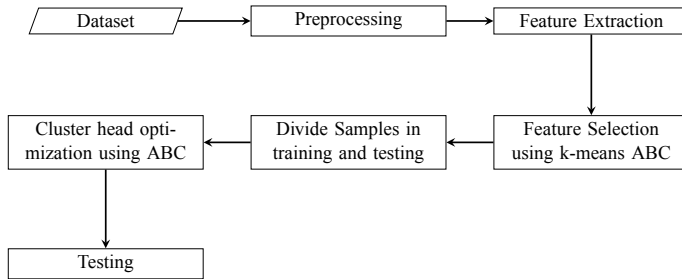


Fig. 1 Experiment process flowchart

4.1 *Preprocessing*

The online reviews most of the time contains noise or words that do not added any meaning to our model so instead of wasting resources in evaluating such entities we completely remove them out of the equation. Following are the operations performed in preprocessing

1. Convert all words into lowercase.
2. Remove stop words like is, or, as etc.
3. Remove symbols like pound, asterisk, etc.
4. Remove punctuation.
5. Replace continuous white spaces with one white space.

4.2 *Feature Extraction*

Feature extraction is done using linguistic inquiry and word count.

4.3 *Feature Selection*

Feature selection is used to remove redundant, noisy, and less significant features so that the learning model can give higher accuracy in a reasonable time. Higher-dimensional data generally tends to increase the training time without giving a significant increase in accuracy (sometimes making it even worse). For these two reasons, feature selection is desirable in most of the machine learning models.

K-means with ABC is used to find out the optimal feature set according to the Algorithm 1. In the proposed method, following steps are taken

1. Every search agent is initialized with random features, and their fitness values are calculated using Algorithm 2.

2. Algorithm 2 in turn uses Algorithm 3 for labeling the cluster heads and Algorithm 4 for calculating the accuracy.
3. In employed bee phase, each search agent's feature subset is changed by replacing one of the current feature with the new one. New fitness is calculated and better one among the current and new is kept.
4. In onlooker bee phase, search agents with higher probability of having a good solution are given the chance to update their feature set.
5. In scout bee phase, search agents whose feature set is not updated for a predefined number of times will be reinitialized randomly.
6. After maximum iteration has been done return the optimal set of features.

Algorithm 1: Feature selection

Input: number of search agents, dimension of search agents, data
Output: optimal features

```

/* Initialization phase */ *
1 while every search agent didn't get a chance do
2   Initialize the search agents with random features
3   Calculate the fitness of each search agent
4 end
5 while maximum iteration not reached do
  /* employed bee phase */ *
  6 while every search agent didn't get a chance do
    7   Select a search agent
    8   Replace one of its feature with a new one
    9   Calculate the new fitness
   10  Apply greedy selection on fitness
  end
  /* onlooker bee phase */ *
  12 Calculate probability of every search agent
  13 while every search agent is not checked do
    14   Select a search agent
    15   if current search agent have good probability then
    16     give it a chance to update its position
    17     apply greedy selection on the fitness
  end
  /* scout bee phase */ *
  20 while every search agent is not checked do
    21   Select a search agent
    22   if current search agent position not changed for a predefined number of times then
    23     Randomly reinitialize the search agent
    24     Calculate fitness
  end
26 end
27 end
28 Return the optimal feature set

```

Algorithm 2: Feature selection fitness function

Input: bee position, samples, samples label
Output: accuracy

- 1 Extract features from samples based on bee position
- 2 Apply kmeans on selected features
- 3 Label the cluster heads
- 4 Calculate accuracy
- 5 Return accuracy

Algorithm 3: Cluster labelling

Input: label of samples(label), to which cluster sample is assigned(belongs)
Output: cluster labels

```

1 while all labels are not checked do
2   if label is positive and belongs to cluster1 then
3     | cluster1.spam++
4   else if label is positive and belongs to cluster2 then
5     | cluster2.spam++
6   else if label is negative and belongs to cluster1 then
7     | cluster1.ham++
8   else if label is negative and belongs to cluster2 then
9     | cluster2.ham++
10 end
11 if cluster1.spam > cluster2.spam then
12   | label cluster1 as spam and cluster2 as ham
13 end
14 else
15   | label cluster1 as ham and cluster2 as spam
16 end
17 Return the label of cluster1 and cluster2

```

4.4 Divide Samples into Training and Testing

The original samples are divided into training samples and testing samples in 7:3 ratio.

4.5 Proposed Artificial Bee Colony Optimizer with K-Means

The proposed method uses ABC to find optimal cluster heads to classify reviews into spam and ham reviews. For finding optimal cluster heads, Algorithm 5 is used in which each search agent represents the position of two cluster heads spam and ham. Followings are the steps for Algorithm 5.

Algorithm 4: Accuracy Calculation Method

Input: label of samples (lable), label of cluster, to which cluster a sample belongs
Output: Accuracy

```

1 Initialize: TP, TN, FP, FN = 0, 0, 0, 0
2 while all samples are not checked do
3   if label is positive and belongs to cluster1 and cluster1.label is spam then
4     | then TP++
5   else if label is positive and belongs to cluster1 and cluster1.label is ham then
6     | then FN++
7   else if label is positive and belongs to cluster2 and cluster1.label is spam then
8     | then TP++
9   else if label is positive and belongs to cluster2 and cluster1.label is ham then
10    | then FN++
11  else if label is negative and belongs to cluster1 and cluster1.label is spam then
12    | then FP++
13  else if label is negative and belongs to cluster1 and cluster1.label is ham then
14    | then TN++
15  else if label is negative and belongs to cluster2 and cluster2.label is spam then
16    | then FP++
17  else if label is negative and belongs to cluster2 and cluster2.label is ham then
18    | then TN++
19 end
20 calculate accuracy
21 return accuracy

```

1. Initialize each search agent randomly within the search space and find the fitness using Algorithm 6.
2. Algorithm 6 will use Algorithm 3 for labeling the clusters and Algorithm 4 for calculating accuracy.
3. In employed bee phase, each search agent is given a chance to update its position using Eq. (2). New fitness value will be compared with the current fitness value, and the best will be kept.
4. In onlooker bee phase, search agents with higher probability of providing a good solution are given the chance to update their position. Probability for each search agent is calculated using Eq. (3).
5. In scout bee phase, search agents whose position is not updated for a predefined number of times will be reinitialized within the search space.
6. Return the optimal cluster position after maximum iterations are done.

4.6 Testing

For testing the efficiency of cluster heads provided by Algorithm 5, Algorithm 7 is used.

Algorithm 5: Cluster head optimization using ABC

```

Input: Number of clusters, data
Output: Optimum cluster heads
/* Initialization phase */ *
1 while every search agent didn't get a chance do
2   Initialize the search agents with random values according to equation (1)
3   Calculate the fitness of each search agent
4 end
5 while maximum iteration not reached do
6   /* employed bee phase */ *
7   while every search agent didn't get a chance do
8     Select a search agent
9     Replace one of its dimension with a new one according to equation (2)
10    Calculate the new fitness
11    Apply greedy selection on fitness
12  end
13  /* onlooker bee phase */ *
14  Calculate probability of every search agent according to equation (3)
15  while every search agent is not checked do
16    Select a search agent
17    if current search agent have good probability then
18      give it a chance to update its solution
19      apply greedy selection on the fitness
20    end
21  end
22  /* scout bee phase */ *
23  while every search agent is not checked do
24    Select a search agent
25    if current search agent position not changed for a predefined number of times then
26      Randomly reinitialize the search agent
27      Calculate fitness
28    end
29  end
30 end
31 Return the optimal cluster heads

```

Algorithm 6: Fitness function for cluster head optimization

Input: search agent position(position), samples, samples label

Output: accuracy

Extract cluster heads from position

Assign samples to cluster heads

Label cluster heads

Calculate accuracy

return accuracy

Algorithm 7: Testing

Input: search agent position(position), testing samples(samples), testing samples label

Output: accuracy

Extract cluster heads from position

Assign samples to cluster heads

Calculate accuracy

return accuracy

5 Experimental Results

The proposed method is tested on three datasets, namely Synthetic spam [11], Yelp [12, 13] and Movie [14], presented in Table 2. Synthetic spam dataset is taken from Database and Information system Laboratory, University of Illinois, and labeled using synthetic review spamming method. Yelp dataset is taken as a subset from restaurant and hotel data, and movie reviews are subset of IMDB dataset. All experiments are done on Python-3.6 on Intel core i5 processor with 6 GB of RAM (Table 1).

For calculating the effectiveness of proposed method, number of true positive, true negative, false positive, and false negative prediction are observed to calculate accuracy, precision, and recall.

- True positive represents spam review predicted correctly.
- True negative represents ham review predicted correctly.
- False positive represents ham reviews predicted incorrectly.
- False negative represents spam review predicted incorrectly.

These four parameters together represent confusion matrix and based on this confusion matrix, precision, recall, and accuracy are computed using Eqs. (5)–(7), respectively.

The proposed model is implemented a total of ten times on each dataset, and average values are considered to evaluate the overall performance of the model. Tables 3, 4, and 5 show the result of synthetic spam review dataset, movie review dataset, and Yelp dataset, respectively. Figure 2 shows the performance of proposed model on all three datasets with different size of feature set (Fig. 3; Tables 6 and 7).

$$\text{Precision} = \frac{\text{TP}}{\text{TP} + \text{FP}} \quad (5)$$

$$\text{Recall} = \frac{\text{TP}}{\text{TP} + \text{FN}} \quad (6)$$

$$\text{Accuracy} = \frac{\text{TP} + \text{TN}}{\text{TP} + \text{TN} + \text{FN} + \text{FP}} \quad (7)$$

Table 1 Parameters for k-Means ABC

S. No.	Parameters	Value
1	Population	30
2	Maximum iteration	500
3	Dimension	Two times number of features
4	Scout bee threshold	$\frac{\text{populationsize} \times \text{Dimension}}{2}$

Table 2 Datasets and their composition

S. No.	Dataset	Total reviews	Spam	Ham
1	Synthetic spam	478	163	315
2	Yelp	4952	3709	1243
3	Movie	8544	3998	4546

Table 3 Synthetic spam review results

Run	TP	TN	FP	FN	Accuracy(%)	Precision(%)	Recall(%)	Time (s)
1	30	86	9	18	81.1188	76.9230	62.5000	464.0110
2	27	78	17	21	73.4265	61.3636	56.2500	461.9867
3	29	85	10	19	79.7202	74.3589	60.4166	465.2193
4	37	70	25	11	74.8251	59.6774	77.0833	478.1129
5	37	69	26	11	74.1258	58.7301	77.0833	463.4829
6	27	84	11	21	77.6223	71.0526	56.2500	464.4838
7	37	67	28	11	72.7272	56.9230	77.0833	460.0673
8	25	85	10	23	76.9230	71.4285	52.0833	460.5071
9	34	69	26	14	72.0279	56.6666	70.8333	462.4235
10	37	69	26	11	74.1258	58.7301	77.0833	461.1607
Average	-	-	-	-	75.6643	64.5854	66.6666	464.1455

Table 4 Movie results

Run	TP	TN	FP	FN	Accuracy(%)	Precision(%)	Recall(%)	Time (s)
1	707	823	540	492	59.7189	56.6960	58.9658	2849.0599
2	683	843	520	516	59.5628	56.7747	56.9641	2880.6256
3	670	842	521	529	59.0163	56.2552	55.8798	2869.1039
4	757	807	556	442	61.0460	57.6542	63.1359	2844.3945
5	813	793	570	386	62.6854	58.7852	67.8065	2897.2389
6	664	899	464	535	61.0070	58.8652	55.3794	2833.30398
7	695	874	489	504	61.2412	58.6993	57.9649	2832.4360
8	761	823	540	438	61.8266	58.4934	63.4695	2813.9950
9	663	875	488	536	60.0312	57.6020	55.2960	2860.8529
10	657	867	496	542	59.4842	56.9817	54.7956	2866.9748
Average	-	-	-	-	60.5620	57.6807	58.9658	2854.7985

Table 5 Yelp results

Run	TP	TN	FP	FN	Accuracy(%)	Precision(%)	Recall(%)	Time (s)
1	1103	2	370	8	74.5111	74.8811	99.2799	1858.1328
2	1104	4	368	7	74.7134	75.0000	99.3699	1888.4344
3	1109	1	371	2	74.8482	74.9324	99.8199	1835.2916
4	1111	0	372	0	74.9157	74.9157	100.0000	1840.2322
5	1111	0	372	0	74.9157	74.9157	100.0000	1877.7144
6	1060	29	343	51	73.4322	75.5523	95.4095	1840.2296
7	1102	4	368	9	74.5785	74.9659	99.1899	1858.2096
8	1111	0	372	0	74.9157	74.9157	100.0000	1850.6239
9	1110	0	372	1	74.8482	74.8987	99.9099	1884.0125
10	1109	1	371	2	74.8482	74.9324	99.819	1881.1705
Average	-	-	-	-	74.6527	74.9910	99.2799	1861.4052

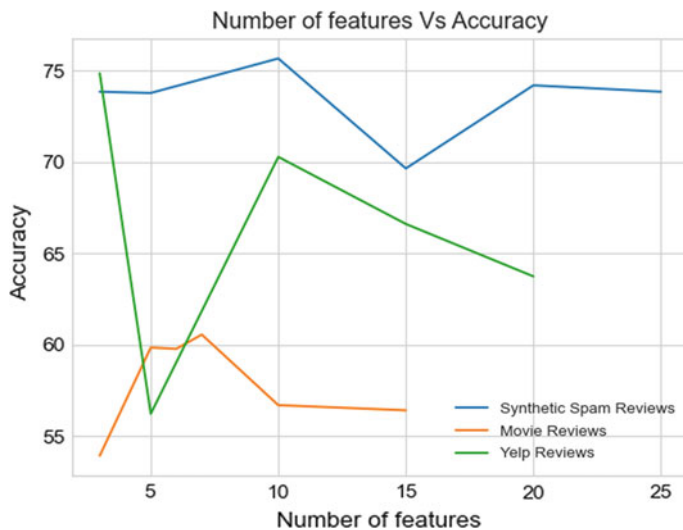
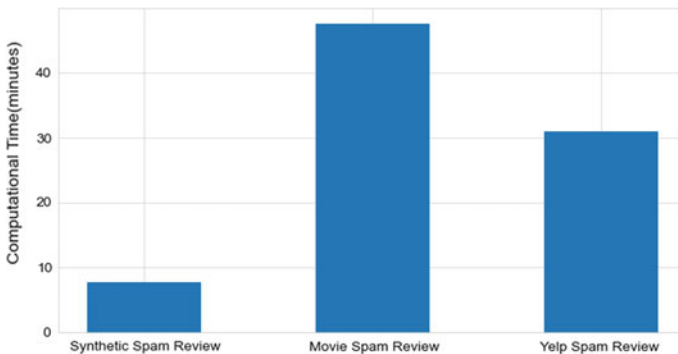
**Fig. 2** Number of features versus accuracy graph**Fig. 3** Average computation time for one run

Table 6 Optimum number of features in each dataset

S. No.	Dataset	Optimum features
1	Synthetic spam review	11
2	Movie review	7
3	Yelp	3

Table 7 Average computation time for one run

S. No.	Dataset	Avg. computational time (min)
1	Synthetic spam review	7.7357
2	Movie review	47.5799
3	Yelp	31.0234

6 Conclusion

In this paper, we have introduced a novel approach by combining k-means and artificial bee colony algorithm for feature selection and cluster head optimization using ABC to detect spam reviews. The proposed method tested on three different datasets and gave us respectable results which shows the potential of the method. In our proposed model, we train on a snapshot of data which makes the model effective for current trend only. In future, the work can be extended to make the model continuously update its knowledge after a period of time. For feature selection, other optimization algorithms can be explored for more optimal set of features.

References

1. Van Deursen AJAM, Helsper EJ (2018) Collateral benefits of internet use: explaining the diverse outcomes of engaging with the internet. *New Media Soc* 20(7):2333–2351
2. Nieto J, Hernández-Maestro RM, Muñoz-Gallego PA (2014) Marketing decisions, customer reviews, and business performance: the use of the toprural website by Spanish rural lodging establishments. *Tour Manage* 45:115–123
3. Bakshi RK, Kaur N, Kaur R, Kaur G (2016) Opinion mining and sentiment analysis. In: 2016 3rd International conference on computing for sustainable global development (INDIACOM). IEEE, pp 452–455
4. Jindal N, Liu B (2007) Analyzing and detecting review spam. In: Seventh IEEE International Conference on Data Mining (ICDM 2007). IEEE, pp 547–552
5. Rajamohana SP, Umamaheswari K, Abirami B (2017) Adaptive binary flower pollination algorithm for feature selection in review spam detection. In: International Conference on Innovations in Green Energy and Healthcare Technologies, pp 1–4
6. Pandey AC, Rajpoot DS (2019) Spam review detection using spiral cuckoo search clustering method. *Evol Intell* 147–164
7. Karaboga Dervis, Akay Bahriye (2009) A comparative study of artificial bee colony algorithm. *Appl Math Comput* 214(1):108–132

8. Sharma Sonal, Kumar Sandeep, Sharma Kavita (2019) Archimedean spiral based artificial bee colony algorithm. *J Stat Manage Syst* 22(7):1301–1313
9. Kumar S, Nayyar A, Kumari R (2019) Arrhenius artificial bee colony algorithm. In: International conference on innovative computing and communications Springer, pp 187–195
10. Nayyar A, Nguyen NG Kumari.R, Kumar S (2020) Robot path planning using modified artificial bee colony algorithm. In: Frontiers in intelligent computing: theory and applications. Springer, pp 25–36
11. Sun H, Morales A, Yan X (2013) Synthetic review spamming and defense. In: Proceedings of the 19th ACM SIGKDD international conference on knowledge discovery and data mining, pp 1088–1096
12. Mukherjee A, Venkataraman V, Liu B, Glance, NS (2013) What yelp fake review filter might be doing? In: ICWSM, pp 409–418
13. Mukherjee A, Venkataraman V, Liu B, Glance N et al (2013) Fake review detection: classification and analysis of real and pseudo reviews. Technical report UIC-CS-2013–03. University of Illinois at Chicago
14. <https://www.kaggle.com/lakshmi25npathi/imdb-dataset-of-50k-movie-reviews>

Mutual Learning-Based Spider Monkey Optimization for Constraint Optimization



Meghna Singh, Nirmala Sharma, and Harish Sharma

Abstract Spider Monkey Optimization (SMO) is a well-known population-based algorithm efficient for its optimizing features. Though, SMO has always been a competitive algorithm when compared with other optimization algorithms and has outperformed them even at times but there are a few limitations associated with it as well like slow convergence and stagnation. The purpose of this article is to overcome such drawbacks and to set a tradeoff between the expedition and exploitation. For the same, a new alternative of SMO algorithm, i.e., mutual learning-based spider monkey optimization algorithm (MuLSMO) has been projected being inspired from the mutual learning concept among individuals. To testify the achievement of the so proposed algorithm, it is proved over a set of 20 standard optimization functions and is compared with standard SMO as well as its recent variants, namely Modified limacon SMO (MLSMO), Fibonacci-based SMO (FSMO), Power law-based SMO (PLSMO) and Levy flight SMO (LFSMO). Intensive statistical analysis of the results shows that MuLSMO came out to be significantly better at validating our newly proposed approach.

Keywords Expedition · Exploitation · Spider monkey optimization algorithm · MuLSMO

1 Introduction

Since decades, it has been in the nature of human to always treasure trove an optimal quick fix for a particular problem with less number of efforts and resources. Swarm intelligence has emerged brilliantly in the field of nature-inspired algorithms and has been solving optimization problems [1–3] since quite a long time. Relyed on the

M. Singh (✉) · N. Sharma · H. Sharma
Rajasthan Technical University, Kota, Rajasthan, India
e-mail: nsharma@rtu.ac.in

H. Sharma
e-mail: hsharma@rtu.ac.in

mutual behavior of social organisms, swarm intelligence-related algorithms discover the solution by a cooperative method of trial and error. The ability of social creatures to learn makes them capable to deal with such intricate tasks. The peer-to-peer learning practice of these social colonies is basically the main driving strength in developing such swarm-based algorithms efficient in every manner. Several researches from the past [4–7] have demonstrated that algorithms based on swarm intelligence have a huge potential to discover solutions for real-world optimization issues. One such algorithm developed under the supervision of swarm intelligence-based algorithms is the Spider monkey optimization algorithm (SMO) [8]. The brilliant food rummaging behavior of these spider monkeys was the keen source of inspiration for the algorithm to be developed. These monkeys belong to the society of fission-fusion relied animals where the individuals form minuscule temporary groups, whose members hail from a huge group to a minute one and converse depending upon the scarcity and sufficiency of food sources. The SMO algorithm improved with nonlinear perturbation rate by some researcher [9–12]. This algorithm is a clear illustration of the food rummaging practice followed by the spider monkeys. Though the algorithm has exceptional performance when it comes to find an optimal solution, it on the other hand also suffers from a few drawbacks like stagnation and slow convergence [8]. To overcome such drawbacks, an enhanced alternative of SMO named as Mutual Learning-based SMO (MuLSMO) has been presented in this paper. This new strategy helps in adjusting the newly produced candidate solution with higher fitness between two individuals that are selected on the basis of a factor known as mutual learning factor [13].

The remaining sections of the paper are framed in the following way: The standard SMO algorithm has been deliberated in Sect. 2. The newly proposed variant of SMO, i.e., MuLSMO is dealt with in Sect. 3. The standard constraint problems and results have been conferred in Sect. 4. Section 5 deals with the closure got on the proposed work done so far.

2 Spider Monkey Optimization (SMO) Algorithm

The algorithm comprises of six steps [8]. These steps are exemplified in the sections below:

2.1 Initialization Step

The algorithm begins with this step where a random populace of ' M ' spider monkeys are procreated and each individual monkey SM_x ($x = 1, 2, \dots, M$) is a vector of dimension Dim and this SM_x serves as the x th monkey in the swarm and being an appropriate solution to the problem under consideration. These SM_x are initialized using the following Eq. 1:

$$SM_{xy} = SM_{\minimy} + RN(0, 1) * (SM_{\maximy} - SM_{\minimy}) \quad (1)$$

here SM_{\minimy} and SM_{\maximy} are the constraints associated with SM_x in x th direction and RN is a random number scattered evenly in between the range $[0, 1]$.

2.2 Step of Local Leader (LLdr)

Every monkey gathers the information from its local leader and other fellow members and based upon that information, these monkeys try to enhance their respective location. A new fitness value is evaluated for this new location. If this value of new location is an improved one, then the monkey adopts this recent location as it is own and discards the previous one.

The location amendment equation for the x th Spider monkey who is a part of the v th local group is given by:

$$SM_{new,xy} = SM_{xy} + RN(0, 1) * (LLdr_{vy} - SM_{xy}) + RN(-1, 1) * (SM_{ry} - SM_{xy}) \quad (2)$$

where $SM_{new,xy}$ is the newly modified solution, $LLdr_{vy}$ is the LLdr in dimension y of v th local group and SM_{ry} is a randomly selected monkey in dimension y .

2.3 Step of Global Leader (GLdr)

In this step all the monkeys are given a chance to update their location after gathering the information from their global leader (GLdr) and its local members of group. The equation of location amendment for this step is as given below:

$$SM_{new,xy} = SM_{xy} + RN(0, 1) * (GLdr_y - SM_{xy}) + RN(-1, 1) * (SM_{ry} - SM_{xy}) \quad (3)$$

where $GLdr_y$ represents the GLdr's location of dimension y where $y \in (1, 2, \dots, Dim)$ is a randomly picked index value. The location of monkeys are modified depending on a probability factor called as $(prob_x)$ which is a fitness function. In such a manner, an individual having high fitness value is given more precedence over the ones who are less fit comparatively. The $prob_x$ values can be deduced using the equation as given below:

$$prob_x = 0.9 * \frac{fitness_x}{MFV} + 0.1 \quad (4)$$

where $fitness_x$ symbolizes the fitness amount of the x th monkey whereas MFV stands for the maximum fitness value in the whole group.

2.4 Learning Step of Global Leader (GLdr)

In this step, the monkey possessing the leading fitness in the whole group will be taken as the new modified location of the global leader applying the concept of greedy selection. Even then if the location of the leader (global) does not seem any enhancing as compared to the old location then the parameter, i.e., global limit count (GLC) is raised by a value of 1.

2.5 Learning Step of Local Leader (LLdr)

Here, in this step, the monkey having a leading fitness in the particular local group will be taken as the new modified location of the local leader (LLdr) by again applying the concept of greedy selection. When this enhanced location of LLdr is contrasted with the previous old location and even then if the LLdr's location does not seem to be enhanced, then the parameter, i.e., local limit count (LLC) is raised by a value of 1.

2.6 Decision Step for Local Leader

In this step, if the LLdr is not modified up to an already planned limit called the Local leader's limit (LLL) then every member of that smallest group will try to modify its location either by initializing randomly or by making use of the mixed information gathered from the leaders (local and global) by using the following Eq. 5 as follows:

$$SM_{new,xy} = SM_{xy} + RN(0, 1) * (GLdr_y - SM_{xy}) + RN(-1, 1) * (SM_{xy} - LL_{vy}) \quad (5)$$

The dimension of this newly enhanced spider monkey will be appealing toward the GLdr and will drift away from the LLdr as per Eq. 5.

2.7 Decision Step for Global Leader

In this step, we keep monitoring the location of GLdr and if it does not show any visible signs in its enhancement to an already planned limit called the Global leader's limit (GLL), the global leader of the group then disbands the group into smaller groups starting from 1,2 and so on until maximum group (MG) formulation is attained. Every time a new group is made as a result of division, every time a learning process is implemented for that group in order to elect a new leader of that particular group. The case where maximum groups are already formed and still there's no such change

in the global leader's location, then this global leader fuses those disbanded groups back into one.

3 Mutual Learning-Based Spider Monkey Optimization Algorithm (MuLSMO)

Mutual learning-based Spider Monkey Optimization algorithm (MuLSMO) as its name suggests is based on the learning behavior among the individuals when they work together coordinately. The source of inspiration for this variant to be developed was the mutually understood behavior among the various learners of the group in which the knowledge is transferred from highly fit solutions to the lower fit solutions [13]. The new solution can be found using Eqs. 6, 7 as shown below:

$$\text{SMnew}_{xy} = \text{SM}_{xy} + \text{RN}(0, \text{MLF}) * (\text{GLdr}_y - \text{SM}_{xy}) + \text{RN}(0, \text{MLF}) * (\text{SM}_{ry} - \text{SM}_{xy}), \quad \text{fitness}_x < \text{fitness}_r \quad (6)$$

$$\text{SMnew}_{xy} = \text{SM}_{ry} + \text{RN}(0, \text{MLF}) * (\text{GLdr}_y - \text{SM}_{ry}) + \text{RN}(0, \text{MLF}) * (\text{SM}_{xy} - \text{SM}_{ry}), \quad \text{fitness}_x \geq \text{fitness}_r \quad (7)$$

where SMnew_{xy} is the enhanced location of the SM_x monkey, GLdr_y signifies the location of the global leader, SM_{ry} denotes the location of the randomly selected monkey, fitness_x signifies the fitness value of the current solution, fitness_r denotes the fitness value corresponding to the random solution and $\text{RN}(0, \text{MLF})$ denotes a random number chosen between 0 and a non-negative constant known as the mutual learning factor.

From Eqs. 6, 7 it can be seen that the value of SMnew_{xy} relates to the difference between the two positions and also to the difference between their fitness values. By making a comparison between the current solution's and random solution's fitness values, it is made sure that the fitness value of the new solution will move to the better solution, which means to say that if the current solution has a higher fitness then each new solution will move toward this current solution otherwise it will move to the random neighbor solution. This mechanism of learning mutually between the two solutions helps in producing a better promising solution. Another thing that needs to be taken care of is the value of mutually learning factor (MLF). It plays an important role in balancing the perturbation between the related solutions. MLF should be a non-negative constant in order to properly ensure that the new solution move toward the better solution only. The value of MLF has been chosen extensively by doing a sensitivity analysis and is discussed in the later section of parameter settings.

The pseudo code of the newly presented mutual learning step is as depicted in algorithm number 1.

Algorithm 1 Mutual Learning Step

```

Initialize the population having solutions,  $SM_x (x = 1, 2, \dots, M)$  using eq 1 and set MLF = 1.5 ;
for  $x=1$  to  $M$  do
    Select a random neighbor solution from the swarm such that neighbor solution  $\neq x^{th}$  solution.
    Evaluate the fitness values of  $r^{th}$  and  $x^{th}$  solution.
    if  $fitness_r > fitness_x$  then
        Enhance the location of  $r^{th}$  neighbor solution using equation 6.
        Select the new location using greedy selection method among the old and new neighbor
        solution's location.
    else
        Enhance the location of  $x^{th}$  solution by using equation 7.
        Select the new location using greedy selection method among the old and new  $x^{th}$  solution's
        location.
    end if
end for

```

Like the basic SMO, MuLSMO algorithm is also disbanded into the equivalent steps, i.e., local leader step, mutual learning step, local and global leader learning steps, local and global leader decision steps. It is briefly discussed in the following algorithm number 2.

Algorithm 2 Mutual Learning based Spider Monkey Optimization Algorithm (MuLSMO)

```

Parameter initialization, namely the Dimension, Population size, MCN (Maximum number of
cycles) and set MLF = 1.5 ;
Initialize the solutions  $SM_x (x = 1, 2, 3, \dots, M)$  using equation. 1
Set cycle = 1.
while cycle <> MCN do
    Step 1.Local Leader (LLdr) Step.
    Step 2.Mutual Learning Step.
    Step 3.Learning Step of Local Leader.
    Step 4.Learning Step of Global Leader.
    Step 5.Decision Step for Local Leader.
    Step 6.Decision Step for Global Leader.
    cycle = cycle+1
end while
Return the best solution.

```

4 Benchmark Problems and Results

To prove how competent the proposed variant is, 20 constrained optimization problems of CEC 2006 are considered [14]. The characteristic properties of these problems are listed in Table 1.

Table 1 CEC 2006 test problems [14] where, Dim symbolizes the dimension, NEq symbolizes equality constraints, NIeq symbolizes inequality constraints and Nact symbolizes active constraints

Problem	Dim	Function type	NEq	NIeq	Optimal function value	Nact
Pr ₁	13	Quadratic	0	0	-15.000000	6
Pr ₂	20	Nonlinear	0	2	-0.803619	1
Pr ₃	10	Polynomial	1	0	-1.000500	1
Pr ₄	5	Quadratic	0	6	-30665.538672	2
Pr ₅	4	Cubic	3	0	5126.496714	3
Pr ₆	2	Cubic	0	2	-6961.813876	2
Pr ₇	10	Quadratic	0	5	24.306209	6
Pr ₈	7	Polynomial	0	4	680.630057	2
Pr ₉	8	Linear	0	3	7049.248021	6
Pr ₁₀	2	Quadratic	1	0	0.749900	1
Pr ₁₁	3	Quadratic	0	1	-1.000000	0
Pr ₁₂	5	Nonlinear	3	0	0.053942	3
Pr ₁₃	3	Quadratic	1	0	961.715022	2
Pr ₁₄	5	Nonlinear	0	38	-1.905155	4
Pr ₁₅	6	Nonlinear	4	0	8853.539675	4
Pr ₁₆	9	Quadratic	0	13	-0.866025	6
Pr ₁₇	7	Linear	5	1	193.724510	6
Pr ₁₈	22	Linear	11	1	236.430976	19
Pr ₁₉	9	Linear	1	2	-400.055100	6
Pr ₂₀	2	Linear	0	2	-5.508013	2

4.1 Experimental Results

The analytical comparison has been taken amid MuLSMO, basic SMO [8] , Modified Limacon SMO (MLSMO) [15], Fibonacci-based SMO (FSMO) [16], Power Law-based SMO (PLSMO) [17], Levy Flight SMO (LFSMO) [18]. In order to test the above mentioned algorithms on the respective testing conditions, the following experimental settings have been adopted:

- Estimated runs/simulation = 100.
- Size of Population (M) = 50.
- Maximum groups (MG) = M/10.
- The value of Mutual learning factor (MLF) has been delicately chosen to be as 1.5 as it is giving the promising mean function values as compared to other values for the two considered optimization problems, namely Pr₁ and Pr₇ chosen randomly for the analysis as shown in Fig. 1 .
- The other parametric settings for the competitors like SMO, MLSMO, FSMO, PLSMO and LFSMO are taken as similar as in their original work.

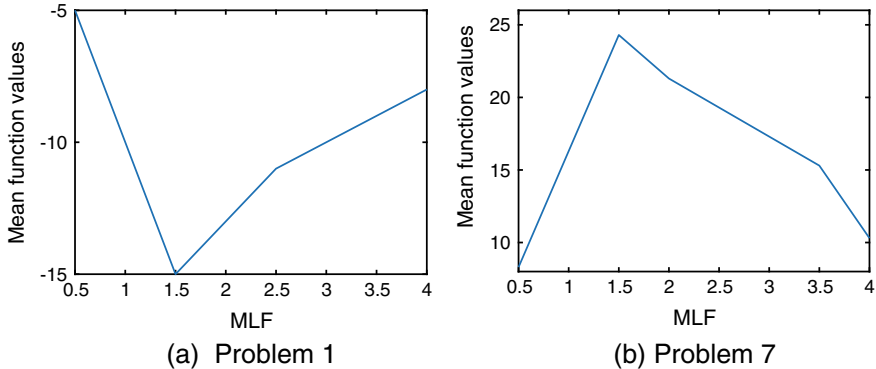


Fig. 1 Variation in the mean function values with change in parameter MLF of MuLSMO

The algorithms are compared on the basis of the mean values, the best values, the worst values and the SD values. Table 2 illustrates this comparison taken amid MuLSMO, SMO, MLSMO, FSMO, PLSMO and LFSMO on the respective parameters so discussed. The bold values signifies the superiority of the algorithm on the respective parameter. The overall results justify that MuLSMO is superior than the other recent variants taken under consideration for comparison. As shown in Table 2, MuLSMO outperforms others in terms of mean value for 9 problems ($Pr_2, Pr_4, Pr_{10}, Pr_{12}, Pr_{14}, Pr_{15}, Pr_{16}, Pr_{17}, Pr_{20}$), 14 problems ($Pr_2, Pr_3, Pr_4, Pr_5, Pr_6, Pr_8, Pr_{10}, Pr_{12}, Pr_{13}, Pr_{14}, Pr_{16}, Pr_{17}, Pr_{18}, Pr_{20}$) on the basis of best values. In addition to it, MuLSMO proves its supremacy on all the parameters considered for 2 problems (Pr_{10}, Pr_{20}).

Along with this, to deduce whether the obtained results have any reasonable difference or not, a statistical test known as Mann Whitney U Analysis [19] has been conducted which is a non-parameterized test in order to compare the non-Gaussian data. The dataset used for the test is the best values of each run. A consequence level of 5% is taken for the study, i.e., $\beta = 0.05$ is taken for the comparison between MuLSMO and SMO, MuLSMO-MLSMO, MuLSMO-FSMO, MuLSMO-PLSMO, MuLSMO-LFSMO.

Table 3 records the outcome of MWU Analysis for the best values of hundred estimated runs. An analysis has been made to check if there is any symbolic difference among the sets of data or not. If there seems no discrepancy then it can be concluded that it is a null hypothesis and for that an “=” operator will be used. The results help us to conclude that out of 20 Problems that were taken for testing purpose, MuLSMO has worked well for 18 problems when compared with SMO, 15 problems when compared with MLSMO, 18 problems when compared with FSMO, 13 problems when compared with PLSMO and on 16 problems when compared with LFSMO.

Table 2 Contrasting results on selected problems

Problem	Algorithms	Mean values	Best values	Worst values	SD
Pr ₁	MuLSMO	-14.97453	-15.00000	-12.45313	2.53411E-01
	SMO	-15.00000	-15.00000	-15.00000	0.00000E+00
	MLSMO	-14.39214	-14.99988	-12.44950	9.56742E-01
	FSMO	-14.98000	-15.00000	-13.00000	1.98998E-01
	PLSMO	-14.95919	-15.00000	-13.00000	2.79884E-01
	LFSMO	-14.98000	-15.00000	-13.00000	1.98998E-01
Pr ₂	MuLSMO	-0.79895	-0.80361	-0.73080	1.30920E-02
	SMO	-0.79678	-0.80358	-0.70813	1.32241E-02
	MLSMO	-0.66762	-0.77038	-0.54404	4.32237E-02
	FSMO	0.13336	-1.00000	-0.77039	1.33557E-01
	PLSMO	-0.79177	-0.79652	-0.75400	6.67627E-03
	LFSMO	-0.79576	-0.80354	-0.75558	8.33598E-03
Pr ₃	MuLSMO	-1.00028	-1.00040	-0.99885	2.29695E-04
	SMO	-1.00033	-1.00030	-0.99925	1.51951E-04
	MLSMO	-0.95699	-1.00024	0.00000	1.95357E-01
	FSMO	-1.00025	-1.00030	-0.99612	4.87935E-04
	PLSMO	-0.99118	-0.99778	-0.99050	1.09109E-03
	LFSMO	-1.00029	-1.00030	-0.99928	1.87544E-04
Pr ₄	MuLSMO	-30665.54000	-30665.54000	-30665.54000	1.39150E-09
	SMO	-30665.53099	-30665.53099	-30665.53099	1.64851E-10
	MLSMO	-30662.60000	-30665.53099	-30465.82000	2.02817E+01
	FSMO	-30665.53099	-30665.53099	-30665.53099	2.75825E-10
	PLSMO	-30665.53000	-30665.53099	-30665.53000	1.41879E-03
	LFSMO	-30665.53099	-30665.53099	-30665.53099	3.41369E-10
Pr ₅	MuLSMO	5216.54100	5126.43400	6009.20600	1.80547E+02
	SMO	5210.56100	5126.43444	6107.68800	1.63973E+02
	MLSMO	5537.33800	5126.44400	7555.62000	4.72758E+02
	FSMO	5262.82700	5126.43444	6096.90400	2.36335E+02
	PLSMO	5136.04300	5126.43444	5223.34400	2.07072E+01
	LFSMO	5219.85300	5126.43444	5794.01400	1.52788E+02
Pr ₆	MuLSMO	-6961.81000	-6961.81400	-6961.78200	4.99903E-03
	SMO	-6961.74100	-6961.81300	-6960.77100	1.64411E-01
	MLSMO	-6959.03800	-6961.64700	-6953.87300	1.71554E+00
	FSMO	-6961.74500	-6961.81300	-6961.11200	1.23741E-01
	PLSMO	-6961.80900	-6961.81300	-6961.78000	6.34016E-03
	LFSMO	-6961.81300	-6961.81300	-6961.80800	8.87047E-04
Pr ₇	MuLSMO	24.76890	24.34744	27.25707	4.98742E-01
	SMO	24.55465	24.33910	25.55106	2.32371E-01
	MLSMO	26.67869	24.36688	31.10798	1.83596E+00
	FSMO	24.61024	24.33498	26.02869	2.71507E-01
	PLSMO	24.48641	24.31224	25.46111	2.11582E-01
	LFSMO	24.52269	24.31825	25.73108	2.37988E-01

(continued)

Table 2 (continued)

Problem	Algorithms	Mean values	Best values	Worst values	SD
Pr ₈	MuLSMO	680.63920	680.63080	680.66680	6.48549E-03
	SMO	680.64150	680.63180	680.66650	7.88807E-03
	MLSMO	681.17580	680.72620	683.25180	4.54205E-01
	FSMO	680.64270	680.63140	680.68360	8.31056E-03
	PLSMO	680.64090	680.63480	680.66000	3.96033E-03
	LFSMO	680.63900	680.63150	680.65690	5.20237E-03
Pr ₉	MuLSMO	7388.90200	7049.71600	10349.18000	4.54584E+02
	SMO	7340.23300	7061.97900	11159.64000	4.89895E+02
	MLSMO	6.57667E+06	7085.47600	2.85339E+08	3.82393E+07
	FSMO	7302.22800	7058.22900	8751.59000	2.32410E+02
	PLSMO	7257.59200	7049.53500	9150.70500	2.49745E+02
	LFSMO	7193.12300	7050.50400	7848.93300	1.40492E+02
Pr ₁₀	MuLSMO	0.74999	0.74999	0.74999	2.15797E-09
	SMO	0.75000	0.75000	0.75001	1.80900E-06
	MLSMO	0.75287	0.75000	0.76079	2.93187E-03
	FSMO	0.75000	0.75000	0.75000	1.48796E-06
	PLSMO	0.75589	0.75025	0.75989	3.10824E-03
	LFSMO	0.75000	0.75000	0.75000	9.86172E-07
Pr ₁₁	MuLSMO	-1.00000	-1.00000	-1.00000	0.00000E+00
	SMO	-1.00000	-1.00000	-1.00000	0.00000E+00
	MLSMO	-0.99966	-1.00000	-0.99128	1.66406E-03
	FSMO	-1.00000	-1.00000	-1.00000	0.00000E+00
	PLSMO	-0.99388	-0.99991	-0.99010	3.52782E-03
	LFSMO	-1.00000	-1.00000	-1.00000	0.00000E+00
Pr ₁₂	MuLSMO	0.11149	0.05392	0.46528	1.54925E-01
	SMO	0.12547	0.05393	0.44327	1.23089E-01
	MLSMO	0.63435	0.06887	1.24852	2.60491E-01
	FSMO	0.13336	0.05393	0.44499	1.33557E-01
	PLSMO	0.14107	0.05431	0.45597	1.45987E-01
	LFSMO	0.16330	0.05393	0.43940	1.22749E-01
Pr ₁₃	MuLSMO	961.91110	961.71510	965.59150	5.92862E-01
	SMO	961.80530	961.71512	965.08230	4.38112E-01
	MLSMO	965.97040	961.74600	972.31750	3.73210E+00
	FSMO	961.89810	961.71512	966.24050	6.48975E-01
	PLSMO	961.89220	961.72290	963.99390	3.96286E-01
	LFSMO	961.73800	961.71512	962.44110	9.33115E-02
Pr ₁₄	MuLSMO	-1.90516	-1.90516	-1.90514	3.92491E-07
	SMO	-1.90510	-1.90510	-1.90515	7.60299E-07
	MLSMO	-1.89809	-1.90434	-1.87672	4.34829E-03
	FSMO	-1.90513	-1.90513	-1.90512	3.76501E-07
	PLSMO	-1.89623	-1.90082	-1.89516	1.37228E-03
	LFSMO	-1.90514	-1.90514	-1.90513	4.24717E-07

(continued)

Table 2 (continued)

Problem	Algorithms	Mean values	Best values	Worst values	SD
Pr ₁₅	MuLSMO	8900.08400	8853.54500	9265.00700	6.48579E+01
	SMO	8912.08300	8853.53000	9232.55100	7.06400E+01
	MLSMO	9057.35500	8897.57900	9312.82900	1.28254E+02
	FSMO	8912.53900	8853.54400	9253.09200	7.07159E+01
	PLSMO	8900.89200	8853.53001	9186.48000	5.87916E+01
	LFSMO	8908.46500	8853.53001	9169.63400	5.39110E+01
Pr ₁₆	MuLSMO	1.27400E+12	1.27400E+12	1.27400E+12	2.30640E+04
	SMO	1.27400E+12	1.27400E+12	1.27405E+12	5.32157E+06
	MLSMO	1.27402E+12	1.27400E+12	1.27409E+12	1.70934E+07
	FSMO	1.27400E+12	1.27400E+12	1.27400E+12	2.11115E+04
	PLSMO	1.27400E+12	1.27400E+12	1.27400E+12	1.39690E+02
	LFSMO	1.27400E+12	1.27400E+12	1.27400E+12	2.20283E+04
Pr ₁₇	MuLSMO	220.45510	187.06450	448.18170	4.49743E+01
	SMO	240.36460	187.35140	481.04840	5.35307E+01
	MLSMO	387.28710	187.09480	583.48210	1.30976E+02
	FSMO	245.07290	187.14590	470.25540	5.09035E+01
	PLSMO	227.31790	187.17090	480.14730	4.65391E+01
	LFSMO	231.74870	187.12420	360.22210	5.22206E+01
Pr ₁₈	MuLSMO	1.09231E+11	154.74900	9.00000E+12	9.13734E+11
	SMO	1.22960E+06	177.62060	1.02970E+08	1.03440E+07
	MLSMO	4.08768E+10	2.34487E+08	2.55926E+11	5.82656E+10
	FSMO	9.00000E+10	167.32920	9.00000E+12	8.95489E+11
	PLSMO	8840.69000	192.18370	2.18939E+04	5.51697E+03
	LFSMO	11790.92000	182.30890	3.61279E+05	3.55969E+04
Pr ₁₉	MuLSMO	109.48200	-358.74180	4741.79600	7.08865E+02
	SMO	83.98234	-382.59420	10763.02000	1.20425E+03
	MLSMO	1560.49300	-300.69600	26185.47000	4.12923E+03
	FSMO	1.21447	-368.48020	1892.66700	2.94824E+02
	PLSMO	-129.15480	-346.17000	252.11140	1.32484E+02
	LFSMO	-114.58180	-341.62300	620.85440	1.87609E+02
Pr ₂₀	MuLSMO	-5.50801	-5.50801	-5.50801	2.71000E-12
	SMO	-5.50800	-5.50800	-5.50800	1.18738E-11
	MLSMO	-5.05369	-5.50766	-4.50904	2.55880E-01
	FSMO	-5.50800	-5.50800	-5.50800	5.59936E-12
	PLSMO	-5.01416	-5.45573	-4.51783	2.46463E-01
	LFSMO	-5.50800	-5.50800	-5.50800	1.96228E-11

Table 3 Best values and MWU test-based comparison ('+' indicates MuLSMO is better, '−' symbolizes that MuLSMO is worse and '=' symbolizes that there is not any distinctive difference)

Problem	MuLSMO versus				
	SMO	MLSMO	FSMO	PLSMO	LFSMO
Pr ₁	+	+	+	+	+
Pr ₂	+	−	+	−	−
Pr ₃	−	−	−	−	−
Pr ₄	+	+	+	+	+
Pr ₅	+	+	+	+	+
Pr ₆	+	+	+	+	+
Pr ₇	−	+	−	−	−
Pr ₈	+	+	+	+	+
Pr ₉	+	+	+	+	+
Pr ₁₀	+	+	+	+	+
Pr ₁₁	+	+	+	−	+
Pr ₁₂	+	+	+	+	+
Pr ₁₃	+	+	+	+	+
Pr ₁₄	+	−	+	−	+
Pr ₁₅	+	+	+	+	+
Pr ₁₆	+	+	+	+	+
Pr ₁₇	+	+	+	+	+
Pr ₁₈	+	+	+	+	+
Pr ₁₉	+	−	+	−	−
Pr ₂₀	+	−	+	−	+
Total Positive Signs	18	15	18	13	16

5 Conclusion

The purpose of this article was to develop a competitive variant of SMO, namely Mutual learning-based SMO. This newly developed variant was testified on a set of 20 constraint optimization functions. The performance of this newly proposed variant MuLSMO has been extensively compared with its parent SMO and its other recent variants, namely MLSMO, FSMO, PLSMO and LFSMO. The results so obtained clearly suggests that MuLSMO has uplifted the SMO algorithm's performance in terms of accuracy, robustness and efficiency terms. Hence, MuLSMO can be considered as a promising alternative of SMO and may also be used to solve a variety of real-world optimization problems in the near future.

References

1. Sharma A et al (2016) Optimal design of PIDA controller for induction motor using spider monkey optimization algorithm. *Int J Metaheur* 5(3–4):278–290
2. Gupta K, Deep K, Bansal JC (2017) Spider monkey optimization algorithm for constrained optimization problems. *Soft Comput* 21(23):6933–6962
3. Gupta K, Deep K, Bansal JC (2017) Improving the local search ability of spider monkey optimization algorithm using quadratic approximation for unconstrained optimization. *Comput Intell* 33(2):210–240
4. Kennedy J, Eberhart R (1995) Particle swarm optimization. In: Proceedings of ICNN'95—International conference on neural networks, vol 4. IEEE
5. Dorigo M, Di Caro G (1999) Ant colony optimization: a new meta-heuristic. In: Proceedings of the 1999 congress on evolutionary computation-CEC99 (Cat. No. 99TH8406), vol. 2. IEEE (1999)
6. Vesterstrom, J, Thomsen R (2004) A comparative study of differential evolution, particle swarm optimization, and evolutionary algorithms on numerical benchmark problems. In: Proceedings of the 2004 congress on evolutionary computation (IEEE Cat. No. 04TH8753), vol 2. IEEE
7. Price K, Storn RM, Lampinen JA (2006) Differential evolution: a practical approach to global optimization. Springer
8. Bansal JC et al (2014) Spider monkey optimization algorithm for numerical optimization. *Memetic Comput* 6(1): 31–47
9. Sharma B, Sharma VK, Kumar S (2020) Sigmoidal spider monkey optimization algorithm. In: Soft computing: theories and applications. Springer, Singapore, pp 109–117
10. Kumar S, Nayyar A, Nguyen NG, Kumari R (2020) Hyperbolic spider monkey optimization algorithm. *Recent Adv Comput Sci Commun (Formerly: Recent Patents Comput Sci)* 13(1):35–42
11. Kumar S, Sharma B, Sharma VK, Sharma H, Bansal JC (2018) Plant leaf disease identification using exponential spider monkey optimization. *Sustain Comput: Inform Syst*
12. Kumar S, Sharma B, Sharma VK, Poonia RC (2018) Automated soil prediction using bag-of-features and chaotic spider monkey optimization algorithm. *Evol Intell* 1–12
13. Rao RV, Savsani VJ, Vakharia DP (2011) Teaching–learning-based optimization: a novel method for constrained mechanical design optimization problems. *Comput-Aided Des* 43(3):303–315
14. Liang JJ et al (2006) Problem definitions and evaluation criteria for the CEC 2006 special session on constrained real-parameter optimization. *J Appl Mech* 41(8):8–31
15. Sharma A et al (2017) Optimal placement and sizing of capacitor using limaçon inspired spider monkey optimization algorithm. *Memetic Comput* 9(4):311–331

16. Sharma A et al (2017) Fibonacci series-based local search in spider monkey optimisation for transmission expansion planning. *Int J Swarm Intell* 3(2–3):215–237
17. Sharma A et al (2017) Power law-based local search in spider monkey optimisation for lower order system modelling. *Int J Syst Sci* 48(1):150–160
18. Sharma A et al. (2016) Optimal power flow analysis using lévy flight spider monkey optimisation algorithm. *Int J Artif Intell Soft Comput* 5(4):320–352
19. McKnight Patrick E, Julius N (2010) Mann-Whitney U test. In: The Corsini encyclopedia of psychology, pp 1–1

Budget-Oriented Reliable WDO Algorithm for Workflow Scheduling in Cloud Systems



Poonam Singh, Maitreyee Dutta, and Naveen Aggarwal

Abstract The Use of Cloud computing for solving complex scientific workflow applications has become very popular nowadays. The cloud infrastructure is equipped with elastic, heterogeneous and cost-efficient resource provision features. It enhances the computing by offering user an on-demand services through Internet. Scheduling these workflow applications under user-defined budget constraint is one of the main challenge in cloud environment. Also taking failure of computing resource into consideration, it becomes imperative to generate reliable schedule while meeting other scheduling attributes like cost, time and deadline. This paper presents a hybrid wind-driven optimization algorithm (HWDO) to generate reliable workflow schedule by maintaining budget within specified limit. The algorithm is simulated using WorkflowSim with real-world scientific applications. The results achieved substantiate 9–17% reliable schedule than other algorithms by meeting the budget constraint.

Keywords Cloud computing · Workflow scheduling · Wind-driven optimization · Reliability · Budget · Failure factor

1 Introduction

Cloud computing has brought a revolution in computing paradigm by offering resource and software services through Internet. The computing services and resources can be provided to the users by following pay-per-use model. So the cloud computing platform has become main choice for researchers to execute large and complex applications. These applications are called workflow applications that normally require high performance computing for their execution. Cloud computing supports resource heterogeneity and elasticity feature to these workflow tasks so that the scheduling process has become very cost-effective. Still this computing era has to face many performance-related issues like resource's performance variations and its

P. Singh (✉) · M. Dutta
NITTTR, Chandigarh, India

N. Aggarwal
UIET, Panjab University, Chandigarh, India

failure factor. The performance variation is examined in case of resource sharing and it is found to be 4–16% over the cloud. Failure of any allotted resource can diminish the efficiency of applications processing. To execute the workflow scheduling process smoothly, we should also take the reliability of resources into consideration along with other scheduling attributes like execution time and cost. In literature, many researchers have proposed heuristics and meta-heuristics-based algorithms to address the reliability issue in workflow scheduling problem.

For scheduling independent tasks, reliable Heterogeneous earliest finish time (HEFT) [1] is presented that maximize the reliability and minimizes the execution time. Pareto-curve approximation is used to trade-off both the objectives. Budget constrained resource provisioning is presented in [2] which is based on modified HEFT algorithm. They considered the cost model using hour-based scheme in IaaS cloud system to minimize the execution time under budget constraint. In [3], authors presented a just-in-time(JIT) and adaptive strategy for fault-tolerant schedule. On-demand and spot instances are used to execute the tasks onto the available resources. This work aimed to minimize the execution cost of the scientific application and also generates reliable schedule meeting user-defined deadline constraint. Bala and Chana [4] used a hybrid algorithm which is a combination of First Come First Serve and Min-Min. The main focus of the algorithm is to optimize the execution time and balancing the load to increase the utilization of resources. The load is distributed in such a way that could results in less resource failure, so hereby enhancing the reliability of the system.

Genetic algorithm has been applied by many authors [5–8] to optimize the reliability along with time and cost of the workflows. Authors [9] have applied a genetic algorithm to produce reliable schedule and optimizes the makespan of applications. Energy consumption and reliability of the system are considered for optimization in [10]. In [11], authors have applied fuzzy dominance sorting to find the Pareto optimal solutions based on particle swarm optimization(PSO). They attempted to optimize the reliability along with time and cost of the schedule under budget and deadline constraints. Their proposed work performed better than the other multi-objective algorithms in grid environment. A hybrid particle swarm optimization(HPSO) is proposed in [12] in which budget and deadline constrained heuristic-based HEFT is used as a initial seed to the PSO algorithm. Their presented work tried to optimize the makespan, lease cost and energy consumption under strict deadline and budget limits. Though this approach assumed the resources provided by IaaS cloud are reliable. Mai and Cheng [13] developed an algorithm for scheduling independent tasks Ant Colony optimization and Harmony search in hybrid form. Their work focused on better resource utilization and reducing makespan along with selecting the reliable schedule. A new swarm algorithm called BAT algorithm is presented by [14] for scheduling scientific workflow applications while optimizing makespan and reliability under budget constraints. Binary version of Bat algorithm [15] is applied to

schedule workflow applications in cloud systems. Authors have worked to generate optimal task to resource mapping while minimizing the overall cost of execution. A fair budget constrained scheduling algorithm (FBCWS) is proposed in [16] for heterogeneous cloud environments. The presented work minimizes the makespan while satisfying budget constraints.

In most of the work found in literature, authors have emphasized on minimizing either time or cost along with maximizing the reliability. None of the work has considered the user-defined budget constraints while generating the schedule. With this motivation, we proposed a hybrid wind-driven optimization algorithm [17] to optimize the makespan and reliability of the schedule while meeting the user-defined budget constraint. Wind-driven optimization(WDO) is a meta-heuristic-based approach which is proposed by Bayraktar [18] to synthesize the linear antenna array. WDO is based on earth's atmospheric motion of wind where it streams to even out the pressure in the air [19].

The structure of the paper is organized as follow. Section 2 describes the problem and Sect. 3 introduces the concept of basic WDO algorithm. Proposed algorithm is explained in Sect. 4 followed by its performance assessment which is done in Sect. 5. Section 6 summarizes the paper with conclusion and the future research work.

2 Problem Description

2.1 Workflow and Application Model

A directed acyclic graph (DAG) $G = (I, P)$, is used to model a task graph or complex scientific workflow consisting of $I = |I|\{i_1, i_2, \dots, i_m\}$ nodes with $|P|$ directed edges p_{yz} depicting the data dependency between the node i_y and i_z . Each node $i_y \in I$ portrays the workflow task holding a workload $WL(i_y)$ measured in million instructions (MI) and each edge p_{yz} indicates a certain amount of data size $data(i_y)$ which is transferred.

A cloud infrastructure consists of n virtual machines (VM) $Q = q_1, q_2, \dots, q_n$, where every VM type q_j is associated with cost $Cost(q_j)$, processing power $Power(q_j)$ and failure rate $\lambda(q_j)$ attributes. The processing power is the time used to process single instruction and its measuring unit is million instructions per second (MIPS). The cost indicates the overall cost for using the virtual machine per unit time.

$$ET(i_y, q_j) = \frac{WL(i_y)}{Power(q_j) \times (1 - PV(q_j))} \quad (1)$$

$$TT(i_y, i_z) = \frac{data(i_y)}{bw} \quad (2)$$

$ET(i_y, q_j)$ is the execution time and $TT(i_y, i_z)$ is the cost of data transfer from task i_y to task i_z , bw is the average bandwidth. The value of $TT(i_y, i_z) = 0$, if i_y and i_z are processed by same VM.

Overall cost of a workflow application is the cost of all the assigned or mapped VMs and it is computed as:

$$\text{Cost(WA)} = \sum_{j=1}^n \text{Cost}(q_j) \times \lfloor \frac{\text{LRT}(q_j) - \text{LAT}(q_j)}{\tau} \rfloor \quad (3)$$

Here n represents total number of allotted virtual machines, τ is the unit time interval used for billing, $LAT(q_j)$ is the time when VM q_j is acquired and $LRT(q_j)$ is the VM release time. It is assumed that VMs are provided from single data center and data transfer charges are also assumed to be zero. Let $\text{Time}_{\text{begin}}(i_y, q_j)$ and $\text{Time}_{\text{end}}(i_y, q_j)$ are the begin and end time of the task i_y on the VM q_j . The begin time of the task with no parent is calculated as:

$$\text{Time}_{\text{begin}}(i_{in}, q_j) = \text{free}(q_j) \quad (4)$$

where $\text{free}(q_j)$ is the time when the VM q_j is available for processing the task. For the remaining tasks in the application, these values are determined as:

$$\text{Time}_{\text{begin}}(i_y, q_j) = \max \left\{ \text{free}(q_j), \max \left\{ \text{Time}_{\text{end}}(i_z) + TT_{yz} \right\} \right\} \quad (5)$$

where $i_z \in \text{child}(i_y)$

$$\text{Time}_{\text{end}}(i_y, q_j) = ET(i_y, q_j) + \text{Time}_{\text{begin}}(i_y, q_j) \quad (6)$$

We assume the storage cost to be zero and also we have a plenty of VMs provided at the data center to avoid conflict to same VM. The total execution time taken for a workflow application (WA) is computed using Eq. 7.

$$\text{Time(WA)} = \max_{y \in I, j \in Q} \{ \text{Time}_{\text{end}}(i_y, q_j) \} \quad (7)$$

2.2 Reliability Model

The reliability model used here makes similar assumptions as taken in [9]. The failure rate of the VM is assumed to be stable and Poisson distribution is followed to model failure of VM. We calculate the probability $FP(q_j^{\text{WA}}) = e^{(-ET(i_y, q_j) * \lambda(q_j))}$ by which the VM q_j can successfully execute all tasks assigned to it in a workflow schedule WS and we name it as probability of success $\text{Prob}_{\text{succ}}$. Thus the reliability

of a schedule Reliability (WA) can be defined as the probability of the VM that it finishes its process correctly using Eq. 8:

$$\text{Reliability(WA)} = \prod_{j=1}^n \text{FP}(q_j^{\text{WA}}) = e^{-\text{Time(WA)} * \lambda(q_j)} \quad (8)$$

2.3 Bi-criteria Budget Constrained Problem

Here we address the problem of scheduling the dependent tasks to the virtual machines provided at cloud infrastructure. The tasks are assigned uniquely and their precedence relation is also followed while making scheduling decision. The fitness function here we use works on two factors: reliability and makespan or execution time of the workflow schedule. We can maximize the reliability by reducing the failure rate $\text{fail(WA)} = \sum_{j=1}^n \text{Time(WA)} * \lambda(q_j)$ of all the VMs. These conflicting factors can be solved by allocating the VM q_j with minimum $\lambda_j \times \gamma_j$ (the product of failure rate λ_j and processing power γ_j) to the tasks. The VMs with minimum product value will be given priority than other VM with maximum product value [7]. A user-defined Budget is used to make this problem as constrained problem along with optimization problem. With this, only that schedule will be generated whose cost will be below the budget otherwise it starts with next iteration. So we define the problem as:

$$\begin{aligned} & \text{Maximize the reliability : Reliability(WA)} \\ & \text{Minimize the Makespan : Time(WA)} \\ & \text{Subject to : Cost(WA)} \leq \text{Budget} \end{aligned} \quad (9)$$

3 Wind-Driven Optimization (WDO)

The wind-driven optimization is an evolutionary algorithm established in 2010 by Bayraktar et al. In this algorithm, air molecule is used to represent a feasible solution for optimization problem [20]. All the molecules have pressure value which is used as a fitness function to select possible solution for a given problem. The velocity and position of the air molecule enable to achieve best solution while moving in the search space. The status of the air molecule expressed by its velocity and position, which are modified in every iteration. For next iteration the value for velocity and position is calculated as given in 10 and 11.

Velocity Vector

$$\begin{aligned} \text{velocity}_{\text{next}} = & (1 - \alpha) \text{velocity}_{\text{prev}} - g \text{Pos}_{\text{cur}} \\ & + \left(|P \text{ value}_{\text{opt}} - P \text{ value}_{\text{cur}}| (\text{Pos}_{\text{opt}} - \text{Pos}_{\text{cur}}) \frac{RT}{P \text{ value}_{\text{cur}}} \right) \\ & + \left(\frac{-2\Omega \times RTv}{P \text{ value}_{\text{cur}}} \right) \end{aligned} \quad (10)$$

where:

α = friction coefficient

T = temperature coefficients

g = gravitational change in velocity

R = gas constant

$P \text{ value}_{\text{cur}}$ = pressure value at current position

$P \text{ value}_{\text{opt}}$ = optimum pressure position

Pos_{cur} = current position

Pos_{opt} = optimum position

$(\Omega \times v)$ = Coriolis force

Position Vector

$$\text{Pos}_{\text{new}} = \text{Pos}_{\text{cur}} + (\text{velocity}_{\text{next}} \times \Delta\text{time}) \quad (11)$$

where Pos_{cur} is old position of the air molecule and Pos_{new} is the new position obtained in upcoming iteration with unit time step, i.e., $\Delta\text{time} = 1$.

3.1 Air Molecule Representation

In WDO, air molecules are used to depict the solution for scheduling problem and solution is optimized by evaluating their fitness function. A air molecule is associated with dimension and range. The dimension is placed equal to the total tasks of the application and range is decided by the number of resources like VMs provided. If we have 5 tasks and 3 VMs are assigned to them, then air molecule representation will be as in Table 1.

Table 1 Representation of air molecule

Tasks	i_1	i_2	i_3	i_4
air_molecule1	1	3	2	1
air_molecule2	3	1	2	2
air_molecule3	2	3	1	3

3.2 Fitness Function

The goodness of the schedule obtained from proposed method is identified by using fitness function. The fitness function is to maximize the reliability and minimize execution time termed as makespan of the schedule while meeting budget constraint of the application. For this, if budget constraint is met, we define the fitness function as:

$$\text{fitness} = \beta \times \text{Time(WA)} + (1 - \beta) \times \text{fail(WA)}, \quad (12)$$

$$(\beta = [0.2, 0.4, 0.6])$$

4 Proposed Algorithm

This section entails the proposed algorithm for scheduling workflow applications based on hybrid WDO algorithm.

Algorithm 1: Proposed Algorithm

Input : Workflow consisting of m tasks, set of n resources called VMs and user-defined *Budget*

Output: Budget constrained Schedule with lower failure rate

- 1 Calculate the *rank_value* of every task of a workflow using Eq. 13 and save the tasks in decreasing order of their rank value in I_{Task_Queue}
- 2 Sort the VMs in ascending order of their failure rate (FR) and put them in Q_{Ready_List}
- 3 Initialize $Budget_Factor = Budget - Cost_{lowest}$
- 4 **while** maximum iterations reached **do**
- 5 | Initialize the population by taking one air molecule as task-VM mapping obtained in step 1
- 6 | Create the remaining air molecules by putting tasks randomly on different VMs available
- 7 | **while** the I_{Task_Queue} is empty **do**
- 8 | Select the current task i_{curr} from $Task_Queue$
- 9 | Assign i_{curr} onto the q_{Sel} VM selected from Q_{Ready_List}
- 10 | Add q_{Sel} to Q_{Sel_list}
- 11 | Calculate fitness function using equation 12 for each air molecule
- 12 | Update the budget factor using equation 15
- 13 | Update the velocity using equation 10
- 14 | Update position of air molecule using equation 11
- 15 | Update the I_{Task_Queue} and Q_{Sel_list} based on fitness function evaluation of the air molecules
- 16 | **end**
- 17 **end**

A number of solutions are possible for a given problem and such solutions are termed as population for meta-heuristic method. In the proposed strategy, for generating superior initial population, the tasks are arranged in descending order as per their rank value calculated using 13.

$$\text{rank}(i_y) = \max_{z \in \text{child}(i_y)} \{\text{AVG}_{\text{value}(p_{yz})} + \text{rank}(i_z)\} + AET(i_y) \quad (13)$$

All the available virtual machines are sorted in increasing order of their failure rate in $Q_{\text{Ready_List}}$. The budget factor is initialized as:

$$\text{Budget_Factor} = \text{Budget-Cost}_{\text{lowest}} \quad (14)$$

Where Budget is the user-defined budget which is used as upper bound for the cost of the schedule and $\text{Cost}_{\text{lowest}}$ is the minimum cost assignment of VM that represents the lower bound for the schedule cost. For all the unscheduled tasks from the task queue $I_{\text{Task_Queue}}$, select the current task i_{curr} and assign it to the VM selected from $Q_{\text{Ready_List}}$. Every time after the VM selection, the budget_factor is recomputed using following equation:

$$\text{Budget_Factor} = \text{Budget_Factor} - [\text{Cost}(i_{\text{curr}}, q_{\text{sel}}) - \text{Cost}_{\text{lowest}}(i_{\text{curr}})] \quad (15)$$

Fitness value of every air molecule is evaluated and its velocity and position are revised at every iteration until we reach the maximum iterations. In the end, the $Q_{\text{Sel_list}}$ is formed that contains the lowest cost VM with lower failure rate.

5 Performance Evaluation

The proposed algorithm is performed using four different scientific workflow applications: Montage, LIGO, Sipt and Epigenomics. The structure of these applications is depicted in Fig. 1. Montage is an I/O intensive astronomical application with reduced CPU requirements. The LIGO inspiral application belongs to physics and used to detect gravitational waves. It is characterized as CPU intensive application. Sipt and Epigenomics applications are based on biology. The portion of these application's structure is presented in Fig. 1. The details of these applications are found in [21].

5.1 Simulation Setup

We assume a IaaS cloud with one data center that provides 4 types of virtual machines (VMs) with varying processing speed on the range of 1000–6000 MIPS. The lease cost is set randomly in a range of 2–10 units per time interval where the highest processing speed VM is assumed to be five units costlier than the lowest speed

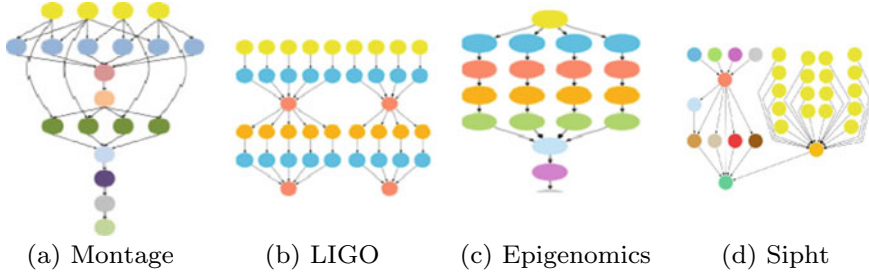


Fig. 1 Structure of various scientific workflows [21]

VM. The average bandwidth between the virtual machines (VMs) is made equal to 20 Mbps. The failure rate of the VMs is considered within the range of 10^{-3} – 10^{-4} failures per hour [9] using uniform distribution. For simulating cloud environment WorkflowSim toolkit [22] is used that efficiently evaluate scheduling algorithms on workflows. The experiments are conducted using the task size of 100 of each workflow. The algorithms are executed 10 times and average values of makespan and reliability are depicted in result graphs. The user-defined budget for the workflow is computed using the following equation:

$$\text{Budget} = \text{LB}_{\text{Cost}} + \phi_B \times (\text{UB}_{\text{Cost}} - \text{LB}_{\text{Cost}}) \quad (16)$$

where LB_{Cost} is the lower bound for the budget which estimated by assigning the tasks on lowest cost VM and UB_{Cost} is the highest cost computed by executing all the tasks on the costliest VM. The value of ϕ_B is taken in the range of 0 and 1. For this paper, the results are demonstrated using the value 0.2, 0.4, 0.6 for ϕ_B .

5.2 Results Evaluation

To validate the results obtained from proposed algorithm, basic genetic algorithm (BGA) [9], bi-criteria priority-based particle swarm optimization (BPSO) [23] and BAT algorithm [14] are used as baseline algorithms for comparisons. The population size and maximum iterations for all the algorithms are taken as 50 and 100, respectively. We set the other parameters for BGA, BPSO and HWDO as given in Table 2. Under Figs. 2 and 3 various graphs indicate makespan and reliability values when scheduling scientific workflows. The results show that HWDO outperforms than BGA, BPSO and BAT by generating reliable schedule with optimized makespan under the budget constraint. HWDO algorithm yields enhancement in the makespan by 34, 31, 38 and 41% for Montage, Inspiral LIGO, Sipht and Epigenomics workflows than the basic genetic algorithm (BGA). Comparing with BPSO, the average makespan found by HWDO is improved with 20, 51, 49 and 53% for Montage, LIGO, SIPHT and Epigenomics workflows, respectively. Similarly, the proposed algorithm

Table 2 Parameter settings for the algorithms

Algorithm	Parameters	Values
BGA	Crossover probability	0.5
	Mutation probability	0.1
BPSO	Inertia weight	0.9
	Acceleration coefficient	2
	Maximum velocity	3
BAT	Emitted pulse rate	rand[0, 1]
	Loudness of bats	rand[0, 1]
	Constants	0.6 and 0.5
HWDO	RT coefficient	3
	Constant in update equation	0.2
	Gravitational constant	0.4
	Coriolis effect	0.4
	Maximum velocity	4

gives improvement in makespan by 45, 40, 45 and 48% for Montage, Inspiral LIGO, Sipht and Epigenomics workflow applications when compared with BAT algorithm. The reliability of the schedule is also increased while using HWDO than BGA, BPSO and BAT algorithms. The proposed algorithm maximizes the reliability by using more reliable VMs and it gave 9–17% better results than other algorithms.

The simulation results substantiate that the HWDO gave potential outcome in generating reliable schedule with minimum makespan under budget condition over the other three algorithms.

6 Conclusion

In this paper, a scheduling algorithm is proposed based on wind-driven optimization in clouds. The proposed method is based on optimization which focuses on minimizing the makespan and assigning the tasks to lower failure rate VMs (resources) while satisfying the budget constraint. Trade-off factor is used to optimize the makespan and reliability of the schedule. The potential of the proposed technique is presented using four scientific workflows with different domains. The simulation results manifest that the HWDO produce quality solutions involving different data sizes when compared with BGA, BPSO and BAT algorithms.

Fig. 2 Average makespan of various workflows with large data size

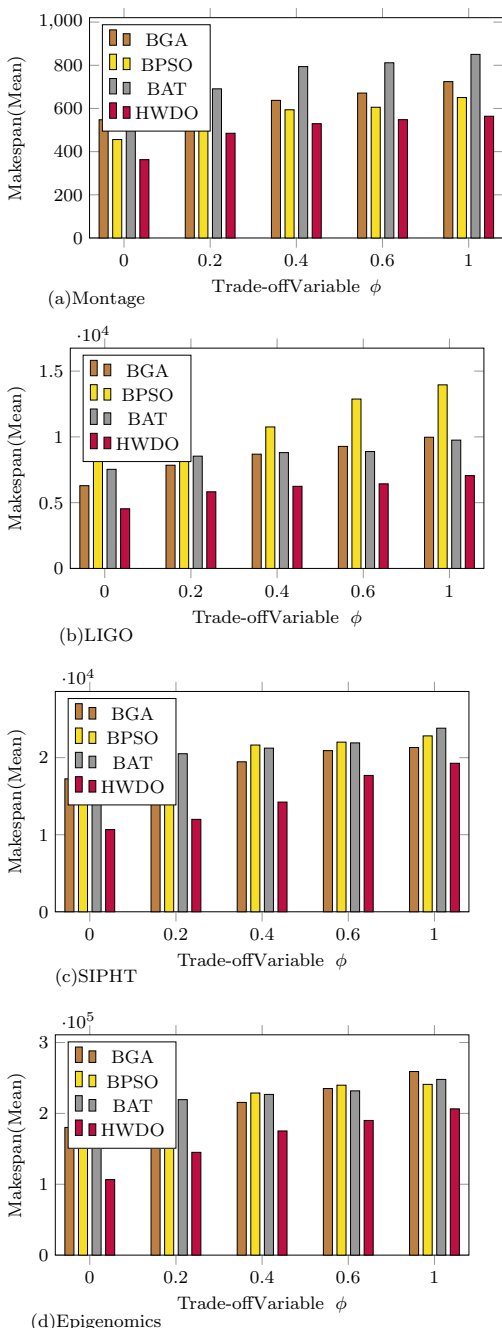
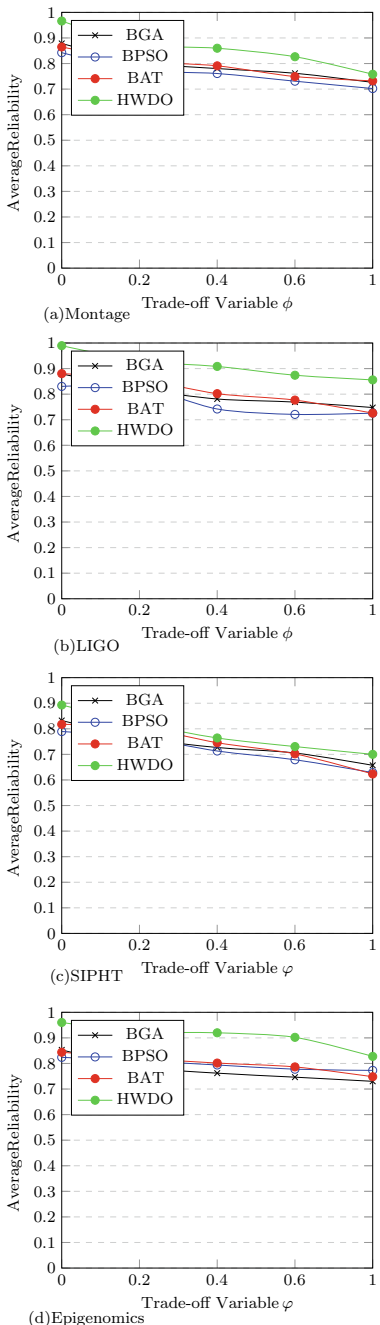


Fig. 3 Average reliability of various workflows with large data size



References

1. Dongarra JJ, Jeannot E, Botanique J, Nancy V, Saule E (2007) Bi-objective scheduling algorithms for optimizing makespan and reliability on heterogeneous systems. In: Proceedings of the nineteenth annual ACM symposium on Parallel algorithms and architectures SPAA 07, pp 280–288
2. Faragardi HR, Fazliahmadi S, Rasouli N, Fahringer T (2019) A budget-constrained resource provisioning scheme for workflow scheduling in IaaS cloud transactions on parallel and distributed systems a Budget-constrained resource provisioning scheme for workflow scheduling in IaaS cloud. No. 2019
3. Poola D, Ramamohanarao K, Buyya R (2016) Enhancing reliability of workflow execution using task replication and spot instances. ACM Trans. Auton. Adapt. Syst. Article 10(21). <https://doi.org/10.1145/2815624>
4. Bala A, Chana I (2015) Autonomic fault tolerant scheduling approach for scientific workflows in cloud computing. Concurr Eng: Res Appl 23(1):27–39
5. Hamed AY (2012) Task allocation for maximizing reliability of distributed computing systems using genetic algorithms. Inte J Comput Netw Wirel Commun (IJCNWC) 2(5):560–569
6. Vidyarthi DP, Tripathi AK (2001) Maximizing reliability of distributed computing system with task allocation using simple genetic algorithm. J Syst Architect 47(6):549–554. <http://linkinghub.elsevier.com/retrieve/pii/S1383762101000133>
7. Wang X, Shin C, Buyya R, Su J (2011) Optimizing makespan and reliability for workflow applications with reputation and look-ahead genetic algorithm. Future Gener Comput Syst 27(8):1124–1134
8. Devi MR, Anju A (2014) Multiprocessor scheduling of dependent tasks to minimize makespan and reliability cost using NSGA-II. Int J Found Comput Sci Technol 4(2): 27–39. <http://www.aircse.org/journal/ijfcst/papers/4214ijfcst04.pdf>
9. Doğan A, Özgürer F (2005) Biobjective scheduling algorithms for execution time-reliability trade-off in heterogeneous computing systems. Comput J 48(3):300–314. <https://doi.org/10.1093/comjnl/bxh086>
10. Faragardi HR, Rajabi A, Shoaee R, Nolte T (2013) Towards energy-aware resource scheduling to maximize reliability in cloud computing systems. In: IEEE international conference on high performance computing and communications & international conference on embedded and ubiquitous computing, pp 1469–1479. <http://www.scopus.com/inward/record.url?eid=2-s2.0-84903978085&partnerID=tZotx3y1>
11. Garg R, Kumar A (2013) Multi-objective workflow grid scheduling using ϵ -fuzzy dominance sort based discrete particle swarm optimization
12. Verma A, Kaushal S (2017) A hybrid multi-objective particle swarm optimization for scientific workflow scheduling. Parallel Comput
13. Mai H, Cheng L (2016) ACO-HS: a hybrid cloud resource scheduling model. Iceta, pp 148–152
14. Kaur N, Singh S (2016) A budget-constrained time and reliability optimization BAT algorithm for scheduling workflow applications in clouds. Procedia Comput Sci 58:199–204 (Euspn). <http://dx.doi.org/10.1016/j.procs.2016.09.032>
15. Raghavan S, Sarwesh P, Marimuthu C, Chandrasekaran K (2015) Bat algorithm for scheduling workflow applications in cloud. In: 2015 International conference on electronic design, computer networks automated verification (EDCAV), pp 139–144
16. Rizvi N, Ramesh D (2020) Fair budget constrained workflow scheduling approach for heterogeneous clouds. Cluster Comput 23:3185–3201
17. Singh P, Dutta M, Aggarwal N (2017) Wind driven optimization based workflow scheduling in cloud computing. In: International conference on communication, computing and networking (ICCCN). Elixir Publications, pp 283–292
18. Bayraktar Z, Komurcu M, Werner DH (2010) Wind driven optimization (WDO): a novel nature-inspired optimization algorithm and its application to electromagnetics (1). In: Proceedings of the antennas and propagation society international symposium (APSURSI), no 1, pp 1–4

19. Bayraktar Z, Komurcu M, Bossard JA, Werner DH (2013) The wind driven optimization technique and its application in electromagnetics. *IEEE Trans Antennas Propag* 61(5):2745–2757
20. Farmer GT, Cook J (2013) Introduction to earth's atmosphere. In: Climate change science: a modern synthesis: vol 1—The physical climate. Springer, Dordrecht, Netherlands, pp 179–198. https://doi.org/10.1007/978-94-007-5757-8_8
21. Juve G, Chervenak A, Deelman E, Bharathi S, Mehta G, Vahi K (2013) Characterizing and profiling scientific workflows. *Future Gener Comput Syst* 29(3):682–692. <https://doi.org/10.1016/j.future.2012.08.015>
22. Chen W, Deelman E (2012) WorkflowSim: a toolkit for simulating scientific workflows in distributed environments. In: 2012 IEEE 8th international conference on e-science, e-Science 2012
23. Verma A, Kaushal S (2014) Bi-criteria priority based particle swarm optimization workflow scheduling algorithm for cloud. In: Recent advances in engineering and computational sciences (RAECS), pp 6–8

Classification of Fundus Images Based on Non-binary Patterns for the Automated Screening of Retinal Lesions



Mekhana Suresh, Sreelekshmi Indira, and Sivakumar Ramachandran

Abstract The prevalence of lesions in the human retina has increased many folds during the past few decades. The two major causes of retinal lesions that affect the visual system are diabetic retinopathy (DR) and age-related macular degeneration (AMD). Digital retinal images obtained from the fundus camera are typically used for lesion screening. Due to the large affected population, manual screening is not a feasible solution for the early diagnosis of the disease. Hence, there exists a high demand for automated computer-aided screening systems that help clinicians to handle the enormous image data. The proposed screening technique relies on the texture analysis of the retinal background using local ternary patterns (LTP). Also, we compared the results obtained using the proposed approach with local binary patterns (LBP) instead of LTP. Three experiments separating, DR from normal, AMD from normal, and DR from AMD are conducted and tested using the proposed pipeline. The feature vectors generated from the proposed technique are analyzed using various classifiers, and the discriminating capabilities of each classifier are reported quantitatively. The results obtained show the effectiveness of LTP in analyzing the retinal texture for diagnosing various lesions.

Keywords Diabetic retinopathy · Age-related macular degeneration · Local binary patterns · Classification

M. Suresh · S. Indira · S. Ramachandran (✉)

Department of Electronics and Communication Engineering, College of Engineering Trivandrum, Thiruvananthapuram, Kerala 695016, India

e-mail: sivan@cet.ac.in

1 Introduction

The retinal fundus camera is a non-invasive diagnostic tool for the screening of various eye diseases, namely diabetic retinopathy (DR), age-related macular degeneration (AMD) and glaucoma. DR and AMD are the two major eye diseases, which are considered to be the leading cause of lifelong vision impairment and blindness. The statistics obtained from the literature shows that the number of DR affected population will rise to 191 million by 2030 [1], and for AMD, the rise goes beyond 196 million by 2020 [2]. Hence, there is a great demand for automated screening techniques due to this large growth of affected inhabitants worldwide. It is worth noting that the early diagnosis by the periodic screening of the retina, with proper medication, will reduce the risks caused due to the diseases. The reported work is a computer-aided automated diagnostic system that is based on the texture analysis of the retinal background using non-binary patterns. To the extent of our knowledge, this is the first work that utilizes non-binary patterns for retinal disease screening.

The major characteristic features of DR and AMD include, but are not limited to, the presence of retinal lesions namely microaneurysms, exudates, or drusen in the retinal surface. Manual delineation of lesions is a very challenging and tedious task, while its automatic segmentation techniques are often prone to errors. In this work, no lesion segmentation is performed and analysis is carried out in the retinal background obtained after the removal of retinal vasculature and optic disk.

The literature contains a fairly good amount of work for the automated screening of various retinal diseases, but the usage of the local binary patterns for screening is very less. The work proposed in [3], classify DR, AMD, and normal fundus images using LBP, and compared the performance with other descriptors such as LBP filtering (LBPF) and local phase quantization (LPQ). Galshetwar et al. [4] used LBP along with color features for content-based image retrieval in DR images. Omar et al. [5] introduced multiscale LBP texture analysis with an artificial neural network (ANN) classifier for automatic exudate detection in DR images. Krishnan and Laude [6] classified DR images using a combination of features obtained from entropy and invariant moments together with LBP. Mookiah et al. [7] used feature vectors obtained from local configuration pattern (LCP) along with linear support vector machine (SVM) to classify normal and AMD images. Garnier et al. [8] used LBP histograms extracted from wavelet coefficients to obtain textural features at various scales. Linear discriminant analysis (LDA) is then performed on the feature sets obtained from the histograms to classify images as healthy or AMD cases. Kumar [9] used LBP for detecting microaneurysms in retinal images by analyzing the retinal background without the need for prior segmentation of suspicious lesions. LBP histogram for each color channel is evaluated and the feature vectors obtained are tested using different classifiers.

The main contributions of this work include a retinal lesion detection technique for the identification of DR and AMD in fundus images. The proposed system inspects the retinal background and avoids the conventional lesion segmentation stage for analysis. The pipeline exploits the discriminating ability of local ternary patterns for

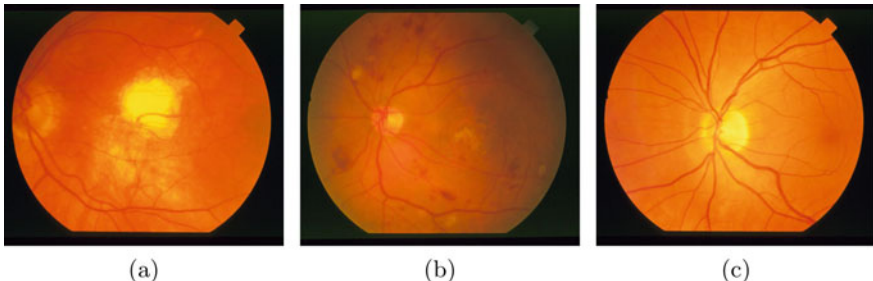


Fig. 1 Examples of retinal images with different disease manifestations obtained from STARE [10] dataset. Case of **a** AMD, **b** DR, and **c** healthy images

achieving the desired objective. A quantitative performance analysis utilizing various classifiers is carried out with the proposed system.

2 Materials and Methods

The resources used for the testing and evaluation consist of retinal images obtained from three publicly available datasets, which are classified as DR, AMD, and healthy based on the opinion of a group of retinal experts. The texture descriptors, namely LBP and LTP, are explored for investigating the texture of retinal background.

2.1 Retinal Images

For studying the effectiveness of the proposed technique, various experiments are performed using the publicly available data sets, namely STARE [10], E-Ophtha [11], and ARIA [12]. A total of 234 images obtained from the three datasets are used for the entire experimentation. From each dataset, the images with doubtful decisions as marked by clinicians and those heavily affected by noise are not considered for the final evaluation. Even though the images present in the datasets have other disease manifestations, we considered DR, AMD, and normal categories, which can be tested using our proposed pipeline. The image resolution of STARE, E-Ophtha, and ARIA datasets are 605×700 pixels, 2544×1696 pixels, and 576×768 pixels, respectively. The images are accompanied by ground truths labels, which help in the training and validation procedures. In Fig. 1, three representative images selected from Stare dataset [10] are shown for illustration.

The images selected from the three datasets are divided into model and validation image sets. The model set is used to train the classifier and is further divided into train and test sets, while validation set is solely used for validating the model trained

Table 1 Number of images used for experiments under each category. Various classifiers are trained and tested under each class, namely DR-Normal, AMD-Normal, and DR-AMD

	AMD	DR	Normal
Model set	25	63	97
Validation set	7	17	25

using the model set. The number of DR, AMD, and healthy images present in the model and validation set are shown in Table 1.

2.2 Local Binary Pattern (LBP)

LBP operator [13] is one of the widely used texture descriptors in the literature for diverse applications, due to its high descriptive power and invariance to local grayscale variations. LBP operator is defined for each pixel in the image based on a circular neighborhood of P pixels of gray level g_p and radius R , around the center pixel of gray value g_c . LBP is computed as:

$$\text{LBP}_{P,R} = \frac{1}{P} \sum_{p=0}^{P-1} S(g_p - g_c) 2^p \quad (1)$$

where

$$S(x) = \begin{cases} 1, & g_p > g_c \\ 0, & g_p \leq g_c \end{cases} \quad (2)$$

LBP for each pixel is obtained as the summation of the binary string weighted with the powers of two by taking the corresponding values in clockwise direction, as shown in Fig. 2a.

2.3 Local Ternary Pattern (LTP)

The inherent noise sensitivity of LBP descriptors in near-uniform image regions can be alleviated using ternary coding [14], achieved by introducing a threshold parameter τ in the canonical LBP function $S(x)$. A user-defined thresholding parameter is required, and the ternary code obtained is bifurcated to form two binary pattern as shown in Fig. 2b, c. The LTP function is computed by modifying LBP function $S(x)$ as:

$$S(x) = \begin{cases} 1, & g_p - g_c \geq \tau \\ 0, & |g_p - g_c| \leq \tau \\ -1, & g_p - g_c \leq -\tau \end{cases} \quad (3)$$

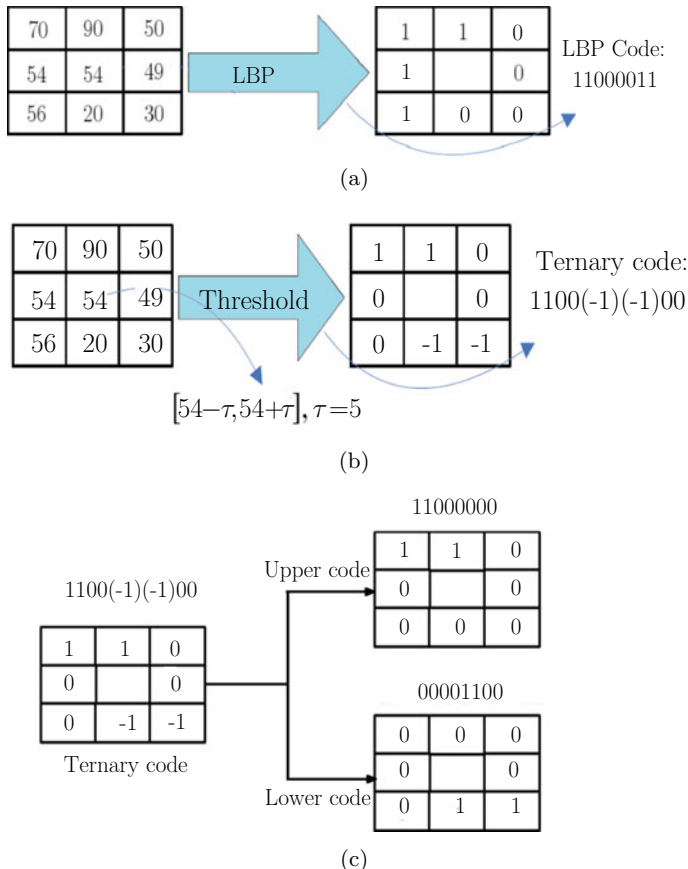


Fig. 2 Illustration of LBP and LTP computation. **a** Extraction of LBP from the gray values of a circular neighborhood of $R = 1$ pixel and $P = 8$ samples. Here, center pixel of gray value 54 is compared with all its neighborhood pixels in the radius $R = 1$ pixel, to obtain the rotation invariant local binary pattern as 11000011. **b, c** Computation of LTP using a set threshold of $\tau = 5$. The generated ternary code 1100(-1)(-1)00 is splitted into upper and lower LBP codes, 11000000 and 00001100, respectively

The selection of a particular threshold value is a critical task as it reduces the sensitivity of LTP operators to noise. The thresholds are set manually to get the best performance for a specific problem in hand.

3 System Methodology

The proposed methodology used the discriminating capability of texture descriptors to highlight the variations between the texture of a healthy and pathological retina for

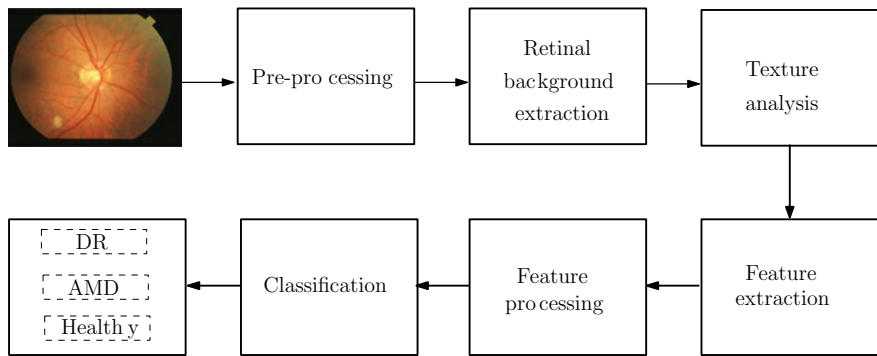


Fig. 3 Proposed method for feature vector extraction and subsequent classification into one of the three classes, namely DR, AMD, or healthy image. First, the input image is re-sized to a designated size followed by filtering of red, green, and blue components present in the image. Then, by using masks retinal background is extracted and feature maps are extracted using LBP and LTP texture descriptors. Finally, the feature vectors formed using statistical values are fed to a classifier to separate into one of the three classes

disease screening. The proposed method consists of six steps, namely preprocessing, retinal background extraction, texture analysis using LTP or LBP, feature extraction, feature processing, and finally classification into one of the three classes, namely DR, AMD, or a healthy image. Figure 3 shows a block schematic of the proposed technique, and in continuation, the six steps are elaborated.

3.1 Preprocessing

In this stage, the input fundus images and its corresponding masks¹ are re-sized based on the horizontal diameter of the image which is taken as the reference. Image resizing is done to make all input images to a fixed size, as they are obtained from different data sets. After resizing, the red, green, and blue components from each image are extracted. Then median filtering is done on each channel for removing noise present in the image. Each pixel value will be re-occupied by the median of its corresponding 3×3 neighborhood.

3.2 Retinal Background Extraction

The retinal background is considered for texture analysis, as the presence of landmark features such as blood vessels and the optic disk does not have much texture

¹Retinal masks obtained from Morales et al. [3] at <https://tinyurl.com/y5833kt4>.

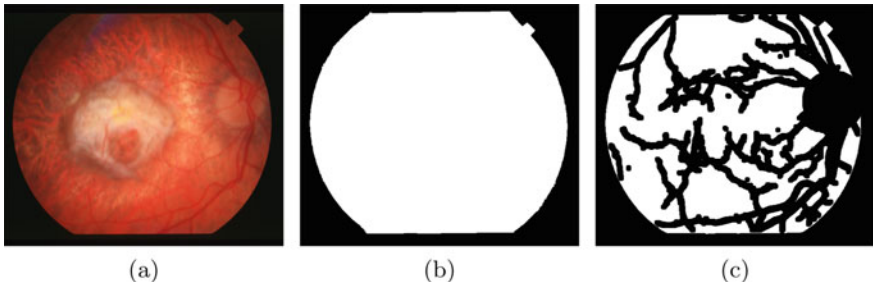


Fig. 4 Sample input retinal image and its masks that is used to define ROI and removal of morphological structures, namely blood vessels and optic disk. **a** Input image, **b** mask for ROI selection, and **c** mask for removal of retinal structures

components present in it. A substantial amount of works have been proposed for retinal vessel segmentation as well as optic disk removal [15–19]. The removal of these structures from the fundus image will give appreciable differences between the texture of healthy and pathological images. In this work, the retinal structures are removed with the help of a masking procedure that used publicly available masks obtained from [3]. Figure 4b and c represents the masks used to remove retinal structures present in a sample image as shown in Fig. 4a. The mask shown in Fig. 4b is used to define the region of interest (ROI) and the second mask Fig. 4c, for removing the morphological structures. After masking operation, the input image contains only the retinal background that holds texture responsible for a typical lesion.

3.3 Texture Analysis

The input image obtained after the masking operation is then subjected to texture analysis. In this work, two texture descriptors are used, namely LBP and LTP (Sects. 2.2 and 2.3). In addition, a contrast measure termed local variance is computed as:

$$\text{VAR}_{P,R} = \frac{1}{P} \sum_{p=0}^{P-1} (g_p - \mu)^2 \quad (4)$$

where

$$\mu = \frac{1}{P} \sum_{p=0}^{P-1} g_p \quad (5)$$

For each pixels in the input image LTP, LBP and local variance values are computed for red, green, and blue channels. Figures 5, 6, and 7 show the LBP, LTP, and variance maps obtained for the input image shown in Fig. 4a.

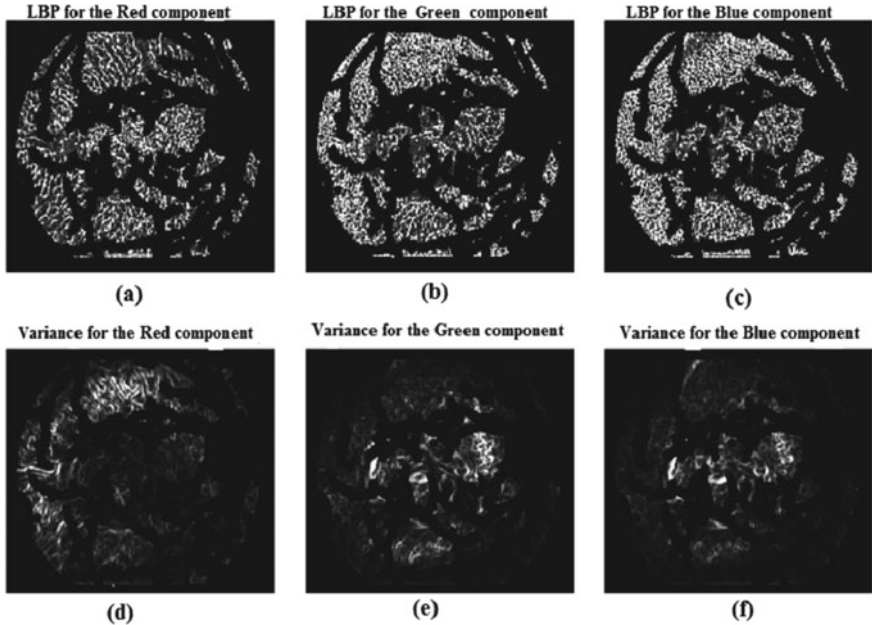


Fig. 5 LBP response map obtained for the input image shown in Fig. 4a. **a–c** represents the LBP response maps for red, green, and blue components of the input image, and **d–f** represents the corresponding variance maps

3.4 Feature Extraction

The LBP, LTP, and variance maps obtained can serve as a descriptor to represent the texture of retinal background. The numerical values of these response maps within the ROI are collected, and their histograms are generated. From the histograms, the statistical parameters such as mean, median, standard deviation, skewness, kurtosis, and entropy are computed for each of the texture descriptors. Here, LBP-based features are also extracted for comparison with the proposed pipeline employing LTP. The proposed technique suitably selects 72 features (For one color channel, six statistical features from each of the upper LTP, lower LTP, upper variance and lower variance images, making a total of 24 features for each channel.) and use it further for classification.

3.5 Feature Processing

The feature maps derived from the texture descriptors are further processed before it is applied to a typical classification model. In this work, two such feature preprocessing

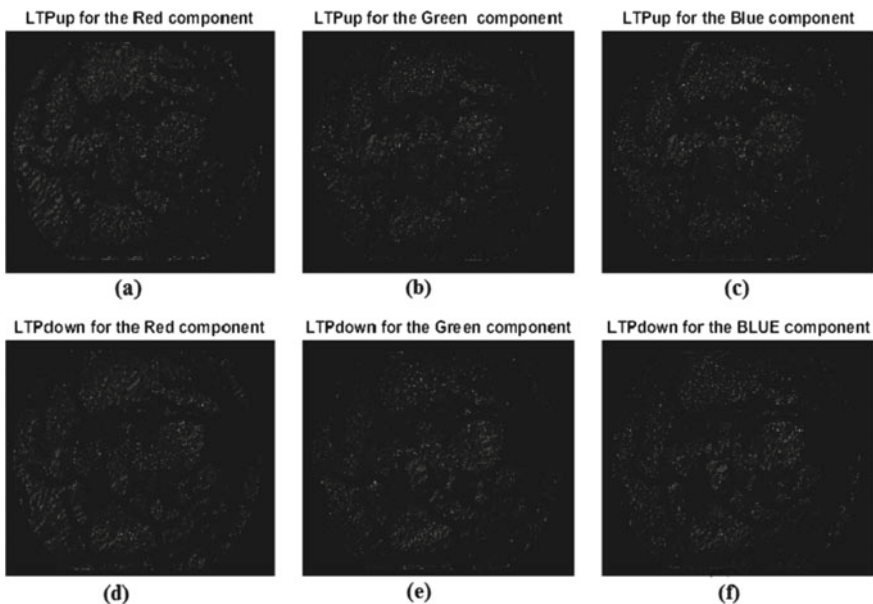


Fig. 6 LTP response map obtained for the input image shown in Fig. 4a. **a–c** represents the upper LTP code response maps for red, green, and blue components of the input image, and **d–f** represents the lower LTP code response maps

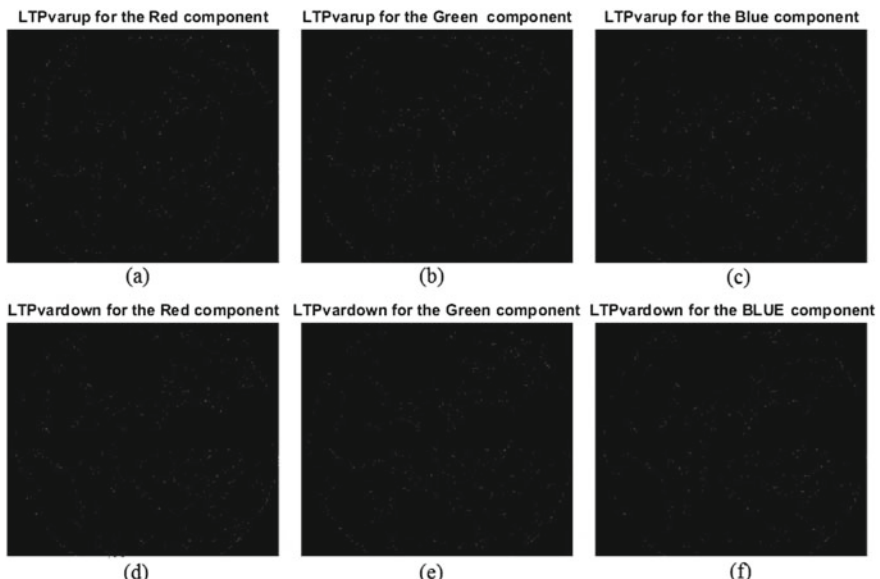


Fig. 7 Variance images obtained while evaluating LTP in the input image shown in Fig. 4a. **a–c** represents the variance for upper LTP image for red, green, and blue components, and **d–f** represents the variance for lower LTP response

techniques are adopted—one for reducing the shifts within the scale and distribution of the given data, and the other for reducing the class imbalance in the experimented dataset. Data normalization is performed to solve the first problem within the used data. In this process, all numeric attributes in the given data are rescaled in the range between 0 and 1.

The next preprocessing step we employed deals with the class imbalance problem in a given dataset, which is alleviated using synthetic minority oversampling technique (SMOTE) [20]. This data re-sampling technique synthesises new minority instances using the existing real data instances and avoids bias in predicted output, which the classifiers are not able to recognize, leading to wrong conclusions.

3.6 Classification

The feature set derived using a particular texture descriptor is then fed to different classifiers for performance analysis. Supervised learning is used here for classifying the extracted features. The classifiers used in this work include random forest [21], naive Bayes [22], AdaBoost [23], SVM [24], logistic regression [25], and C4.5 [26]. As discussed in Sect. 2, the images obtained from various data sets are grouped into model set and validation set. The model set is used for training the classification model and testing is performed by cross-validation. On the other hand, validation set is used for testing the final model. In this work, a fivefold cross-validation is used, where the whole model set is divided into 5 non-overlapping pairs of train and test sets. Training of a particular classifier with each subset of images are carried out followed by its evaluation using the test set. The process is then repeated for every fold of images. After successful training, the model is fixed and the validation set is tested on the final classifier model.

4 Results and Discussions

Here, we present the results obtained for the various experiments conducted using the proposed pipeline that segregates AMD-Normal, DR-Normal, and AMD-DR images. The efficiency of various classifiers using the feature vectors derived from the proposed technique is reported here.

To compare the performance of the proposed system, we compute the true positive rate (TPR) and true negative rate (TNR) measures, which are expressed as:

$$\text{TPR} = \frac{T1}{T1 + F2}, \quad \text{TNR} = \frac{T2}{T2 + F1} \quad (6)$$

where $T1$, $T2$, $F1$, and $F2$ represent true positives, true negatives, false positives, and false negatives, respectively.

Table 2 Number of images used for experiments under each category. Various classifiers are trained and tested under each class, namely DR-normal, AMD-normal, and DR-AMD

	AMD-normal	DR-normal	DR-AMD
Model set	122	160	88
Validation set	32	42	24

In this work, we explored the utility of LTP for retinal pathology detection. It is noticed that there is a significant difference in the feature vectors of retinal background between healthy and diseased fundus images. In addition, we plot the inter-class histograms of the different classes, namely DR, AMD, and healthy. The number of images used for experimentation under each category are given in Table 2. Figure 8 shows the histograms for the three experiments we performed, namely DR-Normal, AMD-Normal, and DR-AMD classification. The distinctions observed show that the derived features can accurately differentiate between classes.

In Tables 3 and 4, we show the comparison results obtained using LTP and LBP descriptors, respectively. The results are expressed in terms of true positive rate (TPR) and true negative rate (TNR) obtained on the model and validation sets, using different classifiers. In LTP-based technique, SVM performs well in DR-normal and AMD-normal classification tasks while for DR-AMD class, random forest outperforms the remaining tested classifiers. On the other hand, for LBP-based system AdaBoost classifier shows optimum performance in DR-normal class while SVM has given maximum performance in AMD-normal classification task. As obtained for LTP, random forest produced maximum output in DR-AMD classification using LBP.

Most of the retinal lesion classification techniques primarily employs a lesion segmentation stage followed by classification of segmented regions into the respective classes. Instead, the proposed method is devoid of lesion segmentation, and hence, time of execution is faster. The method involves retinal background analysis after removing the morphological structures, namely blood vessels and optic disk from the images. It is a fact that there exists substantial amount of research works for blood vessel and optic disk detection, which can be used for generating masks. When compared to similar state-of-the-art retinal lesion classification tasks, the performance of proposed method using LTP descriptors is not optimal but provides useful features for lesion screening in retinal images. Hence, feature maps obtained can be combined with other texture descriptors to enhance the output results.

5 Conclusion

A novel approach based on LTP has been proposed in this paper for the screening of lesions in retinal images. The obtained results demonstrate the effectiveness of LTP as a texture descriptor for lesion screening in retinal images. A comparison between LTP and LBP for screening DR and AMD is also provided for understanding

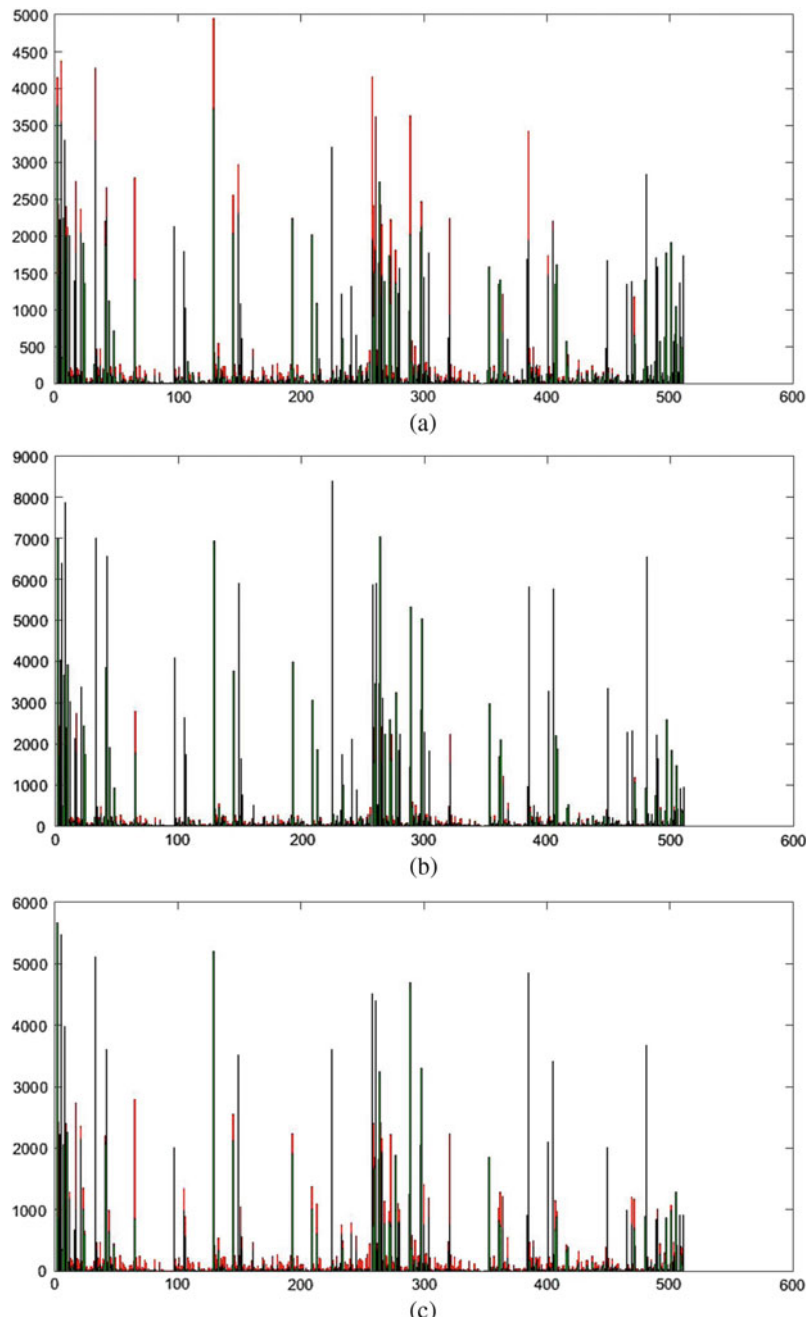


Fig. 8 Histograms obtained for the different experiments performed. **a** DR (green) and normal (red), **b** AMD (green) and normal (red), and **c** DR (green) and AMD (red) experiments

Table 3 Classifier performance in terms of true positive rate (TPR) and true negative rate (TNR) obtained using feature set obtained with LTP texture descriptor

	Classifier	DR-normal		AMD-normal		DR-AMD	
		TPR	TNR	TPR	TNR	TPR	TNR
Model set	Random forest	0.822	0.810	0.950	0.938	0.945	0.924
	Naive Bayes	0.780	0.800	0.832	0.806	0.925	0.979
	AdaBoost	0.935	0.940	0.888	0.850	0.830	0.814
	SVM	0.943	0.923	1.000	1.000	0.828	0.792
	Logistic regression	0.801	0.753	0.804	0.832	0.760	0.755
	C4.5	0.842	0.815	0.861	0.878	0.853	0.885
Validation set	Random forest	0.832	0.843	0.867	0.866	0.837	0.985
	Naive Bayes	0.843	0.830	0.826	0.836	0.880	1.000
	AdaBoost	0.990	0.940	0.879	0.890	0.800	0.920
	SVM	0.922	0.963	1.000	1.000	0.890	0.748
	Logistic regression	0.859	0.883	0.897	0.826	0.874	0.741
	C4.5	0.835	0.877	0.844	0.839	0.999	0.965

Bold indicates the maximum performance

Table 4 Classifier performance in terms of true positive rate (TPR) and true negative rate (TNR) obtained using feature set obtained with LBP texture descriptor

	Classifier	DR-normal		AMD-normal		DR-AMD	
		TPR	TNR	TPR	TNR	TPR	TNR
Model set	Random forest	0.817	0.806	0.957	0.907	0.928	0.938
	Naive Bayes	0.773	0.760	0.928	0.870	0.800	0.800
	AdaBoost	0.955	0.921	0.973	0.920	0.903	0.905
	SVM	0.899	0.881	0.988	0.930	0.887	0.927
	Logistic regression	0.798	0.670	0.902	0.840	0.871	0.870
	C4.5	0.824	0.885	0.937	0.823	0.865	0.877
Validation set	Random forest	0.700	0.673	0.903	0.883	0.944	0.921
	Naive Bayes	0.699	0.686	0.893	0.607	0.808	0.821
	AdaBoost	0.915	0.900	0.887	0.913	0.967	0.902
	SVM	0.876	0.856	0.920	0.902	0.929	0.871
	Logistic regression	0.789	0.660	0.887	0.782	0.850	0.770
	C4.5	0.799	0.707	0.680	0.663	0.725	0.833

Bold indicates the maximum performance

the effectiveness of both the techniques in screening lesions in retinal images. The threshold value selection in the LTP operator for which a classifier will give the best performance varies for different classifiers and is selected manually. The setting of this threshold value is the main challenge while using non-binary patterns for texture analysis.

References

1. World Health Organization et al (2013) Universal eye health: a global action plan 2014–2019. 2013
2. World Health Organization et al (2010) Action plan for the prevention of avoidable blindness and visual impairment, 2009–2013
3. Morales S, Engan K, Naranjo V, Colomer A (2015) Retinal disease screening through local binary patterns. *IEEE J Biomed Health Inf* 21(1):184–192
4. Galshetwar GM, Waghmare LM, Gonde AB, Murala S (2017) Edgy salient local binary patterns in inter-plane relationship for image retrieval in diabetic retinopathy. *Procedia Comput Sci* 115:440–447
5. Omar M, Khelifi F, Tahir MA (2016) Detection and classification of retinal fundus images exudates using region based multiscale LBP texture approach. In: 2016 International conference on control, decision and information technologies (CoDIT). IEEE, pp 227–232
6. Krishnan M, Laude A (2013) An integrated diabetic retinopathy index for the diagnosis of retinopathy using digital fundus image features. In: *J Med Imaging Health Inform* 3(2):306–313
7. Mookiah MRK, Rajendra Acharya U, Martis RJ, Chua CK, Lim CM, Ng EYK, Laude A (2013) Evolutionary algorithm based classifier parameter tuning for automatic diabetic retinopathy grading: a hybrid feature extraction approach. *Knowledge-Based Systems* 39:9–22
8. Garnier M, Hurtut T, Tahar HB, Cheriet F (2014) Automatic multiresolution age-related macular degeneration detection from fundus images. In: Medical imaging 2014: computer-aided diagnosis, vol 9035. International Society for Optics and Photonics, p 903532
9. Kumar A (2018) Detection of microaneurysms in retinal images through local binary patterns
10. STARE database structure analysis of the retina (2004). <http://www.ces.clemson.edu/~ahoover/stare/>. Last accessed on Jan 2020
11. E-Ophtha Database (2006) A color fundus image database, <http://www.adcis.net/en/Download-Third-Party/E-Ophtha.html>. Last accessed on Jan 2020
12. ARIA Online (2006) Retinal image archive. <http://www.eyecharity.com/ariaonline.html>. Last accessed on Jan 2020
13. Ojala T, Pietikäinen M, Harwood D (1996) A comparative study of texture measures with classification based on featured distributions. *Pattern Recogn* 29(1):51–59
14. Nanni L, Brahma S, Lumini A (2011) Local ternary patterns from three orthogonal planes for human action classification. *Expert Syst Appl* 38(5):5125–5128
15. Ramachandran S, Kochitty S, Vinekar A, John R (2020) A fully convolutional neural network approach for the localization of optic disc in retinopathy of prematurity diagnosis. In: *J Intell Fuzzy Syst* 1–10 (IOS Press)
16. Sivakumar R, Eldho M, Jiji CV, Vinekar A, John R (2016) Diagnosis of plus diseases for the automated screening of retinopathy of prematurity in preterm infants. In: 2016 11th International conference on industrial and information systems (ICIIS). IEEE, pp 408–413
17. Sivakumar R, Veena V, John R (2017) A curvature based approach for the automated screening of retinopathy of prematurity in preterm infants. In: 2017 13th International conference on signal-image technology internet-based systems (SITIS). IEEE, pp 503–508

18. Sivakumar R, Eldho M, Jiji CV, Vinekar A, John R (2016) Computer aided screening of retinopathy of prematurity—A multiscale Gabor filter approach. In: IEEE 2016 Sixth international symposium on embedded computing and system design (ISED). IEEE, pp 259–264
19. Ramachandran S, Strisciuglio N, Vinekar A, John R, Azzopardi G (2020) U-COSFIRE filters for vessel tortuosity quantification with application to automated diagnosis of retinopathy of prematurity. In: Neural computing and applications, Springer, pp 1–16
20. Chawla NV, Bowyer KW, Hall LO, Kegelmeyer WP (2002) Smote: Synthetic minority oversampling technique. *J Artif Intell Res* 16:321–357
21. Breiman L (2001) Random forests machine learning, vol 45
22. John GH (1995) Estimating continuous distributions in Bayesian classifiers. In: Proceedings of 11th conference on uncertainty in artificial intelligence
23. Freund Y (1996) Experiments with a new boosting algorithm. In : 13th International conference on machine learning
24. Chang C-C (2011) LIBSVM: a library for support vector machines. *ACM Trans Intelli Syst Technol* 2(27):1–27. <http://www.csie.ntu.edu.tw/~cjlin/libsvm>
25. Le Cessie S, Van Houwelingen JC (1992) Ridge estimators in logistic regression. *J R Stat Soc: Ser C (Appl Stat)* 41(1):191–201
26. Quinlan JR (1993) Program for machine learning. C4:5

A Modulo ($2^n - 2^{n-2} - 1$) Adder Design



Ahmad Hiasat

Abstract This paper presents a modulo ($2^n - 2^{n-2} - 1$) adder. The proposed structure uses a parallel-prefix binary adder with an end-around carry as its skeleton. It splits the parallel-prefix phase into lower ($n - 2$)-bit part and upper 2-bit part. The proposed structure requires the area and delay of a regular parallel-prefix binary adder with an end-around input carry. Compared with functionally-similar modulo ($2^n - 2^{n-2} - 1$) using VLSI synthesis tools, the suggested adder reduces area by (14.2–72.2)%, time by (5.1–19.5)%, and area-time product by (36.5–92.0)%.

Keywords Residue number system · Modular adders · Parallel-prefix structures · Computer arithmetic

1 Introduction

When performing basic arithmetic operations of addition and multiplication using Residue Number System (RNS), there is no carry propagation from one digit to another. Computations can be carried in parallel on all digits of RNS [1]. However, RNS has few major limitations that make its use limited to applications which require the above mentioned arithmetic operations. The limitations include residue-to-binary decoding, sign identification, comparison and division [2–14]. Nevertheless, RNS has been used extensively in digital signal processing, cryptography, communications, and other computation-intensive applications [1, 15–19].

In the remaining of this paper, Sect. 2 introduces the basics of parallel-prefix adders with an End-Around Carry (EAC) and highlights the most relevant works to the proposed one in this paper. Section 3 introduces the newly proposed modulo ($2^n - 2^{n-2} - 1$) adder, while Sect. 4 evaluates and compares the new work with the most relevant and similar modular adders.

A. Hiasat (✉)

Princess Sumaya University for Technology, Amman, Jordan
e-mail: a.hiasat@psut.edu.jo

The variables, definitions, and notations used in this work are:

- The modulus M is a positive integer, where $n = \lceil \log_2 M \rceil$, and where $\lceil \cdot \rceil$ is the ceiling value function (the smallest integer greater than or equal to (\cdot)).
- For integers $X, Y \in [0, M]$, the binary representation of X and Y are given by: $X \xrightarrow{\text{binary}} (x_{n-1} \dots x_2 x_1 x_0)$, $Y \xrightarrow{\text{binary}} (y_{n-1} \dots y_2 y_1 y_0)$, respectively.
- $(\cdot)_M$ refers to the remainder when dividing (\cdot) by M .
- The symbols of \wedge , \vee , \oplus , \odot , and $\overline{(\cdot)}$, refer to logical operators of AND, OR, EX-OR, EX-NOR, and NOT, respectively.

1.1 Parallel Prefix Addition with EAC

Computing $T = X + Y$ produces an $(n + 1)$ -bit number expressed as: $T = t_n \dots t_1 t_0$. In modular adders of the form $(2^n - 1)$, the output carry (i. e. t_n) is re-inserted as an EAC [20–24]. Figure 1 shows the phases of evaluating T , where these phases are:

- Pre-processing phase: this phase produces the “Propagate” vector P , the “Generate” vector G , and the “Half-sum” vector H , where each is an n -bit value, defined as follow:

$$P = p_{n-1} p_{n-2} \dots p_2 p_1 p_0, \quad (1)$$

$$\text{for } 0 \leq i \leq n-1, \quad p_i = x_i \vee y_i$$

$$G = g_{n-1} g_{n-2} \dots g_2 g_1 g_0, \quad (2)$$

$$\text{for } 0 \leq i \leq n-1, \quad g_i = x_i \wedge y_i$$

$$H = h_{n-1} h_{n-2} \dots h_2 h_1 h_0, \quad (3)$$

$$\text{for } 0 \leq i \leq n-1, \quad h_i = x_i \oplus y_i = \overline{g}_i \wedge p_i$$

- Parallel-prefix phase: the basic component of this phase is the black-circle node. This node handles two pairs, namely, (p_{i-1}, g_{i-1}) and (p_i, g_i) , and produces the output $(p_{(i,i-1)}, g_{(i,i-1)})$. The logic equation that governs the node operation is:

$$(p_{(i,i-1)}, g_{(i,i-1)}) = (p_i \wedge p_{i-1}, g_i \vee (g_{i-1} \wedge p_i)) \quad (4)$$

The output of the parallel-prefix phase is an n -pair output, where the pairs are denoted as: $(G_{n-1}, P_{n-1}), (G_{n-2}, P_{n-2}), \dots, (G_1, P_1), (G_0, P_0)$.

- Summation phase with EAC: in modulo $(2^n - 1)$ adders, the output carry resulting from the parallel-prefix phase denoted as c_{out} is re-inserted as an input carry. The c_{out} (which is G_{n-1}) is incorporated in the summation result using the EAC nodes by applying the following logic formula:

$$c_i = G_i \vee (P_i \wedge c_{\text{out}}), \quad 0 \leq i \leq n-2, \quad (5)$$

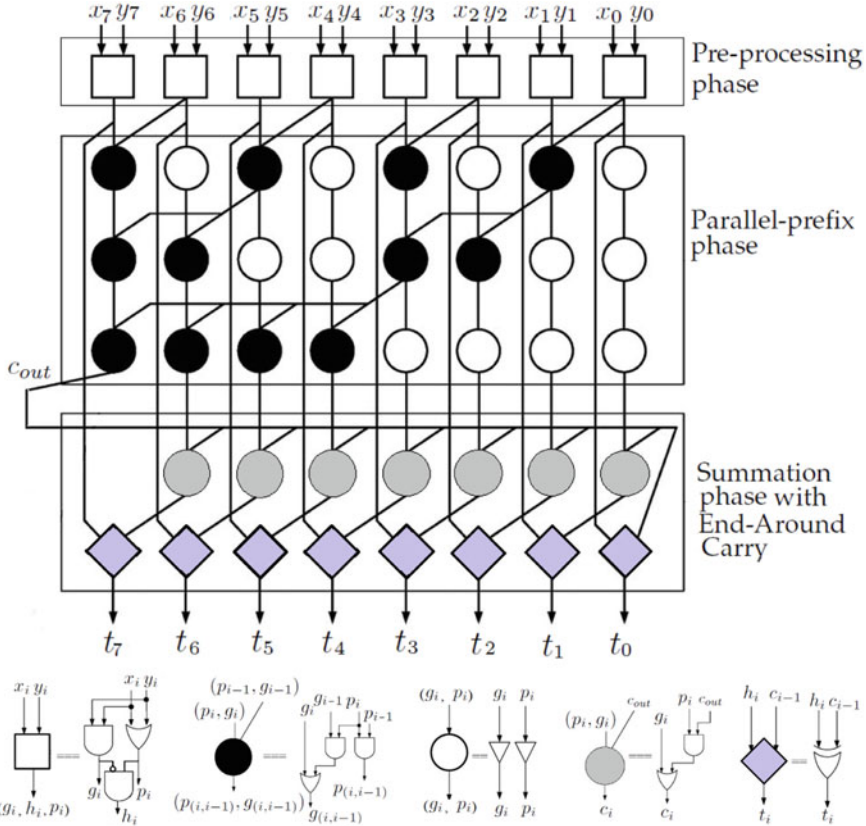


Fig. 1 Parallel-prefix adder with EAC for the case $n = 8$

Computing the summation, $\langle T \rangle_{(2^n-1)} = \langle X + Y \rangle_{(2^n-1)}$, culminates with performing the following logic operations:

$$\begin{aligned} t_i &= h_i \oplus c_{i-1}, \quad 1 \leq i \leq n-1 \\ t_0 &= h_0 \oplus c_{\text{out}} \end{aligned} \quad (6)$$

where the bits t_{n-1} through t_0 constitute $\langle X + Y \rangle_{(2^n-1)}$.

1.2 Modulo-Specific Adders

Modular addition has received a considerable attention. Some adders deal with a general modulus M that can have any form. A general adder requires usually two

binary-adders and a selection circuit to select one of two-outputs. Modulo-specific adders are the ones that deal with moduli of the form $(2^n \pm 1)$ [20–24], or other forms [25–28]. For instance [25, 28], deal with moduli of the form $(2^n - 2^{n-2} - 1)$. While [26] deals with moduli of the form $(2^n - 2^k - 1)$. However, [27] deals with the more general form of $(2^n \pm K)$.

2 New Modulo $(2^n - 2^{n-2} - 1)$ Adder

2.1 Mathematical Model

A general residue-based arithmetic addition operation modulo M is performed according to the following equation:

$$W = \langle X + Y \rangle_M \quad (7)$$

where W represents the result of the modular summation.

Equation (7) can be re-written in the form of:

$$W = \begin{cases} X + Y & , \text{if } X + Y < M \\ X + Y - M & , \text{if } X + Y \geq M \end{cases} \quad (8)$$

Considering the case $M = 2^n - 2^{n-2} - 1$, (8) can be written as:

$$W = \begin{cases} X + Y & , \text{if } X + Y < M \\ X + Y - (2^n - 2^{n-2} - 1) & , \text{if } X + Y \geq M \end{cases} \quad (9)$$

Defining an intermediate variable Z to be

$$Z = X + Y + 2^{n-2} \quad (10)$$

where the binary representation of Z is given by $Z \xrightarrow{\text{binary}} (z_n z_{n-1} \dots z_2 z_1 z_0)$. The formulas in (9) and the definition of Z in (10) implies three different cases described as follows:

- If $0 \leq (X + Y) \leq M - 1 < (2^n - 2^{n-2} - 1)$, then $(2^{n-2} \leq \overbrace{X + Y + 2^{n-2}}^Z < 2^n - 1)$. Hence, this case is identified by the Most Significant Bit (MSB) of Z , namely $z_n = 0$. The value W is obtained by subtracting 2^{n-2} from Z .
- If $(X + Y) = M = (2^n - 2^{n-2} - 1)$, then $\overbrace{X + Y + 2^{n-2}}^Z = 2^n - 1$. Hence, this case is identified by the MSB of Z , $z_n = 0$, and with the n Least Significant Bits

(LSB) of Z ($z_{n-1} \dots z_2 z_1 z_0$) = $\overbrace{11 \dots 111}^n$ bits. Similar to the previous case, the value W is obtained by subtracting 2^{n-2} from Z . Similar to the case of modulo $(2^n - 1)$ adders, which uses two representations for a 0, the modular adder in this paper

uses two representations for a 0, namely, $\overbrace{00 \dots 000}^n$ bits and $\overbrace{101 \dots 111}^n$ bits. Hence, the value W in this and the previous case is computed by removing the bias 2^{n-2} from Z .

- If $2^n \leq (X + Y) < 2M - 1$, then $(2^n \leq \overbrace{X + Y + 2^{n-2}}^Z < 2^{n+1} - 1)$. This case is recognized by the MSB of Z to be $z_n = 1$. The value W is obtained by subtracting 2^n from Z (i. e. clearing z_n to 0) and adding a 1 to $(z_{n-1} \dots z_0)$, which is realized by adding the EAC as an input carry.

The above analysis leads to rewriting (9) in the following form:

$$W = \begin{cases} Z - 2^{n-2}, & \text{if } Z < 2^n \text{ (i. e. } z_n = 0\text{)} \\ Z - 2^n + 1, & \text{if } Z \geq 2^n \text{ (i. e. } z_n = 1\text{)} \end{cases} \quad (11)$$

2.2 Proposed Implementation

The hardware implementation of a regular parallel-prefix adder modulo $(2^n - 1)$, shown in Fig. 1, can be modified to implement the proposed modulo $(2^n - 2^{n-2} - 1)$ adder. The new adder is shown in Fig. 2.

The value of Z in (10) can be computed as follows:

$$\begin{array}{r} x_{n-1} \ x_{n-2} \ x_{n-3} \ \dots \ x_1 \ x_0 \\ + \ y_{n-1} \ y_{n-2} \ y_{n-3} \ \dots \ y_1 \ y_0 \\ + \ 0 \ \ \ \ 1 \ \ \ \ 0 \ \ \ \ \dots \ \ \ \ 0 \ \ 0 \\ \hline z_n \ z_{n-1} \ z_{n-2} \ z_{n-3} \ \dots \ z_1 \ z_0 \end{array} \quad (12)$$

This implies that the pre-processing phase components, which produces the P , G , and H vectors, are re-formulated as:

$$\begin{aligned} P &= p_{n-1} \ 1 \ p_{n-3} \ \dots \ p_2 p_1 p_0, \\ &\text{for } 0 \leq i \leq n-1, \ i \neq n-2 \\ p_i &= x_i \vee y_i, \quad p_{n-2} = 1 \end{aligned} \quad (13)$$

$$\begin{aligned} G &= g_{n-1} g_{n-2} \ \dots \ g_2 g_1 g_0, \\ &\text{for } 0 \leq i \leq n-1, \ i \neq n-2 \\ g_i &= x_i \wedge y_i, \quad g_{n-2} = x_{n-2} \vee y_{n-2} \end{aligned} \quad (14)$$

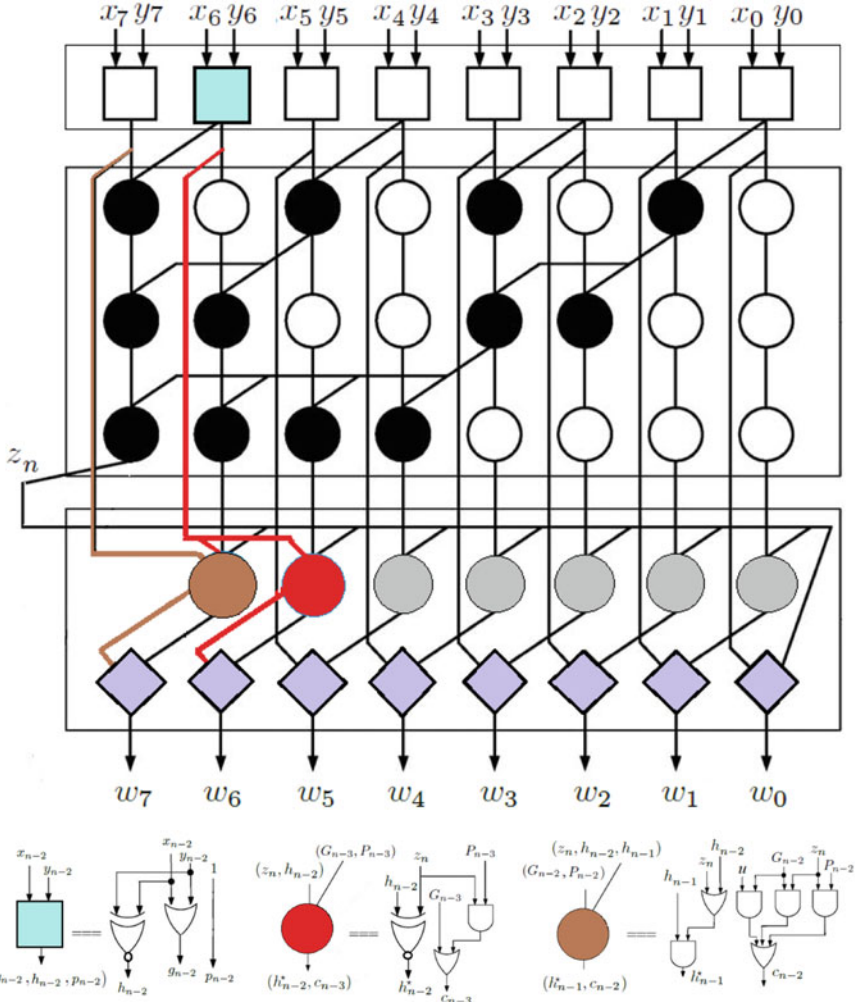


Fig. 2 Proposed modulo $(2^n - 2^{n-2} - 1)$ adder for the case $n = 8$

$$\begin{aligned}
 H &= h_{n-1}h_{n-2}h_{n-3}\dots\dots h_2h_1h_0, \\
 &\text{for } 0 \leq i \leq n-1, \quad i \neq n-2 \\
 h_i &= \bar{g}_i \wedge p_i, \quad h_{n-2} = x_{n-2} \odot y_{n-2}
 \end{aligned} \tag{15}$$

Examining P , G and H vectors given in (13)-(15) shows that they can be computed using $(n-1)$ units of the white-square nodes for $i = 0, 1, 2, \dots, n-3$ and $i = n-1$. For $i = n-2$, the blue square node, shown in Fig. 2, is used. The parallel-prefix circuits of Fig. 2 computes an n -pair output, defined before as:

$(G_{n-1}, P_{n-1}), (G_{n-2}, P_{n-2}), \dots, (G_1, P_1), (G_0, P_0)$, where G_{n-1} is referred to as z_n . Based on (11), the summation phase with EAC of Fig. 2 should add a 1 when $z_n = 1$ and subtract 2^{n-2} when $z_n = 0$. The LS $(n-3)$ gray-circle nodes in the summation phase of Fig. 2 are not affected by subtracting 2^{n-2} . Hence, these LS $(n-3)$ nodes need just to incorporate the value of z_n . However, in the MS 2-bits, adding a 1 or subtracting a 2^{n-2} is realized as follows:

- The Half-Sum vector H given in (15) is formed as: $h_{n-1}h_{n-2}h_{n-3}\dots h_2h_1h_0$. The MS 2-bits, namely $h_{n-1}h_{n-2}$, are the ones affected by subtracting 2^{n-2} .
- If $(h_{n-1}h_{n-2} \neq 00)$, then subtracting 2^{n-2} when $z_n = 0$ is equivalent to:

$$\begin{array}{r} h_{n-1} \quad h_{n-2} \\ - 0 \quad \bar{z}_n \\ \hline h_{n-1}^* \quad h_{n-2}^* \end{array}$$

where h_{n-2}^* and h_{n-1}^* are computed as follows:

$$h_{n-2}^* = \begin{cases} h_{n-2} & \text{if } z_n = 1 \\ \bar{h}_{n-2} & \text{if } z_n = 0 \end{cases} \quad (16)$$

Equivalently, (16) can be written as:

$$h_{n-2}^* = h_{n-2} \odot z_n \quad (17)$$

whereas,

$$h_{n-1}^* = \begin{cases} h_{n-1} & \text{if } z_n = 1 \\ h_{n-1} & \text{if } z_n = 0 \text{ and } h_{n-2} = 1 \\ \bar{h}_{n-1} & \text{if } z_n = 0 \text{ and } h_{n-2} = 0 \end{cases} \quad (18)$$

For the first case of (18), h_{n-1} is not affected because $z_n = 1$. For the second case of (18), h_{n-1} is also not affected because $h_{n-2} = 1$, hence subtraction is realized by clearing h_{n-2} to 0 as indicated in (17). In the third case of (18), subtraction is realized by borrowing a 1 from h_{n-1} which has a weight of 2^{n-1} and, hence, complementing both h_{n-2} and h_{n-1} .

- If $(h_{n-1}h_{n-2} = 00)$, then subtracting 2^{n-2} when $z_n = 0$ can't be performed using $(h_{n-1}h_{n-2})$. Nevertheless, subtraction can still be performed using G_{n-2} , which has a binary value of 1 and a weight of 2^{n-1} by clearing G_{n-2} to 0, while setting h_{n-2} to 1. When $z_n = 0$, it is worth mentioning that the case $G_{n-2} = 0$ and $(h_{n-1}h_{n-2} = 00)$ is impossible. The reasoning for that is the following:
 - If $h_{n-1} = 0$, this implies that $x_{n-1} = y_{n-1} = 0$ or $x_{n-1} = y_{n-1} = 1$. The second possibility is not valid because $z_n = 0$. Hence, $x_{n-1} = y_{n-1} = 0$.
 - If $h_{n-1} = 0$, this implies that $x_{n-2} \neq y_{n-2}$.
 - Reconsidering (12) in light of the above arguments:

$$\begin{array}{r}
 x_{n-1} \quad x_{n-2} \quad 0 \quad 1 \\
 + \quad y_{n-1} \quad y_{n-2} \Rightarrow 0 \quad 0 \\
 + \quad \underline{1} \quad \underline{\quad} \quad \underline{1}
 \end{array} \tag{19}$$

Equation (19) indicates clearly that g_{n-2} , and consequently G_{n-2} , has to be 1 when $h_{n-1} = h_{n-2} = 0$.

All the above results are summarized in Table 1, where “X” in the table refers to a don’t care condition. Moreover, performing standard minimization techniques using Table 1 leads to logic equations governing the three outputs:

$$h_{n-2}^* = h_{n-2} \odot z_n \tag{20}$$

$$h_{n-1}^* = h_{n-1}(h_{n-2} \vee z_n) \tag{21}$$

$$c_{n-2} = (G_{n-2} \wedge z_n) \vee (G_{n-2} \wedge u) \vee (P_{n-2} \wedge z_n) \tag{22}$$

where $u = h_{n-1} \vee h_{n-2}$, and where the red and brown nodes of Fig. 2 realize (20)–(22). Both nodes act similar to other gray nodes at the same level if $z_n = 1$.

3 Evaluation, VLSI Implementation, and Comparison

The modulo $(2^n - 2^{n-2} - 1)$ proposed in this work is compared with other recent, functionally-similar, and competitive works. The most recent competitive published designs that can perform modulo $(2^n - 2^{n-2} - 1)$ additions are [25–28]. The adder in [25] performs modulo $(2^n - 2^{n-2} - 1)$ addition. The adder in [26] performs modulo $(2^n - 2^k - 1)$ addition. For fair comparison, it has been assumed that $k = n - 2$ so the comparison would have the same base in terms of design requirements. The adder in [27] performs $(2^n - K)$ addition. Once more, to unify the base of comparison, it has been assumed that $K = 2^{n-2} + 1$. The authors in [28] proposed two modulo $2^N + 2^{N-1} - 1$ adder designs. The most competitive among the two is the one referred to as totally parallel-prefix (TPP) modulo $2^N + 2^{N-1} - 1$ adder. This adder is actually a modulo $(2^n - 2^{n-2} - 1)$, where $n = N + 1$. Comparison of the proposed work with [25–28] is carried using technology-independent approach (unit-gate model) and simulation-oriented approach (VLSI synthesis tools).

Table 1 The truth table of $h_{n-1}h_{n-2}$ in Fig. 2 which incorporates the corrective measure of subtracting 2^{n-2} from Z whenever $z_n = 0$

h_{n-1}	h_{n-2}	G_{n-2}	P_{n-2}	$z_n = 0$			Explanation of the corrective measure (i.e. subtracting 2^{n-2} from Z) when $z_n = 0$	$z_n = 1$		
				h_{n-1}^*	h_{n-2}^*	c_{n-2}		h_{n-1}^*	h_{n-2}^*	c_{n-2}
0	0	0	0	X	X	X	It is impossible to have $h_{n-1} = h_{n-2} = G_{n-2} = 0$	0	0	0
0	0	0	1	X	X	X		0	0	1
0	0	1	0	0	1	0	Subtracting 2^{n-2} from Z is realized by using G_{n-2} as a borrow, thus, clearing c_{n-2} to 0 and setting h_{n-2} to 1.	0	0	1
0	0	1	1	0	1	0		0	0	1
0	1	0	0	0	0	0	Subtracting 2^{n-2} from Z is realized clearing h_{n-2} to 0	0	1	0
0	1	0	1	0	0	0		0	1	1
0	1	1	0	0	0	1		0	1	1
0	1	1	1	0	0	1		0	1	1
1	0	0	0	0	1	0	Subtracting 2^{n-2} from Z is realized by using h_{n-1} as a borrow, hence, clearing h_{n-1} to 0 and setting h_{n-2} to 1	1	0	0
1	0	0	1	0	1	0		1	0	1
1	0	1	0	0	1	1		1	0	1
1	0	1	1	0	1	1		1	0	1
1	1	0	0	1	0	0	Subtracting 2^{n-2} from Z is realized clearing h_{n-2} to 0.	1	1	0
1	1	0	1	1	0	0		1	1	1
1	1	1	0	1	0	1		1	1	1
1	1	1	1	1	0	1		1	1	1

3.1 Unit-Gate Comparison

The unit-gate comparison model is a theoretical approach used to compare the hardware and time needs of digital arithmetic circuits [29–39]. The comparison is held in terms of unit-gate numbers and unit-gate delays. For this purpose, a unit-gate is a 2-input AND, OR, NAND, or NOR gate. Any of these gates is assumed to have an area of 1 unit and a delay of 1 unit. The EX-OR and EX-NOR gates have the area of 2 units and the delay of 2 units. Based on this technology-independent comparison, the proposed circuit shown in Fig. 2 consists of:

- The Pre-processing phase consists of n white square node (including the blue one). Each node consists of 3 unit-gates in area and one unit gate in delay. The total needs of this phase is $3n$ unit-gates and 1 critical delay. All the h_i 's computed at this phase are not within the critical path delay of the circuit.
- The parallel-prefix phase consists of $\frac{n}{2} \lceil \log n \rceil$ black circle nodes, where each is composed of 3 unit-gates and requires a delay of 2 unit-gates. Hence the area of this phase is $\frac{3n}{2} \lceil \log n \rceil$ and the delay is $2 \lceil \log n \rceil$.
- The EAC phase consists of $(n - 3)$ gray circle nodes in addition to the red and brown nodes. Each gray node consists of 2 unit-gates. The brown and red nodes require 10 gates. The total gate-count of this phase is $(2n + 5)$ and the gate delay is 2 units.
- The summation phase consists of n rhombus nodes, where each consists of 2 unit-area and 2 unit-delays. Hence the total area of this phase is $2n$ units.

Table 2 summarizes the area and time requirements of the proposed adder. Similarly, Table 3 lists and compares the area and delay needs of similar modulo adders reported in [25–28].

Two important concerns regarding the TPP modulo $(2^n - 2^{n-2} - 1)$ adder reported in [28]. The first concern is that the authors have used two representations for each integer $X \in [0, 2^{n-2}]$. The dual representation over the indicated range, which is very uncommon, has resulted in reducing the requirement of the adder design. It also

Table 2 Hardware and time requirements of the proposed modulo $(2^n - 2^{n-2} - 1)$ adder shown in Fig. 2 in terms of unit-gates

Phase	Node type	Number of nodes	Number of gates	Time delay
Preprocessing	White sq. ^a	n	$3n$	1
Parallel-prefix	Black cir.	$n \lceil \log n \rceil$	$\frac{3}{2}n \lceil \log n \rceil$	$2 \lceil \log n \rceil$
EAC	Gray cir. ^b	$n - 1$	$2n + 5$	2
Summation	Rhombus	n	$2n$	2
Total requirements			$\frac{3}{2}n \lceil \log n \rceil + 7n + 5$	$2 \lceil \log n \rceil + 5$

^aIncluding the blue-square node

^bIncluding the red- and brown-nodes

Table 3 Gate-counts and gate-delays of different competitive modulo $(2^n - 2^{n-2} - 1)$ adders as compared with the proposed adder

Modulo adder	Gate count ^a	Gate delay
[25]	$3n \lceil \log n \rceil + 2^{\lceil \log n \rceil - 1} + 11n - 2$	$2 \lceil \log n \rceil + 5$
[26]	$\frac{3}{2}n \lceil \log n \rceil + 8n - 3$	$2 \lceil \log n \rceil + 7$
[27]	$3n \lceil \log n \rceil + 10n$	$2 \lceil \log n \rceil + 6$
[28]	$3n \lceil \log n \rceil + 5n + 40$	$2 \lceil \log n \rceil + 4$
Proposed	$\frac{3}{2}n \lceil \log n \rceil + 7n + 5$	$2 \lceil \log n \rceil + 5$

^aTo ease comparison, it is assumed that $\log(n - 1) = \log n$

imposes additional circuitry if to be interfaced with other arithmetic components that do not use this representation-duality. The dual-representation that is usually adopted in residue arithmetic is for the value of 0. The other concern is that the delay of TPP modulo $(2^n - 2^{n-2} - 1)$ adder, reported in [28] as $(2\lceil \log n \rceil + 3)$, is incorrect. The reported delay has considered the delay of the inverted-triangle \blacktriangledown node (Fig. 6 of [28]) as 2 instead of 3 units (as clearly indicated in Fig. 3 of [28]). Therefore, Table 3 has listed the corrected time requirements of [28] as $(2\lceil \log n \rceil + 4)$ instead.

Table 4 VLSI synthesis results of the proposed modulo $(2^n - 2^{n-2} - 1)$ adder and other competitive works and reductions achieved

Modulo adder	n	Area (μm^2) (% Area reduc.)	Time (ps) (% Time reduc.)	(% A \times T reduction)
[25]	8	658 (68)	519 (15)	(93)
	12	1125 (69)	708 (14)	(92)
	16	1511 (71)	892 (12)	(91)
	24	2582 (74)	1236 (9)	(89)
	32	3536 (79)	1607 (8)	(94)
	(Reduc. average)	(72.2)	(11.5)	(92.0)
[26]	8	455 (16)	559 (24)	(44)
	12	766 (15)	757 (21)	(40)
	16	1019 (15)	949 (19)	(37)
	24	1689 (14)	1335 (17)	(34)
	32	2181 (10)	1715 (16)	(28)
	(Reduc. average)	(14.2)	(19.5)	(36.5)
[27]	8	614 (57)	523 (16)	(82)
	12	1053 (59)	698 (12)	(78)
	16	1429 (61)	883	(11)
	24	2441 (65)	1239 (9)	(79)
	32	3302 (67)	1601 (8)	(80)
	(Reduc. average)	(61.7)	(11.1)	(79.6)
[28]	8	635 (62)	475 (5)	(71)
	12	1035 (56)	660 (6)	(65)
	16	1360 (54)	825 (4)	(59)
	24	2256 (52)	1216 (7)	(63)
	32	2897 (47)	1542 (4)	(52)
	(Reduc. average)	(54.1)	(5.1)	(62.0)
Proposed	8	392	451	
	12	664	623	
	16	886	795	
	24	1482	1139	
	32	1976	1483	

3.2 VLSI Synthesis Comparison

The proposed modular adder, along with the ones published in [25–28], has been synthesized using Synopsys Design Compiler version (G-2012.06). The five designs have been modeled in Verilog HDL and mapped to 65 nm using standard-cell Synopsys DesignWare Logic Libraries. The Synopsis IC Compiler has been used to perform “place and route” phase. Table 4 lists all synthesis results and reduction percentages in Area, Time, and Area-Time product ($A \times T$) achieved by the proposed adder compared with the ones in [25–28]. Table 4 shows that the suggested adder in this paper has achieved, on average, an area, time, and area-time product reductions of 72.2%, 11.5% and 92.0%, respectively as compared with the design published in [25]. It has also achieved an area, time, and area-time product reductions of 14.2%, 19.5%, and 36.5%, respectively as compared with the design published in [26]. Compared with that published in [27], the new design has achieved an area, time, and area-time product reductions of 61.7%, 11.1%, and 79.6%, respectively. Moreover, the new design has shown an area reduction of 54.1%, a time reduction of 5.1%, and an area-time product reduction of 62.0% when compared with [28].

4 Conclusions

This work presented an area- and time-efficient modulo $(2^n - 2^{n-2} - 1)$ adder. The proposed adder was minimally adapted from the modulo $(2^n - 1)$ structure while keeping the regularity of the parallel-prefix phase. The new design has shown significant reductions in area and time-delay. Using VLSI synthesis tools, the proposed work has a reduced area of (14.2–72.2)%, a reduced time-delay of (5.1–19.5)%, and a reduced area-time product of (36.5–92.0)% compared with the most recent competitive published works.

References

1. Mohan P (2016) Residue number systems: theory and applications. Birkhäuser
2. Pettenghi H, Chaves R, Sousa L (2013) RNS reverse converters for moduli sets with dynamic ranges up to $(8n + 1)$ -bit. IEEE Trans Circ Syst I 60(6):1487–1500
3. Hiasat A (2017) An efficient reverse converter for the three-moduli set $(2^{n+1} - 1, 2^n, 2^n - 1)$. IEEE Trans Circ Syst II: Express Briefs **64**(8), 962–966
4. Hiasat A (2017) A residue-to-binary converter for the extended four-moduli set $\{2^n - 1, 2^n + 1, 2^{2n} + 1, 2^{2n+p}\}$. IEEE Trans Very Large Scale Integr (VLSI) Syst **25**(7):2188–2192
5. Hiasat A (2017) A reverse converter and sign detectors for an extended RNS five-moduli set. IEEE Trans Circ Systems I: Regul Pap **64**(1):111–121
6. Niras C, Kong Y (2016) Fast sign-detection algorithm for residue number system moduli set $\{2^n - 1, 2^n, 2^{n+1} - 1\}$. IET CDT **10**(2):54–58
7. Kumar S, Chang C (2016) A new fast and area-efficient adder-based sign detector for RNS $2^n - 1, 2^n, 2^n + 1$. IEEE Trans Very Large Scale Integr (VLSI) Syst **24**(7):2608–2612

8. Sousa L, Martins P (2017) Sign detection and number comparison on RNS 3-moduli sets $\{2^N - 1, 2^{N+x}, 2^N + 1\}$. *Circ Syst Signal Process* 36(3):1224–1246
9. Hiasat A (2016) A sign detector for a group of three-moduli sets. *IEEE Trans Comput* 65(12):3580–3591
10. Hiasat A (2018) Sign detector for the extended four-moduli set $\{2^n - 1, 2^n + 1, 2^{2n} + 1, 2^{n+k}\}$. *IET Comput Digital Tech* 12(2):39–43
11. Kong Y, Phillips B (2009) Fast scaling in the residue number system. *IEEE Trans Very Large Scale Integ (VLSI) Syst* 17(3):443–447
12. Sousa L (2015) 2^n RNS scalers for extended 4-moduli sets. *IEEE Trans Comput* 64(12):3322–3334
13. Hiasat A (2017) Efficient RNS scalers for the extended three-moduli set $\{2^n - 1, 2^{n+p}, 2^n + 1\}$. *IEEE Trans Comput* 66(7):1253–1260
14. Hiasat A, Abdel-Aty-Zohdy HS (1995) A high-speed division algorithm for residue number system. In: Proceedings of ISCAS'95—International symposium on circuits and systems, vol 3, pp 1996–1999
15. Schoinianakis D (2020) Residue arithmetic systems in cryptography: a survey on modern security applications. *J Crypto Eng* 1–19 (2020)
16. Cardarilli G et al (2020) Design space exploration based methodology for residue number system digital filters implementation. *IEEE Trans Emerging Top Comput* (2020) (to appear)
17. Vayalil NC, Paul M, Kong Y (2019) A residue number system hardware design of fast-search variable-motion-estimation accelerator for HEVC/H.265. *IEEE Trans Circ Syst Video Technol* 29(2):572–581
18. Courtois J, Abbas-Turki L, Bajard J (2019) Resilience of randomized RNS arithmetic with respect to side-channel leaks of cryptographic computation. *IEEE Trans Comput* 68(12):1720–1730
19. Hiasat A (2004) A suggestion for a fast residue multiplier for a family of moduli of the form $\{2^n - (2^p \pm 1)\}$. *Comput J* 47(1):93–102
20. Zimmermann R (1999) Efficient VLSI implementation of modulo $2^n \pm 1$ addition and multiplication. In: 14th IEEE symposium on computer arithmetic, pp 158–167
21. Kalamboukas L, Nikolos D, Efstathiou C, Vergos HT, Kalamatianos J (2000) High-speed parallel-prefix modulo $2^n - 1$ adders. *IEEE Trans Comput* 49(7):673–680
22. Vergos HT, Efstathiou C, Nikolos D (2002) Diminished-one modulo $2^n + 1$ adder design. *IEEE Trans Comput* 51(12):1389–1399
23. Juang T, Chiu C, Tsai M (2010) Improved area-efficient weighted modulo $2^n + 1$ adder design with simple correction schemes. *IEEE Trans Circ Syst II* 57(3):198–202
24. Vergos HT, Dimitrakopoulos G (2012) On modulo $2^n + 1$ adder design. *IEEE Trans Comput* 61(2):173–186
25. Patel RA, Benissa M, Boussakta S (2007) Fast modulo $2^n - (2^{n-2} + 1)$ addition: a new class of adder for RNS. *IEEE Trans Comput* 56(4):572–576
26. Ma S, Hu J, Wang C (2013) A novel modulo $2^n - 2^k - 1$ adder for residue number system. *IEEE Trans Circ Syst I: Regul Pap* 60(11):2962–2972
27. Hiasat A (2018) General modular adder designs for residue number system applications. *IET Circ Devices Syst* 12(4):424–431
28. Jaberipur G, Nadimi B (2020) Balanced $(3 + 2 \log n) \Delta G$ adders for moduli set $\{2^{n+1}, 2^n + 2^{n-1} - 1, 2^{n+1} - 1\}$. *IEEE Trans Circ Syst I* 67(4):1368–1377
29. Hiasat A, Hasan O (2003) Bit-serial architecture for rank order and stack filters. *Integr VLSI J* 36(1–2):3–12
30. Hiasat A, Al-Khateeb A (1998) Efficient digital sweep oscillator with extremely low sweep rates. *IEE Proc Circ Dev. Syst* 145(6):409–414
31. Hiasat A, AL-Khateeb A (1999) New high-resolution digital sinusoidal oscillator structure with extremely low frequency and sensitivity. *Int J Electron* 86(3):287–296
32. Hiasat A, Sousa L (2018) On the design of rns inter-modulo processing units for the arithmetic-friendly moduli sets $\{2^{n+k}, 2^n - 1, 2^{n+1} - 1\}$. *Comput J* 62(2):292–300

33. Hiasat A (2019) A residue-to-binary converter with an adjustable structure for an extended rns three-moduli set. *J Circ Syst Comput* 28(8):1950,126:1–1950,126:24
34. Hiasat A (2019) A reverse converter for three-moduli set $(2^k, 2^n - 1, 2^n + 1)$, $k < n$. In: 2019 IEEE Jordan international joint conference on electrical engineering and information technology (JEEIT) (2019)
35. Hiasat A, Sweidan A (2003) Residue number system to binary converter for the moduli set $\{2^n - 1, 2^n - 1, 2^n + 1\}$. *J Syst Archit* 49(1):53–58
36. Hiasat A, Sweidan A (2004) Residue-to-binary decoder for an enhanced moduli set. *IEE Proc Comput Digital Tech* 151(2):127–130
37. Hiasat A, Abdel-Aty-Zohdy H (1997) Design and implementation of an RNS division algorithm. In: Proceedings of 13th IEEE symposium on computer arithmetic, pp 240–249
38. Hiasat A (2000) Rns arithmetic multiplier for medium and large moduli. *IEEE Trans Circ Syst II* 47(9):937–940
39. Hiasat A (2018) New residue number system scaler for the three-moduli set $\{2^{n+1} - 1, 2^n, 2^n - 1\}$. *Computers* 7(3):1–7

Entity-Based Knowledge Graph Information Retrieval for Biomedical Articles



Vikash Kumar Prasad, Shashvat Bharti, and Nishanth Koganti

Abstract In this paper, we present an information retrieval system on a corpus of scientific articles related to COVID-19 and biomedical. We build a heterogeneous entity-based knowledge graph network, where edges are shared between biomedical entities and paper names, where entities appear in abstract of the paper. The biomedical entities are derived from the abstract of the scientific articles using a fine-tuned Bio-BERT model. For a user query, entities are derived using a fine-tuned Bio-BERT model and then semantic similarity to query is employed for the return of the top-most relevant papers on the titles. We also provide a small set of results for the information retrieval system.

Keywords Knowledge graph · BERT · Entity recognition · Natural language processing

1 Introduction

The information surge in research papers has increased exponentially, which is excellent, but extracting relevant information from such a huge ocean of textual research remains challenging [1]. If we have a system which responds to queries like “Lung cancer effect due to COVID-19”, it would be helpful to gather relevant research articles around such queries for the biomedical researchers. In general, information retrieval is finding relevant documents to a respective query. We already have Google, Bing search engines where it’s a standard problem and there are models which particularly do so and rely heavily on domain-specific word embeddings [2],

V. K. Prasad (✉) · S. Bharti · N. Koganti
GEP Worldwide Inc., Hyderabad, India
e-mail: vikash.prasad@gep.com

S. Bharti
e-mail: shashvat.bharti@gep.com

N. Koganti
e-mail: nishanth.koganti@gep.com

e.g., Bio-BERT [3]. Direct use of Bio-BERT would not be recommended since it would be computationally intensive, when we compare a user query to each of the article’s title to find out the most feasible semantic match. It also points out the fact that words like “coronavirus” and “COVID-19” would not be having corresponding word vectors.

1.1 NER-Based Systems

One of the aspects of our paper is Named Entity Recognition (NER), NER is one of the most fundamental tasks in NLP, which involves recognizing numerous domain-specific proper nouns such as in a biomedical corpus. Information retrieval is an upheaval task, especially when searching for near accurate answers, Tan et al. [4] proposed a LSTM-based Question Answering system for sentence matching in which word embeddings of question and answer sentences are fed into a Bi-LSTM network. Yadav et al. [5] proposed a method in which they find the closest match to a question using Glove [6] word embedding and cosine similarity. Yin et al. [7] proposed a Basic CNN (BCNN) model and three attention-based CNN (ABCNN) models for text matching. Recently the focus has shifted to transformer-based models in which Garg [8] proposed the TANDA model, which utilizes BERT [9] and RoBERTa [10] pre-trained language models for modeling the dependency between two sequences of sentences for Answer Sentence Selection (AS2). More recently, on CORD-19 dataset Andre et al. [11] proposed the CO-Search a retriever-ranker semantic search engine designed to handle complex biomedical queries over the COVID-19 literature. The information retrieval system is built from a SiameseBERT [12] encoder that is linearly composed with a TF-IDF vectorizer [13], and reciprocal-rank fused [14] with a BM25 vectorizer.

1. In this paper, the proposal is about an entity-based extraction system which can be used to extract relevant information from an incoming query. The method proposes a system which is designed to decrease the search criteria, hencewise decreasing time complexity, by concentrating only on the papers which corresponds to user query’s entities.
2. The paper also highlights the fact that domain-specific trained models are of utmost importance especially in case of biomedical information retrieval systems. For example, if the query is “Does hydrochloroquine reduces fatality rate?”, the system first filters out using Knowledge graph on the entity nodes, all the papers which have entities [“B-Simple-chemical”] in their abstracts, thus reducing the search space and giving more accurate results.

In Sect. 2 we explain our proposed method, and in Sect. 3 the focus is on the datasets used for experiments and examples from fine-tuned NER model. The results Sect. 4 shows a detailed view of the various results based on relevancy and time complexity and we finally conclude in Sect. 5 with directions for future work.

2 Proposed Method

The below approach is followed for information retrieval. For any query, first the corresponding entities using our fine-tuned Bio-Bert [3] model is extracted. Next the Neighbor Paper names from heterogeneous graph G is extracted by querying on the entity nodes. If more than one entity is found in our query we intersect the common papers between these entities. Then using the paper names the corresponding titles of papers is extracted. The titles are mapped to 768-dimensional vector using pre-trained Bio-BERT [3] embeddings. Bio-BERT embeddings for the query text is also extracted. The last step is to rank the titles and the query text based on semantic cosine similarity on a threshold t, hencewise we get the corresponding paper names to the query.

2.1 Fine-tuning of Bio-BERT

Due to wide use of bio-medical entities and sentences in CORD-19 data, Bio-BERT [3] has been used to fine-tune our entity recognition model. Bio-BERT [3] is specifically trained on PubMed abstracts and is one of the first domain-specific language model, which gives a much higher performance with respect to medical entities in comparison with traditional BERT which is trained on Wikipedia articles.

To suit our paper needs, the fine-tuning of the Bio-BERT [3] for Name Entity Recognition (NER) is based on the weights of pretrained Bio-BERT [3]. Unlike the previous work, Bio-BERT which is based on BERT architecture directly learns Word Piece embeddings during pre-training and fine-tuning.

2.2 Graph Construction

A heterogenous graph is created based on all the information from the CORD-19 data. The reason for using a heterogenous graph instead of multiple homogenous graphs is the ease of retrieval as well as savings in time and space-related resources. The graph created is an undirected graph. The reason for going ahead with the undirected graph is that we do not encounter a situation where retrieval of information fails because it gets stuck in a “sink”.

The heterogenous graph contains three types of vertices, namely, abstract from the papers, name of the papers and entities extracted from the abstract. To avoid any kind of ambiguity, the names of the papers are concatenated with a hash value to make the combination of paper name and hash value unique. The entity vertices contain entities extracted by performing NER on the abstracts. Since the graph is heterogenous, we need an identifier for the type of nodes. The three types of nodes

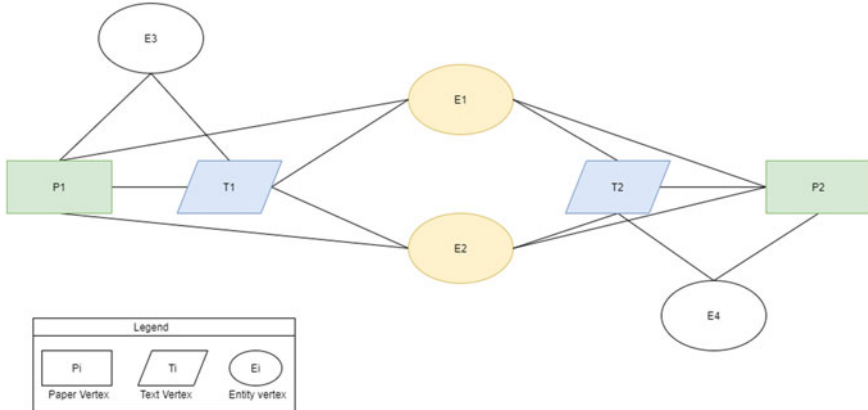


Fig. 1 Structure of the knowledge graph

are given “text”, “paper” and “entity” tag, respectively. These tags are concatenated to the names of the original vertices, e.g., $\langle \text{tag} \rangle _\langle \text{vertex_name} \rangle$.

The vertices tagged “paper” form edges with vertices tagged “entity”. The vertices tagged “entity” also form edges with vertices tagged “text”. Since our knowledge graph is undirected, this means that “entity” vertices are connected to both “paper” vertices and “text” vertices. The “paper” vertices also form edges with “text” vertices.

The relationship between “paper” vertices and “entity” vertices is $1:n$, where n is the number of entities present in its abstract. the value of n has a range of [1, 13] as 13 is the maximum number of entities recognized by our NER. The “text” and the “entity” vertices have a $m:p$ relationship, where m is the number of abstracts associated with the entity and has a range of [1, total number of abstracts] and p is the number of entities associated with a single abstract and has a range of [1, 13]. “paper” vertex and “text” vertex have a $1:1$ relationship as each paper has a single abstract, refer Fig. 1.

2.3 Overview of Information Retrieval System

The CORD-19 corpus is huge and to match a query to the best paper and would incur a very high complexity; if we directly try the semantic similarity approach, in addition vectors for words like “COVID-19” are not even available. Hence if a query “Lung cancer effect due to COVID-19” is passed, the fine-tuned model on BioNLP13cg [15] is first applied on data to get the probable entities which would be [‘O’, ‘B-Cancer’, ‘I-Cancer’, ‘O’, ‘O’, ‘O’, ‘B-Gene_or_gene_product’, ‘O’], refer Fig. 2. Using the thus obtained entities we query the graph G on entity nodes for the neighboring paper names. The entities used to create Graph G have been obtained from the “abstract” provided in metadata. We consider the common paper names

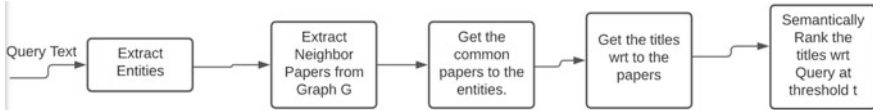


Fig. 2 Flow of incoming query

of the above entities, thus reducing our search size to a significant number, which can then further be ranked using cosine similarity of the query to the titles using Bio-BERT [3].

$$\cos(\mathbf{t}, \mathbf{e}) = \frac{\mathbf{t}\mathbf{e}}{\|\mathbf{t}\| \|\mathbf{e}\|} = \frac{\sum_{i=1}^n \mathbf{t}_i \mathbf{e}_i}{\sqrt{\sum_{i=1}^n (\mathbf{t}_i)^2} \sqrt{\sum_{i=1}^n (\mathbf{e}_i)^2}} \quad (1)$$

3 Experiments

For the information retrieval approach and experimentation purpose COVID-19 Open Research Dataset (CORD-19) has been used which was collected by the Allen Institute for AI and a coalition of research groups and open sourced by Kaggle [16]. The CORD-19 dataset contains around 273,419 scientific articles with full text, abstract and title. Although unique articles can be reduced to 226,999 which is still a marathon dataset to conduct one's research. The focus is to use the metadata for conducting our task, from data cleaning perspective firstly any null present in the data is dropped, also drop those rows which do not have any titles or abstract present. We also drop any duplicate titles present. To create a unique “id” column “cord-uid” + “title” columns are concatenated. Entities from “abstract” column are extracted to be used for Graph construction G . All the entities are considered except “O” [others]. The title column is also used for graph G construction.

Examples of entity recognition as derived from abstracts of paper refer to Table 1.

3.1 Dataset For Fine-tuning

For fine-tuning our NER using Bio-BERT open sourced tagged dataset BioNLP13cg-IOB [15] is used which contains the following tags refer to Table 2.

The CORD-19 dataset contains majorly contains biomedical terms, due to which we chose BioNLP13cg-IOB [15] for fine-tuning the Bio-BERT model. The training and test data is divided as follows for BioNLP13cg, around 86499 labeled lines for training whereas 54675 labeled lines for test data. We obtain a $F1$ -score of 0.93 on the test data after 30 epochs of fine-tuning with very close precision and recall

Table 1 Examples of entity recognition in abstracts

Abstract	Paper	Entities
The BIG project looks at some of the ethical concerns surrounding globalization and health	Bioethical implications of globalization: An International Consortium Project of the European Commission_vw8xjo9t	['O', 'O', 'B-Gene_or_gene_product', 'O', 'O']
Resource allocation during an influenza pandemic	Resource allocation during an influenza Pandemic_sswimukk	['O', 'O', 'O', 'O', 'O', 'O', 'O', 'O']
National public health institutes will play a key role in implementation of the revised International Health Regulations	Global Public Health Security_ge5iri3v	['O', 'O', 'O']
Masao Matsuoka wins the 2011 retrovirology prize	The 2011 Retrovirology Prize winner Masao Matsuoka: forward looking and antisense_132oghxax	['O', 'O', 'I-Organism', 'O', 'O', 'O', 'O', 'O', 'O', 'O']
Please see later in the article for the Editors' summary	Ethical alternatives to experiments with novel potential pandemic Pathogens_qbct63p4	['O', 'O', 'O', 'O', 'O', 'O', 'O', 'O', 'O', 'O']

Table 2 BioNLP13cg entities datasets

Class	Entities
Cancer	["B-Cancer", "I-Cancer"]
Cell type	["B-Cell", "B-Cellular_component", "I-Cell"]
Chemical	["I-Simple_chemical", "B-Simple_chemical"]
Anatomy	["B-Anatomical_system", "B-Developing_anatomical_structure", "I-Developing_anatomical_structure", "I-Immaterial_anatomical_entity", "I-Anatomical_system", "B-Immaterial_anatomical_entity"]
Tissue	["B-Multi-tissue_structure", "B-Tissue", "I-Multi-tissue_structure", "I-Tissue"]
Organ	["B-Organ", "I-Organ"]
Organisms	["B-Organism", "B-Organism_subdivision", "B-Organism_substance", "I-Organism_subdivision", "I-Organism_substance"]
Pathological	["B-PathologicalFormation", "I-PathologicalFormation"]

Table 3 Metrics of fine-tuning

Loss	Precision	Recall	F1-score
0.416734	0.895301	0.896354	0.895827

scores. We also closely monitor the validation score for around 30 epochs. We get the following metrics after fine-tuning which refers to Table 3.

3.2 Graph Structure

There are a total of 13 “entity” vertices as that is the total number entities recognized by our NER. In the knowledge graph, there is an equal number of “paper” and “text” vertices as each paper has a corresponding abstract. There are 193,465 vertices for both. Since there is a 1:1 relationship between “paper” and “text” vertices, there are 193,465 number of edges between the two kinds in total. A “text” vertex can be connected to up to 13 “entity” vertices. This same behavior is mirrored by the “paper” vertices. Each “text” vertex needs to have an edge with at least 1 “entity” vertex otherwise that vertex is of no use to the knowledge graph and is discarded.

4 Results

The fine-tuned entity model is used to get the entities of the input query which helps us concentrate on abstracts and consequently on papers only which contains those entities. The titles are then ranked with user query by setting semantic threshold to be $t=0.90$, and get the relevant titles to the search. The semantic similarity is the result of cosine similarity (1) between each query and the titles that is derived from the graph G . Few results are shown below refer to Table 4.

In introduction, we mentioned the usage of domain-specific models, and we used BioBERT instead of BERT to fine-tune our NER model and get word/sentence embeddings for drawing cosine similarity to rank our findings for the query. The reason for using BioBERT is the following:

1. Non-presence of biomedical specific words in BERT due to which word vectors and consequently sentence vectors would be impossible to derive and hencewise relevant ranking of papers wrt query would not be possible, refer to Table 5.

We compare our results with standard search where plain use of semantic similarity is not able to provide relevant results and the computational complexity is very high, since words like “COVID-19” have no corresponding word vectors, but at least by entity model “COVID-19” is mapped to B-Gene_or_gene_product, resulting in shortening our span of search to fewer sentences, see Table 6.

Table 4 Results of query

RelevantPapers	simScore	query	queryEntities
Acute myocarditis associated with COVID-19 infection	0.964	Myocardial injury disease due to COVID-19	['O', 'B-Multi-tissue_structure', 'O', 'O', 'O', 'O', 'B-Gene_or_gene_product', 'O']
Myocardial injury and COVID-19: possible mechanisms	0.959	Myocardial injury disease due to COVID-19	['O', 'B-Multi-tissue_structure', 'O', 'O', 'O', 'O', 'B-Gene_or_gene_product', 'O']
Stress-induced cardiomyopathy secondary to COVID-19	0.955	Myocardial injury disease due to COVID-19	['O', 'B-Multi-tissue_structure', 'O', 'O', 'O', 'O', 'B-Gene_or_gene_product', 'O']
COVID-19 in patients with lung cancer	0.925	Lung cancer effect due to COVID-19	['O', 'B-Cancer', 'I-Cancer', 'O', 'O', 'O', 'B-Gene_or_gene_product', 'O']
Optimizing lung cancer radiation treatment worldwide in COVID-19 outbreak	0.917	Lung cancer effect due to COVID-19	['O', 'B-Cancer', 'I-Cancer', 'O', 'O', 'O', 'B-Gene_or_gene_product', 'O']
Acute lung injury in patients with COVID-19 infection	0.914	Lung cancer effect due to COVID-19	['O', 'B-Cancer', 'I-Cancer', 'O', 'O', 'O', 'B-Gene_or_gene_product', 'O']

Table 5 Example Of words present in BioBERT

Words	PresentInBert	PresentInBioBERT
Angiotensin	False	True
Staphylococcus	False	True
Glycopeptide	False	True
Dexamethasone	False	True
Cardiovascular	False	True

Table 6 Comparison with semantic search

Methods	Mean time (s)	Num sentences
Semantic search	52.05	2500
Proposed method	22.24	2500

For a typical query like “Lung cancer effect due to COVID-19” if we apply plain semantic similarity on all the titles to get the best probable match, we would have to go through all the papers which would be close to 200,000. On the other hand, our method reduces the search space typically to 10,000 papers, due to querying on entity nodes of graph G, we then apply semantic similarity on the 10000 papers to get the best ranked paper names.

5 Conclusion

The highlight of the paper is that we tried to approach the information retrieval problem from the view of entity-recognition to shorten our search space and then apply semantic similarity to find the best ranked results from the search space. The fine-tuned model with the code in pytorch will be released, so that it helps in various types of tasks such as classification of biomedical articles. Our current work would help in better information retrieval when based on entity-recognition systems which we have shown above with the results.

We would like to improve upon our current work by introducing better annotations for bio-medical words like “coronavirus”/“COVID-19”. This can be done by further adding sentences containing above words specifically from the biomedical articles. In current scenario of fine-tuned model, words like “COVID-19”/Coronavirus/SARS-COV-2 might point at different entities, but we would want them to be annotated under B-Covid/I-Covid (a new entity), this will help in our graph search, since all the papers connected to this entity node will come under one search and one umbrella, thus helping us improve the results further.

References

1. Asai A, Hashimoto K, Hajishirzi H, Socher R, Xiong C (2019) Learning to retrieve reasoning paths over wikipedia graph for question answering. [arXiv:1911.10470](https://arxiv.org/abs/1911.10470)
2. Mikolov T, Sutskever I, Chen K, Corrado GS, Dean J (2013). Distributed representations of words and phrases and their compositionality. In: Advances in neural information processing systems, pp 3111–3119
3. Lee^{1,†} J, Yoon^{1,†} W, Kim² S, Kim¹ D, Kim¹ S, So³ CH, Kang¹ J. BioBERT: a pre-trained biomedical language representation model for biomedical text mining
4. Tan M, dos Santos C, Xiang B, Zhou B (2016) Improved representation learning for question answer matching. In: Proceedings of the 54th annual meeting of the association for computational linguistics (vol 1: Long papers). Association for Computational Linguistics, Berlin, Germany, pp 464–473
5. Yadav V, Sharp R, Surdeanu M (2018) Sanity check: a strong alignment and information retrieval baseline for question answering. In: SIGIR
6. <https://nlp.stanford.edu/projects/glove/>
7. Yin W, Schütze H, Xiang B, Zhou B (2016) ABCNN: attention-based convolutional neural network for modeling sentence pairs. Trans Assoc Computat Linguisit 4:259–272

8. Garg S, Vu T, Moschitti A. Tanda: transfer and adapt pre-trained transformer models for answer sentence selection. In: Thirty-fourth AAAI conference on artificial intelligence
9. Devlin J, Chang M-W, Lee K, Toutanova K. BERT: pre-training of deep bidirectional transformers for language understanding
10. Liu Y, Ott M, Goyal N, Du J, Joshi M, Chen D, Levy O, Lewis M, Zettlemoyer L, Stoyanov V. RoBERTa: a robustly optimized BERT pretraining approach
11. Esteva A, Kale A, Paulus R, Hashimoto K, Yin W, Radev D, Socher R. CO-search: COVID-19 information retrieval with semantic search, question answering, and abstractive summarization
12. Reimers N, Gurevych I (2019) Sentence-bert: sentence embeddings using Siamese bert networks. [arXiv:1908.10084](https://arxiv.org/abs/1908.10084)
13. Cormack GV, Clarke CL, Buettcher S (2009) Reciprocal rank fusion outperforms condorcet and individual rank learning methods. In: SIGIR 2009, pp 758–759
14. Shahmirzadi O, Lugowski A, Younge K (2019) Text similarity in vector space models: a comparative study. In: ICMLA 2019. IEEE, pp 659–666
15. Pyysalo S, Ohta T, Rak R, Rowley A, Chun HW, Jung SJ, Choi SP, Tsujii J, Ananiadou S (2015) Overview of the cancer genetics and pathway curation tasks of bionlp shared task 2013. BMC Bioinf 16(10):1
16. <https://www.kaggle.com/allen-institute-for-ai/CORD-19-research-challenge>

Human Activity Recognition Using Deep Learning-Based Approach



Maruf Rahman and Tanuja Das

Abstract There is a considerable demand for human activity recognition techniques in the area of human perception and also encompasses many other purposes like healthcare monitoring, assisted living for elders, and intelligent video surveillance. There are different approaches to machine learning that have been adapted for the purpose of activity recognition. But these techniques depend heavily on hand-crafted feature extraction which is unable to perform well when dealing with complex scenarios. Deep learning techniques have great potential for human activity recognition. In this paper, a neural network (NN) based approach for classification and evaluation of human activities has been explored. In this method, a convolutional neural network (CNN) is put together with long short-term memory (LSTM). The dataset experimented in this system is the classic Human Activity Recognition (HAR) dataset for classifying the six human activities, viz., walking, walking-upstairs, walking-downstairs, sitting, standing, and laying. Results show that the proposed model is very efficient for recognizing human activity.

Keywords Human activity recognition · Deep learning · Convolutional neural network · Long short term memory

1 Introduction

The classification of human activities by using the data collected by the sensors is known as human activity recognition [1]. Nowadays, social groups, third parties, and end-users are using various applications for activity monitoring available in smart-phones and smart devices. End users operate applications such as fitness and health tracking and self-management apps. The result of activity recognition can be used by third parties for advertisement and management. The results of activity recognition of various persons have the opportunity to possess social applications such as event detection and interfacing individuals with comparable action profiles [2].

M. Rahman (✉) · T. Das

Department of Information Technology, GUIST, Guwahati, Assam, India

Different techniques have been developed for activity recognition using different kinds and locations of sensors. Information representation is the main problem of activity recognition technique where data is taken from the sensors [3]. The features extracted from kinetic signals are used in the traditional methods for classification. However, deep knowledge of the human experience and application domain is required in the process of feature extraction but it still leads to poor features [4]. Moreover, traditional HAR methods in most cases perform really poorly on the data that continually changes after it's collected.

In neural networks, learning methods can be automatically used to learn the features in a network. These methods make an accurate prediction from the raw data fed into the network. Because of these learning methods, various types of new datasets and sensor techniques are approved in an efficient manner. Nowadays, feature learning is achieved by the deep learning models. This led to recent development and cutting edge research advances in the technology of activity recognition [5]. The deep learning models accomplish learning of features automatically from data by unsupervised or supervised learning methods. The deep learning techniques tend to have relatively good performance in feature learning compared to traditional hand-crafted techniques.

The deep learning models perform feature selection and extraction. The feature learning process is automatically done by the neural network and we do not have to develop it manually [6]. Deep learning methods are suitable for performing difficult activity recognition techniques. These methods perform feature learning automatically. The classification of time series data is shown by two kinds of methods. These two methods are used to achieve activity recognition by using the raw data collected from the sensors. Activity recognition is mainly used in healthcare and fitness tracking as an adaptive technology. The two methods are convolutional neural network models and recurrent neural network models [6].

The popularity for automated and deep learning methods for human activity recognition [5] is due to the fundamental idea that the data selecting process is changed to a learning model as soon as we adopt the data-driven approach for signal classification. Among the signals, spatial and temporal dependencies can be detected by the convolutional neural networks (CNNs) and can model the local features [7]. CNNs are developed to use the input as image data to create handwriting recognition, number recognition, and many more. CNN also solved the problems of computer vision techniques successfully. CNNs are mainly used in recognizing and restricting the objects in images to a particular place. It also obtains the information of the images [8].

Recurrent neural networks (RNNs) are a different kind of deep neural network. RNNs are developed for learning from the data that is in sequence. For example, the observation that is in sequence over time or words that are in sequence from a sentence [9]. The long short-term memory (LSTM) is an artificial recurrent neural network (RNN) paradigm that supports sequence prediction and has the capacity to learn sequences of processes from states in an activity [10]. LSTMs are greatly successful in tackling the prediction problems that use the sequence data as input. They are mainly used in recognition of handwriting and the translation of the models.

A CNN-LSTM approach is used in this paper in which the data acquired from the smartphone sensors was provided into the convolution layers and then followed by the LSTM layer. The complete CNN model is enveloped in a time distributed layer. Also, every convolutional layer is succeeded by the max-pooling layer. Then a dropout layer is added. Moreover, a dense fully connected layer with Softmax activation function is used in this model, and in every convolution layer, a ReLU activation function was applied. For experimentation purposes, the UCI-HAR dataset [11] is used in which raw data is acquired from the tri-axial accelerometer and tri-axial gyroscope sensors that are inserted in the smartphone. The dataset consists of tasks carried out by individual subjects that include walking, walking-upstairs, walking-downstairs, sitting, standing, and laying.

The organization of the paper is given as: Sect. 2 presents the related works on human activity recognition using deep learning methods. Section 3 gives the background of our work. Section 4 gives the detailed framework of the CNN-LSTM model. Experimental evaluation is discussed in Sects. 5 and 6 presents the results of the effect of hyper-parameters on the training of the system. In Sect. 7 a summary of the paper is presented and in the last Sect. 8 gives the acknowledgment of the work.

2 Related Works

Many researchers are actively conducting a huge number of researches in investigating different sensing technologies. Different techniques were created for the objective of classification of the human activities. Since there is no working model that can guarantee 100% classification of all the human activities, the problem still exists and requires further research on this topic. In this section, we try to give a summary of some of the relevant works done in this domain.

In the first work to classify the human activities, a random forest (RF) classifier was used [12]. In this work, a monitoring system is developed by using six inertial measurement units. After executing network analysis, the feature set is formed by selecting several network estimates that succeed in the hypothesis test. In another work, human activity recognition is examined with a multi-layer perceptron (MLP) classifier [13]. In the MLP algorithm, the only problem is that it cannot assure that in the training time that the minima stop is the global minima. The resilient back-propagation algorithm has been utilized for building the neural network, thus optimizing the learning time. In the multi-layer perceptron network, the overall parameters have been optimized and because of that, the model accuracy has been improved.

Chen and Xue [14] used a deep learning-based approach on a single accelerometer for human activity recognition. Although the model is capable of isolating the knowledge present in the same axis, the features extracted from the model are not specified clearly. In the paper [15], a technique is presented for the human movement perception. It is used to extract the shapes that are in motion. The movements are classified using SVM Classifier. The SVM Classifier categorize the movements into different groupings. In this work, the evaluation is done by experimenting on a

dynamic video for the efficiency of the technique. The movement of walking is not provided and classified in this technique and it is held on for future research.

In another work [16], a new technique is proposed in which the temporal convolutional network is put together with convolutional auto-encoder. It increases the effectiveness in the classification of activities. It accomplishes great outcomes using this technique. It is more powerful than CNN and LSTMs. The limitation in this technique is to examine the model in a latest domain. In the paper [17], Bagging and Adaboost ensemble classifiers is used for activity recognition structure. Adaboost SVM classifier is proposed in which it gives precise classification of activities for healthcare and elderly people who require constant guidance. It acts as a device for health workers to assist patients. The evaluation of this technique needs extra analysis and procedure to carry out in various other disciplines.

In another paper [18], a deep learning technique is used for the recognition of activities. The deep learning model is to modify the system that is presented for the investigation of a software to translate from one language to another. The model takes advantage of the attention mechanism in deep learning to bring about feature learning. The disadvantage of this technique is that it did not achieve window-wise classification. In the paper [19], a generative graphical model called deep belief network (DBN) is presented for identification of human activity. A real-world dataset from wearable health devices is used in this work. The model performs various evaluations for the accurate results of the developed deep learning methodology. The limitation lies in the fact that the model requires a real-time domain to perform.

Numerous deep learning methods exist for the purpose of recognition of human activities such as convolutional neural networks (CNNs), long short-term memory (LSTM), recurrent neural networks (RNNs) and deep neural network (DNN). In the paper [20], the authors inspect various networks such as DNN, CNN, and RNN to use for the activity dataset. It is decided that recurrent neural networks (RNN) achieve greater performance. It perform much better than the evaluations that are concluded on OPPORTUNITY [21], PAMAP2 [22] and Daphnet Gait [23] dataset. In this work, recurrent neural networks achieve much better results than convolutional neural networks for activity recognition in which time span of the activities is smaller. A deep neural network system is presented in the work given in [24]. It is composed of layers of convolutional and LSTM. The model uses various sensors such as gyroscope, magnetometer and accelerometer in various ways. The model is estimate by analyzing OPPORTUNITY [21] datasets. The model is to a great extent improves the use of suitable hyper-parameters.

In the recent work on deep learning [25], a LSTM technique is used in the system. The model uses the wearable sensing data. This work utilizes deep learning techniques as it can focus on the possibility of developing and research in this domain. In another work [26] it proposed the k-nearest neighbors approach for the identification of the basic human activities. The data of the human activities is gathered together from the wrist and the waist. The evaluation of the model in this paper is done using hand-crafted features and the CNN derived features. The preferable interpretation of the deep learning networks is done using the features obtained from the system. In another paper [26], a multichannel CNN system is presented for the activity recog-

nition. The classifiers use in this model are Decision Tree, kNN, and Naive Bayes classifiers. It improves the model for better classification of activities.

In [27] an attempt was made to utilize the same in order to identify in case of real-world videos. Murad and Pyun [28] used deep RNNs for classifying human activity at each time. But the approach has a major limitation of functioning for a fixed window of data. In [29], a convolutional neural network was applied on the HAR dataset for extracting the significant features related to the respective activities. The major challenge of this model is that it is quite complicated to validate the extracted features which are not generated automatically. Sun et al. [30] uses an approach which combines the basic idea of LSTM and ELM classifier for classifying human activities. However, the approach has yet to be tested for large scale data classification.

In another work, 3D human activity recognition using the help of reconfigurable convolutional neural networks [31] is introduced. The convolutional neural network is benefited from its automatic feature extraction. In the input, the local elements match with one another and it is described as a tensor. CNN does not encode the position and orientation of the object. It cannot be spatially invariant to the input data. Another important method is proposed in [32] where LSTM cells were used on the dataset. LSTM has the ability of sequence prediction and this led to NLP and narrative analysis to support neural networks. The usage of high memory-bandwidth is higher so LSTMs become inefficient hardware-wise.

In the work [33], a deep autoencoder strategy is used for activity recognition on the smartphone. In this strategy, the stacked auto-encoder (SAE) improved accuracy and prediction time. Autoencoders may enhance the performance, produce biologically plausible filters. But as the complexity of the images increase, auto-encoders struggle to keep up with the model and the images start to get blurry. In [34], a review of some of the handcrafted as well as learning-based techniques for activity recognition has been discussed in detail. Because of the disadvantages of the above methods, a method established on the grounds of CNN and LSTM is presented for the recognition of the basic activities of an individual. In this CNN-LSTM model, the automatic feature extraction is done by CNN and the classification of the model for human activities is done with only a small amount of parameters. Enhanced performance is shown in the proposed model.

3 Background

In this part of the paper, we provide a brief description of the CNN-LSTM-based feature extraction approach. Convolutional neural networks (CNNs) are a category of deep neural network in which the framework is very similar to the visual biological system [35] and long short-term memory (LSTM) networks are a type of recurrent neural network which have the knack of acquiring long-term dependencies [36]. The CNN-LSTM is an LSTM architecture that was fabricated for solving sequence prediction problems that can be used for related inputs such as images or videos [37]. Convolutional neural networks (CNNs) are such a type of neural network which is

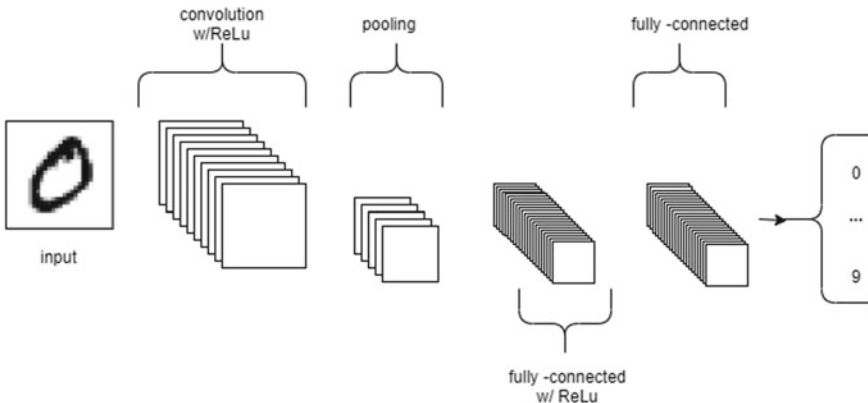


Fig. 1 The basic framework of simple CNN network

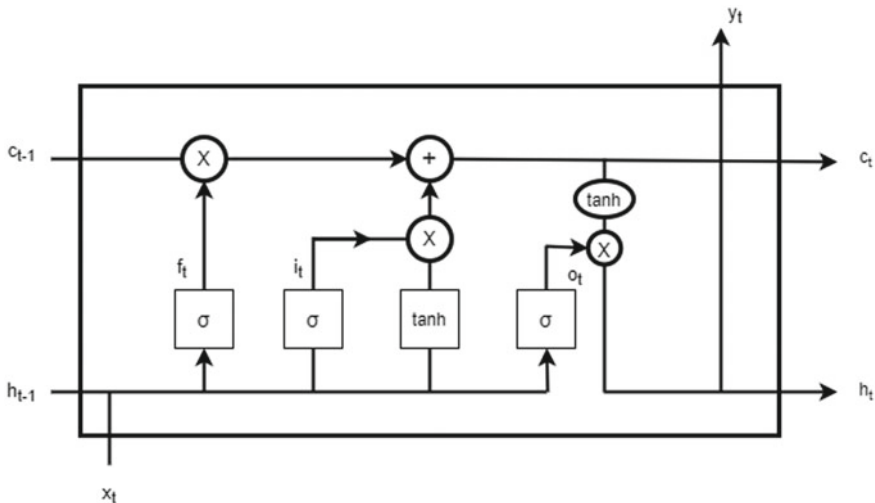


Fig. 2 Architecture of simple LSTM network

primarily exploited in the field of pattern recognition within images [38]. These networks are created from an input layer, an output layer, and several hidden layers. Each hidden layers consist of convolutional layers, pooling layers, fully connected layers, and normalization layers. A basic CNN architecture for analyzing the MNIST data is depicted in Fig. 1.

Long short-term memory (LSTM) is designed for long term dependencies [39]. It is composed of memory blocks called cells. Each cell consist of an input gate, an output gate and a forget gate. LSTM differs from RNN in that it copes with the exploding and vanishing gradient problems. The basic architecture of an LSTM is shown in Fig. 2.

The CNN LSTM framework utilizes the various layers of the CNN for the purpose of feature extraction from the considered dataset and then is subjected to classification using LSTM. A comprehensive summary of the CNN-LSTM [40] is given below:

- *Convolutional layer*: There are two vectors $x \in \mathbb{R}^N$ and a kernel vector $h \in \mathbb{R}^M$. The convolution of the two vectors is a vector $c \in \mathbb{R}^{M+N-1}$ in which the convolution operation is $c = x * h$ in one-dimensional case. The following equation is the convolution

$$c[n] = \sum_{k=-\infty}^{\infty} x[k]h[n-k] \quad (1)$$

for $\forall n \in [1 \dots N]$ in the discrete domain. The convolution filter is referred to as a reflected vector h and it is sliding along signal x . At each n value a dot product is computed.

- *Activation function*: The ReLU activation function is used in this proposal. The ReLU function obtains only positive values of c . Rectified linear unit (ReLU) is defined as

$$\text{ReLU}(C) = \max(0, c) \quad (2)$$

- *Pooling layer*: The output of the convolution is reduced and encapsulated. Max pooling function is used in the training of the CNN-LSTM system. The size of the vector is $[1 \times 2]$.
- *Flatten layer*: The flatten layer translates a two-dimensional matrix of features into vector which has the ability to be inserted into a fully connected neural network classifier.
- *LSTM layer*: The structure of an LSTM network memory cell contains four major elements: an input gate, a neuron with a self-recurrent connection, a forget gate, and an output gate. The adjustment of the connection between the memory cell itself and its surroundings is done by the gates. The modification of the state of a memory cell by the incoming signal is done by the input gate or the input gate can block the incoming signal. The effect on neurons to the state of a memory cell or its prevention is permitted by the output gate. Lastly, The memory cell's self-recurrent connection can be controlled so that the cell can remember or forget its previous state by the forget gate.

The process of updating an LSTM layer is shown in the following equations:

$$i_t = \sigma_i(W_{ai}a_t + W_{hi}h_{t-1} + W_{ci}c_{t-1} + b_i) \quad (3)$$

$$f_t = \sigma_f(W_{af}a_t + W_{hf}h_{t-1} + W_{cf}c_{t-1} + b_f) \quad (4)$$

$$c_t = f_t c_{t-1} + i_t \sigma_f(W_{ac}a_t + W_{hc}h_{t-1} + b_c) \quad (5)$$

$$o_t = \sigma_o(W_{ao}a_t + W_{ho}h_{t-1} + W_{co}c_t + b_o) \quad (6)$$

$$h_t = o_t \sigma_h(c_t) \quad (7)$$

In the equations, the input gate, forget gate, output gate and cell activation vectors are described by i , f , o and c . The latent variable is denoted by h . W_{ai} , W_{hi} , W_{ci} , W_{af} , W_{hf} , W_{cf} , W_{ac} , W_{hc} , W_{ao} , W_{ho} and W_{co} are weights and b_i , b_f , b_c and b_o are bias vectors.

- *Dense layer*: It is also known as fully connected layer. It provides learning features from all the combinations of the features of the previous layer.
- *Soft-max Layer*: It calculates the probability distribution of the fundamental human activities.

4 Materials and Methods

The CNN-LSTM model architecture proposed is shown in Fig. 3. To achieve the optimum feature learning, in this technique, the data is followed to more than one hidden layer. The dataset consists of total acceleration, body acceleration, and body gyroscope signals, and the individual signals contain 3 axes of data as x , y , z . The architecture of the CNN-LSTM contains an input layer, a hidden layer, and an output layer. The input layer consists of 30 neurons and 3 convolution layers with filters 64, 128, 256 are formed in the hidden layer in the CNN-LSTM system. In this proposal, the CNN-LSTM model contains 3 convolutional layers, and individual layers are followed by max-pooling layers. A time distributed wrapper is invoked in both the convolution layer and max-pooling layer, To reduce the dimension pool length 2 is selected. ReLU function is used as an activation technique. It is superseded by a flatten layer and then the LSTM model. It has the ability for sequence prediction. After that to reduce over-fitting, the dropout layer is introduced and then a dense fully connected layer with Softmax activation function is used to classify the human activities.

To optimize the neural network, an RMSprop optimizer is used and the loss function of categorical cross-entropy is selected which is used for multi-class classification. The categorical cross-entropy loss [41] is represented by the below equation:

$$CE = -\log\left(\frac{e^{s_p}}{\sum_j^C e^{s_j}}\right) \quad (8)$$

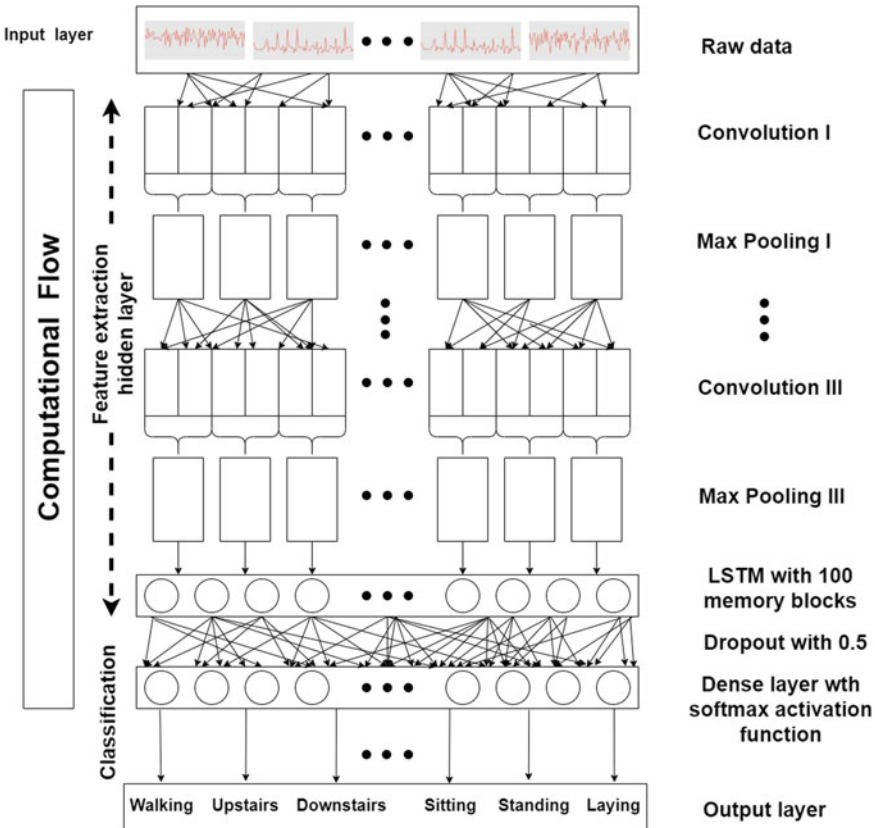


Fig. 3 Architecture of proposed system for detection of human activities

5 Experimental Evaluation

5.1 UCI HAR Dataset

The UCI-HAR dataset is used in the training of the model [11]. The dataset is taken from the UCI machine learning repository. It has been created using the experiments carried out by the 30 volunteers. Smartphones were used by the volunteers to store the raw data by utilizing the inbuilt sensors in the smartphones. The activities performed by each person includes walking, upstairs, downstairs, sitting, standing, and laying activities. The raw data captured by the smartphones where linear acceleration data is collected by accelerometer and angular velocity data is collected by gyroscope sensors. Each activity is processed in fixed-width sliding windows of 2.56 s. The dataset has been split randomly into training and testing sets with the distribution of

Table 1 The distribution of human activities of training and testing sets

Activity	Training	Testing
Walking	1226	496
Ascending stairs	1073	471
Descending stairs	986	420
Sitting	1286	491
Standing	1374	532
Laying	1407	537

training and testing sets being 70% and 30%, respectively. The number of instances of the activities of both the sets from the UCI HAR dataset is shown in Table 1

The entire dataset has been divided into training and testing set in the following manner:

- Training set: The training dataset is formed by 70% (21 persons) of the volunteers from the whole database. There are 7352 instances collected from 21 volunteers. The formation of the training set is done by $7352 \text{ instances} \times 128 \text{ samples} \times 6 \text{ axis}$.
- Test set: The testing dataset is formed by 30%(9 persons) of the volunteers from the whole database. There are 2947 instances collected from 9 volunteers. The formation of the testing set is done by $2947 \text{ instances} \times 128 \text{ samples} \times 6 \text{ axis}$.

5.2 Model Training

The proposed network structure was build using a neural network API known as Keras. The computer language used in the proposed network structure is Python. It is run on Tensorflow, an open-source machine learning platform. Here, the Tensorflow library is used in the CNN-LSTM system. A PC of i5-7200U CPU with 2.50 GHz, 8 GB RAM, and an NVIDIA GeForce 920MX with 2GB memory is used in the training of the CNN-LSTM system and the identification of the human activities. The operating system used is Windows with 64 bits. Also here, the backpropagation of the CNN-LSTM model is from Softmax layer [42] to the Convolution layer. The categorical cross-entropy loss function [43] and RMSprop optimizer [44] is used in this proposed model. The batch size and the total no. of epochs for the training of the model were 128 and 100, respectively. To enhance the performance of the system, the shuffling of the training data and the selection of the learning rate of 0.001 were done. The various values of the specifications of the proposed model are given in Table 2.

Table 2 Specifications of the CNN-LSTM model

Parameter	Value
The size of input vector	128
The number of input channels	6
Filter size	[1 × 3]
Pooling size	[1 × 2]
Activation function	ReLU (rectified linear unit)
Learning rate	0.001
Momentum	0.9
The probability of dropout	0.5
The size of mini-batches	128
Maximum epochs	100

6 Results and Discussion

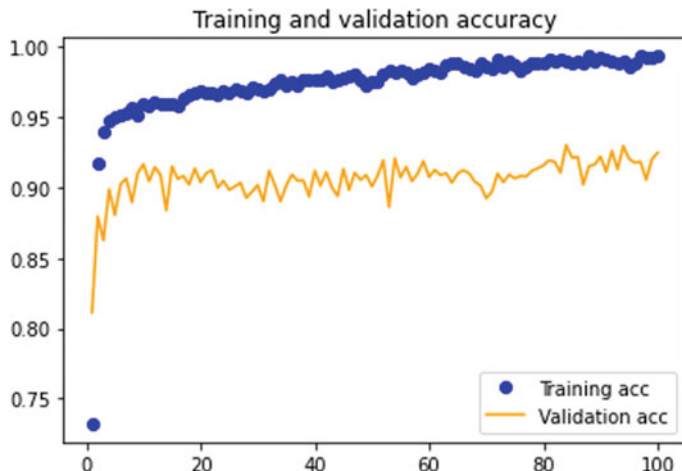
The model so trained was tested on the various instances of the UCI-HAR dataset as given in Table 1. The proposed system is 93.35% accurate as out of the total 2947 instances, 2741 instances of the training set are accurate in the training model. The classification between sitting and standing is deficient as the two activities act the same from the viewpoint of the motion sensors. Table 3 depicts the confusion matrix showing the case of categorical classification of the six human activities. The training and validation accuracy graph in Fig. 4 and the training and validation loss in Fig. 5 is presented in this paper in case of the proposed CNN-LSTM framework. The accuracy of both training and validation is increasing over time. Further, the training loss is decreasing over time but validation loss is fluctuating during the training of the model.

6.1 *The Performance of the CNN-LSTM Model by the Result of Hyper-parameters*

The efficiency of a neural network model is greatly improved by the use of suitable hyper-parameters. The hyper-parameters which include batch size and the type of optimizer which improved the training of the proposed model and enhanced its accuracy are shown in this work. The efficiency of the system is calculated by F1 score to measure its accuracy.

Table 3 Confusion matrix of classification of the considered human activities in the UCI-HAR dataset

Activity	Walking	Walking Upstairs	Walking down-stairs	Sitting	Standing	Laying	Recall (%)
Walking	473	0	1	0	22	0	95
Walking upstairs	6	435	29	1	0	0	92
Walking down-stairs	0	0	420	0	0	0	100
Sitting	0	6	0	418	67	0	85
Standing	3	1	0	43	485	0	91
Laying	0	1	0	0	26	510	95
Precision (%)	98	98	89	90	84	100	93

**Fig. 4** Training-validation accuracy

6.1.1 Effect of Optimizer

The efficiency of a neural network model can be made to be greatly improved by selecting a suitable optimizer. The optimizer calculates the weight parameters and learning rate to give better results. There are many optimizers to select such as Adagrad, RMSprop, SGD, Adam, Adadelta [44] as shown in Fig. 6. In this proposed CNN-LSTM model, RMSprop is selected to train the model as it improves and gives better results to the model.

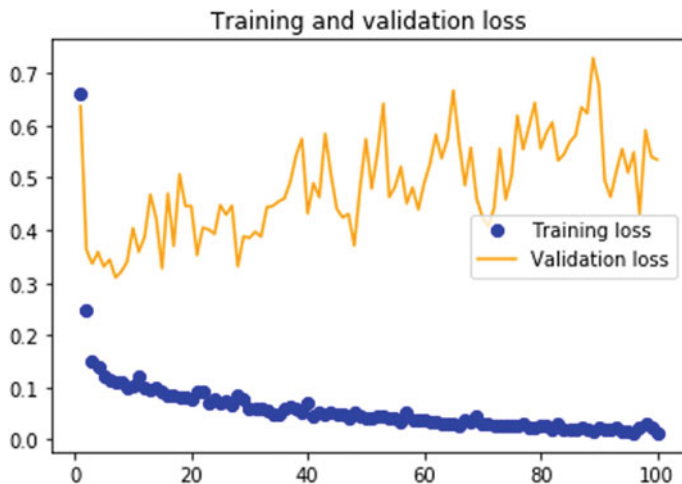


Fig. 5 Training-validation loss

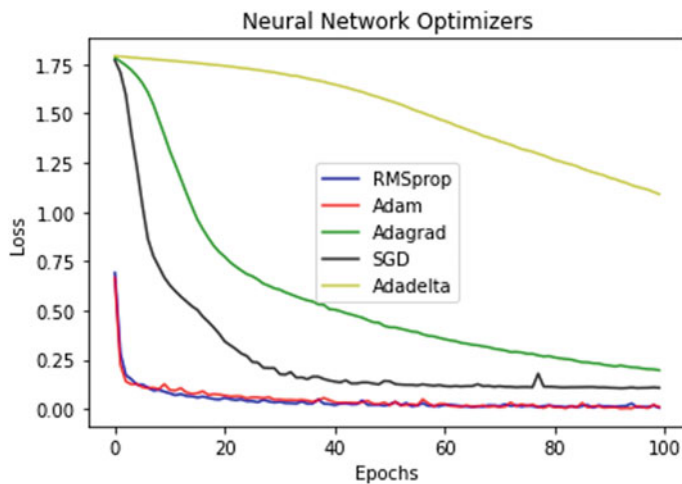


Fig. 6 Impact of optimizer on model performance

6.1.2 Effect of Batch Size:

When training neural networks, mini-batch is used to get high throughput and faster convergence to improve the training of the model. Mini batching allows for a high-quality gradient and this will be really useful allowing one to use high learning rates. Table 4 represents the accuracy of the 5 distinct sizes of the mini-batch. The efficiency of the proposed system is greatly improved if the size of the batch is 128.

Table 4 Impact of batch size on model performance

Batch size	F1 score (%)
64	90.87
128	93.35
192	92.02
256	93
320	89.92

7 Conclusion

A CNN-LSTM model is proposed for classification of human activities. A combination of neural network and convolutional layers with LSTM is used for classification of human activity. The activities selected for classification of activity recognition includes walking, upstairs, downstairs, sitting, standing, and laying activities. A time distributed wrapper is utilized on both the convolution layer and max-pooling layer in the CNN model. CNN-LSTM model takes as input, the raw data is collected from the smartphone, and it consists of total acceleration, body acceleration, and body gyroscope signals, and the individual signals contain 3 axes of data as x , y , z . The CNN-LSTM model uses the UCI-HAR sensor dataset for making the model learn and then predict the activity performed by the person. The proposed model precisely classifies the six categories of human activity. The UCI-HAR dataset is used for training the model that comprises of six categories of human activity. The evaluation of the CNN-LSTM system shows that the prediction of the human activities is mostly correct. The accuracy of the proposed model is of 93.35%. In the field of deep learning, a new person can precisely classify and predict various human activities. Because of this approach, we can use in various device systems including surveillance systems, health care monitoring and human-computer interaction.

The efficiency of the CNN-LSTM system is calculated by the F1 score to measure the model's accuracy. Further, different types of optimizers and batch size are used to understand the impact of the hyper-parameters in the proposed model efficiency to select fitting hyper-parameters to train the CNN-LSTM model. Overall the performance is higher for the proposed CNN-LSTM model. Future work includes more complex activities and can develop a real-time system on a smartphone.

Further studies require in the coming times for the prospective of deep learning techniques in the recognition of human activities. The training of deep learning models requires an abundant quantity of detailed data for human activity recognition. The demand for detailed data can be reduced with the assist of unsupervised learning. Nowadays, unsupervised learning models are mostly required for feature extraction. The models are not used for the classification of human activities. Because of the limitation for the classification of the human activities a new technique is proposed that is deep unsupervised transfer learning [45]. There is another alternative to turn to the data-driven approach which includes ontology [46].

The main problem in human activity recognition is the classification and prediction of interestingly new activities where the proposed models did not work with these activities. The proposed model's main requirement is to comprehend the latest information and accomplish a precise prediction of the activities in the absence of direct observation. There is another method which is feature learning that is scalable to diverse activities. In another paper [47] it proposed a method in which mid-level attributes are utilized for the representation of activities that are associated with special features. In another work [48], a new approach is used that is disentangled representation to depict the classification of novel activities.

Future activity prediction is another part of activity recognition. In the activity prediction methodology, it predicts the actions of humans in advance. The future activity prediction is helpful in the recognition of human intentions. It can be used in criminal detection, driver behavior prediction, and smart services. The activities are mainly in a precise order in several behavior tasks. The future predictions are favorable to predict when the activities are modeled with temporal dependencies. In these kinds of situations, LSTM networks [49] are used for the classification. But the activities that require a long period of time is not suitable for LSTM networks. It did not accommodate long dependencies. In the work [50], an intention recognition method is used which is built on the basis of brain signals that aid future research in activity prediction.

A huge amount of works have been proposed for research in the field of deep learning. The experimental evaluations and the hyper-parameters that affect the performance of human activity recognition changes from paper to paper. In deep learning techniques, it depends mainly on training data. The effects of activity recognition depend on the distribution of training and testing datasets. There are various additional factors such as the processing of data and the execution of the model in various platforms and also lead to skewed comparison. Hence, there is a huge demand for the researcher in researching a fully developed method or technique.

Acknowledgements This research activity is a portion of the TEQIP Collaborative Research Scheme (CRS) project entitled, “Seamless Health Monitoring and Analysis of soldier using Machine Learning Approach” [CRS ID 1-5763896131]. The authors would like to thank NPIU, Government of India.

References

1. Lara OD, Labrador MA (2012) A survey on human activity recognition using wearable sensors. *IEEE Commun Surv Tutor* 15(3):1192–1209
2. Jalal A, Kim Y-H, Kim Y-J, Kamal S, Kim D (2017) Robust human activity recognition from depth video using spatiotemporal multi-fused features. *Patt Recogn* 61:295–308
3. Bevilacqua A, MacDonald K, Rangarej A, Widjaya V, Caulfield B, Kechadi T (2018) Human activity recognition with convolutional neural networks. In: Joint European conference on machine learning and knowledge discovery in databases. Springer, pp 541–552
4. Minar MR, Naher J (2018) Recent advances in deep learning: an overview. arXiv preprint [arXiv:1807.08169](https://arxiv.org/abs/1807.08169)

5. Ramasamy Ramamurthy S, Roy N (2018) Recent trends in machine learning for human activity recognitionla survey. Wiley Interdisc Rev Data Min Knowl Discov 8(4):
6. Wang J, Chen Y, Hao S, Peng X, Hu L (2019) Deep learning for sensor-based activity recognition: a survey. Pattern Recogn Lett 119:3–11
7. Guo S, Lin Y, Li S, Chen Z, Wan H (2019) Deep spatial-temporal 3d convolutional neural networks for traffic data forecasting. IEEE Trans Intell Transp Syst 20(10):3913–3926
8. Nunez JC, Cabido R, Pantrigo JJ, Montemayor AS, Velez JF (2018) Convolutional neural networks and long short-term memory for skeleton-based human activity and hand gesture recognition. Pattern Recogn 76:80–94
9. Medsker LR, Jain L (2001) Recurrent neural networks. Des Appl 5
10. Graves A (2012) Long short-term memory. In: Supervised sequence labelling with recurrent neural networks. Springer, pp 37–45
11. Anguita D, Ghio A, Oneto L, Parra X, Reyes-Ortiz JL (2013) A public domain dataset for human activity recognition using smartphones. Esann 3:3
12. Jalloul N, Poree F, Viardot G, L'Hostis P, Carrault G (2017) Activity recognition using complex network analysis. IEEE J Biomed Health Inf 22(4):989–1000
13. Talukdar J, Mehta B (2017) Human action recognition system using good features and multilayer perceptron network. In: 2017 international conference on communication and signal processing (ICCP). IEEE, pp 0317–0323
14. Chen Y, Xue Y (2015) A deep learning approach to human activity recognition based on single accelerometer. In: 2015 IEEE international conference on systems, man, and cybernetics. IEEE, pp 1488–1492
15. Priya G, Paul SN, Singh YJ (2015) Human walking motion detection and classification of actions from video sequences. Int J Concept Comput Inf Technol 3(1):40–44
16. Browne D, Giering M, Prestwich S (2019) Deep learning human activity recognition. Ceur workshop proceedings, Sun SITE Central Europe 2563:76–87
17. Subasi A, Fllatah A, Alzobidi K, Brahim T, Sarirete A (2019) Smartphone-based human activity recognition using bagging and boosting. Procedia Comput Sci 163:54–61
18. Mahmud S, Tonmoy M, Bhaumik KK, Rahman A, Amin MA, Shoyaib M, Khan MAH, Ali AA (2020). Human activity recognition from wearable sensor data using self-attention. arXiv preprint [arXiv:2003.09018](https://arxiv.org/abs/2003.09018)
19. Hassan MM, Huda S, Uddin MZ, Almogren A, Alrubaian M (2018) Human activity recognition from body sensor data using deep learning. J Med Syst 42(6):99
20. Hammerla NY, Halloran S, Plötz T (2016) Deep, convolutional, and recurrent models for human activity recognition using wearables. arXiv preprint [arXiv:1604.08880](https://arxiv.org/abs/1604.08880)
21. Roggen D, Forster K, Calatroni A, Holleczek T, Fang Y, Troster G, Ferscha A, Holzmann C, Riener A, Lukowicz P et al (2009) Opportunity: towards opportunistic activity and context recognition systems. In: 2009 IEEE international symposium on a world of wireless, mobile and multimedia networks & workshops. IEEE, pp 1–6
22. Reiss A, Stricker D (2012) Introducing a new benchmarked dataset for activity monitoring. In: 2012 16th international symposium on wearable computers. IEEE, pp 108–109
23. Bachlin M, Roggen D, Troster G, Plotnik M, Inbar N, Meidan I, Herman T, Brozgol M, Shaviv E, Giladi N et al (2009) Potentials of enhanced context awareness in wearable assistants for parkinson's disease patients with the freezing of gait syndrome. In: 2009 international symposium on wearable computers. IEEE, pp 123–130
24. Ordóñez FJ, Roggen D (2016) Deep convolutional and LSTM recurrent neural networks for multimodal wearable activity recognition. Sensors 16(1):115
25. Panwar M, Dyuthi SR, Prakash KC, Biswas D, Acharyya A, Maharatna K, Gautam A, Naik GR (2017) CNN based approach for activity recognition using a wrist-worn accelerometer. In: 2017 39th annual international conference of the IEEE engineering in medicine and biology society (embs). IEEE, pp 2438–2441

26. Sami S, Wiratunga N, Massie S (2017) Learning deep features for KNN-based human activity recognition. CEUR workshop proceedings
27. Wei L, Shah SK (2017) Human activity re cognition using deep neural network with contextual information. In: International conference on computer vision theory and applications, vol 6. SCITEPRESS, pp 34–43
28. Murad A, Pyun J-Y (2017) Deep recurrent neural networks for human activity recognition. Sensors 17(11):2556
29. Xue L, Xiandong S, Lanshun N, Jiazheng L, Renjie D, Dechen Z, Dianhui C (2018) Understanding and improving deep neural network for activity recognition. arXiv preprint [arXiv:1805.07020](https://arxiv.org/abs/1805.07020)
30. Sun J, Fu Y, Li S, He J, Xu C, Tan L (2018) Sequential human activity recognition based on deep convolutional network and extreme learning machine using wearable sensors. J Sens
31. Wang K, Wang X, Lin L, Wang M, Zuo W (2014) 3d human activity recognition with reconfigurable convolutional neural networks. In: Proceedings of the 22nd acm international conference on multimedia, pp 97–106
32. Zhao Y, Yang R, Chevalier G, Xu X, Zhang Z (2018) Deep residual bidir-lstm for human activity recognition using wearable sensors. Math Probl Eng
33. Almaslukh B, AlMuhtadi J, Artoli A (2017) An effective deep autoencoder approach for online smartphone-based human activity recognition. Int J Comput Sci Netw Secur 17(4):160–165
34. Sargano AB, Angelov P, Habib Z (2017) A comprehensive review on handcrafted and learningbased action representation approaches for human activity recognition. Appl Sci 7(1):110
35. Wu J (2017) Introduction to convolutional neural networks. National Key Lab for Novel Software Technology. Nanjing University. China, 5, 23
36. Hochreiter S, Schmidhuber J (1997) Long short-term memory. Neural Comput 9(8):1735–1780
37. Ullah A, Ahmad J, Muhammad K, Sajjad M, Baik SW (2017) Action recognition in video sequences using deep bi-directional lstm with cnn features. IEEE Access 6:1155–1166
38. O’Shea K, Nash R (2015) An introduction to convolutional neural networks. arXiv preprint [arXiv:1511.08458](https://arxiv.org/abs/1511.08458)
39. Yu Y, Si X, Hu C, Zhang J (2019) A review of recurrent neural networks: LSTM cells and network architectures. Neural Comput 31(7):1235–1270
40. Tu X, Zhang H, Xie M, Luo Y, Zhang Y, Ma Z (2019) Enhance the motion cues for face anti-spoofing using cnn-lstm architecture. arXiv preprint [arXiv:1901.05635](https://arxiv.org/abs/1901.05635)
41. Martinez M, Stiefelhagen R (2018) Taming the cross entropy loss. In: German conference on pattern recognition. Springer, pp 628–637
42. Du G, Tian C, Li Z, Zhang D, Yin Y, Ouyang Y (2019) Efficient softmax hardware architecture for deep neural networks. In: Proceedings of the 2019 on great lakes symposium on VLSI, pp 75–80
43. Zhou Y, Wang X, Zhang M, Zhu J, Zheng R, Wu Q (2019) Mpce: a maximum probability based cross entropy loss function for neural network classification. IEEE Access 7:146331–146341
44. Kumar A, Sarkar S, Pradhan C (2020) Malaria disease detection using cnn technique with sgd, rmsprop and adam optimizers. In: Deep learning techniques for biomedical and health informatics. Springer, pp 211–230
45. Bengio Y (2012) Deep learning of representations for unsupervised and transfer learning. In: Proceedings of icml workshop on unsupervised and transfer learning, pp 17–36
46. Riboni D, Pareschi L, Radaelli L, Bettini C (2011) Is ontology-based activity recognition really effective? In: 2011 IEEE international conference on pervasive computing and communications workshops (percom workshops). IEEE, pp 427–431
47. Nair H, Tan C, Zeng M, Mengshoel OJ, Shen JP (2019) Attrinet: learning mid-level features for human activity recognition with deep belief networks. In: Adjunct proceedings of the 2019 acm international joint conference on pervasive and ubiquitous computing and proceedings of the 2019 ACM international symposium on wearable computers, pp 510–517
48. Tran L, Yin X, Liu X (2017) Disentangled representation learning gan for pose-invariant face recognition. In: Proceedings of the ieee conference on computer vision and pattern recognition. Human Activity Recognition using Deep Learning based approach 13, pp 1415–1424

49. Baccouche M, Mamalet F, Wolf C, Garcia C, Baskurt A (2010) Action classification in soccer videos with long short-term memory recurrent neural networks. In: International conference on artificial neural networks. Springer, pp 154–159
50. Zhang D, Yao L, Zhang X, Wang S, Chen W, Boots R, Benatallah B (2018) Cascade and parallel convolutional recurrent neural networks on eeg-based intention recognition for brain computer interface. In: Proceedings of the aaai conference on artificial intelligence, vol 32(1)

Time Fractionalized Lattice Boltzmann Model-Based Image Denoising



P. Upadhyay and K. N. Rai

Abstract In this paper, we have proposed the Caputo sense time fractionalized lattice Boltzmann (LB) model for time sub-diffusion equation in Caputo sense recently proposed by Rui Du et al. We have applied this model to denoise white Gaussian noise corrupted images with different noise levels. The denoising results have been compared with some of the recently reported state-of-the-art methods in terms of PSNR and SSIM values. The results found show considerable improvement over other recently reported state-of-the-art methods in terms of both PSNR and SSIM values.

Keywords Time fractionalization · Gaussian noise · Denoising · Caputo fractional partial derivative

1 Introduction

One of the most important areas of image processing is denoising of images. Noise is introduced to images in its different phases including the image capturing phase. Several image denoising methods have been proposed. Every method suffers from its own shortcoming. Therefore, the greatest challenge in the area of image denoising has always been to get maximum information from the denoised images with minimum trade off. Some of the commonly used methods of image denoising include but not limited to total variational-based methods [1, 2], non-local self similarity-based methods [3–6], low-rank-based methods [7, 8], etc.

P. Upadhyay (✉)

DST-CIMS Banaras Hindu University, Varanasi, Uttar Pradesh 221005, India
e-mail: prateep.upadhyay1@bhu.ac.in

K. N. Rai

Department of Mathematical Sciences IIT (B.H.U.), DST-CIMS Banaras Hindu University, Varanasi, Uttar Pradesh 221005, India
e-mail: knrai.apm@itbhu.ac.in

El Helou [9] introduced a blind and universal deep learning image denoising method for Gaussian noise. Tian et al. [10] designed a batch renormalization denoising network (BRDNet) to denoise images. A region-based anisotropic shaped Wiener filtering (ASRWF) along with BayesShrink (ASRBS) algorithms capable of exploiting the characteristics of the region for estimation of the variance of the original signal based on statistical approach is introduced by Verma et al. [11]. An improvement of the low-rank-based image denoising method using an adaptive boosting technique is proposed by Fan et al. [12]. A perceptually motivated blind image denoising problem using a single model is proposed by Uddin et al. [13]. A structure tensor-based fractional order image denoising model is proposed by Han [14]. Wang et al. [15] proposed a fourth order PDE-based image denoising model exploiting the idea of non-convexity property of the diffusion function along with the hypersensitivity of the Laplace operator. Quan et al. [16] used complex valued convolutional neural networks for the recovery of images. Lan et al. [17] proposed an enhanced generative adversarial network (EGAN) for denoising of images.

In this paper, we have proposed the Caputo sense time fractionalized model recently introduced by [18] to denoise Gaussian noise corrupted images with different noise variance. The Caputo fractional derivative is defined as [19]

$${}^cD_0^\alpha(f(t)) = \begin{cases} \int_0^t \frac{f^n(y)}{(t-y)^{\alpha+1-n}} dy & ; n-1 < \alpha < n, n \in \mathbb{N} \\ f^n(t) & ; \alpha = n. \end{cases}$$

We have compared the denoising performance of the proposed method with the recently proposed methods [20–22] and [23] both qualitatively and quantitatively.

2 Statement of Problem

One of the greatest challenges in image denoising tasks has always been to find methods that can

- (a) Retain minute details in the denoised images
- (b) Give better denoised images
- (c) Easy to implement.

Motivated from these facts, we have Caputo sense time fractionalized the model introduced recently by Rui Du et al. [18]. The proposed model has been applied to denoise Gaussian noise corrupted images with different noise variances.

3 Formulation of Problem

The model reported in [18] is given by

$$\sigma \frac{\partial \phi}{\partial t}(X, t_n) = D \nabla^2 \phi + F(X, t_n) \quad (1)$$

where ϕ represents concentration, D represents diffusion coefficient, $\sigma = \frac{\Delta t^{1-\alpha}}{\Gamma(2-\alpha)}$, and $F(X, t_n)$ is given in Eq. (2)

$$F(X, t_n) = \frac{\sigma}{\Delta t} \sum_{m=1}^{n-1} [(n-m+1)^{1-\alpha} - (n-m)^{1-\alpha}] [\phi(X, t_m) - \phi(X, t_{m-1})] + g(X, t_n) \quad (2)$$

Assuming $\phi(X, t_n)$ and $g(X, t_n) \in C^n[a, b]$, we can write the time fractionalized model of (1) in Caputo sense as

$$\begin{aligned} & \frac{\partial^{\beta_2+1}(\phi(X, t))}{\partial^{\beta_2+1}t} \\ &= \begin{cases} \frac{1}{\Gamma(n-\beta_2)} \int_a^t \frac{1}{(t-s)^{\beta_2+1-n}} \frac{\partial^n}{\partial t^n} \left[\frac{1}{\sigma} D \nabla^2 \phi + \frac{1}{\Delta t} \sum_{m=1}^{n-1} [(n-m+1)^{1-\alpha} - (n-m)^{1-\alpha}] \right] \\ [\phi(X, t_m) - \phi(X, t_{m-1})] + \frac{1}{\Gamma(n-\beta_2)} \int_a^t \frac{1}{(t-s)^{\beta_2+1-n}} \frac{\partial^n}{\partial t^n} \frac{g(X, t_n)}{\sigma}; (n-1) < \beta_2 < n \\ \frac{\partial^{n+1}(\phi(X, t_n))}{\partial t^{n+1}}; \beta_2 = n \end{cases} \end{aligned} \quad (3)$$

$$\begin{aligned} & \frac{\partial^{\beta_2+1}(\phi(X, t))}{\partial^{\beta_2+1}t} \\ &= \begin{cases} \frac{1}{\Gamma(n-\beta_2)} \int_a^t \frac{1}{(t-s)^{\beta_2+1-n}} \left[\frac{-(1-\sigma)}{\sigma \Delta t} D \nabla^2 \phi (\phi(X, t_m) - \phi(X, t_{m-1})) \right] + \\ \frac{1}{\Gamma(n-\beta_2)} \int_a^t \frac{1}{(t-s)^{\beta_2+1-n}} \left(\frac{\partial^n \phi(X, t_m)}{\partial t^n} - \frac{\partial^n \phi(X, t_{m-1})}{\partial t^n} \right) \\ \left(\frac{1}{\sigma} D \nabla^2 \phi + \frac{1}{\Delta t} \sum_{m=1}^{n-1} [(n-m+1)^{1-\alpha} - (n-m)^{1-\alpha}] \right) + \\ \frac{1}{\Gamma(n-\beta_2)} \int_a^t \frac{1}{(t-s)^{\beta_2+1-n}} \left(\frac{1}{\sigma} \frac{\partial^n g(X, t_n)}{\partial t^n} - \frac{1}{\sigma^2} \frac{\partial^n \sigma}{\partial t^n} g(X, t_n) \right); (n-1) < \beta_2 < n \\ \frac{\partial^{n+1} \phi(X, t_n)}{\partial t^{n+1}}; \beta_2 = n \end{cases} \end{aligned} \quad (4)$$

where $\phi(X, t)$ is the noisy image and $g(X, t) = \log(\nabla \phi(X, t))$. $\nabla \phi(X, t)$ is the gradient of the noisy image and $m, n \in \mathbb{Z}$.

In this paper, we have used different values of α and β_2 in (4) and have reported the results in tables (1), (2) and (3), respectively.

4 Numerical Computations

The qualitative comparison of the denoising performance of the proposed method with the methods [20–22] and [23] is depicted in Fig. 1 corrupted by white Gaussian noise with variance of noise 0.3. In Fig. 1, the values of the parameters for the proposed method are $\alpha = 0.5$ and $\beta_2 = 0.2$, respectively. The quantitative evaluation of the proposed method with the above-mentioned methods has been done using PSNR(a,b) & SSIM(a,b). The PSNR(a,b) & SSIM(a,b) are given, respectively, as

$$\text{PSNR}(a, b) = 10 \log_{10} \left(\frac{(2^8 - 1)^2}{\text{MSE}(a, b)} \right).$$

$$\text{SSIM}(a, b) = \frac{(2\Omega_a \Omega_b + d_1)(2\epsilon_{a,b} + d_2)}{(\Omega_a^2 + \Omega_b^2 + d_1)(\epsilon_a^2 + \epsilon_b^2 + d_2)}.$$

$$\text{MSE}(a, b) = \frac{1}{kl} \sum_{i=0}^{k-1} \sum_{j=0}^{l-1} [a(i, j) - b(i, j)]^2.$$

a and b are the original and noisy images, respectively, Ω_a and Ω_b are the mean values of orginal and noisy images, d_1 and d_2 are constants, ϵ_a^2 and ϵ_b^2 are, respectively, the variances of original and noisy images, and $\epsilon_{a,b}$ is the co-variance. Size of the image is represented by $k \times l$.

5 Results and Discussions

We have performed all the experiments in MATLAB. For all the experiments, we have taken the value of D of the order 10^{-6} in (3). The value of D is calculated as indicated by the method in [18]. We have performed the experiments by taking $\alpha = 0.2$, $\beta_2 = 0.6$, $\alpha = 0.3$, $\beta_2 = 0.7$ & $\alpha = 0.4$, $\beta_2 = 0.8$, respectively (left to right in the proposed method column of Tables 1, 2 and 3, respectively). Tables 1, 2, and 3 illustrate the comparison of SSIM and PSNR values among different methods. Figure 1 is the visual depiction of denoising performance of different methods with noise variance 0.3.

From Tables 1, 2, and 3, it is evident that the methods reported in [22] and [21] show comparable, and the methods reported in [20] and [23] show inferior performances, respectively, in terms of PSNR and SSIM values in comparison to the proposed method for the entire noise range.

It is clearly evident that the proposed method outperforms all the reported methods of [20–23] for the values of $\alpha = 0.2$, $\beta_2 = 0.6$, $\alpha = 0.3$, $\beta_2 = 0.7$ & $\alpha = 0.4$, $\beta_2 = 0.8$ in terms of both SSIM and PSNR values, respectively. Experimentally, we found that the SSIM and PSNR values fall rapidly with constant value of α and increasing value of β_2 with increasing noise variance. We also found that the PSNR and SSIM



Fig. 1 Denoised images from **a** original Barbara image, **b** adaptive TV^p regularization, **c** Bayesian deep matrix factorization, **d** detail retaining convolutional neural network, **e** non-subsampled contourlet transform, **f** proposed method

Table 1 PSNR(SSIM) values comparison among different methods for Barbara image

Noise variance	Adaptive TV^p regularization	Bayesian deep matrix factorization	Detail retaining CNN	Non-subsampled contourlet transform based CNN	Proposed method		
0.1	35.28 (0.85)	37.14 (0.75)	48.01 (0.94)	48.58 (0.96)	49.76 (0.978)	49.81(0.981)	49.92(0.983)
0.5	32.57 (0.77)	35.24 (0.61)	47.89 (0.91)	46.31(0.94)	49.51 (0.964)	49.38 (0.963)	49.23 (0.961)
1.0	31.77 (0.66)	31.56(0.34)	47.41 (0.89)	46.67 (0.92)	48.11(0.952)	48.26 (0.958)	48.09 (0.951)
1.05	29.96 (0.58)	28.19 (0.23)	46.27 (0.87)	46.53 (0.90)	48.01 (0.948)	48.15 (0.946)	48.12 (0.941)
1.1	29.65 (0.49)	28.79 (0.19)	45.98 (0.86)	45.43(0.88)	47.98 (0.939)	47.96 (0.938)	47.98 (0.936)
1.2	23.45 (0.40)	25.68 (0.17)	45.46 (0.84)	44.19(0.87)	47.08 (0.928)	47.06 (0.929)	47.15 (0.925)
1.5	21.48 (0.31)	23.54 (0.11)	43.77 (0.81)	43.86 (0.85)	46.48 (0.917)	46.54 (0.916)	46.31 (0.914)

values of the proposed method show good results with the constant value of β_2 and varying value of α for increasing noise variance. From Tables 1,2, and 3, we find that the SSIM and PSNR values show mixed trend of rise and fall with gradual increase of α and β_2 values with increased noise variance. We also found that for all the possible increasing decreasing combinations of α and β_2 , the proposed method outperforms aforesaid methods of literature.

6 Conclusion and Future Direction

In this paper, we have proposed the Caputo sense time fractionalized variant of lattice Boltzmann model for time sub-diffusion equation in Caputo sense proposed by Du et al. [18], and we applied it to denoise images, corrupted by additive white Gaussian noise with different noise variances. We found that the proposed method outperforms the recently reported methods of [20–23] in respect of both SSIM and PSNR values for different combinations of α & β_2 . In future, we shall try to study the effects of space fractional model of time fractional lattice Boltzmann model in image denoising.

Table 2 PSNR(SSIM) Values comparison among different methods for Lena image

Noise variance	Adaptive TV^p Regularization	Bayesian deep matrix factorization	Detail retaining CNN	Non-subsampled contourlet transform based CNN	Proposed method		
0.1	34.08 (0.83)	38.11 (0.78)	45.56 (0.97)	46.18 (0.95)	49.76 (0.978)	49.81(0.981)	49.92(0.983)
0.5	32.77 (0.78)	36.23 (0.63)	44.86 (0.92)	46.01(0.93)	50.66 (0.965)	50.28 (0.965)	50.15 (0.976)
1.0	30.12 (0.69)	32.45(0.39)	43.14 (0.87)	45.67 (0.91)	49.12(0.963)	49.28 (0.967)	49.09 (0.962)
1.05	29.01 (0.55)	30.48 (0.21)	42.77 (0.86)	45.35 (0.90)	48.86 (0.957)	48.75 (0.955)	48.68 (0.951)
1.1	28.54 (0.48)	29.09 (0.17)	41.33 (0.88)	45.29(0.87)	47.92 (0.941)	47.90 (0.943)	47.95 (0.945)
1.2	25.55 (0.42)	25.68 (0.15)	40.26 (0.82)	44.39(0.83)	47.01 (0.925)	47.03 (0.929)	47.09 (0.928)
1.5	22.98 (0.27)	24.24 (0.12)	40.11 (0.80)	43.65 (0.81)	46.18 (0.919)	46.24 (0.917)	46.29 (0.915)

Table 3 PSNR(SSIM) Values Comparison Among Different Methods for Boat Image

Noise variance	Adaptive TV^p regularization	Bayesian deep matrix factorization	Detail retaining CNN	Non-subsampled contourlet transform based CNN	Proposed method		
0.1	36.61 (0.89)	38.11 (0.78)	47.56 (0.93)	48.58 (0.96)	49.76 (0.978)	49.81(0.981)	49.92(0.983)
0.5	32.46 (0.75)	36.21 (0.68)	47.32 (0.92)	47.69(0.97)	52.53 (0.966)	52.58 (0.965)	52.37 (0.962)
1.0	31.17 (0.69)	32.64(0.36)	47.11 (0.88)	47.14 (0.90)	49.19(0.958)	49.66 (0.954)	49.78 (0.957)
1.05	29.98 (0.60)	29.15 (0.25)	47.02 (0.88)	47.31 (0.89)	49.14 (0.946)	49.75 (0.948)	49.60 (0.947)
1.1	29.35 (0.50)	29.04 (0.21)	46.84 (0.84)	46.18(0.87)	48.99 (0.944)	48.93 (0.946)	48.91 (0.941)
1.2	27.15 (0.46)	26.64 (0.19)	46.26 (0.81)	45.21(0.86)	48.81 (0.940)	48.78 (0.949)	48.72 (0.943)
1.5	23.58 (0.33)	24.74 (0.15)	45.17 (0.80)	44.88 (0.82)	48.77 (0.935)	48.48 (0.937)	48.33 (0.939)

References

1. Chambolle A (2004) An algorithm for total variation minimization and applications. *J Math Imag Vis* 20(1):89–97
2. Rudin LI, Osher S, Fatemi E (1992) Nonlinear total variation based noise removal algorithms. *Phys D Nonlinear Phenom* 60(1–4):259–268
3. Buades A, Coll B, Morel JM (2005) A non-local algorithm for image denoising. *Comput Vis Pattern Recogn* 60–65
4. Dabov K, Foi A, Katkovnik V, Egiazarian K (2007) Image denoising by sparse 3D transform-domain collaborative filtering. *IEEE Trans. Image Process* 16(8):2080–2095
5. Mairal J, Bach F, Ponce J, Sapiro G, Zisserman A (2010) Non-local sparse models for image restoration. In: *IEEE international conference on computer vision*, pp 2272–2279
6. Zuo C, Jovanov L, Goossens B, Luong HQ, Philips W, Liu Y, Zhang M (2016) Image denoising using quadtree-based nonlocal means with locally adaptive principal component analysis. *IEEE Sig Process Lett* 23(4):434–438
7. Dong W, Shi G, Li X (2013) Nonlocal image restoration with bilateral variance estimation: a low-rank approach. *IEEE Trans Image Process* 22(2):700–711
8. Gu S, Zhang L, Zuo W, Feng X (2014) Weighted nuclear norm minimization with application to image denoising. *Comput Vis Pattern Recogn* 2862–2869
9. El Helou M, Süssstrunk S (2020) Learning blind universal Bayesian image denoising with Gaussian noise level. *IEEE Trans Image Process* 29:4885–4897
10. Tian CC, Xu Y, Zuo W (2020) Image denoising using deep CNN with batch renormalization. *Neural Netw* 121:461–473
11. Verma R, Pandey R (2020) Characterization of local regions for wavelet-based image denoising using a statistical approach. *Int J Wavelets Multiresolut Inf Process*
12. Fan L, Li X, Fan H, Zhang C (2019) An adaptive boosting procedure for low-rank based image denoising. *Sig Process* 164:110–124
13. Uddin AFMS, Chung T, Sung HB (2019) A perceptually inspired new blind image denoising method using L1 and perceptual loss. *IEEE Access* 7:90538–90549
14. Han H (2019) A tensor voting based fractional-order image denoising model and its numerical algorithm. *Appl Numer Math* 149:133–144
15. Wang X, Wa Z, Rui L, Ruoxi S (2019) The UDWT image denoising method based on the PDE model of a convexity-preserving diffusion function. *EURASIP J Image Video Process* 81
16. Quan Y, Chen Y, Shao Y, Xu TH, Ji Hui Y (2021) Image denoising using complex valued deep CNN. *Pattern Recogn* 111
17. Yan L, Zheng W, Wang FY, Gou C, Joint image to image translation with denoising using enhanced generative adversarial networks. *Sig Process Image Commun* 91 (201)
18. Du R, Sun D, Shi B, Chai Z (2019) Lattice Boltzmann model for time sub-diffusion equation in caputo sense. *Appl Math Comput* 358
19. Atangana A (2018) Fractional operators with constant and variable order with application to geo-hydrology. Academic Press
20. Pang ZF, Li Z, Hui, Luo S, Zeng T (2020) Image denoising based on the adaptive weighted TV^p regularization. *Sig Process* 167
21. Lyu Z, Zhang C, Min H (2020) A nonsubsampled countourlet transform based CNN for real image denoising. *Sig Process Image Commun* 82
22. Li X, Xiao J, Zhou Y, Ye Y, Lv N, Wang X, Wang S, Gao S (2020) Detail retaining convolutional neural network for image denoising. *J Vis Commun Image Represent*
23. Xu S, Chunxia Z, Jiangshe Z (2020) Bayesian deep matrix factorization network for multiple images denoising. *Neural Netw* 123

Distributed and Anonymous E-Voting Using Blockchain and Ring Signatures



Nishay Madhani, Vikrant Gajria, and Pratik Kanani

Abstract Digitization of bureaucratic processes has been a long suited method for the growth of a country. E-Voting (Electronic Voting) is a method of casting, tallying and verifying votes from citizens using electronic means. With the advent and boom of Blockchain and Distributed Computing, many methods to improve E-voting have come forward that allows us to assure the privacy of voters and security against voter fraud. In this paper, we analyze the different types of Blockchains and which ones would be suitable for these purposes. In the end, we propose a method using Blockchain and Linkable Ring-Signature that provides the privacy of voters in a large-scale election by deploying smart contracts for “rings” of registered voters and analyze its performance on consumer devices.

Keywords Blockchain · E-voting · Ring signatures

1 Introduction

Elections are an important part of every democracy, they maintain certain standards of democracy for the growth of the nation. Countries such as India, Estonia, and Namibia have used E-Voting to conduct their elections [1–3]. E-Voting can be conducted using a series of methods such as telephone networks and Fax. Slowly and steadily we have now come to a stage where many elections are being conducted using the Internet [4]. Many of the Electronic-Voting-Machines (EVMs) and systems used have been surveyed to have flaws [4], considerable media attention and given the importance of the issue. We require a much more stable as well transparent method for E-Voting.

Blockchain was introduced, with Bitcoin [5]. Thereafter, Bitcoin has been used primarily as a cryptocurrency. Ethereum is another such Blockchain with Ether as its cryptocurrency. However, unlike Bitcoin, Ethereum has focused a lot of its attention on building Decentralized Applications [6] with the help of Smart Contracts. Each application developed on Ethereum is backed by the Blockchain. Agora, [7] a Swiss Company in 2018 developed a Blockchain-based E-voting system for conducting

N. Madhani (✉) · V. Gajria · P. Kanani

Dwarkadas J. Sanghvi College of Engineering, Mumbai, Maharashtra 400056, India

a large proof-of-concept in Sierra Leone [8]. Voatz, an American company with a record dating back to 2015, has developed a Blockchain-based E-voting system for conducting elections in Denver and West Virginia [9].

Blockchain would make a great candidate for digitizing elections and move its responsibilities from fallible humans to trusted computer systems. The key features of Blockchain are:

1. **Decentralized**—Blockchain works on the notions of distributed computing where many computers need to work together to complete a task. Therefore, control of the ledger is distributed among multiple parties. This could be beneficial for E-Voting as the process would not be centrally dependent, which eliminates the concerns of trust and reliability for the system.
2. **Privacy**—Blockchain-dependent systems [5, 6] use many cryptographically backed functions to maintain user anonymity and therefore making it impossible to trace a vote back to its user.
3. **Integrity**—Ledgers stored centrally are vulnerable to attacks [10, 11], however, as Blockchain is decentralized it is almost impossible to change a transaction after it has been accepted.
4. **Accessibility**—A user does not require complex computing machinery to perform transactions and does so from anywhere without any form of restriction.

In this paper, we propose the design of a system using Blockchain and Ring signatures to enforce voter anonymity while mitigating problems such as double voting in an anonymous environment. We use Ring Signatures [12], a cryptographic method of signing messages when given a group of public keys ensuring that the message cannot be traced back to its issuer while maintaining the verification of the message arising from a group of keys.

The major contributions of our methodology are:

Scalability of ballots We divide ballots into several contracts called “Voting Contracts” which manage a small group of voters. We propose a size of 50–100 as shown in the results later. With this division, the task of managing voters is distributed and invulnerable to attacks such as Denial-of-Service attacks.

Offline verification and online anonymity Voter identity is verified offline using Aadhar card or any other nationally recognized unique identification. Later, the voter generates a key pair for membership in the ring which is submitted to the election authority, and a Blockchain wallet account for sending the vote. While the election authority only recognizes the public key required for membership, the Voting Contracts cannot identify which voter has cast a vote due to a different wallet key pair.

Double-voting protection Each Voting Contract checks new votes cast against all previously verified votes to check if the ring-signature sent in the new vote is already cast by the same ring member. This would anonymously link two votes without giving up the identity of the voter.

2 Required Features

Upon analysis of papers such as [3, 7, 13–15], we have enlisted the following as requirements for the election system:

1. **Trust of voters**—Democracy and elections are tightly intertwined and an unstable or untrustworthy system for elections will directly relate to the state of democracy. Therefore, it is necessary for there to be the trust of the voters within the system without which the vote and its result cannot be accepted.
2. **Anonymity**—Each voter must be assured privacy and anonymity in elections. No vote should be capable of being traced back to its voter, which would otherwise jeopardize the election and its results. An excellent example of this is Monero [16] a Blockchain technology that does very well in maintaining the anonymity of parties within a transaction.
3. **Verification of Identity**—No election can be conducted without the authentication of its voters. Verification of identity is vital for the prevention of unwarranted users from accessing the system and registering a vote by impersonating someone else.
4. **Cost-effective**—A computationally costly system for conducting Blockchain-based E-voting may not be affordable for elections with a large number of voters. Similarly, an economically costly system would not be attractive to governments of countries. Hence, keeping computational and operational costs at a minimum is crucial.
5. **Transparency**—An E-Voting system should be free of coercion. No single party or syndicate can use the system to manipulate democracy to its favor. To ensure this, results and votes should be public and verifiable by individual auditors, ensuring no transgressions in the process.
6. **Audit and Verification**—An E-Voting system will not be fool-proof if it does not account for verification of votes and is efficient in doing so. There should be substantial methods for security checks and audits.

3 Related Work

Ring Signature-Based Voting on Blockchain—[14] proposes a solution to solve voter-anonymity issues with the introduction of the Ring Signatures. The architecture proposed by the authors uses a private Blockchain to store the ring signatures acquired from the voters. Exonum [17] is the Blockchain of choice. Exonum is a framework specially designed for the implementation of private Blockchains and maintains all the key aspects of technology such as decentralization and integrity. However, the use of a private Blockchain limits the feasibility of this system to be used in public elections, this system might be suitable for smaller elections even though they propose this system may be viable in Russia.

One of the most crucial aspects of any voting system is the authorization of its voters, the proposed solution does not contain methodologies where identification of users can be done without negating their privacy.

Asset Tokenization is the method used in designing the architecture for registering votes during the voting phase. Each voter is given a token which is spent when the voter casts his ballot. The famous double-spending problem where one token is spent twice is eliminated through this process as each voter is given only one token. However, to give the user a token, the issuing party must know the identity of the voter. This is problematic for an anonymous environment.

A Novel P2P-based System with Blockchain—[18] for secured voting scheme introduces a system that bridges the gap between voters and the system backed by distributed ledger mechanisms. The authors used Blockchain technology as the backbone which provides the trustless Electronic Voting Machine—an EVM without the intervention of a third party.

The architecture proposed has two interfaces and two servers. One of the two interfaces is used by the voter to interact with the system, while the other is used by the admin to maintain control over the election process. An Arbitration Server and an Authentication Server are used by the system, the former is used as an intermediary between the Ethereum and the user and registers the user's vote on the Blockchain, while the latter is mainly for authentication purposes and facilitates the Aadhar authentication of the user. The system also accounts for unregistered votes or votes where the user selects NOTA (None of the above) both of which are good inclusions and cordial to election situations.

Although this paper proposes a system that ensures the security of votes and its integrity, it cannot assure the anonymity of its voters. If each of the voters is to be authorized by a centralized server, this system could be vulnerable to attacks like Denial-of-Service (DOS). All users are to identify themselves with an Aadhar number and the paper does not specify remedies where this cannot be traced to a vote, disregarding voter anonymity.

Chainintegrity: Blockchain-enabled large-scale e-voting system with robustness and universal verifiability—[19] analyzed the different prerequisites of a Blockchain E-Voting solution. The authors found that current solutions do not meet or violate one or more of the conditions surveyed and thereafter proposed a solution to meet the same requirements.

The system proposed in this paper used Blockchain with smart contracts, digital signature using Blind Signature, Homomorphic encryption using Pallier Threshold Encryption, Counting Bloom filter, and Merkel hash tree.

Blind Signatures were introduced in [20] by Chaum, in this algorithm the signer and the author of the message are different, the payload is blinded before it is sent and can be verified by checking against the unblinded message. Threshold Encryptions are suited for distributed systems as the private key is divided, requiring a minimum number of components of the key for use. Counting Bloom filter and Merkel Hash tree are both used for providing the digital signature with an added advantage over cryptographical attacks.

As the paper suggests, the feasibility of such a solution and integration into more advanced and new methods of voting such as Quadratic Voting [21], statement voting [22] requires additional examination.

Agora—[7] proposed an end-to-end verifiable solution for free and fair E-Voting solution which meets the following requirements: transparency, privacy, integrity, affordability, accessibility. Their architecture is custom-built and multilayered. Bulletin Board, a distributed Blockchain ledger derived from the Skipchain Architecture [23]. Agora stores all their transactions on the Bitcoin Blockchain. Contena is a tamper-resistant logging system based on the Catena schema which links the Bulletin Board with the Bitcoin Blockchain. Agora has a mesh of trustless nodes that validate blocks on the Bulletin Board called the Valeda Network. VOTAPP is the final layer, it interfaces with the voter providing them with a Voting Booth, Audit, and a full Node.

Agora has six distinct steps in its voting process:

1. **Configuration**—Creation of election by an authority.
2. **Casting**—Voters cast their votes on Agora's Blockchain.
3. **Anonymization**—All votes are anonymized to secure the privacy of voters.
4. **Decryption**—Anonymized votes are decrypted for later use.
5. **Tallying**—Counting of votes.
6. **Auditing**—Votes are audited before the results are announced.

Agora has proved to be a resilient solution for E-Voting with its proof-of-concept elections held in Sierra Leone in March 2018. Representatives of Agora had manually registered the votes on their network and therefore, proved to be an optimal solution for E-Voting. However, they still have security and legal issues, and the cost of Election heavily depends on voter turnout and the total number of voters.

In [24], a solution is provided using the Bitcoin Blockchain first introduced by Satoshi Nakamoto in [5]. This solution leverages the OP-RETURN field in Bitcoin transactions to store and validate the Ring signatures of voters.

When casting their ballot, each voter signs the candidate's unique identifier using the ring signature algorithm. This message is sent in the OP-RETURN field of the Bitcoin transaction. For tallying the results all such transactions can be retrieved from the ledger and verified. The proposed method, however, does not account for the added cost involved while signing each transaction and does not prove to be scalable due to the mining and verifying time of each block on the Bitcoin Network [5].

In [15], a system is proposed that combines Aadhar data and decentralized Blockchain to provide an integrated solution. The system verifies the user's identity using Aadhar Number, collects the vote, encrypts it, and stores it in a centralized database Oracle for later use and tallying. They have taken a hardware-integrated approach to the solution and provided fingerprint recognition and the voting booth using Arduino [25]. The centralized database as used in this paper, Oracle 9i is vulnerable to SQL injection [26], authentication bypass [27], XSS [28], and database tampering [29]. This seriously threatens the security of the votes and consequently the entire election.

4 Technologies

In [30], a thorough review is conducted into the various types of Blockchain Technology and its applications. For our application which uses Blockchain and ring signature as backbones for E-Voting systems, we have evaluated the feasibility of different Blockchains, and the numerous consensus algorithms supported by it.

4.1 *Types of Blockchain*

Bitcoin—In [5], Nakamoto introduced the first cryptocurrency using the Proof-of-Work algorithm and a Blockchain as a decentralized ledger. It is a permissionless public Blockchain divided into two networks, the Bitcoin Network, and the testnet. The testnet is a test chain created and its coin does not hold any value. Bitcoin includes a Forth-like scripting language called Script for transactions. Using Script we can restrict access of coins to only its owner. It is a list of transactions limiting access to the coin and can be used for performing or programming applications on the network.

Ethereum—The cryptocurrency created by Vitalik Buterin is only behind Bitcoin in terms of market capitalization. Ethereum, akin to Bitcoin, is permissionless and works on the Proof-of-Work consensus algorithm. Ethereum boosted the popularity of creating decentralized applications using Smart Contracts. A Smart Contract is a high-level program code written in many languages that are converted to bytecode specially designed to run on peers in a Blockchain network using the Ethereum Virtual Machine. Smart Contracts are supported in Solidity (C-like), Vyper (Python-like), Serpent, LLL (Low-level Lisp-like Language), and Mutan. Ethereum lacks fast verifiability as its transaction speed per second is only 25.

Quorum—Quorum is Ethereum-fork created by JP Morgan & Chase, currently acquired by ConsenSys [31]. While Ethereum is a public and permissionless Blockchain, Quorum is designed for permissioned and private Blockchain networks. RAFT and IBFT are used as consensus algorithms. RAFT is used for crash fault tolerance and IBFT used for Byzantine Fault Tolerance. Quorum is built with privacy in mind by dividing the ledger into two chains public and private. Private Ledger can only be seen by the transacting parties while the public is open for all.

Exonum—Exonum is an open-source, end-to-end Blockchain implemented in the Rust programming language. Exonum was built to aid developers in building a private Blockchain. Exonum can be used for domains such as finance, legal, and government applications, and supports transactions speeds up to 5000/s. Rust as a programming language limits the developers available for Exonum, due to this the maintainers introduced Java-bindings to make the tools more friendly toward developers and enterprises.

Hyperledger Fabric—part of the Hyperledger project which is an open-source effort aimed to create a decentralized enterprise ledger codebase. The protocol defined by Hyperledger fabric is commanded by two kinds of peers—validating and non-validating. A validating peer is a consensus node responsible for maintaining and validating transactions, a non-validating node acts as a proxy to connect to clients.

4.2 Consensus Algorithms

PoW—Proof-of-Work algorithm is used by both Ethereum and Blockchain. In this consensus algorithm, each node on the network can introduce a new chain with an added block and this chain then needs to be verified by corresponding nodes on the network. A block is said to be verified if it has 6 new blocks are added. Miners are nodes in the network who introduce new blocks, each block is a combination of multiple transactions. For a block to be mined its hash needs to meet certain criteria this is like solving a puzzle for the miner, once solved the miner is awarded a transaction fee for its efforts. Proof-of-Work is a very energy consuming algorithm requiring powerful Graphics Processing Units (GPUs) for competing in the mining competition, hence it has many legal implications that must be taken into consideration.

PoS—Given the limitations of PoW such as inequality where modern and powerful machines dominate mining, Proof-of-Stake was first introduced on the Bitcoin forum in 2011. It is a hybrid PoW and stake-based consensus aimed to be more judicious. Each node is appointed a stake which quantifies the trust that the network has in the node. Using this stake, we can decide which node will be allowed to mine the chain. This gives PoS an advantage over fraudulent actions as more than 50% of the stake in the network would be required to perform a double-spending attack.

4.3 Ring Signature

Ring signatures were introduced in [12], there have been subsequent developments to this method [32–34]. We define a vote as the tuple (C_i, s) where C_i is the candidate ID, and s is the linkable ring signature generated for that ID. A wallet application is a set-up to ease the entire voting process for voters, from registration to key pair generation, Blockchain account generation, and casting the vote. The first step in voting is retrieving a list of approved candidates C with their respective unique identifiers. Next, the wallet application retrieves the ring that the user belongs to through the EMC. This returns the address to the VC that the user must use for casting an anonymous vote. This list of public keys is used for generating the ring signature for the vote. A voter can only cast their vote to the VC allotted to them. In this paper, we have used the algorithm proposed in [35].

5 Proposed Methodology

The Election is divided into 5 distinct phases—**Candidate Registration Phase, Voter Registration Phase, Voter Sampling Phase, Voting Phase, and Tallying Phase**. Voter Registration Phase is a centralized process due to the sheer number of potential voters in a country. Alternate implementations can strive for decentralized methods of storing millions and potentially billions of public key addresses on a distributed network. However, in this paper, we focus more on voter anonymity and decentralized voting rather than the storage of high volumes of data on a Blockchain.

We define an account on Blockchain as a cryptographic key pair of public and private key (P_u, P_r) for signing transactions done on the Blockchain. The following assumptions are made:

1. A Registration Authority (RA) has an account on the Blockchain
2. Each candidate has an account on the Blockchain for registration
3. Each voter has an account on the Blockchain for sending their vote
4. Each voter has generated another key pair (P_u, P_r) for signing the linkable ring signature
5. This generated key pair is in no way linked to the voter's account on the Blockchain

5.1 Candidate Registration Phase

A Candidate Registration Contract (CRC) is deployed as an intermediary between the RA and the candidate who wishes to register. The CRC may set-up a registration fee for all candidates to eliminate spam registrations. The RA can be notified of any new registrations. Initially, the registration is not approved. Once the candidate verifies their identity with the RA, the RA can approve the candidate using the smart contract's available functions. Storage is set-up for candidate details in the CRC. Every candidate is given a unique identifier C_i where $C_i = \{0, 1\}^+$. This restriction makes ring signatures easy to generate, as the message to be signed should be a string of 1s and 0s only (Figs. 1 and 2).

5.2 Voter Registration Phase

A potential voter approaches the RA with the relevant documents. In the case of an Aadhar Card, the voter may use SMS OTP or biometric verification for identification. Additional data of the voter's public address on the Blockchain network needs to be stored by the RA. Once verified, the voter uses a wallet application to generate another key-pair for interacting with the Blockchain.

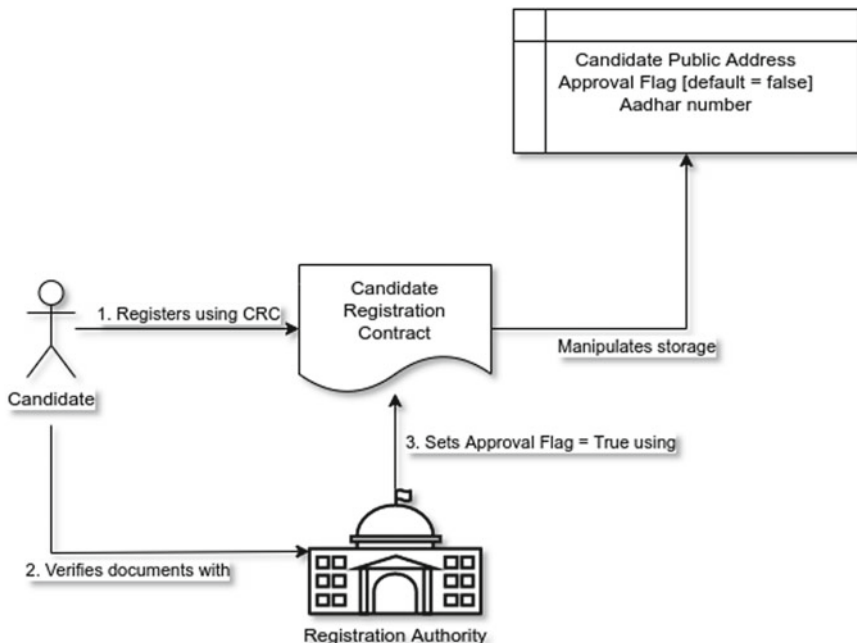


Fig. 1 Candidate registration process

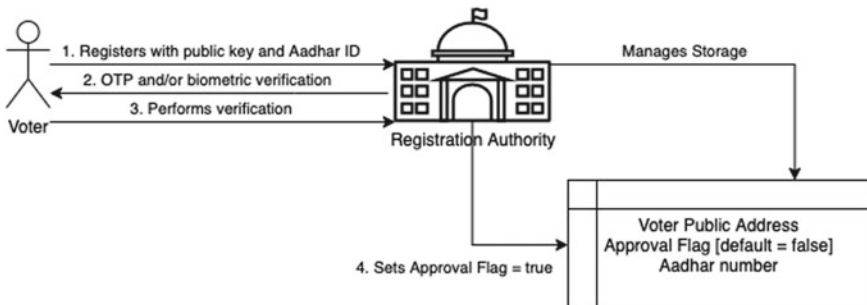


Fig. 2 Voter registration process

Next, the user's wallet/application generates a keypair (P_u, P_r) on elliptical curve altbn128 . The ECC public key P_u for generating linkable ring signatures in the ring and must be submitted to the RA for ring formation. This account on the Blockchain is used only for sending the vote to the Voting Contract by signing the transaction. The message to be sent is signed with the ECC key-pair (P_u, P_r) (Fig. 3).

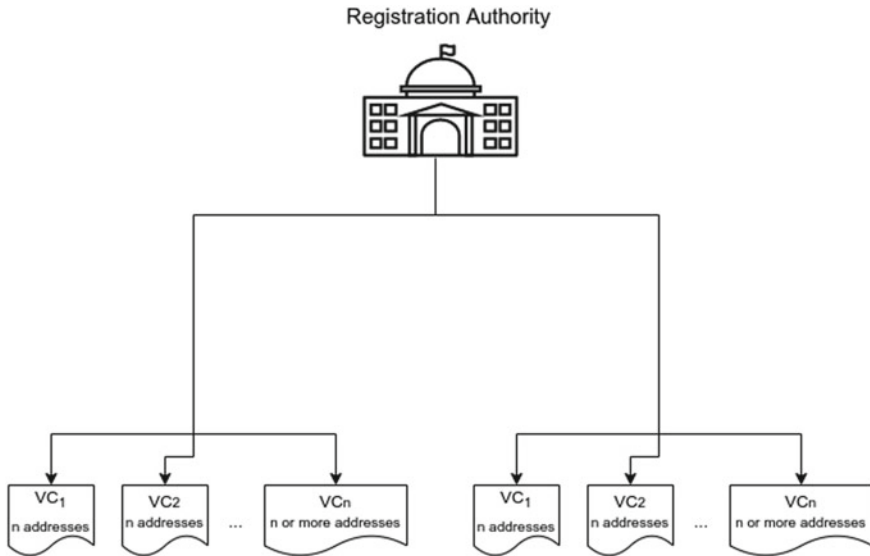


Fig. 3 RA sampling voters into voting contracts

5.3 Voter Sampling

Ring signature performance is linearly dependent on the number of participants and size of the messages (demonstrated in Implementation and Results section). Therefore, any proposed solutions should be implemented considering this limitation. We use a sampling algorithm for distributing voters into aptly sized rings. Each ring can be no smaller than a specified size. A sample algorithm is provided below, which distributes the voters to random rings:

Algorithm 1 Sampling (*voters, min_size*)

```

rings =  $\emptyset$ 
while voters.length  $\geq$  min_size do
    r = remove min_size of voters
    add r to rings
end while
for each voter in voters do
    r = random ring from rings
    add voter to r
end for
return rings
  
```

5.4 Voting Phase

The voter is provided with the candidate list C , and the public address of their ring's Voting Contract (VC). The VC provides the voter with a list of public addresses in their ring. The voter first checks if their generated public address P_u exists in the VC's voter list. If the list does not contain their public address, the VC will reject their vote automatically in the verification process. This ensures that each voter sends votes to the sanctioned VC for tallying and verification, hence combating vote manipulation (Fig. 4).

To vote for a candidate with ID C_i , the voter signs a message m containing the C_i using Linkable Ring Signature LSAG scheme with the list of public addresses in their ring. The voter then sends a message m and the signature s to the VC. If the candidate does not exist in the list, or the signature was invalid, the vote is rejected automatically. Otherwise, the VC adds this vote to its internal tally. Additionally, a list of cast votes is stored for preventing double-voting by a public key. New signatures can be tested against previously cast votes to verify if a generated key pair (P_u, P_r) is being misused for vote manipulation.

The VC can verify and compare ring signatures to detect vote manipulation. Since linkable ring signatures can only link two signatures together, it is impossible to find the culprit in the ring. Instead, votes linked together can be rejected together. The verification process commences immediately after a vote is cast. The algorithm for vote casting function is given below:

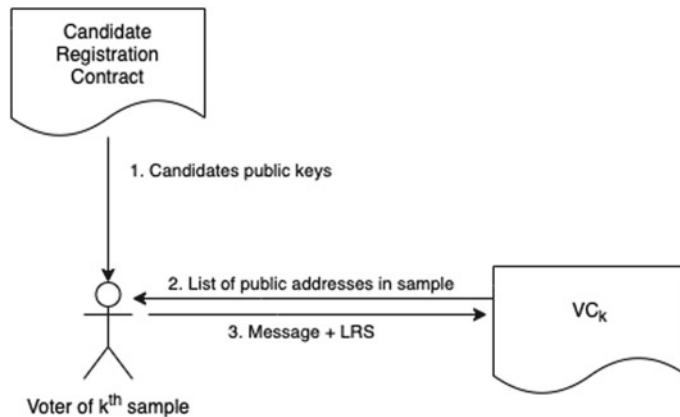


Fig. 4 Voting process

Algorithm 2 VoteCast (*candidate_id*, *s*, *ring*, *cast_votes*)

```

if signature is invalid then
    return
end if
for each vote in cast_votes do
    if vote.signature and signature are signed by same signer then
        return
    end if
end for
add (candidate_id, s) to cast_votes

```

5.5 Tallying Phase

The final phase after all votes are cast is the tallying phase. Here, the manual workload is reduced. The VCs can keep track of the votes per candidate after each vote is cast. Double voting is prevented with verification of ring signatures of new votes with ring signatures of previously verified votes. The only task left is to collect the internal counts of all VCs and add them up. This can be performed in a distributed or centralized manner with the help of a master contract used by the highest authorities. The master contract is used for setting up ballots, as well as deploying and keeping track of potentially millions of VCs. Unlike EVMs which can be easily manipulated or even stolen, VCs are much more feasible, safer, and transparent. The source code of all the contracts proposed thus far can be open-sourced for additional scrutiny.

6 Results

For simulating the above solution we used eth-tester python library available at <https://github.com/ethereum/eth-tester> for prototyping. We generated rings of sizes 10–500 at steps of 10 and benchmarked the time required to sign a Candidate's ID C_i as a message using a linkable ring-signature algorithm. The benchmark test was performed on a Macbook Air 2017 with Intel i5 5th generation processor, hence the performance measure gives a generalized view for the various devices owned by voters (Fig. 5).

It can be deduced that the time required to sign a signature is linearly proportional to the size of the ring. As we increase the size of the ring, the privacy of the voter would get more secure. However, it'll be as expensive to verify the ring signature in a smart contract as each signature has to be checked against all candidate IDs stored in the contract. Hence, we recommend a ring small enough for performance and large enough for maintaining anonymity. We can define an arbitrary size range as between 30 and 100 (Fig. 6).

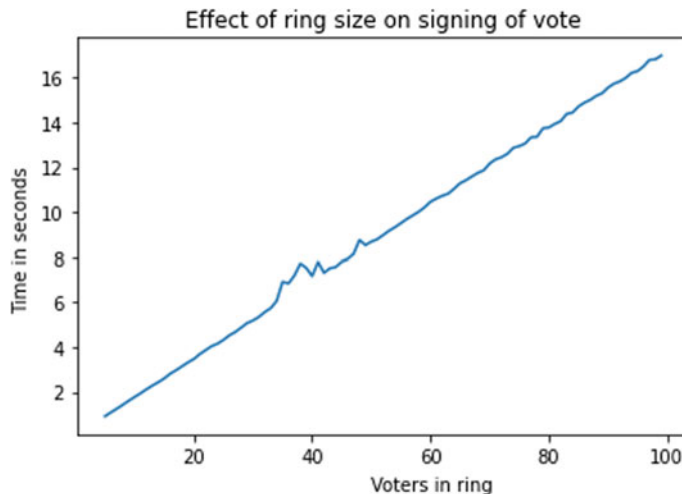


Fig. 5 Benchmark of time to sign a linkable ring-signature to ring size

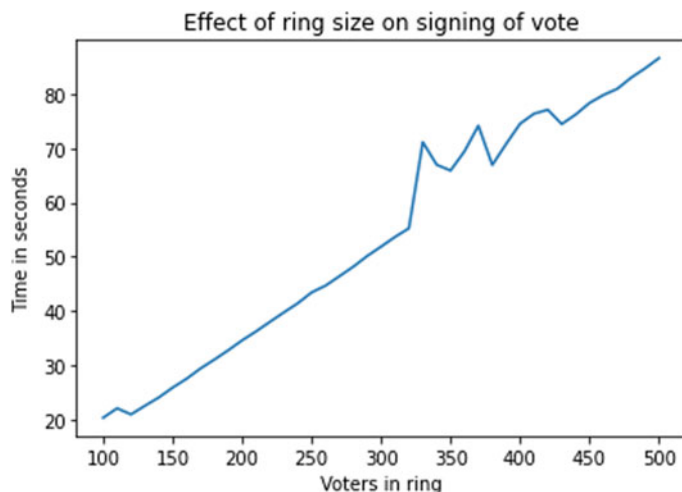


Fig. 6 Benchmark of time to sign a linkable ring-signature to larger ring sizes

Similarly, we benchmarked the time required to verify a ring signature for a single candidate ID as a function of the size of the ring as shown in Fig. 7. We extrapolate a linear relation analogous to the function of signing time to the size of the ring.

With a sampling of voters into appropriately sized rings, we introduced a divide-and-conquer method to ensure that smart contracts aren't faced with long transaction and vote verification times, a problem which was faced by Russia in June 2020. Voters can vote offline at voting booths as well as online from their homes using our

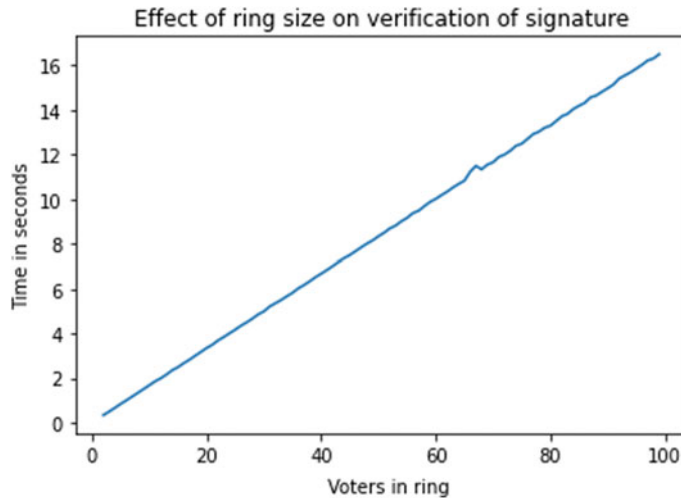


Fig. 7 Benchmark of time to verify a linkable ring-signature to ring size

proposed architecture—a sure advantage in the trying times of a pandemic like that of COVID-19.

A public network like Ethereum MainNet would have more miners, improving the veracity of blocks in the network. However, this would increase the cost of deploying smart contracts and casting votes, making the overall process expensive for the voters as they need to pay a standard transaction fee to interact with a smart contract. Another option is to deploy a private network using Ethereum node implementations like Geth. This would allow for eliminating the transaction costs, however, the network would need a sufficient number of miners to prevent attacks like the 51% attack for manipulating the elections. The discussion is still open as this paper describes the methodology and algorithms required for setting up a scalable e-voting system. From the Blockchain networks that we reviewed, Exonum seems to be suitable for such government applications due to its high transaction rate [17]. However, the choice of network is still an open question for developers to choose as per their financial capability and that of their voters.

7 Conclusion

Blockchain Technology moving forward is likely to be merged with various other Technologies. For our proposed methodology, authentication of Voters is done offline and an online solution with the help of Zero-Knowledge Proofs could be ventured. Furthermore, Big Data and its applications are reviewed in [36] and could prove to be an efficient solution for maintaining voter privacy and the integrity of votes.

A question may arise about the veracity of verifiers of the tally. If a public Blockchain is used, individual auditors can be allowed to retrieve the votes stored in a Voting Contract (VC) either free of cost or by paying a nominal fee. This would allow for more transparency as the individual auditors won't be able to identify the voter, eliminating the role of Returning Officer (RO) in Indian elections. Such a system would save hours or potentially days of manual work done by the Election Commission of India, as well as eliminate the problems of trust put into the vote tallying process and miscounting of votes. The stakeholders who are worried about the future of politics in the country can perform verification of votes stored in Voting Contracts in their district in a decentralized manner.

Thus, we reviewed different Blockchain technologies and networks in this paper. Later, we presented a Blockchain-based solution that tackles the problem of scalability in decentralized applications and that of trust in conventional systems including online and mail-in voting. Through trust-less mechanisms, it is possible to ameliorate the general mistrust in online e-voting solutions and hence supplement the number of potential voters. What started as a surrogate economy, can soon be the backbone of democracies of the future.

References

1. Mpeko N, van Greunen D (2017) E-voting experiences: A case of namibia and estonia. In: 2017 IST-Africa week conference (IST-Africa), pp 1–8
2. Schryen G, Rich E (2009) Security in large-scale internet elections: a retrospective analysis of elections in estonia, the netherlands, and switzerland. IEEE Trans Inf Forens Secur 4(4):729–744
3. Singh VP, Pasupuleti H, Babu NSC (2017) Analysis of internet voting in india. In: 2017 international conference on innovations in information, embedded and communication systems (ICIECS), pp 1–6
4. Gibson JP, Krimmer R, Teague V, Pomares J (2016) A review of e-voting: the past, present and future. Ann Telecommun 71(7):279–286. <https://doi.org/10.1007/s12243-016-0525-8>
5. Nakamoto S (2009) Bitcoin: a peer-to-peer electronic cash system. Cryptography Mailing list at <https://metzdowd.com>
6. Wood G et al (2014) Ethereum: a secure decentralised generalised transaction ledger. Ethereum project yellow paper 151(2014):1–32
7. Agora_whitepaper.pdf. <https://www.agora.vote/resources>. Accessed on 08/21/2020
8. Sierra leone just held the world's first blockchain-powered election. <https://futurism.com/sierra-leone-worlds-first-blockchain-powered-election>. Accessed on 08/21/2020
9. Denver and west virginia deserve praise for voting on blockchain | fortune. <https://fortune.com/2019/03/23/blockchain-vote-election-denver-west-virginia-votz/>. Accessed on 08/21/2020
10. Apnewsbreak: Georgia election server wiped after suit filed. <https://apnews.com/877ee1015f1c43f1965f63538b035d3f>. Accessed on 08/21/2020
11. North Carolina election fraud: board orders new nc-9 house election - vox. <https://www.vox.com/policy-and-politics/2019/2/21/18231981/north-carolina-election-fraud-new-nc-9-election>. Accessed on 08/21/2020
12. Rivest RL, Shamir A, Tauman Y (2001) How to leak a secret. In: Boyd C (ed) Advances in cryptology–ASIACRYPT 2001. Springer, Berlin Heidelberg, Berlin, Heidelberg, pp 552–565

13. Hjálmarsson F, Hreiarsson GK, Hamdaqa M, Hjálmtýsson G (2018) Blockchain-based e-voting system. In: 2018 IEEE 11th international conference on cloud computing (CLOUD), pp 983–986
14. Kugusheva A, Yanovich Y (2019) Ring signature-based voting on blockchain. In: Proceedings of the 2019 2nd international conference on blockchain technology and applications, pp 70–75
15. Patil S, Bansal A, Raina U, Pujari V, Kumar R (2018) E-smart voting system with secure data identification using cryptography. In: 2018 3rd international conference for convergence in technology (I2CT), pp 1–4
16. Whitepaper.pdf. <https://cryptonote.org/whitepaper.pdf>. Accessed on 08/24/2020
17. Yanovich Y, Ivashchenko I, Ostrovsky A, Shevchenko A, Sidorov A (2018) Exonum: byzantine fault tolerant protocol for blockchains. bitfury.com, pp 1–36
18. Vijayalakshmi V, Vimal S (2019) A novel p2p based system with blockchain for secured voting scheme. In: 2019 fifth international conference on science technology engineering and mathematics (ICONSTEM), vol 1, pp 153–156
19. Zhang S, Wang L, Xiong H (2020) Chaintegrity: blockchain-enabled large-scale e-voting system with robustness and universal verifiability. Int J Inf Secur 19(3):323–341. <https://doi.org/10.1007/s10207-019-00465-8>
20. Chaum D (1983) Blind signatures for untraceable payments. In: Advances in cryptology. Springer, pp 199–203
21. Posner EA, Weyl EG (2015) Voting squared: quadratic voting in democratic politics. Vand L Rev 68:441
22. Zhang B, Zhou HS (2019) Statement voting. In: International conference on financial cryptography and data security. Springer, pp 667–685
23. Nikitin K, Kokoris-Kogias E, Jovanovic P, Gailly N, Gasser L, Khoffi I, Cappos J, Ford B (2017) {CHAINIAC}: proactive software-update transparency via collectively signed skipchains and verified builds. In: 26th {USENIX} security symposium ({USENIX} security 17), pp 1271–1287
24. Wu Y (2017) An e-voting system based on blockchain and ring signature. University of Birmingham, Master
25. Arduino SA (2015) Arduino. Arduino LLCs
26. Cve-cve-2006-1705. <https://cve.mitre.org/cgi-bin/cvename.cgi?name=CVE-2006-1705>. Accessed on 08/21/2020
27. Cve-2005-3641 : oracle databases running on windows xp with simple file sharing enabled, allows remote attackers to bypass authenticatio. <https://www.cvedetails.com/cve/CVE-2005-3641/>. Accessed on 08/21/2020
28. Cve-2006-6703: multiple cross-site scripting (xss) vulnerabilities in oracle portal 9i and 10g allow remote attackers to inject arbitra. <https://www.cvedetails.com/cve/CVE-2006-6703/>. Accessed on 08/21/2020
29. Cve-2006-0272 : unspecified vulnerability in the xml database component of oracle database server 9.2.0.7 and 10.1.0.4 has unspecified i. <https://www.cvedetails.com/cve/CVE-2006-0272/>. Accessed on 08/21/2020
30. Hakak S, Khan WZ, Gilkar GA, Assiri B, Alazab M, Bhattacharya S, Reddy GT (2020) Recent advances in blockchain technology: a survey on applications and challenges
31. Quoram whitepaper. <https://github.com/ConsenSys/quorum/blob/master/docs/Quorum>. Accessed on 08/21/2020
32. Fromknecht C (2016) One-time zero sum ring signature
33. Liu JK, Wei VK, Wong DS (2004) Linkable spontaneous anonymous group signature for ad hoc groups. In: Wang H, Pieprzyk J, Varadharajan V (eds) Information security and privacy. Springer, Berlin Heidelberg, Berlin, Heidelberg, pp 325–335
34. Maxwell G, Poelstra A (2015) Borromean ring signatures. Accessed: 8 Jun2019
35. Liu JK, Wei VK, Wong DS (2004) Linkable spontaneous anonymous group signature for ad hoc groups. In: Australasian conference on information security and privacy. Springer, pp325–335
36. Deepa N, Pham QV, Nguyen DC, Bhattacharya SBP, Gadekallu TR, Maddikunta PKR, Fang F, Pathirana PN (2020) A survey on blockchain for big data: approaches, opportunities, and future directions

Neuronal Unit of Thoughts (NUTs); A Probabilistic Formalism for Higher-Order Cognition



Nordin Zakaria

Abstract A probabilistic graphical model, *Neuronal Unit of Thoughts* (NUTs), is proposed in this paper that offers a formalism for the integration of lower-level cognitions. Nodes or neurons in NUTs represent sensory data or mental concepts or actions, and edges the causal relation between them. A node affects a change in the *Action Potential* (AP) of its child node, triggering a value change once the AP reaches a fuzzy threshold. Multiple NUTs may be crossed together producing a novel NUTs. The transition time in a NUTs, in response to a ‘surprise,’ is characterized, and the formalism is evaluated in the context of a non-trivial application: Autonomous Driving with imperfect sensors.

1 Introduction

Deep learning neural networks, riding upon the wide availability of high-end GPUs in recent years, have improved the state-of-the-art significantly in an array of high-profile applications, driving optimism in artificial intelligence to a new high, one with neural network (NN) at the forefront. However, while deep NNs have approached or surpassed human ability in several tasks, they are generally designed for very specific tasks that require low-level cognition.

The main concern in this paper is on the structural representation of higher order cognition. A relatively straightforward approach would be to layer a symbolic reasoning engine, for example, a fuzzy rule-based system, on top of low-level cognition. But the brain is connectionist, structurally graph-theoretic. The intriguing question that motivates this paper is of how a neural structure is capable of carrying the sort of computation that goes in the mind of an intelligent agent.

The language should be able to describe how we park a car, how a cat decides when to steal food over the kitchen counter, how a boxer decides to counter a punch, and so on. And noting that NN outcome for a given input may fluctuate—due to

N. Zakaria (✉)

High-Performance Cloud Computing Center, Universiti Teknologi PETRONAS,
Seri Iskandar, Malaysia

e-mail: nordinzakaria@utp.edu.my

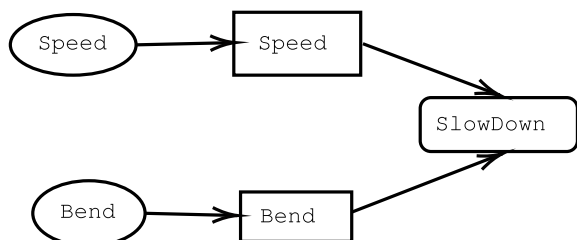
environmental noise, obstruction, viewing angle, etc., it should be able to do so in the face of complex, uncertain input stream. Further, the structure should be syntactically compositional—newer structures should be composable from existing structure through well-defined procedures, allowing for formation of new thoughts, a cognitive capability that we take almost for granted, given that we do it almost all the time, in dreams, in conscious thoughts, and in creative or imaginative thinking.

Previous work proposes largely architectural solutions to the problem, often involving hybridization of existing AI methods (see for example [1]). The solution I am proposing in this paper, *neuronal unit of thoughts* (NUTs), on the other hand, is a graph-oriented formalism for layering over primitive thoughts unit. It is essentially a probabilistic graphical model. The fact that it is probabilistic is consistent with the current view of a probabilistic brain [2–4]. Structurally, it is similar to a Bayesian network (BN), a node in a NUTs representing a variable and interconnecting edges implying causal effects between variables. However, a NUTs variable holds an activation potential (AP) that maps to fuzzy literals. Further, while a node in BN stores a probability table, containing the conditional probability of each possible variable value given its parents' values, in a NUTs,

To present the idea in a concrete setting, I develop and demonstrate NUTs in this paper for autonomous vehicle (AV), a fast-growing AI application area that has been benefiting substantially from deep learning and associated methods [5, 6]. Only highway autonomous driving with a limited set of tasks is considered in this paper; experimentation was done using a modified version of the open-source racing platform TORCS [7]. The main challenge is in dealing with a dynamic environment while moving at high speed [8]. Further, I assume that sensory failure is inevitable. The sensory unit may fail due to hardware or environmental issue, or inaccurate perception [9, 10], and the consequences potentially catastrophic [11].

Figure 1 offers a sneak preview of NUTs in AV context. When driving at high speed, what goes into the mind when approaching a bend, ‘Slow down,’ might be the generic advice for a new (especially teen) driver. The advice implicitly assumes that the current speed is high; further, it assumes recognition, visual presumably, of an approaching bend. Hence, the NUTs in Fig. 1 contain nodes pertaining to *speed* and *bend*. Oval shapes indicate sensory nodes, rectangle a mental concept, and rounded rectangle an action. Hence, as can be seen in the figure, sensory stimulus (*speed* and *bend* in oval nodes) affects an agent's belief about the world (rectangle

Fig. 1 Slow down when you see a bend



nodes). Agent's belief is captured as fuzzy literals, mapped probabilistically from its activation potentials.

A parent node $\text{par}(\eta)$ affects its child η through incremental change to the child's AP, $\hat{\eta}$. This can be expressed in the form of rules, that relates both nodes' literal values, $\text{par}(\eta)$ and $\bar{\eta}$, to an action. Examples are shown below for bend:

$$\overline{\text{Bend}} = \text{low}, \overline{\text{Bend}_D} = \text{high} \xrightarrow{1} ++ \quad (1)$$

$$\overline{\text{Bend}} = \text{high}, \overline{\text{Bend}_D} = \text{low} \xrightarrow{0.8} -- \quad (2)$$

$$\overline{\text{Bend}} = \text{low}, \overline{\text{Bend}_D} = \text{low} \xrightarrow{1} +- \quad (3)$$

The D subscript denotes a data (or sensory) node. $++$, $--$, and $+-$ are *actions* to the AP, $\widehat{\text{Bend}}$, of the subject node bend. $++$ is a small increment $\delta\widehat{\text{Bend}}$, $--$ a decrement $-\delta\widehat{\text{Bend}}$, and $+-$ no change. The parameter above the arrow specifies the probability of the action actually happening when the conditions are true. An action in NUTs hence happens probabilistically.

The NUTs in Fig. 1 may be thought of as a cognitive behavioral plan [8]. It is executed repeatedly in the 'mind' of a cognitive agent, responding reactively to environmental cues or affordances [12] through probabilistic changes in the AP. As in biological brain [13, 14], NUTs are meant to integrate information over time and over multiple channels, potentially allowing for more robustness in dealing with noise and ambiguous input. Nodes are updated incrementally, and multiple nodes may contribute to the AP of a node, possibly in a contradicting manner. Further, since the formalism is graph-theoretic, new NUTs, that is new thoughts, can be derived through simple graph-based operations as will be further elaborated later.

Given the reference to the 'mind,' is NUTs really biologically realistic? While it is not strictly important in the context of building intelligent system [15], I seek a solution that can be mapped in some way, at least at an abstract level, to biological reality. The brain is neuronal, essentially graph-theoretic, so is NUTs. The set of rules in each node, though symbolic, is akin to the activation function in the neuron of an NN, performing computation on the input vector to produce an output scalar (the AP). A stronger point to note is that NUTs advocate a probabilistic view of the brain's inner working, in line with the current dominant view in neuroscience. And there are benefits from the level of biological realism adopted; NUTs naturally encodes surprise [2], as will be shown later, in the context of AV, and it allows for robustness in dealing with noise and uncertainty in the world.

The rest of this paper is organized as follows. The next section covers literature of relevance to NUTs. A more detailed description of NUTs follows. Evaluation of NUTs in an AV context is then presented, following which the paper is concluded.

2 Relevant Work

NUTs deal with thoughts, a higher mental process through which we manipulate and analyze acquired or existing information. Low-level cognition here refers to cognitive capability that are local and automatic, while higher-level cognition are the executive functions [16]. One can think of NUTs as a cognitive formalism, a representation that can describe a cognitive system and its processes. A large part of current effort on computing higher-level cognition focuses on architectural designs. There are efforts as well that focuses on knowledge representation.

2.1 Architectural Solutions

Given the requirements and the complexity of the real world, numerous architectures have been proposed over the past 40 years or so [17] for higher-level cognition. Classical AI approach involves mediated perception [18]—building a world model based on sensor input and then performing symbolic reasoning based on that model in order to arrive at an action.

More reactive systems, often insect-inspired [19] and involving direct perception [20], include the subsumption architecture [21]. The control architecture is partitioned into layers of abstraction. Modules are grouped into layers of competence, with that in a higher lever capable of overriding or subsuming behaviors in the next lower level. A hybrid symbolic-reactive approach is possible too, as shown in [1]; a solution is proposed that combines symbolic planning with reactive behaviour networks, automated task delegation, reinforcement learning, and pattern-based selection of suitable self-organisation mechanisms.

Another line of architectural work seeks to capture more of human cognitive ability, aiming to describe at a system level the ‘representation and processes that produce intelligent thought’ [22, 23]. Such work includes ACT-R [24], Sigma [25], soar [26], and the standard model [27].

In the works cited above, the primary concern has been functionality. Architecture with more concern for biological realism usually involves a connectionist representation. Examples include SPA [28], recommendation [29], Leabra [30], and Darwinian neurodynamics [31]. These systems are usually proposed with the primary goal being cognitive modeling. In work like [22, 32], ambitious effort is made to model large-scale biologically realistic cognitive architecture.

It is important to note that NUTs are not an architectural proposal. It does not supersede the existing proposals. Instead, NUTs add to the repertoire of notational tools that one can use in building a cognitive system.

2.2 *Representational Solution*

At the symbolic level, NUTs are most similar to fuzzy decision system [33], a representation that has actually been used before in AV context, specifically as a TORCS driving controller [34]. There are subtle differences however. First of all, NUTs rules operate not on decision variables, but on AP, as will be further elaborated later in this subsection. Secondly, a simple probabilistic interpretation, rather than a full blown fuzzy logic, is assumed for fuzzy literals in NUTs. Finally, NUTs symbolic rules are embedded within a graphical structures, delegating its roles to neuronal level computation.

At the structural level, NUTs are a graph-based representation, the sort of representation popular during the 1960s and 1970s in AI work. Graph notations, especially notable the conceptual graph [35], are capable of representing first-order logic or a formally defined subset, rendering it suitable as an intermediate language for tasks such as mapping natural language questions [36]. NUTs have similar capabilities too. However, while it is a graph-based representation, the nodes in a NUTs are not just nodes—they are ‘alive’ in the sense of the computation performed.

In a neural network, as in NUTs, the nodes—neurons—are alive too, each performing a simple computation, mapping its many weighted input into an output. Information is represented in a neural network by patterns of activity distributed over the neurons, each neuron representing not a complete concept or feature, but a ‘microfeatures’ [37]. Neural network may be considered as an abstraction of the biological brain; while relatively simple, its distributed structure allows for the ability to deal with noisy, uncertain input. In fact, theoretical psychological models, such as Rao and Ballard’s predictive coding [38] and Friston’s free energy principle [2], have been shown to map well to neural network implementation [39]. But while powerful and currently dominant, as implied in the opening paragraph of this paper, neural networks are naturally best suited for low-level cognitive tasks, one that requires no reasoning (or explaining) or other forms of higher-order thoughts. This has been attributed primarily to the incapability for abstract compositional representations [40], a weakness which invariably is the strength of symbolism, and the AI school of thought that is driven by the explicit representation of knowledge.

At the variable level, NUTs’ primary distinction is that while the majority of work assumes a direct mapping between the primary variables involved in cognitive process, that is $\eta_0 \xrightarrow{F} \eta_1$, where η_0 is the current value of a variable, F the action on it, and η_1 the new value, in NUTs, the activation potential (AP), $\hat{\eta}$, mediates the effect of one variable on another: $\hat{\eta} \xrightarrow{F} \hat{\eta} \pm \delta\hat{\eta}$. Working in this way, we can model psychologically realistic response to surprise [2], as will be discussed later.

In work such as [1, 41] on the other hand, activation refers to a real number that determines selection of behaviour. A behaviour may have multiple sources of activation, including other behaviours. If the total activation of behaviours passes the execution threshold and all preconditions are fulfilled, a planner selects behaviours for execution. Hence, activation in existing work is largely lateral, not longitudinal in temporal dimension.

3 NUTs Brain

A collection of NUTs is referred to as a *brain*. In this paper, I assume a NUTs brain B to be a sequence:

$$B = (\beta_1, \beta_2, \dots, \beta_{|B|}) \quad (4)$$

The sequence is in order of increasing priority. The action due to β_j may then override that due to β_i where $j > i$. More complex forms of organization are possible of course, but for the AV highway context in this paper, this simple organization suffices.

Each NUTs β are a directed graph comprising of a set of nodes $N = \{\eta_1, \eta_2, \dots, \eta_{|N|}\}$ and directed edges $E = \{\eta_i \rightarrow \eta_j : 1 \leq i, j \leq |N|\}$.

A node, η , has a numerical value $\hat{\eta}$ —the activation potential (AP)—and a fuzzy definition Z that probabilistically maps $\hat{\eta}$ to its literal value, $\bar{\eta}$:

$$Z(\hat{\eta}) = \bar{\eta} \quad (5)$$

η may be a sensor node (graphically an oval), a mental concept (rectangle), or an action (rounded rectangle). Note that action here may be either physical or mental. A mental action may be an operation on or the activation of other NUTs. A sensor node has no parent (a root). For other nodes, denote the set of parents of η as $Par(\eta)$

To illustrate in an AV context, the NUTs in Fig. 2a describes a lane-following action. It assumes the presence of an *Angle* sensor node that captures the angular deviation between the car motion direction and that of the lane. The NUTs shown in Fig. 2b ensure that the car slows down when navigating a sharp angle at high speed. A more complex NUTs are shown in Fig. 3, describing the mental process of merging into another lane, say the right lane. If the nearest car to the right is far enough (as captured by *RMargin*, the steering is adjusted (*OffsetSteer*) to move the car into that lane. If not, depending on the speed of the ego car (*Speed*) versus that of the other car (*sSpeed*), one needs to modulate the current acceleration (*ModulateAccel*).

The deeper semantic of a NUTs is actually within its nodes. Each non-root node, η , is associated with a set of rules, each of which defined as follows:

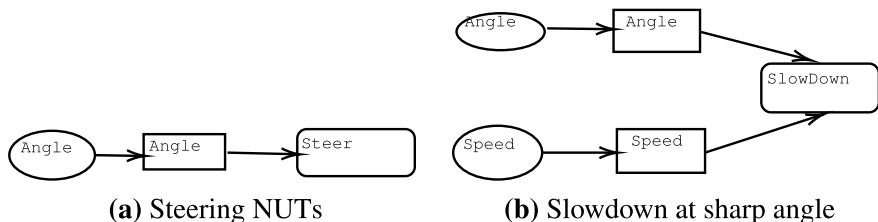


Fig. 2 Two simple NUTs

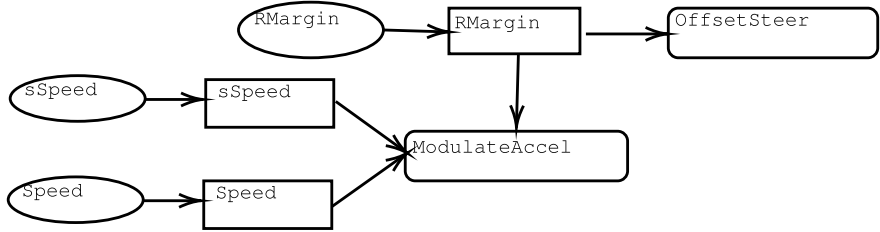


Fig. 3 Merge into a lane

$$R = \bar{\eta}, \overline{Par(\eta)} \xrightarrow{p} A \quad (6)$$

Here, p is a strength factor, and A an action that incrementally changes the AP $\hat{\eta}$. p denotes the probability of A being carried out when the premise is true. The set of literal values of $Par(\eta)$ is written as $\overline{Par(\eta)}$. The rules are the computation within a node or NUTs neuron and basically captures the belief of the NUTs engineer of how the values of one node affects the activation of another. The probabilities affect the transition of NUTs nodes from one state to another. In a later section, a mathematical characterization of this transition is provided, one that can provide guidelines for the probabilities setting.

It is important to note that NUTs operate in a temporal fashion, updating its nodes iteratively and probabilistically over a period of time, each node integrating data from multiple sources. Working in this way, it is potentially more robust against noise and uncertainty in the environment. In fact, biological brain works the same way too. Each neuron's response is inherently variable: repeated presentations of the same stimulus elicit different responses (see for example [42]). Further, in a biological system, as imitated in NUTs, sensory data construes as evidence for or against a proposition [43]. Evidence accumulated beyond a threshold signals a commitment to a proposition or behavioral response.

Due to its probabilistic nature, implementation-wise, a NUTs brain B should be duplicated, with a certain *redundancy factor* κ , forming an ensemble, B^κ . Each brain in the ensemble samples the environment and generates its own action recommendation, the average of which determines the final action value.

4 NUTs Response to a Surprise

The free energy principle (FEP) [2] relates that adaptive organism seeks to minimize the long-term average of *surprise* associated with its sensory input. The term ‘surprise’ in FEP describes the difference between a belief, ϑ about a certain variable in external world, for example the temperature, and a sensory stimulus, φ due to that variable. Agents minimize surprise by changing their expectation or by attempting to change sensory inputs through actions.

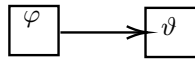


Fig. 4 Effect of sensory input φ on ϑ

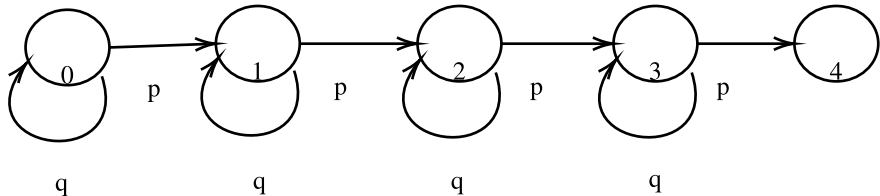


Fig. 5 PFA for NUTs transition

NUTs may be considered as an operational interpretation of the free energy principle (FEP). Consider the NUTs in Fig. 4. The current value in ϑ is a belief about the external state. ϑ moves in response to φ until it reaches an equilibrium. Hence, in NUTs perspective, surprise corresponds to the difference between ϑ and φ .

The amount of surprise correlates to the time it takes for an agent to generate a response—it takes a while to respond to something surprising, like when an obstacle suddenly appear out of nowhere in a highway, but we can respond more immediately to something that we have been anticipating. This is of practical importance in, for example, the design of NUTs for AV. The probabilities in a NUTs should be favorable to a faster response to dangerous situation; the transition can go slower when switching to what is expected to be a safer situation.

The amount of time or the number of steps it takes for a transition in a NUTs can in fact be estimated. Suppose the current value of ϑ , $\vartheta_{\text{curr}} = 0$, and it is subjected to \leftrightarrow with a probability p . Let the maximum value of ϑ , its ‘destination,’ be $\vartheta_{\text{final}} = 4$. There is a probabilistic pressure on ϑ to move from 0 to 4, that is, the surprise value, E , is 4.

Consider now the number of steps or iterations, T , needed to move from ϑ_{curr} to ϑ_{final} . At each integral step from 0 to 4, there is a probability p of an increment and a probability $q = 1 - p$ of repeating a value. We can model the movement of ϑ in the form of a probabilistic finite automata (PFA), A , with 0 the start state and 4 the end state, as shown in Fig. 5.

Possible strings producible by A include 01234, 001234, 011234, 0011222234, and so on. Let T_A be the length of a string producible by A . The length denotes the number of steps it takes to get from 0 to 4.

In general, a NUTs PFA (NPFA) is a PFA with a set of $N + 1$ states where

1. the states are connected into a sequence $Q = (q_0, q_1, \dots, q_N)$ such that there is
 - (a) a transition $q_i \rightarrow q_{i+1}$ for every $i < N$ and
 - (b) a cyclic transition $q_i \rightarrow q_i$ for every $i < N$
2. there is exactly one start state, q_1
3. and exactly one final state, q_N

A complete transition in an NPFA is a sequence of transitions from start to finish, $q_0 \rightarrow q_N$. The minimum length of a complete transition is N , that is one with no repetition. At each state q_i in A , however, the probability of r repetitions before moving forward forms a geometric distribution $p(r) = q^r p$. The generating function encoding the distribution is as follows:

$$F(x) = \frac{p}{1 - qx} \quad (7)$$

where the r th coefficient a_r of the expanded form gives the probability of a transition from start to finish with r repetition.

For an NPFA with $N + 1$ nodes, the generating function is as follows:

$$F(x) = \left(\frac{p}{1 - qx} \right)^N \quad (8)$$

and the probability of a complete transition with r repetitions is given by the r th differentiation of F :

$$\begin{aligned} F^{(r)} &= \prod_{i=0}^{r-1} (N+i)p^N q^r (1-qx)^{-(N+r)} \\ &= \frac{(N+r-1)!}{(N-1)!} p^N q^r (1-qx)^{-(N+r)} \end{aligned} \quad (9)$$

The expected length (or number of time steps) of a transition is then given as

$$E(T) = \sum_{n=0}^{\infty} (N+r-1) F^{(r)} \quad (10)$$

4.1 Composing New NUTs

New networks evolve in the brain, during sleep, dream, and when engaging in imaginative or creative acts. If we assume NUTs as the basic chromosomes of thoughts, then new thoughts or variants of thoughts come about through crossovers and mutations of network. In other words, NUTs lend itself naturally to neuroevolution [44].

A simple form of crossover is presented in this section. Two NUTs can crossover by simply merging at a common node. I illustrate NUTs merger in the context of avoiding head-on collisions from incoming vehicle. Suppose a car agent is endowed with the ability to sense incoming car posing a head-on collision danger, an ability encoded in the NUTs is shown in Fig. 6. Further, it has sensors that provide information on the space or margin to the right or left of an incoming vehicle. As shown in Fig. 7, this sense is activated in the event, an *Avoid*, is needed.

Fig. 6 Impending headon collision detected

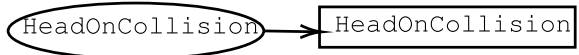
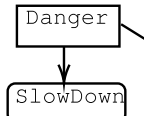
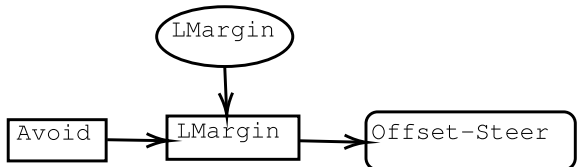


Fig. 7 Offset steer to avoid (something). Similar NUTs assumed for the right margin



(a) Respond to danger



(b) Headon collision is a danger

Fig. 8 Dangerous situation

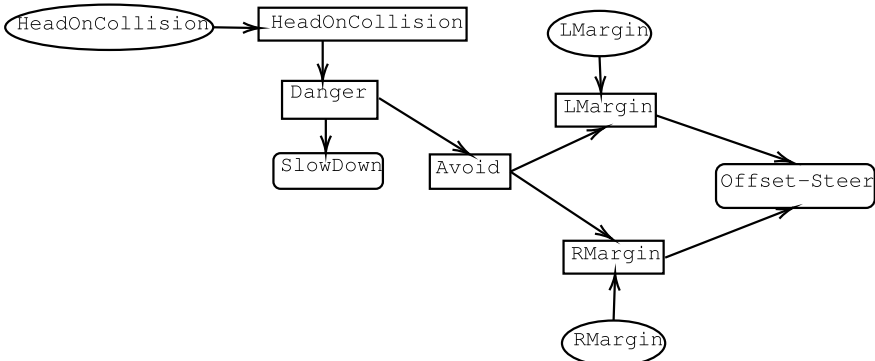


Fig. 9 Respond to headon collision danger

A generic sense of what to do in the event of a *Danger* is needed as well. In the event of a *Danger*, the action to be taken is generally *SlowDown* and *Avoid*, as shown in Fig. 8a. Further assume the presence of the NUTs in Fig. 8b, that relate *HeadOnCollision* with *Danger*.

Compositing it all together, performing unions at common nodes, we obtain the NUTs in Fig. 9.

Can the NUTs in Fig. 9 be derived automatically? Since it is essentially a combinatorial problem, evolutionary algorithm or some other global optimizer matches well; this will be elaborated upon in a future paper though.

5 NUTs AV Experiments

Experimental evaluation for NUTs, in this first exposition on the approach, is on its robustness to errors, specifically errors in Angle_D , the sensor or data node for Angle in Fig. 2b. To perform the evaluation, the open-source TORCS was modified to interface to a Java NUTs engine. The simplest driver provided in TORCS, *bt*, was modified to be a NUTs-controlled driver, *bt-NUTS^k*. The NUTs incorporated are the ones in Fig. 1, 2a, b and 9. κ indicates the NUTs redundancy factor; two versions were considered—*bt-NUTS¹*, one with no redundancy, and *bt-NUTS⁵*, a version with redundancy factor 5.

Gaussian errors, σ , are injected into Angle_D ; the sensor values are then distributed about the true value μ with a Gaussian distribution $N(\mu, \sigma)$, inducing a drunk-like driving profile. Three TORCS-provided autonomous drivers are included as well in the experiment—*berniw*, *damned* and *inferno*. Note that these drivers have been built with sophisticated controllers, making full unlimited use of knowledge of vehicle dynamics and track properties, deploying techniques such as anti-block system (ABS) and traction control limit (TCL) to avoid car skidding. Further a fuzzy controlled driver, *fuzzy-bt*, derived from *bt*, was included as well to pit fuzzy control system against NUTs. *fuzzy-bt* was a translation of the NUTs in this paper to a Mamdani fuzzy system [33].

The cars are made to complete three laps on *CG Speedway 1* with varying values of σ , and the *damages*, as reported by the TORCS engine, recorded. Should a car not complete a lap or a race, due to extensive damage, an arbitrary maximum damage value of 5000 is assumed. The average over three runs were recorded.

Consider first the performance of *bt-NUTS¹* against that of the TORCS drivers *berniw*, *damned* and *inferno*. Figure 10a shows a plot of the outcome. The figure shows that *bt-NUTS¹* sustained lesser damage in coping with erroneous sensors, even though $\kappa = 1$. The average distance from the center of the lane, as plotted in Fig. 10b, is indicative as well of NUTs superior performance.

NUTs effectiveness may be understood by examining how it deals with erroneous sensor signal. Figure 11a shows how the input sensory data Angle_D affects the mental or internal variable Angle , in the presence of no error. Figure 11b illustrates the stability of the mental variable in the presence of noisy input.

bt-NUTS¹, however, cannot be expected to perform well against a deterministic *fuzzy-bt*. *fuzzy-bt* suffers from no crash at all, for the *CG Speedway 1* track. A probabilistic system like *bt-NUTS¹* is meant to deal with difficult input, but as with Monte Carlo sampling, it can only work well with multiple samples or redundancy. For the TORCS environment, I found that a redundancy factor of five is sufficient. In fact, *bt-NUTS⁵* suffers from no crashes at all on the same track, but operates more smoothly at bigger σ compared to *fuzzy-bt*, as can be seen in Fig. 12a. Further, *bt-NUTS⁵* suffers from less speed degradation, as can be seen in Fig. 12b.

Pitting further *bt-NUTS⁵* against *fuzzy-bt*, test runs were conducted on a much more difficult track *Wheel 2*. This time, *fuzzy-bt* suffers crashes, but not *bt-NUTS⁵*, as can be seen in Fig. 13.

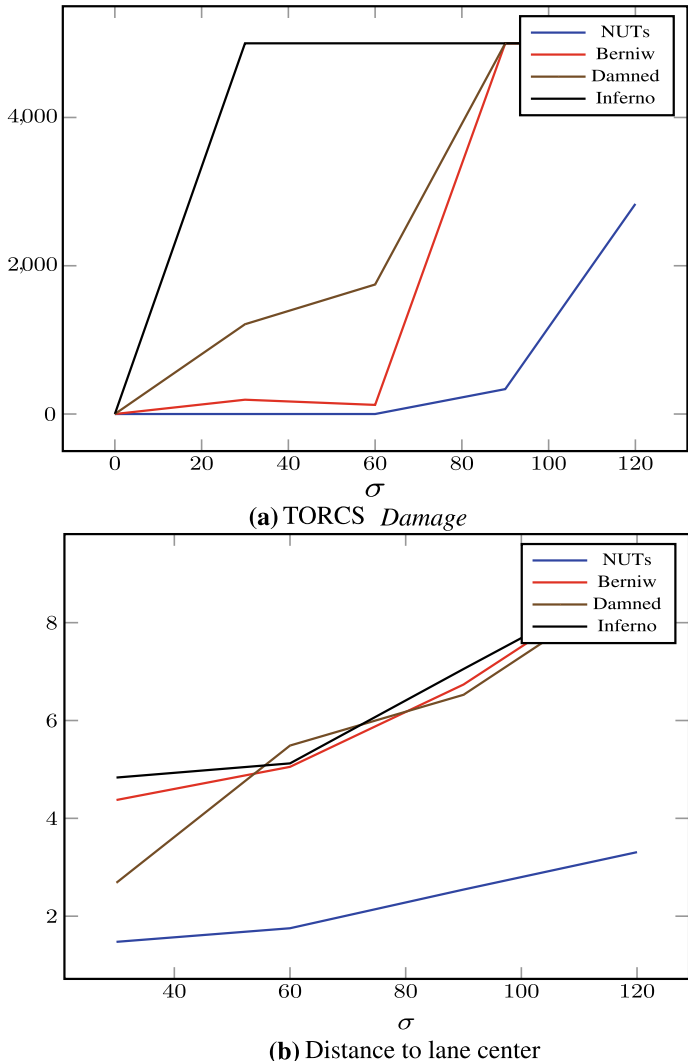


Fig. 10 Variation with σ

6 Conclusion

A graphical formalism, neuronal unit of thoughts (NUTs), has been introduced for building mental models that link up low-level classifiers or regressors. Sensory data, mental concepts, and actions are represented by nodes and causal sequence enforced by edges. A node affects another node through incremental changes in the latter's action potential (AP), and these changes are described by a set of probabilistic rules.

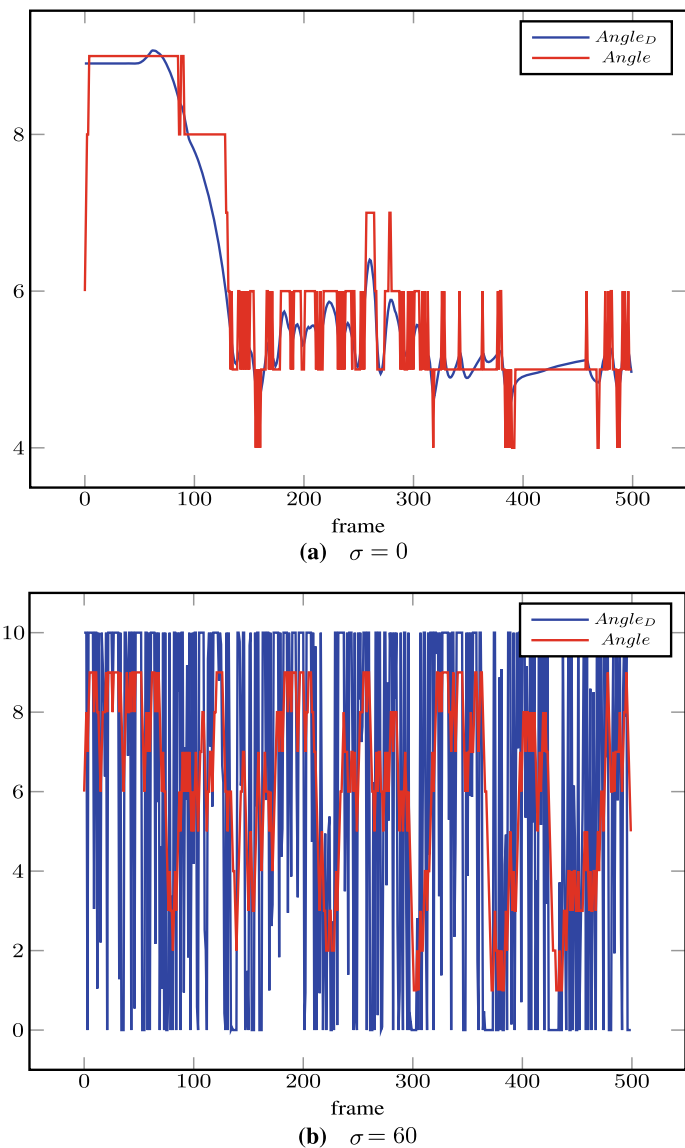


Fig. 11 Variation of $Angle_D$ with $Angle$

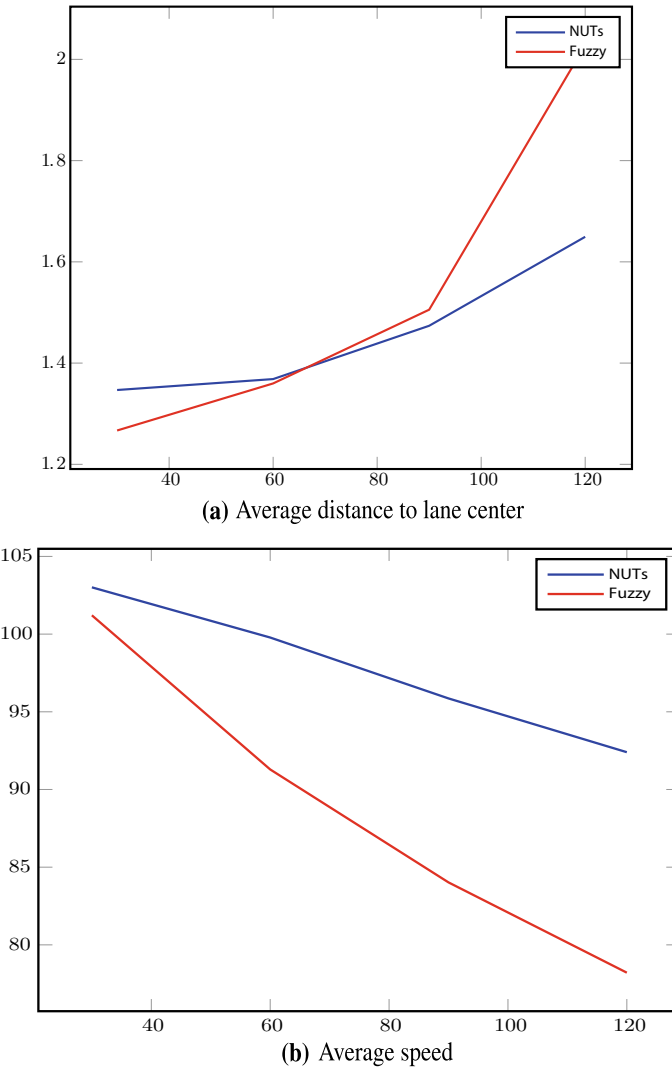


Fig. 12 Variation of σ (horizontal)

The computation at the node represents a generalization of the neuronal-level computation in a conventional neural network. And through its graph-theoretic structure, NUTs enable compositionality [45], implying its potential as a ‘language of thought,’ a language with both combinatorial syntactic and semantic structure [46].

NUTs have been shown in this paper to be capable of expressing higher order cognition, such as that required in autonomous driving. Further, it was shown to be robust to sensory errors. Nevertheless, NUTs potential remains to be further elaborated upon, especially where compositionality is concerned.

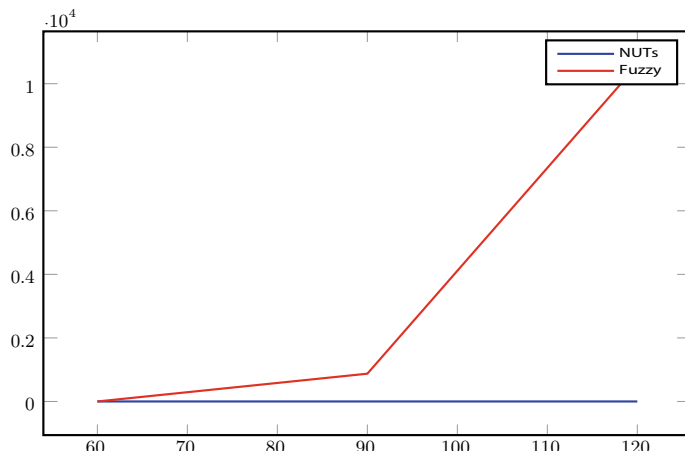


Fig. 13 Variation of σ (horizontal) with damage, on *Wheel 2* track

References

1. Hrabia CE (2019) Self-adaptive and self-organised planning and decision-making for multi-robot systems. Doctoral thesis, Technische Universität Berlin, Berlin
2. Friston K (2003) Learning and inference in the brain. *Neural Netw* 16(9):1325–1352
3. Knill DC, Pouget A (2004) The bayesian brain: the role of uncertainty in neural coding and computation. *Trends Neurosci* 27(12)
4. Yang T, Shadlen MN (2007) Probabilistic reasoning by neurons. *Nature* 447(7148):1075–1080
5. Grigorescu S, Trasnea B, Cocias T, Macesanu G (2020) A survey of deep learning techniques for autonomous driving. *J Field Robot* 37(3):362–386
6. Kuutti S, Bowden R, Jin Y, Barber P, Fallah S (2020) A survey of deep learning applications to autonomous vehicle control. *IEEE Trans Intell Transp Syst*, 1–22
7. Wymani B, Espié E, Guionneau C, Dimitrakakis C, Coulom R, Sumner A (2013) TORCS, the open racing car simulator, v1.3.5. <http://www.torcs.org>
8. Claussmann L, Revilloud M, Gruyer D, Glaser S (2019) A review of motion planning for highway autonomous driving. *IEEE Trans Intell Transport Syst* 21(5)
9. Alcorn MA, Li Q, Gong Z, Wang C, Mai L, Ku WS, Nguyen A (2019) Strike (with) a pose: neural networks are easily fooled by strange poses of familiar objects. In: Proceedings CVPR 2019
10. Michaelis C, Mitzkus B, Geirhos R, Rusak E, Bringmann O, Ecker AS, Bethge M, Brendel W (2019) Benchmarking robustness in object detection: autonomous driving when winter is coming. CoRR abs/1907.07484
11. Yurtsever E, Lambert J, Carballo A, Takeda K (2020) A survey of autonomous driving: Common practices and emerging technologies. *IEEE Access* 8:58443–58469
12. Chen C, Seff A, Kornhauser A, Xiao J (2015) Deepdriving: learning affordance for direct perception in autonomous driving. Proceedings ICCV 2015. IEEE Computer Society, USA, pp 2722–2730
13. Stein B (1998) Neural mechanisms for synthesizing sensory information and producing adaptive behaviors. *Exp Brain Res* 123:124–135
14. Toker D, Sommer FT (2019) Information integration in large brain networks. *PLOS Comput Biol* 15(2):1–26

15. Hassabis D, Kumaran D, Summerfield C, Botvinick M (2017) Neuroscience-inspired artificial intelligence. *Neuron* 95(2):245–258
16. Stuss D, Alexander M (2009) Frontal lobe syndrome. In: Squire LR (ed) *Encyclopedia of neuroscience*. Academic Press, Oxford, pp 375–381
17. Kotseruba I, Tsotsos JK (2018) 40 years of cognitive architectures: core cognitive abilities and practical applications. *Artif Intell Rev* 53
18. Ullman S (1980) Against direct perception. *Behav Brain Sci* 3(3):373–381
19. Wessnitzer J, Webb B (2006) Multimodal sensory integration in insects—towards insect brain control architectures. *Bioinspiration Biomimet* 1(3):63–75
20. Gibson JJ (1972) A theory of direct visual perception. In: Noe A, Thompson E (eds) *Vision and mind: selected readings in the philosophy of perception*. MIT Press, pp 77–89
21. Brooks R (1986) A robust layered control system for a mobile robot. *IEEE J Robot Automat* 2(1):14–23
22. Eliasmith C (2013) *How to build a brain: a neural architecture for biological cognition*. Oxford University Press, Oxford
23. Thagard P (2012) *Cognitive architectures*. Cambridge University Press, Cambridge
24. Anderson JR, Byrne MD, Douglass S, Lebiere C, Qin Y (2004) An integrated theory of the mind. *Psychol Rev* 111(4):1036–1050
25. Rosenbloom P, Demski A, Ustun V, Sigma T, Architecture C (2016) The sigma cognitive architecture and system: towards functionally elegant grand unification. *J Artif Gener Intell* 7(1)
26. Laird JE (2012) *The soar cognitive architecture*. The MIT Press, Cambridge
27. Laird JE, Lebiere C, Rosenbloom P (2017) A standard model of the mind: toward a common computational framework across artificial intelligence, cognitive science, neuroscience, and robotics. *AI Mag* 38(4)
28. Stewart TC, Eliasmith C (2013) Parsing sequentially presented commands in a large-scale biologically realistic brain model. In: 35th annual conference of the cognitive science society, pp 3460–3467
29. Coward LA (2011) Modelling memory and learning consistently from psychology to physiology. Springer, Berlin
30. Chipman SEF, O'Reilly RC, Hazy TE, Herd SA (2015) *The Leabra cognitive architecture: how to play 20 principles with nature and win!* Oxford University Press, Oxford
31. Fedor A, Zachar I, Szilágyi A, Öllinger M, de Vladar HP, Szathmáry E (2017) Cognitive architecture with evolutionary dynamics solves insight problem. *Front Psychol* 8:427
32. Mizutani H, Ueno M, Arakawa N, Yamakawa H (2018) Whole brain connectomic architecture to develop general artificial intelligence. *Procedia Comput Sci* 123:308–313
33. Mamdani E (1974) Application of fuzzy algorithms for control of simple dynamic plant. *Proc Inst Electr Eng* 121:1585–1588(3)
34. Salem M, Mora AM, Merelo JJ, García-Sánchez P (2017) Driving in torcs using modular fuzzy controllers. In: Squillero G, Sim K (eds) *Applications of evolutionary computation*. Springer International Publishing, Cham, pp 361–376
35. Sowa JF (1984) *Conceptual structures: information processing in mind and machine*. Addison-Wesley Longman Publishing Co., Inc, Boston
36. Sowa JF (2008) Conceptual graphs. In: *Handbook of knowledge representation*
37. MacLennan B (2015) Cognitive modeling: connectionist approaches. In: Wright JD (ed) *International encyclopedia of the social and behavioral sciences*, 2nd edn. Elsevier, Oxford, pp 84–89
38. Rao R, Ballard D (1999) Predictive coding in the visual cortex: a functional interpretation of some extra-classical receptive-field effects. *Nature Neurosci* 2:79–87
39. Bogacz R (2017) A tutorial on the free-energy framework for modelling perception and learning. *J Math Psychol* 76:198–211
40. Garnelo M, Shanahan M (2019) Reconciling deep learning with symbolic artificial intelligence: representing objects and relations. *Curr Opin Behav Sci* 29:17–23

41. Blumberg BM, Galyean TA (1995) Multi-level direction of autonomous creatures for real-time virtual environments. In: Proceedings of the 22nd annual conference on computer graphics and interactive techniques. SIGGRAPH '95, Association for computing machinery, New York, pp pp 47–54. <https://doi.org/10.1145/218380.218405>
42. Jazayeri M, Movshon JA (2006) Optimal representation of sensory information by neural populations. *Nat Neurosci* 9(5):690–696
43. Mazurek ME, Roitman JD, Ditterich J, Shadlen MN (2003) A role for neural integrators in perceptual decision making. *Cerebral Cortex* 13(11):1257–1269
44. Stanley KO, Clune J, Lehman J, Miikkulainen R (2019) Designing neural networks through neuroevolution. *Nat Mach Intell* 1
45. Szabó ZG (2017) Compositionality. In: Zalta EN (ed.) The stanford encyclopedia of philosophy. Metaphysics Research Lab, Stanford University, summer 2017 edn
46. Fodor JA, Pylyshyn ZW (1988) Connectionism and cognitive architecture: a critical analysis. In: Pinker S, Mehler J (eds) *Connections and Symbols*. MIT Press, Cambridge, pp 3–71

Real-Time Multi-obstacle Detection and Tracking Using a Vision Sensor for Autonomous Vehicle



Sobers Francis, Sreenatha G. Anavatti, Matthew Garratt, and Hussein A. Abbass

Abstract In this paper, an effective approach for real-time multi-obstacle detection and tracking in the navigation module is discussed. To calculate a feasible path for an autonomous ground vehicle (AGV) from the start position to goal position, efficient Dstar lite global planner is added and adhered to ROS nav_core package. Later, the clustering of points based on distance from a laser scanner data is carried out to perform multi-obstacle detection and followed by tracking. Then, the clusters are categorised as static and dynamic obstacles from their location, orientation, speed and size of an individual cluster. Using this approach, dynamic obstacles' paths are estimated from their respective past positions. To predict the dynamic obstacle for the next five-time steps, linear extrapolation and line fitting are employed. The estimated obstacles' path data are published as a *PointCloud* ROS message, then it is subscribed by the *costmap* node of the ROS navigation package. The *costmap* automatically updates the obstacle map layer and rebuilds the 2D occupancy grid map with new information about obstacles. Then, the path planner replans the path using updated *costmap* to avoid obstacles in the dynamic environment. Finally, real-time experiments are conducted to validate the efficacy of this intelligent system.

Keywords Multi-obstacle tracking · Collision avoidance · Intelligent vehicles · ROS navigation

1 Introduction

AGVs are widely utilised for scientific, commercial, industrial, and military applications for different tasks such as exploration in hazardous environments and unknown areas, military surveillance and reconnaissance, search and rescue missions and industrial automation.

An AGV must be able to adequately sense its surroundings to operate in unknown environments and execute autonomous tasks in which vision sensors provide the

S. Francis (✉) · S. G. Anavatti · M. Garratt · H. A. Abbass
School of Engineering and IT, University of New South Wales, Canberra, Australia
e-mail: s.anavatti@adfa.edu.au

necessary information required for it to perceive and avoid any obstacles to accomplish autonomous path planning. Hence, the vision (perception) sensor becomes the key sensory device for perceiving the environment in intelligent mobile robots, and the perception objective depends on three basic system qualities, namely rapidity, compactness and robustness [1].

The basic operation of mobile robot navigation encompasses the robot's ability to act and react based on partial knowledge about its operating environment and vision sensor readings to reach its goal positions efficiently and reliably as possible [2]. Path planning in a cluttered environment involves identifying a trajectory in a partially known map and with a target location that will cause the mobile robot to reach the location when executed. Obstacle avoidance means modifying the mobile robot's path to avoid collisions using real-time sensor data. The problem in a dynamic environment is that in most real applications as future motions of moving objects are a priori unknown, and it is necessary to predict them based on observations of the obstacles' past and present states, so that the AGVs path can be re-planned in advance to avoid a collision in critical conditions. So, an approach is required to estimate future positions and orientations of moving obstacles [3].

Until recently, most motion prediction techniques [4] have been based on kinematic models that describe how the state (e.g. position and velocity) of an object evolves. The models that are used to improve prediction results are the hidden Markov stochastic models, the grey prediction, least-mean square-error, and Kalman filter. In this paper, numerical prediction approaches, such as linear extrapolation and linear fitting are used to predict future positions and orientations of a moving object in dynamic environments because they are simple and convenient. Light detection and ranging (LIDAR) [5] is widely utilised as a mobile robot's vision sensor in the detection and tracking of obstacles. The supervised machine learning technique is used to classify the detect objects with the help of a clustering algorithm for robust detection and tracking from the lidar data [6]. It requires more computation time than the conventional method during the training phase.

The robotic operating system (ROS) is an open-source, meta-operating robot framework, which was originally developed in 2007 by the Standford Artificial Intelligence Institute and is a set of software frameworks for robotics engineering [7]. In our work, ROS is adopted for implementing the navigation planner, tracking obstacles from laser data, and controlling the AGV. Our main contributions of this paper can be summarised as follows:

1. A simple but effective way of detecting and estimating the dynamic obstacles as clusters with the help of range information from a single laser sensor is developed, by which a mobile robot can navigate the large-scale cluttered map with ease.
2. The estimated obstacles' path data are projected into the *costmap* of the ROS navigation package automatically which helps to update the 2D occupancy grid map regularly. Using this, the path planner replans the path, if needed, without any delay for each cycle.
3. Finally, the effectiveness of the proposed obstacle detection and avoidance approach has been demonstrated by real-time experiments.

Fig. 1 Jackal with laser range finder [autonomous lab @ UNSW Canberra]



The paper is organised as follows: Section 2 discusses the custom ROS navigation stack configuration. The multi-obstacle detection and tracking approach is explained in Sect. 3 along with the obstacle avoidance strategy. In Sect. 4, real-time experiments are demonstrated to validate the performance of the approach. Lastly, Sect. 5 concludes the paper with some recommendations for future work.

1.1 System Overview

The Jackal AGV is a small, fast and entry-level field robotics research platform, which has an on-board computer, GPS and IMU fully integrated with ROS for out-of-the-box autonomous capability [8]. Figure 1 shows one of our SICK LMS 111 laser-rangefinder equipped Jackal AGVs from the UNSW Canberra autonomous system lab. The AGV has the following specifications:

- Processor: Intel i5-4570TE Dual Core, 2.7 GHz Processor with 8GB RAM.
- Sensors: LMS 111 Laser finder, in-built Odometer fused with IMU.
- OS: ROS Kinetic Kame in Ubuntu 16.04.

2 ROS Path Planner

Path planning of mobile robots relies greatly on known information about the immediate environment and the motion constraints of robot kinematics and dynamics. ROS provides a package to navigate from a start position to goal position while avoiding obstacles. The navigation stack [9] is a ROS package that subscribes to

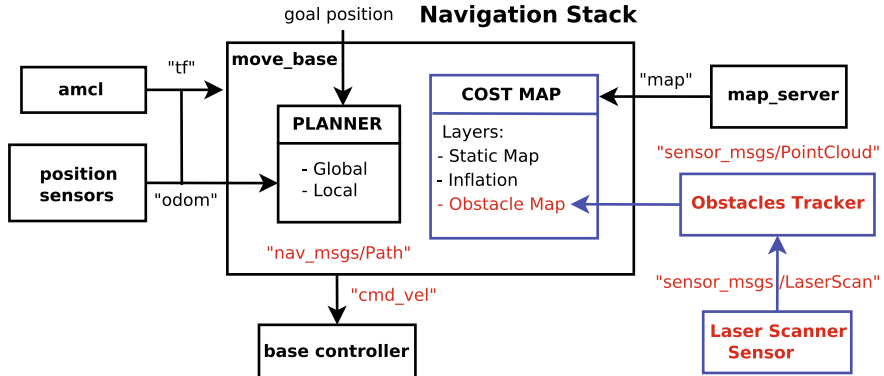


Fig. 2 ROS navigation stack with obstacle tracker

different ROS topics from odometry (robot position and orientation), sensor sources (like Laser scanner (“scan”)) and a goal position (“*move_base_simple/goal*”) and publishes safe velocity commands (“*cmd_vel*”) to a mobile base controller. Then, the mobile base controller converts the “*cmd_vel*” topic into motor commands to send to a mobile base.

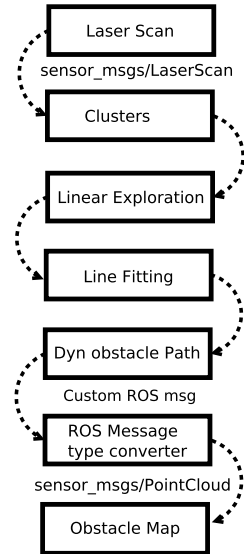
Adaptive Monte Carlo localization (amcl) is a package that deals with mobile robot localisation in which the position and orientation data representing the robot’s pose [10]. Figure 2 illustrates an overview of the navigation stack configuration used for our approach. The occupancy grid path planning method in ROS divides the operating area into cells/map pixels and assigns them as occupied or empty. The path planner finds a feasible path that avoids any of the occupied cells.

An efficient Dstar lite path planner [11] is added and adhered to the *nav_core :: BaseGlobalPlanner C++* interface defined in *nav_core* package [12]. A new path planner is added as a plugin to ROS, so that the AGV determines path sequence to move from starting position to destination in the navigation *move_base* package. The navigation stack uses two different *costmap* (local and global *costmap*) to store information about the obstacles from the static map and obstacles. Global *costmap* is for planning over the entire map, whereas local *costmap* is for local planning and obstacle avoidance. Each ROS topic can be subscribed by the navigation stack cycles at the rate specified by the parameter which determines the frequency, in Hz, at which the topic will run its update loop.

3 Multi-obstacles Detection and Tracking

This section provides a detailed explanation about multi-obstacles tracking of dynamic obstacles. The present navigation stack can only subscribe sensor data published using ROS message type, *sensor_msgs/LaserScan* and *sensor_msgs/Point*

Fig. 3 Flowchart: raw laser data to multi-obstacle information



Cloud. The laser sensor is used to provide information to the navigation stack about the environment. Flowchart (Fig. 3) depicts the step-by-step approach in sequential order to detect and track the obstacles.

The location of the obstacles with respect to the scanner on the robot can be plotted in xy coordinates Eq. (1).

$$\begin{aligned} x_{obs} &= \text{range}[i] * \cos(\text{angle_min} + i * \text{angle_increment}) \\ y_{obs} &= \text{range}[i] * \sin(\text{angle_min} + i * \text{angle_increment}) \end{aligned} \quad (1)$$

where i is the total number of measurement steps varies from zero to maximum values and $\text{range}[i]$ is the distance measurement corresponding to measurement steps.

Initially, laser scan data is subscribed, and their successive time step data are compared to filter the obstacles if any. Followed by the clustering of points based on distance is carried out to perform multi-obstacle detection. Then, the clusters are grouped as static and dynamic obstacles from their location, orientation, speed and size of an individual cluster. Later, dynamic obstacles' paths are estimated from their respective past positions. Linear extrapolation is employed to estimate future values by observing the relationship between the available data values. The range values of a cluster at different time steps are sampled periodically, and these data are used to approximate the future values. Then, the series of cluster position points have fitted a line using line fitting. These estimated obstacles path data are published as a *PointCloud* ROS message, and then it is subscribed by the *costmap* node of the ROS navigation package. The *costmap* automatically updates the obstacle map layer and rebuilds the 2D occupancy grid map with new information about obstacles. Then, the path planner replans the path using updated *costmap* to avoid obstacles in the dynamic environment.

The *costmap* ROS package [13] offers a configurable structure that keeps the information about where the AGV should navigate in the form of an occupancy grid. Each cell in this costmap structure can be either free, occupied or unknown and has assigned to special cost values (one of 255 different cost values). The occupied cells in the *costmap* are allotted a *costmap_2d* :: *LETHAL_OBSTACLE* with cost value = 254, the unknown cells are assigned a *costmap_2d* :: *NO_INFORMATION* cost, and others are allotted a *costmap_2d* :: *FREE_SPACE* with cost value = 0. For each cycle, the *costmap* updates the map information at the rate of update_frequency (5Hz).

3.1 Obstacle Avoidance Strategy

There is a need for a strategy to avoid obstacles, while the AGV is travelling to the goal position in a cluttered environment. In this paper, an obstacle avoidance strategy is followed as explained below. Laser sensor (LMS111) can provide data up to a maximum range of 20 m. In *LaserScan.msg*, LIDAR scans from the start angle which commences along the positive x-axis to the end angle in a counter-clockwise direction. To discard the unnecessary range data, laser scan data is filtered with a start angle of $+90^\circ$ and an end angle of -90° as illustrated in Fig. 4. Our strategy procures obstacle data once their range is ≤ 10 m. When the obstacles enter a 10 m region, the algorithm starts to cluster the obstacles as static and dynamic obstacles and predicts their next trajectory points if it is a dynamic obstacle. Further, when obstacle arrives within a 5 m region, obstacle map layer of *costmap* updates the map about the new obstacles information. Finally, the planner replans the mobile robot's path if there is any chance of collision.

Figure 4 shows the laser scan image with two obstacles *Obs1* and *Obs2*. Both *Obs1* and *Obs2* are clustered and tracked as their distances are below 10 m away from the laser. But the *costmap* updates only *Obs1* information into the map layer that helps the planner to perform re-planning only if necessary. The estimated *Obs1* paths are updated in the map with the cost value assigned to 255 and projected into a *costmap* structure.

4 Experimental Results

To validate the performance of our approach, various experiments are carried out on Jackal's model in Gazebo and mainly in Jackal UGV with LMS111 laser finder as a vision sensor. Though the Jackal is mounted with other vision sensors such as 3D Velodyne, Bumblebee camera and IP camera, only the LMS111 sensor is utilised for obstacle avoidance and estimation. A map is created with gmapping ROS package using a laser camera and is used by the map server. The map of the operating environment is of 4000×4000 pixels with 0.05 m/cell in Fig. 5. During

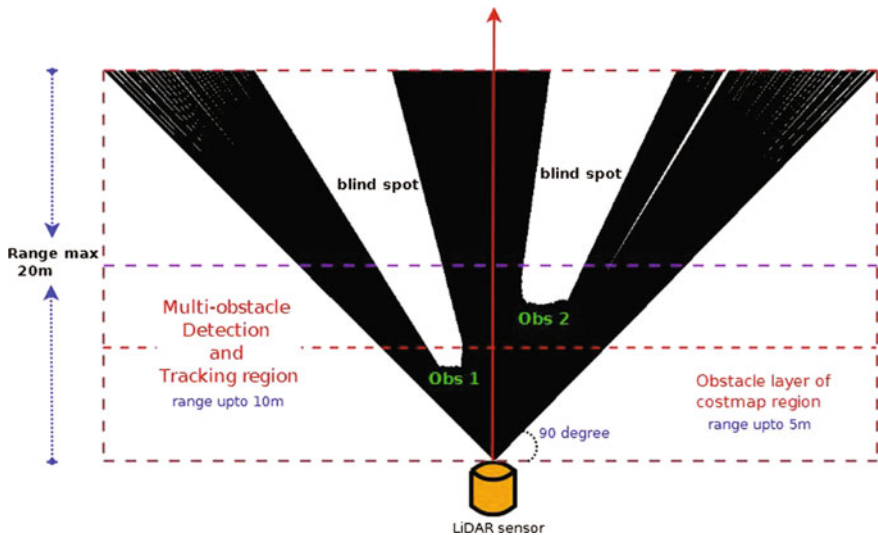
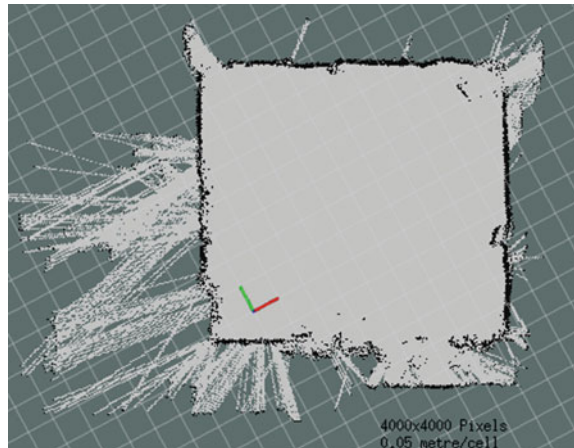


Fig. 4 Top view of laser scan with the obstacles

Fig. 5 Operating map in ROS rviz



the experiments, other Jackal robots, which can be controlled manually through the PS4 gaming controller, are used as the dynamic obstacles as shown in Fig. 7.

The laser range values from LMS 111 are utilised to detect the moving obstacles, and later, their position and orientation are estimated. These estimated trajectories are incorporated with the path planning algorithm, which helps to handle dynamic obstacles, so that AGV can calculate its feasible path without any collision. LIDAR LMS111 sensor has a maximum aperture angle of 270° with a scanning frequency of 25/50Hz. The angular resolution of the scan measurement is of 0.25 or 0.50. In this work, LaserScan Message holds information about a single scan of range data as in Table 1.

Algorithm 1 Costmap updates map with the tracked obstacles

Require: LaserScan.msg provides start angle angle_min , end angle of the Laser scan, angle increment angle_incre , range_min and range_max . The Off_angle is the angle ignored at the sides. The ns is the number of samples per degree. The range_count is the number of range data per scan

Ensure: Clusters of Obstacles, Estimation of dynamic obstacles

```

 $n \leftarrow 0$ 
for  $i \leftarrow off\_ang * ns$  to  $[\text{range\_count} - off\_ang * ns]$  do
    if  $\text{ranges}[i] > \text{range\_min}$  and  $\text{ranges}[i] < 10.0$  then
         $\text{obstacle\_distances}[n] = \text{ranges}[i]$ 
         $y \leftarrow \text{ranges}[i] * \sin(\text{angle\_min} + i * \text{angle\_incre})$ 
         $x \leftarrow \text{ranges}[i] * \cos(\text{angle\_min} + i * \text{angle\_incre})$ 
         $\text{-->} \text{Cluster the obstacles}$ 
         $\text{-->} \text{Estimate the obstacles position}$ 
        if  $\text{ranges}[i] < 5.0$  then
             $\text{LETHAL\_OBSTACLE: cost\_lethal} = 254$ 
             $\text{-->} \text{Insert obstacles information into costmap}$ 
             $\text{-->} \text{Assign cell cost value} = 254$ 
             $\text{-->} \text{Replan the planner if necessary}$ 
        end if
         $n++$ 
    end if
end for

return Obstacles path, costmap updation
```

Table 1 Single laser scan from LMS111

LaserScan.msg

Message definition	Values
angle_min	-1.60570287704 rad
angle_max	1.60570287704 rad
angle_increment	0.00873
time_increment	2.77777780866e-05
scan_time	0.0199999
range_min	0.00999999 m
range_max	20.0 m

In Experiment I, the Jackal is stationary where a dynamic obstacle is moving towards the robot along with a few static obstacles. The consecutive laser scans are compared and then match each grid cells with cells from the previous iteration (based on distance). The location, size and speed of the obstacles as clusters are updated through observations by using a weighted average from cluster matches. ROS packages can also use a static map to help remove static obstacles and also to find out the moving obstacles. Once the obstacle enters the *costmap* region (<

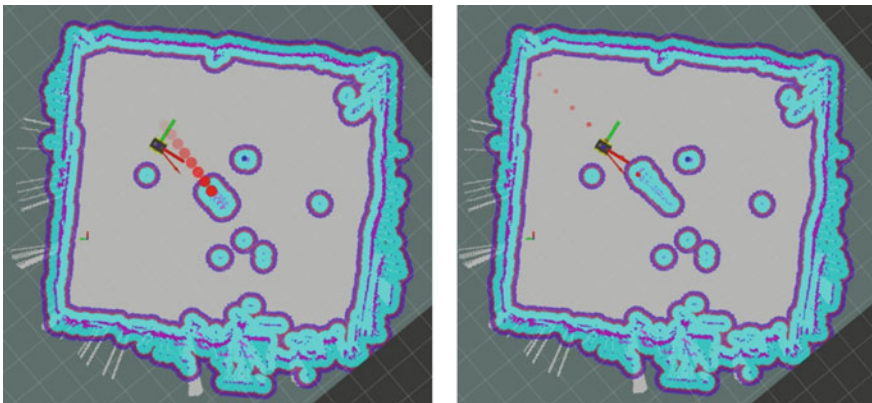


Fig. 6 Experiment I: detection and estimation of trajectories of the dynamic obstacle in ROS 3D visualiser



Fig. 7 Real-time path planning with obstacles

5 m) as proposed, its path is predicted and *costmap* updated. Figure 6 shows the static obstacles as blue circle clusters, dynamic obstacles with the predicted future trajectories as red circles (Fig. 7).

For Experiment II, Jackal has to perform a safe navigation task in a partially known map, and during its traverse towards the goal location, it simultaneously detect, estimate and avoid the obstacles and replan its path if necessary. Once the goal location is selected in the ROS rviz window inside the map, Jackal finds an initial feasible path to reach the goal. The readings from the laser scan on the Jackal help to locate the obstacles and provides information about the cluster whether static or dynamic. The dynamic cluster points are estimated from their past and present locations with the employed linear extrapolation and line fitting approach. Once the obstacles enter the 5-m region, the obstacles' trajectories are projected into the obstacle layer of the ROS *costmap* package. Eventually, Jackal has successfully reached the goal position by avoiding the obstacles, and the snapshots of the experiment are shown in Fig. 8.

The experimental results show that the proposed approach can help Jackal to detect and avoid both static and dynamic obstacles independently while performing navigation.

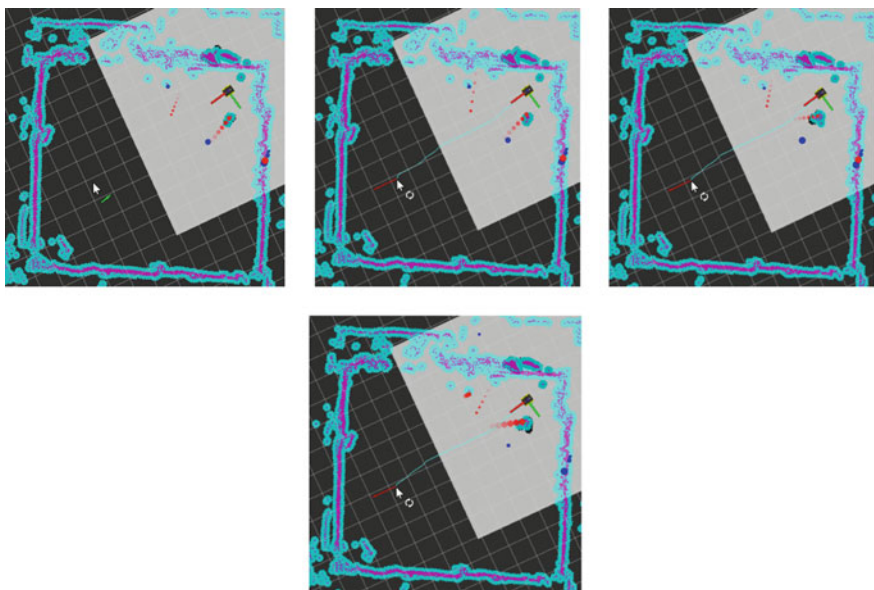


Fig. 8 Real-time path planning with static and dynamic obstacles

5 Conclusion

In this article, an approach for detecting and tracking obstacles is presented. The purpose of obstacle detection and tracking is to obtain the movement state of the moving obstacle, to predict the possible state and trajectory of the dynamic obstacle, which is of great significance to path planning of autonomous ground vehicles.

For future work, more experiments are planned with more complex scenarios to test and validate our approach. The performance of our approach needs to be verified with different scenarios such as when the AGV turns too fast when the surrounding has obstacles with various shapes and sizes and wider laser angles.

Acknowledgement This material is based upon work supported by the U.S. Army Ground Vehicle Systems Centre and International Technology Centre-Pacific under Contract No. FA5209-18-P-0140. Any opinions, findings and conclusions or recommendations expressed in this material are those of the author(s) and do not necessarily reflect the views of the U.S. Army.

References

1. Patnaik S (2007) Robot cognition and navigation—an experiment with mobile robots. In: Cognitive technologies
2. Siegwart R, Nourbakhsh IR, Scaramuzza D (2011) Introduction to autonomous mobile robots, 2nd edn. The MIT Press, Cambridge

3. Volos CK, Jahanshahi H, Sari NN (2020) Recent advances in robot path planning algorithms: a review of theory and experiment. *Robotics research and technology series*. Nova Science Publishers, Incorporated
4. Jiang R, Tian X, Xie L, Chen Y (2008) A robot collision avoidance scheme based on the moving obstacle motion prediction. In: 2008 ISECS international colloquium on computing, communication, control, and management, vol 2, pp 341–345
5. Xie D, Xu Y, Wang R (2019) Obstacle detection and tracking method for autonomous vehicle based on three-dimensional LiDAR. *Int J Adv Robot Syst* 16:172988141983158
6. Karakaya S, Yasar Ocak H, Küçükıyıldız G (2015) A bug-based local path planning method for static and dynamic environments*
7. Quigley M, Conley K, Gerkey B, Faust J, Foote T, Leibs J, Wheeler R, Ng A (2009) ROS: an open-source robot operating system, vol 3
8. Jackal: Unmanned ground vehicle. <https://clearpathrobotics.com/jackal-small-unmanned-ground-vehicle/>
9. Fabro J, Guimarães R, Oliveira A, Becker T, Brenner V (2016) ROS navigation: concepts and tutorial 625:121–160
10. Zheng K (2017) ROS navigation tuning guide. 06
11. Francis S, Anavatti SG, Garratt M (2018) Real-time path planning module for autonomous vehicles in cluttered environment using a 3D camera. *Int J Veh Auton Syst* 14:40
12. Li Y, Shi C (2018) Localization and navigation for indoor mobile robot based on ROS. In: 2018 Chinese automation congress (CAC), pp 1135–1139
13. ROS: Costmap guide. http://wiki.ros.org/costmap_2d

Healthcare Security: Usage of Generative Models for Malware Adversarial Attacks and Defense



Shymala Gowri Selvaganapathy and Sudha Sadasivam

Abstract Digitization of services offered by healthcare sector to enable efficient and convenient patient care demands more attention as security and privacy concerns must be addressed cautiously. Healthcare apps developed to deliver such services are under constant threat of malware attacks. Nowadays, malware-infused medical apps are on the rise, inflicting severe damage to the end user. Attackers are lured by the benefits of hacking electronic protected health information (ePHI). This article takes up a proof of concept approach to validate the hypothesis that malware-infused medical apps try to bypass detection by anti-malware engines utilizing machine learning techniques internally for detection. Evading detection can be achieved by the possibility of adversarial attacks on malware detectors deploying learning-based techniques. The article utilizes a generative adversarial networks (GANs)-based attacking technique to craft adversarial samples which insert perturbations into the malicious apps. These perturbed samples when fed to the malware detector are misclassified as benign. The article takes a stand to provide defense by denoising approach and tries to utilize generative models suitable for denoising such as autoencoders (AE) and variational autoencoders (VAE). The denoised malware samples when fed to the malware classifier are expected to be classified as malware. The current results are not promising but showcase the pathway for improvements.

Keywords Health care · Security · Cyberattacks · Malware · Defense · Generative models

1 Introduction

The soaring high usage of smartphones and digitization of all forms of communications during the pandemic has motivated and pushed healthcare providers to digitize

S. G. Selvaganapathy

Department of Information Technology, PSG college of Technology, Coimbatore, India

S. Sadasivam

Department of Computer Science and Engineering, PSG college of Technology, Coimbatore, India

healthcare services. This has resulted in upsurge of healthcare-related medical apps to connect patients to healthcare platforms for enabling effective and convenient patient care. The healthcare-related apps make use of Internet of Medical Things (IoMT) to enable doctors to remotely observe the patient's medical status through wireless connectivity and digital monitoring of the medical devices connected with patients such as pacemakers, cardioverter defibrillators (ICD), ventilators, infusion pumps, deep brain neurostimulators, glucometers and insulin pump monitors, to name a few. There are applications that offer services telemedicine, fitness tracking, appointments, insurance and reimbursement, to name a few. Epocrates [9], temperature body health recorder [23], paramedic protocol provider [21] TousAntiCovid [26], glucose-buddy [11] and Kareo[15] are a few medical apps offering varied services to deliver better health care.

These healthcare and medical management apps offered by healthcare organizations (HCOs) are at the high risk of cybersecurity attacks [12]. Figure 1 illustrates the statistics of cybersecurity attacks targeting healthcare data as featured by the HIPAA Journal [13]. Attackers are enticed with the benefits obtainable from electronic protected health information (ePHI). This has motivated attackers to infuse healthcare apps with malware contents. Malware-infused healthcare-related apps have the objective of compromising sensitive patient data, carrying out ransomware attacks, performing distributed denial of service to obstruct provision of medical services to patients, healthcare fraud and abuse to name a few [2, 10, 12, 16, 18, 19, 22, 24, 25, 27, 28]. HCOs should also focus on thwarting cyber security attacks from malware-infused medical apps by deploying better malware detectors. This article takes up a proof of concept approach to validate the hypothesis that malware-infused medical apps try to bypass detection by anti-malware solutions in their end point security solutions [17, 20]. But malware detectors deploying learning-based techniques are vulnerable to adversarial attacks. Evading detection can be achieved

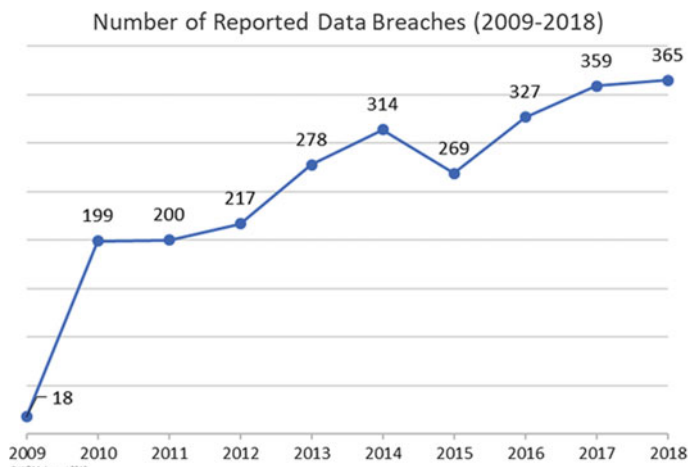


Fig. 1 Statistics of data breach in healthcare industry adapted from [13]

by the possibility of adversarial attacks on malware detectors deploying learning-based techniques. The article utilizes a GAN-based attacking technique [14] to craft adversarial samples which insert perturbations into the malicious apps. The article takes a stand to provide defense by denoising approach and tries to utilize available denoising generative models such as autoencoders and variational autoencoders [6, 24].

The contribution of this article is as follows:

- Conceptualize the possibility of GAN-based adversarial attacks on learning-based anti-malware engine utilized by malware-infused medical apps.
- Gestate defense by denoising through generative learning models like autoencoder and variational autoencoder to make the anti-malware engine robust against evasion attacks.

The article tries to elaborately assess the inherent vulnerability of usage of machine learning models deployed in the AI medical support system.

The rest of this article is articulated as follows: Sect. 2 presents the related works. Section 3 gives background on generative models. Section 4 provides background on adversarial machine learning (AML). Section 5 elaborates on the proposed methodology along with result analysis while Sect. 6 concludes with possible future work.

2 Literature Survey

Hathaliya [12] provides a structured overview of the various security and privacy issues that are faced in Healthcare 4.0 along with possible research directions along with projecting the emerging usage of healthcare apps paired with the rising security and privacy concerns. Ethical issues and biased habits which could be prescribed by medical apps along with the security issues that these apps could carry are discussed by Buijink [7].

Security challenges faced by healthcare sector with specific emphasis on malware-based attacks on healthcare industry are discussed in detail by Ahmed2 [3]. Ransomware attacks on several healthcare organizations are exemplified to illustrate the havoc malware medical apps can cause on a breached healthcare sector.

Argaw [4] provides best practices to be followed by healthcare organizations to keep them against security breaches. Newaz [18] exposes the possible cyber security issues caused by malware-infused medical apps.

3 Background on Generative Models

Learning techniques can be categorized into generative models and discriminative models [6]. In generative models, given training data, it generates new samples from same distribution. The model tries to learn $p_{\text{model}}(x)$ similar to $p_{\text{data}}(x)$. It explicitly

models the actual distribution of each class. Discriminative models, on the other hand, model the decision boundary between the classes. It learns the conditional probability distribution $p(x, y)$. Generative models address the density estimation problem by either explicit density estimation or implicit density estimation. Explicit density estimator models explicitly define and solve for $p_{\text{model}}(x)$ by assuming some prior distribution about the data. Maximum likelihood is an example for the same. Explicit density models define an explicit density function. Then, it tries to maximize the likelihood of that function on the training data. They can be subdivided into tractable density and approximate density. Tractable density models can define a parametric function that is able to capture the distribution effectively. But many of the real-world data generating distributions are complex, and it is difficult to design a parametric function to capture them. Approximate density models are those that do not have a parametric function to capture the distribution. Implicit density estimators model a stochastic procedure that can directly generate data. GANs are an example for the same.

3.1 Autoencoders

Autoencoders (AE) [6] are an unsupervised way for learning the lower-dimensional feature representations and are comprised of two connected components: the encoder (E) and the decoder (D). The aim of E is to take an input (x) and produce a feature map (Z). Z captures the meaningful information that can be used to describe the input data and variation in the data. Autoencoders are trained in an unsupervised way such that the features can be used to reconstruct the original data by the decoder (D).

3.2 Variational Autoencoders

The difference between a traditional autoencoder and variational autoencoder (VAE) [6] is that instead of directly extracting the features from the input data, VAE tries to model the probability distribution of the training data. In VAE, the encoder instead of producing an encoding vector of size n constructs two vectors of size ‘ n ’ which are the mean and standard deviation. In the architecture of VAE, the mean is used to control the position where the encoding of the input should be centered around. The standard deviation is used to control how much the mean encodings can vary. The loss function used to train the VAE is the Kullback–Leibler divergence. KL divergence measures how different the two probability distributions are. VAE has to be trained to minimize the KL divergence by optimizing the parameters of the probability distribution such as the mean and standard deviation.

3.3 *Generative Adversarial Networks*

GANs [6] are unsupervised generative models which constitute two neural networks: the generator G and the discriminator, D competing with each other for a joint learning process. At the end of this minimax game, the G and D interaction renders into a general objective for the GAN architecture as given in Eq. 1 [14]. The generator takes in a latent vector, ‘ z ’ usually sampled from the gaussian distribution to generate fake samples similar to that of the real samples under consideration. The discriminator usually performs the task of categorizing whether the incoming sample is coming from the fake distribution or the real distribution. GANs try to make generated distribution look similar to the real one by minimizing the underlying cost function.

$$\begin{aligned} V(D, G) = \min \theta_g \max \theta_d &[E_{X \sim p_{da}}(X)[\log D_{\theta d}(X)] \\ &+ E_{Z \sim p_Z(Z)}[\log(1 - (D_{\theta d}(G_{\theta g}(Z))))]] \end{aligned}$$

G wants to maximize this cost which infers that D is performing poorly and is classifying fake ones as real; whereas, D wants to minimize this cost function which infers that it is classifying correctly.

As the D has an easy task, it can become superior soon, then D may start providing less informative feedback for updating G . This can lead to vanishing gradient problems and mode collapse issues.

4 Background on Adversarial Machine Learning

Adversarial machine learning (AML) is a confluence of learning techniques and security issues that may affect the learning techniques. Adversarial attacks can be launched on learning techniques by violating few statistical assumptions made underneath such as satisfying the identically and independently distributed (IID) assumption. An adversarial sample is one in which perturbations have been added [17, 20]. In the machine learning model development process, if the attack is launched on the training process, it is known as poisoning attacks, and if it happens during inference phase, it is termed as evasion attacks. Depending upon how much information the attacker has, the adversarial attacks can be classified into white box and black box attacks.

5 Proposed Methodology

This article coheres into security attacks in healthcare sectors. Dataset comprising of medical apps infused with malware is not publicly accessible, so to demonstrate the considered usecase as a proof of concept, the Drebin dataset [5] comprising of 5560

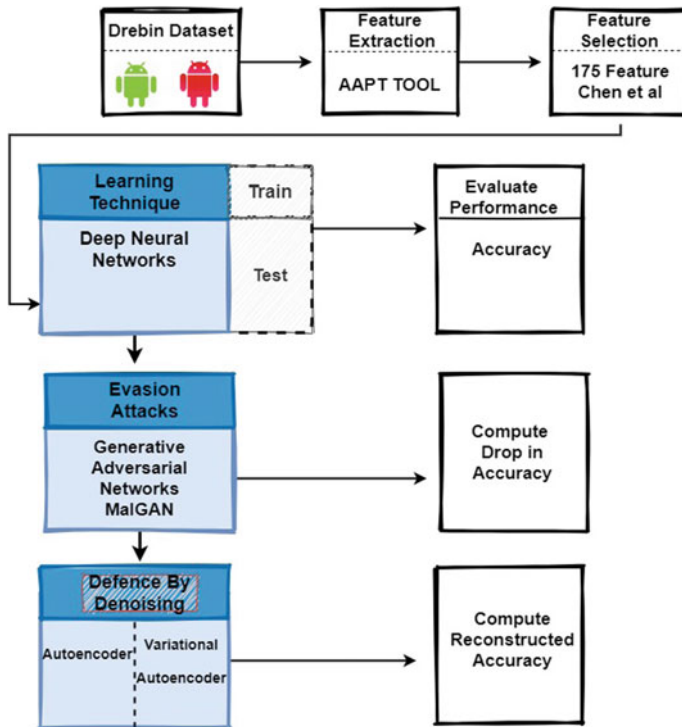


Fig. 2 Flow diagram of the proposed work

malicious and 123,453 benign Android applications is considered for this research. Assumption made is that the malware apps considered can be medical apps or health-care services apps infused with malware simulating a trojan horse effect. Based on this considered assumption, the validity of the hypothesis considered is evaluated. Malware-infused medical apps try to bypass detection by anti-Malware solutions [17, 20]. Malware detectors deploying learning-based techniques are vulnerable to adversarial attacks. Hence, evasion attacks in a black box setting are considered in the proposed work along with possible defense options as given in Fig. 2.

5.1 Feature Extraction

Android applications can be reverse engineered for malware analysis in two ways, namely static analysis and dynamic analysis [17]. Static analysis analyzes the source code of the applications without running them, and dynamic analysis analyzes the

source code by running the application on a sandbox or emulator and gathers the behaviors of the application during run time. In the proposed work, static analysis is performed using AAPT tool [1].

5.2 Feature Selection

Every application exhibits only few features from the entire feature set. Feature selection is an important step since it affects the performance of the classifier by limiting the number of input features. To reduce the computation cost and to speed up the crafting process of adversarial examples, more appropriate features must be selected. To select the features, the method proposed by Chen et al. [8] is utilized for the proposed work which comprises of 175 chosen syntax features as shown in Fig. 3.

5.3 Model Building

A binary feature vector represents each apk file. The presence or absence of a unique API call is represented by a ‘1’ or ‘0’ at a particular index location of the feature vector. A deep neural network (DNN) is considered for model building. The Drebin dataset is split into 80 and 20% for training and testing purposes. The input layer

PERMISSION	SET_WALLPAPER	TelephonyManager.getSubscriberId	LocationManager.addNmeaListener
ACCESS_COARSE_LOCATION	SET_WALLPAPER_HINTS	TelephonyManager.getVoiceMailNumber	LocationManager.addProximityAlert
ACCESS_FINE_LOCATION	STATUS_BAR	TelephonyManager.hasSailfishCard	LocationManager.addTestProvider
ACCESS_LOCATION_EXTRA_COMMANDS	SYSTEM_ALERT_WINDOW	SmallFileTransferManager.setNetworkRoaming	LocationManager.addTestProviderLocation
ACCESS_NETWORK_STATE	USER_DEVICE_STATS	SmsManager.getDefault	LocationManager.getGpsStatus
ACCESS_WIFI_STATE	USE_CREDENTIALS	SmsManager.sendDataMessage	LocationManager.getLastKnownLocation
AUTHENTICATE_ACCOUNTS	VIBRATE	SmsManager.sendMultiPartTextMessage	LocationManager.requestLocationUpdates
BATTERY_STATS	WAKE_LOCK	SmallFileTransferManager.setNetworkRoaming	LocationManager.removeExtraCommand
BLUETOOTH	WRITE_APP_SETTINGS	HttpURLConnection.disconnect	WifiManager.addNetwork
BROADCAST_SMS	WRITE_SETTINGS	HttpURLConnection.getContentEncoding	WifiManager.calculateSignalLevel
BROADCAST_STICKY	WRITE_SMS	HttpURLConnection.getPermission	WifiManager.createWifiLock
CALL_PHONE	WRITE_EXTERNAL_STORAGE	HttpURLConnection.getResponseCode	WifiManager.enableNetwork
CAMERA	INTERNET	HttpURLConnection.getResponseMessage	WifiManager.getBackgroundNetwork
CHANGE_COMPONENT_ENABLED_STATE	action.DELETE	HttpURLConnection.useProxy	WifiManager.getConnectionInfo
CHANGE_CONFIGURATION	action.GET_CONTENT	ContentResolver.bulkInsert	WifiManager.getDhcpInfo
CHANGE_NETWORK_STATE	action.MAIN	ContentResolver.getType	WifiManager.getNetworkResults
CHANGE_WIFI_MULTICAST_STATE	action.MOUDLE_ID	ContentResolver.openAssetFileDescriptor	WifiManager.setWlState
CHANGE_WIFI_STATE	action.SET_WALLPAPER	ContentResolver.query	WifiManager.wifiEnabled
CLEAR_APP_CACHE	action.VIEW	ContentResolver.registerObserver	WifiManager.removeNetwork
CONTROL_LOCATION_UPDATES	category.BROWSABLE	ContentResolver.update	WifiManager.saveConfiguration
DELETE_CACHE_FILES	category.DEFAULT	ContentResolver.unregisterObserver	WifiManager.setConfiguration
DELETE_PACKAGES	category.HOME	Runtime.delete	NotificationManager.cancel
DISABLE_KEYGUARD	category.INFO	Runtime.exec	NotificationManager.notify
EXPAND_STATUS_BAR	category.LAUNCHER	Runtime.addShutdownHook	PackageManager.checkPermission
FLASHLIGHT	HARDWARE	Runtime.setMaxMemory	PowerManager.inInteractive
GET_PACKAGE_SIZE	camera.autofocus	URLConnection.addRequestProperty	PowerManager.setScreenOn
GET_TASKS	sensor.accelerometer	URLConnection.connect	PowerManager.setWakeLock
INSTALL_PACKAGES	telephony	URLConnection.getConnectTimeout	SEMANTIC
INTERNET	touchscreen	URLConnection.getContent	"Install application"
KILL_BACKGROUND_PROCESSES	APN_CALL	URLConnection.getDefaultType	"Uninstall application"
MODIFY_PHONE_STATE	URL.openConnection	URLConnection.getDefaultUseCaches	"Get installed packages"
MOUNT_UNMOUNT_FILESYSTEMS	URL.openStream	URLConnection.getPermission	"Monitor URI"
NFC	URL.getContent	URLConnection.getURL	"Download file"
PERSISTENT_ACTIVITY	TelephonyManager.getCallState	URLConnection.setReadTimeout	"Get location"
PROVIDE_OOOGING_CALLS	TelephonyManager.getCallLocation	URLConnection.setReadTimeout	"Read SD card"
READ_CALL_LOGS	TelephonyManager.getDeviceId	ActivityManager.getLargeMemoryClass	"Write SD card"
READ_CONTACTS	TelephonyManager.getDeviceSoftwareVersion	ActivityManager.getRunningAppProcesses	"Request for chmod"
READ_EXTERNAL_STORAGE	TelephonyManager.getExternalStorageGpsInfo	ActivityManager.isLowRamDevice	"Start http connection"
READ_LOGS	TelephonyManager.getGpsInfo	ActivityManager.killBackgroundProcesses	"Send file"
READ_PHONE_STATE	TelephonyManager.getGsmOperator	ActivityManager.restartPackage	"Receive Sms"
READ_PROFILE	TelephonyManager.getNetworkOperatorName	BluetoothAdapter.cancelDiscovery	"Delete Sms"
READ_SMS	TelephonyManager.getNetworkType	BluetoothAdapter.getAddress	"Intercept Sms receiver"
RECEIVE_BOOT_COMPLETED	TelephonyManager.getPhoneType	BluetoothAdapter.getBondedDevices	"Get wifi info"
RECEIVE_SMS	TelephonyManager.getSimCountryIso	BluetoothAdapter.getConnectedDevice	"Get file"
RECEIVE_WAP_PUSH	TelephonyManager.getSimOperator	BluetoothSocket.connect	"Get Class loader"
RECORD_AUDIO	TelephonyManager.getSimOperatorName	DownloadManager.enqueue	"Get contacts"
RESTART_PACKAGES	TelephonyManager.getSimSerialNumber	DownloadManager.query	"Get account"
SEND_SMS	TelephonyManager.getSimState	LocationManager.addGpsStatusListener	"Get phone type/Sim serial number/device id/subscriber id/IMSI"

Fig. 3 175 features selected from Drebin dataset by Chen et al. [8]

consists of 175 nodes, and the final layer comprises of a single node to classify between benign and malicious applications. Different configurations are set for the neural network by varying the values of the hyperparameters like the number of hidden layers and also by varying the number of neurons per layer in the range (10,300) which are empirically tried, and the resulting performance metrics such as false positive rates (FPR), false negative rates (FNR) and accuracy are listed in Fig. 4. Accuracy is computed as the correct number of predictions made by the model to the total number of possible predictions. Also, for every neuron in the hidden layer, rectified nonlinearity is chosen as the activation function with the final layer having softmax activation function. Based on the tabulation, 175-256-256-1 is chosen as the final model, F with 98.76% test accuracy.

S. No.	No. of Neurons in the hidden layer	Accuracy		FPR		FNR	
		Epoch=6	Epoch=8	Epoch=6	Epoch=8	Epoch=6	Epoch=8
1	[200]	0.9845	0.9853	0.28	0.26	0.07	0.07
2	[256,256]	0.9876	0.9793	0.26	0.22	0.06	0.07
3	[10,10]	0.9782	0.9822	0.35	0.33	0.09	0.12
4	[10,200]	0.9815	0.9866	0.36	0.30	0.07	0.1
5	[200,10]	0.9853	0.9852	0.36	0.24	0.07	0.07
6	[50,50]	0.9843	0.9859	0.38	0.25	0.06	0.08
7	[50,200]	0.9852	0.9865	0.3	0.25	0.07	0.06
8	[200,50]	0.9854	0.9866	0.13	0.22	0.07	0.07
9	[100,200]	0.9846	0.9865	0.27	0.22	0.06	0.07
10	[200,100]	0.9858	0.9871	0.26	0.22	0.06	0.07
11	[200,200]	0.9850	0.9872	0.28	0.22	0.04	0.07
12	[200,300]	0.9852	0.9873	0.26	0.23	0.06	0.06
13	[300,200]	0.9852	0.9874	0.29	0.22	0.04	0.07
14	[200,200,20 0]	0.9851	0.9874	0.24	0.28	0.06	0.09
15	[200,200,20 0,200]	0.9858	0.9875	0.24	0.21	0.06	0.08

Fig. 4 Performance of DNN

5.4 Performing Evasion Attacks

The perturbations added to the malicious sample ($x_{test_mal_clean}$) which when fed to the trained model cause the model to get confused, and the model misclassifies the noisy malware ($x_{test_mal_noisy}$) sample as a benign entity as shown in Fig. 5. Adversarial samples are crafted using black box evasion attacks by utilizing a generative adversarial network, MalGAN as given publicly in [14]. The generator architecture used is tabulated in Fig. 6. The MalGAN simulates a feature vector for an Android application which is malicious with considerable modifications (additions) to the features. The attacked model's test accuracy when injected with adversarial samples is reduced to 8.3%

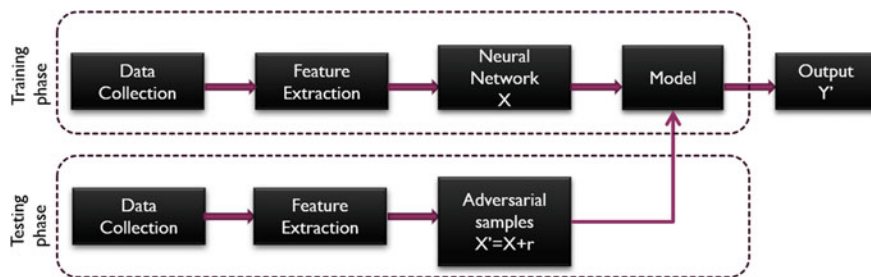


Fig. 5 Adversarial sample (X') crafted at test time for input pair (X, Y) by adding the noise perturbation ' r '

generator- summary:

Layer (type)	Output Shape	Param #	Connected to
input_2 (InputLayer)	(None, 175)	0	
input_3 (InputLayer)	(None, 25)	0	
concatenate_1 (Concatenate)	(None, 200)	0	input_2[0][0] input_3[0][0]
dense_3 (Dense)	(None, 256)	51456	concatenate_1[0][0]
dense_4 (Dense)	(None, 175)	44975	dense_3[0][0]
activation_2 (Activation)	(None, 175)	0	dense_4[0][0]
maximum_1 (Maximum)	(None, 175)	0	input_2[0][0] activation_2[0][0]

Total params: 96,431
Trainable params: 96,431
Non-trainable params: 0

Fig. 6 GAN architecture used for crafting adversarial samples

5.5 Defense by Denoising

Defense techniques for overcoming evasion attacks considered in this proposed method are to actively detect the adversarial perturbations by denoising techniques which would remove the perturbations inserted during evasion attack. The options considered are denoising generative models such as autoencoder and variational autoencoder [6]. The architecture considered for the purpose of denoising is given in Figs. 7 and 8. The samples obtained after denoising are again fed into the trained model F for prediction, and reconstructed accuracy is computed which is tabulated in Table 1. From the results, it can be clearly inferred that the test accuracy of the DNN model built is 98.76% from which the accuracy drops to 8.3% based on the adversarial samples crafted using the MalGAN attack. The reconstruction accuracy obtained is 11.3% when using an AE and 13.2% for a VAE. The results do not show significant improvements in the reconstructed accuracy or in the quality of perturbation elimination on the adversarial samples considered which highlights the need for improvements. Rosenberg in [24] has considered similar approach of using generative models for denoising adversarial samples for the same malware domain but utilizes recurrent neural network for the classification task. Rosenberg et al. [24] also affirm the fact that the considered problem statement in the malware space is an upcoming research area. This motivates for future research to resolve the gaps identified and provide improved comparable results.

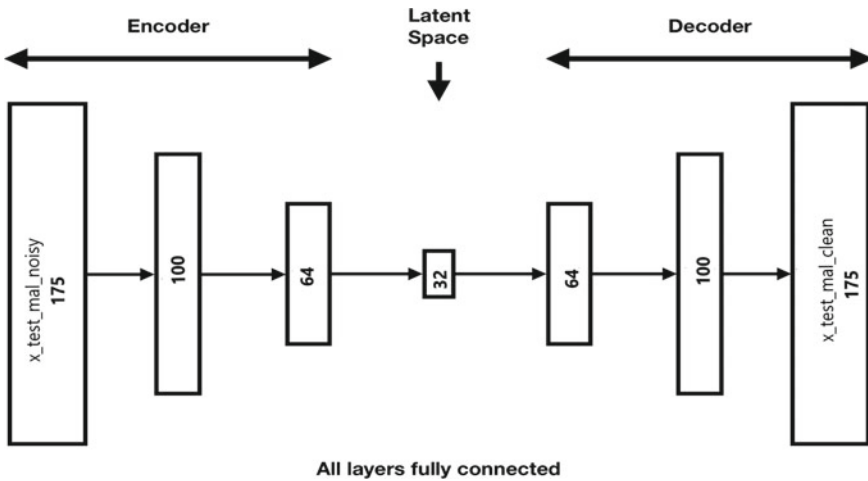


Fig. 7 Autoencoder architecture for denoising

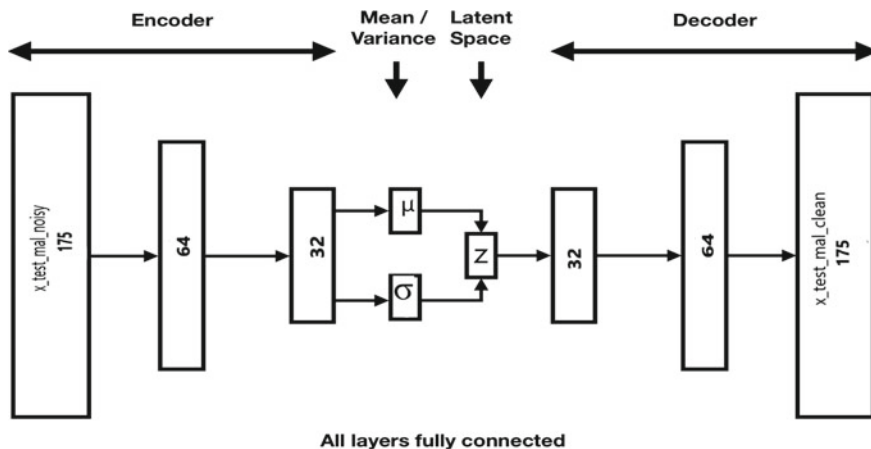


Fig. 8 Variational autoencoder architecture for denoising

Table 1 Performance of DNN classifier for no attack, no defense, defense by denoising approach

Classifier/architecture	Accuracy (Test time) no attack (%)	Accuracy after MalGAN attack, no defense (%)	Accuracy reconstructed from AE (%)	Accuracy reconstructed from VAE (%)
DNN/175-256-256-1	98.76	8.3	11.3	13.2
175-125-75-10-1	97	6.1	7.9	9.4

6 Conclusion and Future Work

Healthcare organizations work toward providing better facilities to patients. HCOs should also focus on thwarting cyber security attacks from malware-infused medical apps by deploying better malware detectors in their end point security solutions. But malware detectors employing learning-based techniques are vulnerable to adversarial attacks. This article takes into consideration a case study of Android applications with the possibility of the dataset comprising malware-infused medical apps to which a DNN model is fitted and computes the test time prediction accuracy. GAN-based adversarial attack technique is utilized to craft adversarial samples by perturbing the malicious samples. These adversarial samples when fed to the trained DNN are misclassified as benign samples. Based on this, the drop in accuracy is computed. Defense techniques suggested are the utilization of generative models available for the purpose of denoising such as AE and VAE. The initial results observed are not satisfactory and suggest for more scope of improvements. HCOs have to adapt to the cyber security aware best practices for being safe against malware attacks [4].

References

1. AAPT. <https://developer.android.com/studio/command-line/aapt2/> (2020)
2. Afianian A, Niksefat S, Sadeghiyan B, Baptiste D (2018) Malware dynamic analysis evasion techniques: a survey. arXiv preprint [arXiv:1811.01190](https://arxiv.org/abs/1811.01190)
3. Ahmed Y, Naqvi S, Josephs M (2019) Cybersecurity metrics for enhanced protection of health-care it systems. In: 2019 13th international symposium on medical information and communication technology (ISMICT). IEEE, pp 1–9
4. Argaw ST, Bempong N-E, Bruce E-C, Flahault A (2019) The state of research on cyberattacks against hospitals and available best practice recommendations: a scoping review. BMC Med Inf Decis Making 19(1):1–11
5. Arp D, Spreitzenbarth M, Hubner M, Gascon H, Rieck K, Siemens CERT (2014) Drebin: Effective and explainable detection of android malware in your pocket. Ndss 14:23–26
6. Bengio Y, Goodfellow I, Courville A (2017) Deep learning, vol 1. MIT Press Massachusetts
7. Buijink AWG, Visser BJ, Marshall L (2013) Medical apps for smartphones: lack of evidence undermines quality and safety. BMJ Evid Based Med 18(3):90–92
8. Chen S, Xue M, Fan L, Hao S, Xu L, Zhu H, Li B (2018) Automated poisoning attacks and defenses in malware detection systems: an adversarial machine learning approach. Comput Secur 73:326–344
9. epocrates. <https://www.epocrates.com/> (2020)
10. Faruki P, Bharmal A, Laxmi V, Ganmoor V, Singh Gaur M, Conti M, Rajarajan M (2014) Android security: a survey of issues, malware penetration, and defenses. IEEE Commun Surv Tutor 17(2):998–1022
11. glucosebuddy. <https://www.glucosebuddy.com/> (2020)
12. Hathaliya JJ, Tanwar S (2020) An exhaustive survey on security and privacy issues in healthcare 4.0. Comput Commun 153:311–335
13. Hipaa. <https://www.atlantic.net/hipaa-compliant-hosting/healthcare-cybersecurity-in-2019-lessons-weve-learned/> (2019)
14. Hu W, Tan Y (2017) Generating adversarial malware examples for black-box attacks based on gan. arXiv preprint [arXiv:1702.05983](https://arxiv.org/abs/1702.05983)
15. Kareo. <https://www.kareo.com/> (2020)
16. Li D, Li Q, Ye Y, Xu S (2020) Enhancing deep neural networks against adversarial malware examples. arXiv preprint [arXiv:2004.07919](https://arxiv.org/abs/2004.07919)
17. Li D, Li Q, Ye Y, Xu S (2020) Sok: arms race in adversarial malware detection. arXiv preprint [arXiv:2005.11671](https://arxiv.org/abs/2005.11671)
18. Newaz AKM, Sikder AK, Rahman MA, Selcuk Uluagac A (2020) A survey on security and privacy issues in modern healthcare systems: Attacks and defenses. arXiv preprint [arXiv:2005.07359](https://arxiv.org/abs/2005.07359)
19. Or Meir O, Nissim N, Elovici Y, Rokach L (2019) Dynamic malware analysis in the modern era—a state of the art survey. ACM Comput Surv (CSUR) 52(5):1–48
20. Papernot N, McDaniel P, Sinha A, Wellman MP (2018) Sok: security and privacy in machine learning. In: 2018 IEEE European symposium on security and privacy (EuroS&P). IEEE, pp 399–414
21. Paramedic Protocol Provider. <https://play.google.com/store/apps/details?id=com.acidremap.paramedicprotocolprovider> (2020)
22. Qamar A, Karim A, Chang V (2019) Mobile malware attacks: review, taxonomy & future directions. Future Gener Comput Syst 97:887–909
23. Temperature Body Health Recorder. <https://play.google.com/store/apps/details?id=com.appcare.bodyrecordhealth/> (2020)
24. Rosenberg I, Shabtai A, Elovici Y, Rokach L (2019) Defense methods against adversarial examples for recurrent neural networks. arXiv preprint [arXiv:1901.09963](https://arxiv.org/abs/1901.09963)
25. Sen S, Aydogan E, Aysan AI (2018) Coevolution of mobile malware and anti-malware. IEEE Trans Inf Forens Secur 13(10):2563–2574

26. TousAntiCovid. <https://play.google.com/store/apps/details?id=fr.gouv.android.stopcovid/> (2020)
27. Ucci D, Aniello L, Baldoni R (2019) Survey of machine learning techniques for malware analysis. *Comput Secur* 81:123–147
28. Veerappan CS, Keong PLK, Tang Z, Tan F (2018) Taxonomy on malware evasion countermeasures techniques. In: 2018 IEEE 4th world forum on internet of things (WF-IoT). IEEE, pp 558–563

Human Identification System Based on Latent Fingerprint



Shashi Shreya and Kakali Chatterjee

Abstract Latent fingerprint is a very sensitive topic in digital forensic as a final verdict can be given to the criminal on its basis. This sensitiveness is due to two main reasons: (1) uniqueness of fingerprint in every human existence is proven to be a universal truth, and (2) latent fingerprint is a type of fingerprint which is not visible through the naked eye and gets deposited to the surface by the person unintentionally, telling the story of his/her presence. From the past 50 years, latent is used as human identification in forensics. These identification phases have many simultaneous steps such as data collection, preprocessing, extraction, matching and decision. Earlier these steps are performed manually but gradually the world moved to the automatic system with invention of technology. Since then there is a lot of evaluation of techniques, methods or algorithms, it happens in different aspects of identification system phases. One of the steps is the extraction phase, which includes three levels. There are a lot of existing models based on Level-1 (features: ridge pattern) and Level-2 (feature: minutiae) but very few have worked in the field of Level-3 (Features: pores) feature extraction. In this paper, we have described an identification framework which uses pores-based feature extraction. This method is compared with some other popular extraction methods like inversion and Gabor filter. Results of experiments in Tables 1 and 2 show that the performance rate of CNN is better than inverse and Gabor filter.

Keywords Latent fingerprint · Feature extraction · Level-1 · Level-2 · Level-3

S. Shreya (✉) · K. Chatterjee

Computer Science and Engineering, National Institute of Technology Patna, Patna, Bihar 800005, India

e-mail: shashis.phd19.cs@nitp.ac.in

K. Chatterjee

e-mail: kakali@nitp.ac.in

1 Introduction

There is a growing demand for personal identification systems that are reliable, supported by advanced technology and having good data handling capacity in today's world. Fingerprint biometric traits are fulfilling these demands in one way and had spreaded its area in forensic and civil applications. Forensic applications such as in access control systems, financial transaction systems, border security, crime scene analysis and civil application such as Aadhar Project [1]. As a result, a lot of law enforcement agencies is utilizing latent fingerprint authentication technique from the past hundred years to prove a crime and provide justice to people [2–5]. Latent fingerprint deposits on the surface unintentionally and is invisible until it goes through some chemical process by the experts, so it becomes a sensitive data in identification process that acts as a clue to the crime investigating officer to catch the criminal. There are two ways for identification—manual and automated. Earlier manual system: "ACE-V" that stands for analysis, comparison, evaluation and verification was in practice. But with the invent of "automated fingerprint recognition system" method for latent fingerprint, it has created a revolution. The automated fingerprint identification system (AFIS) technique includes phases, which is (1) enrolment (2) features extraction, (3) matching and (4) decision. The main aim to shift from manual to automatic identification system is to reduce human intervention. For example, it takes approx 1 h, 53 min and 12 s by FBI's current AFIS to do fingerprint image matching with 73.1 million references enroled fingerprint [1].

Features of latent fingerprint represent the basic building block of person-related identity whose sharing and misplacement are not possible. In technical terms, we can say that its body measurements and its calculations for making a unique password for everyone cannot be forgotten, lost and not even pass further to another individual. Uniqueness depends upon how precise the feature is extracted. Maltoni et al. [6] have categorized latent fingerprint features into three levels, namely Level-1 includes overall ridge flow pattern, Level-2 includes minutiae points which are unique in nature in every human being, and Level-3 includes dots, pores and incipient ridges [1]. Commonly used feature in automatic fingerprint identification systems (AFIS) is minutiae from Level-2 [7] because ridge flow pattern from the Level-1 feature is not a unique feature. Ridge is only a subset from whole details of the latent fingerprint. To make more clear, Level-1 features (ridge) are merged with Level-2 feature(minutiae). Still, existing AFIS is not satisfying the need of identification accuracy to the law enforcement or justice system [8]. This is because of image quality and quantity. A latent fingerprint is lifted from the evidence collected from the crime area, which may contain more than two fingerprints in an overlapped fashion, different types of noise like arch and lines or it can be of very low quality due to less pressure applied by the suspects. Hence, there are very few cases where the whole fingerprint is found; otherwise, a small portion is obtained after segmentation and enhancement for feature extraction. As a result, very less amount of feature from Level-1 and Level-2 is gathered that can be questioned in a court of law. Biometric authentication systems with these two levels (Level-1 & Level-2) have to speed up the court decisions

and lower the human expert's intervention, making investigation easy but it is not enough. The latent fingerprint misidentification due to the small number of details can damage an innocent person's life. Some of the case studies show how wrong matching can harm people.

- Shirley Mckie is Scottish police. He was wrongly charged for the murder of Marion Ross after her fingerprints were found at the crime scene [1]. There was no formal apology.
- Brandon Mayfield is an American lawyer. He was wrongly arrested bombarding in 2004. He suffers from 2 months allegation and 14 d imprisonment. Later FBI announced the formal apology [9].

It has been stated in [7] that to upgrade the AFIS performance, Level-3 features must come into consideration. It works in a small portion with the same accuracy as it works on a large portion. However, pores are not used directly in forensic practices. This can be helpful for the case where image area or minutiae count is too small to make a decision. In this paper, it has been considered that a small portion of the latent fingerprint is obtained after segmentation of all type of noise. So, the system is able to extract very few details of Level-1 and Level-2. It may cause a false decision. For example, there is a small section of two different latent fingerprint images that has the same ridge orientation and minutiae point (bifurcation and ridge ending). This error can be solved using the third level (Level-3) of features. This Level-3 focuses on pores that are categorized in two forms, either open pores or closed pores, depending upon its penetration due to sweat. Pores are fixed feature developed on the ridge of the human body since the sixth month of gestation because of sweat glands ducts reaching the surface of the epidermis of a finger. About 9–18 pores can be found on a ridge within a centimetre [6]. Hence, it becomes an important and sensitive data to be used in identification. The major contribution of this paper is

- A biometric identification framework has been proposed which mainly use latent fingerprint.
- In this proposed framework, Level-3 features have been used for automated identification system.

The organization of the paper is as follows: Sect. 2 describes literature survey; Sect. 3 discusses the proposed framework; Sect. 4 provides a detailed description of results and performance analysis; Sect. 5 concludes the paper with future work discussion.

2 Literature Survey

This section is all about surveys related to Level-3 features of the latent fingerprint which is our main focus in the whole human identification system. Based on the observation from the literature survey, pore extraction methods are changing with time. Earlier in [10–12], fingerprint images are processed to be binarized and then skeletonized, after which the fingerprint skeleton is tracked to find pores. During this

tracking, the system is bound to meet specific criteria to detect a pore. This type of model has limitations like skeletonization computation of fingerprint is expensive, noise sensitivity and restricted to work only on high-resolution and high-quality images.

To resolve the existing model limitations, filtering-based methods are in the spotlight. This type of methods detects pores with the help of pore models such as Ray's model [13], Jain's model [14] and the difference of Gaussian (DoG) model [15]. Ray's model was proposed by Ray et al. to extract pores using modified two-dimensional Gaussian function-based pore model. Moreover, Ray's pore model is isotropic, but the appearance of open pores on real fingerprint images is not isotropic. Jain's model was proposed by Jain et al. to extract pores using the Mexican hat wavelet transform for the specific data set by observing the fact that pore regions typically have a high negative frequency response as intensity values change abruptly from bright to dark at the pores. Moreover, Jain's model is only limited to a specific data set. It cannot work for other fingerprint or other areas on the fingerprint. Coming to difference of Gaussian (DoG) model proposed by Parsons et al., it detects pores by using a band-pass filter, assuming pores as a circle like features. This model also has limitations such as unitary scales which are used instead of considering the pore scales variation within the fingerprint image. All these three models are isotropic pore models.

In 2010 [16], Qijun et al. proposed a novel pore model as well as an extraction method to solve the problem of existing isotropic pore model. They presented a dynamic anisotropic pore model in which orientation and scale parameters are used to obtain more accurate pores. Based on the dynamic anisotropic pore model, an adaptive pore extraction method was also proposed. Although it is better than above-mentioned approaches, but it is limited to adapt a variety of shape and size in terms of single as well as different person [17]. Many different techniques using different algorithms for the different scenario are also proposed such as in 2016, Angelo et al. proposed a first-ever method that will extract the Level-3 features (sweat pores) from the fingerprint images. These images are a touchless acquisition and captured with a shelf camera. In 2017 [18], Jang et al. proposed a pore extraction method using deep ConvNet (CNN). In 2018 [19], Donida et al. proposed a method that can extract the pores coordinates from all type of fingerprint, either touchless or touch-based and latent fingerprint images using ConvNet (CNN). From all the literature survey, it is found that only this model [7] is considering a latent fingerprint image unlike plain and rolled fingerprint of high quality and resolution. Another approach proposed in 2019 [20] by Nguyen, Dinh-Luan and Anil K. Jain is particularly for latent fingerprint images. It first performs enhancement to reduce the noise and then extract the pores by using neighbourhood connected component.

3 Proposed Model

This section represents pore-based latent fingerprint biometric traits for human authentication system in forensic. The proposed human identification framework

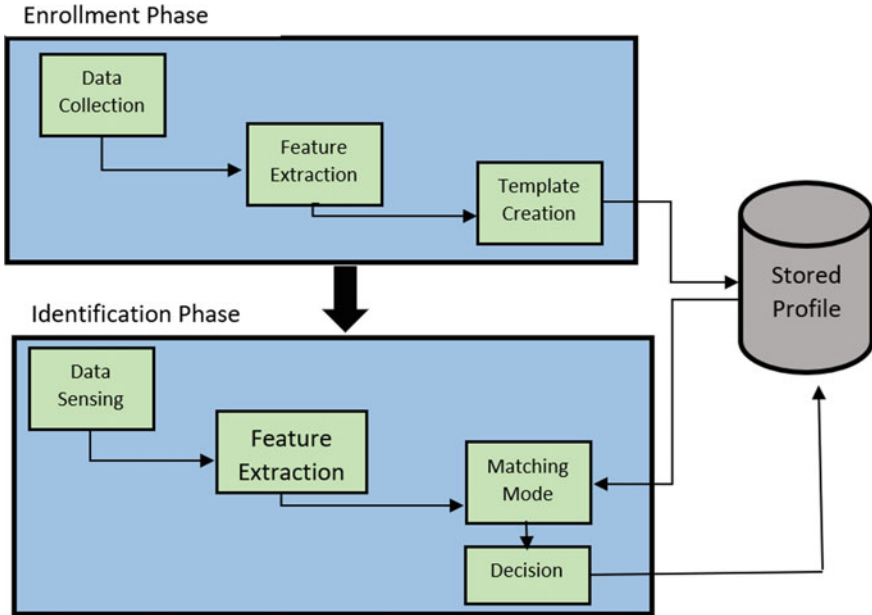


Fig. 1 Framework of the proposed model

for forensic is shown in Fig. 1. This framework is designed by keeping a particular crime scene seized by the forensic particular which is elaborated below in Sect. 3.1.

This framework includes two phases: enrolment phase and identification phase. As discussed previously, a lot of existing approaches are present to deal with identification. As far as feature extraction is concerned, most of the systems are based on ridge orientation flow and minutiae, i.e. Level-1 and Level-2. But they are not suitable for the situation where a forensic officer manages to collect very noisy latent fingerprint from the crime area, and a small portion of the latent fingerprint image is obtained. So in this paper, pore-based feature extraction is taken into consideration. From the literature, it is seen that most of the methods for pores extraction are developed using machine learning (ML) approach [18, 19] and feature-based approach [16] except [17] that have deep machine learning concept. This paper focuses on machine learning algorithm discussed below for pore extraction.

3.1 Description of Forensic's Crime Scenario

In this section, the crime scene is described as shown in Fig. 2. A party club is considered where registered people are allowed. A ticket is collected by a person at the entrance of the club. This entry ticket is generated after filling registration form which includes respective person's details along with the phone number. It is

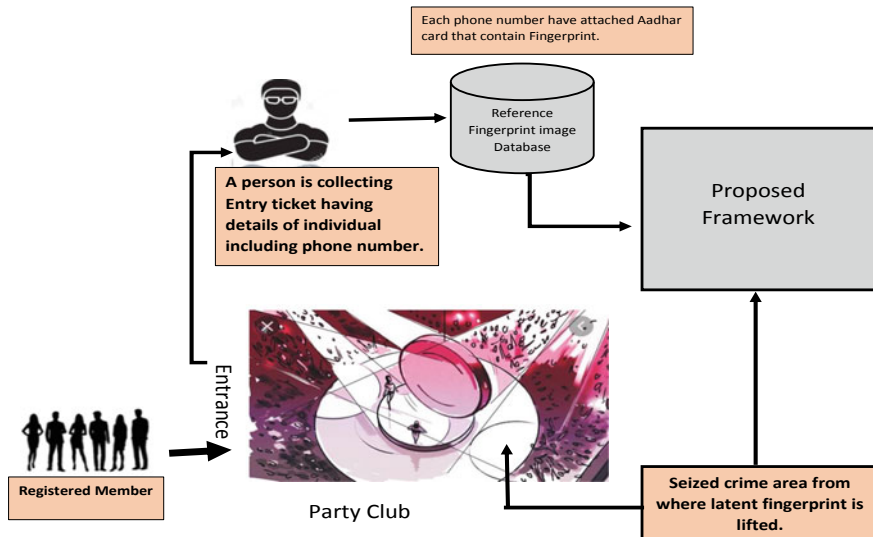


Fig. 2 Description of crime scenario

assumed that a person within the club commits a crime when the light was low and stays salient. After the incident, FIR is filed and an investigation officer is appointed to the crime scene. The officer collected many evidences along with latent fingerprint. As there was a party going on and the area was crowded, very noisy (overlapped fingerprint, cut mark, arc, etc.) latent fingerprint is collected. Hence, it has to go through Level-3 (pores) feature extraction process to get a more accurate result. For that latent image, the input is given in the proposed framework and matched against the reference data. This reference data is a real data, stored by the central agency against registered phone number of the user during the issue of an identity card such as Adhaar card and Voter card.

3.2 Enrolment Phase

Data Collection This is the first step of the automated fingerprint identification system (AFIS). Data collection—the image gathered through some chemical process with the evidence collected by the investigation officer is given as input to the system.

Feature Extraction The observation says that pores have features like very small size, round in shape and present on friction ridges. It uses a high-resolution image, which is not a major concern nowadays with the advancement in cameras and its capture technology. CNN is a technique, which stands robust enough to adapt parameters of feature extraction. It can learn pore's salient features without any image characteristics assumptions.

Pore-based feature extraction through CNN [19] is described below:

- **Step 1: Pore Detection**

Network working: Pores are detected in here through the network as C_D which takes a greyscale image as input, let I_m of $m \times n$ pixel. CNN architecture of this paper uses convolutions layers and pooling layers. There are five layers of the network, out of which three are convolutional layers and two are max-pooling layers.

There are five filters in the first convolutional layer whose size = $(P_1 \times P_1)$ pixels, strides = $(1,1)$ and padding = $(\frac{P_1-1}{2}, \frac{P_1-1}{2})$. Then comes the second layer, that is the max-pooling layer with 3×3 pixel kernel.

About 15 filters are there in third layer of CNN and second convolutional layer whose size = $(P_2 \times P_2)$ pixels, strides = $(1,1)$ and padding = $(\frac{P_2-1}{2}, \frac{P_2-1}{2})$. Then again comes the max-pooling layer with 3×3 pixel kernel in the fourth layer of CNN.

Similarly, the fifth layer of CNN and last convolutional layer is computed but it has only one filter of size = $(P_3 \times P_3)$, strides = $(1,1)$ and padding = $(\frac{P_3-1}{2}, \frac{P_3-1}{2})$.

In this CNN approach, the size of the image remains the same as compared to others, where the size gradually decreases after each layer.

In brief, these process and layers result in the enhancement of the pores by removing the image's ridge pattern. In here the input is taken as I map by the convolutional layers which applies k two-dimensional filters, say F with basis B. The output given for each of the coordinate (x, y) is , say O is given as

$$O_{x''y''} = B + \sum_{x'=1}^{h'} \sum_{y'=1}^{w'} F_{x'y'} \times I_{x''+x'-1, y''+y'-1} \quad (1)$$

with $I \in \mathbb{R}^{h \times w}$, and $F \in \mathbb{R}^{h' \times w'}$, where h is height and w is weight dimensions.

After convolutional layer, the max-pooling layer will compute maximum response of each feature in $h' \times w'$ using max-pooling operator and give output through equation-2 resulting in size = $O \in \mathbb{R}^{h'' \times w''}$.

$$O_{x''y''} = \max_{1 \leq x' \leq h', 1 \leq y' \leq w'} I_{x''+x'-1, y''+y'-1} \quad (2)$$

In between the process, empirical tuning of different layers, kernel's size of convolutional as well as max-pooling and the strides are performed when needed. The image obtained after travelling through the layers is named as I_f .

Training: C_D is trained with the help of stochastic gradient descent with momentum algorithm [21]. Starting with filters weight initialization with the help of Gaussian distribution through random sampling and by putting mean (0) and standard deviation (0.01).

The training aims to develop a CNN which yields pores centre intensity as 1 and other as -1. To achieve this aim, a data set having multiple images is labelled and used for training. These labels are 1 for pore's centroid representing pixels, 0 for pixel across the circle with radius ' r ' as well as the centre of the pore centroid, and -1 for rest of the pixels.

Step 2: Pores Coordinates Estimation

A matrix (M) having Cartesian coordinates of pores centre from image ' I_f ' is estimated. At first, pixels of the output image of I are set to -1 detecting negative intensity as it shows that the region is far from pore's centre. Secondly, binary map (BM) is computed by putting threshold value to the image I with the help of Otsu's algorithm [22]. And, finally the coordinates are computed as $M_x = (I_x, O_y)$ for each pore as (I_x, O_y) is centroid of white region x of BM. Then the white regions with area equal or less than an empirically tuned threshold are discarded.

Step 3: Filtering and Feature Extraction

In this step, four-channel image of size 12×12 pixels is computed that represents pixel-wise features (four features) out of local region which is centred in M_x . These four channels are as follows:

- I_m , local intensity.
- I_f , local intensity.
- Binary ridge map (R), local intensity.
- Radial symmetry image (I_m), local intensity.

Here, ' R ' will provide the information about the ridge–valley pattern of the latent fingerprint to the CNN. R is computed through the algorithm in [23]. Enhancement of the visibility of regions is done by I_C with high radial symmetry of ' I ' and provides the information about the existence of pores (circular shapes) to the CNN. Here, I is computed by fast RST method application proposed in [24] to I_C .

Template Generation In this phase, template of latent image is generated, say T^l and given by,

$$T^l = \{p = (x, y)\}_{i=1}^n \quad (3)$$

Here p is pore on the latent image with labelled coordinate (x, y) , and ' n ' is the total number of pores extracted from the image.

3.3 Identification Phase

Identification phase is the second phase which at last gives the decision. It includes steps like data sensing, feature extraction, matching and decision-making.

Data Sensing In this step, data is collected from a real database. As mentioned in the crime scenario, a registration form was filled before entering the club. This club member database is provided to the investigating officer. He collected fingerprints from the identification card details stored in central agencies. These fingerprints are given in the system to proceed with the identification phase.

Feature Extraction This step is the same as the feature extraction steps followed in the enrolment phase.

Matching Pore-based matching is done using the bipartite graph in this paper [20]. Pores are considered as vertices, and whole fingerprint image is considered as a

densely connected graph. The vertices are coloured, and edges are considered if and only if two vertices are of the same colour. It actually is a graph colouring problem [25]. This colouring problem is solved through graph traversal, and a few data structures are given in [26]. As discussed in the extraction process in Sect. 4.1, a small section image of 100×100 pixels is taken say ‘S’. The other components other than ‘S’ are eliminated. Between the two images, a matching score is computed which is the summation of scores of several matches of the refined pore.

Unlike extraction processes, CNNs are not used in pore matching because of its characteristics dense, very small and large amount of existence in a small section.

Decision This is the final step of the human identification system. It is also based on a threshold value because it is clear from the above discussion that it is not one-to-one matching. If matching score is within threshold value, then only it is accepted, otherwise rejected.

4 Implementation Results and Performance

4.1 Extraction

Before discussing the Level-3 feature extraction, let us first have some spotlight on Level-1 and Level-2 feature extraction. As discussed earlier, Level-1 cannot be used alone, it has to be merged with Level-2 to provide a decision in law enforcement. The system including these two has to extract features: (1) ridge patterns through orientation field estimation and singular points: core and delta and (2) minutiae extraction such as ridge bifurcations, ridge endings, ridge crossovers and small. However, automatic systems are using only two types of minutiae, i.e. ridge bifurcations and ridge endings. In these type of systems, singular points and ridge patterns can be common but minutiae are always unique in nature. So its decision results are used as evidence in the court to address punishments.

To go beyond these minutiae technique, many researchers are extending the feature extraction to Level-3 (pores) to make the decision more robust including certain regions mentioned above in Sect. 1. From the literature survey, works dealing with pore extraction are found in [7, 19, 20] as per my knowledge. The data sets used by them are not currently available. So, the data set of latent fingerprint used in this paper is created and collected in our laboratory. To achieve the data set, forensic procedure as well as digitization of the image through document scanner is performed. This data set consists of 30 latent fingerprints of different fingers with a resolution of 1200 DPI and 320×240 pixels. Total 1585 pores are extracted with labelled coordinates (x, y) in the images. The method is tested using classified pores that will give the validity of the methodology used. Also, a comparison between the used approach with other well-known extraction methods in the literature is done like inversion method and Gabor filtering [14]. Here, a k-fold validation strategy ($k = 5$) [27] is used for the purpose of pores coordinate estimation in every images from the created data set.

Table 1 Average performance metrics in percentage (standard deviation)

	Gabor filter	Inversion	CNN (C_D)
R_{T_r}	31.8(28.8)	32.8(13.0)	51.5(31.3)
$R_{F_{ls}}$	72.8(10.8)	81.3(7.9)	23.0(10.2)

Table 2 Average performance metrics in percentage (standard deviation)

	Gabor filter	Inversion	CNN (C_D)
R_{T_r}	44.2(18.1)	44.0(25.4)	62.6(15.0)
$R_{F_{ls}}$	40.9(20.3)	55.0(27.1)	16.5(10.6)

There are three training folds, one validation fold and one testing fold. Secondly, the true detection rate (R_{Tr}) and the false detection rate (R_{Fls}) concept of [28] are used with consideration of Euclidean distance from the pore coordinates equal or less than pixels (p) labelled by the human to the system, for correct pore detection. Here pixels (p) are given by $p = arw/2$, where ‘arw’ denotes average width of ridge within the specific image. Table 1 shows the performance metrics in an average.

As per our crime scenario taken in Sect. 3.1 of this paper, only a section of the latent fingerprint image is gathered because of the crowded area, increasing the pore extraction complexity. So to study the performance on a small section, a subset of the latent fingerprint is taken. This subset contains 20 images of 100×100 pixels. Again, average performance metrics are compared between the methods used here and inverse as well as the method in [14] as shown in Table 2.

4.2 Matching

Before discussing pore-based matching, again, let us have some spotlight on minutiae-based matching steps in latent fingerprint according to literature survey. These steps include (1) minutiae detection, (2) applying minutiae descriptor to eliminate false minutiae and (3) computing match score. In contrast, pore-based matching uses bipartite graph. A Hamiltonian path concept from [29] is used between testing and reference data pore graphs. Then statistical shape matching from [30] is applied to obtain matched pairs of pore.

4.3 Limitations of the Study

This paper includes different techniques to design a framework that yields an accurate result but it has some limitations as the work is done with clear background of

the image. It is obvious, because data set is created using forensic procedure and digitization, not collected from the crime scene. It becomes complex for arbitrary input.

5 Conclusion and Future Research

Latent fingerprints are an important part of evidence collected by the forensic's investigating officer which provide justice to the people. In this paper, a human identification system is described, keeping a particular crime scene in focus. Apart from the traditional method of AFIS, Level-3 is considered for extraction and matching. In this paper, CNN-based feature extraction has been used, and a comparison is drawn between the inverse method and Gabor filtering method of feature extraction. From the result, it is found that the feature extraction method used in this paper results better.

For future research, more work can be done on improving resolution of the image (more than 1200 dpi). Different matching technique should be experimented to achieve more robust identification framework. Also works can be done to reduce the limitations of the study.

Acknowledgement This research is completed with the support of Information Security Education and Awareness Project (ISEA), Project Phase-II, MeitY, Government of India.

References

1. Sankaran A, Mayank V, Richa S (2014) Latent fingerprint matching: a survey. *IEEE access. IEEE Biometric Compendium RFIC Virtual J* 2:982–1004
2. Li J, Feng J, Jay Kuo C-C (2018) Deep convolutional neural network for latent fingerprint enhancement. *Signal Process Image Commun* 60:52–63
3. Cao K, Jain AK (2018) Automated latent fingerprint recognition. *IEEE Trans Pattern Anal Mach Intell* 41(4):788–800
4. Cao K, Jain AK (2018) Latent fingerprint recognition: role of texture template. In: 2018 IEEE 9th international conference on biometrics theory, applications and systems (BTAS). IEEE
5. Manickam A et al (2019) Score level based latent fingerprint enhancement and matching using SIFT feature. *Multimedia Tools Appl* 78(3):3065–3085
6. Maltoni D et al (2009) Handbook of fingerprint recognition. Springer Science & Business Media
7. Zhao Q, Feng J, Jain AK (2010) Latent fingerprint matching: Utility of level 3 features. *MSU Techical Report* 8:1–30
8. Maltoni D, Cappelli R, Meuwly D (2017) Automated fingerprint identification systems: from fingerprints to fingermarks. In: *Handbook of biometrics for forensic science*. Springer, pages 37–61
9. Oig A (2006) Review of the fbi's handling of the brandon mayfield case. *Office of the Inspector General, Oversight and Review Division, US Department of Justice*, pp 1–330

10. Stosz JD, Alyea LA (1994) Automated system for fingerprint authentication using pores and ridge structure. In: Automatic systems for the identification and inspection of humans, volume 2277. International Society for Optics and Photonics, pp 210–223
11. Kryszczuk K, Drygajlo A, Morier P (2004) Extraction of level 2 and level 3 features for fragmentary fingerprints. In: Proceedings of 2nd COST275 workshop, volume 8388
12. Kryszczuk KM, Morier P, Drygajlo A (2004) Study of the distinctiveness of level 2 and level 3 features in fragmentary fingerprint comparison. In: International workshop on biometric authentication. Springer, pp 124–133
13. Ray M, Meenen P, Adhami R (2005) A novel approach to fingerprint pore extraction. In: Proceedings of the thirty-seventh southeastern symposium on system theory, 2005. SSST'05.. IEEE, pp 282–286
14. Jain A, Chen Y, Demirkus M (2006) Pores and ridges: Fingerprint matching using level 3 features. In: 18th international conference on pattern recognition (ICPR'06), vol 4. IEEE, pp 477–480
15. Parsons NR, Smith JQ, Thöennes E, Wang L, Wilson RG (2008) Rotationally invariant statistics for examining the evidence from the pores in fingerprints. *Law Probab Risk* 7(1):1–14
16. Zhao Q, Zhang D, Zhang L, Luo N (2010) Adaptive fingerprint pore modeling and extraction. *Pattern Recogn* 43(8):2833–2844
17. Genovese A, Munoz E, Piuri V, Scotti F, Sforza G (2016) Towards touchless pore fingerprint biometrics: a neural approach. In: 2016 IEEE congress on evolutionary computation (CEC), . IEEE, pp 4265–4272
18. Jang H-U, Kim D, Mun S-M, Choi S, Lee H-K (2017) Deepore: fingerprint pore extraction using deep convolutional neural networks. *IEEE Sig Process Lett* 24(12):1808–1812
19. Labati RD, Genovese A, Muñoz E, Piuri V, Scotti F (2018) A novel pore extraction method for heterogeneous fingerprint images using convolutional neural networks. *Pattern Recogn Lett* 113:58–66
20. Nguyen D-L, Jain AK (2019) End-to-end pore extraction and matching in latent fingerprints: going beyond minutiae. arXiv preprint [arXiv:1905.11472](https://arxiv.org/abs/1905.11472)
21. Sutskever I, Martens J, Dahl G, Hinton G (2013) On the importance of initialization and momentum in deep learning. In: International conference on machine learning, pp 1139–1147
22. Otsu N (1979) A threshold selection method from gray-level histograms. *IEEE Trans Syst Man Cybernet* 9(1):62–66
23. Watson CI, Garris MD, Tabassi E, Wilson CL, Michael McCabe R, Janet S, Ko K (2007) User's guide to nist biometric image software (nbis)
24. Loy G, Zelinsky A (2003) Fast radial symmetry for detecting points of interest. *IEEE Trans Pattern Anal Mach Intell* 25(8):959–973
25. Jensen TR, Toft B (2011) Graph coloring problems, vol 39. Wiley, New York
26. Pardalos PM, Mavridou T, Xue J (1998) The graph coloring problem: a bibliographic survey. In: Handbook of combinatorial optimization. Springer, pp 1077–1141
27. Duda RO, Hart PE (2001) Dg stork pattern classification. Wiley, New York
28. Zhao Q, Liu F, Zhang L, Zhang D (2010) Parallel versus hierarchical fusion of extended fingerprint features. In: 2010 20th international conference on pattern recognition. IEEE, pp 1132–1135
29. Yuri G, Saharon S (1987) Expected computation time for hamiltonian path problem. *SIAM J Comput* 16(3):486–502
30. Castellani U, Cristani M, Fantoni S, Murino V (2008) Sparse points matching by combining 3d mesh saliency with statistical descriptors. In: Computer graphics forum, vol 27. Wiley Online Library, pp 643–652

Data Quality Requirements Methodology for an Adapted PHM Implementation



N. Omri, Z. Al Masry, N. Mairot, S. Giampiccolo, and N. Zerhouni

Abstract The technologies of digitization allow organizations to rely on data mining for performance improvement. In this context, data-driven Prognostics and Health Management (PHM) is being introduced as a new framework for data management and knowledge extraction. However, the collected data are generally accompanied by quality issues that influence PHM results. Metrics are therefore needed to quantify data suitability for PHM application. The majority of existing works propose to improve PHM tools without taking into account the adequacy of the used data to the fixed objectives. This paper aims to propose a set of data quality requirements for PHM applications and in particular for the fault detection task.

Keywords Data quality metrics · Data quality requirements · Impact of data quality on PHM results · Data detectability

1 Introduction

Prognostics and Health Management (PHM) is a science that studies the health state of a system and predicts its future evolution, which allows to improve its performance [10]. In [9], the authors define PHM as “a set of tools that can be used in cascade or separately to monitor the health state of a system, predict its future evolution and/or optimize decisions.” PHM implementation approaches are divided into model-based and data-driven approaches [6]. The first approach uses the system’s physical process to control its health state. Thus, a good understanding of the physical process of component degradation is necessary. To overcome this problem, the second approach consists in using monitoring data to extract knowledge about the system’s behavior.

N. Omri (✉) · Z. Al Masry · N. Zerhouni
FEMTO-ST Institute, Univ. Bourgogne Franche-Comté, CNRS, ENSMM, 24 rue Alain Savary ,
25000 Besançon Cedex, France
e-mail: nabil.omri@femto-st.fr

N. Omri · N. Mairot · S. Giampiccolo
SCODER 1 rue de la Forêt Z.A. l’Orée du Bois, 25480 Pirey, France

In this case, the results are strongly influenced by the quality of the used data. To take advantage of the strengths of each approach and effectively implement a PHM process, a new approach has recently emerged which is the hybrid approach.

Driven by the emergence of digitization technologies, data-driven approach for product life cycle management has attracted more attention in recent years [13]. Thanks to the huge volume of collected data, scalable, re-configurable and low cost PHM solutions can be easily implemented. The industrial application of the PHM discipline generally concerns decision support for a more efficient and intelligent operation of machines [1]. To satisfy this objective, three main PHM tasks are identified: (i) fault detection, (ii) fault diagnosis and (iii) degradation prediction. These tasks are performed consecutively starting with fault detection. Thus, the success of the fault detection task is a necessary condition for the success of the entire PHM process. Many sophisticated algorithms have been proposed to deal with the problem of fault detection with impressive performances. However, these algorithms become useless in the case when data are not suitable for this task [8]. In this context, data quality has a major impact on the data suitability for the PHM tasks [10].

Data quality (DQ) has been the subject of many research works where several definitions were proposed to characterize this concept. The ISO/IEC 25012 standard [7] definition assumes that high data quality is “the degree to which a set of characteristics of data fulfill requirements.” We here adopt the data quality definition proposed in [10] and which define high-quality data as “all data with a minimum level of quality that guarantees the satisfaction of objectives set by the owner.” Data quality is a multidimensional issue where several data quality dimensions (DQD) are defined to characterize the data requirements [12]. However, some dimensions are studied more than others. Redman [11] offers a short list of the most studied ones which includes accuracy, completeness, consistency, timeliness and consistency. In the industrial context, this list is reduced to three main dimensions:

- Data volume: Evaluate whether the data volume is sufficient for the application.
- Data completeness: Evaluate the ratio of missing values for a variable.
- Data accuracy: Represent the degree of representativeness of the correctly recorded data to the real world.

Despite the huge volume of studies that deal with the data quality problem, only few of them introduce this issue in the PHM context. Thus, the objective of this work is to position the data quality problem in a PHM context and to propose a new metric to assess data suitability for the fault detection task.

The remainder of this paper is organized as follows. Section 2 presents a brief review of related works that concern data quality impact on the PHM tasks. In Sect. 3, an empirical data detectability model is proposed. This model is validated and applied in a real case study in Sect. 4. Finally, conclusions and perspectives are displayed in Sect. 5.

2 Data Quality Problems in the PHM Context

As shown in Fig. 1, data quality management in the PHM context can be seen from two sides: (1) a direct process where data quality is assessed and its suitability for the PHM application is evaluated, and (2) a reverse process where a set of data quality requirements is defined to meet the fixed objectives. Existing data quality studies are part of the direct process (1). We are here interested in the inverse process (2). Nevertheless, there is no generic metric to quantify data quality and its impact on PHM results. Thus, this work aims to define a generic method allowing the understanding and the quantification of the data quality impact on PHM tasks. Based on this quantification, data quality requirements can be defined to meet the fixed objectives.

In this context, three data quality metrics are defined in [8] to characterize data for PHM applications. These metrics concern the aspects of detectability, diagnosability and trendability. However, no generic method has been proposed to quantify these metrics and even those proposed in [8] strongly depends on the used data modeling algorithm and ignore the impact of the data quality. The authors in [9] propose a set of data quality requirements to be suitable with PHM applications. The data issues evoked in the mentioned paper concern mainly: data volume, data completeness and accuracy. Consequently, we propose in this paper to classify the data problems according to these characteristics:

Data volume Data volume is the most important data quality dimensions and it concerns here the imbalanced data. The imbalanced data is a form of between-class imbalance that refers to the non-equivalence in the number of instances between faulty and healthy classes. The following metric is used to quantify this aspect of data volume problem:

$$q_{\text{Im}} = 1 - \frac{|\{o \in S | o \in R\}|}{|R|} \quad (1)$$

where o is an observation and S is the objects ensemble of the subsampled class.

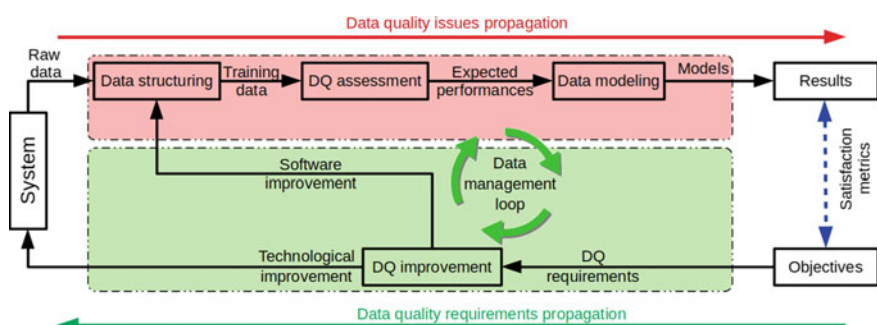


Fig. 1 Data management process in the PHM context

Data completeness Completeness is the data dimension that deals with the problem of missing data. Thus, completeness is explained in this case as the percentage of available values for a variable. The completeness ratio is calculated using the following metric:

$$q_m = \frac{|\{o \in M\}|}{|R|} \quad (2)$$

where M is the ensemble of missing observations for the feature $X_i, i = 1, \dots, n$.

Data accuracy Data accuracy concerns data recorded with an error in relation to the world reality they describe. In [3], authors define accuracy as the “distance” between the data or information and the world reality they describe. We propose here to quantify the accuracy ratio as follows:

$$q_n = \frac{|\{o \in N\}|}{|R|} \quad (3)$$

where N is the ensemble of noisy observations for the feature $X_i, i = 1, \dots, n$.

Recall that the main PHM tasks are fault detection, diagnosis and degradation prediction. The fault detection task is the first one on the PHM process [8] and is considered in the rest of this study. Many factors can affect the fault detection task. These factors can be related to the performance of the used detection algorithm, the data quality issues or the system observability. For the first possibility, many sophisticated algorithms have been proposed to deal with the problem of fault detection with impressive performances. However, these algorithms become useless in the case when the system’s observability is weak or the unsuitability of the collected data. In this paper, we propose to formalize the data quality impact on the fault detection task. Some assumptions are made for our study:

- (A1) The studied system is assumed to be fully observable.
- (A2) The studied system is observed during a sufficient horizon of time to collect the needed data.
- (A3) The used detection algorithms are all able to perform equal results.
- (A4) The detectability task is done in a supervised mode.

One should note that the assumption (A1) is a logical one since the unobservable features can be considered as observable ones with weak quality.

3 The Empirical Data Detectability Model

This section presents an empirical development of the detectability metric. Using 10 datasets (real and simulated datasets), we tested the most used fault detection techniques (see [10]) in order to study their behavior regarding the data quality problems. These algorithms include artificial neural network (ANN), decision tree (DT), support vector machine (SVM), K-Nearest Neighbors (KNN) and Naive Bayes (NB).

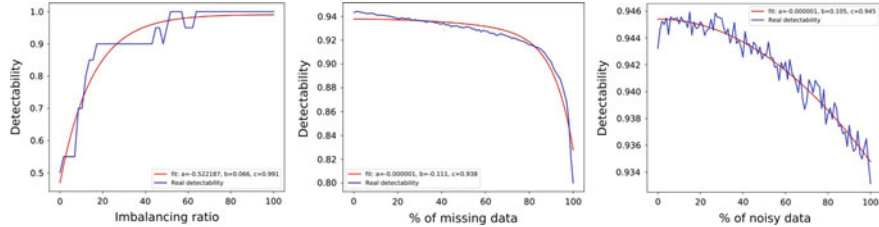


Fig. 2 Detectability evolution as a function of the data quality problems

More than 10^5 simulations have been carried out with different quality configurations. For each configuration, the data detectability is assessed. The overall mean of these simulation results is then used to develop a global detectability model taking into account each data quality issue (Fig. 2).

Figure 2 shows that the detectability evolution regarding to the imbalanced data ratio q_{Im} is then given by

$$\text{Det}(q_{\text{Im}}) = 1 - 0.52 \times e^{-0.07 \times q_{\text{Im}}} \quad (4)$$

where q_{Im} is defined in (1).

For the detectability evolution regarding to the missing data ratio q_{i1} of a feature X_i is given by

$$\text{Det}(w_i, q_{i1}) = \frac{w_i}{w_{i_{\min}}} [1 - 2.10^{-6} \times (q_{i1}^2 + e^{0.11 \times q_{i1}})] \quad (5)$$

where q_{i1} is defined in (2) and the features importance w_i estimation are conducted implicitly by the *Random Forest* classifier based on the “Gini importance” [4].

Therefore, the detectability evolution regarding to the noisy data ratio q_{i2} is given by

$$\text{Det}(w_i, q_{i2}) = \frac{w_i}{w_{i_{\min}}} [1 - 10^{-6} \times (q_{i2}^2 + e^{0.07 \times q_{i2}})]. \quad (6)$$

where q_{i2} is defined in (3).

The previously studied data quality issues are divided into global quality (GQ) and local quality (LQ). The GQ impacts the whole features of the data set (i.e., Imbalanced data) and the LQ impacts each feature according to its quality level (i.e., Noisy and missing data). Thus, the data detectability depends on the product of the global qualities multiplied by the sum of the local qualities for all the features. Thereby and referencing to the previously detailed models, the final detectability model can be defined as follows:

$$\begin{aligned} \text{Det}(q_{\text{Im}}, q_{i1}, q_{i2}) &= (1 - 0.52 \times e^{-0.07 \times q_{\text{Im}}}) \times \sum_{i=1}^n \frac{w_i}{w_{i_{\min}}} [2 - 2.10^{-6} \\ &\quad \times (q_{i1}^2 + e^{0.11 \times q_{i1}}) - 10^{-6} \times (q_{i2}^2 + e^{0.07 \times q_{i2}})]. \end{aligned} \quad (7)$$

4 Model Validation and Case Study

Finally, we come to the application of the developed model to a real case study. However, it is needed to assess its performance before applying it in our production process. For that, a validation step is conducted using public datasets in order to assess the validity of the proposed model.

4.1 Model Validation

To validate the detectability model, a set of numerical simulations are used. Thus, the previously used fault detection algorithms are tested to define their behavior regarding to the data problems. These fault detection algorithms are tested in two real datasets (Spam [2] and Inflammations diagnosis [5]) to assess the performance of the developed detectability model.

As shown in Fig. 3, the expected detectability is compared with the average of real detectability of each algorithm. For each dataset, 500 data quality configurations are tested. Results show that the developed model is able to predict the general evolution of detectability as a function of the used data quality. The detectability is predicted with an RMSE equal to 0.05 and 0.09 for the diagnostic and the spam datasets, respectively. We can notice that the difference between actual and expected detectability does not only belong to the developed model, but also to other data quality issues (i.e., outliers) that are not taken into account in this work. The obtained results prove the validity of the proposed detectability model, which qualifies it to be applied in real case studies.

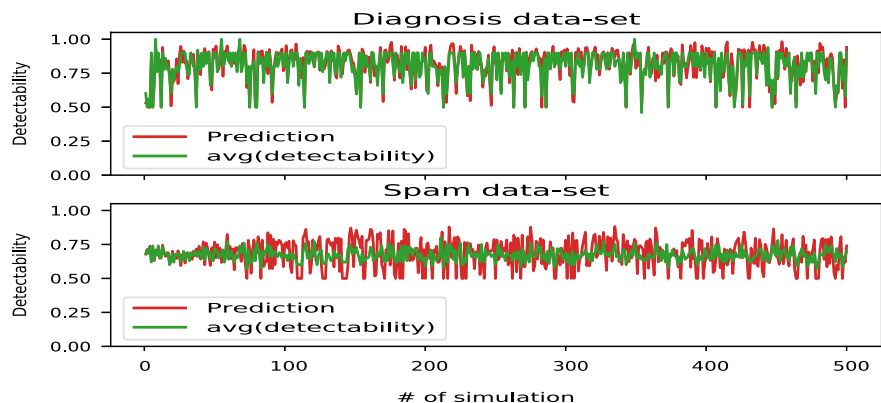


Fig. 3 Results of the model validation step

4.2 Case Study

The detectability model is applied to the Scoder case study. Scoder is a French SME specialized in ultra-precise stamping for automotive applications. The production performance is affected by the used metal coil characteristics. For that purpose, a PHM study is conducted to detect the suitability of each sheet metal for production. Thus, the characteristics of the coil, the caused machine breakdowns, and the quality rate are collected and analyzed. The aim here is to detect the suitability of each metal coil with 80% as minimum rate of performance. A data inventory is first conducted to collect all the data that can be useful for project. Then, 24 variables are identified which consist in 12 metal properties, 6 types of machine's breakdown and 6 kinds of product's non conformity. Samples of these data are collected carefully, and they are used to preliminary analyze the data and to quantify the importance of each feature. Only 5 features are identified as pertinent for the study. Thus, the rest of features are eliminated, and the rest of the study is based on these five variables. Table 1 shows the features importance from the used data subset. It is proven that the *Var5* is the most important one to identify the capacity of the used coil to produce good quality parts.

For the Scoder case study, advanced sensing technologies are required to ensure high data quality level for the *Var5*. As for the other variables, it can be done easily. In addition, it takes a lot of time to have a balanced dataset. For that, a significant cost is allocated to the imbalanced data ratio without forgetting the important cost of a negative detection. Table 1 shows the order of magnitude of these costs. In order to minimize the data acquisition cost, the developed data detectability model is used to identify the data quality requirements to satisfy objectives (80% as accuracy rate).

Table 2 shows a data quality configuration that guarantee 90% of detectability. As a matter of fact, it is allowed to have 29% of missing data for *var5* and up to 60% for some other variables. For the noisy data, the percentages vary between 36 and 77%.

Figure 4 shows the installed data acquisition system for the Scoder case study where the previously defined requirements are respected. The expected installation

Table 1 Features importance in the Scoder case study

Variable	Wi	Costs				Imbalanced	False alarm
		Noisy	Missing				
Var 1	0.11	1	1			8	10
Var 2	0.09	1	1				
Var 3	0.14	1	1				
Var 4	0.09	1	1				
Var 5	0.57	3	3				

Table 2 Data quality requirements for the Scoder application

Det	q_{lm}	q_{11}	q_{21}	q_{31}	q_{41}	q_{51}	q_{12}	q_{22}	q_{32}	q_{42}	q_{52}
90%	30%	25%	60%	6%	28%	29%	53%	36%	77%	71%	67%

cost is 11.05 *MU* which is optimized to be suitable for SMEs with limited resources. The properties of the metal coils are tested in a specialized test station where the previously defined requirements are met. The dataset was collected in more than 6 months during which the data quality has evolved to meet the defined requirements. At the end of this period, the data quality requirements are satisfied for all the variables. Using the detectability model developed in (7), the expected detectability level using this data quality setting was 94%. The actual detectability level is 95% which is obtained by the DT algorithm. These results show that it is possible to predict accurately the performance of the PHM framework and to assess the suitability of the used data for the detection task.

The proposed model makes it possible to optimize the PHM performance according to the available budget. This removes the exclusivity of PHM for large companies and proves that it is also applicable in SMEs with limited budgets.

5 Conclusion and Perspectives

PHM concept is widely used in organizations as a data management framework to optimize their process and improve their performance. However, PHM results are heavily dependent on the used data quality. For that, this paper proposes to study the data quality issues in the PHM context while evaluating their suitability for the faults detection task. The proposed model is developed empirically, and it concerns only the detection task of the PHM process. One should think about studying the impact of data quality issues on the rest of the PHM tasks (diagnostics and prognostics). Thus, further work should be developed to define a technical protocol for data quality

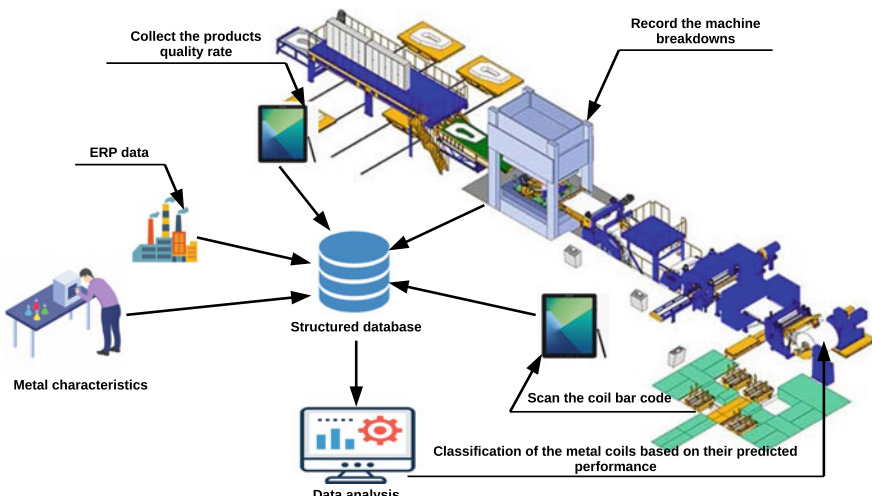


Fig. 4 Details of the Scoder data acquisition system

evaluation and improvements for the whole PHM process. This can reduce the time and the cost of data processing and to improve the obtained results.

References

1. Al Masry Z, Omri N, Varnier C, Morello B, Zerhouni N (2019) Operating approach for fleet of systems subjected to predictive maintenance. In: Euro-Mediterranean conference on mathematical reliability
2. Almeida TA, Hidalgo JMG, Yamakami A (2011) Contributions to the study of sms spam filtering: new collection and results. In: Proceedings of the 11th ACM symposium on Document engineering, pp. 259–262
3. Batini C, Scannapieco M (2016) Data and information quality: concepts, methodologies and techniques
4. Breiman L (2001) Random forests. *Mach Learn* 45(1):5–32
5. Czerniak J, Zarzycki H (2003) Application of rough sets in the presumptive diagnosis of urinary system diseases. In: Artificial intelligence and security in computing systems. Springer, pp 41–51
6. Gouriveau R, Medjaher K, Zerhouni N (2016) From prognostics and health systems management to predictive maintenance 1: monitoring and prognostics. Wiley, New York
7. ISO/IEC: Software engineering—software product quality requirements and evaluation (square)—data quality model. In: ISO/IEC, technical report ISO/IEC 25012
8. Jia X, Zhao M, Di Y, Yang Q, Lee J (2017) Assessment of data suitability for machine prognosis using maximum mean discrepancy. *IEEE Trans Indus Electron* 65(7):5872–5881
9. Omri N, Al Masry Z, Giampiccolo S, Mairot N, Zerhouni N (2019) Data management requirements for phm implementation in smes. In: 2019 Prognostics and system health management conference (PHM-Paris). IEEE, pp 232–238
10. Omri N, Al Masry Z, Mairot N, Giampiccolo S, Zerhouni N (2020) Industrial data management strategy towards an sme-oriented phm. *J Manuf Syst* 56:23–36
11. Redman TC (1997) Data quality for the information age, 1st edn. Artech House Inc., Norwood
12. Sidi F, Panahy PHS, Affendey LS, Jabar MA, Ibrahim H, Mustapha A (2012) Data quality: a survey of data quality dimensions. In: 2012 international conference on information retrieval & knowledge management. IEEE, pp 300–304
13. Trabelsi I, Zolghadri M, Zeddini B, Barkallah M, Haddar M (2020) Fmeca-based risk assessment approach for proactive obsolescence management. In: IFIP international conference on product lifecycle management. Springer, pp 215–226

Scaling Depression Level Through Facial Image Processing and Social Media Analysis



Akshar Bhayani, Pratiksha Meshram, Bhishman Desai, Ayushi Garg, and Shivam Jha

Abstract One of the leading causes of illness and disability among adolescents is depression. Often, a person going through mental health issues hesitate to consult a counselor. Moreover, they are not willing to share their feelings with their near ones. Technology can play a vital role and can be the first line of support in such a situation. As people are more active on social media, it can be used successfully to help or diagnose physical and mental illness. The current literature review focuses on image processing, machine learning algorithms, and sentimental analysis, as stated in recent years of existing approaches. Various techniques used for data analysis and current datasets are summarized with all methods along with their performance reports. Besides, this review includes not only the criteria for clinical depression, but also facial image processing along with online behaviors on social media platforms such as Twitter.

Keywords Depression detection · Facial features · Sentimental analysis · Machine learning · Image processing

1 Introduction

The current work is a structured review of pre-existing methods for depression detection and/or severity evaluation. Focus is given to techniques for the diagnosis of depression by image processing and social media. Depression is one of the main cause of disorder globally. It is estimated that almost 350 million individuals of every age suffer from depression globally [1]. Depressed individuals have different signs of depression expressed by actions that differentiate them.

A. Bhayani (✉) · B. Desai · A. Garg · S. Jha

Information Technology—Bachelor of Technology, SVKM's NMIMS MPSTME, Shirpur, India

P. Meshram

Department of Information Technology, SVKM's NMIMS MPSTME, Shirpur, India
e-mail: pratiksha.meshram@nmims.edu

Individuals are said to be in a state of depression when they find themselves feeling sad and hopeless nearly every single day for two or more weeks continuously. Such people then begin to recuperate from their social lives. They stop doing some of the typical activities they usually liked to do. Research has been conducted to connect people with signs of depression by Internet use. This study found that people with depression accessed the Internet more often to reveal emotions and their personal status. On social media, user-generated content (UGC) immediately represents not just everyday lives, but also user mental states. Social media have been largely used for physical and mental wellness research over the past decade, particularly mental wellness compared to ordinary people.

The most significant means of non-verbal communication is a person's facial expressions. Hence, a system is developed, and this system primarily uses various image processing techniques for face recognition, feature extraction and classification of these faces as depressed or non-depressed. Depression characteristics can be trained in the system. Images of multiple people with a frontal face can then be filmed using a web camera. Then the facial features of these faces will be extracted for prediction of depression. The individual will be categorized as depressed or non-depressed based on the level of depression characteristics [2].

1.1 *Clinical Background of Depression*

Psychological doctors frequently conduct face-to-face interviews with regard to the generally used criteria for the Diagnostic and Statistical Manual of Mental Disorders in clinical diagnosis. In total, there are nine classes of symptoms related to depression interpreted, explaining distinctive behaviours of daily life. Even though it is the most successful method for depression diagnosis, people are in so unaware or ashamed of depression. 70% of individuals do not consult psychological doctors in the early stages of depression. Clinically, distinct depressive disorders encompass a broad variety of aspects.

According to DSM-5 MDD, generally referred as Clinical Depression, the presence of depressed mood most of the day, and continuous decrease in interest or pleasure, together with at least four of these symptoms over a period of two weeks can be diagnosed: (a) A Significant change in weight of more than 5% in a month (b) Sleeping disorders (insomnia or hypersomnia) (c) Repeated thoughts of death or suicide. “Clinically notable distress or damage in social, occupational or other important areas of functioning” is a ordinary feature of all depressive disorders [3]. For depression, in general, “there is no blood test” since the condition lacks biochemical gold standards. Particularly current classification systems (e.g., DSM-5) are at risk of confused normal sorrow with depression, which raises the chance of false positive diagnosis. Depression assessment is a dynamic procedure, and a large degree of ambiguity is involved with diagnosis, including the absence of objective boundaries and the ability to interpret symptoms within the present psycho social context and historical experience of the individual [4].

Usually, diagnosis performance increases as findings from consecutive clinical examinations, carried out for many months, are recorded. Importantly, in order to establish relationships with the patient, a simplistic “symptom checklist” strategy is severely restricted and diagnosis requires significant time commitment. It has also disputed the relevance and the clinical importance of strict grouping systems. Scores on self-report scales and inventories (Self-RIs) can also help clinical diagnosis of depression [5]. The varied types of PHQ-2/8/9 (Patient Well being Questionnaire, consisting of 2, 8, or 9 items, respectively) and BDI (Beck’s Depression Inventory) are the most commonly used self-RIs in effective computing research. SelfRIs are easy and economical, but have some drawbacks, with reported sensitivity and specificity reaching 80–90% (e.g., PHQ-9) [5]. Importantly, as compared to a clinical interview, they do not take into consideration the clinical importance of symptoms and do not allow adjustments for individual trait features, other psychiatric and medical risk factors and significant life events.

1.2 Related Work

Despite the increasing interest in the subject, current reviews differ in their particular emphasis, and seldom attempt to analyse methods and outcomes in detail.

Work on depression detection through Facial image processing. The detection of suicidal individuals has been very common in recent studies. As seen in the reported findings, the previous year’s AVEC depression subchallenges showed papers with respectable precisions via Decision Tree grouping and multimodal integration of visual and text elements, Yang et al. [6] achieved very plausible precision during AVEC 2016. In the AVEC 2014 competition, Jan et al. [7] used Motion History Histogram by capturing Local Binary Pattern (LBP) and Edge Orientation Histogram (EOF) features for depression detection. Other features have also been used for depression identification, such as head posture, blink rate and textual characteristics. A discriminative function to demarcate suicidal individuals from non-depressed is head posture and facial movement. Depressed individuals exhibit less nodding, minimizing eye contact and more likelihood of positioning head down than non-depressed individuals. The Alghowinem et al. used face-related head pose and motion characteristics to perform SVM classification on recognition of depression; and concluded that depressed people’s head movements are distinct from that of a typical person.

Driven by the latest success of deep learning in emotion prediction, Tzirakis et al. [8] proposed a deep learning-based approach in AVEC 2016 to determine the individual’s emotion and depression state. They used the audio Convolution Neural Network (CNN) and the visual data Deep Residual Network (resNet) of 50 layers. They deduced that comparatively better results were obtained by their deep learning methodology than other approaches at the time. Features from the documented verbal contact written in the transcript file given in the data were extracted by Pampouchidou et al. in AVEC 2016. The Arousal Valence ranking of the words that were used as a function of negative sentiment, and they deduced that their elimination had a negative

effect on the total accuracy of the qualified fused model. In AVEC 2013, Cummins et al. have proposed a multimodal method by fusing audio and visual modalities with various depression detection techniques. All current literature, however, stresses the need for the identification of depression in an automated and fruitful manner to assist clinicians and patients.

Work on depression detection through social media analysis. Online depression detection with the evolving age, we are almost unable to live without social media, even suicidal people. In doing so, researchers began to examine the online habits of suicidal users. Park et al. investigated, as a preliminary review, the use of vocabulary in explaining depressed moods using real-time moods recorded from Twitter users. He also conducted face-to-face interviews with 14 involved Twitter users to investigate their suicidal habits in their follow-up work. More recently, from the viewpoint of social networks and linguistic trends, Xu et al. sought to clarify how site users address depression-related topics. Depression detection from the social media became achievable with the aforementioned work. The capability of using social media to identify and treat major individual depressive disorders was explored by Choudhury et al.

In the study of linguistic signs for the diagnosis of depression, Resnik [9] researched subject models. These attempts to diagnose depression showed that large depressive people can be analyzed on social media. There are some drawbacks to the present work, however (a) most of them carried out their studies on a very small number of subjects, so it is impossible to explain the robustness and commonality of their results on a widespread depression population. (b) Some of them described possible suicidal consumers from various social media modalities. (c) They did not extensively study social media depression habits, and relatively little studies explored the recently presented signs of depression as the environment changes.

1.3 *Structure of Paper*

The current review is done in five sections. Section 2 covers the datasets of depression, the procedure of collecting these datasets and enlists the dataset available for the depression analysis till date. The methodology, the entire process, how it takes place is given in Sect. 3 and followed by the system performance in Sect. 4. The conclusion of what the entire review paper talks about and the future work that can be done on the topic is covered in Sect. 5.

2 Depression Detection Datasets

For the assessment of automated depression assessment methods, the availability of clinical evidence is of critical importance. During algorithm creation, and testing, such data is important. Accessibility is neither broad nor free, because of the fragile

existence of clinical data, most study organizations stick to producing their own sets of data. The methods of data collection used and the derived datasets found in studies analyzed are explained in this section.

2.1 *Collection Procedure*

Participant recruitment is probably the most difficult step in research. MDD patients, often clinical psychologists or social workers, were recruited from the population and assessed using DSM-IV criteria and/or patients with HAM-D scores were able to be medicated, unmedicated or in remission. For the data collection for the recorded dataset, the Mini International Neuropsychiatric Interview (MINI) was used to collect user data in order to achieve the diagnosis. Self-RIIs such as PHQ-9 evaluating the intensity of symptoms linked to depression is used for data collection from non-clinical samples [5]. In addition, posters, institutional mailing lists, social networks, and personal contacts were included in the recruiting methods.

Executive tasks include arranging, organizing, and solving problems task by studies. For example, a series of “training tasks” includes vowel pronunciation, solving a task aloud, counting from one to ten, singing, reading novel, and narrating a particular scene presented in illustrated form were inserted into the dataset developed for the AVEC’13.

Formalized interviews are commonly used to capture depressive symptoms, but were also used for asking participants to explain intimate, emotionally charged experiences to produce specific emotions. Interviews can take place multiple days over a week, performed by a counsellor, or led by directions on a digital screen. The subject of the interview usually moves seamlessly from casual to more personal subjects. Again, one or more cameras, usually coloured, are used together to record more than one camera angle and field of vision (e.g., for both face and body separately) depending on the approach. Thermal imaging was used to investigate the clinical severity of depression, as well as to use an infrared eye monitoring device also, in research focusing on saccadic eye movements. In certain cases, depth sensors have also been used. In an interview or narrating activities, microphones are naturally necessary to record the speech of the participants.

On Twitter, which has mature APIs, researchers developed two datasets of depressed and non-depressed users. Biradar and Totad [10] and is widely prevailing, to detect depression through social media. Provided a Twitter user, to infer the mental state, we collected the user’s profile data and an anchor tweet. As individuals should be monitored according to clinical practice for a period of time, all the other tweets released in a month were also collected. Again, the exact setup varies across research, like with emotion elicitation.

2.2 Datasets Till Now

The different datasets that have been recorded in the related work are summarized in Table 1. Two recruited teenagers, many researches and employed matured participants. Methods for the compilation of depressive symptoms included: (a) personal, i.e., interview or contact with friends and family; (b) anti-social, where attendees were introduced on a computer; and (c) a fusion of a and b. The basic reality of the occurrence of depression differed correspondingly, depending in most cases on clinical examination and self-reports.

The screening process used was heavily dependent on the research problem. To diagnose depression or separation from bipolar disorder, DSM and HAM-D criteria were used. In order to track recovery performance, some had more precise requirements, i.e., patients healing from Deep Brain Stimulation [11]. Studies testing the predictive potential of the tool for the possible occurrence of psychiatric depression in adolescents included participants aged 9–12 years in the initial dataset, with a two-year period of clinical reassessment.

AVEC is an only completely accessible dataset for free with respect to the availability of the dataset, although the DAIC-WOZ dataset is also partially accessible. In order to have download access, both of the datasets need to sign End User License Agreement (EULA). The remaining datasets mentioned are proprietary, they were also given to foreign researchers in some cases. The number of participants listed in Table 1 corresponds to the number of participants registered using the relevant dataset in the latest publication.

Researchers developed a depression dataset D1 on the basis of the tweets between 2009 and 2016. Influenced by Coppersmith et al., if user anchor tweets followed the “(I’ve been/I’m) struggling with depression” pattern, users were marked as depressed. A total of 1403 of depressed users and 292,565 numbers of tweets were collected in this manner in just one month [12]. A non-depression dataset D2 was created, where users were classified as non-depressed if they had never published a tweet with the “depress” keyword. Researchers also created an untagged depression participant dataset D3 on the basis of the December 2016 tweets, where users were obtained if

Table 1 Datasets used by the studies for depression evaluation [3]

Dataset	Total participants	Age group	Collection methods	Research type	Availability
DAIC -WOZ	189	Adults	Combination	Detection, severity scale	Audio recordings, audio & video features
AVEC	58	Adults	Anti-social	Severity scale	Audio & video features, full video recordings

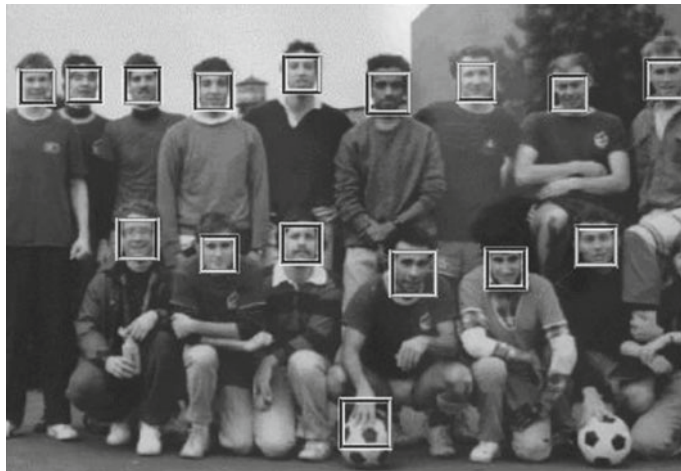


Fig. 1 Example of Face detection using Viola–Jones algorithm [2]

their anchor tweets included the “depress” keyword. While there was a lot of noise in the depression participant dataset, it had more depressed users than randomly sampled. Finally, within one month, they received 36,992 depression participant users and more than 34 million tweets that will be used for online behavior analysis.

3 Methodology

3.1 Pre-processing

Typical necessary preprocessing steps are illumination normalization, alignment and registration between the face detection and image sequences, given a visual input (video). Viola and Jones [2] have proposed a common algorithm used in face detection. Some off-market facial-expression analysis applications were also been commonly used for preprocessing methods, allowing scientists to concentrate on high-level knowledge derivation (Fig. 1).

The OpenFace freeware application 5 is an instance of such a method. Another potentially helpful preprocessing method is using an open-source platform called SEAMAINE API used for developing emotion oriented system. Gaze estimation instruments, such as the one shown in, can assist in deriving important characteristics related to symptoms of depression, such as focus or shorter eye contact. For alignment and landmark identification, Z-Face was also employed.

Twitter allows public access to the tweets of an individual. It offers an API which makes it easy to analyze the user’s behavior. This technique has used a Python library

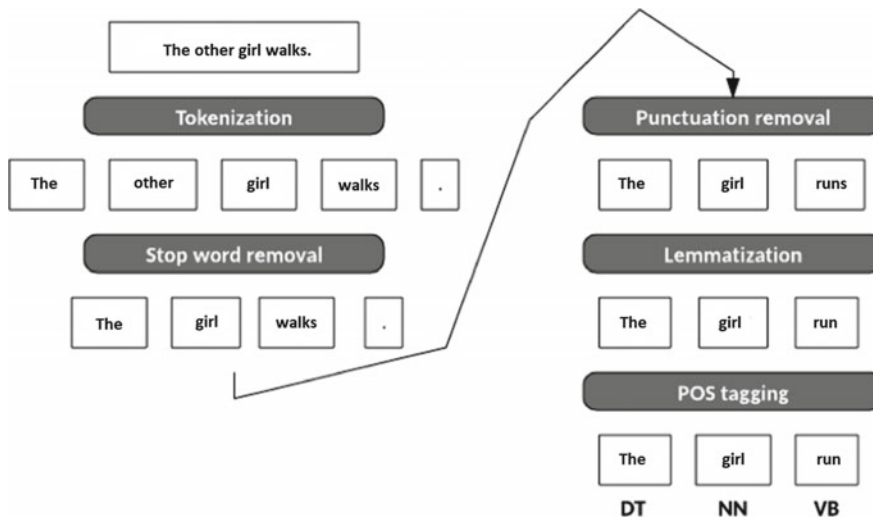


Fig. 2 Example of pre-processing tweets [10]

called Tweepy, [10] which makes it easy to download and collect data from Twitter. This technique has basically four modules:

- Classification
- Sentiment analysis
- Machine learning model
- Data acquisition

So, this technique uses the Twitter API which is used to collect all the tweets made by the user. This data is given as an input for sentiment analysis. Each tweet is assigned with relative sentiment.

Figure 2 is the example of how the tweets get analyzed and processed by searching keywords and using it for the detection of depression. It is then used as training dataset for the model. Then a classification is made based on the type of tweet. Basically, used for the text classification. Words are separated with the help of Tokenizer. Lemmatizer extracts similar words and later transforms them into a similar word. It usually helps keeping samples much smaller.

3.2 Process

This section describes techniques for detecting depression involved in feature extraction for facial recognition and social media analysis. The input for the machine learning stage is generated by the output of this processing stage, where no further manipulation of features takes place.

Facial Image Processing. Firstly, Viola–Jones algorithm is used to detect a face in each frame of the video sequence. Viola–Jones [2] algorithm makes use of Haar-like features as well as AdaBoost learning algorithm, for helping in extracting the background of the image. In this, they applied the Viola–Jones C++ program which was available in the OpenCV library. Secondly, for locating the landmarks on the face after the extraction, they used Landmark Model Matching (LMM) algorithm, this method consists of Active Shape Model and Elastic Bunch Graph matching. Landmark Distribution Model (LDM) was used which was constructed using the pre-defined facial landmarks in training datasets. For features extraction from the landmarks detected by LMM, Gabor wavelet is used. More importance is given to the interior landmarks compared to the landmarks located on the outer boundary for analysis. The training sets used were the mix of depressed as well as non-depressed subjects.

The authors used DCNN algorithm, which viewed the video data into two components. The first part carries the static information as well as the data regarding the appearance of the face. The second part is responsible for capturing the changes in expression as well as the facial dynamics. The only drawback of using DCNN is the data used for training the system is not sufficient; therefore, the authors used two types of data sets, first for pre-training and second to fine-tune the system. During the pre-training stage, the database containing 494,414 images was used to train the network from scratch. This step resulted in the system to capture the facial features effectively. In the next step of fine-tuning, the motive is to calculate the depression value from the individual frames of the image. In addition to the system proposed above, the authors used Dynamics-DCNN. It calculates the difference between the optical flows of multiple frames in a video. Finally, a joint layer is used to combine the results from two models proposed, and loss function is also calculated.

Social media analysis for depression detection. A harmonic analysis technique is being implemented which basically uses textual cues from the daily tweets of the user. Depending upon the major symptoms of MDD, keyword that seems to be negative are depression, sadness, tired, guilt, suicidal, anxiety and mental health. It is the assessment of the online communication may that be in the form of text, and measuring the sentiment in the online text [13]. There exists certain algorithm that makes it really easy and automates the sentiment analysis in an online text. Our sentiment analysis involves short texts as Twitter allows a 280 characters limit per tweet [10]. So, the best suited tool for our project is SentiStrength Sentiment Analysis. Its main highlight:

- Consists of a list of word based on a human's strength and polarity
- Auto spelling correction
- Has a word booster list
- List of negative words
- List of languages to identify common phrases

The tweets are passed through Senti-Strength Sentiment Analysis tool, and based on sentiment assigned to the keyword, it produces positive or negative sentiment to the tweet.

4 Performance

The categorical depression evaluation methods discussed in this section are grouped and compared in accordance with Tables 2 and 3 in terms of the dataset employed. In addition, with respect to the assessed characteristics, the findings are considered.

The various methods were evaluated on datasets or individual subsets of varying sizes, apart from disclosing different performance metrics. Performance standards are explained next in the report.

4.1 DAIC-WOZ Dataset

The method SimSensei kiosk, developed at the Institute of Creative Technologies University of Southern California (ICTUSC), was the basis for the development of the DAIC-WOZ dataset. SimSensei is a system of human–computer conversation developed to perform individual interviews while capturing and analyzing the interviewee's facial image and expression. On this dataset, several methods were tested, mainly from the relevant study, mainly from the relevant research community.

The importance of the audiovisual approach was tested by Scherer et al., gaining 89.74 % precision compared to 51.28 % of each modality characteristics and 64.10 %

Table 2 Comparison of depression assessment techniques according to used datasets [3]

Dataset	Paper	Participants	Features	Algorithm	Accuracy (%)
DAIC-WOZ	Yang et al. [6]	35	Full face, Audio, Ffacial landmarks & Text.	Random forest	86
	Scherer et al. [14]	39	Audio & Full face	SVM	89.74
AVEC	Senoussaoui et al. [15]	50	Full face	SVM	82
	Pampouchidou et al. [16]	200	Full face	Nearest neighbour	74.5

Table 3 Tweets keywords [10]

Keywords	Number of tweets	Accuracy (%)
Depression	6908	79.46
Suicidal	1100	81.00
Sadness	1100	79.56
Tired	1100	81.46

of each one-modality visual characteristics. Scherer et al. investigated linear correlations between the occurrence of particular characteristics and the type of condition in subsequent publications, showing major variations in anxiety, post-traumatic stress disorder (PTSD), depression, and smile behavior.

4.2 AVEC Dataset

The AVEC depression detection dataset, while considered for continuous evaluation, was also used for categorical evaluation using case groupings based on BDI ratings. Senoussaoui et al. gained 82%, accuracy for evaluation of depression. Normal BDI cutoffs considered by Pampouchidou et al. was

- 0 to 9 as low level.
- 10 to 18 as mild-level.
- 19 to 29 as moderate level.
- 30 to 63 as severe level.

In distinguishing cases, the recorded accuracy was 74.5%. The overall accuracy for this dataset was 63.5%.

4.3 Social Media Analysis Dataset

Researchers justified the model performance of depressed users on various scales and are compared and grouped in terms of keywords found in Table 3. Researchers fixed our dataset's capacity to 1500, with depressed users counting 1402 in total and the scale varied from 10 to 90% of depressed users with an increase in 10 %. It can be noticed that while depression users' scale ranged from 40 to 60 %, with the highest results at 50 %, our approach achieved an outstanding performance [10].

They obtained a reasonable performance under imbalanced scales. Therefore, in the tests, non-depressed users counting 1402 on D2 were chosen randomly to make the 50% depressed users scale. Thus, they discovered some fascinating results.

- Time for posting—Users who are depressed (+44 % on average) post tweets between 11:00 PM and 6:00 AM, showing that insomnia is prone to them.
- Catharsis of Emotion—They found positive words up to 0.37 and negative words up to 0.52 per tweet for depressed users,
- Where among non-depressed users, the count was 0.17 for positive words and 0.23 for negative words. More emotions are expressed by depressed users ,especially negative emotions on the social media.
- Knowledge of oneself—in contrast to non-depressed users, approximately 200 % more first personal pronouns were used in tweets of depressed users, which may suggest their silenced speeches and high sense of self-awareness.

5 Future Scope

Automatic depression appraisal research has fallen a long way from McIntyre et al. and Cohn et al. [17], both in terms of technique and results, with some novel methods. The latest systematic state-of-the-art analysis presents a variety of perspectives, while highlighting several issues that remain subject to further study. In clinical psychology and psychiatry, depression detection itself is an active and contentious subject. The development of automated, analytical measurement approaches can be useful for both study and clinical practice, considering the above outstanding problems. In addition, the observations are consistent with depression's social detachment, emotion-context insensitivity, and diminished a reactivity hypothesis.

In addition, through the quantitative research reported in this study, the importance of complex characteristics as well as multimodal approaches was also illustrated. It suggests that continuous methods are more in line with clinical practice. In order to increase the reliability and comparability of information, it is important to facilitate the exchange of similar data and to standardize data collection procedures in many domains. Interestingly, while physiological activity assessed by BVP, respiration, EMG, and skin conductance may be insightful about occurring emotional responses, such data has not been implemented in multimodal studies, excluding Zhou et al. [18], who reported heart rate using non-contact, facial video-based method. Body demonstrations, as well as pupil-related attributes, have also not been sufficiently used for automated evaluation, even though they are shown to be statistically relevant.

6 Conclusion

The systematic analysis of the data available highlights the important potential of using video-based approaches to determine and track the progression of depression. It was also made clear that to obtain clinically relevant outcomes, visual signals need to be accompanied by knowledge from other modalities. While a multitude of techniques are documented in the literature in terms of relevant algorithms, automated depression evaluation is still a very long journey from being well developed, with considerable space for progress on current methods.

Acknowledgements We would like to thank SVKM's NMIMS Mukesh Patel School of Technology Management and Engineering for providing research facilities and to Prof. Pratiksha Meshram (Assistant Professor, Department of Information Technology) for their support and encouragement.

References

1. Islam M, Kabir M, Ahmed A, Kamal A, Wang H, Ulhaq A (2018) Depression detection from social network data using machine learning techniques. *Health Inf Sci Syst* 6(1):8. <https://doi.org/10.1007/s13755-018-0046-0>
2. Viola P, Jones M, Rapid object detection using a boosted cascade of simple features. <https://doi.org/10.1109/CVPR.2001.990517>
3. Zhu Y, Shang Y, Shao Z, Guo G (2017) Automated depression diagnosis based on deep networks to encode facial appearance and dynamics.: *IEEE Trans Affect Comput* 9(4):578–584. <https://doi.org/10.1109/TAFFC.2017.2650899>
4. Alghowinem S, Goecke R, Cohn J, Wagner M, Parker G, Breakspear M, Cross-cultural detection of depression from nonverbal behaviour. <https://doi.org/10.1109/FG.2015.7163113>
5. Jraidi I, Chaouachi M, Frasson C, A dynamic multimodal approach for assessing learners' interaction experience. <https://doi.org/10.1145/2522848.2522896>
6. Yang L, Jiang D, He L, Pei E, Ovemeke M, Sahli H, Decision tree based depression classification from audio video and language information. <https://doi.org/10.1145/2988257.298826>
7. Jan A, Meng H, Gaus Y, Zhang F, Turabzadeh S, Automatic depression scale prediction using facial expression dynamics and regression. <https://doi.org/10.1145/2661806.2661812>
8. Tzirakis P, Trigeorgis G, Nicolaou M, Schuller B, Zafeiriou S (2017) End-to-end multimodal emotion recognition using deep neural networks.: *IEEE J Sel Top in Sig Process* 11(8) 1301–1309. <https://doi.org/10.1109/JSTSP.2017.2764438>
9. Kelly D, Spaderna M, Hodzic V, Nair S, Kitchen C, Werkheiser A, Powell M, Liu F, Coppersmith G, Chen S (2020) Blinded clinical ratings of social media data are correlated with in-person clinical ratings in participants diagnosed with either depression, schizophrenia, or healthy controls. *Psychiatry Res* 113496: <https://doi.org/10.1016/j.psychres.2020.113496>
10. Biradar A, Totad S, Detecting depression in social media posts using machine learning. https://doi.org/10.1007/978-981-13-9187-3_64
11. He L, Cao C (2018) Automated depression analysis using convolutional neural networks from speech. *J Biomed Inf* 83:103–111. <https://doi.org/10.1016/j.jbi.2018.05.007>
12. Shen G, Jia J, Nie L, Feng F, Zhang C, Hu T, Chua T, Zhu W, Depression detection via harvesting social media: a multimodal dictionary learning solution. <https://doi.org/10.24963/ijcai.2017/536>
13. Cacheda F, Ez D, Novoa F, Carneiro V (2019) Early detection of depression: social network analysis and random forest techniques. *J Med Internet Res* 21(6): <https://doi.org/10.2196/12554>
14. Scherer S, Stratou G, Mahmoud M, Boberg J, Gratch J, Rizzo A, Morency L, Automatic behavior descriptors for psychological disorder analysis. <https://doi.org/10.1109/FG.2013.6553789>
15. Senoussaoui M, Sarria-Paja M, Santos J, Falk T, Model fusion for multimodal depression classification and level detection. <https://doi.org/10.1145/2661806.2661819>
16. Pampouchidou A, Simos P, Marias K, Meriaudeau F, Yang F, Pediaditis M, Tsiknakis M (2017) Automatic assessment of depression based on visual cues: a systematic review.: *IEEE Trans Affect Comput*. <https://doi.org/10.1109/TAFFC.2017.2724035>
17. Saragih J, Lucey S, Cohn J, Face alignment through subspace constrained mean-shifts. <https://doi.org/10.1109/ICCV.2009.5459377>
18. Zhang Q, Wu Q, Zhou Y, Wu X, Ou Y, Zhou H (2017) Webcam-based, non-contact, real-time measurement for the physiological parameters of drivers. *Measurement* 100:311–321. <https://doi.org/10.1016/j.measurement.2017.01.007>

Classification of Social Media Users Based on Temporal Behaviors and Interests



Murad Hossen, Tamanna Afrose, Atashi Mani Ghosh,
and Md. Musfiq Anwar

Abstract Most existing works on categorization of social media users in online social networks (OSNs) consider only the topical interest of users as the basis for user classification. The temporal evolution of user topical interests has not been thoroughly studied to identify their effects on the classification of social users. In this paper, we investigate the problem of discovering/classifying and tracking time-sensitive activity-driven social user classification in OSNs. The users in a particular class have the tendency to be temporally similar in terms of their temporal degree of topical interests. Our main idea is based on the observation that the degree of users' topical interests often degrades or upgrades widely over a period of time. The temporal tendency of user activities is modeled as the freshness of recent activities by tracking the social streams with a fading time window.

Keywords Online social network · Temporal activity · Topical interest · Fading time window · Social stream

1 Introduction

OSNs have become one of the mainstream mediums for communication as these platforms provide multiple modes of communication, enable diverse interaction types, and allow sharing of user-generated contents (e.g., blogs, tweets, and videos). On social media platforms, the tendency of users with similar interests, choices, and preferences into common category/class. Many existing works have studied this problem such as [1] clustered user attributes (such as first and last name, location) based on both the communication of users with those attributes as well as content similarity [1–5]. A supervised approach was proposed in [6] which considered properties of users profiles and user-generated contents to classify users. However, the common aspect of the above works is that they did not study the temporal degree of users' topical interests. That is to say, these methods cannot identify the temporal informa-

M. Hossen (✉) · T. Afrose · A. M. Ghosh · Md. M. Anwar
Computer Science and Engineering Department, Jahangirnagar University, Savar, Bangladesh
e-mail: manwar@juniv.edu

tion associated with the network, and thus cannot detect how the classification may evolve over a period of time.

In this work, we introduce a novel concept of user's temporal topical activeness. It refers to the level of participation of a user toward certain topics and emphasizes her degree of interest on those topics at a time period. According to our observation, the interest of users on different topics keeps changing with time based on several external factors.

Given a query Q consisting of a set of topics such as politics, sports, technology, and entertainment, our system will classify users accordingly to Q based on their temporal interests at each time interval. We also classify *active* publishers (users who are highly active) for each of the topic, etc. We choose an overlapping time window that partially overlaps with the prior window to track the changes in each class over time. Our main motives of this work are as follows:

- Introducing a novel concept of user's temporal topical activeness.
- Classifying the Twitter user according to their behavior and interest.
- Monitoring the changing behaviors of users' according to time and their response to different changing events.

In the rest of the paper, we present the related works in Sect. 2 and formulate the problem of classification of social users in Sect. 3. The details of the proposed framework are described Sect. 4. Our experimental results are shown in Sect. 5, and finally, we conclude the paper in Sect. 6.

2 Related Work

Existing research works on classification of users in Twitter mainly considered users' profiles as well as different features such as gender, number of hashtags, URLs, retweets, mentions, emoticon, and symbols. For example, authors in [7] considered users' profiles, behaviors, and content-specific information to classify them into two board categories such as *real user* and *digital user*. This classification method was designed specifically for security purpose, and hence, it did not consider users' topical interests over time.

Pennacchiotti et al. [8] proposed a model based on machine learning model techniques that can automatically determine different attributes of users' such as their political orientation or ethnicity, etc. Rao et al. analyzed both users' profiles and tweet contents and considered features such as gender, age, regional origin, and political orientation to train support vector machine (SVM) classifier in order to classify Twitter users [9]. Munjal et al. [10] also developed a framework for analyzing twits.

Alabdullatif et al. chose to classify Arabic Twitter users' based on their topical interest in recent trends in Twitter as well as the relationships between members of a community [6]. Boyd et al. [11] examines the tweeting and retweeting activities of users in order to differentiate them. The authors in Hofman et al. [12] introduced a method that classifies users into *elite* and *ordinary* groups. They further classified *elite*

users into one of four categories based on their interests related to *media*, *celebrities*, *organizations*, and *bloggers*.

Thelwall et al. [13] focused on gender-based classification by identifying the text patterns of positive and negative emotions in the tweets. Lim et al. [14] proposed a framework that classifies Twitter users into three different categories such as *organization*, *journalists/bloggers*, *individuals* with the help of the information from Wikipedia. Similarly, authors in [8] classify users into three different classes based on their affiliation/involvement in politics, ethnicity, and affinity toward a particular business. They considered features such as users' profiles, tweeting behaviors, and linguistic contents of the tweets. Recently, Munjal et al. [15] developed a new strategy for opinion mining based on Ostwald ripening [16]. All these foregoing investigations did not consider users' temporal topical interests as we observed that social users' topical interests vary widely over time. Again, they have different degrees of interests in different topics.

3 Preliminary and Problem Definition

At first, we focus on some key terminologies used in this work before describing the details of our proposed approach.

Social Network: We model the online social media as a graph $G = (U, E, T)$, where the vertex set U indicates social media users, the edge set E pointing the virtual relations among the users, and the set T indicates those topics that the social users usually pay more attentions [17].

Topic: A topic usually consists of several keywords that are related to that topic. For example, *online social media* topic has words like post, share, follower, upload, etc.

Activity in Twitter: Twitter users conduct different actions at different times such as post new tweets, replies, or retweets of existing tweets. These actions are considered as activities. Each activity ($\langle u_i, T_x, t_j \rangle$) has three things: the owner of the activity (u_i), topic of the activity (T_x), and the time of the action (t_j). A set S indicates all the valid activities in Twitter.

Overlapping Time Window: We consider *overlapping time window* in this work. Total time period is partitioned into equal-length intervals denoted as $\mathcal{I} = \{I_1, \dots, I_m\}$.

Recency Score: Social users perform different actions at different time points as their topical interests vary widely over time. So, we emphasize more to user's recent activities by a measure called *recency score* [18], denoted by $\mu \in [0, 1]$. Equation (1) shows that an exponential time-decay function is used to measure the value of μ .

$$\mu_{\langle u_i, T_x, t_j \rangle} = \exp(-a \times \text{age}_{\langle u_i, T_x, t_j \rangle}) \quad (1)$$

The parameter a is used to control the speed of decay and $\text{age}_{\langle u_i, T_x, t_j \rangle}$ represents the total time that passed since the occurrence of the action.

Query: An input query Q contains a set of topics $\{T_1, T_2, \dots, T_n\}$. At each time interval I_m , our proposed model categories the users according to the given query Q .

User's Interest Score: For each user $u_i \in U$, we compute her interest score to measure her involvement toward a query Q in a time interval I_m , using Eqs.(2) and (3), where $t_j \in I_m$, $T_x \in Q$ and $\psi_{(u_i, Q, I_m)}$ is the user's degree of topical interest compared to the total number of activities performed by all the users.

$$\psi_{(u_i, Q, I_m)} = \sum \mu_{(u_i, T_x, t_j)} \quad (2)$$

$$\sigma_{(u_i, Q, I_m)} = \frac{\psi_{(u_i, Q, I_m)}}{\max_{u_z \in U} \{\psi_{(u_z, Q, I_m)}\}} \quad (3)$$

Problem Definition: Given a social network $G = (U, E, \mathcal{T})$, an activity set S , time interval set \mathcal{I} , and a query Q , our proposed model classifies the users U into set of different categories (according to the query topics) at each time interval I_m .

4 Proposed Framework

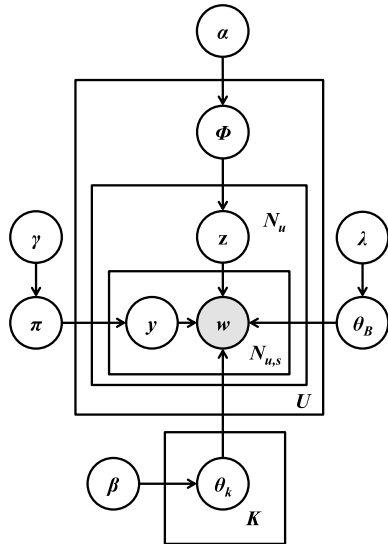
Our proposed framework has two major steps to classify social media users for a given query Q . At first, the system filters out the noisy tweets and apply a topic modeling method on the cleaned tweets to identify the latent topics. Then, it applies an algorithm to perform the desired classification of the users at each time interval I_m .

4.1 Data Pre-processing for Topic Detection

Social users often posts noisy contents (messages or tweets) which may contain misspelled words, grammatically incorrect words/phrases, for example, tmrw for tomorrow, gr8 for great, etc. In this work, we applied a normalization lexicon proposed in [19] to convert those noisy words into their standard meaningful and correct form.

Twitter users often use hashtags (for example, #Trump, #Ronaldo, etc.) in tweets to indicate the topic. There is no standard rule for defining hashtags, and as result, it is not suitable to infer the topic of tweet using hashtags. So, we apply a topic modeling approach named Twitter-LDA (T-LDA) [20], which is an unsupervised learning that generates information and analyzes words from documents by linking words with the same features and differentiate across the uses of words with various meanings. Twitter-LDA (T-LDA) is an effective extension of LDA [21] model and is used for topic distillation. The graphical representation of T-LDA is shown in Fig. 1. The formulation of T-LDA is given below:

Fig. 1 Graphical representation of Twitter-LDA model



- The symbol ϕ_i denotes the topical interests of social users' in Twitter. These topical interests are comprised over N different topics.
- Every topic has background word distribution (θ_{bw}) as well as topic word distribution (θ_{kw}).
- A latent variable y is used to identifies whether a word is from background word distribution (θ_{bw}) if $y = 0$, or from topic word distribution (θ_{kw}) when the value of $y = 1$.
- A variable π is a common factor which is the ratio of background words and topic word. Again, θ_{kw} and θ_{bw} have similar rate at π .

4.2 Query-Oriented Topical Classification Algorithm

We develop an algorithmic framework to detect and track users' topical clusters.

Algorithm overview. The algorithm first computes the users' interest score $\sigma_{(u_i, Q, I_m)}$ at each time interval I_m (line 1–3). Then, it places the users, whose interest score $\sigma_{(u_i, Q, I_m)} \geq 0.25$, into related categories (line 4–5). Finally, it outputs the desired classification of the users Φ^Q at each I_m (line 8).

Algorithm 1 Query-Oriented Topical Classification Algorithm**Input:** $G = (U, E, T), \mathcal{I}, Q$ **Output:** set of topical clusters (categories) $\Phi_Q = \{\mathcal{C}_{T_1}, \mathcal{C}_{T_2}, \dots, \mathcal{C}_{T_n}\}$

```

1: for each  $I_m \in \mathcal{I}$  do
2:   for each  $u_i \in U$  do
3:     compute  $\sigma_{(u_i, Q, I_m)}$ 
4:     if  $\sigma_{(u_i, Q, I_m)} \geq 0.25$  then > each  $u_i \in U$  has to perform certain number of actions related
      to  $Q$ 
5:        $\mathcal{C}_{T_j}.add(u_i)$ 
6:     end if
7:   end for
8:   Output the set of topical clusters  $\Phi_Q$  at each time interval  $I_m$ 
9: end for

```

Table 1 Sample word topic distribution in T-LDA model

Politics	News	Entertainment	Economy
Vote	Report	Media	Job
Democrat	Live	Video	Market
Republican	Weekly	Song	Fund
Elect	Campaign	Awesome	Credit
Senat	Terror	Game	Tax

5 Experimental Results

We conduct the experiment on a Twitter dataset named CRAWL [22]. In CRAWL dataset, we randomly choose 100 users and select their tweets from January 22, 2012 to March 07, 2012. The total number of tweets used in the experiment is 2,60,168. We divide the total time period into several time intervals each of which is 7 d in length, i.e., $\text{len} = 7$ days. Again, we consider overlapping time window that overlaps in every 3 d (i.e., $\Delta t = 3$ days).

We consider total six (6) topics such as $\{politics, news, entertainment, religion, economy\}$, and $technology$. Table 1 shows some representative words for four topics. To classify a user u_i into a particular category according to the given query Q , we want that u_i has to exhibit certain degree of topical interests in a particular time intervals I_m . Hence, in this work, we set a threshold value on users' topical interest score ($\sigma_{(u_i, Q, I_m)} \geq 0.25$) in order to check the eligibility of a user to be considered in a particular classification.

Table 2 shows the number of users in different topics at three different time intervals (T1, T2, and T3) in which the query Q is set to just a single topic. We see that there are different number of users for each topic at different time intervals as their topical interests as well as topical activities vary over time.

In this work, we set a limit to 2–3 topics for a query Q to contain multiple topics. Again, we consider topical cohesiveness in this case with two variations. One of the

Table 2 Number of topical users at different time intervals

Topic	T1 (31/01–06/02)	T2 (03/02–09/02)	T3 (06/02–12/02)
Politics	20	25	23
News	39	33	30
Technology	24	39	36
Entertainment	47	39	51
Economy	42	47	49
Religion	9	13	12

Table 3 Number of topical users for multiple interest at different time intervals

Query	T1 (31/01 – 06/02)		T2 (03/02 – 09/02)		T3 (06/02 – 12/02)	
	Relax	Strict	Relax	Strict	Relax	Strict
News, technology	46	38	61	48	54	43
News, technology, economy	59	31	71	38	63	34
Technology, politics	45	36	61	37	59	34
Technology, politics, religion	47	29	62	30	68	27
Entertainment, economy	56	53	51	50	60	56
Entertainment, economy, religion	60	39	54	35	61	39

variations is *relax* in which a user will be considered as an eligible member of a particular category if she expresses her interest in any one of the topics (T_x) related to the query Q , i.e., $T_x \in Q$. The other variation is *strict* where a user has to show her inclination to all the topics related to Q in order to become a candidate member to a particular class.

Table 3 shows the changes in different categories for different queries consisting of multiple topics both for *relax* and *strict* variation of topical cohesiveness. We can see that the number of users in each category is less in *strict* version compare with the *relax* version for the same query as not all the users have topical interests in all the query topics. For the same reason, the number of users decreases in *strict* version as we add more topic(s) in a query Q . For example, the second row in Table 3 shows that the number of users (for topics {news, technology, economy}) decreases in each time interval compare with the number of users in first row (for topics {news, technology}) as we increase the number of topic (i.e., adding the topic *economy*). We also observe that different combination of topics produce different results, for example, there are more number of users in the category when the query is set to the topics of {technology, politics} compare with the query consisting of the topics of {politics, and religion}.

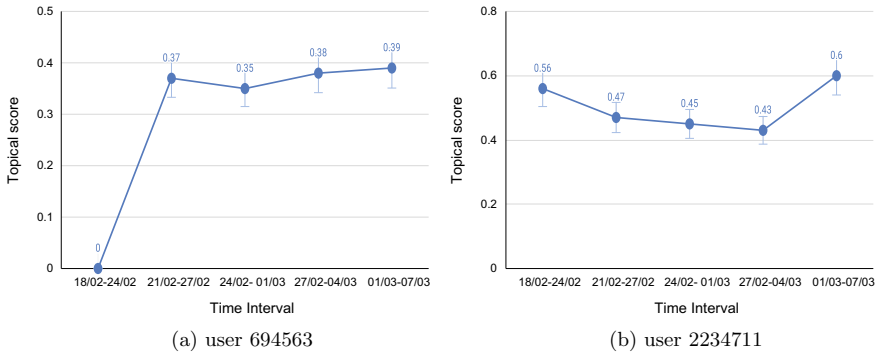


Fig. 2 Tracking topical interest score (σ) of user ID 2234711 for the topic of *news* and user ID 694563 for the topic of *politics* at different time intervals

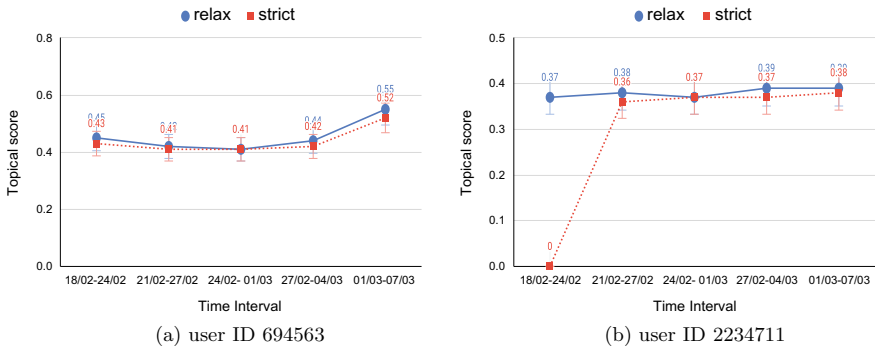


Fig. 3 Tracking topical *relax* and *strict* interest score (σ) of user ID 2234711 and user ID 694563 for the query consisting of *{religion, politics}* at different time intervals

We also track the changes in topical interests of two users for two different topics at different time intervals. Figure 2 show the changes of topical interest scores (σ) of user ID 694563 and 2234711 in *politics* and *news* topic, respectively. We can see that both the users have a different degree of topical interests at different time intervals.

We also track the changes in topical interests of two users for a query having multiple topics at different time intervals with two variants *relax* and *strict*. Figure 3 shows the changes of topical interest scores (σ) of user ID 2234711 and 694563 in both *religion* and *politics* topics for *relax* and *strict* interest. Here, we also see that both the users have different degree of topical interests at different time intervals.

6 Conclusion

In this work, we propose a method to track the online social users' topical interests over time and classify them accordingly into different categories. Experiment results on a real Twitter dataset show that the users in a particular class have the tendency to be temporally similar in terms of their temporal degree of topical interests which keep changes widely over time.

References

1. Bergsma S, Dredze M, Van Durme B, Wilson T, Yarowsky D (2013) Broadly improving user classification via communication-based name and location clustering on twitter. In: Proceedings of the 2013 conference of the North American chapter of the association for computational linguistics: human language technologies, pp 1010–1019
2. Anwar MM, Liu C, Li J (2018) Uncovering attribute-driven active intimate communities. In: Australasian database conference. Springer, pp 109–122
3. Aurora TT, Khan F, Anwar MM (2020) Discovering and tracking query oriented topical clusters in online social networks. In: IEEE region 10 symposium (TENSYMP). IEEE 2020, pp 1054–1057
4. Das BC, Ahmed MS, Anwar MM (2020) Query-oriented active community search. In: Proceedings of international joint conference on computational intelligence. Springer, pp 495–505
5. Das S, Anwar MM (2019) Discovering topic oriented highly interactive online community. *Front Big Data* 2:10
6. Alabdullatif A, Shahzad B, Alwagait E (2016) Classification of arabic twitter users: a study based on user behaviour and interests. In: Mobile information systems 2016
7. Uddin MM, Imran M, Sajjad H (2014) Understanding types of users on twitter. arXiv preprint. [arXiv:1406.1335](https://arxiv.org/abs/1406.1335)
8. Pennacchiotti M, Popescu A-M (2011) A machine learning approach to twitter user classification. In: Fifth international AAAI conference on weblogs and social media
9. Rao D, Yarowsky D, Shreevats A, Gupta M (2010) Classifying latent user attributes in twitter. In: Proceedings of the 2nd international workshop on search and mining user-generated contents, pp 37–44
10. Munjal P, Narula M, Kumar S, Banati H (2018) Twitter sentiments based suggestive framework to predict trends. *J Stat Manag Syst* 21(4):685–693
11. Boyd D, Golder S, Lotan G (2010) Tweet, tweet, retweet: conversational aspects of retweeting on twitter. In: 43rd Hawaii international conference on system sciences. IEEE 2010, pp 1–10
12. Wu S, Hofman JM, Mason WA, Watts DJ (2011) Who says what to whom on twitter. In: Proceedings of the 20th international conference on world wide web, pp 705–714
13. Thelwall M, Wilkinson D, Uppal S (2010) Data mining emotion in social network communication: gender differences in myspace. *J Am Soc Inf Sci Technol* 61(1):190–199
14. Lim KH, Datta A (2013) Interest classification of twitter users using wikipedia. In: Proceedings of the 9th international symposium on open collaboration, pp 1–2
15. Munjal P, Kumar S, Kumar L, Banati A (2017) Opinion dynamics through natural phenomenon of grain growth and population migration. In: Hybrid intelligence for social networks. Springer, pp 161–175
16. Munjal P, Kumar L, Kumar S, Banati H (2019) Evidence of Ostwald ripening in opinion driven dynamics of mutually competitive social networks. *Phys A Stat Mech Appl* 522:182–194
17. Anwar MM, Liu C, Li J (2019) Discovering and tracking query oriented active online social groups in dynamic information network. *World Wide Web* 22(4):1819–1854

18. Anwar MM, Liu C, Li J, Anwar T (2017) Discovering and tracking active online social groups. In: International conference on web information systems engineering. Springer, pp 59–74
19. Han B, Cook P, Baldwin T (2013) Lexical normalization for social media text. ACM Trans Intell Syst Technol (TIST) 4(1):1–27
20. Zhao WX, Jiang J, Weng J, He J, Lim E-P, Yan H, Li X (2011) Comparing twitter and traditional media using topic models. In: European conference on information retrieval. Springer, pp 338–349
21. Blei DM, Ng AY, Jordan MI (2003) Latent Dirichlet allocation. J Mach Learn Res 3:993–1022
22. Bogdanov P, Busch M, Moehlis J, Singh AK, Szymanski BK (2013) The social media genome: modeling individual topic-specific behavior in social media. In: Proceedings of the 2013 IEEE/ACM international conference on advances in social networks analysis and mining, pp 236–242

Stability and Dynamic Power Analysis of Novel 9T SRAM Cell for IoT Applications



Ashish Sachdeva and V. K. Tomar

Abstract With increasing need for on-chip computation of data in Internet of things-based devices, the onboard SRAM memory has remain under renovation phase to eliminate classical obstacles of stability and power dissipation. To resolve the read/write conflict of SRAM cell with lesser power consumption and moderate delay, a novel 9T SRAM cell has been proposed. The power consumption has been found be reduced at least by 28.90% with proposed circuit in strong inversion region. Delay and stability factors are noted and compared with conventional 6T. Furthermore, bit-line leakage reduced to get efficient read and hold power was observed to be 2.509 pW. The dynamic power during read cycle is investigated. In the worst-case scenario, the cell sustains the write ability till 400 mV supply voltage. The area of layout for proposed cell was calculated to be $1.72 \times$ of standard 6T SRAM cell. For simulation purpose, 45 nm CMOS technology node with Cadence Virtuoso tool is used.

Keywords Internet of things · SRAM · Low power · Stability

1 Introduction

The simplicity of connectivity with mobile battery-operated devices used for Internet of things-based applications has resulted in to explosive increase of Internet usage through all over the world. Embedded memories take the supreme space in silicon-on-chip devices, which are frequently realized with standard 6T SRAM cells. All the Internet of things-based applications, where low energy consumption, is the prominent factor, and performance gets minor, requires the circuits which can propose ‘Read’ and ‘Write’ operations at minimum likely voltage level. In many applications like portable devices such as cell phones or some sensor networks in the modern era, low power is a limitation, where the performance or may be the area can be negotiated [1]. The wide spread choice for decreasing the power is scaling the supply voltage

A. Sachdeva (✉) · V. K. Tomar
GLA University, Mathura, India
e-mail: vinay.tomar@ieee.org

which has its effect of quadratic reduction in power by the virtue of CV_{dd}^2 . When this attempt applied to conventional design in order to achieve the minimum power level, it creates the challenges of decreased SNM with certain trade-off of performance [2]. The power alone has a number of components, i.e., static power, dynamic power, average power, and peak power. So far much of the emphasis has been on the static power. However, the maximum consumption has been seen in dynamic power where switching is one of the prominent factors. Swing and supply voltage remain minor summarized by the following Eq. (1)

$$P_{\text{avg}} = p_t(C_L \cdot V \cdot V_{dd} \cdot f_{clk}) + I_{\text{leakage}} \cdot V_{dd} + I_{sc} \cdot V_{dd} \quad (1)$$

The first term explains the switching component of power, C_L is the load capacitance, V is voltage swing, expected to be same as supply voltage V_{dd} . However, swing on internal nodes is slightly less. Clock frequency and p_t probability that power consuming transition occurs are other effecting factors [3]. Therefore, it is evident that superior assistance is expected by reduction in V_{dd} . Though this should also be clearly understood, this meek solution comes at the cost of increase in delay, given by, Eq. (2), determined experimentally in [4].

$$T_d = \frac{(C_L \times V_{dd})}{I} = \frac{(C_L \times V_{dd})}{\frac{\mu C_{ox}}{2} \left(\frac{W}{L} \right) (V_{dd} - V_t)^2} \quad (2)$$

Another move towards low power model was to have dual or multi-threshold transistors and choosing minimal width-length ratio. Due to this minimal design, in nanometer region, the random dopant density fluctuations in source and drain also results in slight increase in threshold voltage V_{th} [5]. It must be understood that stability of SRAM cell design is also affected by changing electrical parameters. Beyond, this variability and scaling down the supply voltage seriously affect the stability of SRAM and result in reduction of SNM. Explicit analytical functions have been investigated in [6–8] that describe SNM as a function of device parameters and supply voltage. This SNM is divided into two separate categories: first read cell stability, which requires both N -curve metrices, i.e., SVNM and SINM, and second write ability which account for WTI and WTV. Read stability is a prominent issue in the 6T cells because the access transistor is moderately weak comparing to the pull-down transistor, so as to keep the read SNM to upright mode. However, this access transistor needs to be very strong then pull-up transistor so as to keep writes ability in order. This confirms the conflicting constraints between the read and write operations of conventional 6T SRAM cell. It can easily conclude by going through carefully in [9, 10] that, with decrease in supply voltage SINM clearly reduces, though the increment in WTI was noted. Another observation shows the simultaneous increase in SVNM and WTV with decrease in supply voltage. However, SNM cannot be explained alone by voltage margins but corresponding current has to be taken in to account. When no significant rise or fall in SVNM is noted, even after changing the

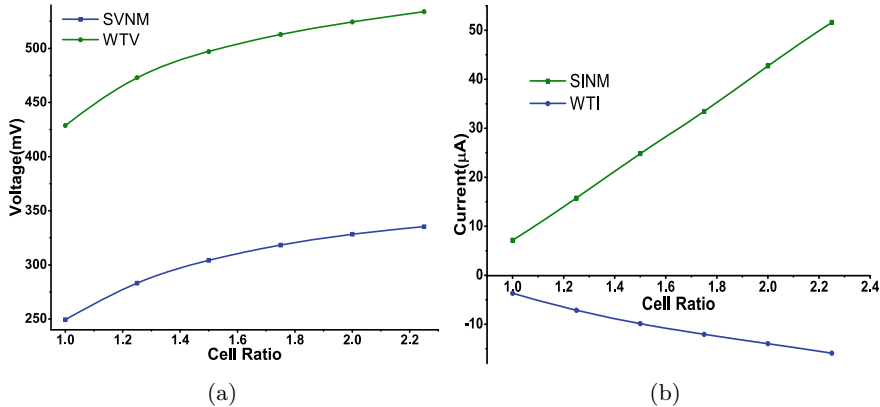


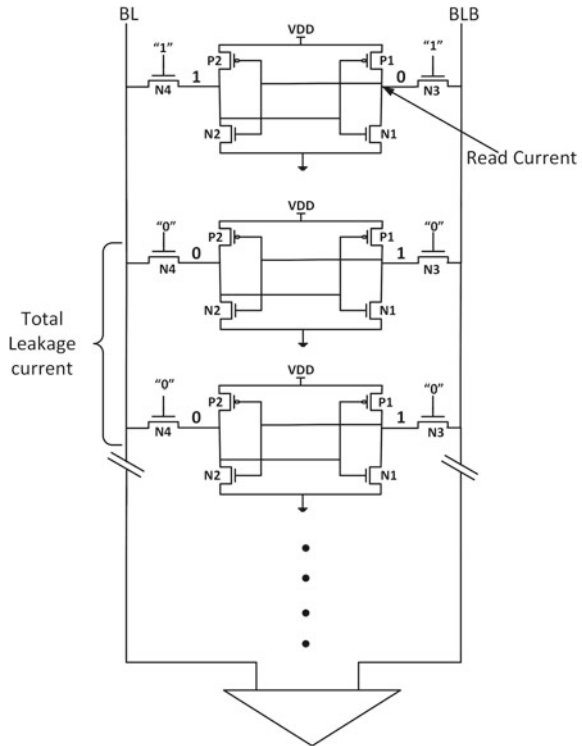
Fig. 1 **a** SVNM, WTV versus cell ratio **b** SINM, WTI versus cell ratio

major electrical parameter, the current explains the change in stability of concerned circuit. SVNM and SINM were plotted with V_{dd} as shown in Fig. 1a, b, respectively.

Some exciting conclusions were drawn such as both parameters decrease with lowering the V_{dd} . It is also worthy to note that, a slight reduction in WTV and a small decrease in absolute value of WTI with lowered supply voltage results in better write ability [9, 11]. Henceforth, for smaller WTI and high SINM at low supply voltage, some trade-off is required. This again leads to the fact that read and write SNM can be improved in conventional 6T SRAM cell up to a certain level only. Therefore, it is a major challenge to develop a topology that can simultaneously improve the read and write metrics with lower supply voltage. Furthermore, in sub-threshold region lower current is expected, because of low gate drive. Taking this consequence to the next level leakage current from the non-accessed cells shared with the bit lines can make the things unrealistic as shown in Fig. 2. In the larger context of array, depending upon the data stored in bit cells, bit-line leakage can exceed read current making the droop on the both bit-line fuzzy [12]. To address these challenges, many of the ways were suggested to get the correct values in read and write operation simultaneously keeping area and performance in control. However, in any of the case trade-off with power or performance (delay) is expected.

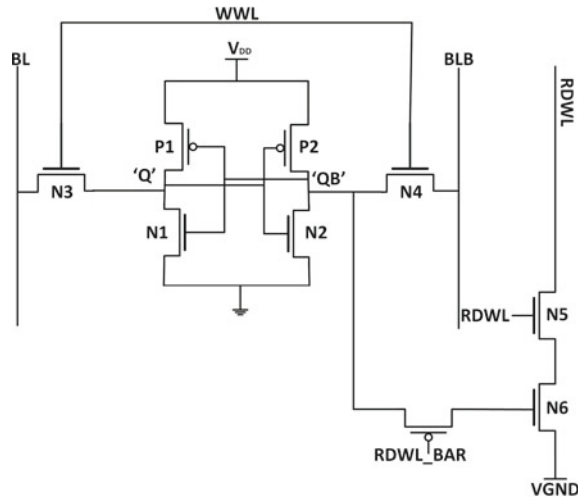
A widespread study has been performed which suggested, a practical approach for decoupling of read and write ports to have a read static noise margin-free read in 7T cell. However, area and other assisting circuits are the additional cost that need to be tolerated. The read performance of 7T cell is also degraded due to single-ended sensing. It may be because of loss of drive of NMOS. Following sections start by explaining a new proposed circuit. Further, the proposed circuit results have been analyzed and compared with conv. 6T design followed by conclusive remarks.

Fig. 2 Bit-line leakage current



2 Proposed Circuit Description

The suggested circuit consists of nine transistors, where N1–N4 along with P1 and P2 form the basic structure of standard 6T SRAM cell. N5 and N6 transistors form decoupled structure for read to get higher SNM, and P3 is linking transistor between the decoupled structure and QB , opposite to data written on Q . In read operation, RDWL input is made high and WL kept low, which in turn gives equal supply at WWL and RDWL. The circuit works in bidirectional mode so as to keep SNM on higher end, and the two outputs for read are BLB and RWBL. Being an obvious fact that in a three bit-line circuit, the power feeding will be on higher side; however, the advantage of separate read and write structure can be taken in this case. P3 transistor has RDWL_BAR as input to its gate. The W/L of P3 is kept on lower side, but the capability of good passage of ‘high’ of PMOS is utilized. Transistor N6 of the decoupled circuit depends upon the bit present at QB. As per convention, to ensure that the circuit read correct bit, access transistor N5 is kept weaker than pulldown transistor N6. Though the W/L ratio of N5 is also kept moderate to keep the resistance low, the trans-conductance and the current competence are directly related to the W/L ratio. A higher W/L ratio works in both ways, on positive side it upsurges the current

Fig. 3 Proposed 9T cell

gain and subsequently a higher current low, and corresponding value is given to RDWL_BAR. It ensures the two things, one is, it disconnects the decoupled circuit from 6T cell, confirming very less leakage while the cell remains in write/standby mode and second is to ensure that during write process the decoupled circuit does not interfere in writing the correct bit and add up to any variations (Fig. 3).

3 Simulation Results

The simulation of the proposed cell has been carried out on 45 nm technology in Cadence virtuoso tool. The dynamic power dissipation, read delay, and write delay have been noted and compared with a few available existing results of standard circuits. Write operation, except the higher voltage at access transistors, is very much parallel to conventional design. For the read operation, the cell has been tested at typical corner. Nevertheless, in the typical corner showed certain delay but bit lines in the presence of variations are also good enough to score right read in sense amplifier [13]. Simulation results also confirm that the differential write eases the writability of the proposed cell at low voltages.

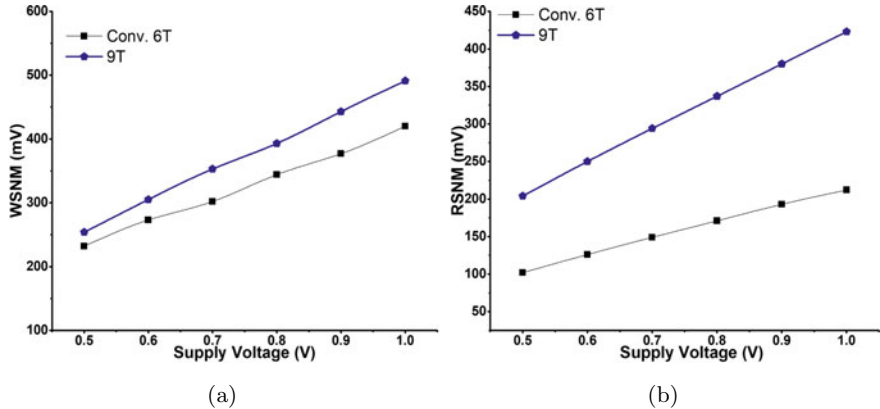


Fig. 4 **a** WSNM versus V_{dd} **b** RSNM versus V_{dd}

3.1 Write and Read Stability

Write margin of memory circuit implies the feasibility of writing with greater ease and less destruction. Write margin needs to be well-adjusted because of two possible scenarios. In first situation, if write margin gets higher the noise susceptibility of the circuit gets enhanced; otherwise, if it gets too low, writing will be harder. To investigate the static noise margin Takeda et al. [14] proposed bit-line sweep method which provides fine correlation of supply voltage and uses butterfly curve. Another method, i.e., word-line sweep proposed by Seevinck et al. [6], has been employed in current work to measure read/write margin of proposed 9T cell. In this method, the node from which the output has been taken is made to store ‘1’. The access transistor is enabled, and the word line is swept from zero to V_{dd} . Figure 4a displays the write margin variation w.r.t. supply voltage. However, the proposed cell maintains better static write margin till 500 mV V_{dd} in comparison with conv. 6T. Figure 4b displays the read margin variation w.r.t. supply voltage. However, the proposed cell maintains improved read static write margin till 500 mV V_{dd} in comparison with conv. 6T.

3.2 Read Dynamic Power and Access Time

The two components responsible for higher end dynamic power dissipation are switching power due to charging and discharging, and second is short circuit power [15]. The critical formulation of the same is explained in Eq. (1). Dynamic power dissipation of the circuit is due to leakage only and that falls in the regime of nanowatt. There are several reasons behind this dissipated power; however, this forms only 10–15% of the total dissipation. Dynamic power consumption has been found to be 0.109 μ w in proposed 9T cell. The reduction in dynamic power during read is due to

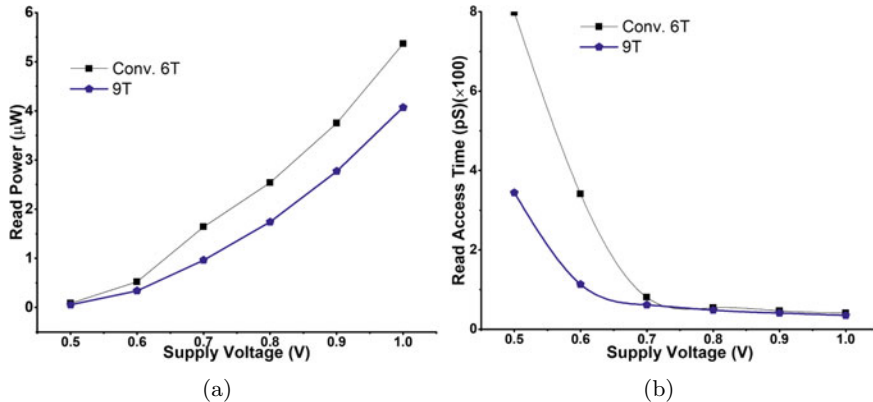


Fig. 5 **a** Read power versus V_{dd} **b** Read access time versus V_{dd}

the presence of P3 that stops the leakage solely via RDWL [16]. The dynamic power dissipation for the proposed cell has been compared with conv. 6T SRAM in Fig. 5a. Comparative analysis shows an effective reduction in dynamic power dissipation in proposed 9T cell in given worst-case scenario and uttered in microwatts.

3.3 Hold State

Essentially, for most of the time SRAM cell remains in standby mode. Therefore, it is also necessary to investigate the power dissipation during the hold state. The bit-line leakage is also the result of hold state and becomes prominent factor during the storage of logic ‘1’ [17]. Figure 6a demonstrates the hold power versus supply voltage, and Fig. 6b demonstrates the hold static noise margin versus supply voltage. It is also worthy to note that the precise value of W/L is responsible to maintain the effective resistance of pull up and pull-down transistors during standby mode. Furthermore, least resistance between QB and ground is required in comparison with off-state resistance of pull up transistor. To achieve this width of the access transistors is enhanced. Hold power was found to be 2.509 pW for read ‘1’ at 500 mV supply. This was also found that hold power increases linearly with supply voltage while reading ‘0’. However, it rises exponentially with upsurge of supply voltage during read ‘1’.

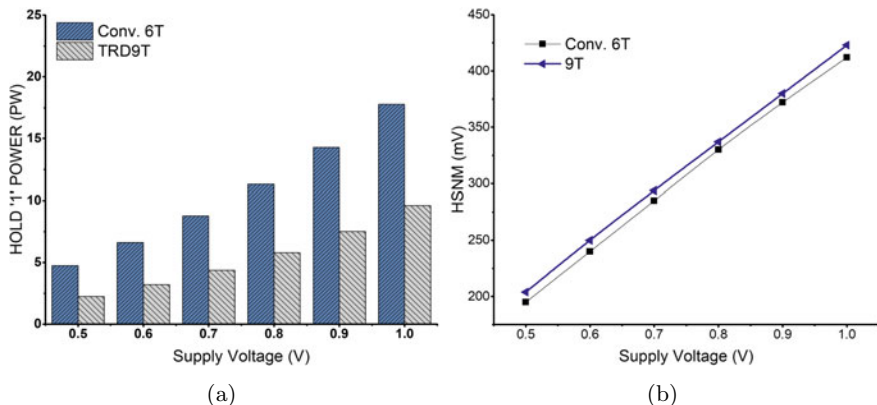


Fig. 6 **a** Hold power versus V_{dd} **b** HSNM versus V_{dd}

4 Conclusion

A Novel 9T cell has been presented in this paper, which has a capability of performing read and write operations in weak inversion regions. This kind of circuit is very much helpful in all applications where low power consumption is required. For completing this task successfully, a write assist power circuit is also proposed which works as dual supply for read and write operations. The novel circuitry reduces the leakage and brings down the total power by 74–80%. The significance of the obtained results will be in most of the low power applications where area and delay are secondary constraints. Overall, proposed 9T cell improves on dynamic power parameters when it is compared to other standard cells in 45 nm technology node.

References

1. Sachdeva A, Tomar VK (2020) Design of a stable low power 11-T static random access memory cell. *J Circ Syst Comput* 29(13):2050206. <https://doi.org/10.1142/S0218126620502060>
2. Azam T, Cheng B, Roy S, Cumming D (2010) Robust asymmetric 6T-SRAM cell for low-power operation in nano-CMOS technologies. *Electron Lett* 46(4):273
3. Sachdeva A, Tomar V (2020) Statistical stability characterization of Schmitt trigger based 10-T SRAM cell design. In: 2020 7th international conference on signal processing and integrated networks (SPIN) (IEEE, 2020), pp 1000–1005
4. Chandrakasan AP, Brodersen RW (1995) Minimizing power consumption in digital CMOS circuits. *Proc IEEE* 83(4):498
5. Kumar H, Tomar V (2020) Design of low power with expanded noise margin subthreshold 12T SRAM cell for ultra low power devices. *J Circ Syst Comput* 30(6). <https://doi.org/10.1142/S0218126621501061>
6. Sevinck E, List FJ, Lohstroh J (1987) Static-noise margin analysis of MOS SRAM cells. *IEEE J Solid State Circ* 22(5):748

7. Sachdeva A, Tomar V (2020) A Schmitt-trigger based low read power 12T SRAM cell. *Analog Integr Circ Sig Process* 1–21
8. Upadhyay P, Kar R, Mandal D, Ghoshal SP (2015) A design of low swing and multi threshold voltage based low power 12T SRAM cell. *Comput Electr Eng* 45:108
9. Grossar E, Stucchi M, Maex K, Dehaene W (2006) Read stability and write-ability analysis of SRAM cells for nanometer technologies. *IEEE J Solid State Circ* 41(11):2577
10. Scientist-E C, Noida U (2011) Characterization and comparison of low power SRAM cells. *J Electron Dev* 11:560
11. Sachdeva A, Tomar V (2020) Design of multi-cell upset immune single-end SRAM for low power applications. *AEU Int J Electron Commun* 153516
12. Sachdeva A, Tomar VK (2020) Design of low power half select free 10T static random-access memory cell. *J Circ Syst Comput* 0(0):2150073. <https://doi.org/10.1142/S0218126621500730>
13. Tomar V, Sachdeva A (2017) Implementation and analysis of power reduction techniques in charge transfer sense amplifier for sub 90 nm SRAM. In: 2017 8th international conference on computing, communication and networking technologies (ICCCNT) (IEEE, 2017), pp 1–3
14. Takeda K, Ikeda H, Hagiwara Y, Nomura M, Kobatake H (2006) Redefinition of write margin for next-generation SRAM and write-margin monitoring circuit. In: 2006 IEEE international solid state circuits conference-digest of technical papers (IEEE, 2006), pp 2602–2611
15. Aly RE, Bayoumi MA (2007) Low-power cache design using 7T SRAM cell. *IEEE Trans Circuits Syst II Express Briefs* 54(4):318
16. Sachdeva A, Tomar V (2016) Investigations of various SRAM cell structures for leakage energy reduction. In: 2016 2nd international conference on communication control and intelligent systems (CCIS)
17. Prabhu CMR, Singh AK (2010) Novel eight-transistor SRAM cell for write power reduction. *IEICE Electron Exp* 7(16):1175

Leveraging Deep Learning Techniques on Remotely Sensing Agriculture Data



Ajaysinh Vikramsinh Kathiya, Jai Prakash Verma, and Sanjay Garg

Abstract Crop yield prediction is very beneficial for the farmers to predict their profit. It can be used by private firms to make business decisions and governments to plan food security as well as planning imports and exports. Several published state-of-the-art techniques rely on handcrafted data. Our model deals with remotely sensed data to predict crop yield using deep learning algorithms such as CNN and LSTM. This model has proved better than existing techniques on evaluation based on its RMSE value. We have leveraged the capabilities of both algorithms to increase the accuracy of crop yield prediction and have successfully closed upon a model that surpassed the accuracy of previously used approaches.

Keywords Crop yield prediction · Remote sensing · Deep learning · LSTM · CNN

1 Introduction

The agriculture sector of a country like India accounts for only 14% of its GDP, though the agriculture sector provides 42% of the total employment. Also, 55% of arable land in India depends on rain. The average investment of a farmer required in agriculture is too high, yet the return of the investment depends on various factors. Computational analysis using deep learning techniques for the agriculture sector mainly focused on the adoption of precision or smart farming [1] with maximizing agriculture production while minimizing investment. Deep learning techniques provide an edge over machine learning for crop disease prediction, crop selection,

A. V. Kathiya · J. P. Verma (✉) · S. Garg
Institute of Technology, Nirma University, Ahmedabad, India
e-mail: jaiprakash.verma@nirmauni.ac.in

A. V. Kathiya
e-mail: 17bce037@nirmauni.ac.in

S. Garg
e-mail: sgarg@nirmauni.ac.in

weather forecasting, and crop yield prediction. Estimating a crop is depending on several external factors and parameters. All exciting approaches are relying on hand-crafted data or manually collected data, which is very time-consuming and expensive. However, remote sensing data is available globally and inexpensive and used in various applications such as weather forecasting, climate modelling. But it has its drawback as high-dimensional and unstructured data [2, 3].

In this paper, we illustrate an approach to predict crop yield based on remote sensing data and deep learning algorithms that led to good improvement in the range of computer vision tasks. Estimation of crop yield, time sequence prediction, and time sequence prediction uses CNN and LSTM as our deep learning model. The model trained on histograms. We evaluate our model on the task of county-level soybean yield in the USA. The proposed model was assessed on RMSE and performed better compared to the existing approach.

1.1 Availability of Agricultural Data

Agriculture is a vast domain and to solve agriculture related problems, dataset [4] that were used, are not of the same type. For a different kind of application, there are different types of data used. For classification purposes, ImageNet [5] and the Flavia leaf dataset [6] used by researchers. Also, for image localization and detection, we have ImageNet Large Scale Visual Recognition Challenge (ILSVRC) dataset [7] and sugar beet dataset for plant classification and localization and mapping [8]. For disease detection, the Plant Village dataset that contains the image of various crops and their diseases is used [9]. For vegetation segmentation masks and crop/weed plant-type annotations, the Crop/Weed Field Image Dataset is used [9]. Several factors can affect agriculture and make prediction tasks difficult. Out of these factors, soil and land types play a very crucial role in crop prediction. Africa Soil Information Service dataset provides continent-wide digital soil maps for sub-Saharan Africa [10]. The US Merced Land use dataset provides us with 21 class land use image datasets [11].

The prediction of agriculture yield before harvesting considered precious information. To collect information, method has been proposed with different types of data. The conventional method uses handcrafted datasets that are generated for each field or county, manually or with UAV. Syngenta Crop Challenge 2017 provides data from 2267 corn hybrids in 2122 locations between 2008 and 2016, together with weather and soil conditions. But the use of this type of data is very time-consuming and costly compared to remotely sensed data [12]. Remote sensing data is available abundantly and is less expensive. Satellite sensors collect electromagnetic waves from the Earth. Plants interact with sunlight, and the light is either absorbed, transmitted, or reflected. Reflected electromagnetic radiation from plants contains information about their physiological status and biophysical compositions. Satellite sensors measure this status. LANDSAT 7 8, SENTINEL, MODIS are widely used satellites for agricultural applications. LANDSAT 8 comes under USGS and takes around 500 images per day. It is capable of monitoring and mapping land surface bio-

physical and geophysical properties and land cover [13]. MODIS 8 day composites surface reflectance at 250 m resolution and land surface temperature product 1 km resolution. It surveys the surface of the entire Earth every 1 to 2 days, in 36 spectral bands between 0.405 and 14.385 um [14]. Apart from MODIS and LANDSAT, other data are also available such as AwIFS, LISS-III, and RapidEye.

1.2 Need of Computational Analysis for Agricultural Data

According to the Global Hunger Index 2019, India is at the 102nd rank. As per the prediction given by Mirkin, 2017, and The Hindu, 2019, the population of India would be around 1.4 billion by 2025. It is estimated that the demand for food would increase to 380 MT by 2025 and 480 MT in 2050. India is currently in the middle of a crisis, and to overcome this situation, India needs to plan its policies and agriculture supply chain from farmer to customer. Analysis of agriculture data can help the government to plan food chain security for the population, in a district/whole county also alert decision-makers about a potential reduction in crop yield, and allow timely import and export decisions.

1.3 Limitations of Traditional Agriculture Analytics

Conventional or traditional approaches work with handcrafted data. The crop estimation is done based on where the data collected from a particular region. Empirical-statistical models, crop growth models, and crop cutting experiments are a few of the approaches commonly used mainly in India to estimate the crop yield. These methods are expensive, time-consuming, and also do not perform efficiently in terms of accuracy. With the availability of remote sensing data, crop yield estimation and prediction has become more efficient and relatively cheap. Currently, crop yield estimation was done through different vegetation indices. NDVI [15], EVI2 [16], and GCVI [17]. Vegetation indices are human-engineered features and measurement of one or two spectral bands. The major drawback of this method is that it discards spectral information on a large scale.

1.4 Contribution

Based on all the discussion mentioned above, we come up with a solution that can overcome the limitation of the previous research work and give a better and more accurate result.

- A robust survey presented for approaches applied for predicting crop yield and leveraging deep learning in agriculture.
- In this paper, we also mention, to convert the high-dimensional digital image into a histogram for better result and to also gain the advantage of soil inversion property.
- The experimental analysis presented in this paper found that LSTM and CNN deep learning algorithms perform well on time serious prediction task. So we tried to leverage the advantage of both of the algorithms in a single approach.

1.5 Organization

This paper is organized into seven sections. Sections 2 and 3 present the related research work in the area of deep learning-based data modelling for agriculture prediction. Section 4 is the problem formulation where the notations used in the paper are defined and the relationship of various entities is represented. Section 5 describes the steps followed for conducting the experimentation including data preprocessing. Section 6 includes results and discussion of the experimental analysis done for the proposed research work. Section 7 presents the conclusions drawn and future direction identified.

2 Deep Learning Architectures for Agriculture

2.1 Convolutional Neural Network (CNN) Architecture

Extracting features from remote sensing data is a difficult task. Deep learning models like convolution neural networks (CNN) have enormous potential to understand the remote sensing data and extract the features efficiently. CNN architecture is mainly into two parts: (1) Convolution layer and (2) fully connected layer.

- (1) Convolution layer: The convolution layer collects features from the image. For extracting the features, convolution layer applies kernel or filter on image and returns feature map.

$$c = (f(W * x + b))$$

Here, as shown in Equation 1, CNN takes x as input image applies filter x with two dimensional convolution operation $*$, followed by nonlinear function $f()$ and sometimes pooling layer $p()$. The b is a bias term and returns the feature map from input image x .

- (2) Fully connected layer: A fully connected layer uses feature maps extracted by the convolution layer to produce output. It converts feature maps into vectors and gives as input to the neural network for predicting and weights updated

through backpropagation. We can leverage the potential of CNN architecture to extract features from remote sensing data and utilize those features for different applications.

2.2 Long Short-Term Memory (LSTM) Network Architecture

Long short-term memory [18] is a specific type of RNN network which takes sequential data as input. In LSTM, the output state depends on the applied input and previous output. This characteristic makes LSTM a better candidate for time-sequential prediction. LSTM generates output from the last executed layer. LSTM has three gates (1) forget gate, (2) input gate, (3) output gate.

$$\begin{aligned} \text{forget } n &= \sigma(\gamma[v, O'] + b) \\ \text{input} &= \sigma(\alpha[[v, h'] + b]) \\ \text{state} &= \text{forget} * \text{state}' + \text{input} * \tanh(W[v, h'] + b) \\ O &= \sigma(\beta[v, h'] + b) * \sigma(\text{state}) \end{aligned}$$

As per equations, O' is previous calculational output and v is current input, $\sigma()$ is the sigmoid function and α , β are W are weighted matrices, and b is biased different for different gates. The ' h ' is stored information. (1) As the name suggests, the forget gate decides which information will be removed from the LSTM cell based on the current input. (2) Input gate takes new input into the cell and decides which information to add to the cell. (3) Output gate based on previous operations done from the input gate and forget gate gives final output from the cell. LSTM takes advantage of temporal patterns of crops across image time series and helps to decrease complexity and improve accuracy.

3 Related Work

Lately, deep learning gained much popularity because of higher accuracy and many state-of-the-art algorithms. Researchers also tried to utilize deep learning for predicting crop yield (refer Table 1). One of the approaches was a backpropagation neural network with a conjugate gradient algorithm for predicting corn in Ottawa [19], which also uses textual indices and vegetation indices for better performance, predicting crop yield in the USA. In another deep learning based model, convolutional architecture was used for fast feature embedding proposed in [20], which uses a network model with two inner product layers. While some researchers try to leverage physicochemical parameters such as pH, MC, TN, Ca, Mg, and NDVI to evaluate wheat yield. The model uses self-organized map methods such as (1) counter propagation artificial neural network, XY fused network, and supervised Kohonen

networks(SKN) [21]. For wheat prediction, a spiking neural network model introduced advantage of this approach is that the model can predict wheat six weeks before harvesting and get an accuracy of around 95.64% with an error of 0.236% t/ha [22]. Another approach was introduced, where the neural network model first predicts the weather parameters, and then the weather parameter along with current agriculture data used as input for support vector regression [23]. You et al. [24] propose a better approach to the previous and discover relevant information from raw data. Most of the models use the mean of the feature, while this model works with pixel distribution over the region directly. Also, they use the Gaussian process top of their model to avoid spatial-temporal dependencies across data. The proposed research work in this paper emphasizes the Jiaxuan model and also takes its result as a benchmark for comparative analysis.

4 Proposed Research Work: Multi-layered Hybrid Model Using CNN and LTSM

CNN and LSTM both are a well-liked model for working with time sequence data. The combination of both models takes advantage of the proposed models. As shown in Fig. 1, data flow in the CNN model presents with a blue arrow line while data flow in the LSTM model with yellow arrows. The CNN model architecture is modified from the basic model by the pooling layer because we do not want location invariance property in our model, so instead of the pooling layer, we use another convolution layer with stride-2. In the proposed architecture of the CNN model, stride-1 convolution layers represent with light blue colour. And stride-2 convolution layers represent light pink colour. However, both types of convolution layers follow the batch normalization and ReLU and also use a dropout layer with a value of 0.5 to avoid overfitting. The number of neurons in each layer represents a particular layer representation with a number.

Completing a series of CNN layers, the output from the last layer is connected to the Global Average Pooling layer to concatenate the CNN model with other layers. The LSTM model is the basic architecture of LSTM that connects with 256 nodes with the dense layer with the ReLU activation function. For preventing the model from overfitting, we set the dropout layer for 0.75 value. For the output, each model is in a concatenated layer with the dropout set as 0.5 with a dense layer as the last layer that has one neuron and the ReLU activation function.

To compare our model, we use previous approaches for prediction analysis of the crop yield. We take some models as our baseline modes that are as RIDGE regression, decision tree, and DNN with three hidden layers. Here, RMSE is applied for comparative analysis. Table 2 compares the root mean square error (RMSE) of our model with other deep learning techniques. The hybrid approach outperforms baseline and other deep learning models.

Table 1 Comparison of different approaches

References	Objective	Approach	Methodology	Pros	Cons
[25]	Yield prediction using TCI, VCI and NDVI	Authors try to use data mining technique with different indices	Utilize temperature condition and vegetation condition for prediction	Climate, agronomic and weather disturbance Variables used for better prediction	handcrafted data used
[26]	Estimation of rice growth, protein content and yield prediction	Monitor rice growth and estimate chlorophyll in rice leaves	Using NDVI and SPAD from satellite, establish a mapping algorithm	Has accuracy of 83 kg/ 10a, Can predict immediately after heading	It uses SPAD and NDVI, which extracts less information
[27]	Compare BRT and SVM for wheat prediction	Select a model which has a high impact in yield prediction	Use single NDVI and incremented NDVI used to select high impact features	Can explain the upward trend, with increasing fertilizer trend for wheat with NDVI	Need to use feature selection first and then apply to model
[28]	Crop yield prediction of Silage maize using satellite data and machine learning algorithms	Leverage the ability to identifying, detection and quantifying patterns for remote sensing data of agriculture	Utilize BRT, RFR, SVM, and GP for prediction task using time series image of Landsat 8 data	It performs better than convention methods	Could not justify the effect of other environmental parameters
[29]	Crop yield prediction using ANN and multiple perceptrons	Predict rice crop from features like precipitation, temperature and evapotranspiration	Using features like precipitation, temperature, and evapotranspiration. Model them through ANN and multiple perceptrons to predict rice	Can identify yield in three types of high yield from 1.11 to 3.16 t/ha, moderate yield 0.61–1.10 t/ha and low yield 0.15–0.60 t/ha	Used handcrafted data or publicly available data is used
[9]	Paradigm for rice yield prediction in Tamil Nadu	Using various parameters such as soil, temp, no of sunshine day, rainfall, bare land and fertilizer to prediction	All features collected are used to predict based on mathematically and statistical functions	A rice yield for any variety can be predicted with nearly real-world values	It used mathematical and fundamental methods, not machine learning methods
[22]	Spiking neural network computational model	Predict the crop yield using spiking neural network computational model	Predict wheat crop yield from data obtained through MODIS satellite China	Has accuracy around 95.64% and the average error is 0.236 t/ha	SNN is had unknown behaviour for spatial, temporal data and large data optimization needed
[23]	Predicting rice yield for Bangladesh by exploiting weather condition	First predict possible weather condition and based on that predict the crop yield	Using model weather-based prediction system for rice yield, we would find weather parameter, and then these parameters and current agriculture data are used in SVR to predict yield	Crop yield prediction is a more promising approach compare to others as it is based on weather prediction first	For predicting crop yet surveyed data or manually collected data is needed

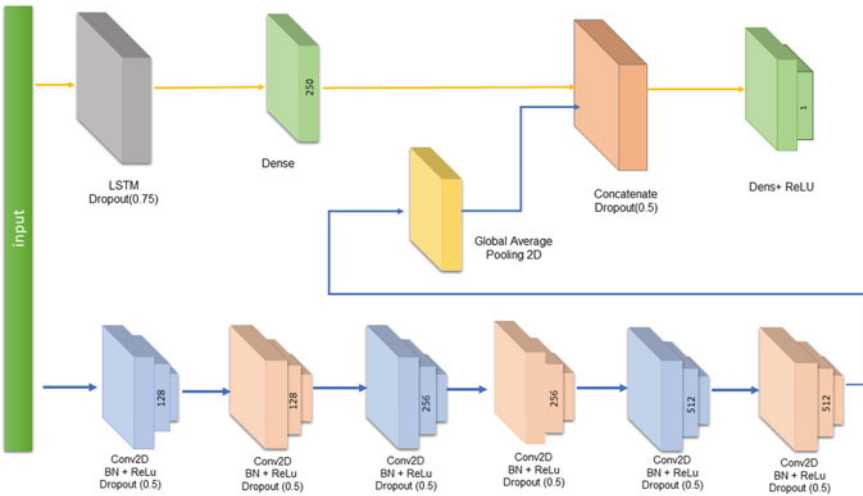


Fig. 1 Execution flow of multi-layered hybrid model using CNN and LTSM

Table 2 Execution

Approach	Baselines			Deep models				
	Ridge	Tree	DNN	LSTM	LSTM + GP	CNN	CNN + GP	Proposed Model CNN + LSTM
2011	9.00	7.98	9.97	5.83	5.77	5.76	5.7	5.29
2012	6.95	7.40	7.58	6.22	6.23	5.91	5.68	4.94
2013	7.31	8.13	9.20	6.39	5.96	5.50	5.83	4.74
2014	8.46	7.50	7.66	6.42	5.70	5.27	4.89	4.39
2015	8.10	7.64	7.19	6.47	5.49	6.40	5.67	4.74
Avg	7.96	7.73	8.32	6.27	5.83	5.77	5.55	4.82

5 Experiment Analysis

For data collection and data preprocessing we used the method proposed by You et al. [24]. For remote sensing data, we used the MODIS satellite, which collects multi-spectral images 30 times a year from 49th day to 281th day, at intervals of every eight days. We take surface reflection, land surface temperature, and land cover as input data from the year 2003–2015. In this approach, we used three features from the MODIS dataset, surface reflection, land surface temperature, and land cover to compare the performance of our model with previous approaches. Moreover, adding a new feature may require that new features must be compatible with other features in terms of the composite period and band characteristics. We convert our remote

sensing data to histograms for dimensionality reduction. After preprocessing our data and converting it into a histogram, we assign USDA data as ground truth USDA is publically available data and provides yearly average soybean yield in each county. The preprocessed dataset was applied to train the proposed model on the dataset.

6 Results and Discussion

Data collected from satellite images from 2003 to 2015 is time-sequential data. So for evaluation, we train the proposed model and compare the results with benchmarks work done by various researchers. We used ‘ADAM’ optimizer and trained our model for 32 batch sizes for 100 epochs. After performing experimental research on hyperparameter with the selected algorithm structure, we found given configuration provides the best result. As the data is time-sequential, it cannot use simple cross-validation for evaluation. Instead of it, a different approach applies by taking data from the starting year to the target year and then evaluates the proposed model for the target year. For example, if our target year is 2015, then train the model from 2003 to 2014 and predictions for 2015. The proposed model is evaluated from the target year 2011–2015 and found that it surpasses the previous approaches for the target years, and moreover that our model provides RMSE value is average 13% less than previous best approaches.

7 Conclusion

This paper presents a model for predicting crop yield based on deep learning and remote sensing data. The model is estimating the average yield of the crop of type soybean before the harvest, based on the sequence of remotely sensed data. It tries to estimate the average yield per county or particular location. This approach is not only limited to predicting crop yield, but we can also estimate whether a new type of crop is suitable or not with the geographical condition in a particular region. We can use the same approach for estimating yield other than soybean. Existing approaches either rely on surveys or parameters related to crop growth. Deep learning-based model such as the multi-layer CNN architecture approach gives comparatively better results.

References

1. Verma JPV, Mankad SH, Garg S (2019) A graph based analysis of user mobility for a smart city project. In: Prateek M, Sharma D, Tiwari R, Sharma R, Kumar K, Kumar N (eds) Next generation computing technologies on computational intelligence. Springer, Singapore, pp 140–151
2. Verma JPV, Mankad SH, Garg S (2020) GeoHash tag based mobility detection and prediction for traffic management. *SN Appl Sci* 2(8):1385. <https://doi.org/10.1007/s42452-020-2870-5>
3. Yadav S, Verma J, Agrawal S (2017) Sutron: IoT-based industrial/home security and automation system to compete the smarter world. *Int J Appl Res Inf Technol Comput* 8(2):193
4. Kamlaris A, Prenafeta-Boldu F (2018) Deep learning in agriculture: a survey. *ArXiv*, abs/1807.11809
5. Deng J, Dong W, Socher R, Li L, Li K, Fei-Fei L (2009) Imagenet: a large-scale hierarchical image database. In: 2009 IEEE conference on computer vision and pattern recognition, pp 248–255
6. Wu SG, Bao FS, Xu EY, Wang Y, Chang Y, Xiang Q (2007) A leaf recognition algorithm for plant classification using probabilistic neural network. In: 2007 IEEE international symposium on signal processing and information technology, pp 11–16
7. Russakovsky O, Deng J, Hao S, Krause J, Satheesh S, Ma S, Huang Z, Karpathy A, Khosla A, Bernstein M, Berg AC, Fei-Fei L (2015) ImageNet large scale visual recognition challenge. *Intl J Comput Vis (IJCV)* 115(3):211–252
8. Chebrolu N, Lottes P, Schaefer A, Winterhalter W, Burgard W, Stachniss C (2017) Agricultural robot dataset for plant classification, localization and mapping on sugar beet fields. *Int J Robot Res* 36:027836491772051
9. Singh D, Jain N, Jain P, Kayal P, Kumawat S, Batra N (2020) Plantdoc: a dataset for visual plant disease detection, pp 249–253
10. Africa Soil Information Service (AfSIS) | ISRIC (2021, April 17) Africa Soil Information Service. <https://www.isric.org/projects/africa-soil-information-service-afris>
11. Fan J, Chen T, Lu S (2017) Unsupervised feature learning for land-use scene recognition. In: IEEE transactions on geoscience and remote sensing, vol 55, no 4, pp 2250–2261. <https://doi.org/10.1109/TGRS.2016.2640186>
12. Bramlett M, Plaetinck G, Maienfisch P (2019) RNA-based biocontrols—a new paradigm in crop protection. *Engineering* 6:12
13. Hansen MC, Loveland TR (2012) A review of large area monitoring of land cover change using landsat data. *Rem Sens Env* 122:66–74 (Landsat Legacy Special Issue)
14. García-Mora TJ, Mas J-F, Hinkley EA (2012) Land cover mapping applications with MODIS: a literature review. *Int J Digit Earth* 5(1):63–87
15. Quaraby NA, Milnes M, Hindle TL, Silleos N (1993) The use of multi-temporal NDVI measurements from AVHRR data for crop yield estimation and prediction. *Int J Rem Sens* 14(2):199–210
16. Bolton DK, Friedl MA (2013) Forecasting crop yield using remotely sensed vegetation indices and crop phenology metrics. *Agric For Meteorol* 173:74–84
17. Lobell DB, Thau D, Seifert C, Engle E, Little B (2015) A scalable satellite-based crop yield mapper. *Rem Sens Environ* 164:324–333
18. Hochreiter S, Schmidhuber J (1997) Long short-term memory. *Neural Comput* 9:1735–1780
19. Serele CZ, Gwyn QHJ, Boisvert JB, Pattey E, McLaughlin N, Daoust G (2000) Corn yield prediction with artificial neural network trained using airborne remote sensing and topographic data. In: IGARSS 2000. IEEE 2000 international geoscience and remote sensing symposium. Taking the pulse of the planet: the role of remote sensing in managing the environment. Proceedings (Cat. No. 00CH37120), vol 1, pp 384–386
20. Kuwata K, Shibasaki R (2015) Estimating crop yields with deep learning and remotely sensed data. In: 2015 IEEE international geoscience and remote sensing symposium (IGARSS), pp 858–861

21. Pantazi XE, Moshou D, Alexandridis T, Whetton RL, Mouazen AM (2016) Wheat yield prediction using machine learning and advanced sensing techniques. *Comput Electron Agric* 121:57–65
22. Bose P, Kasabov NK, Bruzzone L, Hartono RN (2016) Spiking neural networks for crop yield estimation based on spatiotemporal analysis of image time series. *IEEE Trans Geosci Rem Sens* 54(11):6563–6573
23. Hossain MA, Uddin MN, Hossain MA, Jang YM (2017) Predicting rice yield for Bangladesh by exploiting weather conditions. In: 2017 international conference on information and communication technology convergence (ICTC), pp 589–594
24. You J, Li X, Low M, Lobell D, Ermon S (2017) Deep gaussian process for crop yield prediction based on remote sensing data. In: AAAI
25. Manjula A, Narsimha G (2015) Xcypf: a flexible and extensible framework for agricultural crop yield prediction. In: 2015 IEEE 9th international conference on intelligent systems and control (ISCO), pp 1–5
26. Wakamori K, Ichikawa D, Oguri N (2017) Estimation of rice growth status, protein content and yield prediction using multi-satellite data. In: 2017 IEEE international geoscience and remote sensing symposium (IGARSS), pp 5089–5092
27. Stas M, Van Orshoven J, Dong Q, Heremans S, Zhang B (2016) A comparison of machine learning algorithms for regional wheat yield prediction using NDVI time series of spot-VGT. In: 2016 fifth international conference on agro-geoinformatics (agro-geoinformatics), pp 1–5
28. Aghighi H, Azadbakht M, Ashourloo D, Shahrabi HS, Radiom S (2018) Machine learning regression techniques for the silage maize yield prediction using time-series images of landsat 8 oli. *IEEE J Sel Top Appl Earth Observ Rem Sens* 11(12):4563–4577
29. Gandhi N, Petkar O, Armstrong LJ (2016) Rice crop yield prediction using artificial neural networks. In: 2016 IEEE technological innovations in ICT for agriculture and rural development (TIAR), pp 105–110

Unsupervised Classification of Zero-Mean Data Based on L1-Norm Principal Component Analysis



José Luis Camargo, Rubén Martín-Clemente, Susana Hornillo-Mellado,
and Vicente Zarzoso

Abstract This paper shows that L1-norm PCA, a robust variant of principal component analysis (PCA), can distinguish between zero-mean populations by projecting the data onto directions along which the variance is much larger for one population than for the other. Thus, the variance can be used as a criterion for classification.

Keywords Principal component analysis · Machine learning

1 Introduction

Principal component analysis (PCA) is one of the most widely used techniques for analyzing multivariate data. It finds application in fields such as image processing, wireless communications, machine learning and biomedical signal analysis, to name only a few [1]. PCA searches for a *low*-dimensional subspace that minimizes the average squared distance of the data points to it, i.e., the best-fit subspace for the data points. By projecting the data onto this subspace, we also reduce the dimensionality of the data. Therefore, PCA is useful for compression and in pattern recognition and denoising problems. Furthermore, it is well known that the best-fit subspace maximizes the variance of the scalar projections of the data points on it. Therefore, PCA also captures the directions of maximum variability of the data [1].

After simple algebra, it can be shown that the best-fit subspace is spanned by the first few dominant eigenvectors of the data covariance matrix [1]. From a compu-

J. L. Camargo · R. Martín-Clemente (✉) · S. Hornillo-Mellado
Signal Processing and Communications Department, University of Seville, Seville, Spain
e-mail: ruben@us.es

J. L. Camargo
e-mail: jlcamargo@yahoo.es

S. Hornillo-Mellado
e-mail: susanah@us.es

V. Zarzoso
I3S Laboratory, CNRS, Université Côte d'Azur, Sophia Antipolis Cedex, France
e-mail: vicente.zarzoso@univ-cotedazur.fr

tational viewpoint, this subspace can be estimated from the singular value decomposition (SVD) of the data matrix. Unfortunately, the SVD is extremely sensitive to the presence of large outliers in the data. This is a serious drawback, since outliers are usually encountered in experiments due to the imperfections in the measuring instruments.

To overcome this problem, several authors have proposed robust variants of standard PCA in recent years. The most promising option is to replace the variance with the *median absolute deviation statistic* for measuring the spread of the data. This approach leads to the technique known as L1-norm-based PCA (L1-PCA) [2, 3]. Specifically, [2] presented this method with a computationally simple algorithm, whereas [3] identifies the equivalence between L1-norm maximization and ‘binary quadratic programming.’ The relationship between L1-PCA and independent component analysis (ICA) and linear discriminant analysis has been also discussed in [4, 5].

After reviewing L1-PCA in Sect. 2, the present contribution investigates the discriminative properties of L1-norm PCA in Sect. 3. Numerical experiments in Sect. 4 validate demonstrate the ability of this technique to carry out classification in an unsupervised fashion.

2 L1-Norm Principal Component Analysis

Let $\mathbf{x} \in \mathbb{R}^p$ be a multivariate random variable measured or observed during the execution of an experiment. For simplicity, we suppose that \mathbf{x} is of zero-mean, i.e., $E[\mathbf{x}] = \mathbf{0}$, where $E[\cdot]$ is the expectation operator.

PCA uses the low-dimensional subspace defined by the most significant directions of spread of \mathbf{x} . Let $\mathbf{a} \in \mathbb{R}^p$ be the unit-norm vector in the direction of the line that best fits \mathbf{x} in the least squares sense. It can be easily shown that \mathbf{a} can be obtained as the solution to the variance-maximization problem [1]

$$\max_{\|\mathbf{a}\|_2=1} E \left[(\mathbf{a}^\top \mathbf{x})^2 \right] = \max_{\|\mathbf{a}\|_2=1} \mathbf{a}^\top \mathbf{C} \mathbf{a} = \max_{\|\mathbf{a}\|_2=1} \sigma^2 \quad (1)$$

where $\mathbf{C} = E[\mathbf{x} \mathbf{x}^\top]$ is the data covariance matrix and $\sigma^2 = \mathbf{a}^\top \mathbf{C} \mathbf{a}$ is the variance of the projected data. According to the Rayleigh quotient principle, the maximizer of (1) is the eigenvector associated to the largest eigenvalue of matrix \mathbf{C} . To determine the whole Q -dimensional best-fitting subspace, (1) is maximized Q times, under the constraint that the direction obtained in the q th optimization is orthogonal to the previously computed directions. As a result, one obtains the subspace spanned by the Q dominant eigenvectors of \mathbf{C} , which can be efficiently computed by the SVD of the data matrix.

A major drawback of PCA is that the square in (1) emphasizes the importance of large data, typically outliers, causing \mathbf{a} to be aligned with the most significant of them. In order to palliate such a serious weakness, [2] proposed the replacement of the square function by the absolute value, yielding the following alternative criterion:

$$\max_{\|\mathbf{a}\|_2=1} E[|\mathbf{a}^\top \mathbf{x}|] \quad (2)$$

Given a sample $\mathbf{x}_1, \dots, \mathbf{x}_N$ from the random variable \mathbf{x} , (2) is approximated in practice by its sample-based estimate

$$\max_{\|\mathbf{a}\|_2=1} \frac{1}{N} \sum_{i=1}^N |\mathbf{a}^\top \mathbf{x}_i| \quad (3)$$

Note that $\sum_{i=1}^N |\mathbf{a}^\top \mathbf{x}_i|$ is the L1-norm of the vector \mathbf{y} whose k th entry is given by $y_k = \mathbf{a}^\top \mathbf{x}_i$. For this reason, PCA based on criterion (2) is usually referred to as ‘L1-norm-based PCA’ or, simply, ‘L1-PCA.’ To gain some insight into the performance of L1-PCA, let us make the common assumption in data analysis that $f(\mathbf{x})$ is a p -variate normal density function of the form

$$f(\mathbf{x}) = (2\pi)^{-\frac{p}{2}} \det(\mathbf{C})^{-\frac{1}{2}} e^{-\frac{1}{2}\mathbf{x}^\top \mathbf{C}^{-1}\mathbf{x}}. \quad (4)$$

Let $y = \mathbf{a}^\top \mathbf{x}$ be the projection of \mathbf{x} into the direction defined by $\mathbf{a} \in \mathbb{R}^p$. From basic statistics, the probability density function of y is Gaussian as well:

$$f(y) = \frac{1}{\sqrt{2\pi\sigma^2}} \exp\left(-\frac{y^2}{2\sigma^2}\right). \quad (5)$$

Then, by using that

$$\int y e^{-\frac{y^2}{2\sigma^2}} dy = -\sigma^2 e^{-\frac{y^2}{2\sigma^2}}$$

some algebra leads to the result

$$E[|y|] = \int_{-\infty}^{\infty} |y| f(y) dy = \sqrt{\frac{2}{\pi}} \sigma.$$

Consequently, as maximizing the standard deviation σ is equivalent to maximizing the variance σ^2 , L1-PCA behaves like traditional PCA while offering robustness against the presence of large outliers in the data [2, 3, 6]. Practical algorithms for maximizing (2) have been proposed in [2, 3, 7].

Now, let us show in the next section that L1-PCA is also endowed with discriminative properties.

3 Main Contribution: L1-PCA for Classification of Zero-Mean Populations

In binary classification problems, we observe random samples from two distinct zero-mean classes ω_1 and ω_2 . The goal is to find a rule to allocate the random samples into one class or the other. By assumption, ω_1 and ω_2 have respective a priori probabilities of occurrence π_1 and π_2 , as well as covariance matrices \mathbf{C}_1 and \mathbf{C}_2 . It is also supposed that the distribution of the random samples is as a mixture of Gaussians, i.e.,

$$f(\mathbf{x}) = (2\pi)^{-\frac{p}{2}} \sum_{i=1}^2 \pi_i \det(\mathbf{C}_i)^{-\frac{1}{2}} e^{-\frac{1}{2}\mathbf{x}^\top \mathbf{C}_i^{-1} \mathbf{x}}.$$

By proceeding as in above, we easily get that

$$E[|\mathbf{a}^\top \mathbf{x}|] = E[|y|] = \sqrt{\frac{2}{\pi}} (\pi_1 \sigma_1 + \pi_2 \sigma_2) \quad (6)$$

where $\sigma_i^2 = \mathbf{a}^\top \mathbf{C}_i \mathbf{a}$ is the variance of the i th class in the direction of the unit vector $\mathbf{a} \in \mathbb{R}^p$. Unfortunately, no direct conclusions can be drawn from (6) when σ_1 and σ_2 vary independently of each other. To get a more meaningful criterion, let us link the class variances in such a way that when one increases the other decreases, and *vice versa*. This is always possible, without any loss of generality, by a data preprocessing step called *whitening* or *sphering*. *Whitening*, which removes the correlation between the data components, is achieved by linearly transforming the data by any square root of the inverse of the raw data covariance matrix [8]. Thanks to this preprocessing step, the covariance of the data becomes the identity

$$\mathbf{C} = E[\mathbf{x}\mathbf{x}^\top] = \pi_1 \mathbf{C}_1 + \pi_2 \mathbf{C}_2 = \mathbf{I} \quad (7)$$

Then, because \mathbf{a} is of unit norm, it follows that

$$E[y^2] = \mathbf{a}^\top E[\mathbf{x}\mathbf{x}^\top] \mathbf{a} = \pi_1 \sigma_1^2 + \pi_2 \sigma_2^2 = 1 \quad (8)$$

so σ_1 and σ_2 are now linked as desired. The key result is that, as it can be formally proven:

Lemma 1 *The criterion*

$$D = \sqrt{\frac{2}{\pi}} (\pi_1 \sigma_1 + \pi_2 \sigma_2) \quad (9)$$

attains its minimum value, under the constraint $\pi_1 \sigma_1^2 + \pi_2 \sigma_2^2 = 1$, when the variance of the projected data points is maximum for one class and minimum for the other.

We omit the proof due to the lack of space. Nevertheless, some intuition can be gained by observing that the minima of $\alpha + \beta$, subject to $\alpha^2 + \beta^2 = 1$ and $\alpha, \beta \geq 0$, where α and β are any generic variables, are at the limit points of the interval, i.e., $\alpha = 0, \beta = 1$ and $\alpha = 1, \beta = 0$. Similarly, the maximum is attained at $\alpha = \beta$.

The Lemma can be put in connection with the useful technique known as common spatial patterns (CSP), which is widely used in brain–computer interfaces (BCIs). In BCIs, electroencephalogram (EEG) samples are acquired under two different conditions (e.g., imagining tongue and hand movements). CSP projects the data onto directions where the variance of the projected points is larger for one class than for the other [9]. The projected data variances are then used by the BCI as criteria for classification.

Consequently, we see that the L1 criterion clearly possesses discriminative properties, similar to those of CSP. The key here is that CSP is a supervised technique, whose performance relies heavily on the availability of correctly labeled data. On the contrary, minimizing the L1 criterion (6), i.e., $E[|y|]$, *can be performed in a completely unsupervised fashion*.

4 Experiments

In brain–computer interfaces (BCI’s), one imagines a limb moving and the machine tries to detect the imagined movement by analyzing the EEG of the user [10]. The dataset 2a from the BCI competition IV consists of 22-channel EEG signals associated to left hand, right hand, feet and tongue motor-imagery movements [11]. As a preprocessing step, we filter the EEG data to 12–30Hz. By so doing, we ensure that the data are zero-mean and, by central limit arguments, we can also safely make the assumption of Gaussianity.

After applying a *whitening* preprocessing to the data, the gradient descent algorithm in [12] is applied to find orthogonal directions $\mathbf{a}_1, \dots, \mathbf{a}_{22}$ that minimize the criterion

$$\sum_{n=1}^{22} E[|\mathbf{a}_i^\top \mathbf{x}|]$$

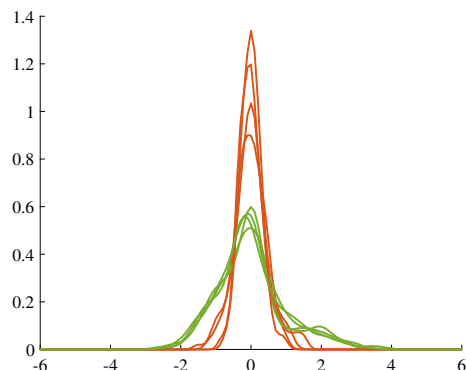
To this end, data samples are drawn from EEG signals from two distinct imagined movements. Table 1 shows the accuracy in the detection of the imagined movements of user 1, where classification is performed by comparing the variances of the projected data (see Fig. 1). A high degree (93%) of accuracy in discriminating between ‘right hand’ and ‘feet’ imagined movements has been obtained, in a completely unsupervised fashion. However, that accuracy reduces to 52% for the same user and the pair ‘feet–tongue.’

Table 1 Accuracy in the discrimination between pairs of imagined movements (L = left hand, R = right hand, F = feet, T = tongue)

L-R	L-F	L-T	R-F	R-T	F-T	Avg
0.66	0.89	0.91	0.93	0.92	0.52	0.84

Results are shown for user 1 of the database. Last column gives the accuracy per user averaged over all movements

Fig. 1 Density functions of several projected ‘left hand’ (orange) and ‘feet’ trials (green) from user 1. The projection direction is that which minimizes the L1-norm-based objective function. The difference between the respective variances is apparent



5 Conclusions

Unsupervised classification can be performed by projecting whitened data onto the few dimensions that minimize the absolute value of the projected data points, thus sparing the need for training data. In the future, we will explore the application of this technique to real data and carry out a more exhaustive comparison with the CSP approach.

Acknowledgements The research of Drs. Martín-Clemente and Zarzoso was partially funded by the project ACACIA (ref US-1264994) awarded by the Junta de Andalucía (Consejería de Transformación Económica, Industria, Conocimiento y Universidades) and I+D+i FEDER Andalucía 2014–2020.

References

1. Jolliffe IT (2002) Principal component analysis. Springer, New York, NY
2. Kwak N (2008) Principal component analysis based on L1-norm maximization. IEEE Trans Pattern Anal Mach Intell 30(9):1672–1680
3. Markopoulos PP, Karystinos GN, Pados DA (2014) Optimal algorithms for L1-subspace signal processing. IEEE Trans Signal Process 62(19):5046–5058
4. Martín-Clemente R, Zarzoso V (2017) On the link between L1-PCA and ICA. IEEE Trans Pattern Anal Mach Intell 39(3):515–528
5. Martín-Clemente R, Zarzoso V (2020) LDA via L1-PCA of whitened data. IEEE Trans Signal Process 68:225–240

6. Markopoulos PP, Kundu S, Chamadia S, Tsagkarakis N, Pados DA (2017) Outlier-resistant data processing with L1-norm principal component analysis. In: Advances in principal component analysis. Springer, Singapore, pp 121–135
7. Markopoulos PP, Kundu S, Chamadia S, Pados DA (2017) Efficient L1-norm principal-component analysis via bit flipping. *IEEE Trans Signal Process* 65(16):4252–4264
8. Kessy A, Lewin A, Strimmer K (2018) Optimal whitening and decorrelation. *Am Stat* 72(4):309–314
9. Martín-Clemente R, Olias J, Thiyam D, Cichocki A, Cruces S (2018) Information theoretic approaches for motor-imagery BCI systems: review and experimental comparison. *Entropy* 20(1):7
10. Lotte F, Bougrain L, Cichocki A, Clerc M, Congedo M, Rakotomamonjy A, Yger F (2018) A review of classification algorithms for EEG-based brain-computer interfaces: a 10 year update. *J Neural Eng* 15(3):031005
11. Blankertz B, Vidaurre C, Tangermann M, Müller KR, Brunner C, Leeb R, Müller-Putz G, Schlogl A, Pfurtscheller G, Waldert S, Mehring C, Aertsen A, Niels B, Miller KJ, Schalk G (2020) BCI competition IV dataset [dataset]. <http://www.bbci.de/competition/iv/>. Last accessed Apr 2020
12. Edelman A, Arias TA, Smith ST (1998) The geometry of algorithms with orthogonality constraints. *SIAM J Matrix Anal Appl* 20(2):303–353

Social Network Analysis Based on Combining Probabilistic Models with Graph Deep Learning



Xuan Truong Dinh and Hai Van Pham

Abstract Social network analysis (SNA) has emerged as a key technique in modern sociology and has gained achievements in demography, communication research, development studies, sociolinguistics, and computer science. Social network data is often in the form of graphs, a significant amount of research on graph to addressing node and graph classification and graph fulfillment has been applied to the SNA. The paper presents the Bayesian graph deep learning framework for the case of classified mixed node random block models to classify the topic of social posts as nodes by creating a homogeneous graph with links between them. The experimental results show that the Bayesian formulation provides better performance in topic classification in social during the training process.

Keywords Social network analysis · Graph data · Bayesian graph deep learning · Probabilistic models · Graph deep learning · Node classification

1 Introduction

Graph structured data are ubiquitous in the real world, representing objects and their relationships such as social networks, physics, chemistry, biology, computer vision, e-commerce networks, traffic networks, to name a few. Although graphs have complicated structures, they contain a rich underlying value [1]. Newly, graph neural networks (GNNs) were shown to be successful in wide applicability because of their good performance and generalization ability [2]. GNN is a deep learning-based method that learns how to iteratively aggregate feature information from local graph neighborhoods [3]. Bruna et al. [4] are the initiator of deep learning on graphs, and the global structure of graphs can be exploited with the spectrum of its graph Laplacian to

X. T. Dinh (✉) · H. Van Pham
Hanoi University of Science and Technology, Hanoi, Vietnam
e-mail: haipv@soict.hust.edu.vn

X. T. Dinh
CMC Institute of Science and Technology, Hanoi, Vietnam

generalize the convolution operator. Henaff et al. have been numerous developments and improvements by developing an extension of spectral networks which incorporate a graph estimation procedure [5]. Although GNNs are a big promise, current implementations have limited in dealing with uncertainty in a graph structure, treat the graph topology as ground truth information, and update information from the neighboring nodes. This leads to the inability to fully describe the uncertainty in the predictions made by the neural network, especially for the SNA that the data is partially hidden [6]. In fact, deep learning model is effective in computing multilayer processing to represent data perception with many levels of abstraction [7]. However, probabilistic graph models are with Bayesian still exhibit more power and flexibility [8–10]. To achieve superiority including perception and inference, it is necessary to integrate probabilistic models like Bayesian models, and graph deep learning is called Bayesian graph deep learning. A graphical probabilistic model is a probability model that uses graphs to visually represent conditional dependencies between random variables. Deep learning can improve higher inference efficiency and vice versa, and feedback from inference can increase the perception of data [11, 12]. Deep learning networks are parameterized nonlinear models used for regression modeling and empirical classification. Their flexibility makes it possible to explore more general relationships in the data than with traditional statistical models. Probability theory provides a consensus for data modeling that offers several benefits. First, the overfitting problem can be solved using Bayesian methods to control the complexity of the model [13]. Second, the probabilistic model naturally deals with uncertainty [14]. Third, we can define more sophisticated probabilistic models that can extract more information from the data [15].

Social post classification plays a fundamental and important role in SNA such as extracting keywords, trending posts, and social summaries in each field and posts topics that the user interacts with, and we can detect their interest, thereby helping to understand the user's behavior and habits [16].

In this paper, we present the approach of the Bayesian and GNN framework for SNA. We focus on the processing of social network data, the posts by creating a homogeneous graph with links between them with a specific random graph model assortative mixed membership block model. We address the task of categorizing posts by semi-supervised classification of nodes in homogeneous graph with nodes as posts.

The proposed method is extensively evaluated on two corpora of Vietnamese and English sets of posts. We have demonstrated that Bayesian graph deep learning model is effective for classifying the topic of social posts in the results section. Our contributions in this research are as follows:

- We represented social posts from a heterogeneous graph—social network type to a homogeneous graph.
- We utilized the Bayesian model and graph deep learning which is capable of the semi-supervised node classification tasks.

- The proposed method is evaluated on Vietnamese as well as English posts on Facebook to demonstrate the language and platform independence property of our approach.

The remainder of this paper is as follow: Sect. 2 summarizes related research addressing the graph deep learning model and method in topic classification, and Sect. 3 describes the proposed method in detail. The results and a discussion set out in Sects. 5 and 6 with concluding observations and future works.

2 Related Work

Frasconi, Gori, and Sperduti in 1998 concentrated on using neural networks to analyze structured data underlying graph describing the relationship between data nodes [17]. Then, Scarselli, Gori, and others in 2009 introduced a novel neural network model that can handle graph inputs. The approach extends into a common framework and based on random walk models [18]. Recursive processing and propagation of information across the graph are the main approaches of these GNNs methods. It can often take a long time to converge in the training process, and the required time scales inevitably relate to the number of nodes in the graph [6].

Graph-based learning methods have emerged more recently, with the first proposals in graph-based embedding including two main subgroups: vertex embedding or node embedding and graph embedding. In general, these methods are on the assumption that nodes that are close together will have similar features. For example, whom you follow on Twitter will help us guess what problems they are interested in on social networks. From there, the researcher will rely on those relationships to propose models for their purposes. DeepWalk is known by Perozzi, Al-Rfou, and Skiena in 2014. DeepWalk, a simple node embedding model, is based on an idea from Word2Vec-Skip gram model using graph sampling with a random walk on graphs, and each node on the network after training process is represented by an embedding vector. Node2Vec is also a node embedding model with the concept of DeepWalk and Word2Vec using the random walk including two parameters P and Q to adjust on the graph [19]. Several node embedding models such as line large-scale information network embedding (LINE) [20], graph representations with global structural information (GraRep) [21] have been applied with some good results. However, narrow domains and few updates in the model are not the problem, but the new nodes in the graph will not have embedding vectors representing them. Additionally, it only uses the information of neighboring nodes to build the model without using other information such as node features in the graph.

Kipf, T. N. and Welling, M. initiated an extensive method on graph data for semi-supervised learning using neural networks [22]. GNNs are quite simple, but there are some limitations concerning memory requirement, directed edges, edge features, limiting assumption, and transductive setting. GraphSage is proposed by Hamilton, W., Ying, Z., and Leskovec, J. with a few improvements in modeling compared to

paper GCN. GraphSage can generalize better with unseen data, and it introduces three aggregate functions to integrate information from neighboring nodes. The mini-batch update gradient descent overcomes the biggest limitation of the GCN which is full-batch gradient descent updates [23]. The graph attention network (GAT) can improve the performance of the GNNs by incorporating attention nodes [24]. Compared to this past work, the primary methodological novelty in the study of Zhang et al. involves the adoption of during the deduction process, and data are supplemented using Bayesian and observational graph processing [6].

In the year 2016, Jotikabukkana et al. developed a useful technique of social text classification by semi-supervised learning utilizing a bag of words taken from news posts that provide the initial keywords related to their category in the form of word vectors with term frequency-inverse document frequency weighting (TF-IDF) and word article matrix (WAM) methods. An improvement of WAM provides an effective model for social text classification [25].

A topic-based classification through unigram unmasking is proposed by Yaakov et al. to show that unmasking was helpful across machine learning models for tasks of online free textbooks belonging to five domains, namely career and study advice, economics and finance, IT programming, natural sciences, statistics, and mathematics [26].

For social network data, in particular, posts have applied methods by processing independent data such as CNN, LSTM, or word graph to classify them [27]. The social network always has links between posts and other entities that are not fully utilized by independent processing methods. This paper will transform social data to citation graph data structure and using Bayesian GNN to improve the performance of topic classification.

3 Background

3.1 *Graph Convolutional Neural Networks (GCNNs)*

In this paper, we focus on the task of identifying the label of the node in the graph. A graph $G = (V, E)$, is defined with components such as a set of N nodes V and a set of edges E . For each node in graphs, we denoted by x_i with the assumption that x_i is detailed and described for node i . We can also denote that y_i is label of node i with labels $Y_S = \{y_i : i \in S\}$ where Y_S is a subset of the nodes $S \subset V$. Task is to use the features x and the graph structure G to estimate the labels of the unlabeled nodes. A GNN performs this task by performing graph convolution collecting the feature vectors as the rows of a matrix X , and A is an adjacency matrix, so the layers of a GNN [22] are of the form:

$$H^{(i)} = f(H^{(i-1)}, A) = \delta(AH^{(i-1)}W^{(i-1)}) \quad (1)$$

With,

$$H^{(0)} = X; H^{(1)} = f(H^{(0)}, A) = \delta(AXW^{(0)}) \quad (2)$$

Here, $H^{(i)}$ is the output representation of layer $i - 1$, each $H^{(i)}$ layer corresponds to a matrix of size $N \times F^{(i)}$ with $F^{(i)}$ shows the number of output features of each node at layer $H^{(i)}$. Matrix $W^{(l)}$ are the weights of the neural network at layer i , and δ is a nonlinear activation function. The matrix A is derived from the relationships between nodes on graph G and determines how the output features are mixed across the graph at each layer. The final output layer L is $Z = H^{(L)}$. Weights of the GNN model are updated during training by minimizing the error between the data set of label Y and the predicted value Z when the data passes through the model. Enhancing the architecture with components has proved useful and improves performance for the standard neural network model, including attention mechanism [24] and dropout connections and gates [28, 29].

There are different types of GNN such as GraphSage [30], GAT [24], Graph-Saint [31], and GIN [32]. Most of them treat a graph with a description of the relationships between the nodes as their reality in graph data [6, 22]. However, in practice, the graph data are often taken from the modeling assumptions or noisy data, so weak edges are sometimes added, and strong edges are removed from the graph. Thus, the current GNNs algorithms have limitations such as the overfitting issue, uncertainty of graph structure, and sensitivity to weak relationships.

3.2 Bayesian Neural Networks

A Bayesian neural network (BNN) is defined as a stochastic artificial neural network trained using Bayesian inference that considering the case where we have a dataset $\mathfrak{D} = \{(x_n, y_n)\}_{n=1}^N$ with training inputs $X = \{x_1, \dots, x_n\}$ and corresponding outputs $Y = \{y_1, \dots, y_n\}$ [33]. The activation function $y = f(x)$ is learnt by a neural network so that the weights W are sufficient statistics for f explanation for the relationship between x and y . A prior distribution over the random variables is modeled for the weights W in a Bayesian approach. By integrating the posterior distribution of W , the prediction is formed with a new data x :

$$p(y|x, \mathfrak{D}) = \int p(y|x, W)p(W|\mathfrak{D})dW \quad (3)$$

In particular, $p(y|x, W)$ can be viewed as a likelihood in a classification task it is modeled using a categorical distribution by applying a softmax function to the output of the neural network. The final prediction is summarized by a few statistics computed using Markov chain Monte Carlo methods. In order to summarize the predictions of a BNN used to perform the regression, the usual procedure is to perform model averaging:

$$p(y|x, \mathcal{D}) \approx \frac{1}{\Theta} \sum p(y|x, W_i) \quad (4)$$

Where Θ is an a collection of samples, and weights W_i are obtained via dropout.

3.3 Homogeneous Graph

Homogeneous graphs are graphs where all the nodes have the same function and a node is interchangeable with the next in the basic function they perform [34]. Citation graph data are known and popular like Cora, Citerseer, Pubmed [35], and the dataset is the homogeneous graph. Nodes mean publications, and edges mean citation relationships. They provided the feature vectors of the training and test instances both labeled and unlabeled instances with the one-hot labels of the labeled training instances and graph as a dictionary with a set of neighbor nodes. Unlike a citer network, a social network is a heterogeneous network with a variety of nodes and edges. Most GNN models work on homogeneous graphs, so we give an algorithm to convert social network posts to bring back the homogeneous graph in order to optimally apply the GNN model in the topic classification of posts or the node classification in academia.

4 Methodology

With a Bayesian approach, the posterior distribution is built for the graph, the node labels, and the weights in the model. From the family of random graph parameters, the probabilistic model considers the observed graph as a realization, then empirically infers the random graph parameters using the Bayes theorem as follows:

$$p(Z|Y_L, X, G) = \int p(Z|W, \tilde{G}, X) p(W|Y_L, X, \tilde{G}) p(\tilde{G}|\lambda) p(\lambda|G) dW d\tilde{G} d\lambda \quad (5)$$

Using a Monte Carlo approximation to achieve this process detailed in Fig. 1 consists of four steps: Bayesian inference for a graph generative model, Bayesian inference for a graph generative model, sampling graph neural network weights, and computing the posterior of labels.

In the first step, V samples λ are drawn from the posterior of a family of graph generative model $p(\lambda|\tilde{G})$, while λ denotes the parameters that characterize a family of random graphs. Depending on the different nature of the graph, these samples will generate different samples. Then, step 2 uses the adopted random graph model sampled N_G graphs from graphs in step 1. After V sampling random graphs we obtain $V N_G$ samples of (λ, \tilde{G}) from the joint distribution $p(\lambda, \tilde{G}|G)$. Thirdly, S weight matrices $W_{s,i,v}$ with W are random variable representing the weights of a Bayesian

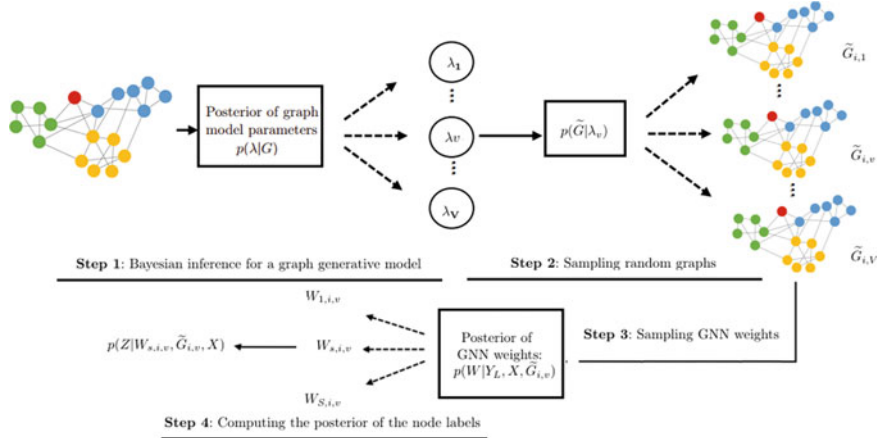


Fig. 1 Generate relationship between the statuses

GNN over graph \tilde{G} , S is sampled from the Bayesian GNNs $p(W|Y_L, X, \tilde{G})$ using the dropout approximation, so we get $VN_{\tilde{G}}S$ samples of GNN weights. The final one, result prediction $p(Z|Y_L, X, G)$ is an average of $p(Z|W_{s,i,v}, \tilde{G}_{i,v}, X)$ from different samples modeled by using a categorical distribution with a softmax function to the output of GNN.

As the integral in Eq. 5 cannot be computed analytically, a Monte Carlo approximation is formed as follows:

$$p(Z|Y_L, X, G) \approx \frac{1}{V} \sum_v^V \frac{1}{N_{\tilde{G}}S} \sum_{i=1}^{N_{\tilde{G}}} \sum_{s=1}^S p(Z|W_{s,i,v}, \tilde{G}_{i,v}, X) \quad (6)$$

We can adopt a number of strategies to approximate it, including variational methods and Markov chain Monte Carlo (MCMC) [36] and using an assortative mixed membership stochastic block model (MMSBM), [37] learn its parameters $\lambda = \{\pi, \beta\}$ by the stochastic optimization, and approximately compute $\{\hat{\pi}, \hat{\beta}\} = \underset{\beta, \pi}{\operatorname{argmax}} p(\beta, \pi|G)$ suitable priors over β and π :

$$p(Z|Y_L, X, G) \approx \frac{1}{N_{\tilde{G}}S} \sum_{i=1}^{N_{\tilde{G}}} \sum_{s=1}^S p(Z|W_{s,i}, \tilde{G}_i, X) \quad (7)$$

The Bayesian GNN model on graph \tilde{G} using Monte Carlo dropped out and its softmax output used to initialize π and β is based on the block structure imposed by π described in Algorithm 1 Bayesian GNN.

Algorithm 1: Bayesian-GNN**Procedure:** Bayesian-GNN**Input:** A observation graph G includes the nodes X with label set Y_L **Output:** The posterior probability of lables $p(Z|Y_L, X, G)$

1: **Initialization:** Train a GNN to initialize the inference in MMSBM and the weights in the Bayesian GNN.

2: **for** $i = 1$ to N_G **do**

3: Make N iterations of MMSBM inference to get $(\hat{\pi}, \hat{\beta})$.

4: Sample graph $G_i \sim p(\tilde{G}|\hat{\pi}, \hat{\beta})$.

5: **for** $s = 1 : S$ **do**

6: Sampling GNN weights $W_{s,i}$ over the graph \tilde{G}_i via MC dropout.

7: **end for**

8: **end for**

9: Approximate $p(Z|Y_L, X, G)$ using Eq. 7

Social network data used in this research are typically the Facebook which includes many types of entities (person, page, group, status) (see Fig. 2). We focus on categorizing the statuses by giving social media data about the status nodes as in the homogenous graph.

The operation process of the status transform in Algorithm 2. The idea here is based on the relationship between writer, page, group, and status. For any two, if both of them belong to the same page/person community, then the probability of a link between them is significantly higher than the case they two belong to different communities. Therefore, posts with the same origin of the agent will be linked together, see Fig. 2 left side, we will see red nodes for people or group nodes, these nodes create posts are green, blue, and yellow nodes, similarly if status are on the same page then they will be linked together in homogenous graph (see Fig. 2 right side).

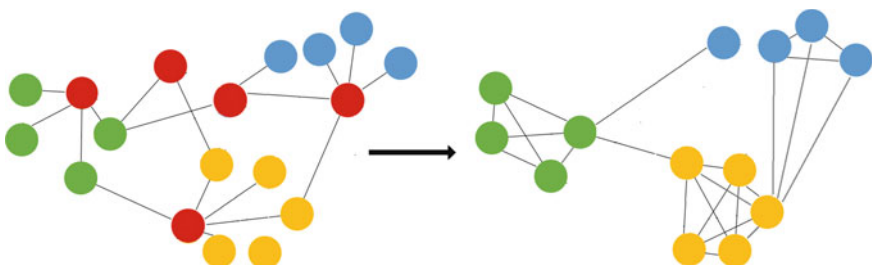


Fig. 2 Generate relationship between the statuses

Algorithm 2: Status Transform to Homogenous Graph**Procedure:** Bayesian-GNN**Input:** Facebook graph dataset G includes set of Person, Group, Status and Page nodes (P, G, S, Pg)**Output:** A Homogeneous Graph for status G_s

```

1: for node ( $N_i$ ) in set ( $P, G, S, Pg$ ) do
2:    $S_i = \emptyset$ 
3:   where  $N_i$  written a Status  $S_i^j$  do
4:     Add  $S_i^j$  in  $S_i$ 
5:     Create connection  $C_i^j$  for all node  $S_i^j$  in  $S_i$ 
6:     Add  $C_i^j$  in  $G_s$ 
7: end for
8: return graph structure  $G_s$  and status node S

```

5 Experimental Results

We explore the performance of the proposed Bayesian GNN on social network data (FacebookNeo4jdataset: <rb.gy/nmgrtt>). In these datasets, each node represents a status, and edges are formed whenever one post is related with another. An undirected graph from posts with an adjacency matrix is constructed. Each node label represents the topic that is associated with the posts. These datasets are represented in Table 1. We are using the method to transform this data to graph data structure that is described in Table 2 with the following steps:

- **Step 1: Data Preprocessing** including tokenization, removing unnecessary punctuation, tags, and stop words.
- **Step 2: Create feature vector** each status is described by a binary-valued word vector indicating the absence or presence of word from the dictionary.
- **Step 3: Label vector** is the labeled status.
- **Step 4 Graph index** as a dict with a set of neighbor nodes.

The hyperparameters of GNN are the same for all of the experiments. The GNN has two layers where the number of hidden units is 16, the learning rate is 0.01, and the dropout rate is 50% at each layer. These hyperparameters are also used in

Table 1 Summary of the datasets used in the experiments

FacebookNeo4jdataset	Quantity
Nodes	362,652
Edges	886,759
Features per node	8243

Table 2 Summary of the datasets to citation graph

Status data graph	Quantity
Nodes	18,419
Edges	58,257
Features per node	5236
Classes	11

Table 3 Prediction accuracy for status dataset

Model	5 labels	11 labels	19 labels
ChebyNet	78.1	78.4	84.0
GCNN	79.7	82.8	85.6
GAT	80.0	81.6	86.9
Bayesian GCN	81.7	82.3	88.6

the Bayesian GNN. The hyperparameters of MMSBM inference are set as follows: $\alpha = 1$, $n = 500$.

We have evaluated the performance of the proposed Bayesian GNN algorithm and compared it to the state-of-the-art methods on the semi-supervised node classification problem. In addition to the 19 labels per class, we evaluate the performance of model in scenarios where only 5 or 11 labels per class are available. We are using accuracy of the ratio between true instance classified and overall classes. We use classification accuracy to measure the performance of our model, it is the ratio of number of correct predictions to the total number of input samples. Table 3 shows the summary of results on datasets. The experiment results prove the improvement in classification by Bayesian GCNN for Facebook status datasets. Bayesian GCNN offers the best performance for 5 and 19 label boxes with classification accuracy ratio of 81.7% and 88.6% higher than other methods (see Table 3) but equivalent performed by other techniques for 11 label cases is 82.3%, it is 0.5% lower than GCNN method.

6 Conclusions and Future Work

In this paper, we have presented a Bayesian neural network, which provides an approach to combining graph uncertainty information through a parametric random graph model. We explored the performance of the Bayesian GNN for the semi-supervised node classification task and found that the improved methodology is based on modern techniques, especially in the case of small number of training labels. This paper presents a preliminary investigation of a Bayes graph convolutional neural network and focuses on a kind of graph model and a graph learning problem. Applying this model and the algorithm of converting Facebook graph data

into homogenous graph data gave better results than other methods to classify posts topics.

In the future, we will extend our approach to Bayesian and graph models for tasks on social data such as relationship prediction or community discovery.

Acknowledgment This research is funded by CMC Institute of Science and Technology (CIST), CMC Corporation, Vietnam. We also thank for administrative support from researchers of Datalake Knowledge Engineering Lab, CIST, CMC Corporation.

References

1. Zhang Z, Cui P, Zhu W (2020) Deep learning on graphs: a survey. *IEEE Trans Knowl Data Eng*
2. Huang Q, Yamada M, Tian Y, Singh D, Yin D, Chang Y (2020) GraphLIME: local interpretable model explanations for graph neural network. [arXiv:2001.06216](https://arxiv.org/abs/2001.06216)
3. Ying R, He R, Chen K, Eksombatchai P, Hamilton WL, Leskovec J (2018) Graph convolutional neural networks for web-scale recommender systems. In: Proceedings of the 24th ACM SIGKDD international conference on knowledge discovery & data mining, 2014, pp 974–983
4. Bruna J, Zaremba W, Szlam A, LeCun Y (2013) Spectral networks and locally connected networks on graphs. [arXiv:1312.6203](https://arxiv.org/abs/1312.6203)
5. Henaff M, Bruna J, LeCun Y (2015) Deep convolutional networks on graph-structured data. [arXiv:1506.05163](https://arxiv.org/abs/1506.05163)
6. Zhang Y, Pal S, Coates M, Ustebay D (2019) Bayesian graph convolutional neural networks for semi-supervised classification. In: Proceedings of the AAAI conference on artificial intelligence, vol 33, pp 5829–5836
7. Wang H, Yeung DY (2016) Towards Bayesian deep learning: a survey. [arXiv:1604.01662](https://arxiv.org/abs/1604.01662)
8. Patel AB, Nguyen MT, Baraniuk R (2016) A probabilistic framework for deep learning. *Adv Neural Inf Process Syst* 2558–2566
9. Sawant SS, Prabukumar M (2018) A review on graph-based semi-supervised learning methods for hyperspectral image classification. *Egypt J Remote Sens Space Sci* (2018)
10. Cheng KP, Mohan RE, Nhan NHK, Le AV (2019) Graph theory-based approach to accomplish complete coverage path planning tasks for reconfigurable robots. *IEEE Access* 7:94642–94657
11. Bishop CM (1997) Bayesian neural networks. *J Braz Comput Soc* 4(1)
12. Wang H (2017) Bayesian deep learning for integrated intelligence: bridging the gap between perception and inference. Hong Kong University of Science and Technology
13. Shridhar K, Laumann F, Liwicki, M (2019) A comprehensive guide to Bayesian convolutional neural network with variational inference. [arXiv:1901.02731](https://arxiv.org/abs/1901.02731)
14. Zhang CY, Zhao Q, Chen CP, Liu W (2019) Deep compression of probabilistic graphical networks. *Pattern Recognit* 96:p.106979
15. Ni Y, Müller P, Wei L, Ji Y (2018) Bayesian graphical models for computational network biology. *BMC Bioinform* 19(3):59–69
16. Truong X, Van Pham H (2020) A proposal of deep learning model for classifying user interests on social networks. In: Proceedings of the 4th international conference on machine learning and soft computing, pp 10–14. 10.1145/3380688.3380707
17. Frasconi P, Gori M, Sperduti A (1998) A general framework for adaptive processing of data structures. *IEEE Trans Neural Netw* 9(5):768–786
18. Scarselli F, Gori M, Tsoi AC, Hagenbuchner M, Monfardini G (2008) The graph neural network model. *IEEE Trans Neural Netw* 20(1):61–80
19. Grover A, Leskovec J (2016) node2vec: scalable feature learning for networks. In: Proceedings of the 22nd ACM SIGKDD international conference on Knowledge discovery and data mining, pp 855–864

20. Tang J, Qu M, Wang M, Zhang M, Yan J, Mei Q (2015) Line: large-scale information network embedding. In: Proceedings of the 24th international conference on world wide web, pp 1067–1077
21. Cao S, Lu W, Xu Q (2015) Grarep: learning graph representations with global structural information. In: Proceedings of the 24th ACM international conference on information and knowledge management, pp 891–900
22. Kipf TN, Welling M (2016) Semi-supervised classification with graph convolutional networks. [arXiv:1609.02907](https://arxiv.org/abs/1609.02907)
23. Hamilton W, Ying Z, Leskovec J (2017) Inductive representation learning on large graphs. In: Advances in neural information processing systems, pp 1024–1034
24. Veličković P, Cucurull G, Casanova A, Romero A, Lio P, Bengio Y (2017) Graph attention networks. [arXiv:1710.10903](https://arxiv.org/abs/1710.10903)
25. Jotikabukkana P, Sornlertlamvanich V, Manabu O, Haruechaiyasak C (2016) Social media text classification by enhancing well-formed text trained model. *J ICT Res Appl* 10(2):177–196
26. HaCohen-Kerner Y, Rosenfeld A, Sabag A, Tzidkani M (2018) Topic-based classification through unigram unmasking. *Procedia Comput Sci* 126:69–76
27. Li C, Zhan G, Li Z (2018) News text classification based on improved Bi-LSTM-CNN. In: 2018 9th International conference on information technology in medicine and education (ITME), pp 890–893
28. Bresson X, Laurent T (2017) Residual gated graph convnets. [arXiv:1711.07553](https://arxiv.org/abs/1711.07553)
29. Li Y, Tarlow D, Brockschmidt M, Zemel R (2015) Gated graph sequence neural networks. [arXiv:1511.05493](https://arxiv.org/abs/1511.05493)
30. Hamilton W, Ying Z, Leskovec J (2017) Inductive representation learning on large graphs. In: Advances in neural information processing systems, pp. 1024–1034
31. Zeng H, Zhou H, Srivastava A, Kannan R, Prasanna V (2019) Graphsaint: graph sampling based inductive learning method. [arXiv:1907.04931](https://arxiv.org/abs/1907.04931)
32. Xu K, Hu W, Leskovec J, Jegelka S (2018) How powerful are graph neural networks? [arXiv:1810.00826](https://arxiv.org/abs/1810.00826)
33. MacKay DJC (1992) A practical Bayesian framework for backpropagation networks. *Neural Comput* 4(3):448–472
34. Gardiner A (1976) Homogeneous graphs. *J Comb Theory Ser B* 20(1):94–102
35. Sen P, Namata G, Bilgic M, Getoor L, Galligher B, Eliassi-Rad T (2008) Collective classification in network data. *AI Mag* 29(3):93–93
36. Li W, Ahn S, Welling M (2016) Scalable MCMC for mixed membership stochastic blockmodels. In: Artificial Intelligence and Statistics, pp 723–731
37. Gopalan PK, Gerrish S, Freedman M, Blei D, Mimno (2012) Scalable inference of overlapping communities. In: Advances in neural information processing systems, vol 25, pp 2249–2257

Data Confidentiality and Integrity in Cloud Storage Environment



Essohanam Djeki, Carlynna Bondiombouy, and Jules Degila

Abstract Cloud services have seen a considerable increase in recent times, as the cloud allows users to outsource their data and IT resources. Storing and backing up data in the cloud have become increasingly popular. However, data security is an increasing concern. With the number of attacks on the cloud and data leakage, users are worried about their data security in the cloud. Several works dealt with data security in the cloud, but most of these solutions largely depend on providers. They do not provide users the control of the security of their data. To deal with data security concerns, we proposed a solution called Encrypt cloud that allows users to encrypt and check their files' integrity before uploading and storing it the cloud storage. We used the encryption technique (AES 256) to ensure the confidentiality of the data. To verify the data integrity, we used the SHA 256 hash function with a two-level integrity check. Performance analysis of the AES encryption algorithm was performed to compare execution time and memory usage during the encryption and decryption process. It should be noted that decryption consumes more resources than encryption.

Keywords Data confidentiality · Data integrity · Cloud storage · Data encryption · Cloud security issues · Encrypt cloud

1 Introduction

Cloud computing is a concept that represents access information and services located on a remote server via Internet. Cloud computing has the potential to revolutionize IT, but it has some disadvantages, like security threats. With the expansion of the

E. Djeki (✉) · J. Degila

Institut de Mathématiques et de Sciences Physiques, Porto-Novo, Benin
e-mail: essohanam.djeki@imsp-uac.org

J. Degila

e-mail: jules.degila@imsp-uac.org

C. Bondiombouy

Centre d'Excellence Africain—Science Mathématiques et Applications, Porto-Novo, Benin

© The Author(s), under exclusive license to Springer Nature Singapore Pte Ltd. 2021

987

H. Sharma et al. (eds.), *Communication and Intelligent Systems*, Lecture Notes in Networks and Systems 204, https://doi.org/10.1007/978-981-16-1089-9_77

cloud, development of its various services and technologies used, new security issues have arisen. Indeed, safety has been a hot topic during forums on privacy and data governance. The controversial issue of confidentiality and data security remains the cloud's major limitation [1]. The risk of seeing the data in a situation of theft, illegal use, or unauthorized use is possible. From an information security perspective, questions are raised about the various threats facing the cloud especially: What are the risks of outsourcing data in the cloud, and how can cloud customers ensure their data security?

In this paper, we were interested in data confidentiality and integrity in the cloud. To address this problem, several research efforts have been undertaken in recent years, to secure and protect data in the cloud. Still, complete security is far from being obvious because of the diversity of possible problems and attacks. We will first start with a cloud overview and its security issues. We will then look at the related works to see what is already achieved for data security in the cloud storage. We will end with our proposed solution to solve problems related to the data protection in transit or at storage and its performance analysis.

2 Cloud Computing

2.1 Overview

In 2018, 26% of European Economic Community enterprises used cloud computing, mostly for hosting their e-mail systems (69%), storing files in electronic form (68%), office software (53%), databases (48%), financial or accounting software applications (38%), CRM software (29%), and computing power for enterprise's software (23%) [2]. Figure 1 shows the comparison between 2014, 2016, and 2018 in using of cloud services by purpose. The use of cloud in 2018 for email, and file storage is still predominant. The use of office software has recorded the highest growth (+19%) since 2014, among all purposes. The more sophisticated purposes of cloud services (for financial and accounting software applications, CRM software applications, and computing power) recorded smaller increases (+7%, +8%, and +6%, respectively) [3].

2.2 Security Issues

The cloud has advantages, but it also has some disadvantages including security issues, i.e., data security issues, networking issues, virtualization issues, organization security management, and backup and recovery issues. In the case of data security, we identified some cloud's challenges such as data confidentiality, data integrity, data availability, data storage, data lock-in, data breaches, data access, data locality,

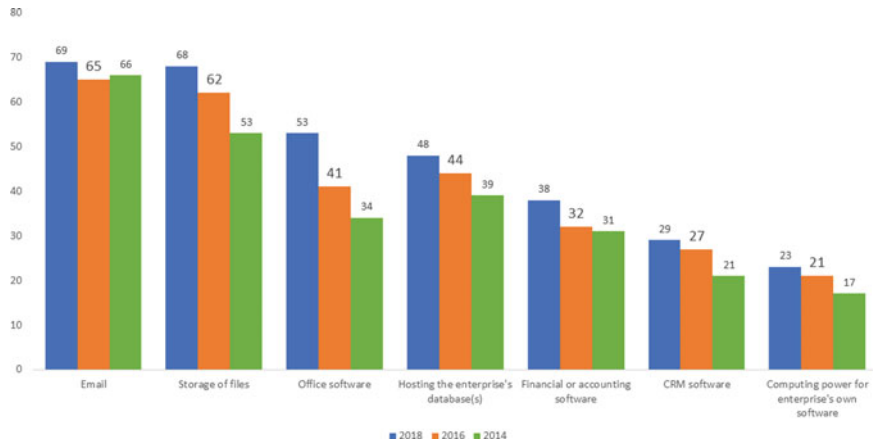


Fig. 1 Cloud computing adoption in services

data privacy, etc. According to Eurostat [2], companies' highest risk is the security breaches, e.g., 57% for large companies and 38% for SME (see Fig. 2). We all know that even a 1% security breach are enough for a criminal hacker to initiate an attack. This is why organizations are increasingly placing more importance on the security of their IT systems. But protection is much more difficult in the cloud environment because of the outsourcing of the system, or servers, or applications leading to loss of control over the system, and the data. Other issues faced by organizations using the cloud are data governance (46% for large enterprises and 31% for SME), data location (46% for large enterprises and 29% for SME), and problems accessing data or services (35% for large enterprises and 27% for SME), insufficient knowledge or expertise in ICT [2]. Thirty-two percent of SMEs using the cloud reported that the problems listed above were a factor limiting the cloud's adoption, compared with 17% of large enterprises. An observation of Fig. 2 shows that security breaches are on the rise.

Data breaches in the USA reached a six-month high of 29% in June 2017, up from the same period the previous year according to the Identity Theft Resource Centre Report (ITRC) [4]. The Equifax data breach example caused considerable damage by exposing users' sensitive personal data, such as names, dates of birth, social security numbers, driver's license numbers, credit card numbers, to the public. IBM's study showed that data breaches come from 53% of insiders and inadvertent of CSP's employees, 42% by outsiders (criminal hackers), and only 5% are caused by insiders malicious [4].

The cloud has excellent potential due to its advantages and has its challenges, among which are security problems. Given a large number of data leaks and the origin of the causes, it is clear that nothing can be done to prevent data leakage 100%. That is why more efforts must be made to enable cloud users to secure their data in transit and at storage. In the next section, we will explore related work in this direction.

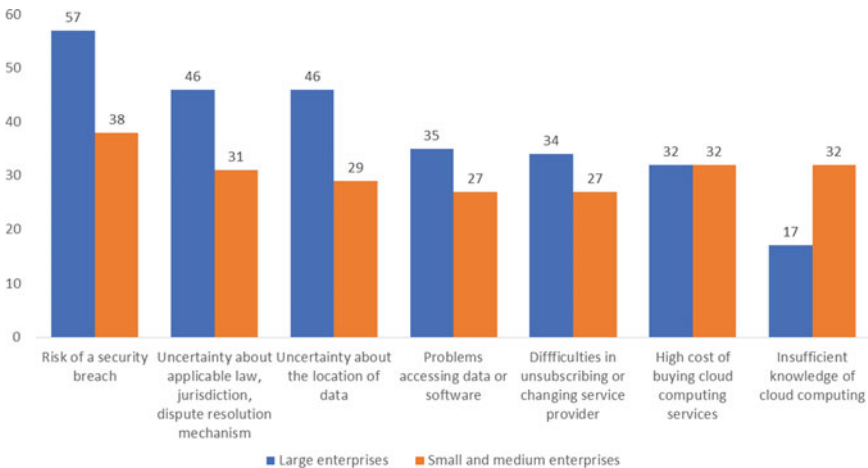


Fig. 2 Cloud computing popular limits

3 Related Works

Data protection often refers to laws concerning the regulation of personal data and privacy. Many states already established data security regulations to prevent abuse and protect users from potential risks. Pfarr et al. [5] highlighted the different necessary current rules to protect the data and privacy of Internet users' that can be applied in cloud environments. Among these regulations, the authors talked about the proposed US Safe Harbor Agreement, the EU General Data Protection Regulation (GDPR), and also the Binding Corporate Rules, which is a regulation ensuring the security of data exchanged between EU countries and third world countries. Laws vary from one country to another depending on the government, while the Internet has no borders, and the duplication of data in geographic areas used by the cloud to ensure data availability, it is becoming increasingly difficult to enforce a law on replicated data.

Ni et al. [6] worked on a new model to ensure data integrity and confidentiality in cloud storage. The authors propose a new secure outsourced data transfer scheme (SODT) based on polynomial-based authenticators and the BCP encryption scheme. They enhance the BCP encryption scheme to handle proxy re-encryption and use it to maintain the outsourced data confidentiality. Using the homomorphism of the enhanced BCP encryption scheme and polynomial-based authenticators, users can efficiently verify the integrity of their data in the cloud to ensure the security of outsourced data transfer in the cloud. Users can also discard data transferred to the cloud by proxy re-encryption method. Their solution focuses on the transfer or migration of data from a cloud provider to a new provider, so the solution is used to ensure data integrity during the migration and to ensure that these data have been adequately removed from the old provider to maintain data confidentiality.

Han and Xing [7] design a novel third party auditor scheme in cloud storage. Their solution is composed of two parts: Users and Advanced Cloud Service Provider (ACSP) in which the third-party auditor function combines with the cloud service provider. To ensure data security, the authors use the RSA algorithm to encrypt all data flow between servers in the ACSP, and bilinear Diffie–Hellman to ensure security while exchanging keys between users and servers in their scheme. A limitation to the cryptographic solution is that CSPs know the encryption and decryption keys to access their customers' data. The cryptographic techniques add computational overhead to CSP, while their primary objective is the optimal resource use.

To solve this problem, Zakaria et al. [8] have thought of using File Assured Deletion (FADE) which is a promising solution to protect user data. FADE ensures the deletion of files by making them unrecoverable for anyone, including cloud storage providers. The system is built by encrypting all data files before outsourcing, then using a trusted party to outsource the key cryptography. But this methodology remains weak because its security largely depend on the key manager's security. To overcome this problem, the authors have proposed a new system to improve the security of the FADE using the Trusted Platform Module (TPM), and the Encrypted File System (EFS).

To protect data from unauthorized users access, the data are supposed to be either in encrypted or unreadable. Sugumar and Arul Marie Joyce [9] propose an obfuscation technique for enhancing data in the cloud storage. This obfuscation technique is used to encrypt and decrypt all data. The authors propose a confidentiality system called SUGUMAR Digits Obfuscation (SUG-DO) to strengthen data security in the cloud environment. The obfuscation technique cannot be used to secure any type of data or large data.

Mahmood et al. [10] propose a new cloud storage system to enhance data security (images), while ensuring a secure and reliable cloud storage service. A secret image is encrypted using the AES algorithm. The encrypted image is embedded into the host image using a steganography technique, which combines discrete wavelet transformation (DWT) and singular value decomposition (SVD) to produce the stego image. To preserve the data integrity, a hash value is computed from the stego image using the SHA-512 before storing the image in the cloud. Once the image is retrieved from the cloud, its hash value is generated using the same algorithm (i.e., SHA-512). The two hash values are then compared to check if the data stored in the cloud changes and to get the secret image.

To ensure the confidentiality of outsourced data, Manikandasaran et al. [11] propose a technique called MONcrypt which is based on obfuscation technique. Generally, obfuscation is done without using any key to obfuscate users' data, but the authors have developed a method that uses a key for de-obfuscation. During the process of obfuscation, a count value is produced from the original text. This count value is used as a de-obfuscation key. The key is stored as metadata in the client part. The authors conducted an experience with sample data, and performance analyzed in terms of time taken for obfuscation and de-obfuscation show that the MONcrypt offers maximum security for outsourced data in less time. Unfortunately, MONcrypt is only applied to numerical data.

Abolghasemi et al. [12] worked on improving the data encryption technique used in cloud storage. The authors proposed a data encryption method based on the user's geolocation, called geo-encryption, to add a new security layer to the existing security measures. Anti-spoof and accurate GPS are required to give the latitude and longitude accurately. The geo-encryption algorithm is implemented in the cloud, and the user's computer, which is connected to the GPS, is used to encrypt-decrypt the data. When uploading data to the cloud, the spatial location is used to generate the encryption and decryption key. To retrieve and decrypt the data, the user had to be in the same location. As a result, they can limit the data access to a specific location at a particular time. Their solution is more appropriate for banks, big companies, institutions, and examples like this.

Sood [13] proposed a model that combined various techniques to perform data security in the cloud. His solution uses encryption as the main fundamental protection scheme. The framework introduces the notion of classification of data based on sensitivity rate (SR), which is computed from the combination of confidentiality, availability, and integrity provided by the user himself, and according to SR, the system decide where to upload the data (public, private, or owner limited access storage), e.g., if $SR < 3 \Rightarrow$ Public, $3 < SR \leq 6 \Rightarrow$ Private, and $6 < SR \leq 10 \Rightarrow$ Owner limited access storage. His solution provides data availability by surpassing many issues like data leakage, tampering of data, and unauthorized access even from the CSP, as he says.

Pitchai et al. [14] proposed a new protocol called availability and integrity verification protocol (AIVP) to predict the available space in the cloud and verify the integrity of the data stored in it. The authors have separated public and private data for integrity checking, thus ensuring data confidentiality. The private data is uploaded by the service providers in the cloud, and the public data will be uploaded by the third-party auditor. In the results of the simulation, the AIVP proposed by the authors outperformed high performance and throughput, which they say will reduce latency, computing, and communication costs.

Wei et al. [15] conducted a study on the use of blockchain techniques to improve data integrity checking by reducing the excessive complexity of calculations, or the problem of lack of scalability. The authors deployed a model of a distributed virtual machine agent in the cloud using mobile agent technology. The virtual machine agent allows multiple tenants to cooperate to ensure data trust verification. The integrity protection framework based on the blockchain is constructed by the proxy model of the virtual machine. The unique hash value corresponding to the file generated by the Merkle hash tree is used to monitor data change through the intelligent contract on the blocking chain, and data is held on time. Besides, a "block-and-response" mode is used to build a data integrity verification scheme in the cloud based on the blocking chain.

Li et al. [16] proposed a new method for proving data integrity (PDI) for customers whose data is hosted on non-trusted servers in cloud computing. An advantage of their model is low cost to the customer since a consistent volume of metadata is generated. The authors propose a simple and efficient audit service for public verification of non-trusted outsourced storage based on a bilinear group. In comparison with existing

PDI methods, they aim to ensure integrity by considering the cost of generating the audit metadata at the customer's side. Besides, their method supports data dynamics and public verifiability.

4 Our Proposed Model

With the growing number of collaboration tools which require resources (files) to be shared, artificial intelligence that involves data (structured and unstructured) for learning, big data, and also the emergence of the bring your own device concept, which requires resources (data or files) to be accessible at any time, from anywhere, and on any device. We estimate that the use of the cloud for storage is and will be increasing. For these reasons, we have decided to make our contribution to data (files) protection in the cloud and mostly focused on the client side.

With the traditional architecture, when a user sends file to the cloud, the files are transmitted and stored in plain text. An unauthorized person can intercept it during the sending (man in the middle attacks), or even access the files in the cloud because of pooling. Sometimes the connection with the CSPs' servers is made securely, i.e., encrypted, and they use security protocols such as SSL/TLS, SSH, IPSec or VPN, but the data sent is stored in plain text on the CSPs' storage servers. According to the service-level agreement (SLA) of some providers, the data is encrypted in storage, and there is still a problem with the encryption–decryption keys. This stipulates that the storage provider has access to the encryption–decryption keys; with this information, the provider can illegally access and use users' data without their permission and consent. Our solution aims to enable users to encrypt their data (files) before uploading it. Users are, therefore, in control of the security of their data. It is an application solution we called Encrypt cloud, i.e., it is about offering an application that allows users to encrypt and verify the integrity files before sending them to the cloud.

At the macro-level, Fig. 3 shows the architecture. In the proposed architecture, users interact with an interface that acts as an intermediary between the users and their CSP by integrating an additional security layer. Before uploading a file, the user chooses whether he wants to encrypt or not, or whether he wants to check the file's integrity or not.



Fig. 3 Generic architecture of the proposition

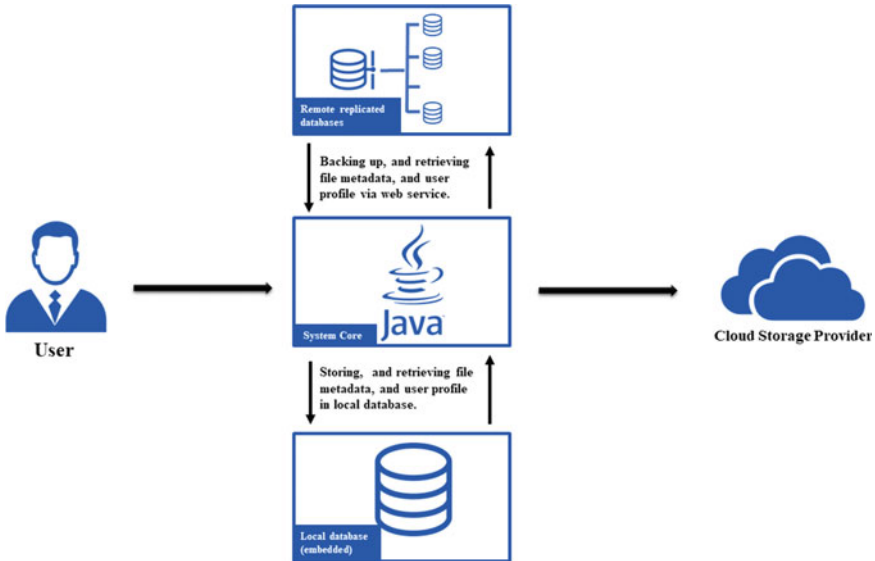


Fig. 4 Architecture of encrypt cloud

The Encrypt cloud architecture is shown in Fig. 4. Encrypt cloud consists of three types of components, *System Core*, *Local Database*, and *Remote Replicated Databases*.

The *System Core* is the engine of the application, it uses both components to ensure effective processing of the application.

The *Local Database* is the data repository and used to store all high-level data; the aim is to allow users to work offline. The storage system is an embedded database, and all tables follow a certain degree of database standardization. There are two main entities in the database, namely *user profile* and *file metadata*. The *User profile* contains information about the system's users, including user id, username, password, email, csp, access token, which allows linking their account to the cloud, among other personal information. *File metadata* store metadata about each file uploaded by the user. This information includes user id, filename, the date and time, hash of the file, encryption key associated with the file, and other information. Why associate an encryption key with each file? We could have generated a single encryption key for users. Still we would like to share files between users without compromising the security of the owners of the shared files. By assigning an encryption key to each file, a file can be shared without worrying about other files' protection.

The *Remote Replicated Databases* provides the availability and continuity of the service, and data also. Before starting, users must create an account by providing a username, password, recovery email, and information about their CSP. This information is stored locally (an embedded database). Suppose the user loses his machine, or reinstalls it, or wants to access data using another machine or device, he or she

will no longer be able to use his encrypted data or check the integrity of his data, because he no longer has the encryption-decryption key, or the hashes of his files. The remote replicated databases will therefore be used to save user information and file meta data remotely.

When a user sends a file, depending on his choice, the system will decide to calculate and save the hash of the file using SHA-256 to ensure the file's integrity. With user's information, the file will be encrypted using the AES-256 (Advanced Encryption Standard) algorithm according to his choice. The encrypted file will be sent to the user's appropriate cloud using the API published by his CSP, and the metadata will be saved on local, and remote database as we can see on Algorithm 1.

Algorithm 1 File uploading process

- 1: Select the file to be uploaded from local storage.
 - 2: **if** the user chooses to check the file's integrity **then**
 - 3: Compute hash(file).
 - 4: **if** the user chooses to encrypt the file **then**
 - 5: Generate an encryption key, and encrypt(file).
 - 6: Send the file to the cloud using CSP's API.
 - 7: Save file's metadata in the local database, and remote replicated databases.
-

After authenticating, the user can retrieve, exploit, or download his files. To download a file, as described with Algorithm 2, the user selects the file he wants; the system recovers the file metadata; if the file is encrypted, it is decrypted with AES-256. Encrypt cloud uses a double integrity check to ensure the file's integrity and of the databases containing the metadata. Once we have the file's metadata, we compare the signatures contained in the databases, if a database is corrupted, i.e., all signatures do not match, we then make a hash comparison and choose the majority hash. Finally, we calculate the hash of the file and compare it with the hash from the databases.

Algorithm 2 File downloading process

- 1: Select the file to be downloaded.
 - 2: Retrieve file's metadata (including the signature, and encrypt-decryption key) from the local database, and from remote replicated databases.
 - 3: **if** the file is encrypted **then**
 - 4: decrypt(file).
 - 5: Compare local signature (from local database) with remote signatures (from replicated databases). If all signatures do not match, then select the majority signature.
 - 6: Compute hash or signature of the downloaded file.
 - 7: Compare the majority hash with the downloaded file's hash.
-

5 Sample User Sessions Using Encrypt Cloud

In this section, we provide detailed examples to illustrate how a user interacts with *Encrypt cloud*. You must log in by providing a username and password before using the application. You must have an account.

The creation process follows three steps:

- First step: provide your profile information, i.e., username, recovery email, and password;
- Second step: select your cloud provider;
- Third step: link your cloud account to your *Encrypt cloud* account. Once you have selected your provider, a web page will be launched from your web browser asking you to log in to allow your cloud account to be linked to *Encrypt cloud*. Your provider will provide you with an authorization code that you will copy and paste into the *Encrypt cloud* and click on “Finish” button to finish the process.

Once the account is successfully created, the application automatically takes you back to the authentication page. Log in with your credentials and you will be on the home page (Fig. 5).

The home page is mainly composed of three columns: The first column presents the user’s folders; the second column presents the files and/or sub-folders of the parent directory, and the last one presents a detailed view of the items. From the home page, we can send files via the “Upload File” button or send a whole folder via the “Upload Folder” button.

Once you click on the “Upload File” button, a window will open (Fig. 6), you will have to specify the folder where the file(s) will be stored, choose the file(s) from your machine, decide whether to encrypt the file or not, and decide

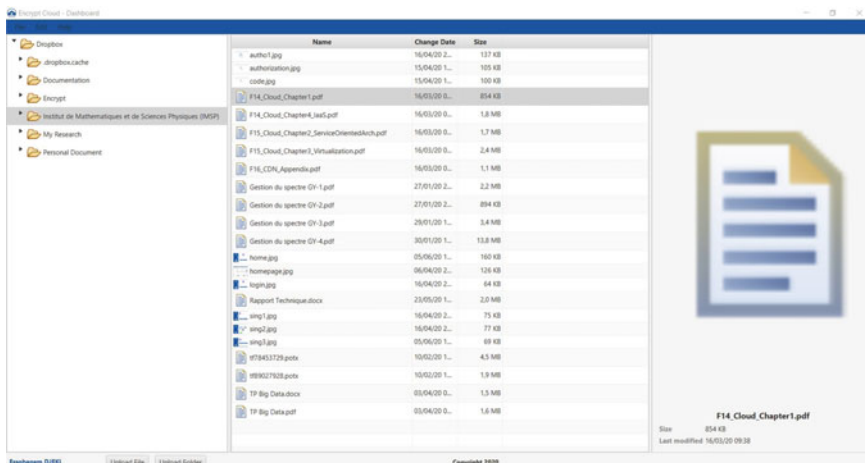


Fig. 5 Encrypt cloud home page

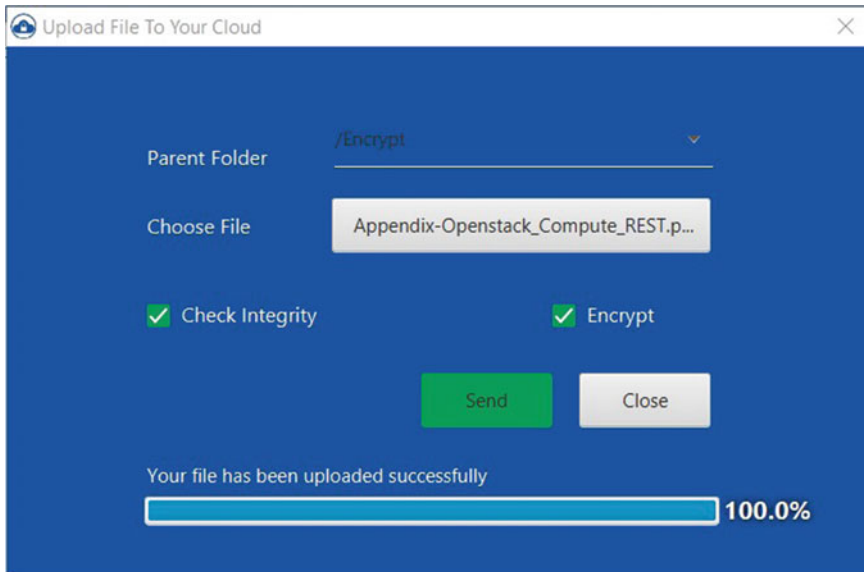


Fig. 6 File uploading window

if the integrity of the file(s) should be checked. In our case, we sent the file “*Appendix-Openstack_Compute_REST.pdf*” in Dropbox, we encrypted it and verified its integrity. A double click on a file opens a window displaying file’s information, whether the file is encrypted or not, whether the file integrity check is enabled or not, whether the file has been altered or not. Figure 7 shows that the file has been altered. The system has detected that the file has been modified. The system asks to know if we are at the origin of the modification, if yes, we have the possibility to update the hash by checking “Yes” or “No” otherwise.

6 Other Encryption Tools

We have found some applications that offer solutions acceptable. Among these solutions, we have: EnCrypted cloud, which shifts your Google Drive, Dropbox, Box, and Egnyte folders into an enCrypted folder; Encrypto, which focuses on sending, and sharing (via USB, or email) encrypted files, but also works for encryption of local, and cloud storage (Dropbox); Boxcryptor, you can create a folder anywhere on your computer, and everything in that folder is encrypted, and in case you use a cloud storage service like Google Drive, or Dropbox, this folder can be placed in the synchronization folder of the corresponding application; Sookasa works very similarly to BoxCryptor; Cryptomator saves the files in an encrypted folder in the vault somewhere on your computer, or on your Google Drive, or Dropbox folder;



Fig. 7 File information window

NordLocker works similarly to Cryptomator; Odrive is a desktop, and web tool which enables you to link all your online storage accounts (Google Drive or Dropbox), its particularity is that files are only encrypted on the cloud storage, not on the local computer; AxCrypt; BitLocker; Perfecto Encryptor; VeraCrypt; and EncFSMP.

These encryption tools use the AES encryption algorithm (Table 2) and are available on, almost all platforms, generally on Windows, Mac, Android, iOS and sometimes on Linux, and available in free or evaluation version and paid version (see Table 1).

We have noticed that most of these tools are applications that are specifically designed to manage files by introducing the notion of “Vault.” And that these vaults can be synchronized with cloud accounts. These vaults are protected by a unique password, which means that the vault remains inaccessible in the event of loss or forgotten password, files are lost. Beyond its limitations, we have noticed that these tools do not support file integrity checking (see Table 2).

7 Performance Analysis

The performance of systems or applications needs to be evaluated based on a number of criteria. These criteria determine whether a system or application is efficient/effective or not: These parameters are known as performance metrics. To ana-

Table 1 Encryption tools: platforms, and prices

Software	Platforms	Pricing
EnCrypted cloud	Win, Mac, Android, and iOS.	Free
Encrypto	Windows, and Mac.	Free
Boxcryptor	Win, Mac, Android, and iOS.	Free
Sookasa	Win, Mac, Android, and iOS.	Free Premium (\$10 /month)
Cryptomator	Win, Mac, Android, and iOS.	Free (Pay what you want)
NordLocker	Win, Mac.	Free (5Go) Premium (\$2.99/month)
Odrive	Win, Mac, Linux.	Free-Premium
VeraCrypt	Win, Mac, Linux.	Free
Perfecto Encryptor	Win, Mac, Linux.	Free
EncFSMP	Win, Mac, Linux.	Free
AxCrypt	Win, Mac, Android, and iOS.	Free
EnCrypt cloud	Win, Mac, Linux.	Free*

Table 2 Encryption tools features

Software	Confidentiality	Integrity
EnCrypted cloud	Yes (AES 256)	No
Encrypto	Yes (AES 256)	No
Boxcryptor	Yes (AES 256)	No
Sookasa	Yes (AES 256)	No
Cryptomator	Yes (AES 256)	No
NordLocker	Yes (AES 256-RSA 4095)	No
Odrive	Yes (AES 256)	No
VeraCrypt	Yes (AES 256)	No
Perfecto Encryptor	Yes (AES 256)	No
EncFSMP	Yes (AES 256)	No
AxCrypt	Yes (AES 256)	No
EnCrypt cloud	Yes (AES 256)	Yes (SHA 256)

lyze our solution's performance, we need to analyze the application's performance when uploading and downloading files. Uploading and downloading files depend on encryption and network speed. Since the network speed varies from one user to another, we have analyzed the performance of the AES algorithm encryption, while sending and receiving based on the metrics used by Lemma et al. [17], which are:

- Encryption, and Decryption Time: the execution time it takes for an encryption algorithm to produce cipher text from plain text or plain text from cipher text;
- Encryption, and Decryption Memory Usage: is the amount of memory (RAM) consumed when the encryption or decryption process;

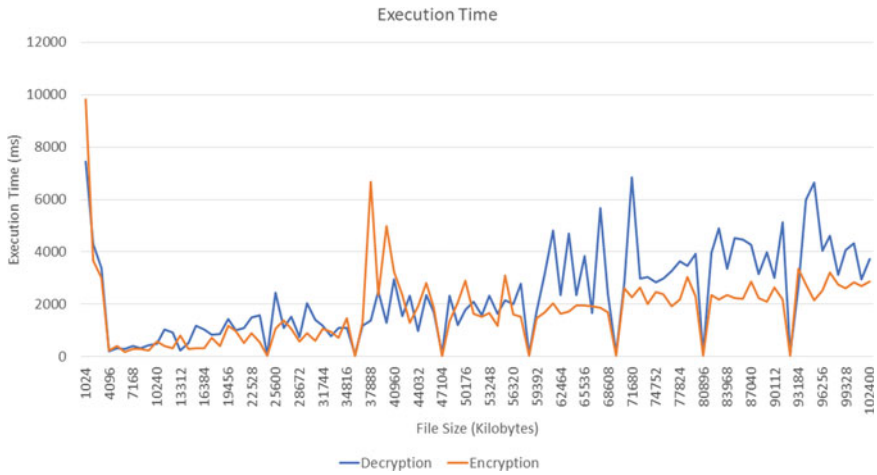


Fig. 8 Execution time

- Encryption, and Decryption Throughput: are calculated from the file (plain text or cipher text) size and the time it takes to process encryption or decryption using the following formula:

$$\text{Throughput} = \frac{\text{Text Size}}{\text{Execution Time}}$$

Many works in the literature have been carried out with the aim of making a comparative study of the performance of encryption algorithms. Their work generally consists of making a comparative study between the encryption algorithms in order to know which one is more efficient and with which metric(s). Their studies have shown that AES and RSA are the most efficient, RSA consumes more resources but is more secure than others, including AES, and AES consumes fewer resources, which is why all encryption tools use AES (see Table 2). Our performance analysis focuses on AES by comparing the performance of encryption and decryption regarding execution time, memory used, and throughput.

The machine used for the simulation described in this paper is a Core i7 CPU @ 2.70 GHz, 8 GB RAM, Processor x64, Windows 10. The solution we propose is developed in Java Fx, so the encryption and decryption performance analysis is simulated with JDK (jdk1.8.0_172) with NetBeans IDE 8.2. To evaluate the performance, we generated files with sizes ranging from 1024 to 102400 KB, and each time a file is encrypted or decrypted we collect the data (execution time and memory usage) that we save in an excel file that allowed us to draw charts.

Figure 8 shows the comparison between the encryption and decryption execution time relative to the files' size. We can see that the encryption and decryption times have the same trends, the times are almost the same for sizes between 1 and 59 MB, and that the decryption time is higher than the encryption time for files larger than 60 MB. We also noticed that as the files' size increases, the encryption time increases slowly while the decryption time increases rapidly.

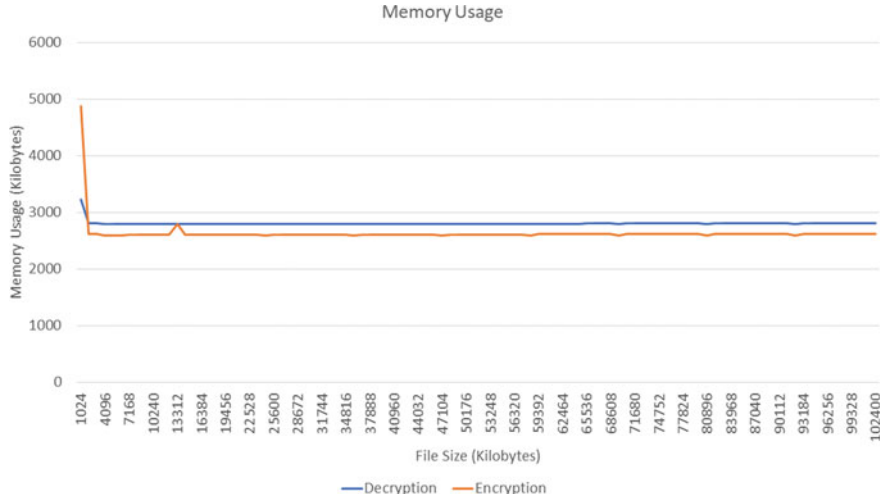
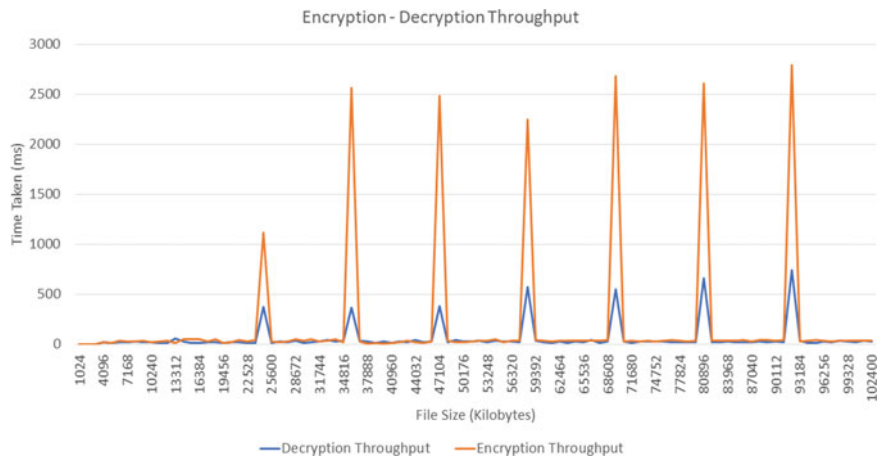
**Fig. 9** Memory usage**Fig. 10** Throughput

Figure 9 shows the memory used for encryption and decryption; we can see that the size used is more or less stable and that the memory used for decryption is slightly higher than the memory used for encryption. A little surprising thing that we can observe on Figs. 8 and 9 is the high peaks at the beginning; for 1024 KB, we notice an encryption time of 9817 ms and 4876 KB of memory usage, and 7435 ms (execution time) and 3220 Kb (memory usage) for decryption. You may be surprised by this result. But it makes sense, because of the “javax.crypto.Cipher” class needs a little “warm-up” when it is first used in the program.

The throughput results of the encryption and decryption are shown in Fig. 10, and these results show that the decryption process has the lowest throughput, while the encryption process has the highest throughput.

8 Conclusion

In this paper, we proposed an architecture primarily based on encryption to secure data during its transmission over the network and its storage in the cloud. Thus, we have introduced a third party, which is an application that acts as an intermediary between the user and his cloud by providing an additional security layer. This application has been designed to be implemented at the customers' level to give them the possibility to ensure the security of their files in the cloud. Several tools are available for encrypting files before sending them to the cloud. However, they do not allow users to know whether their files are corrupted, or not. Encrypt cloud, which we are proposing, brings a new functionality, offering users the possibility to check their files' integrity, by proposing a double-checking approach of file, and database integrity. Another feature our solution provides is encrypted file sharing, allowing users to collaborate on files without compromising the security of other files. Users can also encrypt their sensitive data (files) to ensure that no unauthorized person can exploit it, even in a data leak. To encrypt the data, we have used AES 256, which is a symmetrical encryption algorithm because we will have to encrypt files of varying sizes ranging from MB to GB.

To evaluate our system's performance, we performed a performance analysis based on execution time, memory usage, and throughput of encryption–decryption using files ranging in size from 1024 to 102,400 KB. This analysis showed that the execution time of encryption and decryption is almost the same for files smaller than 60 MB. The execution time of decryption is higher than the execution time of encryption for files larger than 60 MB. The performance study also showed that memory usage is more or less stable for both processes (between 2595 and 2794 KB), and that the encryption throughput is high compared to the decryption throughput. It should be noted that decryption consumes more resources than encryption in the case of AES.

Currently, all information, especially encryption and decryption keys and signatures, are stored in a database, whether local or replicated is a single point of failure, making the solution vulnerable. In our future work, we will work on the architecture of the solution to decentralize the information.

References

1. Kaur S, Kaur A (2015) Survey of security algorithms in cloud
2. Eurostat. https://ec.europa.eu/eurostat/statistics-explained/index.php?title=Archive:Cloud_computing_-_statistics_on_the_use_by_enterprises_-_2016_data
3. Magdalena K, Maria S (2018) Cloud computing—statistics on the use by enterprises. Dec 2018. https://ec.europa.eu/eurostat/statistics-explained/index.php?title=Cloud_computing_-_statistics_on_the_use_by_enterprises#Use_of_cloud_computing:_highlights
4. UnfoldLabs (2017) 8 trends in cloud computing for 2018, Nov 2017. <https://medium.com/@UnfoldLabs/8-trends-in-cloud-computing-for-2018-d893be2d8989>
5. Pfarr F, Buckel T, Winkelmann A (2014) Cloud computing data protection—a literature review and analysis. In: 2014 47th Hawaii international conference on system sciences. IEEE, pp 5018–5027
6. Ni J, Lin X, Zhang K, Yu Y, Shen XS (2016) Secure outsourced data transfer with integrity verification in cloud storage. In: 2016 IEEE/CIC international conference on communications in China (ICCC). IEEE, pp 1–6
7. Han S, Xing J (2011) Ensuring data storage security through a novel third party auditor scheme in cloud computing. In: 2011 IEEE international conference on cloud computing and intelligence systems. IEEE, pp 264–268
8. Zakaria I, Mustapha H, Igarramen B (2019) A data confidentiality system based on trusted platform module in cloud storage environment. *J Theoret Appl Inf Technol*
9. Sugumar R, Arul Marie Joyce K (2017) Ensure and secure data confidentiality in cloud computing environment using data obfuscation technique. *Int J Adv Stud Comput Sci Eng* 16–21
10. Mahmood GS, Huang DJ, Jaleel BA (2019) Achieving an effective, confidentiality and integrity of data in cloud computing. *IJ Netw Secur* 326–332
11. Manikandasaran SS, Arockiam L, Sheba Kezia Malarchelvi PD (2019) MONcrypt: a technique to ensure the confidentiality of outsourced data in cloud storage. *Int J Inf Comput Secur* 11(1):1–16
12. Abolghasemi MS, Sefidab MM, Atani RE (2013) Using location-based encryption to improve the security of data access in cloud computing. In: International conference on advances in computing, communications and informatics (ICACCI). IEEE, pp 261–265
13. Sood SK (2012) A combined approach to ensure data security in cloud computing. *J Netw Comput Appl* 35(6):1831–1838
14. Pitchai R, Babu S, Supraja P et al (2019) Prediction of availability and integrity of cloud data using soft computing technique. *Soft Comput* 23:8555–8562. <https://doi.org/10.1007/s00500-019-04008-0>
15. Wei PC et al (2020) Blockchain data-based cloud data integrity protection mechanism. *Future Gen Comput Syst* 102:902–911
16. Li A, Tan S, Jia Y (2019) A method for achieving provable data integrity in cloud computing. *J Supercomput* 75(1):92–108
17. Lemma A, Tolentino M, Mehari G (2015) Performance analysis on the implementation of data encryption algorithms used in network security. *Int J Comput Inf Technol* 04(04):711–717

Social Media Analytics: Current Trends and Future Prospects



Sonam Srivastava, Mahesh Kumar Singh, and Yogendra Narain Singh

Abstract Social media analytics (SMA) has recently emerged as a dominant research field due to the usage of social media platforms, globally. The SMA usually involves the primary steps of data acquisition, preprocessing and analysis. Due to voluminous, heterogeneous, imprecise and noisy data, challenges at each step are inevitable. The need for unparalleled storage, computing power and efficiency have rendered traditional data modeling methods inapplicable. There is substantial literature available on the challenges and issues related to particular analysis approaches. However, there hardly exists any study on the steps of social media analytics. To enlighten this gap, this paper presents the current trends and proposes a novel framework for SMA. This framework provides a roadmap to the five stages of SMA, i.e., data acquisition, preprocessing, data representation, analysis and presentation along with its challenges at each stage. The potential of the state-of-the-art machine learning techniques such as deep learning and transfer learning for addressing issues of SMA are described. Further, the article puts emphasis on the future prospects of SMA in terms of knowledge discovery, recommendation and trust in social media.

Keywords Social media · Big data · Social media analytics

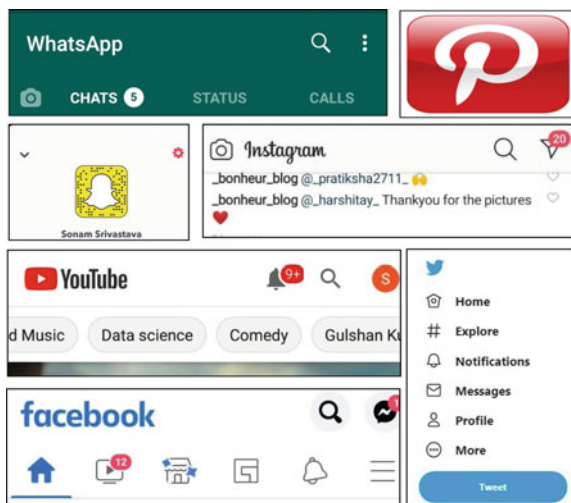
1 Introduction

Dominant trends of the present time to reshape the world is the global connectivity through Internet. Nowadays, one of the most common practices online is the use of social media. Social networking includes blogs, microblogs, business networks, forums, social gaming, photograph sharing sites and chat apps. The social networks have emerged as the core of the World Wide Web and their penetration rate reached 49% in 2020, globally [1]. The number of people using social media worldwide is growing and expected to rise 4.41 billion by 2025 from present 3.6 billion [2].

S. Srivastava (✉) · M. K. Singh · Y. N. Singh

Institute of Engineering and Technology, Dr. APJ Abdul Kalam Technical University, Lucknow, Uttar Pradesh 226021, India

Fig. 1 Social media platforms



Social media is an Internet-based technology that facilitates the exchange of thoughts, ideas and knowledge through creating virtual networks and communities. The dissemination of information takes place through various social media platforms, i.e., Facebook, YouTube, WhatsApp, Instagram, etc. Information floats through these social media platforms in the form of text, images, audio, video, etc., are shown in Fig. 1. As of July, 2020, the Facebook and YouTube are the most popularly used social networks, ranked by the number of active users [3]. This results in the generation of huge amount of social media data. It is characterized by high volume, high velocity, variety, veracity and value [4]. The rise of these sites has rendered distinct applications of social media, i.e., businesses, health care, academics, etc., with new source of insights to base their social and strategic plans.

Social media analytics (SMA) is the technique used to devise intelligence strategies from voluminous data of application specific domain. It facilitates informed decision making and useful insights to address the specific challenges of distinctive applications [5]. It is an interdisciplinary area of research that attempts to integrate, broaden and adapt social media data analytics methods. Although social media big data has substantial benefits, numerous challenges are associated with it. These issues must be addressed to completely realize the capabilities of social media data. The acquisition of social media data across distinct platforms along with the constantly evolving nature of the designs and concepts of social media platforms is a bigger challenge. The social media data is semi-structured and unstructured that causes heterogeneous information overload. It poses challenges for massive computational resources that are needed for advanced sampling, extraction and analysis. To derive useful insights from such vast and complex data raises critical knowledge discovery challenges, we need efficient analysis strategies that utilize voluminous datasets and articulate in a structured form. In order to manage social media big data, the novel strategies to be devised that have maximum impact and business value. In the

present era of digitization, preserving the privacy and maintaining security of users using automated means are other issues of social media analytics [6]. The scarcity of efficient analytical strategies to interpret, analyze and make sound predictions along with data privacy gathered from diverse sources and locations are the future challenges.

The objective of this paper is to present the prospective scenarios of social media analytics (SMA). In particular, the current strategies of SMA are evaluated critically and a novel framework for SMA is presented. The proposed framework is derived from [4, 7] with different aims of data preprocessing, data representation and data analysis highlighting social media analytics challenges. Most of the current SMA strategies available in the literature can be categorized as descriptive, diagnostic, predictive and prescriptive [8]. We evaluate descriptive analytics that deals with understanding and describing situations using historical and present data to gain insights for future challenges. An inspection to locate and find the root cause of events and their behaviors is done for diagnostic analytics. The prediction of the possibilities for a particular event to occur is evaluated for predictive analytics. Finally, the evaluation of techniques to construct composite alternatives that prescribe the most appropriate solution from the existing dataset for prescriptive analytics. Further, the future prospects of SMA are given. Specially, the role of the state-of-the-art machine learning techniques such as deep learning and transfer learning to address the problem of heterogeneity, noise, uncertainty and multimodality are described.

Rest of the paper is organized as follows. The literature review of SMA is given in Sect. 2. The current trends of SMA along with its challenges are presented in Sect. 3. The proposed framework of social media analytics is described in Sect. 4 and the future directions of research with respect to social media analytics are highlighted in Sect. 5. Finally, the conclusion is drawn in Sect. 6.

2 Literature Review

Social media analytics refers techniques of collecting and analyzing data from social media to address specific issues. It aims to analyze social media data to extract novel ideas from customers and strengthen customer relationships. Recently, enterprises have shown growing interest in social media analytics. Lee has presented a four-stage analytics process model [9]. This model shows different stages to facilitate social media analytics management.

The social media big data can upgrade decision making and organizational performance when an appropriate selection of analytical method is done to derive value from data [10]. In this context, different researchers have discussed various analytics methods. Rehman et al. have performed big data analytics using descriptive analysis that extracts features from unstructured data [11]. Diagnostic analytics is employed to find the reasons behind the occurrence of any event [12]. Predictive analytics leverages past and transactional data patterns to detect risks and market opportunities. It is based on supervised and unsupervised learning methods [13]. Prescriptive analyt-

ics determine the cause-effect relationship between analytical outcomes and policies for optimizing business processes [10, 12]. Volume is often the only dimension that spans the major aspects of big data. Gandomi et al. have presented a consolidated description of social media analytics [14]. They have reviewed analytics approaches for text, video and audio and obtain valuable insights from big data.

Social media are constantly being used in political context. The need to continuously collect, observe, interpret, summarize and visualize social media data that is politically relevant. Stiglitz et al. have proposed a methodological framework for social media analytics in the political context [15]. Their framework sums up politically relevant issues from the viewpoint of political institutions. In an another research, Stiglitz et al. have highlighted four stages of social media analytics, i.e., data discovery, collection, preparation and analysis [4]. They have discussed various challenges that might be encountered during the analytics process and suggest possible solution to them.

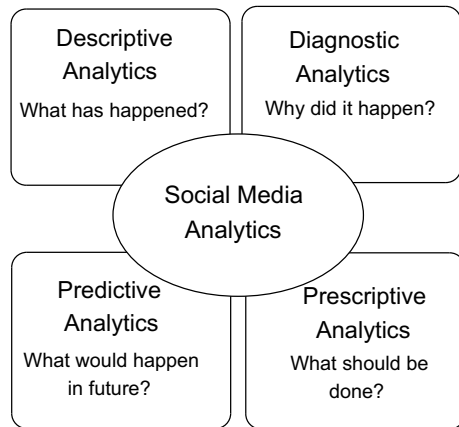
Within the phenomenon of social spread, the emergence of opinions is a large category that is encouraged by the diffusion of information. Information transmission is often a word-of-mouth phenomenon, and online social media platforms have recently facilitated [16]. Social networking sites such as Facebook or microblogging sites such as Twitter have become so prominent nowadays that more and more users are joining these sites. Twitter is utilized to evaluate users' opinion to boost services and quality of products. In this context, Munjal et al. have presented a visualization framework that detects opinions from tweets using the method of lexical analysis [17]. The existing opinion exchange models for characterizing the real-world social networks possess limited potential. Therefore, in their other works, Munjal et al. have developed the Ostwald ripening social network model [18]. This model could be used to explain the growth of particles at nanoscale and help in the observation, prediction and control of complex processes in social networks.

3 Social Media Analytics: Current Trends

Traditionally, enterprises have obtained the information from consumers and other focus groups that post publically on social media platforms. The conventional analytics techniques with less computational capabilities have to analyze free text, i.e., unstructured data. With the advent of artificial intelligence and machine learning techniques, organizations easily quantify social media posts in a scalable way. It helps businesses to extract data on how the audience perceives their brand, what sort of goods people want and dislike, etc. Social media analytics makes it possible to measure, compute and analyze business needs using data of focus groups. In this context, social media analytics refers to the techniques used to analyze and grab intelligence from social media big data.

Most techniques of social media analytics presented in the past can be broadly categorized in four different classes [8]. These classes of techniques seek answer to different questions and provide different prospects of SMA as shown in Fig. 2.

Fig. 2 Current trends of social media analytics



Descriptive analytics is one of the basic forms of analytics adopted by most of the organizations presently. It deals with understanding and describing situations on the basis of historical and current data. The most elementary way of specifying descriptive analytics is to make use of business intelligence to answer the questions like, “what has happened?” or “what is happening?”. For example, Netflix uses data mining to recognize correlation between different events [8].

Diagnostic analytics refers to mining, correlation and data discovery using techniques. It enables easy and speedy understanding of data to answer questions like, “why did it happen?”. Diagnostic analytics inspects the performance of posts and campaigns to discern their success. The predictive analytics is used to predict any possibility for a particular event to occur [14]. It is undertaken by businesses to closely observe the data and find out the answer to the questions like, “why will it happen?” or “what would happen in future?”. Sentiment analytics is the most usual type of predictive analytics. Organizations use it to recognize sales trends and forecast inventory levels.

The prescriptive analytics utilizes mathematical models and advanced technologies like artificial intelligence/machine learning, natural language processing to construct a set of composite alternatives from the existing dataset. This set is then considered to prescribe the most appropriate solution. It adopts the optimization and simulation to cross examine “what should be done?”. The effect of predictive analytics is based on the adequacy of the decision model in apprehending the repercussions of decision being analyzed [12]. It also handles uncertainty and prescribes strategies to alleviate the risks that arise from it. Both predictive and prescriptive analytics are proactive in nature, and they forecast patterns, events based on existing data.

4 Social Media Analytics: Proposed Framework

We propose a framework of social media analytics that overcome various issues of social media big data. It is motivated from [4] and designed with different aims of data preprocessing, data representation and data analysis highlighting social media analytics challenges. More formally, the proposed SMA framework consists of the following stages, i.e., data acquisition, preprocessing, data representation, analysis and presentation as shown in Fig. 3. The data acquisition stage involves collecting data from different social media sources using tracking methods, e.g., application programming interface (API) offered by the corresponding source. All data gathered from different sources of social media may not be useful, i.e., data consists of elements of both structured as well as unstructured type. The unstructured social media data is noisy and inconsistent. Thus, following the data acquisition stage, the data needs to be preprocessed for quality check and further analysis. Hence, filtering of noisy data, removal of spam, stop words, stemming and lemmatization is done.

The preprocessed data is represented in various categories, i.e., trend related, opinion related and based on structural attributes. In order to present the useful data in an understandable form, the analysis is done using an appropriate data representation category, e.g., content analysis, trend analysis, sentiment analysis, statistical analysis and social network analysis. Content analysis is used to identify issues and to draw valid inferences from unstructured contents present in text and multimedia [19]. Trend analysis identifies and predicts future results and behavior based on his-

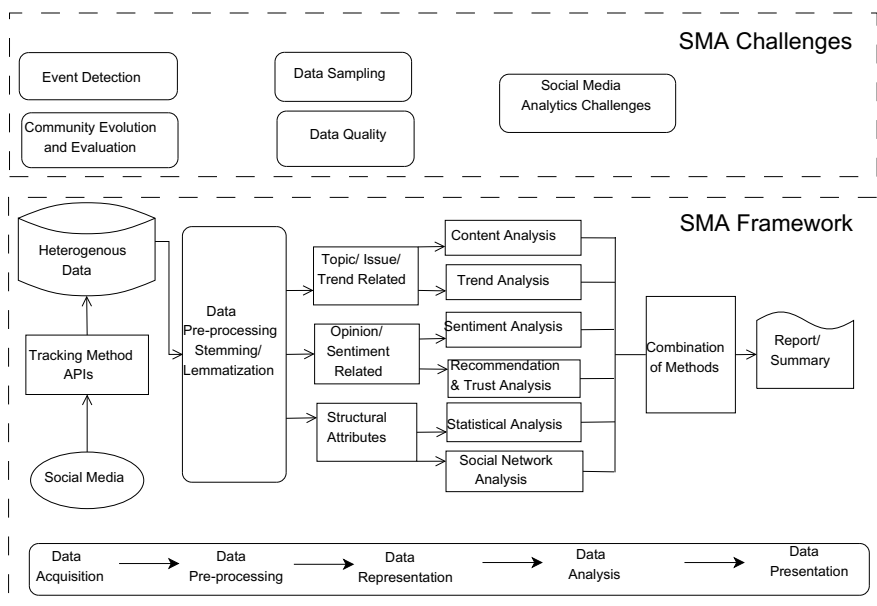


Fig. 3 Proposed framework of social media analytics (motivated from [4])

torical data gathered over time [20]. Sentiment analysis studies the subjective details in an expression, that is, the views, assessments, feelings or attitudes toward a subject, individual or entity [21]. Statistical analysis is the methodology of extracting statistics from stored data and interpreting the results to deduce significance from the underlying dataset [22]. Social networks analysis is the method of analyzing social systems by using networks and graph theory [23]. Finally, evaluated results are presented to handle the issues related to public safety and peace.

Let us describe the SMA framework in more detail. The stage of data collection involves gathering of data from distinct social media sources as described in Sect. 2.1. The stage of data acquisition includes data tracking and monitoring. There exist various means of data collection, however, primarily it can be done with an API offered by respective application [24]. The API exposes the end points of URL which the developers can utilize for retrieving data from an application. The registered and authenticated developers can freely access the API for applications such as Facebook, Twitter and Instagram.

The gathered social media data provides an insight into daily habits of users and about those who comment on their posts. Data collected from different sources of social media is heterogeneous in nature. The elements of this data are both structured as well as unstructured. The structured data comprises of temporal and spatial data, user profile demographics, likes, retweets, mentions and comments. Unstructured data takes the form of all user-generated textual content. Such data is converted into essential formats and consumed into databases.

The task of preprocessing is to make textual data qualitative for further analysis. It involves elimination of words those have grammatical significance, i.e., stop words. In addition, other tasks performed are stemming that involves reducing derived words or inflected words to their word stem along with lemmatization which combines together various inflected word forms so that they can be analyzed as a single entity. Overall, this step prepares the textual data for the extraction of essential information.

Data is represented in various categories like trend, opinion and structural attributes [25]. Recent advancements in have led to the development of numerous algorithms for predicting emerging trends [26]. Content analysis and text mining techniques are adopted for identifying topics and predicting trends [27]. People express their emotions, views and opinions over different social media platforms. Opinions are essential for decision making in almost every application domain of social media [28]. Thus, the sentiment analysis has emerged as the notable method for thorough analysis of people's attitudes, sentiments, views and their emotions.

The spread of social media has provided numerous platforms to let people express their opinions, emotions or views. Assessing people's opinions, attitude, sentiments, evaluations and judgment toward intangible or tangible entities and events is referred to as sentiment analysis [21]. Facebook, Twitter and Instagram are very enticing sources for sentiment analysis because of the data availability in huge volume, velocity and variety. Thus, an automated summarization systems and opinion discovery can be achieved by sentiment analysis.

There exist various descriptive and deductive approaches of content classification including supervised and unsupervised learning [29, 30].

Social network is a social structure of the people, communities, organizations and states of common interests linked together. In the context of social media analytics, social network analysis is the key technique in identifying influential users, i.e., opinion leaders or applicable user communities in social media. However, social network analytics still confronts several challenges in finding changing clusters in such large-scale environment and with dynamic data. Thus, it demands for the novel approaches mainly when decision is to be sought in real time. The content analysis is used to identify topics for forming valid inferences from massive unstructured content like text, multimedia and images [31, 32]. Enormous growth of social media data necessitates the adoption of automated quantitative content analysis methods. These methods are capable of providing answers to a wide variety of research questions, classification of text and identification of the recurring topics [31].

Finally, trend analysis identifies and predicts future results and behavior based on historical data gathered over time. Recent advances in the field of computer science and statistics have devised many techniques to predict emerging issues [33]. Most trend analysis algorithms use hidden Markov models to train subject observations which are in turn stored for topic prediction [34]. Trend analysis can also be done using statistical methods, i.e., regression analysis, time-series analysis and other modern modeling techniques such as support vector machines [35] and neural networks [36].

Data presentation is the final stage of our proposed social media analytics framework. The summarized and evaluated results from different analytics presented to users in understandable format to handle the issues related to public safety. Distinct visualization techniques assist in portraying information to the users.

5 Social Media Analytics: Future Prospects

The potential directions to address the issues of social media analytics using the state-of-the-art machine learning techniques are deep learning and transfer learning. Social media has become an integral part of people connected online across the globe. The challenges associated with globally rising statistics of social media usage include cyber-bullying, distribution of fake evidences and the coordination of militant organizations. Individuals, usually adolescents, harass others in the digital spaces particularly on social networking platforms. It is often difficult to distinguish truth from fiction because of the rapidity of the distribution of knowledge. This results in the spread of massive digital misinformation as one of the major threats for the modern society.

Deep learning is the characteristic learning that derives data representations using a hierarchical mechanism using convolution neural network (DenseNet [37]) as shown in Fig. 4. Deep learning has a versatile architecture that tackles data heterogeneity and other data veracity related challenges, i.e., noisy and uncertainty. The problem associated with nonlinearity of data is addressed by its multiples layers using nonlinear transformations. Deep learning frameworks are proved and well

suited to solve complex problems with larger datasets [38]. The social media is a source of online community networking that relies predominantly on user-generated contents. Deep learning provides methods to evaluate the user's behavior, trends, learning associations between their previous and present characteristics. The areas where deep learning require further investigations for SMA include unstructured data of higher dimension, mining from streaming data, model security, scalability and users' privacy.

Social media platforms span a range of social relationships that need trustworthy recommendations. In recommendation systems, trust metrics have a major role to play. Deng et al. made a deep learning-based attempt to recommend trust-aware relationships to social media users [39]. Social media users use variety of natural languages to post their opinions and reviews. For example, English, Hindi, Chinese, Arabic, Spanish, etc. In order to address these text-related challenges, efforts are made to explore sentiments from languages using recursive deep learning [40]. The challenges of deep learning methods, i.e., heterogeneity, scalability and multimodality can be resolved by network diffusion-based embedding [41].

Alike, humans transfer their experiences from one domain to another, transfer learning adapts knowledge acquired in one domain to a new domain. Transfer learning is a technique to enhance learning by training the learning model with other datasets from multiple sources. Transfer learning possesses the potential to address the challenges related to big data [42]. It addresses heterogeneity because of ability to learn from one domain and then transfer knowledge between datasets of the target domain [43]. Yang et al. proposed an automatic transfer learning algorithm for handling big data [42]. It analyzes small text data using knowledge from lengthy text available online. Likewise, ensemble learning integrates multiple learning models as shown in Fig. 4. This learning model may be adopted to handle heterogeneity and suitable when we have insufficient knowledge about users of different platforms and

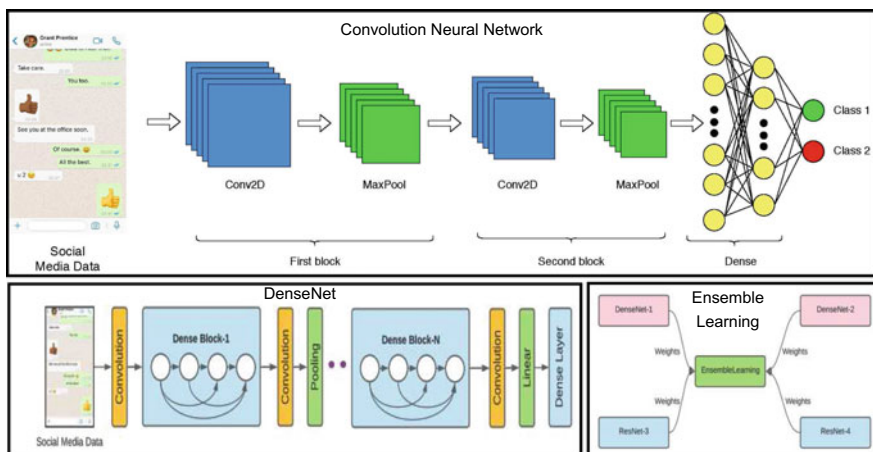


Fig. 4 Prospects of deep learning for social media analytics

wish to learn their behavior from existing and other familiar platforms. The potential of ensemble learning may be evaluated to study and understanding of trust in social media and identify users with specific roles.

6 Conclusion

Recently, social media analytics has gained widespread recognition. It assembles the data from distinctive social media platforms and examines it for better decision making. This paper has critically evaluated the current trends of SMA, i.e., descriptive, diagnostic, predictive and prescriptive analytics of SMA. The study lets the organizations know what strategy is to be implemented to optimize their roles. It is observed that social media data is continuously updating and expanding. Thus, a novel framework of SMA is proposed in this paper. This framework has provided a roadmap to data collection, preprocessing, representing, analyzing and presenting along with social media analytics challenges.

Further, the paper has addressed heterogeneity, uncertainty, impreciseness, noise, etc., as the significant hurdles in the analytics process. Therefore, the potential of the state-of-the-art machine learning techniques such as deep learning and transfer learning act as the ultimate savior in the context of social media analytics. Finally, the article has emphasized on knowledge discovery, recommendation and trust in social media as the future prospects of social media analytics.

References

1. Social media—statistics & facts. <https://www.statista.com/topics/1164/social-networks/>. Last accessed 18 Oct 2020
2. Number of social network users worldwide from 2017 to 2025. <https://www.statista.com/statistics/278414/number-of-worldwide-socialnetwork-users/>. Last accessed 18 Oct 2020
3. Most popular social networks worldwide as of July 2020, ranked by number of active users. <https://www.statista.com/statistics/272014/global-social-networks-ranked-by-number-of-users/>. Last accessed 19 Oct 2020
4. Stiglitz S, Mirbabaie M, Ross B, Neubeger C (2018) Social media analytics—challenges in topic discovery, data collection, and data preparation. *Int J Inf Manage* 39:156–168
5. Srivastava, S, Singh YN (2020) Big social media analytics: Applications and Challenges. In: 3rd international conference on computer networks, big data and IoT to be held on 15–16 Dec, 2020, India. to appear in Lecture Notes on DECT, Springer. TBA
6. Singh YN, Singh SK (2013) A taxonomy of biometric system vulnerabilities and defences. *Int J Biometr* 5(2):137–159
7. Stiglitz S, Xuan LD, Bruns A, Neubeger C (2014) Social media analytics: an interdisciplinary approach and its implications for information systems. *Bus Inf Syst Eng* 6:89–96
8. Ghani NA, Hamid S, Hashem IAT, Ahmed E (2019) Social media big data analytics: a survey. *Comput Hum Behav* 101:417–428
9. Lee I (2018) Social media analytics for enterprises: typology, methods, and processes. *Bus Horiz* 61(2):199–210

10. Joseph RC, Johnson NA (2013) Big data and transformational government. *IT Prof* 15(6):43–48
11. Rehman MH, Chang V, Batool A, Teh YW (2016) Big data reduction framework for value creation in sustainable enterprises. *Int J Inf Manage* 36(6):917–928
12. Bihani P, Patil ST (2014) A comparative study of data analysis techniques. *Int J Emerg Trends Technol Comput Sci (IJETTCS)* 3(2):95–101
13. Waller MA, Fawcett SE (2013) Data science, predictive analytics, and big data: a revolution that will transform supply chain design and management. *J Bus Logist* 34(2):77–84
14. Gandomi A, Haider M (2015) Beyond the hype: big data concepts, methods and analytics. *Int J Inf Manage* 35:137–144
15. Stiglitz S, Xuan LD (2012) Social media and political communication: a social media analytics framework. *Soc Netw Anal Min* 3:1277–1291
16. Munjal P, Kumar S, Kumar L, Banati A (2017) Opinion dynamics through natural phenomenon of grain growth and population migration. In: Banati H, Bhattacharyya S, Mani A, Koppen M (eds) *Hybrid intelligence for social networks*. Springer, Cham, pp 161–175
17. Munjal P, Narula M, Kumar S, Banati H (2018) Twitter sentiments based suggestive framework to predict trends. *J Stat Manag Syst* 21(4):685–693
18. Munjal P, Kumar L, Kumar S, Banati H (2019) Evidence of Ostwald ripening in opinion driven dynamics of mutually competitive social networks. *Phys A* 522:182–194
19. Reddick CG, Chatfield AT, Ojo A (2017) A social media text analytics framework for double-loop learning for citizen-centric public services: a case study of a local government Facebook use. *Gov Inf Q* 34:110–125
20. Monitoring and analyzing social media trends: the best practices. <https://blog.digimind.com/en/trends/monitoring-and-analyzing-social-media-trends-the-best-practices>. Accessed 5 Dec 2017
21. Pang B, Lee L (2008) Opinion mining and sentiment analysis. *Found Trends Inf Retr* 2:1–135
22. Slavakis K, Giannakis GB, Mateos G (2014) Modeling and optimization for big data analytics: (statistical) learning tools for our era of data deluge. *IEEE Sig Process Mag* 31:18–31
23. Chang V (2018) A proposed social network analysis platform for big data analytics. *Technol Forecast Soc Chang* 130:57–68
24. Kennedy H, Moss G (2015) Known or knowing publics? Social media data mining and the question of public agency. *Big Data Soc* 2:1–11
25. Sivarajah U, Kamal MM, Irani Z, Weerakkody V (2017) Critical analysis of big data challenges and analytical methods. *J Bus Res* 70:263–286
26. Marquez JLJ, Carrasco IG, Cuadrado JLL, Mezcua BR (2019) Towards a big data framework for analyzing social media content. *Int J Inf Manage* 44:1–12
27. Hassani H, Beneki C, Unger S, Mazinani MT, Yeganegi MR (2020) Text mining in big data analytics. *Big Data Cognit Comput* 4:1–34
28. Pavaloaia VD, Teodor EM, Fotache D, Danileț M (2019) Opinion mining on social media data: sentiment analysis of user preferences. *Sustainability* 11:1–21
29. Liu W, Luo X, Xuan J, Xu Z, Jiang D (2016) Cognitive memory inspired sentence ordering model. *Knowl Based Syst* 104(C):1–13
30. Doerfel ML, Barnett GA (1996) The use of CATPAC for text analysis. *Sage* 8:4–7
31. Krippendorff K (2004) Content analysis: an introduction to its methodology. Sage Publications London
32. Aggarwal CC, Wang H (2011) Text mining in social networks. In: Aggarwal CC (ed) *Social network data analytics*. Springer, Boston, pp 353–378
33. Boutaba R, Salahuddin MA, Limam N, Ayoubi S, Shahriar N, Solano FE, Caicedo OM (2018) A comprehensive survey on machine learning for networking: evolution, applications and research opportunities. *J Internet Serv Appl* 9:1–99
34. Rabiner LR (1989) A tutorial on hidden Markov models and selected applications in speech recognition. *Proc IEEE* 77(2):257–286
35. Kannan N, Sivasubramanian S, Kaliappan M, Vimal S, Suresh A (2018) Predictive big data analytic on demonetization data using support vector machine. *Clust Comput* 22:1–12

36. Sigo MO, Selvam M, Maniam B, Kannaiah D, Kathiravan C, Vadivel T (2018) Big data analytics-Application of artificial neural network in forecasting stock price trends in India. *Acad Account Finan Stud J* 22
37. Huang G, Liu Z, Maaten LVD, Weinberger KQ (2017) Densely connected convolutional networks. In: Proceedings of the IEEE conference on computer vision and pattern recognition (CVPR), 4700–4708
38. Hayat MK, Daud A, Alshdadi AA, Banjar A, Abbasi RA, Bao Y, Dawood H (2019) Towards deep learning prospects: insights for social media analytics. *IEEE Access* 7:36958–36979
39. Deng S, Huang L, Xu G, Wu X, Wu Z (2017) On deep learning for trustware recommendations in social networks. *IEEE Trans Neural Netw Learn Syst* 28(5):1164–1177
40. Li C, Xu B, Wu G, He S, Tian G, Hao H (2014) Recursive deep learning for sentiment analysis over social data. In: IEEE/WIC/ACM international joint conferences on web intelligence (WI) and intelligent agent technologies (IAT) 2, 180–185
41. Shi Y, Lei M, Yang H, Niu L (2019) Diffusion network embedding. *Pattern Recogn* 88:518–531
42. Yang L, Chu Y, Zhang J, Xia L, Wang Z, Tan KL (2015) Transfer learning over big data. In: International conference on digital information management (ICDIM'15) 63–68
43. Torrey L, Shavlik J (2010) Handbook of research on machine learning applications and trends. IGI Global

A Study on Application of Interplanetary File System



Ankur Biswas, Riya Sil, and Abhishek Roy

Abstract With the advancement of information and communication technology (ICT), people are exchanging sensitive information through open communication channel like Internet. This tendency of digital communication has increased exponentially during the days of global pandemic where people are forced to maintain social isolation to break the chain of coronavirus (COVID-19) transmission within the society. Moreover, renowned corporate entities have implemented Work From Home for employees to continue their regular functioning. As a result, adversaries have found ample scope to mount active and passive attacks over these huge digital traffic to compromise the integrity of an electronic mechanism and fulfill their ill intention. In this situation, it becomes pertinent to ensure information security by establishing privacy, integrity, non-repudiation and authentication (PIN) of electronic transaction. To fulfill this objective, in this paper, authors have implemented secured electronic file management using Interplanetary File System (IPFS) over banking and legal datasets.

Keywords Information security · Blockchain · IPFS

1 Introduction

With the advancement of information and communication technology (ICT)-based applications, people are exchanging sensitive information related to banking, legal, health care, education, business administration, etc., through open communication channel like Internet. This tendency of digital communication has increased exponentially during the days of global pandemic where people are forced to maintain social isolation to break the chain of corona virus (COVID-19) transmission within

Ankur Biswas: International Association of Engineers (Number: 257255), Hong Kong.
Cryptology Research Society of India (Number: L0949), ISI Kolkata 700108, India.
IEEE (Number: 95002369) R10-Asia and Pacific.

A. Biswas (✉) · R. Sil · A. Roy

Department of Computer Science and Engineering, Adamas University, Kolkata, India
URL: <http://adamasuniversity.ac.in/>

the society. This situation has compelled us to practice electronic mode of operations like electronic education, electronic medical consultancy, electronic business, etc. Moreover, renowned corporate entities have implemented Work From Home for employees to continue their regular functioning and keep economy rolling, which is badly affected due to long haul lockdown. Due to this chaotic situation, adversaries have found ample scope to mount active and passive attacks over these huge digital traffic to compromise the integrity of an electronic mechanism and fulfill their ill intention. For instance, the recent data leak of hi profile Twitter [1] account may be cited as an example of similar threat [2]. In this situation, it becomes pertinent to regain trust of end user and ensure information security by establishing privacy, integrity, non-repudiation and authentication (PIN) of electronic transaction. To fulfill this objective, in this paper, authors have implemented secured electronic file management using Interplanetary File System (IPFS) over banking and legal datasets.

The risk factors of electronic file system are studied in Sect. 2. The basic concepts of Interplanetary File System (IPFS) are discussed in Sect. 3. The proposed electronic file management using Interplanetary File System (IPFS) over legal and banking dataset is explained in Sect. 4. Conclusion is finally drawn in Sect. 5.

2 Risk Factors of Electronic File Management

Data security and privacy issues are the key concerns of electronic file management. To gain trust of users, the integrity of any electronic communication should be maintained at its highest level. For a better understanding of any electronic file management, its user-centric risk factors [3] should be studied thoroughly.

1. User training is of low quality—most IT project-based software firms perform training sessions for its users, during which developer prepares user manual assuming that they can accomplish their operation with this new software system. Document management is usually crowded and complicated as large number of users access software system to obtain their desired information. To make users confident about the software system [4], its training should be conducted with highest level of professional efficiency, else it will adversely affect the user.
2. Traditional circulation of document in public sector—public sector [5] may be considered as the most conventional organizational structure. Since inception, officials have been working with hard copy [6] (i.e., paper) documents, and hence searching of any document from a huge pile of papers becomes a hectic task. However, for any Naive user, working with hard copy (i.e., paper) is more convenient compared to electronic document due to lack of proper training.
3. Fragile legislation environment—the action of workers in public sectors is controlled by many legislative documents at central and individual institution level [7]. Few of the regulation of document management system includes record-keeping and safety policy rules, regulation for document circulation, job responsibilities, etc. These regulations are followed systematically by officials who are

usually unwilling to accept any alternative approach (i.e., electronic documents). Absence of basic legislative rules at the public and private sectors can have negative impact over electronic document management.

To ensure the integrity of any electronic transaction and gain trust of end user, advanced technology like Interplanetary File System (IPFS) [8–12] may be applied, which is discussed below.

3 Fundamentals of Interplanetary File System (IPFS)

Interplanetary File System (IPFS) [8, 13] is a peer-to-peer (P2P) [14] file sharing system that helps in changing the process of information distribution across the globe. Interplanetary File System (IPFS) consists of distributed systems and communication protocols that are combined to produce file system. Communication protocols are known as set of rules defined for electronic transaction between its connected users. It consists of several layers where each layer is responsible for specific function. Client-server model and HTTP Web-based model are enhanced further to Interplanetary File System (IPFS) over P2P file sharing system which is actually a combination of numerous novel and existing approaches. Its main component is discussed below:

Distributed Hash Table (DHT): Hash table mainly stores information as a pair of keys. In distributed hash table (DHT) [15], data is proficiently coordinated and spread over network of computers to allow access and search among the nodes. The advantages of distributed hash function (DHF) include scalability, decentralization and fault tolerance. The system is able to function reliably even after node failure as central coordination is not required. It is also important to state that distributed hash table (DHT) can accommodate abundant number of nodes.

This electronic file security system may be applied over multivariate electronic mechanisms like banking, legal, education, health care, etc., which are discussed below.

4 Applications of Interplanetary File System (IPFS)

In this paper, authors have proposed a distributed hypermedia protocol [16], namely Interplanetary File System (IPFS) [17, 18]-based electronic file management. It is a simple and exceptionally secure procedure with many major and significant ramifications over the Web-based structure. As shown in Fig. 1, user interface (UI) consists of three sections, namely (i) document issuer, (ii) citizen part, and (iii) document seeker (i.e., third party service provider).

At first, document issuer issues a digital document to citizen through their software system. After issuance and validation of file, the document is uploaded through the cloud, which can be accessed from dashboard of citizen. In case a document seeker

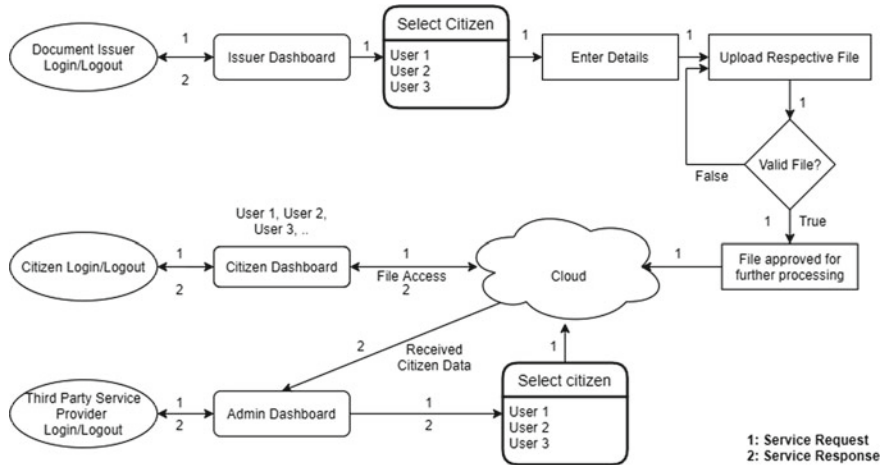


Fig. 1 General data flow of any electronic transaction

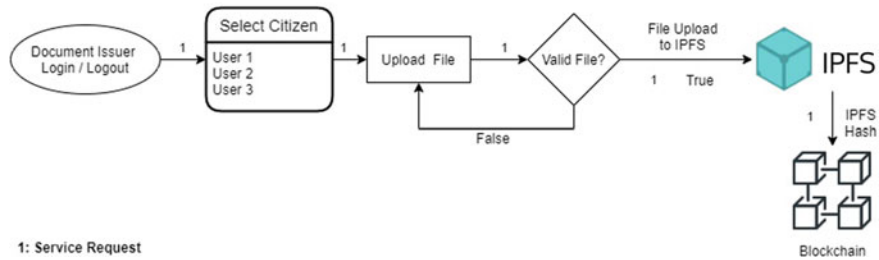


Fig. 2 Proposed electronic file management using IPFS: Phase-I

(i.e., third party service provider) wants any document from citizen, citizen can give its access directly to the document seeker (i.e., third party service provider). As that document is already verified, document seeker (i.e., third party service provider) does not need to invest resource (i.e., time, computation, etc.) to verify it further.

We have explained our proposed secure electronic file management using Interplanetary File System (IPFS) [19] through Phase-I and Phase-II. In this paper, Fig. 2 shows the issuance of document through Phase-I. To issue a document, issuer selects the citizen. After selecting the citizen, issuer uploads the document, which passes through prefixed file type validation [20]. After successful validation of file type, system uploads it into Interplanetary File System (IPFS) node. On upload to Interplanetary File System (IPFS), it returns an Interplanetary File System (IPFS) Hash for the uploaded document. To make it more robust, Interplanetary File System (IPFS) Hash is stored into the smart contract of blockchain. As blockchain [21, 22] is immutable in nature, after storing the Interplanetary File System (IPFS) Hash into a blockchain [23, 24], system becomes more robust in nature.

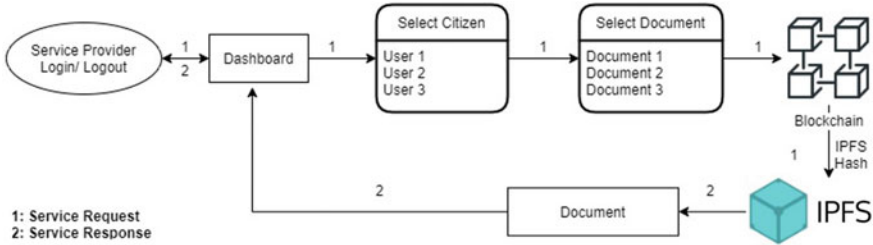


Fig. 3 Proposed electronic file management using IPFS: Phase-II

As shown in Fig. 3, Phase-II shows how the third party service provider can view the issued document. At first, the third party service provider selects citizen and then the particular document name from list of documents. Each and every document has a unique Interplanetary File System (IPFS) Hash. After getting the Interplanetary File System (IPFS) Hash from blockchain, Inter Planetary File System (IPFS) node will return the original document as a service response to the third party service provider. Transfer of issued document in the decentralized file storage is accessible only to citizen and its approved document seeker to guarantee that issued data is tamper proof due to its hash-based access. As a result, the tampering of document becomes extremely difficult for the adversary.

In this paper, authors have implemented Inter Planetary File System (IPFS) over banking and legal dataset to ensure data security, which is described below.

4.1 Application of IPFS over Banking Dataset

As shown in Fig. 4, Interplanetary File System (IPFS) is implemented over existing banking system. At first, document issuers like Pan Card Authority, Voter ID card Authority, Ration Card Authority, Birth Certificate Authority, etc., login into their respective section of the proposed system and open their respective dashboard [25, 26]. Then, the issuer selects citizen to issue its document. After the selection of citizen, issuer input details about desired document and verifies it to upload into Interplanetary File System (IPFS). Once Interplanetary File System (IPFS) confirms its upload procedure, it will return Interplanetary File System (IPFS) Hash, for the uploaded document. This Interplanetary File System (IPFS) Hash is stored in smart contract of blockchain. Citizen can access the issued file by login into the system and can grant its access to the service provider (i.e., bank).

Service providers like bank can access the document after login into their system. After a successful login, bank initiates **SERVICE REQUEST** to system by selecting user and respective document. Document's Interplanetary File System (IPFS) Hash is validated with blockchain to receive corresponding **SERVICE RESPONSE**. In this process, citizen is relieved from any physical document submission to bank. On

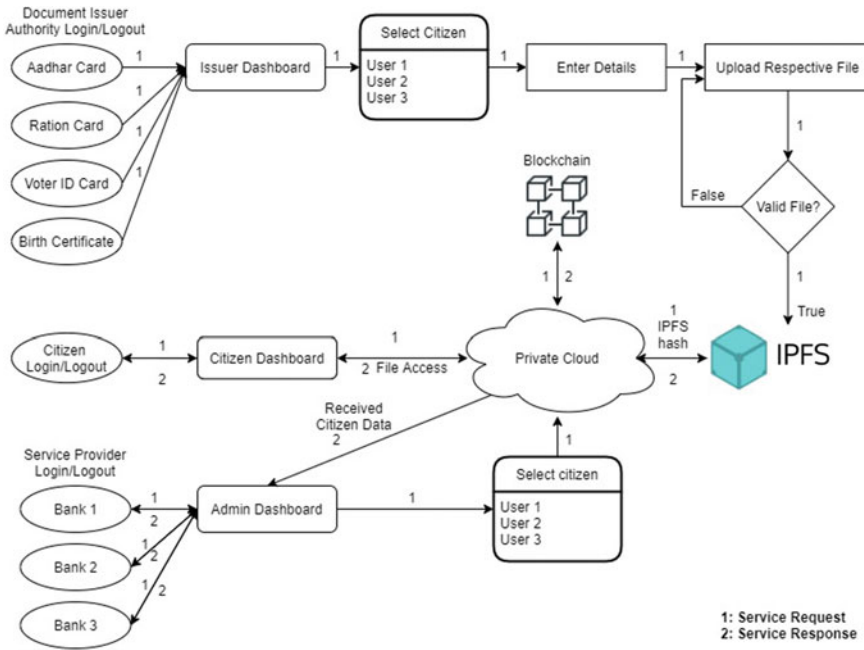


Fig. 4 Application of Interplanetary File System (IPFS) over banking dataset

the other side, bank is also relieved from verification of the document as it is already verified by the document issuer. In this way, an electronic document can be secured from any illicit attempts of adversaries.

Similarly, Interplanetary File System (IPFS) can also be applied to secure other datasets like legal dataset, which is discussed below.

4.2 Application of IPFS over Legal Dataset

As shown in Fig. 5, Interplanetary File System (IPFS) may be applied to secure electronic version of legal dataset [27]. In this case, legal professionals may login into their respective section in the proposed system and open their respective dashboard. After the selection of case number, legal professional [28] selects hard copy of plaintiff's case document, which are collected from several trial courts of West Bengal. These hard copy documents are converted into soft copy format (i.e., PDF format) using optical character recognition (OCR). These soft copy legal documents are validated and uploaded into Interplanetary File System (IPFS). After receiving confirmation about the uploaded file, Interplanetary File System (IPFS) returns Interplanetary File System (IPFS) Hash which is stored in smart contract of blockchain. For future retrieval of any case document [29], legal professional just login to its

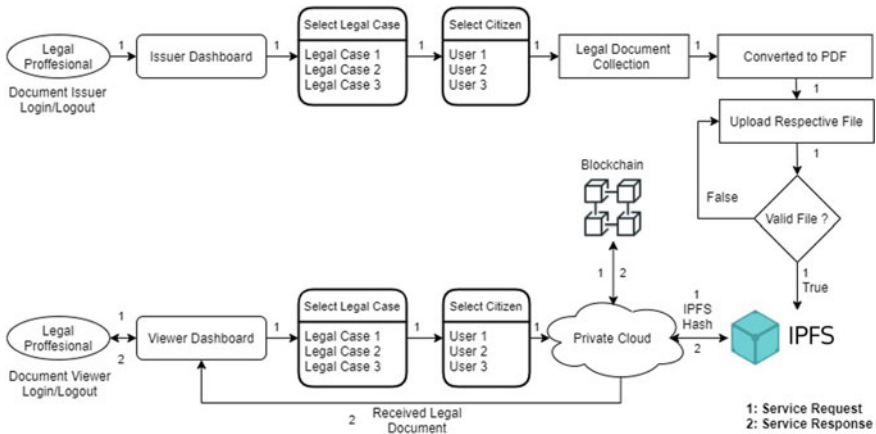


Fig. 5 Application of Interplanetary File System (IPFS) over legal dataset

portal and select the desired plaintiff case document. After obtaining the desired case document, a **SERVICE REQUEST** is sent to blockchain. As its corresponding **SERVICE RESPONSE**, blockchain will return Interplanetary File System (IPFS) Hash, which represents the desired case document from Interplanetary File System (IPFS).

5 Conclusion

In this paper, authors have discussed Interplanetary File System (IPFS)-based monitoring of electronic document to defend against any illicit attempts of adversary. Moreover, due to the application of Inter Planetary File System (IPFS) Hash, the computation time required for searching and physical verification of any document can be reduced to a significant level. Finally, blockchain-based multivariate application of Interplanetary File System (IPFS)-based electronic file management may be considered as future scope of this work.

References

1. BBC News (2020) Indian Prime Minister Modi Twitter Account Hacked. [online] Available at: <https://www.bbc.com/news/business-54007995>. Accessed 01 Oct 2020
2. Refugees U (2020) RefworldIndia: availability and prevalence of fraudulent identity documents, including membership cards of political parties (2011-April 2014), [online] Available at: <https://www.refworld.org/docid/538c369f4.html>. Accessed 04 Oct 2020
3. Rosa J, Teixeira C, Sousa Pinto J (2013) Risk factors in e-justice information systems. *Govern Inf Q* 30:241–256. <https://doi.org/10.1016/j.giq.2013.02.002>

4. Swaminathan V, Lepkowska-White E, Rao B (2006) Browsers or buyers in cyberspace? An investigation of factors influencing electronic exchange. *J Comput-Mediated Commun* 5: <https://doi.org/10.1111/j.1083-6101.1999.tb00335.x>
5. Gander P, Hartley L, Powell D, Cabon P, Hitchcock E, Mills A, Popkin S (2011) Fatigue risk management: organizational factors at the regulatory and industry/company level. *Accident Anal Prevent* 43:573–590. <https://doi.org/10.1016/j.aap.2009.11.007>
6. Guan Y, Shi W, Wu D (2012) The design and development of a school file management system for standardized. In: 2012 international conference on computer science and electronics engineering. <https://doi.org/10.1109/ICCSEE.2012.506>
7. Dickersin K (1990) The existence of publication bias and risk factors for its occurrence. *JAMA: J Am Med Assoc* 263:1385. <https://doi.org/10.1001/jama.1990.03440100097014>
8. Singhal N, Sharma M, Samant S, Goswami P, Reddy Y (2020) Smart KYC using blockchain and IPFS. Lecture Notes in Electrical Engineering, pp 77–84. https://doi.org/10.1007/978-981-15-3125-5_9
9. Steichen M, Fiz B, Norvill R, Shbair W, State R (2018) Blockchain-Based, decentralized access control for IPFS. 2018 IEEE international conference on internet of things (iThings) and IEEE green computing and communications (GreenCom) and IEEE cyber, physical and social computing (CPSCom) and IEEE smart data (SmartData). <https://doi.org/10.1109/Cybermatics.2018.2018.00253>
10. Tenorio-Fornés A, Jacynycz V, Llop-Vila D, Sánchez-Ruiz A, Hassan S (2019) Towards a decentralized process for scientific publication and peer review using blockchain and IPFS. In: Proceedings of the 52nd Hawaii international conference on system sciences. <https://doi.org/10.24251/HICSS.2019.560>
11. Nizamuddin N, Salah K, Ajmal Azad M, Arshad J, Rehman M (2019) Decentralized document version control using ethereum blockchain and IPFS. *Comput Electr Eng* 76:183–197. <https://doi.org/10.1016/j.compeleceng.2019.03.014>
12. Dias D, Benet J (2016) Distributed web applications with IPFS, tutorial. Lecture Notes in Computer Science 616–619: <https://doi.org/10.1007/978-3-319-38791-8-60>
13. Muralidharan S, Ko H (2019) An InterPlanetary file system (IPFS) based IoT framework. In: 2019 IEEE international conference on consumer electronics (ICCE), pp 1–2. <https://doi.org/10.1109/ICCE.2019.8662002>
14. Sicilia M, Sánchez-Alonso S, García-Barriocanal E (2016) Sharing linked open data over peer-to-peer distributed file systems: the case of IPFS. *Commun Comput Inf Sci* 3–14: <https://doi.org/10.1007/978-3-319-49157-8-1>
15. Nasir M, Muhammad K, Bellavista P, Lee M, Sajjad M (2020) Prioritization and alert fusion in distributed IoT sensors using Kademia based distributed hash tables. *IEEE Access* 8:175194–175204. <https://doi.org/10.1109/ACCESS.2020.3017009>
16. Benhamouda F, Halevi S, Halevi T (2018) Supporting private data on hyperledger fabric with secure multiparty computation. In: IEEE international conference on cloud engineering (IC2E)
17. Politou E, Alepis E, Patsakis C, Casino F, Alazab M (2020) Delegated content erasure in IPFS. *Future Gener Comput Syst* 112:956–964. <https://doi.org/10.1016/j.future.2020.06.037>
18. Shen J, Li Y, Zhou Y, Wang X (2019) Understanding I/O performance of IPFS storage. In: Proceedings of the international symposium on quality of service. <https://doi.org/10.1145/3326285.3329052>
19. Zheng Q, Li Y, Chen P, Dong X (2018) An innovative IPFS-based storage model for blockchain. In: 2018 IEEE/WIC/ACM international conference on web intelligence (WI). <https://doi.org/10.1109/WI.2018.000-8>
20. Ying N, Yao Z, Hua Z (2009) The study of multi-level authentication-based single sign-on system. In: 2009 2nd IEEE international conference on broadband network and multimedia technology, pp 448–452
21. Pinno OJA, Gregio ARA, De Bona LCE (2017) ControlChain: blockchain as a central enabler for access control authorizations in the IoT. In: GLOBECOM 2017. IEEE global communications conference. Singapore

22. Tapas N, Merlino G, Longo F (2018) Blockchain-based IoT-cloud authorization and delegation. In: 2018 IEEE international conference on smart computing (SMARTCOMP), Taormina, pp pp 411–416
23. Odelu V (2019) IMBUA: identity management on blockchain for biometrics-based user authentication. Advances in intelligent systems and computing, pp 1–10. <https://doi.org/10.1007/978-3-030-23813-1-1>
24. Nizamuddin N, Hasan H, Salah K (2018) IPFS-Blockchain-Based Authenticity of Online Publications. Lecture Notes in Computer Science 199–212: <https://doi.org/10.1007/978-3-319-94478-4-14>
25. Roy A (2019) Smart delivery of multifaceted services through connected governance. In: 3rd international conference on computing methodologies and communication (ICCMC). IEEE. India, pp 476–482. <https://doi.org/10.1109/ICCMC.2019.8819851>
26. Biswas A, Roy A (2019) A study on dynamic ID based user authentication system using smart card.: ajct [Internet]. [cited 26Feb.2020];5(2). <http://www.asianssr.org/index.php/ajct/article/view/871>
27. Sil R, Roy A (2020) A novel approach on argument based legal prediction model using machine learning. In: International conference on smart electronics and communication, 487–490.<https://doi.org/10.1109/ICOSEC49089.2020.9215310>
28. Saha D, Sil R, Roy A (2021) A study on implementation of text analytics over legal domain. In: Bhateja V, Peng SL, Satapathy SC, Zhang YD (eds) Evolution in computational intelligence. Advances in intelligent systems and computing, vol 1176. <https://doi.org/10.1007/978-981-15-5788-0-54>
29. Sil R, Roy A, Bhushan B, Mazumdar A (2019) Artificial intelligence and machine learning based legal application: the state-of-the-art and future research trends. In: 2019 international conference on computing, communication, and intelligent systems (ICCCIS). <https://doi.org/10.1109/ICCCIS48478.2019.8974479>

A Hybrid LWT and DCT-Based Lossless Watermarking Scheme for Color Images



Roop Singh, Alaknanda Ashok, and Mukesh Saraswat

Abstract This paper introduces a hybrid lossless color image watermarking scheme using lifting wavelet transform (LWT) in discrete cosine transform (DCT) domain. A scrambled watermark image corresponds to Arnold transform is embedded. The two-level LWT is performed on a host image and LL subband is chosen, followed by DCT for embedding the scrambled watermark. The performance of the proposed scheme has been validated in terms of PSNR and NC. The various image processing attacks are encountered to investigate the robustness.

Keywords Color watermarking · LWT · DCT · Arnold transform · PSNR · NC

1 Introduction

The fast advancement in multimedia technology has increased the possibility of manipulating, copying, and transferring data among the public in an unfair manner which leads to the violation of digital management rights. It is a serious issue for the researchers to provide security to multimedia content in the present scenario [1]. The researchers have presented many techniques such as stenography, encryption, and cryptography to protect multimedia contents but fail. Digital watermarking is an efficient scheme to prevent unauthorized users from [2–4]. Digital watermarking incorporates a watermark that can be recovered back later.

R. Singh (✉)

Department of Electronics and Communication Engineering, Uttarakhand Technical University, Dehradun, Uttarakhand, India

A. Ashok

Dean College of Technology, G.B. Pant University of Agriculture and Technology, Pantnagar, Uttarakhand, India

M. Saraswat

Jaypee Institute of Information Technology, Noida, India

Generally, watermarking schemes are of two types, i.e., frequency domain scheme and spatial domain scheme. A message as a watermark is directly concealed into the cover image in spatial domain schemes. However, these schemes are computationally fast but vulnerable to image processing attacks. In another type of scheme, the watermark is incorporated into the frequency coefficients rather than direct insertion. Frequency domain schemes are more reliable and robust than the spatial domain schemes [5]. The most powerful techniques used in frequency domain are DWT [6], DCT [7], and RDWT [5].

In the present scenario, the researchers are focusing on color watermarking schemes rather than grayscale watermarking schemes. In 2007, Agreste et al. [8] described a watermarking method to insert images into the HH subband of DWT. In 2010, Golea et al. [9] offered a blind watermarking scheme based on SVD for color images. In 2012, Vahedi et al. [10] invented a three-level DWT-based watermarking technique to improve the performance. In 2014, Su et al. [11] suggested a color watermarking approach to embed a color watermark by using OR decomposition. In 2015, Gupta et al. [12] presented a watermarking technique which uses three-level DWT in uncorrelated color space (UCS). In 2016, Chaturvedi et al. [13] employed mid-band DCT. In 2017, Zhang et al. [14] suggested a watermarking algorithm by using SVD in the spatial domain. Sharma et al. [15] deployed firefly for image segmentation. In 2018, Roy et al. [5] introduced a watermarking scheme by utilizing SVD in RDWT domain. Gupta et al. identified race [16] and age [17] using color images. In 2019, Yadav et al. [18] used dither-based block truncation for image retrieval. In 2020, Sharma et al. [19] utilized Kapur and Tsallis entropy for thresholding. However, the existing techniques suffer information loss caused by the truncation of pixels value. Hence, the aforementioned schemes are not capable to provide lossless data recovery. Therefore, this paper presents a lossless robust watermarking (LWT-DCT) scheme using LWT-DCT for color images.

The remaining paper is structured as follows: Sect. 2 explains the related watermarking schemes. The proposed scheme is discussed in detail in Sect. 3. The experimental results are presented in Sect. 4. Finally, Sect. 5 concludes the paper.

2 Preliminaries

2.1 Lifting Wavelet Transform

The lifting wavelet transform (LWT) is an extended version of DWT, introduced by Sweldens [20]. LWT partitioned an image into four subbands namely, LL (approximation), LH (horizontal), HL (vertical), and HH (diagonal) coefficients respectively. Unlike DWT, LWT converts an image pixel's value from integers to integers which results in lossless, computationally faster, and reliable execution. There are mainly three steps, namely split, predict, and update. The lifting scheme is depicted in Fig. 1.

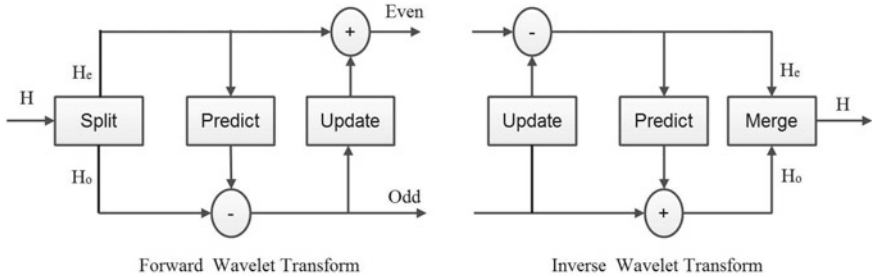


Fig. 1 Lifting scheme

Splitting: Divide an image into even and odd parts.

$$H_e = A[2n]$$

$$H_o = A[2n + 1]$$

Prediction: each odd pixel value is calculated by subtracting even pixel values from odd pixel values.

Updation: Predicted odd samples are added with the even samples to obtain updated new even samples.

2.2 Discrete Cosine Transform

The image information can be extracted by converting image into frequency domain. DCT is a compression tool especially for lossy compression because of its energy compaction property.

The 2D-DCT of a host image $c(a, b)$ having size $r_1 \times c_1$ can be described by Eq. (1):

$$\begin{aligned} D(p, q) &= \frac{2}{\sqrt{r_1 c_1}} \beta(p) \beta(q) \sum_{a=0}^{r_1-1} \sum_{b=0}^{c_1-1} c(a, b) \\ &\quad \times \cos \frac{(2a+1)p\pi}{2r_1} \times \cos \frac{(2b+1)q\pi}{2c_1} \end{aligned} \quad (1)$$

The inverse DCT is given by Eq. (2).

$$\begin{aligned} c(a, b) &= \frac{2}{\sqrt{r_1 c_1}} \sum_{p=0}^{r_1-1} \sum_{q=0}^{c_1-1} \beta(p) \beta(q) D(p, q) \\ &\quad \times \cos \frac{(2a+1)p\pi}{2r_1} \times \cos \frac{(2b+1)q\pi}{2c_1} \end{aligned} \quad (2)$$

where $\beta(p), \beta(q)$ is defined by Eq. (3)

$$\beta(p), \beta(q) = \begin{cases} \frac{1}{\sqrt{2}} & \text{if } p, q = 0 \\ 1 & \text{else} \end{cases} \quad (3)$$

2.3 Arnold Transform

The Arnold transform shuffles pixel's value within image to enhance security and provides scrambled image. The pixel's values are mapped into a new pixel's value through an iterative process in Arnold transform.

The two-dimensional Arnold transform of a host image can be described by Eq. (4):

$$\begin{bmatrix} x_p \\ y_p \end{bmatrix} = \begin{bmatrix} 1 & c \\ d & cd + 1 \end{bmatrix} \begin{bmatrix} x_{p-1} \\ y_{p-1} \end{bmatrix} \mod (n) \quad (4)$$

where c and d denote real and positive values. After p iterations, the output of Arnold transform is x_p , and y_p according to coordinates x_{p-1} and y_{p-1} , n represents the size of a square transformed output image.

3 Proposed Scheme

This section presents the two phases, i.e., embedding and extraction of the proposed scheme. The proposed scheme is depicted in Fig. 2.

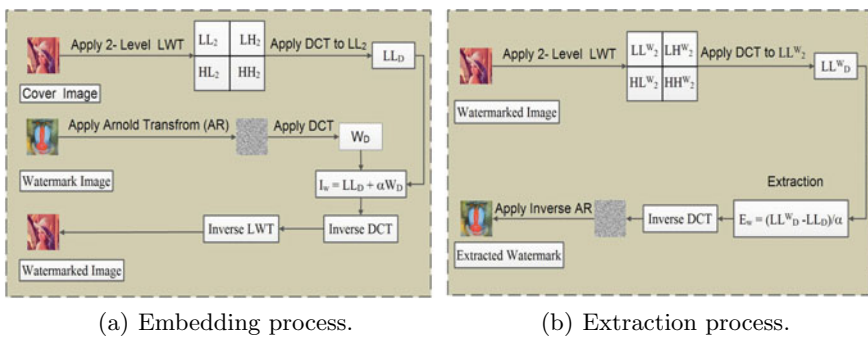


Fig. 2 The proposed watermarking scheme

3.1 Embedding Scheme

The followings steps are taken into consideration while embedding a watermark.

1. Select a color host image (H) of size $L \times L$.
2. Select color watermark image (W) of size $\frac{L}{4} \times \frac{L}{4}$.
3. Perform two-level LWT on a color image (H), to form four subbands namely, LL_H^2 , LH_H^2 , HL_H^2 , and HH_H^2 .
4. Select subband LL_H^2 followed by DCT to obtain LL_D for insert watermark image.
5. Perform Arnold transform on a watermark image (W) followed by DCT to obtain W_D .
6. Embed both LL_D and W_D through a constant embedding factor (0.15) according to Eq.(5).

$$I_w = LL_D + \alpha \times W_D \quad (5)$$

7. Compute IDCT on I_w followed by two-level IWT to obtained watermarked image.

3.2 Extraction Scheme

In watermarking scheme, reverse operation of the watermark embedding scheme is the extraction. To recover the watermark, following steps are taken.

1. Select a color watermarked image (W_m) of size $L \times L$.
2. Perform two-level LWT on a color watermarked image (W_m), to obtain four subbands, namely LL_W^2 , LH_W^2 , HL_W^2 , and HH_W^2 .
3. Select subband LL_W^2 followed by DCT to obtain LL_D^W .
4. Extract watermark E_w by Eq.(6).

$$E_w = \frac{(LL_D^W - LL_D)}{\alpha} \quad (6)$$

5. Compute IDCT on E_w to obtain scrambled watermark image.
6. Finally, perform inverse Arnold transform to get extracted watermark image.

4 Result Analysis and Discussions

The practical implementation of the proposed scheme has been carried out on MATLAB along with eight standard test images of size 512×512 , envisioned in Fig.3 and taken from the database USC-SIPI [21]. The efficacy of the proposed scheme is investigated by performing ten well-known image processing attacks, namely (i) Gaussian noise, (ii) Localvar noise, (iii) Poisson noise, (iv) Salt and pepper noise, (v)



Fig. 3 The input images **a** Lena, **b** Barbara, **c** Airplane, **d** Sailboat, **e** Peppers, **f** Tulip, **g** Splash, and Watermark image **h** Baboon

Speckle noise, (vi) Rotation, (vii) Gaussian filtering, (viii) Median filtering, (ix) Histogram equalization, and (x) JPEG compression. The results of the proposed scheme is compared with Su et al. [11], Gupta et al. [12] and Zhang et al. [14].

4.1 Performance Parameters

The imperceptibility and robustness can be evaluated through PSNR and NC matrices, respectively. The imperceptibility and robustness indicate the visual quality of watermarked and extracted watermark images respectively. PSNR measures the imperceptibility (cover image, color watermarked image of size $L \times L$).

Mathematically, PSNR is given by Eq. (7)

$$\text{PSNR}(C, W) = 20 \log_{10} \left(\frac{H_{\max}}{\sqrt{\text{MSE}}} \right) \quad (7)$$

where MSE represents mean squared error which is computed by Eq. (8)

$$\text{MSE}(C, W) = \frac{1}{R^2} \sum_{u=1}^R \sum_{v=1}^R (C(u, v) - W(u, v))^2 \quad (8)$$

To assess the robustness, NC is used and calculated between the watermark image and the extracted watermark image of size $R_1 \times R_1$.



Fig. 4 Visual quality of watermarked images and extracted watermark images

Mathematically, NC is expressed by Eq. (9)

$$\text{NC}(w, E_w) = \frac{\sum_{u=1}^{R_1} \sum_{v=1}^{R_1} w(u, v) E_w(u, v)}{\sqrt{\sum_{u=1}^{R_1} \sum_{v=1}^{R_1} w(u, v)^2} \sqrt{\sum_{u=1}^{R_1} \sum_{v=1}^{R_1} E_w(u, v)^2}} \quad (9)$$

Imperceptibility analysis: For qualitative analysis, Fig. 4 depicts that the quality of watermarked image, as well as extracted watermark image, is quite closer to the host images shown in Fig. 3. Table 1 shows that the proposed (LWT-DCT) scheme has

Table 1 Comparative analysis of imperceptibility

Host image	Watermark image	Proposed (LWT-DCT)	Su et al. [11]	Gupta et al. [12]	Zhang et al. [14]
Lena	Baboon	40.03	38.71	36.85	37.42
Barbara	Baboon	39.99	38.01	37.59	37.61
Airplane	Baboon	40.01	38.79	37.74	37.57
Sailboat	Baboon	40.57	38.57	36.42	37.39
Peppers	Baboon	40.52	38.23	36.71	37.72
Tulip	Baboon	40.51	38.36	37.32	37.52
Splash	Baboon	40.96	38.81	37.77	37.97

Table 2 Comparative analysis of robustness for Lena image

S. No.	Description of attack	Proposed (LWT-DCT)	Su et al. [11]	Gupta et al. [12]	Zhang et al. [14]
1	Gaussian noise (10%)	0.9878	0.9796	0.9714	0.9632
2	Localvar noise (5%)	0.9827	0.9745	0.9663	0.9581
3	Poisson noise	0.9960	0.9878	0.9796	0.9714
4	<i>Salt and pepper noise</i> (5%)	0.9980	0.9898	0.9816	0.9734
5	Speckle noise	0.9905	0.9823	0.9741	0.9659
6	Rotate 30° in anticlockwise	0.9745	0.9663	0.9581	0.9499
7	Gaussian filtering (3 × 3)	0.9999	0.9917	0.9835	0.9753
8	Median filtering (3 × 3)	0.9990	0.9908	0.9826	0.9744
9	Histogram equalization (0, 255)	0.9878	0.9796	0.9714	0.9632
10	JPEG compression ($Q = 20$)	0.9999	0.9917	0.9835	0.9753

acquired PSNR above 40 for all images. Table 1 illustrates the comparative analysis of imperceptibility with other related schemes. It can be depicted from the table that the LWT-DCT scheme outperforms the related schemes.

Robustness analysis: Table 2 depicts the qualitative analysis of robustness in terms of NC corresponds to each considered attack. It can be envisioned from the table that the LWT-DCT scheme has higher robustness than the considered schemes against each attack. For quantitative analysis, Table 3 shows that the LWT-DCT scheme returns back a recognizable watermark corresponding to each attack. Hence, the LWT-DCT scheme shows robustness.

Table 3 Quality of watermarked image and extracted watermark image after performing various attacks.

S.No.	Attack	Attacked image	Extracted watermark	S.No.	Attack	Attacked image	Extracted watermark
1	Gaussian noise (10%)			6	Rotation 30° in anticlockwise		
2	Localvar noise (5%)			7	Gaussian filter (3 × 3)		
3	Poisson noise			8	Median filtering size 3 × 3		
4	<i>Salt&pepper noise</i> (5%)			9	Histogram equalization [0, 255]		
5	<i>Speckle noise</i>			10	JPEG compression (20)		

5 Conclusion and Future Work

This paper introduces a lossless robust hybrid watermarking scheme based on LWT and DCT for color images. This approach uses the significant features of the lifting scheme and DCT scheme to acquire transparency and robustness. The proposed scheme resists image processing attacks.

References

- Tripathi AK, Sharma K, Bala M, Kumar A, Menon VG, Bashir AK (2020) A parallel military dog based algorithm for clustering big data in cognitive industrial internet of things. *IEEE Trans Ind Inf* 17(3):2134–2142
- Singh R, Ashok A, Saraswat M (2020) Optimised robust watermarking technique using CKGSA in DCT-SVD domain. *IET Image Process* 14(10):2052–2063
- Singh R, Gupta R (2011) Digital watermarking with visual cryptography in spatial domain. In: International conference on advanced computing, communication and networks, pp 948–951

4. Dubolia R, Singh R, Bhadoria SS, Gupta R (2011) Digital image watermarking by using discrete wavelet transform and discrete cosine transform and comparison based on PSNR. In: 2011 international conference on communication systems and network technologies. IEEE, pp pp 593–596
5. Roy S, Pal AK (2018) An SVD based location specific robust color image watermarking scheme using RDWT and Arnold scrambling. *Wirel Pers Commun* 98(2):2223–2250
6. Liu XL, Lin CC, Yuan SM (2016) Blind dual watermarking for color images-authentication and copyright protection. *IEEE Trans Circuits Syst Video Technol* 28(5):1047–1055
7. Singh D, Singh SK (2017) DCT based efficient fragile watermarking scheme for image authentication and restoration. *Multimedia Tools Appl* 76(1):953–977
8. Agreste S, Andaloro G, Prestipino D, Puccio L (2007) An image adaptive, wavelet-based watermarking of digital images. *J Comput Appl Math* 210(1–2):13–21
9. Golea NEH, Seghir R, Benzid R (2010) A bind RGB color image watermarking based on singular value decomposition. In: ACS/IEEE international conference on computer systems and applications-AICCSA 2010. IEEE, pp 1–5
10. Vahedi E, Zoroofi RA, Shiva M (2012) Toward a new wavelet-based watermarking approach for color images using bio-inspired optimization principles. *Digital Sig Process* 22(1):153–162
11. Su Q, Niu Y, Wang G, Jia S, Yue J (2014) Color image blind watermarking scheme based on QR decomposition. *Sig Process* 94:219–235
12. Gupta M, Parmar G, Gupta R, Saraswat M (2015) Discrete wavelet transform-based color image watermarking using uncorrelated color space and artificial bee colony. *Int J Comput Intell Syst* 8(2):364–380
13. Chaturvedi R, Sharma A, Dwivedi U, Kumar S, Praveen A (2016) Security enhanced image watermarking using mid-band DCT coefficient in YCbCr space. *Int J Control Theory Appl* 9(23):277–284
14. Zhang H, Wang C, Zhou X (2017) A robust image watermarking scheme based on SVD in the spatial domain. *Future Int* 9(3):45
15. Sharma A, Chaturvedi R, Dwivedi U, Kumar S, Reddy S (2018) Firefly algorithm based effective gray scale image segmentation using multilevel thresholding and entropy function. *Int J Pure Appl Math* 118(5):437–443
16. Gupta R, Yadav P, Kumar S (2017) Race identification from facial images using statistical techniques. *J Stat Manag Syst* 20(4):723–730
17. Gupta R, Kumar S, Yadav P, Shrivastava S (2018) Identification of age, gender, and race SMT (scare, marks, tattoos) from unconstrained facial images using statistical techniques. In: 2018 international conference on smart computing and electronic enterprise (ICSCEE). IEEE, pp 1–8
18. Yadav P, Gupta R, Kumar S (2019) Video image retrieval method using dither-based block truncation code with hybrid features of color and shape. In: Engineering vibration, communication and information processing. Springer, pp 339–348
19. Sharma A, Chaturvedi R, Kumar S, Dwivedi UK (2020) Multi-level image thresholding based on Kapur and Tsallis entropy using firefly algorithm. *J Interdiscip Math* 23(2):563–571
20. Sweldens W (1998) The lifting scheme: a construction of second generation wavelets. *SIAM J Math Anal* 29(2):511–546
21. Ali M, Ahn CW, Pant M (2014) A robust image watermarking technique using SVD and differential evolution in DCT domain. *Opt Int J Light Electron Opt* 125(1):428–434

Author Index

A

- Abbas, Hussein A., 873
Abdy Sayyed, Mohd Abbas H., 133
Abubacker, Nirase Fathima, 315
Acharyulu, B. V. S., 717
Afrose, Tamanna, 935
Aggarwal, Naveen, 759
Ahmad, Mohiuddin, 147
Ahuja, Yogesh Kumar, 533
Alaidah, Albtool, 315
Alamoudi, Eman, 315
Al Masry, Z., 911
Alnamshan, Hajar, 315
AlQahtani, Malak, 315
Al-Salamee, Baidaa A., 241
Al-Shammari, Dhiyah, 241
Amitha, I. C., 435
Amrita, 309
Anavatti, Sreenatha G., 873
Anwar, Md. Musfiqur, 935
Arya, Chandrakala, 111
Arya, Shobha, 111
Ashok, Alaknanda, 1027
Awoyera, Paul, 133
Azar, Ahmad Taher, 717

B

- Balyan, Vipin, 21
Bappy, Akash Shingha, 147
Baral, Vishal, 59
Baranidharan, B., 503
Bausys, Romualdas, 335
Bhandari, Manish, 275
Bharti, Shashvat, 803
Bhayani, Akshar, 921

- Bhosale, Hrushikesh, 629
Biswas, Ankur, 1017
Bondiombouy, Carlyn, 987

C

- Camargo, José Luis, 967
Cardoz, Lester, 157
Chakraverty, Shampa, 365
Chandra, Arunesh, 265
Chandrashekhar, D. K., 659
Chaplygin, Sergey, 545
Chatterjee, Kakali, 899
Chaturvedi, Yatender, 265
Chen, Zhengxin, 409
Choudhary, Shubhra, 533

D

- Dao, Thi-Kien, 69
Das, Tanuja, 813
Datt, Gopal, 617
Degila, Jules, 987
Desai, Bhishman, 921
Desai, Chitra, 99
Dhilsath Fathima, M., 691
Dinh, Xuan Truong, 975
Diwakar, Manoj, 111
Djeki, Essohanam, 987
Dutta, Maitreyee, 759

F

- Flores, Silvana, 709
Flores, Susana, 709
Francis, Sobers, 873

G

- Gajria, Vikrant, 839
 Gajula, Anuj, 157
 Galarce-Miranda, Claudia, 585
 Garg, Ayushi, 921
 Garg, Sanjay, 955
 Garratt, Matthew, 873
 Ghasiya, Piyush, 447
 Ghosh, Atashi Mani, 935
 Giampiccolo, S., 911
 Gobinath, R., 133
 Goel, Ankit, 265
 Gormaz-Lobos, Diego, 585
 Gorripotu, Tulasichandra Sekhar, 717
 Goyal, Ankur, 31
 Goyal, Rajni, 289
 Grewal, Harshit, 289
 Grover, K. S., 375
 Gupta, Mukesh Kumar, 355
 Gupta, Prateek, 309
 Gupta, Varun, 265
 Gupta, Yogendra, 13

H

- Hamdan, Lamia, 709
 Hayet, Mouss Leila, 235
 Hegade, Prakash, 489
 Hiasat, Ahmad, 789
 Hilgarth, Alexander, 585
 Hornillo-Mellado, Susana, 967
 Hossen, Murad, 935

I

- Indira, Sreelekshmi, 773
 Irani, Arshan, 157
 Islam, Md. Tobibul, 147
 Ivaschenko, Anton, 545

J

- Janamala, Varaprasad, 201
 Jangid, Amita, 355
 Jangid, Amit Kumar, 375
 Jha, Shivam, 921
 Jindal, Gaurav, 81
 Jones, Santiago, 709
 Joshi, Aditya, 121
 Joshi, Tanvi, 629
 Joykutty, Anu Maria, 503
 Justin Samuel, S., 691
 Juyal, Amit, 121

K

- Kalathil, Abhishek Thazheth, 395
 Kamal, Nashwa Ahmad, 717
 Kamat, Pooja, 157
 Kanani, Pratik, 839
 Karwal, Ramesh, 275
 Kathiya, Ajaysinh Vikramsinh, 955
 Kaur, Gaganpreet, 81
 Khatti, Jitendra, 375
 Kini, Gopalakrishna N., 575
 Koganti, Nishanth, 803
 Kolesnikova, Katerina, 1
 Kolsanov, Alexandr, 545
 Kumari, E. Kusuma, 461
 Kumar, M. Vinod, 461
 Kumar, Pradeep, 275
 Kumar, Sachin, 45
 Kumar, Sandeep, 31, 717
 Kumar, Satish, 157
 Kumawat, Renu, 557

L

- Lahorkar, Ashwin, 629
 Lima, Rui, 211, 223
 Loganathan, D., 643

M

- Madhani, Nishay, 839
 Mairot, N., 911
 Makhija, Nishkarsh, 533
 Mallya, Girish P., 489
 Marndi, Ashapurna, 595
 Marni, Pallavi, 157
 Martín-Clemente, Rubén, 967
 Meriem, Benbrahim, 235
 Meshram, Pratiksha, 921
 Mezentseva, Olga, 1
 Mishra, Sumita, 45
 Mittal, M. L., 275
 Mohan, Sherna, 513
 Mohanty, Banaja, 717
 Mohanty, Nirjharini, 59
 Montenegro, Sergio, 585
 Murugan, S., 461

N

- Nadjiha, Hadjidj, 235
 Nagaraja, S. R., 187
 Nagaraju, T. V., 133
 Narayanan, N. K., 435
 Nayak, Soumen, 59

- Nazaryan, Aikush, 545
 Ngo, Truong-Giang, 69
 Nguyen, Trong-The, 69
- O**
 Ojha, Priyanka, 575
 Okamura, Koji, 447
 Omri, N., 911
- P**
 Paiva, Sara, 211, 223
 Pandraju, Thandava Krishna Sai, 201
 Patra, G. K., 595
 Pham, Duc-Tinh, 69
 Pilla, Ramana, 717
 Polley, Dipan, 395
 Popli, Garima, 475
 Prasad, Vikash Kumar, 803
- R**
 Rahman, Maruf, 813
 Rai, K. N., 831
 Rai, Shwetha, 575
 Rajesh, M., 187
 Rajitha, B., 533
 Ramachandran, Sivakumar, 773
 Ramya, Prakash, 669
 Rao, B. Ashwath, 575
 Rathore, Likhita, 31
 Reddy, Preneer, 173
 Renuga Devi, S., 669
 Ribeiro, Jorge, 211, 223
 Rizvi, Syed Wajahat Abbas, 297
 Rout, Imlee, 59
 Roy, Abhishek, 1017
- S**
 Sachdeva, Ashish, 945
 Sadasivam, Sudha, 885
 Saha, Akash, 157
 Saha, Monarch, 59
 Saha, Pratim, 423
 Saini, Prateek, 731
 Sane, Aamod, 629
 Sangwan, Anju, 475
 Sangwan, Anupma, 475
 Saraswat, Mala, 365
 Saraswat, Mukesh, 1027
 Satapathy, Santosh Kumar, 643
 Savielieva, Olena, 1
- Selvaganapathy, Shymala Gowri, 885
 Semenas, Rokas, 335
 Serrano, Fernando E., 717
 Shalabi, Dauaa, 315
 Sharathkumar, S., 643
 Sharma, Ashish, 13
 Sharma, Harish, 13, 731, 745
 Sharma, Niketa, 13
 Sharma, Nirmala, 731, 745
 Sharma, Purnima K., 461
 Sherly Puspha Annabel, L., 607
 Shreya, Shashi, 899
 Shringi, Sakshi, 731
 Shukla, Apratim, 395
 Sil, Riya, 1017
 Singh, Mahesh Kumar, 1005
 Singh, Meghna, 745
 Singh, O. P., 45
 Singh, Poonam, 759
 Singh, Pratibha, 575
 Singh, Rishi Pal, 475
 Singh, Roop, 1027
 Singh, Yogendra Narain, 1005
 Solanki, Brijraj Singh, 557
 Sreenidhi, S., 607
 Srikanthiah, K. C., 659
 Srinivasan, Seshadhri, 557
 Srivastava, Sonam, 1005
 Subhashini, N., 395
 Sugandhi, Rekha, 157
 Sultana, Naznin, 423
 Suresh, Mekhana, 773
 Swart, Theo G., 173
- T**
 Tangudu, Srihitha, 533
 Tarek, Berghout, 235
 Tewari, Naveen, 617
 Thandapani, Jothiswaran, 69
 Tharun, V. P., 669
 Tikhe, Gaurav, 629
 Tolani, Mayank K., 395
 Tomar, V. K., 945
 Torrero, Claudia, 709
 Torrero, Everardo, 709
- U**
 Upadhyay, P., 831
- V**
 Valadi, Jayaraman K., 629

Van Pham, Hai, [975](#)
Venugopal, K. R., [659](#)
Verma, Jai Prakash, [955](#)
Verma, Shubhangi, [45](#)
Vimina, E. R., [513](#)
Vishali, N., [607](#)
Vu, Van-Dinh, [69](#)

W

Wyk van, Dirk, [21](#)

X

Xing, Zexi, [409](#)

Z

Zakaria, Nordin, [855](#)
Zarzoso, Vicente, [967](#)
Zerhouni, N., [911](#)